CONF-821026--

NOTICE

PORTIONS OF THIS REPORT ARE ILLEGIBLE. It has been reproduced from the best available copy to permit the broadest possible availability.

HYDROGEN AND WATER REACTOR SAFETY

Proceedings of the Second International Conference
on the Impact of Hydrogen on Water Reactor Safety
Albuquerque, New Mexico
October 3-7, 1982

NUREG/CP--0038

TI84 016099

Sponsored by

US Nuclear Regulatory Commission
Electric Power Research Institute

Hosted by

Sandia National Laboratories

NUREG/CP-0038
EPRI RP 1932-35
SAND82-2456

MASTER

DISCLAIMER

This report was prepared as an account of work sponsored by an agency of the United States Government. Neither the United States Government nor any agency thereof, nor any of their employees, makes any warranty, express or implied, or assumes any legal liability or responsibility for the accuracy, completeness, or usefulness of any information, apparatus, product, or process disclosed, or represents that its use would not infringe privately owned rights. Reference herein to any specific commercial product, process, or service by trade name, trademark, manufacturer, or otherwise does not necessarily constitute or imply its endorsement, recommendation, or favoring by the United States Government or any agency thereof. The views and opinions of authors expressed herein do not necessarily state or reflect those of the United States Government or any agency thereof.

DISTRIBUTION OF THIS DOCUMENT IS UNLIMITED

DISCLAIMER

This report was prepared as an account of work sponsored by an agency of the United States Government. Neither the United States Government nor any agency Thereof, nor any of their employees, makes any warranty, express or implied, or assumes any legal liability or responsibility for the accuracy, completeness, or usefulness of any information, apparatus, product, or process disclosed, or represents that its use would not infringe privately owned rights. Reference herein to any specific commercial product, process, or service by trade name, trademark, manufacturer, or otherwise does not necessarily constitute or imply its endorsement, recommendation, or favoring by the United States Government or any agency thereof. The views and opinions of authors expressed herein do not necessarily state or reflect those of the United States Government or any agency thereof.

DISCLAIMER

Portions of this document may be illegible in electronic image products. Images are produced from the best available original document.

CONFERENCE ORGANIZING COMMITTEE

M. Berman, Sandia National Laboratories
J. Larkins, U.S. Nuclear Regulatory Commission
L. Thompson, Electric Power Research Institute

TECHNICAL PROGRAM COMMITTEE

M. Berman, Sandia National Laboratories
J. Carey, Electric Power Research Institute
J. Larkins, U.S. Nuclear Regulatory Commission
L. Thompson, Electric Power Research Institute

FOREWORD

The first Workshop on the Impact of Hydrogen on Water Reactor Safety was held in Albuquerque, New Mexico, January 26-28, 1981 and sponsored by the U.S. Nuclear Regulatory Commission. Interest was even higher than expected and nearly 200 attendees from 9 countries gathered to hear 44 papers in 5 sessions. That conference included tutorials on hydrogen behavior, presentations of analyses and research plans, and surveys of work largely performed prior to the Three Mile Island accident.

The ensuing year and a half has seen an accelerated interest in hydrogen control as research programs have developed and as regulatory issues have been debated. Utilities and industry have become more deeply involved: the second Workshop was sponsored by both EPRI and the USNRC, and 'International' was properly added to the title. Held October 3-7, 1982, 8 sessions were necessary for the presentation of 73 papers, with 169 people attending from 10 countries. Keynote addresses were given by J. J. Taylor, Director of the Nuclear Regulatory Research, USNRC, and by H. R. Denton, Director of the Office of Nuclear Reactor Regulation, USNRC.

Several trends are apparent with respect to the 1981 and 1982 agendas. Utilities and architect engineers presented four times as many papers in 1982 than in 1981, amounting to 25 percent of the 1982 total. The number of papers describing USNRC-sponsored research also rose although the percentage dropped slightly from 50 to 45 percent. The number of papers from other countries did not change, and EPRI-sponsored work rose to about 15 percent of the 1982 total.

Due to the wide interest in each workshop topic, the sessions were held in series so that all attendees could participate. Overview presentations of several large research programs were included in the first session. (This is in contrast to the first workshop which saw research plans presented on the last day.) Sessions followed on hydrogen behavior during accidents, combustible gas generation, mixing, combustion models and experiments, accelerated flames and detonations, mitigation and control, and equipment survivability.

About one-quarter of the papers reported new experimental results, the remainder dealing with evaluations or analyses. The experimental results to date are very encouraging, and strides are rapidly being made in the understanding of hydrogen and its control in containment buildings.

Loren Thompson
Electric Power Research Institute
Palo Alto, CA 94303

John Larkins
U.S. Nuclear Regulatory Commission
Washington, D.C. 20555

CONTENTS

	Page
FOREWORD	ii
LIST OF ATTENDEES	xi
INTRODUCTION J. J. Taylor	
SESSION I: HYDROGEN RESEARCH PROGRAMS CHAIRMAN: MARSHALL BERMAN	
"Regulatory Perspectives on Hydrogen Control for Degraded Core Accidents" W. R. Butler and C. G. Tinkler	
"Hydrogen Research & Nuclear Safety--A Utility Perspective" W. Lau	2
"EPRI Research on Hydrogen Combustion and Control" L. Thompson	2
"The NRC Hydrogen Behavior and Mitigation Research Programs" J. T. Larkins and P. Worthington	4
"IDCOR Approach to Hydrogen Generation, Combustion and Burn Control" E. L. Fuller and E. P. Stroupe	7
"Research Programs Performed by ENEA Pisa University and Ansaldo Impianti on the Impact of Hydrogen on LWR Safety" F. Fineschi, A. Morici and R. Zinnari	9
SESSION II: HYDROGEN BEHAVIOR DURING LWR ACCIDENTS CO-CHAIRMEN: JOHN T. LARKINS AND LOREN THOMPSON	115
"Hydrogen Behavior and Control at Light Water Reactors During Normal Operations and During Accidents" C. F. Kupiec and A. L. Camp	117

CONTENTS (Cont.)

	Page
"Training for Power Plant Personnel on Hydrogen Production and Control" G. J. Dickelman	131
"The CONTEMPT-DG Containment Analysis Code" R. E. Deem and K. Rousseau	145
"Effects of Hydrogen Burning and Associated Engineered Safety Features on Containment Building Responses" S. S. Iyer and R. E. Deem	161
"Applications of HECTR to Reactor Containments" S. E. Dingman, M. J. Wester and A. L. Camp	175
"Multiple Hydrogen-Air Deflagrations in Containment and the Resulting Thermal Environments" S. N. Kempka, A. C. Ratzel and M. R. Baer	191
"Evaluation of Post-Accident Combustible Gas at Millstone Unit I" J. H. Bickel	209
"BWR Mark III Pressure Suppression Containment Response to Hydrogen Deflagration G. M. Fuls and A. D. Gunter	225
"Effect of Hydrogen Control on the Risk From Severe Accidents in a BWR/6 Mark III Standard Plant" D. A. Hankins and K. W. Holtzclaw	257
"Assessment of Hydrogen Combustion Effects in the BWR/6 Mark III Standard Plant" J. S. Elliott, L. B. Nesbitt, P. F. Gou, S. S. Dua and D. A. Hankins	265 ~~257~~
"A Utility Perspective on Hydrogen Control" J. D. Richardson and S. H. Hobbs	283
SESSION III: COMBUSTIBLE GAS GENERATION CO-CHAIRMEN: DANA A. POWERS AND JOHN J. HAUGH	301
"Zircaloy-Oxidation and Hydrogen-Generation Rates in Degraded Core Accident Situations" H. M. Chung, C. H. Bowers and G. R. Thomas	303
"H_2 Production From the Steel-Water Reaction During a Postulated Core Meltdown Accident" W. S. Yu and W. T. Pratt	317

CONTENTS (Cont.)

	Page
"Hydrogen Production During Fragmented Debris/ Concrete Interactions" W. W. Tarbell and R. Blose	333
"Hydrogen Generation During Molten-Fuel-Coolant Interactions" M. L. Corradini	351
"Gas Release and Containment History During Melt-Concrete Interaction" K. Hassmann, W. Schwarzott and R. Reimann	369
"Combustible Gas Generation From Molten Fuel-Concrete Interactions" R. K. Cole and D. P. Kelly	385
"Corrosion of Aluminum and Zinc in Containment Following a LOCA and Potential for Precipitation of Corrosion Products in the Sump" K. K. Niyogi and J. S. Mackenzie	401
"Effects of Temperature, pH and Boron on Rates of Hydrogen Generation From Zinc Corrosion" V. M. Loyola	425
"Hydrogen Generation From Aluminum Corrosion in Containment Spray Solutions" W. Frid and G. Karlberg	432 439
SESSION IV: HYDROGEN TRANSPORT AND MIXING CO-CHAIRMEN: HERMANN L. JAHN AND LOUIS MUHLSTEIN	451
"Hydrogen Distribution in a Containment With a High Velocity Hydrogen-Steam Source" G. R. Bloom, L. D. Muhlestein, and A. K. Postma	453
"Assessment of RALOC MOD1 and 1980 Updates" L. D. Buxton	469
"Recent Improvements in the RALOC Code" H. L. Jahn, P. Papadimitriou, T. V. Pham and G. Weber	
"HMS: A Model for Hydrogen Migration Studies in LWR Containments" J. R. Travis	489
"Application of COBRA-NC to Hydrogen Transport" M. Thurgood	509

CONTENTS (Cont.)

	Page
"Application of the Tempest Computer Code for Simulating Hydrogen Distribution in Model Containment Structures" D. S. Trent and L. Eyler	531
"Development of a Mixing Analysis Computer Code on Behavior of Hydrogen in a Subcompartmented Containment Vessel After a LOCA" T. Fujimoto, O. Ukai, J. Ogata, M. Kinoshita, A. Tsuge, T. Koor, Yama K. Shimamura, K. Takahasi, K. Onishi, S. Inase, A. Nakamura, T. Morota	553
BANQUET SPEAKER "Hydrogen Management and the Metamorphosis of NRC Policy on Severe Nuclear Accident Risk" Harold R. Denton	569
SESSION Va: COMBUSTION MODELLING AND EXPERIMENTS CO-CHAIRMEN: JOHN H. S. LEE AND ROBERT ZALOSH	579
"Ignition of Hydrogen/Oxygen/Nitrogen Mixtures Exposed to Two Configuration Dependent Ignition Sources" F. J. Benz	581
"Extinction of Corrugated Hydrogen/Air Flames" M. Mizomoto, Y. Asaka, S. Ikai, and C. K. Law	595
"Flame Temperature Criteria Tests" S. S. Tsai, N. J. Liparulo, J. E. Olhoeft, and D. F. Paddleford	609
"A Review of Recent WNRE Experiments on Hydrogen Combustion" H. Tamm, R. K. Kumar, and W. C. Harrison	633
"Hydrogen Control Tests in Intermediate Scale" R. C. Torok, K. Siefert, and L. B. Thompson	651
"Experimental Results From Combustion of Hydrogen: Air Mixtures in an Intermediate Scale Tank" W. B. Benedick, J. C. Cummings, and P. G. Prassinos	665
SESSION Vb: COMBUSTION MODELLING AND EXPERIMENTS CO-CHAIRMEN: GARRY L. SCHOTT and MARTIN HERTZBERG	681
"Medium-Scale Tests of H_2:Air:Steam Systems" S. F. Roller and S. M. Falacy	683
"Water Fog Inerting of Hydrogen-Air-Steam Mixtures" R. G. Zalosh and S. N. Bajpai	709

CONTENTS (Cont.)

	Page
"Fog Inerting Criteria for Hydrogen/Air Mixtures" S. S. Tsai and N. J. Liparulo	727
"Vaporization of Sprays in Superheated Atmospheres" C. F. Guenther and R. J. Tosetti	741
"A Hydrodynamic Model of Hydrogen Flame Propagation in Reactor Vessels" M. R. Baer and A. C. Ratzel	7
"Turbulent Condensation in the Presence of a Noncondensible Gas" M. L. Corradini	775
"Combustion Modelling in MARCH, Developments and Limitations" F. E. Haskin and W. R. Trebilcock	791
"Lean Hydrogen-Air-Steam Mixture Combustion Models" R. G. Zalosh and V. W. S. Hwa	807
"HECTR: A Computer Program for Modelling the Response to Hydrogen Burns in Containment" A. L. Camp, M. J. Wester, S. E. Dingman, and M. P. Sherman	827
"Steam:Hydrogen Flame Jet Experiments" J. E. Shepherd and O. B. Crump, Jr.	843
SESSION VI: ACCELERATED FLAMES AND DETONATIONS CO-CHAIRMEN: ROGER STREHLOW AND ROBERT ZALOSH	871
"Turbulent Burning of Hydrogen: Upper-Bound Chemical Kinetic Models Accounting for the Influence of Temperature Fluctuations" K. N. Tennankore and H. Tamm	873
"Hydrogen: Air Deflagrations--Recent Results" J. H. S. Lee, C. Chan, and R. Knystautas	889
"Discrete Vortex Simulation of Flame Acceleration Due to Obstacle-Generated Turbulent Flow" W. T. Ashurst and P. K. Barr	915
"The Relation Between Energy and Power for Direct Initiation of Hydrogen-Air Detonations" E. K. Dabora	931
"Large-Scale Hydrogen-Air Detonations" W. B. Benedick	953

CONTENTS (Cont.)

	Page
"Hydrogen:Air Detonations" J. H. S. Lee, R. Knystautas, C. Guirao, W. B. Benedick, and J. E. Shepherd	961
"Predictions of Detonability of H_2 Air:Steam Systems S. F. Roller and J. E. Shepherd	1007
SESSION VII: COMBUSTION MITIGATION AND CONTROL CO-CHAIRMEN: PATRICIA WORTHINGTON AND DAVID RENFRO	1027
"Development and Testing of Hydrogen Ignition Devices" D. Renfro, L. Smith, L. Thompson, and R. Clever	1029
"Review of the Grand Gulf Hydrogen Igniter System" J. C. Cummings, et al.	
"A Technical Evaluation of a Post-Accident CO_2 Inerting Hydrogen Control System" M. A. Harris, S. H. Hobbs, and D. H. Ashton	1061
"Mitigation Effects of Continuously Pressurized, Partially Inerted Containment Building Atmospheres" A. L. Berlad, R. Jaung, and W. T. Pratt	1077
"Hydrogen Combustion in Aqueous Foams" M. R. Baer, S. K. Griffiths and J. E. Shepherd	1089
"Study of Hydrogen Removal Systems" W. Baukal, A. Koehling, G. Langer, and E. Poeschel	1109
SESSION VIII: EQUIPMENT SURVIVABILITY CO-CHAIRMEN: GEORGE SLITER AND ROBERT G. LaGRANGE	1115
"EPRI Research on Equipment Survivability Under Hydrogen Burn" G. Sliter	1117
"Hydrogen Burn Survival Program Review" V. J. Dandini, W. H. McCulloch, and D. T. Furgal	1127
"Hydrogen Burn Survival Experiments FITS Series One" B. Richards, W. H. McCulloch, J. Aragon, and D. T. Furgal	1145
"Survivability of Essential Equipment at the Sequoyah Nuclear Plant for Hydrogen Burn Temperatures" R. H. Bryan, Jr.	1157
"An Analysis of Equipment Survivability in Hydrogen Burn Environments" P. S. Kepley, S. H. Hobbs, and A. T. Vieira	1181

CONTENTS (Cont.)

Page

"Electrical Cable Insulation Pyrolysis and Ignition Resulting From Potential Hydrogen Burn Scenarios for Nuclear Containment Buildings" 197
A. L. Berlad, R. Jaung, and W. T. Pratt

"Remarks on Regulatory Issues of Maintaining Containment Integrity" 1213
Ahearne*

*Commissioner Ahearne had intended to discuss the hydrogen question at this workshop, but was unable to because of other commitments arising from Chairman Palladino's illness. At the request of Commissioner Ahearne, his paper is included with the other papers of the Hydrogen Workshop, since much of the material deals with the potential threats to containment that could result from hydrogen combustion.

LIST OF ATTENDEES

John Aragon
Sandia National Laboratories
Division 9445
Albuquerque, NM 87185

W. T. Ashurst
Sandia National Laboratories
Division 8523
Livermore, CA 94550

Thomas Auble
EPRI
P. O. Box 10412
Palo Alto, CA 94303

Mel R. Baer
Sandia National Laboratories
Division 1513
Albuquerque, NM 87185

P. K. Barr
Sandia National Laboratories
Division 8523
Livermore, CA 94550

Lake Barrett
US Nuclear Regulatory Commission
Washington, DC 20555

V. L. Behr
Sandia National Laboratories
Division 9411
Albuquerque, NM 87185

Victor Benaroya
US Nuclear Regulatory Commission
7920 Norfolk Avenue
Bethesda, MD 20014

W. B. Benedick
Sandia National Laboratories
Division 1131
Albuquerque, NM 87185

A. S. Benjamin
Sandia National Laboratories
Division 9411
Albuquerque, NM 87185

Pauline Bennett
Sandia National Laboratories
Division 9411
Albuquerque, NM 87185

Frank J. Benz
NASA JSC
P. O. Drawer MM
White Sands
Las Cruces, NM 88001

Abraham L. Berlad
UCSD - Energy Center
P. O. Box 6908
Point Loma Station
San Diego, CA 92106

Marshall Berman
Sandia National Laboratories
Division 9441
Albuquerque, NM 87185

Charles Bergeron
Stone & Webster Engrg. Corp.
Mail Stop 245/9
P. O. Box 2325
Boston, Mass. 02107

G. R. Bloom
Westinghouse Hanford Co.
W/221-T(HE)
P. O. Box 1970
Richland, WA 99352

J. H. Bickel
Northeast Utilities
Safety Analysis/PRA Unit
P. O. Box 270
Hartford, Conn. 06101

John L. Boccio
Brookhaven National Laboratory
Bldg. 130
Upton, NY 11973

Robert H. Bryan, Jr.
Tennessee Valley Authority
W10 D 203
400 Commerce Avenue
Knoxville, TN 37922

T. Daniel Butler
Group T-3, MS B216
Los Alamos National Laboratory
Los Alamos, NM

Walter R. Butler
US Nuclear Regulatory Commission
Office of Nuclear Reactor Regulation
MS P-904
Washington, DC 20555

L. D. Buxton
Sandia National Laboratories
Division 9444
Albuquerque, NM 87185

Eileen M. Buzzelli
The Cleveland Electric Illuminating Company
P. O. Box 5000
Cleveland, Ohio 44101

R. K. Byers
Sandia National Laboratories
Division 9444
Albuquerque, NM 87185

A. L. Camp
Sandia National Laboratories
Division 9441
Albuquerque, NM 87185

H. M. Chung
Argonne National Laboratory
9700 Cass Avenue
Argonne, IL 60439

M. J. Clauser
Sandia National Laboratories
Division 9424
Albuquerque, NM 87185

R. K. Cole, Jr.
Sandia National Laboratories
Division 9441
Albuquerque, NM 87185

M. Corradini
University of Wisconsin
Nuclear Engineering Department
Madison, WI 53706

L. O. Cropp
Sandia National Laboratories
Division 9446
Albuquerque, NM 87185

J. C. Cummings
Sandia National Laboratories
Division 9441
Albuquerque, NM 87185

R. T. Curtis
US Nuclear Regulatory Commission
Washington, DC 20555

Peter Cybulskis
Battelle Columbus Laboratories
505 King Avenue
Columbus, Ohio 43201

Eli K. Dabora
University of Connecticut
Mechanical Engrg.
U-139ME
Storrs, Connecticut 06268

D. A. Dahlgren
Sandia National Laboratories
Dept. 9440
Albuquerque, NM 87185

V. J. Dandini
Sandia National Laboratories
Division 9445
Albuquerque, NM 87185

Richard E. Deem
Power Authority State of
New York
10 Columbus Circle
17th Floor
New York, NY 10019

Harold R. Denton
US Nuclear Regulatory Commission
MS P-428
Washington, DC 20555

G. J. Dickelman
General Physics
1000 Century Plaza
Columbia, MD 21044

S. E. Dingman
Sandia National Laboratories
Division 9441
Albuquerque, NM 87185

Constantino Economos
Brookhaven National Lab
Bldg. 130
Upton, NY 11973

Fred Edeskuty
Los Alamos National Laboratory
Los Alamos, New Mexico

James C. Elliott
General Electric company
175 Curtner Avenue
M/C 157
San Jose, CA 95125

Norman A. Evans
Sandia National Laboratories
Division 9441
Albuquerque, NM 87185

Duane Faletti
Math Building
Battelle Northwest
P. O. Box 999
Richland, WA 99352

James W. Fisk
Technadyne Engrg. Consultants
3033 Palo Alto Dr., NE
Albuquerque, NM 87111

Tetsuo Fujimoto
Mitsubishi Heavy Inds. Ltd.
Penn Center
Bldg. 3, Rm. 600
P. O. Box 355
Pittsburgh, PA 15230

G. Martin Fuls
Offshore Power Systems
P. O. Box 8000
Jacksonville, FL 32211

E. Goodwin
Stone & Webster
P. O. Box 5200
Cherry Hill, NJ 08034

Stewart K. Griffiths
Sandia National Laboratories
Division 1513
Albuquerque, NM 87185

Charles F. Guenther
Bechtel Power Corporation
P. O. Box 3965
San Francisco, CA 94119

Dale Gunter
Offshore Power Systems
Box 8000
Jacksonville, FL 32211

J. R. Haley
Mississippi Power and
Light Company
P. O. Box 1640
Jackson, MS 39205

Deborah A. Hankins
General Electric Company
175 Curtner Avenue
MC 738
San Jose, CA 95125

M. A. Harris
Bechtel Power Corporation
15740 Shady Grove Rd.
Gaithersburg, MD 20877

F. E. Haskin
Sandia National Laboratories
Division 9411
Albuquerque, NM 87185

John J. Haugh
EPRI
3412 Hillview Avenue
P. O. Box 10412
Palo Alto, CA 94303

J. O. Henrie
Rockwell International Corp.
2750 East Bldg.
200 East Area
Richland, WA 99352

Martin Hertzberg
Pittsburgh Research Center
U. S. Bureau of Mines
P. O. Box 18070
Pittsburgh, PA 15236

S. H. Hobbs
Mississippi Power and
Light Company
P. O. Box 1640
Jackson, MS 39205

John Hosler
EPRI
3412 Hillview Avenue
P. O. Box 10412
Palo Alto, CA 94303

S. S. Iyer
Power Authority State of
New York
10 Columbus Circle
17th Floor
New York, NY 10019

J. K. Jacoby
EG&G-TMI
P. O. Box 88
Middletown, PA 17057

R. Jaung
Brookhaven National Laboratory
Upton, New York 11973

D. P. Kelly
Sandia National Laboratories
Division 9441
Albuquerque, NM 87185

Steven N. Kempka
Sandia National Laboratories
Division 1513
Albuquerque, NM 87185

J. E. Kennedy
Sandia National Laboratories
Division 2513
Albuquerque, NM 87185

Pat S. Kepley
Bechtel Power Corporation
15740 Shady Grove Road
Gaithersburg, MD 20877

C. Kupiec
General Physics
1000 Century Plaza
Columbia, MD 21044

Robert G. LaGrange
US Nuclear Regulatory Commission
Washington, DC 20555

Ernest A. Lamont
Rockwell International Energy
Systems Group
8900 DeSoto Avenue
Canoga Park, CA 91304

John T. Larkins
US Nuclear Regulatory Commission
Washington, DC 20555

Tim Lee
US Nuclear Regulatory Commission
MS-1130SS
Washington, DC 20555

B. D. Liaw
US Nuclear Regulatory Commission
Washington, DC 20555

John Locante
Westinghouse Electric Corp.
Monroeville Nuclear enter
P. O. Box 355
Pittsburgh, PA 15230

V. M. Loyola
Sandia National Laboratories
Division 2516
Albuquerque, NM 87185

Bob Marshall
Battelle Northwest
Box 990
Richland, WA 99352

Ken Marx
Sandia National Laboratories
Division 8523
Livermore, CA 94550

W. H. McCulloch
Sandia National Laboratories
Division 9445
Albuquerque, NM 87185

William J. McLean
Sandia National Laboratories
Division 8513
Livermore, CA 94550

David Medek
American Electric Power
Room 1158-D
2 Broadway
New York, NY 10004

R. P. Minogue
US Nuclear Regulatory Commission
Washington, DC 20555

Dennis Mitchell
Sandia National Laboratories
Division 9441
Albuquerque, NM 87185

Louis Muhlestein
Westinghouse Hanford Co.
P. O. Box 1970
Richland, WA 99352

Lloyd S. Nelson
Sandia National Laboratories
Division 9441
Albuquerque, NM 87185

Lloyd Nesbitt
General Electric Company
175 Curtner Avenue
San Jose, CA 95125

Kalyan Niyogi
United Engineers and
Constructors, Inc.
30 S. 17th Street
Philadelphia, PA 19101

K. I. Parczewski
US Nuclear Regulatory Commission
Washington, DC 20555

Roy D. Peak
Westinghouse Hanford Company
P. O. Box 1970
Richland, WA 99352

V. Thinh Pham
GRS/EPRI
3412 Hillview Avenue
P. O. Box 10412
Palo Alto, CA 94303

Henry B. Piper
Energy Incorporated
5345 Wyoming, NE
Albuquerque, NM 87109

Steve Polkinghorne
EG&G Idaho
P. O. Box 1625
Idaho Falls, ID 83415

P. G. Prassinos
Sandia National Laboratories
Division 9441
Albuquerque, NM 87185

Gerald J. Presby
Cleveland Electric
Illuminating Company
P. O. Box 97
Perry, Ohio 44081

Gary Quittschreiber
Advisory Committee on
Reactor Safety
US Nuclear Regulatory Commission
Washington, DC 20555

Arthur C. Ratzel
Sandia National Laboratories
Division 1513
Albuquerque, NM 87185

David G. Renfro
Tennessee Valley Authority
W10D216 C-K
400 W. Summit Hill Dr.
Knoxville, TN 37902

Clyde Richards
Route 3
Box 352
Los Lunas, NM 87031

E. H. Richards
Sandia National Laboratories
Division 9445
Albuquerque, NM 87185

S. F. Roller
Sandia National Laboratories
Division 2513
Albuquerque, NM 87185

Keith Sanders
Rockwell International
8900 DeSota Avenue
Canoga Park, CA 91304

B. R. Sanders
Sandia National Laboratories
Division 8523
Livermore, CA 94550

M. A. Schoppman
NUS Corporation
910 Clopper Road
Gaithersburg, MD 20878

Garry L. Schott
Los Alamos National Laboratory
Los Alamos, NM 87545

S. L. Seiffert
The BDM Corporation
1801 Randolph Rd., SE
Albuquerque, NM 87106

James H. Shepard
Illinois Power Company
2859 Forrest Lane
Decatur, IL 62521

E. W. Shepherd
Sandia National Laboratories
Division 9780
Albuquerque, NM 87185

J. E. Shepherd
Sandia National Laboratories
Division 2513
Albuquerque, NM 87185

M. P. Sherman
Sandia National Laboratories
Division 9441
Albuquerque, NM 87185

Martin S. Shinko
NUS Corporation
910 Clopper Rd.
Gaithersburg, MD 20878

G. S. Shukla
Virginia Electric & Power Co.
P. O. Box 26666
Richmond, VA 23261

Jim Sicilian
Flow Science, Inc.
P. O. Box 933
Los Alamos, NM 87544

Ashok K. Singhal
CHAM of North America Inc.
3400 Blue Spring Road
Huntsville, Alabama 35810

George Sliter
EPRI
P. O. Box 10412
Palo Alto, CA 94303

A. W. Snyder
Sandia National Laboratories
Organization 9400
Albuquerque, NM 87185

Siavash Sohrab
Northwestern University
Dept. of Mech. Engineering
Evanston, IL 60201

Bob Spulak
Sandia National Laboratories
Division 9412
Albuquerque, NM 98185

V. Srinivas
Westinghouse Electric Corporation
P. O. Box 355
Bay 416
Pittsburgh, PA 15230

Roger A. Strehlow
University of Illinois
505 S. Pine Street
Champagne, IL 61820

E. P. Stroupe
Technology for Energy Corp.
One Energy Center
Pellissippi Parkway
Knoxville, TN 37922

T. M. Su
US Nuclear Regulatory Commission
Washington, DC 20555

A. L. Sudduth
Duke Power Company
P. O. Box 33189
Charlotte, NC 28242

David Swanson
Consultant NRC
P. O. Box 2687
Palos Verdes Pennisula
California 90274

John J. Taylor
EPRI
3412 Hillview Avenue
Palo Alto, CA 94303

Loren Thompson
EPRI
3412 Hillview Avenue
Palo Alto, CA 94303

Richard T. Thompson
EG&G, Inc. G-01
P. O. Box 1912
Las Vegas, NV 89125

S. L. Thompson
Sandia National Laboratories
Division 9444
Albuquerque, NM 87185

M. Thurgood
Battelle Northwest Laboratory
P. O. Box 999
Richland, WA 99352

Sheldon Tieszen
Sandia National Laboratories
Division 9441
Albuquerque, NM 87185

Charles Tinkler
US Nuclear Regulatory Commission
Washington, DC 20555

Raymond C. Torok
Acurex Corporation
485 Clyde Avenue
Mountain View, CA 94042

John R. Travis
Los Alamos National Laboratory
Group T-3, MS B216
Los Alamos, NM 87545

S. S. Tsai
Westinghouse Electric Corp.
P. O. Box 355
Pittsburgh, PA 15230

Erdem Ural
Factory Mutual Research
1151 Boston-Providence Turnpike
Norwood, MASS 02062

W. A. von Riesemann
Sandia National Laboratories
Division 9442
Albuquerque, NM 87185

Kenneth Vehstedt
American Electric Power
Room 1158-D
2 Broadway
New York, NY 10004

J. V. Walker
Sandia National Laboratories
Dept. 9420
Albuquerque, NM 87185

Bev Washburn
US Department of Energy
NE12
MS B-107
Washington, DC 20545

M. L. Wester
Sandia National Laboratories
Division 9441
Albuquerque, NM 87185

A. J. Wickett
Sandia National Laboratories
(Dept. 9420)
Albuquerque, NM 87185

Foreman Williams
Princeton University
Dept. of Mech. Engineering
Princeton, NJ 08544

P. Worthington
US Nuclear Regulatory Commission
Washington, DC 20555

W. S. Yu
Brookhaven National Laboratory
Upton, NY 11973

Robert Zalosh
Factory Mutual Research
1151 Boston-Providence Turnpike
Norwood, Mass. 02062

Erwin J. Zoch
Gulf States Utilities Co.
P. O. Box 2951
Beaumont, TX 77704

CANADA

Karl T. Chung
Chalk River Nuclear Labs
AECL
Chalk River
Ontario, Canada

R. Knystautas
McGill University
Dept. of Mech. Engrg.
Montreal, PQ
Canada H3A-2KG

Joseph Lau
Ontario Hydro
700 University Avenue
Toronto, Canada M5G 1X6

John H.S. Lee
McGill University
Dept. of Mech. Engrg.
Montreal, PQ
Canada H3A-2KG

D. W. McKean
Ontario Hydro
700 University Avenue
Toronto, Ontario N5G 1X6
Canada

T. K. Min
Atomic Energy of Canada, Ltd.
Engineering Company
Sheridan Park Research Community
Mississauga, Ontario L5K 1B2
Canada

Duane Pendergast
Atomic Energy of Canada, Ltd.
Engineering Company
Sheridan Park Research Community
Mississauga
Ontario L5K 1B2
Canada

K. R. Shultz
Atomic Energy Control Board
P. O. Box 1046
Ottawa, Ontario
Canada K1P 5S9

Heiki Tamm
Atomic Energy of Canada, Ltd.
Whiteshell Nuclear Research Estb.
Pinawa, Manitoba
Canada ROE 1LO

Kannan N. Tennankore
Atomic Energy of Canada, Ltd.
Whiteshell Nuclear Research Estb.
Pinawa, Manitoba
Canada ROE 1LO

FRANCE

J. Michel Evrard
Commissariat A L'Energie Atomique
(CEA)
Centre d'etudes nucleaires de
Fontenay-aux-Roses
92260 Fontenay-aux-Roses
France

GERMANY

Dr. Werner Baukal
Battelle-Institut E.V.
Am Roemerhof 35
6000 Frankfurt am Main 90
West Germany

Werner Geiger
Battelle-Institut E.V.
Am Roemerhof 35
D-6000 Frankfurt am Main 90
West Germany

Klaus Hassmann
Kraftwerk Union
Aktiengesellschaft
Kraftwerk Union AG
Hammerbacherstrabe 12+14
Postfach 3220, 8520 Erlangen 2
Federal Republic of Germany

Hermann Jahn
Gesellshaft fur
Reaktorsicherheit
Forschungsjelaende
8046 Garching
Federal Republic of Germany

Guenter Langer
Battelle-Institut E.V.
Am Roemerhof 35
6000 Frankfurt 90
Federal Republic of Germany

Michael Untucht
TUV Baden
Dudenstr. 28, P.O.B. 2420
D 6800 Mannheim
Federal Republic of Germany

ITALY

Fabio Fineschi
University of Pisa
Dipartimento di Costruzion,
Meccaniche E Nucleari
2 Via Diotisalui
Pisa, Italy

Corrado Kropp
AMN
Via G D'Annunzio 113
Genova, Italy 16121

Alessandro Morici
ENEA-DISP
125 Viale Regina Margherita
Rome, Italy

KOREA

Thomas K. Min
AECL

MEXICO

Carlos Arredondo
Comision Nacional de Seguridad
Nuclear y Salvaguardias (Mexico)
Insurgentes Sur 1806
Mexico D.F.
Mexico

SWEDEN

Wiktor Frid
Swedish State Power Board
S-16287 Vallingby
Sweden

UNITED KINGDOM

Alain B. H. Chevalier
National Nuclear Corp., Ltd.
Cambridge Road
Whetstone,
Leicester-LE8 3LH
United Kingdom

S. F. Hall
UKAEA Safety & Reliability
Directorate
Wigshaw Lane
Culcheth
Warrington,
United Kingdom WA 4NE

Roger May
National Nuclear Corp., Ltd.
Cambridge Road
Whetstone
Leicester LE8 3LH
United Kingdom

Welcome and Introduction

SECOND INTERNATIONAL WORKSHOP ON THE IMPACT OF HYDROGEN ON WATER REACTOR SAFETY

J.J. Taylor
Electric Power Research Institute

The hydrogen burn at Three Mile Island raised many questions regarding hydrogen safety in nuclear reactor containment buildings. The complexity of the issue was apparent during the first hydrogen workshop in Albuquerque. That meeting in January 1981 elicited more than 40 papers, most of them involving analyses or literature surveys. This week about 70 papers will be presented and there will be a heavier emphasis on data. Now that we have very encouraging reseach results we feel much more confident that the nuclear safety issues regarding hydrogen can be successfully and finally resolved.

Several owners of PWR ice condenser and BWR Mark III containments have now installed hydrogen control systems and have received interim approvals from the NRC Office of Nuclear Reactor Regulation. Each of the systems incorporates 70 to 100 distributed ignition devices which would assure hydrogen combustion prior to substantial accumulation during a degraded core accident. Several alternative hydrogen mitigation concepts were studied prior to the decision, first made by TVA, that deliberate ignition was the most viable option for hydrogen control.

EPRI began an active research program early in 1981 to evaluate the effectiveness of this approach. All three of the PWR ice condenser plants owners participated (Duke, TVA, and AEP). Four experimental facilities were constructed in the spring of 1981 to support this examination and the first experiments were performed in late summer of that year. The results of all four experimental projects have now been reported in connection with NRC evaluations of the Sequoyah (TVA) and McGuire (Duke) hydrogen control systems. Hydrogen control in BWR Mark III containments is being addressed as a separate issue and EPRI is working with an owners group to establish a research program for Mark III-specific concerns.

The small and intermediate-scale EPRI projects that are now completed have provided several important results which increase confidence that simple hydrogen control systems will be adequate.

- o Hot surface igniters (of the type installed by utilities) are effective for deliberate ignition of hydrogen in wide-ranging environments of air, steam, water spray, and water fog.

- o Initial simulations of several degraded core accidents, with continuous injection of hydrogen into a vessel containing an activated igniter, have resulted in maximum combustion pressures of less than 2 atmospheres, which appears to be within the ultimate capacity of all containments. Injection of steam with the hydrogen provides an additional mitigating effect, and water sprays have a dramatic limiting effect on combustion pressures in such experiments.

- o Safety-related electrical equipment operated successfully during and after repeated combustion events with no apparent degradation.

- o Hydrogen mixing experiments showed rapid uniform mixing for a small break degraded core accident. Hydrogen concentrations at any time normally differed by less than 3 volume percent.

- o No tendency toward detonation was observed in intermediate-scale tests, even with stoichiometric dry hydrogen/air mixtures.

Details regarding these points will be provided in several technical papers to be delivered at this Conference.

Where do we go from here? In reactor safety research the question of scaling has often proven difficult. We do not expect to find important safety-related differences in hydrogen combustion behavior as we increase scale. However, we believe that it is prudent to conduct experiments in a large volume to demonstrate that there are indeed no safety-related surprises due to scale.

In the fall of 1981 EPRI established a contract with DOE to utilize a very large vessel at the Nevada Test Site for hydrogen combustion experiments. [The spherical vessel has a diameter of 52 feet (16 m) and a design pressure (87 psig, 600 kPa) that is substantially higher than that of commercial nuclear containment buildings.] Several organizations have joined in the sponsorship of this testing program including EdF, Kansai Electric Power Company, Ontario Hydro, Swedish State Power Board, Taiwan Power Company, and very recently, the NRC Office of Nuclear Regulatory Research. The site is now nearing the latter stages of preparation for shakedown in late 1982. It will be utilized for several important tasks:

- o verification of the data base from small-scale testing,
- o validation of computer codes for combustion,
- o examination of equipment survivability, and
- o testing of methods for hydrogen control during simulated degraded core accidents.

We expect that many organizations will continue to perform research on hydrogen behavior during postulated severe nuclear accidents for some time, and such research is needed for the refinement of our understandings. We now believe that the state of technology has advanced sufficiently so that licensing decisions can be made at an early point in time. The serious concerns which developed after Three Mile Island have now been replaced by a judgement in the nuclear community that the potential threat due to hydrogen in nuclear containment buildings can be successfully understood and controlled.

SESSION I

HYDROGEN RESEARCH PROGRAMS

REGULATORY PERSPECTIVES ON HYDRODEN CONTROL FOR DEGRADED CORE ACCIDENTS

by

W.R. Butler and C. G. Tinkler
U.S. Nuclear Regulatory Commission

I. INTRODUCTION

This paper presents the current regulatory perspectives relative to hydrogen control for postulated degraded core accidents in light water reactor plants. These perspectives should be an important element in decision making regarding research programs that deal with the various aspects of hydrogen management during postulated severe accidents in licensed nuclear power plants.

A paper on the same subject was presented during the first workshop in January 1981 (See NUREG/CR-2017, Volume 1, August, 1981). Numerous regulatory decisions have been made, licensing actions taken, and rulemaking activities completed since the January 1981 workshop. The objectives of this paper are to summarize those events and to indicate the areas where the regulatory views have changed and /or crystallized since January 1981.

A few preliminary matters need some attention, however. The matter of resource limitations warrants some discussion. Research in the broad field of hydrogen control is no different from research in any other field of reactor safety. The research manager must always be conscious of the balance between resource cost and the safety benefits to be gained from each project. If excessive resources are being allocated to one area of research, then since the total available resources is fixed, other important areas of research may have to be deferred at some cost to overall nuclear plant safety.

Another matter involves the potential for "re-inventing the wheel". Wherever there is rapid growth of research activities and hydrogen control appears to be one of these areas, the research manager should be particularly concerned that some elements of his research program may already have been completed by someone else. A responsible program of literature search and field surveys should always precede major outlays for new research. If the configurations, circumstances or accuracy of the prior work are different from today's needs, consideration should be given to adapting the results of the prior work to meet todays needs before embarking on the new program.

Finally, the researcher and the research manager should be ever conscious of one aspect of human nature. The researcher, by nature, is seldom inclined to want to conclude his work. He generally wants more time and more resources so as to improve on his prior work. On the other hand, the research manager is charged with deciding when enough has been done so that his scarce resources can be allocated to other jobs.

Both the researcher and the research manager must develop a healthy understanding of this aspect of human nature.

The above comments should not lead one to conclude that enough research work has already been done to meet the objectives of having all licensed LWR plants provided with the capability for successfully accommodating the large amounts of hydrogen releases associated with degraded core accidents. Clearly, mork work needs to be done. However, it does point out a need to be particularly resource-conscious when new programs are proposed.

In this regard, while implementation of the new requirements spawned by the TMI-2 accident has made the occurrence likelihood for degraded core accidents more remote, it is far from being extinguished. As evidence, I would cite a recent experience at a nuclear plant where the maintenance personnel left disengaged both battery packs from the d.c. power system. Since the normal operating d.c. power requirements of the facility were met by the battery chargers which derive their power from the a.c. power system, the facility operators were unaware of the incorrect hookup. An accident with loss of offsite power under these circumstances could have had serious consequences.

II. DISCUSSION

In this discussion, we will summarize the recently completed regulatory activities and will identify those research areas where better information is needed to support those future regulatory requirements that deal with hydrogen control for degraded core events (excluding core melt events).

A. Summary of Recent Regulatory Activities

The TMI Action Plan, NUREG-0061, dated May 1980 provided the early guidance on what the Nuclear Regulatory Commission (NRC) believed had to be done to improve the hydrogen control capability at licensed nuclear facilities. Further guidance evolved from subsequent Commission action on pending licensing cases, e.g., Sequoyah, McGuire, Floating Nuclear Plant, Grand Gulf, and North Anna, and on the various proposed changes to the Commission's regulations. As a result, a substantial momentum has been achieved in the various NRC and industry supported research activities dealing with severe accidents as shown in Figure 1.

The NRC sponsored severe accident research has been designed to support its near term licensing decisions and the various related rulemaking activities. It consists of a two-phase plan for first producing and later confirming the information needed for regulatory decisions on severe accidents and technical assistance programs. The Industry Degraded Core Rulemaking (IDCOR) activities are designed to study the

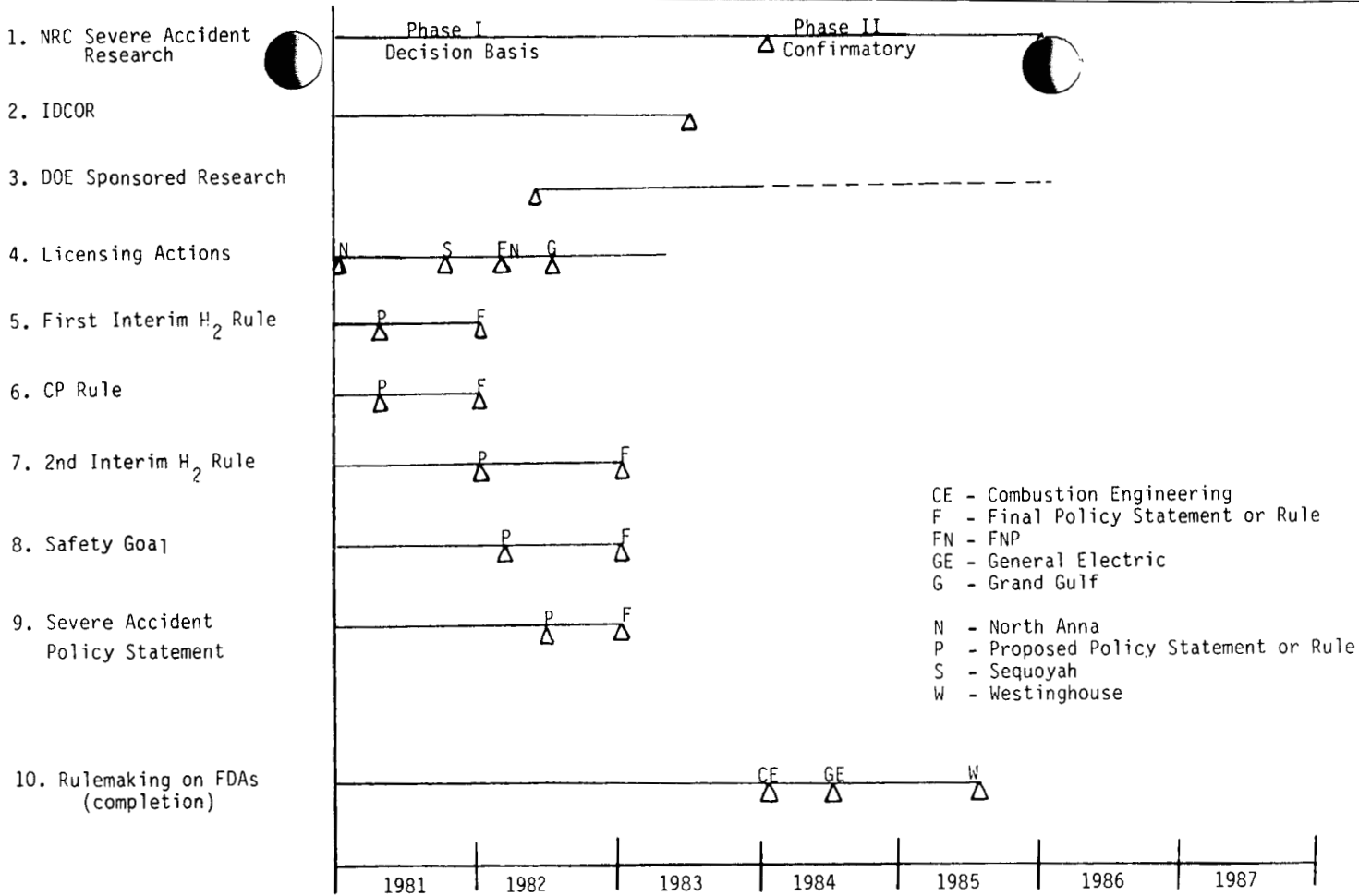


Figure 1 Proposed Schedules for Programmatic Activities of NRC and the Nuclear Industry as Related To Severe Accident Policy Development, Regulatory Decisions and Rulemaking.

costs and benefits of various design features to deal with severe accidents. The results will also be useful in supporting the various regulatory requirements that are instituted by the upcoming rule char The Department of Energy is also in the process of sponsoring researc work in the field of hydrogen control.

The NRC's rulemaking activities address current containment designs and apply to plants ranging from those already in operation to those for which applications for a construction permit are currently under Staff review. The rule changes include the following:

(1) "Interim Requirements Related to Hydrogen Control." This rule, published in the Federal Register, December 1, 1981 (46FR 58484) as a final rule, deals with the requirement for inerting Mark I and II containments, among other requirements.

(2) "Interim Requirements Related To Hydrogen Control." This rule, published in the Federal Register, December 23, 1981 (46 FR 62281) as a proposed rule, provides the proposed interim requirements for hydrogen control systems in Ice Condenser and Mark III containments and a proposed requirement that hydrogen analyses be performed for large dry containments.

(3) "Licensing Requirements for Pending Construction Permits and Manufacturing License Applications." This rule, published in the Federal Register, January 15, 1982 (47 FR 2286) as a final rule, specified hydrogen licensing requirements for pending construction permit and manufacturing license applications.

1. Mark I and Mark II BWR Containments

The interim requirements related to the Mark I and II containments were issued in the form of a final rule 46 FR 58484. These requirements were intended to address several concerns over hydrogen control in a post accident environment.

It should be made clear that the requirements of this rule were adopted to improve hydrogen control capability for both degarded core accidents involving a significant fuel cladding water reaction and those accidents considered as design basis accidents with a relatively small cladding reaction as considered in 10 CFR 50.46 and modified by 10 CFR 50.44, paragraph 2. The requirement to inert the smaller pressure suppression containments was instituted because of the limited ability of these designs to tolerate the range of consequences stemming from hydrogen

combustion, coupled with the knowledge that the Mark I and II containments have successfully operated for a number of years with a preinerted containment. The consequences of hydrogen combustion, principally with regard to containment pressurization, were judged to be sufficiently severe at metal water reaction fractions much less than that estimated to order at TMI (approximately 45%). Thus it was on the basis of the experience of TMI, a degraded core accident,that the Mark I and II containments are required to be inerted.

A separate provision of the rule, 46 FR 58484 (December 1, 1981), was to require the utilities relying upon the various methods of purging to control hydrogen to provide a recombiner capability. This provision is applicable to all containments, including the Mark I and II designs, which purge to prevent the combustion of hydrogen. It does not address those plants which already have recombiner systems and a backup purge system as required by other regulations. It does, however, apply to plants which are inerted but rely on purging (other than recombiners) to control the oxygen concentration.

The genesis of this requirement was again the experience following the TMI accident but from a different perspective. It was clear, though the TMI accident was a degraded core accident that even if a less severe accident were to occur, a design basis accident for example, flexibility in handling hydrogen control is a desirable option. It became obvious that even if purging meant release of relatively small amounts of radioactivity to the environs that under certain circumstances it is preferable to control combustible gases with recombiners. Thus it was not the fact TMI was a degraded core accident but the realization that design basis accidents may dictate the need for options other than purging.

2. Ice Condenser & Mark III Containments

The interim requirements related to those ice condenser and plants for which a construction permit was issued prior to March 28, 1979 were published as a proposed rule on December 23, 1981 (46 FR 62281).

This rule would require the subject containments be designed to accommodate the consequences of a degraded core accident with a postulated metal-water reaction of up to and including 75% of the active fuel cladding. In this regard the owners of these plants are required to install a hydrogen control system such that the containment atmosphere pressure is maintained below the value corresponding to ASME code Service Level C or Factored Load Category limits. Furthermore, systems necessary to establish and maintain safe shutdown and maintain containment integrity must be demonstrated to be capable of performing

their functions during and after conditions created by the burning or detonation of hydrogen.

Dry Containments

The proposed interim requirements related to those plants for which a construction permit was issued prior to March 28, 1979 are again addressed by the proposed rule 46 FR 62281. This rule requires owners of the subject plants to perform and and submit by two years after the effective date of the rule or the date of issuance of a license authorizing operation above five percent of full power, whichever is later (i) analyses to assure that during degraded core accidents, containment structural intergrity will be maintained; and (ii) equipment survivability analyses to assure continued containment integrity and safe shutdown capability. These postulated degraded core accidents will be assumed to produce hydrogen releases to the containment resulting from the reaction of up to and including 75% of fuel cladding surrounding the active fuel region with water.

4. NTCP & ML Applications

A separate set of requirements have been issued as a final rule (47 FR 2286) to address hydrogen control for pending construction permit and manufacturing license applications. In this regard, the principal requirements are:

(1) provisions of a dedicated penetration for possible use with a filtered-vent system;

(2) containment structural integrity is assured for internal pressures of at least 45 psig;

(3) analyses of alternative hydrogen control systems are to be performed assuming 100% fuel clad-water reaction and the resultant containment uniform hydrogen concentration must be less than 10% by volume or the mixture rendered non-flammable;

(4) essential systems must be shown to survive the environment associated with the accidents considered.

B. Areas Where A Greater Data Base Is Needed

Our understanding of the response of the various containment types to large releases of hydrogen has improved substantially during the recent past. The areas receiving the most attention include: hydrogen source terms, hydrogen combustion phenomena, containment pressure and temperature responses to hydrogen combustion, and containment structural response.

1. Hydrogen Source Term

The first technical issue cited was the hydrogen source term, which refers to the subject of mass and energy releases involving the conditions of hydrogen, steam, and water releases from the primary system. For different containment designs, the influence of the mass and energy release is seen to vary. For the dry containment with its large volume and high pressure capacity, the effect of varying the mass and energy release is generally acknowledged to be minimal. In the case of large dry containments without additional hydrogen control features, the maximum pressure consequences naturally stem from the combustion of hydrogen in a manner which depletes all the combustible gas present in containment. The uncertainty over the rate at which hydrogen and steam are released to containment is seen to be relatively unimportant since the dry containments are judged to be capable of tolerating the complete combustion of all the hydrogen that can be produced during postulated degraded core accidents. Because there are certain questions concerning the precise nature of the combustion phenomenon, the NRC has proposed to require, through the proposed rule published in the Federal Register (46 FR 62281) December 23, 1981, that utility owners of dry containments confirm the plant capability.

The effect of the hydrogen source term was originally considered to be of significant impotance in evaluating the efficacy of hydrogen control systems; i.e., igniter systems, proposed for pressure suppression containments. This is due to the fact that, within limits, the pressure suppression containments are generally sensitive to the mass and energy release rate, especially in instances where the pressure suppression mechanism, i.e., ice bed or supression pool, is bypassed. As part of the licensing activities on ice condenser plants, utilities have opted to evaluate the sensitivity to the type of degraded core accident scenario by performing sensitivity studies around the base case, which was selected as a small break LOCA with failure of ECCS injection (S D). This approach serves two functions: it provides a mechanism for evaluating the effect of uncertainties in the base case mass and energy releases which were calculated using the MARCH code and it provides a measure of the capacity to accommodate different unique accident sequences.

While the preliminary assessments of hydrogen ignition systems proposed for ice condenser and Mark III containment plants indicated a significant effect may result due to changes in the effluent release rates, sensitivity studies performed by the utilities do not indicate this to be a strong influence. This appears to be true for several reasons. The pressure suppression chamber acts as a focusing mechanism

in that through the steam condensation process hydrogen burning is concentrated immediately downstream of the suppression chamber. If the downstream volume, upper plenum or wetwell, can be assured of an adequate supply of oxygen, then the process can be carried on somewhat independent of the hydrogen release rate. The analytical assumptions regarding combustion also play a role in the demonstration of this relative insensitivity. Furthermore, all of the codes currently employed to perform hydrogen combustion analysis assume complete mixing within the control volumes. Thus while much of the containment hydrogen analyses related to ignition systems demonstrates a second order sensitivity to the hydrogen and steam release rates, a closer scrutiny of the individual elements which make up the analyses may reveal that safety margins are more greatly affected.

With regard to post-accident inerting systems, the principal interest related to the hydrogen source term involves the time period needed to inert the atmosphere. In other words, can the post-accident inerting system inert the containment atmosphere prior to any significant release of hydrogen into containment? Several factors weigh on this issure including the time it takes the operator to identify the accident as a degraded core accident relative to the time for onset of hydrogen generation and the interval necessary to introduce the inerting agent inside containment. Part of this latter factor includes the time required to insure mixing of the inerting agent.

2. Combustion Phenomena

Much of the resources directed at resolving hydrogen control issues has been focused on combustion testing. Early in the application of ignition systems to nuclear plants it was necessary to test the proposed igniters to determine their performance characteristics, durability and efficacy in promoting ignition of various mixtures. The tests, in general, were carried out in relatively small vessels representing a single volume geometry. The importance of various combustion phenomena examined through testing, e.g., flammability limits and flame speed, would seem to vary depending upon the containment type that is under consideration. In the case of large dry containments without supplemental hydrogen control systems such as igniters, it is necessary to evaluate the consequences of inadvertent ignition of the hydrogen released to containment. Although nuclear plants contain random sources of ignition, as evidenced by the hydrogen burn at TMI, in the absence of accountable, demonstrated ignition sources, it must be assumed that a random ignition event occurs under less than favorable conditions. This results in the assumption that combustion occurs after all the hydrogen produced by the postulated metal-water reaction has been released. Thus, worst case pressure

depends on identification of the most aggravating set of initial conditions. Adiabatic calculations indicate that the most severe consequences are usually produced when the containment atmosphere steam concentration is high enough to depress the relative hydrogen concentration to a value which approaches the lower limit for coherent flame propagation. Therefore, the principal matter of interest when considering adiabatic calculations is establishing the lower limit at which complete combustion is achieved. It is our view to date, that sufficient theoretical models have not been developed to predict this limit with confidence in situations representative of a large dry containment that does not have intentional ignition capability.

Testing of quiescent combustible mixtures of hydrogen produces consistent results, which indicate complete combustion is achieved at approximate concentrations of 8.5 to 9 v/o hydrogen in air. The effect of steam addition to the mixtures is not seen to be as reproducible between various test programs, though steam in relatively low concentrations (less than 30 v/o) is seen to only modestly affect flammability limits. Testing of mixtures with induced turbulence shows less consistency with regard to establishing the pertinent flammability limits although turbulence is acknowledged to produce complete combustion in leaner mixtures. This variance in results may result from the differences in testing; various fans and directed velocities undoubtedly alter the turbulence produced in different configurations. In any event, as stated before, these items contibute to the uncertainty over establishing exact flammability limits for use in evaluating reactor plants.

Another parameter of interest when considering the non-adiabatic pressure rise is the flame speed or rate at which hydrogen combustion occurs. It is again our view that sufficient data have not yet been presented to predict the pressurization rate with any degree of confidence though this matter appears to be of less importance for the dry containments.

However, the uncertainty over combustion phenomena assumes greater significance in pressure suppression containments because of their greater degree of vulnerability to the effects of hydrogen combustion. In addition, due to the design of these plants, it is necessary to pursue in greater depth a more comprehensive range of combustion issues, i.e., flame acceleration, deflagration transition to detonation and mixing of combustible gases. Since the NRC and the industry have conducted numerous programs to investigate these issues the logical question is how far have we progressed in resolving the pertinent issues.

First let us examine the means by which the pressure suppression containments (ice condenser and Mark III) with their small design pressure capacity, are able to withstand the combustion of large quantities of hydrogen. Basically, there are two processes which will allow these containments to burn hydrogen and still ensure containment integrity: 1) combust hydrogen in smaller subvolumes of the

containment which promote expansion of the gases; and 2) combust hydrogen in large volumes but at lower relative concentrations (6-7 v/o). The first method enjoys the advantage of generally allowing the hydrogen to be ignited at higher concentrations dependent upon the relative sizes of the combustion volume and the expansion volume.

One means by which we evaluate the adequacy of testing is to determine if the scope of testing is comprehensive enough to permit the confirmation of analysis. In this regard the combustion testing performed to date has not addressed the complex nature of the thermodynamic and flow processes involved in a pressure suppression containment together with hydrogen combustion. The approach rather has been to conduct tests using simple configurations and procedures and to use these results to verify the adequacy of individual input assumptions for simplified analytical models. This is not to imply that this approach is wholly unsatisfactory; it simply places a greater burden on the analytical solution, versus experimental verification, to the problem. In this case it means that multitudinous sensitivity studies are necessary to investigate the effects of the various uncertainties in the combustion process. The primary difficulty in opting for simple tests is that the analytical capability may be quite inadequate and the requisite bounding sensitivity studies may cause potentially large and unwarranted reductions in safety margins.

3. Pressure and Temperature Responses

The analyses of the consequences of hydrogen combustion within containment is currently treated as a basic energy balance problem in the current state of the art computer codes. The codes which have been developed to calculate the bulk atmosphere pressure and temperature are essentially design basis containment analysis codes which have been modified to simulate, in a simplistic fashion, the burning of hydrogen. The codes generally have the following common features:

(a.) Model constituent gases; e.g., N , O , H ;

(b.) Steam table properties up to 3000 F (in some cases steam as ideal gas);

(c.) Models for containment heat removal system (sprays, fans);

(d.) Structural heat transfer; and

(e.) User specified combustion control parameters.

As stated previously, the current containment hydrogen combustion codes are modifications of basic containment codes, e.g., COMPARE and CONTEMPT. In this regard the mass and energy released to the containment atmosphere in the form of steam, hydrogen, or nitrogen is a user input parameter for the code. The one notable exception to this is the MARCH code which calculates the response of the reactor coolant system, and therefore the mass and energy release to containment, as well as the containment atmosphere pressure and temperature transient.

The burning of hydrogen is calculated based on simplified user inputs to control the rate of energy addition to a volume(s). Hydrogen combustion is generally dictated by the following input parameters: (1) hydrogen volume concentration at which ignition is initiated in a given volume; (2) burning rate; (3) completeness of combustion; (4) minimum requisite oxygen concentration; and (5) conditions under which hydrogen burning is assumed to propagate to other volumes. There is no attempt in current analytical codes to model the precise nature of multidimensional flame propagation. Existing containment codes have the capability to simulate the deflagration of hydrogen but do not have the capability for performing detonation calculations. Several codes employed by the industry and NRC have the capability of modeling multicompartment containments. Additionally, models may be provided for specific regions unique to pressure suppression containments such as an ice condenser or suppression pool. Flow between volumes is generally treated by simplified forms of the momentum equation used in conventional containment codes.

Flow rates are typically calculated based on pressure differences with little or no accounting of thermal and density induced convection or the influence of turbulence introduced by the momentum of the jetting effluent.

While we have briefly discussed the limitations of the current containment hydrogen combustion codes, it should be stated that advanced computer models with the predictive capability to calculate the complex phenomena associated with the transport and combustion of hydrogen in a reactor containment are at least several years away. It is also quite plausible that mathematical modeling may never be adequate to analyze these situations. What is needed now is to determine the proper balance between future confirmatory efforts in testing, including large or full scale simulation, and analytical development.

4. Structural Response

The conclusion that various containment designs (including both those with supplemental hydrogen control features and those without) will

retain containment integrity in the event of a degraded core accident relies in large measure on the understanding that the pressure capacity of containments well exceeds the stated design pressure. Numerous analyses have been performed to demonstrate that the pressure capacity of containments extends to 2-4 times the design pressure. What has been lacking, however, is the evaluation of leakage characteristics for pressures beyond those tested as part of ILRT programs called for in Appendix J to 10 CFR Part 50. Thus we are left with the consensus that basic structural integrity is maintained with little confirmation of the expected offsite dose releases. It is our view that future efforts should address this issue in order to provide an integrated assessment of degraded core accidents and a confirmation of the maintenance of adequate safety margins.

5. Recombiner Capability

Switching now to another matter, that of the recently imposed requirement for a"recombiner capability, "a BWR plant licensee has filed a preliminary report, which proposed that an alternative and less conservative prescription for evaluating radiolysis effects be considered by the staff for reviewing licensee compliance with the requirements of 10 CFR Section 50.44. A staff review program, including assistance from a number of consultants, has been initiated to evaluate this report. In this regard, the staff finds that sufficient data do not appear to exist for prescribing the production of oxygen by radiolysis in non-boiling water, when the water is contaminated with fission product iodine and various metal oxides. However, the G-values in Regulatory Guide 1.7 are recognized as being conservative.

The licensee's report relies primarily on the assumption that bulk boiling can reasonably be expected to terminate some 12 hours following the onset of postulated design basis accidents. The objective of this discussion is to examine the acceptability of the "bulk boiling assumption" from the perspective of degraded core accidents.

The staff's prior determination that inerting of Mark I and Mark II containments was necessary for accommodating the consequences of degraded core accidents was based on the assumption that the provisions of 10 CFR Section 50.44 for dealing with design basis accidents would remain in effect. This means, among other things, that use of the source term methodology prescribed in Regulatory Guide 1.7 (Revision 2) would continue as the basis for complying with the rule.

HYDROGEN RESEARCH AND NUCLEAR SAFETY--A UTILITY PERSPECTIVE*

Wang Lau, Head Nuclear Engineer
Tennessee Valley Authority, Knoxville, Tennessee

I. Introduction

In making decisions on hydrogen-related nuclear safety issues, as in other decisionmaking, one has to consider two major factors: Information and Perspective.

Nearly all the papers in the 4-day workshop will be dealing with the first factor. There will be experimental data, computer analysis, future program descriptions, etc., so that there will be a large amount of information.

In this paper, we shall discuss perspectives, at least from a utility's point of view: Are the key issues identified? Is there enough information for decisions to be made? Are the scope, depth, and schedule of the research consistent with the safety concern? Is the emphasis correctly placed? What should be the future actions, if any?

Before we begin to discuss the utility's perspective on the specific subject of hydrogen research, we should briefly discuss the utility's perspective on nuclear safety. Some people believe that the utilities are interested in doing nothing and spending nothing. The truth is that the utilities realize that there is "utility risk" as well as "public risk." If there is a major nuclear accident, the operators are the closest to the reactor, not the public. In addition, the utilities' investment is at stake. Unquestionably, there are incentives for the utilities to take steps to protect their personnel and their investment, in addition to protecting the public.

The utilities also realize that given certain manpower and budget in the regulatory agencies and national laboratories, a certain amount of information and questions will be produced. If they are not on one subject, they will be on another subject. Inherently, therefore, the utilities are living with the fact that there will always be safety concerns and questions. What the utilities want is to have safety issues placed in perspective; make the best allocation of resources, both monetary and human; and reduce the public risk and the utility risk, if they are found to be too high. That, of course, is only one of the elements in having "perspective."

Two years ago, after an intensive study period, the Tennessee Valley Authority (TVA) voluntarily proposed the use of thermal igniters inside a reactor containment building, and together with Duke Power and American Electric Power, helped initiate an industry hydrogen research program (now known as the EPRI hydrogen program). This focused attention on the hydrogen issue

*This is a Government publication and not subject to copyright.

and triggered an extensive industry-wide research program. It is perhaps fitting that two years later, TVA publishes this paper and tries to look at a bigger picture and put things in the right perspective.

Another item must be mentioned before we get to the specific hydrogen issue. We would not have proposed the hydrogen ignition system had we not believed that it is a desirable thing to do and that it contributes to risk reduction, even though the risk was low to begin with. What followed in this particular case was that the NRC asked a lot of questions and demanded much more information that we originally envisioned. The analytical cost was extremely high. That is an important point. When a stick is used instead of a carrot in response to a voluntary action by a utility, it may destroy some of the utilities' incentives in the future. That, of course, is another element in having "perspective."

II. Scope and Approach

We identified three and only three major concerns:

1. Containment integrity due to pressure generated by hydrogen burns.
2. Equipment survivability due to transient temperature by hydrogen burns.
3. Containment and equipment survivability due to local hydrogen detonation, if any.

Our preliminary investigations indicated that if a degraded core situation with hydrogen release is assumed, then a mitigative system would be beneficial. We considered eleven (11) options:

1. Nitrogen inerting
2. Carbon dioxide postinerting
3. Halon postinerting
4. Distributed ignition (spark and thermal)
5. Filtered-vented containment
6. Coupled containment
7. Larger and stronger containment
8. Passive containment
9. Gas turbine
10. Catalytic combustor
11. Fog

A twelfth option of using foam was later considered by Sandia Laboratory.

Before we started our intensive research effort, we laid down three ground rules for our approach to the specific degraded core accident situation:

A. Limited Scope--When we got started, we did not set out to solve all the problems of the degraded core issue, neither did we attempt to come up with an optimized mitigative system. We wanted to have a reasonably practical system that would contribute to the reduction of risk and without significant negative effects.

B. Consequential studies--We realized that if an accident takes place at a plant, that plant is going to respond based on the hardware it has at that time, the configuration it is in at that time, the emergency operating procedure it has at that time, and the knowledge and actions of the operators it has at that time. If a piece of research does not lead to actual changes in equipment or procedures at a plant, it is not "consequential." The plant would not know if that research was done or not, even though the research may confirm an engineer's judgement and make the documentation more complete.

C. Streamlined Effort-- Judgements were made periodically to identify projects that reached dead ends and those projects were terminated. Emphasis was made on key issues. No attempt was made to have equal and parallel projects at all fronts. Rather, we tried to assure that the level of the studies was consistent with the overall objective of the program.

We also recognized that a data base (information) was needed to support the eventual decision and that research was needed. We started to prioritize and classify research projects into three categories to aid in our administration and decision process:

1. Research needed for decisions--These are "consequential" research projects to answer specific questions and provide key data, such as hydrogen mixing effectiveness, since the decisions had potential impact on plant hardware and emergency operating procedural changes. These research projects were targeted to be completed in a timely manner.

2. Confirmatory research --The data from these studies leads to fundamental understandings of various processes, but most likely will not affect plant equipment or procedures. These research projects are "inconsequential" and are necessary only to defend a licensing decision.

3. Licensing research--These are research projects made necessary by questions posed by the regulatory agencies. Often it is easier for the utilities to do research than to continue debating issues. In most cases of this type, the human and monetary resource allocations are not optimized, and the levels of studies are not necessarily consistent with the risk or safety concerns.

With the above three major concerns, 11 mitigative system options, three ground rules, and three research categories as

starting points, we formed a task force and moved quickly. Within a matter of months, scoping documents were prepared, requests for proposals were sent, proposals were received and evaluated, contracts were awarded to various contractors, design studies were made, and the key issues were evaluated, reports were received, followup cost estimates were made inhouse, and a decision to use the thermal igniters were made, backed up by preliminary computer analysis and tests.

The distributed thermal ignition system was selected through the process of elimination of the other options. The key technical issues that we concentrated on were:

- hydrogen source (sequences and rates)
- mixing (detonable concentrations?)
- functional capability and endurance of igniters
- containment capability
- equipment survivability (tests)
- emergency operating procedures
- potential negative effects

III. Major Concerns and Conclusions

The three major concerns are now discussed:

A. Containment integrity--It was found by many organizations' independent calculations that the Sequoyah ice condenser freestanding steel containment can withstand at least three times the design pressure before gross failure would take place. We proceeded to confirm that the local penetrations are at least as strong.

Our best estimate study using the computer codes MARCH and CLASIX showed that the containment pressure following hydrogen burns with igniters operational was very close to the design pressure, while a reasonable parametric study showed that the pressure was within the containment ultimate capability. This was based on our conclusions that a constant hydrogen release rate of 1 lb/sec is a nominal value and 3 lbs/sec is a upper bound for most degraded core accidents. These were confirmed later by a Battelle Columbus study (NUREG/CR-2540), again using MARCH. In all likelihood, when a better computer code than MARCH is available, it will be found that there is additional conservatism in these release rates.

We concluded that containment integrity was no longer a major concern as far as hydrogen burn issue is concerned.

We believe that failure of the containment boundary leakage path configuration control, unrelated to hydrogen burn, is a more likely containment failure mode. To put things in the right perspective, it is believed that we may not be working on the issue with the greatest potential for risk reductions, except that the hydrogen problem has been an

important licensing issue.

B. Equipment survivability--The most convincing test in this area was the one done at our own Singleton Laboratory. This will be covered in detail in a separate paper by our Mr. Robert Bryan later. The evidence is so strong, the margin is so abundant, and the cross checking through heat flux and total energy calculations is so fundamental that there leaves little doubt that temperature transients due to hydrogen burns are not a real concern, at least for the ice condenser containments.

Earlier, we were required to identify the safety systems needed after a hydrogen burn, identify the safety components needed, identify the locations of the components, and perform various analysis and computer benchmarkings, etc. Some of these analyses were done by TVA but, in retrospect, most of this was wasted effort, since the Singleton test was simpler, more conservative, and more conclusive.

C. Local detonation--We concluded very early in our study that local detonation in an ice condenser containment is incredible because:

1. There is no reasonable source location in confined space.
2. There is good spatial distribution (mixing).
3. There is no shock tube geometry for the pressure wave to accelerate in.
4. Combustible limit is reached prior to detonable limit.

Later in the conference, there will be papers by people from Hanford and others to show that mixing is indeed very good. We are aware that during the last few years, there have been many studies about transition to detonation. In some of these studies, a 22-percent hydrogen concentration was, on occasion, referred to as "lean" mixture. In another study, detonators were used to "detonate" mixtures at about 12 percent at some very special conditions. Before we draw conclusions from these experiments, we must keep in mind that detonators are not ordinary equipment inside a containment and 22 percent hydrogen is not easily obtained when a distributed ignition system is functional.

We should add that in some of our dynamic tests, such as the Fenwal and Acurex tests, we introduced pure hydrogen (and in some cases also steam) into a closed vessel with an igniter operating nearby. The hydrogen concentration varied from 100 percent near the source to a few percent near the igniters. Detonations were not observed.

We have concluded that local detonation is not a problem, at least in the ice condenser containments.

These three major concerns have been resolved to TVA's satisfaction,

and we hope to the NRC's. With the three major concerns resolved to our satisfaction, we are operating our Sequoyah Nuclear Plant units 1 and 2 at full power.

Perhaps we should add that while there have been numerous research projects, multiple sets of questions from the regulatory agencies, meetings, etc., in the last two years, the equipment and procedures that we proposed originally have not undergone any significant changes.

IV. Future Studies

Before people come to the conclusion that we are one of those who have done everything and therefore will do nothing and spend nothing, we do have a few items that we think merit further studies:

1. Better quantify the hydrogen source (sequences and rates)--This is in conjunction with other severe accident studies of core behavior. The objective is to understand the phenomena of hydrogen generation in light water reactor cores during degraded core conditions, to reduce conservatism, if it exists, and to better quantify the reduction in risk.

2. Burn above suppression pool--This is a phenomenon unique to the uninerted Mark III containments. Instead of studying flame height, however, we believe that people should study the energy release rate and perform heat flux calculations instead. Also, the space industry routinely releases and burns hydrogen through a pool of water in the open. Perhaps quite a bit of information is already in existence.

3. Burn in rich hydrogen/lean oxygen environments--This is a phenomenon that may exist in the Mark III drywells. It may also exist in preinerted Mark I and Mark II containments a long time after a severe accident takes place. Steam and nitrogen may not play a significant role, but a small scale confirmatory test has merit.

4. Confirm that for uninerted containments, the most likely hydrogen release points are not in confined regions.

5. Containment boundary leakage path configuration control--This is not a hydrogen-related item but we believe it is the most likely failure mode for containments. This issue should receive the proper human resource allocation when other required fixes and studies are completed.

V. Summary Remarks

The main thrust of this paper is to emphasize the fact that while most people are busy in quantification and information gathering, the decision makers should put things in perspective. In this case, he should have taken the following steps:

1. Identify clearly what decisions are needed.
2. Develop an overall decision logic chart and identify the information required for each of the decisions.
3. Distinguish confirmatory research from research needed for decisionmaking information.
4. Recognize that an optimized mitigation system is generally not the objective, neither is minimum risk required.
5. Assure that the level of studies be consistent with the risk.

We have taken the above steps, and we have concluded that a deliberate and distributed ignition system is a viable solution for the hydrogen problem for certain nuclear power plants. We also have concluded that the issue can and should be closed out for ice condenser plants.

The objective of the inerting requirement in the Interim Rule (46 FR 58484) is to eliminate the potential for a major hydrogen combustion in the Mark I and Mark II containment. If the inerted conditions were lost (such as by radiolysis effects) within a short time following onset of the postulated degraded core accident, then the above stated objective would not have been achieved.

Some elaboration on the inerting requirement of the Interim Rule is appropriate at this point. The Mark I and Mark II containments are being required to be inerted to deal with a postulated degraded core accident. Radiolysis is a known anism for the production of oxygen which could cause the dei ng of the containment.

If the radiolysis source term we t analyzed for the conditions associated with degraded core accidents and dealt with appropriately, then the inerting requirement would have been for naught.

The analysis of the radiolysis source term in the licensee's report was confined to design basis accident scenarios. These analyses concluded that bulk boiling of the reactor coolant can reasonably be postulated to be terminated some 12 hours following onset of the design basis accident. A similar conclusion cannot be justified for the various degraded core scenarios. In degraded core scenarios, bulk boiling must be postulated for a protracted period following onset of the accident because the coolant flow channels will be substantially blocked. The results of analyses performed to determine the effect of radiolysis in post-accident management of combustible gases for a typical Mark I containment reveal that prolonged radiolysis produces sufficient oxygen to support combustion. These analyses were performed assuming design basis values for metal-water reaction G-valves, and for the fission product energy releases (Regulatory Guide 1.7).

It should be recognized that the use of a metal-water reaction fraction typical of design basis accidents elevates the required oxygen concentration for supporting combustion. However, considering a 5% metal-water reaction and an assumed G-value of 0.5, the environment will be comprised of 13 v/o hydrogen and 5 v/o oxygen in less than 1 1/2 days. Thus if nonflammable conditions are to be maintained, then positive action additional to the initial preinerting must be taken.

Accordingly, even if reduced G-values for radiolysis relative to those prescribed in Regulatory Guide 1.7 (Revision 2) were found acceptable for assessment of design basis accidents on the basis of the "bulk boiling argument," such related G-values would not be appropriate for dealing with degraded core accidents. Therefore, since the inerted condition needs to be maintained for protracted periods following onset of the accident for both degraded core and design basis accidents, use of the conservatively prescribed source terms in Regulatory Guide 1.7 (Revision 2) should continue to serve as a method for complying with 10 CFR Section 50.44.

EPRI RESEARCH ON HYDROGEN COMBUSTION AND CONTROL

L. Thompson
Electric Power Research Institute
Nuclear Safety Analysis Center
3412 Hillview Avenue
Palo Alto, California 94303

ABSTRACT

EPRI is conducting a program to study hydrogen combustion behavior in the LWR containment building environments that could follow severe postulated nuclear accidents. Flammability limits, deflagrations, combustion control methods, equipment survivability, and hydrogen mixing and distribution in hydrogen, air, steam, and water spray environments have been investigated in several projects. Analytic models and computer codes are also being developed and evaluated for combustion behavior and for hydrogen mixing and distribution processes.

1.0 INTRODUCTION

EPRI's research program on hydrogen control in postulated degraded core accidents began in early 1981 with the development of several small and intermediate-scale experimental facilities. The program focused on studies of premixed combustion in potential accident environments, hydrogen mixing and distribution in a compartmentalized geometry, and on the deliberate ignition approach to hydrogen control. Concerns related to nuclear plant licensing prompted an accelerated schedule, and a substantial data base has now been developed. Program activity is currently geared toward preparation of a very large scale combustion facility for the further evaluation and demonstration of hydrogen control methods.

Results of the small and intermediate-scale work to date are very encouraging and indicate that relatively simple means of hydrogen control may be adequate. A brief overview of the program and some results are presented in this paper; more detailed results may be found in other papers to be presented at this Conference.[1-8]

As the generic work enters a new phase, participation has broadened with international support. The completed experimental work was co-funded by the three U.S. PWR ice condenser utilities (Duke, TVA, and AEP). Several foreign organizations are now participants, including EdF, Kansai Electric Company, Ontario Hydro, Swedish State Power Board, and Taiwan Power Company. The NRC Office of Nuclear Regulatory Research has very recently also become a partner in the large scale test project.

2.0 OUTLINE OF PROGRAM

The generic research program is formed by five experimental and two analytic projects, the experimental facilities involving vessels ranging in size from 0.017 to 2100 m^3. The projects are related and consist of the following.

- Hydrogen combustion studies at the Whiteshell Nuclear Reserach Laboratory, Atomic Energy of Canada, Ltd., in Manitoba (combustion behavior and igniter effectiveness in steam environments, using 0.017-m^3 and 6-m^3 vessels), continuing.

- Hydrogen control studies by Acurex Corporation at a test site near Livermore, California (simulated accident conditions and deliberate ignition with dynamic hydrogen injection, water spray, water fog, and equipment survivability in a 18-m^3 vessel), completed.

- Hydrogen mixing and distribution studies at the Hanford Engineering Development Laboratory (HEDL) in Richland, Washington (hydrogen-steam injection into a compartmentalized 850-m^3 vessel; study of mixing behavior), continuing.

- Large-scale demonstration at DOE's Nevada Test Site (simulation of accident environments in a 2100-m^3 vessel; study of hydrogen control systems and equipment survivability), continuing.

- Effects of water fog on lower flammability limits at Factory Mutual Research Corporation in Norwood, Massachusetts (bench-scale study of fog effects on flammability limits), completed.

- Modeling of hydrogen combustion at Factory Mutual, continuing.

- Calculation of hydrogen distributions at Battelle, Pacific Northwest Laboratory in Richland, Washington, completed.

Figure 1 shows the volume and design pressure characteristics of several of the larger test vessels and provides a comparison with the characteristics of reactor containments.

The nature and extent of each experimental study is indicated in the matrix of Table I. Flammability and ignition limits were determined in the smallest vessels as a function of steam, turbulence, water spray and water fog. Premixed combustion has been studied in three vessels of distinctly different volume. The most complete work was performed in a sphere of 6 m^3 volume, complemented by experiments in a larger cylinder and in bench scale. Hydrogen and steam concentrations were varied over a wide range (to 40 and 55 volume percent respectively), and igniter location, temperature, and fan turbulence were parameters. Tests in the largest volume included water fogs, using a fog nozzle evaluated in a bench scale project. Some studies of compartmentalization effects and concentration gradients on hydrogen combustion were included using a pipe-sphere configuration.

Simulations of degraded core accident situations were undertaken in addition to ignition-limit and premixed combustion studies. Gas mixtures were injected into a large volume to study mixing and distribution, and into an intermediate

size volume in order to study combustion and the deliberate ignition concept. Flows in the mixing tests were scaled by the Froude Number for a small-break degraded core accident. The same flows were scaled by volume ratio for the combustion tests. Results of these experiments and the premixed combustion tests have helped form the basis and rationale for selection of a test matrix for the large scale demonstration tests in Nevada.

3.0 PROGRESS AND RECENT RESULTS

Figure 2 summarizes the maximum combustion overpressure observed in tests using a 2.3 meter diameter sphere.[3] The observed pressures for dry mixtures are about 10% lower than the adiabatic combustion pressures for 100°C. The presence of only 20 volume percent water vapor further reduces the peak pressure at stoichiometry by almost 20%, and 30 volume percent water vapor causes a 30% reduction. The highest flame speeds were on the order of 100 m/sec, far below the condition required for a deflagration to detonation transition.

Other experiments in the sphere have examined completeness of combustion for lean hydrogen/air/steam mixtures, the qualitative effects of gratings and fan turbulence, and combustion in a pipe/sphere geometry.[3] During the latter tests large acoustic pressure oscillations were found in the 6 m long, 0.3 m-diameter pipe for dry hydrogen mixtures of more then 20 volume percent. Oscillations were small in the open sphere, and flame speeds quickly decelerated on approaching the pipe end.

Bench scale tests have been conducted to determine ignition limits in steam and flammability limits in water fog. Thermal igniters of the types proposed by some utilities for use in deliberate ignition systems have been employed in order to carefully map ignition limits as a function of steam concentration.[3,7] Both the General Motors AC-7G diesel engine glow plug, requiring 12 to 14 volts for operation, and a newer hot surface device operable on 110-120 volts was tested. Even with 30 volume percent steam a static mixture of less than 8 volume percent hydrogen will ignite, and the limit is under 6 volume percent hydrogen with fan-turbulence.[3,7] Glow plug surface temperatures at ignition increased with steam concentration but were always less than 850°C (1560°F) even with 50% steam. Furthermore experiments with fog showed that even a dense fog of small droplets has little effect on flammability.[5]

Larger scale premixed combustion experiments were performed to assess the capability of water fog for mitigating pressures and temperatures.[4] Tests with about 7.5 and 10 volume percent hydrogen in air produced about the same combustion overpressure with or without microfog spray. Spray of about 5 l/min (1.1-1.4 gpm) from 9 nozzles in a cylindrical tank of cross sectional area 3.5 m^2 (38 ft^2) was used. The number-mean diameter drop size was estimated at 10 microns. It appears that the density of droplets fine enough to vaporize and absorb energy during the combustion period (about one second) was too low to have an appreciable effect. In the lean mixture tests with about 7.5 v% hydrogen the fog spray may have increased turbulence, enhancing burn completness. In all cases ignition took place approximately 20 seconds after the igniter was turned on.

Hydrogen control by deliberate ignition has been studied in several degraded core accident simulations in intermediate scale.[4] Most of the experiments

feature continuous injection of a hydrogen-steam source into an 18-m^3 cylinder containing a preenergized glow plug. The vessel was fitted with the standard containment spray nozzle used in many LWRs, as well as with several microfog nozzles, three standard glow plug igniters, a nozzle for premixed hydrogen-steam injection, and a series of 35 flame front detectors.

The dynamic injection tests were intended to simulate the amount of hydrogen released to containment following a small-break degraded core accident. Several parameters were varied in these tests, including the amount of hydrogen and steam flow; the ignition location; presence of water spray, water fog, and fans; and microfog drop size. Pressures are generally lower when steam is injected with the hydrogen and are much lower when water sprays are activated prior to the hydrogen injection.

The effects of ignition location on hydrogen combustion behavior in tests with continuous injection of dry hydrogen can be seen in Figure 3. With the bottom igniter activated hydrogen bypassed the ignition source, building up throughout the volume until a global burn took place at about 450 seconds. The peak overpressure was 193 kPa (28 psi). Use of the central ignition position allowed earlier and frequent intermittent local combustion to take place. The highest single overpressure was only 41 kPa (6 psi). With the top igniter activated, some combustion took place at about 300 seconds as the ignition limit for upward propagation was reached. A volume-average concentration of 4.7 v% hydrogen had been injected up to that time. As hydrogen was further introduced the limit for downward propagation was apparently reached at about 580 seconds and a global burn took place producing an overpressure of 139 kPa (20 psi). Most of the injected hydrogen was consumed in all three cases.

The addition of steam or water spray can have a dramatic mitigating effect on combustion in dynamic hydrogen injection tests. Typical effects can be seen in Figure 4 which shows three cases having an activated central igniter. The top curve is for injection of dry hydrogen, resulting in a number of intermittent local burns which consume most of the hydrogen and produce a maximum pressure of 41 kPa. For the center figure, steam was added to the hydrogen flow in a mass ratio of 60 to 1 (volume ratio of about 7 to 1). The highest combustion overpressure is reduced slightly, however the major effect is to make the combustion somewhat more erratic, taking place over a longer time period. In the lower figure, Test 2.9, both steam and water spray are added. Now the multiple combustion events are much more uniform, and peak combustion overpressures are less than 20 kPa (3 psi).

A series of experiments on equipment survivability has also been completed in this intermediate scale vessel.[8] All items of equipment -- which included a solenoid valve, pressure transmitter, valve operator, limit switch, resistance temperature device, thermocouple, and electrical cable -- operated successfully both during and after exposure to multiple hydrogen burns.

Hydrogen mixing and distribution has been studied in a large 20 m-high, 7.6 m-diameter vessel.[1] The vessel was fitted with a deck, and with provision for some convective flow from the lower to the upper compartment and for forced flow from upper to lower. Hydrogen-steam releases from a small break are simulated, and two nozzle locations were used. Figure 5 shows the vessel configuration. Gas sample, air velocity, and temperature measurement locations are concentrated in the annular lower compartment at locations indicated by the 'star' symbol in the figure.

Four preliminary tests were performed in order to determine the separate and combined effects of natural and forced convection air recirculation. Seven mix tests were performed with a 10 minute injection of a scaled hydrogen/steam or helium/steam jet, followed by about one hour of continued measurements. Concentrations were monitored continuously.

Figure 6 shows concentration measurements for the case of a vertical helium/-steam release corresponding to 550 kg/min (1200 lb/min) steam and 9 kg/min (20 lb/min) hydrogen in a small break degraded core accident. The maximum concentration difference observed at any time during the test was about 2.5 volume percent, occurring during the release period. The largest difference decayed to less than 1 volume percent soon after the release ended. In other experiments with horizontal jet sources concentration differences tended to be less.

Predictions of hydrogen distribution have been made with an existing code.[2] TEMPEST is a general hydrothermal code which solves time-dependent turbulent, momentum, and heat transport in three dimensions. In spite of several limitations the current code logic is able to provide good comparisons with Battelle-Frankfurt data on hydrogen mixing and distribution (Figure 7). The code has also been applied to the EPRI mixing tests in connection with a blind 'standard problem' exercise.

Models are being developed and improved in the case of combustion.[6] For lean mixtures the combustion is incomplete, nonadiabatic, and governed by buoyant flame propagation. For rich mixtures combustion is assumed to be complete, adiabatic, and to involve spherical flame propagation.

Calculations with the complete combustion model are compared to test results with hydrogen volumetric concentrations ranging from 8 - 15.1% and steam concentrations from 0 - 25% in Figure 8. Percentage peak pressure deviation is plotted against burning velocity. The deviation is greater for smaller burning velocities, corresponding to low hydrogen concentration (and/or high steam concentration), because the adiabatic assumption is questionable for these slow-burning gas mixtures. For burning velocities greater than 0.45 m/s (approximatly 11% dry hydrogen) the deviation is within 8%.

Difficulties of predicting combustion behavior for lean mixture combustion reflect the importance of heat transfer processes and assumed burning velocities. Figure 9 indicates pressure-time signatures for combustion events at Three Mile Island and in a 2.3 m-diameter sphere. Substantially different pressure-decay (and temperature decay) characteristics occur in part due to differences in surface area-to-volume ratio and in the rates of radiative and convective heat losses to surfaces.

The large-scale hydrogen combustion and control demonstration project at the Nevada Test Site will provide data needed for validating existing computer models. Other objectives of the project are

- verification of the data base from small-scale testing
- examination of equipment survivability, and

- o testing of the deliberate ignition hydrogen control approach during simulated degraded core accidents.

The Nevada dewar, once used to store liquid hydrogen, has a diameter of 52 feet, a design pressure of 87 psig (600 kPa), and a 1 m annulus containing high grade pearlite insulation. The vessel was pressure tested to 75 psig (520 kPa) for 24 hours in December 1981 as one of the initial steps leading facility activation. Fluid system additions to the facility include:

- o a heated water spray system (16 standard containment nozzles with 910 1/m (240 gpm) total capacity);
- o a boiler to generate 7,700 kg/hr (17,000 lb/hr) steam at 1030 kPa (150 psi);
- o a steam control and measurement system for steam flows from 2.3 to 135 kg/min (5-300 lb/m);
- o a hydrogen delivery manifold for 0.45, 0.91, 1.8, or 3.2 kg/min (1, 2, 4 or 7 lb/min) of H_2 gas;
- o a hydrogen/steam mixing chamber outside the dewar;
- o two mixing fans in the dewar, each 85 m^3/min (3000 cfm); and
- o an air compressor with a 17 m^3/min (600 cfm) rating.

Figure 10 provides a schematic of the primary systems. Hydrogen supplied from gas cylinders in a 'tube trailer' will enter the dewar through a nozzle at the bottom and will be released at an interior elevation of about 5 ft (1.5m). Steam is released at the same point. Standard Spraco water spray nozzles will be used as well as an array of flame front detectors and up to 12 igniters. Transducers will measure heat flux, pressures, temperatures, gas concentrations, wall strain, and liquid level. Methods for visualization are being investigated. Facility shakedown is expected in December 1982.

The test matrix includes premixed combustion experiments as well as simulations of hydrogen/steam release during degraded core accidents, and has been based on results of the completed small and intermediate scale tests. The source nozzle geometry will be a variable, and equipment survivability testi will be incorporated while concurrently serving other project objectives.

4.0 SUMMARY AND CONCLUSION

Several small and intermediate-scale experimental projects have been completed which have increased confidence that simple hydrogen control systems will be adequate. Deliberate ignition devices have been found effective in various environments of hydrogen, air, steam, water spray, and water fog. The maximum pressures observed in intermediate scale tests of the deliberate ignition concept were less than 2 atmospheres. Hydrogen mixing in a small-break accident simulation was rapid and nearly uniform, and no tendency toward detonation was observed in combustion tests covering a wide range of conditions. Electrical equipment operated successfully during and after multiple combustion events.

Codes for prediction of combustion and mixing behavior require improvements. Data to help benchmark codes and to validate current experience will soon be obtained in a very large scale combustion and control demonstration facility.



REFERENCES

1. G.R. Bloom, L.D. Muhlestein, and A.K. Postma, "Hydrogen Distribution in a Compartment with a High Velocity Hydrogen-Steam Source," Second International Workshop on the Impact of Hydrogen on Water Reactor Safety, Albuquerque, New Mexico, October 4-7, 1982. (Session IV).

2. D.S.Trent and L.L. Eyler, "Computation of Hydrogen Distribution Using the TEMPEST Computer Code, Ibid. (Session IV)

3. H. Tamm, R.K. Kumar, and W.C. Harrison, "A Review of Recent WNRE Experiments on Hydrogen Combustion," Ibid. (Session Va).

4. R. Torok, et.al., "Hydrogen Control Tests in Intermediate Scale, Ibid. (Session Va).

5. R.G. Zalosh and S.M. Bajpai, "Water Fog Inerting of Hydrogen-Air-Steam Mixtures," Ibid. (Session Vb).

6. R.G. Zalosh, E. Ural, and V.W.S. Hwa, "Lean Hydrogen-Air Mixture Combustion Models," Ibid. (Session Vb).

7. D. Renfro, et.al., "Development and Testing of Hydrogen Ignition Devices," Ibid. (Session VII).



G. Sliter, "EPRI Research on Equipment Survivability Under Hydrogen Burn," Ibid. (Session VIII).

Table I
EPRI Hydrogen Combustion and Control Program
Test Parameters

Parameter	Facility					
	FMRC (Fog)	Whiteshell (Combustion)		Acurex (Control)	HEDL (Mixing)	Nevada (Demon.)
Volume (m^3)	0.018	0.017	6	18	850	2100
Shape	Cyl.	'Sph.'	Sph./Pipe	Cyl.	Cyl.	Sph.
Igniter	Spark, GP(1)	GP	Spark	GP	-	GP
Ignition Limit	X	X	-	-	-	-
Premixed H_2/Steam	-	X	X	X	-	X
H_2/St. Flow	-	-	-	X	X	X
Water Spray	X	-	-	X	-	X
Water Fog	X	-	-	X	-	-
Initial T	X	-	X	X	X	X
Igniter Loc.	-	-	X	X	-	X
Multiple Ign.	-	-	-	-	-	X
Fan	-	X	X	X	X	X
Compartments	-	-	X	-	X	X
Mixing & Distrib.	-	-	-	-	X	X
Equip. Surviv.	-	-	-	X	-	X

(1)Glow Plug

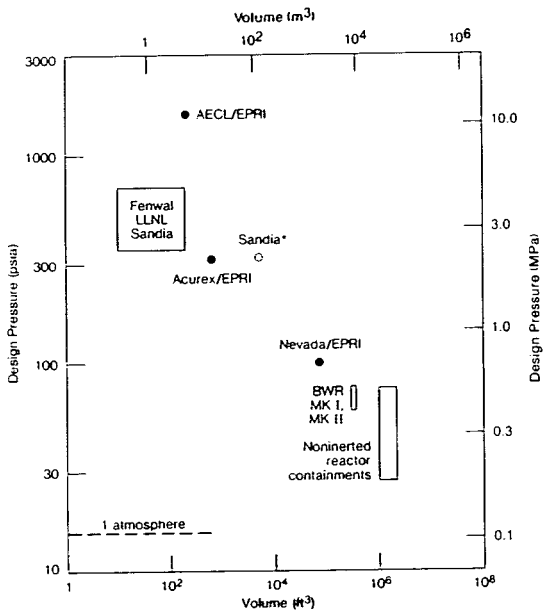


Figure 1--Volume and design pressure characteristics of hydrogen combustion test vessels and containments.

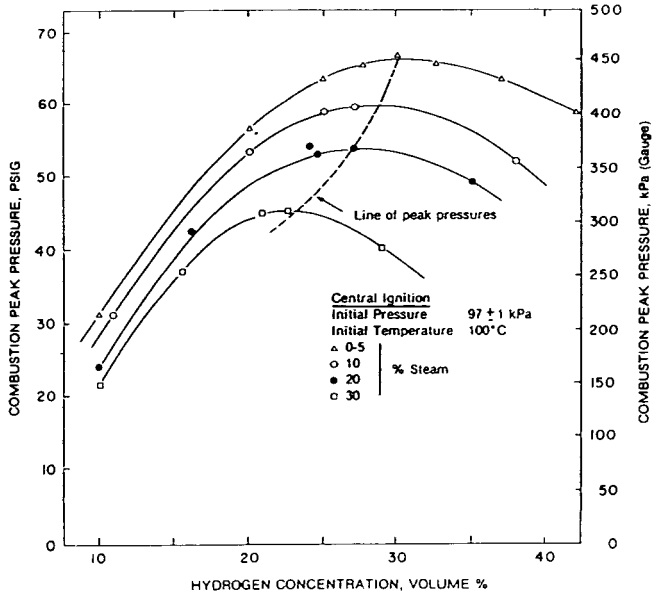


Figure 2--Maximum combustion overpressure as a function of hydrogen and steam concentration in a 2.3 m-diameter sphere.

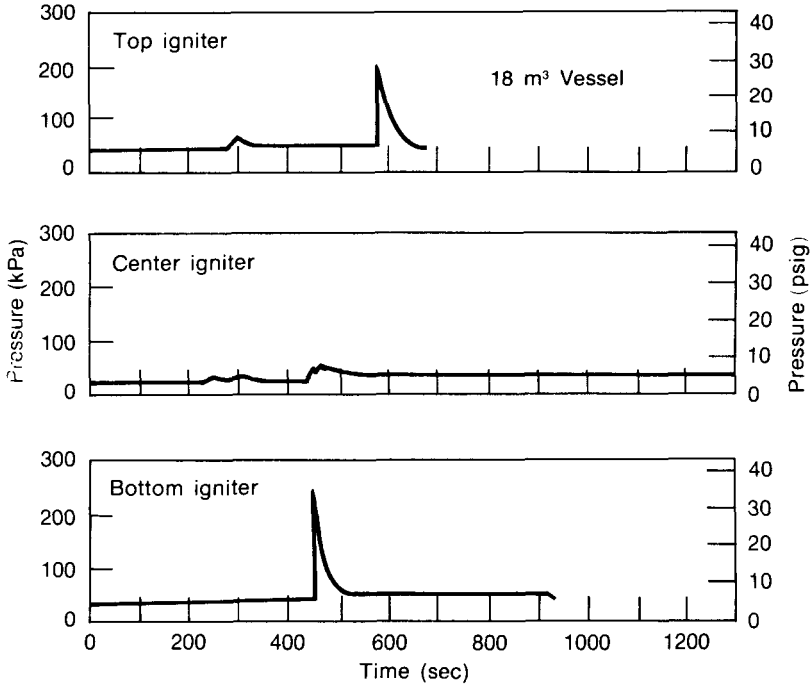


Figure 3--Effect of igniter location on pressure during injection of hydrogen into an 18 m^3 cylindrical vessel.

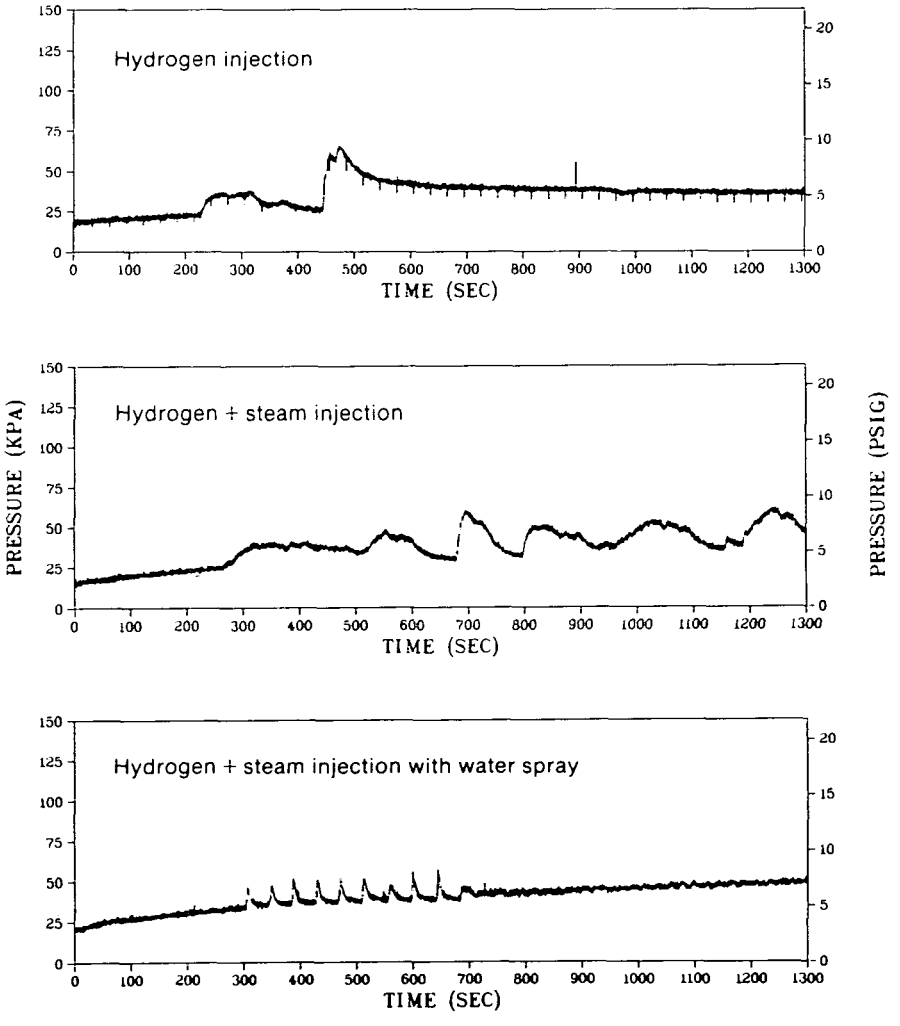


Figure 4--Effect of steam injection and water spray on pressure during continuous injection of hydrogen into a cylindrical 18 m^3 vessel.

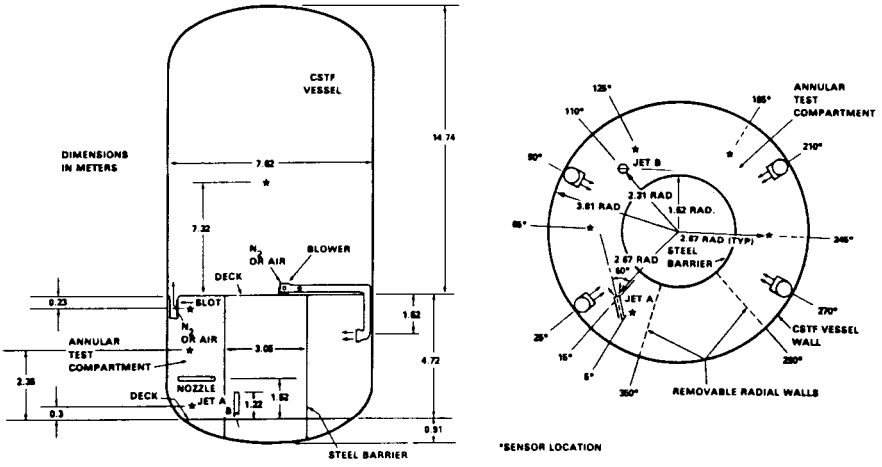


Figure 5--Schematic of 850 m^3 vessel used in hydrogen and helium mixing and distribution tests.

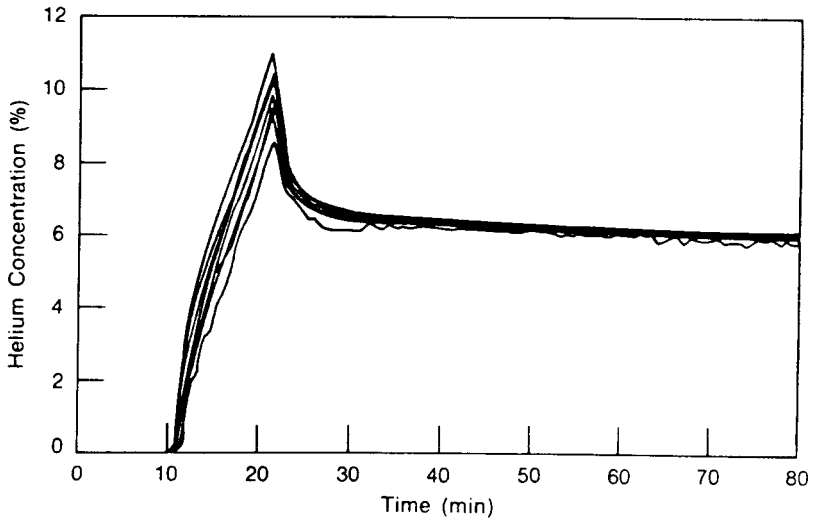


Figure 6--Gas concentrations at several locations during and following injection of a vertical helium/steam jet into the lower compartment of a 850 m^3 vessel.

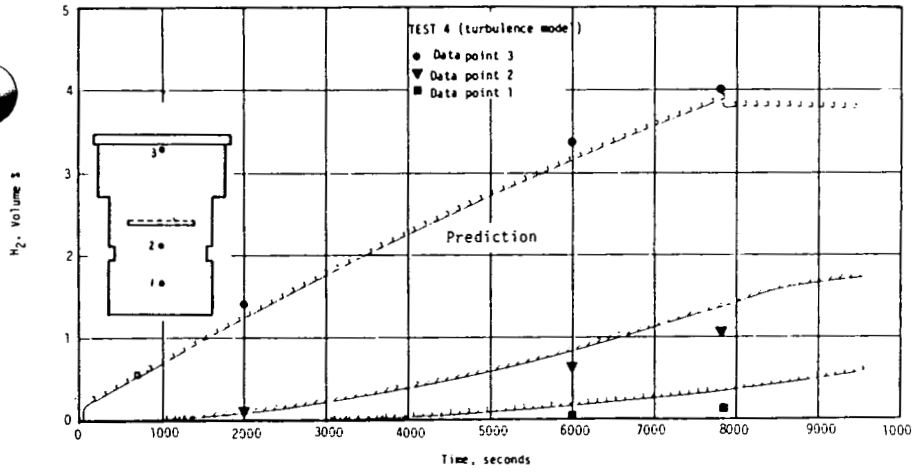


Figure 7--Computer code prediction of Battelle-Frankfurt hydrogen mixing data for an 8000-second experiment.

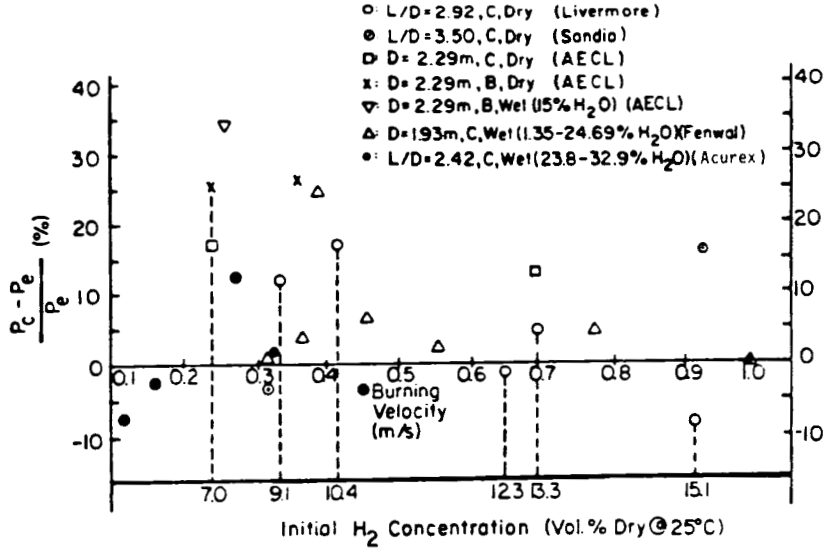


Figure 8--Comparison of calculated and actual pressures during complete combustion tests at several facilities.

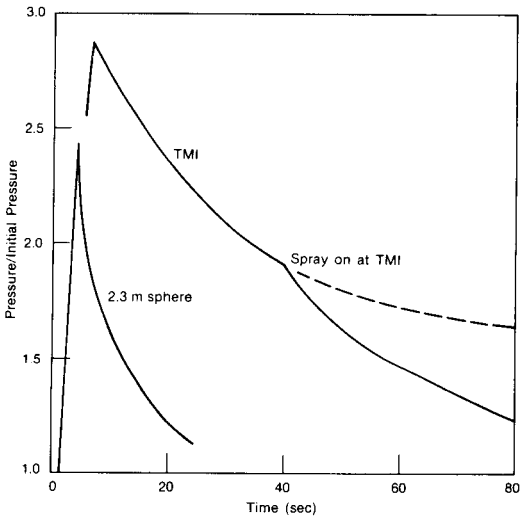


Figure 9--Pressure decay at Three Mile Island and (typical) rate for 2.3 m-diameter sphere.

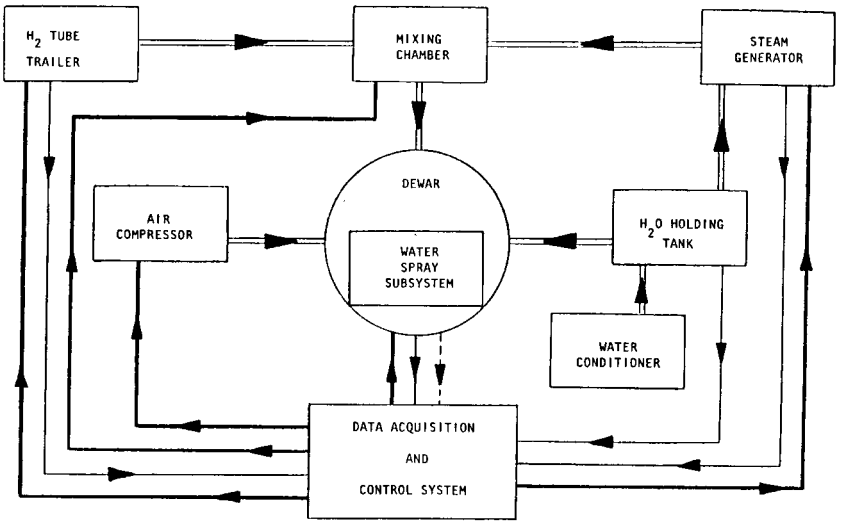


Figure 10--Schematic of principal systems at Nevada Hydrogen Test Facility.

THE NRC HYDROGEN BEHAVIOR AND MITIGATION RESEARCH PROGRAM

by

J. T. Larkins and P. Worthington
Office of Nuclear Regulatory Research
United States Nuclear Regulatory Commission

THE NRC HYDROGEN BEHAVIOR AND MITIGATION RESEARCH PROGRAM

I. Introduction

As a result of the accident at TMI-2, the potential for hydrogen combustion in nuclear plant containments has received increased consideration in terms of safety implications. Two final rules related to hydrogen control and a third rule on the interim requirements for hydrogen are currently under Commission review; additionally, the Office of Research of the NRC has prepared a research plan, draft NUREG-0900, to develop a technical basis for decisions related to severe accidents. This plan will provide information to assess the risk reduction benefits of various proposed add-on systems for the prevention and mitigation of severe accidents. Part of the work being done at Sandia on hydrogen safety is directed at assessment, with the major emphasis of the program on developing information for near term regulatory decisions and to support the various rulemaking activities. To address these hydrogen-related issues, the Office of Nuclear Regulatory Research (Divisions of Accident Evaluation and Engineering Technology) has initiated a comprehensive research program whose objective is to quantify the threat posed by hydrogen released during severe reactor accidents, and to generate information, procedures and concepts which will prevent or mitigate that threat. The products of this research program will include:

1. Assessment of the threat for several classes of reactors and containment designs;

2. Assessment of the adequacy of existing safety systems and mitigation strategies;

3. Identification and concept demonstration of improved mitigation and detection systems;

4. Publication of manuals and reports on: evaluation of the state-of-the-art; phenomena important to threat assessment; operator strategies and training; and reactor safety issues;

5. Development and applications of computer codes for addressing the generation, transport, combustion and mitigation of hydrogen during hypothetical reactor accidents.

From its inception, this program has been planned and executed in close cooperation with the Office of Nuclear Reactor Regulation and with the industry research effort conducted by the Electric Power Research Institute and various interested

utilities. Considering the large diversity of issues related to the hydrogen problem, the elements of the various research programs have remained, to a large extent, complementary to each other, as can be seen from the papers at this workshop. Even in the areas where overlap has occurred, the data have frequently supported each other and raised our confidence in the accuracy and reliability of the results; in some cases, possible discrepancies have arisen, and further research will be required to resolve these questions.

II. Research Program Elements

There are several aspects to the hydrogen issue: hydrogen generation (sources), detection, transport and mixing, combustion, and ultimately mitigation and control. Figure 1 illustrates the interdependence of these aspects; phenomenological information from these areas must eventually be incorporated into models which can predict reactor and containment responses during hypothetical accidents. The NRC research program is addressing many areas within each of these groups; current research emphasizes those aspects of the problem which are considered to be most urgent, based on current information; future research directions will obviously depend on information produced from the current research.

Sandia National Laboratories is the prime contractor for 5 hydrogen-related programs supported by the Office of Research. The Combustible Gas in Containment program (A-1255) is primarily aimed at determining the rates and total quantities of hydrogen which could be generated from corrosion of coatings (galvanized material, aluminum, paints, etc.) in containments during reactor accidents. Another major aspect of this research is to determine the quantity and morphology of debris and residues which might be produced during the corrosion reactions. The concern here is the potential that large quantities of debris might have for adversely affecting the performance of the reactor sump and water recirculation system.

The Hydrogen Burn Survival program (A-1270) is evaluating the response of safety-related equipment to the severe environments which might develop during or subsequent to a hydrogen combustion event. Of immediate interest is the determination of equipment response to the pressures and temperatures characteristic of ordinary single isolated deflagrations, or sequences of such deflagrations as might occur for plants equipped with deliberate ignition mitigation systems. Future research will address the loads that might be generated by accelerated flames or detonations. This program is complementary to a technical assistance program supported by NRR (A-1306).

The primary objective of the Code Assessment and Applications program (A-1205) is to evaluate the major thermalhydraulic computer codes (TRAC, RELAP4 and 5, etc.). A major subtask, however, is the assessment of the German (GRS) hydrogen transport code, RALOC. This code has been used to evaluate hydrogen transport and mixing times in various containments as a functio of source rates and other initial conditions.

The objectives of the Hydrogen Combustion Mitigative and Preventive Schemes program (A-1336) include:

1. The evaluation of the effectiveness and feasibility of the control methods currently considered to be most promising (deliberate ignition; pre- and post-accident inerting; oxygen depletion; water fogs and foams);

2. The identification and assessment of new ideas for mitigation and control;

3. The investigation of deliberate flaring of steam: hydrogen jets;

4. Identification of the net advantages and disadvantages of the various schemes under accident and post-accident conditions.

The Hydrogen Behavior program (A-1246) is the first, the largest, and the most comprehensive of the NRC hydrogen programs. It addresses most of the items shown in Fig. 1 which are not specifically addressed by the other programs. The primary emphasis of this program is on the combustion aspects of the hydrogen problem; it also ensures that the research elements are well organized, and integrates these elements into the reactor accident analysis tasks.

Several philosophies have been incorporated into the various hydrogen programs to maximize their utility to the NRC. First, the programs contain both experimental and analytical elements. This facilitates the use of the experimental data, as well as providing guidance to and assessment of the code development efforts. Secondly, the programs are designed to provide interim, scoping information to assist in current decision-making processes and in answering urgent licensing questions. The programs are also designed to address long-term research goals; i.e., experimental facilities of broad scope and equipped with adequate instrumentation are being designed and built to comprehensively address important reactor safety issues; these facilities will be intimately coupled with longer-term code development activities. This two-pronged approach is consistent with meeting urgent licensing needs,

without compromising the more detailed information that will be needed in the long-term evaluation of the consequences of severe reactor accidents. Figure 2 lists the prime contractor and major subcontractors involved with the NRC-funded hydrogen programs.

Figure 3 illustrates the relationships between the various code development tasks and their applications. The HECTR code is intended to be a fast-running reactor accident analysis tool which will calculate the transport and combustion of the fuel and oxidant gases during hypothetical reactor accidents. It is a one-dimensional, multicompartment, control-volume code, which will model the various engineered safety features in different containments. It will include heat transfer (radiation, convection, conduction, droplet evaporation), flame initiation and propagation, and a rudimentary model for transport and mixing. It will employ other codes for the definition of the source term (e.g., MARCH, CORCON, MELCOR, etc.), or internally calculate this term by means of tables or simple formulas. It may also incorporate simplified versions of more complex flame propagation codes. HECTR has been and will continue to be used for reactor accident calculations; it may also provide models for incorporation into the large, second-generation accident analysis codes such as MELCOR. HECTR is also being used to provide pressure and temperature histories for the evaluation of equipment survival. These histories are used directly in heat transfer codes to predict the response of equipment to hydrogen burns; they are also being used to guide the design of experimental facilities which will simulate temperature histories at reactor scales.

An analytic effort is underway at Sandia Livermore (SNLL) to predict the possibility and consequences of flame acceleration in reactor accidents. This effort includes the modification and application of complex vortex dynamics codes as well as simpler codes, and even empirical correlations when appropriate. This code development effort will be closely coupled to the experimental study of accelerated flames at Sandia Albuquerque (SNLA) and at McGill University.

Under NRC sponsorship, several hydrogen transport codes are currently being evaluated. The best of these codes will be pursued, both for comparisons to experiments, and to provide benchmark calculations. However, with the extension of HECTR's capability to the modelling of transport and mixing, the need for simplified 1-D pure transport codes will diminish. Code storage limitations and run time constraints, however, may extend the utility of RALOC for pure transport calculations.

Detonation loads have been calculated by a modified version of the Sandia CSQ code for several plants. The code can sometimes calculate non-conservative loads (i.e., less than the classical Chapman-Jouguet predictions), because it empirically assumes a finite run distance for transition to detonation. Nevertheless, it provides pressure-time behavior for calculating impulses delivered to structures (which are needed for structural failure calculations); note that the delivered impulses, however, (i.e., the time integrals of pressure) are generally quite accurate. Although refinement and improvement of CSQ for these calculations is quite possible, it is not planned for the immediate future.

Figure 4 lists the various experimental facilities available for the hydrogen research effort. A large pre-existing capability has been tapped for this work (e.g., the VGES 16-ft tank, the FITS tank, two large sites for high explosive testing at SNLA, and 10 tubes and channels of various lengths and diameters at McGill University). Some new facilities have been built or modified (e.g., FITS and the steam:hydrogen jet facility), or will be built shortly (FLAME). These facilities, together with those employed by EPRI and the utilities should suffice for most experimental investigations. Figure 5 shows those facilities which are being used to address questions dealing with deflagration phenomena. Figures 6 and 7 connect the appropriate facilities to studies of detonations and accelerated flames, respectively.

III. Research Highlights

Table I lists the important accomplishments of the hydrogen program through the end of FY81. Many of these items were discussed in the last Workshop in January, 1981. Table II lists tasks which have been completed in FY82. Most of these results will be discussed in considerably more detail in the following sessions. What we would like to do here is present a general overview of the work, emphasizing the important research highlights and how the results can be used by the NRC and others.

A. WORKSHOPS

This workshop and the one that preceded it in 1981 are an important means of disseminating information and airing different viewpoints. The published proceedings are documents of major utility to the reactor community, both for their technical content and their insights into the opinions of the different users of the research.

B. COMPENDIA AND MANUALS

The state-of-the-art on hydrogen was summarized in NUREG/CR-1561, published in August 1980. We anticipate a major revision of this document will be completed in FY84. A "Light Water Reactor Hydrogen Manual," NUREG/CR-2726, will be available in a few months. This manual is intended to provide information at a general but comprehensive level on the subject of hydrogen behavior during normal reactor operation and during accidents. The manual is directed toward readers who have a limited knowledge of this subject, and is not intended to provide in-depth information.

Although the manual's purpose is not to provide procedural directions to reactor operators, it should nevertheless prove useful to designers and operators when they formulate their own plant-specific procedural guides. Several utilities and vendors have participated in the review and format of this document.

C. DEFLAGRATIONS

C.1. Code Development and Applications

The purpose of the HECTR code (Hydrogen Event: Containment Transient Response) is to calculate the gas temperatures, pressures and compositions, and wall temperatures during and after a deflagration in multicompartment reactor containments. HECTR will be a generic hydrogen combustion code in that models will be available for ice condensers, Mark III's and large dry containments. The MOD1 version of this code will be released this fiscal year. It has already been used to calculate hydrogen combustion events for hypothetical accidents in the Grand Gulf, Sequoyah, and Zion nuclear plants. The MOD1 version will model spray evaporation, heat transfer (radiation, convection with and without wall condensation, and conduction into walls), flame initiation and propagation between compartments, transport in a rudimentary way, and several engineering safety features (air-return fans, ice condensers, fan coolers, suppression pools, etc.). Future versions of the code will contain models for all remaining safety features, more refined transport and mixing models, and a more detailed treatment of flame propagation within and between compartments. We also anticipate significant improvements in existing models as better experimental data become available. HECTR has also been coupled to a heat transfer code to determine the thermal loading of equipment. HECTR is expected to become a very important tool for experiment analysis, reactor accident studies, equipment survival calculations, and for comparison against industry codes (e.g., CLASIX).

C.2. Experimental Programs

The acronym VGES (Variable Geometry Experimental System) describes a group of experimental facilities located at the Explosive Test Site 9920, at Sandia Albuquerque. Facilities which are currently operational include 3 buried tanks (all 4' in diameter, 16' long) used for studying deflagrations, accelerated flames, mitigation concepts and the effects of aerosols; 4 large horizontal tubes (4' x 10', 2 @ 3' x 7', and 2.5' x 10') used for critical tube diameter and critical energy studies; and several smaller tubes of various lengths. Two new facilities will become operational in FY83: the FLAME channel (6' x 8' x 100') for large-scale flame acceleration and detonation studies; and a 1.5' diameter by 42' long heated tube for detonation studies in steam:hydrogen:air mixtures. The FITS tank at Explosive Test Site 9940, SNLA, was originally built to investigate steam explosions. It has been modified to permit studies of combustion in steam:hydrogen:air mixtures, and became operational in FY82. Deflagration experiments in FITS and the appropriate VGES facilities have addressed the following issues: flame shape and speed; combustion completeness; effects of igniter type and location; quiescent versus dynamic (turbulent) initial conditions; effects of steam, carbon dioxide and water foams; equipment survivability; and the effects of initial pressure, temperature, and gas concentrations. Some very important conclusions can be drawn from this body of experimental data, many of which have also been confirmed in studies conducted by EPRI and the utilities. It is important now to understand that the earlier concept of "flammability limits" is insufficient (and sometimes misleading) for reactor safety applications. The experiments show that such limits are not based on physical and chemical properties of the component gases alone; rather, they depend on ignition type and strength, vessel geometry and size, the nature and geometry of obstacles which may be present (and their heat transfer properties), and the velocity of the gases (quiescent versus moving). In addition, flame ignition must clearly be distinguished from flame propagation; e.g., hydrogen can be burned in the neighborhood of an igniter or on the surface of a catalyst, without any flame propagation occurring. This clearly complicates the job of the reactor safety analyst. If he wishes to know if a particular mixture of gases will sustain a propagating deflagration (and to know the resulting pressure rise), he will need to describe the initial and boundary conditions of the problem sufficiently accurately to determine flame speeds, combustion completeness and the important heat transfer mechanisms. In fact, an important result of the NRC-sponsored deflagration research program will be to produce curves and formulas which will allow such predictions. The data base already gathered to date will be expanded to permit such predictions. In addition, we plan to experimentally investigate

the effects of nonhomogeneous concentrations, multiple simultaneous or sequential ignitions, the effects of aerosols on combustion (and combustion on aerosols), and the performance of various mitigation schemes.

Laboratory-scale experiments are frequently employed when the feasibility of concepts is being tested. A set of such tests measured fog densities by means of x-ray absorption; this work is documented in NUREG/CR-2767. The potential for water foam mitigation of combustion-generated pressures and temperatures was also tested at small scale. These results have been published in NUREG/CR-2865, and will be discussed in Session VII.

The steam:hydrogen jet facility has two major objectives: to understand the behavior of such jets issuing from breaks in the primary system as functions of hydrogen and steam concentrations, flow velocities, gas temperatures, break size, and the nature and placement of flameholders (i.e., obstacles); and to investigate deliberate flaring through high-point vents as a mitigation concept. The facility is operational, and the highlights of this work will be discussed in Session Vb.

D. Detonations

D-1. Code Development and Applications

Most analysts believe that the development of a fully established detonation wave during a reactor accident is an unlikely event. However, the potential for damage is considered to be sufficiently high to justify the research necessary to better understand this phenomenon. The pressure amplification due to detonation waves and their reflections can be easily calculated from thermodynamic data alone, for classical Chapman-Jouguet detonations. These pressure ratios are shown in Fig. 8. The pressures alone, however, are insufficient for calculating structural failure probabilities; in the case of such brief dynamic loads, structural failure depends more on impulse delivered ($\int P(t)dt$) than on peak pressures. For this reason, the two-dimensional hydrodynamics code, CSQ, was modified to calculate the time-dependent pressure behavior, P(t), resulting from detonations. The waves may be weaker than C-J predictions; this is a consequence of modelling the energy deposition rate in an empirical, and somewhat arbitrary way; depending on the run-up distance available, CSQ will predict peak pressures that range from about 50% to 100% of the C-J pressures. The impulse calculations, however, are expected to be quite close to what would be generated by a C-J wave. Hence, the CSQ calculations can provide fairly reliable impulse histories, which can then be used in structural calculations to estimate the probability of dynamic failure. The code has been used to calculate the pressure histories due to postulated detonations in the Sequoyah, Grand Gulf and Zion containments (see NUREG/CR-2385). No further code development is planned at this time.

D-2. Experimental Programs

A very desirable result of the detonation research would be to either demonstrate that the probability of detonation occurrence is so small as to present a negligible threat, or to make that probability small by means of preventive measures or mitigation features. For example, at the inception of this program, the "accepted" values for "detonability limits" of hydrogen:air mixtures was 18-59% hydrogen. If such concentrations could be ruled out for reactor accidents, then detonations would be impossible. Unfortunately, our research has already shown that "detonability limits" (in the classical sense of specific numbers independent of geometry and size) are no more fundamental properties of nature than were "flammability limits". A very extensive program at McGill University (using hydrocarbons as well as hydrogen) coupled with large-scale critical tube diameter experiments at the VGES site, has led to the production of U-shaped curves as shown in Figs. 9-10. The detonation cell width, λ, appears to be a fundamental parameter of detonations; small values of λ correspond to highly detonable gases (such as acetylene and hydrogen) or to near-stoichiometric mixtures; the larger the value of λ, the more difficult it is to establish and maintain a steady detonation wave. It now appears that the cell width can be related to other important parameters of detonations such as initiation energy, critical tube diameter, and detonability limits. The critical tube diameter d_c, is the minimum diameter which will permit a steady planar detonation wave to propagate into an open volume (i.e., become a spherically expanding wave). The solid curve in Fig. 9 shows the critical tube diameter as a function of hydrogen concentration (in air) calculated by the empirical equation, $d_c = 13\ \lambda$; the specific points refer to direct measurements of d_c. A similar curve can be drawn where the ordinate is the critical energy for direct initiation of a detonation. Hence, Fig. 9 relates detonability limits to geometry, size, and the relative concentrations of the gases. Figure 10 is a direct plot of detonation cell width, λ, as a function of the relative fractions of hydrogen and air, and including additions of carbon dioxide gas. This curve can agai be employed to indicate detonability limits. As the concentrations move away from stoichiometric conditions (29.6% hydrogen in air), the establishment of steady propagating detonation waves require larger volumes; i.e., λ, and also d_c, become larger, indicating that the mixture is becoming less detonable. Similarly, the addition of carbon dioxide also reduces the detonability of the mixture. Figure 11 pictorially represents our current thinking concerning the relationships between geometry, size, and concentration and the possibility of a sustained propagating detonation wave. For cylindrical tubes, detonations can propagate if the tube diameter exceeds about

1/2 λ; a cloud should be about 1.5-5 λ in height above a surface (one degree of confinement) for propagation to occur; and finally, a spherical detonation (zero degrees of confinement) should be possible for a cloud of diameter 6.5 λ or larger. It should be emphasized that these results are tentative, and further work is clearly required to increase our confidence in the results.

U-shaped curves such as Fig. 10, but with the CO_2 additions replaced by steam, would also be valuable for reactor accident analyses. We plan t[illegible]uct these experiments (i.e., measure λ as a function of th[illegible]tive concentrations of hydrogen, air and steam) in t[illegible]S 1.5' x 42' tube in FY83.

We expect these results to be very valuable to reactor analysts and plant designers. For example, if one wishes to rule out the possibility of a detonation occurring within a particular duct, and then exiting into a large open volume, he needs only to know the duct dimensions and a conservative estimate of the local hydrogen concentrations. If the duct height is less than about 1/2 λ, a detonation probably could not develop in the duct; if the duct height is less than about 3-13 λ at its exit, then even a propagating detonation wave would be quenched in the larger room. Hence, important questions such as these can be answered without considering the more complex phenomenological questions dealing with transition to detonation. All these results will be discussed in more detail in Sessions V and VI.

E. Accelerated Flames

E-1. Code Development and Applications

There is an intermediate form of combustion between slow deflagrations and classical C-J detonations that is sometimes called accelerated flames. Flame speeds in the laboratory coordinate system are vastly greater than the laminar burning velocities, but can still be well below the C-J conditions. These flames are of interest in reactor accident analysis since they can lead to pressures and temperatures in excess of the adiabatic, isochoric combustion predictions for equivalent concentrations. There is also the possibility that an accelerated flame can become a "strong" jet ignition source capable of direct initiation of a detonation in a neighboring region. In contrast to the low probability of detonations, the existence of some degree of flame acceleration during a combustion event in a hypothetical accident is probably quite likely. The modelling of these flames is an extremely difficult, ambitious, and perhaps impossible task. The NRC effort is directed at providing NRR with some means of estimating the probability of the occurrence of flame acceleration

under given accident conditions, and the anticipated mechanical and thermal loads. Two approaches are being pursued. One is to modify an existing two-dimensional vortex dynamics code at SNLL to account for gas motion ahead of the flame, and the effects of obstacles. The other approach is to employ simple 1-D flame co and empirical correlations to explain the experimental results and extrapolate those results to reactor environments. We do not expect either of these approaches to definitively explain flame acceleration phenomena; but we do, however, expect them to be useful in making informed licensing decisions.

E-2. Experimental Programs

An extensive experimental investigation of flame acceleration has been underway at McGill University for many years, primarily studying various hydrocarbons. The NRC is supporting part of this effort, which is aimed specifically at reactor accident simulations using hydrogen. The small-scale experimental effort at McGill is strongly coupled to the larger-scale program at SNLA, where the FLAME (Flame Acceleration Measurements and Experiments) facility is being built. This experimental program has already produced a significant body of data with important applications to reactor safety. It now appears that hydrogen is very sensitive to flame acceleration (as is acetylene). Significant flame acceleration (flame speeds on the order of hundreds of m/s) has been observed in hydrogen:air mixtures as lean as 10% H_2. The degree of acceleration depends strongly on tube geometry and size, obstacle nature and blockage ratio, and gas concentrations. Recent data have also shown an extreme sensitivity to the degree of confinement along a channel (note that the downstream end of the channel is always fully open); e.g., vent areas representing about 10% of the top face of the channel can lead to order-of-magnitude reductions in flame speed. If this strong dependency on venting persists in the large-scale tests in FLAME, it would indicate that flame acceleration in large channels (e.g., the ice condenser upper plenum) could be significantly moderated by partial venting.

Experiments to date indicate that the mechanisms governing flame acceleration may represent a precarious balance of positive and negative factors associated with flame folding and turbulence. Two positive factors that lead to an increase in burning rate are the increase in flame area due to folding, and the increase in the local burning velocity of the folds due to higher turbulent diffusivities associated with fine-scale turbulence; the increase in flame areas is a result of the gas flow ahead of the flame being greatly perturbed by the presence of obstacles. In the absence of negative factors, the volumetric burning rate would continue to increase until a transition to detonation occurred.

The negative factors that lead to a decrease in the burning rate are reaction quenching due to excessive flame stretching, and rapid cooling due to turbulent mixing. If the negative factors are strong enough, the flame could be quenched; if they are of intermediate strength, then a steady, strong flame can be produced which does not undergo transition; if the factors are sufficiently weak, then transition to detonation may take place.

This particular approach can be extended to the more general problem of intercompartmental transmission of flames. Considering accelerated flames to be a subclass of deflagrations, there are six possible modes of transmission. The upstream (or donor) compartment can be either in the deflagration or detonation mode; the downstream (receiver) compartment can be in either the deflagration or detonation modes, or the flame could be extinguished. Research on these questions is also being actively pursued. The flame acceleration work being supported by the NRC program is discussed in more detail by the researchers themselves in Session VI.

F. Hydrogen Combustion Mitigation and Control

Many operating plants already have hydrogen mitigation and control systems in place (e.g., recombiners, sprays, deliberate ignition systems); some are contemplating the deployment of new schemes. The NRC will need to develop the capability to assess these schemes for licensing purposes. Consequently, a major task of the research effort includes the evaluation of proposed equipment, concepts and operational schemes to prevent or mitigate the effects of hydrogen combustion during LWR accidents. One of the first accomplishments in this area was the analysis of three mitigation schemes being considered for the Sequoyah nuclear power plant: deliberate ignition, water fogging, and post-accident inerting with Halon. The results of this study were published in NUREG/CR-1762. The Grand Gulf hydrogen igniter system was also reviewed in a study funded by NRR; the results were documented in NUREG/CR-2530. Laboratory experiments were conducted on water fogs and foams, as discussed earlier in Section III. C.2.

All the analytical and experimental facilities described previously are available for mitigation research. The candidate schemes with the highest potential (as currently perceived) are being studied now; these include deliberate ignition; deliberate flaring; the addition of diluents (water fogs and foams) in combination with deliberate ignition; and (partial or total) pre-and post-accident inerting. More advanced schemes will be addressed in the later stages of the research, if that proves to be necessary.

G. Equipment Survivability

Current research may show that some reactor containments are strong enough to survive hydrogen combustion events without failing. However, it still is necessary to show that important safety equipment will not only survive, but will continue to perform their intended function, in order to bring the plant to a safe shutdown condition after an accident and maintain it in that condition. It is reasonable to assume that the primary threat to equipment during deflagration is thermal overloading. If significant flame accelerations occur, or transitions to detonations, then mechanical loads may be of concern. The basic elements of the hydrogen research program are being utilized to predict the range of pressure and temperature environments that might occur during reactor accidents. These combustion environments are then used in the Hydrogen Burn Survival (HBS) program to experimentally and analytically assess the effects of hydrogen combustion on equipment. Our primary goal is to develop a method the NRC can use to evaluate licensee submittals regarding the survivability of safety-related equipment. We expect to accomplish a major part of this goal (dealing with deflagration-produced loads) by the end of FY83.

The current program on hydrogen burn survivability is a cooperative effort between the Offices of Research and Reactor Regulation; RES sponsors the experiments and NRR the analyses. The program is phased in two parts: (1) to provide information to NRR in the short-term on the effects of hydrogen combustion on equipment for near-term licensing decisions and (2) to develop reliable methods to predict the response of equipment to the temperature and pressure environments produced during multiple hydrogen deflagrations. The need to investigate hydrogen detonations is also being considered. The program has already combined an early version of the HECTR code with a standard heat transfer code to calculate thermal responses to single burns. In addition, heat flux gages, simulated equipment surfaces, and some actual pieces of equipment have been subjected to single burn environments in the experimental facilities at SNLA. A report (NUREG/CR-2730) has been issued based on preliminary tests and analyses; it concludes that the hydrogen burn environment may pose a threat to some components.

Future efforts include additional burn tests in the FITS facility as well as large scale simulation tests planned for the Radiant Heat Facility and the Solar Thermal Test Tower. These facilities would be used to perform scoping tests on actual components in simulated full-scale hydrogen burn environments. The purpose of these tests would be to identify potential failure modes, if any. In addition, the analyses will be extended to include the effects of multiple burns. Details of this program are discussed in Session VIII.

G. Combustible Gas in Containment

As indicated earlier, the objective of this program is to determine the rates and quantities of hydrogen that could be generated by corrosion of coatings in containments, and to determine the nature and quantity of the debris resulting from the corrosion process. Preliminary estimates of hydrogen generation were made in NUREG/CR-1561. Zinc inventories in some PWR and BWR plants were gathered and published in NUREG/CR-2021. The first test series addressed the rate of hydrogen production from galvanized steel samples immersed in solutions with varying properties; viz.; temperature, pH and boric acid concentration. These results have been published in NUREG/CR-2812. Research on this program will continue to address the effects of other initial conditions of hydrogen production (e.g., spraying of solution versus immersion); debris will be collected and studied. The status of this work is discussed in Session III.

H. Transport Code Development and Applications

A major task of the Code Assessment and Applications program (A-1205) is to assess various existing codes for applications to hydrogen transport and mixing problems. Three laboratories are currently involved in this effort. Los Alamos National Laboratory is evaluating the HMS code; Battelle Pacific Northwest Laboratories is using the COBRA code; and Sandia National Laboratories is evaluating the GRS code, RALOC, developed by H. Jahn. The EPRI-sponsored tests at Hanford Engineering and Development Laboratories are being used as a benchmark problem for code comparisons. We expect to evaluate these programs in the near term, and focus on the one or two most promising paths. The transport and mixing of hydrogen is an important question relating to the extent and duration of concentration gradients that could develop during reactor accidents. These gradients could strongly influence the potential for accelerated flames or detonations. The current codes, however, are not intended to model combustion. They are therefore limited in their capability to analyze accidents in which deliberate ignition is available. For those accidents, the combustion event itself will play an important role in subsequent convective mixing, as well as determining the relative concentrations of hydrogen, oxygen, and other gases available for subsequent combustion. Session IV will provide information on the latest results from the transport and mixing studies.

IV. CONCLUSIONS

It is clear from the preceding discussion that the current research program has already produced results of significant value to reactor safety analyses. Several other programs supported by

the Office of Research are also contributing to the resolution of hydrogen related questions. The Molten Core-Concrete Interactions program (A-1019) and the Core Melt Technology program (A-1218) will provide information on the production of combustible gases (carbon monoxide and hydrogen) due to core-concrete interactions (Session III). The Molten Core-Coolant Interactions program (A-1030) can provide information on the amounts and rates of hydrogen generated by the explosive and nonexplosive interactions of molten metals and water.

There are also several research programs that will use the codes and experimental data generated by the hydrogen programs. The Safety Margins for Containment program (A-1219) will use the predictions for mechanical loads resulting from combustion. The Containment Analysis (A-1198), MELCOR (A-1339), and SASA (A-1258) programs will all use the models and codes developed for hydrogen behavior analyses.

In the short time that the hydrogen research programs have been in place, we have already advanced our understanding of many hydrogen-related phenomena pertinent to reactor safety questions. We are quite optimistic that the ultimate result of these research efforts will be the resolution of hydrogen-related issues to the satisfaction of the NRC and most other affected parties, including the utilities, the industry and the general public.

TABLE I. HYDROGEN BEHAVIOR PROGRAM:
ACCOMPLISHMENTS THROUGH FY81

- COMPENDIUM PUBLISHED.
- HYDROGEN DETECTOR DRAFT REPORT RELEASED.
- HYDROGEN WORKSHOP HELD, PROCEEDINGS PUBLISHED.
- SEQUOYAH MITIGATION STUDY COMPLETED, REPORT PUBLISHED.
- GRAND GULF MITIGATION STUDY INITIATED.
- COMPREHENSIVE PROGRAM PLAN DEVELOPED.
- ACCIDENT ANALYSES FOR VARIOUS LWR CONTAINMENTS INITIATED.
- DEFLAGRATION, DETONATION, HEAT TRANSFER CODES DEVELOPED.
- RALOC CODE OBTAINED, EVALUATION BEGUN.
- CSQ DETONATION CALCULATIONS FOR ZION AND SEQUOYAH.
- WORK INITIATED ON HYDROGEN EMERGENCY MANUAL.
- EXPERIMENTAL TEST PLAN DEVELOPED, PRESENTED, APPROVED.
- LABORATORY EXPERIMENTS INITIATED ON FOGS AND FOAMS.
- VGES 16'-TANK TS #1 THROUGH 8 COMPLETED.
- H_2:STEAM JET FACILITY TO BE DESIGNED AND CONSTRUCTED.
- FITS TANK TO BE MODIFIED.
- EXPERIMENTS ON ACCELERATED FLAMES AND DETONATIONS INITIATED AT McGILL UNIVERSITY.

TABLE II

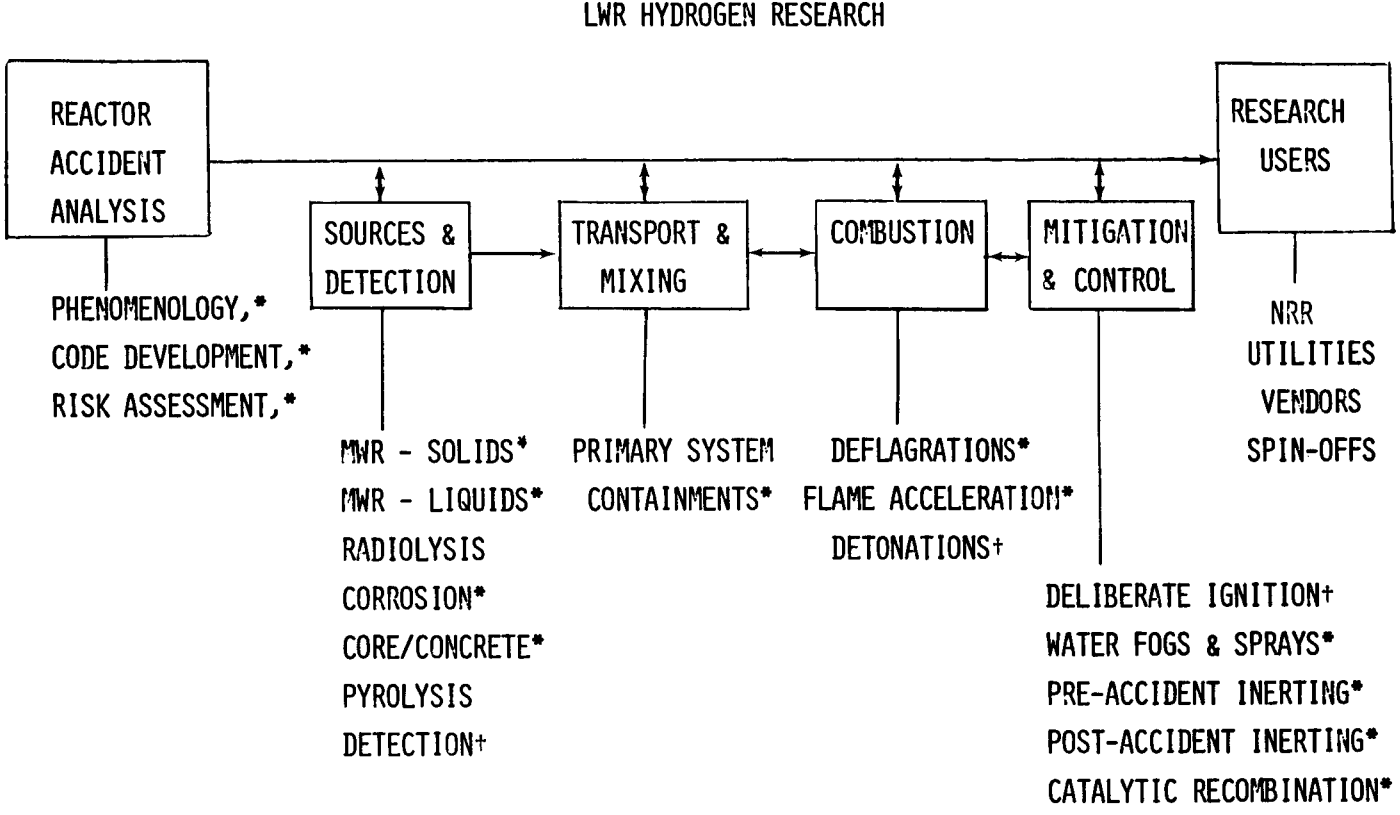
HYDROGEN BEHAVIOR PROGRAM

ACCOMPLISHMENTS THROUGH FY82

- CSQ REPORT ON ZION/SEQUOYAH PUBLISHED.
- PERFORM CSQ DETONATION CALCULATIONS FOR GRAND GULF
- HYDROGEN DETECTOR REPORT PUBLISHED.
- COMPLETE ACCIDENT ANALYSES WITH MARCH.
- COMPLETE DEFLAGRATION CODE (HECTR-MOD1).
- COMPLETE RALOC CODE ASSESSMENT AND PUBLISH REPORT.
- PREPARE MANUAL ON HYDROGEN BEHAVIOR DURING LWR ACCIDENTS.
- PLAN SECOND INTERNATIONAL WORKSHOP ON HYDROGEN (OCTOBER 3-7, 1982).
- INITIATE EFFORT AIMED AT MODELLING ACCELERATED FLAMES.
- COMPLETE MODIFICATION OF FITS FACILITY AND PERFORM TESTS ON DEFLAGRATIONS AND DETONATIONS IN TERNARY MIXTURES OF HYDROGEN:AIR:STEAM.
- COMPLETE CONSTRUCTION OF STEAM:HYDROGEN JET FACILITY AND PERFORM TESTS ON AUTOIGNITION (AND INTENTIONAL FLARING UNDER A-1336).
- DRAFT REPORT ON EXPERIMENTS IN VGES 16'-TANK.
- CONTINUE EXPERIMENTS IN VGES 16'-TANK (MITIGATION, FLAME ACCELERATION, DETONATION).

TABLE II CONTINUED

- BEGIN CONSTRUCTION OF FLAME ACCELERATION FACILITY.
- CONTINUE EXPERIMENTS ON FLAME ACCELERATION AND DETONATION AT McGILL UNIVERSITY.
- DRAFT REPORT ON H_2 GENERATION FROM CORROSION OF ZINC.
- PUBLISH REPORT ON PRELIMINARY RESULTS ON EQUIPMENT SURVIVABILITY.
- PUBLISH REPORTS ON WATER FOG AND WATER FOAM STUDIES.
- COMPLETE PHASE 1 OF GRAND GULF STUDY AND PUBLISH REPORT.



*ADDRESSED BY NRC HYDROGEN OR OTHER RELATED PROGRAMS

+SUBTASK COMPLETED OR MAJOR MILESTONE ACHIEVED.

FIGURE 1

NRC/RES HYDROGEN PROGRAMS

PRIME CONTRACTOR: SANDIA NATIONAL LABORATORIES/
ALBUQUERQUE, NM (SNLA) AND
LIVERMORE, CA (SNLL)

MAJOR SUBCONTRACTORS:
- SWACER, INC./McGILL UNIVERSITY
- GENERAL PHYSICS CORP., COLUMBIA, MD
- PROTEUS CORP., ALBUQUERQUE, NM
- DIKEWOOD CORP., ALBUQUERQUE, NM
- TECHNADYNE CONSULTANTS, ALBUQUERQUE, NM
- M. L. CORRADINI, UNIVERSITY OF WISCONSIN
- C. RICHARDS, ATMOSPHERIC PHYSICS, INC. SAN DIEGO, CA.
- KTECH CORP., ALBUQUERQUE, NM

LOS ALAMOS NATIONAL LABORATORIES AND BATTELLE PACIFIC NORTHWEST LABORATORIES ALSO PARTICIPATE IN TRANSPORT CODE ASSESSMENT PROGRAM.

FIGURE 2. PROGRAM CONTRACTORS

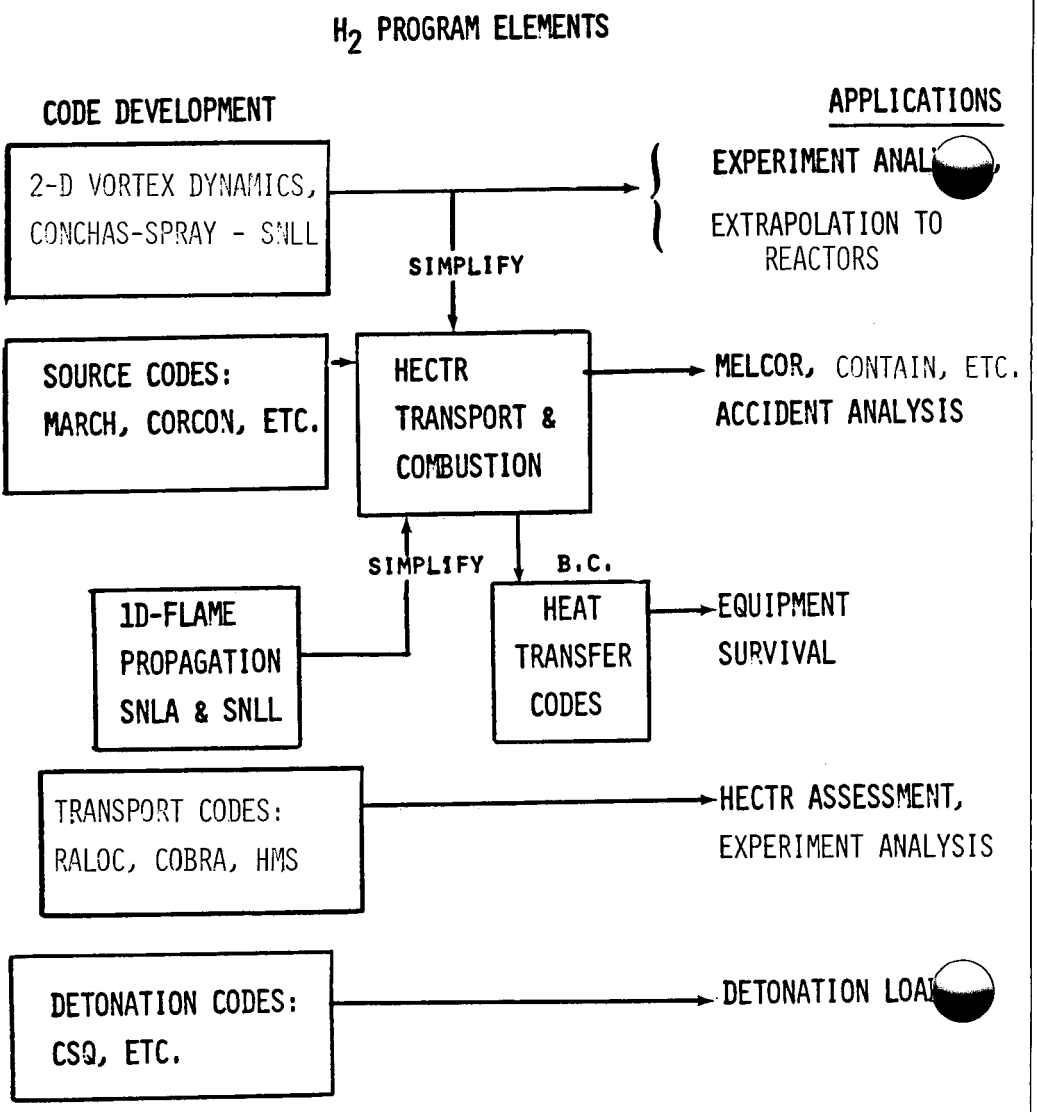


FIGURE 3. CODE DEVELOPMENT AND APPLICATIONS

EXPERIMENTAL PROGRAM FACILITIES

OPERATIONAL:

- LABORATORY-SCALE (FOG & FOAM)
- VGES 16-FT TANK
- McGILL TESTS
- FITS TANK
- STEAM:HYDROGEN JET
- VGES PLASTIC BAG DETONATIONS

OPERATIONAL IN FY83:

- VGES ACCELERATED FLAME FACILITY, "FLAME"
- VGES 18" STEAM:HYDROGEN DETONATION TUBE

PLANNED ACCORDING TO NEED:

- CHARGED DROPLET APPARATUS

FIGURE 4

H_2 PROGRAM ELEMENTS

DEFLAGRATION EXPERIMENTS

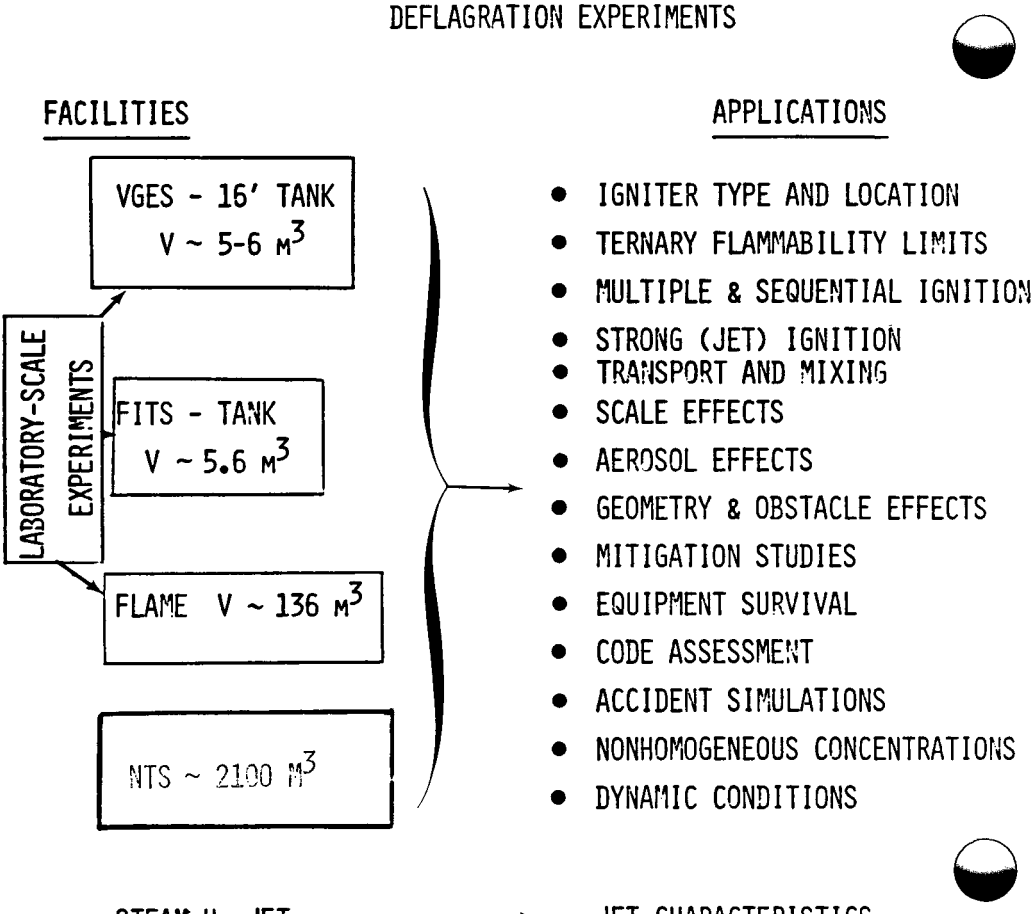


FIGURE 5

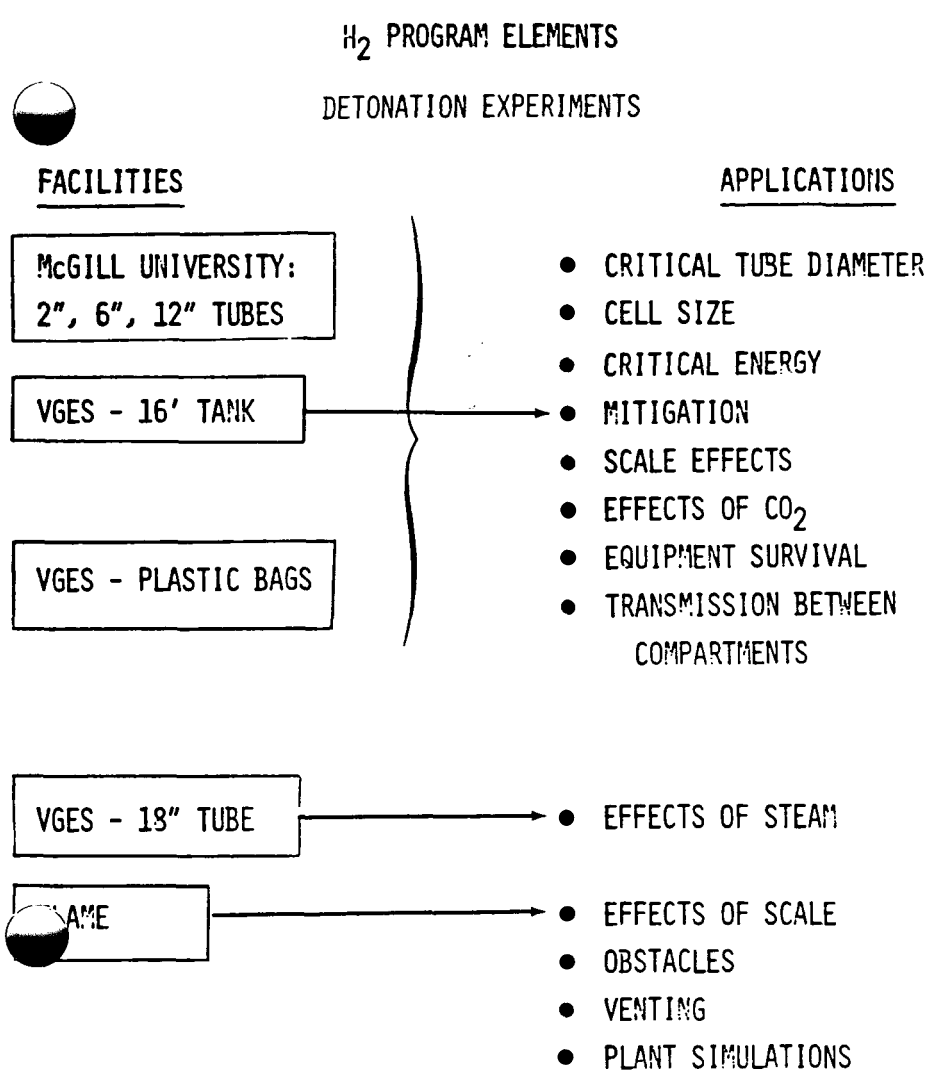

H_2 PROGRAM ELEMENTS
DETONATION EXPERIMENTS
FACILITIES
APPLICATIONS
McGILL UNIVERSITY:
2", 6", 12" TUBES
VGES - 16' TANK
VGES - PLASTIC BAGS
CRITICAL TUBE DIAMETER
CELL SIZE
CRITICAL ENERGY
MITIGATION
SCALE EFFECTS
EFFECTS OF CO_2
EQUIPMENT SURVIVAL
TRANSMISSION BETWEEN COMPARTMENTS
VGES - 18" TUBE
EFFECTS OF STEAM
AME
EFFECTS OF SCALE
OBSTACLES
VENTING
PLANT SIMULATIONS

FIGURE 6

H_2 PROGRAM ELEMENTS

ACCELERATED FLAME EXPERIMENTS

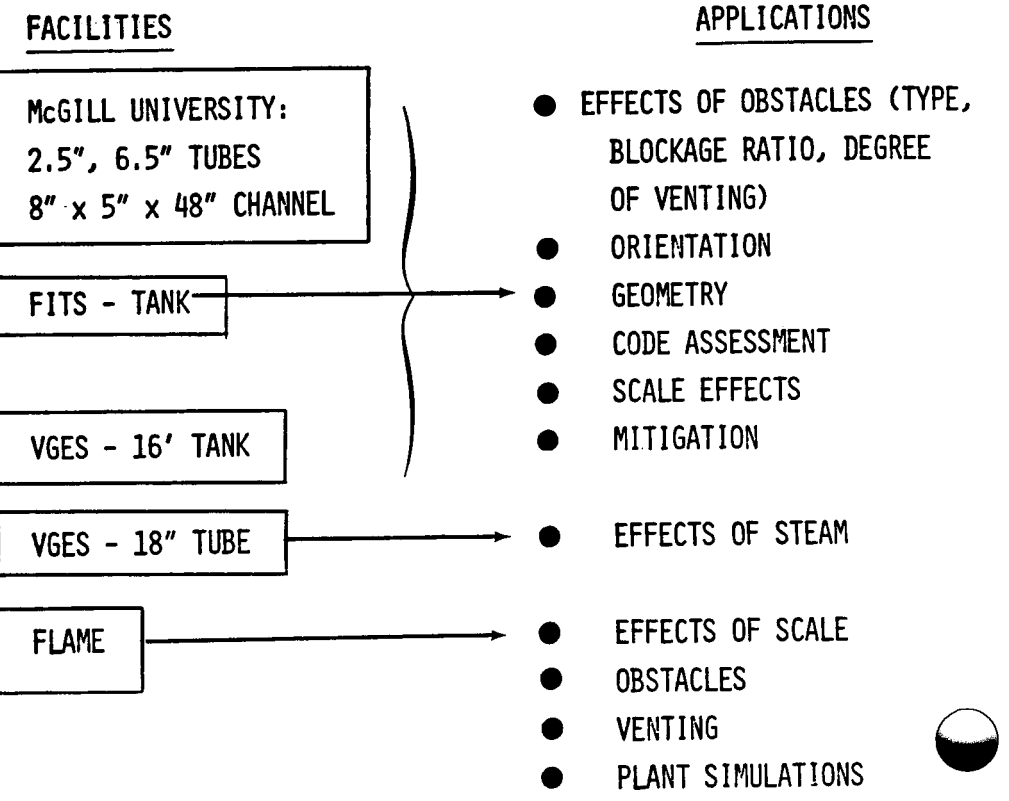


FIGURE 7

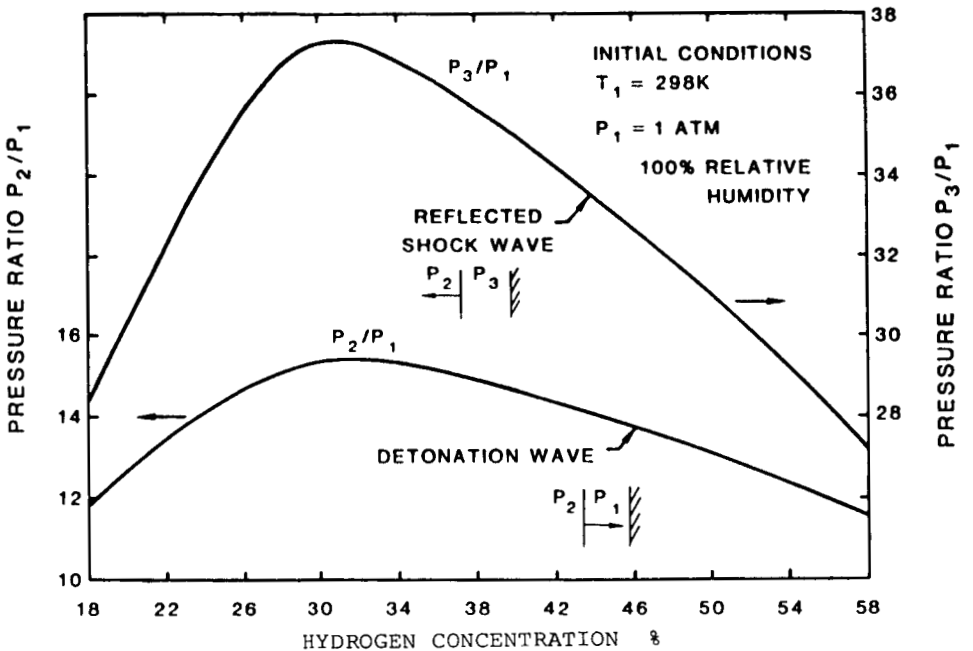


FIGURE 8. THEORETICAL DETONATION PROPERTIES

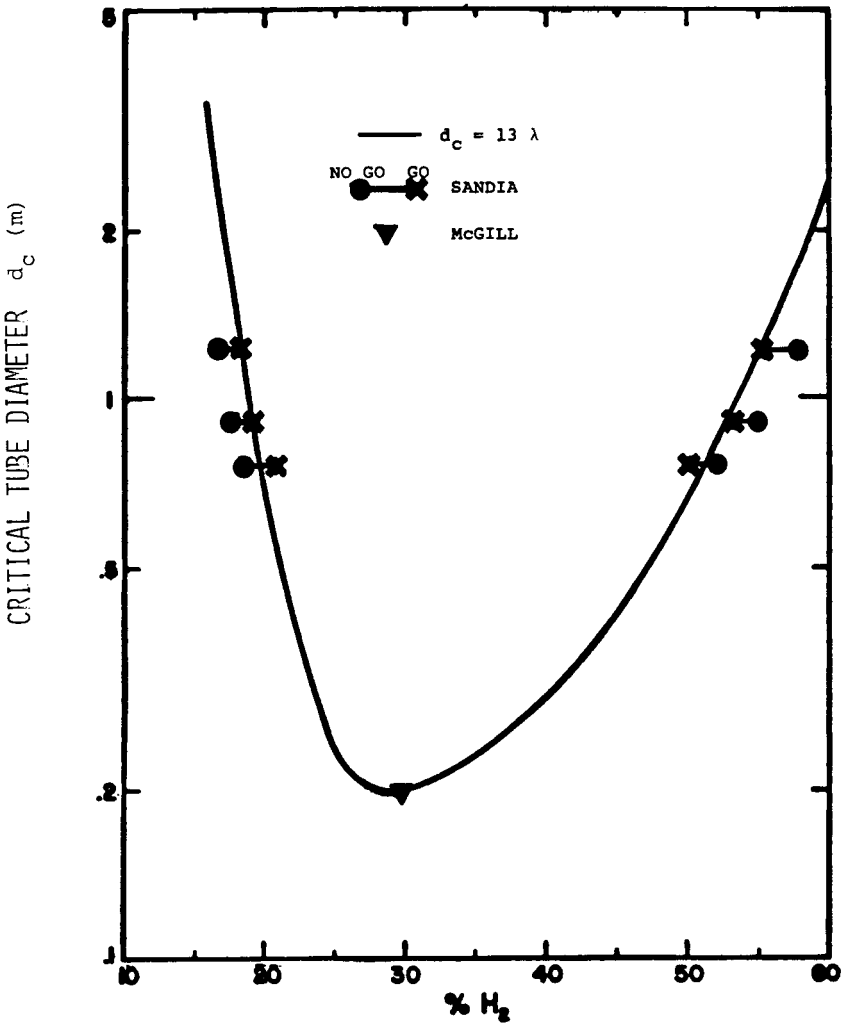


FIGURE 9. MEASUREMENTS OF THE CRITICAL-TUBE-DIAMETER AT SANDIA AND McGILL COMPARED TO THE 13 λ CORRELATION (BASED ON λ MEASUREMENTS AT McGILL).

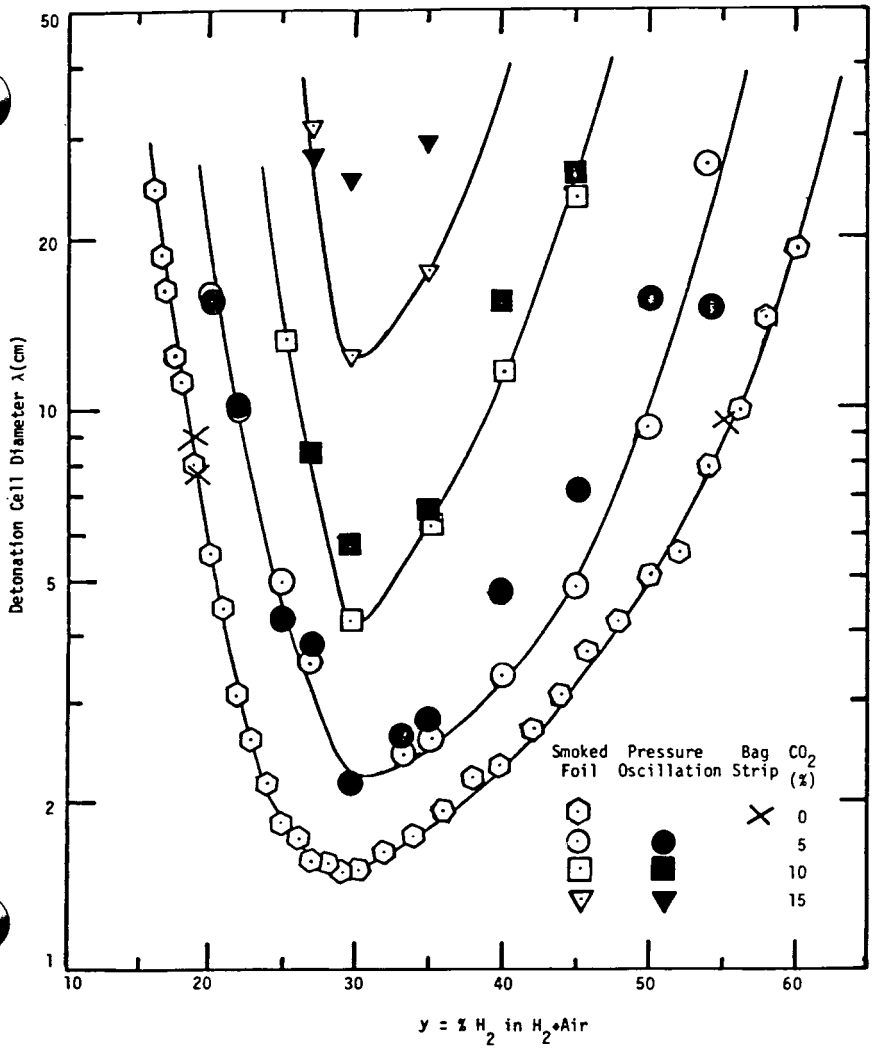
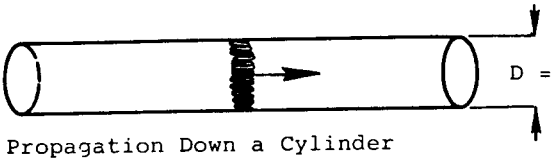
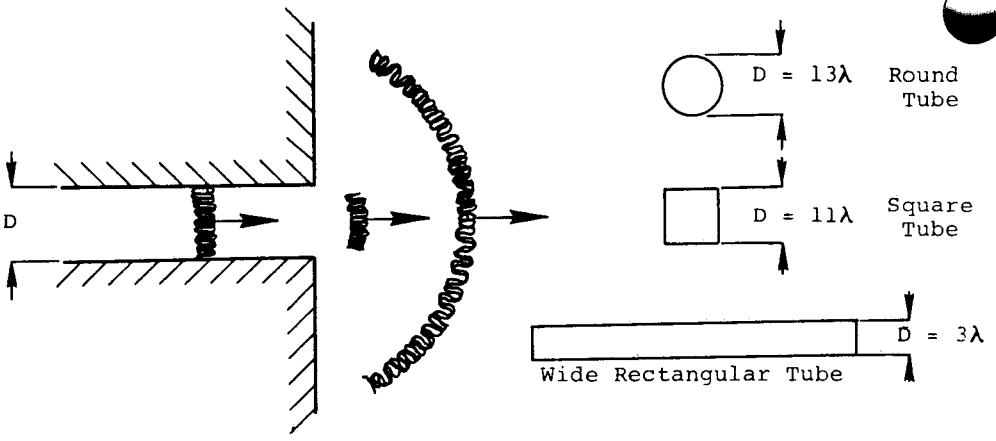


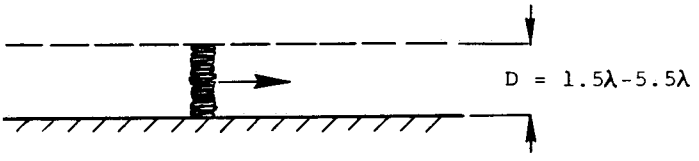
FIGURE 10. λ VERSUS H_2 AND CO_2 CONCENTRATIONS.



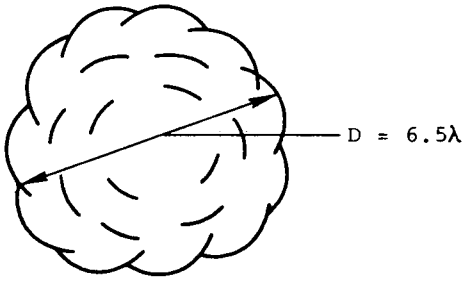
Propagation Down a Cylinder



Propagation from a Tube into a Large Open Space
"Critical Tube Diameter"



Minimum Cloud Thickness for Propagation Confined on Any One Side



Minimum Diameter for Propagation of Unconfined Detonation

Figure 11. Minimum Dimensions for Propagation of Detonations

IDCOR APPROACH TO HYDROGEN GENERATION, COMBUSTION, AND BURN CONTROL

By

E. L. Fuller and E. P. Stroupe

Technology for Energy Corporation
One Energy Center, Pellissippi Parkway
Knoxville, Tennessee 37922
September 1982

DISCLAIMER

This report was prepared as an account of work sponsored by the IDCOR Policy Group through the Atomic Industrial Forum. Neither the Policy Group, the Atomic Industrial Forum, nor any of its employees, makes any warranty, expressed or implied, or assumes legal liability or responsibility for the accuracy, completeness, or usefulness of any information, apparatus, product, or process disclosed, or represents that its use would not infringe on privately-owned rights.

The opinions, conclusions, and recommendations set forth in this report are those of its authors and do not necessarily represent the views of the Atomic Industrial Forum, Inc., its members, or its consultants.

ABSTRACT

The IDCOR Program is developing the appropriate information and methodology to predict the following phenomena during severe accidents:

1. hydrogen generation, both in-vessel and ex-vessel, primarily from metal-water reactions,
2. hydrogen distribution in reactor containments, and
3. potential hazards of overpressurization or combustion of hydrogen.

The information is being assembled into reports describing the phenomenology and incorporated into the IDCOR Modular Accident Analysis Program (MAAP), in order to determine the behavior of hydrogen during accident sequences in four reference plants. From these analyses, conditions will be determined so that hydrogen burn control measures can be evaluated.

A review is being made of various approaches for suppression of combustion or controlled burning to limit hydrogen to concentrations below the detonation range. The review considers the advantages and disadvantages of various hydrogen control systems concepts for reactor and containment combinations and, in addition, addresses the various concepts for eventual removal of hydrogen from containment.

INTRODUCTION

In order to properly assess containment effectiveness and the potential for equipment survivability during severe accidents, it is necessary to properly understand phenomenological behavior, both in-vessel and ex-vessel, and integrate this understanding into models for carrying out realistic analyses of temperature, pressure, and fission product loads on containment from a spectrum of dominant accident sequences. These loads must then be compared with the capabilities of the containment, and with the equipment within containment that will be required to function during such accidents. In this context, a proper understanding of the phenomenology associated with hydrogen generation, distribution, and combustion will enable sound strategies for managing and controlling the accidents to be developed. The various hydrogen burn control measures that have been implemented or proposed can then be evaluated properly, and appropriate recommendations can be made for the various containment types.

This procedure is being followed in the IDCOR Program for four "reference" plants, namely, Zion, Sequoyah, Peach Bottom, and Grand Gulf. The phenomenology is being studied in IDCOR Task 12, the models are being integrated for analysis into the Modular Accident Analysis Program (MAAP)[1] in IDCOR Task 16, the integrated analyses of the dominant sequences are being carried out in Task 23, hydrogen burn control measures are being reviewed in IDCOR Task 13, and equipment survivability is being assessed in IDCOR Task 17.

The remainder of this paper will outline in more detail the approach taken by IDCOR toward hydrogen generation, distribution, combustion, and burn control. Both the phenomenology and burn control evaluations will be discussed in the contexts of plant design detail, and expected behavior during the accident sequences.

HYDROGEN GENERATION

In severe accidents, hydrogen could be generated either in-vessel or ex-vessel (in the case of meltdown and vessel failure). The principal source of hydrogen generation in-vessel would be from high-temperature oxidation of Zircaloy in the core. Once oxidation begins, the upper core region is exposed to a mixture of hydrogen and steam. IDCOR is utilizing models describing such conditions in conjunction with models describing core heatup and fuel melting. These models, developed by Fauske and Associates (FAI) and the Electric Power Research Institute (EPRI) for IDCOR, both for PWR and BWR cores, are integrated into MAAP. They are experimentally based, and are in the Cathcart-Pawel[1] formulation below 1600°C, and in the Baker-Just[2] formulation above 1600°C, with proper accounting of hydrogen-steam mixture conditions. Consistent application of these models during the core uncovery and heatup phases enables accurate estimations of heatup from Zircaloy oxidation, meltdown rates, rates and amounts of hydrogen generation, and fission product release rates from fuel to be made. The hydrogen produced is then carried to release points from the primary system, such as break locations or relief valves, and released to containment. In addition, some of the hydrogen remains within the primary system subsequent to core melt, and is available for release upon vessel failure. If blowdown is rapid upon vessel failure, such as in small-break LOCAs or transients, this hydrogen can be rapidly released to the containment. MAAP is currently being used to calculate this behavior for dominant accident sequences in the four reference plants. Preliminary results indicate similar rates and amounts of hydrogen generation are predicted during this phase to previous evaluations.[4,5]

In addition to treating hydrogen generated during the initial core uncovery and heatup process, additional hydrogen generated in-core as a result of water addition prior to core melting (such as at TMI-2) is also determined. Such water can be added as a result of operator action to implement upper head injection, hot-leg injection, core sprays, etc., and such actions can augment the hydrogen generated. Analysis of sequences in which partially damaged cores are recovered is possible with MAAP, and is a very important activity in the IDCOR Program. From these analyses, realistic association of hydrogen release rates with the degree of core damage will be made, so as to enable rational rules on hydrogen control to be implemented.

Hydrogen production in the lower vessel head from metal-water reactions is also determined. In this phase, however, mechanistic treatments incorporated into MAAP, considering both fragmentation models[6] and design details in the lower head, show that very little additional hydrogen can be generated prior to vessel failure. This is in contrast to previous, non-mechanistic calculations using MARCH[7] that lead to gross overestimation of hydrogen production via core melt-water interactions.

Preliminary MAAP evaluations for the reference plants also show that ex-vessel hydrogen generation will be very small, provided that water is continually available to first quench, and then maintain, the coolability of the core debris, thus minimizing concrete attack. It has been found that the availability of water is both design and sequence dependent. For those cases where the core debris is released from the reactor

pressure vessel and water is not available to the debris, thermal attack of the concrete would ensue, the concrete would decompose, and water would be liberated. As long as the debris stays molten, the steam released would penetrate the upper melt stratum, oxidize unreacted zirconium and steel in the molten mixture in a very efficient manner, and thus form significant quantities of hydrogen. The concrete attack model in MAAP accurately determines the rate and amount of hydrogen produced in this manner, as a function of the amount of water available for cooling the debris, the temperature of the melt, and the available surface area between the melt and the concrete as concrete attack continues.

HYDROGEN DISTRIBUTION

Under severe accident conditions, hydrogen will enter the containment atmosphere as a buoyant, turbulent jet or plume. The degree to which hydrogen becomes mixed within the containment atmosphere is important because it can affect the design of control methods, such as the placement of igniters, and the effect of a hydrogen burn on structures and equipment.

Several processes may act to mix the hydrogen and limit the extent of stratification: gas motion due to momentum of the H_2-steam jet, forced convection due to the operation of blowers and sprays, natural convection arising from temperature gradients and nonhomogeneous fluids, and molecular diffusion.

The modeling of hydrogen mixing in a containment atmosphere has proceeded along several lines. On the one end is the empirical approach wherein experimental data obtained from scale models are applied to full-scale plants using similarity parameters. At the other end are numerical solutions to the differential equations of fluid flow. The experimental results of ongoing programs, particularly those of EPRI at Hanford Engineering Development Laboratory (HEDL), are being compared to various predictive methods for IDCOR by EPRI, so as to enable the regions of applicability of each method to be better identified.

These recent experimental data are encouraging, in that they demonstrate that jet mixing and natural convection are effective mechanisims for mixing hydrogen exiting into a containment volume. On this basis,

hydrogen is currently assumed to be perfectly mixed within the compartment that it is released to for purposes of analysis with MAAP. In addition, transfer of hydrogen to other compartments is based upon conservation of mass and energy considerations, and computing the gas flow rate through a given area. More sophisticated modeling will be incorporated when recommended by EPRI.

HYDROGEN COMBUSTION

Hydrogen which mixes with air in the containment atmosphere may react with oxygen, forming water and liberating energy. The characteristics of hydrogen combustion depend strongly on the hydrogen concentration and other conditions. Key aspects of hydrogen burns are addressed by IDCOR, based upon the work carried out by EPRI. These aspects include: flammability limits, including the effects of temperature, pressure, inert diluents, turbulence, and suspended particles and drops; ignition, including spontaneous ignition, ignition by electric sparks and by hot surfaces; deflagrations; transition from deflagration to detonation; diffusion flames; and containment response. In this regard, it is assessed that detonations are not realistic events in reactor containments.

At present, MAAP models hydrogen combustion with a simple flame temperature criterion, and burning is assumed to be complete, thus predicting a conservatively high pressure rise. More sophisticated modeling, based upon models developed from work currently in progress, will be incorporated soon. The modeling that will be adopted will be that which EPRI recommends, based upon an ongoing review of hydrogen combustion computer models applicable to building burn scenarios.

The computer codes and models being surveyed differ considerably in degree of rigor and sophistication. They include: empirical deflagration models, such as those appearing in MARCH, CLASIX,[8] and HECTR,[9] phenomenological deflagration models based upon simulations of flame front propagation, such as the complete and incomplete combustion

models, being developed by Factory Mutual Research Corporation (FMRC) and detailed hydrodynamic and chemistry models. Based on this review, IDCOR has decided to incorporate the FMRC phenomenological models into MAAP.

HYDROGEN CONTROL

Once hydrogen has been released to the containment, it can be controlled to prevent hydrogen-caused containment failure from being a dominant risk contributor. If not controlled, hydrogen or other combustibles may threaten containment integrity by overpressurization due to (1) buildup of noncondensable gases, (2) large amounts of hydrogen burned without removing the resulting energy, or (3) a pressure wave resulting from detonation. IDCOR Task 13 is evaluating various means of controlling hydrogen to minimize the risk to the containment. This task is being performed by Acurex Corporation, Factory Mutual Research Corporation, Mollerus Engineering, and S. Levy, Inc. The work scope of this task is to critically review existing studies to determine the advantages and disadvantages of various hydrogen control system concepts. Independent engineering studies and calculations are limited to scoping analyses required to determine the merits of a particular concept. The final report is under preparation.

The hydrogen control concepts under evaluation are...

1. Preinerting with nitrogen.
2. Postinerting with carbon dioxide.
3. Postinerting with Halon 1301.
4. Postinerting with water fog.
5. Postinerting with distributed torches burning a fuel.
6. Postinerting with gas turbines.
7. Atmospheric preconditioning (partial preinerting) with postinerting.

8. Hydrogen getters or catalytic removal of hydrogen.

9. Distributed ignitors.

10. Distributed ignitors with water fog or foam.

11. Catalytic burners inside or outside the containment.

12. Primary system bleed to burners inside or outside the containment.

The parameters chosen for evaluating the merits of hydrogen control systems are

State of the art. State of the art is determined by the extent and type of testing required prior to application of a system in a nuclear power plant.

Intrinsic interaction. These are the characteristics that have the potential to adversely affect plant personnel and public safety, normal operations, and plant response to abnormal events. Specific examples are toxicity, pathogenic properties, effect on containment temperature and pressure, chemical activity, and disposal difficulty.

Initiation logic. The decision processes required to initiate the system are being evaluated for ambiguities, availability of adequate time, and for such inhibiting factors as the severity of the consequence of an erroneous initiation of the system. The consequences of initiation may be reduction in safety; risks to personnel, the public, and the plant; or a plant shutdown.

Support and services. These parameters include instrumentation, electric power, service, air, heating and ventilating, containment sprays, and service water systems. The existence and suitability of existing systems to provide support and services when required can have a significant impact on the incremental cost of a system.

Flexibility. Flexibility refers to the capability of a hydrogen control system to mitigate a range of accidents. The range over which the evaluation extends includes the spectrum of loss of coolant accidents which may terminate in a degraded core or continue on to a full meltdown and containment basemat interaction. The evaluation also includes the potential to enhance or reduce the system's capability to mitigate consequences by such means as increasing its size or capacity.

Backfit potential. This is the system's potential for being implemented into plants which exist, are under construction, or are in the design process. Elements of this evaluation are availability of space, accessibility, schedule delay, downtime, and changes required in plant systems and structures.

Reliability. Reliability is being evaluated by studying the reliability of similar equipment and systems under comparable environmental stress.

Cost. Cost is being evaluated as indicated by the initial size, quantity of equipment and materials required, as well as by expendable materials and labor needed to maintain the system throughout its service life.

The hydrogen control systems are being evaluated by assigning four levels of acceptability to each of the parameters identified above. These acceptability measures are relatively judgmental and qualitative. They are simply high, medium, low, and unacceptable. A parameter for a given system received an unacceptable rating if that parameter made the concept clearly unsuitable for application. The high and low ratings are defined below for each of the evaluation parameters.

State of the art

High: Straightforward design application with components readily available.

Low: Design requires extrapolation of technology or one or more critical components must be developed.

Intrinsic interaction

High: Negligible adverse effects on plant personnel, public safety, normal operations, and plant response to abnormal events.

Low: Significant adverse effects on any one of the above.

Application interaction

High: Negligible interference with safety system functions, maintenance, and surveillance.

Low: Incompatible with at least one safety system function or with maintenance or surveillance.

Initiation

High: Clear, unambiguous accident parameters for initiation of the system with negligible consequences of erroneous operation on plant safety, personnel, capacity factor, and the time needed to achieve a functioning system is not critical to the control of the accident.

Low: Complex anticipatory initiation logic required for initiation or severe consequences of erroneous operation or system response time is critical to the control of the accident.

Support and service

High: Minimum requirement for monitors, power, air, water, ventilating systems, and the availability and suitability of existing systems for support, such as containment sprays.

Low: High additional power or other services required or additional ventilation or incompatibility with existing safety systems.

Flexibility

High: Capability to mitigate a wide range of accident conditions.

Low: Applicable to narrow range of specific accident conditions.

Backfit potential

High: Minimum change in plant system or structure for plants which exist or are under construction.

Low: Major changes in plant design required.

Reliability

High: Similar systems under similar operating conditions are in use and have a record of reliable performance.

Low: New design never applied or a component must be developed and proven to be reliable.

Cost

High: System with estimated relatively low costs for installation and operation.

Low: System with high relative cost, with unknown costs of design or development, or with high operating costs.

Using these evaluation parameters and ratings, preliminary results have been obtained for the candidate systems. These results will not be finalized until they have been reviewed by Technology for Energy Corporation (TEC) (the IDCOR Program Manager), the Technical Expert Review group (selected experts from industry), and by the IDCOR Steering Committee.

The preliminary results indicate that the concepts of postinerting with Halon, water fog, distributed torches, or gas turbines have at least one parameter which makes the use of the system unacceptable. Likewise, the use of "getters" or catalysts to remove hydrogen and the controlled combustion systems of catalytic burners, recombiners, and bleeding to burners were found to be unacceptable.

Preinerting with nitrogen for BWR Mark I and II containments and deliberate ignition using glow plugs for all containments were found to be acceptable. Two marginally acceptable systems were postinerting with CO_2 and atmospheric preconditioning with postinerting.

IDCOR TASKS RELATED TO HYDROGEN CONTROL

IDCOR Task 10, Containment Structural Capability, consisted of holding a workshop to study the structural capability of various containment structures. This workshop was attended by experts who have performed capability assessments for a variety of containment structures. One of the conclusions of this meeting was that a hydrogen deflagration is a static load on the containment and thus, relatively simple analysis techniques can be used.

Equipment Survivability, IDCOR Task 17, is a study of the capability of critical equipment to function during a degraded core event. Critical equipment is defined as instrumentation required to monitor the state of the core and containment and the equipment required to bring the plant to a safe stable state. This task will include a review of previous studies as well as an analysis to determine the capability of equipment and instruments to survive. The environment created by a hydrogen deflagration will be investigated along with the radiation, pressure, temperature, and aerosols present in a degraded core environment.

SUMMARY

The IDCOR Program includes several tasks directly related to the control of hydrogen. These tasks examine work done to date to assure that the necessary research is being done to achieve timely resolution of hydrogen issues.

REFERENCES

1. R. E. Henry, et al., "Analysis of Postulated Severe LWR Accidents," International Meeting on Thermal Reactor Safety, Chicago, Illinois, September 1982.

2. J. V. Cathcart, et al., "Zirconium Metal-Water Oxidation Kinetics IV. Reaction Rate Studies," ORNL/NUREG-17, August 1977.

3. L. Baker, Sr., and L. C. Just, "Studies of Metal-Water Reactions at High Temperatures III. Experimental and Theoretical Studies of the Zirconium-Water Reaction," ANL-6548, May 1962.

4. Zion Probabilistic Safety Study, Commonwealth Edison Company, 1981.

5. Steven W. Hutch, et al., "Reactor Safety Study Methodology Applications Program," Grand Gulf No. 1 BWR Power Plant, NUREG/CR-1569, SAND 80-1897, October 1981.

6. Henry & Fauske, Sun Valley paper.

7. R. O. Wooten and H. I. Avci, "MARCH (Meltdown Accident Response Characteristics) Code Description and User's Manual," NUREG/CR-1711, BMI-2064, October 1980.

8. G. M. Fuls, "The CLASIX Computer Program," Offshore Power Systems Report No. 36A31, October 1981.

9. J. B. Rivard, ed., "Interim Technical Assessment of the MARCH Code," SAND 81-1672, NUREG/CR-2285, 1981.

RESEARCH PROGRAMS IN DEVELOPMENT IN ITALY BY ENEA, PISA UNIVERSITY AND ANSALDO IMPIANTI ON THE IMPACT OF HYDROGEN ON LIGHT WATER REACTOR SAFETY

by

F. Fineschi - Pisa University
A. Morici - ENEA/DISP - Rome
R. Zinnari - A.I. - Genoa

Ansaldo Impianti - Via G. D'Annunzio, 113 - 16121 Genoa (ITALY)

ENEA - DISP - Viale Regina Margherita, 125 - 00198 Rome (ITALY)

Università di Pisa - Dipartimento Costruzioni Meccaniche Nucleari
Via Diotisalvi, 2 - 56100 Pisa (ITALY)

A B S T R A C T

This report presents the italian research activities developed and to be carried out in the next two years concerning hydrogen impact on reactor safety and design.
A short description of three experimantal facilities (HYDRO facility, PIPER-ONE loop and PEGASUS facility) is also included.

1. INTRODUCTION

The problem of hydrogen control in a reactor containment after a loss of coolant accident has been considered very carefully in Italy also before the TMI accident with the intent to minimize the probability of hydrogen explosion.

Some of the works performed in Italy between 1975 and 1980 have been presented during the workshop on the impact of hydro - gen on water reactor safety, held here in Albuquerque on January 1981. The main items discussed during that workshop are listed below.

a) A critical analysis of the design criteria that US NRC recom mended during 1980 for the safety analysis of the light water reactor nuclear power plants. An indipendent approach to hydrogen risk assesment has been presented.

b) The theoretical and experimental analyses of hydrogen concen tration and distribution in the drywell of a Mark II contain ment, performed with the cooperation of the Von Karman Insti tute for Fluid Dynamics in Belgium. The study was performed to evaluate the hydrogen concentration distribution inside the drywell and to verify the behaviour of the PACAM system provided in Caorso Power Plant in order to avoid the forma - tion of high hydrogen concentration packets.

c) The survey program on hydrogen monitoring systems, in order to extende the knowledge on the hydrogen sensors, performed with the cooperation of the NUS Corporation in Maryland. This survey program allowed to identify the tendency in USA to provide the nuclear power plants with hydrogen monitoring

systems using thermal conductivity sensors, frequently located outside the reactor containment.
The survey was extended to 75 nuclear power plants, 48 PWR type and 27 BWR type.

d) The experimental program, started in 1980, to test the hydrogen sensors in order to evaluate their capability to operate with elevated reliability and availability also in an atmosphere characterized by high temperature and high water vapor content.
This program utilizes the PEGASUS test facility existing at ANSALDO IMPIANTI research center, and described in paragraph 3.1.
During 1980 just two sensor have been tested : a catalytic combustion type and a thermal conductivity type. The first one demonstrated a poor repeatability and an excessive pressure and temperature sensitivity. The second one presented an excellent behaviour with a dry sample while, with a wet sample, showed an increasing inaccuracy with the increase of the water vapor content.

During the 1981 and the first months of 1982, the research program was continued in order both to analyze other types of hydrogen sensors and to reevaluate the hydrogen production rate after a LOCA.

For what concerns the experimental program, three hydrogen sensors of electro-chemical type have been tested during the last year; then the PEGASUS test facility has been put in maintenance before initiating the new test program on thermal conductivity sensors recived by qualified manufacturers.

For what concerns the evaluation of hydrogen production rate, studies have been performed with particular regard to the evaluation of the metal-water reaction and the aluminium corrosion. In these frame, many calculation methods have been acquired, with special reference to the computer programs HYDRO and COHCO; this second program has been developed in General Electric with the participation of ANSALDO IMPIANTI technicians.

Besides, studies on hydrogen distribution and combustion inside the containment have been carried out at PISA UNIVERSITY.

Details of the performed works and on the future programs are discussed in the present paper.

2. RESEARCH ACTIVITIES PERFORMED AT PISA UNIVERSITY

2.1. Generalities

In 1975 at DCMN (Dipartimento di Costruzioni Meccaniche e Nucleari) in a cooperation agreement with ENEA (Ente Nazionale Energie Alternative) experimental and theorical research concerning Hydrogen behavior in containment systems began.
The main issues carried out have been :

- study of H2 distribution in containment;
- critical analysis of design criteria involving Hydrogen release from primary circuit;
- drawing of a SOAR (State of The Art Report), together with other CEC (Commission of the European Communities) experts concerning most of the aspects linked with hydrogen generation,distribution, controll and explosion potential in LWRs.

Particularly the last items followed TMI accident.
The above studies lead to the definition of two high proprity research goals :

a) to prevent large core damage and then to limit hydrogen production;
b) to limit the consequences of hydrogen combustion with particular regard to safety systems.

Point a) doesn't require further discussion; the importance of point b) derives from the consideration that once a certain amount of H2 has been produced, it is quite difficult to show the impossibility of combustion in some part of the plant. This item doesn't excludes needs of studies aiming at the control of the gas or, however, at preventing H2 bubbles (bags) to build up and to coalesce.

Taking into account of the above, at Pisa University in cooperation with ENEA, two facilities, allowing to study combustion, generation and release of H2 will be build up within 1983.

2.2. HYDRO facility for experiments of hydrogen deflagration

The HYDRO facility flow diagram is shown in figure 2.1., and the main components of this apparatus are :

- the PROCO vessel, (pressure = 0.65 Mpa, volume = 6.88 m^3, height = 2.5 m) which has already been used to simulate thermalhydraulics transients arising in Mark II and Mark III types of BWR containment, will also be used to study PWR containment systems;
- steam injection system;
- spray system;
- mixing system;
- gas injection system;
- flammable mixture composition measurement system;
- ignition system;
- pressure and temperature detection systems;
- control panels.

In this facility an experimental work to define flammability limits, pressure and temperature time transients of combustion and the possibility of flame acceleration under realistic condition will be carried out. Special attention will be paid in detecting concentration gradients, temperature, humidity, droplets, turbulence, obstacles and containment geometries, particularly in

areas not covered by present researches. In addition the survival ability of small safety related equipments during hydrogen explosion could be checked.
The availability (in 1984) of PSICO 10 vessel (pressure = P.6 Mpa volume = 100 m^3 , height = 7 m) in place of PROCO vessel will permit to study scale effects and the testing of greater safety related equipments.

2.3. PIPER-ONE LOOP for experiments of hydrogen generation and realease from reactor coolant system

PIPER-ONE is an experimental facility designed to simulate thermalhydraulic behaviour of BWR reactor coolant system after small LOCA; the flow diagram is shown in figure 2.2.
The main characteristics of the loop design are the monodimensionality of the various zones (as far as possible), the considera - tion of piezometric heads of the real plant which are the same in the model and the scaling ratios of the pressures and times which are provided to be equal unity.
Besides, flowrates and electric power are scaled down as the overall volume scaling ratio (1/2200). Phenomena connected with ECCS intervention also played an important role in the design of the apparatus.
The heated zone has the same geometry (rod diameter and height pitch, etc.) of the nuclear plant and the allows to reproduce a real time scale the pin surface temperature and the complex heat exchange phenomena arising between the rods and the coolant in the phases of blowdown and reflood.
In this paper the proposal of planning in PIPER-ONE loop experience related to hydrogen production and diffusion in the primary system of a LWR is presented. Particularly the main problem to be taken into consideration during LOCA simulation is as follows :

- the amount of hydrogen produced in the core per unit time having been assigned, what is the gas release in the containment system when break area and position are varied ?

A second more expensive research which coul be carried out later in time is :

- a power transient in a zircaloy or in a stainless steel sheated rod having been assigned, what is the actual hydrogen production in a thermalhydraulic situation similar to the one arising in a real plant during small LOCAs ?

The final objective of the first issue should be the development and the qualification of a theorical model studying the distribution of hydrogen in the primary circuit and then the interaction with the thermalhydraulics of steam-water mixtures;furthemore the maximum realistic fraction of the produced gas really exiting from the break should be the result of the anlysis. With regard to the second issue the effects of the local temperature, quality and velocities of the mixture in the metal-water reaction kinetics should be investigated; taking into account that in PIPER-ONE the above thermalhydraulic parameters are very near to the correspondent ones in real plants during various transient, it follows that the proposed research could produce more realistic correlations for the oxidation process than those commonly used.
In order to realise the above proposals, a feasibility analysis possibly considering the impact of modifications to the hardware of the facility is required.
Considering that from a chemical point of view there is no difference between water and steam and that hydrogen has no physical preferential affinity with water or steam, it results that the laws regulating the gas behaviour inside the vessel are the same governing steam-water flows. With this respect it has been shown, using RELAP4/MOD6 code, that the trends of the main varia

bles (flowrates among various zones, pressures, temperatures , heat exchange, etc.) in PIPER-ONE loop are very similar to the correspondent ones calculated for the real plants : this depends on the chosen scaling laws and in particular on the fact that gravity heads are imposed to be the same in the model and in the real plant. These considerations, although a deeper analysis is necessary, allow us to conclude that hydrogen diffusion in the primary circuit could have the same features, also quantitatively, in PIPER-ONE and in the real plant, if multidimensional effects do not influence appreciably the phenomenon.

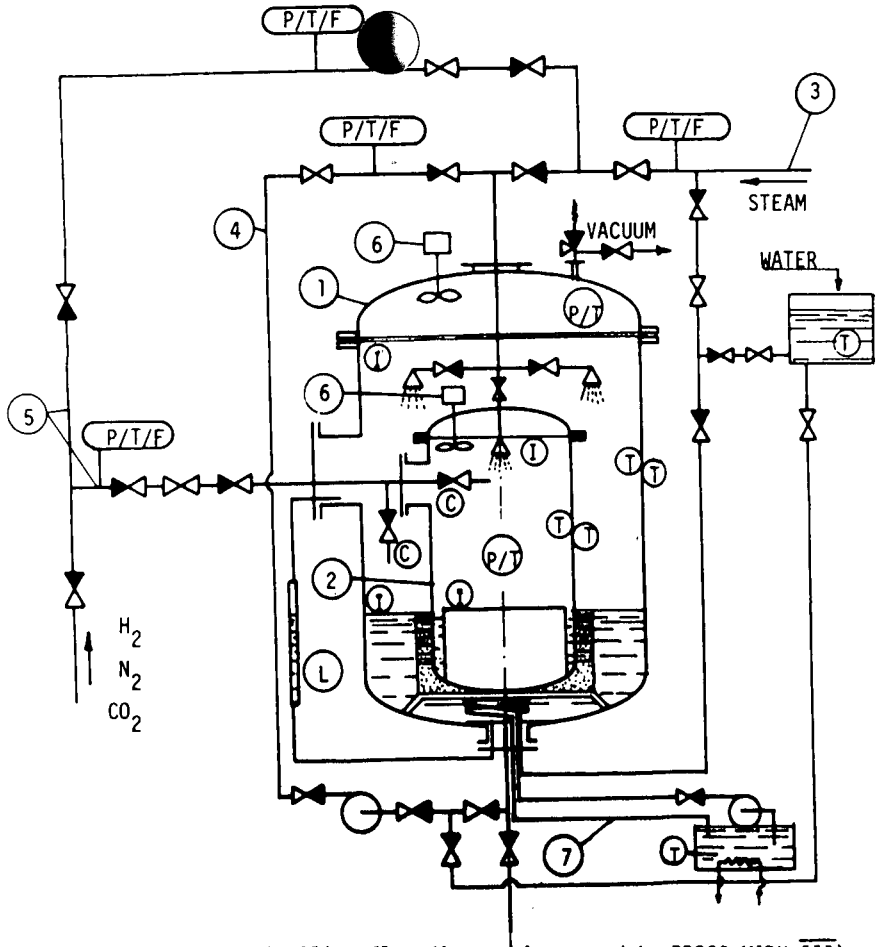


Fig. 2.1. HYDRO facility flow diagram (arranged by PROCO-MARK III)

LEGENDA

1 - PROCO wet-well

2 - PROCO dry-well

3 - Steam injection system

4 - Spray sistem

5 - Gas injection system

6 - Mixing system

7 - Coolant system

C - Concentration measurements

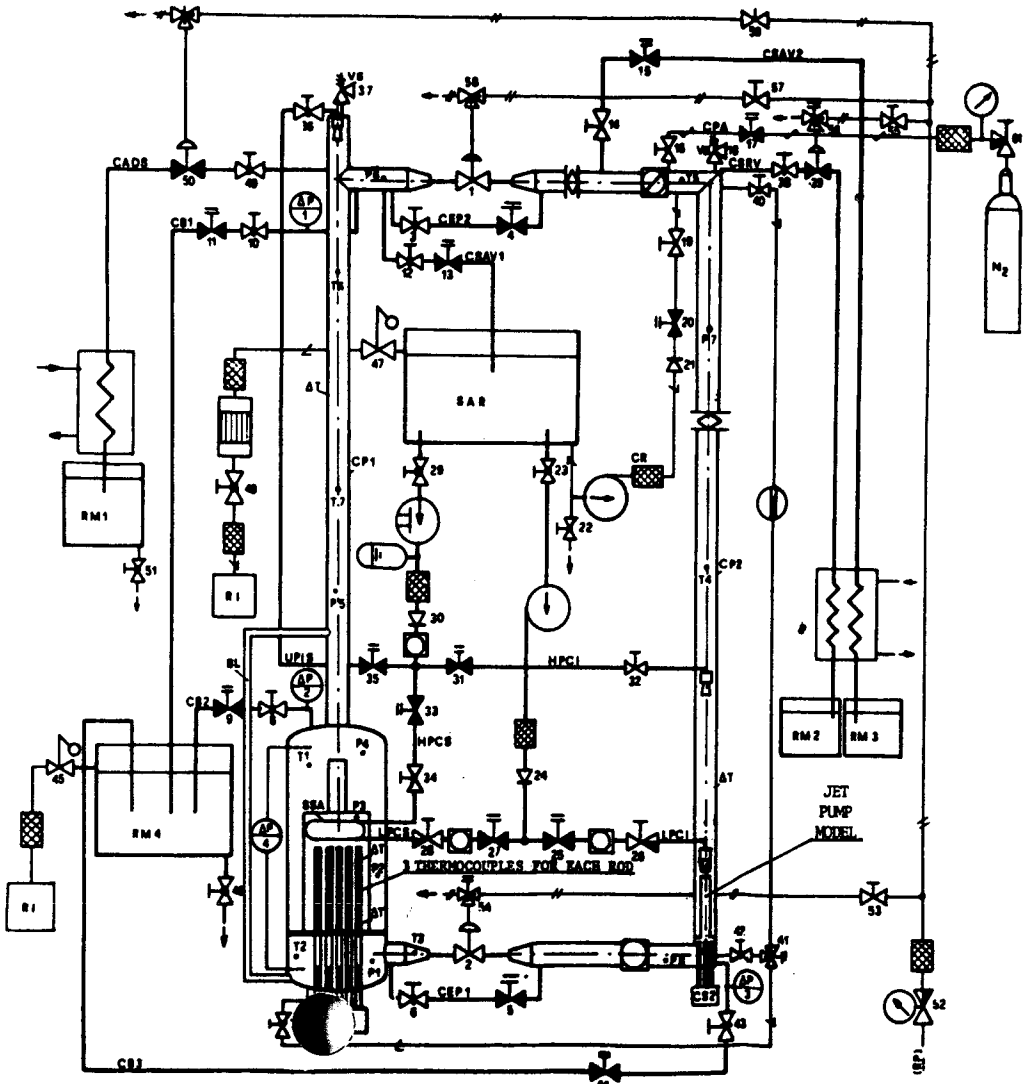
F - Flow rate measurements

I - Ignitors

L - Level measurements

P - Pressure measurements

T - Temperature measurements



LEGEND

- Diaphragm drive
- Hand drive
- Level drive
- Solenoid drive
- Safety valve
- Control valve
- Check valve
- Normally closed valve
- Three-way valve
- Valve (Globe-valve, Gate-valve)
- Turbine (+ DRAG BODY)
- Spray nozzle
- Piston pump
- Centrifugal pump
- Level transducer
- Manometer
- Expansion joint
- Filter
- Deionizer
- Condenser
- Expansion tank

VS	Safety valve
SSA	Spray annulus
SAR	Deionized feed water tank
RP	Feed air
RM	Measurement tank
RI	Feed water
CSRV	Safety-relief system
CSAV	Air-steam relief system
CS	Heater rods
CR	Filling system
CPA	Pressurized nitrogen system
CP	Main [illegible]
CEP	Pre[illegible]qualization system
CB	Blo[illegible]loop
CADS	Automatic depressurization system
BL	Bypass loop

3. RESEARCH ACTIVITIES PERFORMED AT AMN

3.1. Generalities

Since 1977 ANSALDO IMPIANTI, a firm of IRI Group, and CNEN (actually ENEA), the Italian Nuclear Authority, signed an agreement in order to improve design of nuclear reactor systems and components.

In this frame many test facilities were been erected both at the AMN Testing Center in Genoa, and at the CNEN Testing Center in Casaccia, near Rome.

One of the above said facility, is the PEGASUS plant, designed to perform the test of hydrogen sensors in the same ambient conditions of temperature, pressure and water vapor content that are expected in the containment atmosphere after a LOCA. The testing conditions are :

- test gas flow rate	0 ÷ 600	dm^3/h
- test temperature	10 ÷ 100	°C
- test pressure	0,5 ÷ 4,0	ata
- relative humidity	10 ÷ 95	%

The system flow diagram is shown in figure 3.1.

During the first part of 1982 the agreement has been renewed for further 5 years between ENEA and ANSALDO Group; this new agreement will cover all the researches on light water reactor both BWR and PWR.

A significant part of the researches proposed for the next years will cover the behaviour of the containment after LOCA, with particular reference ot the analysis of the hydrogen behaviour.

3.2. Development of computer programs

One of the most significant activities will be performed on the reevaluation of the hydrogen production rate and on the hydrogen concentration build-up in the containment atmosphere, taking into account both the expected metal-water reaction and the action of hydrogen recombiners, ignitors, venting system and other devices provided to control the hydrogen concentration.

This study will bring to the development of a computer code chain, comprehending the HYDRO Code and the COHCO Code.
The HYDRO Code evaluates the hydrogen mass flow rate producted versus the time after LOCA, essentially due to water-metal reaction.
The COHCO Code evaluates the hydrogen concentration inside the drywell and the containment (Mark III type).

Actually these two codes are under testing and sensitivity analyses are performed in order to evaluate the code capabilities.

3.3. Qualification of hydrogen sensors

This activity, which started in 1980 will be completed within the first months of next 1983, when the qualification tests of the hydrogen sensors acquired by ANSALDO IMPIANTI will be completed.
The main purpose of this activity is to define experimentally the effectivness of the hydrogen sensors both versus the type (cathalitic, thermoconducibility, etc.), and versus the operating conditions (ambient pressure and temperature, water vapor content, etc.).

Figure 3.2. shows the PEGASUS facility with on hydrogen sensor ready to be submitted to the qualification tests.
The results of this program will be immediatly applied to the design of Montalto di Castro power plant (two BWR units of 1000 MWe each) which is under erection by ANSALDO IMPIANTI at north of Rome.

3.4. Hydrogen control and monitoring systems design

The activity will include the feasibility analysis of new systems for the control and the monitoring of hydrogen concentration inside the primary containment after a LOCA, taking into account the most updated hypotheses on the hydrogen production rate.
The main goal of the activity is to design a hydrogen monitoring system equipped with hydrogen sensors installed outside the containment. This solution will assure a better maintenance and a prompter adjustment of the sensors, in comparison to the present situation with the sensors installed inside the containment.
The feasibility study will be completed within the next 1983, and this assures the possibility to apply the new system to Montalto di Castro power plant.

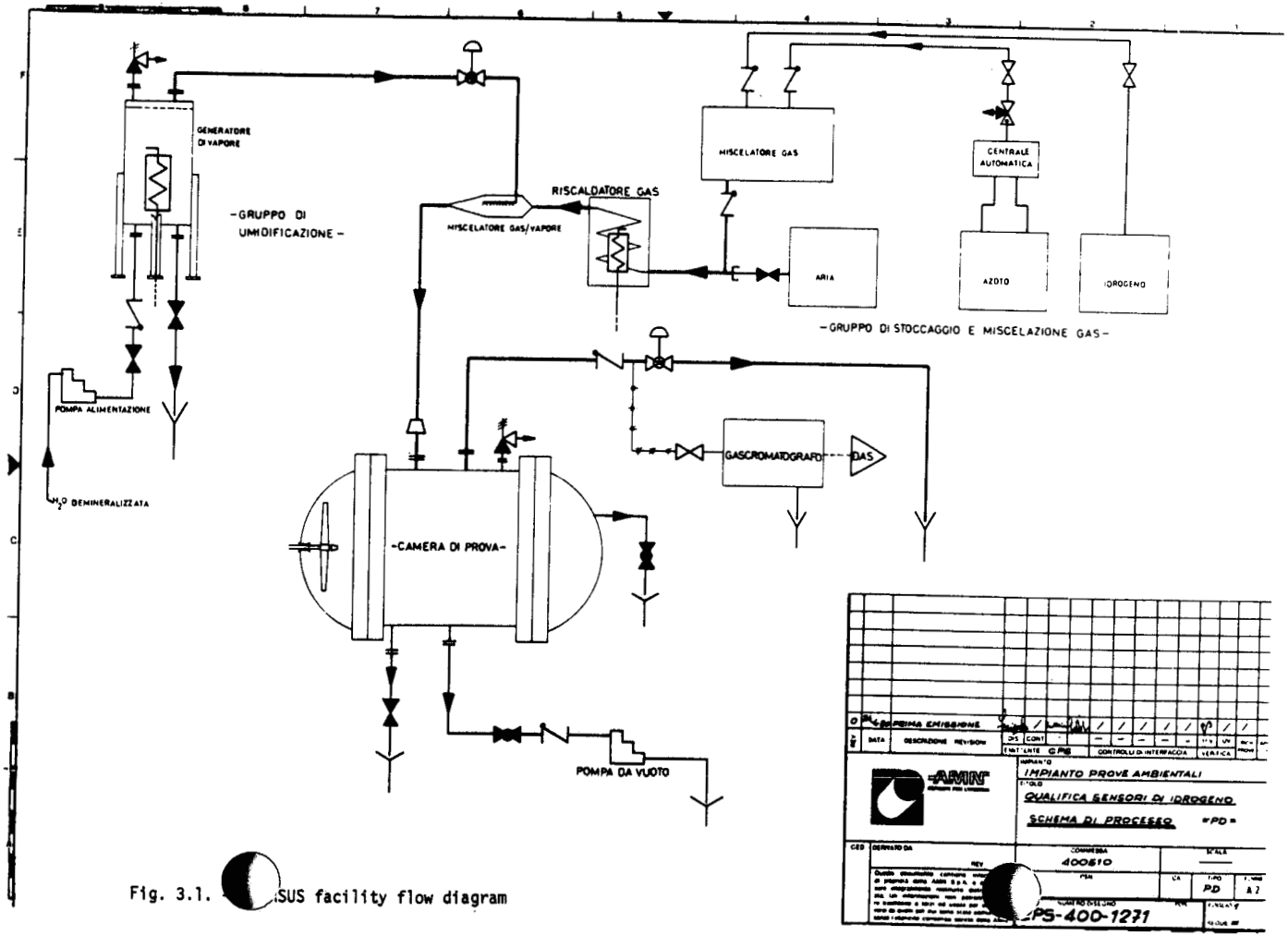


Fig. 3.1. SUS facility flow diagram

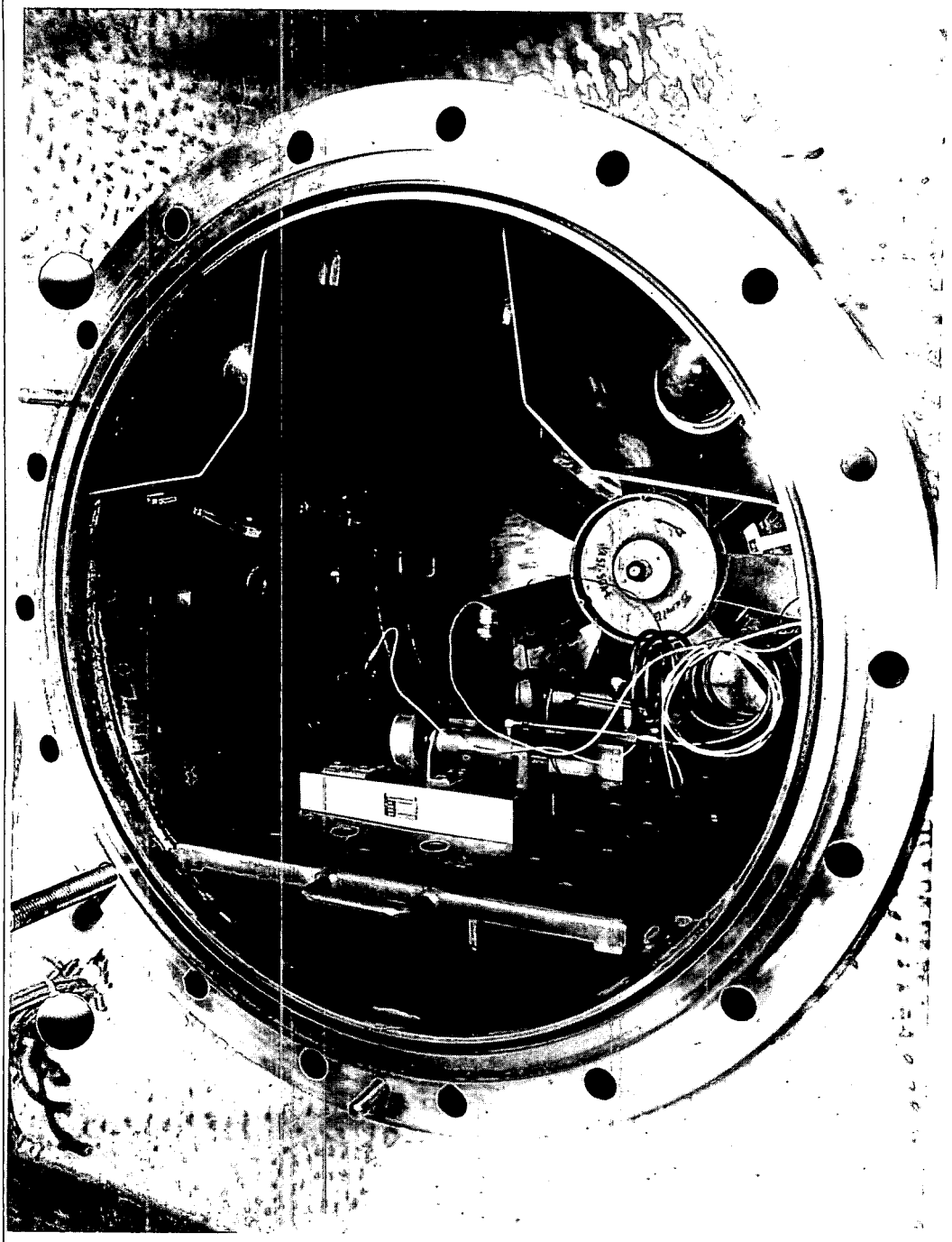


Fig. 3.2. - PEGASUS test chamber with hydrogen sensor

4. CONCLUSIONS

4.1. Time schedule

The annexed table 4.1. presents the time schedule of the activities planned up to the end of next 1983: the milestones shown in this bar-chart don't represent the whole research activity on hydrogen, which will be completed in the subsequent years, as reperted in the next point 4.2..

4.2. Future programs

After 1983, the availability of HYDRO facility and of PIPER-ONE loop will allow the execution of experimental tests concerning:

a) hydrogen flammability limits versus pressure, temperature, water vapor content, water droplets and inerting gas concentration;

b) pressure time transients due to hydrogen deflagration versus the initial hydrogen concentration for the various atmosphere conditions, as defined above;

c) effects of turbolence due to the action of fans, on the fraction of hydrogen burned;

d) effectivness of spray systems on mitigation of the deflagration conseguences;

e) hydrogen behaviour in primary loop during small LOCA and interaction with thermal-hydraulics of two-phase mixture;

f) hydrogen generation during a temperature transient arising in electrically heated zircaloy or stainless steel rods in realistic LOCA conditions.

The detailed test programs will be defined during 1983 both taking into account the results of the researches performed in other countries, and in agreement with the research program developed by the Working Group 2 on "Water Reactor Safety Research" of the Commission of the Euroepan Communities.

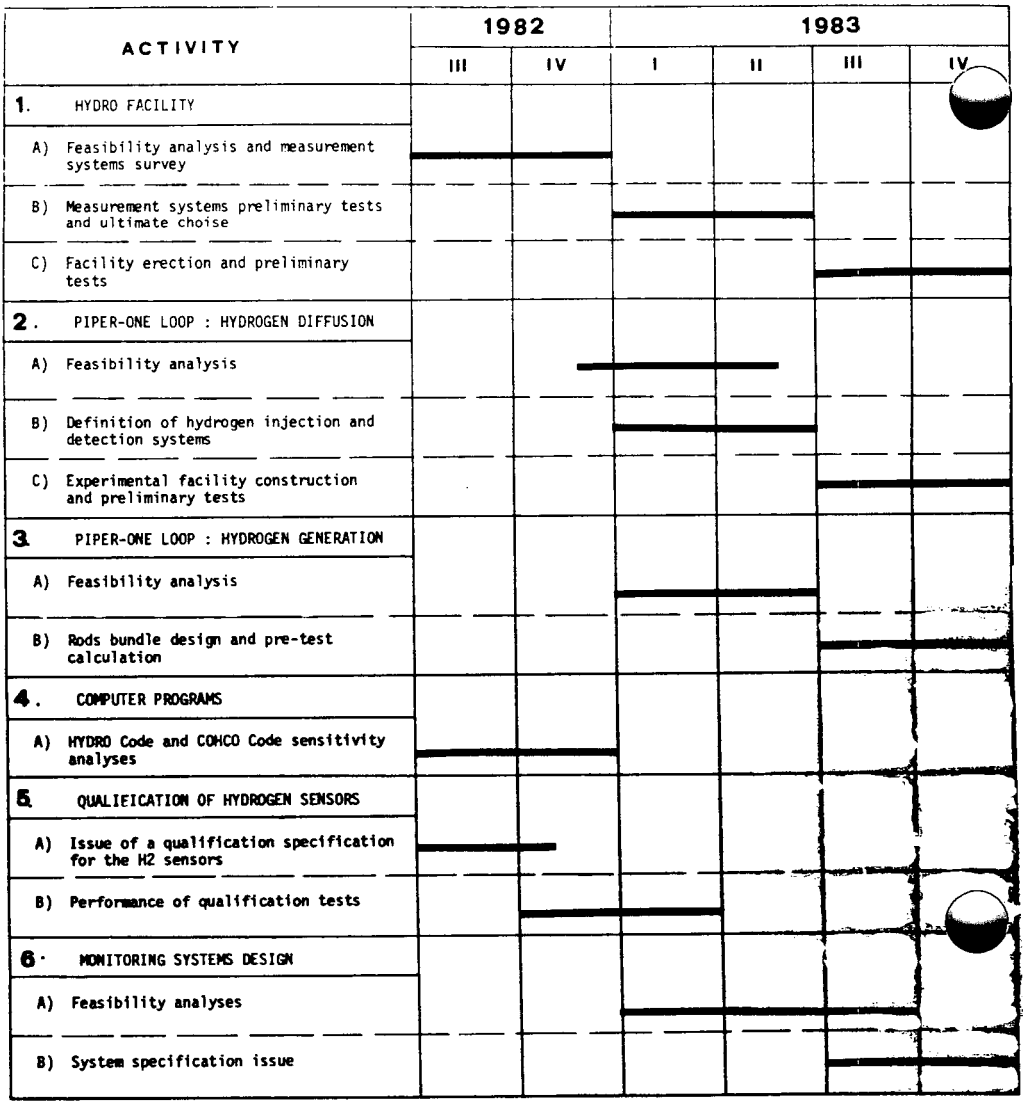


TABLE 4.1. - ESTIMATED SCHEDULE FOR THE RESEARCH ACTIVITIES TO BE PERFORMED WITHIN 1983

BIBLIOGRAPHY

1. GUERRIN, LANZA, MAZZINI, MIRANDOLA, PETRANGELI - "PSICO 10 : A Facility for Testing in the Field of Containment Technology for Nuclear Plants". Ingegneria Nucleare 1969.

2. GUERRINI, MAZZINI - "L'apparecchiature sperimentale SOPRE 1 per la ricerca sui sistemi di contenimento a soppres - sione di pressione". Ingegneria Nucleare 1976.

3. BOZZOLO, KORHERR, PESENTI - "Experimental Verification of PACAM System Performance". AMN-RS-75-013 1976.

4. OLIVARI, THIRY - "Helium Dispersal in the Model of the Drywell of the Caorso Power Plant". Von Karman Inst-AMN 1977.

5. FINESCHI, LANZA - "Mixing of Hydrogen in a Closed Containment". ENS/ANS International Meeting on Reactor Safety, Brussels 1978.

6. FINESCHI, LANZA - "Problemi di modellistica nello studio sperimentale del miscelamento dell'idrogeno con l'atmosfera dei contenitori di sicurezza degli impianti nucleari in condizioni di post-LOCA". Università di Pisa RP 365 (79) 1979.

7. NAHUM - "Survey on Containment Hydrogen Recombiners and Hydrogen Monitoring Systems in the USA L.W.R. Power Plants". Ansaldo RT-400-DRO-203 1980.

8. NAHUM, PERUGINI - "Alternative Solution for Caorso Primary Containment Hydrogen Monitoring System. Sensor Types and Sampling System Analysis". Ansaldo NT-DDR-8001 1980.

9. D'AURIA, LAZZERI, MAZZINI, RUGAI, VIGNI - "Analisi di fattibilità del circuito PIPER-ONE, un'apparecchiatura per esperienze sui transitori termoidraulici che si verificano in un BWR in seguito ad un piccolo LOCA". Università di Pisa RP 416 (80) 1980.

10. BELLI - "Test Results on Hydrogen Sensors Obtained by Ansaldo Impianti". Ansaldo PT-DPC-7910 1980.

11. FINESCHI, LANZA - "An Approach to Hydrogen Risk Assesment in LWRS". Workshop on Hydrogen Impact on Reactor Safety Albuquerque 1981.

12. ZINNARI, NAHUM - "Research Activities on the Hydrogen Behaviour inside BWR Containment after LOCA Developed under the CNEN-AMN Agreement". Workshop on Hydrogen Impact on Reactor Safety Albuquerque 1981.

13. THE EXPERT SUBGROUP OF THE EUROPEAN COMMISSION WORKING GROUP N. 2 ON WATER REACTOR SAFETY - "Assesment of Hydrogen Generation, Distribution and Esplosion Potential Associated with Accidents in LWRs". DG.CEE XII-D-3 1981.

14. MAZZINI, D'AURIA, VIGNI - "PIPER-ONE : an Experimental Apparatus to Evaluate Thermal-hydraulic Transients in BWRs after Small Breaks". ANS Specialists Meeting Monterey-California 1981.

15. CARBONE, D'AURIA, LAZZERI, MAZZINI, RUGAI, VIGNI - "Analisi con il codice RELAP 4-Mod del transitorio preso a riferimento per il calcolo di progetto del circuito PIPER-ONE". Università di Pisa, RP 492 (81) 1981.

16. DIPARTIMENTO COSTRUZIONI MECCANICHE E NUCLEARI - "PIPER-ONE : Progetto concettuale e valutazione economica di massima dell'apparecchiatura con 16 canne scaldanti". Università di Pisa, 1982.

Hydrogen Behavior and Control at Light Water Reactors During Normal Operations and During Accidents

Chester F. Kupiec, General Physics Corporation
Allen L. Camp, Sandia National Laboratories

Introduction

Since the accident at Three Mile Island Unit 2 (TMI-2) there has been a very significant interest regarding the problem of hydrogen production and combustion in light water reactors (LWRs). From the available TMI accident data, it appears that the TMI-2 core was uncovered for a time and significant quantities of hydrogen were produced and released into containment. This hydrogen eventually ignited and produced about a 26 psig (179 kPa) pressure rise within containment. While this particular event did not endanger the TMI-2 containment, there is concern that other, weaker containments might be vulnerable to hydrogen combustion or that more severe pressure rises might be seen under other accident conditions. In addition to the TMI-2 accident, there have also been several incidents where hydrogen combustion occurred in Boiling Water Reactor (BWR) Off-Gas Systems.

Because of the above concerns and the interest shown regarding these problems, Sandia National Laboratories and General Physics Corporation, under the sponsorship of the Nuclear Regulatory Commission, have prepared The Light Water Reactor Hydrogen Manual*.[1] This manual is intended to provide information at a general but comprehensive level on the subject of hydrogen behavior. Numerous references are cited in the manual for readers who wish for more details on particular subjects. The manual addresses the basic theory of hydrogen production, transport, and combustion, along with various proposed control and mitigation schemes. Some of the subjects addressed are topics of current research efforts, and therefore contain some uncertainties. In later chapters, the basic theory is applied to specific hydrogen problems at reactors during both normal operations and accident conditions. The sections on basic theory and mitigation schemes should be useful to plant designers. The sections on hydrogen behavior during normal operations should be useful to plant operators and supervisors, and the sections on hydrogen behavior during accidents may be of value to utility personnel and to NRC staff. Note that no part of this manual is intended to replace specific plant manuals, or to provide procedural directions to operators. Rather, this report is intended as a guide to utility staff when they are formulating their own plant-specific procedures.

*The Light Water Hydrogen Manual is currently at the final stage of preparation and should become available early in 1983.

This paper is an overview of those portions of the manual dealing with hydrogen behavior and control at LWRs during normal operations as well as during accident conditions.

The hydrogen manual consists of the following:

- Chapter 1--Introduction and Objectives
- Chapter 2--Hydrogen in Light Water Reactors
- Chapter 3--Hydrogen Behavior and Control--Normal Operation
- Chapter 4--Hydrogen Behavior and Control--Accident Conditions
- Appendix I--The Three Mile Island Incident Scenario
- Appendix II--A Guideline for Reactor Coolant System Gaseous Void Detection and Sizing
- Appendix III--Reactor Vessel Head Vent Venting Time Period
- List of Abbreviations
- Glossary of Terms

Hydrogen Behavior and Control at LWRs During Normal Operations

Hydrogen can be found in both Pressurized Water Reactors (PWRs) and Boiling Water Reactors (BWRs) during normal operating conditions; its presence is not necessarily a cause for concern. To properly judge whether its presence in a particular location or at a particular concentration is unusual or undesirable requires an understanding of its role during routine operating conditions. An effort is made in this hydrogen manual to examine the role of hydrogen at both of these types of light water reactor facilities.

It was found, for example, that some hydrogen considerations are common to both PWRs and BWRs alike. For example, some plant locations in which hydrogen can be found in both BWRs and PWRs include the following:

- Reactor Coolant System (hydrogen is produced by radiolysis and various corrosion processes)
- Bulk Storage Facility (hydrogen is stored here)
- Electrical Generators (internal cooling of the generator is done by hydrogen)

- o Gas Cromatograph (used at nuclear facilities and employs hydrogen as a calibration gas or carrier gas for gas analysis)

- o Battery Room (Hydrogen is released during the battery charging process)

- o Resin Beds (hydrogen can be formed in the demineralizer resin beds)

Insofar as Pressurized Water reactors (PWRs) are concerned, hydrogen is introduced directly into the Reactor Coolant System (RCS) for corrosion control. If the hydrogen concentration becomes too high locally, such as in the top of the reactor vessel head, or becomes concentrated in the pressurizer steam space, it can cause control problems for the plant.

In addition, reactor coolant which is being letdown from the RCS in a PWR for purification is degassed. The hydrogen gas is then released from the RCS water and concentrated in the Gaseous Waste Disposal System for the plant. As a result the gas decay tanks in this system contain a hydrogen-rich mixture, which can cause a problem for the station.

For example, one Pressurized Water Reactor (PWR) station* experienced a hydrogen ignition in one of the gas decay tanks during a cold shutdown. This incident resulted in release of about 8.8 Curies of noble gases and in minor damage to the tank. The hydrogen ignition was caused by the presence of air contamination in the inert nitrogen system that is used to minimize the oxygen concentration in the tank. (The increasing oxygen concentration was not detected because the gas analyzer in the system was inoperable.) The apparent source of the ignition was the oxygen recombiner in the cryogenic waste gas treatment assembly.** In this incident, the source of air was instrument air that leaked through check valves at the cross connection between the instrument air and nitrogen lines. Leakage occurred in this direction since, under normal operating conditions, the pressure in the instrument air system is higher than that in the nitrogen system. To eliminate the possibility of recurrence at this plant, those portions of the nitrogen system that are a

*This incident occurred in July 1981, at San Onofre Nuclear Generating Station Unit 1. This plant is operated by Southern California Edison Company. It is located near San Clemente, California

**Not all PWR facilities employ a cryogenic waste gas treatment assembly as part of the Gaseous Radwaste Disposal System.

backup supply to the air system have been completely separated from the balance of the nitrogen system that supplies cover gas. Bottles of compressed nitrogen are now used to provide the backup to the air system.

There are also those hydrogen considerations that are pertinent to Boiling Water Reactors (BWRs). Figure 1 illustrates the basic BWR cycle. In this cycle, the reactor coolant absorbs energy as it passes up through the reactor core. The energy absorption causes a water-to-steam transformation. The steam passes through steam dryers in the upper part of the reactor pressure vessel and then flows to the turbine.

As previously discussed, some of the water passing through the core undergoes radiolytic decomposition because of the intense radiation field that is present. Some of the hydrogen and oxygen produced during this process is carried with the steam to the turbine and main condenser. These gases are removed from the condenser by the steam jet air ejectors (SJAEs), along with other noncondensable gases that are present (such as trace amounts of the noble gases, krypton and xenon), and processed through the Off-Gas System.

A BWR nuclear power plant produces a relatively substantial volume of gaseous wastes. In order to properly control these gases, plants employ an Off-Gas System that takes noncondensable gases from the main condenser and processes them in an appropriate manner before releasing them to the atmosphere. One of the most critical aspects of the Off-Gas System is the disposal of the large amounts of hydrogen contained in the off-gas mixture. The lower combustible limit of hydrogen in air is 4.1 percent by volume, while an off-gas mixture typically contains 6 to 8 percent hydrogen. Thus, the Off-Gas System is a potentially hazardous area, in which a spark may cause an ignition. Combustion of hydrogen in the Off-Gas System has not been a rare occurrence during operation. The industry average has been about one combustion for every four years of plant operation. Changes have been made in Off-Gas System design since the early BWR models to reduce the hydrogen concentration in the system, but the system still must be properly and carefully operated to ensure that hydrogen ignition does not occur. In recent generation BWRs, the primary method of reducing hydrogen concentrations in the Off-Gas System is through the use of recombiners.

Hydrogen Behavior and Control at LWRs During Accident Conditions

The possibility of hydrogen combustion inside the reactor vessel was a major concern of the public and of utility personnel during the Three Mile Island Unit-2 incident. There was no such combustion in the vessel, but the question comes to mind: "Was the fear justified?" Although the possibility exists for substantial amounts of hydrogen to be produced in the reactor

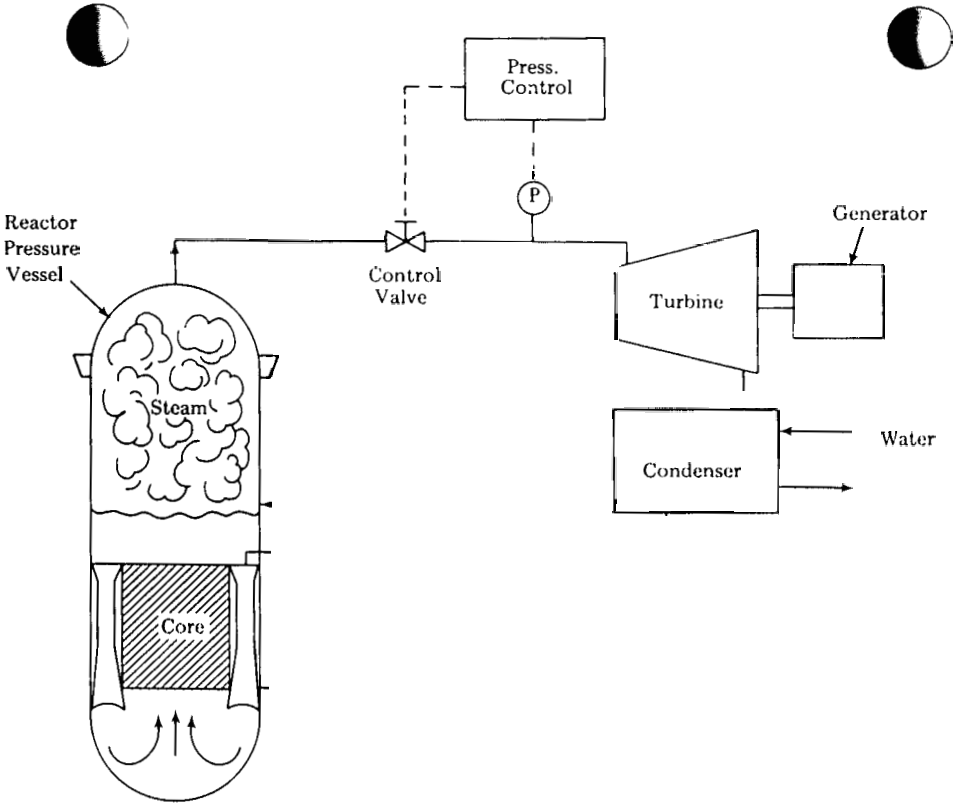


Figure 1. Schematic Diagram of a Typical BWR System

vessel during accident conditions, it is highly unlikely that detonation or deflagration limits would be reached because of the low oxygen concentration in the Reactor Coolant System. However, a large portion of the hydrogen eventually would be transferred to the containment atmosphere (eg, via venting or through a Reactor Coolant System break), possibly creating an environment capable sustaining a detonation or deflagration.

Therefore, one chapter of the hydrogen manual is devoted to a discussion of hydrogen behavior and control under accident conditions. The principal topics covered include containment integrity, indications of a loss-of-coolant accident (LOCA), indications of hydrogen production, hydrogen transport and mixing, indications of hydrogen combustion, and mitigation schemes. An effort has been made to integrate the theoretical aspects of hydrogen production, transport, mixing, and combustion with the operational and emergency aspects that could arise during an accident condition. The hydrogen manual addresses the following for Pressurized Water Reactors (PWRs) and Boiling Water Reactors (BWRs):

- Indications of possible hydrogen production within the reactor as a result of an inadequate core cooling condition (ICC) in the reactor core
- Hydrogen indications external to the Reactor Coolant System
- Transport and mixing of hydrogen
- Potential sources of accidental hydrogen ignition
- Hydrogen detection methods
- Evidence of hydrogen combustion
- Methods of controlling liberated hydrogen

A loss of coolant accident (LOCA) in a light water reactor (LWR) has the potential for hydrogen production if emergency co cooling is not adequately supplied. An inadequate core cooling (ICC) condition can create a degraded reactor core in which hydrogen may be liberated. This degraded core would be the principal source of hydrogen that could be liberated into the containment and transported to other buildings or structures. For example, during the TMI-2 incident the hydrogen generated, principally by the zirconium-steam reaction in the reactor core, was transported throughout the RCS, as shown in Figure 2. This figure shows a sketch of the TMI-2 Reactor Coolant System at a time when hydrogen was most probably being generated. The great loss of reactor coolant inventory enabled hydrogen to spread

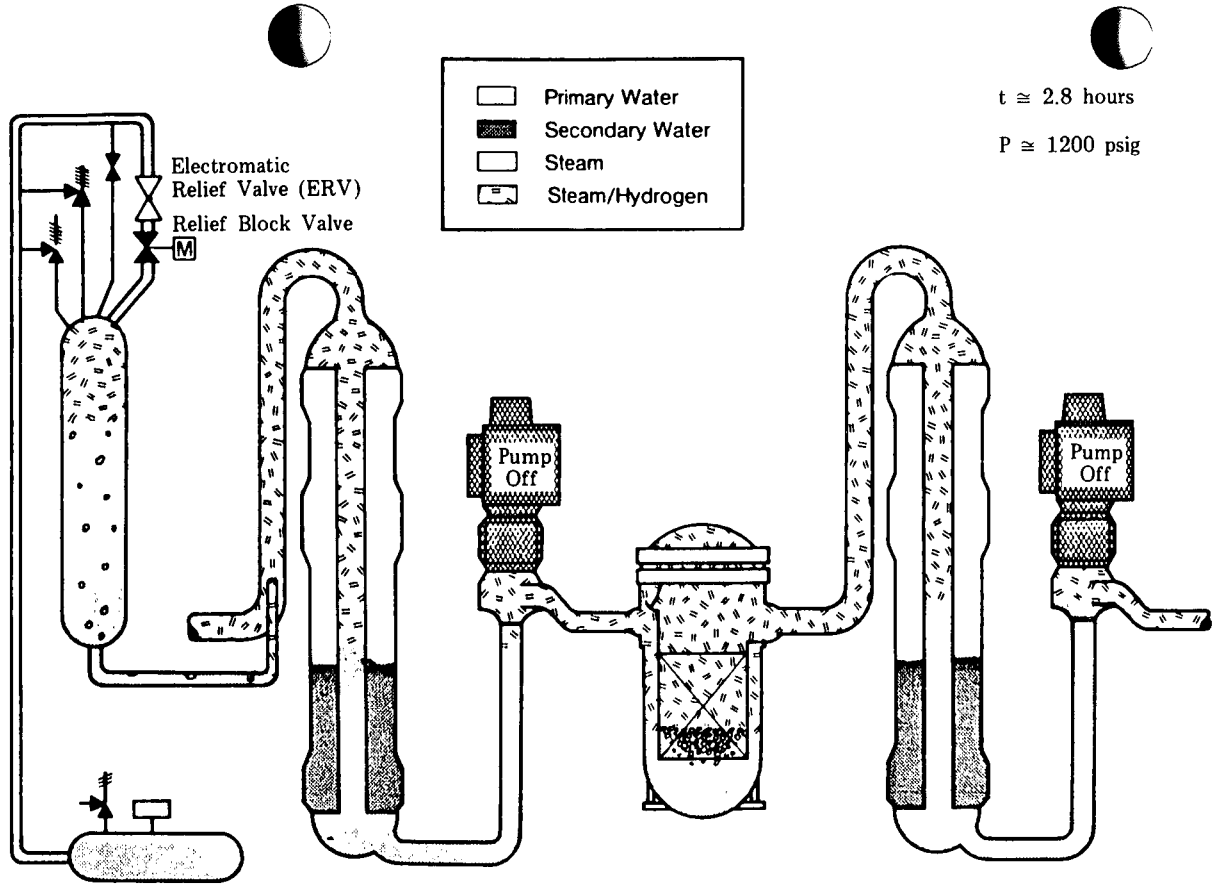


Figure 2. The TMI Reactor Coolant System Showing Hydrogen Generation During the Inadequate Core Cooling Condition

freely throughout the system. The lack of water inventory also made it impossible to establish single-phase natural circulation once the reactor coolant pumps (RCPs) had been tripped.

There are many potential hydrogen release paths through components in the RCS or through systems that interface with the RCS. For a PWR these paths include, but are not necessarily limited to, the following:

- Reactor vessel head vent (as required by NUREG-0737)
- Through the hot leg or cold leg piping (as might occur because of a break in one of these piping sections)
- By way of the pressurizer and pressurizer relief tank (quench tank)
- By way of auxiliary and emergency systems that interface with the RCS. These include:
  - -- Chemical and Volume Control System (CVCS)
  - -- Emergency Core Cooling System (ECCS)
  - -- Residual Heat Removal System (RHR)
  - -- Sampling System (SS)

Similarly, for the BWR a number of potential hydrogen release paths exist that include the following:

- Through a Reactor Coolant System break into the containment
- By way of auxiliary, emergency, and steam systems for the drywell to the secondary containment (or another building). These potential bypass leakage paths include:
  - -- Main steam lines
  - -- Feedwater lines
  - -- Reactor water cleanup line
  - -- Recirculation pump seal mini-purge line
  - -- Main steam line drains
  - -- Suppression pool purification line
  - -- Drywell Ventilation and Purge System
  - -- High Pressure Coolant Injection (HPCI) lines (when there is a suction taken from the suppression pool)
  - -- Reactor Core Isolation Cooling (RCIC) lines (when there is a suction taken from the suppression pool)
  - -- Residual Heat Removal (RHR) lines
  - -- Core Spray (CS) lines
  - -- Drywell Reactor Building (primary-to-secondary containment) Vacuum Breaker System
  - -- Drywell floor and/or equipment sump to Radwaste System
  - -- Control Rod Drive Hydraulic System

It is theoretically possible, then, for hydrogen to be transported into the containment building (or drywell) during a loss-of-coolant accident (LOCA) in which inadequate core cooling (ICC) has resulted. It is also possible for the hydrogen to be transported to other buildings by means of those systems that interface with the Reactor Coolant System. The release of hydrogen into the containment volume is, of course, the more probable event following a condition of inadequate core cooling (ICC). Combustion of this gas in the containment building could pose a threat to safety-related equipment and, possibly, to the containment itself. At TMI, the 28 psig (193 kPa)* maximum pressure that occurred was substantially less than the 60 psig (510 kPa) containment design pressure. However, for a containment building with a smaller volume or a lower design pressure a more severe threat could have resulted.

Some combustion properties for hydrogen-air-steam mixtures on a large scale are not well known. However, the manual examines some current work pertaining to hydrogen distribution and combustion following an accident. It also introduces information regarding hydrogen flame acceleration channels that may occur in a reactor containment and some work currently being performed to further study flame acceleration.

Accidental ignition of hydrogen could be caused by several sources in the containment structure if the hydrogen concentration in air were to reach sufficient levels. In air at 77°F, 14.7 psia (25°C, 101 kPa), and 100 percent relative humidity, the lower limit for hydrogen combustion is approximately 4.1 percent hydrogen concentration by volume. Table 1 indicates the approximate hydrogen concentrations required for combustibility (burning) and detonability in air.

TABLE 1

Hydrogen Concentration vs. Possible Reactions

Hydrogen Concentration in Air**	Possible Reaction
0% - 4%	Noncombustible
4% - 14%	Combustible
14% - 60%	Combustible (possibly detonable)
60% - 75%	Combustible
75% - 100%	Noncombustible

* The pressure was elevated about 2 psig before the burn, which produced an additional 26 psig pressure rise.

**Recent experiments have indicated that the range of concentrations for which detonations may be achieved may be wider than that indicated.

Some containment systems include intentional ignition devices, such as glow plugs, to keep the hydrogen concentration in containment below about 4 percent to 9 percent in the event of a LOCA. These systems are also considered in the hydrogen manual.

Hydrogen generation, and its subsequent release to the containment structure, is a concern primarily in a post-accident mode. In the event of an accident, hydrogen will either collect in the reactor head or vent to containment through the reactor head relief valves or a coolant pipe break. If this happended, any unsealed electrical component or any valve movement that created a spark could provide the necessary energy for an ignition. Depending on the location of the leakage, the vented hydrogen might pass or remain near many possible ignition sources as it left the Reactor Coolant System.

If hydrogen is vented from the reactor vessel head, the many motors and valves near it could provide the necessary spark for ignition. The control rod drive motors (in a PWR) and power-operated relief valve motors (in both PWRs and BWRs) are located near the reactor vessel head relief valves. In addition, in a PWR, there are the control rod drive mechanism (CRDM) cooling fans.

Solenoids, which actuate many motors, generally are not considered to be a probable ignition source because most solenoids are sealed, thus preventing exposure of any sparks to the vented hydrogen. A motor, however, is not completely sealed and can be an ignition source.

Global burns of hydrogen in containment could result in large, short-duration temperature and pressure increases. Multiple local burns or continuous flaring could result in a more gradual increase in containment ambient temperature and pressure (possibly with high local temperatures). Any systems and equipment inside containment whose use may be required after a burn must be able to survive both burn and post-burn environments. The following is a sample list of systems and equipment for a BWR6/Mark III facility whose use may be required after a burn:

- Containment isolation valves, penetrations, locks, and hatches
- Hydrogen Igniter System
- Hydrogen recombiners
- Containment Spray (CS) System
- Safety/relief valves

- Low pressure core spray, low pressure coolant injection, and residual heat removal systems
- Reactor level and pressure instruments
- Hydrogen analyzers
- Containment pressure and high-range radiation instruments
- Containment and suppression pool temperature instruments
- Drywell pressure instruments
- Associated instruments and controls
- Associated power and control cables

The list for a PWR facility would be similar, minus the drywell equipment, and with the addition of pressurizer and steam generator equipment and instruments.

During the TMI-2 accident, the pressurizer level transmitters, pressurizer pressure transmitters, and RCS flow transmitters, all located at the six-foot elevation in containment, failed when the water level rose (due to the LOCA) to the seven-foot elevation. The TMI-2 Instrumentation and Control staff has recommended that any transmitters positioned at lower elevations in the containment building be repositioned at a higher elevation to prevent a transmitter failure by submergence in water. An alternate solution to this problem would be to enclose transmitters in watertight casings.

Also of concern in burn and post-burn environments are nuclear radiation, pressure, and temperature effects. Instrumentation can be damaged due to excessive radiation exposure. Although this was probably not a cause of any instrument failure at TMI, it is certainly one of the factors to be considered in instrumentation reliability. Some data have been generated regarding the integrated dose required for given vital instrumentation to fail.[2] It is expected that more data will be made available regarding this parameter in the future.

During a hydrogen burn there is a rapid temperature increase in the vicinity of the burn. For a short duration, the temperature may exceed 1000 K, causing concern over radiative as well as convective heat transfer. Radiation heat transfer can be adequately controlled by shielding susceptible instrumentation with a cover insulated on the inside.

As a result of multiple burns, the ambient containment temperature could rise. Typically, vital instrumentation transmitters are designed to operate in ambient conditions ranging

from -40°F to 160°F. This range is below the maximum temperature expected in containment under severe conditions. Therefore, the reliability of such instrumentation would be questionable. An exception to this rule is containment pressure instrumentation. One manufacturer, for example, has a containment pressure transmitter capable of operating in an environment of 90 psig and 318°F. A specially designed transmitter such as this should, therefore, be more reliable during the maximum temperature transient.

There have also been a number of proposed hydrogen mitigation schemes. These include:

- Deliberate Ignition
- Deliberate Ignition and Water Fogs
- Carbon Dioxide Post-Inerting
- Halon Post-Inerting
- Nitrogen Pre-Inerting
- Flame Recombiners
- Thermal Recombiners
- Catalytic Recombiners
- Purging or Venting
- Oxygen Removal by Gas Turbine

Each of these methods is examined in the hydrogen manual. An outline of their relative advantages and disadvantages is also presented.

In summary, then, the hydrogen manual which has been jointly prepared by Sandia National Laboratories and General Physics Corporation will become available early in 1983. This manual not only examines the theoretical aspects of hydrogen production, transport, mixing and mitigation, but also makes a strong effort to apply these principles to light water reactors. It is hoped that the manual will serve as a reference document for LWR design and operations personnel alike. Hydrogen behavior and control is closely examined for both normal operating conditions as well as postulated accident conditions at both Boiling Water Reactors (BWRs) and Pressurized Water Reactors (PWRs).

References

1. A. L. Camp, C. F. Kupiec, Jr., et al, "Light Water Reactor Hydrogen Manual," NUREG/CR-2726, SAND82-1137, Sandia National Laboratories and General Physics Corporation, to be published.

2. L. L. Bonzon, W. H. Buckalew, "Evaluation of Simulator Adequacy for the Radiation Qualification of Safety-Related Equipment," NUREG/CR-1184, SAND79-1787, Sandia National Laboratories (May 1980).

SESSION II

HYDROGEN BEHAVIOR DURING LWR ACCIDENTS

Training for Power Plant Personnel on Hydrogen Production and Control

Gary J. Dickelman, General Physics Corporation

It has been our experience that every utility is interested in the hydrogen issue. From the Three Mile Island Unit-2 (TMI-2) incident to the many Off-Gas System Combustions that have taken place over the years, utility managers and training personnel have been asking pertinent questions concerning how well the plant operating staff is versed on this issue. Does the operating staff understand the basic physics involved? Do the operations personnel know how to mitigate the consequences of a hydrogen combustion? Do the operators and plant engineers know where hydrogen can be encountered during everday routine plant operation?

It is the purpose of this paper to address the issue of training for power plant personnel in the area of hydrogen control. Our experience in the training business seems to indicate that most of the operations and engineering personnel have a very limited awareness of this phenomenon. The average member of a power plant operating staff can explain that the zirconium-water reaction occurs above 1500°F. This same individual also might know that a 4% hydrogen concentration has some significance in terms of combustion (for example, those familiar with the augmented off-gas system at a Boiling Water Reactor (BWR) facility.) Generally speaking, however, not much more theory regarding hydrogen usually is known by most operations personnel at a Light Water Reactor. In fact, the vast majority of questions asked during our training programs (related to mitigating the consequences of reactor core damage) are in regard to the hydrogen considerations as applied to their facility. The questions , range from the basic chemical kinetics of hydrogen combustion to the various hydrogen release paths from the reactor vessel into the containment and possibly other buildings. Such questions have broadened our approach to the topic and have forced us to organize our thoughts in terms of a rigorous training program. It is our purpose, therefore, to share with you our ideas on training, that are, in turn, based on the specific needs of the power industry.

Theory

The very first question asked deals with numbers: What concentration(s) of hydrogen will support combustion? Here, even the word combustion is used very loosely. Some small percentage of the operating personnel understand the difference between a detonation and a deflagration, but the language in which these issues are couched is often ambiguous ("explosion," "burn," "blast," etc.). We feel, therefore, that it is best to first discuss the combustion phenomenon in somewhat formal terms. Our approach has been to spend some time on chemical kinetics. In this way the terms involved (detonation, deflagration) can be clearly defined to avoid ambiguity. Several other advantages are the following:

- Operators, having studied neutron diffusion as part of their licensing programs, are familiar with the language of gas kinetics.
- Operators have dealt with rate-type equations when studying radioactive decay.

- Hydrogen control in containment using Halon 1301 (CF_3Br) is discussed later, for which a minimal understanding of free radical propogation is necessary.

To be sure, one could spend weeks on the topic of chemical kinetics; we are merely proposing a presentation that would last between one and two hours to cover the gist of the phenomenon. The operational aspects of control, of course, deserve the most attention. Basically, one should briefly cover the following topics:

- Chain branching of free radicals
- Detonation and deflagration as functions of pressure, temperature, hydrogen concentration
- H_2 concentrations that support deflagration and detonation

(The latter item provides the numbers that the operating staff should have at their fingertips).

Under the general heading theory one should also include information on the consequences of detonations and deflagrations. Specifically, how the containment is affected by each type of combustion. This leads to a more down-to-earth discussion of these issues, now in terms of the physical dimensions of the containment and the type of loads (quasi-static, dynamic or impulsive) produced. The issue of flammability limits may seem clear-cut in the context of chemical kinetics, however the large size of the containment produces variations in these limits. Moreover, a large number of obstacles (such as in the lower portion of a PWR containment) alters the lower detonation limit. If the containment atmosphere is altered by the addition of steam, carbon dioxide or nitrogen, for example, the upper and lower flammability limits decrease and increase, respectively, until the containment is inerted. Most operating personnel are aware of the inerting process, however they are not familiar with the dynamics of the flammability limits as a function of diluent addition. Grasping this idea, at least qualitatively, lends itself to a better understanding, or a more educated operating staff, in terms of hydrogen control.

Incidents

Digressing for a moment from the physics of the combustion phenomenon, is undoubtedly a good idea to discuss (or at least list) many of the hydrogen incidents that have occurred. The impetus is simply to allow the operating staff to come to grips with the issue of hydrogen control in terms that are free from obstraction. It might be the case that no incident has occurred at "our station," so why must we study this? To be sure, the incidents we have in mind are not simply of the "TMI-2 variety," but rather the deflagrations that have occureed in waste gas decay tanks at Pressurized Water Reactors, (PWRs) and Off-Gas Systems of Boiling Water Reactors (BWRs). For example, on February 4, 1982, the Palisades Nuclear Power Station (South Haven, Michigan) experienced a hydrogen leak from its electrical generator's cooling system to the exciter area. The subsequent ignition caused considerable damage and injury to one person. In July of 1977 the Zion Nuclear Station (Zion, Illinois) experienced a fire in the vent stack to the roof of the turbine

building. A combustible mixture of hydrogen had apparently been released through the stack. Such incidents comprise a long list, with a multitude of details in equipment damage and personnel injury to choose from for pedagogical purposes. It has been estimated, for example, that at BWR facilities the average occurrence of Off-Gas System hydrogen combustion is once for every four years of plant operation. The following table, excerpted from EPRI NP-1839, May 1981 (BWR Off-Gas Systems - Operating Experience and Plannning Study) lists several such incidents and the results.

Table 1: Chronological list of Hydrogen Combustion Events

Date	Plant	Cause/Description	Injury	Damage
4/73	Dresden 2	Unrelated welding vicinity of an off-gas pipe purge exhaust point.	Minor burns to two persons	None
11/75	Cooper	Gas accumulated in sump ignited while sampling. Improperly installed valve caused the accumulation.	Major burns to one person, minor burns to another.	Sump lines became separated
1/76	Cooper	Ice blocked the stack. Off-gas backed up into the stack building and was ignited by electrical equipment.	None--missed 2 operators by a few minutes.	Major damage to roof slabs, equipment in the stack building.
1/76	Brunswick	High filter differential pressure by frozen moisture. Loop seals blown. Accumulated gas ignited.	None	Glass items broken. Hatch blown open in roof of room at stack base.
10/77	Brunswick	Similar to that which occured at this same station in 1/76. Cause of back pressure unknown. Possibly only a deflagration.	None	None
12/77	Millstone 1	Loop seals in stack base blown by internal combustion ignited by a welder's arc strike. Accumulated gas was subsequently ignited by electrical equipment.	One person sustained abrasions and a concussion	4" concrete ceiling instruments, and fixtures in stack base damaged. Door blown off.

Discussing the various incidents such as those listed in Table 1 at a number of nuclear generating stations has the added advantage of leading into the issue of where hydrogen is to be found in a power plant during normal operations. This serves to familiarize the operating staff with potential release pathways that will be considered later when accident conditions are discussed. The next section, therefore, deals with training of personnel on hydrogen issues during normal plant operations.

Normal Operations

The first item should be a review of those plant systems that interface with hydrogen and provide hydrogen release pathways. Specifically, those systems which interface with the reactor coolant system and the containment (or drywell) should be studied. Generally, it is the loss of coolant accident (LOCA) that has the potential for deteriorating into an inadequate core cooling (ICC) event in which hydrogen is liberated. The degraded core, being the primary source of hydrogen via the zirconium-steam reaction, is therefore viewed as a central point from which hydrogen is relased. For a BWR, the interfacing systems and components are listed in Table 2. Those for a PWR are listed in Table 3.

Table 2: BWR Systems and Components Interfacing With Hydrogen

Main steam lines
Feedwater lines
Reactor water cleanup line
Recirculation pump seal mini-purge line
Main steam line drains
Suppression pool purification line
Drywell Ventilation and Purge System
High Pressure Coolant Injection (HPCI) lines (when there is a suction taken from the suppression pool)
Reactor Core Isolation Cooling (RCIC) lines (when there is a suction taken from the suppression pool)
Residual Heat Removal (RHR) lines
Core Spray (CS) lines
Drywell Reactor Building (primary-to-secondary containment)
Vacuum Breaker System
Drywell floor and/or equipment sump to Radwaste System
Control Rod Drive Hydraulic System

Table 3: PWR Systems and components Interfacing With Hydrogen

Reactor Vessel Head Vent
Hot Leg and Cold Leg Piping
Pressurizer and Pressurizer Relief Tank
Reactor Coolant Pumps (seal leakoff)
Reactor Vessel flange seal leakoff
Reactor coolant loop drain header
Steam Generator Tube Leaks
Chemical and Volume Control System (Letdown and Charging System)
Emergency Core Cooling System (Safety Injection System)
Residual Heat Removal System
Sampling System
Safety Injection Tank Drains (Nitrogen Accumulators or Core flood Tanks Drains)
Post Accident Sampling System
Gaseous Waste Disposal System
Liquid Waste Disposal
Containment Purge and Ventilation System

During such a review of power plant and component systems, the issue of hydrogen control should be emphasized. Merely lifting the existing system descriptions (for example, from an operator existing training program) is not necessarily advisable. For example, at Pressurized Water Reactor (PWR) much time is devoted to the review of the pressurizer (that device which is half-filled with water and half-filled with steam serves to control pressure in the system during normal operation along with anticipated transients). Generally, for most licensed operators normal pressure operation tends to be well understood. However, over the years a number of facilities have determined that hydrogen in the Reactor Coolant System can accumulate in pressurizer steam space and create significant pressure control problems (a so-called "hard bubble" phenomenon). As a result, it is very worthwhile to include a discussion of this so-called "hard bubble" hydrogen phenomenon to the existing pressurizer pressure control review discussion with the operations staff. One should spend some time explaining how it can be detected and the resultant control problems that can result from the presence of hydrogen in the pressurizer steam space. Adding a discussion of this type is relevant, useful and cost-effective in that it can truly serve to minimize unnecessary down-time of the plant in the long run. Specific behavioral objectives referenced to a task analysis of hydrogen control measures should therefore be attached to such a review. The previous example suggests that without such objectives it is plausible that control operators would look upon the review as somewhat pointless. A workshop environment is an excellent alternative (as a pilot program, for example), wherein several scenarios of hydrogen release are suggested. The participants armed with Piping and Instrumentation Diagrams, Technical Specifications and the like could be split into groups in order to formulate action plans for the various scenarios. Clearly a detailed systems review would ensue, as well as sufficient information on which to base behavioral objectives for the next session. The following simplified diagrams, Figures 1 and 2 (for BWR and PWR stations, respectively) could be used for such workshops. In each case the participants could be issued a general scenario. For example for a PWR one might consider how. Hydrogen is released through the Reactor Coolant System into the containment. Further the

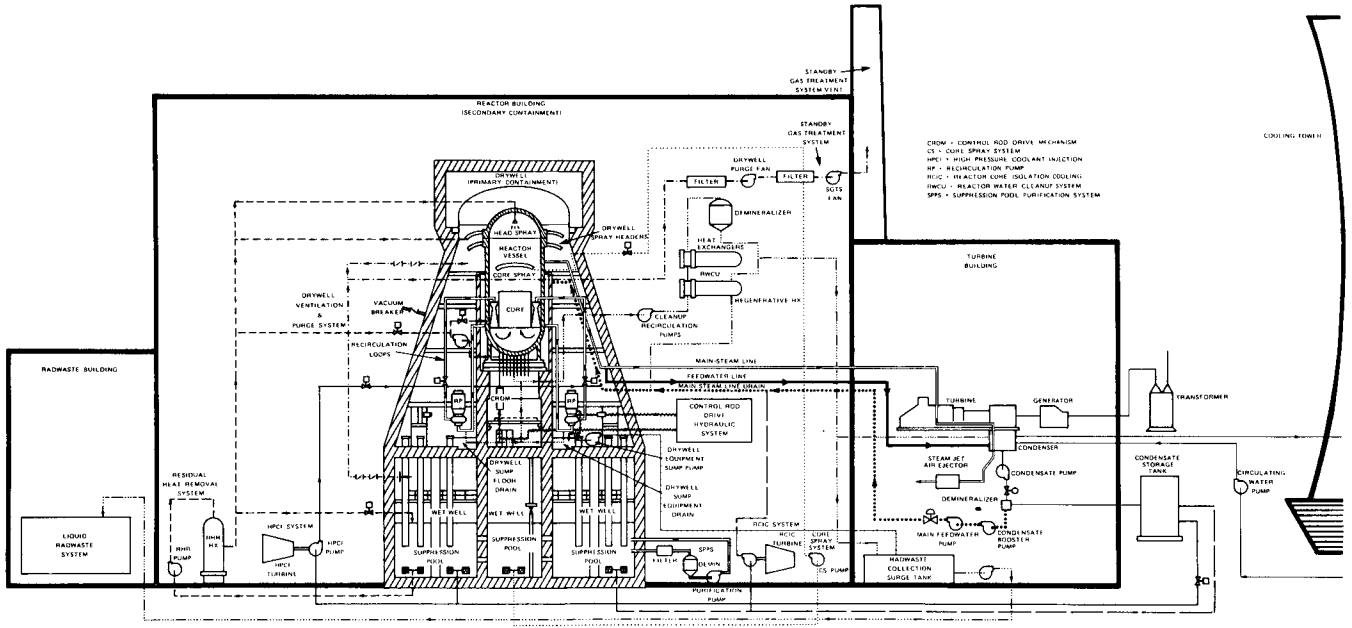


Figure 1. Potential Hydrogen Release Pathways (BWR)

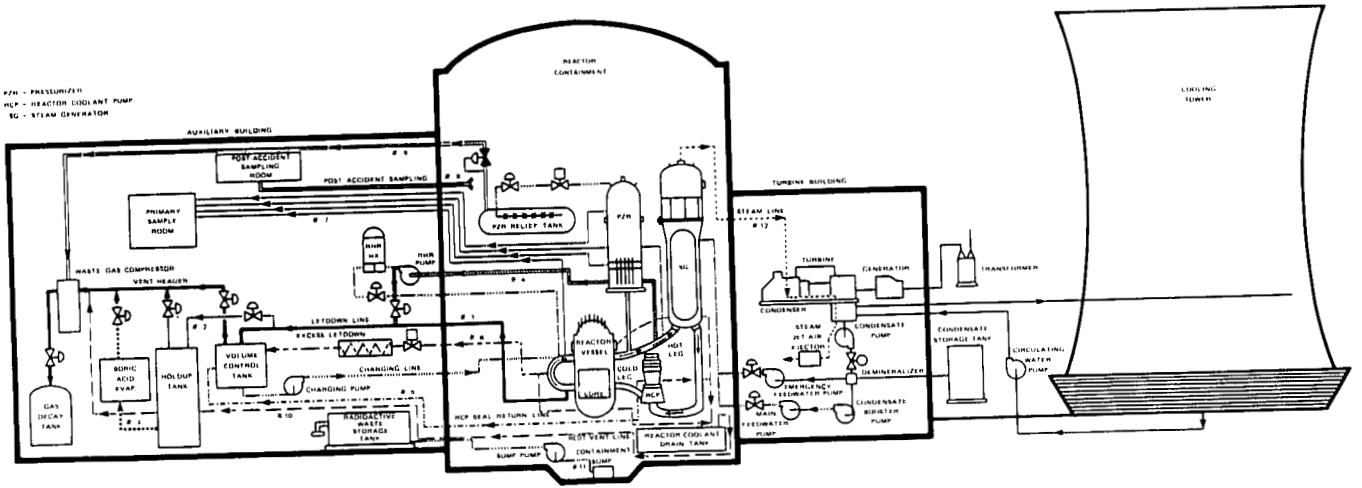


Figure 2. Potential Hydrogen Release Pathways (PWR)

workshop discussion groups could examine how the systems and components listed in Table 3 may become involved. In addition, the workshop discussion groups could examine how a hydrogen release could be accomplished by way of auxiliary and emergency systems that interface with the Reactor Coolant System (RCS). (Similar questions for BWRs. can also be prepared.)



Accident Conditions

For the accident conditions, the operating personnel must first understand the basics of hydrogen generation. The majority are familiar with radiolysis of water and the zirconium-water reaction to some degree, but feedback becomes almost nonexistent when questions are posed on the steel-steam reaction, aluminum-steam reaction and the core-concrete reaction. The systems review of the previous section is an obvious prerequisite. The locations and quantities of steel, aluminum, zinc and zirconium must be known in order to assess hydrogen production as a function of time. For some stations this is simply a matter of reviewing the Accident Analysis portion of the FSAR; for others (in our experience), such plant-specific information is difficult to come by or non-existent. Vendors generally supply excellent generic information, for which a good program can be written.

A loss-of-coolant accident (LOCA) scenario which progresses to an inadequate core cooling (ICC) condition provides an excellent vehicle for studying hydrogen production as presented above. Table 4 lists, in time-dependent order, production of hydrogen during such an accident.

Table 4: Reactions Resulting in Significant Hydrogen Production as an Inadequate Core Cooling Event Progresses

Early in accident	1. Steam : zirconium reaction 2. Steam : steel 3. Core : concrete
Significant over long periods of time	4. Radiolysis of water 5. Corrosion of zinc-based paint and galvanized steel 6. Corrosion of aluminum

Each item in Table 4 should be discussed in some detail. In the case of radiolysis, for example, a review of the types of radiation from fission products should be reviewed.



Once hydrogen is being produced in large quantities from the above reactions, the stage is already set for discerning the release paths to the containment. Hydrogen mixing in the containment atmosphere must also be discussed. On the latter point, we find that little is known among the operating staff. A general misimpression is that any hydrogen released into the containment will collect in the upper regions. A thorough treatment of mixing, including bulk gas motion due to pressure difference, natural convection, forced convection (e.g. from fans or steam jets) is therefore considered an integral part of such a training program. Concentrations of Air : Steam : Hydrogen within the containment must also be addressed, at least qualitatively. This depends on the rate of hydrogen release, location of

hydrogen release, steam removal (e.g., supression pool, ice condenser, etc.), and other systems-related issues. A firm qualitative grasp of the dynamics should be the minimal objective. Finally, a hypothetical calculation of the fraction of the core that would have to react to produce sufficient hydrogen to support a deflagration or detonation should be performed. In this regard, pressure rises within the containment could be correlated and compared with the containment design pressure. Damage to safety related equipment should also be considered here as a function of a deflagration or a detonation.

Mitigation Schemes

A training program for control and mitigation of hydrogen should not only include a study of those hydrogen control systems employed at the individual facility, but should study the gamut of control measures. Hydrogen recombiners are familiar to most personnel, however there isn't much familiarity with water fogging, glowplugs (and other deliberate ignition schemes) in general. Table 5 lists those hydrogen control measures that have been either implemented, proposed and/or studied.

Table 5: Methods of controlling Liberated Hydrogen

- Hydrogen Recombiners
- Deliberate Ignition
- Venting
- Halon Suppressant System
- Containment Spray and Fogging
- Fogging Combined with Deliberate Ignition
- Inerting (Post-accident)
- Pre-inerting and Partial Pre-Inerting

A presentation of all of these systems should be accompanied by a discussion of the relative advantages and disadvantages of the control systems. Criteria should include whether or not...

...deflagrations are prevented;
...detonatons are prevented;
...large scale hydrogen generation is reduced;
...containment pressure rise is reduced;
...there is a danger associated with inadvertent actuation
...installation is difficult/expensive;
...maintenance is difficult/expensive

A sample table is given in Table 6 for Deliberate Ignition With a Water Fog.

Summary

In conclusion, we would like to outline a training program on the control and mitigation of hydrogen. Detailed information, references and the like for the individual topics can be obtained from the LWR Hydrogen Manual when it appears early in 1983, a discussed in the previous talk. Of course, the needs of the individual utility ultimately dictates the extent of such training. We present this summary on the basis of our experience in training at many facilities on this topic, a well as a sincere desire to share that experience with those in the process of developing their own training programs.

Table 6: Advantages & Disadvantages of Deliberate Ignition with a Water Fog

Advantages	Disadvantages
Deliberate ignition distributes the energy addition to containment over a period of time, which allows the pressure and temperature changes inside containment to be gradual.	• It requires additional containment penetrations for electrical connections.
• It will control a large-scale generation of hydrogen.	• It is an active system requiring power to pump water to maintain the fog.
• The system is no threat to personnel since it is not required during normal operation, and inadvertent actuation would not present a threat.	• If the loss rate of drops is as high as predicted by aerosol codes, then the water flow rate required to maintain the fog may be impractically high.
• It has a relatively short warm-up time.	• The technology is not fully developed
• Maintenance would be minimal.	• Burns may damage equipment in containment.
• The cost is moderate.	
• It will condense steam, reducing containment steam pressure during a LOCA.	
• It may prevent detonations. This issue is not yet resolved.	
• It could effectively remove fission products and aerosols from the containment atmosphere.	
• It will reduce the pressure and temperature increase of the combustion of deliberate ignition alone.	

Table 7: Outline of a Mini-Course for Power Plant Operating Personnel on Hydrogen Generation, Control and Mitigation

Topic Covered	Items Addressed	Presentation Time
Combustion Theory	• Chemical Kinetics • Free Radical Propagation • Flammability Limits • Containment Integrity • Recognizing Combustion	2-4 hours
Incidents	• BWR Off-Gas System deflagrations • PWR waste gas tank ignition general operating experience	1-2 hour
Normal Operations	• Systems Review • Workshop exercises • Transport of Hydrogen	4-8 hours (Depending on depth of systems review necessary)
Accident Conditions	• Accident Analysis: Review of LOCA scenarios leading to ICC events • Steam : metal reactions • Radiolysis • Corrosion • Mixing of Hydrogen in the containment atmosphere • Calculations (% core reacted, pressure rise in containment) • Damage to containment and safety - related equipment	3-4 hours
Mitigation Schemes	• Recombiners • Deliberate Ignition • Venting • Halon • Fogging & Spray • Fogging & Deliberate Ignition • Inerting • Advantages/Disadvantages	2-4 hours

THE CONTEMPT-DG CONTAINMENT ANALYSIS CODE

by

Richard E. Deem and Kenneth Rousseau

A B S T R A C T

The assessment of hydrogen burning in a containment building during a degraded core event requires a knowledge of various system responses. These system responses (i.e. heat sinks, fan cooler units, sprays, etc.) can have a marked effect on the overall containment integrity results during a hydrogen burn. In an attempt to properly handle the various system responses and still retain the capability to perform sensitivity analysis on various parameters, the CONTEMPT-DG computer code was developed. This paper will address the historical development of the code, its various features, and the rationale for its development. Comparisons between results from the CONTEMPT-DG analyses and results from similar MARCH analyses will also be given.

1.0 Historical Background

The Zion/Indian Point (ZIP) Near Site Study commenced in the latter part of 1979. Early in the study, technical exchange meetings took place between the utilities involved, the NRC staff, and various consulting organizations. At that time, some of the discussions dealt with the use and applicability of the MARCH [1] computer code as an analytical tool for Probabilistic Risk Analysis (PRA). Exception was taken by various consultants and NRC staff members with the MARCH code and some of the results it calculated. During the same time period, EPRI developed the RECAP [2] code package, which contained a computer that was supposed to perform similar analyses to that of MARCH. This code had, as its basis, CONTEMPT-LT with the subroutines BOIL, PVMELT, and INTER added to it. A copy of this code was obtained and after approximately one month of concentrated effort the code was made functional. Sample cases were then run to determine the accuracy and the cost of running the code. Results showed that various minor errors existed in the code and that for the size of the problem and level of complication of the model, the code was not very cost-effective. As a result of the above, a decision was made to use MARCH for the ZIP study and make the necessary changes to it as the phenomenology was developed. A parallel effort was also embarked upon to rewrite the CONTEMPT-LT based code from the RECAP package. The rationale for this type of approach was as follows:

1.) The NRC consultants had used the MARCH code for their analyses. If the utilities with their consultants used a different code, there would not be a common basis for comparison of results.

2.) Although many people took issue and had anxiety about the use and methodology of the MARCH code, none took the position that it had definite errors. CONTEMPT-LT (RECAP) did have various minor errors.

3.) In order to meet the ZIP study completion date, work had to commence immediately. Therefore, the time required to make CONTEMPT-LT (RECAP) functional would have had a major impact on the study schedule.

2.0 CONTEMPT-LT (RECAP) Code Rewrite

As stated in Section 1.0, this rewrite was performed as a parallel effort to the ZIP study. The goals of the rewrite, in their order of priority, are described in the following text with the salient results of each achieved goal.

First and of foremost importance was the correction of the errors that existed in the code. The major errors that were corrected were as follows:

1.) All noncondensible product amounts produced in INTER (the corium-concrete interaction subroutine) were not being accounted for in the containment response tracking subroutine (GO).

2.) The downstream pressure in subroutine EXITBL was changed to the upstream pressure on the flow calculation iteration. This was causing a mass/energy balance failure during vent clearing.

3.) Some of the unit conversions from British to SI units were in error for PVMELT input variables.

4.) The final flow rates for intercompartmental leakages were being totaled incorrectly in subroutine LEAK 1. This was causing excessive iterations to balance the mass and energy of the donar and receiver compartments.

The second goal of the rewrite was to restructure and optimize the code to make it as cost-effective and user oriented as possible. To achieve this goal, the following major items contributed greatly to enhancing the code performance:

1.) Elimination of approximately 2300 lines of redundant coding.

2.) Rewriting the code specifically for the Control Data Cyber-200 vector mainframe.

3.) Elimination of the calling of the interpolation subroutines for tabular data

entries that were not input for specific computer runs.

The above items resulted in reducing the cost of running the code by an overall factor of 12.4. Individual reduction contributions for each of the above items were; a factor of approximately 4 for item 1, approximately a factor of 6 for item 2, and approximately a factor of 2.4 for item 3.

2.1 Enhancements made to the code

As the ZIP study progressed, analyses performed utilizing the MARCH code showed that certain engineered safety features had a significant effect on the results in terms of risk contribution. In particular, the operation of fan cooler units, containment sprays, and how they were modeled. Another key element for consideration was where the blowdown and the core melt were to be received if a subcompartment analysis is to be performed. This item can be extremely important when dealing with hydrogen burns and the associated pressure spike the containment structure is subjected to as a result of hydrogen burning. Lastly, from a user and cost viewpoint, it was felt that a progressive, segmented restart option should be incorporated in the code. This item would be of particular importance if parametric studies were desired during specific times of an accident sequence.

Enhancements made to the code as a result of the above were as follows:

1.) The fan cooler heat removal capacity was fractionalized to reflect the actual flow rates between compartments.

2.) The code was modified to allow the core melt and the blowdown to go to differenct compartments for dry containment cases.

3.) A progressive restart option as included in the code rewrite which would allow the user to change any input variable to the code, if the variable has not produced any intermediate results prior to the restart tape being written.

4.) An optional hydrogen addition table was added to the input description of the code. This would allow the user to input hydrogen addition rates to the containment if desired. For example, if the user had hydrogen production rates which were calculated by another computer code or experimental data, it could be utilized in this code to examine response of the containment via use of this option.

5.) A logic change was made to the code to allow for a large timestep parameter to be utilized even though a subcompartment analysis is performed. This was achieved by writing an interface subroutine which would take the large timesteps and subdivide them into small timesteps just for subcompartment analysis purposes.

3.0 Comparison of Results between CONTEMPT-DG & MARCH

After completing the rewrite of the code and incorporation of the above stated enhancements, the code was substantially exercised to ensure the results calculated were reasonable. Having assured that the basic logic and mathematical models were correct, various scenarios were analyzed and compared with MARCH analyses. Even though the two codes handle various aspects of the analysis differently, the inputs were "adjusted" to make the internal models function similarly. For example, the PVMELT input was adjusted to conform to the MARCH models and the heat structure specification in CONTEMPT-DG had to be made consistent with the MARCH specification. The basic model employed for the comparison calculations is depicted in Figure A. Three basic scenarios were selected for analysis, an AD, S_2D, and an S_2B sequence. All data used in the analyses were for the Indian Point 3 plant.

3.1 Results for the AD sequence

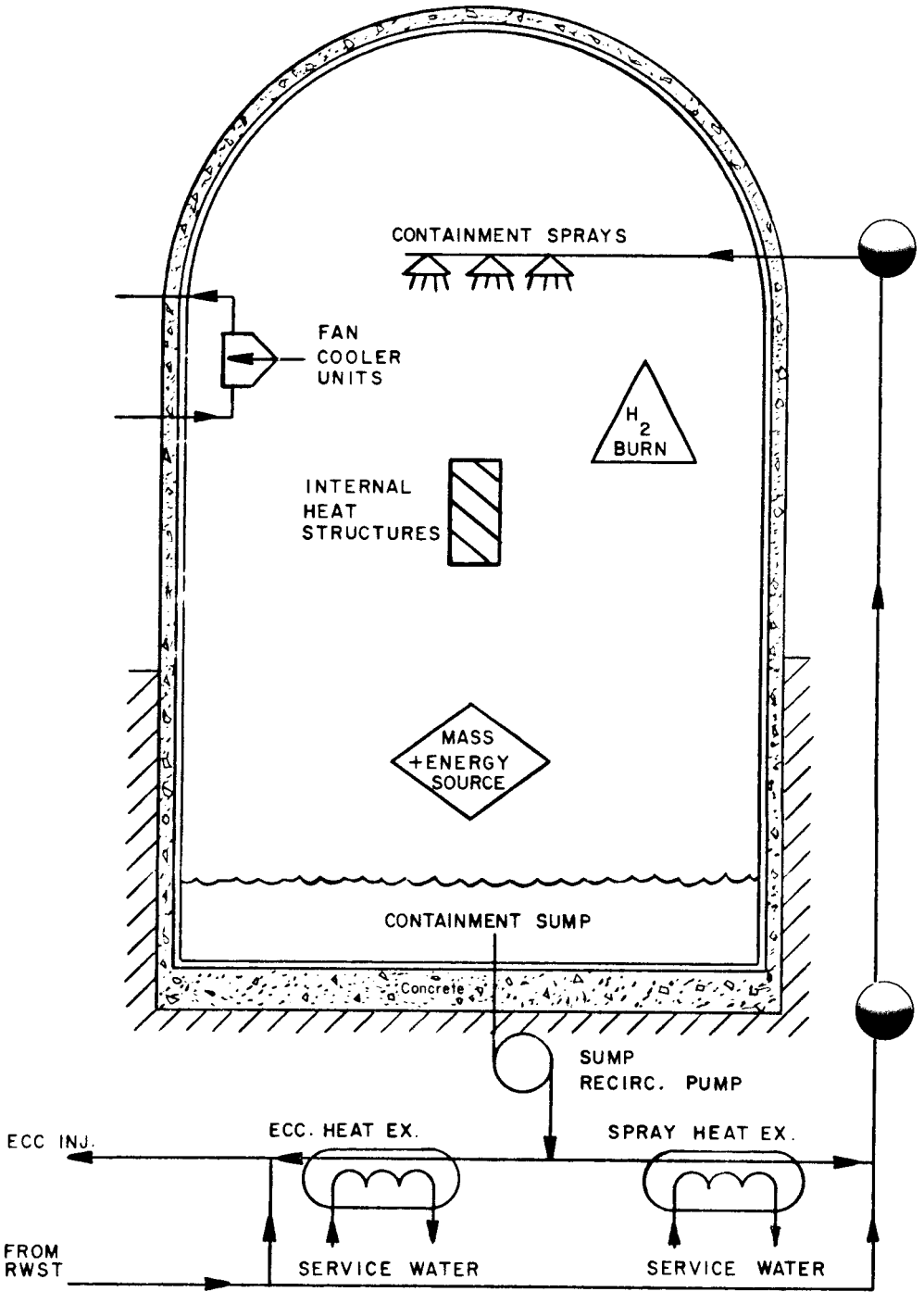
This section contains the results of the MARCH and CONTEMPT-DG calculations for the AD sequence. Table I contains the relevant timings of events predicted and peak pressures for each code. Figure I shows the containment pressure profiles for this scenario. As can

be seen, the blowdown phase of the primary system requires approximately 21 seconds for this case. Comparison of the containment responses during this time indicates a pressure difference of about 15 psia. This is attributed to different modes of energy addition to the containment by the two codes. MARCH assumes 50% of the blowdown coolant is being added to the pool region and the other 50% is added to the vapor region as steam. CONTEMPT-DG assumes all of the blowdown mass is added directly to the vapor region of the containment. The MARCH analysis also predicted a small hydrogen burn approximately 58 minutes into the accident while CONTEMPT-DG predicted none. This was due to steam blanketing of the containment atmosphere, precluding hydrogen burning for the CONTEMPT-DG case. The different blowdown modes, slightly compounded by calculational differences in the heat structures, results in the differences in pressure observed. The main pressure spike occurs just following vessel failure (69.3 min.) as a result of hydrogen burning. Subsequent to that, the containment sprays and fan cooler units reduce the containment pressure and the scenario remains relatively benign.

TABLE I
SEQUENCE: AD

	MARCH	CONTEMPT-DG	
SPRAY ON:	.55	1.0	MIN.
CORE UNCOVER:	1.3	1.0	MIN.
CORE MELT START:	21.3	26.4	MIN.
CORE SLUMP:	41.3	42.1	MIN.
VESSEL FAIL:	69.3	69.3	MIN.
HYDROGEN BURN:	69.4	69.3	MIN.
MAX. PRESSURE--NON-ADIABATIC H_2 BURN AT VESSEL FAILURE:	89.8	77.9	PSIA

FIGURE A



ONE REGION CONTAINMENT SYSTEM

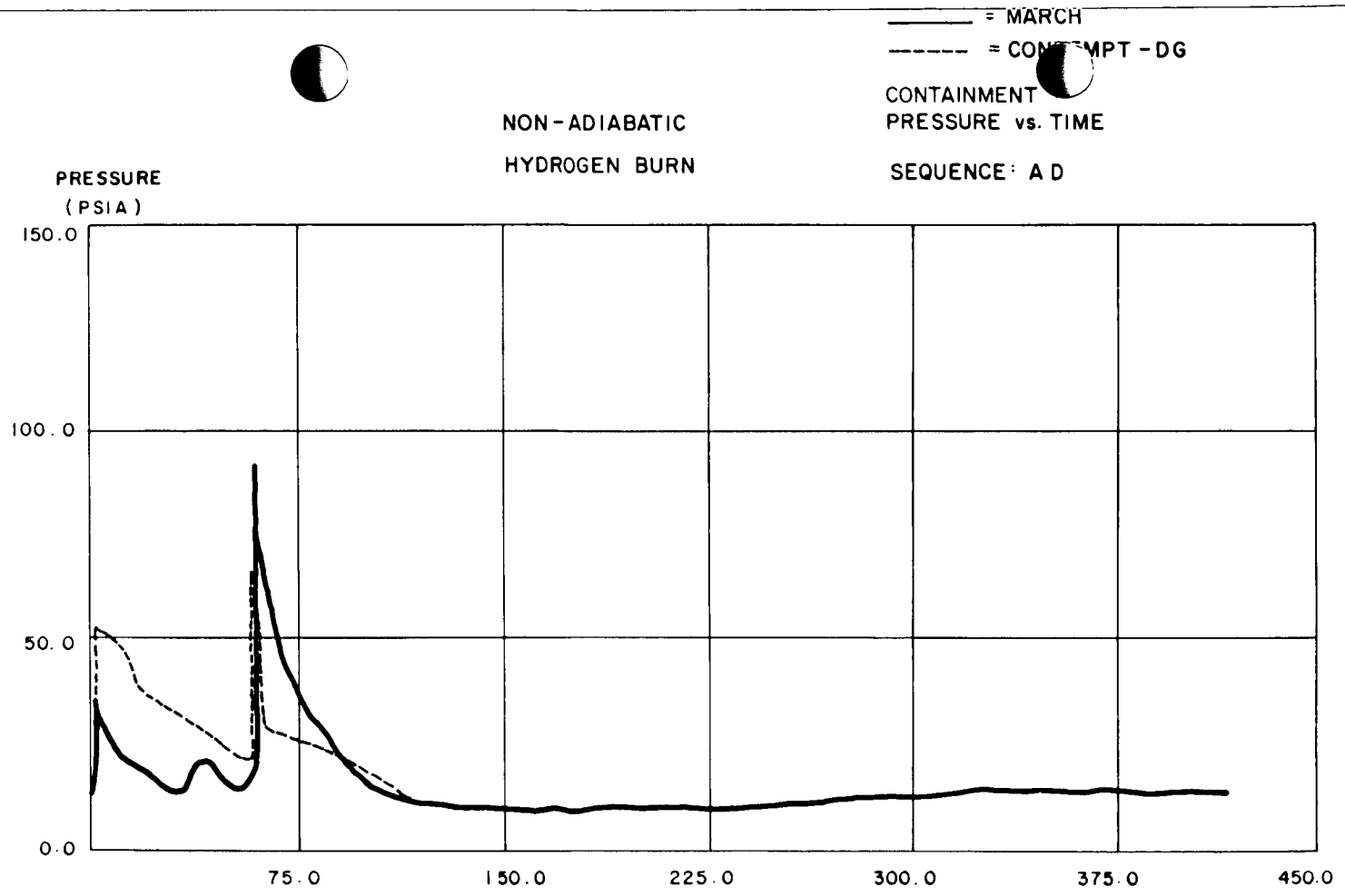

= MARCH
= CONTEMPT - DG
CONTAINMENT
PRESSURE vs. TIME
NON-ADIABATIC
HYDROGEN BURN
SEQUENCE: A D
PRESSURE
(PSIA)
150.0
100.0
50.0
0.0
75.0
150.0
225.0
300.0
375.0
450.0
TIME (MIN.)

FIGURE I

3.2 Results for the S_2D sequence

This section contains the results of the MARCH and CONTEMPT-DG calculations for the S_2D sequence. Table II contains the relevant timings of events predicted and peak pressures for each code. Figure II shows the containment pressure profiles for this scenario.

As can be seen, the containment pressures during the blow-down phase of the sequence are slightly different. The reason for this is simply the calculational differences for primary system leakage. CONTEMPT-DG assumes an ideal gas for its penetration (primary system) leakage. Since the density of the steam-gas mixture is substantially higher than the expected densities that the equations were designed for, a higher mass transfer rate is calculated, resulting in a slightly higher containment pressure during the blow-down phase. The main pressure spike again occurs following vessel failure as a result of hydrogen burning.

TABLE II
SEQUENCE: S_2D (2" break)

	MARCH	CONTEMPT-DG
SPRAY ON:	90.3	30.0 MIN.
CORE UNCOVER:	44.6	42.1 MIN.
CORE MELT START:	70.5	69.6 MIN.
CORE SLUMP:	89.5	93.9 MIN.
VESSEL FAIL:	89.8	94.7 MIN.
HYDROGEN BURN:	89.9	94.8 MIN.
MAX. PRESSURE--NON-ADIABATIC H_2 BURN AT VESSEL FAILURE:	84.0	76.4 PSIA

3.3 Results for the S_2B sequence

This section contains the results of the MARCH and CONTEMPT-DG calculations for the S_2B sequence. Table III contains the relevant timings of events predicted and peak pressures for each code. Figure III shows the

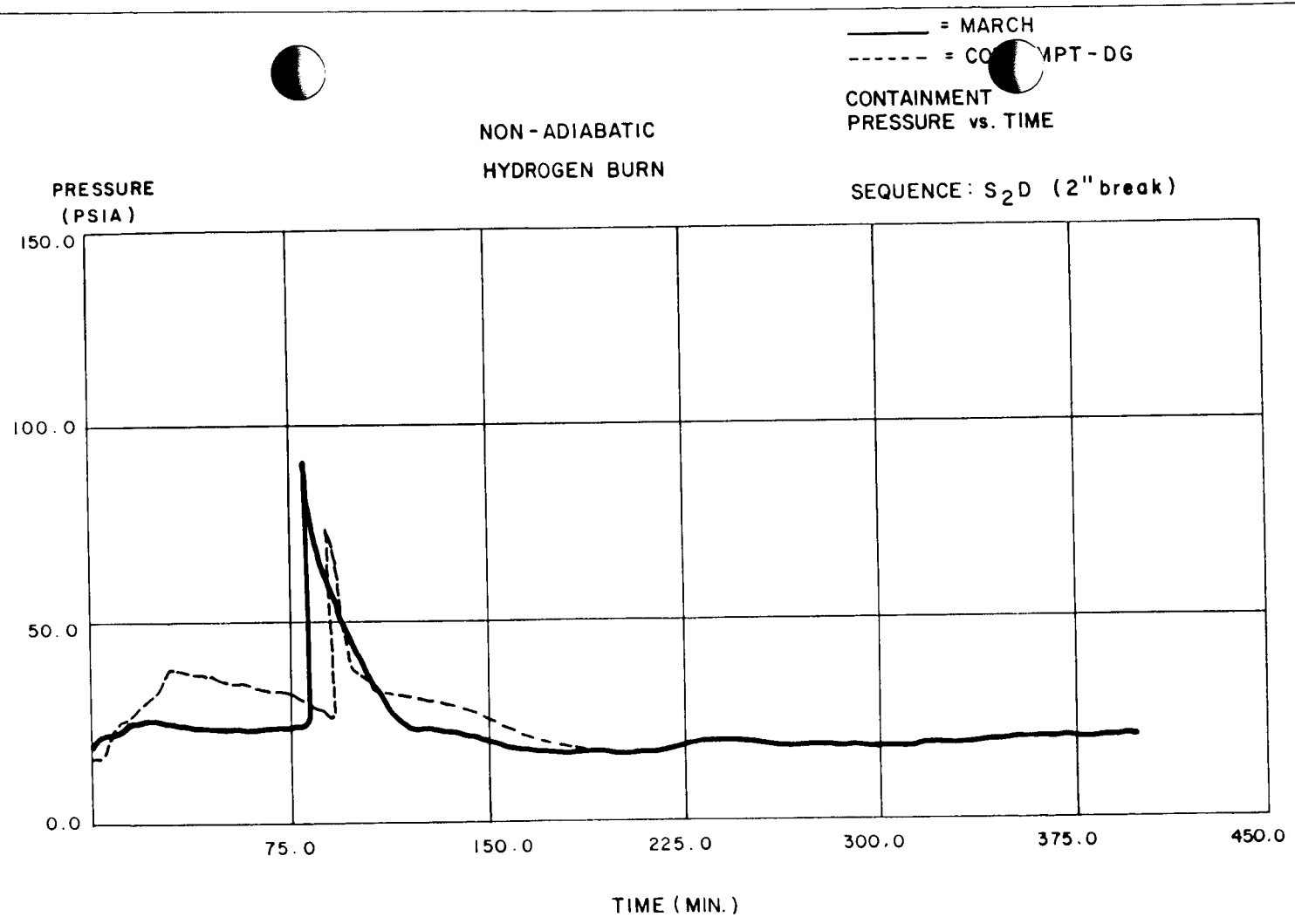

_____ = MARCH
------ = COMPT-DG
CONTAINMENT
PRESSURE vs. TIME
NON-ADIABATIC
HYDROGEN BURN
SEQUENCE: S2D (2" break)
PRESSURE
(PSIA)
150.0
100.0
50.0
0.0
75.0
150.0
225.0
300.0
375.0
450.0
TIME (MIN.)

FIGURE II

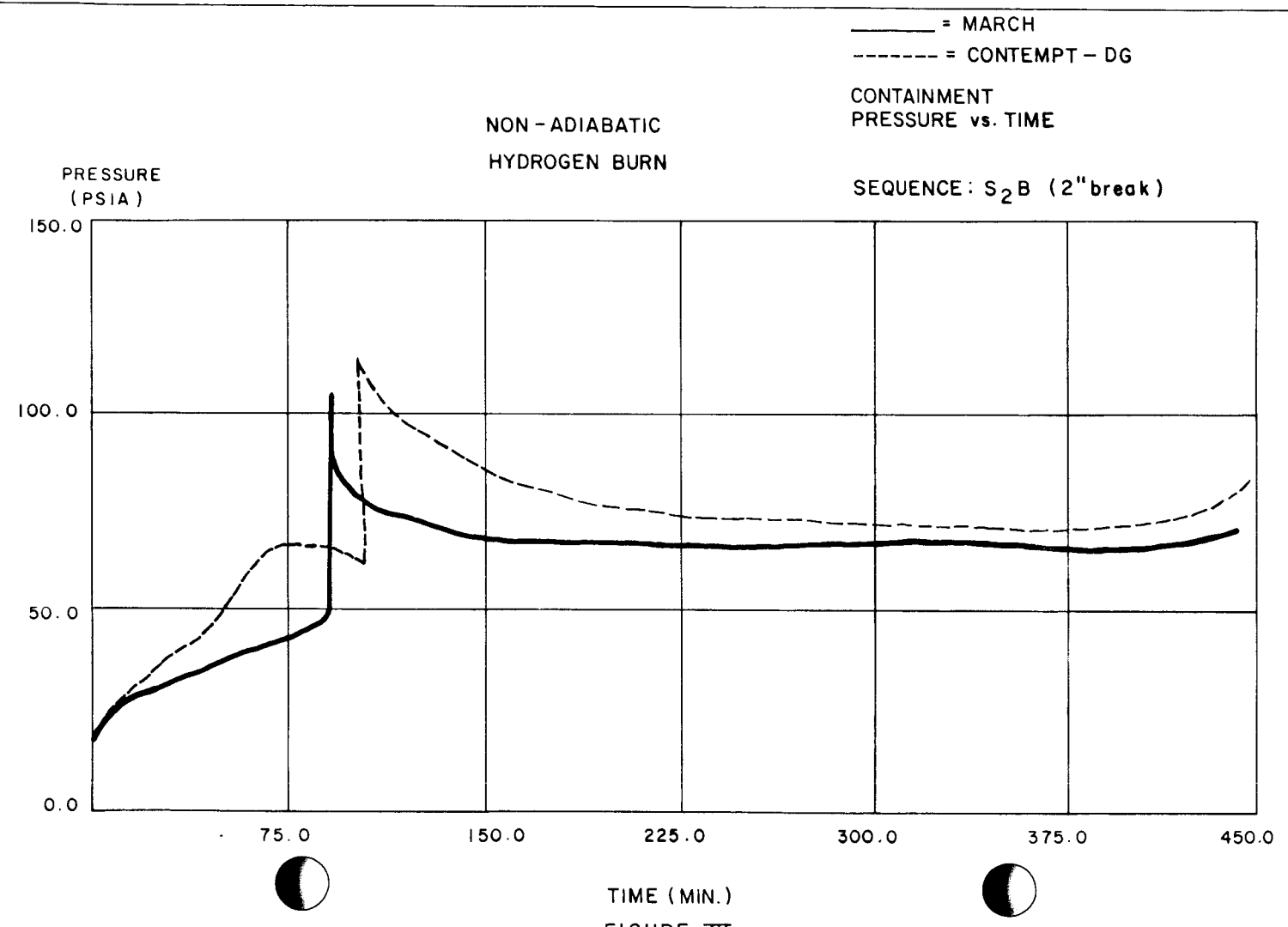

_____ = MARCH
------- = CONTEMPT – DG
CONTAINMENT
PRESSURE vs. TIME
NON-ADIABATIC
HYDROGEN BURN
SEQUENCE: S2B (2"break)
PRESSURE
(PSIA)
150.0
100.0
50.0
0.0
75.0
150.0
225.0
300.0
375.0
450.0
TIME (MIN.)

FIGURE III

containment pressure profiles for this scenario. The containment pressure profiles during the blowdown phase are similar to those seen for the S_2D case and the slight difference between the code results is again due to calculational differences for primary system leakage. The main pressure spike again occurs following vessel failure as a result of hydrogen burning. However, in this case, CONTEMPT-DG predicts a higher containment peak pressure than MARCH, approximately 8.7 psi. The reason for this is because in this sequence there are no containment sprays or fan coolers operating. Since the differences in leakage modelling in CONTEMPT-DG result in a slightly higher containment pressure during the blowdown phase this increase would also be superimposed on the pressure peak because there are no sprays or fan coolers operating to reduce it in this scenario.

TABLE III
SEQUENCE: S_2B (2" break)

	MARCH	CONTEMPT-DG	
SPRAY ON:	--	---	MIN.
CORE UNCOVER:	44.6	42.1	MIN.
CORE MELT START:	70.5	69.5	MIN.
CORE SLUMP:	88.9	95.4	MIN.
VESSEL FAIL:	89.8	99.3	MIN.
HYDROGEN BURN:	90.0	103.0	MIN.
MAX. PRESSURE--NON-ADIABATIC H_2 BURN AT VESSEL FAILURE:	103.5	112.2	PSIA

4.0 Conclusions

Results from the previous section demonstrate that in spite of variations in models for the two computer codes, both give similar results. The sensitivity of each code to various parameters, however, is not similar. These differences in sensitivity will be addressed in another paper which is to be given at this conference.[3] How various safeguard systems are modelled in each code can have a marked effect on the overall results (i.e., containment peak pressure). It

is felt however, that each code has various limitations and various good points. In the two tables below, what is felt to be limitations and good points for each code relative to the other are shown.

MARCH

Good Points	Limitations
1) Inexpensive and easy to use.	1) Questionable conservation of mass and energy.
2) Can perform compound/ sequential event analyses relatively easily.	2) Cannot perform subcompartment analyses.
3) Can perform sensitivity analyses on hydrogen burns.	3) Questionable model for BWR's.
4) Can perform debris bed. particle size parametric studies (i.e., HOTDROP).	4) Constant heat removal rates for fan coolers.
	5) Limited heat structure modeling capabilities.

CONTEMPT-DG

1) Has conservation of mass and energy.	1) Ice condenser plants are very difficult to model
2) Can perform hydrogen volume parametric analyses.	2) Has limited in-vessel phemomenology.
3) Has good flexibility and versatility (containment sensitivity analyses).	3) Has very simple hydrogen burn mode (flame-temperature criteria only).
4) Can perform subcompartment analyses.	4) Blowdown model may be overly conservative.
5) Models for engineered safety features reflect more accurately real plant conditions.	

4.1 Future enhancements to CONTEMPT-DG

A substantial amount of research and development work has been done recently and more is contemplated for the future for degraded core phenomena. Based on the review of exisitng work done, certain enhancements to CONTEMPT-DG are planned. The various enhancements planned are listed below and whether the enhancement requires an extensive (major) or minor re-programming effort.

1) Incorporate two-phase flow subroutines associated with BWR's in intercompartmental leakage calculations for PWR cases. (Major)

2) Make CORCON an option for core-concrete interactions. (Minor)

3) Incorporate ablation model (subroutine Henry) in vessel failure section of the code. (Minor/ Major)

4) Review and modify blowdown model. (Major)

5) Correct error in large timestep option for intercompartmental flow calculations. (Minor)

REFERENCES

1). R.O. Wooton, H.I. Avci, "MARCH (Meltdown Accident Response Characteristics) Code Description and Users Manual", Battelle Columbus Laboratories, NUREG/CR-1711, BMI-2064, October, 1980.

2). R.L. Ritzman, Z.T. Mendoza, V.E. Denny, D.E. Stevenson, "RECAP (Reactor Accident Consequence Analysis Program) Code", Electric Power Research Institute, Palo Alto, California, July, 1980.

3). S.S. Iyer, R.E. Deem, "Effects of Hydrogen Burning and Associated Engineered Safety Features on Containment Building Response", 2nd International Workshop on the Impact of Hydrogen on Water Reactor Safety, Alburquerque, New Mexico, October, 1982.

EFFECTS OF HYDROGEN BURNING AND ASSOCIATED ENGINEERED SAFETY FEATURES ON CONTAINMENT BUILDING RESPONSE

by

Shrinivas S. Iyer and Richard E. Deem

A B S T R A C T

It is established that large amounts of hydrogen can be generated during degraded core events. The burning of this hydrogen can produce resulting loads which may represent a serious challenge to containment integrity.

This paper will present some perspectives on hydrogen behavior during various degraded core events for a large dry containment. The analysis addresses the hydrogen transport and its subsequent diffusion once released to the containment. Since the distribution of hydrogen in the containment depends on the rate of release and various driving forces, the effects from various subsystems (i.e. fan coolers, sprays, heat structures, etc.) are examined to determine the sensitivity of each effect on the overall containment response. The sensitivity of results due to sub-compartmentalization of the containment will also be examined. Effects from localized hydrogen pocketing and burning will be addressed with emphasis on its relative impact on containment integrity.

1.0 Introduction

The purpose of this paper is to present results of studies conducted on hydrogen behavior in the containment after its release during degraded core accidents and its effect on containment integrity. Rates and amounts of hydrogen released depend on the nature of the accident sequence. Transport of the released hydrogen and its subsequent combustion can be tracked by establishing the progression of the accident sequence taking into account effects of various subsystems in the plant, namely fan coolers, containment sprays, and effects of heat structures. Analysis discussed in the subsequent sections has been performed with the CONTEMPT-DG computer code[1]. The computer code itself was discussed in the paper previously presented by Richard Deem.

1.1 Accident Sequences Analyzed

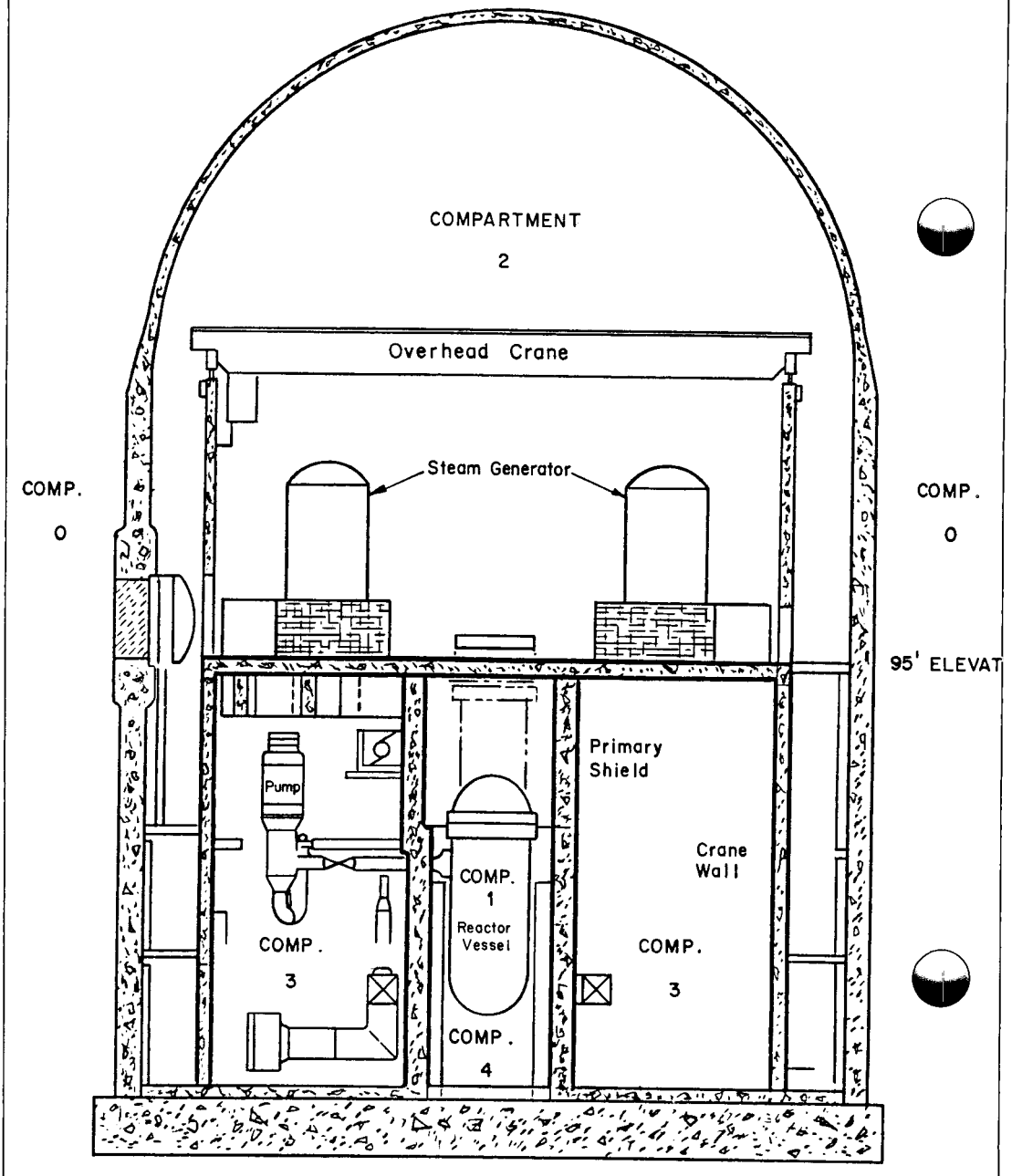
The selection of accident sequences for these studies has as its basis existing work involving complete core meltdown. Probablistic safety studies for a PWR have identified the following initiating events as the dominant ones leading to core meltdown and important in the study of hydrogen behavior. It is felt that they also represent the greatest probability of challenge to containment integrity.

1) Small break loss of coolant accident with failure of emergency core cooling (S_2D).

2) Transient involving total loss of onsite and offsite power and steam driven auxiliary feedwater pump (TMLB').

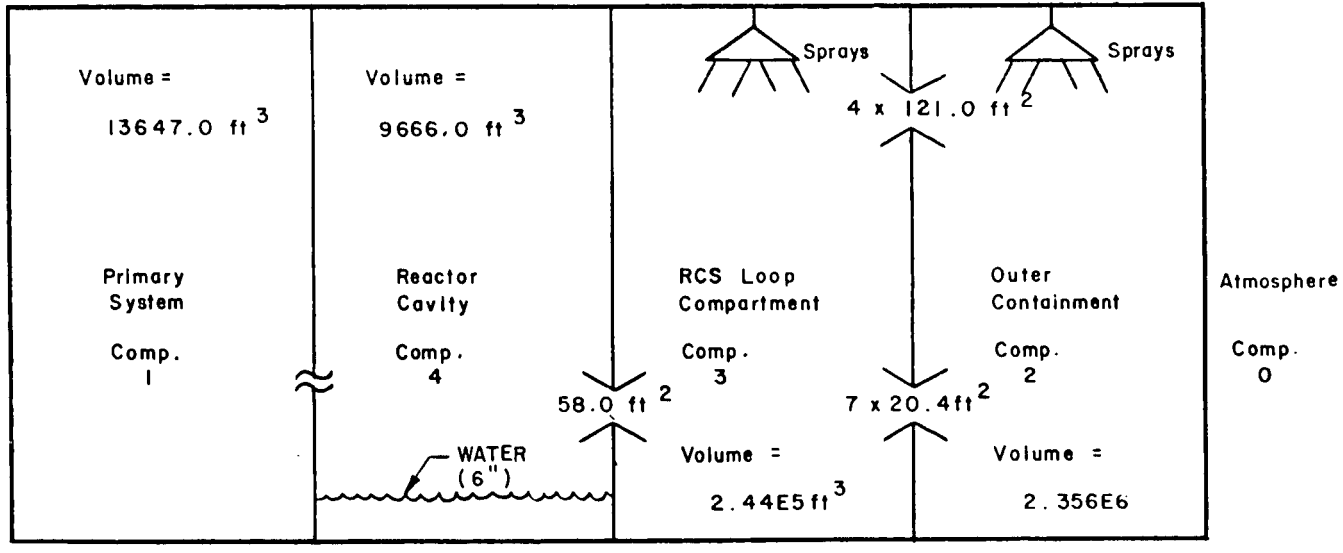
2.0 Model and Boundary Conditions Utilized

All data utilized in both analyses is based on the Indian Point 3 nuclear plant design[2]. The containment model employed in both analyses is shown in Figure I. A multi-region arrangement was used and is depicted with relative vent sizes in Figure II. Both sequences had the primary system blowdown going into compartment 4. Also, both sequences assumed that at least 6 inches of water was present in the reactor cavity (compartment 4) at the time of reactor vessel



CONTAINMENT ARRANGEMENT CROSS – SECTION

FIGURE I



MULTI-REGION CONTEMPT-DG CONTAINMENT ARRANGEMENT
FIGURE II

failure. Preliminary calculations indicated that this would probably be more conservative than the dry cavity case from the standpoint of containment pressure.

For the S_2D scenario, a nominal break size of four inches was selected. Minimum safeguards, excluding ECCS and auxiliary feedwater, were considered operable (i.e. 3 of the five fan coolers and 1 of the 2 containment spray pumps operable). In the TMLB' scenario, none of the engineered safeguards were considered operable.

3.0 Results

Figure III shows the amount of heat lost to the outside (compartment 0) as a function of time for an S_2D sequence. The amount of heat loss is depicted as a percentage of the total decay heat present in the containment. As can be seen, heat losses to the outside amount to approximately 0.55 percent of the total. However, during and just after the calculated hydrogen burn, this amount jumps to approximately 1.30 percent. Although this does not appear to be a very large percentage, considering that three fan coolers remove approximately 27.0 percent of the total amount, from the standpoint of sequence timing and the calculated amount of condensation in the containment building, it can be significant. Also, the amount of heat lost to the outside is sequence dependent. Since the amount of heat loss is proportional to the containment bulk (atmosphere) temperature, it will be greater for a TMLB' and less for a large break (i.e. AD) sequence.

Another aspect which can be important is the mode of heat transfer selected for the heat structures. Figure IV shows the heat transferred to the walls of compartment 3 during a hydrogen burn for an S_2D sequence. The dotted line depicts the amount of heat transfer by radiation while the solid line represents heat transfer by convection. As can be seen, there is a significant difference. Although the additional amount of heat transferred via radiation would ultimately return to the containment atmosphere, during the hydrogen burn interval the additional heat capacity would result in lowering the compartment atmosphere temperature. This would be translated directly to a lower compartment pressure. For an S_2D sequence, the change in heat transfer mode to radiation results in approximately a six psi decrease in compartment pressure during the hydrogen burn. Therefore, the pressure peak during the hydrogen burn would be less pronounced. Again, the magnitude of

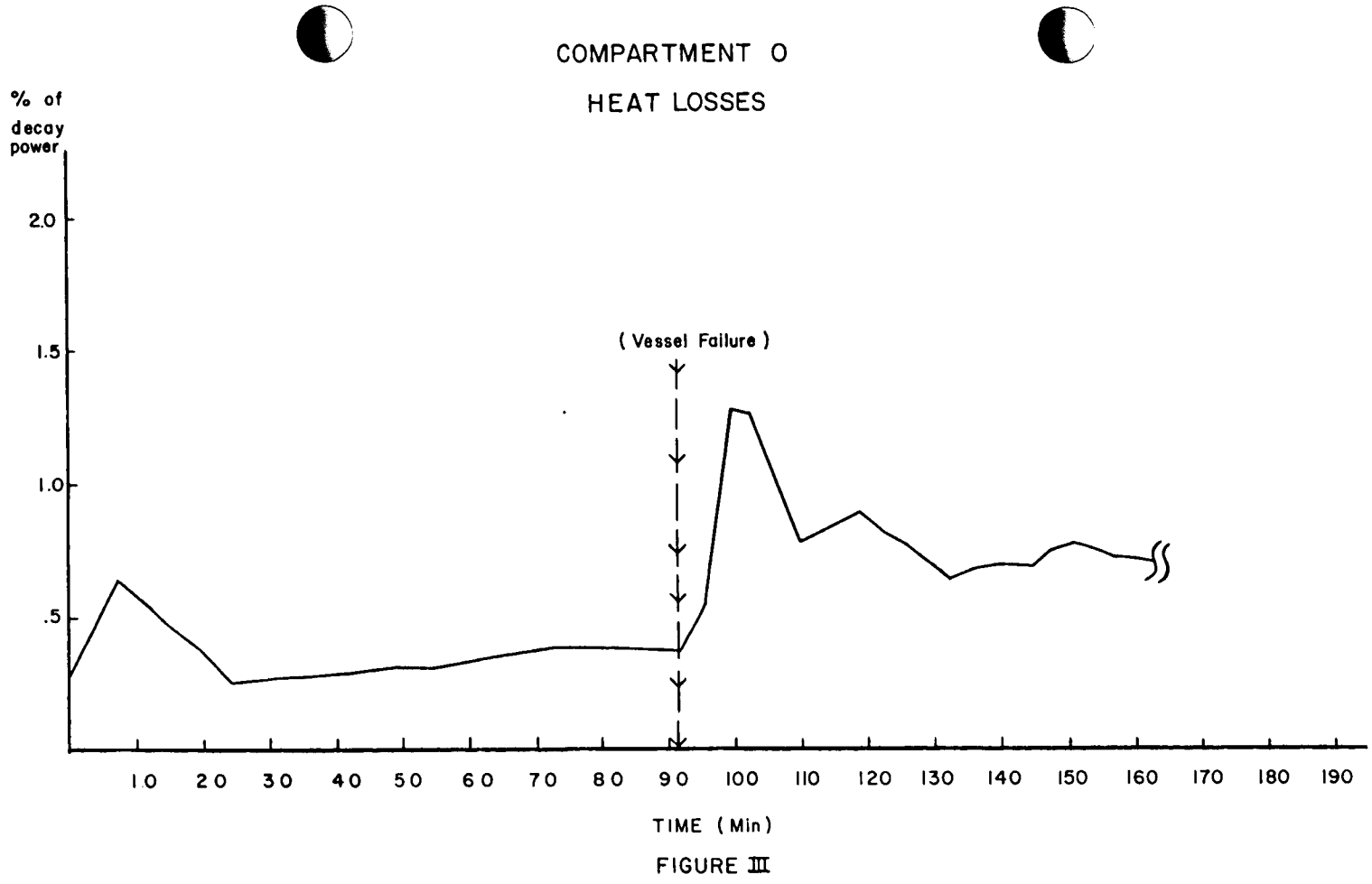

COMPARTMENT O
HEAT LOSSES
% of
decay
power
2.0
1.5
1.0
.5
(Vessel Failure)
10 20 30 40 50 60 70 80 90 100 110 120 130 140 150 160 170 180 190
TIME (Min)

FIGURE III

COMPARTMENT 3

MODE OF HEAT TRANSFER TO STRUCTURES DURING HYDROGEN BURN

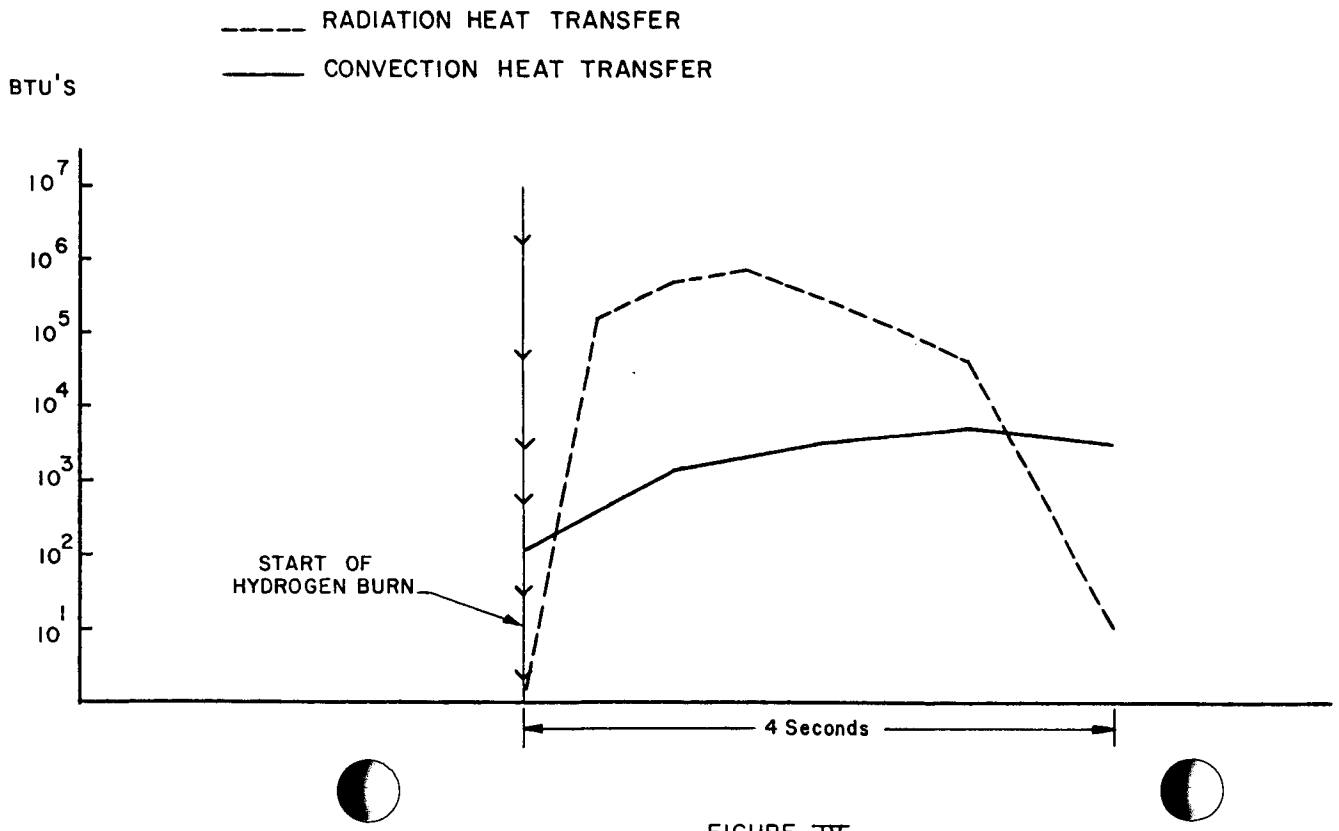


FIGURE IV

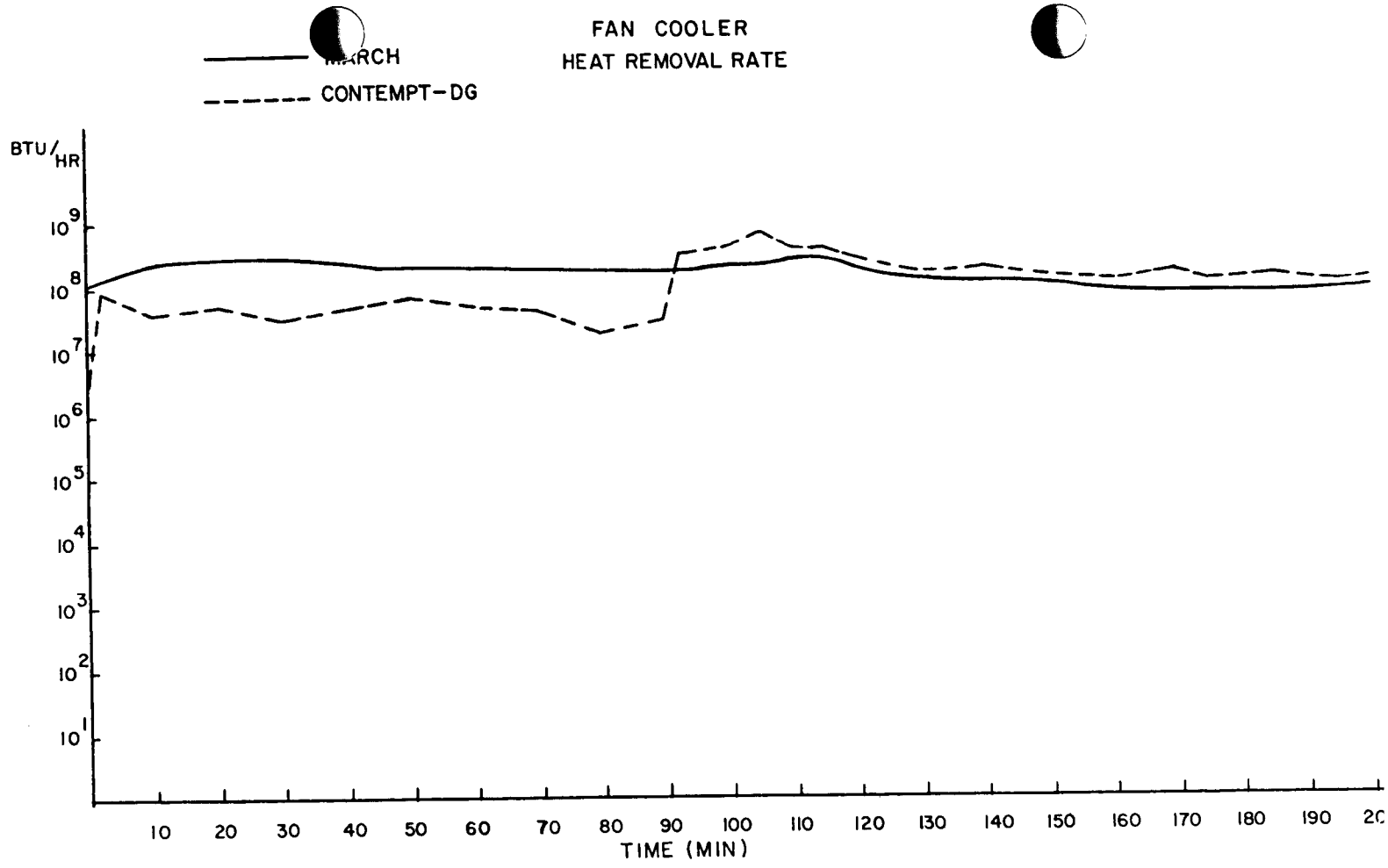

FAN COOLER
HEAT REMOVAL RATE
MARCH
CONTEMPT-DG
BTU/HR
10^9
10^8
10^7
10^6
10^5
10^4
10^3
10^2
10^1
10 20 30 40 50 60 70 80 90 100 110 120 130 140 150 160 170 180 190 20
TIME (MIN)

FIGURE V

this effect will vary with the timing and type of sequence being investigated.

Fan cooler units are an important safeguard feature in most dry containment analysis. Figure V depicts the fan cooler heat removal rate for an S_2D sequence analyzed with both the MARCH[3] computer code and the CONTEMPT-DG computer code. As can be seen on the figure, the MARCH fan cooler heat removal rate remains fairly constant while the CONTEMPT-DG case varies considerably. This is due to calculational difference, between the two computer codes. In MARCH, the rated fan cooler system heat removal capacity is input. With this rate as a basis, MARCH calculates an equivalent heat transfer area based on a normal operating condition heat transfer coefficient, and given the temperature difference between the containment atmosphere and the secondary cooling water, a resultant heat transfer removal rate is determined. CONTEMPT-DG utilizes a table of heat removal capability as a function of temperature. Heat removal differences in the early part of the scenario (blowdown phase) result in a predicted containment pressure for CONTEMPT-DG being approximately 11 psia higher than the MARCH case. This difference in modeling of the fan cooler system can have a marked effect on the predicted results. Timing of events during various scenarios can be radically changed, thereby impacting the final containment pressure. Due to the delayed accuation of the containment sprays in the MARCH case, more steam was removed (condensed) from the containment atmosphere, thus allowing for the possibility of a hydrogen burn. Also, the pressure peak during a hydrogen burm may be greater because less heat is removed from containment during this period in the MARCH case. In terms of the magnitude of this modeling difference between the two codes, it will be sequence dependent and a function of which additional engineered safety features are operational (i.e. containment spray).

In past conferences and workshops dealing with PRA analysis, various questions were raised regarding hydrogen pocketing and its impact on containment integrity. Figures VI and VII reflect subcompartment analyses for an S_2D and TMLB' sequence, respectively. Both figures consider time zero to be reactor vessel failure. For the S_2D sequence the compartment pressures equalize after approximately eight seconds. This is due primarily to the large vents between compartments, especially compartments 4 and 3. The large (first) pressure spike in compartment 4 is due to primary system blowdown and a large steam generation rate caused by the corium interacting with the

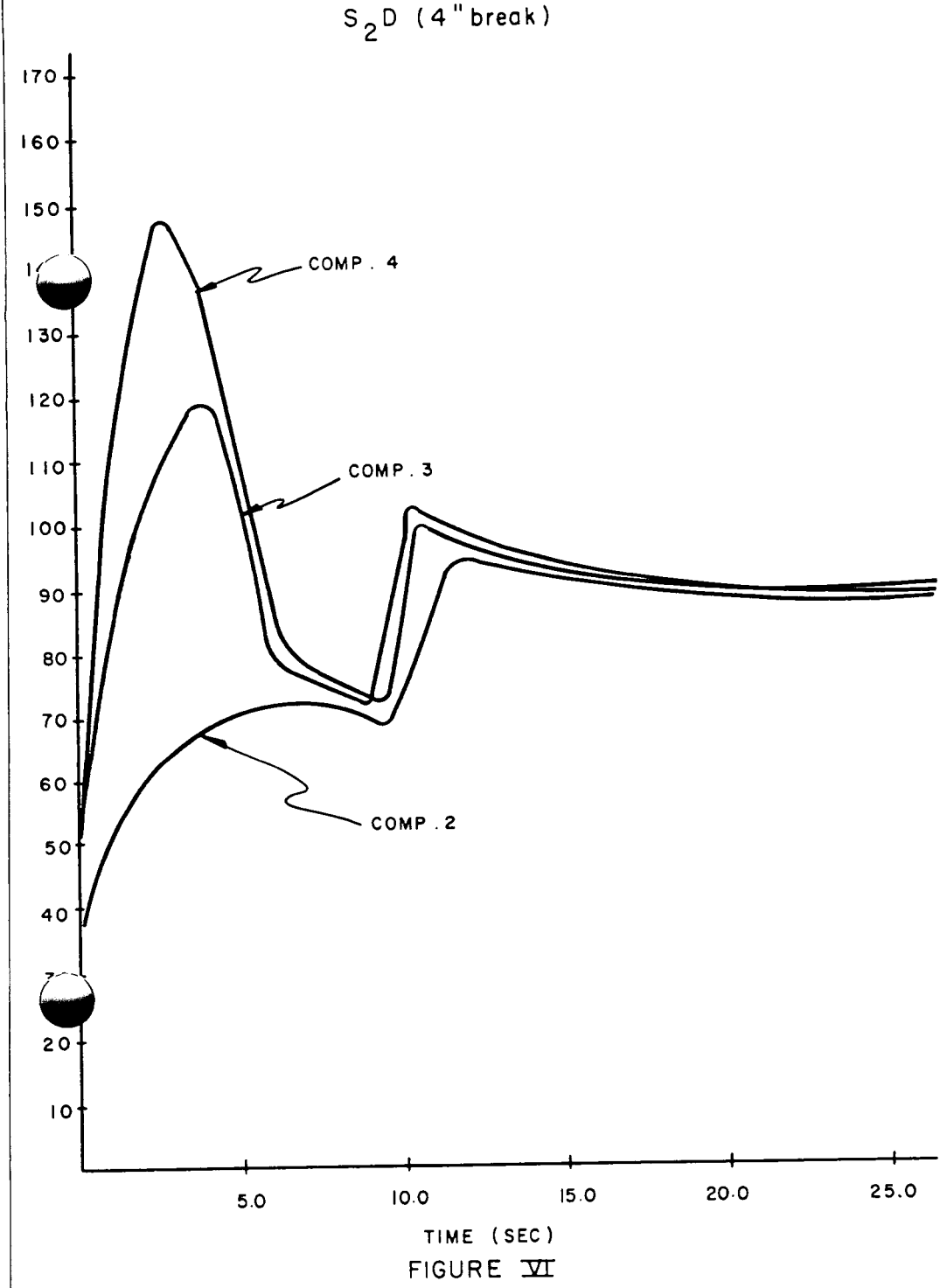

S_2D (4" break)
170
160
150
140
130
120
110
100
90
80
70
60
50
40
20
10
COMP. 4
COMP. 3
COMP. 2
5.0
10.0
15.0
20.0
25.0
TIME (SEC)

FIGURE VI

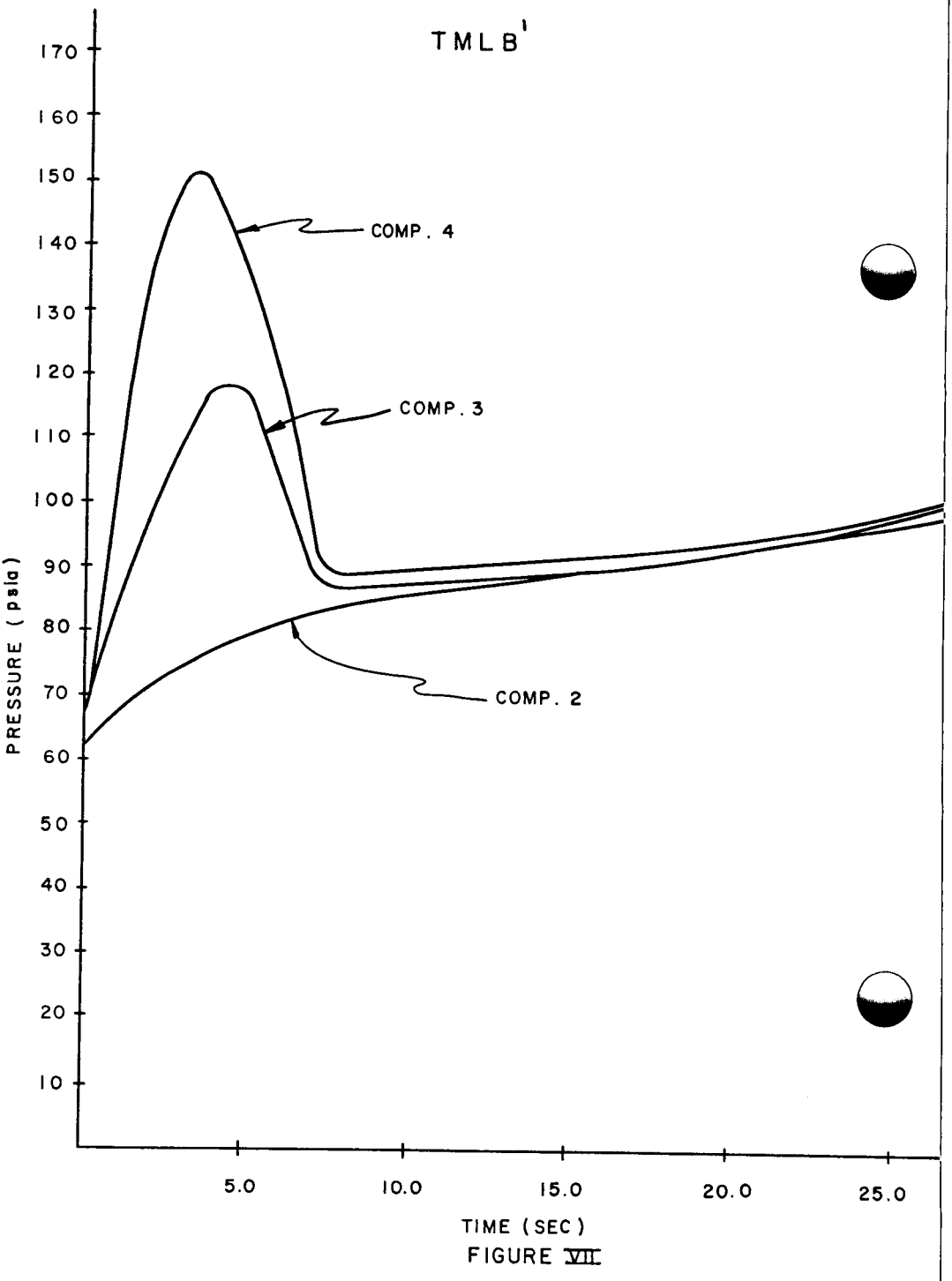

TMLB'
170
160
150
140
130
120
110
100
90
80
70
60
50
40
30
20
10
PRESSURE (psia)
COMP. 4
COMP. 3
COMP. 2
5.0
10.0
15.0
20.0
25.0
TIME (SEC)

FIGURE VII

six inches of water in the cavity area. The second spike, occurring approximately two seconds after the first pressure spike has dissapated, results from a hydrogen burn in compartment 3. Important results from this analysis are that the hydrogen burn does not occur simultaneously with vessel failure and the fact that although the pressure in compartment 3 and 4 is quite large, the pressure in compartment 2 remains relatively low. It should be noted that the containment pressure boundary is located in compartment 2. The reason for the hydrogen burn not occurring simultaneously with vessel failure, it is felt, is primarily due to the large amount of steam generated from corium interacting with cavity water. This conclusion is further demonstrated in the TMLB' case. CONTEMPT-DG did not predict a hydrogen burn subsequent to vessel failure. Since no engineered safeguards are functional during this sequence, steam blanketing has to be the primary reason for inhibiting the hydrogen burn.

4.0 Conclusions

Various conclusions can be drawn from the results contained in this paper. However, for the values obtained, the results have a relative error associated with them of ± 10%. This is due to limitations in the codes utilized and in some cases, simplification of the phenomenology involved in this type of analysis.

Heat transfer to the outside atmosphere should be considered for certain sequences. This will effect the timing of various sequences which can change the consequences resulting from these scenarios, in particular, the sequences involving total loss of onsite and offsite power. Similarly, the modeling of the fan cooler can have a rather large effect on sequence timing and overall containment pressure response, in that it may inhibit a hydrogen burn or cause actuation of the containment spray system. It is felt that CONTEMPT-DG more accurately reflects how the fan cooler system functions under accident conditions.

Heat transfer mode of heat sinks during a hydrogen burn is also important. Effects of radiation heat transfer should be considered during hydrogen burns. Although results presented in this paper were pronounced, it is felt they may be conservative. Results calculated by CONTEMPT-DG were low compared to results obtained by hand calculations in a paper[4] given at the first workshop on hydrogen behavior.

Certain conclusions can be drawn from the subcompartment analysis performed in this paper. However, it should be pointed out that results for this type of analysis are highly dependent on containment arrangement (i.e. intercompartmental vent sizes), boundary conditions selected, and limitations that exist in the computer code modeling. In the S_2D case, the hydrogen burn in compartment 3 rapidly occurs following vessel failure blowdown. Hand calculations showed that the time interval between the end of vessel failure blowdown and commencement of the hydrogen burn should be 4.5 seconds rather than the code predicted 2 seconds. Even with this conservatism it is not possible for a hydrogen burn to occur concurrently with the vessel failure pressure pulse for wet cavity cases. The most salient conclusion of the subcompartment analysis is that hydrogen burns in subcompartments may not necessarily be more deleterious, as is currently advocated. Depending on the particular containment arrangement, it may be advantageous from a containment integrity standpoint.

Lastly, what we attempted to show in this paper is that various aspects of the phenomenology associated with degraded core events are very important to the overall results (i.e. containment integrity). It is hoped that the results presented will assist others in their studies of degraded core events.

REFERENCES

1.) R.E. Deem, Kenneth Rousseau, "The CONTEMPT-DG Containment Analysis Code", 2nd International Workshop on the Impact of Hydrogen on Water Reactor Safety, Alburquerque, New Mexico, October, 1982.

2.) Indian Point Nuclear Generating Unit No. 3, FSAR, Docket No. 50-286

3.) R.O. Wooton, H.I. Avei, "MARCH (Meltdown Accident Response Characteristics) Code Description and Users Manual", Battelle Columbus Laboratories, NUREG/CR-1711, BMI-2064, October, 1980.

4.) R.J. Tosetti, C.F. Guenther, "Evaluation of H_2 Combustion and Control Under Degraded Core Conditions for Pilgrim-2", 1st International Workshop on the Impact of Hydrogen on Water Reactor Safety, Alburquerque, New Mexico, January, 1981.

Applications of HECTR to Reactor Containments

Susan E. Dingman
Michael J. Wester*
Allen L. Camp

SANDIA NATIONAL LABORATORIES
Albuquerque, New Mexico 87185

*The Dikewood Corporation

Introduction

This paper presents the results of calculations performed with HECTR[1], a computer program developed at Sandia National Laboratories to model nuclear plant containment responses to transients that include hydrogen burns. Calculations were performed for Grand Gulf, a Mark III boiling water reactor, and Sequoyah, a pressurized water reactor with ice condensers. The transients analyzed were for a stuck-open relief valve and a small break loss-of-coolant accident (LOCA). Failure of emergency core coolant injection was assumed for both transients, leading to the production of a significant amount of hydrogen. Both Grand Gulf and Sequoyah are equipped with deliberate hydrogen ignition systems which were designed to ignite hydrogen/air mixtures at low hydrogen concentrations; the intent is to subject the containment to lower peak pressures than would occur if larger concentrations accumulated and were accidently ignited. HECTR calculations were performed for both plants to determine the containment response to the transients including burns due to deliberate ignition.

Grand Gulf Calculations

A schematic of the Grand Gulf containment is shown in Figure 1. The containment can be divided into four discrete regions: drywell, wetwell, annular region, and dome region. The drywell is located in the center of the containment. The wetwell is an open annular region that surrounds the drywell and extends from the surface of the suppression pool to the 135' elevation. Above the wetwell is another annular region, which extends from the 135' elevation to the 209' elevation. This annular region is very cluttered with equipment and structures. The final region in the containment is the dome, a large, relatively empty volume which extends from the 209' elevation upward to 290'.

Calculations were performed for the Grand Gulf reactor using three different compartmentalizations. The HECTR base-case calculation used the two compartment model shown in Figure 2A. The dome region was modelled as one compartment and the annular and wetwell regions were lumped together for the second compartment. The drywell was not included in the model. A stuck-open relief valve transient was analyzed in which all of the steam was assumed to condense in the suppression pool, such that only hydrogen was injected into the wetwell. The injection rate was calculated by MARCH[2] and was used in similar utility calculations.[3] The HECTR calculations started when significant hydrogen generation began, rather than at the beginning of the accident. The hydrogen ignition and upward propagation limits for this calculation were assumed to be 8 percent and 4.1 percent, respectively. Combustion was assumed to be 100% complete.

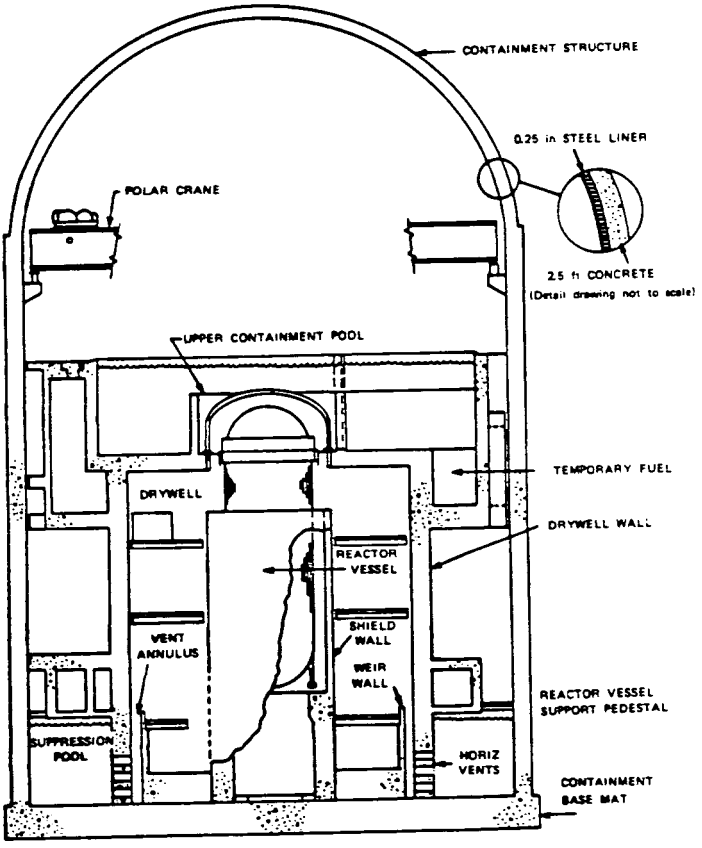


Figure 1. Schematic of Grand Gulf Containment

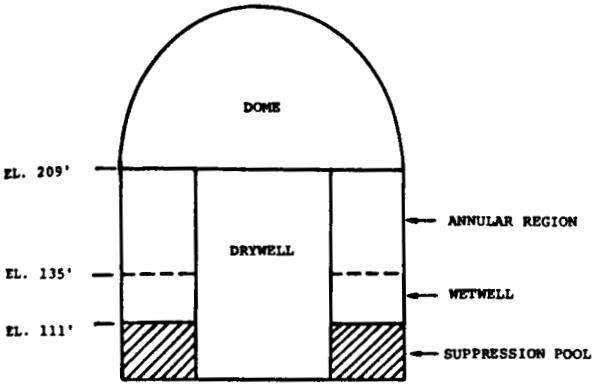


Figure 2A. Base Case Model

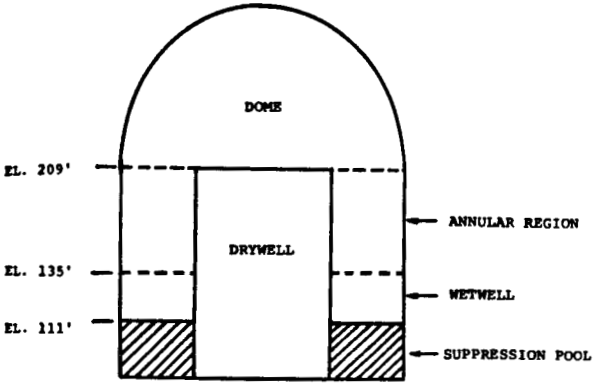


Figure 2B. One-compartment Model

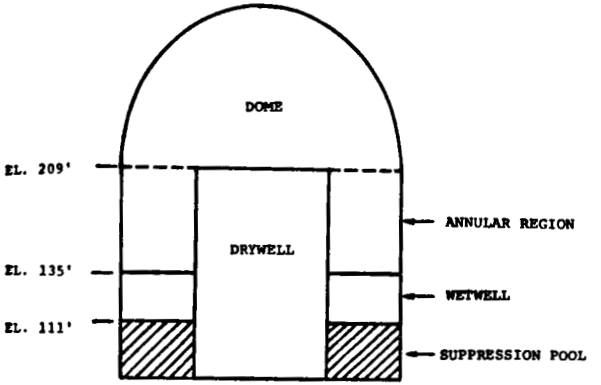


Figure 2C. Alternate Two-compartment Model

The containment pressure for the base case is shown in Figure 3. There were several relatively small pressure spikes corresponding to burns in the bottom compartment and one larger pressure spike that corresponded to a burn that started in the bottom compartment and then propagated into the top compartment. The pressure spikes for the burns occurring in the bottom compartment were small because the combustion gases expanded into the larger volume of the second compartment as it burned, relieving the pressure. The pressure spike for the burn which propagated into the top compartment was larger because more total hydrogen was burned and less gas expansion occurred as the top compartment burned. However, the pressure was still relatively small because the hydrogen concentration in the top compartment was only slightly above the 4.1 percent propagation limit.

Figure 4 shows the containment pressure calculated for the same transient but with the two compartments used in the base case combined into a single compartment (see Figure 2B). Since the hydrogen injection rate is the same as in the base case but the volume of the compartment it enters is larger, it takes longer for the hydrogen concentration to reach the ignition limit. Therefore, there are fewer burns than in the base case. However, they are more severe, because more total hydrogen is consumed in each burn and the one-compartment model does not allow pressure relief by venting to another compartment.

A calculation was also performed using the two compartment model shown in Figure 2C which considered the wetwell as one compartment and combined the annular and dome regions into the second compartment. This two compartment model gave significantly different results from the two compartment model used in the base case Figure 5 shows the containment pressure for the calculation. As in the base case, there are several small pressure spikes corresponding to burns in the bottom compartment. The pressure spikes are smaller than in the base case because the ratio of the top to bottom volumes is higher in this model, allowing more pressure relief. The burns are also more frequent since it takes less time for the hydrogen to reach the ignition limit in this smaller volume. At about 3400 seconds, enough oxygen has been depleted, due to the repeated burns, to inert the bottom compartment. This inerting did not occur in the base case because more oxygen was available in the bottom since its volume was larger. After the bottom compartment inerted, the hydrogen was gradually pushed into the top compartment until it reached the ignition limit and burned. The burning then pushed oxygen back down into the wetwell and the flame was able to propagate into the lower compartment. This burn was much more severe than the propagating burn in the base case because it occurred in an about 8 percent hydrogen mixture rather than about a 4 percent hydrogen

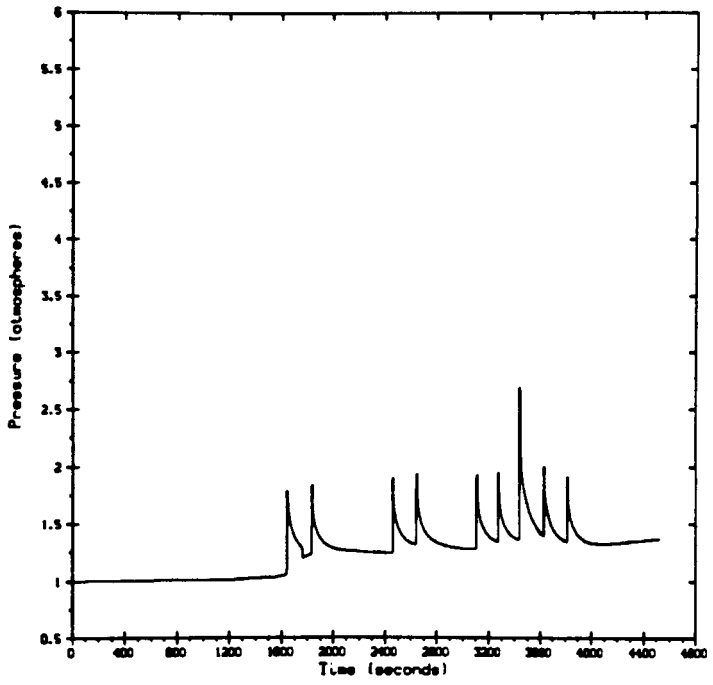


Figure 3. Containment Pressure for Grand Gulf Base Calculation

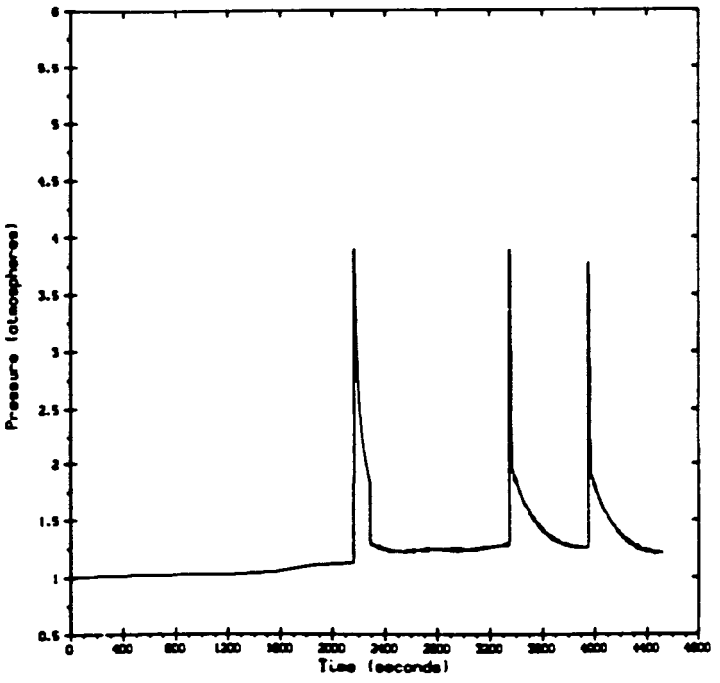


Figure 4. Containment Pressure for Grand Gulf Calculation using the One-compartment Model

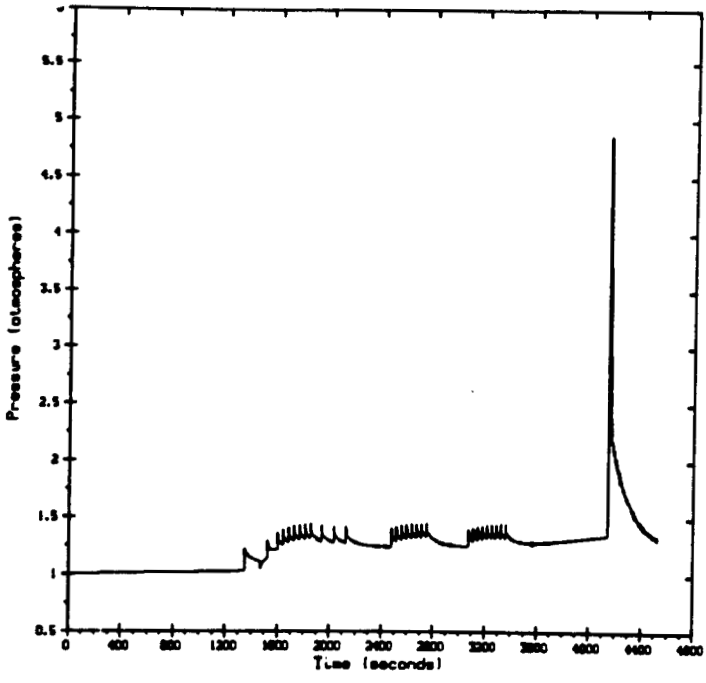


Figure 5. Containment Pressure for Grand Gulf Calculation using the Alternate Two-compartment Model

mixture. The wet-well inerting that resulted in this more severe burn may not be realistic. Codes such as HECTR do not properly model convective mixing. The mixing within a compartment is overpredicted and the mixing between compartments is underpredicted. Therefore, the amount of oxygen returning to the well from the top compartment as well as the amount of hydrogen reaching the top are underpredicted. This problem is currently being investigated.

The three calculations discussed above have shown that the HECTR results for Grand Gulf calculations are sensitive to the compartmentalization used. One-compartment models are typical of very rapid mixing, and the two-compartment models are typical of slower mixing. Even when the same number of compartments were used, very different results were calculated when the volume distribution between the compartments was changed. Further details of these and other cases considered for the Grand Gulf reactor are discussed in reference 4.

A sensitivity study was also performed to evaluate the effects of varying the flame speed (and hence, the burn time) for the one-compartment model undergoing a 10 percent hydrogen burn. The flame speed was varied over a range of two orders of magnitude, from 42 to 0.42 m/s. The results are presented in Figure 6, in which the ratio of the peak pressure calculated with HECTR to the pressure that would result from an adiabatic burn is plotted against the burn time. Results are plotted both with sprays on and sprays off. In both cases, longer burn times resulted in peak pressures that were further below adiabatic than for shorter burn times since there was more time available for heat transfer from the gas. The pressure reduction was more pronounced with the sprays on than with the sprays off due to the large heat absorbing capacity of the sprays.

Sequoyah Calculations

A schematic of the Sequoyah containment is shown in Figure 7. The containment can be divided into the following regions: lower compartment, dead-ended region, ice condenser, and upper compartment. The lower compartment is the center region of the containment enclosing most of the primary system components. Surrounding the lower compartment is the dead-ended region. Both of these regions are very cluttered with equipment and structures. The upper compartment is a large, relatively open region above the lower compartment and dead-ended region. The primary flow path from the lower compartment to the upper compartment is through the ice condenser. Air return fans circulate air from the upper compartment down to the dead-ended region and into the lower compartment during accident conditions. The ice condenser consists of a lower plenum, the region containing the ice, and an upper plenum. Three sets of doors are included in the ice condenser which are

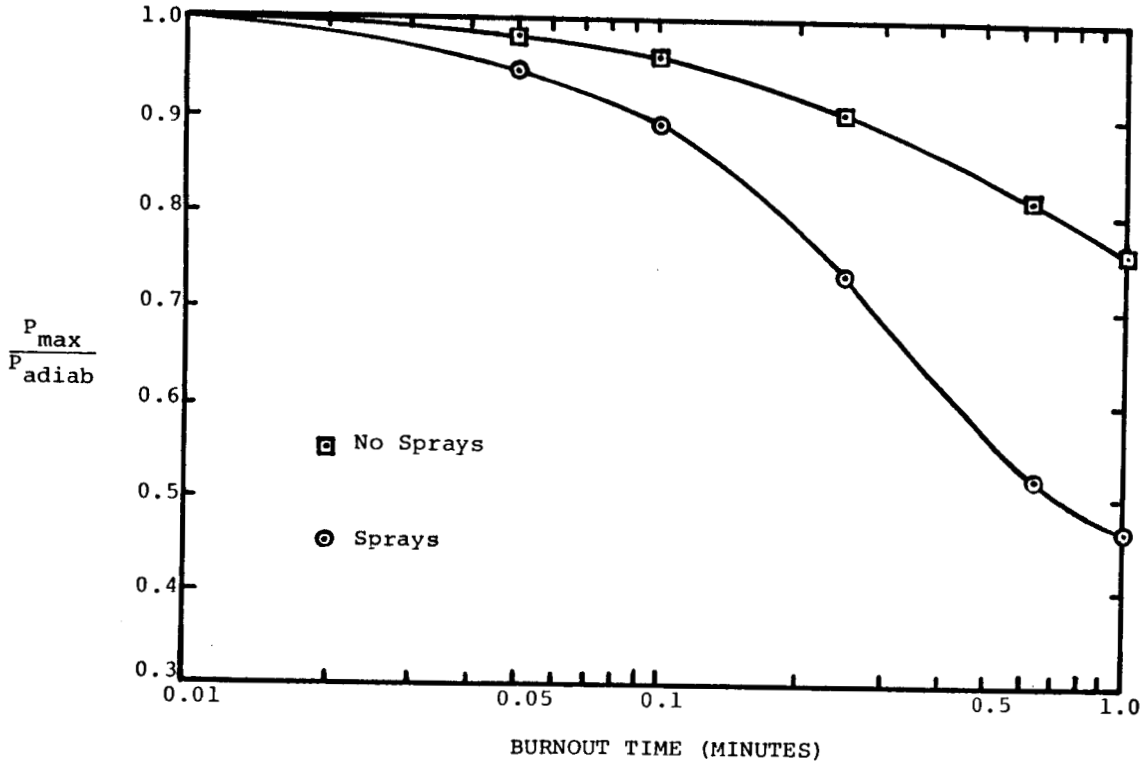


Figure 6. Effect of Hydrogen Combustion Burn Time on the Peak Pressure P[illegible]cted by HECTR

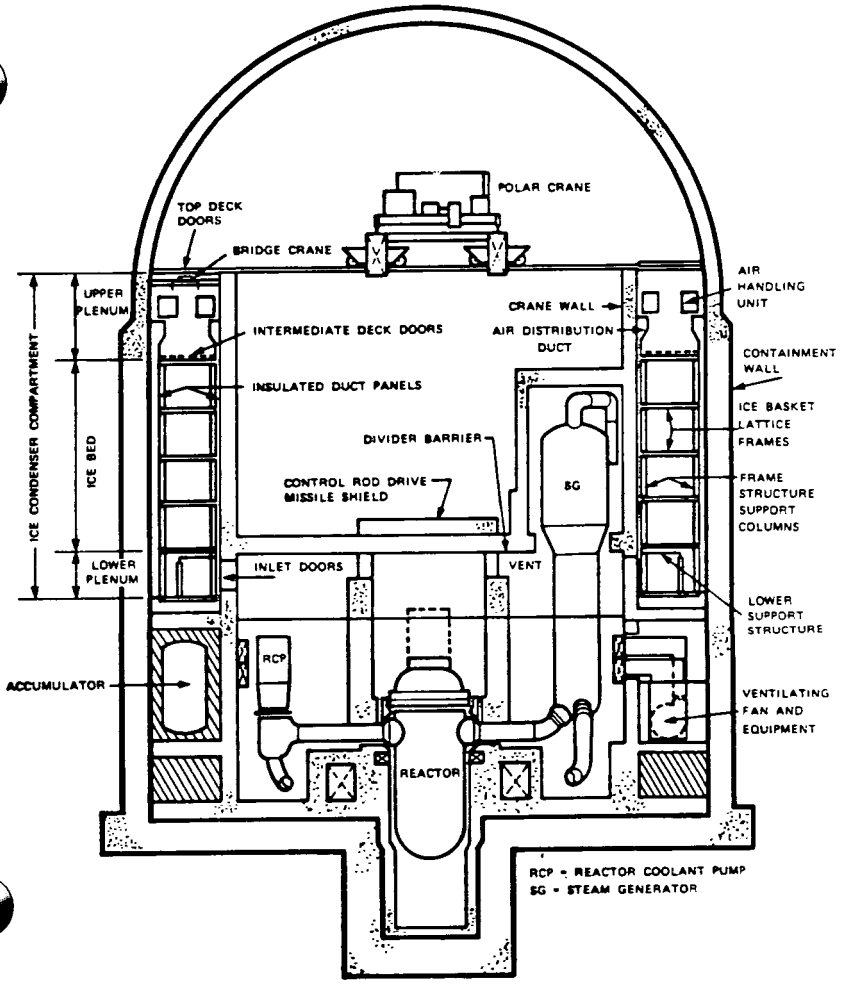


Figure 7. Schematic of Sequoyah Containment

closed during normal operating conditions. The doors located at the lower plenum inlet and those located between the ice region and the upper plenum open when a small differential pressure is exceeded, then re-close when the differential pressure returns a lower value. Once fully open, the doors which separate the upper plenum and the upper compartment are expected to remain open. Igniters are located in all regions of the containment except the lower plenum and the ice basket region of the ice condenser.

The compartmentalization used for the HECTR calculation is shown in Figure 8. The upper compartment, lower compartment, and dead-ended region were each modelled as a separate compartment. The ice condenser was modelled as three compartments. The upper plenum was modelled as a separate compartment since there are igniters located in this region. The remainder of the ice condenser was divided into two equal-sized compartments. Flow through the doors at the lower plenum inlet and the doors above the ice was only allowed in one direction. Both fans, but only one spray train, were assumed to be operating. The ignition limit was 8 percent hydrogen and the upwards, horizontal, and downward propagation limits were 4.1 percent, 6 percent, and 9 percent hydrogen, respectively. Ignition was suppressed in the ice region where there are no igniters. Hydrogen and steam were injected into the lower compartment using injection rates calculated by MARCH for a small break LOCA.[5]

The upper compartment pressure history calculated by HECTR is shown in Figure 9. Between about 4200 and 5200 s, burns occur in the upper plenum because the condensation of steam in the ice condenser yields a higher concentration of hydrogen in the mixture leaving the ice condenser than exists in the lower compartment. Most of the pressure rises during this time are small because the gas can expand into the upper compartment as it burns. The larger pressure spikes during this time correspond to burns that start in the upper plenum, then propagate into a relatively lean mixture in the upper compartment. After all the ice melts, no steam is removed from the flow, so the hydrogen concentration is unchanged in the ice condenser. Thus, no further deflagrations are initiated in the upper plenum. Since the hydrogen injection rate is relatively small by this time, the hydrogen can be spread fairly uniformly through the containment, rather than accumulating and then burning in the lower compartment. By the time the lower compartment reaches the ignition limit, the rest of the containment is just below the limit. Thus a severe burn occurs which starts in the lower compartment, then propagates into a relatively uniform mixture throughout the containment.

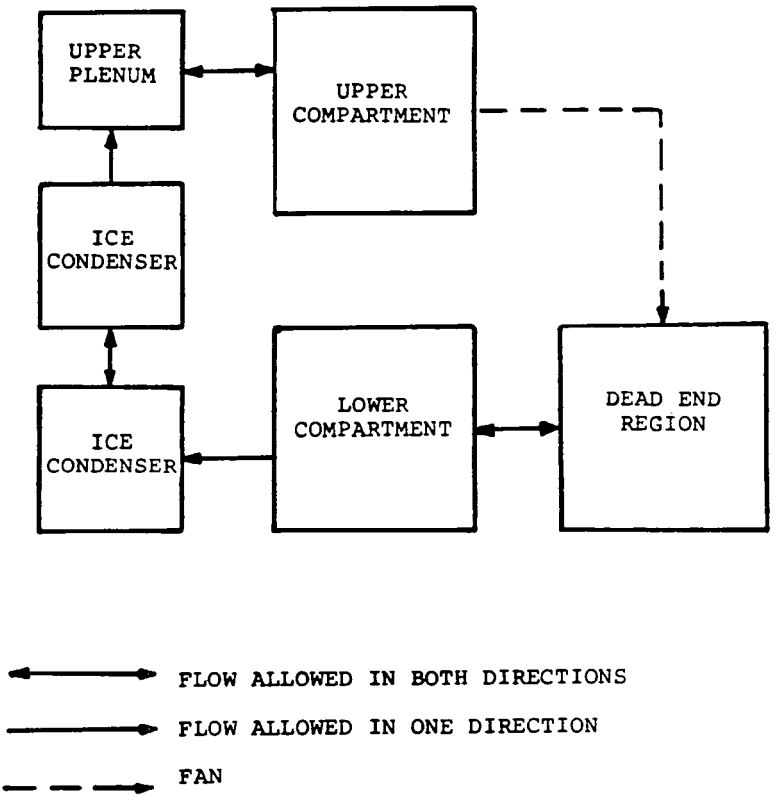


Figure 8. Sequoyah Compartmentalization

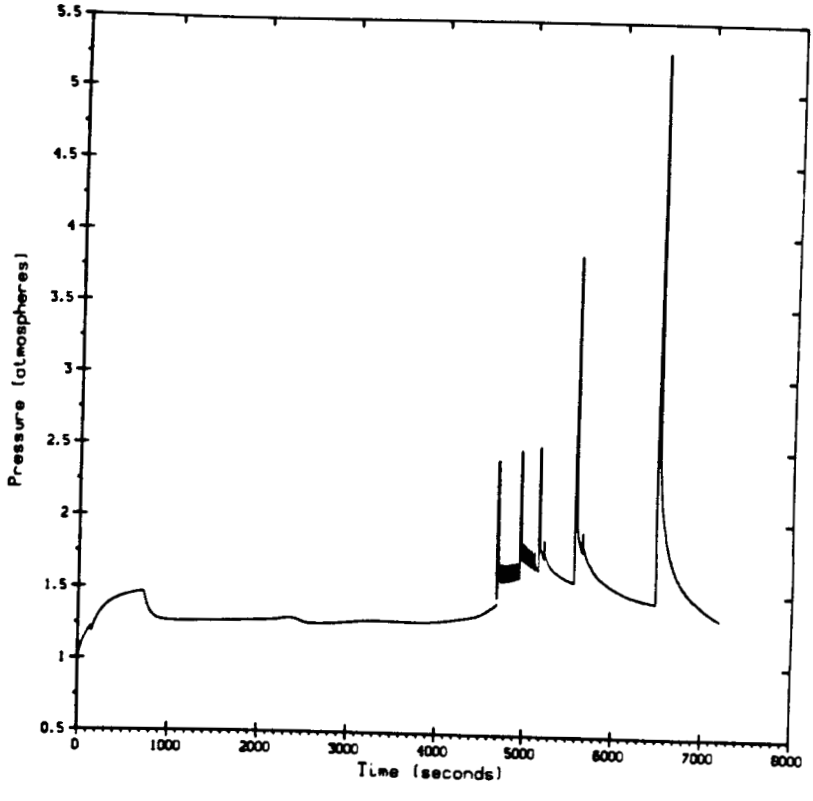


Figure 9. Upper Compartment Pressure for Sequoyah Calculation

The HECTR calculation discussed above was made using some preliminary models that are still being evaluated. The ice condenser model is currently being upgraded and including small leakage paths between compartments is being considered. The Sequoyah calculation discussed above will be reconsidered after these upgrades are completed to determine whether or not they influence the results.

Summary

HECTR calculations were performed for Grand Gulf and Sequoyah. The Grand Gulf results were found to be very sensitive to the compartmentalization used. Flame velocity also affected the calculations, especially with sprays on. The preliminary Sequoyah calculation predicted a series of relatively minor burns in the upper plenum, followed by a severe burn that started in the lower compartment, then propagated into a relatively uniform mixture (~ 8% hydrogen) throughout the containment. Several preliminary models used in the calculations are currently being upgraded. The calculations will be reconsidered after the upgrades are complete.

References

1. A. L. Camp, et al, "HECTR: A Computer Program for Modelling the Response to Hydrogen Burns in Containment," to be presented at the Second International Workshop on the Impact of Hydrogen on Reactor Safety, Albuquerque, NM, October 3-7, 1982.

2. R. O. Wooton and H. I. Avci, "March (Meltdown Accident Response Characteristics) Code Description and Users Manual," Battelle Columbus Laboratories, BMI-2064, October 1980.

3. "Report on the Grand Gulf Nuclear Station Hydrogen Ignition System," Mississippi Power and Light Company, August 31, 1981.

4. J. C. Cummings, et al, "Review of the Grand Gulf Hydrogen Igniter System," Sandia National Laboratories, NUREG/CR-2530, to be published.

5. Sequoyah Nuclear Plant Core Degradation Program, Volume 2, "Report on the Safety Evaluation of the Interim Distributed Ignition System," December 15, 1980.

References

1. NUREG/CR-2726
   SAND82-1137

   Light Water Reactor Hydrogen Manual

   Co-authors:
   Allen L. Camp
   John C. Cummings
   Martin P. Sherman
   Chester F. Kupiec, Jr.
   Robert J. Healy
   John R. Sandhop
   Jeffrey S. Caplan
   James H. Saunders

2. Mitigating Reactor Core Damage for Pressurized Water Reactors, General Physics Corporation, 1981

3. Mitigating Reactor Core Damage for Boiling Water Reactors, General Physics Corporation, 1981

MULTIPLE HYDROGEN-AIR DEFLAGRATIONS IN CONTAINMENT AND THE RESULTING THERMAL ENVIRONMENTS*

S. N. Kempka, A. C. Ratzel and M. R. Baer
Sandia National Laboratories
Albuquerque, New Mexico 87185

ABSTRACT

The computer program HECTR-ES has been developed to determine component thermal responses to combustion and post-combustion environments in nuclear reactor containments. The computer model is described and results obtained from the model are compared to experimental data obtained from hydrogen-air deflagration tests conducted at Sandia Laboratories. Predicted results for multiple-burn simulations are presented for the Grand Gulf Mark III boiling water reactor utilizing hydrogen generation rates obtained from a MARCH computer simulation of an S_2D accident scenario. These results indicate that safety-related equipment in containment will exceed LOCA qualification temperature limits if the spray systems in containment are inoperative for either an 8% or 10% (hydrogen volume) ignition criterion.

*This work performed at Sandia National Laboratories supported by the U. S. Nuclear Regulatory Commission, Office of Nuclear Regulatory Research.

INTRODUCTION

A significant consequence of a loss-of-coolant accident (LOCA) in a nuclear reactor is the generation of combustible hydrogen gas from steam-zirconium reactions. If this gas is allowed to accumulate in the nuclear containment to volume concentrations in excess of 6%, possible hydrogen-air deflagrations may result. The ensuing temperature and pressure increases might threaten nuclear reactor containment integrity and damage safety-related equipment within containment. To avoid such events, halon or carbon dioxide inerting and/or water addition using sprays or foam to mitigate combustion effects are currently under investigation in conjunction with deliberate ignition. However, the possibility of uncontrolled ignition (i.e., automatic ignition at specified hydrogen concentrations) in the absence of a mitigation scheme may represent a worst case to consider.

This work considers deliberate multiple ignitions of hydrogen in a reactor containment and the resulting thermal environment (pressure and temperature history) which occurs during and following combustion. A representative hydrogen gas generation scenario resulting from an S_2D pipe break accident sequence has been obtained from a MARCH [1] analysis. ("S_2D" refers to a small-break, loss-of-coolant accident with concurrent failure of the emergency core coolant system.) The predicted hydrogen generation rates are used as input for a computer simulation of the combustion and post-combustion environment using HECTR-ES. This computer program, portions of which were assembled from previously developed Sandia Laboratories thermal codes for studying post-deflagration environments, incorporates a hydrogen flame propagation model with molecular gas band radiative energy transfer. Conductive and convective heat transfer models and a condensation model are also included in the simulation. The primary purpose of this study is to determine component thermal responses following combustion within containment. The thermal response of representative large and small mass components are studied and temperature extremes resulting from multiple deflagration scenarios are obtained. In addition, the sensitivity of the thermal response to the hydrogen ignition criterion (deliberate ignition at 8% or 10% hydrogen concentrations) is investigated.

Representative benchmarking studies compare the thermal model with experimental data obtained from hydrogen deflagrations in the 5.7 m^3 VGES (Variable Geometry Experimental System) facility at Sandia National Laboratories in Albuquerque (SNLA). The problems associated with modeling large nuclear containments are discussed and the trends observed from the analyses are reviewed to provide insight for further analytical modeling efforts.

DESCRIPTION OF THE COMPUTER MODEL

The computer model HECTR-ES was developed to predict thermal responses of safety-related equipment to hydrogen-air deflagrations in nuclear reactor containments. This code simulates the transient heat exchange during and after single or multiple hydrogen deflagrations in a single compartment containment. The single burn option has been used primarily to model small-scale experiments and requires the temperature, pressure and gas species concentrations prior to ignition. Multiple deflagration computations are intended to simulate nuclear reactor LOCA scenarios and require representative steam and hydrogen release rates (source terms) in addition to the necessary single burn input information. In both cases, the containment geometry and the material properties of each surface must also be specified. The relative positions of the surfaces with respect to each other are defined by mean beam (path) lengths and configuration factors. Since hydrodynamic models are omitted in the post-deflagration model, the orientation of the component surfaces with respect to gas flow is not included and the code is essentially a global analysis model (i.e., zero-dimensional).

Multiple burn routines in HECTR-ES maintain an inventory of all gas species, burned and unburned, throughout the analysis and determine when the hydrogen ignition criterion (a user input) has been realized. Deflagrations can be simulated either as an adiabatic, isochoric instantaneous energy release or with a one-dimensional (1-D) flame propagation model developed by Baer and Ratzel [2]. In this hydrodynamic model, the flame front is treated as a density and entropy discontinuity which propagates at prescribed burning velocities, corresponding to laminar or turbulent flames. The 1-D flame model can be applied to axisymmetric, variable area geometries and includes radiation heat transfer to containment surfaces and to the unburned gases during the combustion process. If the heat loss mechanisms are omitted from the analysis, this model yields pure adiabatic pressure and temperature results following completion of the combustion.

Post-combustion heat exchange between the hot gases, containment walls and components is calculated using heat transfer routines from the computer program HECTR developed at SNLA [3,4]. The heat transfer mechanisms include thermal radiation, convection, wall conduction and steam condensation. The radiative model simulates gas band radiation using exponential wide-band models [5] and includes radiative energy exchange between gray surfaces. Convective heat transfer coefficients are calculated from empirical correlations for forced and natural convection on vertical plates and the greater of the two heat transfer rates is used for each time step. Since the post-combustion analysis does not model the hydrodynamics, the user must specify a characteristic length for each surface and a bulk velocity which are used in the forced convection energy calculations. A Nusselt, air-steam condensation model [6] includes the effects of mass diffusion and superheating when thermodynamic conditions are appropriate. Additional information on the heat transfer models incorporated in HECTR-ES have been documented previously in reference [4].

The post-combustion environment is assumed to be spatially uniform in pressure, temperature and gas species concentrations. Because of these assumptions, a global energy balance can be performed during each time step without solving the field equations for velocity and temperature. The post-deflagration heat exchange continues until the ignition criterion is again satisfied, whereupon flame calculations are initiated to simulate another deflagration. This process continues until the hydrogen, oxygen or simulation time (a user input) are depleted or until the environment is steam-inerted.

COMPARISON OF MODEL RESULTS WITH EXPERIMENTAL DATA

A qualitative assessment of HECTR-ES predictive capabilities was sought prior to applying the code to deflagration scenarios in nuclear reactor containment buildings. To this end, HECTR-ES was used to simulate hydrogen deflagration experiments conducted in the Variable Geometry Experimental System (VGES) for the Hydrogen Burn Survival Program [7]. The VGES facility is a 5.7 m^3 cylindrical vessel used for combustion experiments at SNLA. The facility was equipped with pressure transducers, thermocouples and with representative calorimeters and instrumented components (flat plates and cubes) for evaluating the post-combustion thermal environment. Geometry data on the VGES tank and on the components are summarized in Table 1. A detailed description of the procedures and equipment used in the hydrogen deflagration experiments is provided in reference [7].

Data from a nominal 15% hydrogen (volume fraction) deflagration (test no. B92) were chosen for the analytical-experimental comparison Initial conditions, beam lengths and configuration factors used in the calculations to simulate the experiment are given in Table 2. Analytical predictions, with and without the convection and condensation models, and experimental data are shown together in Figures 1a through 1d. Gas temperature data in Figure 1a were obtained from a slow response thermocouple. Consequently, the measured gas temperature can be expected to lag behind the actual gas temperature during and immediately following combustion. However, for times greater than ten seconds after complete combustion, the thermocouple measurement errors are expected to diminish, and the data agree with HECTR-ES predictions. The calculated temperature profiles for the two flat plates (Figure 1b) and for the representative thin-wall component (Figure 1c) bracket nearly all the experimental data. The early-time thick-wall component data (Figure 1d) are anomalous as a result of thermocouple measurement errors. Comparison of the two computed temperature profiles in each figure indicate that radiative energy exchange is the dominant heat transfer mechanism. Note, for example, that the combined heat transfer temperature profile is not appreciably different from the shape of the pure radiation profile.

Overall, the comparison of VGES experimental data with HECTR-ES simulations indicates that the computer model yields reasonable estimates of temperatures for components exposed to hydrogen deflagrations in small-volume enclosures. Although exact comparison of early time gas temperature data and predictions was not possible, the component thermal response comparisons indicate that the gas environment is adequately modeled. While the HECTR-ES heat transfer models have been verified at least to some degree for the VGES facility, it should be noted that applying the code to full-scale containments requires careful review of the phenomenological modeling. The relative importance of each heat transfer mechanism may vary with containment size and geometry, and with the pre- and post-combustion thermal environments.

GRAND GULF ANALYSIS

HECTR-ES simulations of an S_2D LOCA in the Grand Gulf Mark III boiling water reactor (BWR) were performed to predict the thermal response of representative components to multiple deflagration scenarios. The Grand Gulf BWR can be treated as a single compartment containment and thus is suitable for modeling by HECTR-ES. The containment building was modeled as an annulus with a hemispherical cap as shown in Figure 2. The inner structure enclosing the reactor vessel is referred to as the dry well. The wet well constitutes the annular region of the containment in this analysis. The variations in the dry well wall diameter represent regions known to be obstructed by structures or equipment.

In the event of a LOCA, hot air, steam and hydrogen from the dry well are vented into a suppression pool at the bottom of the wet wall. The suppression pool "scrubs" (removes) steam from the vented gases, allowing only saturated air and hydrogen to enter the wet well volume. This scrubbing system prevents large, steam-induced pressure rises in the wet well, but allows hydrogen to accumulate in the containment. Since ignition of high concentrations of hydrogen (greater than 10% by volume) could damage the reactor building, deliberate ignition at low concentrations is proposed to protect the integrity of the containment. Such deflagrations prevent structural damage but could impair the performance of safety-related equipment, especially if spray-cooling systems are inoperative. Such a worst-case scenario is considered in this analysis of the Grand Gulf reactor containment.

Containment walls and structures in the Grand Gulf reactor building were modeled by 23 surfaces as described in reference [8]. The representative components considered in the analyses are hollow and solid aluminum cubes (10 cm sides, similar to those in the VGES experiment). Each component type was positioned in the dome region and in the lower wet well region (shown in Figure 2) to assess the effects of (1) thermal mass and (2) location on component thermal responses. Further details on the component

radiative and geometric conditions are given in Tables 1 and 3. Hydrogen release rates utilized in the Grand Gulf analyses were obtained from MARCH calculations [1,9]. Molar flow rates of hydrogen used in the analyses were taken from reference [9] and are summarized in Table 4 (Case B1). The initial number of moles of oxygen in containment (3.08×10^5 moles) was sufficient to reduce (i.e., react with) the total molar influx of hydrogen (5.83×10^5 moles), indicating that combustion was not oxygen-limited. Analyses were peformed comparing 8% and 10% hydrogen (volume fraction) ignition criteria with spray cooling systems inoperative. For each ignition criterion, three cases were considered; heat exchange by: (1) radiation, convection and condensation with heat transfer during combustion, (2) radiation only, with heat transfer during combustion, and (3) radiation, convection and condensation with adiabatic combustion. The flame is initiated as a planar surface at the suppression pool surface with upward flame propagation to the dome. Each combustion process was assumed to be a laminar flame propagation and to burn to 100% completion. Typical flame propagation results for a single ten percent deflagration are summarized in reference [2] for the Grand Gulf geometry used in this study.

GRAND GULF RESULTS

Combustion gas temperatures and pressures characterizing deflagration environments for 8% and 10% hydrogen ignition criteria are shown in Figures 3a & 3b and 3d & 3e, respectively. Three deflagrations occurred in the 10% ignition case, and four deflagrations resulted when the 8% ignition criterion was employed. The four 8% deflagrations consumed nearly 100% of the hydrogen generated in the accident scenario, whereas a 3% mole fraction of hydrogen remained after the 10% hydrogen deflagrations (see Figures 3c and 3f). Hence, a greater quantity of energy was released in the multiple 8% deflagration analysis, indicating that this case may yield the more severe thermal environment for equipment survival. Further evidence of this premise is given in Figures 3a, 3b and 3c, which show that the time between deflagrations are reduced in the 8% hydrogen ignition criterion analysis. The combustion gases thus have a shorter period to cool prior to the next deflagration. Total energy release and ignition frequency, however, may not be the only factors to consider in the determination of a worst-case. Peak gas temperatures and pressures can also strongly influence which thermal environment is more severe. In these analyses, the 10% ignition analysis resulted in the greater peak gas temperatures and pressures (see Figures 3a & 3b and 3d & 3e). This observation indicates that a worse case ignition criterion cannot be determined from environmental characterizations alone; the transient component thermal responses must be included. As a final note, it should be pointed out that multiple deflagrations affect the local maxima of the gas temperature and pressure differently. In both the multiple burn scenarios, the local peak gas temperatures are nearly the same following each deflagration. However, the local gas pressure maxima increase with successive ignitions resulting in a final maximum pressure approximately 15% greater than the first maximum.

Thermal response predictions for representative equipment surfaces (i.e., thin- and thick-wall components) indicate that component thermal mass and location in the containment can play important roles in equipment survival analyses. Figures 4 and 5 show that a single deflagration (8% or 10% hydrogen) will not increase equipment surface temperatures above the LOCA qualification temperature (> 433 K). However, multiple deflagrations successively elevate the component temperatures above the LOCA specification since there is not sufficient time between deflagrations for the components to cool significantly. Thick-wall components cool very little after each deflagration so that the temperature increases resulting from each deflagration are nearly additive. Thin-wall components exhibit greater cooling between deflagrations as a consequence of their small thermal capacitance; however, they also show a greater temperature increase during each burn. This ultimately leads to higher temperatures for the thin-wall components. The maximum temperature for a given component is not strongly dependent on the choice of ignition criteria. However, the time periods during which the components exceed the LOCA qualification temperature are greater in the 8% hydrogen deflagration analyses. This finding indicates that the 8% hydrogen ignition criterion provides the worse thermal environment in this analysis.

An interesting result observed from Figures 4 and 5 is that thermal capacitance effects on maximum component temperature are influenced by component location. In the lower wet well, the difference between thin- and thick-wall maximum temperatures is 20 K, while in the dome region this difference is 200 K. Radiative beam lengths in the dome region are significantly greater than in the lower wet well (see Table 3);thus, radiative energy transfer from the combustion gases to the surfaces in the dome region is much greater. Similarly, Figures 4 and 5 show that components in the dome region cool more rapidly than do components in the lower wet well. The large beam lengths between surfaces in the dome region cause the components to more closely follow the gas temperature, which cools rapidly after combustion (see Figure 3). Components in the lower wet well are less affected by the gas temperatures (smaller beam lengths). Instead, these component cooling rates are dominated by radiative energy exchange with containment walls.

Inspection of the local maximum temperature data points from adiabatic flame propagation calculations shows the importance of heat transfer during the combustion process. The component thermal response calculations in each figure indicate that the maximum temperatures obtained from the adiabatic flame propagation computations were lower than in other analyses which included radiation heat transfer during the deflagrations. This result is surprising since the peak adiabatic isochoric combustion pressures and temperatures are always greater than non-adiabatic flame results. The lower component temperatures in spite of higher peak gas temperatures and pressures are attributed to the omission of pre-heating the containment surfaces during deflagrations. The local

maxima obtained from analyses where only radiative energy exchange is considered are also presented in Figures 3, 4 and 5. As was noted previously in the VGES simulations, the maximum component temperatures obtained from these analyses are always greater tha those obtained with convection and condensation included.

In summary, the multiple deflagration analyses for the Grand Gulf Mark III BWR show that components within the containment building may be subjected to temperatures above the LOCA qualification temperature for extended periods of time. This does not necessarily indicate component failure, but satisfactory performance of safety-related equipment in these extreme environments thus far has not been demonstrated. These analyses are subject to the limitations of the heat transfer models and hydrodynamic assumptions. Local gas temperature gradients and gas velocity variations in the combustion environments may significantly impact the thermal responses predicted in these analyses. Also there is uncertainty in applying the HECTR-ES convection and condensation models to large volume containments. (That is, the appropriate large-geometry length scales to be used in the convective heat transfer models are unknown.) Overall, the accuracy of these calculations cannot be estimated without comparison of the model with large-scale geometry experimental data, and thus, error estimates of HECTR-ES calculations obtained from VGES studies are not applicable to the Grand Gulf analyses. Results obtained from these Grand Gulf analyses should be considered only as preliminary estimates of the expected temperatures resulting from the complex heat transfer phenomena.

SUMMARY

The computer program HECTR-ES was developed to simulate the transient heat exchange resulting from hydrogen deflagrations in enclosures, for specific application to obtaining equipment thermal responses during LOCA scenarios in nuclear reactors. Comparison of computer simulations of small-scale hydrogen combustion experiments and measured data indicate that the heat transfer and flame propagation models provide good estimates of component thermal responses. Simulations of multiple hydrogen deflagrations in the Grand Gulf reactor were performed using two different ignition criteria (8% and 10% hydrogen concentrations) to evaluate the effects of different severe environments on component thermal response. The analyses indicate that for both ignition criteria, the resulting thermal environments substantially exceed the LOCA qualification temperature. Therefore, subject to the validity of the assumptions made in the analyses, these environments comprise a potential threat to the safe operation of the nuclear power plant.

ACKNOWLEDGEMENTS

The development of HECTR-ES involved personnel from several organizations. The authors gratefully acknowledge Susan Dingman, Allen Camp and Michael Wester of Division 9441 and W. H. McCulloch, project coordinator of Division 9445, for their contributions to this work.

REFERENCES

1. Wooten, R. D. and Avci, H. I., "MARCH (Meltdown Accident Response Characteristics) Code Description and Users Manual," Battelle Columbus Laboratories, BMI-2064, October 1980.

2. Baer, M. R. and Ratzel, A. C., "A Hydrodynamic Model of Hydrogen Flame Propagation in Reactor Vessels," included in Second International Workshop on the Impact of Hydrogen on Water Reactor Safety Proceedings, 1982.

3. Berman, M., "Light Water Reactor Safety Research Program Semiannual Report, April-September 1981," Sandia National Laboratories, SAND82-0006, (NUREG/CR-2481), February 1982.

4. Wester, M. J., et al., "Development and Application of a Computer Program for Modelling the Response to Hydrogen Burns in Containment," submitted to 2nd International Topical Meeting on Nuclear Thermalhydraulics, to be held in Santa Barbara, California, January 11-14, 1983.

5. Edwards, D. K., "Molecular Gas Band Radiation," Advances in Heat Transfer, 12, T. F. Irvine and J. P. Hartnett, ed., Academic Press, New York, 1976.

6. Whitley, R. H., "Condensation Heat Transfer in a Pressurized Water Reactor Dry Containment Following a Loss of Coolant Accident," Ph.D Dissertation, University of California at Los Angeles, 1976.

7. McCulloch, W. H., et al., "Hydrogen Burn Survival: Preliminary Thermal Model and Test Results," Sandia National Laboratories Report SAND82-1150, (NUREG/CR-2730), August 1982.

8. Cummings, J. C., et al., "Review of the Grand Gulf Hydrogen Igniter System," Sandia National Laboratories Report SAND82-0218 (NUREG/CR-2530), Draft Report, January 1982.

9. "Report on the Grand Gulf Nuclear Station Hydrogen Ignition System," Mississippi Power and Light Company, August 1981.

Table 1. Geometry Information for Simulations of 15% Hydrogen Deflagration Experiment in the VGES Facility and for Multiple Deflagrations in the Grand Gulf BWR Containment

VGES Geometry (carbon steel, vertical, right circular cylinder)

height	4.9 m
diameter	1.2 m
wall thickness	.016 m
volume	5.7 m^3
area	21.1 m^2

Grand Gulf Reactor Containment (steel and concrete)

height	57.7 m
area	11201. m^2
enclosed volume	37922. m^3
geometry	(see Figure 2)

Flat Plate Calorimeter (brass, back surface insulated, square)

length	.152 m
area	.023 m^2
thickness	.635 mm

Cubical Components (aluminum, solid and hollow, modeled as equivalent flat plates)

Hollow Cube		Solid Cube	
area	.0619 m^2	area	.0619 m^2
thickness	.00317 m	thickness	.01693 m
height	.1016 m	height	.1016 m

Table 2. Pre-ignition Conditions and Radiative Input Information for Simulations of 15% Hydrogen Deflagration Experiment in the VGES Facility

Pre-ignition Conditions

temperature of gas and surfaces	297. K
gas (air and hydrogen) pressure	.971 atm
hydrogen volume fraction	.15
humidity ratio	.001
uniform bulk velocity	.3 m/s (assumed)

Radiative Inputs

Surface	Beam Length (m)	Configuration Factor ($F_{vges-cal}$)
flat plate 1	1.46	.0011
flat plate 2	1.46	.00117
aluminum cubes	1.46	.00295
VGES wall	1.08	.9918

Table 3. Pre-ignition Conditions and Radiative Input Information for Simulations of Multiple Deflagrations in the Grand Gulf BWR

Initial Conditions

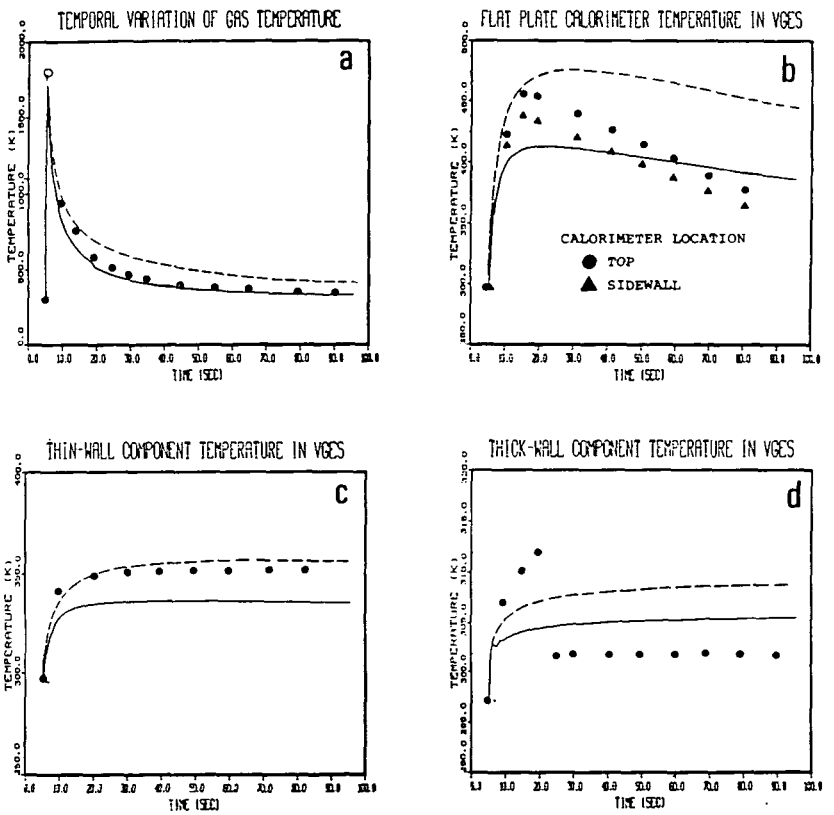
gas pressure at start of LOCA	1.1 atm
gas temperature	310 K
steam volume fraction	2.0%
pre-ignition conditions	(see Figure 3)
ignition criterion	8% or 10% volume fraction
uniform bulk velocity	.3 m/s (assumed)

Radiative Inputs

Surface	Beam Lengths (m)	Configuration Factors $F_{cube-sfc}$
Dome Region		
steel dome	14.9	.622
crane	25.4	.335
grating @ 63.4 m	29.5	.043
Lower Wet Well Region		
lower wet well	9.6	.558
grating @ 34 m and 41 m	5.1	.221

Table 4. Hydrogen Source Terms (Case B1) Used in HECTR-ES Simulations of Multiple Deflagrations in the Grand Gulf BWR

Time (s)	Release Rate (moles/s)	Time (s)	Release Rate (moles/s)
0	.867	1863	63.03
306	1.802	2163	122.4
336	6.397	2463	120.9
606	10.87	2763	105.3
906	41.36	3063	216.4
1246	153.2	3064	234.6
1563	172.6	4512	0.0



Legend

- - - - - - -	radiative transfer only
———	radiative, convective and condensation energy transfer
○	adiabatic, isochoric temperature
● ▲	experimental results

Figure 1. Comparisons of model predictions and experimental data for a 15% hydrogen-air deflagration in the VGES facility

a: gas temperature
b: flat plate calorimeter
c: thin-wall (hollow cube) component
d: thick-wall (solid cube) component

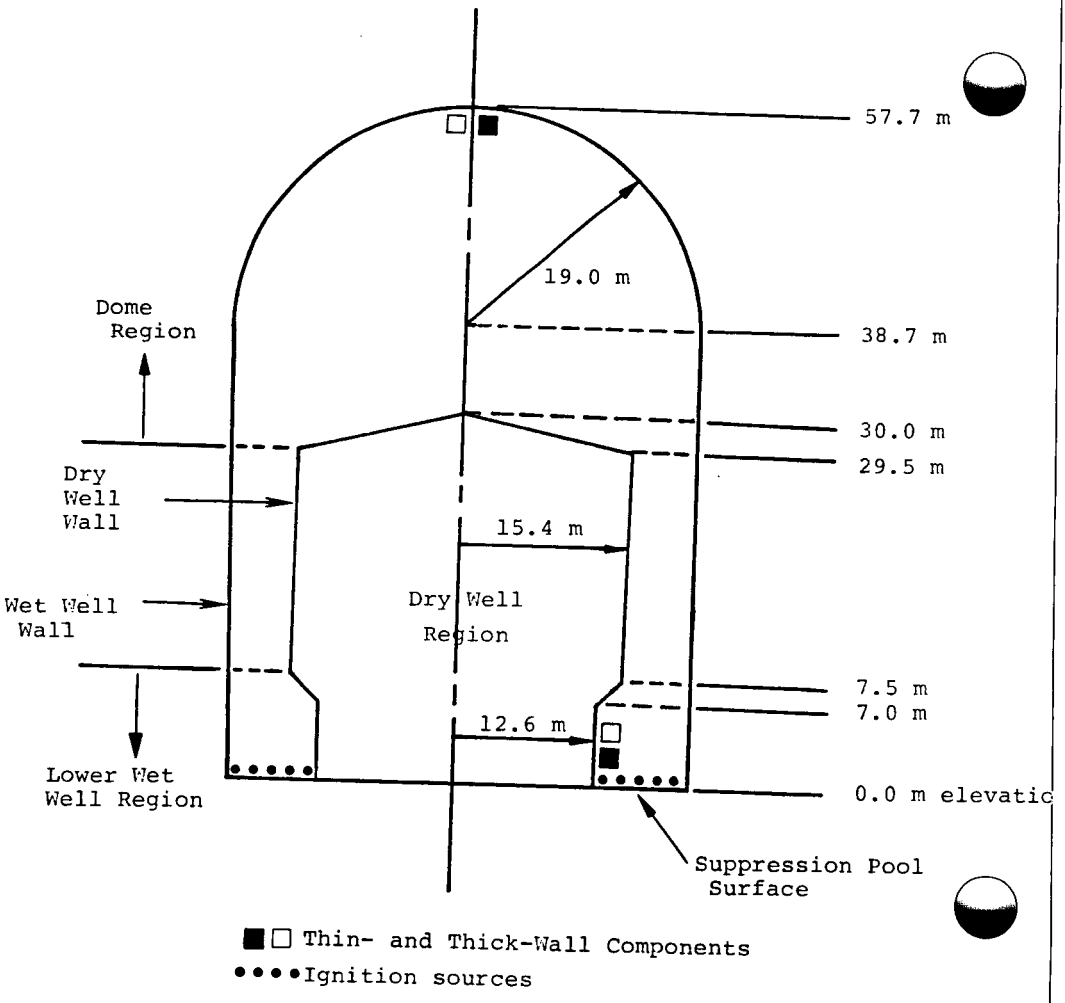
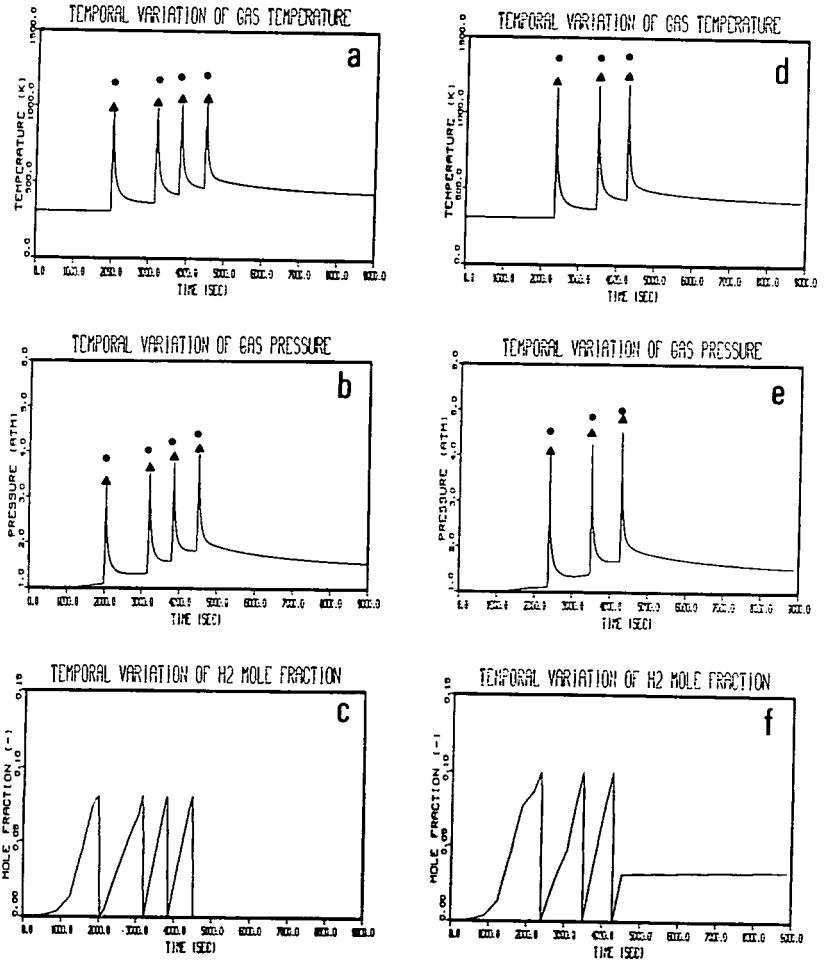


Figure 2. Schematic of Grand Gulf Mark III BWR containment (3.79×10^4 m^3 total volume)



Legend

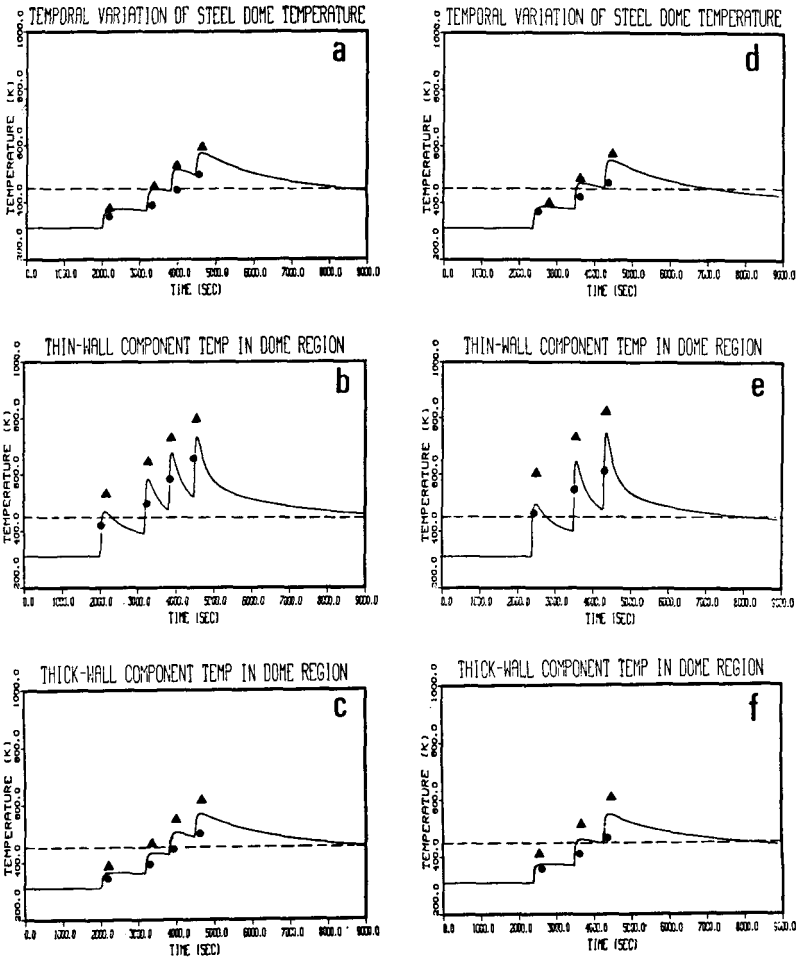
——— nonadiabatic flame propagation with radiation, convection and condensation

● adiabatic flame propagation with radiation, convection and condensation (maxima)

▲ nonadiabatic flame propagation with radiation (maxima)

Figure 3. Grand Gulf containment environments resulting from 8% (a,b,c) and 10% (d,e,f) multiple ignition accident scenarios

a & d: gas temperature
b & e: gas pressure
c & f: hydrogen concentrations



Legend

——— nonadiabatic flame propagation with radiation, convection and condensation

- - - - - - - LOCA qualification temperature (433 K)

● adiabatic flame propagation with radiation, convection and condensation (maxima)

▲ nonadiabatic flame propagation with radiation (maxima

Figure 4. Thermal responses of representative components and containment surface in the dome region of the Grand Gulf containment for 8% (a,b,c) and 10% (d,e,f) multiple ignition accident scenarios

a & d: steel dome
b & e: thin-wall (hollow cube) component
c & f: thick-wall (solid cube) component

EVALUATION OF POST-ACCIDENT COMBUSTIBLE GAS CONTROL AT MILLSTONE UNIT I

Dr. J. H. Bickel, Sr. Eng.
Safety Analysis Department
Northeast Utilities Service Co.
Hartford, Connecticut 05101

Introduction and Summary

On December 2, 1981 the NRC published 10CFR 50.44, "Interim Requirements Related to Hydrogen Control". The major impact of this regulation on Mark I BWR Containments was to require inerting and to eliminate containment purging as a post-accident combustible gas control scheme. This rule in effect required installation of hydrogen recombiners on all plants originally licensed assuming purge/pressurization for hydrogen control. Because of the high costs ($6-$10 million) of backfitting hydrogen recombiners on operating Mark I Containment B.W.R.s, such as Millstone I, it was decided to more thoroughly investigate the technical bases of the need to purge containment for hydrogen control if the containment was initially inerted (with O_2 content less than 4%). It should be pointed out that such an investigation to define the technical bases for purging had never been carried out before.

Northeast Utilities Service Co. (NUSCO) on behalf of Northeast Nuclear Engergy Co. (NNECO) the operating company for Millstone Unit I conducted this investigation and identified the following:

a. Preinerting of a Mark I Containment with excess N_2 is so effective that no extent of metal-water reaction can directly lead to flammable H_2-O_2 gas mixtures.

b. Production of hydrogen via large metal-water reactions actually makes the containment more inert by further diluting the initial O_2 content. (O_2 concentration is the limiting factor affecting flammability).

c. With removal of oxygen (air) in-leakage to the containment from the M.S.I.V. and Safety/Relief Valve control air lines, radiolysis is the only credible oxygen source present in the post-accident containment environment.

d. Post-accident boiling phase radiolysis, which is the most rapid source of oxygen generation, is insufficient to yield a flammable mixture.

e. Post-accident subcooled phase radiolysis in which natural recombination is strongly favored, yields stable equilibrium levels of H_2 and O_2 below the flammable mixture level.

The major difference between the approach taken by NUSCO and that defined in Reg. Guide 1.7 is the utilization of a detailed treatment of chemical kinetics of recombination reactions occurring during the subcooled long term decay heat removal phase. Taking credit for these natural recombination effects, eliminates the need for post-accident containment purging and hence, installation of recombiners.

Bases of NUSCO's Analyses

The analysis of post-accident combustible gas control at Millstone Unit I was based on assuming:

- o A net containment volume conservatively estimated at 7.29×10^6 liters.
- o This volume contains conservatively 2.7×10^5 moles of gas of which 4% is O_2 (upper Tech. Spec. Limit) and 96% is N_2 and other inert gases.
- o Mixing between the drywell and torus volumes due to the initial blowdown and long term coolant recirculation phases.

Impacts of Metal-Water Reaction and Boiling Phase Radiolysis

The changes in the hydrogen and oxygen mole fractions as a result of the metal-water reaction and net radiolysis may be conservatively defined by noting that the increase in moles of H_2 gas from the metal-water reaction is:

$$\Delta n_{H_2} = 2 f_{Zr\text{-}H_2O} n_{Zr} \qquad (1)$$

- where: $f_{Zr\text{-}H_2O}$ is the fractional extent of the metal water reaction (0.0 to 1.0)

  n_{Zr} is the total number of moles of Zirconium in the core (3.529×10^5 moles Zr)

The increase in hydrogen due to net radiolysis is:

$$\Delta n_{H_2}' = \varepsilon_{H_2O} \chi_{H_2} \qquad (2)$$

- where: ε_{H_2O} is the extent of radiolysis lbs. of H_2O decomposed

  χ_{H_2} is 25.178 moles H_2 produced per lb. H_2O decomposed

The increase in oxygen due to net radiolysis is:

$$\Delta n_{O_2}' = \varepsilon_{H_2O} \chi_{O_2} \qquad (3)$$

- where: χ_{O_2} is 12.589 moles O_2 per lb. H_2O decomposed

Utilizing these increases, the mole fractions of H_2 and O_2 in the post-accident phases can be assessed as follows:

$$f(H_2) = \frac{n_{H_2} + \Delta n_{H_2} + \Delta n_{H_2}'}{n_{H_2} + \Delta n_{H_2} + \Delta n_{H_2}' + n_{O_2} + \Delta n_{O_2}' + n_{N_2}}$$

$$= \frac{n_{H_2} + 2 f_{Zr\text{-}H_2O} n_{Zr} + \varepsilon_{H_2O} \chi_{H_2}}{n_{H_2} + 2 f_{Zr\text{-}H_2O} n_{Zr} + \varepsilon_{H_2O} (\chi_{H_2} + \chi_{O_2}) + n_{O_2} + n_{N_2}} \qquad (4)$$

$$f(O_2) = \frac{n_{O_2} + \Delta n_{O_2}'}{n_{H_2} + \Delta n_{H_2} + \Delta n_{H_2}' + n_{O_2} + \Delta n_{O_2}' + n_{N_2}}$$

$$= \frac{n_{O_2} + \varepsilon_{H_2O} \chi_{O_2}}{n_{H_2} + 2 f_{Zr\text{-}H_2O} n_{Zr} + \varepsilon_{H_2O} (\chi_{H_2} + \chi_{O_2}) + n_{O_2} + n_{N_2}} \qquad (5)$$

These results are parametric in f_{Zr}-H_2O (the extent of the metal-water reaction) and H_2O (the extent of net radiolysis) Parametric analyses are then carried out to ascertain what amount of radiolytic decomposition is necessary to reach the Coward-Jones[1] Flammability limits (which were curvefitted to a third order polynomiial). The results of these parametric calculations are shown in Figure 1.

One unanticipated result was the existence of particular metal-water reaction extent which required a minimal value of radiolysis in order to reach flammability. For Millstone Unit I, f_{Zr}-H_2O=0.00612 required only a minimal 273.25 lbs. of H_2O in order to reach flammable limits. This metal-water reaction extent curiously lies between the f_{Zr}-H_2O=0.0019 predicted for DBA LOCA via Appendix K type calculations and the five times DBA LOCA f_{Zr}-H_2O value which is the normal bases for combustible gas control systems.

To understand the impacts of boiling phase radiolysis on containment flammability, additional parametric studies were carried out for the extent of boiling (equivalent to radiolysis from full core boiling) for various net yields: $G(H_2)$, $G(O_2)$

$$\varepsilon_{H_2O} = \int_0^{T_B} \dot{M}_{H_2O}(t)\, dt \qquad (6)$$

- where: T_B is the boiling time in seconds

$\dot{M}_{H2O}$ is the H_2O decomposition rate in lbs./sec.

$\dot{M}_{H2O}(t)$ may be expressed:

$$\dot{M}_{H_2O}(t) = \frac{2.2\times10^{-5}\, P_o\, E_{\beta,\gamma}(t)\,(G(H_2)M_{H_2} + G(O_2)M_{O_2})}{A_o} \qquad (7)$$

- where: Po is the initial core power level (Po=2.051 MW_t)

Ao is Avogadro's number (Ao=6.023 x 10^{23})

$G(H_2)$=0.44 molecules/100eV, conservatively assuming no vapor phase recombination

$G(O_2)$=o.22 molecules/100eV, based on stoichiometry considerations and assuming no vapor phase recombination

M_{H_2} is the molecular weight of H_2 gas (M_{H_2}=2.106 grams/mole

M_{O_2} is the molecular weight of O_2 gas (M_{O_2}=31.999 grams/mol

$E_{\beta,\gamma}(t)$ is the β,γ decay energy function and is defined as in Reg. Guide 1.7

$$E_{\beta,\gamma}(t) = 10^{22} f_{\beta,\gamma} \sum_i k_i e^{-\lambda_i t} \qquad (8)$$

The results of these parametric calculations were then compared to the flammability limits. This comparison is shown in Figure II. As noted in this figure, the range of post-boiling phase radiolysis for all ranges of metal-water reactions is substantially outside the flammability limits. Hence, the metal-water reaction and boiling phase radiolysis does not pose a threat of flammability in the inerted containment.

Subcooled Phase Radiolysis

Long term post-accident decay heat removal in a BWR involves an injection and breakout of subcooled water. In this state, liquid phase recombination of dissolved H_2 and O_2 gases is favored under certain conditions. To evaluate the dissolved gas concentrations, a net molar partition coefficient is defined as the ratio of moles of gas in the containment gas region to the moles of gas in containment liquids. By noting that:

$$\text{Moles of gas "X" in gas region} = \frac{P_x V_{cont.}}{RT}$$

$$\text{Moles of gas "X" in liquid region} = \frac{S_x P_x}{M_x} V_{liq.}$$

- where: P_X is the gas partial pressure in atmospheres
  S_X is the gas solibility in 10^{-3}gr/liter H_2O
  M_X is the molecular weight in grams

The partition coefficient can then be defined:

$$\gamma_x = \frac{M_x}{S_x RT}\left(\frac{V_{cont.}}{V_{liq.}}\right) \qquad (9)$$

Using these partition coefficients, the hydrogen and oxygen concentrations can be defined:

$$[H_2] = \frac{1}{V_{liq}}\left(\frac{1}{\gamma_{H_2}+1}\right)\left[n_{H_2} + 2f_{Zr-H_2O} n_{Zr} + \varepsilon_{H_2O}\chi_{H_2}\right] \qquad (10)$$

$$[O_2] = \frac{1}{V_{liq}}\left(\frac{1}{\gamma_{O_2}+1}\right)\left[n_{O_2} + \varepsilon_{H_2O}\chi_{O_2}\right] \qquad (11)$$

Figures III and IV show the results of parametric variations in f_{Zr-H2O} and H_2O at 25°C and 100°C respectively. These concentrations define the initial conditions for the analysis of subcooled phase radiolysis.

To carry out the simulation of subcooled phase radiolysis with recombination a three node model of the Millstone Unit I containment was developed using the FACSIMILE Code[2] written and owned by the United Kingdom Atomic Energy Authority. The FACSIMILE (or Flow and Chemistry Simulation) Code is a very fast running code specifically suited for the treatment of linear homogeneous chemical kinetics problems and other general initial value problems arising from stiff systems of differential equations. The simple three node model developed to simulate post-accident subcooled phase radiolysis is shown in Figure V.

This model assumes H_2 and O_2 gas transport to and from the torus liquid volume and the containment gas volume as defined by the following system of differential equations.

$$\frac{d}{dt}[H_2]_T = \frac{1}{RT}\left(\frac{V_{cont}}{V_{torus}}\right) k_T(H_2) P_{H_2} - k_R(H_2)[H_2]_T + \left([H_2] - [H_2]_T\right)\frac{V_{core}}{\dot{V}_{core}} \quad (12)$$

$$\frac{d}{dt}[O_2]_T = \frac{1}{RT}\left(\frac{V_{cont}}{V_{torus}}\right) k_T(O_2) P_{O_2} - k_R(O_2)[O_2]_T + \left([O_2] - [O_2]_T\right)\frac{V_{core}}{\dot{V}_{core}} \quad (13)$$

- where:

$[H_2]_T$ $[O_2]_T$ are respectively the torus' liquid concentrations of hydrogen and oxygen in moles/liter

$[H_2]$, $[O_2]$ are the core liquid concentrations in moles/liter

V_{cont} is the containment gas volumes (7.29×10^6 liters)

V_{torus} is the torus liquid volume (2.605×10^6 liters)

V_{core} is the core liquid volume (2.5×10^5 liters)

$\dot{V}_{core}$ core volumetric flow rate

P_{H_2}, P_{O_2} are respectively the containment H_2 and O_2 gas partial pressures in atmospheres

$k_T(H_2)$, $k_T(O_2)$ are the rates of gas transport from the gas region to the torus liquid volume

$k_R(H_2)$, $k_R(O_2)$ are the rates of gas transport from the torus liquid volume to the gas volume

The values of the rate constants $k_T(X)$, $k_T(X)$ were specifically chosen to agree with Henry's Law gas solubility data when equilibrium is reached.

$$\left(\frac{[X]_T}{P_X}\right)_{eq.} = \frac{1}{RT}\left(\frac{V_{cont.}}{V_{torus}}\right)\frac{k_T(X)}{k_R(X)} = \frac{S_X}{M_X} \quad (14)$$

Hence, for a given $k_T(X)$, $k_R(X)$ was chosen as:

$$k_R(X) = \frac{k_T(X)}{RT}\left(\frac{V_{cont.}}{V_{torus}}\right)\frac{M_X}{S_X} \qquad (15)$$

In the FACSIMILE Simulation of mass transport of liquid (out the break path or relief valve discharge path) from the core liquid volume to the torus liquid volume, the liquid was assumed to carry dissolved concentrations of H_2, O_2, and H_2O_2. These species were tracked because:

- o In the subcooled phase, (temperatures $\leq$100°C)they are long lived stable species from a radiation chemistry point of view (e.g., the concentrations of all other radiation induced radicals and ions decay away within seconds).
- o These species all have concentrations greater than 10^{-6} moles/liter.

In the core liquid volume, the initial radiolytic yields shown in Figure VI were utilized based on a compilation by Cohen[3]. The chemical reactions shown in Figure VII were assumed to proceed within the core liquid volume based on published kinetic rate constants from the National Bureau of Standards (Ref.4, 5, 6, and 7). A system of fourteen linear homogeneous chemical kinetics equations was derived in FACSIMILE to define the time dependent core liquid, concentrations of H_2, O_2, e_{aq}^-, H, H^+, H_2O_2, OH, OH^-, HO_2, HO_2^-, and O_2^-.

As examples, the rate equations governing H_2 and O_2 concentrations are:

$$\frac{d}{dt}[H_2] = \frac{P_o E_{\beta,\gamma}(t)}{A_o V_{core}} G_{H_2} + k_5[H]^2 + k_8[e_{aq}^-]^2 + k_{13}[H][e_{aq}^-]$$
$$-k_{18}[H_2][OH] + ([H_2]_T - [H_2])\frac{\dot{V}_{core}}{V_{core}} \qquad (16)$$

$$\frac{d}{dt}[O_2] = k_{10}[OH][HO_2] + k_{11}[OH][O_2^-] + k_{24}[HO_2][O_2^-]$$
$$+k_{25}[HO_2]^2 + k_{26}[O_2^-]^2 - k_7[e_{aq}^-][O_2]$$
$$-k_{21}[H][O_2] + ([O_2]_T - [O_2])\frac{\dot{V}_{core}}{V_{core}} \qquad (17)$$

Typical results for a pure water simulation are shown in Figures VIII and IX, which are based on initial conditions defined in the analysis of boiling phase radiolysis, where: f_{Zr-H2O}=0.01 (five times the DBA number) and ϵ_{H_2O}= 110.0 lbs. Figure VIII shows the time dependent concentrations of all critical radical, ionic, and molecular species produced via radiolysis and removed by natural back reactions. Figure IX shows the time dependent behavior of the H_2 and O_2 gas partial pressures. Of significance, it is noted that an overall net recombination of H_2 and O_2 gas is predicted.

A large number of sensitivity studies were conducted to bound areas where certain uncertainties were felt to exist. In particular:

- o Gas Transport Rates to and from the torus liquid

  Sensitivity studies indicated shifts in the dynamics but no significant impact on the final achieved equilibrium values.

- o Core Volumetric Flow Rates

  Sensitivity studies where flow rate was varied over several orders of magnitude indicated shifts in the dynamics but no significant impact on the final achieved equilibrium values. Figure X shows the results of this study.

- o Extent of Metal-Water Reaction

  Because large overpressures of H_2 gas are known to favor net recombination by promoting the reaction: $H_2 + OH \rightarrow H_2O + H$, the case of $f_{Zr\text{-}H_2O}=0.0$ was studied. In this case, the only initial source of hydrogen was from the boiling phase radiolysis, with $\epsilon_{H_2O}=110.0$ lbs. Figure XI shows the results of this scenario.

- o Temperature

  As temperature is increased, the rate of the dominant back reaction should increase substantially. This was simulated by adjusting all kinetic rate constants to rates based on the extrapolation of Arrehnius' Law:

$$k(T) = k(T_o) \exp\left[-\frac{E_a}{R}\left(\frac{1}{T} - \frac{1}{T_o}\right)\right] \qquad (18)$$

  Additionally, the gas solubility required adjustment. The results of this simulation at just below the boiling point are shown in Figure XII. Of particular interest is the substantially faster removal rate of H_2 and O_2.

Impacts of Chemical and Fission Product Impurities

The natural recombination mechanisms, in general, are chain reactions which convert dissolved H_2 and O_2 back to water. The rate of recombination is, in fact, limited by the concentration of OH and H radical species and the aqueous electron. The potential impact of chemical and fission product impurities is their potential in breaking up the chain back reactions by scavenging too many of the limiting radicals effecting recombination.

In this regard, it is noted that the OH radical is an appreciable oxidizing agent, whereas the H radical and aqueous electron (e_{aq}^-) act as reducing agents. To properly address the impacts of impurities, a systematic screening process must be employed to identify the significant impurities capable of participating in oxidation-reduction reactions which could block recombination. Such a systematic screening must address the following three critical factors:

- o The relative concentration of the impurity species.
- o The relationship of the impurity concentration to the extent of fuel damage (e.g. extent of metal-water reaction) and excess H_2 gas generation (and whether or not such a relationship exists).
- o The chemical kinetic rate constant for reaction of the impurity with the radicals OH, H, and the aqueous electrons (e_{aq}^-).

NUSCO carried out this screening by classifying the potential impurities as either:

a. Impurities related to the oxidation of Zircaloy cladding (the concentration of these impurities are directly proportional to the extent of the metal-water reaction).

b. Fission product impurities, whose concentration in appreciable quantities result from extensive fuel damage (e.s. beyond the normal Appendix K limits).

c. Normal BWR water chemistry impurities whose existence is independent of the extent of the metal-water reaction.

The impurities related to oxidation of the cladding will be various zirconium oxide and hydroxides. Gordon, Schmidt, and Honekamp[8] have noted that due to solubility considerations, the amount of zirconium in solution as either a hydroxide or ion form would be negligible. Because of this, impurities related to the metal-water reaction will have no real effect on the radiolytic stability of the coolant water.

Fission product impurities physically cannot be present in any substantial concentrations unless a substantial metal-water reaction has occurred in the process. These impurities appear along with the generation of excess H_2 gas, a portion of which becomes redissolved in the coolant. To understand the relative concentrations likely from a severly damaged core accident, the results of the chemistry samples taken at TMI-2[9] were examined. By converting the measured activities to molar concentrations, the following was obtained:

$[^{131}I] = 8.6 \times 10^{-7}$ moles/liter $[^{133}I] = 4.5 \times 10^{-8}$ moles/liter
$[^{134}Cs] = 3.5 \times 10^{-7}$ moles/liter $[^{136}Cs] = 1.8 \times 10^{-8}$ moles/liter
$[^{137}Cs] = 2.3 \times 10^{-5}$ moles/liter
$[^{89}Sr] = 2.1 \times 10^{-9}$ moles/liter $[^{90}Sr] = 4.1 \times 10^{-6}$ moles/liter
$[^{106}Ru] = 1.0 \times 10^{-7}$ moles/liter
$[^{140}Ba] = 2.1 \times 10^{-9}$ moles/liter $[^{136m}Ba] = 2.8 \times 10^{-15}$ moles/liter

$[^{140}La] = 2.0 \times 10^{-9}$ moles/ liter

$[^{99}Mo] = 3.8 \times 10^{-9}$ moles/liter

$[^{132}Te] = 5.0 \times 10^{-9}$ moles/liter

$[^{141}Ce] = 2.6 \times 10^{-8}$ moles/ liter

Based on this review, the fission products ^{137}Cs, ^{90}Sr, ^{131}I, ^{133}I were identified as being appreciable from a concentration point of view. Based on a review of the chemical properties of these potential impurities, however, only iodine based impurities were concluded to be of significance to the question of radiolytic stability. This is because chemically, Cs is a Group IA Alkali Metal whose normal oxidation state is +1. The oxidation of any member of the Group IA Alkali Metal Family beyond the +1 oxidation state is extremely difficult. Sr, on the other hand, is a member of the Group IIA Alkaline-Earth Metal Family. Oxidation of any member of this chemical family beyond the +2 oxidation state (such as, by reaction with the OH radical) is also extremely difficult.

Equilibrium proportionation studies[10] indicate that for the iodine impurities present, the iodide ion (I^-) would predominate in concentration by several orders of magnitude over the iodate ion (IO_3^-). Furthermore, the measured chemical kinetic rate constant for the reaction of OH with I^- is 1.2×10^{10} $(\frac{\text{sec. mole}}{\text{liter}})^{-1}$ whereas, the reaction with IO_3^- is 5.0×10^7 $(\frac{\text{sec. mole}}{\text{liter}})^{-1}$.

In assessing iodine effects, it is also important to recognize the existence of appreciable quantities of stable and relatively long-lived iodine isotopes. By multiplying the ^{131}I concentration by a factor of 3.736, the relative amounts of ^{133}I, ^{129}I, and ^{127}I can be conservatively accounted for. (The factor 3.736 = $[I_{tot}]/[^{131}I]$ was determined based on results obtained from the ORIGEN Code.)

To complete the systematic screening of impurities, the normal BWR water chemistry impurities were also assessed. Chloride ions (Cl^-) nominally maintained in the range of 20 ppb (or 5.6×10^{-7} moles/liter) pose no significant threat to radiolytic stability due to their low concentration and relatively small kinetic rate constant for reaction with OH radicals. (Published NBS data indicates a chemical kinetic rate constant of less than 1×10^6 in the pH range of interest.)

A detailed review of the worst case soluble metallic ion impurities likely to be present and their chemical kinetic rate constants revealed the following:

	Reaction Mechanism	Impurity Concentration	Rate Constant
(1)	$Fe^{+2} + OH \rightarrow Fe^{+3} + OH^-$	$[Fe^{+2}] = 1.2 \times 10^{-7}$ moles/liter	$k = 3.4 \times 10^8 (\frac{\text{sec.mole}}{\text{liter}})^{-1}$
(2)	$Cu^{+2} + OH \rightarrow Cu^{+3} + OH^-$	$[Cu^{+2}] = 2.7 \times 10^{-7}$ moles/liter	$k = 3.5 \times 10^8 (\frac{\text{sec.mole}}{\text{liter}})^{-1}$
(3)	$Co^{+2} + OH \rightarrow Co^{+3} + OH^-$	$[Co^{+2}] = 4.75 \times 10^{-9}$ moles/liter	$k = 2.0 \times 10^6 (\frac{\text{sec.mole}}{\text{liter}})^{-1}$
(4)	$Ni^{+2} + OH \rightarrow Ni^{+3} + OH^-$	$[Ni^{+2}] = 2.0 \times 10^{-7}$ moles/liter	$k = 5.0 \times 10^5 (\frac{\text{sec.mole}}{\text{liter}})^{-1}$
(5)	$Zn^{+2} + OH \rightarrow Zn^{+3} + OH^-$	$[Zn^{+2}] = 1.1 \times 10^{-8}$ moles/liter	$k = 5.0 \times 10^5 (\frac{\text{sec.mole}}{\text{liter}})^{-1}$
(6)	$Mn^{+2} + OH \rightarrow Mn^{+3} + OH^-$	$[Mn^{+2}] = 2.6 \times 10^{-8}$ moles/liter	$k = 1.4 \times 10^8 (\frac{\text{sec.mole}}{\text{liter}})^{-1}$

Based on this review, Fe, Cu and Mn impurities were determined to be of greatest significance to the question of radiolytic stability.

To quantitatively assess the impact of I^-, Fe^{+2}, Cu^{+2}, and Mn^{+2} impurities on radiolytic stablility, a simple model developed by Jenks and Greiss[11] was utilized. Based on their work, the effective net rate of recombination can be expressed as:

$$R_{Rec.} = Dose \cdot \frac{3G_{OH} + 2G_{H_2O_2} + G_{e_{aq}^-} + G_H}{2 + \frac{\sum_i k_i [M_i]}{k_{18}[H_2]}} \qquad (19)$$

with k_i as the rate constant for reaction of impurity species Mi with the OH radical, $k_{18} = 4.5 \times 10^7 (sec \cdot mole/liter)^{-1}$

The net rate of decomposition is:

$$R_{Dec.} = Dose \cdot G_{-H_2O} \qquad (20)$$

A simple criteria for assessing radiolytic stability can be written as:

$R_{Rec.} > R_{Dec.}$ Net Recombination

$R_{Rec.} = R_{Dec.}$ Equilibrium

$R_{Rec.} < R_{Dec.}$ Net Decomposition

By substituting in for the known initial yields: $G_{OH} = 2.34$, $G_{H_2O_2} = 0.70$, $G_{e_{aq}^-} = 2.31$, $G_H = 0.55$, $G_{-H_2O} = 3.74$, this stability criteria can be simplified to the following:

$0.95\, k_{18}[H_2] > \sum_i k_i [M_i]$ Net Recombination

$0.95\, k_{18}[H_2] = \sum_i k_i [M_i]$ Equilibrium

$0.95\, k_{18}[H_2] < \sum_i k_i [M_i]$ Net Decomposition

Using this criteria, it can be shown:

- Insignificant fuel damage results in a net recombination of the H_2 and O_2 evolved from the boiling phase radiolysis.
- When insignificant fuel damage exists, but there are worst case corrosion product impurities present, additional net radiolysis will occur which produces the H_2 overpressure necessary to stabilize the coolant against further decomposition. In all cases, the H_2 and O_2 evolved are less than one-half that needed to achieve flammability.

- When significant fuel damage exists, the H_2 evolved from the metal-water reaction is sufficient to block further radiolysis. The excess H_2 evolved also tends to make the containment more inert than it was initially, hence, very large H_2O values are needed to reach flammability.

Thus, by merely assuring adequate pre-accident inerting of the containment, a passive combustible gas control is found to exist whereby, the combustible gas concerns of a severe accident are self-limiting in nature.

References Cited:

(1) Coward, H. F., and Jones, G. W., "Limits of Flammability of Gases and Vapors", U. S. Bureau of Mines Bulletin No. 503, 1952.

(2) Curtis, A. R., et al, "FACSIMILE: A Computer Program for Flow and Chemistry Simulation", A.E.R.E./Harwell Report AERE-R 8775, December 1977.

(3) Cohen, P., "Water Coolant Technology of Power Reactors", Gordon and Breach, New York, 1969.

(4) "Selected Specific Rates of Reactions of Transients from Water in Aqueous Solution, Hydrated Electron Data", National Bureau of Standards NSRDS-NBS-43, 1973.

(5) "Selected Specific Rates of Reactions of Transients from Water in Aqueous Solution, Hydrated Electron, Supplemental Data", National Bureau of Standards NSRDS-NBS-43, Supplement, 1975.

(6) "Selected Specific Rates of Reaction of Transients from Water in Aqueous Solution, Hydrogen Atom Data", National Bureau of Standards NSRDS-NBS-51, 1975.

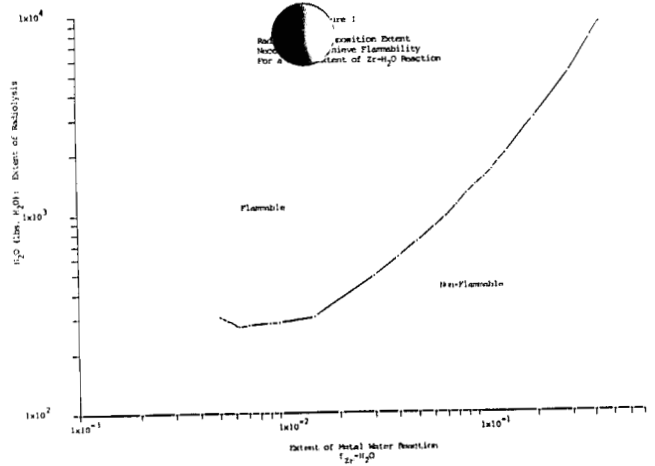
(7) "Selected Specific Rates of Reactor of Transients from Water in Aqueous Solution, Hydroxyl Radical, Perhydroxyl Radical, and Their Radical Ions", National Bureau of Standards NSRDS-NBS-59, 1977.

(8) Gordon, S., Schmidt, K. H., and Honekamp, J. R., "An Analysis of the Hydrogen Bubble Concerns in the Three Mile Island Unit 2 Reactor Vessel", Journal of Rad. Phys. and Chem., June 1982.

(9) "Technical Staff Analysis on Chemistry to the President's Commission on the Accident at Three Mile Island", October 1979.

(10) "Technical Bases for Estimating Fission Product Behavior During LWR Accidents", U.S.N.R.C. NUREG-0772, June 1981.

(11) Jenks, G. H. and Greiss, J. C., "Water Chemistry in Pressurized and Boiling Water Power Reactors", Oak Ridge National Laboratory ORNL-4173, November 1967.



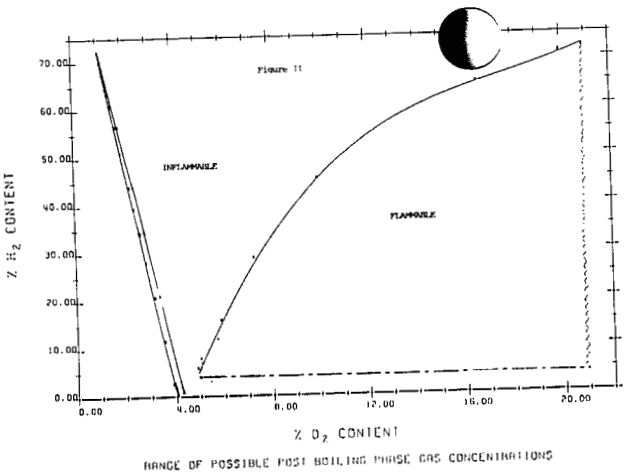


Figure III

Equilibrium Post-Boiling Phase Dissolved Gas Concentrations

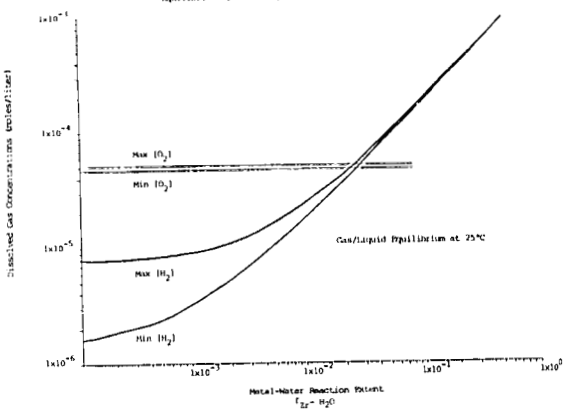
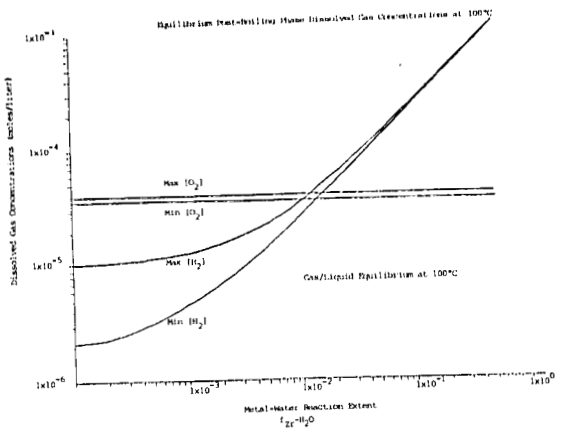


Figure IV

Equilibrium Post-Boiling Phase Dissolved Gas Concentrations at 100°C



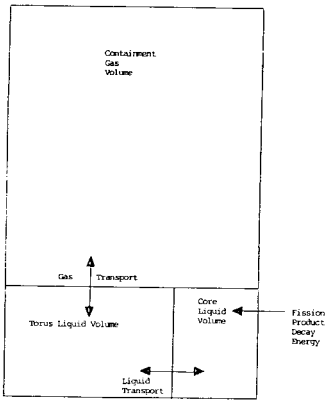


Figure V

Millstone Unit 1 Reactor and Containment Noding for Radiolysis/Recombination Simulation

	e^-_{aq}	H + e^-_{aq}	H	H_2	H_2O_2	OH	HO_2	AVERAGE L.E.T
mixed γ, β	2.31	2.86	0.55	0.44	0.70	2.34	0.00	.02 eV
γ	2.60	----	0.55	0.45	0.70	2.60	0.02	.02 eV
n	0.36	0.72	0.36	1.12	1.00	0.47	0.17	4.0 eV
$^{10}B(n,\alpha)^7Li$	0.04	0.20	0.16	1.70	1.30	0.10	0.30	24.0 eV

Initial Radiolytic Yields G_x in $\frac{\text{molecules}}{100\ eV}$

Figure VI

HIGAM VIII
RADIOLYTIC DECOMPOSITION AND RECOMBINATION REACTIONS

Chemical Reaction	Rate Constant at 25°C	Activation Energy kcal/mole
(1) $e^-_{aq} + H_2O \rightarrow H + OH^-$	1.8×10^1	3.0
(2) $e^-_{aq} + H^+ \rightarrow H$	2.4×10^{10}	3.0
(3) $e^-_{aq} + OH \rightarrow OH^-$	3.0×10^{10}	3.0
(4) $e^-_{aq} + H_2O_2 \rightarrow OH + OH^-$	1.3×10^{10}	3.0
(5) $H + H \rightarrow H_2$	1.0×10^{10}	3.0
(6) $e^-_{aq} + HO_2 \rightarrow HO_2^-$	2.0×10^{10}	3.0
(7) $e^-_{aq} + O_2 \rightarrow O_2^-$	1.9×10^{10}	3.0
(8) $2e^-_{aq} + \rightarrow 2OH^- + H_2$	5.0×10^9	3.0
(9) $2OH \rightarrow H_2O_2$	4.5×10^9	3.0
(10) $OH + HO_2 \rightarrow H_2O + O_2$	1.2×10^{10}	3.0
(11) $OH + O_2^- \rightarrow OH^- + O_2$	1.2×10^{10}	3.0
(12) $OH^- + H \rightarrow e^-_{aq} + H_2O$	2.0×10^7	3.0
(13) $e^-_{aq} + H + H_2O \rightarrow OH^- + H_2$	4.5×10^8	3.0
(14) $e^-_{aq} + HO_2^- \rightarrow H_2O + OH + 2OH^-$	2.0×10^7	3.0
(15) $H^+ + OH^- \rightarrow H_2O$	1.4×10^{11}	3.0
(16) $H_2O \rightarrow H^+ + OH^-$	2.6×10^{-5}	3.0
(17) $H + OH \rightarrow H_2O$	3.0×10^{10}	3.0
(18) $OH + H_2 \rightarrow H + H_2O$	4.5×10^7	7.0
(19) $OH + H_2O_2 \rightarrow H_2O + HO_2$	4.3×10^7	4.5
(20) $H + H_2O_2 \rightarrow OH + H_2O$	9.0×10^7	4.5
(21) $H + O_2 \rightarrow HO_2$	1.9×10^{10}	3.0
(22) $HO_2^- + O_2^- \rightarrow H^-$	8.0×10^7	3.0
(23) $O_2^- + H^+ \rightarrow HO_2$	5.0×10^{10}	3.0
(24) $HO_2 + O_2^- \rightarrow O_2 + HO_2^-$	9.5×10^7	4.5
(25) $2HO_2 \rightarrow H_2O_2 + O_2$	2.7×10^6	4.5
(26) $O_2^- + O_2 + H_2O_2 \rightarrow O_2 + 2OH^-$	Base Chem 10^2	4.5
(27) $H + HO_2 \rightarrow H_2O_2$	2.0×10^{10}	3.0
(28) $K + O_2^- \rightarrow HO_2^-$	2.0×10^{10}	3.0
(29) $e^-_{aq} + O_3^- \rightarrow HO_2^- + OH^-$	1.3×10^{10}	4.5
(30) $OH^- + H_2O_2 \rightarrow HO_2^- + H_2O$	1.0×10^8	4.5
(31) $HO_2^- + H_2O \rightarrow OH^- + H_2O_2$	1.022×10^5	3.0

Figure VIII

BASE CASE Time Dependent Concentrations of Radiolytically Induced Species (at 25°C)

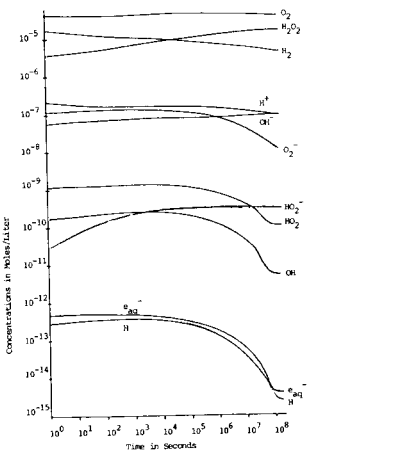


Figure IX

BASE CASE Containment Gas Partial Pressures vs. Time (at 25°C)

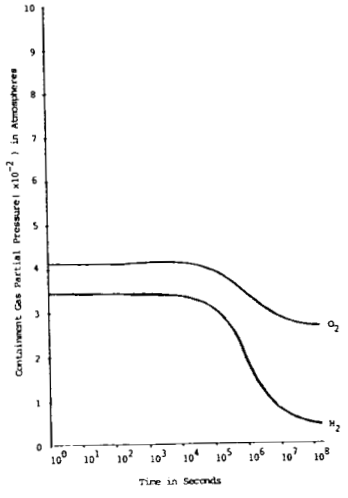


Figure X

BASE CASE SENSITIVITY TO CORE VOLUMETRIC FLOW RATE

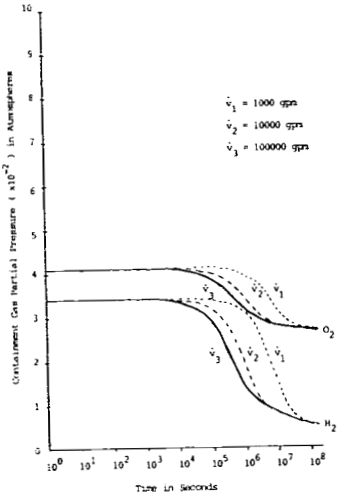


Figure XI

BASE CASE Sensitivity to Extent of Fr-H_2O Reaction

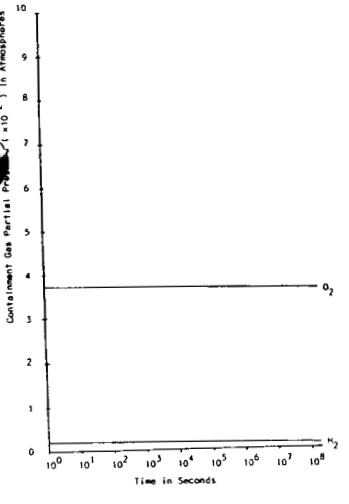
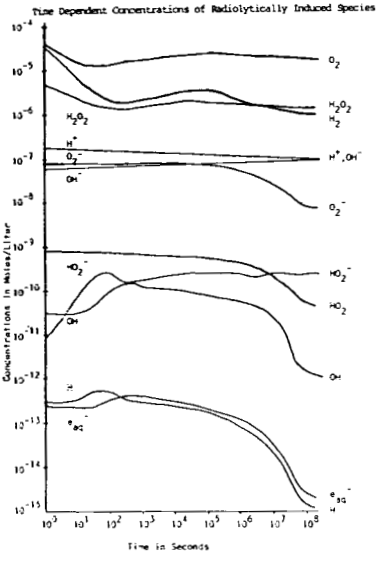
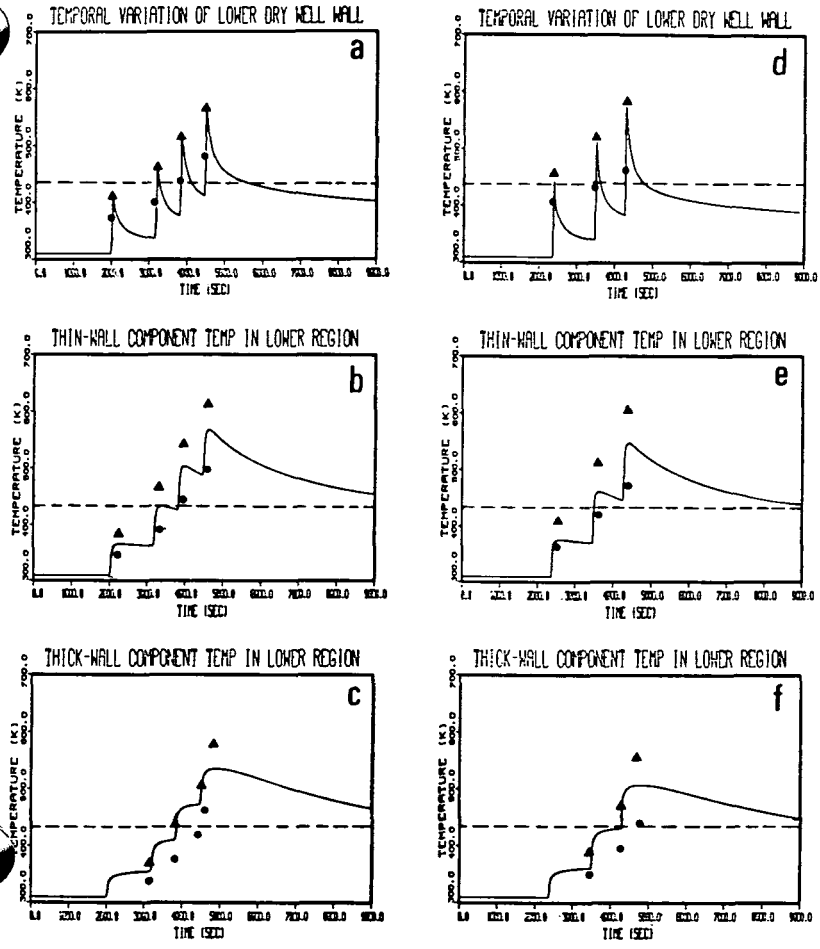


Figure XII

Time Dependent Concentrations of Radiolytically Induced Species (at 100°C)





Legend

——— nonadiabatic flame propagation with radiation, convection and condensation

- - - - - - LOCA qualification temperature (433 K)

● adiabatic flame propagation with radiation, convection and condensation (maxima)

▲ nonadiabatic flame propagation with radiation (maxima)

Figure 5. Thermal responses of representative components and containment surface in the lower wet well region of the Grand Gulf containment for 8% (a,b,c) and 10% (d,e,f) multiple ignition accident scenarios

a & d: steel dome
b & e: thin-wall (hollow cube) component
c & f: thick-wall (solid cube) component





BWR MARK III PRESSURE SUPPRESSION CONTAINMENT RESPONSE TO HYDROGEN DEFLAGRATION

by

Dr. G. M. Fuls - Mr. A. D. Gunter
Westinghouse Offshore Power Systems
7960 Arlington Expressway
Jacksonville, Florida

Report No. OPS-38A94

ABSTRACT

The CLASIX-3 computer program has been used to evaluate the temperature and pressure response of the BWR Mark III Suppression Containment System to hydrogen deflagration resulting from a degraded core condition. The CLASIX-3 computer program is an extension of the CLASIX program which was originally developed to analyze ice condenser containments. A brief description is given of the modifications made to CLASIX to increase its flexibility and versatility to include the capability of analyzing the Mark III Containment. Analytical results are presented for the two base case transients. The two base cases are the stuck open steam relief valve and the small break LOCA, both of which are assumed to lead to a degraded core condition and the release of hydrogen to the containment. Results include pressure and temperature response, gas concentrations and suppression pool response.

BWR MARK III
PRESSURE SUPPRESSION CONTAINMENT RESPONSE
TO HYDROGEN DEFLAGRATION

I. INTRODUCTION

At the first Workshop on the Impact of Hydrogen on Water Reactor Safety in January 1981, a paper was presented on an early version of the CLASIX computer program (Reference 1)*. The analytical model in CLASIX was a fixed array of control volumes and flow paths with a one to one correspondence with those of an ice condenser containment. As a result of this rigid modeling, the applicability of CLASIX to other types of containment, such as dry containments and pressure suppression containments, was limited. However, some CLASIX analysis of these types of containment had been attempted.

Because of the need for licensing support for the BWR Mark III Pressure Suppression Containment of the Mississippi Power and Light Grand Gulf Nuclear Station, significant modifications to CLASIX were required to adequately represent the pressure suppression type containment. To distinguish between the two versions of the program, the numeral three was appended to the name to form CLASIX-3 for the Mark III containment.

II. MODIFICATIONS TO THE PROGRAM

The first need was to generalize the program. The rigid model construction was eliminated so that flow paths can connect any two active control volumes. Similarly, doors, or check valves, can be specified in any active flow path. Passive heat sinks, sprays and addition tables can also be associated with any active control volume. Once this generalization was completed, the following additions were made to the model.

* References are listed at the end of the text.

a. Suppression Pool

The most significant addition to the program was the suppression pool. The analytical model of the pool simulates the dynamic response of the water in the drywell and wetwell pools and in the vents connecting the two pools. The model is based on the one developed in Reference 2. The model in the reference was developed for analysis of the first few seconds of the design basis accident during which the drywell is pressurized and suppression pool vents cleared. Changes in the model were required to permit reverse flow through the vents.

The pressures in the wetwell and drywell provide the external forces which change the water levels, clear vents and cause gas flow through the vents. A schematic diagram of a Mark III containment is shown in Figure 1. An enlarged schematic diagram of the analytical model of the suppression pool is shown in Figure 2. This model consists of six control volumes. Because of the large length to area ratio of the wetwell pool, its inertia is negligible.

Associated with the suppression pool dynamics is the assumption that any gas exiting a vent is assumed to reach instantaneous thermal equilibrium with the pool and that the non-condensibles are released at the surface of the pool at the equilibrium conditions. Thus there is no pool swell due to entrained bubbles in the pool.

b. Steam Relief Valves

Actuation of the steam relief valves and/or Automatic Depressurization System in a Mark III containment results in discharge directly into the wetwell side of the suppression pool. This is simulated in the program the same as the discharge from a vent. The non-condensibles, if any, are instantaneously released at the surface of the pool at thermal equilibrium conditions with the pool.

c. Holdup Volume

During certain transients, the water level in the drywell side of the suppression pool will exceed the height of the weir wall and flow into the depressed area inside the weir wall. This volume is termed the holdup volume. An inventory of the water overflowing the weir wall is maintained and only that amount exceeding the holdup volume is allowed to return to the suppression pool when the pool level again drops below the top of the weir wall.

d. Upper Pool Dump

In most Mark III containments, a large amount of water from the upper pool can be dumped to the suppression pool. The purpose of this feature of the plant is to maintain sufficient mass inventory in the suppression pool during certain postulated severe accidents. This action results in a significant increase in the containment volume and an increase in mass inventory and water levels in the pool.

e. Drawdown of the Suppression Pool

The suppression pool is the source of water for all low pressure injection and containment spray. Recirculation to the sprays will result in a negligible net reduction in the mass inventory in the suppression pool. However, use of the suppression pool water to refill the reactor system can result in a significant net reduction in the pool inventory.

For a stuck open relief valve transient, any reactor system makeup water removed from the pool in excess of the amount necessary to fill the system is returned to the pool through the open relief valves. However in the event of a small break LOCA, the water level in the reactor system would eventually reach the break and be released into the drywell to accumulate in the holdup volume discussed above.

The program permits the removal of two volumes of water from the suppression pool. Each may occur at a different rate and occur at different times in the transient. The volume of water going to fill the reactor system is effectively removed from future calculations. The second volume of water is added to the inventory in the holdup volume discussed above. For a stuck open relief valve transient, the second volume would not be used.

f. Spray Carryover

With the containment represented by more than one volume, some of the spray generated at the spray header will eventually pass through open areas and grating into a physically lower volume. As shown in Figure 1, some of the spray from the containment volume will pass through annular openings into the wetwell volume. In the program, a fraction of the spray terminating its fall in one volume may be specified as carrying over to another volume.

g. Inverted Flame

For the small break LOCA transient, the drywell atmosphere at the end of hydrogen generation is almost equal parts of steam and hydrogen. With the Combustible Gas Control System (CGCS) and/or vacuum breakers introducing relatively dry air from the containment into the drywell, it is possible for an inverted flame to occur in the vicinity of the discharge of the CGCS and/or vacuum breakers. This phenomenon is modeled in the program.

III. SAMPLE ANALYTICAL RESULTS

Extensive analyses have been performed with CLASIX-3 on the Mark III containment. The majority of these analyses have been performed as generic studies utilizing parameters appropriate to the Grand Gulf Nuclear Station. Only the two cases considered the base cases will be discussed here. In the stuck open relief valve case all releases are directed into the suppression pool on the wetwell side and consequently all of the hydrogen is first introduced into the wetwell

volume. The second case is the small break LOCA which initially discharges directly into the drywell but, because of the manual or automatic activation of the depressurization system later in the transient, some of the discharge is directed to the wetwell side of the suppression pool. In both transients, discharge rates of steam, hydrogen and fission product energy are based on MARCH analytical results. Since recovery of some core cooling capability is assumed to limit the zirconium/water reaction to 75% of the active fuel cladding, the MARCH results were modified to eliminate core slump and the corresponding high rate of hydrogen generation.

For the analysis, a schematic of the containment as shown in Figure 3 was used. The major assumptions for the two transients are shown in Tables 1 and 2.

Results from the drywell break are shown in Figures 4 to 15 inclusive. As discussed above, initially all releases are to the drywell, but after actuation of the depressurization system, it is assumed that one-half the discharge is released through the relief valves into the wetwell side of the suppression pool. At the same time that depressurization is begun, the CGCS is also activated. The reactor system discharges continue until 7800 seconds when the core is recovered and no more hydrogen is released. During the period of discharge numerous burns occur in the wetwell with a peak containment pressure of 27 psia (12 psig).

However, at the end of discharge, the drywell atmosphere consists of about half hydrogen and half steam. Eventually the steam in the drywell will condense sufficiently and the CGCS will supply sufficient air to cause a combustible mixture and ignition in the drywell. This portion of the transient is shown in Figures 10 through 15. Because the CGCS continues to pressurize the drywell relative to the containment, some hydrogen passes through the suppression pool vents to cause several additional wetwell burns. At about 11,200 seconds, sufficient oxygen accumulates in the drywell to cause ignition. As pressure rises due to deflagration, excess hydrogen is rapidly

discharged through the suppression pool to cause rapid burning throughout the containment and wetwell. The result is a containment pressure spike on the order of 47 psia (32 psig).

Comparable results for the stuck open relief valve (SORV) base case are shown in Figure 16 to 21 inclusive. Many burns occur in the wetwell during this transient and, based on the initial criteria for ignition, no burns would occur elsewhere. However, at the end of reactor system discharge, the hydrogen concentration in the containment is so close to the ignition setpoint that a burn was forced to occur in the containment volume to evaluate its effects. The result is a peak pressure of 39 psia (24 psig). This is 8 psi lower than the peak obtained with the drywell transient.

In comparing the two cases, the responses are generally similar with the differences being reasonable based on the differences in the transients.

IV. SUMMARY

The analytical model developed for the CLASIX-3 computer program provides a detailed model for the evaluation of hydrogen deflagration in a Mark III containment. Based on the extensive use of the two CLASIX programs, the numerous sensitivity studies and the verification of the analytical model to date, a high level of confidence can be placed in the analytical results produced by CLASIX-3.

REFERENCES

1. "Containment Pressure Response to Hydrogen Combustion," Proceedings of the Workshop on the Impact of Hydrogen on Water Reactor Safety, NUREG/CR-2017, Vol. 1, pp 227-251, August 1982.

2. "The General Electric Mark III Pressure Suppression Containment System Analytical Model," W. J. Belanin, NEDO 20533, June 1974.

TABLE 1

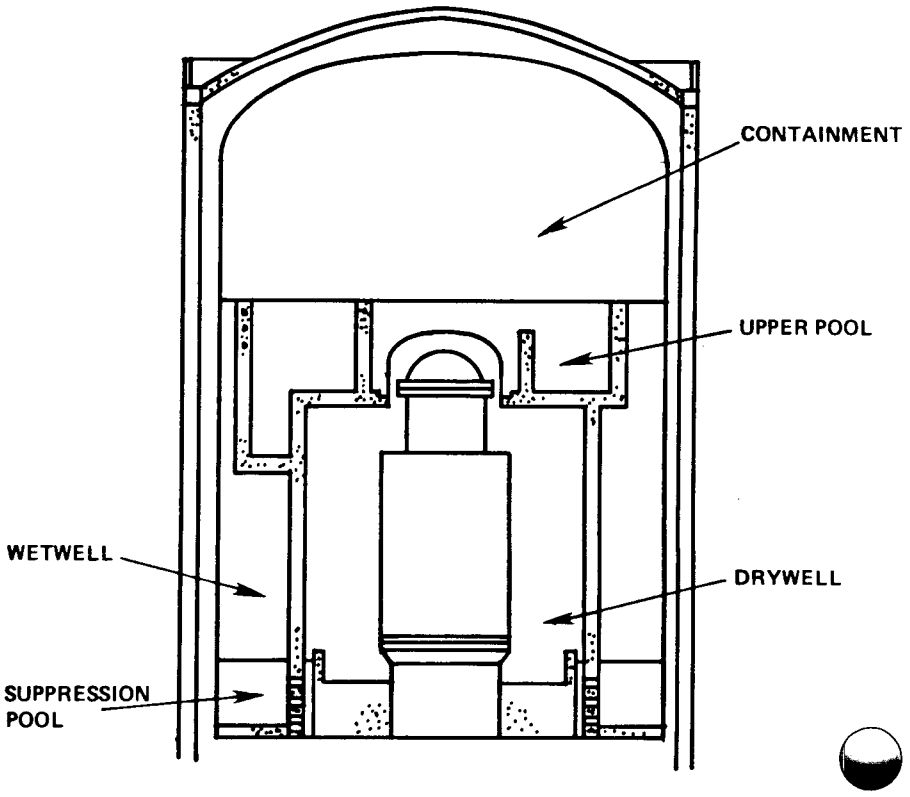
Drywell Break Base Case Description

- Modified MARCH Release Rates
- 50/50 Release Rate Split between drywell and suppression pool at 20 minutes
- CGCS and Igniters - Initiated at 20 minutes
- Upper Pool Dump - Initiated at 30 minutes
- Suppression Pool Drawdown - Initiated at 30 minutes
- 8 ^{v}/o hydrogen for ignition & 85% completion
- 6 ft/sec flame speed
- 1 Spray Train - Initiated after first burn
- Wetwell spray carryover

TABLE 2

SORV Base Case Description

- Modified MARCH Release Rates
- CGCS and Igniters - Initiated at 20 minutes
- Upper Pool Dump - Initiated at 30 minutes
- 8 $^{v}/_{o}$ hydrogen for ignition & 85% completion
- 6 ft/sec flame speed
- 1 Spray Train - Initiated after first burn
- Wetwell spray carryover
- Forced Containment Burn at end of Hydrogen Release



MARK III CONTAINMENT

FIGURE 1

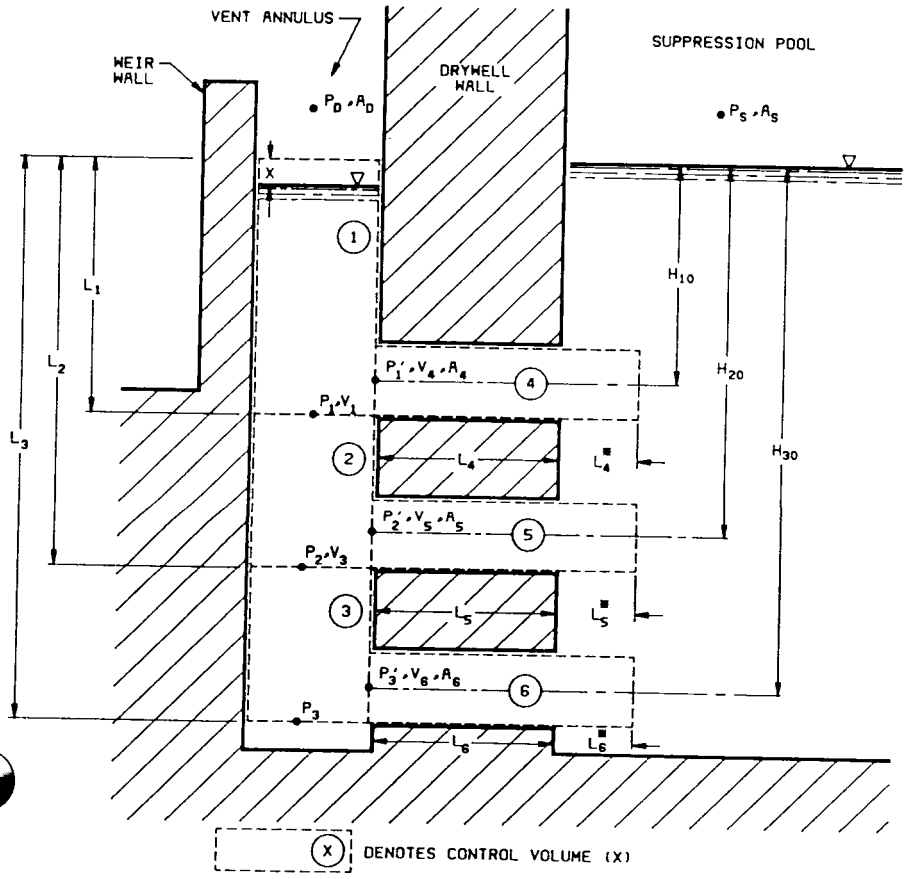
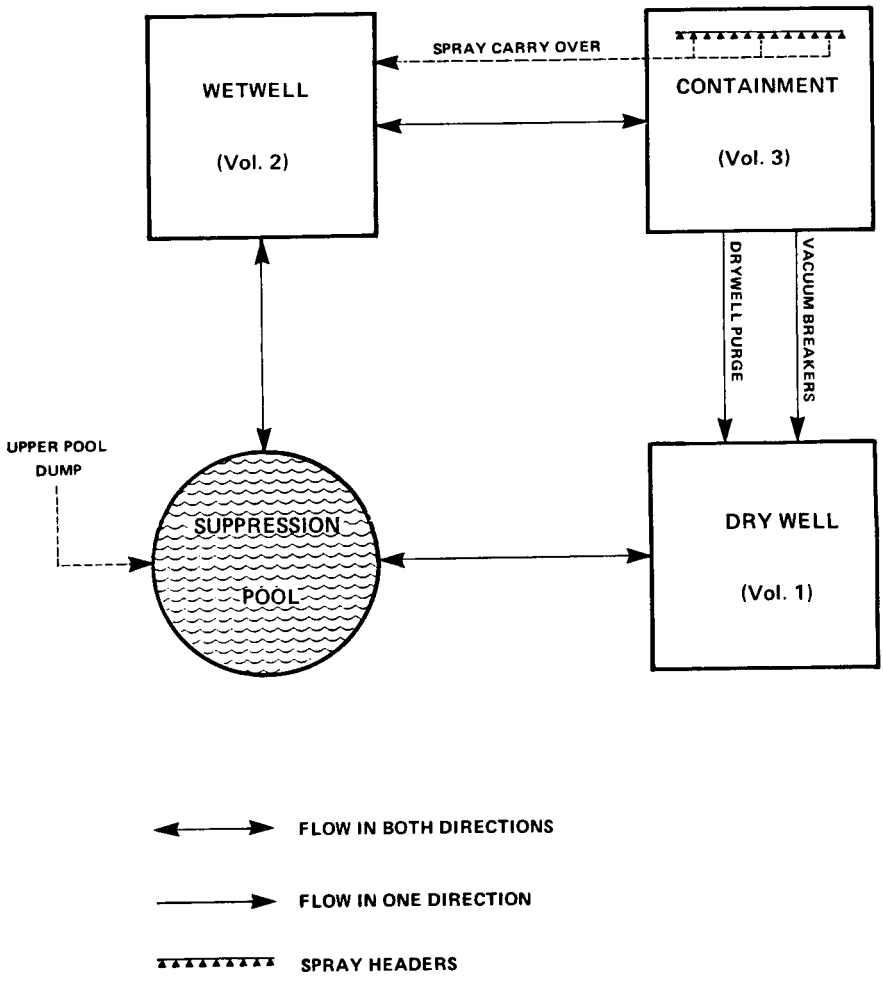
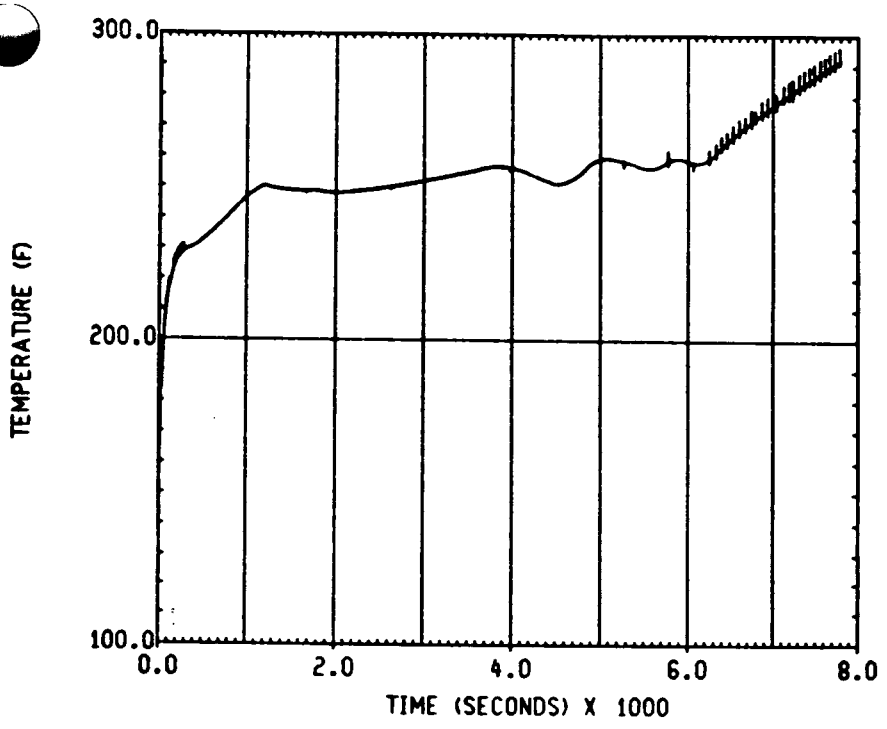


FIGURE 2
SUPRESSION POOL MODEL IN CLASIX-3 COMPUTER PROGRAM

FIGURE 3

GRAND GULF CLASIX-3 MODEL

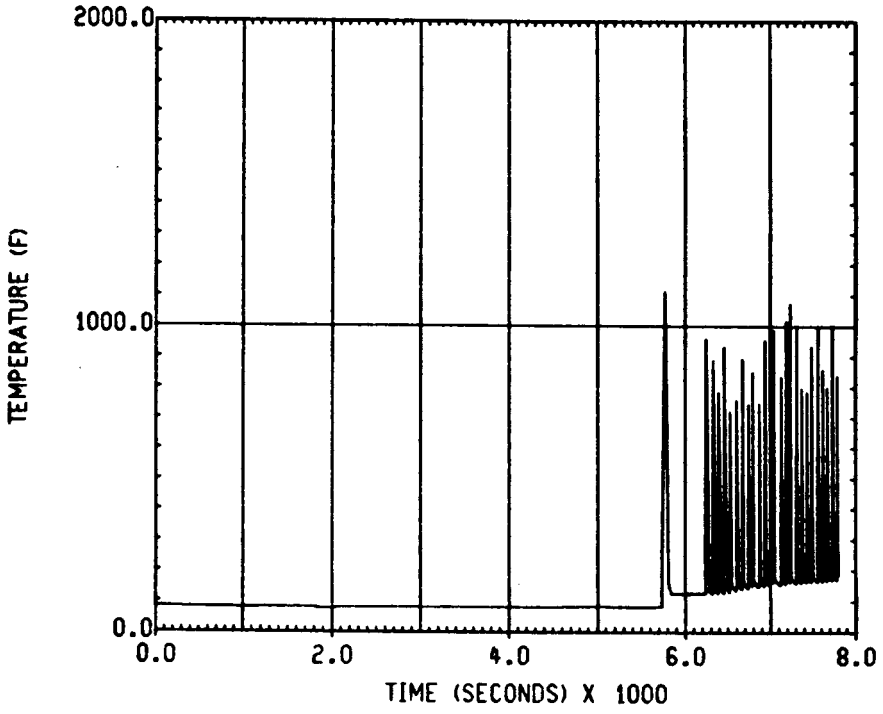




GGNS BASE CASE DRYWELL BREAK

DRYWELL TEMPERATURE

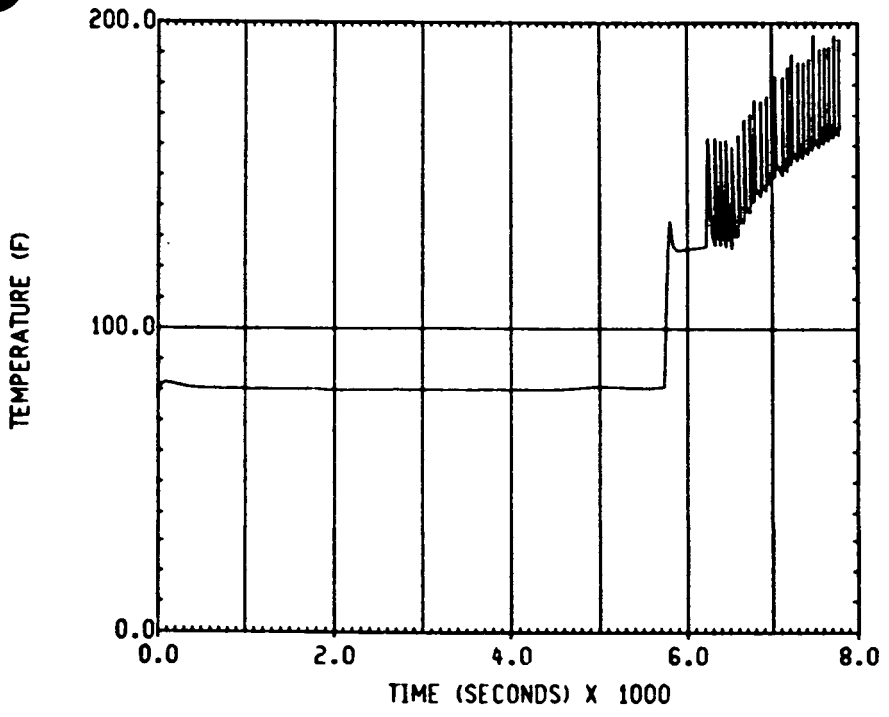
FIGURE 4



GGNS BASE CASE DRYWELL BREAK

WETWELL TEMPERATURE

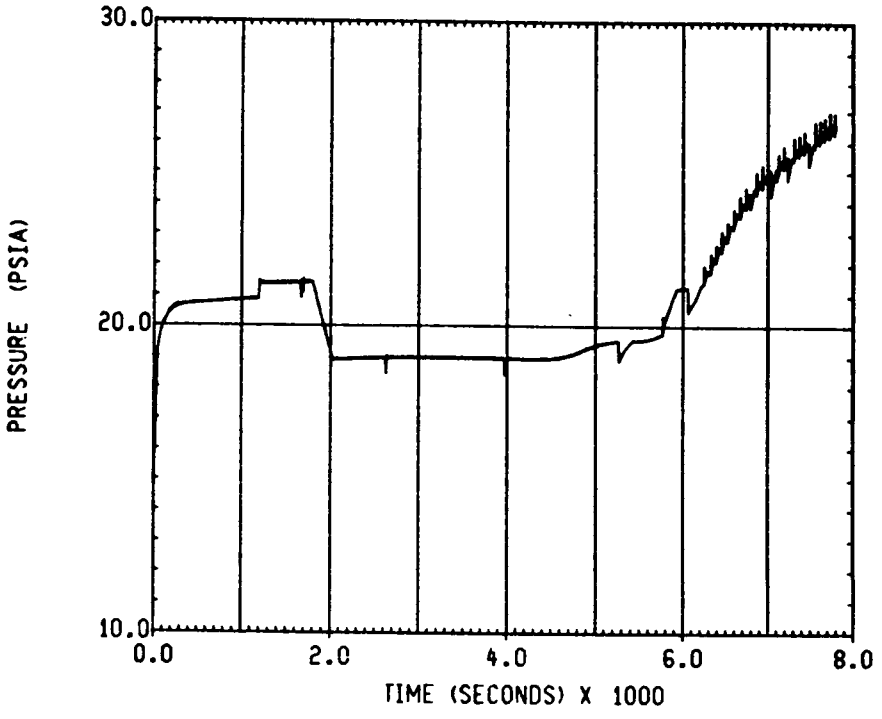
FIGURE 5



GGNS BASE CASE DRYWELL BREAK

CONTAINMENT TEMPERATURE

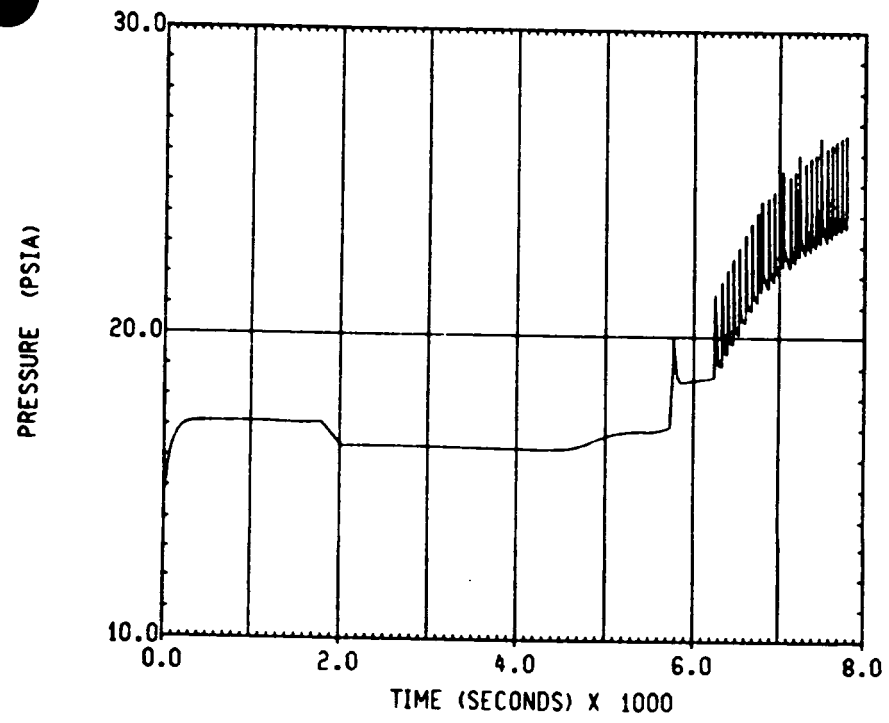
FIGURE 6



GGNS BASE CASE DRYWELL BREAK

DRYWELL PRESSURE

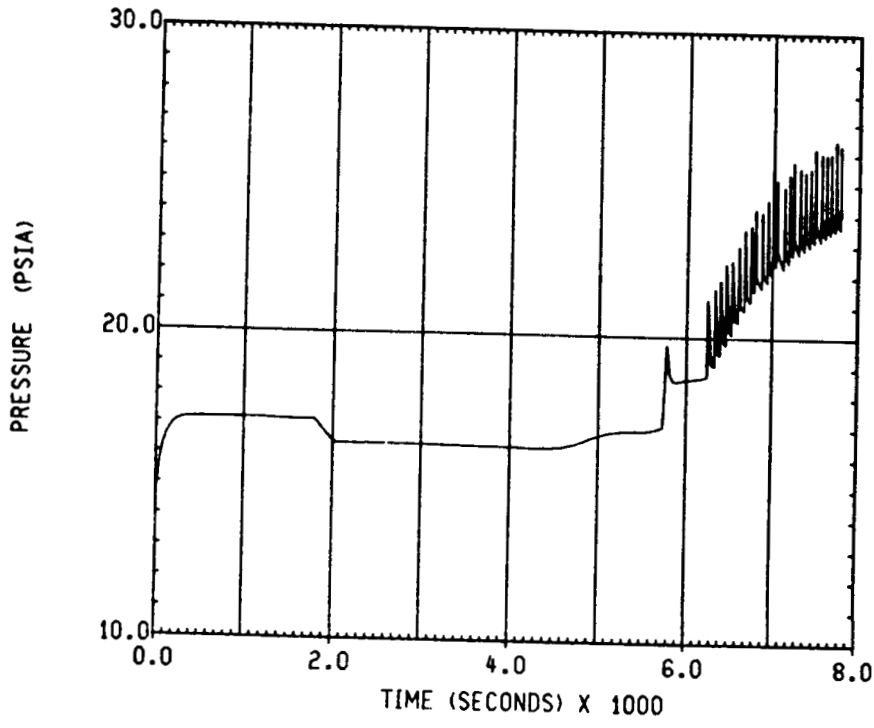
FIGURE 7



GGNS BASE CASE DRYWELL BREAK

WETWELL PRESSURE

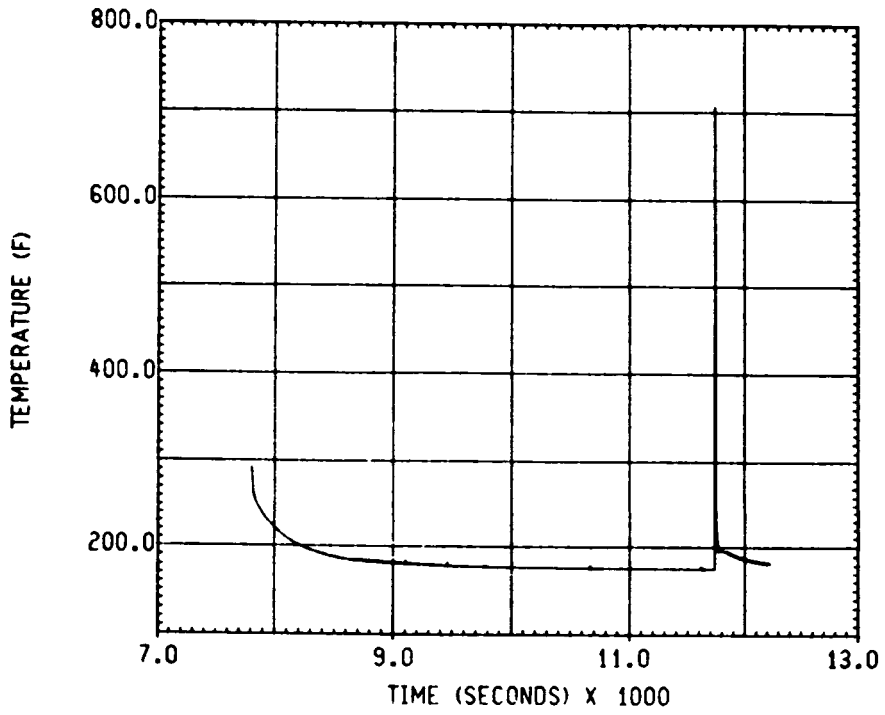
FIGURE 8



GGNS BASE CASE DRYWELL BREAK

CONTAINMENT PRESSURE

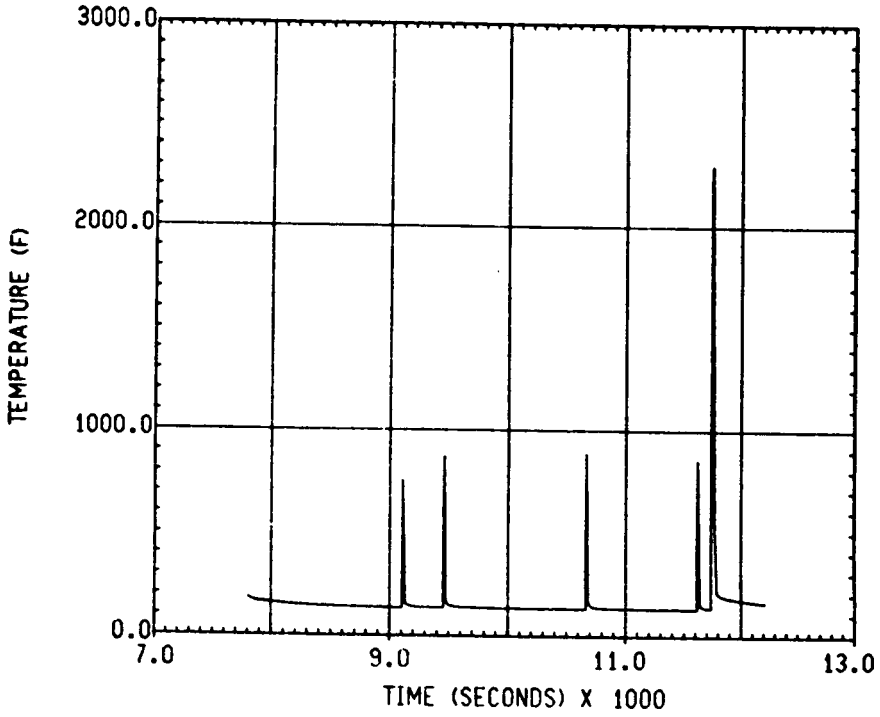
FIGURE 9



GGNS BASE CASE DRYWELL BREAK

DRYWELL TEMPERATURE

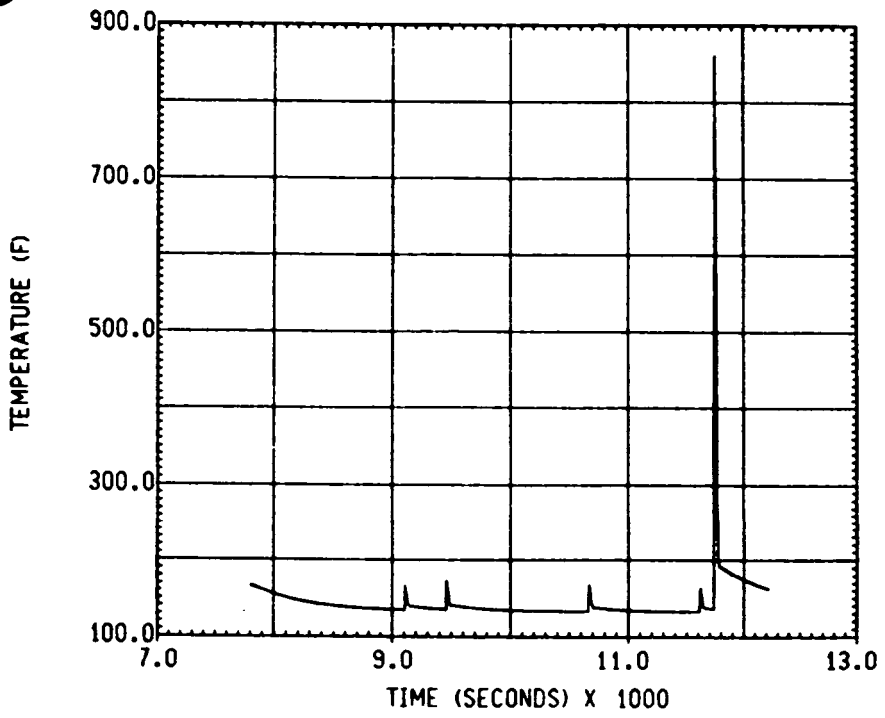
FIGURE 10



GGNS BASE CASE DRYWELL BREAK

WETWELL TEMPERATURE

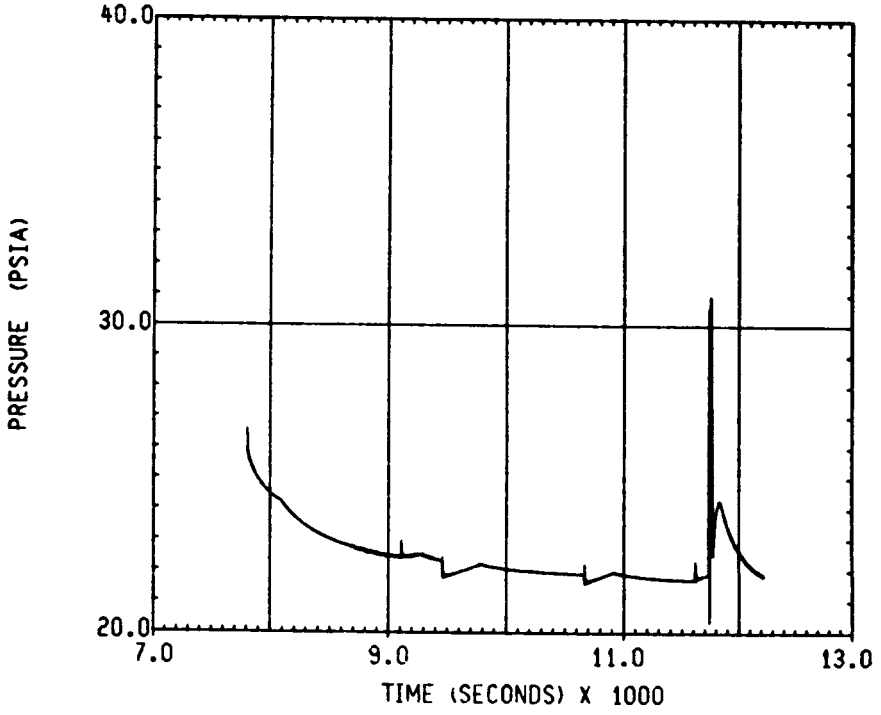
FIGURE 11



CGNS BASE CASE DRYWELL BREAK

CONTAINMENT TEMPERATURE

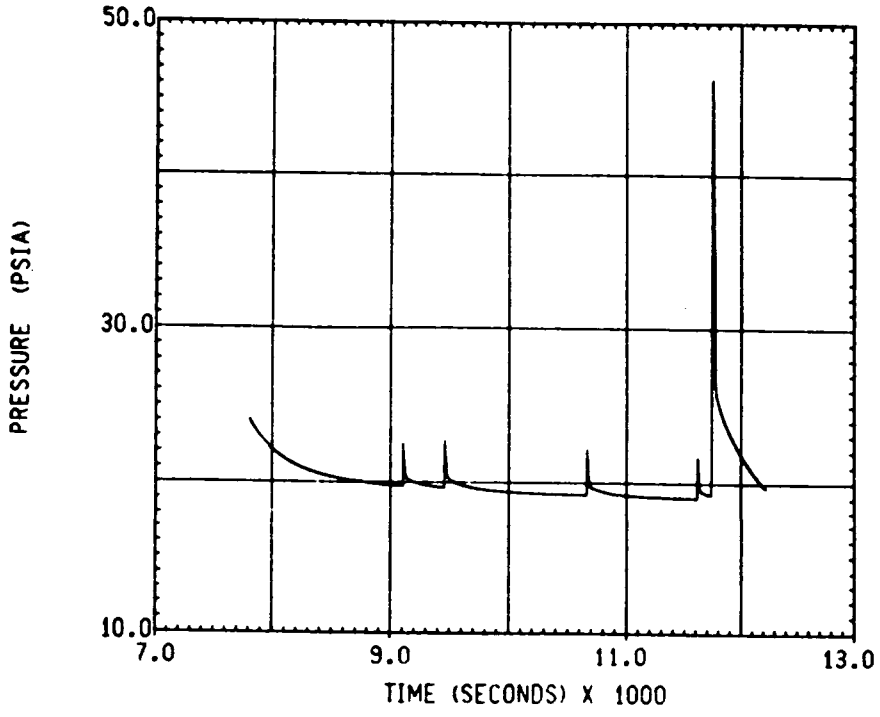
FIGURE 12



GGNS BASE CASE DRYWELL BREAK

DRYWELL PRESSURE

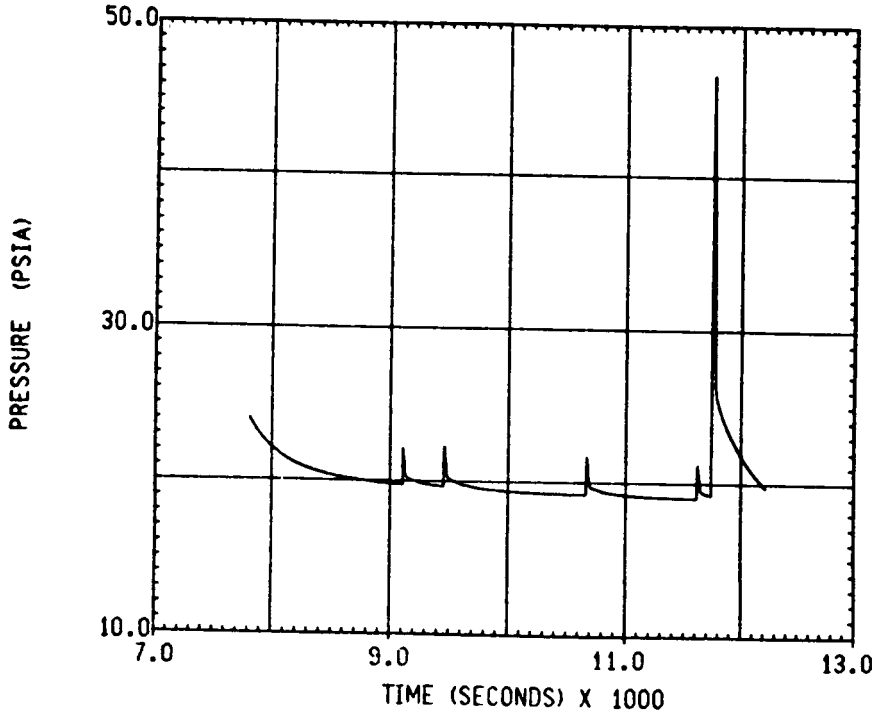
FIGURE 13



GGNS BASE CASE DRYWELL BREAK

WETWELL PRESSURE

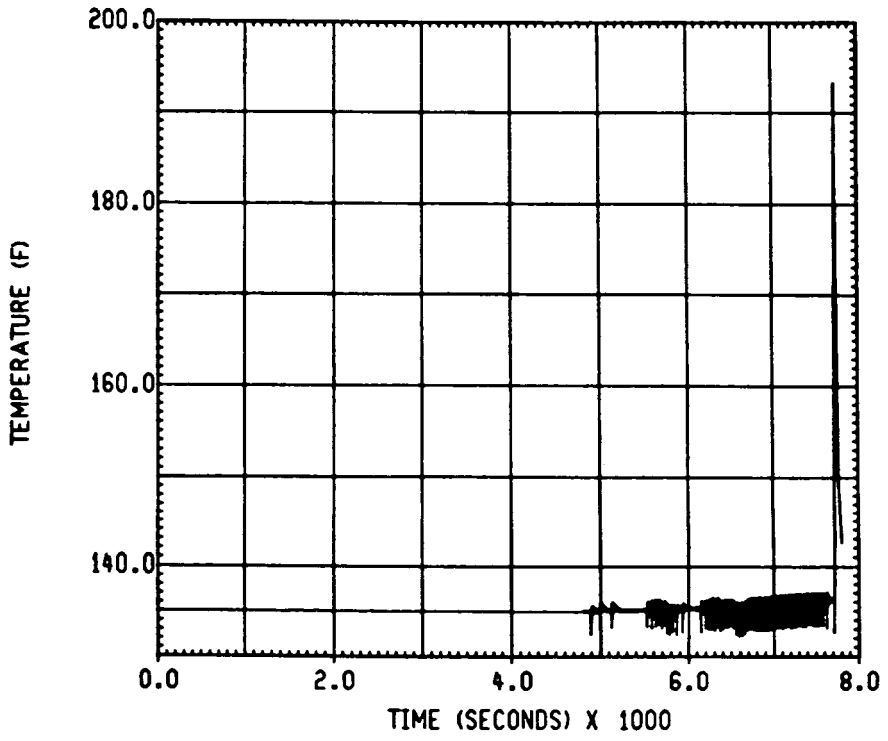
FIGURE 14



GGNS BASE CASE DRYWELL BREAK

CONTAINMENT PRESSURE

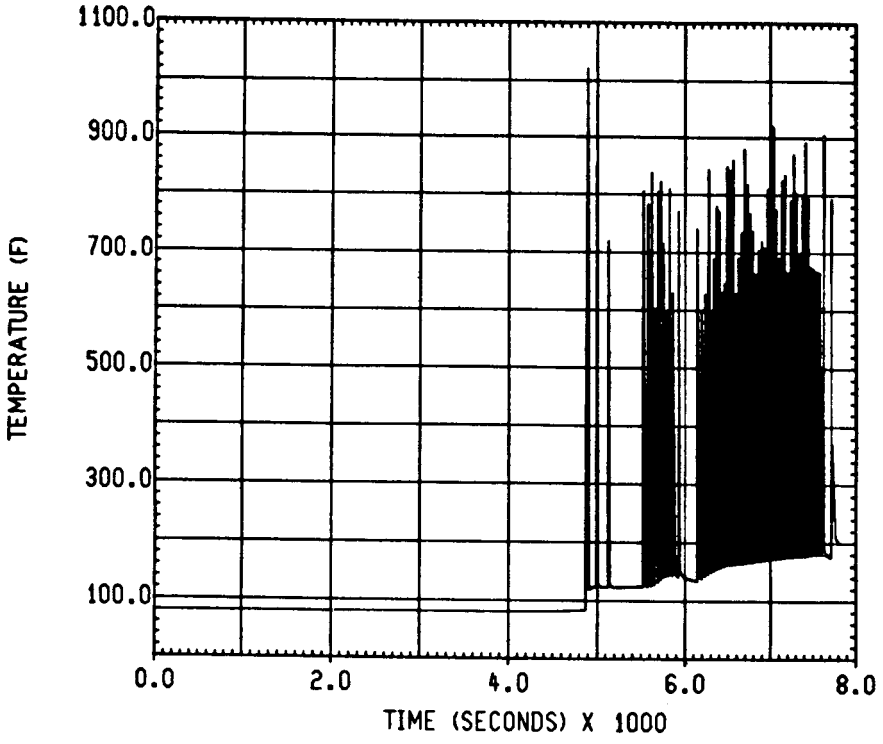
FIGURE 15



GGNS BASE CASE SORV

DRYWELL TEMPERATURE

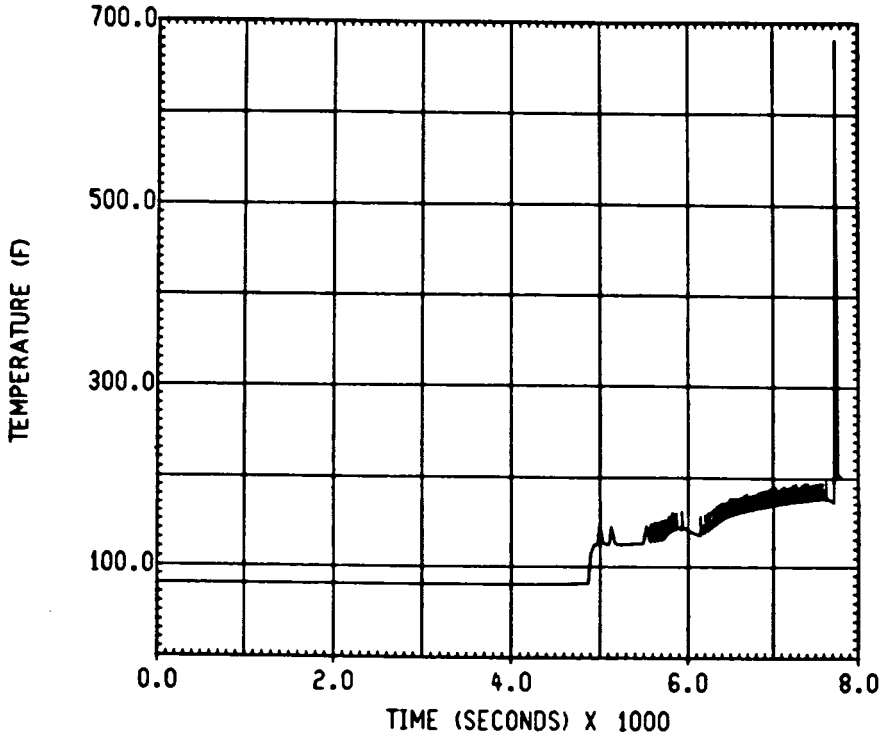
FIGURE 16



GGNS BASE CASE SORV

WETWELL TEMPERATURE

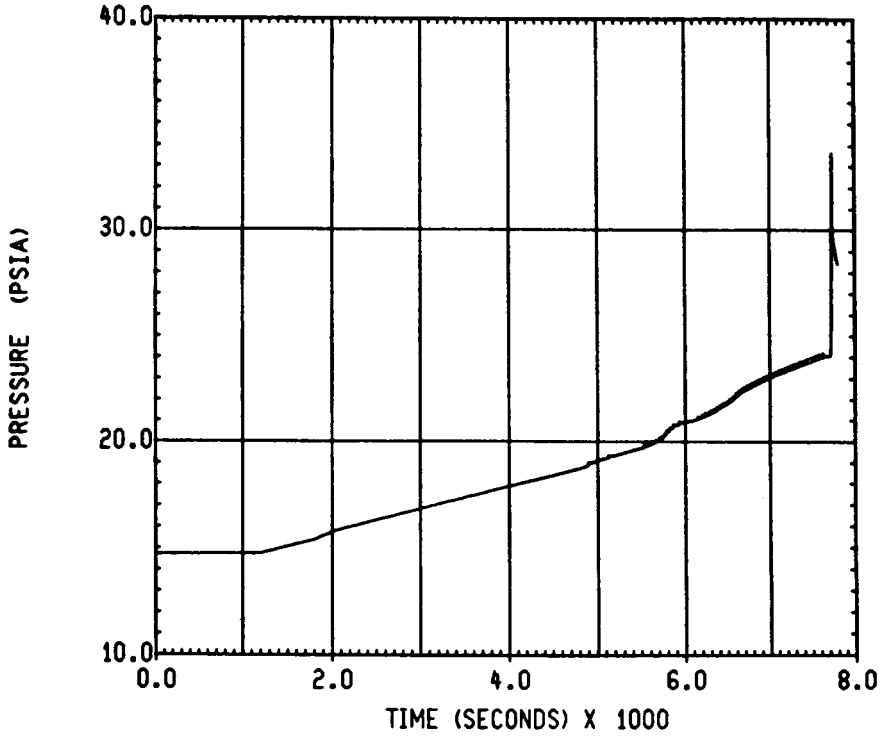
FIGURE 17



GGNS BASE CASE SORV

CONTAINMENT TEMPERATURE

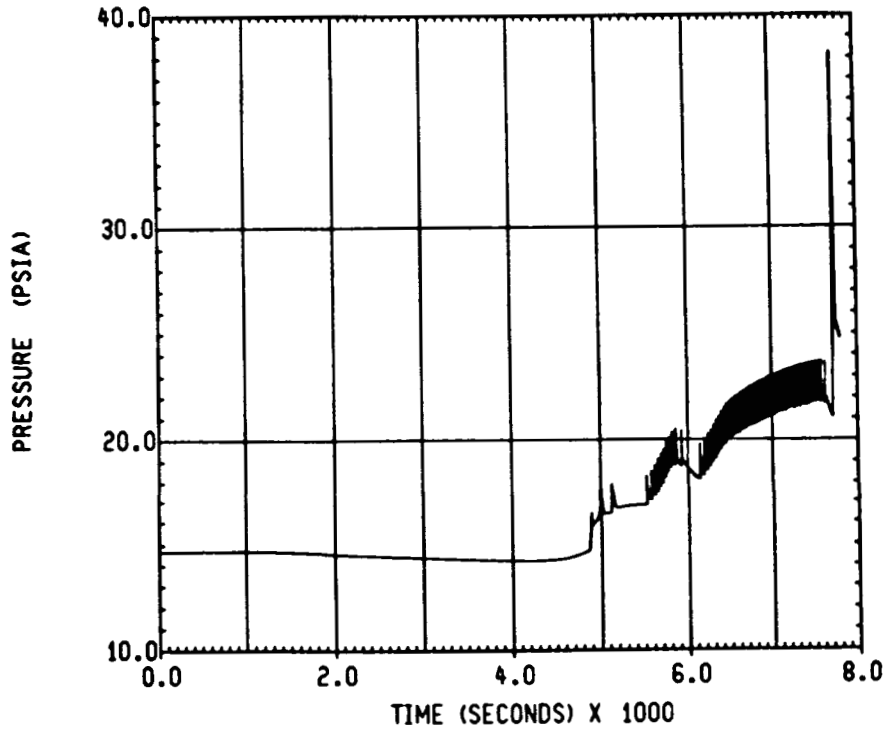
FIGURE 18



GGNS BASE CASE SORV

DRYWELL PRESSURE

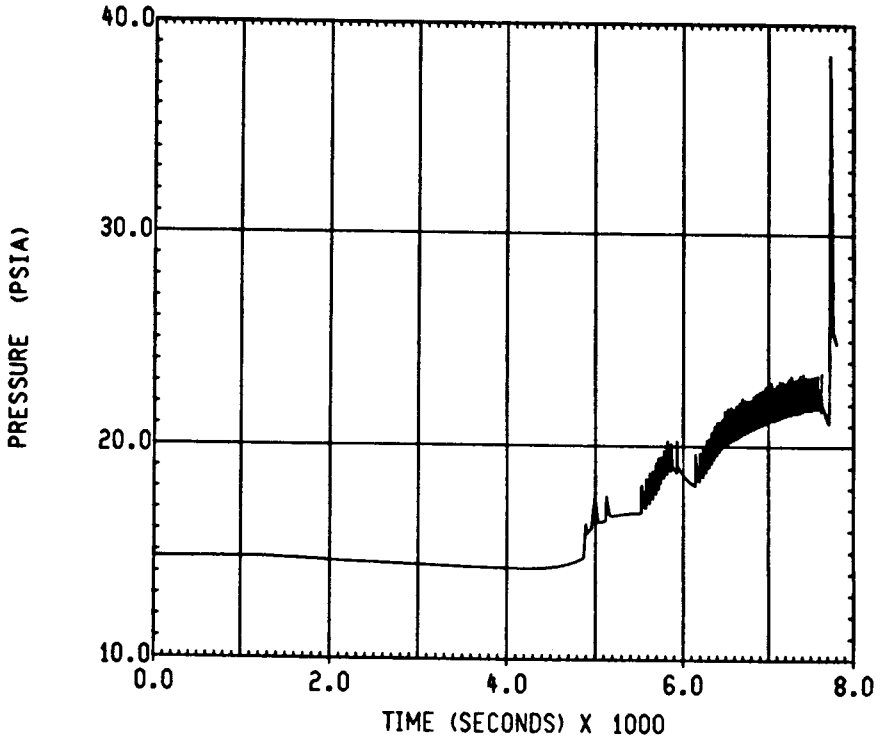
FIGURE 19



GGNS BASE CASE SORV

WETWELL PRESSURE

FIGURE 20



GGNS BASE CASE SORV

CONTAINMENT PRESSURE

FIGURE 21

TITLE: Effect of Hydrogen Control on the Risk from Severe Accidents in the BWR/6 Mark III Standard Plant

AUTHORS: D. A. Hankins, K. W. Holtzclaw
General Electric Company
San Jose, California

Introduction

One of the key issues identified by the NRC related to severe accidents has been hydrogen control. In the notice of Proposed Rulemaking on Interim Requirements Related to Hydrogen Control in December, 1981, the NRC has proposed additional hydrogen control systems for the BWR/6 - Mark III design to accommodate hydrogen release from postulated severe accidents. The proposed rule would require applicants to demonstrate maintenanc of containment integrity for events which release an amount of hydrogen equivalent to 75% metal-water reaction of the active fuel cladding.

This quantity of hydrogen can only be generated from a severely degraded core and most probably an accident with substantial core melt. Core meltdown accidents may lead to core-concrete interaction and loss of containment integrity by the generation of non-condensible gases such as carbon monoxide and carbon dioxide. Precluding hydrogen combustion in the accident sequence will not prevent eventual loss of containment integrity. Overpressurization of containment by concrete decomposition products can occur in all current light water reactor containment designs.

This paper discusses the potential risk reduction for precluding hydrogen combustion in a Mark III containment. The potential risk reduction is minimal because the Mark III containment is designed to mitigate the effects of loss of containment integrity caused by either hydrogen combustion or concrete decomposition.

The BWR/6 Standard Plant Probabilistic Risk Assessment[1] (PRA) considered hydrogen generation for severe accidents. The PRA quantified the consequences of hydrogen combustion events taking account of the structural capability of the drywell and suppression pool to assure scrubbing of potential fission product releases even for cases with loss of primary containment integrity. Fission product retention by suppression pool scrubbing means that the containment function (limiting offsite doses) is maintained even for severe accidents.

Quantification of the fission product scrubbing capability of the suppression pool during severe accidents was based on GE's Fission Product Scrubbing Program[2]. A first principles analytical model was developed to describe fission product scrubbing in the suppression pool. Experimental verification of this model was obtained by mass-transfer and hydrodynamic testing. This model predicts that the suppression pool would reduce particulate fission product releases by a factor of 10,000 in the unlikely event of a severe accident. These results confirm that the BWR suppression pool would effectively retain fission products released during severe accidents.

Utilizing the accident sequence results developed in the PRA for full core meltdown accidents and an assessment of partial core melt accidents (where the melt progression is terminated inside the reactor pressure vessel), the maximum potential risk reduction for a hydrogen control system in the BWR/6 Standard Plant was evaluated.

Methodology

Two approaches were used to assess the maximum risk reduction afforded by the addition of a hydrogen control system to the BWR/6 Standard Plant design. The first approach used PRA techniques to assess the plant risk in terms of man-rem/year. The PRA assumes that all core damage sequences result in full core meltdown and loss of containment integrity.

The results from all accident sequences were grouped into fifteen fission product release categories (compared to five used in WASH-1400). These fifteeen release categories were input to the analysis which determines offsite consequences. In seven of the fifteen categories loss of primary containment integrity was postulated to result from hydrogen combustion. In the remaining eight categories containment overpressurization by steam or noncondensible gases was postulated. The effect of precluding hydrogen combustion for the first seven categories is to shift the loss of containment integrity from the time of hydrogen combustion to the time of containment overpressurization from noncondensibles generated primarily by core concrete interaction. This delay in the time of fission product release could reduce risk by allowing additional time for fission product decay before the loss of containment integrity.

Mean risk was calculated using the CRAC code with the WASH-1400 site 6 meteorology and population within 50 miles of the plant. Site 6 was used as a representative site because it has average site characteristics. The population within 50 miles was used to allow comparison with the proposed NRC safety goal[5]. Relative to the proposed safety goal, the BWR/6 Standard Plant risk is well below the proposed numerical guidelines for core melt probability and risk.

The second method of assessing the maximum effect of hydrogen control on severe accident risk considered partial core melt sequences. Partial core melt is defined as an accident where core cooling is restored in time to arrest the melt progression and establish coolable geometry within the reactor pressure vessel. Partial core melt was analyzed since the NRC has focused on less than a full core meltdown for consideration in hydrogen control rulemaking. Two cases were analyzed: ten percent of the core melted and fifty percent of the core melted. These two cases were chosen to represent approximate bounds for partial core melt conditions. Events with less than ten percent core melt do not produce substantial amounts of hydrogen (less than twelve percent metal-water reaction). For events with greater than fifty percent core melt, termination of the event within the reactor pressure vessel cannot be assured and the event would then fall into one of the full meltdown sequences previously discussed.

Fuel releases of fission products were calculated as a function of temperature and time at temperature. Six transient-initiated accident sequences were modeled. These sequences contribute 98% of the assessed frequency of core damage (see Table 1.0) for the BWR/6 Standard Plant.

Results

Risk results of the full core melt accident sequences are given in Table 2.0. The results are expressed as man-rem per reactor year for a population to 50 miles) and the BWR/6 Standard Plant PRA result (for a population to 500 miles). The BWR/6 PRA result is provided for comparison only. These results combine the probability of the accident and its consequences. It can be concluded that the maximum risk reduction achievable is 0.14 man-rem /reactor year which is a small risk reduction when compared to the safety goal numerical guidelines discussed below.

Table 3.0 gives the results of the partial core-melt analyses in man-rem. A comparison is made to the natural background radiation (100 millirem) received by the same population in one-year. The partial core melt results are expressed in terms of consequences only with no regard for the probability of accident occurrence (i.e., accident probability assumed equal to one). It can be seen that for the fifty percent core melt case the total exposure from the accident is equivalent to 3% (24,360 man-rem) of the annual background radiation exposure. Therefore, in absolute terms, any reduction in this exposure is not significant.

Comparison to Proposed NRC Safety Goal

In February, 1982 the NRC published for public comment a proposed policy statement on safety goals for nuclear power plants. In addition, a separate report (NUREG-0880) discussing the development of the proposed policy statement was published. Although the NRC safety goal policy is only in draft form, it provides a useful comparison in assessing the results of the BWR/6 Standard Plant PRA.

The proposed NRC policy statement proposes the following numerical guidelines:

1. Individual and Societal Mortality Risks

   The risk to an individual or to the population in the vicinity of a nuclear power plant site of prompt fatalities that might result from reactor accidents should not exceed one-tenth of one percent (0.1%) of the sum of prompt fatality risks resulting from other accidents to which members of the U.S. population are generally exposed.

   The risk to an individual or to the population in the area near a nuclear power plant site of cancer fatalities might result from reactor accidents should not exceed one-tenth of one percent (0.1%) of the sum of cancer fatality risks resulting from all other causes.

2. Benefit-Cost Guideline

The benefit of an incremental reduction of risk below the numerical guidlines for societal mortality risks should be compared with the associated costs on the basis of $1,000 per man-rem averted.

3. Plant Performance Guideline

Large-Scale Core-Melt: The likelihood of a nuclear reactor accident that results in a large-scale core melt should normally be less than one in 10,000 per year of reactor operation.

A comparison of the PRA results to the NRC proposed guidelines is provided in Table 4.0. Comparison is made to all the numerical guidelines dealing with mortality risks and plant performance.

The calculated core melt probability of ~5 x 10^{-6} per reactor year for the BWR/6 Standard Plant is a factor of 20 below the proposed guideline. There were no calculated early (prompt) fatalities for the sequences considered. Consequently, the BWR/6 results are well below the NRC guidelines for individual and societal prompt fatality risks. The NRC numerical guideline for individual latent fatality risk is based on 0.1% of national statistics[3] and is equivalent to ~2.0 x 10^{-6}. The PRA result of 1.7 x 10^{-5} latent fatalities (the mean of the risk curve for fatalities within 500 miles) when divided by the population within 1 mile of the site (168 people) yields an individual latent fatality risk of 1.0 x 10^{-7}. The societal latent fatality risk is calculated to be 1.7 x 10^{-5} and is five orders of magnitude below the guideline value of 3.2.

Comparison of the results in Table 2.0 to the proposed cost-benefit guideline of $1000 per man-rem averted shows that an estimated $10 million hydrogen control system fails the proposed cost-benefit comparison by orders of magnitude. If a system could avert all man-rem from the accident (which is clearly impossible), the system should cost less than $140 per year (0.14 man-rem x $103) to be cost-beneficial. Considering partial core melts without regard to accident probability, the maximum risk reduction afforded by a hydrogen control system is insignificant (24,000 man-rem) compared to background radiation (800,000 man-rem).

Conclusions

Therefore, relative to natural background radiation, the addition of a hydrogen control system provides minimal risk reduction. Further, the BWR/6 Standard Plant risk is already low compared to the proposed NRC Safety Goal and thus the provision of an additional hydrogen control system is not cost effective.

TABLE 1.0

BWR/6 PRA RESULTS:

BREAKDOWN OF THE ASSESSED FREQUENCY OF CORE DAMAGE PER REACTOR YEAR

Event Description	Frequency of Core Damage Per Reactor Year	Percent of Core Damage Probability
o Transients		98.
o Loss of Offsite Power	4.1×10^{-6}	(88)
o All others	5×10^{-7}	(10)
o Loss of Heat Removal	2×10^{-8}	0.4
o ATWS	6×10^{-8}	1.3
o LOCA	2×10^{-9}	0.04
Total	4.7×10^{-6}	

TABLE 2.0

BWR/6 PRA RISK RESULTS FOR FULL CORE MELTDOWN SEQUENCES

	Risk (Man-rem per reactor-year)
o Standard Plant PRA Result, All accident sequences Population within 500 miles	0.26
All accident sequences Population within 50 miles	0.14

TABLE 3.0

PARTIAL CORE MELT RESULTS

	MAN-REM PER EVENT*
o 100 percent core melt	30,120
o 50 percent core melt	24,360
o 10 percent core melt	19,430
	MAN-REM PER YEAR
o Background Radiation**	820,000

* It should be noted that the probability of this event is only ~5 x 10^{-6} per year whereas the background radiation occurs every year.

** Annual exposure to 8.2 million people within 50 mile radius of plant.

TABLE 4.0

COMPARISON OF BWR/6 STANDARD PLANT PRA RESULTS TO PROPOSED NRC SAFETY GOALS

Criteria Per Reactor Year	Proposed NRC Guideline	BWR/6 Standard Plant Result
Core Melt Probability	1.0×10^{-4}	$\sim 5.0 \times 10^{-6}$
Individual Prompt Fatality Risk	5.0×10^{-7} (1)	0 (4)
Individual Latent Fatality Risk	2.0×10^{-6} (1)	2×10^{-10}
Societal Prompt Fatality Risk	1×10^{-4} (2)	0 (4)
Societal Latent Fatality Risk	3.2 (3)	1.7×10^{-5}

NOTES:

(1) 0.1% of National Fatality Statistics.

(2) Assuming 1-mile average population of 168 people.

(3) Assuming 50-mile average population of 1.7 million people.

(4) No prompt fatalities were calculated in any of the 238 Nuclear Island PRA accident sequences.

REFERENCES

(1) ''GESSAR II, BWR/6 Nuclear Island Design,'' General Electric Company, March 1982 (22A7007 Rev 2) Section 15D.3

(2) ''GESSAR II, BWR/6 Nuclear Island Design,'' General Electric Company, May 1982 (22A7007 Rev 2) Section 15D.2

(3) U.S. Nuclear Regulatory Commission, ''Safety Goals for Nuclear Power Plants: A Discussion Paper,'' USNRC Report NUREG-0880, February 1982.

ASSESSMENT OF HYDROGEN COMBUSTION EFFECTS IN THE BWR/6 - MARK III STANDARD PLANT

by

J. C. Elliott
L. B. Nesbitt
P. F. Gou
S. S. Dua
D. A. Hankins

General Electric Company
San Jose, California

ABSTRACT

This report discusses General Electric's study of potential hydrogen combustion effects on the Standard Mark III containment during postulated severe accidents. This study was performed as part of the Probabilistic Risk Assessment of the BWR/6 - Mark III Standard Plant. The methodology of determining the accident event sequence and modeling of the Boiling Water Reactor (BWR) core response, including hydrogen generation by metal-water reaction, is described. Combustion of hydrogen released to the containment is analyzed and effects on the Mark III containment system are assessed. It is concluded that even for those cases where containment integrity may be lost, the containment function (i.e., limiting offsite doses) is maintained by the drywell and suppression pool.

1.0 INTRODUCTION

As part of General Electric's Probabilistic Risk Assessment (PRA) of the BWR/6 - Mark III Standard Plant, a study was made to determine the potential effects of hydrogen combustion in the pressure suppression containment. First, accident-initiating events which might lead to core damage and subsequent hydrogen generation were identified, then consistent accident sequences were developed. For each accident sequence, estimates of the timing, rates, and extent of hydrogen generation and transport to the containment were made. Next, the various possible hydrogen combustion modes in the containment were analyzed, and probabilities for a given mode assigned consistent with the accident sequence parameters. Finally, the containment response to the combustion pressure and temperature was analyzed. The following discussion describes the above steps in more detail.

2.0 ACCIDENT SEQUENCE INITIATORS

A comprehensive Probabilistic Risk Assessment (PRA) of the BWR/6 - Mark III Standard Plant (238 Nuclear Island) has been performed.(1.) The objective of this PRA was to assess the core damage probability and associated risk for the 238 Nuclear Island. Accident initiating events which may lead to core damage and subsequent hydrogen generation are listed in Table 2.0 with the corresponding frequency of core damage. Accident initiators are separated into two general groups, transients and loss of coolant accidents (LOCAs). The individual transient accident initiator frequencies were calculated from BWR operating experiences modified to reflect BWR/6 Design features. This data base represents 100 plant-years of experience. WASH-1400 provided the primary basis for the LOCA initiating event frequencies. It can be seen in Table 2.0 that the LOCA contribution to core damage frequency is negligible. Therefore, the most likely hydrogen generating event is a degraded transient which discharges hydrogen directly to the suppression pool through the safety relief valves.

Given the initiating event and assumed system failures, individual accident sequences were modelled to determine the core damage progression. Hydrogen generation during core damage is discussed in the following section.

3.0 HYDROGEN GENERATION AND TRANSPORT TO THE CONTAINMENT

As mentioned previously, postulated accidents are characterized by an accident initiating event (e.g., either an operational transient or a LOCA) with the assumed loss or unavailability of all reactor water makeup systems. Assessment of the hydrogen generation by metal-water reaction (MWR) was based on an integrated analysis of the reactor pressure vessel (RPV) thermal-hydraulic system response, which determines the core heatup, and the behavior of the core as the core temperatures reach the melting point. The total amount of hydrogen generation is limited by the availability of the steam inside the RPV. During the accident, hydrogen and steam are released from the RPV either through the safety/relief valve (S/RV) discharge lines and/or through the vents to the containment, depending on the accident sequence.

TABLE 2.0

BREAKDOWN OF THE ASSESSED FREQUENCY OF CORE DAMAGE

EVENT DESCRIPTION	FREQUENCY OF CORE DAMAGE PER REACTOR YEAR	PERCENT OF CORE DAMAGE PROBABILITY
o Transients		98.
o Loss of Offsite Power	4.1×10^{-6}	(88)
o All others	5×10^{-7}	(10)
o Loss of Heat Removal	2×10^{-8}	0.4
o ATWS	6×10^{-8}	1.3
o LOCA	2×10^{-9}	0.04
TOTAL	4.7×10^{-6}	

For this study, the MARCH code (2.) was used to analyze the thermal-hydraulic behavior of the reactor and containment for postulated highly degraded core cooling accidents. The physical phenomena considered during the accidents include loss of reactor water inventory by boiloff, RPV blowdown (by the operator action according to emergency procedure guidelines or through a break if a LOCA is considered), core uncovery and heatup, and resultant MWR in the core region. The subsequent core meltdown and further MWR during the quenching phase as the molten core debris slumps into the lower plenum water are also modelled. MWR in the intact core as well as the MWR during the quenching phase of the molten part of the core were calculated by using the Baker-Just correlation.

For a representative event, i.e., reactor isolation transient without any water makeup for the entire duration of event progression, the hydrogen generation inside the RPV is determined to be limited to the equivalent reaction of approximately 45% of the cladding surrounding the active fuel for a standard BWR/6-238 plant. However, the amount of MWR is expected to be significantly reduced if the recovery of a water makeup system is postulated within a reasonable time after the accident initiation. For example, the hydrogen generation is calculated to be limited to the equivalent reaction of about 12% of the cladding surrounding the active fuel if a water makeup of about 5000 gpm is assumed to be recovered at about 45 minutes from the event initiation.(3.)

4.0 HYDROGEN COMBUSTION PHENOMENA IN A MARK III CONTAINMENT

Hydrogen combustion phenomena can be divided into four major categories which depend on the hydrogen concentration, spacial

distribution, and the time of ignition. The four categories are: (1) global combustion, (2) local combustion, (3) global detonation, and (4) local detonation. Each of these categories is defined below for the purposes of this study:

4.1 COMBUSTION

Burning of hydrogen at a concentration between 4 and 18 volume percent hydrogen in air.

(1) Local combustion is combustion of hydrogen involving less than 50 percent of the entire volume (e.g., compartments, pockets) within a structure where the hydrogen concentration is not uniform throughout the entire volume. A local combustion which is sustained for more than a few minutes is called a continuous burn. Combustion of local pockets of hydrogen for shorter periods of time are referred to as local combustions. The duration of the continuous burn corresponds to the duration of hydrogen generation after ignition.

(2) Global combustion is combustion of hydrogen involving more than 50 percent of the entire volume within a structure where the hydrogen concentration is approximately uniform within this volume.

4.2 DETONATION

Detonation is combustion where the combustion front moves at supersonic speeds. Detonations can occur at hydrogen concentrations between 18 and 59 volume percent hydrogen in air.

(3) Local detonation is a detonation involving less than 50 percent of the entire volume (e.g., compartments or regions within a structure. The hydrogen concentration is not uniform within the entire volume.

(4) Global detonation is a detonation involving more than 50 percent of the entire volume within a structure. The hydrogen concentration is approximately uniform within this volume.

4.3 APPLICATION OF FLAMMABILITY LIMITS

For the purpose of this study, it was assumed that the following types of combustion occur under the indicated conditions:

(a) Local or Global Combustion occurs when the hydrogen concentration is above 6% by volume and less than 19% by volume at the time of ignition. The combustion is global if the hydrogen has had time to distribute uniformly prior to ignition. The combustion is taken as local if ignition occurs prior to the time needed for uniform distribution. A continuous burn is possible if hydrogen ignites during the

period of hydrogen release from the RPV.

(b) Local Detonation can occur when the hydrogen concentrations exceed 19% by volume at the time ignition occurs. The detonation is taken as local or global depending on whether ignition takes place before or after the time needed for sufficient mixing.

For accident sequences with steam concentrations in the volume of interest greater than 60%, the combustion probability was assessed to be zero. Steam inerting prevents combustion of hydrogen in the drywell for most LOCAs.

4.4 IGNITION SOURCES

For the purposes of estimating ignition sources, accident sequences were divided into events with and without the availability of AC power. If AC power is available, the presence of a large number of electrical contactors in the containment will lead to a very high probability of ignition in a relatively short time. The major sources of ignition in a Mark III containment, assuming the presence of AC power, are located in the annular region between the drywell and the primary containment wall. These sources are primarily at an elevation above the floor that holds the hydraulic control units, and below the operating floor at the upper pool surface level. There are few, if any, ignition sources located on the steel containment wall.

In the absence of AC power (onsite as well as offsite), the probability of ignition is smaller, but not zero, as existing data from BWR off gas system operation indicate hydrogen ignition and combustion have occasionally occurred in systems which have no moving parts and no electrical connections. Also, ignitions could be expected in the BWR containment following an event generating large quantities of hydrogen due to the large amount of electrical instrumentation and equipment which are powered by station batteries.

4.5 APPLICATION OF IGNITION SOURCES

For all events with AC power available, the probability of ignition within the first 24 hours is assessed to be unity because of the multiple ignition sources. Further, the hydrogen is likely to ignite as soon as a combustible concentration is reached, and therefore it is unlikely that the concentration will reach detonable levels.

For events where AC power is not available, ignition is less likely and will most probably occur when AC power is restored. Based on the times for power restoration, it is likely that the hydrogen will be uniformly distributed at the time of ignition, which may result in a global combustion or a global detonation.

In all cases of ignition, the most likely ignition points are around the CRD hydraulic control units. The impact of ignition at this location on the drywell and containment structures is described later in the report. In the case of global combustion, the exact point of

ignition is usually not significant as the combustion front spreads throughout the containment.

4.6 GENERAL CHARACTERISTICS OF HYDROGEN COMBUSTION

If the hydrogen concentration in a volume is non-uniform, it is possible for ignition to initiate local combustion in a mixture approximately 8-12% H_2 by volume and burn at a velocity of ~6.5 to 500 ft/sec to a region of ~19% H_2 where the local combustion becomes a local detonation. It is possible for a local detonation to progress to a region where the concentration of hydrogen is not sufficient to support detonation and to change to a local combustion. It is also possible for the combustion front to progress to an area where a hydrogen stream is being added to the volume and to transform to a continuous burn. Unless ignited by a strong shock wave, an ignition in a hydrogen mixture in the detonable range requires some distance of flame motion before the detonation is produced. This distance is a function of the local hydrogen steam and air concentrations.

4.6.1 PRESSURE RISE FROM LOCAL OR GLOBAL COMBUSTION

Local or global combustion results in a pressure rise caused by the exothermic heat of reaction. Local high temperatures from hydrogen flames, in the case of a continuous burn, can result in equipment damage as well as increased containment pressure.

The pressure rise in a closed volume as a result of the burning of hydrogen is the consequence of two competing phenomena: The exothermic heat of reaction and heat transfer to the walls of the vessel. If combustion occurs after all the hydrogen is added, the reaction is complete in less than a minute (with an initial concentration of 12%, it would take only a few seconds) and the entire energy goes into heating the air space with negligible loss to the walls.

For local or global combustion cases, the pressure rise can be simply calculated from the amount of reactants, the exothermic heat of reaction and the heat capacity of the system. From this it can be seen that the peak pressure is a function of the mass of hydrogen averaged over the whole containment volume. The rate of rise of pressure is a function of the local concentration and heat transfer. The decay in pressure is a function of the heat transfer from the hot reactants to the structures.

For local and global combustion, the presence in the air of fine particle water sprays reduces the resulting pressure rise, by absorbing heat by vaporization. Some experiments report an increase in reaction rate due to the turbulence introduced by water sprays while others report a decrease. The effect of sprays upon the pressures due to a local or global detonation is negligible, although there are some reports that indicate sprays make the propagation of a detonation more difficult.

If global combustion were to occur with an initial concentration of 24

volume percent H_2 for example, the resulting containment pressure would be about 120 psig for an initial pressure of about 20 psia. For the MARK III containment, the combustion of 24 volume percent hydrogen over a period of about 6 minutes results in a peak pressure less than 60 psig (20 psig for early ignition). Therefore, containment integrity will be maintained for some local and global combustion cases.

4.6.2 PRESSURE RISE FROM DETONATION

Ignition of a mixture of hydrogen in air, where the H_2 concentration is greater than 19 volume percent, may result in a detonation. The pressure due to the detonation is not uniform in space or constant with time. Walls parallel to the path of the detonation experience pressures approximately 250 psia (assuming initial conditions of 14.7 psia). Walls perpendicular to the path of the detonation can cause reflections that raise the peak pressure to ~600 psia. The rise time for the pressure is less than 1 μsec. The decay time is a function of the distance the detonation has traveled.

The capability of the containment barriers to maintain their integrity when subjected to hydrogen combustion pressures is discussed later in this report. The pressure effect of local detonations upon objects smaller than walls (e.g., pipes) is a function of the detonation front and pipe detail geometry. However, it is difficult to get a 180° direction reversal of a plane detonation front from a cylindrical pipe surface. Therefore, it is apparent that the effect on pipes is about that of the effect on walls parallel to the motion of the front or about 17 times the initial pressure (~250 psia).

4.7 ACCIDENT SEQUENCES AND COMBUSTION PROBABILITIES

A potential challenge to the BWR containment integrity results from the combustion of hydrogen in a degraded core accident. The extent of this challenge is dependent upon the details of the accident sequences, the potential combustion process, the location of the hydrogen, the location and timing of the ignition and the details of the structure which may be threatened.

The most probable route of hydrogen from the RPV to the primary containment is through the safety relief valve (S/RV) quenchers. Hydrogen rises vertically at about 10 feet/second because it is less dense than the air. The lateral dispersion of this rising column of hydrogen will be influenced by the geometry of the equipment and structures in its path and the rate of release.

The ignition probability for drywell combustion was assessed to be zero due to steam inerting. Employing the phenomena and principals discussed in the preceding sections, judgments were made to determine the relative probabilities of local or global combustion and local or global detonation. Continuous burns take place only during the period of hydrogen generation, therefore, after 1 hour, the continuous burn probability is zero. Because of the many ignition sources, the ignition probability is high and hydrogen will ignite once the

flammability limits are exceeded. For these reasons, local or global combustion is more likely than local or global detonation. The distribution of probabilities among these events is not of major significance since primary containment integrity is similarly affected in almost all cases. Drywell integrity is not affected by global combustion or local detonations, therefore, the relative distribution of probabilities between these two events has not significant effect on the risk results.

POTENTIAL EFFECTS OF HYDROGEN COMBUSTION IN A STANDARD MARK III CONTAINMENT

The primary containment pressure vessel is designed to withstand the maximum pressure and temperature conditions which might occur in a design basis LOCA event. Due to conservative design practices, however, the ultimate capability is much higher. Additionally, a unique feature of the Mark III containment is that the containment function is maintained even if the primary containment is breached, as long as integrity of the drywell and the suppression pool are maintained. Containment function (limiting of offsite doses) is achieved by the suppression pool which scrubs or filters any potential fission product release to the environment.

5.1 CONTAINMENT ULTIMATE STATIC PRESSURE CAPABILITY

A containment pressure capability study was conducted to determine the maximum pressure at which the Mark III Standard Plant containment structural system can be expected to maintain its integrity. The pressure carrying capability is different for each structural component. Loss of containment integrity is determined when a calculated pressure exceeds the pressure capability of the limiting structural component. The major structural components in the containment structural system of a Mark III Standard Plant consist of a free-standing primary containment vessel, suppression pool wall structure, anchorage for the containment vessel, drywell wall, drywell roof/ceiling slab and drywell head. A typical section through the containment structure system is shown in Figure 5.1.

This investigation consisted of two major steps:

1. The pressure-carrying capability of the major structural components in the containment structural system was determined based on acceptance criteria defined in Subsection NE of ASME III for steel structures and in Division 2 of ASME III for reinforced concrete structures and identifying the region in the structure with the least capability, and

2. Applying the theory of plasticity to the high stress region identified in Step 1 to calculate the pressure level at which the structure loses its integrity.

The pressure-carrying capabilities of the containment pressure vessel, suppression pool wall and the anchorage for the containment shell based on Level A and Level C acceptance criteria for steel structures,

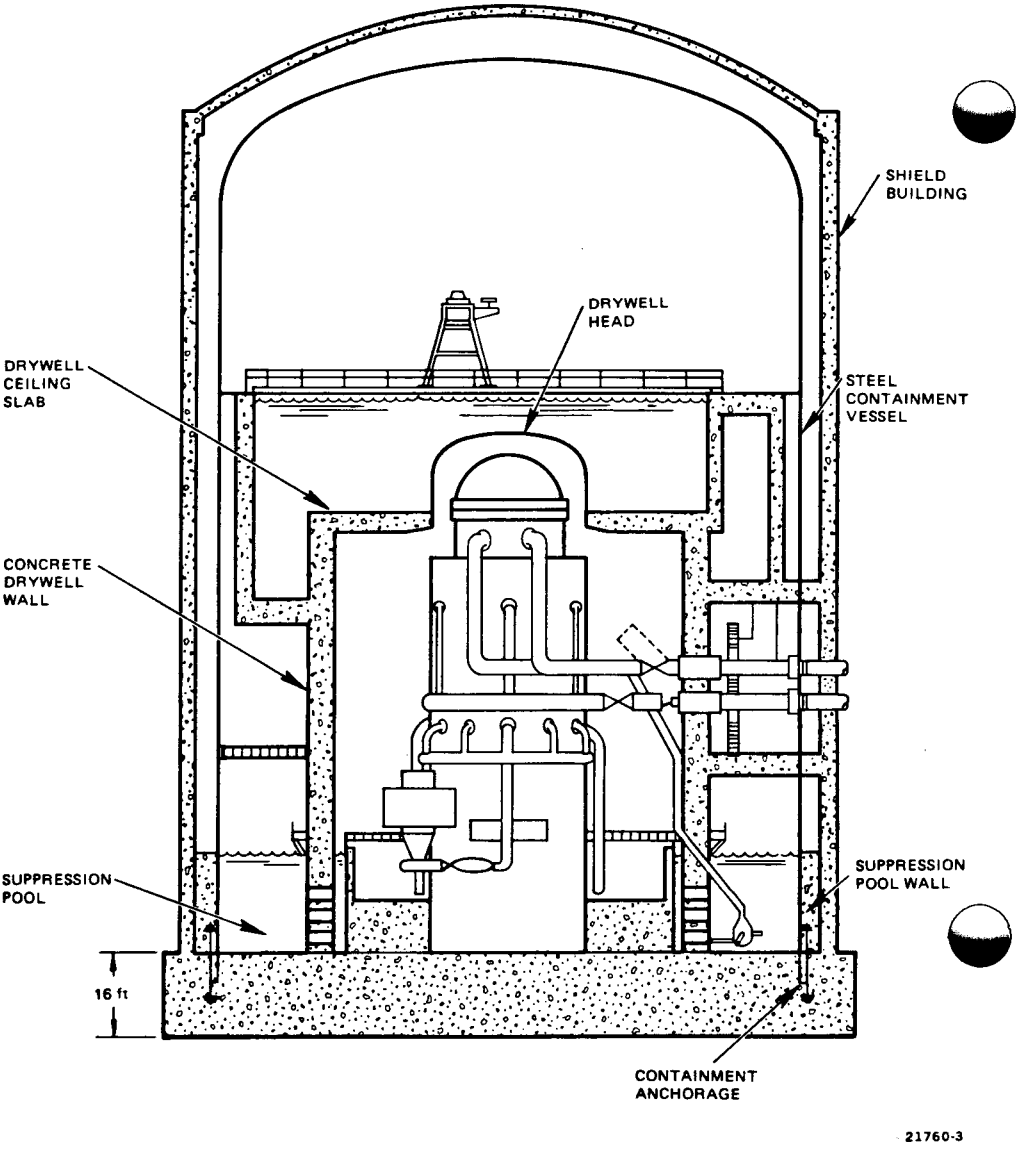


Figure 5.1 Cross-Section of Standard Mark III Containment

service category and factored category acceptance criteria for reinforced concrete structures are in Table 5.1. The pressure-carrying capabilities for the drywell wall, drywell roof/ceiling slab and drywell head based on their respective acceptance criteria, are summarized in Table 5.2.

A comparison of the values shown in these two tables reveals that the dome of the steel containment vessel has the lowest pressure capability. Thus, if pressure increased continuously and steadily, it is expected that the dome of the steel containment vessel will reach yield stress first. Loss of integrity of the containment dome is assumed to occur when either the ultimate tensile strength in the high stress region is reached or when cracks develop. The theory of plasticity has been applied to determine the pressure level at which the stress in the high stress region reaches ultimate tensile strength. It is assumed that cracks will be developed when the stress in the high stress region reaches a value between the yield strength and the ultimate strength of the steel of the containment vessel. Based on the findings from numerous studies, the distributions of ultimate and yield strengths are approximately normal. When the means and standard deviations of the ultimate strength and yield strength of a steel are known, the probability of a pressure causing loss of integrity of the containment dome can be found by applying standard probabilistic methods. Detailed calculations and a discussion can be found in reference 5.

Using the ultimate tensile strength and yield strengths of SA 516, Gr.70 steel and the geometry of the containment, it is found that, when the applied internal pressure is 58 psig, the probability of loss of integrity for the containment dome is 50%. This pressure is higher than the applicable level C stress limit for the containment dome, but less than the pressure-carrying capabilities of the cylindrical shell portion of the containment vessel, suppression pool wall, drywell wall, drywell head and containment vessel anchorage system (Table 5.1). If the containment building were to experience continuous, gradual, and unabated pressurization, loss of containment integrity would eventually occur in the torispherical dome region. Loss of integrity in this region would be expected to lead to gradual depressurization of the containment building which would leave the containment shell, suppression pool boundary and containment anchorage system intact.

During degraded core accidents, if the interior of the drywell is pressurized relative to the containment, drywell pressure is relieved by gas flow through the weir wall vents into the suppression pool. As a result of this pressure equalization capability and significant strength, the drywell is expected to maintain its integrity for gradual containment pressurization phenomena.

Therefore, though slow pressurization under degraded core conditions can potentially lead to loss of containment integrity in the dome region, the integrity of the drywell and the suppression pool boundary is expected to be maintained.

TABLE 5.1

CONTAINMENT STRUCTURES

Structural Components	Nominal Design Pressure (psig)	Internal Pressure Capability: Level A for Steel/Service Allowable for Concrete (psig)	Internal Pressure Capability: Level C for Steel/Factored Allowable for Concrete (psig)
Steel Containment	15		
- Dome		15	30
- Cylindrical Shell		33.5	63
Suppression Pool			
- Wall	15	75	141
Anchor System	15		
- Anchor Bolts		62	104
- Concrete Bearing under Anchor Bolts		25	72

TABLE 5.2

DRYWELL STRUCTURES

Structural Components	Nominal Design Pressure (psig)	External Pressure Capability: Level A for Steel/Service Allowable for Concrete (psig)	External Pressure Capability: Level C for Steel/Factored Allowable for Concrete (psig)
Drywell Wall	21	136	272
Drywell Roof	21		
(1) Slab under water		51	96
(2) Slab exposed to air		118	200
Drywell Head	21	75	160

5.2 DYNAMIC EFFECTS OF HYDROGEN COMBUSTION

Based on the natural periods of the steel containment vessel, the suppression pool wall, the reinforced concrete drywell wall and the drywell head, it was determined, by consideration of the maximum Dynamic Load Factor (DLF) for constant force with finite rise time, that pressure increases longer than one second can be considered static loads. For all the severe accidents except those where a detonation occurs, the pressurization within the containment vessel increases slowly. Thus, the results based on static analysis can be applied. For hydrogen detonation, the pressure pulse effects are converted into a static equivalent pressure with which the pressure-carrying capabilities of each structural component are compared. The ECCS suction piping is not expected to fracture and drain the pool because the piping pressure capability (~250 psig) exceeds the pressure challenge.

5.3 EFFECTS OF LOCAL COMBUSTION ON DRYWELL INTEGRITY

An investigation was performed to determine the potential for suppression pool bypass resulting from high temperature effects of local hydrogen combustion. While the major drywell structural components, which consist of thick concrete sections, are not susceptible to local high temperature effects (albeit some local spalling), the numerous penetrations might be affected. A failure of the piping or penetration assemblies in the annular space between the drywell and containment, could allow bypass of the suppression pool, either from the reactor to the containment, or from the drywell to the containment.

For the purposes of this investigation, a hydrogen flame was postulated to emanate from the suppression pool surface, directly above one or more of the 19 safety-relief valve discharge quenchers, or above the drywell horizontal vents which are distributed uniformly around the drywell. A flame height of 20 to 40 feet with a duration of 30 minutes was assumed.

Heat transfer from a hydrogen flame burning after release of the gas below a pool surface has been calculated. Dr. B. Lewis predicted flame velocities of 10 ft./sec and flame temperature of about 4400°R.(4) With these as working inputs the heat transfer can be as high as 45,000 BTU/hr/ft^2. Using normal steel heat capacity, about 12,000 BTU/ft^2 will cause the steel containment wall to melt. This could be achieved in about 15 minutes of burn.

All the drywell penetrations were examined and most were found not be susceptible to a flame-induced failure which would allow pool bypass. Most pipes have normally-closed isolation valves or check valves inside the drywell so that failure of the piping in the containment-drywell annulus would not allow drywell bypass. Much of the piping and many of the penetrations are shielded from a potential flame by the solid floor which supports the CRD modules (see Figure 5.2). Many of the penetrations assemblies (see Figure 5.3, Type 5) would not be exposed to the flame.

Out of the hundreds of drywell penetrations, the following were

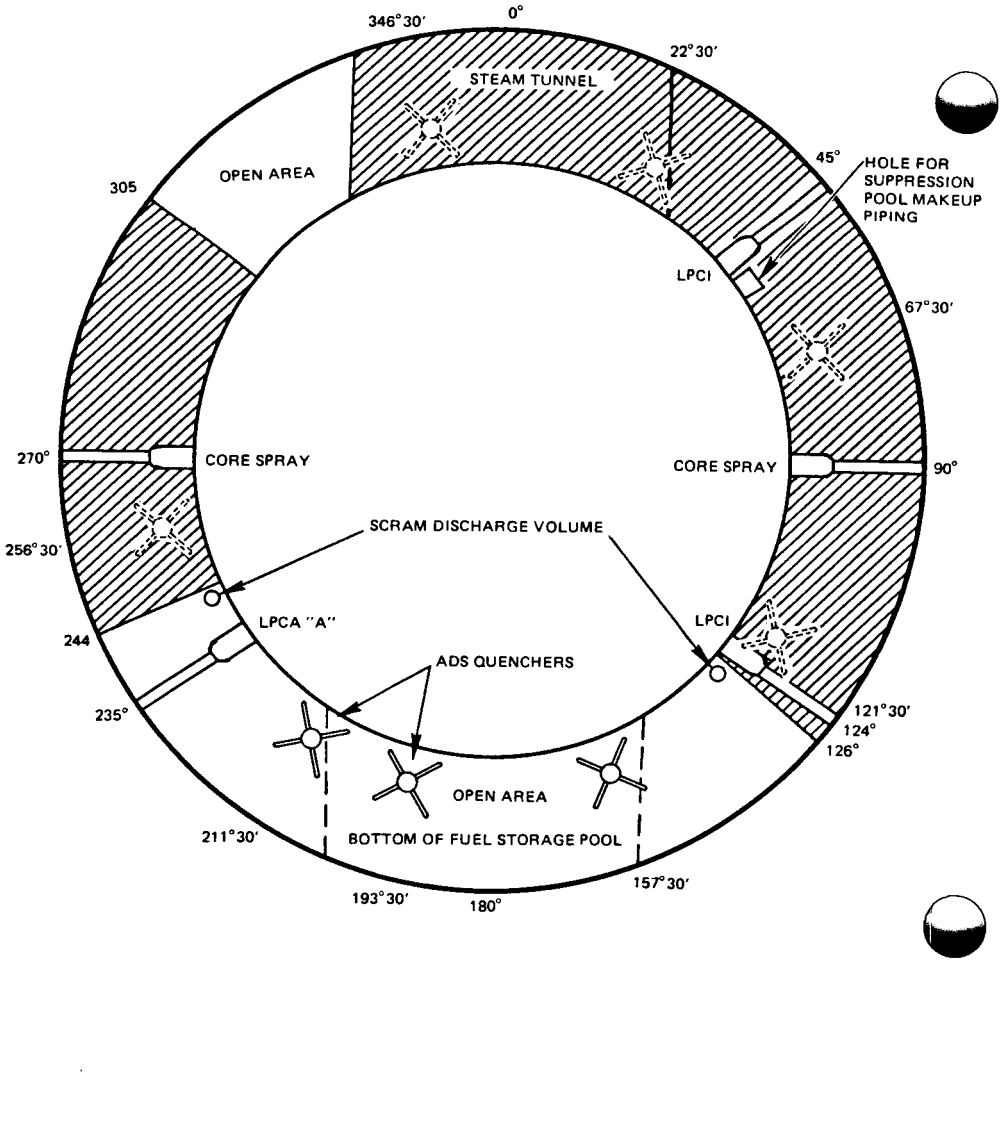


Figure 5.2 Plan View of Standard Mark III Containment at CRD Module Elevation

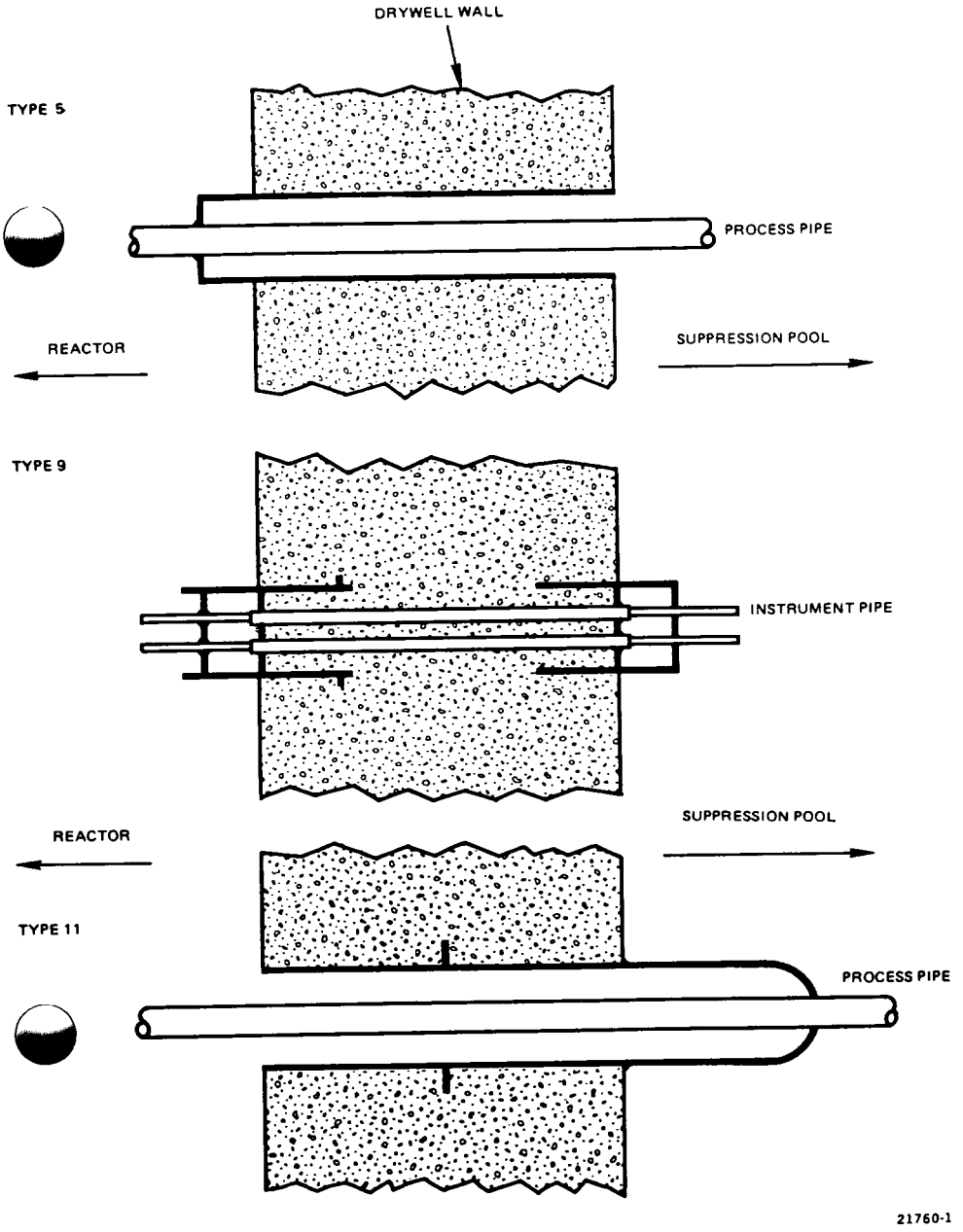


Figure 5.3 Standard Mark III Drywell Pentrations

identified as susceptible:

DESCRIPTION	BYPASS ROUTE	COMMENT
LPCI ''A'' Penetrations (see Figure 5.3, Type 5)	Drywell to Containment	
30 Instrument Penetration Assemblies (Type 9)	Drywell to Containment	Potential flow path is 1/16'' wide and aerosol plugging is expected
45 Electrical Penetrations	Drywell to Containment	Penetrations are tightly packed and aerosol plugging is expected
3/4'' Instrument Lines from RPV to containment	Reactor to Containment	All instrument lines have 1/4'' orifice

It was concluded from this study that there is a low probability of significant drywell bypass in the event of a degraded core event.

6.0 SUMMARY AND CONCLUSIONS

The GE Probabilistic Risk Assessment has shown that the probability of core damage for the BWR-6 Mark III Standard Plant is very low. The most likely initiating event for a degraded-core event is a transient rather than a LOCA. Hydrogen generation is limited by BWR design features to approximately 45% of active fuel cladding. Conclusions from this study of potential hydrogen combustion effects on the Standard Mark III containment are:

(1) Local or global combustion is the most likely mode for hydrogen to burn if released to the containment. A local detonation may occur, but is less likely. A global detonation is unlikely to occur.

(2) Given a continued, slow pressure increase, the containment would eventually fail in the torospherical dome region.

(3) The structural integrity of the drywell is expected to be maintained during a slow pressure increase by its pressure-equalizing capability and high strength, and during a local detonation by its high strength.

(4) Drywell bypass due to failure of a penetration assembly or piping has a low probability of occurring.

(5) Even though containment integrity may be lost in some cases, containment function is maintained by the continued integrity of

A UTILITY PERSPECTIVE ON HYDROGEN CONTROL

by

John D. Richardson and Sam H. Hobbs
Mississippi Power & Light Company

ABSTRACT

A description of the hydrogen control measures at the Grand Gulf Nuclear Station through September 1982 is provided as well as a discussion of the organizational interfaces between Mississippi Power & Light and other participating organizations and a utility perspective on hydrogen control.

Introduction

Nuclear Power Plants which utilize a Boiling Water Reactor (BWR) as a Nuclear Steam Supply System (NSSS) customarily make use of a pressure suppression containment to house the reactor and many associated components. There are many significant advantages to the use of a pressure suppression containment. The primary advantage is that peak containment pressure which is reached a few seconds after the limiting Design Basis Accident (DBA) is substantially reduced in comparison to peak pressures reached in other types of containments even with a substantially smaller containment volume. The combination of the resulting lower design pressure and smaller containment

result in a substantial cost reduction for containment construction. The customary design of a BWR containment uses a suppression pool which consists of a large volume of water through which the steam blowdown resulting from an accident is discharged. This volume of water also acts as a substantial passive heat sink in the hours following such an accident and allows a more deliberate response to the accident. In addition, the use of the suppression pool as the steam quenching mechanism following the actuation of safety-relief valves during normal operation allows increased operational flexibility.

The Grand Gulf Nuclear Station(GGNS) is the lead domestic BWR/6 and utilizes a Mark III pressure suppression containment. Prior to October 1980, hydrogen control at GGNS complied with existing Nuclear Regulatory Commission (NRC) regulations which required that hydrogen concentrations be maintained at less than 4 ^{v}/o during the post-DBA period. The hydrogen source terms included a small but presumably conservative metal-water reaction (MWR) of the zircalloy clad which occured during the first few seconds following the onset of the DBA as well as hydrogen resulting from radiolytic decomposition of water and the chemical reaction of steam with such metals as zinc and aluminum. In the days following a DBA, it could have been anticipated (using conservative NRC dictated assumptions) that the concentration of hydrogen would have eventually exceeded 4 ^{v}/o unless hydrogen control measures were implemented. The design features at GGNS which precluded this included purge compressors which forced circulation and mixing between the containment and drywell atmospheres, low capacity (100scfm) hydrogen recombiners and the availability of backup containment purge.

The accident at Unit 2 of Three Mile Island (TMI-2) in March 1979 produced unexpectedly large releases of hydrogen primarily because of operator error in defeating the operation of emergency core cooling systems (ECCS). The hydrogen source was almost entirely MWR with the fuel clad. Estimates of the amount of MWR range from twenty to fifty per cent which are far in excess of the approximately one per cent which would have been "conservatively" estimated by calculations using the then existing regulatory assumptions.

One of the first nuclear power plants to receive an operating license following the TMI-2 accident was the Tennessee Valley Authority (TVA) Sequoyah plant which utilizes a Pressurized Water Reactor (PWR) and an ice-condenser containment (another type of small volume, pressure suppression containment). The NRC required Sequoyah to implement design measures to deal with amounts of hydrogen which might result from a degraded core accident such as the one at

TMI-2. The use of a Distributed Ignition System was chosen by TVA as an optimum interim solution, and, since then, a somewhat modified system of igniters has been chosen by TVA as the final hydrogen control design.

The NRC requested that Mississippi Power & Light Company (MP&L) provide hydrogen control measures for degraded core events at GGNS in October 1981. A comprehensive program was initiated at that time. The first step involved an engineering study to select an optimum hydrogen control system. The use of a Hydrogen Ignition System (HIS) was determined to be the appropriate design measure for hydrogen control following a degraded core event. In addition to the preliminary analysis which was done prior to selecting igniters, substantial analysis has been done including the determination of containment ultimate capacity, evaluation of containment response to various controlled burn scenarios, consideration of local detonations, a determination of equipment which must survive burn environments associated with the postulated combustion, and evaluation of the ability of such equipment to actually survive burn environments. Based on these evaluations (and on independent evaluations conducted by the NRC and their consultants), GGNS has been granted a low power operating license and has satisfied the NRC that a full power license can be granted with the condition that substantial additional evaluation (including testing) be completed satisfactorily within approximately one year. The remaining work is in progress.

System Selection

Criteria were developed for use in system selection. These criteria are summarized below:

- preclude detonations
- preclude significant pocketing
- system operation should not result in unacceptable plant damage or decrease plant operational safety
- system must be reliable, controllable, testable, and able to handle a spectrum of hydrogen generation events (HGE)

- system operation should not endanger public health or safety

- equipment required for the system must be readily available and suited to the functional and survivability requirements of system

- the least costly system which satisfies all other criteria should be used.

The following systems were evaluated against the above criteria:

- containment pre-inerting

- additional recombiners

- post-accident halon injection

- purge and filtered vent

- post accident inerting (nitrogen and CO_2 were considered)

- post accident inerting with filtered vent

- water fog or steam spray

- oxygen depletion

- igniters.

The use of igniters was found to be substantially more desirable and costly than any other alternative. The only other system which was found to be feasible with current technology was post accident inerting with CO_2, and it was the considered engineering judgement of MP&L that there were more problems associated with that option and that the problems were less amenable to resolution than the evaluations which were anticipated to be associated with demonstrating the adequacy of an igniter system. In retrospect, although the preliminary resolution of the issues associated with igniters was

lengthier and more difficult than anticipated, it is believed that this judgement was correct.

Accident Scenarios and Hydrogen Release Rates

In order to evaluate the adequacy of the proposed GGNS HIS, two basic accident scenarios were used. The first of these scenarios is a transient followed by a stuck open relief valve (SORV). The second is a small break loss-of-coolant accident (LOCA) in the drywell. The steam and hydrogen release rates associated with these two scenarios is assumed to be the same. The primary difference in the scenarios is the location of the release. Both scenarios assume that no makeup water is provided to cool the core until after a significant amount of hydrogen (corresponding to a degraded core event from which a recovery is made prior to a core melt) is released. The SORV scenario results in a release of steam and hydrogen into the suppression pool. The small break LOCA (sometimes designated S-LOCA) initially has a release point of steam into the drywell where it then bubbles through the drywell vents into the suppression pool. Later in the event, but prior to hydrogen release, several safety-relief valves (SRV) are open and the hydrogen/steam release is partly distributed directly to the drywell and partly directly to the suppression pool.

The reasons for choosing these two scenarios were:

1. The precursor events (SORV's and S-LOCA's) are thought to be particularly significant. The SORV has a relatively high probability for BWR's, and the S-LOCA is commonly a relatively high risk contributor in probabilistic risk analyses (PRA) for light water reactors.

2. The use of these two scenarios forced consideration of the effects of hydrogen releases in the two major possible locations for hydrogen releases.

The sequence of events for both scenarios is as follows:

- initiating event occurs (SORV or S-LOCA)

- no vessel inventory makeup occurs

- as water level falls without makeup, the operators initiate the HIS and the Combustible Gas Control System (CGCS) which for analysis purposes is assumed to consist of enabling the post accident drywell vacuum breakers and initiating operation of the purge compressors

- as water level continues to fall, the operators begin opening SRV's which provides steam cooling flow across the fuel elements and extends the time prior to significant core degradation

- hydrogen is generated due to MWR and released from the vessel

- prior to core melt, core cooling is restored and the hydrogen generation is terminated.

As a part of the Mark III Hydrogen Control Owners Group (HCOG) efforts, later studies were done to identify probable HGE's. Although the most probable events did not involve SORV's, it was found that the primary assumptions resulting from the SORV scenario (i. e., depletion of vessel inventory and depressurization prior to hydrogen generation) were consistent with the most probable precursor events so that the SORV base case adequately represents the mechanistic results which are anticipated to result.

The steam and hydrogen release rates used in the containment response evaluation were based on the RSSMAP TPE sequence (an SORV event with a failure of safety injection) MARCH analysis which was originally run by the Battele-Memorial Institute in Columbus for the Sandia National Laboratory in connection with studies which were being conducted for the NRC. The results were modified to be consistent with a degraded core event rather than the melt event which was depicted in the particular calculation which was available. Significant amounts of hydrogen began to be released at approximately 3600 seconds into the event. The event was assumed to terminate at approximately 7800 seconds into the event with a peak hydrogen release rate of approximately 1 lbm/sec. This corresponded to a 75% MWR which was consistent with proposed hydrogen rules which had been published at the time scenario selection was made.

As a part of the same later studies done to identify probable HGE's, estimates were made by General Electric of hydrogen release rates and of plausible MWR per centages for HGE's. Sensitivity studies indicated that between 7.6% and 34.2% MWR were plausible depending on the precise assumptions made about recovery, but the best engineering judgement indicated that no more than about 12.5% MWR should be assumed for degraded core events in which core recovery prior to core melt is assumed. This study indicates that the assumption of 75% MWR is quite conservative.

System Design

The HIS consists of two trains of seismically designed sets of igniters which are fully qualified in accordance with current NRC equipment qualifications requirements. Each set is powered from a separate engineered safety feature electrical bus which can be powered from diverse offsite and onsite AC power supplies.

The igniters are located so that the separation between igniters located in large areas does not exceed about 30 ft (60 ft if it is assumed that one train of igniters fails). In addition, the individual igniters are located so that there are generally two igniters (one from each power supply) in each compartment. There is a group of igniters located above the suppression pool and below the HCU floor to provide an ignition source as close as practical to the anticipated source of hydrogen releases into the containment atmosphere.

The actual igniter assemblies consist of General Motors AC Division Model 7G glow plugs mounted in a welded metal enclosure which contains the transformer and associated wiring for reducing the 120 VAC power supply to the 12 VAC power required for operation of the igniter. The choice of these glow plugs was based on the satisfactory previous demonstration of their suitability for such service in extensive tests which were conducted to support their service in ice condenser containments. The design basis of the assembly includes the ability to withstand seismic forces and dynamic forces associated with specific locations where pool swell loads associated with a large break LOCA may be able to affect particular assemblies, degraded power supply voltage, environmental conditions associated with LOCA's including elevated temperatures and a high radiation environment, ability to withstand spray and brief periods of submergence, and to withstand the environmental conditions associated with a postulated combustion environment without

degradation of the ability to maintain surface temperatures of at least 1700°F at the end of a 40 year plant life. A test program which will demonstrate these abilities is in progress.

Containment Response Analysis

The containment response analyses required to demonstrate the adequacy of the HIS was performed using the CLASIX-3 computer code. This code is based on the CLASIX code which was originally developed by Offshore Power Systems for use in the hydrogen control analysis of the ice condenser containment used on the Floating Nuclear Plant. CLASIX was subsequently used in the analysis of the ice condenser containments at Sequoyah, McGuire, and the D. C. Cooke plants. The code was modified to handle variable volumes (resulting from variations in suppression pool level and upper pool dump) and to model suppression pool dynamics in the interface between the drywell and containment volumes. The modified code was entitled CLASIX-3.

Output which is generated routinely as a part of the results include pressures, temperatures and volume fractions of oxygen, nitrogen, hydrogen and steam at each containment model node (usually 3 - the main containment volume, the wetwell, and the drywell) as well as differential pressure between the containment and the drywell. Substantial additional information is available and is saved in online files. Portions of this information are needed from time to time and may be generated as output in specific cases on an as needed basis (e. g., suppression pool level).

Combustion is modeled in CLASIX-3 as a series of puff burns which occur when a predetermined concentration of hydrogen is reached in one of the volumes being modeled.

In addition to the two base cases discussed above, a large number of containment sensitivity studies were run. These studies include the following categories:

- drywell breaks (the largest category)

- hydrogen release rate variations

- burn parameter variations

- containment spray variations

- passive heat sink variations

- miscellaneous studies (convection flow and gas specific heats)

- volume nodalization variations

- heat sink modeling variations

Generally the results of these studies are that the pressure transients resulting from igniter induced combustion is quite benign. It should be noted that this view is not universally held. The most severe predicted pressure occurs due to a global burn with no containment spray. The HECTRE code which was developed by Sandia National Laboratory as a part of studies conducted for the NRC predicts higher pressures for such cases (probably due to different burn parameters used in calculations in the two codes), but the pressures are still within the calculated containment ultimate capacity.

One of the most interesting cases studied involves the drywell break case and the resulting differential pressures between the containment and the drywell. In this case, which occurs after the core has been recovered, the drywell is inerted with a mixture of hydrogen and steam, and air is being added to the drywell atmosphere from the containment atmosphere by the purge compressors. Eventually the concentration of oxygen is sufficient to support a large burn in the drywell. Due to this burn, the pressure increases dramatically and a substantial amount of the hydrogen rich drywell atmosphere is forced into the containment through the suppression pool. There is a burn in the wetwell, but the large volume of hydrogen being forced through the suppression pool causes a substantial volume of hydrogen to be swept into the containment atmosphere where there is a global burn. This burn causes a relatively high pressure in the containment which forces the suppression pool to depress rapidly. Simultaneously, the hot water vapor in the drywell is being condensed by the flow of water from the break location which causes a low pressure to occur in the drywell at the same time that the high pressure is occuring in the containment. The combined negative differential pressure transient causes the violent overflow of the suppression pool into the drywell. This overflow further condenses water vapor in the drywell

atmosphere which increases the net effect to some extent. This analysis is still being finalized. Based on the results, the effects of the violent pool overflow will be evaluated to determine what adverse effects there are on essential equipment which is needed for long term accident recovery.

It should be noted, as discussed below, that it is anticipated that t particular sequence of events will eventually be shown not to be a concern since it is believed that, instead of a large drywell burn, continuous inverted diffusion flames will form at the purge compressor discharge into the drywell resulting in a slow, nominal pressure increase.

General Combustion Phenomena

MP&L retained Messrs. Lewis and Karlovitz of Combustion and Explosives Research, Inc. (COMBEX) to provide an independent evaluation of the adequacy of the use of igniters for hydrogen control in the GGNS containment. Specific conclusions of interest are:

- igniters provide an adequate measure of hydrogen control in the GGNS containment

- the geometry is not conducive to transition from deflagration to detonation

- rather than periodic puffs of hydrogen burning in the wetwell, continuous flames will exist above the suppression pool

- it is believed that the flame height will be such that heat transfer effects will not be a significant problem, but the uncertainty is such that testing is appropriate

- burning in the drywell will be in the form of inverted diffusion flames at the discharge of the purge compressors into the drywell

- testing to determine ignition and flammability limits in hydrogen rich, steam rich environments is needed.

Structural Capability

The design pressures for the containment and drywell are 15 psig and 30 psid respectively. There are substantial margins between the design pressures and the pressure at which containment integrity would be threatened. There are no unambiguous criteria, however, for calculation of such containment failure pressures. In lieu of such calculations, a calculation was done of the pressure at which a general yield state in a critical containment section would be reached. This pressure is labeled the containment ultimate capacity. The margins implied by this ultimate capacity are conservative since the actual failure pressure exceeds the pressure associated with the onset of yield. The calculated lower bound containment ultimate capacity based on actual material strengths for the GGNS containment is 62 psig. The drywell ultimate capacity is 67 psid positive pressure differential, and the negative pressure capability of the drywell is higher. The pressure capability of other pressure retaining components exceeds the containment and drywell ultimate capacities.

A major NRC concern is the ability of the GGNS containment to withstand the effects of local detonations. This is in spite of the fact that local detonations are believed to be extremely improbable. Since such detonations cannot be ruled out entirely, the consideration of local detonations and demonstration of the ability to withstand postulated local detonations without degrading containment integrity was mandated. The most recent evaluation in this area was based on a 28,000 cubic foot local detonation, corresponding to the largest wetwell volume which exists below a solid surface. This is an extremely conservative assumption. The pressure time history for an appropriate geometry was modeled by Sandia National Laboratory using the CSQ code. A detailed structural analysis demonstrated the ability of the containment to withstand such a postulated detonation without loss of containment integrity.

Equipment Survivability

A major concern in the area of deliberate ignition as a hydrogen control measure is the evaluation of the combustion environment on equipment which must be available either to mitigate HGE's or to accomplish long term accident recovery. This has been evaluated in detail for GGNS. The first step was the establishment of functional criteria for the identification of essential

equipment. Based on these criteria, a generalized list of equipment was generated (at the system level) and a detailed list of critical components was developed. Typical components were selected based on thermal sensitivity and sophisticated analyses were done to demonstrate that the components would survive and remain operable.

The limiting thermal environment is the wetwell environment (because of the large number of closely spaced small burns which allow relatively little time for thermal recovery between burns). The temperature results from the SORV CLASIX-3 base case were conservatively modified (for ease of input) and used as input for the HEATING3 code. The selected components were modeled as 2-D heat transfer models. The 2-D modeling was done in a conservative fashion. The results demonstrated the survivability of essential equipment.

The methodology was validated by modeling the McGuire igniter assembly and comparing the computed thermal response to actual burn tests done for that assembly. The results of the calculation, as expected, were conservative.

Testing

As a part of the required long term resolution of hydrogen control issues on the GGNS containment, MP&L is participating in a sophisticated testing program which will evaluate suppression pool burn phenomena, mixing, and flammability limits. The particular tests planned at this time include:

- $^{1}/_{20}$th scale combustion tests
- $^{1}/_{4}$th scale, 360° combustion tests
- hydrogen rich, steam rich, flammability limit tests

Evaluation is underway with regard to the need for inverted flame tests to confirm appropriate modeling assumptions for the effects on the drywell the predicted inverted diffusion flame.

Organizational Interfaces

The number of separate organizations involved in analysis, testing, system design and engineering, equipment assembly and procurement, and construction is large. Added to that is the interface with regulatory

organizations and their consultants. A summary list of the organizations with which there has been significant interface on the HIS for GGNS follows:

- Nuclear Regulatory Commission - direct licensing interface concerning overall evaluation and acceptability of HIS

- Sandia National Laboratory - served as consultants to both the regulatory and research staffs of the NRC, primary concerns were containment response evaluations, local detonations and an overall evaluation of HIS adequacy

- Brookhaven National Laboratory - served as consultants to the NRC staff regarding containment ultimate capacity (interface limited to NRC run meetings)

- Advisory Committee on Reactor Safeguards - provide an overall recommendation to the NRC Commissioners on acceptability of hydrogen control (interface limited to formal committee meetings)

- Los Alamos Scientific Laboratory - a member of LASL staff served as a consultant to ACRS regarding hydrogen control (interface limited to formal committee meetings)

- Bechtel Power Corporation - serve as engineer/constructor for GGNS and were responsible for system selection study, system design, equipment survivability analysis, containment ultimate capacity analysis, portions of the detonation calculations, procurement of components, component testing, and system installation.

- Power Systems Corporation - provided igniter assemblies under contract to Bechtel

- equipment testing facilities - provided specific igniter assembly qualification testing under contract to Bechtel

- various component suppliers - provided information and/or analysis regarding pressure retention capability of particular components

- Offshore Power Systems - provided containment response evaluations and general consulting in the area of hydrogen control

- COMBEX - provided general combustion consulting under contract to Offshore Power Systems

- other Mark III containment owners - provided alternate sources of technical advice and financial and manpower support of HCOG activities

- Electric Power Research Institute - serve as program manager for HCOG, provide technical information on various hydrogen related areas including areas related to IDCOR, and are conducting the testing program for the HCOG

- IDCOR participants and contractors - serve as information source as certain information becomes available; also GGNS is the prototypical Mark III containment being analyzed for IDCOR and there are many demands for technical hydrogen control information to be provided to various contractors

- General Electric - provided scenario probability and hydrogen generation calculations as confirmatory work for the HCOG

- ice condensor containment owners - serve as sources of information which have aided in hydrogen control work on Mark III containments

- other consultants - provide manpower and/or analytical services on an as needed basis

The demands for coordination have, needless to say, been considerable. In addition, MP&L serves as the chairman of the HCOG and as the owner of the lead domestic BWR/6 Mark III plant has unavoidably been the industry leader on licensing issues on Mark III containments.

Utility Perspective

The summary presented above is a sparse sketch of the actual information, but it leads naturally into a discussion of our perspective on hydrogen control. Discussions of both a utility technical perspective and a more general perspective on cooperation and commonality of interest are presented below.

The technical perspective is involved primarily with the appropriate hydrogen source term and accident scenario for BWR's, relative risks, resource allocation, and the state of current regulatory criteria.

The NRC has invoked a de facto regulatory requirement to design pressure suppression containments to withstand a degraded core event which produces a 75% metal water reaction. This is based primarily on the large hydrogen releases during the accident at TMI-2 with a substantial margin to assure conservatism. It is certainly understandable that following such a dramatic and unexpected sequence of events at TMI-2 there would be dramatic new regulatory requirements; indeed there are so many dramatic recent developments in regulatory requirements that it is quite safe to state that the likelihood of having a similar set of events is dramatically reduced. In particular, improvements in instrumentation, emergency operating procedures, and operator training as well as improvements in various automatic systems probably have a noticeable effect in decreasing the probability of a degraded core event similar to the TMI-2 accident for all domestic light water reactors.

For BWR's in particular, there were significant differences even prior to the TMI-2 induced round of regulatory changes which made the generation of significant amounts of hydrogen much less likely than for a comparable PWR:

- BWR instrumentation provides direct indication of vessel water level which is the only parameter needed to assess adequacy of core cooling

- BWR water delivery systems to the reactor vessel are highly diverse and redundant consisting of six high pressure and seven low pressure pumps and an Automatic Depressurization System. Of the thirteen pumps available, any one of the eleven larger pumps is sufficient to keep the core covered in most circumstances, and either of the two remaining pumps is capable of core cooling if

the vessel is still pressurized and provided the equivalent steady state power level did not exceed 65% prior to the transient or accident.

- The source of water for the injection systems is diverse consisting of three readily available normal sources.

- The electrical power supply for the injection systems is diverse including offsite and onsite AC power supplies. The onsite power supplies (at least for the BWR/6) are less susceptible to common mode failures than traditional onsite electrical power because there are two different types of diesel generators.

- Even in the event of a station blackout, a steam turbine driven injection system can keep the core covered for several hours.

- The suppression pool provides a large passive heat sink which effectively decouples the reactor from the balance of plant for short term decay heat removal and enables operations to be fully devoted to maintaining reactor water inventory.

- BWR operations inherently include natural circulation and operations with a void fraction in the core. These features enable core cooling to continue whenever water inventory is available.

- A critical difference between hydrogen generation in a PWR and a BWR is commonly neglected in calculating hydrogen generation in a BWR. This feature is that steam cooling flow across BWR fuel elements will continue to provide cooling until the steam is virtually exhausted which leaves very little steam or water to react in the postulated metal water reaction, but it is nevertheless commonly assumed at least in regulatory MARCH calculations for BWR's that there is an unlimited amount of steam available so that the metal water reaction is maximized. This means that such assumptions as the 75% metal water reactor are excessively conservative. As discussed previously, a more

appropriate metal water reaction based on actual metal water reaction calculations for BWR's is 12.5% between 10 and 35%.

In addition to such features, probabilistic risk assessment (PRA) results which are being reported have generally not found that hydrogen related events are significant risk contributors. Many recent results are not readily available, but as an example, the RSSMAP study for GGNS which is a very conservative PRA sponsored by the NRC concluded that risk from hydrogen events as an insignificant contributor to risk.

It is our belief, at least for BWR's, that a critical assessment is needed to determine the allocation of risk reduction resources. Considering the status of regulatory compliance on hydrogen control by GGNS and other BWR/6 Mark III owners, this is probably a moot point for hydrogen control.

As a final primarily technical point, we would like to observe that there is a dearth of firm regulatory criteria such as regulatory guides or standard review plans. The regulatory guidance which does exist is sometimes in the form of NUREG or NUREG/CR reports which in many cases are frankly speculative and which provide little firm guidance. The usefulness of solid regulatory criteria for ice condenser and Mark III containments at this time is debatable, but prior to extending requirements to the large dry containments, it would be highly desirable to establish appropriate criteria.

When dealing with a subject of this compexity where a large number of organizations are involved, the need for an integrated approach and assertive coordination cannot be overemphasized. Effective and frequent communications are an essential part of such an effort. It is all too easy for a licensee to proceed with very substantial technical considerations and to resolve issues to his satisfaction with very little communications with the appropriate NRC personnel. Effective communications are probably the most important single contributor to resolving the issues to the mutual satisfaction of the NRC and the licensee.

As implausible as it may sometimes seem, there is a real commonality of interest between utility license applicants and the NRC. That common interest is safety. Although utilities are nominally charged with providing economical power generation and making a fair profit for their investors, there are several urgent reasons why concern with safety is also a prime concern:

- nothing will devastate the utilities' customers and investors as critically as a severe accident

- the image of a utility as a good corporate citizen depends partly on directing an appropriate level of effort to assuring safety

- the management and employees of a utility are susceptible to the same effects on public health and safety as the general public.

The NRC has safety as its primary consideration. All too frequently however, this commonality of interest is lost in the day to day business of resolving issues. Effective and frequent communications may not eliminate conflicts, but in combination with a recognized commonality of interest it will probably make them far easier to resolve.

Conclusion

Three years ago, in the aftermath of the accident at TMI-2, there was evidently a general regulatory perspective that hydrogen control had a high priority which could not wait for a more general rulemaking. There was also evidently a belief that hydrogen control measures could be implemented quickly and easily. In retrospect, the belief that there was a quick or easy resolution can be seen to be quite naive. There has been no quick, easy or inexpensive resolution. We believe that it is now clear that there are no insurmountable obstacles to resolution of the hydrogen control issue, but a substantial amount of additional work is needed before that resolution can be achieved in today's regulatory climate.

The question of whether the high priority was justified remains. We believe that a more deliberate approach would not have endangered public health and safety and would have enabled a far more effective resource allocation in the area of risk reduction.

the drywell and suppression pool which provides scrubbing of any fission product release.

7.0 REFERENCES

1. GESSAR II, BWR/6 Nuclear Island Design, General Electric Company, March 1982 (22A7007, Rev. 2)

2. R. O. Wooton and H. I. Avci, ''MARCH (Meltdown Accident Response Characteristics) Code Description and User's Manaul'', prepared by Battelle Columbus Lab. for Nuclear Regulatory Commission, NUREG/CR-1711, Oct. 1980.

3. S. S. Dua, J. T. Teng, B. W. Shaffer, and A. S. Rao, ''BWR Hydrogen Generation and Control with Postulated Delayed Water Makeup'', Second International Workshop on the Impact of Hydrogen on Water Reactor Safety, Albuquerque, New Mexico, Oct. 3-7, 1982.

4. Bela Karlovitz and Bernard Lewis, ''Report on Study of Hydrogen Control in the Grand Gulf Nuclear Station'', Combustion and Explosives Research, Inc., 11/25/81.

5. P. F. Gou and J. E. Love, ''Pressure Carrying Capability of the Containment Structural System of the Mark III Standard Plant'', a paper presented at the International Workshop on Containment Integrity, Washington D.C., June 7-9, 1982.

SESSION III

COMBUSTIBLE GAS GENERATION

ZIRCALOY-OXIDATION AND HYDROGEN-GENERATION RATES IN DEGRADED-CORE ACCIDENT SITUATIONS*

H. M. Chung
Materials Science and Technology Division
Argonne National Laboratory
Argonne, Illinois 60439

and

G. R. Thomas
Nuclear Safety Analysis Center
Electric Power Research Institute
Palo Alto, California 94303

ABSTRACT

Oxidation of Zircaloy cladding is the primary source of hydrogen generated during a degraded-core accident. In this paper, reported Zircaloy oxidation rates, either measured at 1500–1850°C or extrapolated from the low-temperature data obtained at <1500°C, are critically reviewed with respect to their applicability to a degraded-core accident situation in which the high-temperature fuel cladding is likely to be exposed to and oxidized in mixtures of hydrogen and depleted steam, rather than in an unlimited flux of pure steam. New results of Zircaloy oxidation measurements in various mixtures of hydrogen and steam are reported for >1500°C. The results show significantly smaller oxidation and, hence, hydrogen-generation rates in the mixture, compared with those obtained in pure steam. It is also shown that a significant fraction of hydrogen, generated as a result of Zircaloy oxidation, is dissolved in the cladding material itself, which prevents that portion of hydrogen from reaching the containment building space. Implications of these findings are discussed in relation to a more realistic method of quantifying the hydrogen source term for a degraded-core accident analysis.

INTRODUCTION

The rate of high-temperature Zircaloy oxidation during a severely undercooled degraded-core accident in a light-water reactor has a major influence on core heat-up, related damage, and hydrogen generation. Oxidation of Zircaloy fuel cladding by steam molecules (contained in the reactor coolant) is the predominant source of hydrogen generation, in contrast to the reactions of water with other core materials, i.e., stainless steel, Inconel, UO_2, and control rod materials. Two moles of hydrogen are generated for each mole of zirconium oxidized, as shown in the equation

$$Zr + 2H_2O = ZrO_2 + 2H_2 + 140 \text{ kCal/mol}.$$

*Work supported by the Nuclear Safety Analysis Center, Electric Power Research Institute, Palo Alto, CA.

Kinetics of the reaction at ≤1500°C have been extensively investigated under conditions of sufficient supply of pure steam.[1-12] The sufficient steam supply in those investigations means that the incident rate of steam molecules per unit area of zirconium-oxide surface is such that the overall kinetics is controlled only by the oxygen diffusion in Zircaloy material. Under such a condition, the oxidation kinetics are parabolic and the rate constant is a function of Zircaloy temperature only. The uncertainty limit of the reported rate constants for ≤1500°C is fairly significant, and is usually attributed to uncertainties in Zircaloy specimen temperature[7] or temperature gradient across the specimen thickness.[12]

Under a degraded-core accident situation, kinetics for >1500°C are relatively more important, because most oxidation and hydrogen generation takes place in the high-temperature region. However, the literature regarding rate constants for >1500°C is relatively limited.[1-4,10] A number of aspects must be carefully examined with respect to the reported rate constants for >1500°C. For the high-temperature region, uncertainty associated with inaccurate temperature measurement is likely to be inherently large. Rate constants measured at >1580°C may be influenced by the tetragonal-to-cubic transformation of the oxide, as originally suggested by Klepfer[4] and later shown by Urbanic and Heidrick.[10] Another important consideration is that, under a degraded-core accident situation, Zircaloy fuel cladding at >1500°C is likely to be exposed to and oxidized in mixtures of hydrogen and depleted steam, rather than in an unlimited flux of pure steam. Examples of lesser oxidation in a hydrogen-steam mixture, compared with the case of pure steam, have been reported by Westerman[13] for 750°C, by Furuta and Kawaskai[14] for 1000-1100°C, and by the authors[15] for 1375 and 1500°C. Attention has been called to two possible mechanisms for the oxidation-rate limitation when the hydrogen fraction in the coolant mixture is high: (1) chemical reduction of adsorbed oxygen on the zirconium oxide surface by gaseous hydrogen, and (2) retardation of the rate of oxygen transport in oxide that may contain a significant amount of dissolved hydrogen.[15] In view of these complexities associated with the kinetics at >1500°C, it is necessary to examine critically the oxidation rates reported for the high-temperature range, with emphasis on their applicability to a degraded-core accident.

In analyzing hydrogen behavior during a degraded-core accident, Zircaloy fuel cladding is usually considered only as a source of hydrogen production through oxidation with steam. However, it can also act as a hydrogen sink because hydrogen is highly soluble in β-phase Zircaloy.[16] Hydrogen absorption by Zircaloy cladding under accident situations can take place via two routes, i.e., from the outer surface of the cladding, by penetrating the growing oxide layer, and from the inner surface of the ballooned and ruptured cladding. The oxide barrier in the latter process is negligible, except in the limited area near the rupture opening. Information on the hydrogen absorption by deformed and ruptured cladding during an accident situation is limited.[16,17] In this paper, available data on the subject are analyzed, to provide a better method of quantifying the hydrogen release term. New results on hydrogen absorption by Zircaloy-4 tubes oxidized in hydrogen-steam mixtures are also shown and discussed relative to similar data obtained in pure steam environments.

OXIDATION RATES MEASURED IN STEAM

There have been reported indications that the oxidation rates determined for ≳1600°C are significantly higher than the values extrapolated from the data obtained at lower temperatures.[4] Bittel and Sjodahl[4] suggested that the higher rates they observed for ≳1600°C could be explained on the basis of tetragonal-to-cubic transformation of the zirconium oxide phase. However, the early day oxidation rates[1-4] apparently reflect significant uncertainties associated with temperature measurements and limited data base. Later works[5-12] (prior to the Three Mile Island reactor accident) were directed primarily to rate constant measurements for ≲1500°C. The more extensive data base obtained from those later works clearly indicated that the high-temperature rates obtained in the early days are not consistent with values extrapolated from the data for lower temperatures. Thus, in contrast to the single Arrhenius-type rate equation reported by Baker and Just,[3] Urbanic and Heidrick[10] represented rate constants by two equations, one for 1580-1850°C and the other for 1000-1580°C.

Urbanic and Heidrick showed that the higher rates at >1580°C are associated with the cubic crystal form of the oxide that is stable at the high-temperature range. The transport rate of oxygen ion is therefore, expected to be higher in the cubic oxide than in the tetragonal form. In this regard, the discontinuity at ~1580°C can be best shown by oxide layer growth rate constants, rather than by rate of total weight gain. Figure 1 shows oxide layer growth rate constants (plotted as a function of inverse temperature) that were determined recently for 1200-1705°C in unlimited flux of pure steam. The details of experimental procedures and oxide layer thickness versus isothermal-oxidation-time plots have been reported elsewhere.[18] For comparison, the Arrhenius equations for rate constants reported by Urbanic and Heidrick[10] and Cathcart and Pawel[7] are plotted in the same figure. Although the present rate constants are somewhat smaller than the ones reported by Urbanic and Heidrick, the results of Fig. 1 confirm their finding that there is a discontinuous jump of oxidation rates at ~1580°C. It appears that the rate constant determined by Urbanic and Heidrick was obtained from single oxidation test for each temperature, in which specimen weight gain was continuously recorded as a function of time.[10] Thus, an oxide layer growth rate constant for a given temperature may have been determined from the slope of the line connecting the origin and the one data point obtained for the temperature, i.e., the oxide layer thickness measured for the single oxidation test.

OXIDATION RATES MEASURED IN HYDROGEN-STEAM MIXTURES

In a prolonged core uncovery, exemplified by events during the Three Mile Island reactor accident, a large amount of hydrogen can be generated and can blanket the high-temperature (>1500°C) fuel cladding in the upper level of the core.[15] Under such a situation, the oxidizing environment is likely to be a mixture of hydrogen gas and depleted steam, rather than an unlimited flux of pure steam. High-temperature oxidation kinetics of Zircaloy-4 in hydrogen-rich steam-hydrogen mixtures have been measured from simulated oxidation tests, and reported recently.[18] Zircaloy tube specimens described in the report were oxidized at 1200-1705°C by steam molecules that impinged on the oxide surface through natural convection in a static hydrogen overpressure of

~33 kPa. Steam impingement rate was varied by changing the steam supply rate into the reaction chamber. Because the hydrogen overpressure was kept constant, a decreased steam supply rate corresponds to an increased hydrogen mole fraction at the oxide/mixture boundary for a given test temperature. Under these experimental conditions, the oxide layer growth rate constant was a function of the steam supply rate as well as of the Zircaloy temperature. However, it was not possible to quantify in the experiments the fundamental thermal-hydraulic parameters that influence the overall oxidation rate in hydrogen-steam mixture, i.e., the local partial pressures of hydrogen and steam at the oxide/mixture boundary.

Both linear and parabolic oxidation regimes were observed from the oxidation tests in a hydrogen-steam mixture.[18] The linear regimes were observed only for the initial period, and attributed to overall kinetics controlled by the net rate of dissociation of steam molecules on the oxide surface, minus the rate of chemical reduction of the adsorbed oxygen by the hydrogen gas molecules. In the parabolic regime, oxide layer growth rate constants were smaller than those obtained in pure steam, and decreased with decreasing steam supply rate and, hence, increasing hydrogen mole fraction at the oxide/mixture boundary. Figure 2 shows the ratio of the oxide layer growth rate constants for the hydrogen-steam mixture to those in pure steam, plotted as a function of steam supply rate and Zircaloy temperature.

Similar results were obtained under somewhat different thermal-hydraulic conditions, and are shown in Fig. 3. The results in Fig. 3 were obtained from oxidation tests in which the Zircaloy-4 tube specimens were surrounded by a quartz flow shroud that simulated a fuel rod channel. Under those conditions, the hydrogen-steam mixture flow was confined within a well-defined boundary. Therefore, it was possible to determine the average hydrogen mole fraction of the input mixture. Hydrogen flow was kept constant at 10 standard liter^3/min. Steam flow rate was varied between 0.5 and 3.2 g/min. to establish input hydrogen mole fractions of between 0.94 and 0.71 at the mixture inlet plane of the shroud. The Reynolds number for the mixture flow was in the range similar to those calculated for the Three Mile Island reactor accident.

The zirconium oxide formed during oxidation in a hydrogen-steam mixture may contain a significant amount of dissolved hydrogen as either interstitial or substitutional impurity. The smaller parabolic rate constants observed for the hydrogen-steam mixtures (see Figs. 2 and 3) can be interpreted in terms of lower transport rates of oxygen ions in such oxide.[18] To evaluate the model in more detail, fine powders were obtained from the "surface oxide skin" by mechanical abrasion and were analyzed for oxygen and hydrogen content by the inert-gas fusion technique.

The powder specimens obtained in this manner contain only the surface oxide layer that was exposed to the hydrogen-steam mixtures. Figure 4 shows the results obtained from several specimens oxidized at 1705°C for ~120 s in various hydrogen-steam mixtures that were described in association with Fig. 2. Weight percentages of hydrogen and oxygen in the "surface oxide skin" are plotted as a function of steam supply rate. For comparison, similar results obtained from comparable specimens oxidized in pure steam are also shown in the figure. The oxide formed in pure steam contained less than

0.03 wt % hydrogen and corresponds to a composition close to ZrO_2. However, as the steam supply rate (hence, the steam mole fraction) decreased in the test, the hydrogen content dissolved in the oxide increased and the oxygen content decreased in proportion. The composition of the oxide skin observed for the smallest steam supply rate in Fig. 4 corresponds to $ZrO_{0.996}H_{0.965}$, which is close to ZrOH. For this composition, it is very possible that the crystal structure is different from the structure of the ZrO_2 that is normally produced in pure steam. The result of Fig. 4 supports the validity of the [18] for the smaller rate constants of Fig. 2, in which oxygen transport in the oxide was assumed to be modified by the significant amount of dissolved hydrogen.

In view of the results shown in Figs. 2-4, it appears unrealistic to assume the applicability of the oxidation rates obtained under conditions of unlimited flux of pure steam (e.g., Fig. 1) to a degraded-core accident situation, in which a fuel cladding is likely to be exposed to mixtures of hydrogen and depleted steam at >1500°C.

ZIRCALOY CLADDING AS HYDROGEN SINK

Some fraction of hydrogen gas produced as a result of Zircaloy-steam reaction has been known to be dissolved in the cladding material itself. Lemmon[2] reported that 6.8% and 12.5% of produced hydrogen were dissolved in Zircaloy-2 specimens at oxidation temperatures of 1000 and 1600°C, respectively. Dissolved hydrogen contents of up to 0.22 and 0.4 wt % have been reported, respectively, by Uetsuka et al.[17] for ballooned and ruptured Zircaloy-4 tube specimens oxidized in steam, and by Furuta and Kawasaki[14] for short undeformed tube specimens oxidized in hydrogen-steam mixtures at 950-1100°C. Although corresponding oxygen contents have not been reported for the tube specimens and, hence, no fraction of dissolved hydrogen can be determined from those test results,[14,17] it appears that the fractions are considerably large for the large hydrogen uptakes.

Oxygen as well as hydrogen contents in oxidized Zircaloy-4 specimens have been analyzed and reported from a recent investigation[16] in which Zircaloy-4 tubes were internally pressurized, ballooned, ruptured, and oxidized isothermally in a steam environment, in simulation of an accident situation. The report shows that the hydrogen uptake was strongly influenced by the morphology and thickness of the inner surface oxide layer, which indicates that the primary route for the absorption was through the inner surface of the ruptured cladding tube. From the oxidation and hydrogen uptake data in the rt, the fraction of the dissolved hydrogen (i.e., the ratio of hydrogen s dissolved in Zircaloy cladding to hydrogen atoms produced as a result of Zircaloy-steam reaction) was calculated and plotted (Fig. 5) as a function of oxidation temperature. In the same plot, similar values obtained from the similar tube specimens oxidized in hydrogen-steam mixtures[18] and described in association with Fig. 2 are also shown. For the latter data set, oxygen and hydrogen weight contents were determined by inert-gas fusion techniques, as for the case of Fig. 4.

From Fig. 5, it seems clear that the hydrogen absorption fraction is not negligible. The apparent maximum of the fraction at ~1140°C is believed to be associated with the formation of porous breakaway-type oxide layer, primarily

at the cladding inner surface, which has been reported[16] to be limited to temperatures $\lesssim$1140°C. Under transient oxidation conditions during a degraded-core accident, formation of the porous oxide is not likely. For temperatures $\gtrsim$1200°C, in which no porous oxide was observed, the absorption fraction is still considerable, i.e., as much as ~20%.

Because the steam molecules are the only source of oxygen during oxidation in a hydrogen-steam mixture, each dissolved oxygen atom in the Zircaloy (in either oxide, α-, or β-phase) still corresponds to one molecul of steam dissociated or two atoms of produced hydrogen. Therefore, a numbe of data obtained from specimens oxidized in hydrogen-steam mixtures and shown in Fig. 5 still signify the fraction of hydrogen atoms absorbed per unit number of hydrogen atoms produced by oxidation of the specimen in the mixtures. The specimen showing as much as 18.5% of absorption at 1705°C (see Fig. 5) contained 0.1993 and 8.63 wt % hydrogen and oxygen, in that order. It was oxidized in a hydrogen-steam mixture for 180 s and had an oxide layer of 0.214 mm at the outer surface.

The information contained in Fig. 5 clearly demonstrates that Zircaloy cladding itself can act as a considerable sink for hydrogen. A better understanding in this area, which requires a more comprehensive data base, would be helpful for a more realistic quantification of hydrogen release rate during a degraded-core accident situation.

SUMMARY AND CONCLUSIONS

(1) Zircaloy-oxidation and corresponding hydrogen-generation rates reported in the literature have been critically reviewed with respect to their applicability to the analysis of hydrogen behavior during a degraded-core accident situation.

(2) New oxidation rate constants obtained for >1500°C in mixtures of hydrogen and steam are shown. The rate constants are a function of thermal-hydraulic parameters of the mixture flow as well as of the Zircaloy temperature.

(3) Zircaloy cladding can act as a considerable sink of hydrogen during high-temperature oxidation in either steam or hydrogen-steam environments. An absorption fraction of as much as ~20% of the produced hydrogen was observed for 1200-1700°C.

ACKNOWLEDGMENTS

The authors gratefully acknowledge the experimental contributions of L. P. Burkel and R. A. Conner, Jr. They are also grateful to D. Graczyk for performing the hydrogen analysis.

REFERENCES

1. W. A. Bostrom, "High Temperature Oxidation of Zircaloy in Water," WAPD-104, Westinghouse Electric Corporation, March 1954.

2. A. W. Lemmon, Jr., "Studies Relating to the Reaction Between Zirconium and Water at High Temperatures," BMI-1154, Battelle Columbus Laboratories, January 1957.

3. L. Baker and L. C. Just, "Studies of Metal-Water Reactions at High Temperatures. III. Experimental and Theoretical Studies of the Zirconium-Water Reaction," ANL-6548, May 1962.

4. J. T. Bittel and L. H. Sjodahl, "Reaction Mechanisms and Kinetics - Oxidation of Zirconium Alloys by Steam or Air," in Seventh Annual Report - AEC Fuels and Materials Development Program, GEMP-1004, General Electric Company, March 1968.

5. R. G. Ballinger, W. G. Dobson, and R. R. Biederman, "Oxidation Reaction Kinetics of Zircaloy-4 in an Unlimited Steam Environment," J. Nucl. Mater. 62, 213-220 (1976).

6. M. Suzuki, S. Kawasaki, and T. Furuta, "Zircaloy Steam Reaction and Embrittlement of the Oxidized Zircaloy Tube Under Postulated Loss-of-Coolant Accident Conditions," JAERI-M 6879, Japanese Atomic Energy Research Institute, Tokai, Japan (NUREG-tr-0014), January 1977.

7. J. V. Cathcart, R. E. Pawel, R. A. McKee, R. E. Druschel, G. J. Yurek, J. J. Campbell, and S. H. Jury, "Zirconium Metal-Water Oxidation Kinetics IV. Reaction Rate Studies," ORNL/NUREG-17, Oak Ridge National Laboratory, Oak Ridge, TN, August 1977.

8. A. F. Brown and R. Healy, "The Kinetics of Total Oxygen Uptake in Steam Oxidized Zircaloy-2 between 1000-1400°C," RD/B/N4117, Central Electricity Generating Board, Berkeley, United Kingdom, September 1977.

9. S. Leistikow, G. Schanz, and H. r. Berg, "Kinetik und Morphologie der isothermen Dampf-Oxidation von Zircaloy 4 bei 700-1300°C," KfK-2587, Kernforschungszentrum Karlsruhe, Germany, March 1978.

10. V. F. Urbanic and T. R. Heidrick, "High Temperature Oxidation of Zircaloy-2 and Zircaloy-4 in Steam," J. Nucl. Mater. 75, 251-261 (1978).

11. A. F. Brown, M. O. Tucker, T. Healey, and C. J. Simpson, "Oxide/α and α/β Phase Interface Advance Kinetics in Steam Oxidized Zircaloy-2," RD/B/N4882, Central Electricity Generating Board, Berkeley, United Kingdom, July 1980.

12. H. Ocken, "An Improved Evaluation Model for Zircaloy Oxidation," Nucl. Tech. 47, 343 (1980).

13. R. E. Westerman, "High Temperature Oxidation of Zirconium and Zircaloy-2 in Oxygen and Water Vapor," HW-73511, Hanford Laboratories, Hanford, Washington, April 1962, pp. 21-23.

14. T. Furuta and S. Kawasaki, "Reaction Behavior of Zircaloy-4 in Steam-Hydrogen Mixtures at High Temperature," J. Nucl. Mater. 105, 119-131 (1982).

15. H. M. Chung and G. R. Thomas, "Rate-Limiting Effects of Gaseous Hydrog on Zircaloy Oxidation," NUREG/CR-2017, SAND 81-0661, Vol. II, Sandia National Laboratories, Albuquerque, New Mexico, September 1981, pp. 39-65.

16. H. M. Chung and T. F. Kassner, "Embrittlement Criteria for Zircaloy Fuel Cladding Applicble to Accident Situations in Light-Water Reactors: Summary Report," ANL-79-48, Argonne National Laboratory, Argonne, Illinois, January 1980.

17. H. Uetsuka, T. Furuta, and S. Kawasaki, "Zircaloy-4 Cladding Embrittlement due to Inner Surface Oxidation under Simulated Loss-of-Coolant Condition," J. Nucl. Sci. Tech. 18, 705-717 (1981).

18. H. M. Chung and G. R. Thomas, "High-Temperature Oxidation of Zircaloy in Hydrogen-Steam Mixture," in Proc. Sixth Intl. Conf. on Zirconium in the Nuclear Industry, June 28-July 30, 1982, Vancouver, Canada, in press.

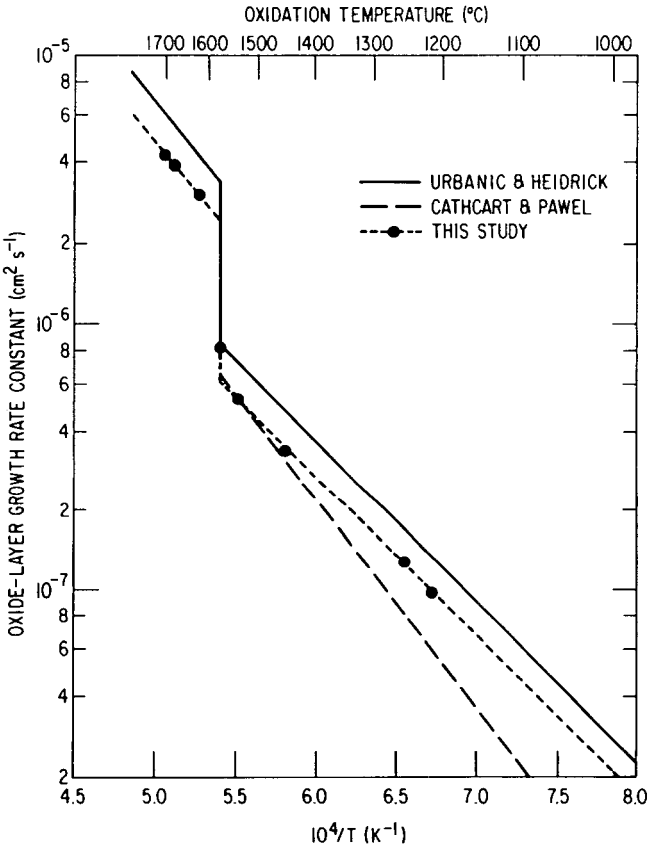


Fig. 1. Parabolic Oxide Layer Growth Rate Constants Obtained for Pure Steam Environments vs Inverse Temperature. Similar results reported by Cathcart and Pawel[7] and Urbanic and Heidrick[10] are shown for comparison.

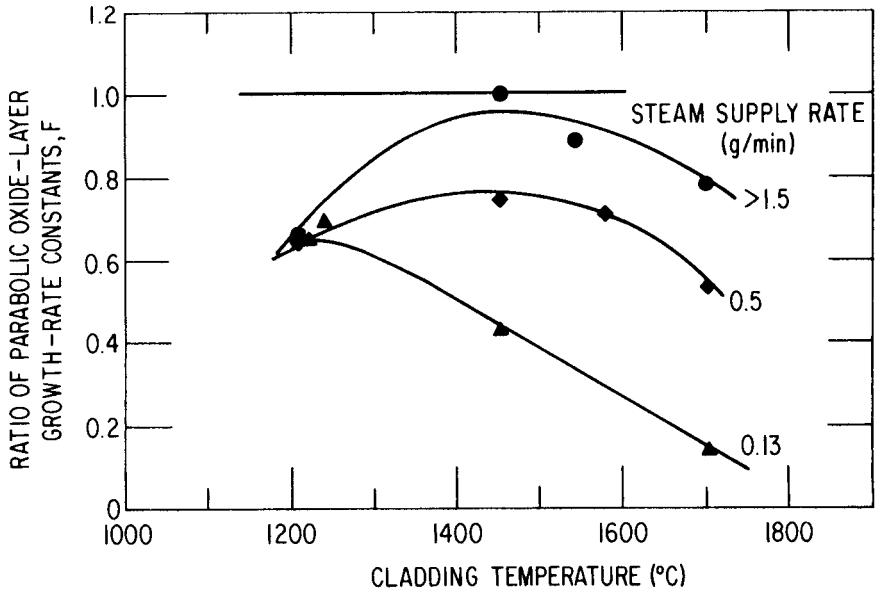


Fig. 2. Ratio of Parabolic Oxide Layer Growth Rate Constant Obtained in Hydrogen-Steam Mixtures to that Obtained in an Unlimited Flux of P Steam as a Function of Zircaloy-4 Temperatures and Steam Supply Rate. The static hydrogen overpressure was kept constant at ~36 kPa and the specimen was oxidized by steam molecules impinging the oxide surface through natural convection. The parabolic growth rates obtained without the hydrogen overpressure, but with steam supplies of similar rates, are shown in Fig. 1.

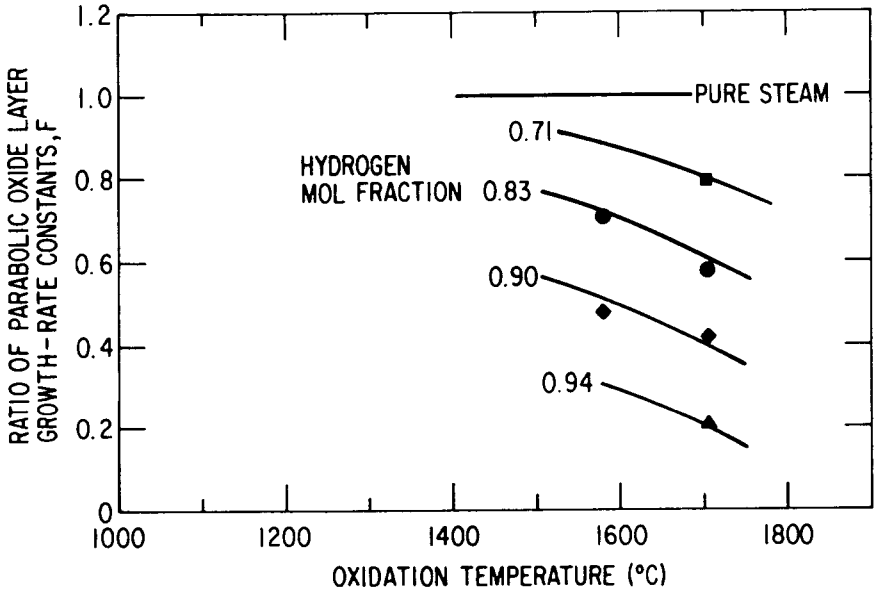


Fig. 3. Ratio of Parabolic Oxide Layer Growth Rate Constant Obtained in Flowing Hydrogen-Steam Mixtures to that Obtained in an Unlimited Flux of Pure Steam as a Function of Zircaloy-4 Temperature and Average Hydrogen Mol Fraction in the Inlet Mixtures. Hydrogen input to the shrouded reaction channel was 0.446 mol/min and steam flow was varied 0.5-3.2 g/min.

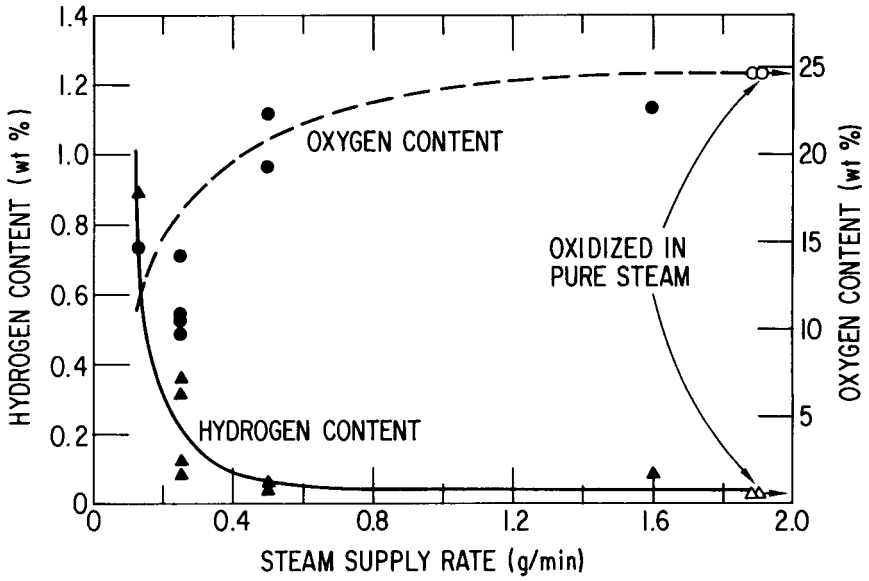


Fig. 4. Hydrogen and Oxygen Contents of the Fine Powders Obtained from Surface Skin of the Oxide Formed During Oxidation at 1705°C for ~120 s in Various Hydrogen-Steam Mixtures Described in Association with Fig. 2. For comparison, similar contents for specimens oxidized in pure steam are shown.

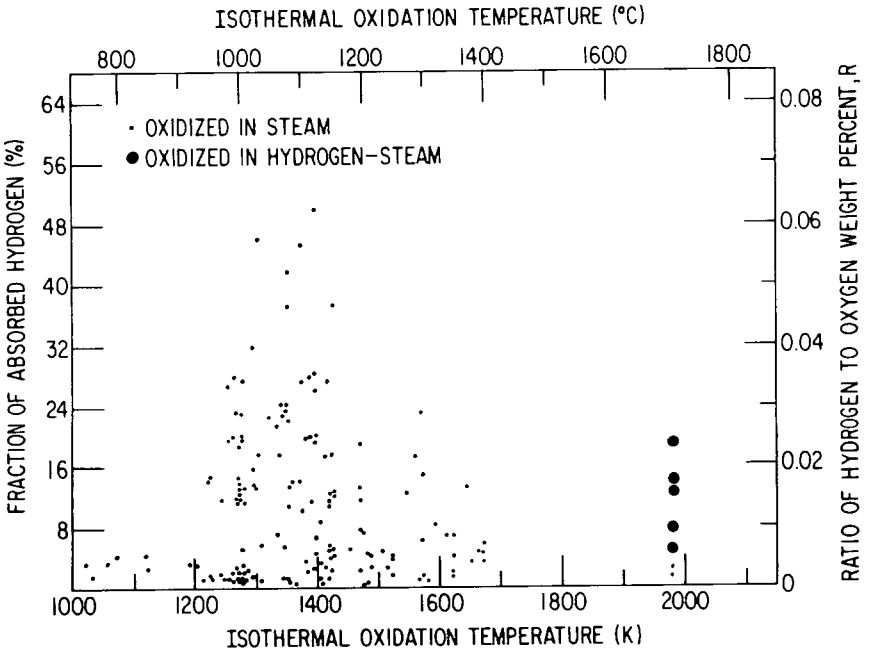


Fig. 5. Fraction of Hydrogen Atoms Dissolved in a Cross Section of Zircaloy-4 Cladding Tube Out of Total Hydrogen Atoms Produced as a Result of Zircaloy-Steam Reaction at Isothermal Oxidation Temperatures Between 1000 and 1700°C. The fractions from oxidation tests in pure steam were obtained from Ref. 16 and similar values for oxidation in hydrogen-steam mixtures were obtained from specimens described in association with Figs. 2 and 4.

H_2 PRODUCTION FROM THE STEEL-WATER REACTION DURING A POSTULATED CORE MELTDOWN ACCIDENT*

W. S. Yu and W. T. Pratt
Department of Nuclear Energy
Brookhaven National Laboratory
Upton, New York 11973

ABSTRACT

The MARCH code has been modified to model H_2 generation from the steel-water reaction during core meltdown accidents. Descriptions of the modifications are given for the Fe-water reaction model. A number of accident sequences were considered to determine the potential amount of H_2 generated during postulated core meltdown events. The results indicate that the Fe-water reaction provides a minor contribution ($\sim$ 10% of the total) to H_2 generation (compared with the Zr-water source) during core uncovery and slumping within the reactor vessel. However, after head failure, the Fe-water reaction in the cavity can potentially make a significant contribution to H_2 generation. The results also indicate that the H_2 generation is very sensitive to the size of the debris particles formed when the molten core materials contact water.

1. INTRODUCTION

The occurrence of a hydrogen burn during the TMI-2 accident highlighted the possibility of H_2 concentrations reaching the containment building in excess of the present design basis for LWRs. It has been noted [1] that the metal-water reaction is a potential source of H_2 generation during core degraded accidents. However, previous analyses [2] of degraded core accidents have emphasized the importance of the Zr-water reaction as a source of H_2 but ignored the steel-water reaction.

The objective of this study is to estimate the additional quantity of H_2 that could be generated from the steel-water reaction and determine its relative importance during the various stages of core degradation. In addition, we extend our analysis beyond degraded core accidents (TMI) to postulate full core meltdown events, which involve the release of core materials from the reactor vessel. An initial summary of the work has been presented [3] at a recent ANS meeting. The present paper describes the work in more detail and considers additional accident sequences.

The MARCH code [4] has been used to predict H_2 generation during core meltdown accidents. However, MARCH models the steel-water reaction only when the core debris interacts with concrete. Our approach has been to incorporate steel-water reaction models into MARCH prior to core-concrete interactions during the following stages:

*This work was carried out under the auspices of the U. S. Nuclear Regulatory Commission.

1) during core uncovery;

2) during core slumping into water in the vessel;

3) during core debris-water interactions in the reactor cavity.

The above BNL modifications to MARCH are at present being incorporated into a new version of MARCH at BCL. Details of the models used and the modifications are further discussed below.

2. DESCRIPTION OF MARCH MODIFICATIONS

The modifications have been incorporated into the BOIL and HOTDROP subroutines of the MARCH code to model the steel-water reaction. There are three major modifications in the following areas: (1) from core uncovery to meltdown, (2) after core meltdown (melted core drops into the bottom head), and (3) after vessel head failure (core debris interacts with the water in the reactor cavity).

The subroutine BOIL and its associated subroutines in the MARCH code analyze the events and conditions in the primary system during the core heatup and meltdown stages of the accident. After the core is uncovered, the fuel rods become overheated and hydrogen is generated from the exothermic Zr-water reaction. BOIL calculates the amount of hydrogen generated during the core heatup stage until the core melts and relocates into the bottom head. As the hot core debris contacts water in the bottom head, steam is generated, which creates the potential for further metal-water reaction. After all the water in the bottom head has either reacted or evaporated, the MARCH code then assumes that the core debris attacks the bottom head. The reactor pressure vessel eventually fails and the core debris is assumed to fall into the reactor cavity and to react with any water that may be present. The steel-water reaction model has been implemented into these various stages to determine the generation of hydrogen.

The steel-water reaction model is basically similar to the zirconium-water reaction model already in the MARCH code. The objective of the present modification is to estimate the additional quantity of hydrogen generated as a result of the steel-water reaction and to determine its relative importance.

2.1 General Assumptions

(1) The reactor vessel internals use 304L stainless steel which consists of 18% Cr, 8% Ni and 74% Fe; however, iron is the only constituent considered in the proposed steel-water reaction model.

(2) The possible reactions between iron and water are:

$$2\ Fe + 3\ H_2O \rightarrow Fe_2O_3 + 3\ H_2$$

$$3\ Fe + 4\ H_2O \rightarrow Fe_3O_4 + 4\ H_2$$

It is assumed that Fe_3O_4 is the major oxide from the steam oxidation of steel.

(3) The oxidation rate of iron is assumed to follow the parabolic rate law [5].

(4) The heat generated from the oxidation reaction,

$$3\ Fe + 4\ H_2O \rightarrow Fe_3O_4 + 4\ H_2$$

is on the order of 155 kcal/g-mole of oxide formed.

2.2 Steel-Water Reaction Models

The iron-steam reaction is assumed generally as a two-step process. First, it is controlled by the gaseous diffusion of steam toward the control rod, and second, by the gaseous diffusion of the hydrogen away from the control rod.

2.2.1 Reaction Rate Controlled by Gaseous Diffusion

The rate of iron-steam reaction at the first stage is calculated by the following expression [6]:

$$\frac{dX}{dt} = \frac{1.3824 \times 10^{-7} \times R_p \times (T_f)^{0.68}}{(R_p - \Delta X/30.48)^2} \qquad (1)$$

where X = radius of unreacted metal (cm)

R_p = original radius of unreacted metal (ft)

ΔX = the thickness of the oxidized layer (cm)

T_f = $(T_s + T_w)/2$

T_s = the metal surface temperature (°K)

T_w = the bulk steam temperature (°K)

t = time (sec)

The units of the variables in Eq. (1) are consistent with the zirconium-steam reaction model in the MARCH code, so that they would cause less confusion for the user.

2.2.2 Reaction Rate Controlled by Solid State Process

The oxidation of 304L stainless steel in the temperature range of 1000 to 1350°C, which is of interest in the analysis of a reactor loss-of-coolant accident, is characterized by an initial linear rate followed by a parabolic rate. The reaction rates are given by J. T. Bittel, L. H. Sjodahl and J. F. White [5] as,

$$\text{LINEAR:} \quad W/t = 1.1 \times 10^{-5} \text{ Exp } \left(\frac{-44350 \pm 2300}{RT}\right) \tag{2}$$

$$\text{PARABOLIC:} \quad W^2/t = 2.4 \times 10^{12} \text{ Exp } \left(\frac{-84350 \pm 2300}{RT}\right) \tag{3}$$

where W = weight gain per unit area (mg/cm^2)

t = time in seconds

R = gas constant (cal/mole °K)

T = absolute temperature (°K)

Linear kinetics, Eq. (2), are indicative of a reaction process limited in rate by chemical reaction at an interface. Parabolic kinetics, Eq. (3), are indicative of a reaction process limited by the transport of reactants. The rate of oxidation of iron, at which the thickness of the oxidized layer increases, is controlled by solid state diffusion. The parabolic rate law is usually considered to apply at this stage. Equation (3) is used in the calculation and can be expressed in terms of thickness of oxidized iron as:

$$\frac{dX}{dt} = \frac{0.2662 \times 10^6}{\Delta X} \text{ Exp } \left(\frac{-76411.68}{T}\right) \tag{4}$$

where $\frac{dX}{dt}$ = the advancement rate of the oxidized layer in cm/sec

T = absolute temperature of the rod surface, °R.

In the program, both Eqs. (1) and (4) are calculated and the smaller of these is used.

2.3 Incorporating the Steel-Water Reaction Model Into MARCH

2.3.1 BOIL Subroutine

The basic structure of BOIL is unchanged by these BNL modifications. The number of radial and axial nodes remains the same. The steel-water reaction is simply added to those stages of the accident where the zirconium-water reaction was previously modeled. In this subroutine the model can be described as follows:

A. At core uncovery:

(a) The oxidation of steel is limited by the availability of steam in the coolant channels associated with the control rods.

(b) The amount of steel reaction at this stage is limited to the control rod cladding.

B. At core meltdown, molten core material begins to fall into the bottom head of the pressure vessel. There are two options in the MARCH code to calculate the oxidation rate of zirconium cladding. Modifications have been made in both options to include the steel-water reaction.

(a) Option 1: The user can simply specify the fraction of zirconium and steel to be oxidized. The availability of water in the bottom head can further limit oxidation.

(b) Option 2: A new subroutine called MWDRPS has been added to the MARCH code to calculate the oxidation of the steel cladding. The calculation assumes that all the material dropped into the bottom head takes the form of spheres. The amount of oxide formed is limited by either the amount of water available in the bottom head, or if the temperature of spheres drops below 2000°F.

2.3.2 HOTDROP Subroutine

In the original MARCH code, the molten core debris is assumed to fragment and form spherical particles upon contact with water in the reactor cavity. The spheres are assumed to contain a central region of uranium fuel and iron, an inner shell of zirconium, and an outer shell of zirconium oxide. In the modified version of HOTDROP, it is assumed that two distinct types of spheres of different compositions will be formed. One type contains uranium fuel, zirconium and zirconium oxide, and the other type contains iron and iron oxide. At this stage, the iron in the spheres is assumed to consist of material from the steel cladding, the lower internal vessel support structures and the bottom vessel head. The iron is assumed to form the inner region and iron oxide forms the outer shell. The iron particles are assumed to be the same size as the zirconium fuel particles.

3. RESULTS AND DISCUSSION

In order to assess the amount of H_2 generation from the iron-water reaction, a number of accident sequences that result in core degradation and melting were analyzed using the modified MARCH code. The analysis was based upon the following table.

Reactor Design Parameters Used in Analysis

		Pressurized Water Reactor (PWR)
Power Level		3400 MWt
Weight of zirconium cladding	=	41990.0 lbs
Zirconium cladding thickness	=	0.00213 ft
Weight of steel cladding	=	3986.0 lbs
Steel cladding thickness	=	0.001583 ft
Weight of total steel in core	=	20,410 lbs
Weight of total steel in grid plates	=	200,000 lbs
Weight of total steel in bottom head	=	78,130 lbs

and average debris particle sizes:

In-vessel particle diameter	= 0.001 to 1.0 in
Ex-vessel particle diameter	= 0.01 to 2.0 in

During core uncovery and heat-up, the modified MARCH code calculates that the Fe-water reaction contributes only about 10% of the total H_2 generation (the remainder coming from the Zr-water reaction). This is due to the relative quantities of Zr and Fe in the core region. The fraction of Zr and Fe oxidized can vary over a wide range depending on the accident sequences and the assumptions made about flow blockage and steam flow rates through the core region. A description of how MARCH can be used to predict oxidation rates for various accidents with a range of flow blockage assumptions was given by Cybulskis at the first H_2 workshop.[7] We carried out a similar sensitivity study with our modified MARCH code and found that the Fe-water reaction was always a relatively minor contribution to H_2 generation during this phase of the accident.

As the core materials melt and relocate into the bottom of the reactor vessel, significant additional quantities of steel could be melted and added to the core debris mass. Therefore, at later stages of core meltdown, the Fe-water reaction has a greater potential for contributing to H_2 generation. We consider two potential accident sequences in order to assess the relative contribution of Fe and Zr oxidation to H_2 generation. We will concentrate our sensitivity study on in-vessel slumping and ex-vessel core debris-water interactions because we have noted above that Fe oxidation has a minor impact during core uncovery. The accident sequences considered are a TMLB' transient and a S_2D LOCA. Here we use the nomenclature of WASH-1400 [8] and defined the accidents in greater detail in the following sections.

3.1 TMLB' Transient

The TMLB' transient assumes a loss of the turbine-driven pump train of the auxiliary feedwater system, coupled with a loss of total AC power for an extended period. H_2 generation rates from the metal-water reaction during the various stages of core meltdown are correlated on logarithm plots in Figures 1-4.

The contribution of the iron-water reaction to H_2 generation during three stages of core degradation is compared with that of the zirconium-water reaction in Figure 1. The results shown in Figure 1 are for an in-vessel particle diameter of of 0.012" and a range of ex-vessel particle diameters of 0.01" to 2.0". Note that the H_2 generation before the core slump is obviously independent of the assumed particle size. For the particular assumptions made during core uncovery, the amount of H_2 generated is 608 lbs. from the zirconium-water reaction and 66 lbs. from the iron-water reaction. As core materials melt and fall into the bottom head, there is an additional 467 lbs. of H_2 generated from the Zr-water reaction, as well as 36 lbs. of H_2 generated from the Fe-water reaction. As a result, before the head failure, the total H_2 generated is 1,075 lbs. and 102 lbs. from the Zr-water and the Fe-water reactions, respectively.

The above results confirm that the Fe-water reaction provides a minor contribution ($\sim$10% of the total) to the H_2 generation, compared with the Zr-water source during core uncovery and slumping within the reactor vessel. However, after head failure, the Fe-water reaction in the cavity makes a significant contribution to the H_2 generation. If 0.01" diameter particles are assumed, 8,465 lbs. of H_2 are produced as a result of the ex-vessel Fe-water reaction, as compared with 794 lbs. of H_2 produced from the ex-vessel Zr-water reaction. The H_2 generation would be reduced to 195 lbs. from the Fe-water reaction and 1.4 lbs. from the Zr-water reaction if the particles formed in the cavity are assumed to be larger (1.8" diameter). The area between the two upper curves in Figure 1 shows the total H_2 contribution from the Fe-water reaction for the range of the ex-vessel particle diameters (0.01" to 1.0"). It is apparent that the H_2 generation is strongly dependent upon the particle sizes. The reliability of MARCH predictions depends on a knowledge of the fragmentation of the debris particles during molten core interactions with water. If the debris particles are large, the total H_2 generation would be limited to $\sim$1,200 lbs. for this particular case. On the other hand, if very fine particles are assumed, the model would predict very high H_2 generation.

Figure 2 shows the percentage of reacted zirconium as a function of the in-vessel particle diameter for various ex-vessel particle diameters. Assuming a particle diameter of 0.1", 38% of Zr would react as the debris falls into the bottom head, as indicated in Figure 2. As the particle diameter decreases, the amount of reacted Zr increases to 98% at 0.0012" diameter. When the head fails, the debris drops to the reactor cavity. The percentage of reacted Zr is also a function of the ex-vessel particle diameter. If the in-vessel particles are assumed to be very fine, Zr is completely reacted prior to head failure. However, at an in-vessel particle diameter of 0.1", and an

ex-vessel particle diameter of 2", 38% of Zr is reacted. 100% of Zr would be reacted only if the ex-vessel particle diameter were decreased to 0.012". Note that the amount of reacted Zr is very sensitive to the size of the particles formed, which can vary from 32% to 100% according to the in-vessel and ex-vessel particle diameter.

The percentage of reacted iron during the three stages of the postulated core meltdown accident is not correlated because the amount of iron considered in the oxidation reaction is different during the various stages of core meltdown.

Figure 3 illustrates the total amount of H_2 generated from the metal-water reaction versus the in-vessel particle diameter for various ex-vessel particle diameters. If a fine particle diameter is assumed, a large amount of H_2 will be produced. As the particle diameter increases, the total amount of H_2 produced decreases sharply. For example, 10^4 lbs. of H_2 would be produced at a particle diameter of 0.012" to 700 lbs. of H_2 at a diameter of 2". The broken line in Figure 3 shows the H_2 production if the size of the particle diameter formed remains the same before and after the head failure.

A cross plot of Figure 3 is given in Figure 4. Since the modified model assumes that there is more Fe participating in the ex-vessel oxidation reaction, the results indicate that the H_2 production is even more sensitive to the ex-vessel particle sizes.

3.2 S_2D LOCA

In addition to a TMLB' transient, an S_2D LOCA was also studied by the modified MARCH code. S_2D is a small LOCA with break area equivalent to a 2" diameter. The S_2D sequence results in a failure of the active ECC system to inject. The H_2 generation of the metal-water reaction is given in Figure 5 as a function of the ex-vessel particle diameter at an in-vessel particle diameter of 0.012". Before the core slumping, the H_2 generation is 681 lbs. from the Zr-water reaction, and 78 lbs. from the Fe-water reaction. The H_2 generation in the bottom head of the reactor is 310 lbs. and 24 lbs. from the Zr-water and Fe-water reaction, respectively. At the head failure the H_2 contribution is 991 lbs. from the Zr-water reaction and 101 lbs. from the Fe-water reaction, resulting in a total of 1,092 lbs. of H_2 production from the metal-water reaction. For an in-vessel particle diameter of 0.012", the H_2 contribution from the Fe-water reaction can be represented by the area between the two upper curves in Figure 5 for various ex-vessel particle diameters (0.01" to 2.0"). Results show that the H_2 generation from the metal-water reaction is similar for an S_2D LOCA and a TMLB' transient.

4. CONCLUSIONS

Some final comments before we make our concluding remarks. It is important to note that the purpose of this paper was not to change the basic phenomenological modeling in the MARCH code but rather to correct an inconsistency. Our conclusions are therefore based upon the existing MARCH models and in particular the HOTDROP model, which predicts core debris/water interactions. This model is rather controversial and in fact we at BNL have suggested [9] an alternative approach based upon debris bed considerations. It has also been suggested that H_2 blanketing could inhibit metal oxidation. However, it should be noted that the above alternative models imply significantly longer times to cool the core debris such that extensive core debris/concrete interactions would occur. Oxidation of the steel would therefore occur as a result of core debris/concrete interactions in these alternative models. The present version of MARCH is able to model (HOTDROP bypass model) steel oxidation during core debris/concrete interactions.

The MARCH computer code has been modified to model H_2 generation from the Fe-water reaction during three stages of core meltdown. Calculations with the modified MARCH code indicate that the Fe-water reaction provides a minor contribution (< 10% of the total) to H_2 generation (compared with the Zr-water reaction) during core uncovery and slumping within the reactor vessel. However, this conclusion is based on the amount of Fe included (assumed to be limited to the control rod cladding) during this stage of core meltdown. After head failure, the Fe mass associated with the grid plates and bottom head is also included in the core debris mass so that the potential for Fe to react with the water is greater in the reactor cavity. Consequently, the Fe-water reaction in the reactor cavity could potentially make a significant contribution to H_2 generation. Finally, our analysis indicates that the H_2 formed as the molten core materials contact water in the bottom of the vessel and in the reactor cavity is a strong function of the core debris particle size. If the particle size is relatively large (> 2 inch equivalent diameter) then the model indicates that relatively small quantities of H_2 are formed as the core slumps into water. However, if relatively fine particles are formed, then significant additional H_2 can be generated during these stages of core meltdown.

5. ACKNOWLEDGEMENTS

The authors wish to acknowledge Sen Sun Tsai for his contributions to the initial stage of this work. The authors also thank R. A. Bari and J. F. Boccio for helpful discussions and for reviewing and commenting on the manuscript.

6. REFERENCES

1. D. A. Powers, "Review of Steel-Steam Oxidation Reactions - The Forgotten H_2 Source," Proceedings of the Workshop on the Impact of H_2 on Water Reactor Safety, NUREG/CR-2017, SAND81-0661 (Aug. 1981).

2. R. O. Wooton, R. S. Denning and P. Cybulskis, "Analysis of the Three Mile Island Accident and Alternative Sequences," NUREG/CR-1219 (Jan. 1980).

3. W. S. Yu and W. T. Pratt, "Effects of Steel-Water Reaction During a Postulated Core Meltdown Event," Trans. Am. Nucl. Soc., 39, 604 (1981).

4. R. O. Wooton and H. I. Avci, "MARCH", NUREG/CR-1711, BMI-2064, Battelle Columbus Laboratories, Columbus, Ohio (Oct. 1980).

5. J. T. Bittell, L. H. Sjodahl and J. F. White, "Oxidation of 304L Stainless Steel by Steam and by Air," Corrosion NACE, 25, No. 1 (1969).

6. L. Baker and L. C. Just, "Studies of Metal-Water Reactions at High Temperatures, III. Experimental and Theoretical Studies of the Zirconium-Water Reaction," Argonne National Laboratory, ANL-6548 (May 1962).

7. P. Cybulskis, "MARCH Predictions of Hydrogen Behavior in LWR Meltdown Accidents," Proc. of the Workshop on the Impact of H_2 on Water Reactor Safety, Volume 1, NUREG/CR-2017, SAND81-0661, (Aug. 1981).

8. U. S. Nuclear Regulatory Commission, "Reactor Safety Study - An Assessment of Accident Risks in U. S. Commercial Nuclear Power Plants," WASH-1400 (NUREG-75/014), (Oct. 1975).

9. J. W. Yang and W. T. Pratt, "Steam Pressure Spike in PWR Plant Under Severe Accident Conditions," presented at the International Meeting on Thermal Nuclear Reactor Safety, (Aug. 29-Sept. 2, (1982).

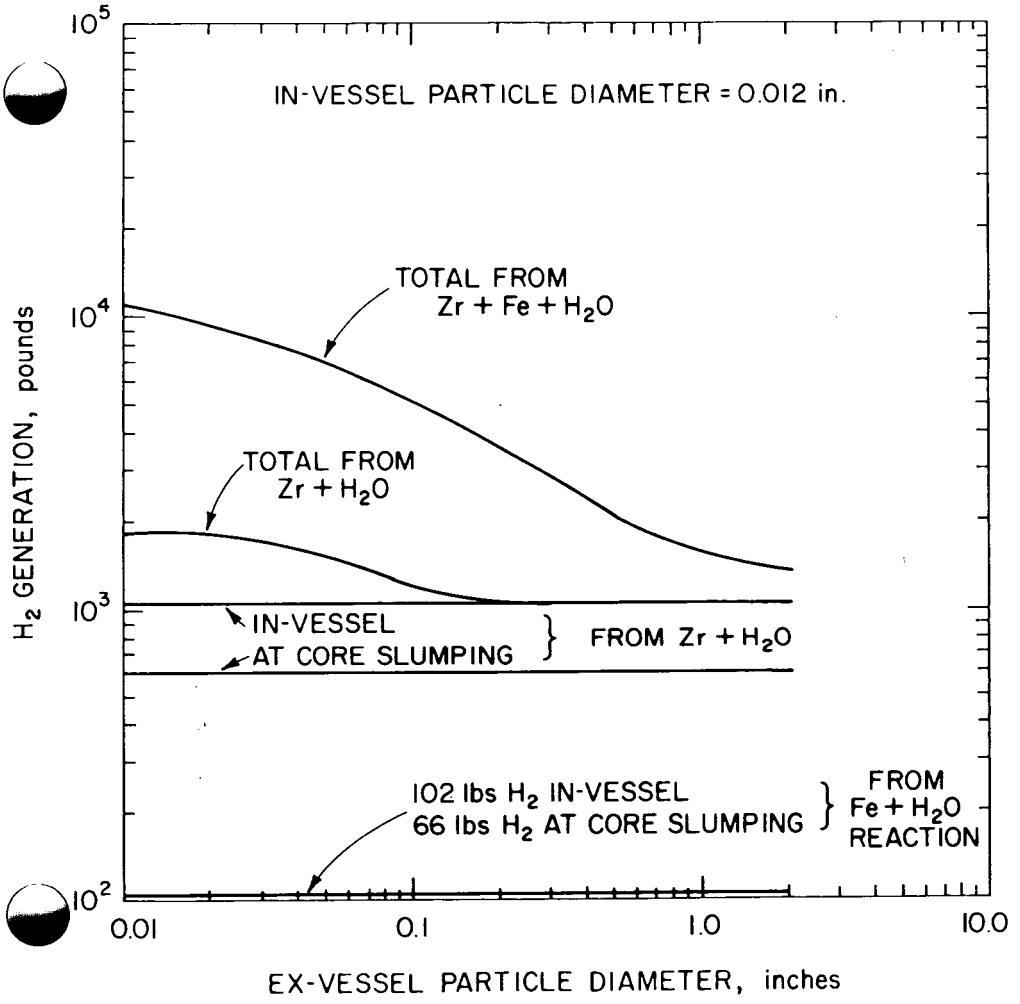


Figure 1. H_2 Generation - TMLB' Transient

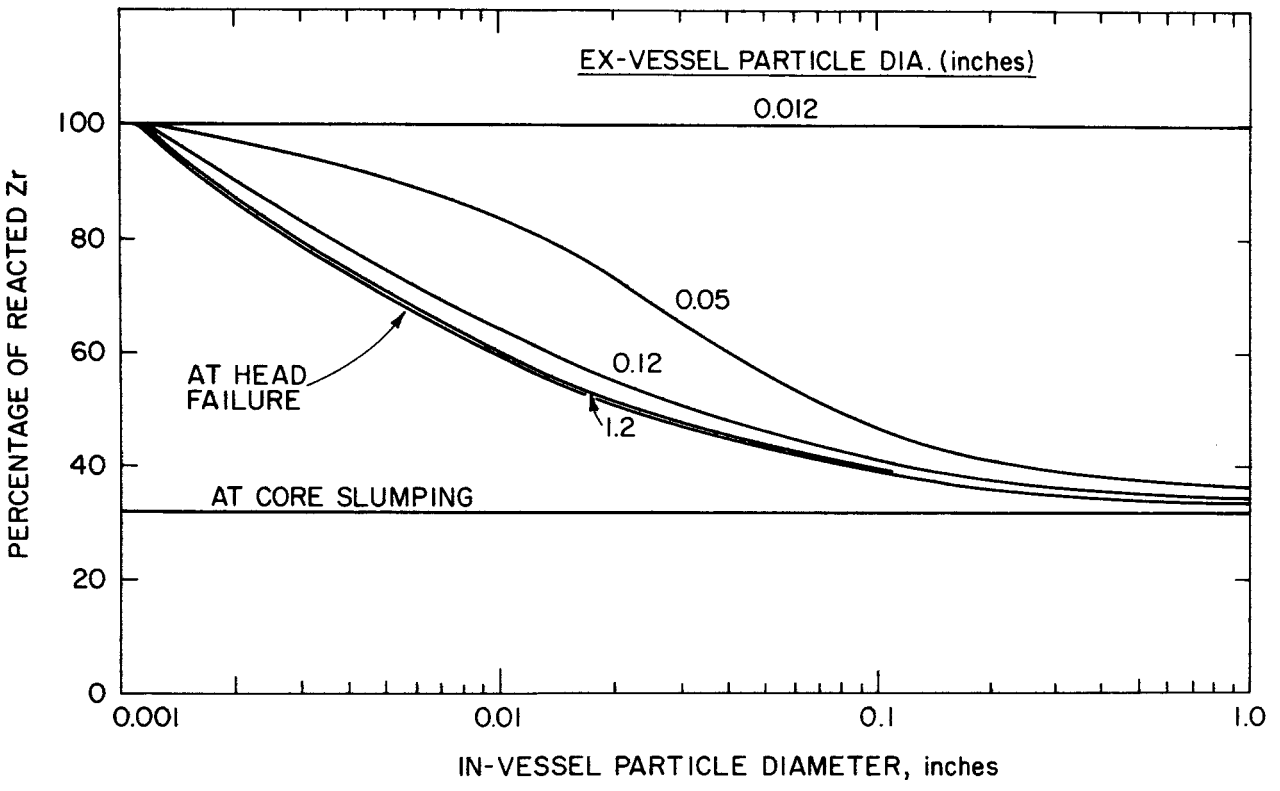


Figure 2. Percentage of Zr-Cladding Reacted - TMLB' Transient

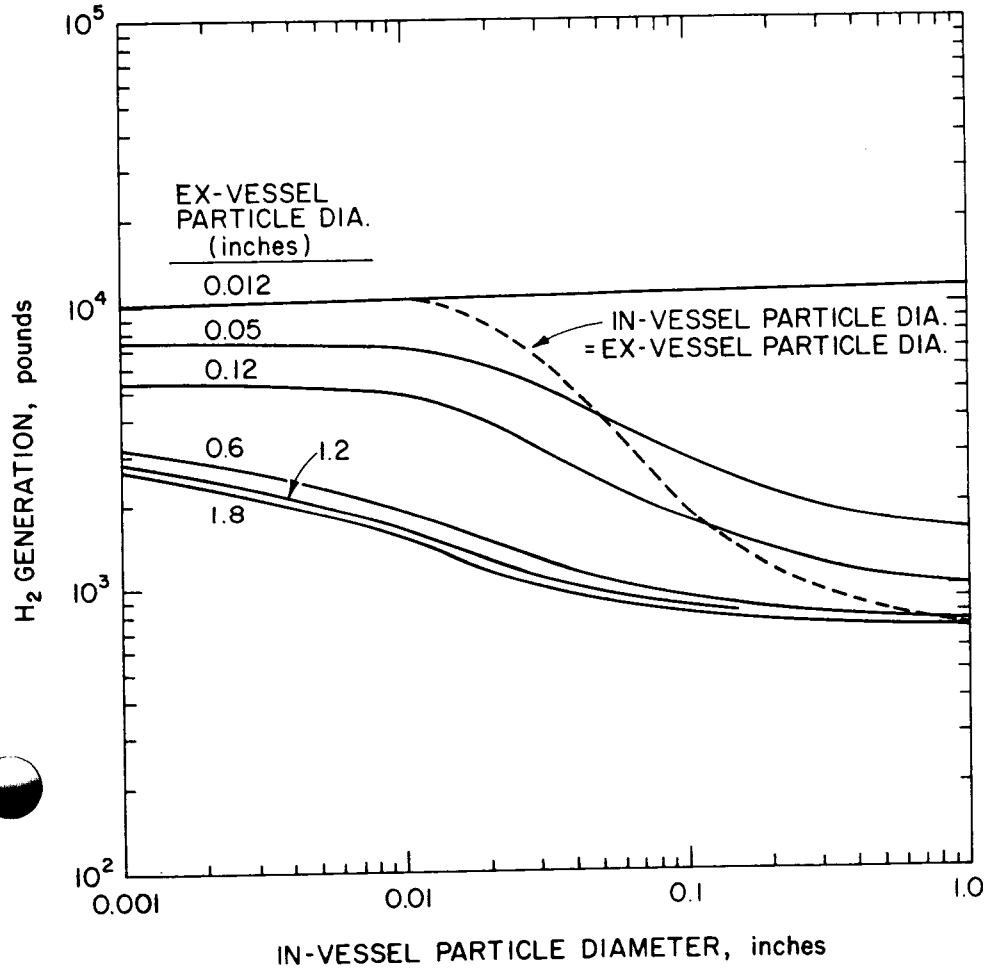


Figure 3. H_2 Generation - TMLB' Transient

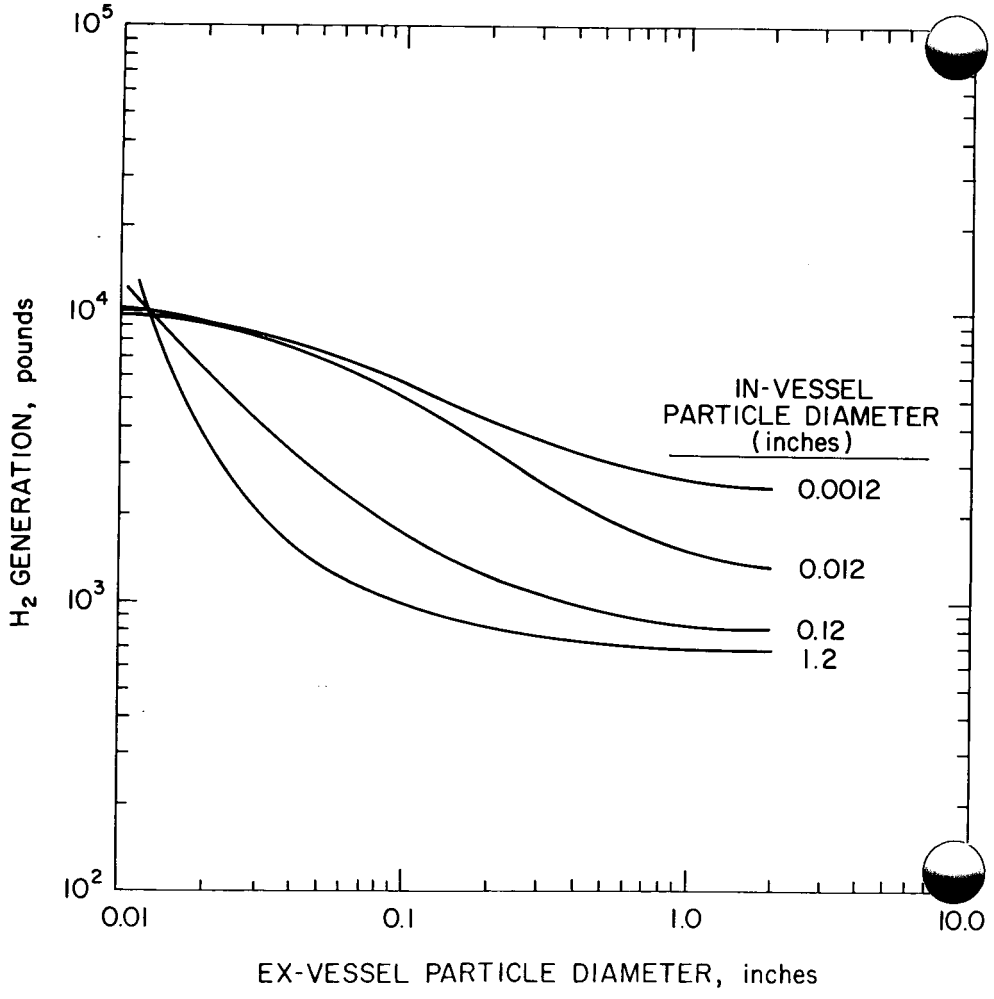


Figure 4. H_2 Generation - TMLB' Transient

HYDROGEN PRODUCTION DURING FRAGMENTED DEBRIS/CONCRETE INTERACTIONS*

William W. Tarbell
Richard E. Blose
Ktech Corp.***

* This work sponsored by the United States Nuclear Regulatory Commision

** Operated for the United State Department of Energy under Contract No. DE-AC04-76DP00789.

***Employees of Ktech Corporation, under contract to Sandia National Laboratories.

Background

In the unlikely event that molten core debris escapes the reactor pressure vessel, the interactions of the debris with concrete and structural materials become the driving forces for severe accident phenomena. The Ex-vessel Core Debris Interactions Program at Sandia Laboratories is a research effort to characterize the nature of these interactions and the magnitude of safety-related phenomena such as hydrogen generation, aerosol production, and fission product release that arise because of the melt/concrete interactions.

Figure 1 shows the temperature history during a hypothetical accident sequence that can lead to hot, but not molten debris attacking the concrete basemat. In this sequence, the temperature history of the debris follows a decay heating curve through to the point where the solidification of the debris material occurs. At the conclusion of the solidification phase, the interaction enters a low temperature phase where the solid debris are at temperatures above the concrete ablation point. Depending on the conditions of the plant at the time of the accident and the types of materials involved (both debris and concrete), the low-temperature phase may be of long duration.

Figure 2 illustrates a second, different accident sequence also leading to the interaction of hot, solid debris and concrete. In this event, the debris initially undergoes an energetic reaction with water to cause fragmentation and quenching of the molten core debris. Subsequently, the decay-power heating of the debris causes the water to boil off and the temperature of the debris to increase. Conceivably, the heating can follow any of the three curves depicted in the figure. Path 2 describes the evolution of the sequence leading to the interaction of hot, fragmented debris with concrete.

Within the Ex-Vessel Core Debris Interactions Program, the Fragmented Debris test series is directed towards the study of the second accident sequence described above. The specific objective of this effort is to quantify gas production, concrete attack, and the effect of coolant associated with these events. This paper addresses specifically the gas generation from the decomposition of concrete exposed to hot solid debris.

Description of Tests

The tests have been performed with concretes of basaltic or limestone aggregate. The test crucible is a right-circular cylinder nominally 41 cm in diameter and 75 cm in height. An internal cavity (22 cm diameter x 60 cm depth) contains the simulated debris. The cavity is filled to a height of 25 cm, with mild steel spheres (approximately 3 mm diameter). An inductive coil placed around the crucible causes magnetic currents to circulate and heat the debris. The temperatures produced during the test are monitored by thermocouples placed in the steel balls and in the concrete.

An insulated and heated instrumentation tower is placed on the

crucible to permit channeling and measuring the decomposition by-products. In addition to diagnostics for measuring flow, gas species, aerosol, and heat flux; video and framing cameras are used to observe the upper debris surface.

A test is initiated with the debris and crucible at ambient temperature. The strength of the magnetic field is varied to control the temperatures generated in the debris. Figure 3 is a thermocouple temperature record from four sensors located on the axial centerline of the debris. At early times, the spread in the individual profiles is small except for the lowermost sensor that is affected by the large thermal sink provided by the concrete base. The amount of heat lost to the base becomes less pronounced at later times as the concrete dehydrates and its effective thermal conductivity decreases. As the temperature of the debris increases (greater than 500°C) the radiative heat transfer to the relatively cool instrumentation tower becomes significant (see M-07 Figure 3) cooling the upper debris regions. However, the cooler portion of the debris generally extends to a depth of two centimeters or less.

The concrete surfaces exposed to the debris increase in temperature because of heat conduction at the metallic sphere/concrete interface. At late times when melting of the concrete occurs, the heat transfer mechanisms become more complicated due to the liquid/solid interface and the movement of molten concrete through the debris. Figure 4 illustrates embedded concrete thermocouple records. For times up to three hours, the records are dominated by the influence of free water migration within the concrete. When this water is depleted in a region, the temperature increases much more rapidly. An abrupt change occurs in the profiles beginning at the 10 hour point in the test, caused principally by the downward movement of the debris.

Table 1 outlines some details of the four fragmented debris (FRAG) tests. Two characteristics are addressed, the type of concrete and the absence or presence of water in the debris bed. Basalt and limestone-common sand are generic reactor-plant compositions commonly used in the USA. The chemical compositions given in Table 2 show that the principal differences are in the CaO and SiO_2 ratios and the large CO_2 contribution in the limestone concrete. The test matrix allows comparison of the behavior of the two concretes under nearly identical conditions and study of the effect of water on the interaction.

The strategy in each test is to heat the debris bed to a nominal temperature of 1350-1400°C. These debris temperatures are sufficient to cause concrete decomposition and melting. Once the concrete is melted, the hydrostatic force exerted by the debris causes molten concrete material to flow through and around the debris. As the concrete material moves upward, it reaches a location where it quenches and forms a crust layer. The relative location of the crust to the debris appears to be linked to the concrete type by the viscosity of the molten material. The more viseous basalt typically forms a crust above the debris while the limestone concrete forms a layer within the debris bed.

For FRAG 1 And FRAG 2A, the concrete attack was allowed to proceed until the debris escaped through the sidewall or the bottom of the crucible. Up to 15 centimeters of erosion has been observed on some tests. The two subsequent tests, FRAG 3 and FRAG 4, differed in that coolant was added on top of the debris after concrete attack was initiated. In both these cases, the water failed to penetrate the debris bed, primarily because of the barrier provided by the crust layer.

The evolution of noncondensable gases during ex-vessel melt interactions will contribute to containment pressurization. If these gases bubble through and react with the debris, flammable gases such as hydrogen and carbon monoxide may lead to detonation and deflagration hazards. Therefore, gas generation during small scale experiments must be understood and mechanisms for predicting and scaling gas composition data must be derived. Some immediate questions that can be addressed are:

(a) Can a thermochemical formalism be used to describe and predict gas compositions or do the kinetics of reaction have to be considered?

(b) How does the overlying water pool affect the gas/debris reactions?

(c) What chemical reactions are responsible for the reduction of CO_2 and H_2O from the concrete to create flammable gasses such as CO and H_2?

For the premise considered in (a) above, the approach will to develop thermodynamic relationships for the reactions occurring in the FRAG tests, then to use these relationships to analyze the data to determine the feasibility of the results. If the results using the thermodynamic relationships appear reasonable, then it can be assumed that these experiments may be modeled thermodynamically rather than kinetically.

Gas Generation

The temperature ranges of thermally induced decomposition of both concrete types are qualitatively similar. Upon heating, water is lost over the range of 30 to 240° C. This "free" water comes from evaporable water within the concrete structure and loss of molecular water from some cementitious species. A second loss occurs over the range 360-485°C when decomposition of hydroxide-species releases bound water. The magnitudes of these two losses are similar for both concrete types.

Above 600° C another loss occurs in concrete because of the decomposition of calcareous species that are in the cementitious phase of concretes owing to the action of air on calcium salts. The limestone aggregate also decomposes to yield carbon dioxide. The aggregate carbonates decompose at somewhat higher temperatures and over a narrower range than do the cementitious species.

For the thermodynamic analysis, the gas is assumed to be in equilibrium with the surrounding media at some time. Further, all chemical reactions are assumed to stop when the temperature of the gas falls below the last equilibrium temperature. The reaction of interest in the gas phase is then:

$$CO_2 + H_2 \leftrightharpoons CO + H_2O \qquad (1)$$

This study is concerned with the influence of the metallic debris in reduction of the CO_2 and H_2O liberated from the concrete.

The gases may be considered ideal so that the thermochemistry of the reaction is given by:

$$\Delta G_{Rxn} = \Delta G_f(CO) + \Delta G_f(H_2O) - \Delta G_f(CO_2) - \Delta G_f(H_2) = -RT \, Ln \left[\frac{P_{H_2O} \, P_{CO}}{P_{H_2} \, P_{CO_2}} \right] \qquad (2)$$

where: $G_f(i)$ = free energy of formation of i^{th} species
R = gas constant
P_i = partial pressure of i^{th} species
ΔG_{Rxn} = free energy of the reaction

Defining the free energy of formation of an elemental species to be zero, yields:

$$\Delta G_f(H_2) = 0$$

Knowing any heterogeneous equilibrium, such as $CO/CO_2/Fe$, the above equation allows other heterogeneous equilibria to be determined, for example $H_2/H_2O/Fe$. There are two possible heterogeneous reactions in the $CO/CO_2/Fe$ equilibria:

$$3\,Fe + 4CO_2 \leftrightharpoons Fe_3O_4 + 4\,CO \qquad (3)$$

or

$$x\,Fe + CO_2 \leftrightharpoons Fe_xO + CO \qquad (4)$$

Writing the free-energy equation for both cases gives:

$$\Delta G_f(Fe_3O_4) + 4\Delta G_f(CO) - 4\Delta G_f(CO_2) = -RT \, Ln \left[\frac{P_{CO}^4}{P_{CO_2}^4} \right] = -4\,RT \, Ln \left[\frac{P_{CO}}{P_{CO_2}} \right] \qquad (5)$$

and

$$\Delta G_f(CO) + \Delta G_f(Fe_xO) - \Delta G_f(CO_2) = -RT \, Ln \left[\frac{P_{CO}}{P_{CO_2}} \right] \qquad (6)$$

where: R = gas constant
T = absolute temperature

Either equation, (5) or (6), allows calculation of P_{CO}/P_{CO_2}. The correct treatment depends on the ratio P_{CO}/P_{CO_2} determined from the combined reaction:

$$3/x\ Fe_xO + (4 - 3/x)\ CO_2 \rightleftharpoons Fe_3O_4 + (4 - 3/x)\ CO \qquad (7)$$

and

$$\Delta G_f(Fe_3O_4) + (4 - 3/x)\left[\Delta G_f(CO) - \Delta G_f(CO_2)\right] - 3/x\ \Delta G_f(Fe_xO) = (4 - 3/x)\ RT\ Ln\left[\frac{P_{CO}}{P_{CO_2}}\right] \qquad (8)$$

This reaction defines the ratios of P_{CO}/P_{CO_2} that keeps Fe_xO in equilibrium with Fe_3O_4. If P_{CO}/P_{CO_2} is larger than the equilibrium ratio, then Fe_xO is formed and Fe_3O_4 is formed when the converse is true.

The equilibrium partial pressure of oxygen in a CO/CO_2 mixture is given by:

$$-2\left(\Delta G_f(CO) - \Delta G_f(CO_2) + RT\ Ln\left[\frac{P_{CO}}{P_{CO_2}}\right]\right) = RT\ Ln\ P_{O_2} \qquad (9)$$

Data from the JANAF tables for the free-energy of formation of gaseous species were fit by a nonlinear least squares method to the equation:

$$\Delta G_f = aTLn(T) + b \times 10^{-3}\ T^2 + c \times 10^6\ T^3 + d \times 10^5/T + eT + h \qquad (10)$$

In general, values calculated in this manner agree with the JANAF tabulated values to $\pm$ 1 cal/mole. In no case is the disagreement greater than 15 cal/mole.

Test Results

Gas specimens were obtained using "grab" samples of the gas stream within the instrumentation chamber. Gas chromatography was subsequently used to determine gas composition. Some impurities such as air and water vapor in the apparatus are present in these samples. When the data are corrected for these impurities, the values obtained effectively become a measure of the molar ratios of H_2, CO_2, and [illegible]. These sample molar ratios must be the same as in the equilibrated [illegible] yielding:

$$m_{CO} + m_{CO_2} + m_{H_2O} + 1 = \frac{P}{P_{H_2}} \qquad (11)$$

where: m_i = the molar ratio of i relative to H_2
P = the total pressure

From the thermodynamic reaction (equation 2) and using P_i/P_{H_2} =

m_i,

$$\frac{m_{CO}}{m_{CO}} + \frac{m_{CO_2}}{m_{CO}} \exp\left[\frac{G_{Rxn}}{RT}\right] \cdot \frac{P}{P_{H_2}} \qquad (12)$$

This equation can then be solved for P_{H_2} and subsequently P_{H_2O}, P_{CO} and P_{CO_2}. Figures 5, 6, and 7 are plots of the results for each of three tests. Included with each set of results is the equilibrium temperature calculated for each sample. In all cases the calculated equilibrium values are within the range of debris bed temperatures at the time the samples were taken. The calculated values of P_{CO} / P_{CO_2} can be compared to values published by Darken and Curry (Ref 1) to determine the feasibility of the Fe_xO equilibrium. The results indicate that the formation is wustite in equilibrium with iron near the lower phase boundary. The consistency of the calculated quench temperature and composition results from the thermodynamic analysis for these data suggests that kinetic effects do not strongly influence the reaction. Apparently, equilibrium was reached by the gases passing through the debris bed.

The data from FRAG 3 provide the opportunity to study the effect that an overlying water pool has on the reaction. Two possible effects are considered; first, the availability of excess water could provide an additional source of hydrogen generation and second, the quenching of a portion of the debris causes a reduction in the hot pathway involved in the reaction. To determine the magnitude of these effects, the data of FRAG 3 are plotted in Figure 8 as a fraction of reduced gas species relative to total gas generation. Additional hydrogen developed by the water would cause the the H_2 plus CO fraction to increase immediately upon the addition of the water. The results are constant before and after the water addition suggesting that the added water is not being reduced.

Thermocouple records for FRAG 3 indicate that within ten minutes of initiation the water had penetrated to its maximum depth in the debris. Those portions of the debris in contact with the water (nominally the upper third of the bed) were quenched to approximately 100°C within the time period. For a kinetically controlled reaction between the debris and the evolved concrete gases the amount of time the gases are in contact with the debris will determine the extent of reaction. In particular, water added to the debris causes the hot pathway for the evolved water and carbon dioxide to be reduced by approximately one-third. Thus, for a constant gas velocity through the bed, the interaction time will also be reduced by a similar amount. However, Figure 8 shows the general trend of the data beyond the time water was added to be remarkably constant. The constancy suggests that the loss of bed height (reduction of reaction time) does not affect the extent of the reduction reaction. Therefore, the reaction must occur rapidly indicating the process is thermodynamically, not kinetically, controlled.

Thermodynamic analysis can be also used to determine the chemical reactions responsible for the flammable gas production. The approach

is to determine the ratio of hydrogen to carbon in the evolved gas for comparison to that obtained from the stoichiometry of the concrete. The ratio of hydrogen to carbon in the gas is defined as:

$$H_2/C = \frac{P_{H_2} + P_{H_2O}}{P_{CO} + P_{CO_2}} \quad (13)$$

where the partial pressures are determined from equation (12).

The pyrolysis of the basalt concrete composition given in Table 2 yields a molar H_2/C ratio of greater than 10. If the organic contaminants remaining from the casting process are included, this ratio is 5 or less. Stoichiometric limestone concrete composition yields a molar H_2/C ratio of 0.64 due to the large CO_2 concentration. If the free water were not included in this determination, the ratio would approach 0.29.

Figures 9 through 11 give the temperature-location results at various times for the three tests, FRAG 1, 2A and 3. These data are used to calculate isotherm velocities to determine the extent of reaction at each time interval. Only base thermocouple data are given, although similar plots for sidewall sensors are also used in the analysis. Because these processes are occuring over time scales of many minutes, smooth curves have been drawn on the figures to approximate the data points. The extent of reaction can be estimated by the depth of penetration for each of the three temperature ranges of interest and the amount of gas evolved from the stoichiometry of the concrete. This procedure is less certain for the basalt concrete due to the large influence caused by the presence of contaminants.

Isotherm velocities determined from the FRAG 1 temperature-location profiles show that the 120° C isotherm propagates at a velocity of 13 to 38 cm/hr. The 450°C and 800°C isotherms travel at correspondingly lower speeds, 4.3 ± 0.8 and 4.1 ± 0.5 cm/hr. Isotherm velocities can be related to the heat flux transmitted to the concrete. The thermal conductivity of the concrete is the highest early in the test, causing the velocity to be high. As the concrete dehydrates, less heat is transferred into the material and the isotherms are slower. The increase in the isotherm velocities at late times appears to be the result of improved heat transfer as the concrete melts and contacts the debris more intimately.

The relative velocities of the three isotherm indicate that the H_2/C ratio will be altered in favor of increased H_2. This means that in accident sequences, the gases will not be evolved in stoichiometric proportions. The basemat of a reactor plant is essentially infinite with respect to the interaction area. This behavior cannot be simulated in the FRAG test geometry due to the presence of finite boundaries, causing the water content to be depleted before the end of the test. Thus, when the 120° C isotherm reaches the outer surface of the crucible, the concrete is no longer behaving prototypically and the measured gas generation will underpredict the accident case. In addition, because the gases are not released in concrete stoichiometric proportions, predictive tools that evoke the concrete

stoichiometry for the evolved gases will underpredict gas production.

The thermodynamic analyses of the FRAG 1 data are consistent with the expected trend for basalt of greater H_2/C concentration. The effect of the organic contaminents for this test is unknown, and therefore, the correspondance of the H_2/C ratios to the stoichiometry of the concrete is uncertain. The data presented in Figure 9 show that almost all the free water is depleted within the first hour after starting the test. The bound-water loss occurs at a slower rate. Calculation of the H_2/C ratios from the isotherm profiles yields values ranging from 18 to 0.9, with the values decreasing with time. The initially higher values illustrate that the concrete rapidly loses the free and bound water in proportions well beyond the concrete stoichiometry. As the concrete becomes dehydrated the ratios approach stoichiometric, with the final ratios indicating water depletion. These results correspond relatively well with the ratios calculated from the gas samples, but the influence of the contaminents is not considered in the isotherm calculations. The gas samples, however, are sensitive to contamination and its effect would be manifested in the analysis. Figure 12 is a plot of the H_2/C ratios calculated by each method.

The gas analysis results of FRAG 2A for the period 441 to 585 minutes shows concentrations higher than expected from the concrete stoichiometry. The first sample (at 312 minutes) yields an H_2/C ratio similar to that expected for concrete without the free water contribution (0.29). The data indicate that the 120° C isotherm propagated to a depth of greater than 3 inches at the time the first sample was obtained (Figure 10). The depletion of free water should also be manifested in the period 441 to 661 minutes, but the ratios determined from the gas samples are abnormally high. The samples during this period may be influenced by contamination caused by foreign materials used to support the thermocouple assemblies. Ratios obtained from the concrete temperature profiles also indicate the loss of free water. The value determined at 600 minutes is inconsistent, possibly because of the moisture released during the decomposition of the thermocouple supports (located at a depth of 5 cm). The last point (660 minutes) occurs during the time when rapid movement of the debris was observed. The movement caused improved heat transfer at the debris/concrete interface, resulting in some distortion in the trend of the 800° C isotherm movement.

Calculation of the 450°C and 800° C isotherm velocities from the FRAG 2A data of Figure 10 yields values of 1.4 ± 0.3 cm/hr and 1.0 ± 0.1 cm/hr, respectively. These values are considerably less than those determined for FRAG 1, owing to the lower heating rate used in this test. At times later than 661 minutes, the calculated H_2/C ratios are reasonable, but may still be artifically high because of the added moisture contained in the foreign structures. As with FRAG 1, the evolution of gas suggests that the dehydration reaction is proceding into the concrete more rapidly than the decarboxylation reaction front.

The FRAG 3 results provide a study of the effect of added water on the gas generation mechanism. The H_2/C ratios shown in Figure 12

are consistent with the stoichiometry of the limestone-common sand concrete. For samples drawn between 494 and 647 minutes the observed ratios are close to the bound water/CO_2 pyrolysis ratio. This fact is supported by the temperature-depth plot (Figure 11) that indicates most of the free water is depleted by 360 minutes.

Figure 12 shows the calculated H_2/C ratios from the FRAG 3 gas samples. The results are fairly consistant at or below the bound water/CO_2 limit. Two data points (546 and 586 minutes) are significantly higher, possibly attributed to erosion of a water-rich area, the effect of contaminents, or the penetration of the water pool into a hot zone. The appreciable data shift demonstrates that the measurement technique is responsive to changes in hydrogen concentration. This sensitivity to increases in hydrogen production validates the previously stated assumption that the water addition did not cause large increases in the hydrogen generation. The large scatter in the early-time data is caused by the extended period of time (up to 325 minutes), in which water was heated within the cavity. During this time, the concrete was very nearly isothermal at 100° C on the surface, causing the propagation of the free water to be very inconsistent. The data do indicate, however, that the free water was probably depleted to a depth of 7.6 centimeters or more at times greater than 350 minutes.

The temperature profiles for FRAG 3 are not as consistent as previously observed for FRAG 1 & 2A. The inconsistency is particularly evident in the velocity of the 800° C isotherm. Calculated values range from 0.6 cm/hr to 2.5 cm/hr with no discernable trend.

Conclusions

The results of the FRAG test series show that flammable gas species are produced during the interaction of low-temperature fragmented debris and prototypic concretes. Thermodynamic analysis of the gas samples from these tests illustrates that the water and carbon dioxide released during the decomposition of the concrete are rapidly reduced to form hydrogen and carbon monoxide. The consistency of results obtained from the thermodynamic analysis suggests that the reaction processes are not kinetically controlled. Records from embedded thermocouple show that the loss of free water from the concrete occurs more rapidly than the loss of bound water or the decarboxylation reaction. This behavior indicates that the gases are not evolved in concrete stoichiometric proportions and at higher rates than those normally assumed in analytical models.

Analysis of the gas samples for all tests show that the reduction is not complete and that the gas stream has a large inert content. The influence of the inert components will affect detonation and flammability characteristics in accident situations. The calculated contribution of each gas species suggests that the gas/metal reaction is characteristic of wustite equilibria near the lower phase boundary.

The effect of an overlying water pool appears to be negligible in that the H_2/C ratio of the gas stream was not changed by enhanced

hydrogen production. The lack of gas sample compositional change with the decrease in the hot bed height caused by the water pool also indicates that the process is thermodynamic rather than kinetic.

References

1. Darken & Gurry "The System Iron-Oxygen I. The Wustite Field and Related Equilibria" Journal of American Chemical Society, Vol. 67, 1945.

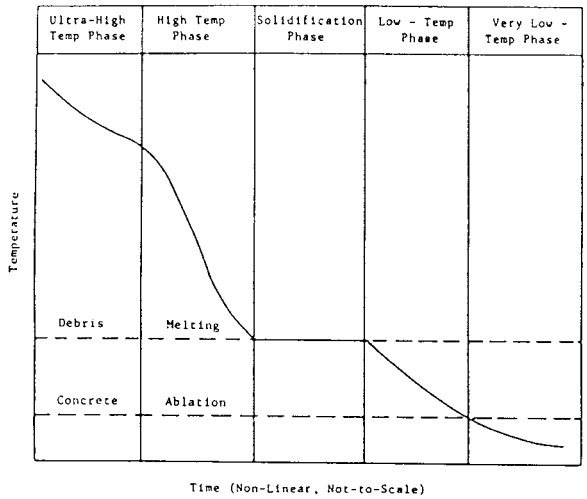


Fig. 1 - Hypothetical Temperature - Time History for Debris/Concrete Interactions

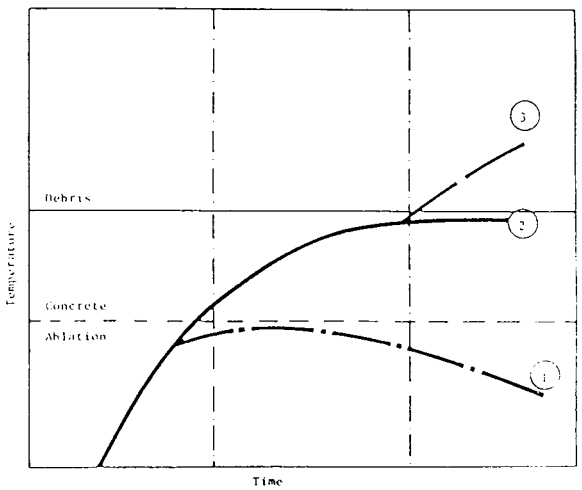


Fig. 2 - Debris Reheat Sequences

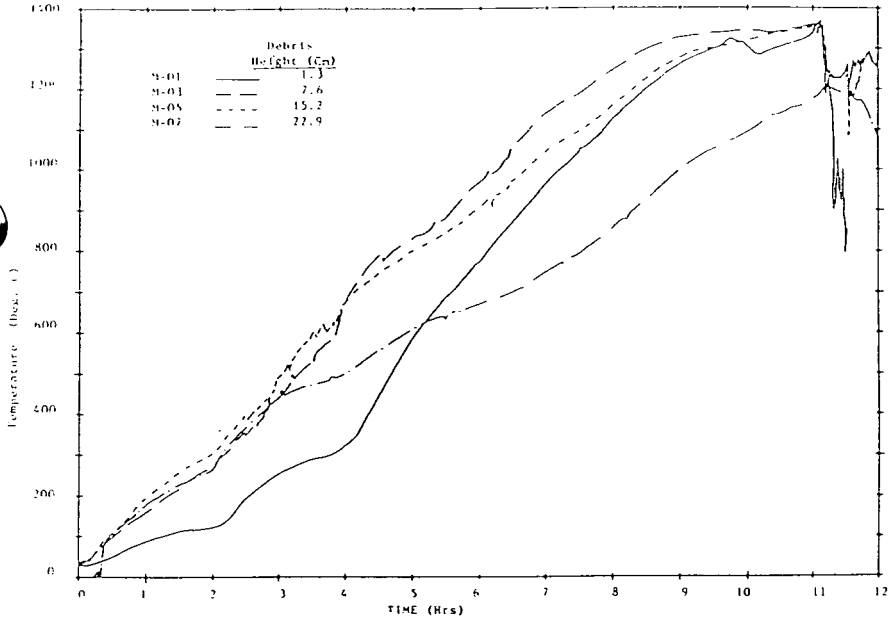


Fig. 3 - FRAG 2A Debris Temperature Histories

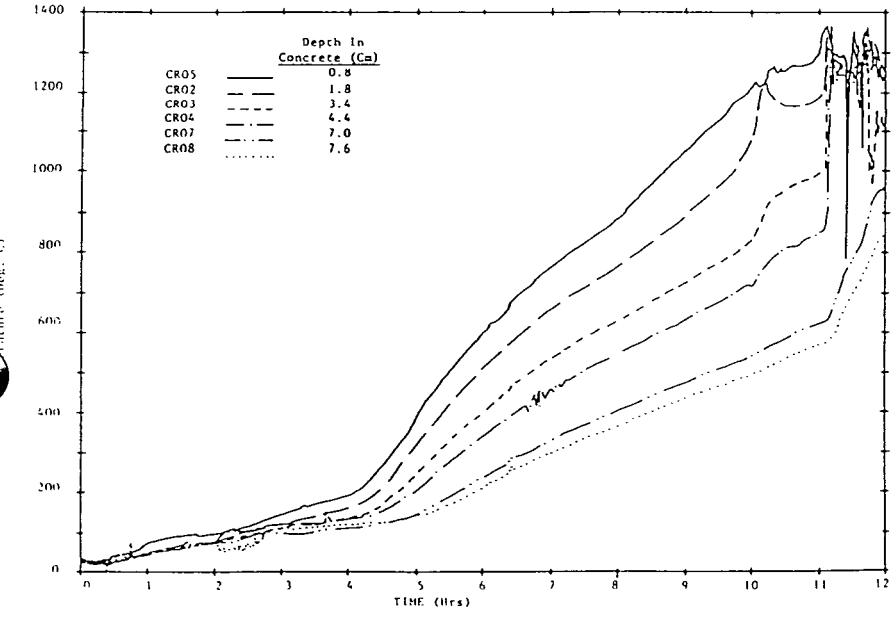


Fig. 4 - FRAG 2A Concrete Temperature - Time Histories

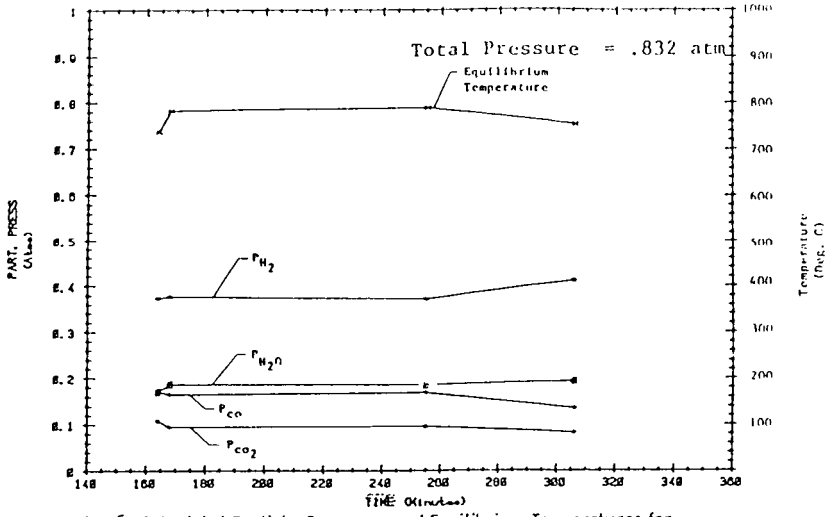


Fig. 5 Calculated Partial Pressures and Equilibrium Temperatures for FRAG 1 Gas Samples

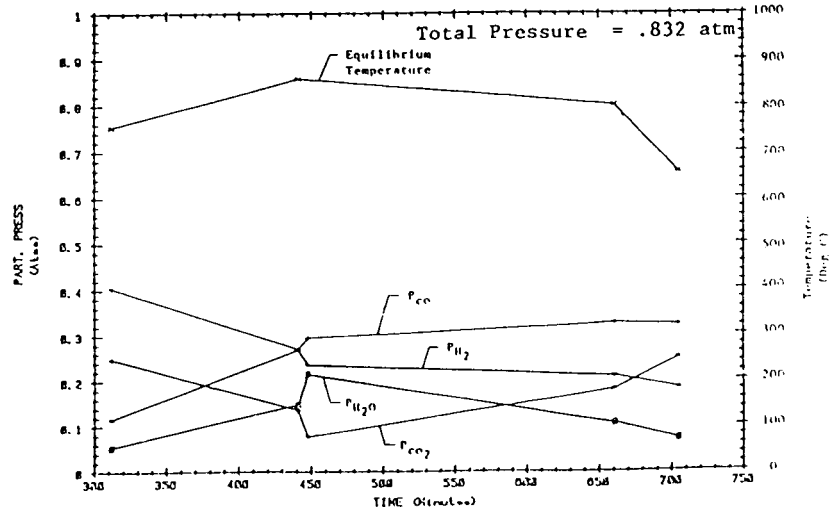


Fig. 6 Calculated Partial Pressures and Equilibrium Temperatures for FRAG 2A Gas Samples

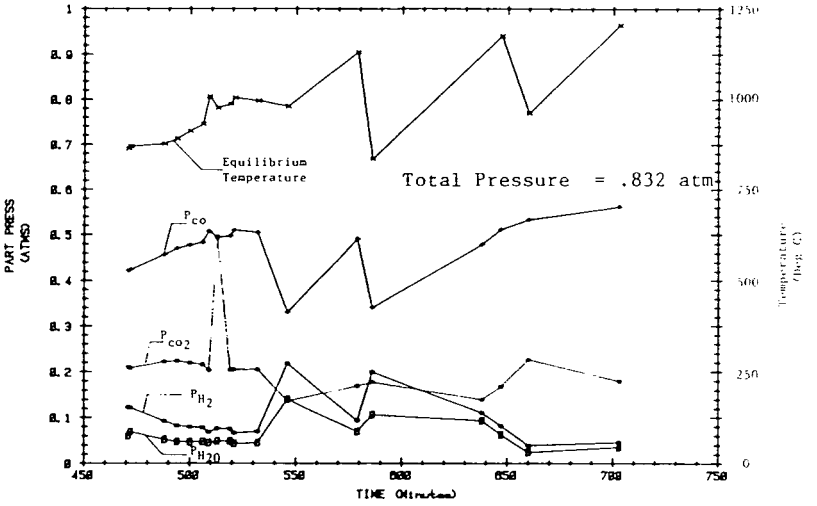


Fig. 7 Calculated Partial Pressures and Equilibrium Temperatures for FRAG 3 Gas Samples

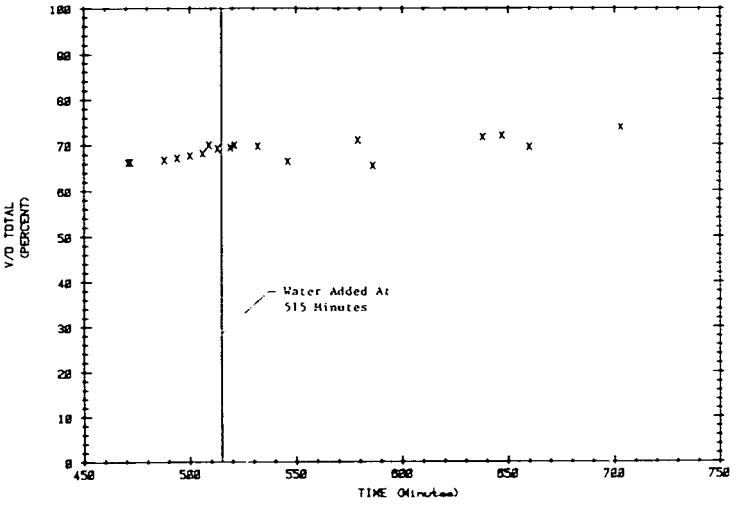


Fig. 8 FRAG 3 Volume Fraction of Flammable Gas Species

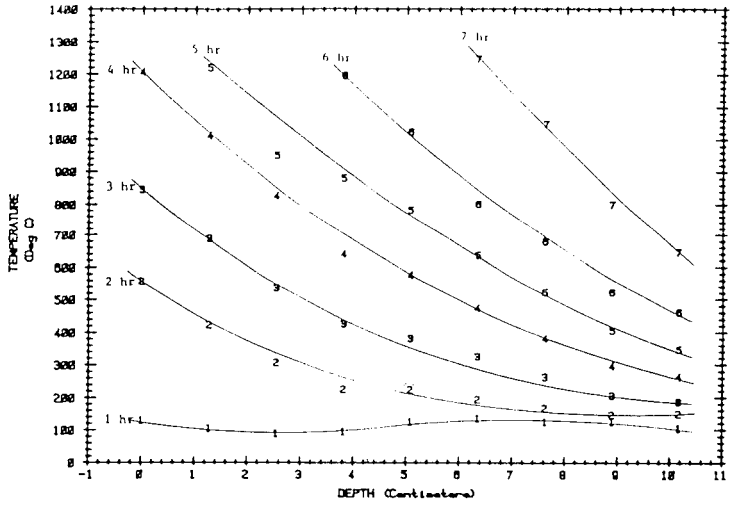


Fig. 9 FRAG 1 Concrete Temperature versus Depth for Various Times

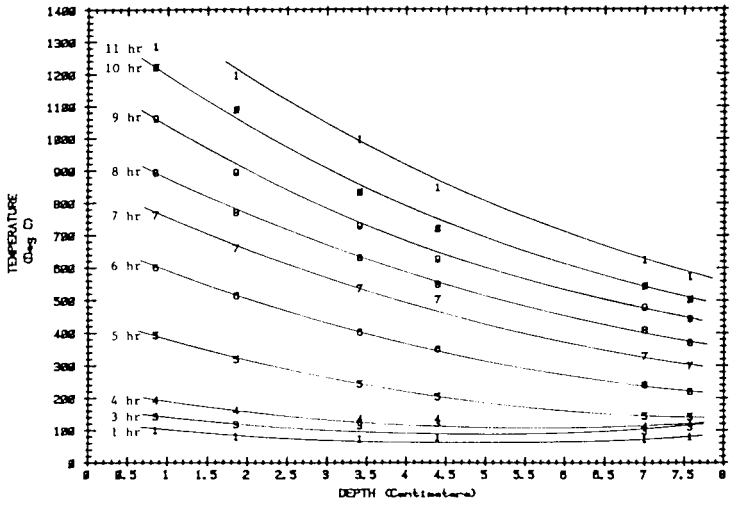


Fig. 10 FRAG 2A Concrete Temperature verses Depth for Various Times

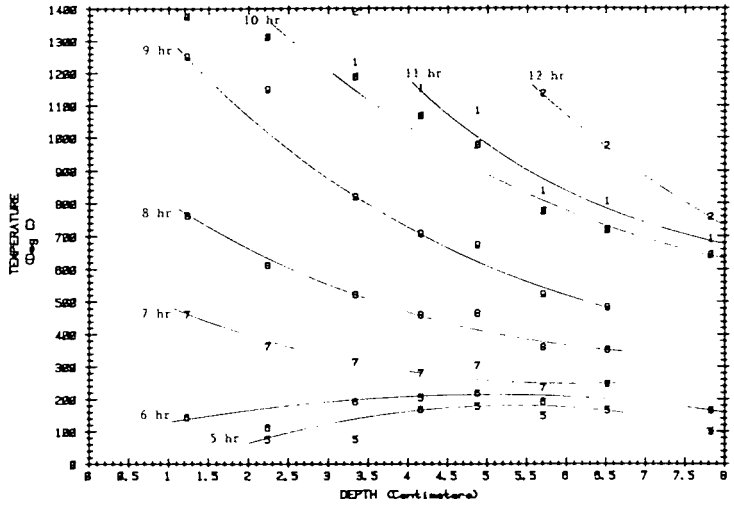


Fig. 11 FRAG 3 Concrete Temperature versus Depth for Various Times

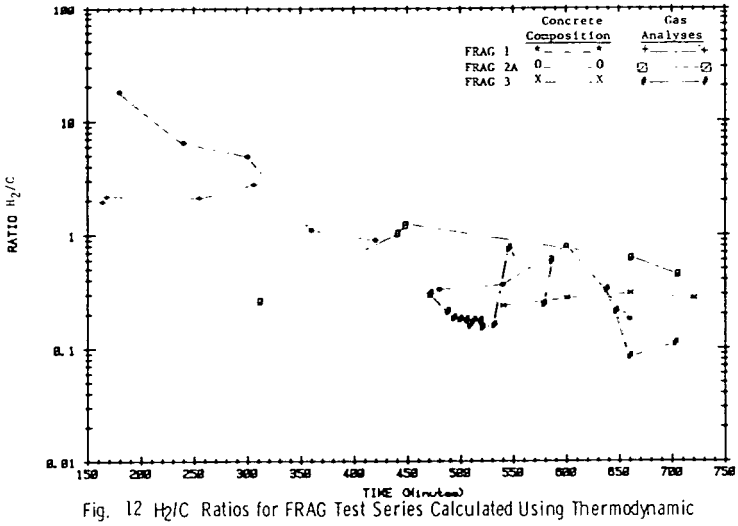


Fig. 12 H_2/C Ratios for FRAG Test Series Calculated Using Thermodynamic Gas Analyses and Concrete Temperature Profiles

TABLE 1
Fragmented Debris Test Description

Test Name	Concrete Type	Debris Size (mm)	Debris Quantity (kg)	Water In Cavity
FRAG 1	Basalt	3.4	44.5	No
FRAG 2A	Limestone-common sand	3.4	45.0	No
FRAG 3	Limestone - common sand	3.8	45.5	Yes
FRAG 4	Basalt	3.8	45.5	Yes

TABLE 2

Chemical Composition of Concretes (weight percent)

Species	Basalt	Limestone Common - Sand
Fe_2O_3	6.25	1.44
Cr_2O_3	ND	0.01
MnO	ND	0.03
TiO_2	1.05	0.18
K_2O	5.38	1.22
Na_2O	1.8	0.82
CaO	8.8	31.2
MgO	6.2	0.48
SiO_2	54.73	35.7
Al_2O_3	8.3	3.6
CO_2	1.5	22.0
H_2O	5.0	4.8
SO_2	<0.2	<0.2
Melting Temperature	1080 - 1380°C	1150 - 1400°C

HYDROGEN GENERATION DURING

MOLTEN-FUEL-COOLANT INTERACTIONS

Michael Corradini
Assistant Professor

Nuclear Engineering Department
University of Wisconsin-Madison

INTRODUCTION

Given the absence of adequate cooling water to the core of a light-water reactor (LWR), the fission product decay heat would eventually cause the reactor fuel and cladding to melt. This could lead to slumping of the molten core materials into the lower plenum of the reactor vessel, possibly followed by failure of the vessel wall and pouring of the molten materials into the reactor cavity. Recent analyses [1-5] have indicated that residual water is likely to be present both in the lower plenum and in the reactor cavity. Therefore, when the molten core materials enter either region, there is a strong probability of molten core contacting water. The physical process by which the molten core ('fuel') contacts and mixes with the water ('coolant') is important for two reasons--(1) because of its potential for rapid steam generation from a fuel-coolant interaction (FCI) either energetic (steam explosion) or non-energetic (steam spike), and (2) because it is a source of combustible hydrogen from the oxidation of the metallic components of the molten core (e.g. iron, chromium, zirconium).

In this paper the rate of hydrogen generation due to fuel-coolant mixing is the major topic. To predict this one must understand two physical processes. The first is the degree of fuel breakup during the mixing phase and during the FCI. By understanding this process one is able to calculate the surface area available during the chemical reaction. The second is the rate of hydrogen generation per unit area when the fuel is molten and as it cools and solidifies. Let us first review past work in this area.

Past research into fuel-coolant mixing (sometimes called 'premixing') has been directed at predicting the physical limits for which mixing could or could not occur. Fauske [6,7] originally proposed that the fuel-coolant interface temperature upon liquid-liquid contact must exceed the spontaneous nucleation temperature (approximately the homogeneous nucleation temperature) to allow premixing and an energetic FCI; the homogeneous nucleation temperature for water is 583K. The physical picture was that stable film boiling is established above this limit for a liquid-liquid system and this allows the fuel time to penetrate and mix with the coolant. For the LWR system, the fuel (UO_2, ZrO_2 steel) and coolant (water) easily satisfy this first criterion (interface temperature calculated to be well in excess of the water critical temperature, 647K). This criterion could be considered necessary but not sufficient.

Cho et al [8] proposed that beyond this criterion, consideration must be given to the energy used in fuel-coolant mixing that creates more surface area and overcomes frictional effects. He concluded that frictional effects dominate the mixing process and developed a simple model to estimate the minimum required energy, E_m, for progressive mixing of the fuel and coolant.

$$E_m = 1.81\ \rho_m\ V_f \left(\frac{V_f^{2/3}}{t_b^2}\right) \left(1 - \frac{D_{FR}^2}{4V_f^{2/3}}\right) \ln\left(\frac{2V_f^{1/3}}{D_{FR}}\right) \qquad (1)$$

where v_f is the initial fuel volume, ρ_m is the density of the coolant (it could be a two-phase mixture), t_b is breakup and mixing time for

the fuel to reach a diameter, D_{FR}. Using this approximate model the energy required for fuel-coolant mixing can be calculated and compared to that available as thermal energy in the fuel, Efth. If E_m is substantially less than Efth, then it indicates that mixing is possible from an energy standpoint.

Recently, Fauske and Henry [9,10] have proposed a simple model to predict the minimum fuel diameter possible during fuel-coolant mixing. They base this model on the physical concept that the fuel can breakup and premix with the water to a uniform size no smaller than that which prevent liquid water from entering the zone; i.e. the fuel surface area increases (diameter decreases) to such a degree that steam outflow stops liquid inflow. To determine this minimum diameter, DMIN, they equated the energy transferred from fuel to coolant in the mixture to be critical heat flux in pool boiling (q''_{CHF}) multiplied by the cross-sectional area of the coolant. The critical heat flux was viewed as an approximate hydrodynamic limit for steam outflor and water inflow (one-dimensional, counterflow, steady state). The minimum diameter is given by

$$D_{MIN} = \frac{6 m_f q''_{DROP}}{\rho_f A_c q''_{CHF}} \tag{2}$$

$$\text{where } q''_{DROP} = \sigma_r (T_f^4 - T_c^4) + h_{film} (T_f - T_c) \tag{3}$$

and m_f is the fuel mass, ρ_f, the fuel density, q''_{DROP} the heat flux per drop, A_c, the coolant cross-sectional area, T, the temperature (f - fuel c - coolant), σ_r, the Stephan-Boltzman Constant, and h_{film}, the film boiling heat transfer coefficient.

Again this model can be viewed as an approximate physical limit. In fact, this physical model is geometrically approximate in two respects: it assumed that the critical limit is reached neglect system dynamics and it assumes that a counterflow of water and steam occurs neglecting the possibility of steam outflow from one surface and water inflow from another surface (multi-dimensional effects). These ommissions cause the model to neglect two possibly important effects: (1) time is not considered relative to that allowed due to geometry characteristics; such as coolant depth or width; (2) mixing is not a discrete process which occurs regardless of time, rather it is a dynamic process always occurring allowing the fuel to fragment to smaller and smaller sizes. These omissions may prompt one to seek strict limits to mixing which are time independent; rather the physics seem to suggest such limits are highly time dependent.

During the FCI, the rate of fragmentation and the final debris size is empirically known from small intermediate scale experiments [11]. These experiments indicate that the fuel fragments quickly (~100-300 μsec) to small sizes (from 1-10 mm to 50-150 μm). Knowing the empirical debris size distribution one can calculate the available surface area.

Knowing the surface area, one then needs information on the chemical kinetics of hydrogen generation by steam oxidation of metallic materials (Zr, stainless steel) or with oxide materials that are not fully oxidized (U-O-Zr) in the molten as well as a solid state. The kinetic rate of

oxidation and hydrogen generation is a function of three important variables; the temperature of the fuel surface at which oxidation is occurring, the rate of diffusion of the vapor to the fuel surface, and the rate of diffusion of the oxygen into the fuel bulk phase.

For oxidation of solids, zirconium and stainless steel at high temperatures have been investigated early in reactor safety research (for example see References 12-15). In an environment of excess steam, diffusion through the solid surface and the oxide film which accumulates controls the rate of oxidation; the kinetic rate can be described in terms of parabolic (zirconium) or a linear rate law (steel). For example, Cathcart and Pawel determined the parabolic rate law for zirconium to be

$$W_{H_2} = 0.00044 \sqrt{t\ K(T)} \quad [kg/m^2] \tag{4}$$

where

$$K(T) = 3(10^6)\ \exp\ (-39940/1.987\ T\ (K)) \tag{5}$$

If the amount of steam is limited, then the rate of hydrogen generation could be controlled by the rate of steam diffusion to the fuel surface. This rate depends on the diffusion coefficient and the pressure and temperature of the steam.

Currently there is no experimental data available for the kinetic rate of reaction for molten metallic materials (zirconium or stainless steel). It is expected that diffusion through the molten phase could also control the oxidation rate given sufficient steam. Baker [12] approximated the molten zirconium kinetic rate (just above melting) by assuming that steam diffusion to the surface was the limiting process.

In this paper we analyze the mixing data from current FCI experiments [11,16] to determine a model for fuel-coolant mixing and then deduce the rate of hydrogen generation for these experiments.

FUEL-COOLANT INTERACTIONS

During a severe accident, fuel-coolant contact may occur in one of two ways; the fuel may pour into a water filled cavity by gravity (or under pressure), or the water may reflood a cavity containing molten fuel. In the former case the fuel falls through the coolant and mixes with it. In the latter case the fuel is stratified with the coolant on top, and a slow quenching is the most likely result. In regard to hydrogen production from fuel-coolant contact the former circumstance is of more interest.

This pouring contact mode was used extensively in FCI tests at Sandia [11,16]. In these tests the hot fuel enters the water pool in film boiling and begins to distort in shape. As it continues to fall through the pool it breaks apart into smaller pieces and mixes with the surrounding water while still in film boiling. These smaller pieces may subdivide further as the steam produced in film boiling flows out through the top of the fuel-coolant mixture and escapes the pool as water

flows in from the sides. This mixture grows radially as the fuel, now mixed with water and steam, continues to fall through the pool finally reaching the chamber base (Figure 1). At or near base contact two possible events can occur, an energetic FCI (steam explosion) is triggered or the 'premixed' molten fuel settles on the chamber base and eventually quenches. During this transient fall phase of the fuel through the water pool one reason for fuel breakup is inertial forces generated by the fuel relative velocity, v_f, and differences in density (ρ_f to ρ_c) [17-19]. If the fuel mass is large (characteristic diameter, D_f, large) or its relative velocity high, its characteristic Weber number, We, (ratio of destabilizing inertial force, $\rho_c v_f^2$, to stabilizing surface tension force, σ/D_f) will be greater than a critical value (We_{crit} = 7-12 for relatively inviscid fluids [19]). The fuel will begin to distort and break apart.

One could develop an empirical model for this mixing phenomena, if the assumption is made that hydrodynamic forces are the major cause of fuel-coolant mixing as in the case of isothermal experiments [17-19]. The major difference in these FCI experiments is that film boiling separates the two liquids; one might presume that the film acts like a low impedance fluid which delays the fuel breakup relative to the isothermal case. The Sandia data can be plotted in dimensionless form. The dependent variables would be the depth of the fuel-coolant mixture, H_m, the lateral dispersion diameter of the fuel-coolant mixture, D_m, the mixture volume, V_m, the displaced water volume V_D (i.e. the fuel and steam volume in the mixture), and the average fuel diameter during mixing, D_{FR}. The independent variables are the fuel mass, m_f, its diameter, D_f, initial entry velocity, v_f, properties and time, t. To nondimensionalize these variables one can use the fuel diameter, the velocity and properties, the resulting groups are H_m/D_f, D_m/D_f, V_D/V_f, V_m/V_f, D_{FR}/D_f, T^+ and We where the independent groups are defined as for example

$$V_f \equiv \pi D_f^3/6 \tag{6}$$

$$T^+ \equiv \frac{t\, v_f}{D_f}\left(\frac{\rho_c}{\rho_f}\right)^{1/2} \tag{7}$$

$$We \equiv \frac{\rho_c\, V_f^2\, D_f}{\sigma_f} \tag{8}$$

In the Sandia FITS experiments (fully instrumented test series), a wide range of conditions were investigated with iron-alumina and Corium fuel; $1 < m_f < 20$ kg, $3.5 < \rho_f/\rho_c < 7$, $4 < v_f < 8$ m/s, $30 < m_c < 250$ kg, $0 < T^+ < 6$, $2000 < We < 8000$. The variation in coolant mass in these tests primarily effected the coolant water depth, H_c (thereby T^+); the width of water cavity, W_c was always large compared to the fuel diameter. Further tests should specifically investigate these parameters.

When the mixing data are plotted in dimensionless form (Figures 2-4), one can make a few observations. First, the data from various experiments follow similar trends and are not subject to a large amount of scatter. Subsequent experiments might be performed at larger scales to determine if these dimensionless groups can still successfully correlate the data. In particular, the fuel fragment diameter, the mixture volume, and displaced water volume are important since they determine the fuel surface area and the average volume fraction of fuel and steam. Knowing these quantities aid predicting hydrogen generation. Second, no effect of the fuel Weber number was observed. This may be partially due to the small range over which it varied. Finally, if one compares the trends of H/D_f and D/D_f for this FITS data with previous data from isothermal tests, it is obvious that the rate of growth of the fuel-coolant mixture in FITS is slower than for isothermal tests. This seems to confirm the notion that the steam generated in these tests adds compliance to the fuel-coolant system and slows fuel-coolant mixing for a given time span.

The data for the observed fuel fragment size, D_{FR}/D_f, are not plotted, but tabulated in Table 1. This is because the visual data could only be obtained at the end of the test near base contact when the fuel-coolant mixture was large and the fuel droplets could be individually measured. It is recognized that visual measurement is prone to some error, therefore, these data should be considered preliminary. The diameter measured is probably larger than the actual diameter due to the luminous image the drop creates on the film; the post-test debris data bear this observation out for two FITS experiments (FITS-1A and 4A).

The previous correlation of test data applies as the fuel falls through the coolant. If coolant chamber is narrow or its depth shallow mixing during the fall phase would be impeded or stopped. Likewise, if the steam generation rate becomes too large, causing the fuel (or coolant) to be rapidly carried out (fluidized) of the mixture then the fuel-coolant mixing would be limited. It is important that one identifies these physical limits to mixing because they represent the bounds that would be set on this dynamic mixing process.

The effect of the physical boundaries is qualitatively obvious, although not quantitatively known. Base contact would most likely trigger an energetic FCI (steam explosion) as the FITS data indicates. If not, the fuel would settle on the chamber base. In the tests it would slowly quench; however, in the accident the decay heat power combined with the fuel molten state may cause prolonged thermal attack of the solid base.

Limits on fuel-coolant mixing due to steam generation could cause the fuel (or coolant) to be carried away with the steam flow. One would expect the mixing process to be self-limiting; i.e. given sufficient time, the fuel would mix and break up to an average size no smaller than that which would cause the liquids to be fluidized and swept away. The fuel droplet distribution and the average diameter, D_{FR}, may be larger than this limit if time is short (due to a small water depth or a triggered explosion). In addition, because the fuel enters the water in a pouring mode of contact, the mass first to reach the coolant chamber bottom would be better mixed than fuel at the top of the water pool. Therefore, if one were to identify this limit on mixing it would represent the minimum average fuel diameter to which all the fuel falling through the coolant could fragment before the mixture would begin to be swept away.

To find this minimum fuel diameter, D_{FR_l} for the case of fluidization one of the fuel droplets, one would equate the velocity needed to fluidize a particle, v_{FL} to the steam velocity, v_v, at any location in the fuel-coolant mixture caused by fuel-coolant heat transfer. Based on a steady state momentum balance the fluidization velocity is given by

$$v_{FL} = \left[\frac{4}{3} \frac{D_{FR_l} g}{C_D} \rho_{f/\rho_v} \right]^{1/2} \tag{9}$$

where ρ_v is the steam density, g is the gravitational acceleration, and C_D is the drag coefficient, corrected for the effect of an array of droplets [20,21] ($C_D \sim 1.5$). Now the steam velocity cannot exceed this value or else the fuel droplets will be swept away. This would first occur at the top of the mixture where all the steam from the whole mixing zone exits to maintain equal pressure with the ambient. Let us consider the steam velocity at the top of the mixture, realizing that the fuel droplet diameter determined from this simple analysis would signal the beginning of the fuel sweep out. Actually the average fuel diameter in a test could fall slightly below this limit before a majority of the fuel begins to be swept away. The steam velocity at the top of the pool is found by an energy balance to be

$$v_{v_{TOP}} = \frac{\dot{m}_{v_{TOP}}}{\rho_v A_m \alpha_v} \tag{10}$$

where A_m is the area of the mixture, α_v the steam volume fraction of the mixture, and

$$\dot{m}_{v_{TOP}} = \frac{6\alpha_f V_m q''_{drop}}{D_{FRAG_f} i_{fg}} \tag{11}$$

where α_f is fuel volume fraction, i_{fg} the coolant latent heat, and

$$q''_{DROP} = \sigma_r (T_f^4 - T_{sat_c}^4) + h_{film}(T_f - T_{sat_c}) \tag{12}$$

where σ_r is Boltzman's constant, h_{film} is the film boiling heat transfer coefficient, and T is the temperature. Notice that all the enegy transferred from the fuel to the coolant was assumed to go into producing steam primarily by blackbody radiation. These assumptions neglect subcooling of the coolant and the reduction of the radiation view factor due to properties and radiation to other fuel particles. Although one may consider these second order effects both would reduce the predicted minimum mixing diameter. When all of these terms are substituted back into equ. 10 the result is

$$v_{v_{TOP}} = \left(\frac{\alpha_f}{\alpha_v}\right) \left(\frac{6 q''_{DROP}}{\rho_v i_{fg}}\right) \left(\frac{H_M}{D_{FR_l}}\right) \tag{13}$$

where H_M is the mixture height. When the two velocities are equated one gets for the average minimum diameter

$$D_{FR_I} = \left(\frac{3}{4}\right)^{1/3} \left(\frac{\alpha_f}{\alpha_v}\right)^{2/3} \left(\frac{6q''_{DROP}}{\rho_v i_{fg}}\right)^{2/3} \left(\frac{C_D H_M^2}{g}\right)^{1/3} \left(\frac{\rho_v}{\rho_f}\right)^{1/3} \qquad (14)$$

Remember that all the assumptions used to derive this simplified mixing diameter limit predict the threshold for fuel sweep out from the top of the mixture. Average fuel sizes could fall slightly below this limit before a major fraction of the fuel would begin to be fluidized. For example, if one equated these velocities near the bottom of the mixture (e.g. the lower third of V_m) to assure a majority of the fuel would be swept out the predicted D_{FR_I} would decrease by a factor of two. Also realize that this is a quasi-steady limit and applied only insofar as one knows the mixing zone conditions (i.e. volume fractions in mixing zone - Fig. 3) at any point in time. The empirical correlations developed from FITS tests that were just presented would give one the initial conditions needed to use this model.

Notice that this physical limit is different from the model proposed by Henry [9,10]. In this model, the physical picture is that the steam flows out the top of the fuel-coolant mixture, water flows in from the bottom and sides, and the fuel falls and disperses radially. A counter-flow hydrodynamic criteria is not the limitation here, rather it is liquid fluidization. This picture is more in line with the debris bed sweepout concepts put forth by Rivard [22].

To find this minimum fuel diameter for the case of fluidization of the coolant which enters the mixing zone, $D_{FR_{II}}$, one would perform the same analysis as before except the fluidization velocity is based on the coolant length scale, D_c.

$$v_{FL} = \left[\frac{4}{3} \frac{D_c\, g\, \rho_c/\rho_v}{C_D}\right]^{1/2} \qquad (15)$$

A reasonable assumption is that the ratio of the coolant volume surrounding a fuel droplet to the fuel drop volume is proportional to the ratio of the total coolant volume to the fuel volume in the mixing zone

$$\frac{D_c^3}{D_{FR_{II}}^3} = \frac{\alpha_c V_M}{\alpha_f V_M} \qquad (16)$$

where α_c is the coolant volume fraction in the mixture. This gives a relation between D_c and $D_{FR_{II}}$.

$$D_c = D_{FR_{II}} \left(\alpha_c/\alpha_f\right)^{1/3} \qquad (17)$$

This result in combination with equs. 9 and 13 gives an estimate of $D_{FR_{II}}$

$$D_{FR_{II}} = \left(\frac{3}{4}\right)^{1/3} \left(\frac{\alpha_f}{\alpha_c}\right)^{1/9} \left(\frac{\alpha_f}{\alpha_v}\right)^{2/3} \left(\frac{6q''_{DROP}}{\rho_v i_{fg}}\right)^{2/3} \left(\frac{C_D H_M^2}{g}\right)^{1/3} \left(\frac{\rho_v}{\rho_c}\right)^{1/3} \qquad (18)$$

The same comments concerning D_{FR_I} are applicable here; the volume fractions of fuel and steam are needed from the experiments (Fig. 4) to employ this model.

A prediction of the minimum fuel mixing diameter due to fluidization can be made using equs. 14 and 18. These calculations could be compared to the actual data of D_{FR} (Table 1) to determine if the model is in agreement with the observed data. The results of the calculation are presented on Table 2, and the agreement between the model and the data is good. Also included in the table are the predictions one would obtain using the model proposed by Henry (equ. 2). The agreement between the proposed mixing limit and the data also suggests that the fall time was sufficiently long enough ($2.5 < T^+ < 4$) to allow the fuel to break apart to a small diameter. One could use this criteria of dimensionless time to predict the mixing time and minimum diameter for larger scale FCI events.

Note that in all the tests the fuel mass was a mixture of an oxidic phase (UO_2 - ZrO_2 or Al_2O_3) and a metallic phase (stainless steel or iron). In the calculation, it was assumed that the heterogeneous mixture behaved as a homogeneous fuel with average mixture properties. This is a reasonable first approximation based on the data [11,16] indicating that post-test debris was compositionally homogeneous for different fuel debris diameters.

In the event that a spontaneous trigger is present as the fuel and coolant mix a steam explosion would occur. The individual fuel droplets would then be rapidly fragmented down to even smaller sizes as the fuel is quenched. Even for this physical process the metallic fuel can produce hydrogen as it cools down and solidifies. The amount of surface area generated by this process depends on the efficiency of the explosion. In the single droplet experiments of Nelson [11] the explosion conversion ratio was 1-2% and the fuel was fragmented in 100-300 μs down to mass average fuel debris diameters of 100-200 μm. From separate droplet breakup tests it is known that complete drop breakup occurs in a time of $3 < T^+ < 6$; this implies that Nelson's single droplets were subjected to hydrodynamic forces with Weber numbers on the order of 10^4 to 10^5. One can use this empirical information to estimate the fuel surface area during this explosion process. Currently there are no accepted models for the fuel fragmentation mechanism during a steam explosion; therefore, only estimates based on empirical data can be made.

HYDROGEN GENERATION

Now that one can estimate the fuel surface area, the next step is to predict the rate of oxidation of the fuel. As stated previously, there are no correlations for the kinetic rate of hydrogen production when the fuel is molten.

To model this phase of hydrogen production one could assume that the rate of steam diffusion to the molten surface controls the oxidation process [12]. This assumption is a reasonable approximation. The molten drop, if metallic or not fully oxidized, would initially have a very steep oxygen concentration gradient in the liquid phase; this steep oxygen gradient would allow for rapid oxidation of the fuel in a very short time. The hydrogen released from the fuel surface would then become a noncondensible gas layer around the fuel drop through which steam must diffuse to react even more of the fuel metallic constituents. The actual mass

transfer problem is, like the FCI phenomena, transient and quite complex. However, if one again assumes quasi-steady-state behavior then a simple model can be derived for the rate of hydrogen generation [23].

To model this mass transfer problem for fuel-coolant mxing, one first needs to know the time during which the fuel surface is molten. If the heat flux from the droplet is given by equ. 12, then the overall heat transfer coefficient can be calculated

$$h_{TOT} \equiv \frac{q''_{DROP}}{(T_f - T_{sat_c})} \tag{19}$$

Using this value for h_{TOT} one can estimate the time for the fuel surface to cool from its initial temperature to its melting temperature by using the transient conduction graph for a sphere [23]. For example, for the FITS test MD-8, the time for the surface to reach the melting temperature, Δt_m, was 1-2 sec. This is well in excess of the mixing time ($\sim$0.2 sec) and indicates that hydrogen generation during mixing for the FITS tests occurs while the fuel is molten. If this was not the case, for times greater than Δt_m the fuel oxidation would be controlled by solid surface oxidation (e.g. equ. 4).

If the steam diffusion through the hydrogen layer to the fuel droplet surface is considered to be a steady-state process then the governning mass transfer equation [23] can be written in spherical coordinates as

$$\frac{dN_{H_2}}{dt} = - 4\pi r^2 \frac{D_o}{R_o T} \frac{dp_{H_2}}{dr} \tag{20}$$

where p is the hydrogen partial pressure, $^{dN}/_{dt}$ is the rate of hydrogen generation, D_o is the diffusion coefficient and R_0 is the gas constant. This expression can be integrated over the radius to the coolant interface giving

$$\frac{dN_{H_2}}{dt} = \frac{4\pi D_o \Delta P_{H_2}}{R_o T_v} \left(\frac{1}{R_{FR}} - \frac{1}{R_c} \right)^{-1} \tag{21}$$

Now if one knows the radial distance to the coolant interface, R_c, then the hydrogen generation rate for a fuel droplet can be calculated. Based on single droplet FCI tests [11] the vapor film thickness is on the order of 1 mm.

Using the simple model just derived one can estimate the maximum amount of hydrogen generated during the fuel-coolant mixing for the FITS experiments. The total generation rate is found by multiplying the rate for one droplet by the total number of droplets at the minimum mixing diameter. The metallic fuel droplet will cool down as it falls in the fuel-coolant mixture; the rate of cooldown will be slow because the oxidation reaction is exothermic and this tends to keep the metallic fuel temperature high. An energy balance on the fuel droplet gives

$$\rho_f c_f \left(\frac{\pi D_{FR}^3}{6} \right) \frac{dT_f}{dt} = - q''_{DROP} \pi D_{FR}^2 + \frac{dN_{H_2}}{dt} i_{ox} \tag{22}$$

where i_{ox} is the energy released due to the reaction per mole of hydrogen produced. The fuel is modelled as a lump because the characteristic Biot number is small (< 0.16). The total amount of hydrogen generated during the fall time to base contact can now be calculated by numerically integrating the previous equations. These calculations were done for the FITS experiments where the metallic phase was iron and stainless steel. The results of the calculation are also given in Table 2. It is interesting to note that during the fall phase the cooldown of the metallic fuel droplets is small ($\Delta T \sim 100K$). This suggests that a constant temperature calculation is a good first approximation. These FITS tests did not measure the amount of hydrogen generated; this is planned in future tests.

Notice that the predicted amount of hydrogen generated is on the order of a few moles. This suggests that only a few moles of the metallic phase interacted with the steam during the mixing phase. This represents about 5-10% of the metallic molten mass (iron or stainless steel). More of the metallic phase would react with the steam after the molten fuel has settled on the chamber bottom; however, in the absence of a steam explosion this additional oxidation would be small, because the exposed surface area would decrease markedly.

To estimate the amount of hydrogen generated during the steam explosion process one could consider the isolated case of a single molten metallic fuel droplet undergoing a steam explosion [11] and estimate the percentage of metallic fuel (Fe) reacted. In this case the same governing equations are relevant but the length scale and pressure for diffusion of the steam to the surface is time dependent. If one assumes an average length scale of the fuel debris radius ($\sim$100 μm) and an average pressure in the bubble of 10 MPa (based on dynamic analysis) the calculation indicates that at most a few percent of the metallic phase would interact during the steam explosion to produce hydrogen. This result is strongly dependent on the fuel debris diameter ($m_{H_2} \sim D_{FR}^{-2}$) and, therefore, is only an indication of the order of magnitude of the hydrogen produced for an energetic steam explosion.

IMPLICATIONS FOR REACTOR SAFETY

In the event of a severe accident in a LWR, the molten material could pour into water in-vessel and/or ex-vessel. In either case hydrogen could be generated. To estimate the amount of hydrogen generated one could use the models developed in this paper. In this case one would seek to find the maximum single molten fuel mass that could mix with the water and break up to its minimum diameter before reaching the bottom of the coolant chamber. Once the bottom surface is reached a steam explosion may result, quenching the molten fuel, or the fuel would settle and stratify on the chamber bottom. Based on the FITS data the molten fuel mixed with the water with a diameter near the predicted minimum diameter when $2 < T^+ < 4$. The time for the fuel to penetrate the coolant depth is given by Fig. 1 to be

$$t_c \sim 1.6 \, {}^{H_c}/_{v_f} \tag{23}$$

If one now substitutes this into the equation for T^+ and solves for the maximum molten fuel diameter, the result is

$$D_{f_{MAX}} \sim {}^{H_c}/_{1.2T^+} \tag{24}$$

The associated minimum mixing size is given by equs. 14 and 18 for $H_m = H_c$ and for values of α_f and α_v gotten from Figure 4.

Using the same calculational procedure as that for the FITS tests the initial molten fuel diameter, mass (sphere), mixing diameter and amount of hydrogen generated can be found as a function of the dimensionless time for mixing and the coolant depth. Table 3 gives some sample results for $2 \leq T^+ \leq 4$ and for coolant depths appropriate to full scale conditions. Separate calculations indicate that the cooldown of the fuel during the fall through the water is again small ($\Delta T < 100K$), and therefore, the fuel temperature was considered to be constant. The major influence is the amount of fuel surface area available due to mixing. The most important point to emphasize is that amount of hydrogen generated is a few percent of the metallic fuel mass (2-5%). This indicates how as the scale increases the amount of hydrogen generated decreases. This should be expected because the oxidation is a surface reaction and the surface to volume ratio decreases as the scale increases.

CONCLUSION

The current FCI experiments conducted by Sandia are analyzed to determine the fuel-coolant mixing behavior as a function of the independent variables. The results are correlated in terms of dimensionless groups. Using this data to determine volume fractions of fuel and steam in the mixing zone, a mixing model is derived which predicts the minimum average fuel diameter that can mix with water before fluidization occurs and limits the mixing process. The model is in reasonable agreement with available data.

Using this model to determine the available surface area, the rate of hydrogen generated during fuel-coolant mixing is determined assuming steam diffusion limits the rate of reaction at the fuel surface. The results indicate that a few moles of hydrogen are produced accounting for an oxidation of 5-10% of the metallic fuel. Also it is found that the fuel does not cool down substantially during its mixing with water because the fuel oxidation reaction is exothermic enough to keep the fuel temperature high.

When this modelling is employed to predict behavior at full scale accident conditions, the calculations indicate only a few percent (2-5%) of the metallic fuel is oxidized during the fuel-coolant mixing process. This result is considered to be important, because it suggests that fuel-coolant mixing in the absence of a steam explosion may not generate substantial quantities of hydrogen.

REFERENCES

(1) L.D. Buxton, Molten Core-Water Contact Analysis, SAND77-1842, Sandia National Laboratories (1979).

(2) W.B. Murfin, Editor, Report of the Zion/Indian Point Study: Volume I, SAND80-0617/1, NUREG/CR-1410, Sandia National Laboratories (1980).

(3) J.F. Meyer et al, Preliminary Assessment of Core Melt Accidents at the Zion and Indian Point Nuclear Power Plants and Strategies for Mitigating Their Effects, NUREG-0850, Vol. 1, USNRC Report (1981).

(4) G. Klopp et al., Zion Probabilistic Safety Study, Commonwealth Edison Co. (1981).

(5) R.E. Henry et al., "Establishment of a Permanently Coolable State," Trans. Am. Nucl. Soc., 39, 368 (1981).

(6) H.K. Fauske, "Some Aspects of Liquid-Liquid Heat Transfer and Explosive Boiling," Proc. Fast Reac. Safety Mtg., Beverly Hills, CA (1974).

(7) R.E. Henry, H.K. Fauske, "Nucleation Characterstics in Physical Explosions," Proc. of Third Spec. Mtg. on Sod. Fuel Int. in Fast Reac., Tokyo, Japan (1976).

(8) D.H. Cho et al., "Mixing Considerations for Large-Mass, Energetic Fuel-Coolant Interactions," Proc. ANS/ENS Fast Reac. Safety Mtg., Chicago, IL (1976) CONF-761001.

(9) R.E. Henry, H.K. Fauske, "Core Melt Progression and the Attainment of a Permanently Coolable State," Proc. of Ther. Reac. Fuels Mtg., Sun Valley, ID (1981).

(10) R.E. Henry, H.K. Fauske, "Required Initial Conditions for Energetic Steam Explosions," Fuel-Coolant Interactions, ASME HTD-V19, Wash. D.C. (1981).

(11) M. Berman, Light Water Reactor Safety Quarterly, Sandia National Laboratories, SAND80-1304; Jan.-March, 1 of 4 (1980), April-June, 2 of 4 (1980), July-Sept., 3 of 4 (1981), Oct.-Dec., 4 of 4 (1981).

(12) L. Baker, L.C. Just, Studies of Metal-Water Reactions at High Temperatures, III Experimental and Theoretical Studies of the Zirconium-Water Reaction, ANL-6548, Argonne National Laboratory (May 1962).

(13) J.V. Cathcart et al., Zirconium Metal-Water Oxidation Kinetics IV. Reaction Rate Studies, ORNL/NUREG-17, Oak Ridge National Laboratory (August 1977).

(14) G.F. Lien (editor), Superheater Alloys in High Temperature High Pressure Steam, ASME, New York (1968).

(15) J.T. Bittle et al., "Oxidation of 304L Stainless Steel by Steam and by Air," Corrosion NACE, 25, No. 1 (Jan. 1969).

(16) D.E. Mitchell, M.L. Corradini, W.W. Tarbell, Intermediate Scale Steam Explosion Phenomena: Experiments and Analysis, SAND81-0124, Sandia National Laboratories (1981).

(17) M. Pilch, Acceleration Induced Fragmentation of Liquid Drops, Doctoral Thesis, Univ. of Virginia (1981).

(18) M. Pilch and C.A. Erdman, "Consideration of Liquid Fragmentation in Safety Analysis," Trans. Am. Nucl. Soc., 38, 403 (1981).

(19) J.O. Hinze, "Fundamentals of the Hydrodynamic Mechanism of Splitting in Dispersion Processes," AIChE Jnl, 1, No. 3 (1981).

(20) J. Collier, Convective Boiling and Condensation, 2nd Ed., McGraw-Hill (1981) NY.

(21) G. Wallis, One-Dimensional Two-Phase Flow, 2nd Ed., McGraw-Hill (1981) NY.
(22) J.B. Rivard, Chapter 6, Report of the Zion/Indian Point Study: Volume 1, SAND80-0617/1, NUREG/CR-1410, Sandia National Laboratories (1980).
(23) R.B. Bird et al., Transport Phenomena, Wiley and Sons Pub., New Jersey (1960).

NOMENCLATURE

- A - area
- C_D - drag coefficient for sphere ($\sim$1)
- D_o - diffusion coefficient between H_2 and H_2O
- D - diameter
- E_m - mixing energy
- g - gravitational acceleration
- h - heat transfer coefficient
- H_c - depth of the water pool
- i_{fg} - latent heat of vaporization
- m'' - mass flux (kg/m^2s)
- N - number of moles
- ΔP - steam partial pressure difference between the ambient and at the fuel surface
- q'' - heat flux
- R_o - universal gas constant
- T - temperature
- T_V - $(T_{sat} + T_f)/2$
- v - velocity
- V - volume
- W_{H_2} - mass flux of H_2 generation
- α - void fraction
- δ_V - vapor film thickness
- ρ - density

Subscripts

- b - breakup
- c - coolant
- d - displaced
- FR - fuel fragment
- f - fuel
- H_2 - hydrogen
- M - mixture
- v - vapor
- sat - saturated

Table 1

Fuel Fragment Size Data During Mixing for FARS Experiments [11,16]

FITS TEST	MOLTEN FUEL COMPOSITION	DENSITY (kg/m^3)	MASS (kg)	ENTRY VELOCITY (m/s)	COOLANT DEPTH (m)	TIME TO BASE CONTACT t (msec)	t*	MASS AVG. FUEL FRAGMENT SIZE AT BASE CONTACT FISSUM* D_{Fr} (mm)	D_{Fr}/D_f	POST-TEST D_{Fr} (mm)	D_{Fr}/D_f
MD-8	IRON-ALUMINA	3850	4.7	6.4	0.71	180	4.42	8	0.057	EXPLOSION‡	
MD-11	IRON-ALUMINA	3850	4.7	4.7	0.71	162	2.62	8	0.057	EXPLOSION‡	
MD-19	IRON-ALUMINA	3850	5.9	5.9	0.61	122	3.8	7	0.053	EXPLOSION‡	
MDC-2	CORIUM	6890	4.1	6	0.53	150	3.25	11	0.11	EXPLOSION‡	
MDC-16	CORIUM	6890	8.5	6	0.53	140	2.6	12	0.105	EXPLOSION‡	
FITS-1A	IRON-ALUMINA	3850	1.95	6.2	0.43	115	3.64	2	0.1	2	0.002
FITS-4A	IRON-ALUMINA	3850	4.3	2	0.61	140	3.65	2	0.025	4	0.03

* Using high-speed camera @ 2000-9000 fps

‡ A steam explosion occurred at base contact; so post-test fuel debris are not indicative of mixing

Table 2

Prediction of Minimum Fragment Diameter and Associated Hydrogen Production

FITS TEST	TIME TO BASE CONTACT (ms)	t*	MINIMUM DIAMETER (HENRY MODEL) D_{min} (mm)	MINIMUM DIAMETER D_{Fr_I} (mm)	$D_{Fr_{II}}$ (mm)	HYDROGEN GENERATED BY METALLIC PHASE OXIDATION g moles for D_{Fr_I}	g moles for $D_{Fr_{II}}$
MD-8	180	4.42	14	6.5	8.3	1.1	0.93
MD-11	162	2.62	13	8.3	10.4	0.82	0.74
MD-19	122	3.8	15	7	8.8	1.02	0.85
MDC-2	150	3.25	14	6	12	0.5	0.2
MDC-16	140	2.6	28	6	12	1.1	0.5
FITS-1A	115	3.64	12	5.8	7.3	0.83	1.5
FITS-4A	140	3.65	15	7.3	9.3	1.01	0.84

Calculations were based on the following initial conditions from FITS data.

T_f = 2700 K

i_{fg} = 2.25 MJ/kg = 0.3 MPa

σ_c, σ_o } based on Fig. 4 data

Table 3

Sample Calculation of Hydrogen Production for Full Scale Conditions

Water Depth (m)	Mixing Time t*	Maximum Initial Diameter (m)	Maximum Initial Mass (kg)	Metallic mass† (kg)	Minimum mixing Diameter D_{Fr_I} (mm)	Hydrogen Generated for D_{Fr_I} (g moles)
0.5	2	0.21	33	10	6.4	3.7
0.5	4	0.8	4.2	1.25	6.4	0.48
1.0	2	0.42	265	80	10.2	32
1.0	4	0.21	33	10	10.2	4.6
2.0	2	0.83	2120	645	16.2	327
2.0	4	0.42	265	80	16.2	42
4.0	2	1.67	17000	5166	25.6	3823
4.0	4	0.83	2120	645	25.6	429

† Based on an average exposed metallic composition of 30%

†† Based on an entry velocity of 5 m/s + 0.3 MPa and fuel temperature of 2700 K

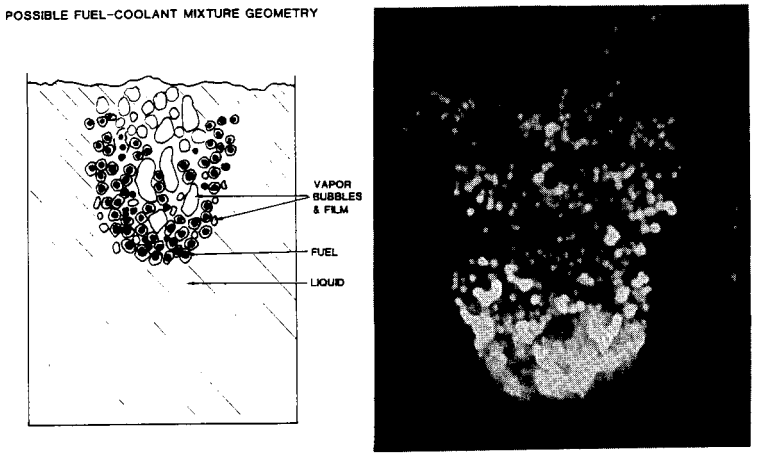


Figure 1 Conceptual Picture of the Fuel-Coolant Mixing Process

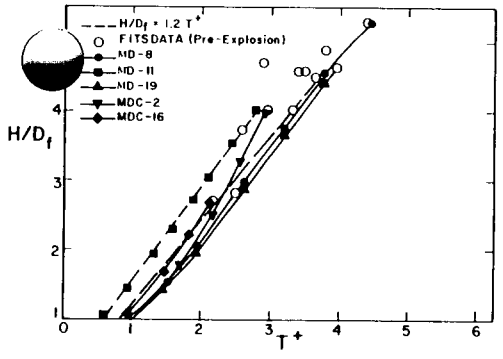


Figure 2 Dimensionless Depth, $^{H}/_{D_f}$, of the Fuel-Coolant Mixture as a Function of Dimensionless Time, T^+

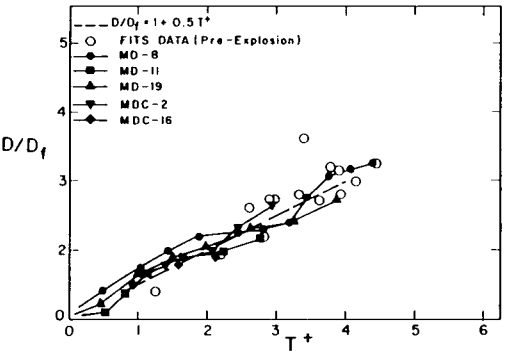


Figure 3 Dimensionless Diameter, $^{D}/_{D_f}$, of the Mixture as a Function of Dimensionless Time

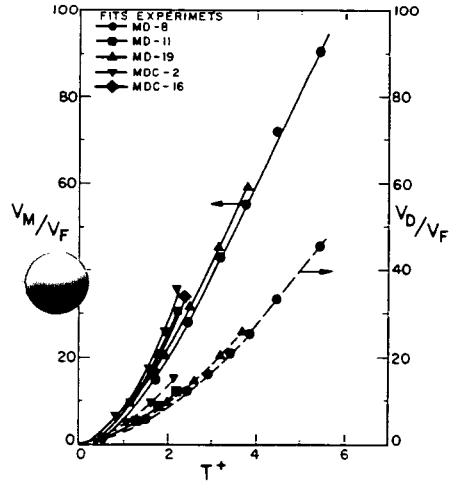


Figure 4 Dimensionless Mixture Volume, $^{V_M}/_{V_f}$, and Displaced Water Volume, $^{V_D}/_{V_f}$, as a Function of Dimensionless Time

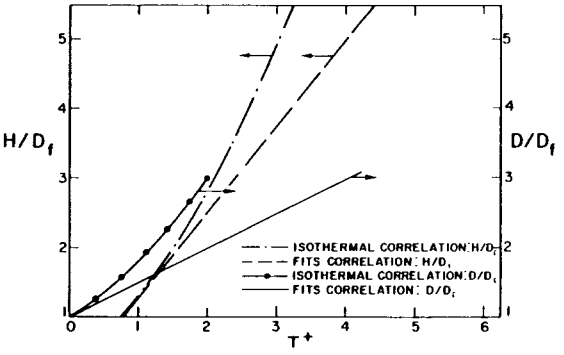


Figure 5 Comparison of FITS Data to Isothermal Data from Previous Experiments [17]

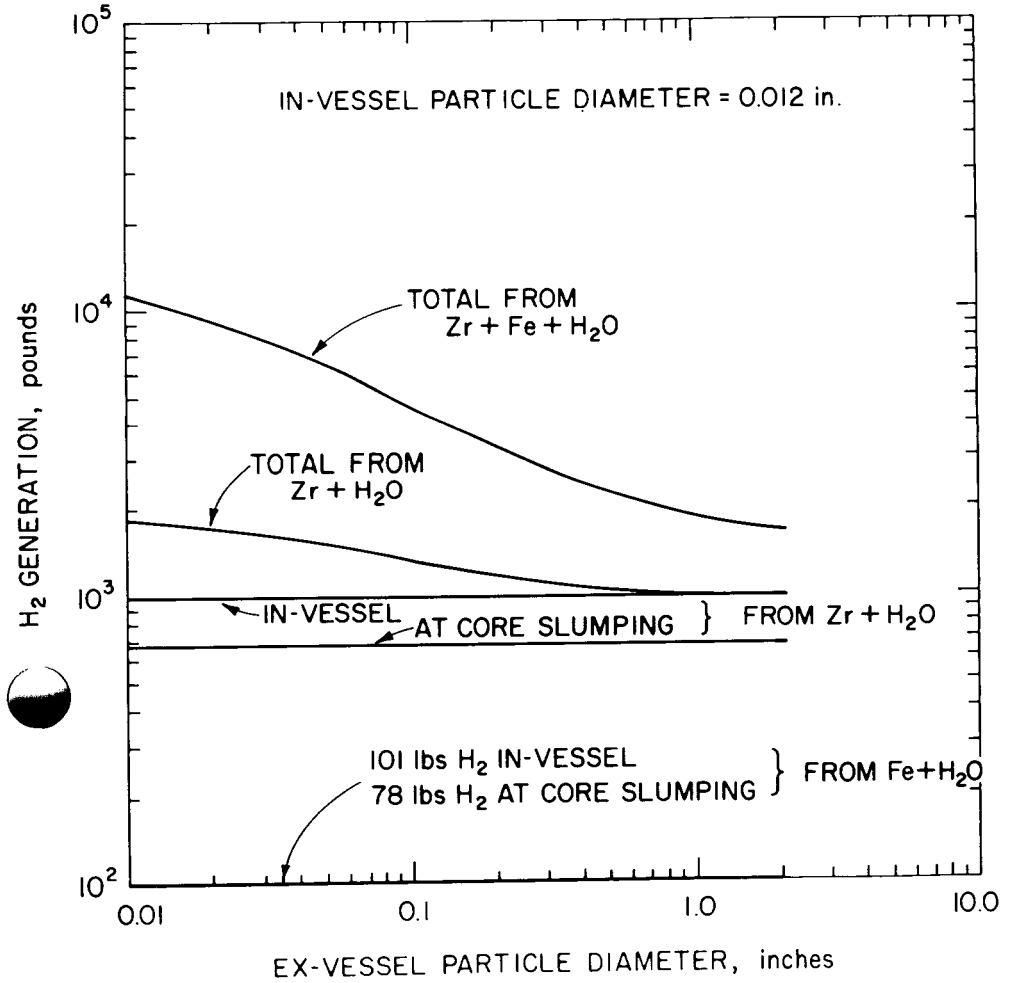


Figure 5. H_2 Generation - S_2D LOCA

GAS RELEASE AND CONTAINMENT HISTORY DURING MELT-CONCRETE INTERACTION

K. Hassmann, W. Schwarzott

Kraftwerk Union Aktiengesellschaft
Postfach 3220, 8520 Erlangen, FRG

M. Reimann

Kernforschungszentrum Karlsruhe
Postfach 3640, 7501 Leopoldshafen, FRG

ABSTRACT

In risk studies, paramount attention is paid to hypothetical accidents with nuclear reactor core melt down because of possible physical health impacts resulting from this type accidents. In the Federal Republic of Germany the research project "Core melting" was initiated by the Federal Ministry of Research and Technology in 1971 in order to investigate melt down phenomena. One of the main objectives within the research project is the development of experimentally verified models and computer codes to predict the events during melt/concrete interaction. It is the purpose of this paper to summarize the present state of the art-melt concrete interaction models developed so far and to show update results with respect to gas release and pressure time history within the containment by varying some sensitive parameters. In addition, the sequence of two different accident scenarios is given in detail which - with respect to overpressurization of the containment building - are expected to cover all other melt down sequences.

INTRODUCTION

In accordance with the licensing rules, the control of loss of coolant accidents must cover the entire range of ruptures from the double ended break of the main coolant pipe up to a break of the smalles connection leading to the primary system. The variety of accident sequences and different leakage rates gave rise to the development of coolant injection and recirculation systems designed and realized with a very high degree of redundancy. In this connection it should be emphasized, that for licensing purposes emergency core cooling calculations are always performed on the basis of highly conservative assumptions.

The highest fission product release rates from the fuel occur during hypothetical melt down accidents. Therefore, such events are of utmost interest in risk studies / 1, 2 /. Contrary to the licensing procedure, analyses in risk studies have to be performed on a best estimate basis. This best estimate procedu should cover all physical phenomena which influence the public risk during and after heavy nuclear accidents.

In the Federal Republic of Germany (FRG) the research project "Core melting" was initiated by the Ministry of Research and Technology (BMFT) in 1971 to study basic problems connected with melt down accidents. In this context, the beneficial cooperation and information exchange between the US and the German program ought to be mentioned here. The following sections summarize the course of the melt down accident as well as the influence of sensitive parameters determining melt concrete interaction.

SEQUENCE OF MELT DOWN ACCIDENT

Melt down scenarios in Light Water Reactors are extremely improbable. Only highly unlikely events with simultaneous failure of almost all safety systems result in melt down processes in the reactor core.

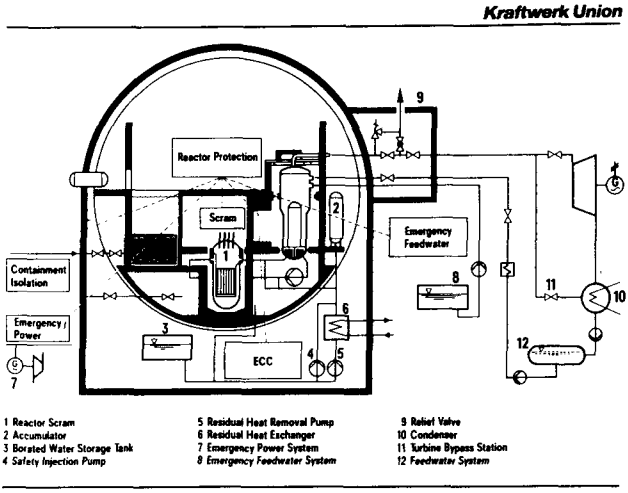


Fig. 1 **Engineered Safety Features for Small Break LOCAs**

The engineered safety features for small break LOCA's available KWU-type PWR's to fullfil the German regulation rules are ven in Fig. 1. In addition, the information given in this scheme is sufficient to demonstrate even the sequence of the melt down accident with large LOCA's and transients as initiating events. Two different accident scenarios, the high pressure and low pressure cases have been analysed in detail up to now; they are in respect of the containment history - assumed to comprise all other melt down sequences.

LOW PRESSURE CASE

Within both, the Reactor Safety Study and the German Risk Study, the initital event of a detailed analysis of the melt down behaviour was considered to be a double-ended break of the hot leg of the primary coolant loop. The analysis being the lower bound of all melt down scenarios will occur, if after a major LOCA the low pressure recirculation systems totally fail. As a consequence of this initial condition, the core melt down accident starts with a totally reflooded reactor pressure vessel about 20 minutes from blow down.

After about 35 min, the water level is calculated to be reduced below the upper grid plate level. As soon as the water level has dropped significantly in the core region, the generated steam flow does not provide sufficient cooling to remove the decay heat in the dry zones of the core. Consequently, the fuel rods are heated up in this region. At a temperature level of about 1000 °C, the exothermal $Zr-H_2O$-reaction starts. This results in an additional heat source within the uncovered core region. The heat production by $Zr-H_2O$-reaction increases exponentially with the temperature of the Zirconium cladding. During this period, melting of the fuel rods starts.

er about 1.3 hours, more than 50 % of the whole core material s heated up to its failure temperature. At that time, the lower grid plate of the core is assumed to fail and the molten part of the core is ecpected to slump into the residual water in the lower plenum of the reactor pressure vessel. The residual water in the lower plenum will evaporate during a short period of time. Subsequently, the refrozen core material heats up and melts again. About 1.8 hours after blow down, a molten pool has formed in the lower plenum. In contact with the pool of molten material, the pressure vessel is heated up. After about 1.9 hours, thermal failure of the reactor pressure vessel is expected to occur.

At that time, the molten material contacts the basement of the containment building and the melt concrete interaction starts. In recent years, many efforts have been made in the FRG to analyse this accident phase which has been identified to influence considerably the sequence of the melt down accident. In particular, sump water evaporation - which starts after the melt has penetrated the innermost shielding in the reactor cavity, separating melt and sump water - influences drastically the pressure time history in the containment. In addition the generation of noncondensible gases during melt concrete interaction contributes to the pressure increase. Although modeling work with respect to the long term behaviour of the melt interacting with concrete is not completed, sufficient evidence is available to demonstrate that overpressurization of the containment steel shell will occur after 5 days at the earliest.

HIGH PRESSURE CASE

Core melt down also can occur at full system pressure following transients with emergency power case and loss of all redundant auxiliary power supplies. The combination of all these highly hypothetical events cause loss of feed water supply of the steam generators, causing the secondary side of the steam generators to become dry. Then the pressure within the primary system increases until the pressurizer relief valves open, inducing primary coolant to flow into the pressurizer relief tank. Then the rupture disk fails and saturated steam enters the containment atmosphere.

After about 2 hours, the water level in the reactor pressure vessel reaches the upper grid plate level of the core, after 2.9 hours the core support structure is assumed to fail. During all the evaporation and core heat up procedure, the pressure in the primary system is at the pressure level of the pressurizer relief valves. As Tab. 1 shows, the pressure vessel is assumed to fail about 1 hour later as compared to the low pressure case, followed by depressurization of the primary system.

Late in the depressurization period the accumulators will be activated and the melt will be quenched partially by the accumulator water. Failure of the innermost shielding in the reactor cavity, caused by the mechanical forces during depressurization of the primary system, cannot be excluded. Therefore, melt and refrozen core material is expected to be flooded by accumulator water and sump.

MELT DOWN SCENARIO	LOW PRESSURE CASE	HIGH PRESSURE CASE
Initiating event	Large LOCA and failure of LPR 20 min from blow down	Emergency power case and loss of auxiliary power supplies
Residual water at upper core level	35 min	2 m
Failure of core support structure	~1.3 m	~2.9 m
Melt concrete interaction	1.9 m	5 m
Sump water ingression	8 m	3 m

Tab.1 COMPARISON OF IMPORTANT RESULTS (GKU 1300 MWe-PWR)

Compared with US-standard, the reactor cavity of German PWR's is designed in a multicompartment mode. Therefore, the melt contacts only small surfaces and volumes after failure of the reactor pressure vessel and the presence of a long term coolable configuration can be eliminated. Consequently, refrozen material is assumed to remelt again and a situation comparable to the high pressure case is anticipated to occur. This case can be considered to be the other bound of the melt scenarios as compared to the low pressure melt down sequence.

Caused by the relatively low release rates to the containment, pressure is only slightly above atmospheric pressure until depressurization of the primary system occurs. The failure mode of the RPV results in a pressure spike due to the rapid release of the steam-hydrogen mixture into the primary system As can be seen in Fig. 2, the long term pressure history within the containment equals the situation during the low pressure case.

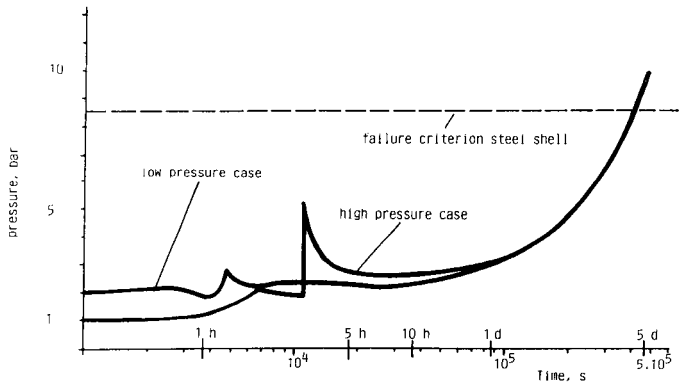


Fig.2 CONTAINMENT, PRESSURE-TIME HISTORY

CONCRETE EROSION - PARAMETRIC INVESTIGATION

The events during melt-concrete interaction have a drastic influence on the pressure time history within the containment and determine the time interval until threat of the containment steel shell occurs. Then a significant amount of fission products is released to the environment during depressurization of the containment atmosphere. This has been demonstrated in the previous sections for all melt down sequences with operating containment isolation. To analyse the sensitivity of different parameters, several computer runs have been performed varying

- the type of concrete aggregates
- the water content of concrete
- the amount of concrete reinforcement.

The objective of this work has been to investigate the influence of different parameters on the release of condensible and non-condensible gases and consequently on the pressure-time history in the containment as well as the possible formation of burnable and/or detonable mixtures. Fig. 3 illustrates in detail the range of variation for the main parameters. Based upon the internal and external impacts tó be considered in licensing procedures, the possibility in varying the amounts of concrete reinforcement within the lower part of the reactor cavity is extremely small.

No significant influence with respect to gas release is expected to occur in the range of reinforcement given in Fig. 3.

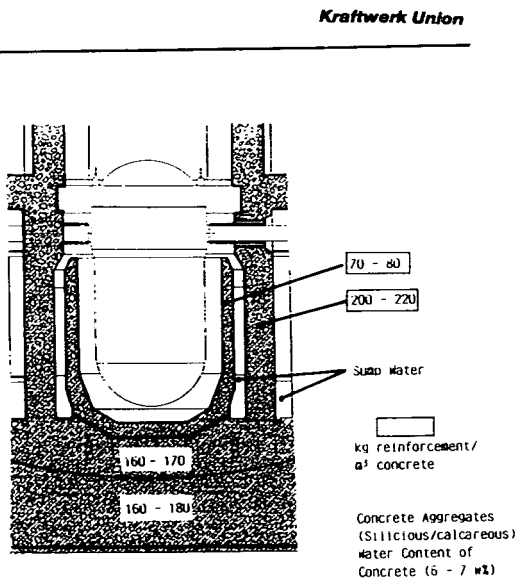


Fig.3 Main Parameters Influencing Long Term Pressure History in the Containment

The low pressure case is taken as a basis for the analysis. Because of the insignificant differences in the long term behaviour with respect to containment pressure during the high and low pressure case, the results are assumed to be tendentiously valid for all other initiating events.

In the FRG, concrete with predominantly silicious aggregates is being used. Nevertheless, one of the reasons for analysing calcareous concrete was to find the envelope covering the consequences for all types of concrete.

All experimental investigations indicate a rapid seggregation of the core melt interacting with concrete. The steel and the

metallic Zirconium, remnants of the melt down process within the RPV, form the metal layer. The oxidic layer consists of fuel and the Zirconium, oxidized by the Zr-H_2O-reaction. During the melt concrete interaction, the concrete will be thermally decomposed into gaseous and liquid products. The portion of the released gases, steam and carbon dioxide, rising through the metal layer of the melt is partly reduced to hydrogen and carbon monoxide forming metal oxides. The metal oxides as well as the liquid decomposition products of the concrete, i. e. silicates, calcium and aluminium oxides, mix with the constituents of the oxide layer. Therefore, the oxidic layer is changing its properties continously with time.

As noted before, the modelling work with respect to the long term melt concrete interaction, in particular crust formation and refreezing phenomena are not completed up to now. In the FRG the KAVERN (KWU) / 3 / and WECHSL (KfK) / 4 / code is being developed in order to predict the phenomena during melt concrete interaction with, to some extent, different physical models. For verification of all codes, the BETA test facility is under consturction at KfK. In this facility, up to about 600 kg thermite melt with metal and oxide layers are designed to interact in concrete crucibles / 5 /. Within these crucibles the metal melt is heated by an induction coil to maintain a high temperature level. The experimental program planned will simulate in different crucibles the interaction of melt with concrete within temperature levels between about 2000 °C and the resolidification temperature which varies with time. The lower temperature limit varies between 1300 °C (silicious concrete) and 1500 °C (calcareous concrete). An investigation of the concrete erosion by resolidified layers is also planned. For the heat transfer from the molten pool to the concrete, both a film and a bubble model have been developed. In the film-model the existence of a continous gas film between the pool and the concrete is assumed. The bubble model assumes heat transport to the concrete by convection caused by rising single gas bubbles. Both models are expected to be valid for different temperature levels ofthe melt. As identified and reported in / 6 /, gas bubbles generated during concrete heat up perculate the metallic and the oxidic phase. Therefore, solidification of the metal layer preventing gas penetration through the melt doesn't occur.

Both, the KAVERN and WECHSL code have been used for the performance of the parametric calculations. Although only preliminary versions are available, good agreement of the results was achieved with respect to integral gas release into the containment atmosphere. As mentioned before, the long term behaviour in the low temperature range, in particular refreez-

ing phenomena, are not modelled satisfactorily in the actual versions of both codes. To be able to run the codes in real times of several days, some assumptions had to be made. The most important ones with respect to gas release and sump water evaporation are:

- in KAVERN heat transfer to the concrete is switched from Film to Bubble model depending upon melt temperature. WECHSL models the heat transfer by the Film model influenced by crust formation in the low temperature range.

- Although KAVERN and WECHSL are developed to model heat removal from the melt to the basement, calculations have been performed without transient heat conduction in the concrete. This assumption is based on parametric studies showing no significant influence of heat removal to the basement during the first couple of days.

- Sump water evaporation starts as soon as the innermost shielding in the reactor cavity is penetrated. The evaporation itself is influenced by crust formation on the surface of the molten pool.

	Type I	Type II	Type III
Steam release during heat up	5.8/7.0	5.8/7.0	5.8/7.0
Aggregates (dry)			
SiO_2 %	81.4	62.9	8.6
CaO %	9.8	18.0	51.8
Al_2O_3 %	5.7	9.4	5.7
CO_2 %	3.1	19.7	33.9
	100.0	100.0	100.0
melting temperature of concrete, °C	1300	1300	1500
desintegration enthalpy, J/g	2284	2284	2608

Tab.2 DIFFERENT CONCRETE COMPOSITIONS ANALYSED

The analysis of the different concrete compositions as well as the main properties are listed in Tab. 2. The steam release has been varied between 5.8 and 7 weight percent concrete which has been figured out to be the upper and lower bound of concrete mixtures manufactured at nuclear power sites. Because of the small range of variation with respect to the water content, the main differences in gas generation are expected to be produced by the chemical composition of the concrete aggregates itself. The most important constituents summarized in Tab. 2 are related to the dry mass before water is added to the different concrete compounds. Due to experimental measurements / 7 / Type I as well as Type II concrete behaves like silicious concrete with a melting temperature of 1300 °C and a desintegration enthalpy of 2284 J/g. Only in case of a relative clean calcareous concrete characterized by a small SiO_2- and a large CaO content, higher values for the melting temperature (1500 °C) and the disintegration enthalpy (2608 J/g) has been demonstrated experimentally / 7 /.

The overall volume flow of noncondensibles composed of CO_2, CO and H_2 versus time, generated during melt-concrete interaction is shown in Fig. 4 for all three types of concrete mixed with the lower bound of water. All values are valid for a

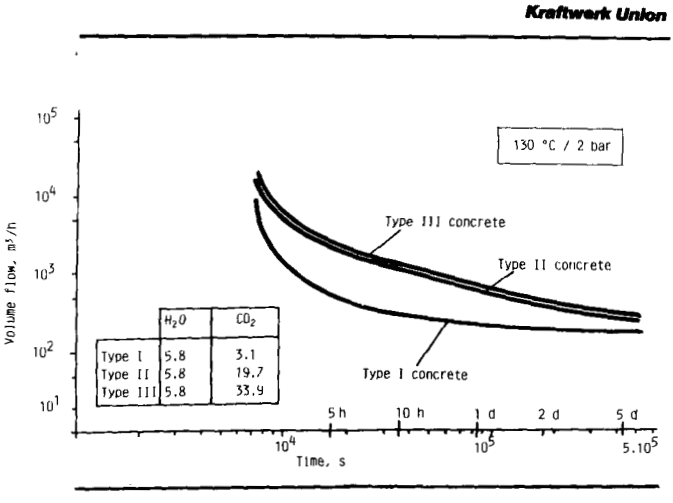


Fig.4 Release of noncondensibles during melt/concrete interaction

situation within the containment of 130 °C and 2 bars and may differ slightly if the correct time-dependent state of the atmosphere will be taken into account which varies between 2 bars/100 °C and 8 1/2 bar/160 °C. As illustrated in the case of Type I concrete, significant less noncondensible gases are released during the first days of melt concrete interaction caused mainly by silicious aggregates. In particular, less CO and CO_2 volume flow is produced. Type II and Type III concrete only differs slightly, because the difference in CO_2-release of 19.7 to 33.9 percent, as shown in Tab. 2, will be equalized by the advantageous behaviour of calcareous concrete as a consequence of its higher melting temperature and its larger disintegration enthalpy.

Pressure and temperature in the containment atmosphere were analysed with the COCMEL code. This model uses a one-compartment containment model taking into account all masses and energies entering the containment atmosphere during the four phases of the melt down sequence. Fission products released during the melting process are assumed to be airborne and homogeneously mixed. Heating up of the steel and concrete structures is considered by conduction. Fig. 5 illustrates the influence of aggregates characterized by Type I - Type III concrete, water content and sump water evaporation on the pressure-time history within the containment.

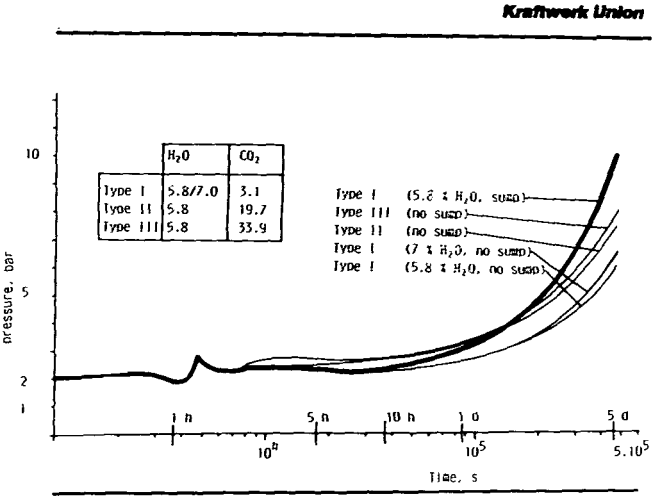


Fig.5 PRESSURE-TIME HISTORY FOR THREE TYPES OF CONCRETE

The reference low pressure-case represented by the bold-face line, has been discussed in detail before (see Fig. 2). The significance of sump water evaporation can be extrapolated by comparing the reference case with the two lowest curves representing different water contents of the Type I concrete. Without sump ingression to the surface of the melt, the pressure increase amounts only to about 5 bars, 5 days from the beginning of the accident and is 4 bars less than compared to the sump water evaporation case. The water content of the concrete itself does not influence the pressure-time history if the amount of water increases from 5.8 to 7 weight percent. Calcareous aggregates mixed with silicious ones behave like basaltic concrete (1300 °C melting temperature, 2284 J/g disintegration enthalpy). In contact with melt it produces a similar amount of gases as Type III limestone concrete. In both cases the pressure increases to about seven bars after 5 days. Taking into account homogeneous mixing of the H_2-CO-CO_2-steam-air-mixture, Fig. 6 shows the course of the enrichment of burnables in the containment. The bold-face line representing the

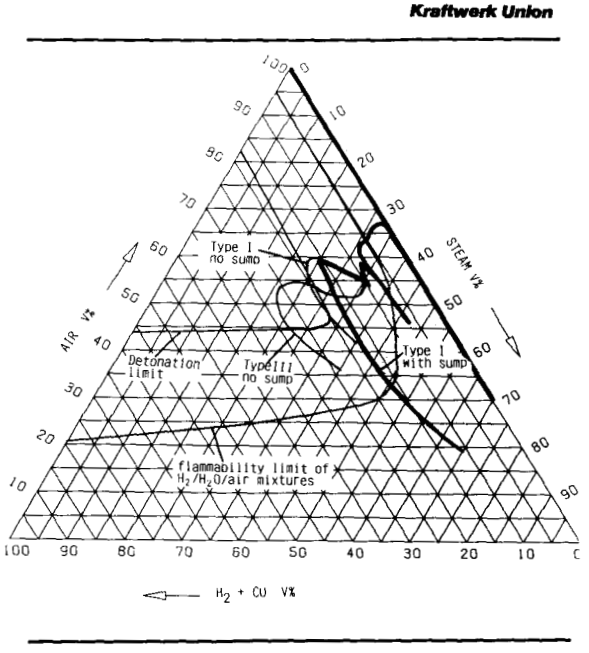


Fig.6 ENRICHMENT OF BURNABLES WITHIN THE CONTAINMENT

low pressure case with sump water ingression to the surface of the melt, exceeds the flammability limit of H_2/H_2O/air-mixtures and shows a considerable distance from the detonation limit. In the same case without sump water evaporation, the detonation limit is analysed to be touched slightly. If Type III concrete as well as Type II is in contact with the melt, the detonation limit is expected to be exceeded. Starting 5 hours from the initiating event burnables are detonable for about 2 1/2 days. However, conclusions on how burnables will influence containment integrity cannot be drawn until more details have been gained from experimentally evaluated models with respect to pocketing and stratification of the different constituents in the containment and the burning procedure of CO/H_2 mixtures in H_2O, CO_2, air atmospheres.

CONCLUSION

Two different melt down sceanarios analysed in this paper:

- the large LOCA as inititating event and failure of the low pressure recirculation systems (low pressure case) and

- the emergency power case with loss of all auxiliary power supplies (high pressure case)

are expected to envelop all other melt down sequences with respect to the containment pressure time history. On the basis of the present status, results of melt down analyses for both, the low and the high pressure case are available for a large dry KWU-type containment indicating threat of the containment building in any case about 5 days from the beginning of the accident. In the high pressure case pressurization of the primary system results in a pressure spike below the design pressure of the containment. The long term pressure increase is drastically influenced by evaporation of sump water.

However, in the long term range of the accident, noncondensible gases generated during concrete heat up, melting and oxydation of the metal constituents of the melt, contribute considerably to the pressure increase of the containment atmosphere. Therefore, a parametric study has been performed to analyse the importance of the concrete aggregates, water content and reinforcement with respect to the containment history. Two types of silicious concrete with (Type II) and without (Type I) significant calcareous admixtures as well as the almost pure calcareous concrete (Type III) have been analysed. The results indicate that

- varying the amount of reinforcement and water content of the concrete within reasonable bounds, does not significantly influence the long term pressure history.

- in any case, a large amount of burnables is released to the containment atmosphere

- Type II and Type III concrete only differ slightly with respect to the long term pressure increase of noncondensible gases, generated during melt concrete interaction as well as the enrichment of burnables

- if no sump water evaporation is considered, pressure in the containment amounts to about 5 bars after 5 days with Type I concrete. By using Type II and Type III concrete, pressure is calculated to rise about 7 bars during the same time interval.

- for Type III concrete, the radial erosion seems to be less than that of Type I and II. Therefore, in the low pressure case, sump water ingression is expected to occur later by using Type III concrete. In the high pressure case, the innermost shielding in the reactor cavity, separating the melt and the sump water will fail by mechanical forces during depressurization of the primary system. Therefore, radial erosion and consequently the composition of concrete does not influence the time history with respect to the sump water ingression.

Summarizing, emphasis should be laid on the fact that the long term behaviour of the melt interacting with concrete is not modelled satisfactorily up to now. Nevertheless, trends given in the paper are expected to be confirmed by improved experimentally validated theoretical models.

REFERENCES

/ 1 / Bundesminister für Forschung und Technologie, "Deutsche Risikostudie Kernkraftwerke", Verlag TÜV Rheinland, Köln 1979

/ 2 / N. C. Rasmussen
Reactor Safety Study - "An Assessment of Accident Risks in US Comercial Nuclear Power Plants", USNRC, WASH 1400 (NUREG-75/014), 1975

/ 3 / BMFT 150379, Detaillierung von KAVERN und Modellentwicklung zur Gasabströmung aus der Schildgrube, Final report to be published

/ 4 / M. Reimann, W. B. Murfin
The WECHSL-Code: A Computer Program for the Interaction of a Core Melt with Concrete, KfK 2890, November 1981

/ 5 / H. Rininsland et al.,
Fortschritte der Reaktorsicherheitsforschung im Projekt Nukleare Sicherheit, PNS Jahreskolloquium 81

/ 6 / K. Hassmann, M. Reimann,
Analyses of Hypothetical Core Melt Down Accidents, ANS/ENS Topical Meeting Reactor Safety Aspects of Fuel Behaviour, August 2 - 6, 1981, Sun Valley, Idaho, Proceedings p 2-496/2-510

COMBUSTIBLE GAS GENERATION FROM MOLTEN FUEL-CONCRETE INTERACTIONS

by

R. K. Cole, Jr. and D. P. Kelly

The CORCON-MOD1 code has been developed at Sandia National Laboratories to evaluate phenomena associated with molten-core concrete interactions. The code is currently being applied for plant calculations and comparison against experiments. An important prediction from this code is the amount and rate at which gases leave the reactor cavity region. Two of these gases are combustible, carbon monoxide, and hydrogen. Calculations have been performed to predict the generation of these gases under various initial and boundary conditions. We will discuss the results of these calculations and their associated uncertainties.

INTRODUCTION

Studies of the risk of operating nuclear power plants must consider hypothetical accidents with very low probabilities, but potentially large consequences. These include sequences where loss of normal and emergency cooling systems leads to melting of the core, failure of the pressure vessel, and deposition of molten core and structural materials onto the concrete floor of the containment building. This can result in a molten pool of material which is maintained above the ablation temperature of the concrete by tens of megawatts of decay heat from nonvolatile fission products retained in the melt. The resulting ablation of concrete raises the possibility of failing containment by melt-through. In addition, the decomposition of concrete produces large volumes of water vapor and carbon dioxide which, if they come into contact with molten metals, can be reduced to hydrogen and carbon monoxide. All four gases contribute to the risk of overpressurizing containment; hydrogen and carbon monoxide are also combustible, presenting an additional risk.

The CORCON code is being developed at Sandia National Laboratories to model the interaction of molten materials with concrete. It treats a variety of internal heat transfer, mass transfer, and chemical phenomena as well as heat transfer to, and ablation of, concrete and heat loss from the surface of the pool. The MOD1 version of the code,[1] available since late 1980, treats the early stages of the interaction. It assumes that the pool is entirely molten, an assumption which fails after several hours because of the decrease in decay power and the dilution of the melt by molten concrete oxides. Also,

interaction with water in the reactor cavity is not permitted in MOD1. A MOD2 version of the code is under development in which these restrictions will be removed. The calculations to be reported here were performed with an intermediate version of the code which has significant structural differences from MOD1, but does not yet include the extended MOD2 models which are being developed and tested outside of CORCON.

EXAMPLE RESULTS AND DISCUSSION

The CORCON code has the capability of modeling plant- and accident-specific problems in some detail. Here, however, we will attempt to develop some insight into the production of combustible gases by examining a few generalized cases. Gas production clearly depends on the decay power in the pool, on the partition of pool heat loss between concrete and the pool surface, and on the energy necessary to ablate concrete combined with the fraction which decomposes to gas. For a given plant, the first is largely a function of time after SCRAM, decreasing rapidly at first and then more slowly. The second is strongly influenced by the geometric proportions of the pool, which determine heat-transfer areas and the fraction of the generated gas which is subjected to chemical reduction. The third depends on concrete properties, of which the most important is the relative silicate/carbonate content. High-silicate concretes are relatively easy to ablate, but produce relatively little gas, mostly water vapor. High-carbonate concretes, while much more refractory, decompose to produce large amounts of carbon dioxide in addition to water vapor.

We have examined the effects of these variables by performing a number of CORCON calculations. In each case the melt, described in Table 1 and typical of a large PWR, was deposited into a right-circular-cylindrical cavity. Decay power was calculated using WASH-1400 retention factors for fission products. Melt deposition might take place as early as 1 hour after SCRAM (for a large-break LOCA with complete loss of power) or be delayed for 6 hours or more (for a small-break LOCA with failure of the recirculation system). Depending on building design, the size of the pool can vary considerably; a reasonable range might be 2.5 m to 4.5 m in radius. Concrete is highly variable, and CORCON allows the user to specify a composition in detail. Three "built-in" compositions are also available corresponding to typical basalt aggregate/silica sand, limestone aggregate/ silica sand, and limestone aggregate limestone sand concretes. (The third is often referred to as "CRBR concrete.") The compositions and melting ranges of these concretes are given in Table 2, as are the ablation temperatures and corresponding heats of ablation used in our calculations.

The increases in ablation temperature, enthalpy, and in gas generation with increasing carbonate content are obvious. The calculations reported are summarized in Table 3.

The first comparison involves early (1 hour) and late (6 hour) deposition into a small (2.5 m radius) cavity in CRBR concrete. The calculation was carried out for 6 hours of interaction in each case. We will examine the early-deposition case in detail. The oxidic phase of the melt is initially denser than the metallic phase and, as the two are immiscible, the pool initially consists of a layer of fuel oxides below a layer of molten metal. A third "slag" layer of molten concrete and steel oxides quickly forms on top. As time progresses, the fuel oxides are diluted by concrete oxides until the fuel oxide layer becomes less dense than the metal. At this time, after a little more than an hour of interaction, it rises through the metallic layer and combines with the slag to produce an oxide-over-metal configuration. This may be seen in the layer-mass and density plots in Figures 1 and 2; the temperature history is shown in Figure 3. The evolution of the cavity shape is shown in

TABLE 1

Initial Melt

UO_2	97.89 tonne
ZrO_2	25.73
FeO	5.0
Fe	111.9
Cr	17.54
Ni	9.744
Initial Temperature	2550 K

TABLE 2

Concrete Properties

	Basalt Aggregate Silica Sand	Limestone Aggregate Silica Sand	Limestone Aggregate Limestone Sand "CRBR"
SiO_2	54.84 w/o	35.80 w/o	3.60
CaO	8.82	31.30	45.40
Al_2O_3	8.32	3.60	1.60
Metal Oxides	13.47	2.144	7.004
Alkali Oxides	7.19	1.302	0.758
CO_2	1.50	21.154	35.698
H_2O	5.86	4.70	5.94
Melt Range	1350-1650 K	1420-1670 K	1690-1875 K
T_{abl}	1450 K	1503 K	1752 K
ΔH_{abl}	1839 J/g	2615 J/g	3620 J/g

TABLE 3

Summary of Calculation

Case	Deposition Time (hours)	Cavity Radius (m)	Concrete	Gas Production (kg-moles) after 2 hours CO	2 hours CO_2	2 hours H_2	2 hours H_2O	4 hours CO	4 hours CO_2	4 hours H_2	4 hours H_2O	6 hours CO	6 hours CO_2	6 hours H_2	6 hours H_2O
1	1	2.5	CRBR	132.	285.	53.	117.	225.	422.	90.	173.	284.	502.	114.	206.
2	6	2.5	CRBR	85.	207.	34.	85.	156.	303.	63.	124.	213.	379.	86.	155.
3	1	2.5	Limestone	105.	199.	56.	109.	194.	361.	104.	197.	(284.	566.	153.	308.)*
4	1	4.5	Limestone	(260.	73.	140.	41.)	(378.	116.	198.	70.)	(476.	164.	239.	108.)
5	6	2.5	Basalt	(11.	14.	104.	132.)	(15.	18.	139.	178.)	(17.	24.	166.	228.)
6	6	2.5	Limestone	85.	151.	46.	83.	(151.	230.	81.	125.)	(204.	311.	110.	170.)

*Parentheses indicate freezing of the metal in CORCON-MOD1. Entries are therefore upper bounds on generation and on reduction to CO and H_2.

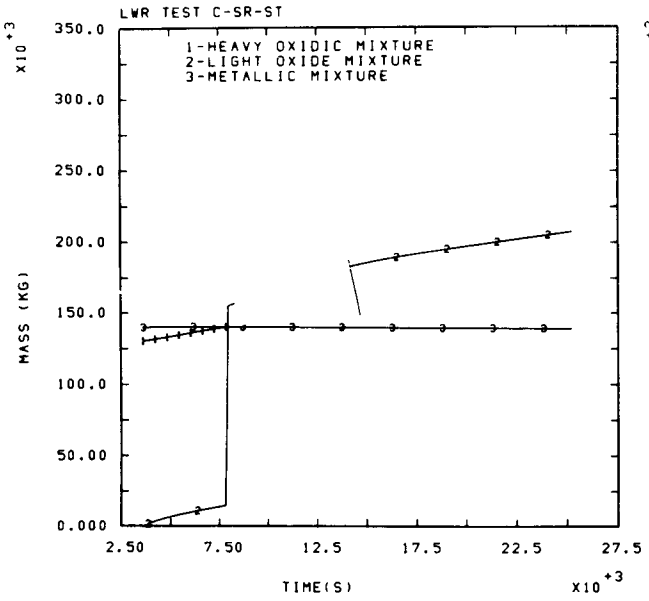


Figure 1: Layer Masses for Case 1

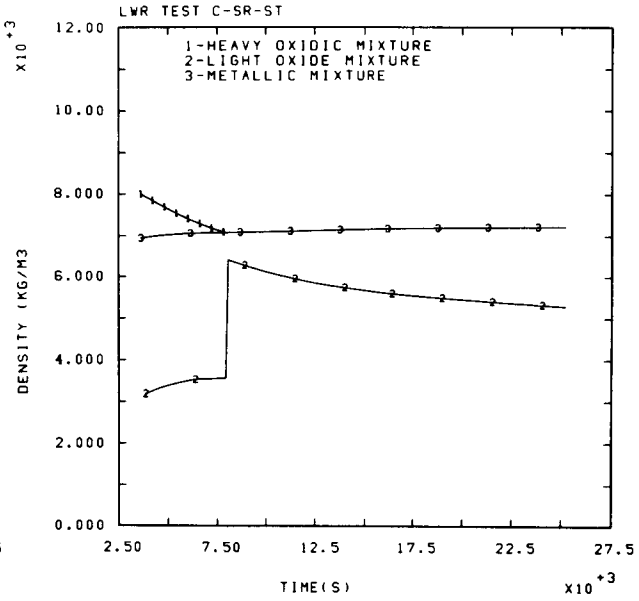


Figure 2: Layer Densities for Case 1

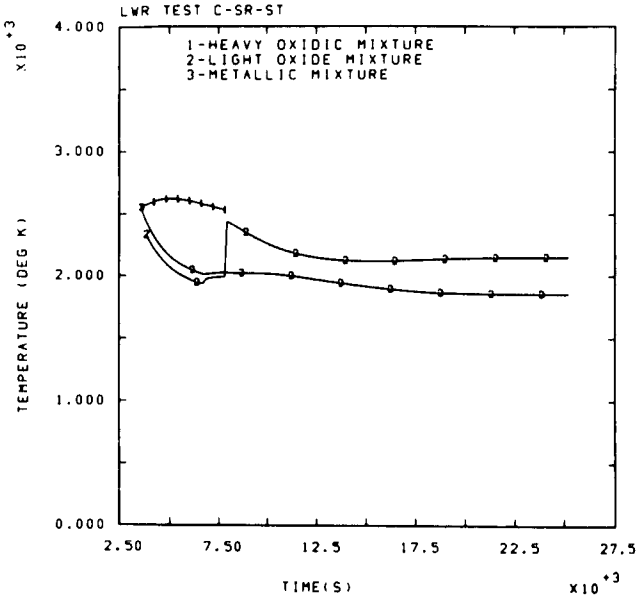


Figure 3: Layer Temperatures for Case 1

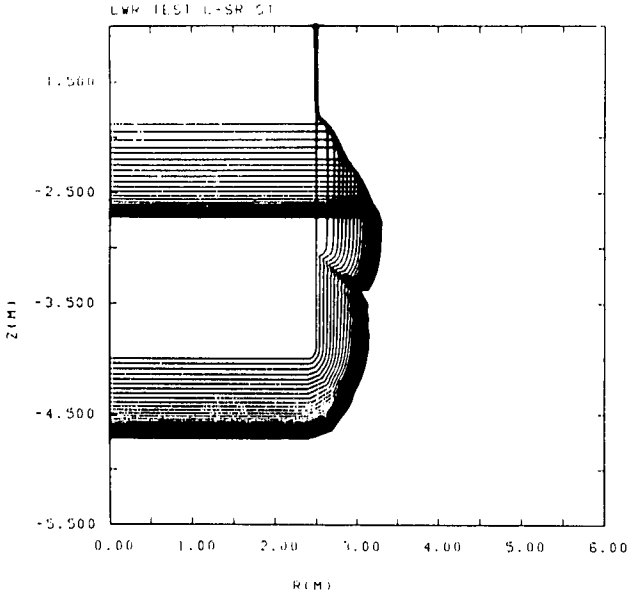


Figure 4: Cavity Profiles for Case 1

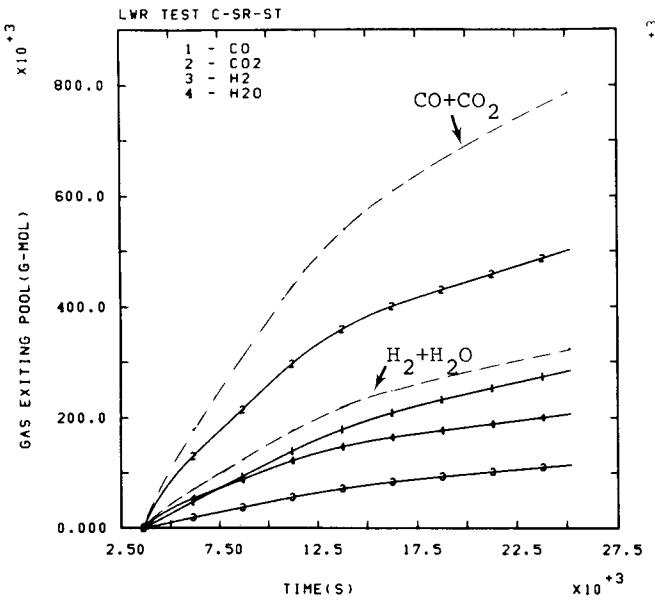


Figure 5: Gas Generation for Case 1

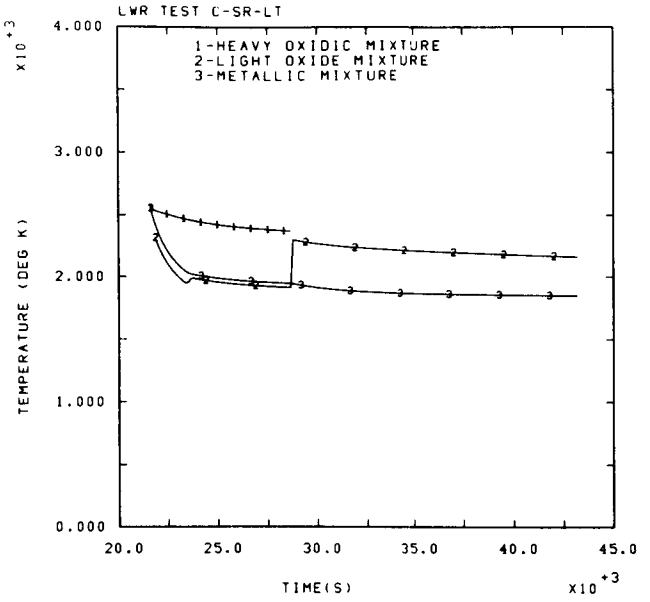


Figure 6: Layer Temperatures for Case 2

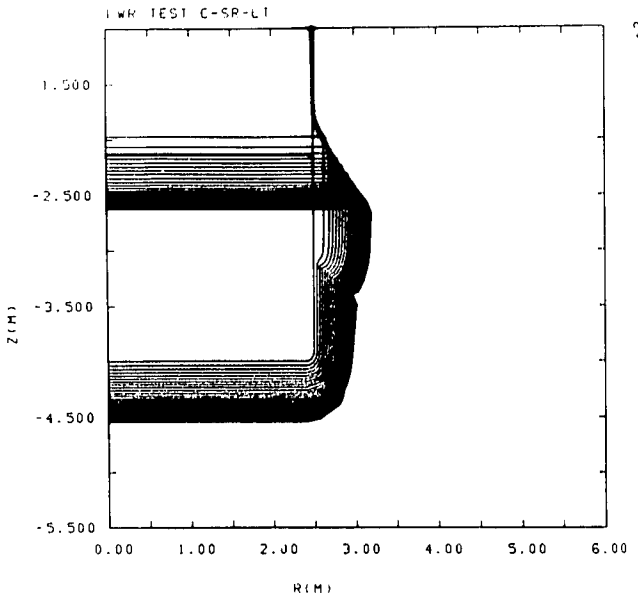


Figure 7: Cavity Profiles for Case 2

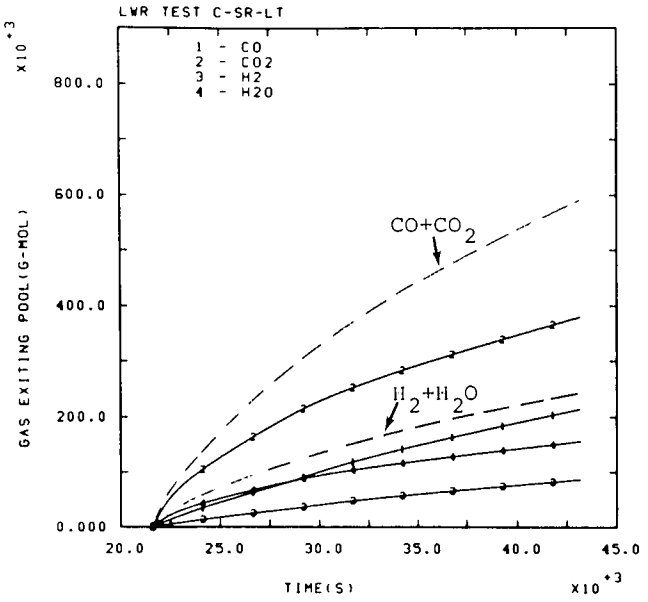


Figure 8: Gas Generation for Case 2

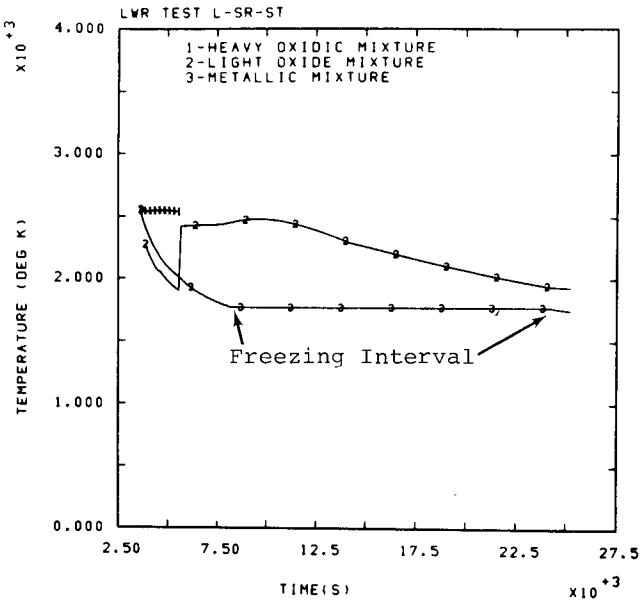


Figure 9: Layer Temperatures for Case 3

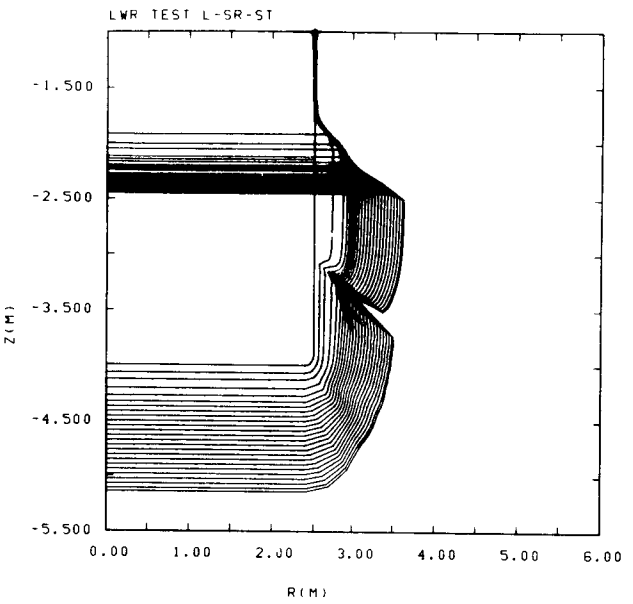


Figure 10: Cavity Profiles for Case 3

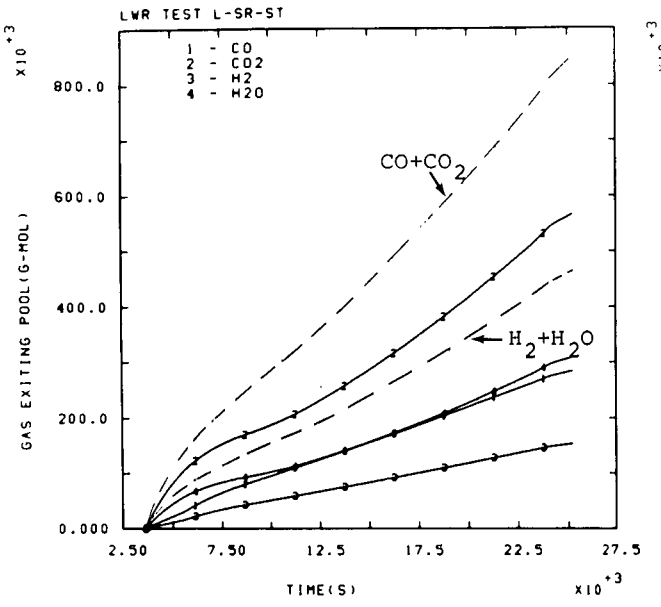


Figure 11: Gas Generation for Case 3

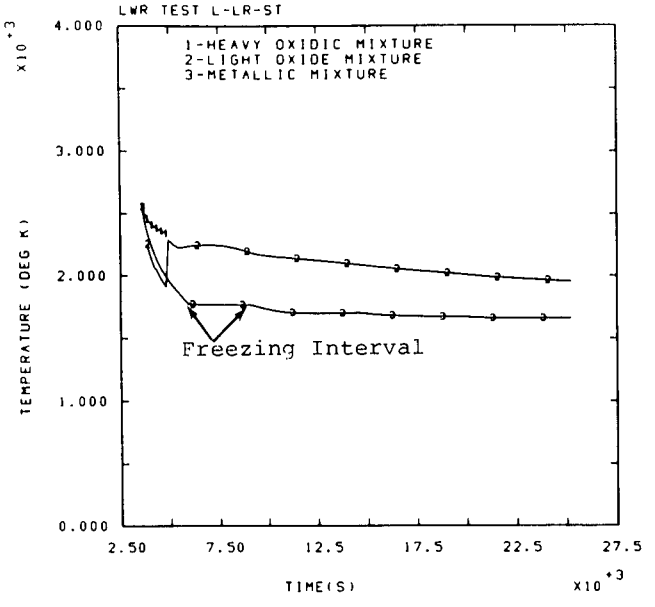


Figure 12: Layer Temperatures for Case 4

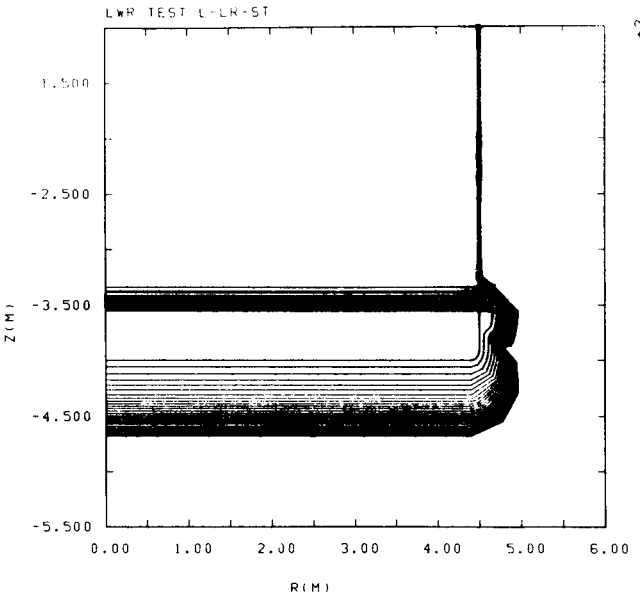


Figure 13: Cavity Profiles for Case 4

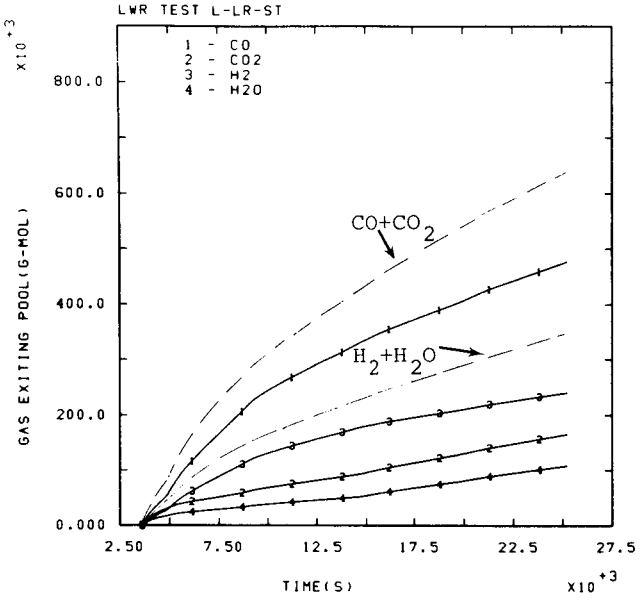


Figure 14: Gas Generation for Case 4

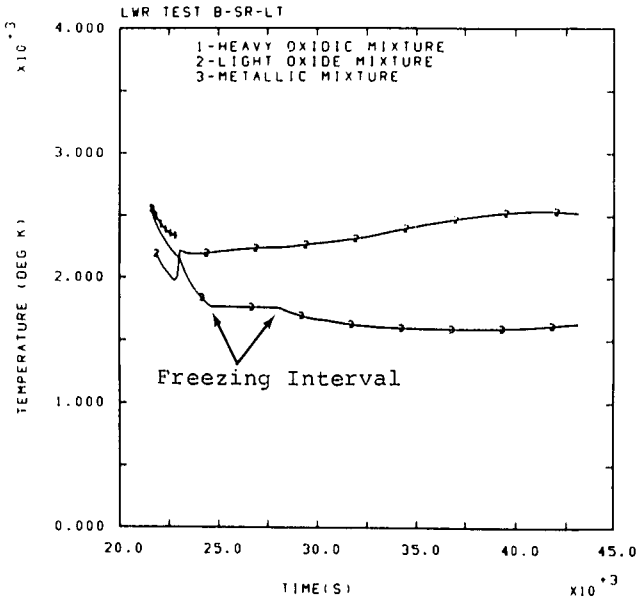


Figure 15: Layer Temperatures for Case 5

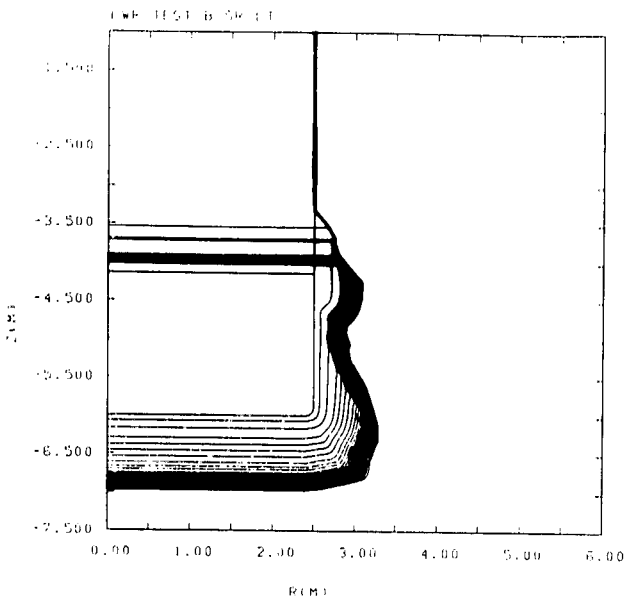


Figure 16: Cavity Profiles for Case 5

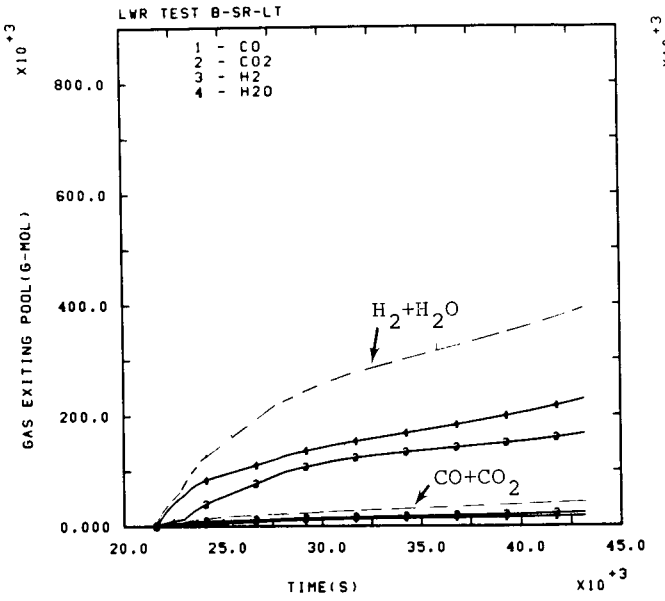


Figure 17: Gas Generation for Case 5

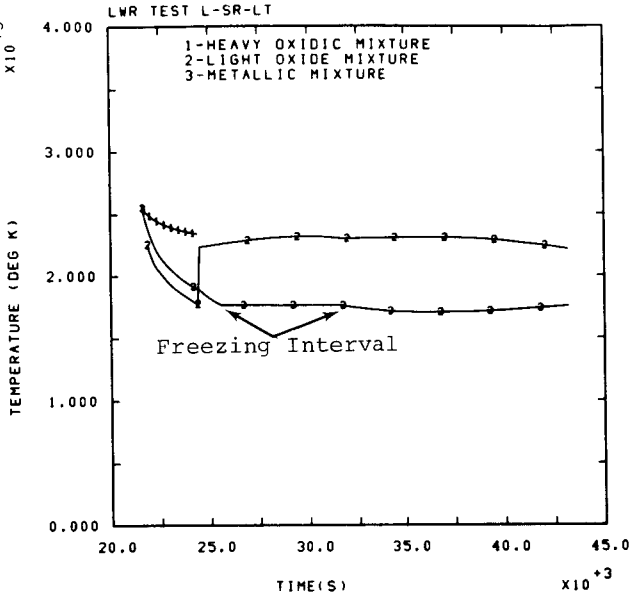


Figure 18: Layer Temperatures for Case 6

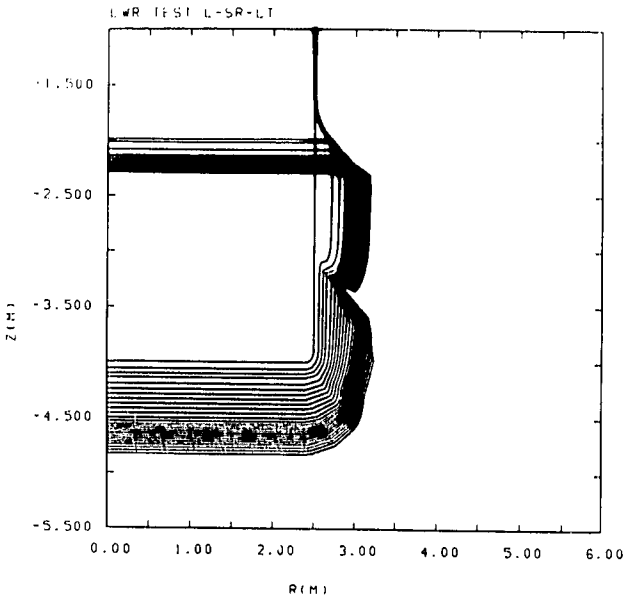


Figure 19: Cavity Profiles for Case 6

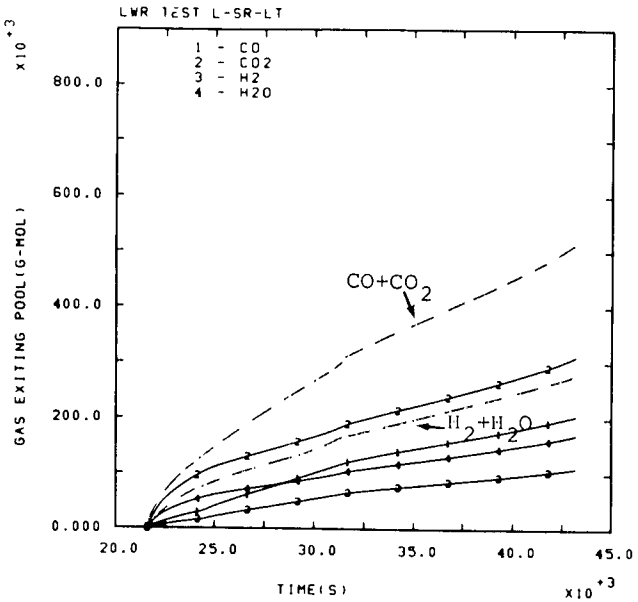


Figure 20: Gas Generation for Case 6

CORROSION OF ALUMINUM AND ZINC IN CONTAINMENT FOLLOWING A LOCA AND POTENTIAL FOR PRECIPITATION OF CORROSION PRODUCTS IN THE SUMP

K. K. NIYOGI

R. R. LUNT

J. S. MACKENZIE

united engineers & constructors inc

30 South 17th Street,
Post Office Box 8223
Philadelphia, PA 19101

1.0 INTRODUCTION

Following a loss-of-coolant accident (LOCA) in a LWR containment, certain materials in the containment come in contact with alkaline emergency cooling and containment spray solutions and may corrode yielding hydrogen gas. The problems associated with the production of hydrogen gas and the control of combustible gas concentration have been extensively explored in recent years. However, the phenomenon of corrosion and its consequences in the long term cooling of the reactor and the containment have drawn very little attention. United Engineers & Constructors Inc. has made an extensive effort to study through literature survey the solubility of the corrosion products from aluminum and zinc in order to assess the potential for precipitation in the containment sump. The NRC has initiated just recently some limited activities in this area by extending the scope of one of the experimental programs conducted at the Sandia National Laboratories. This experimental facility was originally set-up for the determination of the corrosion rates of zinc.

2.0 ANALYSIS

The analysis presented in this article is based on parameters for a typical large dry reactor containment with caustic/boric acid buffered spray solution. Parameters used in this study may vary from one plant to another. However, they are not expected to affect the overall conclusions.

2.1 Aluminum and Zinc Inventory in Containment

The aluminum and zinc inventories in a typical containment building are illustrated in Tables 1 and 2, respectively. There are approximately 1 ton of aluminum and 12 tons of zinc with exposed surface areas of 2,500 sq. ft. and 233,000 sq. ft., respectively, in the containment. It is to be noted that most of the aluminum components are associated with reactor control systems and made of structural grade alloy (6061 - T6), The amount of aluminum is not expected to vary much for the same type of reactor. Most of the zinc present in the containment is in the form of galvanization and the amount varies significantly from plant to plant. Paints containing zinc are also found in containments for some plants.

2.2 Composition of Spray Water

During the initial phase of the accident, spray water is drawn from the Refueling Water Storage Tank (RWST) and Spray Additive Tank (SAT). The concentration of NaOH in the SAT is (20 + 1)% by weight. Boron concentration in the RWST is (1900 $\pm$ 95) ppm. The usable volume of the SAT is approximately 10,000 gallons and that of the RWST is 350,000 gallons. This initial phase lasts for

less than one hour to about two hours depending on the number of safety injection and spray trains operating. The spray pH may vary from 9.0 to 10.6 and remains within the acceptable range of variation from 8.5 to 11, dictated by the Standard Review Plans (SRP)(3), during this period.

During the recirculation mode the spray water is drawn from the containment sump. Other than the RWST and SAT liquid, about 500,000 lbs. of reactor coolant with maximum boron concentration of 4,000 ppm and 225,000 lbs. of liquid from the accumulator tank with nominal concentration of 2,000 ppm are also discharged to the sump, resulting in approximately 3.71×10^6 lbs. of liquid in the sump. The sump pH varies from 8.9 to 9.8 during a 30-day cooling period.

2.3 Corrosion of Aluminum and Zinc

The corrosion rates of aluminum and zinc are functions of spray pH and chemistry and of material temperatures. For the estimation of corrosion rates, the containment spray temperature and material temperatures are assumed to be reaching the containment atmospheric temperature. The applicable metal corrosion research to date is rather limited. A wide spectrum of corrosion data is found in the literature. However, the corrosion rates used in this study are considered acceptable in the industry.

2.3.1 Aluminum

Following ANS WG56.1 recommendation(1), the corrosion rate of aluminum can be expressed as

$C_{al} = A \exp (BT)$,

where C_{al} is in mils/year, T is temperature in ^{o}F, A and B are constants. A = 32.9859 and B = 0.02398 for $T > 220^{o}F$; and A = 13.4456 and B = 0.02796 for $T \leq 220^{o}F$.

According to RESAR[2], the corrosion rates of aluminum are significantly lower and can be expressed as

$C_{al} = 1.143 \exp (0.0334T)$.

However, SRP 6.2.5(3) suggests a constant amount of 200 mils/year as a long term corrosion rate with appropriate correction in the upward direction considering higher temperature early in the accident.

The amount of aluminum corroded in the containment following a LOCA has been calculated according to the ANS method and presented in Table 3. Similar calculations have been made following the SRP

with correction for higher temperature (above 153°F) using RESAR, and the results are presented in Table 4. Figure 1 shows the comparison of corrosion obtained by these two methods. Based upon the ANS method about 300 lbs of aluminum would be corroded during the first eight hours of containment spray operation and almost 1000 lbs. of aluminum would be corroded after 30 days. The RESAR/SRP method results in only about half this amount of corrosion. From one-quarter to one-half of the initial amount of aluminum may corrode in 30 days, corresponding to 30 day solution concentrations of 9.2×10^{-3} gm moles Al/l by ANS and 4.4×10^{-3} gm moles Al/l by RESAR/SRP.

2.3.2 Zinc

The zinc corrosion rate, according to ANS 56.1, is expressed as

$$C_{zn} = 5.577 \times 10^{9} \exp \{26{,}100/R(T+460)\}$$

where, C_{zn} is in mills/year, T is temperature in °F, and R is 1.986 Btu/lbm mole - °R.

There is no recommendation in SRP 6.2.5 regarding corrosion of zinc.

Table 5 presents the corrosion of zinc. Figure 2 also shows the amount of zinc corrosion. After eight hours of containment operation about 400 lbs of zinc would be corroded. Approximately 10% (about one ton) of the initial amount of zinc may corrode in 30 days. This would result in a potential concentrations of 8.8×10^{-3} gm moles Zn/l.

2.4 Solubility of Aluminum and Zinc

Solubility product data for the predominant compounds expected to control the solubility of aluminum and zinc in a caustic/boric acid buffered system are summarized in Table 6. These data represent a compilation of selected published values, calculated solubilities based upon recent literature on thermodynamic properties, and, in the case of aluminum, limited data from relevant, unpublished solubility tests. It should be noted that these data are for a temperature range of 20-30°C.

In general, it can be anticipated that the hydroxides of aluminum and zinc will be solubility limiting over the range of conditions of the containment spray solution. Both aluminum and zinc hydroxide are amphoteric, dissolving readily under strongly acidic and strongly basic conditions. At intermediate pH values, such as the slightly basic containment spray solutions, aluminum and zinc hydroxide are relatively insoluble.

The solubilities of the various aluminum and zinc compounds considered were estimated using the extended Debye-Hückel equation to calculate activity coefficients as shown in Table 7. Estimates were based upon a solution ionic strength of 0.1M, which is approximately that expected for the containment spray solution. Variations in ionic strength between 0.05M and 0.15M actually have very little effect on the estimated solubilities, since the calculated activity coefficients shown in Table 7 would vary by only a few percent.

2.4.1 Aluminum

There have been numerous studies published on the solubility and solution chemistry of aluminum. A number of different forms of aluminum hydroxide precipitate have been observed depending upon solution compositions and experimental conditions. These range from amphorous solids (sometimes gelatinous in appearance) to crystalline forms of diaspore and Gibbsite, $Al_2O_3 \cdot 3H_2O$, one of the most stable forms.

There has been some disagreement over which form(s) actually represent the true "equilibrium" solid phase for freshly precipitated aluminum hydroxide. In fact, a number of forms may exist, including simple hydroxides, as well as more complex polymeric compounds. However, it has been established that under certain conditions, aluminum hydroxide precipitates undergo an "aging" (recrystallization) process through intermediate hydration states to more stable, and inevitably, less soluble forms. A prevalent view is that aluminum hydroxide initially precipitates in a somewhat amorphous form as $Al(OH)_3$, and then slowly converts to Gibbsite. This is probably more characteristic of precipitation behavior under acid conditions.

Solubility products reported for "freshly precipitated" aluminum hydroxide, under alkaline conditions, have generally been in the range of 5×10^{-13} to 10^{-13} (12-15). More recent information(7,8,11) indicates that, under the alkaline conditions of the containment spray solution, aluminum hydroxide can be expected to precipitate as boehmite, AlO(OH), or possibly diaspore, the latter being the more stable form to which boehmite may convert after "aging" for a period of days or weeks. Gibbsite is not expected to be the prevalent form in the pH range of the containment spray system. Reported values of the solubility product of boehmite are in range of 10^{-15} to 10^{-16} (at 25°C).

Because of the uncertainty in the form (and manner) of aluminum precipitation, consideration must be given to the formation of "fresh precipitate" as well as boehmite. Boehmite may or may not be the form of the initial precipitate; however, it is likely to be the form to which a less stable "fresh" precipitate converts after "aging". Hence its solubility product should be that ultimately limiting solubility.

The effect of pH on the solubility of aluminum in P_{CA1}/pH at an ionic strength of 0.1M is shown in the plot of Figure 3. In the pH range of 8 to 10, aluminum solubility is predicted to be 10^{-4} to 10^{-2} gm moles/liter based upon "fresh" precipitate; and about 3×10^{-7} to 3×10^{-5} gm moles/liter for boehmite.

As noted earlier, the solubility product data discussed above are for temperatures in the range of 20°C to 30°C. At higher temperatures characteristic of initial spray operations, the solubility of aluminum corrosion products is expected to be somewhat higher based upon published temperature/solubility data and thermodynamic properties for aluminum oxides and hydroxides (7,8,10,14,16). Dillion (16) reports that the solubility of aluminum corrosion products in tap water experiments roughly doubles between 30°C and 100°C.

2.4.2 Zinc

In caustic/boric acid buffered solutions, zinc can precipitate as $Zn(OH)_2$ or possibly as $Zn(BO_2)_2 \cdot 2H_2O$. Solubility products reported for these compounds are given in Table 6.

The effect of pH on $Zn(OH)_2$ solubility is illustrated in the pC_{Zn}/pH diagram in Figure 4. In the pH range of 8 to 10, the solubility for dissociated $Zn(OH)_2$ would range from about 10^{-3} gm moles/liter (at a pH of 8), to about 10^{-7} gm moles/liter (at a pH of 10), for a solution with an ionic strength of 0.1M.

However, zinc hydroxide may be somewhat more soluble than suggested above due to the solubility of un-ionized (associated triple ion) $Zn(OH)_2$ (aq). Unfortunately, there is little data available on un-ionized $Zn(OH)_2$, although its existence is referenced by Cotton and Wilkinson(6). Based upon Cotton and Wilkinson and calculations using thermodynamic properties, a maximum activity of $Zn(OH)_2$ is estimated to be in the range of 1.5×10^{-5}. If the activity coefficient were assumed to be approximately equal to 1.0, this would represent the maximum concentration of un-ionized zinc hydroxide.

The solubility of $Zn(BO_2)_2 \cdot H_2O$ may also be a factor limiting soluble zinc concentrations. The reported solubility product for $Zn(BO_2)_2 \cdot H_2O$(1) is 6.6×10^{-11}. Since the concentration of BO_2^- is unknown, it is difficult to determine what impact zinc metaborate will have on overall solubility. As a first estimate of the maximum solubility, it can be assumed that the concentration of BO_2^- is very low, say 10% of the total boron present. In this case, the maximum soluble zinc concentration would be on the order of 3×10^{-6} gm moles/liter, within the range for $Zn(OH)_2$.

As in the case of aluminum, the solubility products for these zinc compounds can be expected to increase with increasing temperature.

2.5 Precipitation Potential

The following discussion of precipitation potential is intended as a preliminary examination based upon the comparison of estimates of metal inventory lost to corrosion with solubility limitations. In this regard, a number of simplifying assumptions have been made:

- Only the formation of simple, single-salt solid phases is addressed. The potential for formation of combination aluminum/zinc compounds or mixed precipitates (e.g., solid solutions) is not considered.

- No consideration is given to the mechanisms of corrosion product formation and transport. The intent is to assess whether corrosion can result in the formation of solids or whether the metal will be solubilized. Therefore, the following discussions only compare the amount of metal that could be released up to the estimated solubilities.

- Potential solution concentrations are compared to solubilities estimated at 20-30°C. Solubility would be expected to increase with increasing temperature; however, temperature dependence over the range of 30-130°C should be relatively small(16) in comparison to the uncertainties in the solubility product data. Further, temperatures on the order of 30°C will be experienced in the containment water cooling system and, longer term, in the sump itself.

2.5.1 Aluminum

Table 8 and Figures 5 through 7 summarize corrosion concentrations and predicted solubilities for aluminum at pH's of 8.9 and 9.8, the range expected for the containment spray solution.

At a pH of 8.9, the maximum solubilities of aluminum either as "fresh" precipitate (1.3-4.9 x 10^{-4} gm moles/l) or as boehmite (1.5-22 x 10^{-5} gm moles/l) are roughly one to two orders of magnitude lower than the concentrations that can be attained due to corrosion from eight hours to one-day of containment spray operation. Assuming aluminum hydroxide solubility to be limiting solution concentrations, then 70-99 + % of the aluminum would be expected to precipitate -- a quantity of solids ranging from a few hundred pounds to almost one-half ton, as AlO(OH).

At a pH of 9.8, aluminum hydroxide is about an order of magnitude more soluble, however the preponderance of the data still indicate

that aluminum precipitation can occur. Only under the most optimistic conditions -- the highest reported solubility product for "fresh"-precipitate and the lowest corrosion rate estimates (RESAR/SRP) -- does the solubility exceed the potential 8-hour and 1-day concentrations. But even under these conditions, the solubility limit and 30-day corrosion concentrations are roughly equal.

2.5.2 Zinc

Table 9 and Figures 8 and 9 summarize corrosion concentrations and predicted solubilities for zinc compounds at pH's of 8.9 and 9.8.

Unlike aluminum, the solubility resulting from dissociated zinc hydroxide decreases with increasing pH over this range -- 1×10^{-5} gm moles/l at a pH of 8.9 and 2×10^{-7} gm moles/l at a pH of 9.8. These solubilities are roughly two and four orders of magnitude, respectively, lower than concentrations due to corrosion. The solubility of un-ionized $Zn(OH)_2$ may produce slightly higher soluble zinc concentrations at a pH of 9.8; however, the solubility level will still be orders of magnitude less than the potential concentration.

Assuming that zinc hydroxide solubility is limiting, then it can be expected that 99+% of the estimated quantity of zinc corroded can precipitate -- an amount of solids equal to about one and one-half tons (as $Zn(OH)_2$) after thirty days.

In addition to zinc hydroxide, it is possible that zinc metaborate may also result in precipitation of zinc. The solubility of zinc metaborate is very low. It is difficult to quantify the effects of zinc metaborate on overall solution concentrations because concentration of $(BO2)^-$ cannot be accurately predicted. If $(BO_2)^-$ amounted to half of the total boron present, then the associated zinc concentration would amount to about 10^{-7} gm moles/l. If only about 10% of the boron were present as metaborate, then the zinc concentration would roughly equal that of unionized $Zn(OH)_2$.

2.6 Precipitation Impacts

The fact that the potential for metal loss due to corrosion exceeds the solubility of aluminum and zinc in the containment spray solution does not in itself indicate that precipitation will occur; or that, if it does, it will create operational problems. Whether the presence of solid corrosion products or formation of precipitates in the containment system will have any significant impact will depend upon a variety of factors, including:

- how the corrosion products are formed on surfaces and transported to the cooling water;
- the characteristics of the solids formed; and
- the amount of solids in the cooling water.

These in turn are a function of the design of the containment and the transient conditions in the containment following a LOCA. Any number of scenarios can be envisioned, but lacking empirical data, it is difficult to predict with confidence what may actually happen. Investigative work on aluminum and zinc published to date offers little insight regarding the nature and fate of corrosion-related precipitates that can form in containment spray wash systems. There is information though, particularly on aluminum precipitates, which can give some perspective.

Areas that could be of concern with regard to precipitation and solids deposition, include:

- containment spray pumps and nozzles;
- heat exchange surfaces;
- reactor core; and
- treatment equipment for water cleanup.

Pluggage of spray pumps and nozzles is not likely to be a short-term problem should precipitation occur, at least with respect to aluminum hydroxide alone. Studies of aluminum precipitates in alkaline systems(13, 17, 18) indicate particle sizes in the colloidal range, generally less than 0.1 micron. It is difficult to envision this type of suspension having a measurable affect on the performance or spray pumps or nozzles. However, little has been reported on the nature of zinc, or combined zinc and aluminum precipitates.

The possibility of precipitated corrosion products adversely affecting cooling of the reactor core and containment water heat exchangers cannot be easily dismissed. Hatcher(13) has postulated that precipitated aluminum corrosion products can be adsorbed onto metal surfaces. He has reported strong evidence of this occuring on the heat exchange surfaces at Chalk River, although the mechanism is not clear. The potential impact of deposition or adsorption of corrosion products can be at least partially addressed. A deposition of 10-15 mil thickness may reduce the heat transfer effectiveness by 50%. Since the deposition is a gradual process, it may not affect the containment peak pressure significantly, however, the long term

cooling may be greatly affected. The cooling surfaces are the most likely place for solid deposition, although the nature and the extent of deposition are extremely difficult to predict.

Finally, there is a strong possibility that precipitates, if formed, can have a major impact on clean-up efforts following a LOCA. These precipitates can form a "Smutzdecke" on the surfa of filter and ion-exchange units that will result in very low service runs due to the development of high differential pressure. At Chalk River[13], reactor primary loop purification prefilters and deep bed demineralizers were ineffective for removal of aluminum corrosion products (extremely short service runs due to high ΔP), and evaporators were required. Such problems need to be considered in pre-accident planning.

3.0 CONCLUSIONS

This assessment of post-LOCA corrosion and the solubilities of aluminum and zinc in containment lead to the following conclusions.

(1) The hydroxides of aluminum and zinc are expected to be the principal compounds limiting solubility. The relatively low solubilities of these hydroxides compared with potential concentrations resulting from corrosion raises concern regarding precipitation and possible deposition of solids. There is also the possibility that mixed zinc and aluminum compounds can be formed, however, those were not considered in this preliminary evaluation.

(2) While solubility data at temperatures of the containment spray are not available for an accurate quantitative analysis, solubility products are reported for low temperatures 20-30°C. As a first approximation of precipitation potential, these solubility products indicate that most, if not essentially all, of the aluminum and zinc may precipitate, as discussed below.

   (a) There is some uncertainty regarding the form in which aluminum hydroxide will precipitate. Recent literature indicates that boehmite, AlO(OH), would be the form in which aluminum will likely precipitate at the slightly alkaline conditions of the containment spray solutions. Since it is the least soluble form reported for these conditions, it must be considered the most conservative measure of precipitation potential. The solubility of boehmite over the pH range of 8.9 to 9.8 is predicted to be a fraction of the eight-hour and one-day corrosion rates.

   (b) The solubility of zinc hydroxide (amorphous) over the pH range of 8.9 to 9.8 is predicted to be two to three orders of magnitude lower than both the eight-hour and one-day corrosion rates. It is possible that zinc metaborate might

limit zinc solubility to even lower concentrations than zinc hydroxide; however, the concentration of metaborate in solution cannot be accurately predicted.

(c) There is no pH level within the range of 8 to 12 where the predicted solubilities for both zinc hydroxide and aluminum hydroxide simultaneously exceed potential corrosion concentrations.

The above conclusions have been derived considering a set of accepted techniques and assumptions, reported experimental data and a postulated accident scenario. In reality, the uncertainties may prove the conclusions to be invalid. The major uncertainties lie in the areas of the determination of corrosion rates of aluminum and zinc under appropriate conditions of pH, chemical composition and temperature of spray solutions, the transport of the corrosion products from the metal surface to the sump water, and the possibility of the formation of a protective coating on the surface resulting in reduction in corrosion rates.

If the conclusions prove realistic, it raises certain very important concerns. The major concern is the consequences of the precipitation in the sump water and on the cooling surfaces, e.g., heat exchangers and reactor core channels. The post-accident clean-up can also be a difficult problem.

The manner in which precipitation occurs and the deposition/fouling potential of any precipitate was not specifically addressed within the scope of this work. However, based upon literature reviewed, it may be difficult to assess the issues of precipitation kinetics and deposition/fouling without experimental studies.

The focus of this work has been on caustic/boric acid buffered systems. The potential for corrosion and precipitation also exists in other buffered systems including those using phosphate (e.g., hydrazine/disodium phosphate/boric acid).

4.0 REFERENCES

1. ANS Work Group 56.1 (Unpublished) Report - Private Communication between K.K. Niyogi (UE&C) and C. Tinckler (NRC), also, ANS 56.1, Draft 6 (1982).

2. Westinghouse RESAR 35, Vol. VII, September (1975)

3. NRC's Standard Review Plan Section 6.2.5, Rev. 1, (1975).

4. Lange's Handbook of Chemistry, edited by JA Dean, Twelfth Edition, McGraw Hill Book Co., (1979)

5. Kolthoff, et al, Quantitative Chemical Analysis, Fourth Edition, MacMillan Co., (1979).

6. Cotton, F.A. and Wilkinson, G., Advanced Inorganic Chemistry, John Wiley and Sons, Inc., (1962).

7. Hemingway, B.S., et al, Geochimica et Cosmochimica Acta, 42, 1533-1543, (1978).

8. May, H.M., et al, Geochimica et Cosmochimica Acta, 43, 861-868, (1979)

9. Chen, D.T.Y., Can. J. Chem., 51, 3528-3533, (1973).

10. Singh, S.S., Soil Sci. Soc. Amer. Proc., 38, 415-417, (1974).

11. Arthur D. Little, Inc., Studies of Aluminum Solubility in Na_2SO_4/ Na_2SO_3 Solutions, (1979-80), Unpublished.

12. Snoeyink, V.L. and Jenkins, D., Water Chemistry, John Wiley and Sons, 1980.

13. Hatcher, S.R. and Kae, H.K., Nuclear Sci. and Eng., 10, 316-330, (1961).

14. Szabo, A.G., et al, Z. Anal Chem., 146, 401-414, (1955).

15. Uhlig, H.H., The Corrosion Handbook, John Wiley and Sons, (1955).

16. Dillon, R.L., AEE-Euratom Conf. Aqueous Corrosion of Reactor Materials, Brussels: TID-7587, 134-152 (1959).

17. Packter, A. and H.S. Dillon, Colloid & Polymer Science: 252, 249-256 (1974).

18. Packter, A., Colloid and Polymer Science = 257, 977-980 (1979).

TABLE 1

CONTAINMENT BUILDING ALUMINUM INVENTORY

Item	Weight (lb)	Volume (ft^3)	Exposed Surface (ft^2)
Nuclear Instrumentation	244	1.452	83
Flux Map Drive System	205	1.220	88
Rod Position Indicator Connectors	302	1.798	162
CRDM Connectors	218	1.298	69
Miscellaneous Valves	230	1.369	86
Containment Elevator Fans	10	0.060	100
Excore Detector Supports	115	0.687	28.6
CRD Fans, Blades and Hubs	180	1.071	1798.4
Polar Gantry Crane	114	0.679	28
Contingency	250	1.488	85

TABLE 2

CONTAINMENT BUILDING ZINC INVENTORY

Item	Weight (lb)	Volume (ft^3)	Exposed Surface (ft^2)
Ductwork, Angles and Supports	5,459	12.637	75,950
Decking	483	1.118	4,120
Checker Plate	594	1.375	2,066
Grating	2,634	6.097	7,661
Treads	126	0.292	366
Cable Trays	1,419	3.285	22,710
Tray Supports	4,108	9.509	36,517
Conduit	1,462	3.384	13,000
Conduit Supports	8,011	18.544	71,209

TABLE 3

CORROSION OF ALUMINUM IN CONTAINMENT
(ANS WG 56.1)

TIME AFTER LOCA (day)	TEMPERATURE (°F)	CORROSION RATE (mils/yr)	INTEGRATED CORROSION Thickness (mils)	INTEGRATED CORROSION Mass (lbm)
0.00	271	21,910	0.00	0.0
0.042	271	21,910	2.52	89.2
0.134	253	14,230	7.07	250.2
0.136	253	14,230	7.15	253.1
0.152	250	13,240	7.75	258.4
0.407	230	8,200	15.24	324.4
0.766	210	4,770	21.61	380.6
1.0	196	3,230	24.17	403.1
5.0	161	1,210	48.50	617.8
10.0	138	640	61.17	729.5
20.0	115	340	74.59	847.8
30.0	103	240	82.53	917.9

TABLE 4

CORROSION OF ALUMINUM IN CONTAINMENT
(RESAR SRP)

TIME AFTER LOCA (day)	TEMPERATURE (°F)	CORROSION RATE (mils/yr)	INTEGRATED CORROSION Thickness (mils)	INTEGRATED CORROSION Mass (lbm)
0.0	271	9,750	0.00	0.0
0.042	271	9,750	1.12	39.6
0.134	253	5,345	3.02	106.9
0.152	250	4,835	3.27	115.7
0.407	230	2,480	5.83	206.3
0.643	217	1,610	7.15	253.1
0.766	210	1,270	7.64	257.4
1.0	196	795	8.23	262.6
5.0	161	245	14.00	313.5
6.75	153	200	15.06	322.8
10.0	138	200	16.84	338.5
20.0	115	200	22.32	386.9
30.0	103	200	27.80	435.2

TABLE 5

CORROSION OF ZINC IN CONTAINMENT
(ANS WG 56.1)

TIME AFTER LOCA (day)	TEMPERATURE (°F)	CORROSION RATE (mils/yr)	INTEGRATED CORROSION Thickness (mils)	INTEGRATED CORROSION Mass (lbm)
0.0	271	86.80	0.0	0.0
0.042	271	86.80	0.01	84.1
0.134	253	55.10	0.0279	234.6
0.152	250	50.90	0.0305	256.5
0.407	230	29.80	0.0587	493.7
0.766	210	16.90	0.0816	686.3
1.0	196	11.10	0.0906	761.9
5.0	161	3.51	0.1707	1435.6
10.0	138	1.59	0.2056	1729.1
20.0	115	0.661	0.2364	1988.1
30.0	103	0.406	0.2510	2110.9

TABLE 6

SUMMARY OF REPORTED ALUMINUM AND ZINC SOLUBILITY PRODUCTS (20^{o}-30^{o}C)

ALUMINUM		K_{sp}	REFERENCES*
$Al(OH)_3$ (s) "Fresh Precipitate"	$Al^{+++}(aq) + 3OH^-(aq)$	1.78×10^{-31} to 1.26×10^{-34}	5,7-14
$Al(OH)_3$ (s) "Fresh Precipitate"	$AlO_2^-(aq) + H^+(aq)$	6×10^{-13} to 1.3×10^{-13}	12-15
$AlO(OH)$ (s) + $2H_2O$ (1) Boehmite	$Al(OH)_4^-(aq) + H^+(aq)$	2.25×10^{-15} to 1.51×10^{-16}	7,(8),11
ZINC			
$Zn(OH)_2$ (s)	$Zn^{++}(aq) + 2OH^-(aq)$	3.16×10^{-16}	5
$Zn(OH)_2$ (s)	$HZnO_2^-(aq) + H^+(aq)$	1.27×10^{-17}	(4)
$Zn(OH)_2$ (s)	$ZnO_2^-(aq) + 2H^+(aq)$	2.19×10^{-30}	(2),(4)
$Zn(OH)_2$ (s)	$Zn(OH)_2$ (aq)	1.53×10^{-5} to 10^{-6}	6,(4)
$Zn(BO_2)\cdot H_2O$ (s)	$Zn^{++}(aq) + 2BO_2^-(aq) + H_2O(1)$	6.6×10^{-11}	4

*( ) - indicates source(s) of thermodynamic properties data from which solubility products were calculat

TABLE 7

BASIS FOR SOLUBILITY ESTIMATES

$M_mX_n = mM+nX$ General Equilibrium Equation

$a_M^m \, a_X^n = K_{sp}$ Solubility Product

Where: $a_i = c_i \, f_i$

and: $$\frac{\log f_i}{z_i^2} = \frac{0.511(I)^{\frac{1}{2}}}{1+0.329\overset{o}{a}_i(I)^{\frac{1}{2}}} - 0.2(I)$$

a_i = ion activity
f_i = ion activity coefficient
c_i = ion concentration
z = ion valence
$\overset{o}{a}$ = effective ionic radius
I = ionic strength = $\frac{1}{2}\varepsilon c_i z_i^2$

Ion	$\overset{o}{a}$	f(at I = 0.1M)
H^+	9	0.86
OH^-	3.5	0.87
Al^{+++}	9	0.27
Zn^{++}	6	0.48
AlO_2^-	(4)	0.81
$Al(OH)_4^-$	(4)	0.81
$HZnO_2^-$	(4)	0.81
$ZnO_2^=$	(4)	0.81
BO_2^-	(4)	0.81

$\overset{o}{a}$ values from reference 4 except for values in parentheses which were assumed.

TABLE 8

COMPARISON OF ALUMINUM CORROSION AND SOLUBILITY

POTENTIAL CONCENTRATION VIA CORROSION

Time After LOCA	8 Hours	1 Day	30 Days
Concentration (gm moles/l)			
by ANS WR 56.1	3.1×10^{-3}	4.1×10^{-3}	9.2×10^{-3}
by RESAR/SRP	1.8×10^{-3}	2.7×10^{-3}	4.4×10^{-3}

ESTIMATED SOLUBILITY (gm moles/l)

	Range	Root-Mean Square Value	No. Pts.
pH = 8.9			
"Fresh" Precipitate	$1.3\text{-}5.9 \times 10^{-4}$	2.5×10^{-4}	5
Boehmite	$1.5\text{-}22 \times 10^{-5}$	5.5×10^{-5}	3
pH = 9.8			
"Fresh" Precipitate	$1.0\text{-}4.7 \times 10^{-3}$	2×10^{-3}	5
Boehmite	$1.2\text{-}17.5 \times 10^{-4}$	4×10^{-4}	3

TABLE 9

COMPARISON OF ZINC CORROSION AND SOLUBILITY

POTENTIAL CONCENTRATION VIA CORROSION

Time After LOCA	8 Hours	1 Day	30 Days
Concentration (gm moles/l)			
by ANS WG 56.1	1.8×10^{-3}	3.2×10^{-3}	8.8×10^{-3}

ESTIMATED SOLUBILITY (gm moles/l)

pH = 8.9	Dissociated $Zn(OH)_2$	1×10^{-5}
	Unionized $Zn(OH)_2$	$\sim 10^{-6}$
	$Zn(BO_2)_2 \cdot H_2O$	$(\sim 10^{-6})$*
pH = 9.8	Dissociated $Zn(OH)_2$	1.7×10^{-7}
	Unionized $Zn(OH)_2$	$\sim 10^{-6}$
	$Zn(BO_2)_2 \cdot H_2O$	$(\sim 10^{-6})$*

* Assuming $[BO_2^-] = 1/10$ total $[H_3BO_3]$

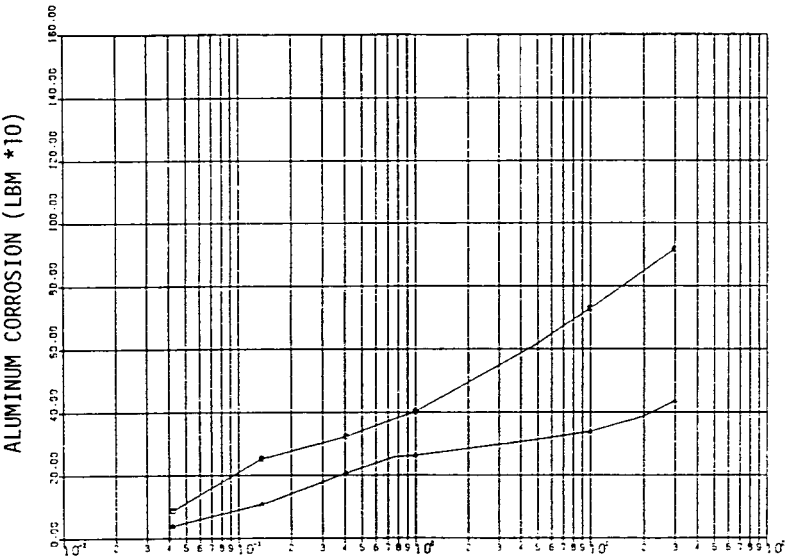


FIGURE 1: CORROSION OF ALUMINUM IN CONTAINMENT FOLLOWING A LOCA

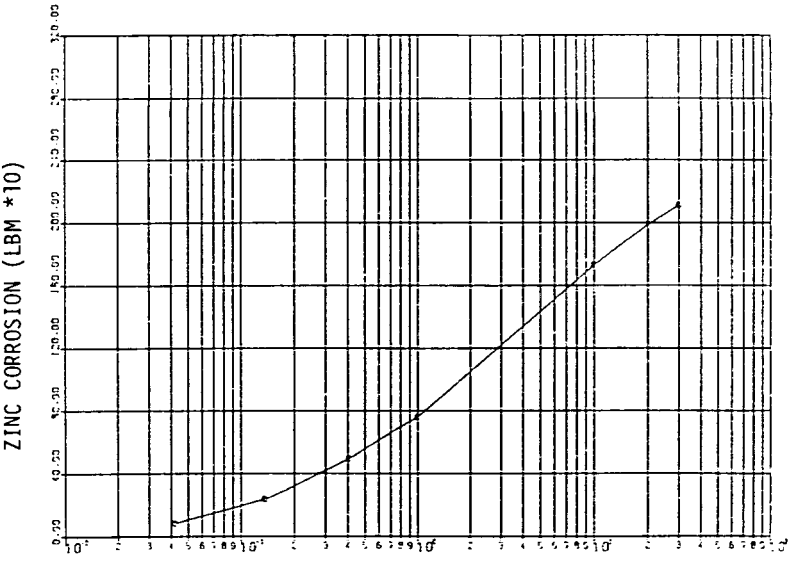
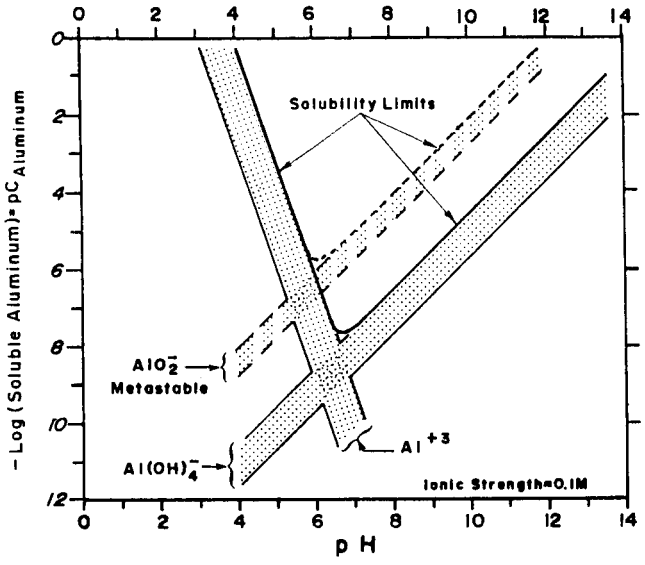


FIGURE 2: ZINC CORROSION IN CONTAINMENT FOLLOWING A LOCA



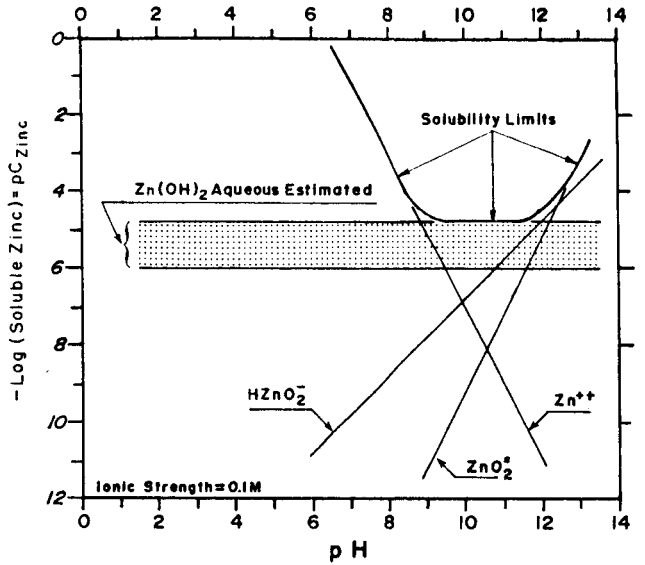
EQUILIBRIUM RELATIONSHIPS:

(1) $Al(OH)_3(s) \rightleftharpoons Al^{+++} + 3OH^-$ $K_{sp} = (0.13 \text{ to } 17.8) \times 10^{-33}$
Fresh Precipitate
$-\text{Log } C_{Al^{+++}} = pC_{Al^{+++}} = (-11.8 \text{ to } -9.0) + 3pH$

(2) $Al(OH)_3(s) \rightleftharpoons AlO_2^- + H^+$ $K_{sp} = (1.34 \text{ to } 6) \times 10^{-13}$
Fresh Precipitate
$-\text{Log } C_{AlO_2^-} = pC_{AlO_2^-} = (12.1 \text{ to } 12.8) - pH$

(3) $AlO(OH)(s) + 2H_2O \rightleftharpoons Al(OH)_4^- + H^+$ $K_{sp} = (1.5 \text{ to } 22.5) \times 10^{-16}$
Boehmite
$-\text{Log } C_{Al(OH)_4^-} = pC_{Al(OH)_4^-} = (14.6 \text{ to } 15.7) - pH$

FIGURE 3: ALUMINUM SOLUBILITY VS. pH



EQUILIBRIUM RELATIONSHIPS:

(1) $Zn(OH)_2 \rightleftharpoons Zn^{++} + 2OH^-$ $K_{sp} = 3.16 \times 10^{-16}$
$-\text{Log } C_{Zn^{++}} = pC_{Zn^{++}} = 2pH - 12.8$

(2) $Zn(OH)_2 \rightleftharpoons HZnO_2^- + H^+$ $K_{sp} = 1.27 \times 10^{-17}$
$-\text{Log } C_{HZnO_2^-} = pC_{HZnO_2^-} = 16.8 - pH$

(3) $Zn(OH)_2 \rightleftharpoons ZnO_2^= + 2H^+$ $K_{sp} = 2.19 \times 10^{-30}$
$-\text{Log } C_{ZnO_2^=} = pC_{ZnO_2^=} = 29.3 - 2pH$

(4) $Zn(OH)_2 \rightleftharpoons Zn(OH)_{2\,aq}$ $K_{sp} = (1 \text{ to } 15) \times 10^{-6}$
$-\text{Log } C_{Zn(OH)_{2\,aq}} = pC_{Zn(OH)_{2\,aq}} = 4.8 \text{ to } 6.0$

(5) $Zn(BO_2)_2 \cdot H_2O \rightleftharpoons Zn^{++} + 2BO_2^- + H_2O$ $K_{sp} = 6.6 \times 10^{-11}$
$-\text{Log } C_{Zn^{++}} = pC_{Zn^{++}} = 6.5 \text{ to } 7.5$?

FIGURE 4: ZINC SOLUBILITY VS. pH

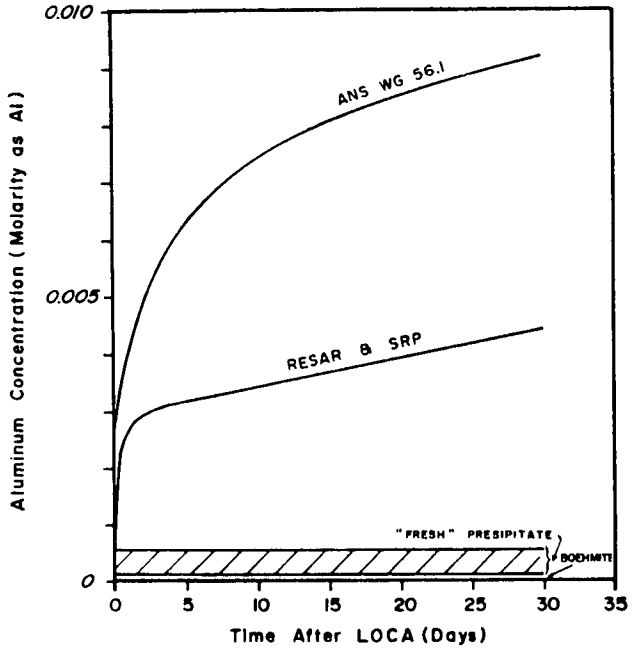


FIGURE 5: ALUMINUM CORROSION AND SOLUBILITY (pH = 8.9)

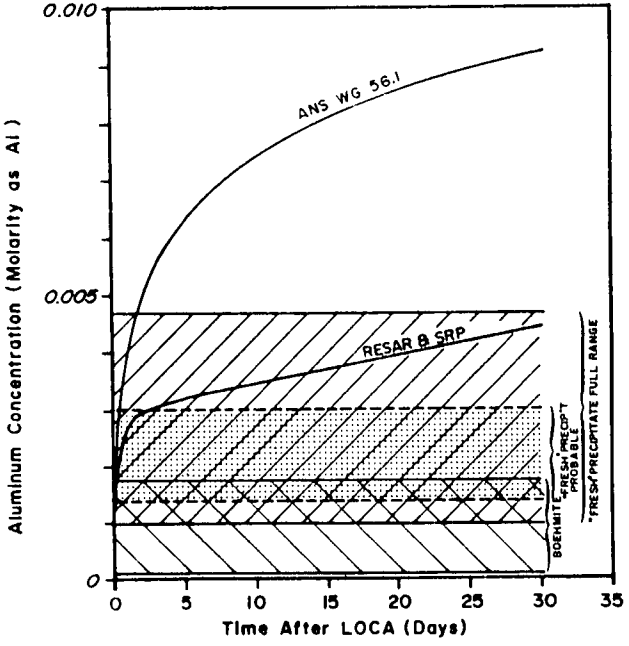
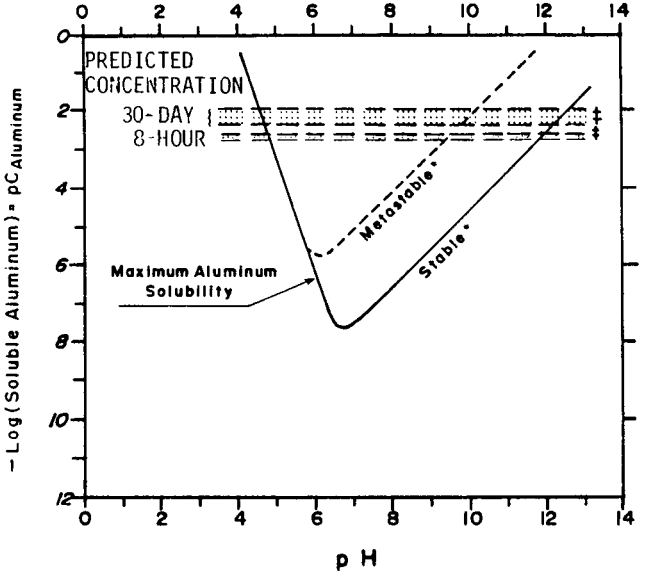


FIGURE 6: ALUMINUM CORROSION AND SOLUBILITY (pH = 9.8)



* REFERENCE FIGURE 3

‡ REFERENCE TABLES 3 & 4

FIGURE 7: ALUMINUM SOLUBILITY LIMITS VS. CORROSION CONCENTRATIONS (IONIC STRENGTH 0.1M)

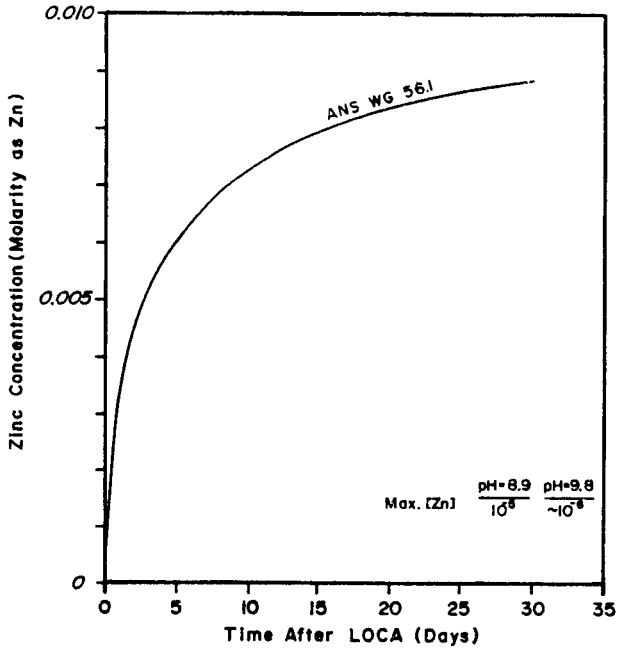
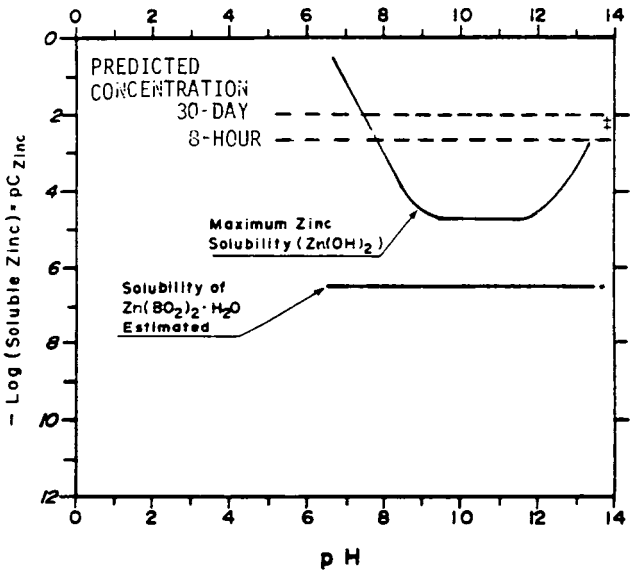


FIGURE 8: ZINC CORROSION AND SOLUBILITY (pH = 8.9, 9.8)



* REFERENCE FIGURE 4
‡ REFERENCE TABLE 5

FIGURE 9: ZINC SOLUBILITY LIMITS VS. CORROSION CONCENTRATIONS (IONIC STRENGTH = 0.1M)

THE IMPORTANCE OF TEMPERATURE, pH, AND BORIC ACID CONCENTRATION ON RATES OF HYDROGEN PRODUCTION FROM GALVANIZED STEEL CORROSION

V. M. Loyola

Division 2513

Sandia National Laboratories

Prepared for
Office of Nuclear Regulatory Research
U. S. Nuclear Regulatory Commission
Washington, D. C. 20555

Introduction

One of the known sources of hydrogen gas within a nuclear plant containment building during a LOCA is the high temperature corrosion of galvanized steel according to reactions of the type shown in Equations 1 and 2.

$$Zn + H_2O \rightleftharpoons ZnO + H_2 \quad (1)$$

$$Zn + 2H_2O \rightleftharpoons Zn(OH)_2 + H_2 \quad (2)$$

The importance of this source of hydrogen will vary depending on the severity of the accident. In an accident which resulted in core degradation, for example, the major source of hydrogen would probably be the metal-water reaction of the zircaloy cladding according to Equation 3,

$$Zr + 2H_2O \rightleftharpoons ZrO_2 + 2H_2 \quad (3)$$

and the corrosion of galvanized steel would then become a relatively minor source of hydrogen. However, in an accident in which core degradation is avoided or limited to minor damage, the corrosion of galvanized steel, and presumably of other materials as well, would then become a major contributor to the buildup of hydrogen within containment. It is important, therefore, to know how much hydrogen can be generated by these sources and how fast it can be expected to do so.

Chemical reactions of all types, including reactions 1 and 2, are generally affected by changes in temperature, pH, and the presence chemical additives. Furthermore, unlike the effect of temperature, which generally tends to accelerate a reaction as it is raised, the effects of pH and chemical additives are not as readily predicted. In a system where two, and possibly more, reactions are operating simultaneously it becomes increasingly difficult to predict an overall

response to a change in reaction conditions. For a system such as Equations 1 and 2 one could reasonably expect a different response from each reaction to the same change in parameters; thus, one might expect the overall rate of hydrogen generation to exhibit a more complex dependence to that change than either one of the reactions alone. The purpose of this study was to determine the overall effects of temperature, pH, and boric acid concentration on the rate of hydrogen generation over a broad range of each parameter, and not to do a detailed study of the effects of each parameter.

Approach

In order to attain our goal, we selected a factorial experiment, shown schematically in Figure 1, designed to identify the important parameters, and their interactions, and to rank them in order of importance. The experimental design and treatment of results is well documented in the literature[1] and will not be discussed here. Only the results and conclusions will be discussed. The factorial design measures the response of the system, i.e., the hydrogen generation rate constant, for various combinations of the three parameters, represented by the corners of the cube in Figure 1, and uses statistics to determine which parameters and interactions are important and which are not. Figure 1 shows that the ranges for the three parameters were 48°C to 168°C for the temperature, 4.0 to 10.0 for the pH, and 2000 ppm to 4000 ppm for the boric acid (measured as total boron). The measured rate constant, and the uncertainty at any one corner of the cube, is mathematically compared to the values obtained at all of the other corners in order to determine whether an observed difference is statistically significant or within the experimental error of the system. For example, Table 1 summarizes the results of this work and gives the

measured rate constants, and their uncertainties, for each set of conditions. Comparison of the results obtained at low temperature to those obtained at high temperature indicates that a change of about two orders of magnitude can be expected for the rate constant over this temperature range. On the other hand, comparison of trials 1 and 3 at low temperature and pH 4 and trials 6 and 8 at high temperature and pH 10.0 shows that a change in boric acid concentration from 2000 ppm boron to 4000 ppm boron does not result in a statistically-significant change in rate constant in either case. In both cases, the measured rate constants are within experimental error of each other.

The factorial design also allows for testing at conditions which correspond to the combined mid-points of the three parameters. Those conditions are shown as the center point of Figure 1 and the results obtained are trial 9 of Table 1. The center point result is used to determine if the response, i.e., the rate constant in our case, is a nonlinear function of one or more of the parameters. Unfortunately, the factorial experiment does not produce sufficient data to allow us to identify the parameter, or parameters, inducing the curvature. In our case nonlinearity is indicated and could be due to temperature and/or pH.

Experimental Details

The corrosion reactions were carried out in a stainless steel vessel, shown schematically in Figure 2, which was designed specifically for this work. The reactor is comprised of two major parts: a condenser which is the upper portion of the Figure 2, and a boiler which is the lower portion of Figure 2. The sample to be tested is placed in a sample holder, shown as number 9 in Figure 2, and isolated from its surroundings until the test commences. With the sample and

sample holder in place the boiler is filled with the solution of interest and attached to the condenser. Heat is applied to the boiler by a resistance heater which is wound around the outer surface of the boiler, and is regulated by a temperature controller via a thermocouple (No.11, Figure 2), which is immersed in the solution. All flange seals are made leak tight with high-temperature, steam-service O-rings, number 2 in Figure 2. When the solution has reached the temperature of interest, the reaction is initiated by exposing the sample to the hot solution. The hydrogen generated by the corrosion reaction will rise, along with the hot water vapor, into the upper portion of the vessel; the water vapor will condense on the relatively cool walls of the condenser and flow back into the boiler, thereby providing convective mixing of the internal atmosphere.

The rate of hydrogen generation was measured by a gas chromatograph which was programmed to periodically sample the internal atmosphere and to perform a hydrogen analysis. Each test was carried out over a twenty-four hour period, and the results of one such test are shown in Figure 3.

Discussion and Conclusions

Figure 3 shows a nearly linear increase in hydrogen concentration over the entire test period; this implies a constant rate of hydrogen generation for this set of conditions. At other conditions, the early part of the reaction shows a short induction period which makes a linear rate constant somewhat more difficult to fit. The complete test results are summarized in Table 1 and, as discussed above, indicate that the temperature is a very important parameter and that boric acid concentration is not. Table 1 also shows that, within experimental error,

the worst case conditions are high temperature and high pH (trial 8, Table 1). Figure 4 shows an Arrhenius plot of the data of Table 1 and contrasts our results to those of other workers. Our rate constants are consistently higher than those measured by other workers; part of the discrepancy may be due to differences in experimental approach. Much of the data collected in the literature was not collected at isothermal conditions, the samples were immersed in the test solution during heating to test conditions and the quantity of hydrogen generated was measured only after the test was complete. Also, some of the other data are for zinc suspended in a paint-like coating.

In any case, the statistical evaluation of the data gives the following results:

(1) The important parameters are temperature and pH, with the temperature dependence being approximately four times as great.

(2) The important interactions are temperature/pH, temperature/pH/boric acid, and pH/boric acid. The importance of these interactions is approximately the same, and considerably less than that of temperature.

(3) The dependence on boric acid concentration and on the temperature/boric acid interaction are statistically insignificant.

Having determined that the temperature and pH are the most important factors for hydrogen generation, one can now take the rate constant for the worst case conditions (trial 8, Table 1) and carry out hypothetical calculation. For a reactor containment building having the following characteristics[3] -- Height 185 ft., free volume of 2.03×10^6 ft^3, and 15,601 lbs of zinc as galvanized steel over a surface area of 137,971 ft^2 -- one could expect to generate 131 standard

cubic meters of hydrogen per hour. This is assuming that all of the galvanized steel is immersed in the spilled solution, an assumption which is obviously conservative. At this rate, after the first hour the containment air would have a 0.2% hydrogen concentration and the hydrogen concentration would be expected to increase to approximately a 5% level only if accident mitigation did not occur for 24 hours. The calculation assumes complete and efficient mixing of the containment atmosphere and makes no corrections for the presence of steam. In any case, the present work indicates that, for this containment at worst case conditions, the corrosion of galvanized steel alone could become a hazard if accident mitigation were delayed.

References

1. Strategy of Experimentation, Applied Technology Division; E.I. DuPont de Nemours and Co. (1975).

2. (a) G. P. Wachtell; Test of Materials in a Simulated Reactor Containment Post-Accident Steam Environment; FIRL Report F-C2928; January 1971.

   (b) H. E. Zittel; Post-Accident Hydrogen Generation from Protective Coatings in Power Reactors; Nuclear Technology; Vol. 17, February 1973.

   (c) NUS Report, NUS: CD-SET-112; March 1977.

   (d) L. Wichter, E. Hillman, and R. Yaeger; Hydrogen Evolution from Zinc Corrosion Under Simulated Loss-of-Coolant Accident Conditions; FIRL Report F-C4290, August 1976.

   (e) J. R. Lopata; Control of Containment H_2 Levels Evolved from Zinc Primers During a LOCA; Power Engineering, November 1974.

3. Data are for San Onofre Nuclear Generating Station, Units 2 and 3 from:

   (a) Zinc Inventories in Containment for Some PWR and BWR Power Plants; J. E. Womelsduff, V. M. Loyola; NUREG/CR-2021; SAND81-0688 AN; Sandia National Laboratories (1981).

   (b) License Application, Final Safety Analysis Report; Southern California Edison Company; 21 March 1977.

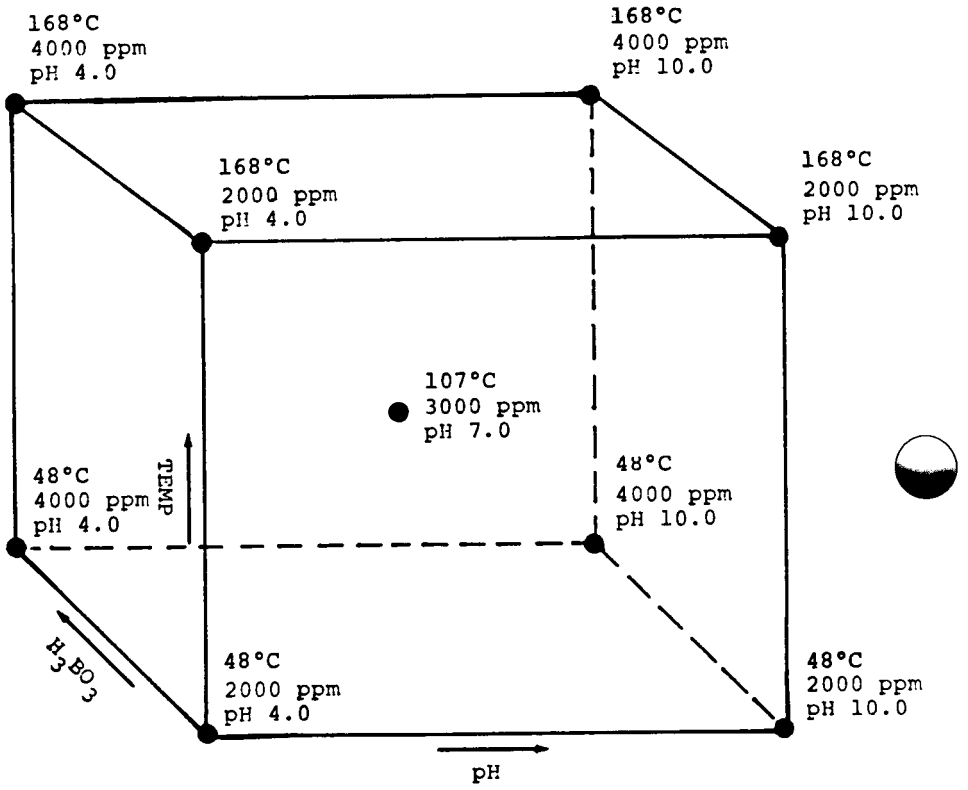
Table 1. Averaged Results for Two-Level, Three Factor Factorial Experiment

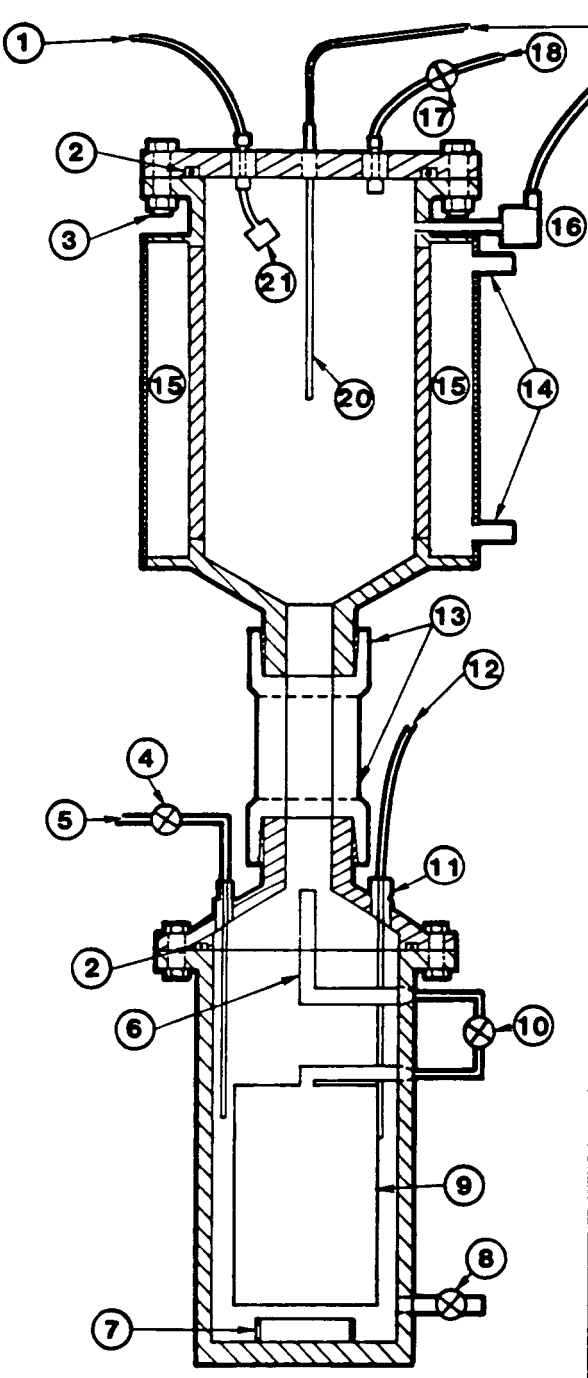
Trial	Temp., ^{o}C	pH	H_3BO_3 (ppm B)	Rate Const. (SCM/m^2-hr)
1	47.2 $\pm$ 3.5	4.0	2000	1.92 $\pm$ 1.02 x 10^{-5}
2	47.8 $\pm$ 2.6	10.0	2000	1.80 $\pm$ 0.39 x 10^{-5}
3	46.8 $\pm$ 3.4	4.0	4000	2.19 $\pm$ 0.64 x 10^{-5}
4	48.0 $\pm$ 3.4	10.0	4000	1.10 $\pm$ 0.43 x 10^{-5}
5	168.0 $\pm$ 1.3	4.0	2000	7.22 $\pm$ 1.46 x 10^{-3}
6	167.4 $\pm$ 1.2	10.0	2000	8.32 $\pm$ 1.57 x 10^{-3}
7	167.1 $\pm$ 0.9	4.0	4000	3.96 $\pm$ 0.87 x 10^{-3}
8	167.0 $\pm$ 1.5	10.0	4000	10.24 $\pm$ 1.87 x 10^{-3}
9	107.5 $\pm$ 2.8	7.0	3000	4.40 $\pm$ 1.32 x 10^{-4}

Figure 1

TWO-LEVEL, THREE-FACTOR EXPERIMENT

PARAMETER FORMAT: TEMP. / H_3BO_3 / pH





LEGEND	
1	G.C. 1/16 s.s. TUBE
2	O-RING SEAL
3	0.375" BOLTS 304 s.s.
4	METERINGVALVE
5	TO PRESSURIZED FRESH SOLUTION RESERVOIR
6	EVACUATING TUBE FOR SAMPLE HOLDER
7	RETAINER CUP FOR MAGNETIC STIR BAR
8	METERING VALVE FOR SAMPLING HOT SOLUTION
9	SAMPLE HOLDER
10	BELLOWS VALVE
11	THERMOCOUPLE IN COMPRESSION FITTING
12	TO TEMP. CONTROLLER AND RECORDER
13	1.500-11.5 NPT
14	COOLANT INLET & OUTLET 1/4" s.s.
15	AIR
16	PRESSURE TRANSDUCER
17	s.s. BALL VALVE
18	TO AIR BOTTLE
19	TO RECORDER
20	s.s. CLAD 1/16" THERMOCOUPLE FOR MEASURING VAPOR PHASE TEMP.
21	s.s. FRIT

Figure 2. Stainless Steel Vessel for Corrosion of Galvanized Steel Measurements

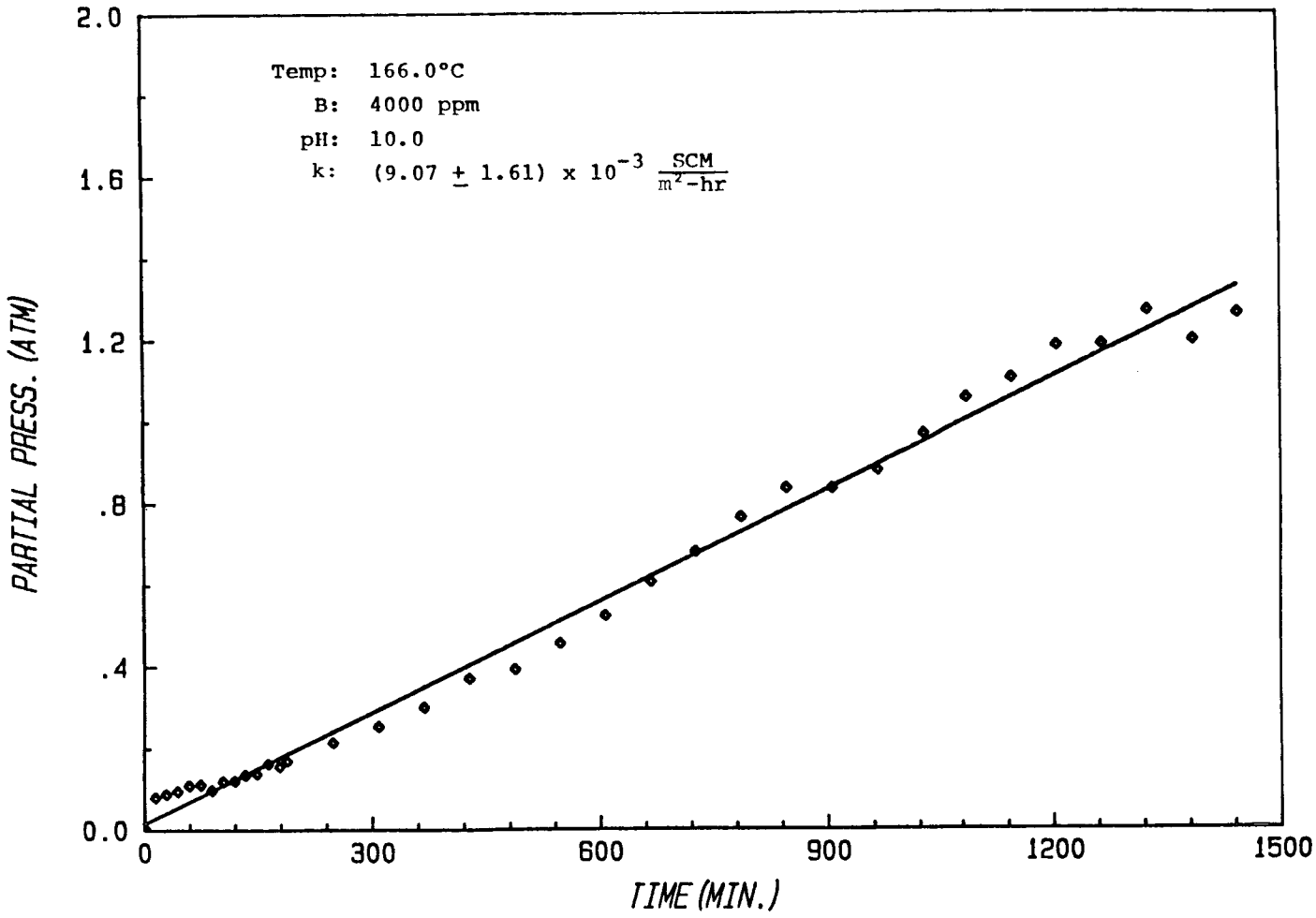


Figure 3

Hydrogen Generation from Corrosion of Galvanized Steel

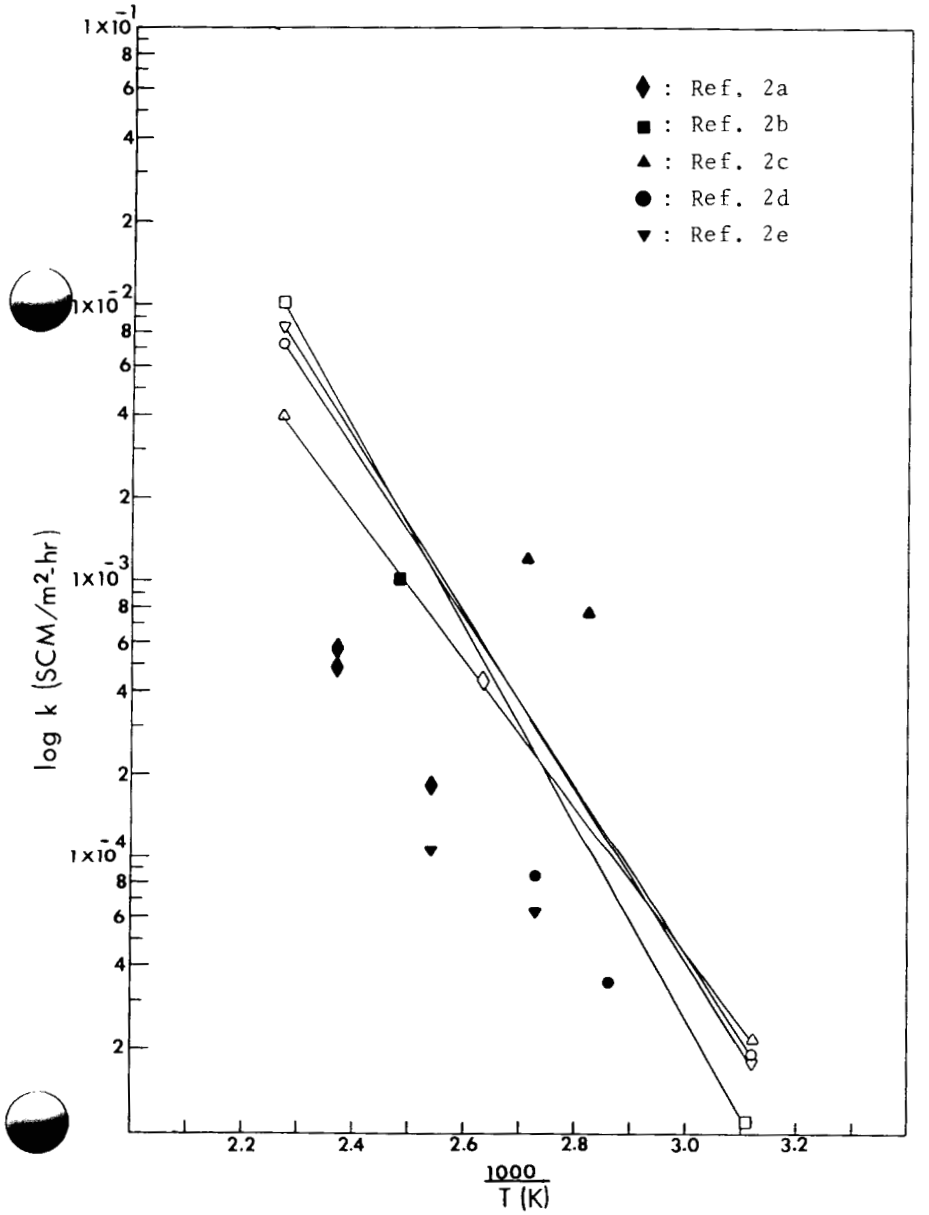


Figure 4. Comparison of data from this study to literature values. Data from this study are shown as unfilled geometric figures.

HYDROGEN GENERATION FROM ALUMINIUM CORROSION IN REACTOR CONTAINMENT SPRAY SOLUTIONS

by

W. Frid
Swedish State Power Board

and

G Karlberg, S B Sundvall
Studsvik Energiteknik AB, Sweden

ABSTRACT

The aluminium corrosion experiments in reactor containment spray solutions, under the conditions expected to prevail during LOCA in BWR and PWR, were performed in order to investigate relationships between temperature, pH and hydrogen production rates.

In order to simulate the conditions in a BWR containment realistic ratios between aluminium surface and water volume and between aluminium surface and oxygen volume were used.

Three different aluminium alloys were exposed to spray solutions: AA 1050, AA 5052 and AA 6082.

The corrosion rates were measured for BWR solutions (deaerated and aerated) with pH 5 and 9 at 50, 100 and 150°C. The pressure was constantly 0.8 MPa. The hydrogen production rate was measured by means of gas chromatography.

In deionized BWR water the corrosion rates did not exceed about 0.05 mm/year (2 mpy) in all cases, i.e. were practically independent of temperature and pH. Hydrogen concentrations were less than 0.1 vol. % in cooled dry gas.

Corrosion rates and hydrogen production in PWR alkaline solution measured at pH 9.7 and 150°C were very high.
AA 5052 alloy was the best material.

1. BACKGROUND

The main goal of experiments described in this paper was to investigate the contribution of aluminium corrosion to hydrogen production after a loss of coolant accident (LOCA) in the older Swedish BWRs where aluminium amounts are considerable.

Due to the lack of experimental data on aluminium corrosion rates in BWR spray solutions, especially at elevated temperatures, it was very difficult to calculate the contribution of this hydrogen source to the total hydrogen production after LOCA. A parametric study /1/ was performed where the

experimental data obtained by Griess and Bacarella in 1971 /2/ were extrapolated to conditions which are expected to prevail in BWR containments after LOCA.

The hydrogen amounts obtained in this way were relatively high having negative effects on the recombiner system in terms of higher thermal loads and earlier start demands.

The problem of aluminium corrosion was found especially important when the inerted BWR containment is temporary filled with air.

2. INTRODUCTION

A BWR station like Forsmark 1 contains about 4 000 m^2 of aluminium surface as the heat insulation sheet. The volume of the containment is 6 900 m^3 containing 3 000 m^3 water. The spray water initially will have a pH of about 8 due to manual LiOH addition but may decrease to pH 5.6 if spraying is performed without pH adjustment. The temperature will vary between 150 and 50°C.

In the unlikely event of loss of coolant accident in a nuclear power plant the containment spray systems will be used for pressure reduction and fission product absorption. Aqueous sodium borate solutions at a pH of about 9 (PWR) or neutral water (BWR) will be used at temperatures up to 150°C. In the open literature insufficient data are published to establish highly accurate and reliable relationships between temperature and hydrogen formation rates during corrosion of aluminium alloys. Under neutral, non-borated conditions, there are even fewer available data than from alkaline solutions (1, 3).

The thermodynamic suppositions of aluminium to react with hydrogen release can be visualized in a potential-pH diagram. MacDonald and Butler (4) in a series of such diagrams show the obvious effect of temperature on the ability of the metal to form a protective passive film. Figure 1 is valid for 150°C and shows that passivity then is possible only between pH 2 and 5. At a higher pH aluminium dissolves to AlO_2^- with H_2 formation and oxygen consumption.

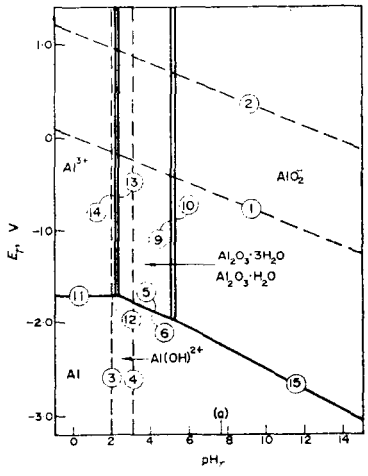


Figure 1 - Potential-pH diagram for the aluminium-water system at 150°C. (a) refers to the pH of a 10^{-4} M OH^- solution (4).

Experimental work on corrosion of aluminium in spray solutions has been published by Griess and Bacarella (2). They used alkaline borate solutions (0.15 M NaOH + 0.28 M H_3BO_3) either with or without sodium thiosulfate (0.064 M) added in order to simulate PWR conditions. At 55°C the data indicated essentially constant corrosion rates of 130 - 190 mpy (3.3 - 4.8 mm/year) in the spray and 45 - 87 mpy (1.1 - 2.2 mm/year) on submerged specimens after a brief period of accelerated attack. At 100°C the only aluminium alloy that showed relatively good corrosion resistance was 5052 aluminium. At 140°C this alloy was the only one tested. During 24 hours the weight losses were about 20 mg/cm^2 in the spray and 16 mg/cm^2 in the solution. The 5052 alloy thus corroded much less than other aluminium alloys tested at higher temperatures but at about the same rate as the other ones at lower temperatures.

Berzins et al (5) studied aluminium BS S1B in deionized water of pH 5 - 8 at 50°C with oxygen or nitrogen as cover gas. The mirror-bright specimens became dulled and in some cases developed a chalky film on the surface within a few days but the weight gain was low, in the order of $50 \cdot 10^{-5}$ g/cm^2/ /10 days (0.06 mm/year).

3. EXPERIMENTAL

The following three alloys were tested with normal delivery surface finish:

Standards			Al	Mg	Mn	Si
SS 4007	BS S1B	AA 1050	≥99.50			
SS 4120	BS NS4	AA 5052	97.2	2.5		
SS 4212	BS H30	AA 6082	97.4	0.9	0.7	1

Triplet specimens were exposed just once and were degreased prior to exposure. The specimens were cut from sheet to the dimensions 50 x 20 x 2 mm with a hole 7.2 mm in diameter, resulting in a specimen surface of 22.4 cm^2.

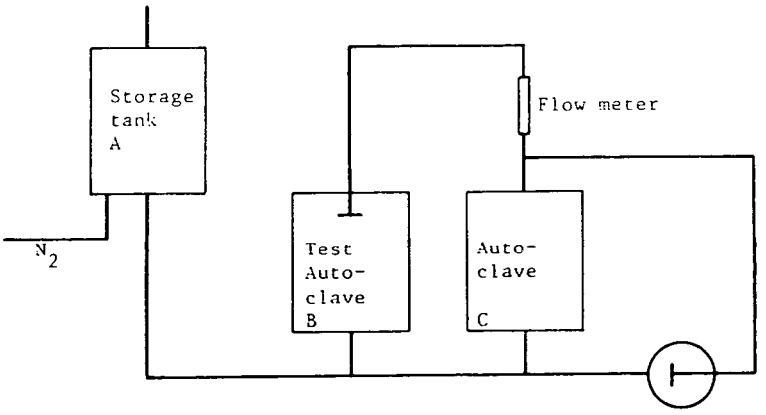


Figure 2 - Test equipment

Figure 2 shows the test equipment. Deionized water was aerated or deaerated in the vessel A. B and C were two titanium lined 37 dm^3 autoclaves. Water could be pumped from C to the top of B where it was sprayed into the autoclave. B was half filled with water and half with nitrogen gas or air. The specimen holder in autoclave B had room for 48 specimens of which 24 specimens were in the spray zone above the water surface. The specimens were electrically insulated. During heating and cooling the spray was cut off and the holder put in an upper position where all specimens were above the water surface.

pH could be measured and adjusted if necessary. The temperature was 50, 100 or 150°C and the pressure constantly 0.8 MPa. Specimens were taken out from the autoclave after certain times and weighed.

The hydrogen production rate was measured by means of gas chromatography. The 5 ml gas sample from the test autoclave was cooled before the registration of hydrogen concentration.

At Forsmark 1 and Ringhals 1 the ratios between aluminium surface and water volume are 4:3 and 3.6:2.6 m^2/m^3 respectively. 34 specimens inside the autoclave gave the same conditions. In order to simulate the conditions in a containment with 5 % radiolytically formed oxygen in the gas phase we could start with aerated water. With 20 specimens in the autoclave the ratio between aluminium surface and oxygen volume was 12 m^2/m^3 which is comparable to the ratio between aluminium surface and oxygen volume in a reactor.

Tests were performed on the three alloys in deaerated deionized water at pH 5 and 9, in aerated water at pH 9 and in a PWR solution referred to by Griess and Bacarella (2). In order to get the corrosion rates att different temperatures isothermal tests were run at 50, 100 and 150°C.

4. EXPERIMENTAL RESULTS

4.1 BWR solution

4.1.1 Deaerated water at pH 5

The specimens were weighed after 48, 93, 190 and 448 hours exposure in spray and water at 50, 100 and 150°C. All specimens got a grey tarnish. Their weight increases varied between $6 \cdot 10^{-4}$ and $29 \cdot 10^{-4}$ g per specimen independent of position, time, temperature and aluminium grade. Before weighing the specimens were stored in a desiccator for 24 hours. Assuming that the passive layer on the metal consists of Al_2O_3 and that the weight gain increased linearly with time with a rate of $6 \cdot 10^{-4}$ - $29 \cdot 10^{-4}$ g/specimen and 48 hours the corrosion rate was at most 0.046 mm/year (1.8 mpy).

The rate of hydrogen evolution, based on this corrosion rate, is $8 \cdot 10^{-4}$ mol $H_2 \cdot m^{-2} \cdot h^{-1}$.

4.1.2 Deaerated water at pH 9

The experiments were repeated at pH 9 instead of pH 5. The actual potential-pH diagrams may lead to the expectations of considerably increased corrosion rates at least at 100 and 150°C but this was not observed. The maximum weight gain at 150°C was 0.0027 g/specimen/48 hours without significant further weight gain after longer exposure times corresponding to a corrosion rate of 0.04 mm/year (1.6 mpy) independent of alloy. Once again the conservative assumption is made that the corrosion rate is equal to the rate during the first 48 hours.

The calculated rate of hydrogen evolution is $7 \cdot 10^{-4}$ mol $H_2 \cdot m^{-2} \cdot h^{-1}$.

4.1.3 Aerated water at pH 9

The preceding results gave about the same corrosion rates and consequently were obtained under cathodic control. Containment spraying may be performed under aerated conditions however, and Griess and Bacarella also used aerated solutions. Because of that a series was started with aerated water. The temperature was 150°C and the exposure time 20 hours. The oxygen content in the water after this time was measured to 6.5 ppm.

Like in the earlier tests the differences in weight losses between the three alloys were small and in the magintude of 0.08 mm/year (3 mpy). The hydrogen evolution from aluminium corrosion was measured by means of gas chromatography. Eighteen specimens inside the autoclave produced 0.042 volume % H_2 in dry gas after 6 minutes, 0.081 % H_2 after 20 minutes, 0.096 % H_2 after 45 minutes and 0.098 % H_2 after 20 hours (see Figure 3).

The rate of hydrogen evolution, calculated from measured production and averaged over the first hour of exposure, is 0.07 mol·H_2·m^{-2}·h^{-1}.

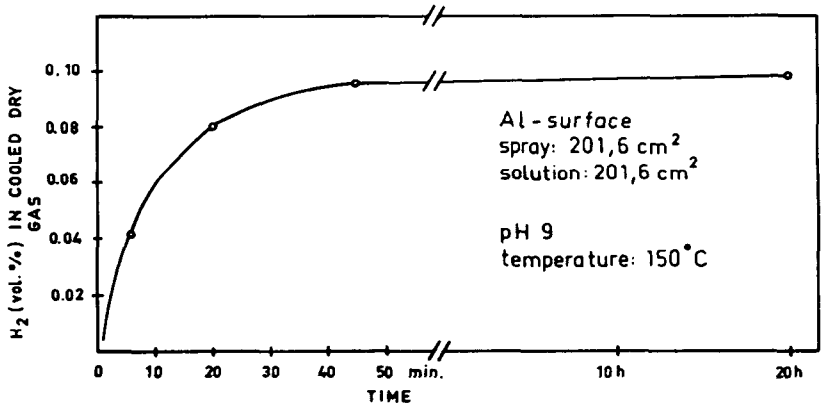


Figure 3 - Hydrogen production, measured in cooled dry gas, due to aluminium corrosion in BWR non-borated spray solution.

4.2 PWR solution

In order to demonstrate the striking difference between the behaviour of aluminium alloys in BWR water and in PWR spray solution, experiments according to those reported by Greiss and Bacarella were performed but with simultaneous registration of hydrogen evolved. The solution contained 0.15 M NaOH and 0.28 M H_3BO_3. pH was measured to 9.7 before the temperature was increased to 150°C.

After 15 minutes 18 specimens in the autoclave had produced 3.9 % H_2, after 25 minutes 5.0 % H_2 and after 35 minutes 7.8 % H_2 in cooled dry gas (see Figure 4).

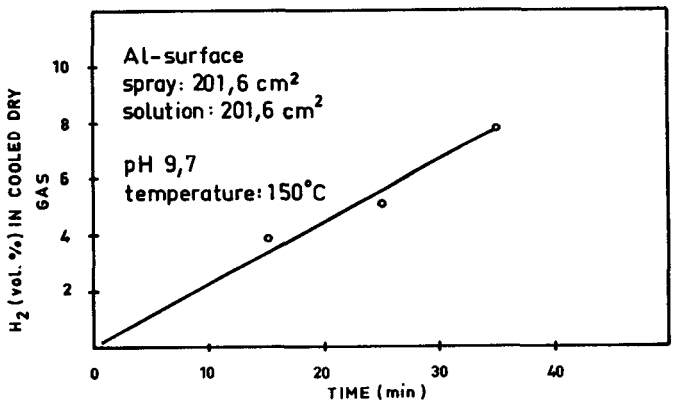


Figure 4 - Hydrogen production, measured in cooled dry gas, due to aluminium corrosion in PWR spray solution.

In this alkaline environment with high conductivity a clear difference was seen between the corrosion rates of the alloys. The mean value of AA 1050 in spray was 0.45 g/specimen/35 minutes and in water 0.46 g/specimen/35 minutes. Corresponding corrosion rate is 570 mm/year ($2.28 \cdot 10^4$ mpy). For AA 5052 and AA 6082 the corresponding values were 0.06, 0.04 (spray) and 0.25, 0.23 g/specimen/35 minutes (water), respectively. Corresponding corrosion rates are 63 mm/year ($2.5 \cdot 10^3$ mpy) for AA 5052 and 300 mm/year ($1.2 \cdot 10^4$ mpy) for AA 6082. Corrosion rates are summarized in Table 1. AA 1050 got a white appearance, AA 5052 was light brown with white spots on specimens exposed to the spray. AA 6082 became grey and white when exposed to the spray, and brown and white when exposed in water.

The rates of hydrogen evolution, calcultated from corrosion rates and measured, are given i Table 2.

5. DISCUSSION

A. The objective of hydrogen concentration measurement was to verify the reliability of hydrogen production calculations based on aluminium corrosion rates. Registration of hydrogen was performed only in two tests: for BWR solutions at pH 9, 150°C and for PWR solutions at pH 9.7, 150°C. The pressure in autoclave was 0.8 MPa.

TABLE 1

PWR solution. Corrosion rates

Alloy	Corrosion rate (mm/year)*
AA 1050	570
AA 6082	300
AA 5052	63

t = 150°C
pH 9.7

* 1 mm/year = 40 mpy

TABLE 2

PWR solution. [illegible] of H_2 evolution

Alloy	Calculated rate (mol $H_2 \cdot m^{-2} \cdot h^{-1}$)*
AA 1050	10.0
AA 6082	5.2
AA 5052	1.1

t = 150°C
pH 9.7

Measured rate of H_2 evolution (averaged over 35 minutes for three alloys):

$$5 \text{ mol } H_2 \cdot m^{-2} \cdot h^{-1}$$

* 1 mol $H_2 \cdot m^{-2} \cdot h^{-1} = 7.3 \cdot 10^{-2}$ SCF $H_2 \cdot ft^{-2} \cdot h^{-1}$

Hydrogen evolved due to aluminium corrosion is distributed in the gas and water phases of the autoclaves. Hydrogen amounts and partial pressure p_{H2} in the gas phase is easily calculated from measured concentrations in cooled dry gas using the ideal gas law.

The amount of hydrogen which is dissolved in the water phase is calcultated applying Henry's law.

$$p_{H2} = H(T, p) \cdot x_{H2}$$

where p_{H2} - partial pressure of hydrogen in gas

x_{H2} - mole fraction of hydrogen in liquid

$H(T, p)$ - Henry constant

Due to the fact that the Henry constant is a weak function of pressure the effect of pressure is neglected.

The Henry constant is obtained from /6/. For temperature ranges between 151°C and 374°C:

$$H = -9.01 \cdot 10^4 + 5.83 \cdot 10^7 / T$$

Table 3 shows the hydrogen amounts calculated with two different methods under the assumption that the passive layer on the aluminium specimens consists of Al_2O_3.

TABLE 3

Comparison between hydrogen amounts obatined from gas chromatography measurement and calcultated from aluminium corrosion rates. Aluminium surface is 403.2 cm^2.

Spray solution	H_2 (mg) Gas	H_2 (mg) Water	H_2 (mg) Total	H_2 (mg) $2Al+3H_2O \rightarrow Al_2O_3+3H_2$
BWR after 20 h pH 9 t = 150°C	3.4	0.4	3.8	2.5
PWR after 35 min pH 9.7 t = 150°C	240	10	250	268

As expected the hydrogen amounts dissolved in water are very small.

Data in Table 3 indicates that calculation of hydrogen production based on corrosion rates gives reasonable results, under the assumption that corrosion products consists of Al_2O_3.

B. In deionized water a more or less passivating film forms which results in a weight gain of the specimens, the velocity of which decreases with time. Even if one supposes that the corrosion rate is the same as during the first 24 hours the corrosion rate will not exceed 0.05 mm/year which is in good agreement with literature data at 50°C (5).

The conservative corrosion rate of 0.05 mm/year corresponds to a metal loss of 200 dm^3/year in a station (Forsmark 1) or 540 kg/year or 20 kmol/year. The corrosion reaction

$$2Al + 3H_2O \rightarrow Al_2O_3 + 3H_2$$

shows that after 24 hours 0.085 kmol H_2 is formed which occupies 1.9 m^3 ideally at 0°C and atmospheric pressure i.e 0.03 % of the gas volume.

Hydrogen concentration in the reactor containment can also be estimated using the measured hydrogen evolution rate i.e. 0.07 mol $H_2 \cdot m^{-2} \cdot h^{-1}$. After one hour the concentration for normal conditions would be 0.09 vol. % and no essential increase is expected based on the experimental results. Direct measurements 20 hours after start of an experiment gave a value of 0.1 vol % hydrogen.

Tests under PWR conditions on the contrary showed very high corrosion rates in good agreement with the results of Griess and Bacarella.

At 150°C AA 5052 was the best material.

SUMMARY AND CONCLUSIONS

In BWR deionized water the three alloys in spray or water give corrosion rates of at most 0.05 mm/year (2 mpy) and hydrogen concentrations less than 0.1 %. On the contrary PWR alkaline solutions give very high corrosion rates and hydrogen contents.

One unexpected result was that aluminium corrosion rates in BWR spray solutions were practically independent of temperature and pH.

In accordance with Regulatory Guide 1.7 the corrosion rate for aluminium exposed to alkaline solution shall be 200 mpy. This value should be adjusted upward for higher temperatures early in the accident sequence.

It means, in view of presented experimental results, that applying Regulatory Guide 1.7 method to BWR non-borated solutions is extremely conservative and should not be used.

The contribution of aluminium corrosion to hydrogen production after LOCA in BWR containments is very small compared with other hydrogen sources such as zirconium-water reaction and radiolysis of water and therefore has no significant effects on combustible gas control systems.

Results of our experiment in PWR aqueous sodium borate solutions at pH 9.7 and temperature 150°C confirm Griess and Bacarella data and support the recommendation of Regulatory Guide 1.7.

ACKNOWLEDGEMENT

This work was financed by the Swedish Nuclear Power Inspectorate. The technical assistance of Mr Jörgen Gjödestöl, Ingemar Larsson and Stig Lindgren is greatfully acknowledged.

REFERENCES

1. FRID, W
Statens Vattenfallsverk EV-20/79
Stockholm (1979).

2. GREISS, J C and BACARELLA, A L
Nucl Technol 10, 546 (1971).

3. VAN ROOYEN, D
Hydrogen release rates from corrosion of zink and aluminium.
Brookhaven Nat Lab, New York (1978).
BNL-NUREG-24532.

4. MACDONALD, D B and BUTLER, P
Corros Sci 13, 259 (1973).

5. BERZINS, A, EVANS, J V and LOWSON, R T
Australian Atomic Energy Commision
AAEC/E270 (1973)
ISBN 0 642 99585 0.

6. The Behaviour of Hydrogen During Accidents in Light Water Reactors.
NUREG/CR-1561
SAND 80 - 1495.

SESSION IV

HYDROGEN TRANSPORT AND MIXING

HEDL-SA-2682

HYDROGEN DISTRIBUTION IN A CONTAINMENT WITH A HIGH VELOCITY HYDROGEN-STEAM SOURCE

G. R. Bloom
L. D. Muhlestein
A. K. Postma
S. W. Claybrook

September, 1982

HANFORD ENGINEERING DEVELOPMENT LABORATORY
Operated by Westinghouse Hanford Company, a subsidiary of Westinghouse Electric Corporation, under the Department of Energy Contract No. DE-AC06-76FF02170
P.O. Box 1970, Richland, Washington 99352

COPYRIGHT LICENSE NOTICE
By acceptance of this article, the Publisher and/or recipient acknowledges the U.S. Government's right to retain a nonexclusive, royalty-free license in and to any copyright covering this paper.

HYDROGEN DISTRIBUTION IN A CONTAINMENT WITH A HIGH VELOCITY HYDROGEN-STEAM SOURCE

G. R. Bloom, L. D. Muhlestein, A. K. Postma and S. W. Claybrook

Westinghouse Hanford Company
Richland, Washington 99352

ABSTRACT

Hydrogen mixing and distribution tests are reported for a modeled high velocity hydrogen-steam release from a postulated small pipe break or release from a pressurizer relief tank rupture disk into the lower compartment of an Ice Condenser Plant. The tests, which in most cases used helium as a simulant for hydrogen, demonstrated that the lower compartment gas was well mixed for both hydrogen release conditions used. The gas concentration differences between any spatial locations were less than 3 volume percent during the hydrogen/steam release period and were reduced to less than 0.5 volume percent within 20 minutes after termination of the hydrogen source. The high velocity hydrogen/steam jet provided the dominant mixing mechanism; however, natural convection and forced air recirculation played important roles in providing a well mixed atmosphere following termination of the hydrogen source.

INTRODUCTION

The presence of hydrogen, following a postulated accident beyond the design basis in a Light Water Reactor, may challenge containment integrity either because of the pressure build-up due to the quantity of hydrogen gas generated, or perhaps more importantly due to the pressure which could result from an uncontrolled hydrogen combustion. Thus, hydrogen generation, distribution, combustion, and control are issues which are addressed in regard to light water reactor safety.

Once hydrogen is assumed to have been generated following a postulated accident sequence, it is important to know how the hydrogen is distributed throughout multi-compartmented regions of a reactor containment as a function of time. Hydrogen distribution, mixing, and stratification play important roles, for example, in determining the location of gas sample sensors and/or hydrogen control devices; analyzing potential trouble areas where gas pocketing may lead prematurely to hydrogen combustion; and designing compartments and/or air recirculation systems to minimize the potential for hydrogen stratification.

The objective of the present program was to determine hydrogen mixing and distribution in simulated light water accident environments, and provide an experimental data base to evaluate analytical methods used to predict the hydrogen distribution. These tests were part of a well integrated Electric

Power Research Institute (EPRI) hydrogen program. Two specific accident scenarios were chosen for the lower compartment region of an ice condenser pressurized water reactor. They were a horizontal hydrogen release from a postulated break of a 5-cm (2-in.) pipe connected to the reactor coolant system, and hydrogen release from the rupture of a 25-cm (10-in.) rupture disk on a pressurizer relief tank. In the second scenario the exit velocity of the steam/hydrogen gas mixture was somewhat slower than the exit velocity for the first case and was directed upward.

MODELING METHOD

Similarity theory was used to apply the results of scale model tests to full-scale prototype systems. One of the inherent requirements of similarity theory is that important physical variables must be identified and incorporated into applicable dimensionless groups which have the same numerical value in the model and in the prototype (1, 2, 3). Modeling is said to be ideal if all dimensionless groups (including geometric scale factors) are identical in the model and in the prototype (4). However, as in this complex model, it is often difficult or impossible to select model test parameters so that all dimensionless groups are identical to those of the prototype. For this reason non-ideal modeling was used and some dimensionless groups were distorted so that reasonably convenient experiments could be carried out to evaluate the dominant controlling phenomena. Dominant similarity parameters were identified and the test conditions selected to yield parameters which were essentially the same in the model as in the prototype. Parameters which were not expected to significantly affect the physical processes of interest were allowed to be distorted.

The lower annular compartment of an ice condenser type reactor is bounded internally by the walls of the reactor cavity. The crane wall forms the outer cylindrical wall of the compartment. This volume is ventilated by air fans which circulate air from the upper containment volume. Air exits from this annular compartment through a series of spring-loaded doors located along the outer cylindrical wall at the ceiling elevation. An examination of this annular volume region, together with the assumed accident scenarios have allowed the dominant mixing processes to be identified. The assumed steam and hydrogen release rates were 544 kg/min (1200 lb/min) and 9 kg/min (20 lb/min) respectively at 316°C (600°F) for both cases.

In the first case, it is postulated that a hot jet of steam-hydrogen gas will exit as a horizontal jet into the annular volume from a 5-cm (2-in.) pipe break. Shortly after the sonic jet exits from the pipe, it will expand, become supersonic and then undergo a supersonic/subsonic transition by means of a normal shock wave. The momentum of this jet will impart motion to much of the fluid in the room, and thereby mix the expelled hydrogen with the surrounding atmosphere. In the near field region (close to the end of the pipe) momentum effects will dominate the mixing processes. However, in the far field (many pipe diameters from the end of the pipe), buoyancy forces will start to play an important role because the gas is significantly less dense than the surrounding atmosphere.

In the second case, hydrogen-steam gas mixtures will exit as a larger, relatively slower speed jet directed vertically from a 25-cm (10-in.) rupture

disk opening on a pressurizer relief tank. While both momentum and buoyancy forces will play a role, buoyancy will be relatively more important for this case than for the higher speed jet. The upward directed momentum of the jet will act along with buoyant forces to distribute the plume in the upper part of the room. Mixing will occur as a result of the initial momentum, that generated by buoyant forces, by forced convection, and by natural convection. Buoyant forces will tend to retard mixing after hydrogen reaches the top of the chamber. The jet momentum will be imparted to the room fluid and will mix the hydrogen with the surrounding atmosphere.

Fans are included in all ice condenser containments to mix upper and lower compartment atmospheres after a loss of coolant accident occurs. Air enters the lower annular room through four openings in the crane wall which forms the outer cylindrical wall of the room. The air enters at low velocity, and is appreciably cooler and more dense than the atmosphere in the annular room. The relatively low momentum of this stream, combined with its significant negative buoyancy, will cause a downward flow of inlet air to the bottom of the room.

Natural convective flows develop along walls if temperature differences exist between the wall and the bulk gas. The temperature differences which apply to the two accident scenarios were not explicitly specified, but it was judged that temperature differences of at least a few degrees would persist throughout the accident cycle. Mixing of the room atmosphere would be enhanced by momentum generated from buoyancy forces due to the temperature differences.

The degree of mixing that is caused by the hydrogen-steam jet can be expected to vary with time. The time available for mixing within the annular compartment depends on the turn-over time of the atmosphere. The scaled times for the jet and the volumetric turn-over should be equal. Relative time was defined for the jet as the length divided by the velocity. For the ventilation flow the relative time was defined as the volume divided by the volumetric flow rate. The criterion was that the ratio of these two times be the same in the model as in the plant. Note that the volumetric flow rate is the sum of recirculation air flow rate and jet flow rate which included hydrogen plus steam.

For the preceding mixing process, the following modeling criteria were adopted for the hydrogen mixing test program:

1. Preserve geometric similarity - all length ratios were preserved with a 0.3 linear scale factor.

2. Preserve densimetric Froude Number of the jet and four inlet air recirculation plumes. This criterion determined the steam and helium mass flow rates.

3. Preserve scaled relative times because of the competing mixing processes.

4. Preserve the density ratio of the expanded jet to the ambient atmosphere.

The model compartment was designed and test conditions were determined based on the above modeling criteria. This resulted in the time scale of the mixing process for the test compartment being 1.7 times faster than the time scale of the reactor mixing process.

The calculated modeling parameters for the reference plant and the target modeling parameters for the test are listed in Table 1.

TABLE 1

COMPARISON OF PARAMETERS FOR PLANT AND TESTS

	Mixing Process Time Scale	Modeling Parameters: Length	Froude Number: Jet	Froude Number: Recirculation	Density Ratio: Jet	Density Ratio: Recirculation
Reference Plant	1.0	1.0	200	0.5	0.44	1.5
Test	0.6	0.3	200	0.5	0.45	1.1

TEST FACILITY DESCRIPTION

The test compartment, which simulated a simplified lower compartment area of an ice condenser plant, was fabricated in the lower area of the Containment System Test Facility (CSTF) vessel. The vessel is 20.4 m (67 ft) high, 7.6 m (25 ft) in diameter, with a volume of 850 m^3 (30,000 ft^3). The horizontal jet nozzle simulating a break of a 5-cm (2-in.) pipe was located 25° from one radial wall of the annulus. The vertical jet nozzle simulating the release from the 25-cm (10-in.) rupture disk on a pressurizer relief tank was directed vertically into the test compartment at 120° from the radial wall. A blower was used to recirculate air from the upper to the lower compartment atmospheres. The size and location of the air inlet ducts were scaled, as far as possible, from the reference plant design, except the air register was internal to the vessel walls.

The test compartment conformed to the modeling criteria but did not contain the many geometrical objects such as pipes, tanks, or structural elements that are present in the plant. The test vessel outer walls simulated the plant crane wall, and the height to diameter ratio of the test compartment was equal to that of the reference plant design. Figure 1 is a schematic of the annular test compartment. In the reference plant air flow is from the fan rooms to the lower compartment. The air flow rate, determined by the modeling criteria to be 104 m^3/min (3730 ft^3/min), was distributed through four openings each 0.73 m (2.4 ft) in height by 1.41 m (4.63 ft) wide at a velocity of 0.43 m/sec (1.40 ft/sec).

The outlet air flow passages, which represented the partially opened ice compartment doors were 24 vertical slots 0.64-m (2.1 ft) high by 4.3-cm (1.7-in.) wide. The slots were made in the wall of circular duct segments suspended from the ceiling of the compartment and equally spaced along the periphery of the compartment, over the 300° segment.

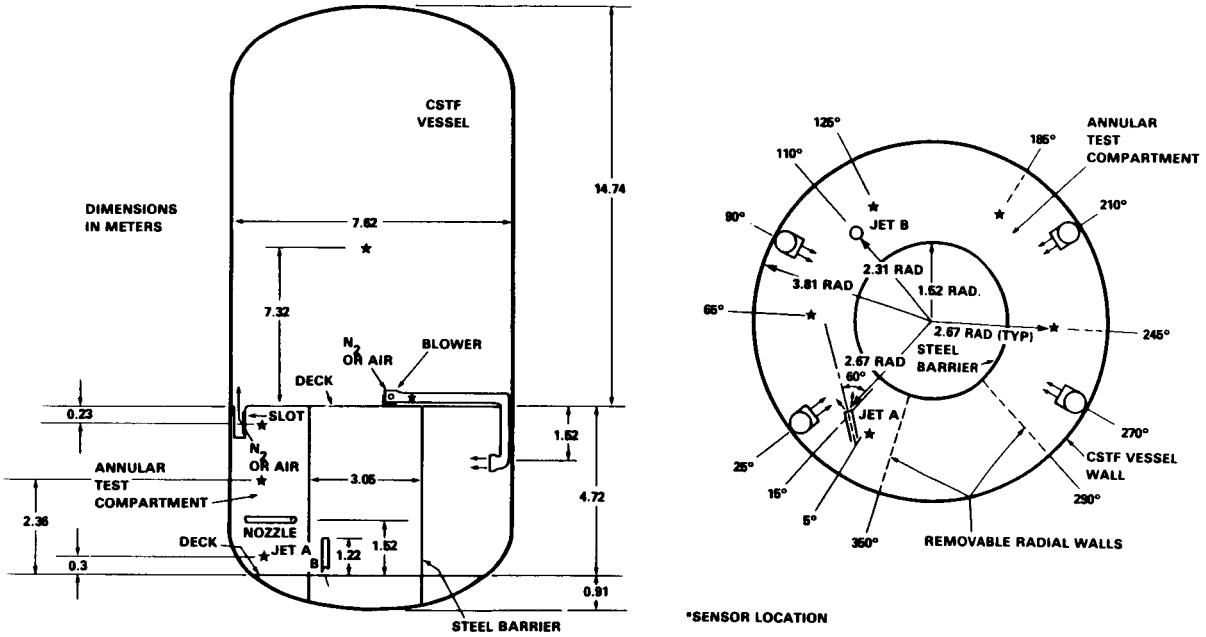


Figure 1. Test Compartment Geometry

The hydrogen and helium concentrations in the test compartment were measured continuously by 12 gas sampling systems which provided constant gas sample flow from the sample points to the gas analyzers. Gas velocities in the test compartment were measured using 10 hot film anemometer systems.

TEST DESCRIPTION

Gas mixing and distribution characteristics were determined for three general types of tests listed in the Test Matrix of Table 2; preliminary, high velocity horizontal jet release, and high velocity vertical jet release. The preliminary tests without a jet release involved air only, while a helium-steam release into air or a hydrogen-steam release into nitrogen were incorporated with the jet release tests. The test conditions of Table 2 were target conditions only and actual test conditions varied from these values. Hydrogen or helium concentrations, gas velocities, and temperature profiles were measured during simulations of two hydrogen release scenarios.

The objective of the four preliminary tests (HMP-1 through HMP-4) was to determine the separate and combined effects of natural and forced air recirculation on gas mixing in the annular compartment. Tests HMP-1 and HMP-2 had relatively lower natural convection effects due to the smaller temperature difference between the bulk air and the vessel wall. Tests HMP-3 and HMP-4 were conducted with the bulk air temperature elevated which increased the temperature difference across the air boundary layer next to the wall and increased natural convection effects on gas mixing. Tests HMP-2 and HMP-4 were provided with forced air recirculation scaled to simulate the air recirculation provided to the ice condenser plant lower containment region.

Mixing tests HM-1 through HM-5 were all simulations of a steam-hydrogen release from a 5-cm (2-in.) pipe break. The tests included cases with and without air recirculation. Air recirculation is normally provided during an accident scenario for an ice condenser lower containment region. Tests HM-1 and HM-3 were conducted with helium-steam release rates arbitrarily set at one half the reference release rate to determine the effect of reduced jet momentum on mixing in the test compartment volume. Mixing test HM-5 was modeled to be "similar" to HM-4 with the difference that hydrogen was used as the source gas and nitrogen was used as the containment gas. This test was conducted to demonstrate that helium was a valid simulant for hydrogen in these tests.

The final tests, HM-6 and HM-7, simulated a vertical hydrogen steam jet release directed upward from a location geometrically similar to that of a pressure relief tank rupture disk vent. The helium-steam source rates were identical to those of tests HM-3 and HM-4, respectively. These test flow rates were representative of the releases from a 5-cm (2-in.) pipe break, as well as a rupture of the pressure relief tank rupture disk.

RESULTS AND DISCUSSION

Preliminary Tests

The preliminary tests demonstrated the separate and combined effects of

TABLE 2

HYDROGEN MIXING TEST MATRIX AND TARGET CONDITIONS

Test No.	Cont. Gas	Recirc. Flow M^3/Min	Recirc. Flow (Ft^3/Min)	Source Gas	He or H_2 Steam Flow kg/Min	He or H_2 Steam Flow (lb/min)	Steam Flow kg/Min	Steam Flow (lb/min)	Initial Lower Cont. Gas Temp. °C	Initial Lower Cont. Gas Temp. (°F)
Preliminary Tests										
HM-P1	Air	0	0	---	---	---	---	---	29	(85)
HM-P2	Air	104	(3700)	---	---	---	---	---	29	(85)
HM-P3	Air	0	0	---	---	---	---	---	66	(150)
HM-P4	Air	104	(3700)	---	---	---	---	---	66	(150)
High Velocity Horizontal Jet Tests										
HM-1	Air	0	0	He-Steam	0.4	(0.9)	12.3	(27)	66	(150)
HM-2	Air	0	0	He-Steam	0.8	(1.8)	24.5	(54)	66	(150)
HM-3	Air	104	(3700)	He-Steam	0.4	(0.9)	12.3	(27)	66	(150)
HM-4	Air	104	(3700)	He-Steam	0.8	(1.8)	24.5	(54)	66	(150)
*HM-5	N_2	104	(3700)	H_2-Steam	*0.4	(0.9)	24.5	(54)	66	(150)
High Velocity Vertical Jet Tests										
**HM-6	Air	104	(3700)	He-Steam	0.4	(0.9)	12.3	27	66	(150)
HM-7	Air	104	(3700)	He-Steam	0.8	(1.8)	24.5	54	66	(150)

* Actual H_2 release rate was ∿0.3 kg/min (0.66 lb/min).

** Actual He release rate was ∿2 x target during last 1 minute of jet release.

natural convection due to temperature differences and forced convection due to air recirculation. Averaged gas velocities in the test compartment for the floor, middle, and top regions are summarized in Table 3.

TABLE 3

SUMMARY RESULTS OF PRELIMINARY TESTS
WITH NO JET RELEASE

	*Local Average Air Velocities m/min (ft/min)		
	Near Floor	Middle	Near Top
Natural Convection Only Ambient Temperature HM-P1	5 (16)	3 (9)	4 (12)
Natural Convection Only Elevated Temperature HM-P3	17 (57)	---	20 (67)
Natural Convection + Forced Convection HM-P2	5 (16)	7 (24)	13 (43)
Natural Convection + Forced Convection Elevated Temperature HM-P4	27 (87)	---	26 (85)

*Uncertainty in flow velocity magnitude measurements

$\begin{bmatrix} +\ 50\% \\ -\ \ 0\% \end{bmatrix}$ Due to unknown flow direction

[± 3.6 m/min (12 ft/min)] Calibration error.

Natural convection velocities resulting from increased ambient gas temperatures were of the same order of magnitude as air velocities resulting from forced air recirculation at the sensor locations. When the compartment air temperature was elevated, the average local air velocity in the lower and upper volume region increased by a factor of approximately four. Air recirculation, for the lower gas temperature test, increased the average local air velocity at the top of the compartment but did not at the bottom. The recirculating air entering near the top of the compartment evidently channeled toward the outlet vents with little effect near the compartment floor. When the compartment was heated, the cool recirculated air spilled onto the floor region and local air velocities were increased at the floor, as well as at

the ceiling. The key observation was that natural convection tends to increase mixing of the entire test compartment. It is important to note that compartment atmosphere to wall temperature differences would be significant during a reactor loss-of-coolant accident and forced air recirculation would be provided. Thus, the elevated temperature was more typical of reactor accident conditions and the compartment atmosphere would be mixed with significant natural and forced convection mechanisms.

Hydrogen and Helium Release Tests

Seven gas release tests were completed which simulated two hydrogen release scenarios. A high velocity jet was released for approximately 10 minutes into the test compartment during each of these tests. The measured concentrations spanned both the horizontal and vertical distances of the test compartment. Hydrogen and helium were measured as volume percent gas on a "dry basis". Water vapor in the gas sample was removed prior to analysis by cooling the gas sample, condensation collection and passage through a drying bed. The "dry basis" volume percent helium and hydrogen are defined by the expressions:

$$\text{volume \% He} = \left(\frac{\text{volume He}}{\text{volume He + volume air}}\right) \times 100, \text{ and}$$

$$\text{volume \% } H_2 = \left(\frac{\text{volume } H_2}{\text{volume } H_2 \text{ + volume air}}\right) \times 100.$$

The ten test compartment hydrogen concentrations for the horizontal jet release of test HM-5 are shown in Figure 2. The measured helium concentration curves for all but the vertical helium release test, HM-6, were of the same general shape as observed for the hydrogen test. The helium concentration curves for test HM-6, shown in Figure 3, had a high spike at the end of the helium release period. The spike was due to an inadvertant high helium release rate during the last minute of the release period. The maximum peak hydrogen or helium concentration for each test is listed below in Table 4.

The maximum measured helium or hydrogen concentration differences between spatial locations in the test compartment for the gas release tests are plotted in Figures 4 and 5. The maximum helium or hydrogen concentration difference reached a relatively steady state value during the source release period for all tests. Consequently, it is concluded that the maximum gas concentration difference for each source release rate was measured during the tests. Extension of the source release period would not have resulted in larger hydrogen concentration differences between spatial locations in the test compartment. Note the maximum concentration difference was not plotted from 10 to 12 minutes during test HM-6. The helium release rate was inadvertantly high during the last minute of the helium-steam release. The previous 8 minutes had a constant helium release rate and that period should be used to determine the maximum helium concentration difference for test HM-6.

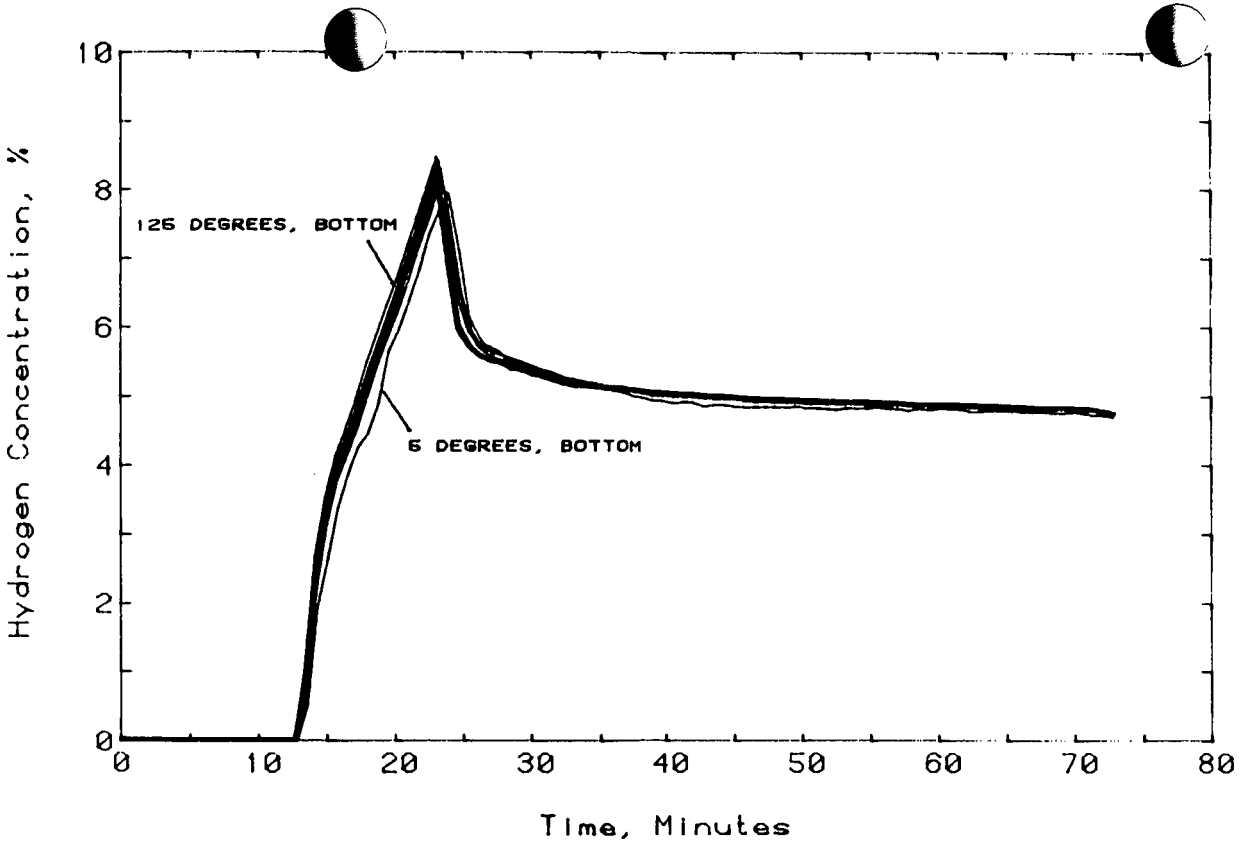


Figure 2. Test: Compartment Hydrogen Concentrations Measured at Ten Sample Points During Test HM-5A.

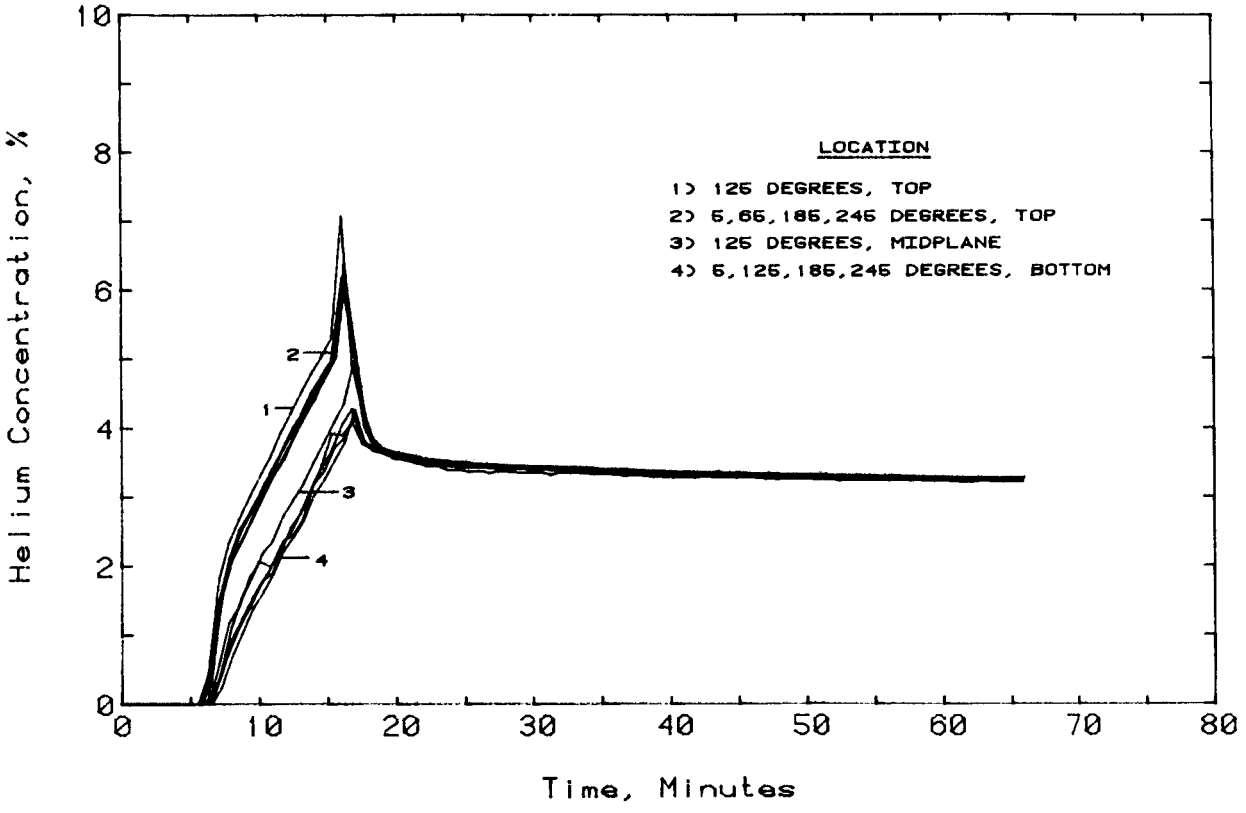


Figure 3. Compartment Helium Concentrations Measured at Ten Sample Points During Test HM-6.

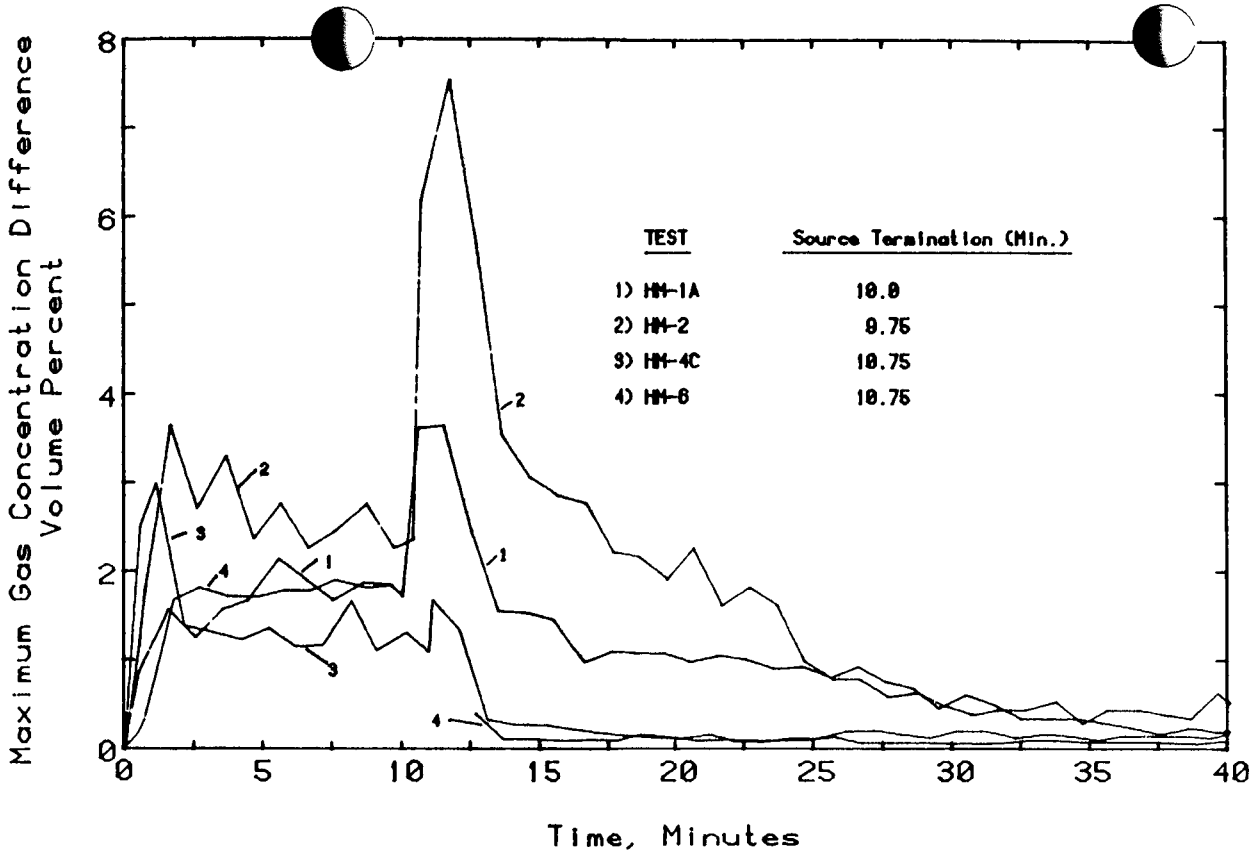


Figure 4. Maximum Gas Concentration Differences Between Ten Test Compartment Sample Points for Tests HM-1A, HM-2, HM-4C and HM-6.

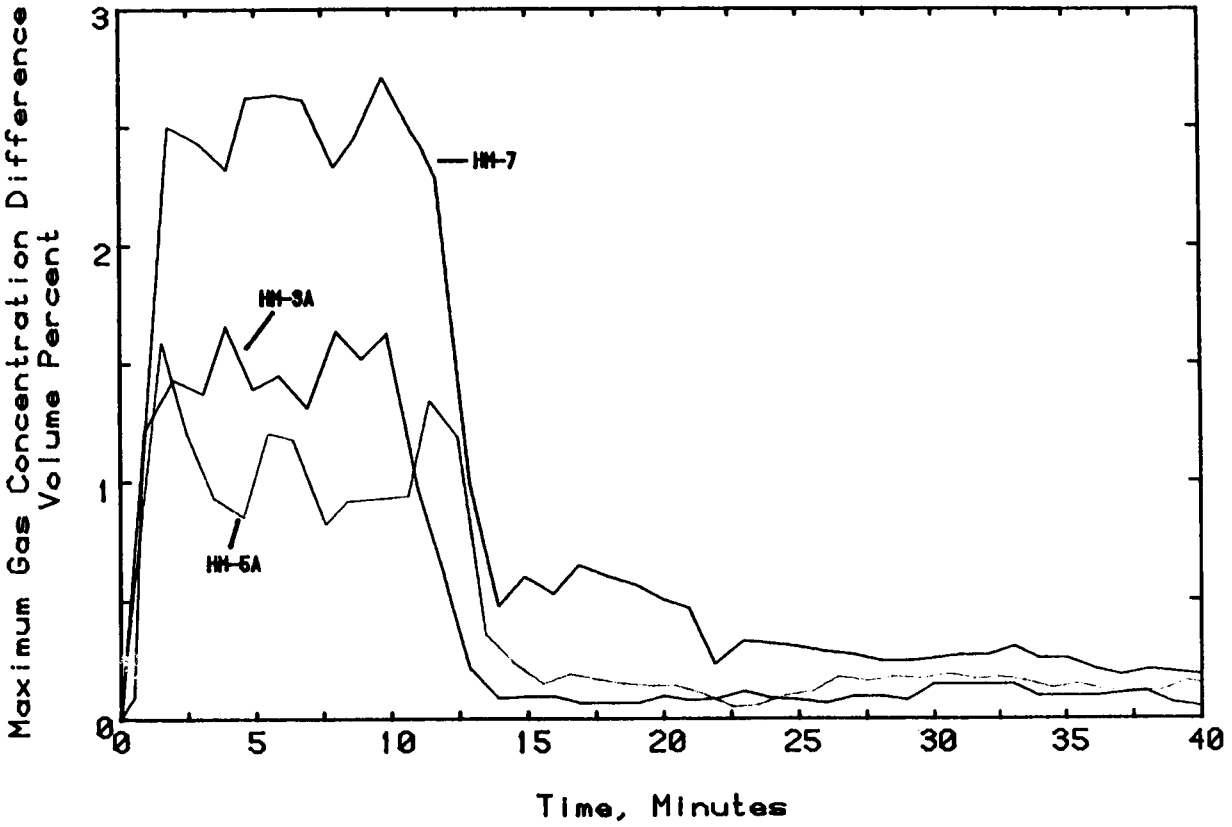


Figure 5. Maximum Gas Concentration Differences Between Ten Test Compartment Sample Points for Tests HM-3A, HM-5A, and HM-7.

TABLE 4

TEST COMPARTMENT PEAK He/H_2 CONCENTRATIONS

Test No.	Release Gas	Temp. at Peak Conc. °C	(°F)	Maximum Peak Conc. Dry Basis (Vol. %)
HM-1	He	81	(176)	13.5
HM-2	He	92	(198)	27.7
HM-3	He	67	(152)	5.4
HM-4	He	79	(174)	10.7
HM-5	H_2	74	(164)	8.5
HM-6	He	67	(152)	*5.5
HM-7	He	81	(178)	11.0

*Estimate based on extropolated data since there was inadvertant high He release rate for last one minute of test.

The largest concentration difference between locations in a test compartment were observed during the horizontal jet release test with a high source flow rate and no air recirculation. Normal air recirculation significantly decreased the maximum measured concentration difference as demonstrated by comparing results of tests HM-2 and HM-4 in Figure 4.

The high velocity jet provided the dominant mixing action during periods of gas release. When the jet was initiated, the local gas velocities, even far from the source, increased by a factor of three to five times over background velocities caused by natural convection and fan induced recirculation. The high momentum of steam released with the hydrogen was transferred to the compartment atmosphere, and significantly increased local gas velocities providing good gas mixing.

The peak concentration differences of 7.5 and 3.8 volume percent helium, measured approximately 2 minutes after termination of the helium source during tests HM-2 and HM-1, respectively, were not typical of the reactor plant postulated accident conditions. Following termination of the helium-steam source, the test compartment pressure decreased below the upper containment pressure as the temperature decreased and the steam in the compartment condensed. Pressure forces caused a reverse migration which, coupled with a lack of a mixing mechanism from either the fans or the jet itself, created an abnormally high concentration difference. This reverse flow condition was not prototypic of ice condenser plant conditions since the ice condenser is provided with upper doors which would simply close once the lower containment pressure is lower than upper containment pressure.

All tests demonstrated that the compartment atmosphere was well mixed after termination of the source jet, and atmosphere recirculation decreased

the time required to obtain a uniform concentration. The recirculation system also decreased the maximum observed concentration in the lower compartment by dilution of the test gases with the upper containment atmosphere during the source release period. The test performed with hydrogen as the source gas produced results that were identical to the corresponding helium test. This demonstrated that helium was a valid simulant for hydrogen in the mixing processes modeled.

Dry basis helium and hydrogen concentrations were measured and reported for these tests which provided a conservative determination of maximum hydrogen concentration difference and peak hydrogen concentration. Actual helium and hydrogen concentration differences were less than those measured since the presence of water vapor would dilute the helium or hydrogen.

SUMMARY AND CONCLUSIONS

The combination of mixing processes anticipated to be in operation in the lower compartment region of an ice condenser containment during a small break loss-of-coolant accident are sufficient to provide a well mixed atmosphere. The high velocity jet resulting from the hydrogen-steam release would provide the dominant mixing; however, natural convection and forced air recirculation would aid in the mixing process. Small concentration differences of the order of less than 3.0 volume percent hydrogen may exist during the gas release period, but natural convection and forced convection would provide uniform gas concentrations very quickly after the source is terminated.

Specific conclusions which were drawn from analysis of the experimental results are summarized as follows:

1. The compartment was well mixed with maximum concentration differences less than 3 volume percent during the source release from a horizontal pipe or a vertical vent.
2. The degree of mixing was not strongly dependent on source jet release orientation.
3. Gas entrainment caused by the high velocity jet was the dominant mixing process for the test compartment during the jet release period.
4. The test compartment was well mixed by natural convection after termination of the source gas for all cases; and forced air recirculation decreased the time required for good mixing.
5. Helium was a valid simulant for hydrogen in these hydrogen mixing and distribution tests.

REFERENCES

1. B. Gebhart. Heat Transfer 2nd Ed. McGraw-Hill Book Company, New York, 1971 (pp 292-295).
2. J. G. Knudsen and D. L. Katz. Fluid Dynamics and Heat Transfer, McGraw-Hill Book Company, New York, 1958 (pp 129-145).
3. W. H. McAdams. Heat Transmission, McGraw-Hill Book Company, New York, 1954, (pp 126-139).
4. D. S. Trent. "Applications of Geometric Models for the FFTF Hydraulic Core Mockup", BNWL-575, Battelle Pacific Northwest Laboratories, Richland, Washington, November 1967.

Assessment of RALOC-MOD1 With 1980 Updates*

Lawrence D. Buxton

Thermal/Hydraulics Analysis
Division 9444
Sandia National Laboratories
Albuquerque, NM 87185

ABSTRACT

"RALOC-MOD1 With 1980 Updates" is an interim version of the RALOC hydrogen transport code which was developed by Hermann Jahn of the Gesellschaft fuer Reaktorsicherheit (GRS) in the Federal Republic of Germany. This code was provided to Sandia National Laboratories by the GRS for use in NRC-sponsored hydrogen transport projects. Since receiving the code from GRS in 1981, we have been assessing the ability of the RALOC code to predict the transport of gases in LWR containments following various hypothetical degraded-core accidents. The assessment has been based on comparisons with experimental data from Battelle-Institut e.V. Frankfurt (BF) for hydrogen/nitrogen injection into a model containment, several thought experiments (using the BF test geometry) which were designed to test the code's capabilities under more unusual and perhaps adverse boundary conditions, and two standard problems based on the EPRI-sponsored steam/hydrogen and steam/helium injection tests which were performed at the Hanford Engineering Development Laboratory (HEDL).

As a result of the assessment analyses which we have performed, we have determined that this version of the RALOC code is capable of providing reasonable hydrogen transport results over a wide range of accident conditions, but code improvements should be made in various modeling areas in order to allow an even wider range of hypothetical accidents to be treated. A summary of the status of the RALOC assessment effort at Sandia will be presented, including a discussion of the limitations of the assessed version.

*This work was performed under the auspices of the U. S. Nuclear Regulatory Commission (NRC).

INTRODUCTION

The ability to predict hydrogen gas concentrations in LWR containments following a hypothetical degraded-core accident is extremely important for both safety analyses and the design of hydrogen-combustion mitigation schemes. Consequently, Sandia National Laboratories in Albuquerque (SNLA) has undertaken a program for the NRC which was designed to develop the capability to predict the concentration of containment gases as a function of position and time for such accidents. As an initial step in attaining this objective, SNLA acquired an interim version of the RALOC code from the Gesellschaft fuer Reaktorsicherheit (GRS) in the Federal Republic of Germany. When RALOC was initially obtained, it was the only known code which was specifically designed to predict gas transport in reactor containments, although several much more generalized mass- and energy-transport codes were available which could perhaps be suitably modified for such purposes.

This report discusses the results of some of our efforts to assess the ability of RALOC to perform the analyses for which it was originally designed and to determine the extent of the modifications necessary to allow more extensive analyses. The assessment of RALOC at SNLA has been based on: comparisons with experimental data from Battelle-Institut e.V. Frankfurt (BF) for hydrogen/nitrogen injection into a model containment; several thought experiments (using the BF test geometry) which were designed to test the code's capabilities under more unusual and perhaps more adverse boundary conditions; and comparison with experimental data from Hanford Engineering Development Laboratory (HEDL) for injection of hydrogen/steam and helium/steam mixtures into a two-room geometry.

RALOC DESCRIPTION

RALOC is a computer program developed by H. L. Jahn of the GRS under the sponsorship of the Bundesministerium des Innern (BMI).[1] The interim version "RALOC-MOD1 With 1980 Updates" [2] was acquired by SNLA under an NRC-BMI agreement, consistent with the existing NRC-BMFT (Bundesministerium fuer Forschung und Technologie) agreement. RALOC was designed to calculate local gas concentrations in subdivided containments. In particular, RALOC was developed to determine the hydrogen distribution in a nuclear power plant containment following a loss-of-coolant accident. The code was, however, only designed to analyze the late time portion of such accidents when radiolysis is the dominant source of hydrogen production. The interim version was not intended to be used at early accident times (during and just after blowdown) when metal/water

reaction is the dominant source of hydrogen generation.[3] Special modifications were made by H. L. Jahn to the interim version to allow simulation of the BF tests, primarily in the injection source logic.

In solving the hydrogen transport problem, RALOC uses lumped parameter zones connected by flow junctions. Within a given zone, up to five constituents can be present: liquid water, steam, hydrogen, helium, and air. Thermodynamic equilibrium and saturated steam/water conditions are assumed in each computational zone. Junction gas flow is driven by both convection and diffusion, and is opposed by a velocity-dependent flow resistance between zones. Provisions were made in the original coding for the transport of dissolved gases between zones via pumped liquid coolant, but that gas transport option has been disabled in the assessed version.

In the code received, one computational zone can be specified as having a hydrogen/air source. That source is defined via a table of injection rate versus time. The injection temperature and the volumetric ratio of the two gases must also be specified. The same or a different zone can be specified as having a helium source, but the limitations on that source are much more strict. The helium injection rate and temperature are hardwired into the code. As mentioned above, the only built-in hydrogen generation mechanism is radiolysis. The split between radiolytic hydrogen generation in the vessel and sump is controlled via user input. Other code options include fans/recombiners, optional heat transfer to constant temperature sinks, and optional heat transfer to and from variable temperature heat slabs with one heat slab allowed per zone.

The overall solution technique used by RALOC is based on the numerical integration of ordinary first-order non-linear differential equations step-wise in time over the total problem time range. The differential equations which are integrated result from considering the energy balance in each zone, the mass balance of each of the five constituents in the zone, the atmospheric flow at each junction, and the diffusion at each junction. Two separate integration techniques are employed by RALOC. The first is explicit while the second is implicit. Normally, the explicit technique is used to initiate the calculation and then a switch is made to the implicit method after certain convergence criteria have been met.

After we obtained RALOC from the GRS, it was converted from the GRS Amdahl computer to the CDC 7600 and CRAY-1 systems used at SNLA. Four partial test calculations were successfully reproduced to ensure that no significant differences were introduced during the conversion process.

Several modifications were made to RALOC-MOD1 with 1980 Updates after it was installed at SNLA. These modifications served either to correct Fortran errors which were discovered in the source deck or to improve the overall use of the code. These changes included modifications to allow an exact restart during the fully implicit integration, the addition of frequency control cards for the plot/restart dumps, modifications to the fan/recombiner logic to correct an error and change hardwired features not relevant to our needs, and routines to allow steam injection. A plot program was also developed at Sandia since the plot routines used at GRS could not be easily converted to our system.

RALOC ASSESSMENT CALCULATIONS

Calculations performed for assessment purposes fell into three groups: predictions of actual experiment data from Battelle-Frankfurt model containment tests; "gedanken" experiments performed with the BF test geometry; and single blind predictions of actual experimental data from Hanford Engineering Development Laboratory mixing tests. These three groups will be separately discussed below.

Battelle-Frankfurt Experiments

RALOC assessment calculations have been made at Sandia for BF tests 2, 6, 10, and 19. Tests 2 and 6 were performed using the two rooms R1 and R2 of the model containment shown in Figure 1.[4] Tests 10 and 19 were performed with the six rooms R1, R2, R5, R6, R7 and R8 of the model containment.[5] Tests 2 and 10 were begun with isothermal conditions, while tests 6 and 19 each had an initial temperature inversion present. The temperature at the top of the test facility was approximately 16 K greater than the temperature at the bottom when test 6 was begun. The initial temperature difference was approximately 30 K for test 19. The injected gas mixture for these experiments was about 2/3 hydrogen and 1/3 nitrogen by volume. The injection technique used was designed to produce a fairly uniform distribution over a $0.8 m^2$ area 0.4 m above the floor of room R1. The volumes of rooms R1 and R2 totaled about 75 m^3. Rooms R5-R8 totaled about 160 m^3.

The RALOC nodalization for the BF tests is shown in Figure 2. The large numbers in the boxes represent zone numbers, the smaller numbers indicate the connection numbering, and the arrows show the originally assigned gas flow directions. Only zones 1-16 were used for tests 2 and 6. Zones 1-6 represent room R2 and 7-16 represent R1. Zone 15 was used as the injection source cell in all cases. For tests 10 and 19, rooms R5 and R7 were modeled as a single compartment by cell 17 and rooms R6 and R8 were combined to make cell 22. The

large holes connecting the various rooms are represented by cells 18, 19, 20 and 21. No modeling provisions were made for horizontal recirculation to the outer rooms (R5-R8) since the exact room connections were unknown.

The gas mixture input rate for experiment 2 was reported as 1.19 m^3/h for 3.78 hours. Figure 3 shows comparisons made between the RALOC predictions (solid lines) of hydrogen concentrations and the experimental data (dashed lines) for that experiment. Comparisons are shown for the upper compartment of the test facility near the centerline and for the bottom compartment near the source. The agreement between the predictions and the data looks reasonably good in both cases, but further examination of these results indicates that too much mixing was predicted by RALOC at early times and not enough mixing at late times. The experimental data clearly exhibit a larger difference in hydrogen concentration between the top and bottom rooms at early times and less difference at late times. The perturbation in the predicted values at 13,620 s corresponds to cessation of the source. The discrepancy in the final hydrogen concentration values may reflect gas leakage from the test facility during the test.

Figure 4 shows comparisons made between the RALOC calculational results and the BF test 6 data. The inverted initial temperature distribution present in test 6 inhibited the convective transport of hydrogen to the upper room of the test facility as seen by comparing the results for zones 1 and 13. The RALOC calculations qualitatively predict the trends in the data; however, too much hydrogen was transported from the bottom compartment to the top one past about 4000 s. There may have also been some leakage out of the facility in this test.

Figure 5 shows the code and experimental results for the first 10,000 seconds of isothermal test 10 which was performed in the six-room geometry. The average injection rate in that test was 1.53 m^3/h. As indicated, the agreement between the RALOC predictions and the experimental data is very good and indicates a well mixed atmosphere. Creating an initial temperature inversion in test 19, as was done in test 6, again leads to lower hydrogen concentrations in the upper compartments. This can be seen by comparing the results in Figure 5 for test 10 with the corresponding results for test 19 in Figure 6. The agreement with the experimental data for test 19 is not as good, but the qualitative trends in the data are reasonably well predicted. We only modeled the first 6700 s of test 19 since helium injection was also started after that time in the experiment. The average hydrogen/nitrogen injection rate was 1.70 m^3/h.

Based on our assessment calculations for the BF data, it appears that RALOC predictions of hydrogen concentrations are somewhat qualitative as has been previously indicated by Dr. Jahn [3]. Trends in the experimental data were predicted and only minor indications of stability problems were found. Further refinements might be obtained by using better source and initial temperature distribution definitions. More detailed nodalizations might be of some benefit also, but studies at GRS have indicated that no dramatic improvements are seen when 34 zones are used for these tests.[3]

"Gedanken" Experiments

Several "gedanken" or thought experiments were performed with RALOC to evaluate how well the code behaved under conditions for which there was no experimental data available. These calculations were done using the nodalizations and initial temperature profiles used for BF tests 2 and 6. The only changes which were made involved the injection source and the initial quantity of hydrogen present in the models.

The first calculations investigated the effects of initialization. No injection sources were used; the calculations were merely initiated from the stagnant initial input conditions for the gases in the volumes. Large convective flows developed early in the explicit portion of the integration of the differential equations. These flows then damped out very slowly during the implicit portion of the calculations. Attempting to increase the user-specified flow resistance in the connections had no effect on the results. We later discovered that the code logic for that additional flow resistance was not in the assessed version of RALOC.

A second set of calculations was performed in which one zone (zone 15) at the bottom of the model for tests 2 and 6 was initialized with a 10% initial hydrogen volumetric concentration instead of the usual "prestress" value of .001%. Again, large convective flows developed during the explicit portion of the calculations, leading to a rapid mixing of the hydrogen "bubble" throughout the model containment. For isothermal conditions, the final hydrogen concentrations were the same in all of the zones. An inverted initial temperature distribution produced a final hydrogen concentration distribution which had more hydrogen at the bottom of the containment than at the top when the calculation was stopped at 10,000 seconds. Convection was apparently inhibited by the temperature gradient. As in the case of the no-source calculations, the convective flows asymptotically decreased during the implicit portion of the integration.

The final set of thought experiments performed with RALOC in the BF test 2 and 6 configuration used hydrogen injection rates intended to be more representative of those that might exist early in a hypothetical degraded-core accident as a result of extensive metal/water interaction. The purpose of these final calculations was to determine whether the RALOC numerics would fail under such large relative injection rates (50 m^3/h and 500 m^3/h). The calculations all proceeded smoothly, and predicted a very rapid dispersal of the hydrogen from the source zone.

None of our "gedanken" experiment calculations produced unexpected results or unreasonable amounts of instability. They indicated that the code numerics appear to be able to successfully handle a wide range of input boundary conditions, including relative source rates greater than or equal to those which might be expected in a degraded-core accident. It should also be noted, however, that we never discovered why the large flow perturbations developed during the explicit integration.

HEDL Experiments

Sandia has also used RALOC to simulate some tests which were performed for the Electric Power Research Institute (EPRI) at HEDL.[6] Those tests involved hydrogen/steam (test A) and helium/steam (test B) mixtures injected into the two-room geometry of the Containment Systems Test Facility (CSTF) shown in Figure 7. The total volume of the CSTF is about 850 m^3; the volume of the bottom compartment is about 150 m^3.

The version of RALOC which we received could not be used to model these tests directly. However, simulation of the HEDL tests was possible after: the existing source logic was modified to allow time-dependent injection of helium/steam and hydrogen/steam mixtures; the water/steam mass and energy balance equations were modified to account for steam sources; and the fan model was altered to merely mix the input gases instead of having a constant outlet temperature. Even with these modifications, there were several recognized problems with the analyses of the HEDL tests. The tests did not start from saturated conditions, as assumed by RALOC, and the artificial water mass required in each zone of the RALOC nodalization to keep it from drying out can adversely affect the energy distribution within the containment.

The nodalization used for the HEDL test calculations is shown in Figure 8. Zones 1-15 represent 60 degree annular segments in the bottom compartment. Likewise, zones 16-33 represent 60 degree annular segments around the periphery of the top compartment. Zones 34-36 are located in the center of the upper compartment and each communicates with its

surrounding cells via the junctions indicated. The fan intake is from zone 34 and it exhausts equally to zones 6, 7, 9, and 10. Zone 37 is a very large artificial volume used to simulate an atmospheric vent system which was present in the tests. The slots connecting the top and bottom compartments are represented by reduced flow areas for junctions 23-27. The hydrogen/steam mixture for test A was injected into zone 6; th helium/steam mixture for test B was injected into zone 8.

Test A comparisons of the RALOC-predicted and the measured hydrogen concentrations (on a dry atmosphere basis) for three 125° measuring stations which are well away from the source are given in Figure 9. Reasonable agreement is seen during the injection period from 12 to 24 minutes, particularly at the middle elevation. The predicted concentrations are all to high and decay too slowly at later times. The temperatures exhibit similar behavior. This disagreement is probably the result of inadequate heat loss from the steam via condensation, particularly in the colder upper compartment.

Test B comparisons for the helium concentration at two 5° measuring stations, again well away from the source zone, are given in Figure 10. The same general trends are seen as in test A; RALOC tends to overpredict the helium concentration, probably because the steam condensation is not treated accurately.

Since these analyses were done in a single blind mode, i.e., we only had the measured boundary conditions until the analyses were completed, we hope to be able to improve the agreement in post-test analyses by simulating wall condensation more accurately Better simulation of the system vent may also be required.

CONCLUSIONS AND RECOMMENDED IMPROVEMENTS

RALOC results were generally in good qualitative agreement with the experimental data from the BF and HEDL tests. RALOC is also fairly well behaved numerically, even under severe source conditions. However, while the trends see in the data were well predicted by the code, there were sometimes up to 40% differences in the magnitude of the predicted and measured hydrogen and/or helium concentrations. Consequently, this version of RALOC appears to be most useful as a fast running transport code for parametric-type studies.

RALOC is capable of producing qualitatively reasonable results over a wide range of accident conditions, but code improvements must be made in various modeling areas in order to allow a wider variety of hypothetical accidents to be treated. Further assessment should also be done as more and better

experimental data become available. If RALOC is pursued and expanded to be applicable to more problems of current interest, we recommend the following code changes or improvements:

1. Make the base set of gases considered by the code be hydrogen, oxygen, nitrogen and steam. The reason for this change is that the modified code might be used to provide starting conditions for combustion calculations. If oxygen is not separately tracked this would be impossible.

2. Provide the option for additional gases to be considered. This option will be required if analyses are desired for transport of additional combustible gases such as carbon monoxide which might result from fuel/concrete interactions.

3. Generalize the source logic to essentially allow the injection of an arbitrary gas mixture into any cell as a function of time. The BF tests could have been modeled more accurately if multiple injection points could have been used for the source.

4. Improve the heat slab model. H. L. Jahn has already improved the model in a later version of RALOC. That new version may be sufficient for more general modeling.

5. Allow user-controlled junction flow resistances. It is not clear that more complicated geometries can be appropriately modeled without such an option to account for multiple connections being treated as one.

6. Generalize the pumped coolant transport model and reinstate the dissolved gas transport option. The current coolant transport model will not be satisfactory for analyzing accident situations in which the analysis begins before containment recirculation pumps are turned on.

7. Develop ice condenser and suppression pool models. As steam and hydrogen pass through such pressure suppression devices, the properties of the gases are changed. Models are needed to account for these changes.

8. Improve the fan/recombiner model. Many modifications were made to the fan model in preparation for the HEDL assessment calculations, but they were kept as minimal as possible.

9. Remove the requirement of always having two-phase saturated conditions in containment. Some work in this area has already been done, but more work remains. The use of an artificial water supply in each zone which can vaporize as the zone heats up causes the steam enthalpy to be in error which in turn alters the enthalpy of the other gases in an indirect manner.

10. Generalize the code initialization conditions. A general set of arbitrary, but thermodynamically consistent, starting conditions cannot be set via input for each cell; certain conditions are hardwired into the initialization procedure. This is expected to have a critical effect on possible future analyses of gas transport in containment after a hydrogen burn has occurred, but presents some problems in almost every analysis.

The ordering in the list of items above has no correlation either with the difficulty of the modification or with the priority which might ultimately be assigned to that particular modification. Also, the list is probably incomplete. As more possible uses of RALOC are suggested by the user community, the list will more than likely grow. Implementation of the changes suggested above should, however, lead to a much more useful analytic tool for a variety of gas transport problems of current interest in the degraded-core accident area.

REFERENCES

1. Hermann L. Jahn, "Hydrogen Distribution After a Loss of Coolant Accident in the Subdivided Containment of Light Water Reactors--Translation," NUREG/CR-1831 (SAND80-6031), Translation of a Dissertation submitted on March 26, 1979, to Munich Technical University.

2. RALOC-MOD1 with 1980 Updates, an undocumented version of RALOC-MOD1 which is documented in: H. Jahn, "RALOC-MOD1, A Computer Program for the Determination of Local Gas Concentrations in Subdivided Vessels (Particularly H_2 Distribution in PWR Full Pressure Containments Following a Loss of Coolant Accident)," NRC Translation #654 of GRS-A-263 (January 1979).

3. H. L. Jahn, "Status Report on the Hydrogen Distribution Following a Coolant Loss Accident," NRC Translation #796 of GRS-A-333 (August 1979).

4. G. Langer, et al., "Experimental Investigation of the Hydrogen Distribution in the Containment of a Light Water Reactor Following a Coolant Loss Accident," NRC Translation #801 of BF-F-63.363-3 (May 1979).

5. Battelle-Frankfurt, "Experimentelle Untersuchung der Wasserstoffverteilung in einem Modell-Containment (Grundlagenversuche Phase II)," Technisher Bericht BF-R-64.036-1 (July 1980).

6. Private Communication, L. D. Buxton with G. R. Bloom, HEDL (1982).

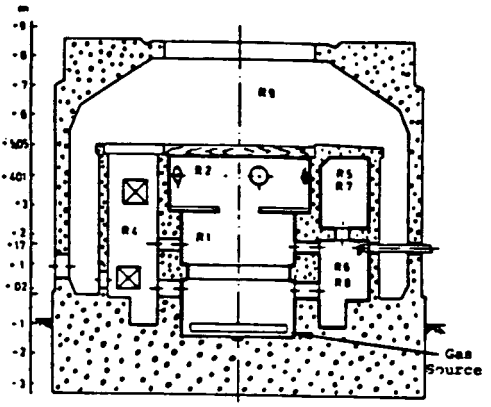


Figure 1. Cutaway of Battelle-Frankfurt (BF) Model Containment

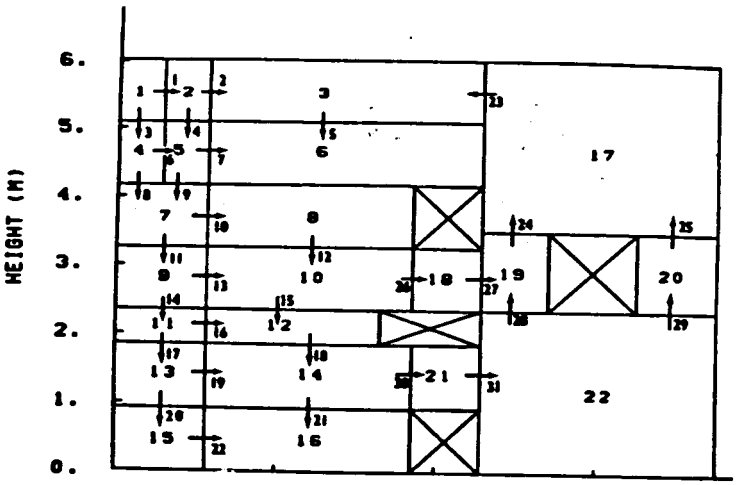


Figure 2. RALOC Nodalization for BF Tests

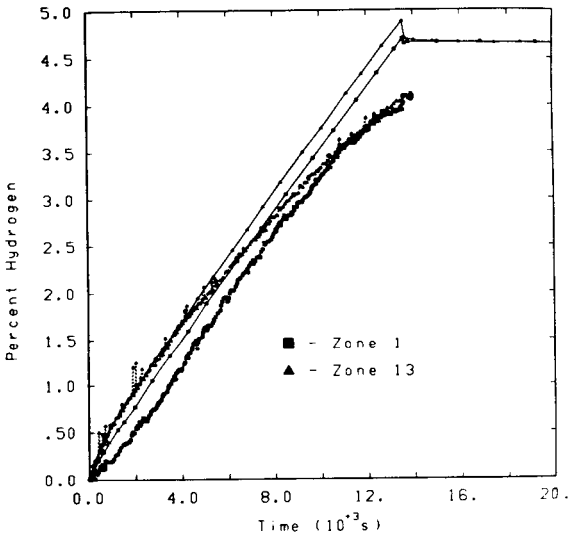


Figure 3. RALOC Predictions vs. BF 2 Data

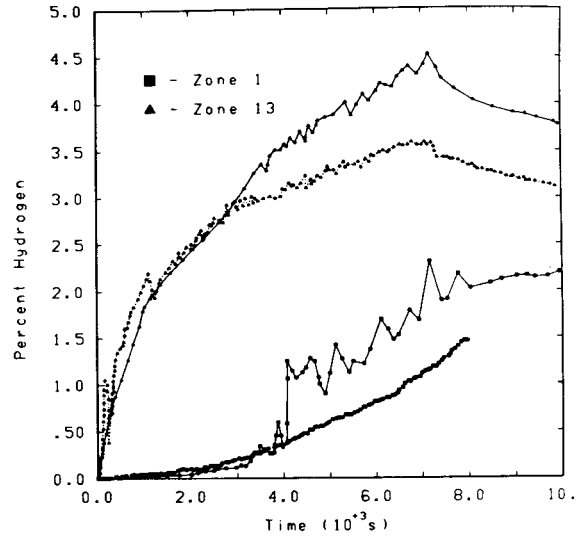


Figure 4. RALOC Predictions vs. BF 6 Data

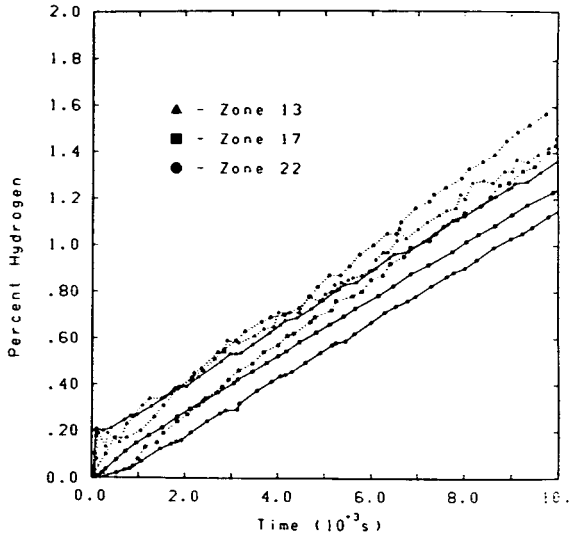


Figure 5. RALOC Predictions vs. BF 10 Data

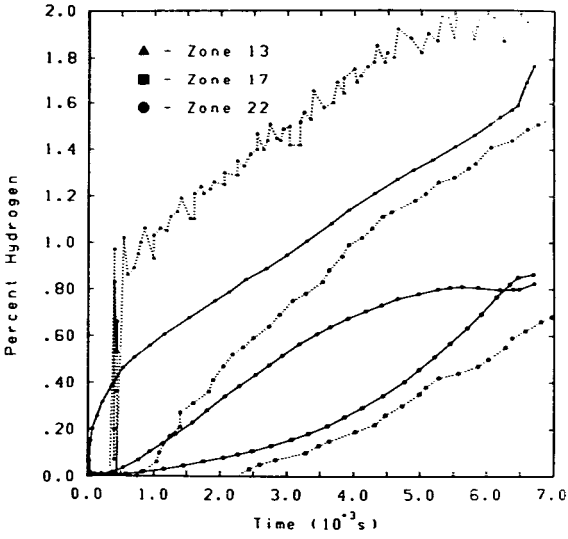


Figure 6: RALOC Predictions vs. BF 19 Data

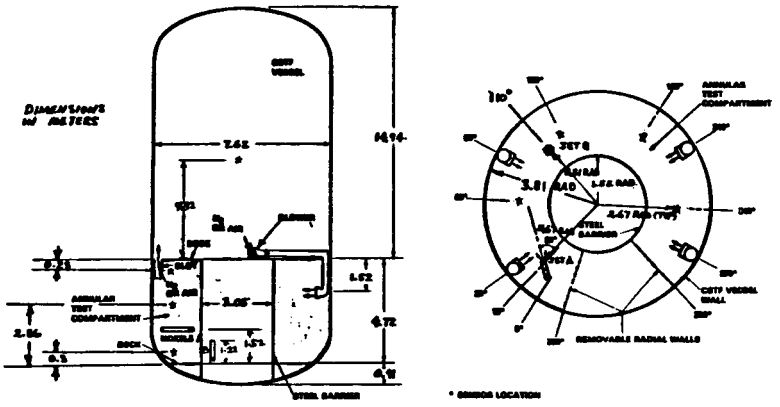


Figure 7. HEDL CSTF Geometry

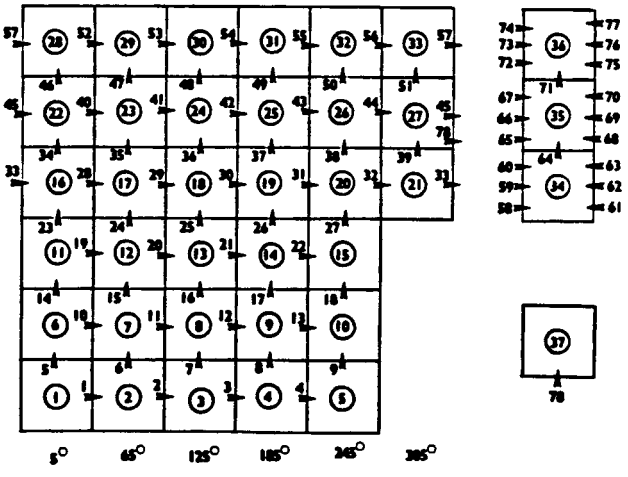


Figure 8. RALOC Logical Discretization for HEDL Problems

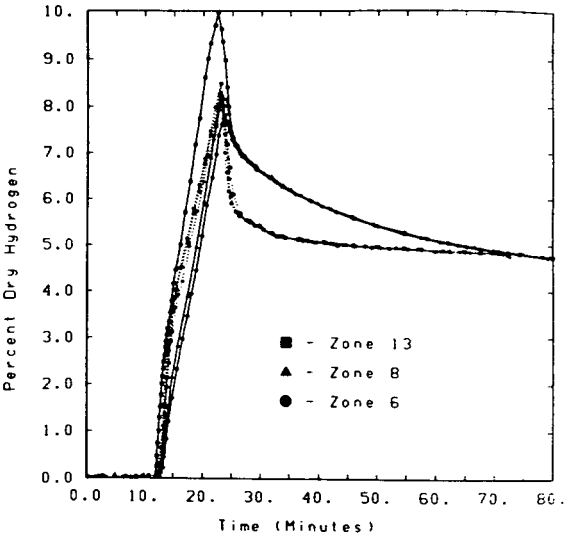


Figure 9. RALOC Predictions vs. HEDL Test A Data

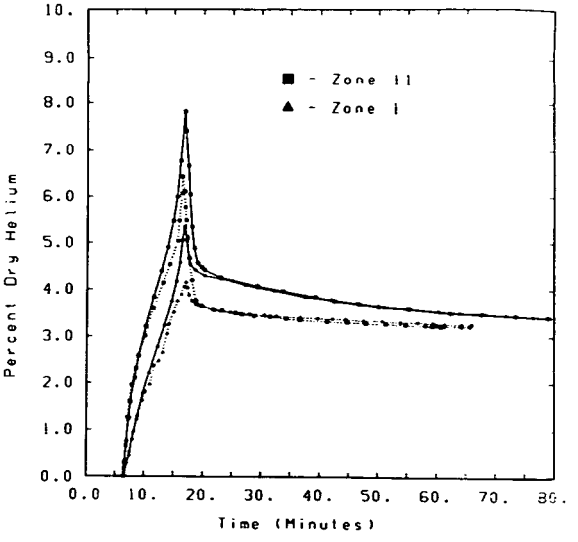


Figure 10. RALOC Predictions vs. HEDL Test B Data

RECENT IMPROVEMENTS IN THE RALOC CODE

H.L. Jahn, P. Papadimitriou, V.T. Pham, G. Weber

The knowledge of the distribution of components of a post LOCA containatmosphere is considered to be of great importance. Especially for severe accidents this concerns not only the hydrogen but as well the distribution of oxygen, inert gases (nitrogen, steam) and of course that of fission products released to the containment atmosphere. The design of all mitigation measures, realistic calculations on burning processes within real plants and risk analyses aspects on the failure of safety related equipment or the containment integrity must be based on such knowledge.

The code RALOC was designed and improved to simulate the distribution of atmosphere in consequence of a LOCA. It is a system code with the intention to deal as a best estimate tool for application on design basis and degraded core accidents. A variation of this code called FIPLOC shall handle the fission product localization problem.

Former calculations done by RALOC MOD1/80 for the Battelle H_2-distribution tests /4/ and first FIPLOC CSE post test calculations confirmed the strong necessity to simulate

1. the prehistory of a test
2. the whole containment systems
3. heat exchange with structures and sumps.

Otherwise completely different results may be expected. Free convection very sensibel on the composition of the atmosphere and its temperature. Both may equally depend on the prehistory and on actual heat exchange processes. Distribution codes need sufficient accuracy to predict temperature profiles if they shall be expected to deliver distribution data. This may be of special importance for the hydrogen problem if high steam rates are released prior, during and possibly after the hydrogen release. It certainly will also be most important for the fission product distribution and behaviour (wet sedimentation).

RALOC MOD1/81 was therefore improved by a comfortable heat transfer and heat slab model. This version was now first applied for the blind

calculations of the HEDL standard problems A and B /3/ and to exp. 16 of the Battelle Frankfurt hydrogen distribution tests /4/. Both test series provided very helpful informations for code verification as well for

- DCA and short term (HEDL) as for
- DBA and long term (Battelle Frankfurt)

The way of simulation and first results of these calculations are shown in the attached figures. A more detailed report on the standard problem calculations and its interpretation was generated but could not be published in time /1/. A more detailed german report will be prepared soon to describe the very new Battelle test calculations done by GRS with RALOC-MOD1.

All calculations show good agreement to the experiments. Therefore the code is considered to be a best estimate systems code. It my be used to study special accident sequences and some important aspects concerning mitigation measures. One phenomenon which was predicted by the code already some time ago /2/ but not yet verified by any experiment is the separation of air and hydrogen caused by the steam release. Some ideas and results are presented for discussion in the attached figures.

It also should be mentioned that a specialist group of the Commission of the European Communities dealing with all aspects of the hydrogen problem advanced a further indepth study of the separation method and generally more detailed investigations of the distribution problem, which was considered to be of high priority within the whole subject /5/.

The FIPLOC work is still at its beginning. Present experiences and the results of CSE experiments 5 and 11 /6/ indicate that adequate analytical methods have to be applied within the field of fission products investigation. Both experiments only differ about the steam supply which was allowed to compensate the vessel-condensation rate at test A-5 and terminated at test A-11 after fission products were injected. The attached figures confirm the necessety of further FIPLOC improvements and its great potential

Literature

/1/ H.L. Jahn, P. Papadimitriou, T.V. Pham
RALOC MOD1/81 Blind Calculations on Standard Problems A and B on Hydrogen Distribution (HEDL-Tests)
To be published

/2/ H.L. Jahn, P. Papdimitriou, T.V. Pham
Quick Look Report on RALOC-Calculations to the HEDL-Test Facility
GRS-Technical Note, January 1982

/3/ G.R. Bloom, S.W. Claybrook
Standard Problems on Hydrogen Mixing and Distribution, Westinghouse Hanford Company, Richland, Washington
March 1982

/4/ G. Langer
Experimentelle Untersuchung der Wasserstoffverteilung in einem Modell-Containment (Grundlagenversuche Phase II)
Bericht BleV-R-64.036-3 des Battelle-Instituts, Juli 1982

/5/ Assessment of Hydrogen Generation, Distribution and Explosion Potential Associated with Accidents in Light-Water Reactors
State of the art report produced by the expert subgroup of the European Commission Working Group No. 2 on Water Reactor Safety Research Commission of the European Communitites, Brussels, to be published

/6/ G. Weber
Rechnungen mit dem Modell FIPLOC-01 zur orts- und zeitabhängigen Methyljodidverteilung für die Versuche A-5 und A-11 des Containment-Systems-Experiment
GRS-A-681, Februar 1982 (restricted distribution)

HMS: A MODEL FOR HYDROGEN MIGRATION STUDIES IN LWR CONTAINMENTS *

J. R. Travis
Theoretical Division, Group T-3
University of California
Los Alamos National Laboratory
Los Alamos, NM 87545

ABSTRACT

A numerical technique has been developed for calculating the full three-dimensional time-dependent Navier-Stokes equations with multiple species transport. The method is a modified form of the Implicit Continuous-fluid Eulerian (ICE) technique to solve the governing equations for low Mach number flows where pressure waves and local variations in compression and expansion are not significant. Large density variations, due to thermal and species concentration gradients, are accounted for without the restrictions of the classical Boussinesq approximation. Calculations of the EPRI/HEDL standard problems verify the feasibility of using this finite-difference technique for analyzing hydrogen dispersion within LWR containments.

I. INTRODUCTION

During and after a loss-of-coolant accident in a light-water reactor, water may be decomposed by chemical reactions and radiolysis to release gaseous hydrogen. Should hydrogen be released, two deleterious effects could occur. The noncondensable gas can increase the containment pressure. In sufficient amounts, the hydrogen could burn in the presence of air, causing considerable loads on the containment walls or harm to crucial control devices. Each effect represents an additional safety risk. To better assess the problem, we have developed a multidimensional fluid dynamics finite-difference code to calculate the details of hydrogen transport through containment structures.

This detailed model of the full three-dimensional time-dependent Navier-Stokes equations with species transport is solved by a variant of the Implicit Continuous-fluid Eulerian (ICE)[1] technique. We make use of the idea that for low-speed flows pressure wave propagation need not be resolved in detail and therefore the local fluid density is a function of the average fluid pressure, local temperature, and relative concentrations of available species. This further allows accurate representation of flows driven by large density variations which the Boussinesq approximation may not provide sufficient accuracy.[2]

Ultimately this detailed model, together with relevant experimental data, will help to benchmark existing hydrogen migration systems codes that are necessarily based on simpler models. This paper presents the governing equations, develops the solution procedure, and presents numerical results for comparison of experimental results in the three-dimensional geometry of the EPRI/HEDL standard problems.[3]

*This work performed under the auspices of the U.S. Dept. of Energy.

II. MATHEMATICAL DESCRIPTION

The partial-differential equations that govern the fluid dynamics and species transport are presented in this section. They are written in cylindrical coordinates; however, the equations for plane coordinates are easily obtained by setting the radial distance r equal to unity and the terms with the β multiplier equal to zero; i.e., $\beta = 1$ for cylindrical coordinates and $\beta = 0$ for planar coordinates.

A. The Mixture Equations

The mixture mass conservation equation is

$$\frac{\partial \rho}{\partial t} + \nabla\cdot(\rho\bar{u}) = \sum_{\alpha=1}^{3} S_\alpha \quad , \tag{1}$$

where

$\rho = \sum_{\alpha=1}^{3} \rho'_\alpha$; ρ'_α = macroscopic density of the individual species (air, steam, or hydrogen),

$\bar{u}$ = mass-average velocity vector, and

S_α = mass source (+) and/or sink (-) of species α per unit volume and time.

The mixture momentum conservation equations are given by

$$\frac{\partial(\rho\bar{u})}{\partial t} + \nabla\cdot(\rho\bar{\bar{u}}\bar{\bar{u}}) = -\nabla p + \nabla\cdot\bar{\bar{\sigma}} + \hat{\rho}\bar{g} + \bar{M} \quad , \tag{2}$$

where

p = pressure,

$\bar{\bar{\sigma}}$ = viscous stress tensor,

$\hat{\rho}$ = local density relative to the average density (see next section), and

$\bar{M}$ = momentum source vector per unit volume and time (see Sec. IV).

In these equations, the viscous force per unit volume and time, $\nabla\cdot\bar{\sigma}$, is given for the

r- or x-component

$$\nabla\cdot\bar{\sigma} = \frac{1}{r}\frac{\partial}{\partial r}(r\,\sigma_{rr}) + \frac{1}{r}\frac{\partial}{\partial\theta}\sigma_{r\theta} - \beta\frac{\sigma_{\theta\theta}}{r} + \frac{\partial}{\partial z}\sigma_{rz} \quad ,$$

θ- or y-component

$$\nabla\cdot\bar{\sigma} = \frac{1}{r^2}\frac{\partial}{\partial r}(r^2\,\sigma_{r\theta}) + \frac{1}{r}\frac{\partial}{\partial\theta}\sigma_{\theta\theta} + \frac{\partial}{\partial z}\sigma_{\theta z} \quad , \text{ and}$$

z-component

$$\nabla\cdot\bar{\sigma} = \frac{1}{r}\frac{\partial}{\partial r}(r\,\sigma_{rz}) + \frac{1}{r}\frac{\partial}{\partial\theta}\sigma_{\theta z} + \frac{\partial}{\partial z}\sigma_{zz} \quad .$$

The components of the viscous stress tensor are defined as follows:

$$\sigma_{rr} = 2\mu\frac{\partial u}{\partial r} + \lambda\nabla\cdot\bar{u} \quad ,$$

$$\sigma_{\theta\theta} = 2\mu\left(\frac{1}{r}\frac{\partial w}{\partial\theta} + \beta\frac{u}{r}\right) + \lambda\nabla\cdot\bar{u} \quad ,$$

$$\sigma_{zz} = 2\mu\frac{\partial v}{\partial z} + \lambda\nabla\cdot\bar{u} \quad ,$$

$$\sigma_{r\theta} = \sigma_{\theta r} = \mu\left[r\frac{\partial}{\partial r}\left(\frac{w}{r}\right) + \frac{1}{r}\frac{\partial u}{\partial\theta}\right] \quad ,$$

$$\sigma_{\theta z} = \sigma_{z\theta} = \mu\left[\frac{\partial w}{\partial z} + \frac{1}{r}\frac{\partial v}{\partial\theta}\right] \quad , \text{ and}$$

$$\sigma_{zr} = \sigma_{rz} = \mu\left[\frac{\partial v}{\partial r} + \frac{\partial u}{\partial z}\right] \quad ,$$

where μ and λ are the first and second coefficients of viscosity, respectively, and

$$\nabla\cdot\bar{u} = \frac{1}{r}\frac{\partial}{\partial r}(ru) + \frac{1}{r}\frac{\partial w}{\partial \theta} + \frac{\partial v}{\partial z} \quad .$$

The mixture internal energy equation is

$$\frac{\partial}{\partial t}(\rho I) + \nabla\cdot(\rho I\bar{u}) = \nabla\cdot(K\nabla T) + Q \quad , \tag{3}$$

where

I = mixture specific internal energy,
K = thermal conductivity,
T = mixture temperature, and
Q = energy source and/or sink per unit volume and time.

We assume viscous dissipation is negligible for the low-speed flows of interest.

The equation-of-state for the average fluid pressure P_o is given by the ideal gas mixture equation

$$P_o = T\sum_{\alpha=1}^{3}(\gamma_\alpha - 1)(C_v)_\alpha \rho'_\alpha \quad , \tag{4}$$

where γ_α is the ratio of specific heats for species α and $(C_v)_\alpha$ is the specific heat at constant volume for species α.

B. The Species Transport Equations

The dynamics of the individual species are determined by

$$\frac{\partial \rho'_\alpha}{\partial t} + \nabla\cdot(\rho'_\alpha\bar{u}) = S_\alpha \quad .$$

Summing Eq. (5) over all species results in the mixture mass Eq. (1).

III. THE FINITE DIFFERENCE EQUATIONS AND SOLUTION PROCEUDRE

Equations (1) - (3) and (5) are written in finite difference form for their numerical solution. The nonlinear finite-difference equations are then solved

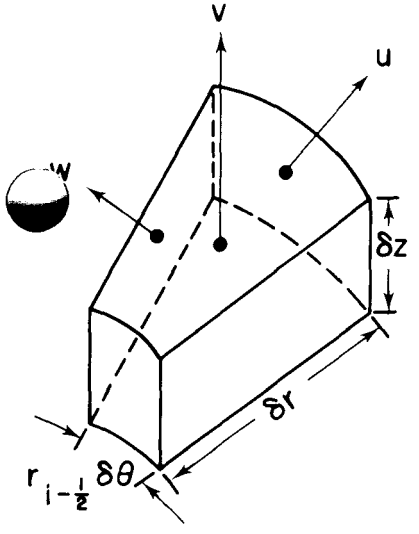


Fig. 1.
Locations of velocity components for a typical cell in cylindrical geometry.

iteratively using a point relaxation method. Since we are interested in low-speed flows where the propagation of pressure waves need not be resolved, we are therefore utilizing a modified ICE[1] solution technique where the species densities are functions of the global or compartment pressure, and not of the local pressure. Time-dependent solutions can be obtained in one, two, and three space dimensions in plane and in cylindrical geometries. The geometric region of interest is divided into many finite-size, space-fixed zones called computational cells that collectively form the computing mesh. Figure 1 shows a typical computational cell with the velocities centered on the cell boundaries. All other quantities, such as I, p and (ρ'_α)'s, are positioned at the cell-center designated (i,j,k). The finite-difference equations for the quantities at time $t = (n+1)\delta t$ form a system of coupled, non-linear algebraic equations. The equations are given below and the solution method follows.

For the problems of interest (See Sec. IV), the source/sink terms in the species transport equations are:

(1) Air (a); $S_a = 0$;

(2) Hydrogen or helium (h); S_h = hydrogen or helium mass per unit volume and time in the jet; and

(3) Steam(s), $S_s - C_s$ = (steam mass per unit volume and time in the jet) - (condensation mass per unit volume and time).

The sources of hydrogen or helium and steam are specified by the experiment; how- the condensation rate must be modeled. We propose the simple but effective ionship, based on the assumption of local equilibrium,

$$C_s = R[\rho'_s(\text{local steam density}) - \rho'_{sat}(T)]$$

where

$\rho'_{sat}(T)$ = saturation steam density at temperature T,

$R = 10^{10}$ /s for ρ'_s(local steam density) $> \rho'_{sat}(T)$, or

$R = 0$, otherwise.

For cell i,j,k we will implicitly solve for the n+1 steam density, $(\rho'_s)^{n+1}_{i,j,k}$, by writing

$$(C_s)^{n+1}_{i,j,k} = R[(\rho'_s)^{n+1}_{i,j,k} - \rho'_{sat}(T^n)] \quad ,$$

which allows any degree of condensation while the numerical scheme remains stable. The steam transport equation is then written

$$(\rho'_s)^{n+1}_{i,j,k} = \{(\rho'_s)^{n}_{i,j,k} + \delta t[- <(\rho'_s)^{n+1}u^{n+1}r>_{i,j,k}/(r_i \delta r)$$

$$- <(\rho'_s)^{n+1}v^{n+1}>_{i,j,k}/\delta z - <(\rho'_s)^{n+1}w^{n+1}>_{i,j,k}/(r_i \delta\theta)$$

$$+ (S_s)_{i,j,k} + R\,\rho'_{sat}(T^n)]\}/(1 + \delta tR) \quad .$$

The flux quantities, for example $<\rho'_s ur>_{i,j,k}$, are calculated using donor-cell differencing, so that

$$<\rho'_s ur>_{i,j,k} = u_{i+\frac{1}{2},j,k} r_{i+\frac{1}{2}} \cdot \begin{cases} (\rho'_s)_{i,j,k} & \text{if } u_{i+\frac{1}{2},j,k} \geq 0 \\ (\rho'_s)_{i+1,j,k} & \text{if } u_{i+\frac{1}{2},j,k} < 0 \end{cases}$$

$$- u_{i-\frac{1}{2},j,k} r_{i-\frac{1}{2}} \cdot \begin{cases} (\rho'_s)_{i-1,j,k} & \text{if } u_{i-\frac{1}{2},j,k} \geq 0 \\ (\rho'_s)_{i,j,k} & \text{if } u_{i-\frac{1}{2},j,k} < 0 \end{cases} \quad .$$

The transport equations for hydrogen or helium and air and the mixture mass equation are written in similar fashion.

The finite-difference representation of the mixture momentum equations is

$$(\rho u)^{n+1}_{i+\frac{1}{2},j,k} = (\widetilde{\rho u})^{n}_{i+\frac{1}{2},j,k} - \delta t\left(p^{n+1}_{i+1,j,k} - p^{n+1}_{i,j,k}\right)/\delta r \quad , \tag{6}$$

$$(\rho v)^{n+1}_{i,j+\frac{1}{2},k} = (\widetilde{\rho v})^{n}_{i,j+\frac{1}{2},k} - \delta t\left(p^{n+1}_{i,j+1,k} - p^{n+1}_{i,j,k}\right)/\delta z \quad , \text{ and} \tag{7}$$

$$(\rho w)^{n+1}_{i,j,k+\frac{1}{2}} = (\widetilde{\rho w})^{n}_{i,j,k+\frac{1}{2}} - \delta t\left(p^{n+1}_{i,j,k+1} - p^{n+1}_{i,j,k}\right)/(r_i\,\delta\theta) \quad . \tag{8}$$

The momentum density quantities designated by the superscript tilde $(\widetilde{\ })$ account for the effects of momentum convection, gravity, source, and viscous stress. For example, consider

$$\begin{aligned}(\widetilde{\rho v})^{n}_{i,j+\frac{1}{2},k} = (\rho v)^{n}_{i,j+\frac{1}{2},k} + \delta t\{ &- \langle \rho^n v^n u^n r\rangle_{i,j+\frac{1}{2},k}/(r_i\,\delta r) \\ &- \langle \rho^n v^n v^n\rangle_{i,j+\frac{1}{2},k}/\delta z - \langle \rho v^n w^n\rangle_{i,j+\frac{1}{2},k}/(r_i\,\delta\theta) \\ &+ \hat{\rho}^{n}_{i,j+\frac{1}{2},k} g + (M_z)^{n}_{i,j+\frac{1}{2},k} \\ &+ \left[r_{i+\frac{1}{2}}(\sigma_{rz})^{n}_{i+\frac{1}{2},j+\frac{1}{2},k} - r_{i-\frac{1}{2}}(\sigma_{rz})^{n}_{i-\frac{1}{2},j+\frac{1}{2},k}\right]/(r_i\,\delta r) \\ &+ \left[(\sigma_{zz})^{n}_{i,j+1,k} - (\sigma_{zz})^{n}_{i,j,k}\right]/\delta z \\ &+ \left[(\sigma_{\theta z})^{n}_{i,j+\frac{1}{2},k+\frac{1}{2}} - (\sigma_{\theta z})^{n}_{i,j+\frac{1}{2},k-\frac{1}{2}}\right]/(r_i\,\delta\theta)\} \quad .\end{aligned}$$

Representing the gravity term by

$$\hat{\rho}^{n}_{i,j+\frac{1}{2},k} g = \left[\rho^{n}_{i,j+\frac{1}{2},k} - \frac{\sum_k \sum_i \rho^{n}_{i,j+\frac{1}{2},k} r_i}{\sum_k \sum_i r_i}\right] g$$

removes the necessity for resolving the hydrostatic pressure gradient, but it allows accurate representation of buoyancy forces developing from large density variations due to species concentration and temperature gradients. The momentum source (M_z) will be addressed in the next section.

The components of the viscous stress tensor are differenced in a similar manner, e.g.,

$$(\sigma_{zz})^n_{i,j+1,k} = 2\mu(v^n_{i,j+3/2,k} - v^n_{i,j+\frac{1}{2},k})/\delta z$$
$$+ \lambda[(r_{i+\frac{1}{2}}u^n_{i+\frac{1}{2},j+1,k} - r_{i-\frac{1}{2}}u^n_{i-\frac{1}{2},j+1,k})/(r_i\,\delta r)$$
$$+ (w^n_{i,j+1,k+\frac{1}{2}} - w^n_{i,j+1,k-\frac{1}{2}})/(r_i\,\delta\theta)$$
$$+ (v^n_{i,j+3/2,k} - v^n_{i,j+\frac{1}{2},k})/\delta z] \quad .$$

In the mixture internal energy equation, the source and/or sink term $Q_{i,j,k}$ is written

$$Q_{i,j,k} = (S_h I_h)^n_{i,j,k} + (S_s I_s)^n_{i,j,k} - (C_s I)^n_{i,j,k} - \frac{AH^n}{Vol_{i,j,k}}(T^{n+1}_{i,j,k} - T_w) \quad ,$$

where

I_h = internal energy of the hydrogen or helium in the source,

I_s = internal energy of the steam in the source,

H = local wall heat transfer coefficient,

A = wall area, and

Vol = volume of the computational cell adjacent to the wall.

Note that in the wall heat transfer term the temperature is written at the vanced time level (n+1). This allows for a stable solution for all physical values of the heat transfer coefficient. By making use of the caloric equation-of-state

$$I = \bar{C}_v T \quad ,$$

where the average specific heat is expressed in terms of the species, densities, and constant specific heats

$$\bar{C}_v = \rho^{-1} \sum_{\alpha=1}^{3} \rho'_\alpha (C_v)_\alpha \quad ,$$

the wall heat transfer term is rewritten

$$\frac{AH^n}{Vol_{i,j,k}} \left[\frac{(\rho I)^{n+1}_{i,j,k}}{\sum_{\alpha=1}^{3} (\rho'_\alpha)^{n+1}_{i,j,k} (C_v)_\alpha} - T_w \right] \quad .$$

The finite-difference equation for the mixture specific internal energy equation is then given by

$$(\rho I)^{n+1}_{i,j,k} = \Bigg\{ (\rho I)^n_{i,j,k} + \delta t \Bigg\{ - \langle \rho^n I^n u^n r \rangle_{i,j,k} / (r_i \delta r) - \langle \rho^n I^n v^n \rangle_{i,j,k} / \delta z$$

$$- \langle \rho^n I^n w^n \rangle / (r_i \delta\theta) + \left[r_{i+\frac{1}{2}} K^n_{i+\frac{1}{2},j,k} \left(T^n_{i+1,j,k} - T^n_{i,j,k} \right) \right.$$

$$\left. - r_{i-\frac{1}{2}} K^n_{i-\frac{1}{2},j,k} \left(T^n_{i,j,k} - T^n_{i-1,j,k} \right) \right] / (r_i \delta r^2)$$

$$+ \left[K^n_{i,j+\frac{1}{2},k} \left(T^n_{i,j+1,k} - T^n_{i,j,k} \right) \right.$$

$$\left. - K^n_{i,j-\frac{1}{2},k} \left(T^n_{i,j,k} - T^n_{i,j-1,k} \right) \right] / \delta z^2$$

$$+ \left[K^n_{i,j,k+\frac{1}{2}} \left(T^n_{i,j,k+1} - T^n_{i,j,k} \right) \right.$$

$$\left. - K^n_{i,j,k-\frac{1}{2}} \left(T^n_{i,j,k} - T^n_{i,j,k-1} \right) \right] / (r_i \delta\theta)^2$$

$$+ (S_h I_h)^n_{i,j,k} + (S_s I_s)^n_{i,j,k} - (C_s I)^n_{i,j,k}$$

$$\left. + \frac{AH^n T_w}{Vol_{i,j,k}} \right\} \Bigg\} \Bigg/ \left[1 + \frac{\delta t A H^n}{Vol_{i,j,k} \sum_{\alpha=1}^{3} (\rho'_\alpha)^{n+1}_{i,j,k} (C_v)_\alpha} \right] \quad (9)$$

The solution method starts with the calculation of S_h^n, S_s^n, $(\widetilde{\rho u})^n$, $(\widetilde{\rho v})^n$, $(\widetilde{\rho w})^n$, H^n, K^n and estimates of $<\rho^{n+1}u^{n+1}r>$, $<\rho^{n+1}v^{n+1}>$, $<\rho^{n+1}w^{n+1}>$, u^{n+1}, v^{n+1} and w^{n+1}, are made. The solution method proceeds with the iteration phase:

(1) The $(\rho'_\alpha)^{n+1}_{i,j,k}$'s are found from the species transport equations using the latest iterates for $(\rho'_\alpha)^{n+1}$ and $\bar{u}^{n+1}$.

(2) The global or average fluid pressure, P_o^{n+1} is determined from integrating the equation-of-state (4) over the computational volume

$$\iiint_{Vol} \frac{P_o}{T}\, dVol = \iiint_{Vol} \sum_{\alpha=1}^{3} (\gamma_\alpha - 1)(C_v)_\alpha \rho'_\alpha dVol$$

or,

$$P_o^{n+1} = \frac{\sum\sum\sum_{ijk} r_i \sum_{\alpha=1}^{3} (\gamma_\alpha - 1)(C_v)_\alpha (\rho'_\alpha)^{n+1}_{i,j,k}}{\sum\sum\sum_{ijk} r_i / T^n_{i,j,k}} .$$

(3) The equation-of-state is modified slightly to find the mixture density using the $(\rho'_\alpha)^{n+1}$'s and P_o^{n+1} from steps (1) and (2)

$$\rho^{n+1}_{i,j,k} = \frac{P_o^{n+1} \sum_{\alpha=1}^{3} (\rho'_\alpha)^{n+1}_{i,j,k}}{T^n_{i,j,k} \sum_{\alpha=1}^{3} (\gamma_\alpha - 1)(C_v)_\alpha (\rho'_\alpha)^{n+1}_{i,j,k}} .$$

(4) With $\rho^{n+1}_{i,j,k}$ [from step (3)] and the latest iterates for $\bar{u}^{n+1}$ the residual, $D_{i,j,k}$, in the mixture mass equation is calculated

$$D_{i,j,k} = \rho^{n+1}_{i,j,k} - \rho^{n}_{i,j,k} + \delta t\left[\langle \rho^{n+1} u^{n+1} r\rangle_{i,j,k}/(r_i \delta r)\right.$$

$$+ \langle \rho^{n+1} v^{n+1}\rangle_{i,j,k}/\delta z + \langle \rho^{n+1} w^{n+1}\rangle_{i,j,k}/(r_i \delta\theta)$$

$$\left. - (S_h)^{n}_{i,j,k} - (S_s)^{n}_{i,j,k} + (C_s)^{n+1}_{i,j,k}\right] \quad .$$

If the convergence criterion is met, for example, $|D_{i,j,k}| < \varepsilon$ where $\varepsilon = 10^{-4}\ \rho^{n}_{i,j,k}$, then no adjustment is made to the local pressure, $p^{n+1}_{i,j,k}$, and the velocities $\bar{u}^{n+1}_{i,j,k}$ for cell (i,j,k). If the convergence criterion is met for all cells in the computational mesh, then the iteration phase of the cycle is complete.

(5) For any cell that the criterion is not met, the local pressure is changed by an amount

$$\delta p_{i,j,k} = - \frac{\Omega\ D_{i,j,k}}{\left(\frac{\partial D}{\partial p}\right)_{i,j,k}} \quad ,$$

where

$$\left(\frac{\partial D}{\partial p}\right)_{i,j,k} = \frac{2\delta t^2}{\delta r^2 + (r_i \delta\theta)^2 + \delta z^2} \quad ,$$

and Ω is a constant over-relaxation factor selected $1.0 \leq \Omega < 2.0$, and the momenta are changed as shown in Eqs. (6) - (8). The velocities are found by simply evaluating

$$u^{n+1}_{i+\frac{1}{2},j,k} = \frac{2(\rho u)^{n+1}_{i+\frac{1}{2},j,k}}{\rho^{n+1}_{i,j,k} + \rho^{n+1}_{i+1,j,k}} \quad ,$$

$$v^{n+1}_{i,j+\frac{1}{2},k} = \frac{2(\rho v)^{n+1}_{i,j+\frac{1}{2},k}}{\rho^{n+1}_{i,j,k} + \rho^{n+1}_{i,j+1,k}} \quad , \text{ and}$$

$$w^{n+1}_{i,j,k+\frac{1}{2}} = \frac{2(\rho w)^{n+1}_{i,j,k+\frac{1}{2}}}{\rho^{n+1}_{i,j,k} + \rho^{n+1}_{i,j,k+1}} \quad .$$

Steps (1) - (5) are repeated until the convergence criterion as presented in step (4) is satisfied on the entire computational mesh. After the iteration phase is complete, the specific internal energy is calculated by Eq. (9) and the computational time step is finished with the advancement of the time step.

More details of the HMS solution methodology, code description, and a listing of the code are given in Ref. (4).

IV. NUMERICAL RESULTS

This computer code was developed to analyze the EPRI/HEDL standard problems "A" and "B".[3] The standard problems A and B, tests HM-5 and HM-6 in reference 5 respectively, were proposed as a bases for comparing blind predictions of detailed hydrogen distribution in reactor-like containment compartments. In both experiments a high velocity steam-hydrogen or steam-helium jet is released into the compartment. The reader is referred to Ref. 5, which is part of these proceedings, for a detailed discussion of the experimental facility.

Figure 2 presents the discretization of the containment compartment. We have modeled the blower which provides recirculation from the upper to lower compartments as four time-dependent prescribed inflow boundary cells. These are shown on the outer circumference (R = 3.81 m) at the axial position 2.36 m $\leq$ Z $\leq$ 3.15 m and in the azimuthal positions 20° $\leq \theta \leq$ 40°, 80° $\leq \theta \leq$ 100°, 200° $\leq \theta \leq$ 220°, and 260° $\leq \theta \leq$ 280°. Flow is allowed to exit the computational mesh by the eight continuative outflow boundary cells shown on the outer circumference (R = 381 m) at the axial position 3.93 m $\leq$ Z $\leq$ 4.72 m and in the azimuthal positions 0° $\leq \theta \leq$ 20°, 40° $\leq \theta \leq$ 60°, 80° $\leq \theta \leq$ 100°, 120° $\leq \theta \leq$ 140°, 160° $\leq \theta \leq$ 180°, 200° $\leq \theta \leq$ 220°, 240° $\leq \theta \leq$ 260°, and 280° $\leq \theta \leq$ 300°. Both tests started with the compartment at 65°C and 10^5 Pa (1 bar), with test A containing nitrogen and test B containing air. Table I lists the timing of events for each test.

TABLE I. Timing of Events

Test A		Test B	
Time (minutes)	Event	Time (minutes)	Event
11.50	Recirculator blower on	4.00 (4.50)*	Recirculator blower on
11.75	Steam source on	4.75	Steam source on
12.50	Hydrogen source on	6.25	Helium source on
12.75	Nitrogen becomes saturated in recirculators	6.50	Air becomes saturated in recirculators
13.5	Hydrogen begins entering compartment through recirculators	7.00	Helium begins entering compartment through recirculators
23.75	Sources shut off	17.00	Sources shut off

*Blind calculation started at 4.00 minutes and the posttest calculation started at 4.50 minutes.

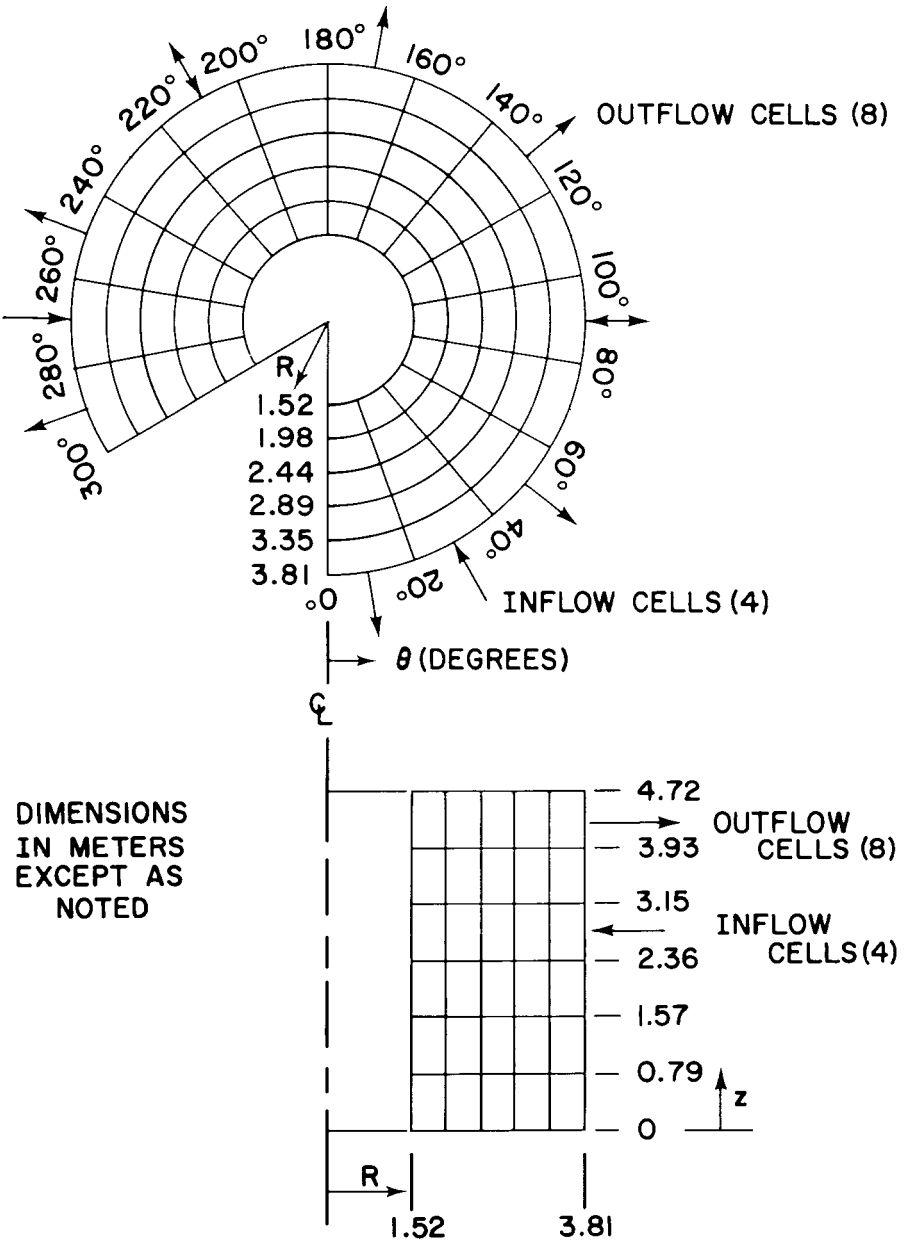


Fig. 2. HMS computing mesh for EPRI/HEDL Standard Problems A and B.

Compartment wall temperatures were assumed constant at 65°C through both tests, while time-dependent prescribed inflow data consistent with the events of Table I are tabulated in Table II.

Experiment A had a horizontal steam-hydrogen jet that was centered in the annulus at 275° at a height of 1.52 m from the floor. The average jet velocity was assumed to be 150 m/s, and it was directed inward at 60° to a radial ray, which led to a momentum source:

$$(M_r)_{R = 2.44m,\ 0.79\ m \leq Z \leq 1.57\ m,\ 260° \leq \theta \leq 280°} = -\frac{1}{2}(S_s + S_h)(150),$$

$$(M_\theta)_{2.44m \leq R \leq 2.89\ m,\ 0.79\ m \leq Z \leq 1.57\ m,\ \theta = 260°} = -0.866(S_s + S_h)(150), \text{ and}$$

$$(M_z) = 0 \quad ,$$

TABLE II. Time-Dependent Prescribed Inflow Data†

Test A		Test B	
Time (minutes)	Inlet Temperature (°C)	Time (minutes)	Inlet Temperature (°C)
0.0	35.0	0.0	35.0
8.0	35.0	4.0	35.0
10.0	35.5	7.0	42.0
13.0	40.0	10.0	43.0
18.0	53.0	11.0	46.5
21.0	57.0	16.0	52.0
23.0	58.25	17.0	52.5
24.0	58.5	20.0	49.5
32.0	53.5	29.0	46.5
35.0	52.5	31.5	46.5
46.0	51.0	32.5	48.0
60.0	50.0	70.0	47.5

Time (minutes)	Hydrogen Concentration (%)*	Time (minutes)	Helium Concentration (%)*
0.0	0.0	0.0	0.0
13.5	0.0	7.0	0.0
15.0	0.6	17.0	3.45
24.0	5.4	19.0	3.55
25.0	5.5	24.0	3.45
32.0	5.1	65.0	3.2
47.0	4.9		
70.0	4.8		

†The inlet velocity is held constant at 0.434 m/s throughout both tests.

*Hydrogen and Helium concentrations are given in volume % on a dry basis; i.e., the steam has been removed.

where the time-dependent mass sources S_s and S_h are tabulated in Table III. Experiment B had a vertical steam-helium jet that was located at 180°, 1.2 m from the floor, and 2.31 m from the compartment axis. The average jet velocity was assumed to be 80 m/s which led to a momentum source:

$(M_r) = 0$,

$(M_\theta) = 0$, and

$$(M_z)_{1.98\ m \leq R \leq 2.44\ m,\ Z = 1.57\ m,\ 160° \leq \theta \leq 180°} = (S_s + S_h)(80).$$

The energy source due to the jet is calculated $S_h I_h + S_s I_s$, where $I_h = (C_v)_h T$ and $I_s = (C_v)_s T$, and T is the time-dependent jet temperature listed in Table IV. For tests A and B the mass and energy sources are associated with cells ($2.44\ m \leq R \leq 2.89\ m$, $0.79\ m \leq Z \leq 1.57\ m$, $260° \leq \theta \leq 280°$), and ($1.98 \leq R \leq 2.44\ m$, $0.79\ m \leq Z \leq 1.57\ m$, $160° \leq \theta \leq 180°$), respectively.

Intermediate values of the parameters in Tables II - IV may be found by linear interpolation.

TABLE III. Time-Dependent Mass Source

Test A

Steam Mass		Hydrogen Mass	
Time (minutes)	Flow Rate (kg/min)	Time (minutes)	Flow Rate (kg/min)
0.0	0.0	0.0	0.0
11.75	0.0	12.5	0.0
12.50	21.0	13.0	0.31
14.0	24.0	23.0	0.31
23.0	24.0	23.75	0.0
23.75	0.0	60.0	0.0
60.0	0.0		

Test B

Steam Mass		Helium Mass	
Time (minutes)	Flow Rate (kg/min)	Time (minutes)	Flow Rate (kg/min)
0.0	0.0	0.0	0.0
4.75	0.0	6.25	0.0
5.50	14.5	7.0	0.405
16.0	14.5	15.25	0.405
17.0	0.0	16.0	0.94
60.0	0.0	17.0	0.0
		60.0	0.0

TABLE IV. Time-Dependent Jet Temperature

Test A		Test B	
Time (minutes)	Temperature (°C)	Time (minutes)	Temperature (°C)
10.0	108.0	2.0	110.0
16.5	101.0	7.0	96.0
18.0	103.0	12.5	96.0
18.5	124.0	17.0	124.0
19.0	130.0	18.0	113.0
20.0	133.0	19.0	109.0
21.0	136.0	21.0	107.0
23.0	140.0	60.0	94.0
24.0	140.0		
26.0	128.0		
28.0	125.0		
60.0	109.0		

In Figs. 3 and 4, we present the test data and the blind (i.e., pretest) concentration predictions for tests A and B, respectively. The curve designated "E" represents the experimental data while the curve designated "C" represents the calculation. For test A, the horizontal jet, there is total mixing throughout the compartment as evidenced by the similarity of the concentration curves and maximum concentrations at various locations in the compartment. All concentrations in this paper are reported in volume percent on a dry basis; i.e., the steam was condensed and the gas sample passed through a drying bed in the tests. Concentrations for test B, the vertical jet, are presented for the same locations as test A. Here we see a definite concentration gradient of roughly 2 to 3 concentration percent during the gas injection phase with maximum values at the compartment top and minimum values at the bottom. This gradient quickly decays to about 1% after the jet to shut off. Our blind calculations of the concentrations are seen to predict the test data very well. The blind temperature predictions were not very good as depicted in Fig. 5. We recognized this at the time,[6] but nevertheless judged our concentrations to be substantially correct. The reason that concentration is not sensitive to temperature in these tests is because the steam is mostly superheated vapor throughout the compartment.

During the posttest analysis, an error was found in the solution of the energy equation. Recalculations showed negligible change in the concentrations and good agreement with the temperatures, as shown in Fig. 6. The corrected energy equation also includes the Uchida[7] correlation for wall-heat transfer and the assumption that K = 0.

For roughly 15 minutes of physical time, these problems required between 5 and 6 hours of CDC 7600 CPU times, or about 2.5 hours of Cray CPU time.

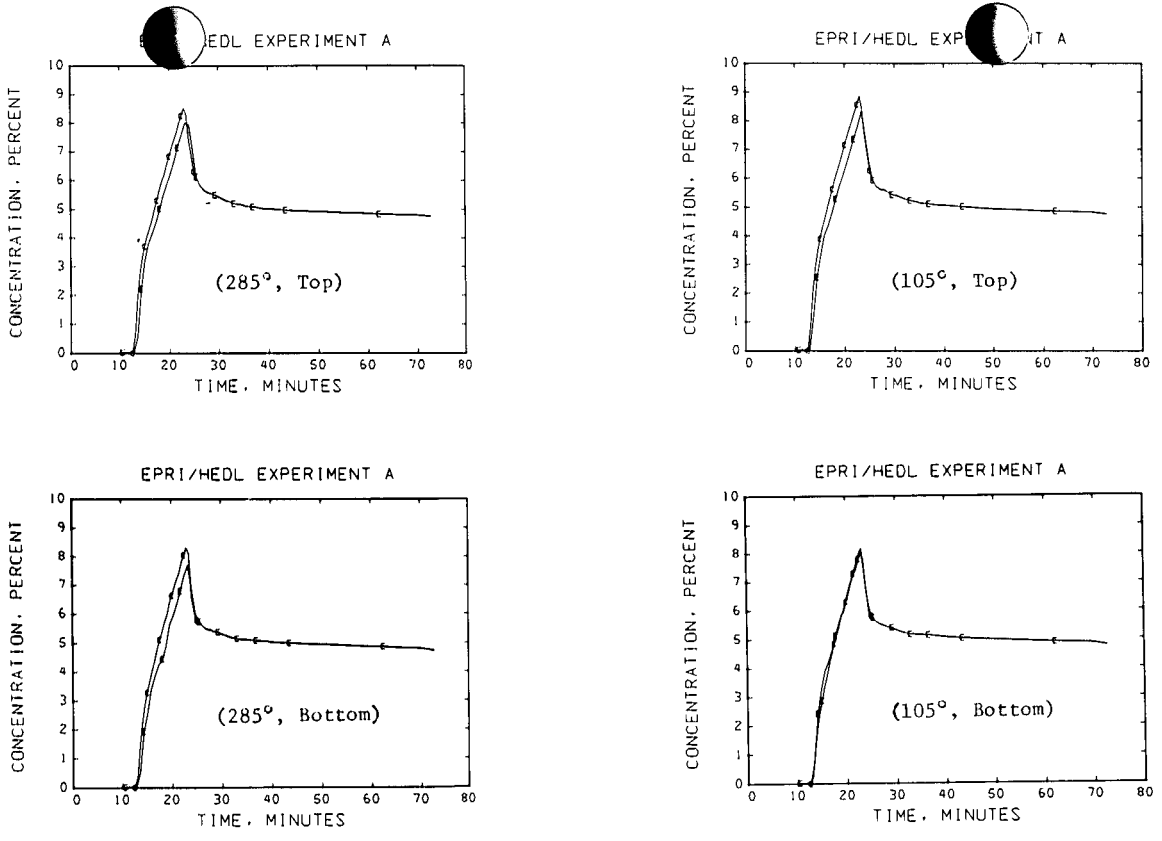


Fig. 3. Hydrogen concentrations for Test A on a dry basis for the indicated locations. The Top and Bottom designations are 0.23 m below the ceiling and 0.3 m above the lower deck, respectively. The curves labeled "E" depict experimental data and those labeled "C" represent the blind calculated results.

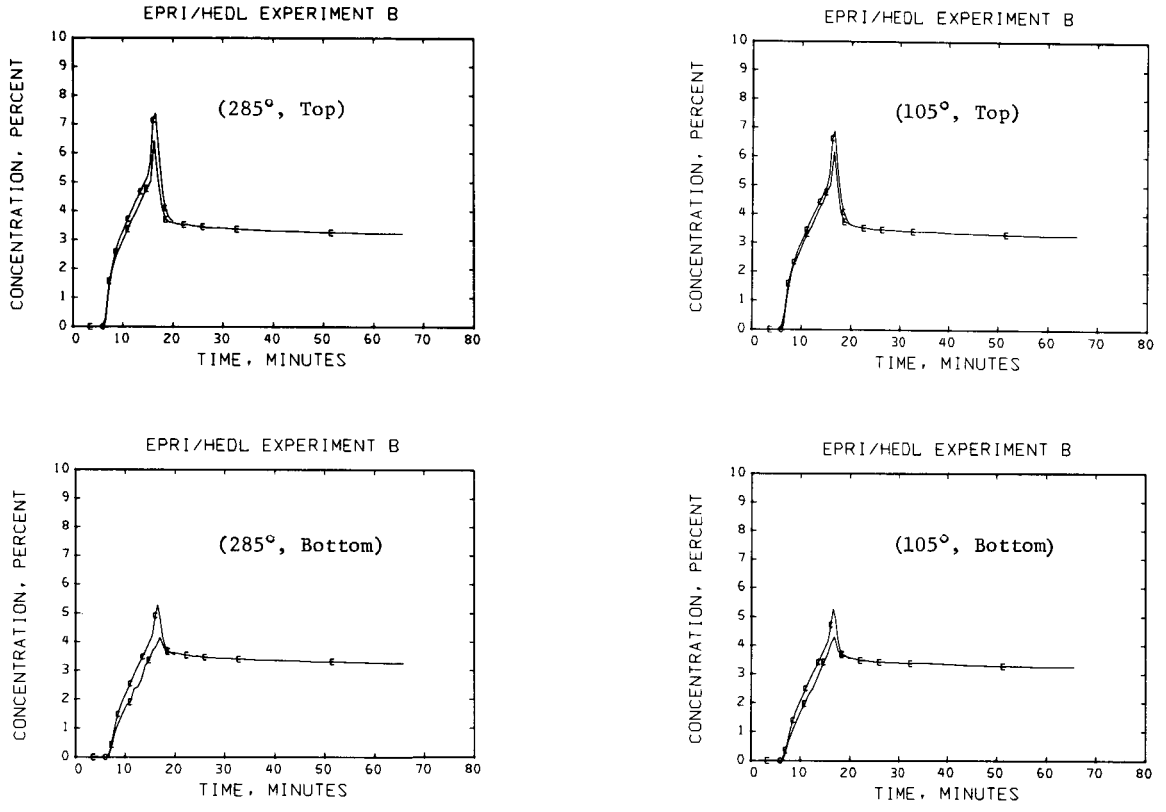


Fig. 4. Helium Concentrations for Test B on a dry basis for the indicated locations. The Top and Bottom designations are 0.23 m below the ceiling and 0.3 m above the lower deck, respectively. The curves labeled "E[illegible]ict experimental data and those labeled "C" represent the blind [illegible]lated results.

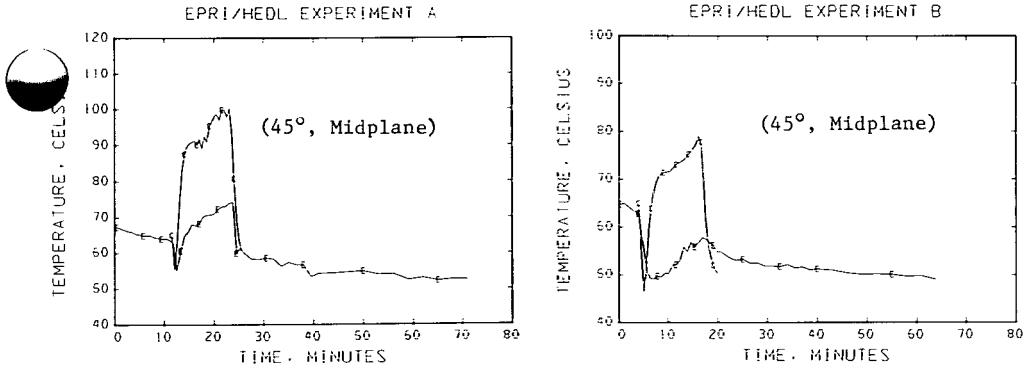


Fig. 5. Compartment temperatures for tests A and B for the indicated locations. The Midplane designation is 2.36 m above the lower deck. The curves labeled "E" depict experimental data and those labeled "C" represent the blind calculated results.

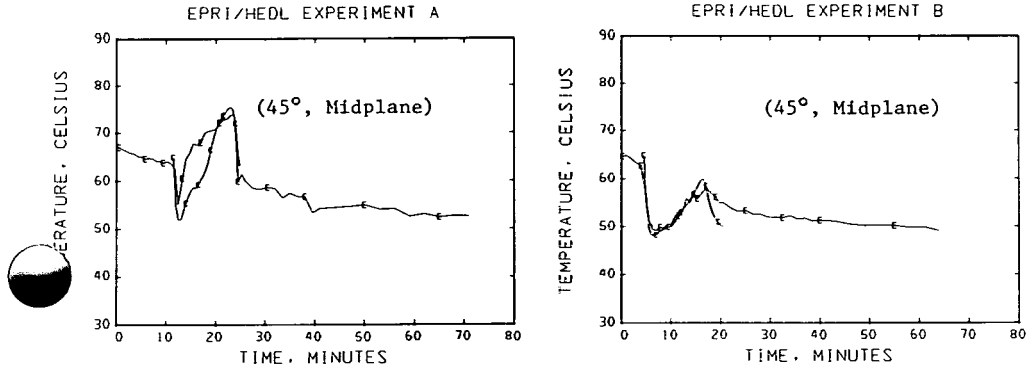


Fig. 6. Compartment temperatures for tests A and B for the indicated locations. The Midplane designation is 2.36 m above the lower deck. The curves labeled "E" depict experimental data and those labeled "C" represent the posttest calculated results.

V. CONCLUSIONS

The mathematical model and solution technique outlined above has proved to be an accurate method for calculating low speed flows with large density variations such as those found in hydrogen mixing within LWR containments. For the time-dependent, fully three-dimensional EPRI/HEDL standard problems, the calculated results compare very closely with the test data even with a fairly coarse computing mesh.

ACKNOWLEDGMENTS

It is a pleasure to express appreciation to F. H. Harlow for his helpful and guiding discussions throughout the course of this work. Additional appreciation is expressed to L. R. Stein and M. D. Torrey for their help in writing the computer programs and to N. C. Romero for his help in producing the graphics. This work was performed under the auspices of the United States Nuclear Regulatory Commission.

References

1. F. H. Harlow and A. A. Amsden, "Numerical Fluid Dynamics Calculation Method for All Flow Speeds," J. Comput. Phys. 8, 197 (1971).
2. C. K. Forester and A. F. Emergy, "A Computational Method for Low Mach Number Unsteady Compressible Free Convective Flows," J. Comput. Phys. 10, 487 (1972).
3. G. R. Bloom and S. W. Claybrook, "Standard Problems on Hydrogen Mixing and Distribution," Westinghouse Hanford Company, Richland, Washington, March 26, 1982.
4. J. R. Travis (in preparation), "A Finite-Difference Method for Time-Dependent, Three-Dimensional Low-Speed Gas Flows with Large Density Variations," Los Alamos National Laboratory report.
5. G. R. Bloom, L. D. Muhlestein, and A. K. Postma, "Hydrogren Distribution in a Compartment with a High Velocity Hydrogen-Steam Source," Second International Workshop on the Impact of Hydrogren on Water Reactor Safety, Albuquerque, NM, October 1982.
6. J. R. Travis, Letter to G. R. Bloom and S. W. Claybrook submitting standard problem results, April 27, 1982.
7. H. Uchida, A. Ogama, and Y. Togo, "Evaluation of Postincident Cooling Systems of Light-Water Power Reactors," Proc. of the Third Inter. Conf. on the Peaceful Uses of Atomic Energy, Geneva, Switzerland (August 31 - Sept. 9, 1964); Vol. 13, 93-104, United Nations, A/CONF.28, p. 436 (1965).

APPLICATION OF COBRA-NC TO HYDROGEN TRANSPORT

M. J. THURGOOD

ABSTRACT

COBRA-NC, a thermal-hydraulic computer code for the analysis of Light Water Reactor (LWR) containment system transients is presented. A brief description of the code is provided While the code is being developed for all phases of a containment transient, data comparisons with hydrogen distribution test data obtained in the Hanford Engineering Development Laboratory te facility and in the Battelle Memorial Institute's test facility are presented in this paper. advantages this code features over other containment codes is also discussed.

INTRODUCTION

The COBRA-NC computer code has been developed to analyze the transient response of LWR containment system's to reactor transients and accidents that result in the release of steam, water and noncondensible gases into the containment atmosphere. The code has been designed to predict two-phase jet impingement loads, room pressurization and the migration of hydrogen and other noncondensable gases within the containment. COBRA-NC thus has the capability to simulate the containment transient from the initiation of the break or release through the hydrogen distribution phase of the transient. No combustion models are currently available in the code.

The ability to compute the blowdown or initial release portion of the transient may be a very important once since the initial conditions in the containment atmosphere for hydrogen release and distribution are established during this period. There is much experimental evidence which indicates that thermal stratification and circulation patterns within the containment atmosphere may have significant effects on the distribution of hydrogen within the containment system. These conditions would be established during the initial phases of the transient.

This paper is concerned primarily with COBRA-NC predictions of hydrogen distribution experimental data. However, the reader should bear in mind that the code is also being assessed against steam/water blowdown data and two-phase jet impingement data. The two-phase flow, thermal nonequilibrium equations that are solved in COBRA-NC also provide for the simulation of containment sprays, suppression pools and ice condensors. The condensation of steam on cold surfaces, or cold water and through mixing with cooler gases is accounted for, as is heat transfer to or from solid structure within the containment.

A brief description of COBRA-NC is presented in the following section. Following this description, COBRA-NC predictions of some hydrogen distribution experiments will be discussed.

CODE DESCRIPTION

The COBRA-NC computer code utilizes a multicomponent, two-fluid, three-field representati of two-phase flow. Conservation equations are solved for water and its vapor and for a noncondensible gas mixture comprised of n species. There are eight noncondensible gas species currently coded. Water and steam provide the two-fluid definition and steam and the mixture of n-noncondensible gases provide the multicomponent definition.

The three velocity fields are 1) the steam and noncondensible gas mixture, 2) the continuous liquid field and 3) the entrained droplet field. Three temperature fields are included. These are 1) the gas-vapor mixture temperature, 2) the continuous liquid and liquid drop mixture temperature, and 3) the temperature of solid structures within the flow field. The field

equations are finite differenced on a three-dimensional mesh in Cartesian coordinates and are solved using a Block-Newton Rapheson linearization technique.

All of the capabilities provided by the two-fluid model are not required if one is solely interested in the distribution of hydrogen within a dry or superheated steam atmosphere. The two-fluid capabilities are not even required in the presence of condensing steam if the condensate has no significant effect on the behavior of the flow field. The two-fluid model is required when 1) the hydrogen/steam mixture flows through liquid pools (e.g., suppression pools) 2) when sprays (or condensate in drop or mist form) impart significant momentum, condensation or turbulence to the containment atmosphere (e.g., containment sprays, two-phase jets, etc.) and 3) when phase changes can significantly alter local gas concentrations and effect transfer rates (e.g., ice condensers and liquid films on containment walls).

The conservation equations solved in the code are as follows:

MOMENTUM

$$\frac{\partial}{\partial t}(\alpha_v \rho_{vg} \vec{U}_v) + \nabla \cdot (\alpha_v \rho_{vg} \vec{U}_v \vec{U}_v) = -\alpha_v \Delta P + \alpha_v \rho_{vg} \vec{g} - \vec{\tau}'''_{wv} - \vec{\tau}'''_{I_{\ell v}} - \vec{\tau}'''_{I_{ev}} + (\Gamma''' \vec{U})$$

$$+ \nabla \cdot (\alpha_{\ell} \underline{\underline{I}}_{v=vg}^{\Gamma}) + \nabla \cdot (\alpha_v \underline{\underline{\sigma}}_{v=vg})$$

$$\frac{\partial}{\partial t}(\alpha_{\ell} \rho_{\ell} \vec{U}_{\ell}) + \nabla \cdot (\alpha_{\ell} \rho_{\ell} \vec{U}_{\ell} \vec{U}_{\ell}) = -\alpha_{\ell} \Delta P + \alpha_{\ell} \rho_{\ell} \vec{g} - \vec{\tau}'''_{w\ell} + \vec{\tau}'''_{I_{\ell v}} - (\Gamma''' \vec{U}) - (S''' \vec{U})$$

$$+ \nabla \cdot (\alpha_{\ell} \underline{\underline{I}}_{\ell=\ell}^{\Gamma}) + \nabla \cdot (\alpha_{\ell} \underline{\underline{\sigma}}_{\ell=\ell})$$

$$\frac{\partial}{\partial t}(\alpha_e \rho_{\ell} \vec{U}_e) + \nabla \cdot (\alpha_e \rho_{\ell} \vec{U}_e \vec{U}_e) = -\alpha_e \nabla P + \alpha_e \rho_{\ell} \vec{g} + \vec{\tau}'''_{I_{ev}} - (\Gamma'''_e \vec{U}) + (S''' \vec{U})$$

Rate of change of momentum + Rate of momentum change by convection = Pressure gradient + Gravity force + Wall shear

+ Interfacial drag between vapor and *continuous* liquid + Interfacial drag between vapor and drops + Interfacial momentum exchange + Momentum exchange due to entrainment

+ Turbulent stresses + Viscous stresses

MASS

$$\frac{\partial}{\partial t}\alpha_v\rho_v + \nabla\cdot(\alpha_v\rho_v\vec{U}_v) = \Gamma''' + \nabla\cdot\alpha_v\rho_{mg}\varepsilon_D\nabla W_v$$

$$\frac{\partial}{\partial t}\alpha_\ell\rho_\ell + \nabla\cdot(\alpha_\ell\rho_\ell\vec{U}_\ell) = \Gamma_i''' - S'''$$

$$\frac{\partial}{\partial t}\alpha_e\rho_\ell + \nabla\cdot(\alpha_e\rho_\ell\vec{U}_e) = -\Gamma_e''' + S'''$$

$$\frac{\partial}{\partial t}\alpha_v\rho_g + \nabla\cdot(\alpha_v\rho_g\vec{U}_v) = \Gamma_{mg} + \nabla\cdot\alpha_v\rho_{mg}\varepsilon_D\nabla W_g$$

Rate of change of mass	+	Rate of mass gain by convection	=	Rate of mass gain by interfacial transfer or chemical reaction	+	Rate of mass gain by entrainment	+	Rate of mass efflux due to turbulent diffusion

ENERGY

$$\frac{\partial}{\partial t}(\alpha_v\rho_{vg}h_{vg}) + \nabla\cdot(\alpha_v\rho_{vg}h_{vg}\vec{U}_v) = \Gamma''' h_g + q_{iv} + Q'''_{vg}$$

$$- \nabla\cdot(\alpha_v q_{vg}) - \nabla\cdot(\alpha_v\underline{\underline{\tau}}_{vg}) + \alpha_v\frac{\partial P}{\partial t}$$

$$\frac{\partial}{\partial t}(\alpha_\ell + \alpha_e)\rho_\ell h_\ell + \nabla\cdot(\alpha_\ell\rho_\ell h_\ell\vec{U}_\ell) + \nabla\cdot(\alpha_e\rho_\ell h_\ell\vec{U}_e) = -\Gamma'''h_f + q_{i\ell} + Q'''_L$$

$$- \nabla\cdot(\alpha_\ell\underline{q}_\ell) - \nabla\cdot(\alpha_\ell\underline{\underline{\tau}}_\ell) + (1-\alpha_v)\frac{\partial P}{\partial t}$$

Time rate of Change	+	Convection	=	Energy Transport Due to Phase Change	+	Interfacial Heat Transfer

+	Wall Heat Flux	-	Conduction Heat Flux	-	Turbulent Heat Flux	+	Pressure Derivative

The following gas transport equation is solved for n-1 species of the gas mixture.



GAS TRANSPORT EQUATION

$$\frac{\partial \alpha_v \rho_A}{\partial t} + \nabla \cdot \alpha_v \rho_A \bar{V} - \nabla \cdot \alpha_v \rho_{mg} \varepsilon_D \nabla w_A - r_A = 0$$

Rate of change of mass for gas component A	+	Rate of mass flux for component A	-	Rate of mass efflux for component A due to turbulent diffusion	-	Rate of mass creation for component A due to chemical reaction, etc.	= 0

An additional transport equation is solved for the interfacial area of liquid drops:

TRANSPORT EQUATION

$$\frac{\partial A_i}{\partial t} = -\frac{\partial A_i V}{\partial x} + \frac{6Se}{\rho_\ell Ds} + S_\Gamma$$

Net Rate of Change of Interfacial Area Concentration	Rate of Interfacial Area Concentration Change Due to Convection	Rate of Interacial Area Concentration Change Due to Entrainment and Deposition of Drops	Rate of Interfacial Area Concentration Change Due to Phase Change

DROP SIZE



$= 6.0\alpha_e / A_i$

Constitutive relations to affect closure of the above equations include models for interfacial shear, interfacial mass and heat transfer, wall heat transfer, wall shear, turbulent shear stresses, entrainment and de-entrainment rates and thermodynamic properties for water and for the noncondensible gases.

Comparisons between the predictions made using the above described model and hydrogen distribution experimental data will now be discussed.

HYDROGEN DISTRIBUTION DATA COMPARISONS

COBRA-NC has been used to simulate hydrogen migration tests conducted in the HEDL Containment System Test Facility (CSTF) and the Battelle Memorial Institute's (BIF) model containment at Frankfurt Ge

HEDL Tests

Comparisons with two HEDL tests designated Jet A and Jet B and Battelle Frankfurt tests, 6, 12 and 15 are reported here. The HEDL facility consists of a larger steel vessel 20.4 m high and 7.6 m in diameter with a annular test compartment constructed in the bottom half of the vessel. The test compartment was a 300 degree segment of an annular ring 7.62 m O.D, 3.0 m I.D. and 4.72 meters high. A blower in the upper compartment provided air recirculation from the upper to lower compartment through four inlet ducts. The outlet air flow passages consisted of 24 vertical slots cut into the wall of circular duct segments connected to the ceiling of the test compartment. Gas concentrations were measured at 15 instrumentation locations at 5 circumferential locations around the annulus. Measurements were made at the bottom, middle and top elevations at each circumferential location.

The horizontal Jet A was located 25° from one radial wall of the test section and was centered in the annulus at a height of 1.52 m from the floor. The vertical Jet B was directed vertically at 120° from one radial wall and 1.2 m from the floor of the test compartment. A schematic of the test section and the COBRA-NC mesh used in the calculation is shown in Figure 1. A mesh of 51 cells on a level and 5 levels high was used in this simulation. A variable mesh was used to allow a smaller mesh size in the vicinity of Jet A. The same mesh was used for the test with Jet B since this prediction was submitted as a blind calculation and time did not allow us to use a different mesh that would provide a finer mesh around Jet B.

The jet hydrogen and steam flowrates and the jet temperature specified for Jet A are shown in Figure 2. The specified blower inlet temperature and hydrogen concentration are shown in Figures 3 and 4. All gas concentrations are shown on a "dry" basis (i.e., the concentration after the steam condensed out).

The hydrogen concentrations calculated on a dry basis for the measurements located at 125° from the radial wall for the "blind" calculation are shown in Figure 5 for the bottom sensor, and Figure 6 for the top sensor. The code prediction at the lower elevation is in reasonable agreement with the data both in shape and magnitude. The observed time shift between the data and the calculation is accounted for in part by a time lag in the experimental measurement systems for which the data shown here has not been corrected. The magnitude of the predicted concentration at the top elevation is a bit low, however even

more significantly the shape of the calculation differs from the measured data. The irregular spiked shape of the calculated curve shown in Figure 6 is the result of a restart error in the code. The calculation was run in two segments and data from the first segment was dumped to a restart file. This file was read by the code in the second restart run and the calculation was continued. A variable was [illegible]ut of the restart dump causing the perturbation to the flow field observed in Figure 6. That this was the problem was demonstrated by a post test calculation in which the restart was not used. A coarser mesh was also used in the post test calculation, Figure 7. All other initial and boundary conditions remained the same and no changes were made to the code between the "blind" and "post test" calculation. The code prediction for the 125° top elevation is shown in Figure 10. Notice that the shape and magnitude of the prediction compares very well with the measured data. Also, there is no disturbing jaggedness to the curve (compare with Figure 6). All calculated values at the top and middle elevations showed the same concentration as did the experimental data. The bottom elevation was slightly underpredicted using the coarse mesh while they were predicted very well using the fine mesh (Figure 5). The bottom concentrations were underpredicted by 17% using the coarse mesh. The coarse mesh causes the jet momentum to be rapidly dissipated resulting in less circulation within the test compartment. The finer mesh preserved more of the jet's momentum allowing a complete mixing of the test compartment. However, one should consider the additional computational cost required to obtain the more accurate solution. The fine mesh calculation required 8 CPU hours on a CDC 7600 computer for 15 transient minutes while the coarse mesh calculation only required 0.72 hours of CPU time for a 23.3 minute transient. Note that the full set of two-fluid equations are solved even though they are not necessarily needed for this test and so one should expect this code to be slower than corresponding single-phase codes. The predicted temperatures at the corresponding measurement locations for the fine mesh calculation are shown in Figure 8 and 9. The reasonable comparison with the data is a good indication that about the right amount of condensation, thermal mixing and wall heat transfer has been calculated.

The "blind" results for the vertical helium Jet B using the original mesh are shown in Figures 11 through 14. The location of the jet was artificially raised in the calculation to avoid the jet crossing [illegible]he narrow level of mesh cells provided for Jet A. This was done to avoid the small timestep dictated by the courant limitation at this location thereby reducing the computational time. The predicted concentrations at the top elevation compare very well with the data in shape and magnitude (Figure 11). The concentrations at the middle and lower elevations were underpredicted. This is a result of the high jet elevation and the coarseness of the mesh in the vicinity of Jet B. It can be assumed that if a finer mesh were used to preserve the momentum of Jet B then there would be increased mixing within the compartment. The temperature predictions for this test were also reasonable (Figure 14).

Battelle Frankfurt Test 12

One of the features of COBRA-NC is that it can be used in either a multidimensional finite difference mode or in a lumped parameter mode. Test 12 of the hydrogen distribution series conducted in the Battelle Frankfurt model containment was simulated to assess the lumped parameter capability.

A schematic of the Battelle facility is shown in Figure 15(a). Rooms 1, 2, 5, 6, 7 and 8 were used during test 12 and all other rooms were sealed off resulting in the test section shown schematically in Figure 15(b). The gas source was in room 1. All rooms were initially at the same temperature. The nodalization used in the calculation along with the boundary conditions is shown in Figure 16. The code predictions are shown in Figure 17 through 20 for sensors located in rooms 1, 2, 7 and 6 respectively. The code predictions are very good for the isothermal test using a lumped parameter approach. The analyst should be cautioned to test the solution for accuracy by varying the time step size when using the lumped parameter approach as some sensitivity to time step size was observed in this calculation. A maximum time step size of 10 seconds was used. The calculation required 5 minutes of CPU time on a CDC 7600 for the 23.6 hour transient.

Battelle Frankfurt Test 15

Test 15 was conducted with the same geometry used in test 12. However, the upper rooms were initially heated to 35°C and the lower rooms to 16°C. The injection rate and composition of the gas mixture were nearly the same as in test 12. A calculation was run using the same nodalization as for test 12. A complete stratification was predicted with all the injected hydrogen remaining in the lower rooms. Additional nodes were added to provide computational circulation paths between the upper and lower compartments. This nodalization is shown in Figure 21. The results for this calculation are shown in Figure 22. The upper curves are the concentraiton in room 1 and the lower curves in room 2. An initial stratification is calculated and then a convection loop is established that completely mixes the compartments. The data indicates a continued separation. The thermal energy stored in the walls of the upper rooms and the heat transfer from these walls was not modeled in this calculation. It is believed that this stored energy is sufficient to maintain the temperature of the upper atmosphere and sustain a thermal stratification. The lack of wall heat transfer in the calculation could explain the early destratification. The wall heat transfer will be modeled in a future calculation. However, the results are sensitive to nodalization so that an increased number of nodes may be required to obtain a closer data comparison. That the code can in fact calculate stratification is demonstrated in the next simulation.

Battelle Frankfurt Test 6

All rooms except rooms 1 and 2 of the Battelle containment were sealed off during this test. A schematic of the resulting test geometry is shown in Figure 23. As in test 15 the upper room was heated to 35°C and the lower room to 17°C. The mesh used for this calculation is shown in Figure 24. The gas source boundary conditions are also shown. The results of the calculation are compared with the experimental data measured at the top of room 1 in Figure 25 and at the top of room 2 in Figure 26. The correct trend of the data is predicted by the code. A significant concentration difference betweem the upper and lower rooms is predicted. The predicted concentration at the top of room 1 is lower than the measured value. The reason for this is uncertain. It is possible that the thermal layer extends down below the orifice between the two rooms thereby increasing the hydrogen concentration in the lower room. It is also uncertain if the volume fraction of hydrogen injected was correctly measured. The wall heat transfer was also not modeled in this calculation and it is possible that this could contribute to the error. However, the capability to predict hydrogen stratification due to a thermal layer has been demonstrated.

CONCLUSIONS

COBRA-NC, a computer code developed for the analysis of LWR containment systems has been briefly described. This code has been assessed against a variety of data. Comparisons with hydrogen distribution test data has been reported here. The overall capability of the code to predict hydrogen distribution in experimental tests has been demonstrated in both the finite difference and lumped parameter modes. These data comparisons are in general very good and indicate that COBRA-NC can be used to reliably predict hydrogen distribution in LWR containment systems. The need for the improvement of some of the input models has been indicated, in particular the modeling of hot walls during thermal stratification tests. The code will continue to be assessed against available data.

A very important feature of COBRA-NC has been demonstrated. This is the capability to do either a finite difference calculation or a lumped parameter calculation or a mixture of both. This may be an essential feature when the code is applied to real containment systems that are very large and complex. This feature will allow the analyst to obtain a reasonably accurate calculation of hydrogen distribution within the containment while using an economically reasonable number of mesh cells. This feature combined with the codes capability to predict steam condensation and two-phase flow make it a very attractive choice for containment analysis.

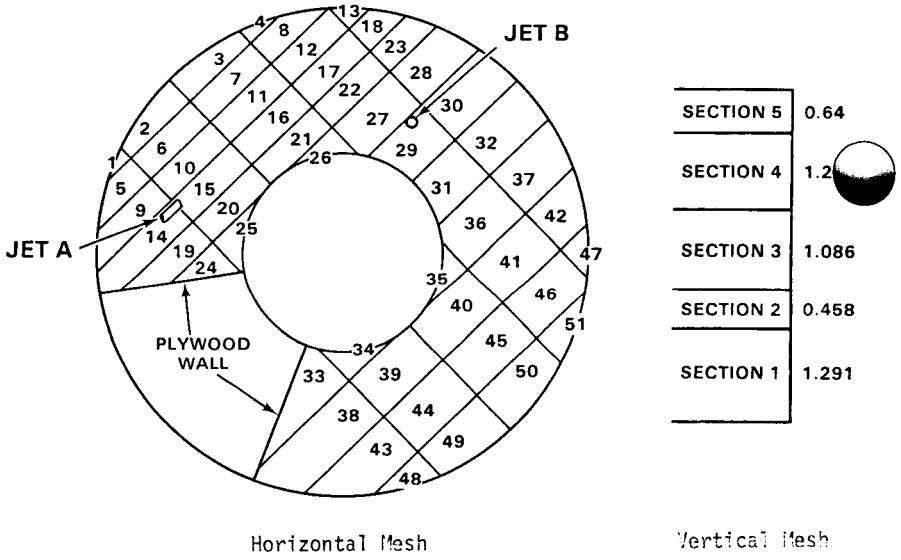


FIGURE 1. Geometry and Mesh for the HEDL Hydrogen Distribution Tests

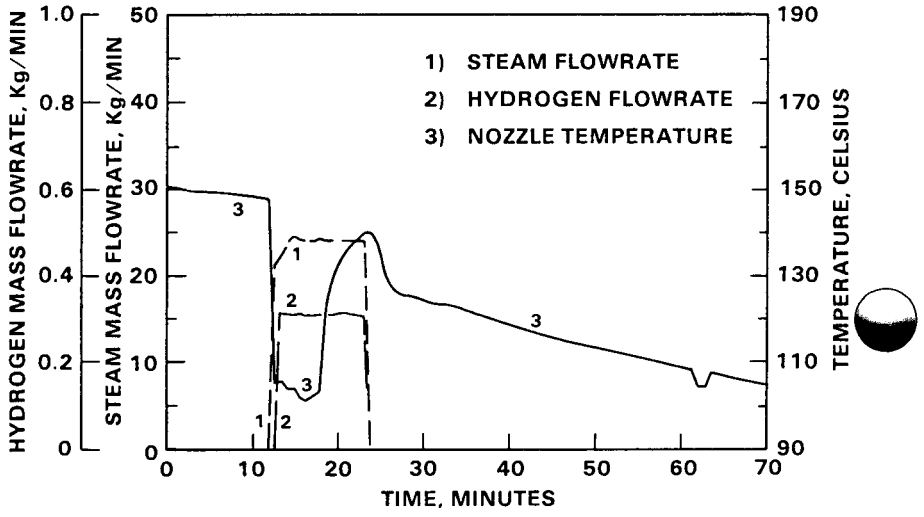


FIGURE 2. Test A Nozzle Gas Flow Rates and Temperature

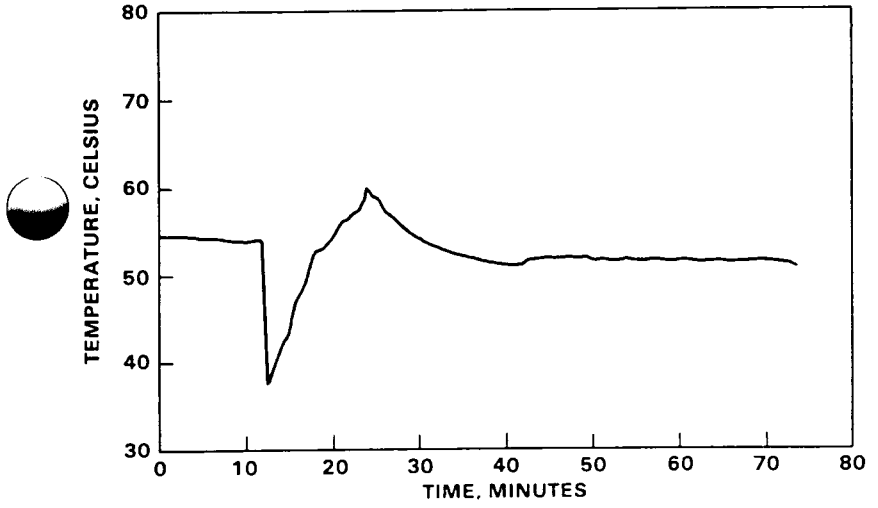


FIGURE 3. Test A Recirculation N_2 Temperature

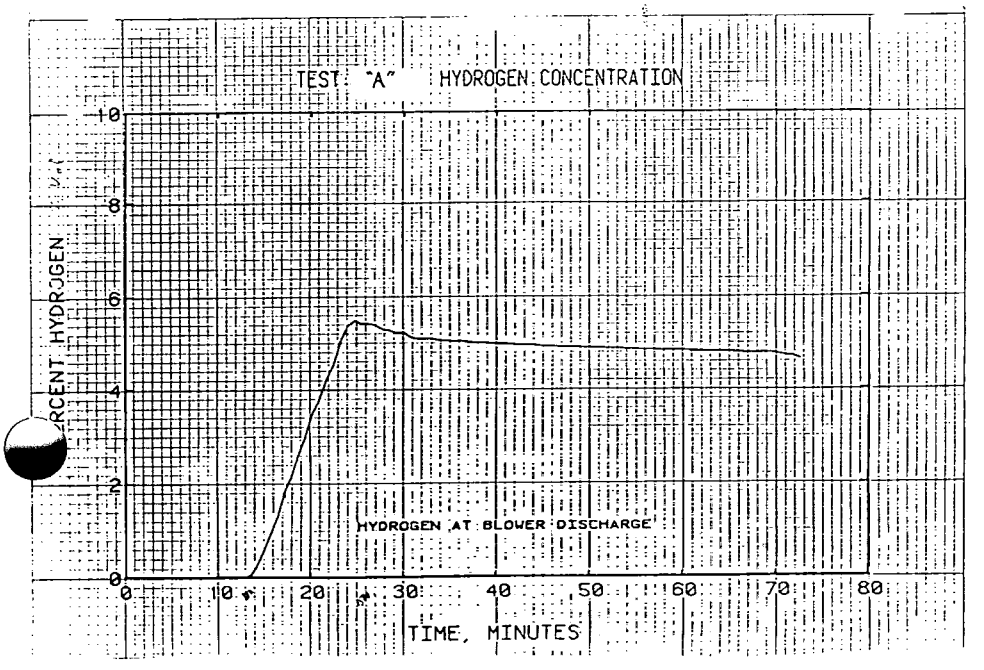


FIGURE 4. Test A Blower Hydrogen Concentration

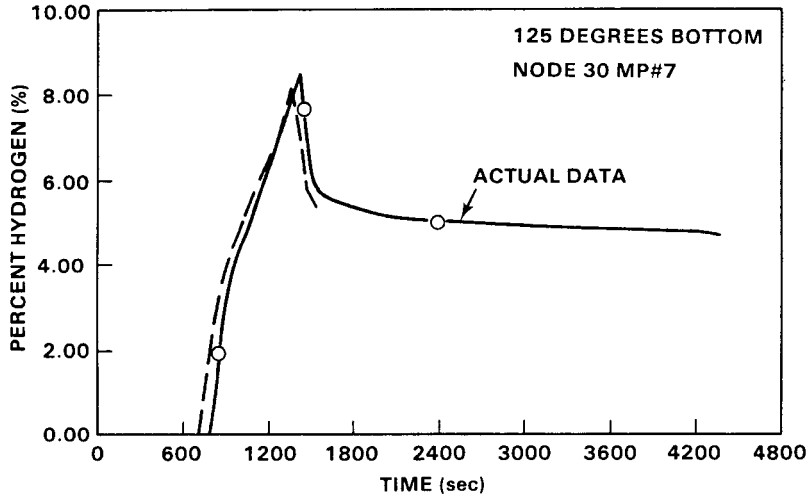


FIGURE 5. Test A Hydrogen Concentration at the Bottom of 125 Degree Location - Blind Calculation

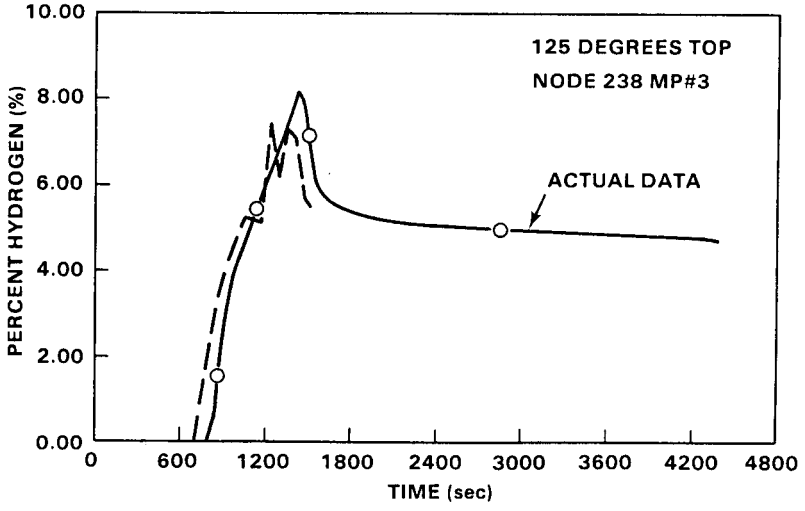


FIGURE 6. Test A Hydrogen Concentration at the Top of the 125 Degree Location - Blind Calculation

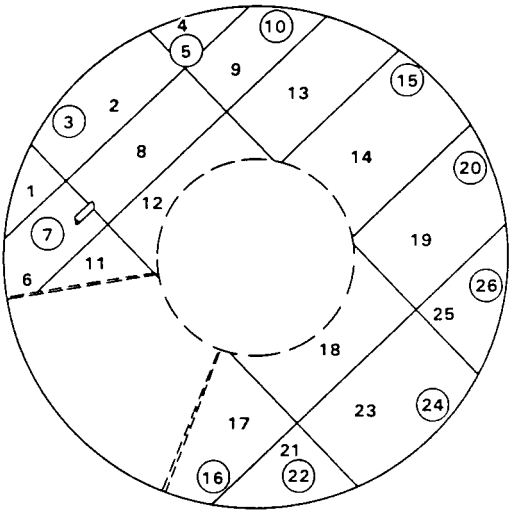


FIGURE 7. Coarse Mesh for the HEDL Post-Test Calculation

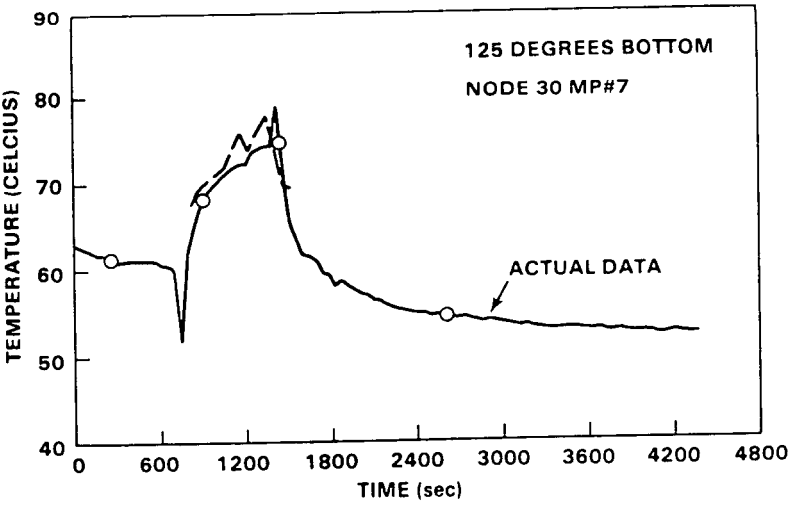


FIGURE 8. Test A Gas Temperature at Bottom of the 125 Degree Location

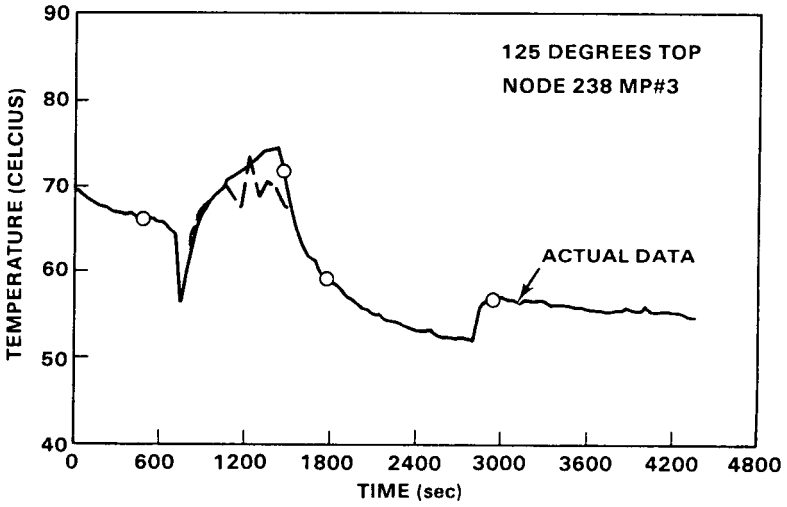


FIGURE 9. Test A Gas Temperature at the Top of the 125 Degree Location

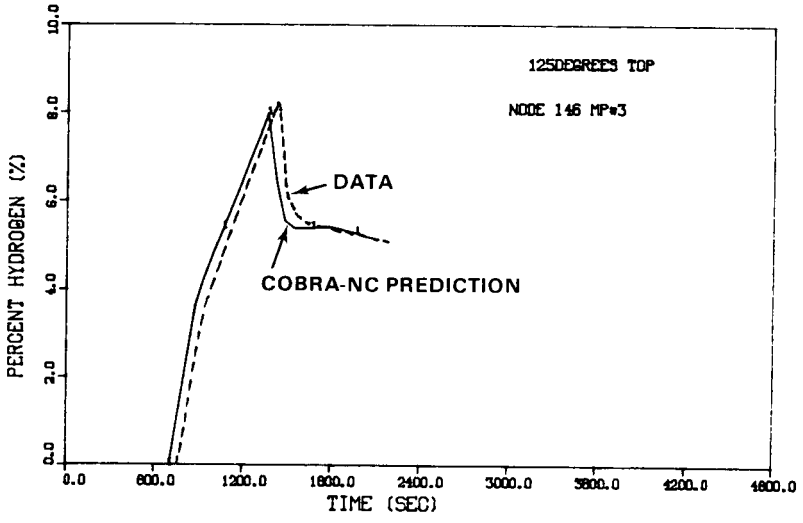


FIGURE 10. Test A Hydrogen Concentration at the Top of the 125 Degree Location - Post-Test Calculation

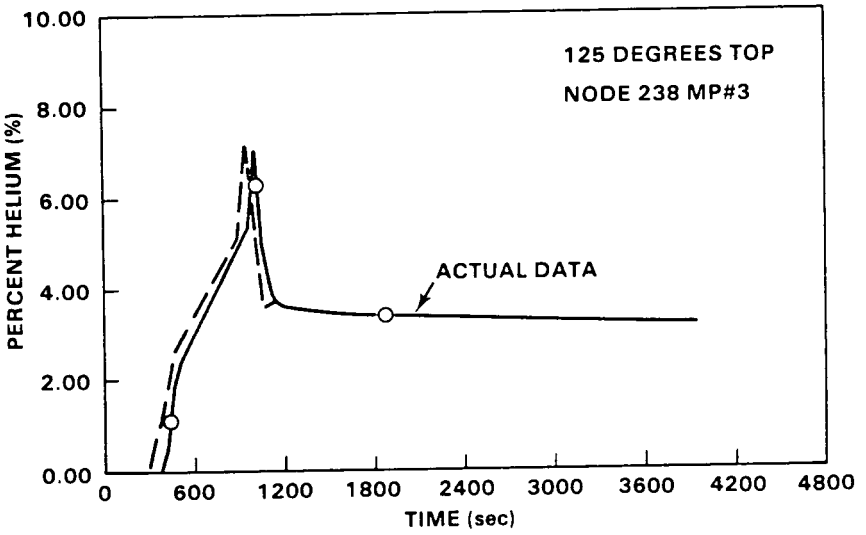


FIGURE 11. Test B Helium Concentration at the Top of the 125 Degree Location - Blind Calculation

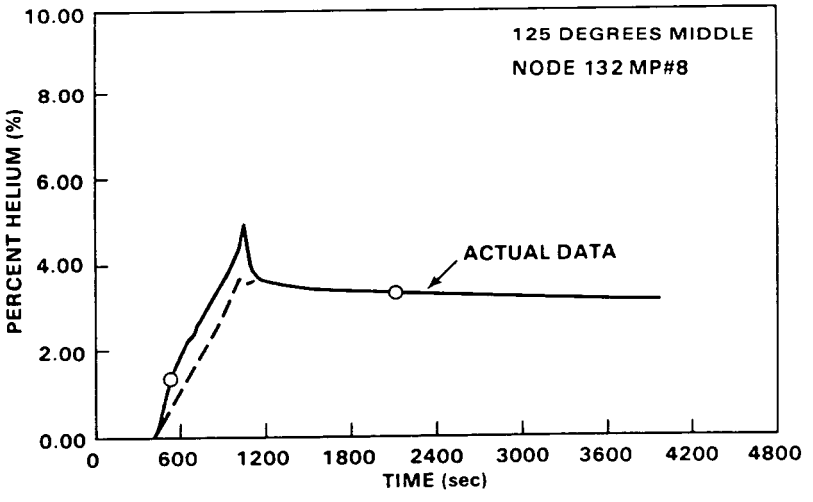


FIGURE 12. Test B Helium Concentration at the Middle of the 125 Degree Location - Blind Calculation

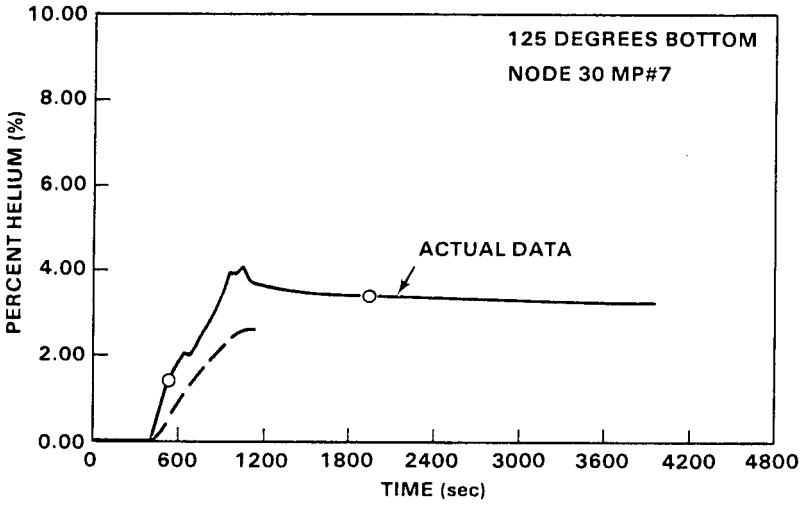
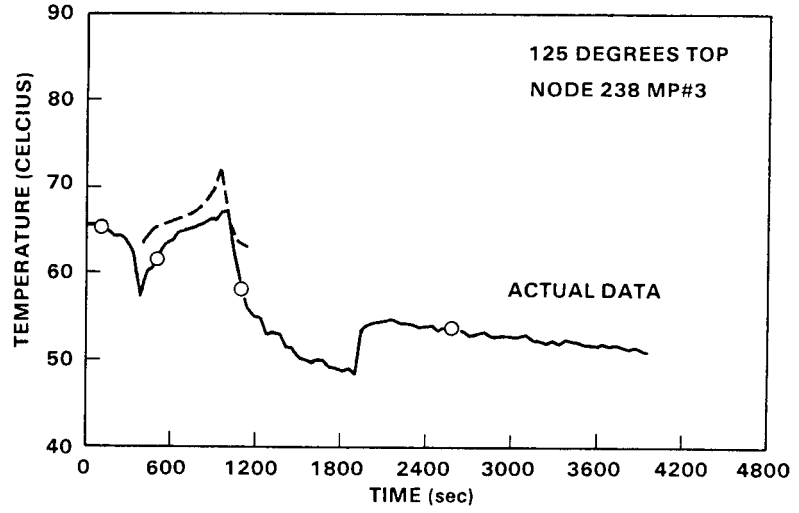


FIGURE 13. Test B Helium Concentration at the Bottom of the 125 Degree Location - Blind Calculation



TEST 14. Test B Gas Temperature at the Top of the 125 Degree Location - Blind Calculation

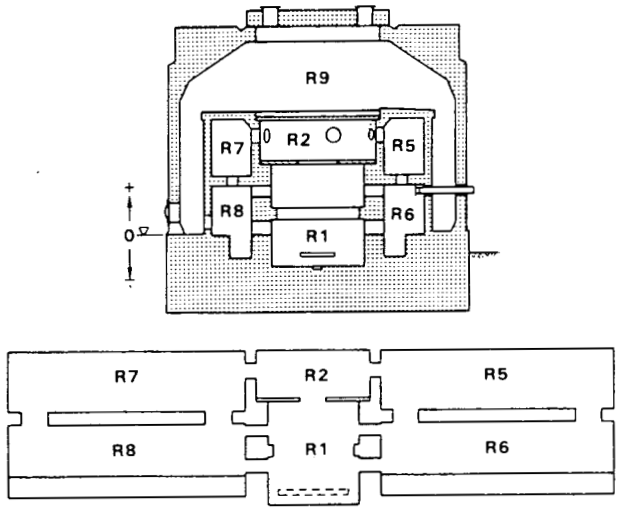
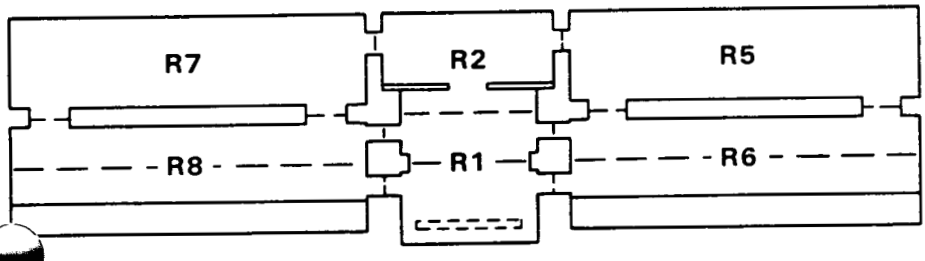


FIGURE 15. Schematic of Battelle Memorial Institute Model Containment



GAS SOURCE
MEAN INJECTION RATE: 0.32m³/hr
MIXTURE: 66.8% H_2 BY VOLUME
33.2% N_2 BY VOLUME

FIGURE 16. Nodalization and Boundary Conditions for Battelle Frankfurt Test 12

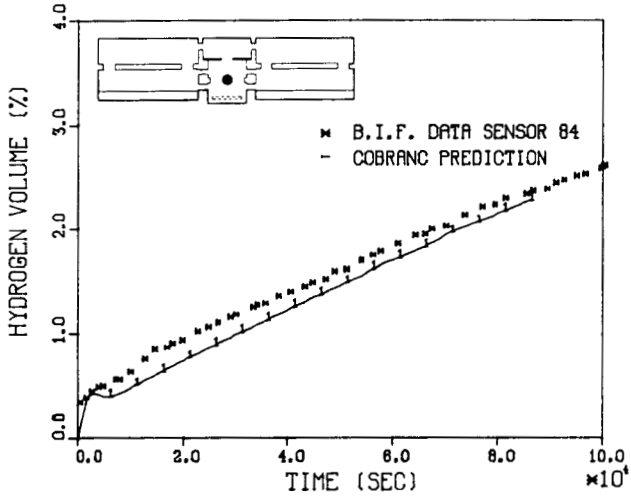


FIGURE 17. Test 12 Hydrogen Concentration in Room 1

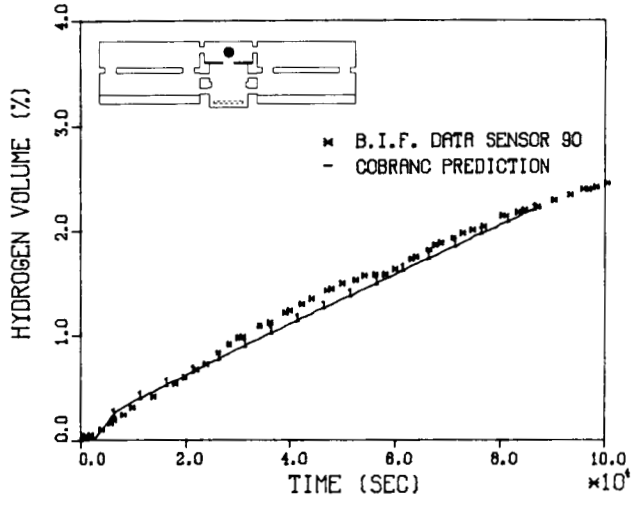


FIGURE 18. Test 12 Hydrogen Concentration in Room 2

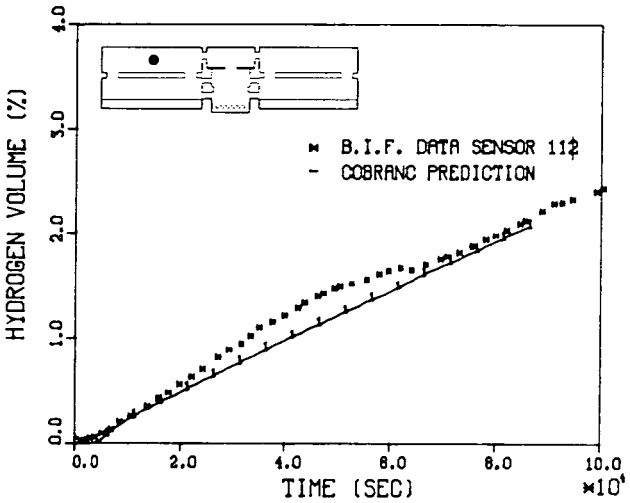


FIGURE 19. Test 12 Hydrogen Concentration in Room 3

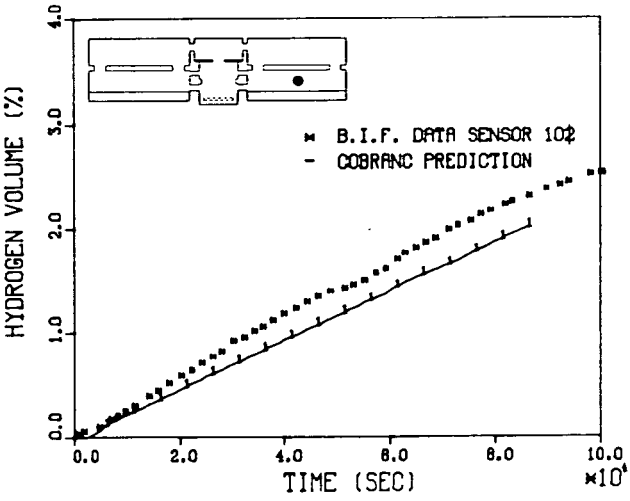


FIGURE 20. Test 12 Hydrogen Concentration in Room 6

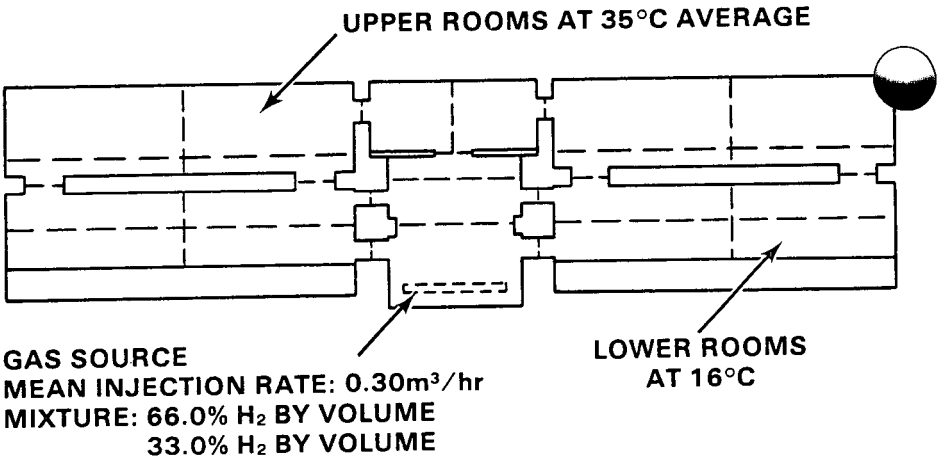


FIGURE 21. Nodalization and Boundary Conditions for Battelle-Frankfurt Test 15

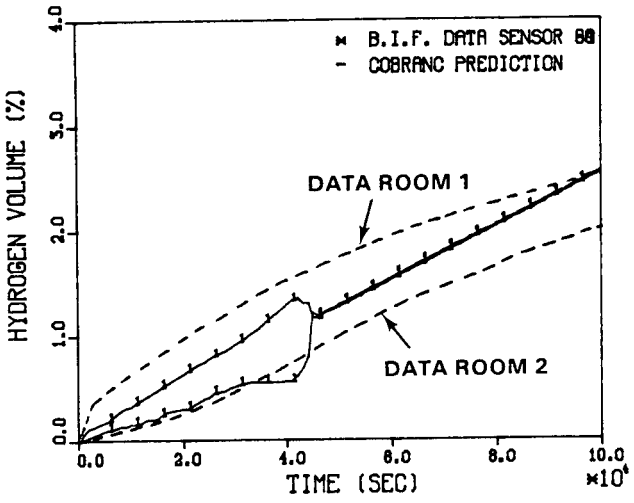


FIGURE 22. Test 15 Hydrogen Concentrations in Rooms 1 and 2

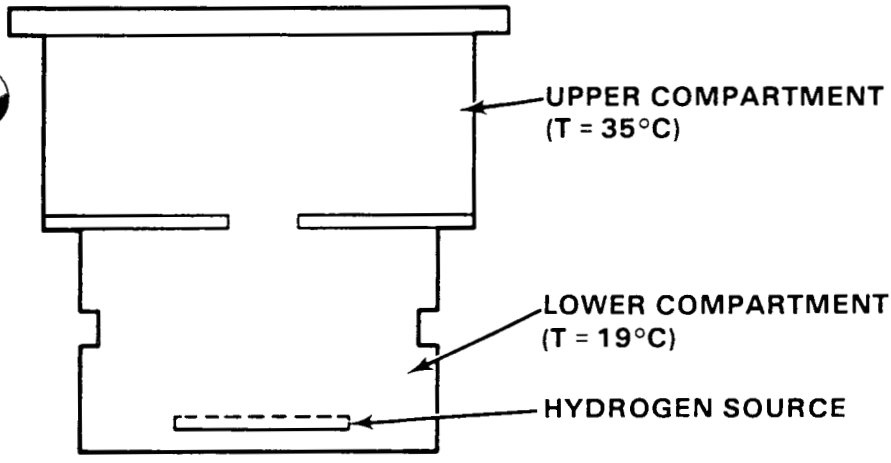


FIGURE 23. Schematic of Geometry for Test 6

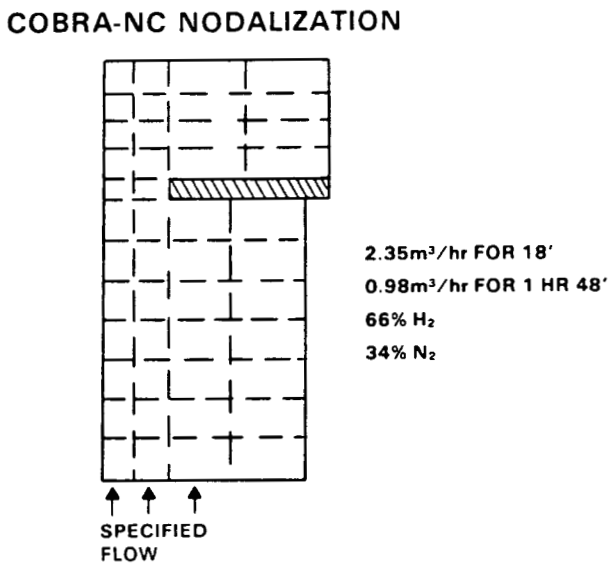


FIGURE 24. Mesh and Boundary Conditions for Test 6

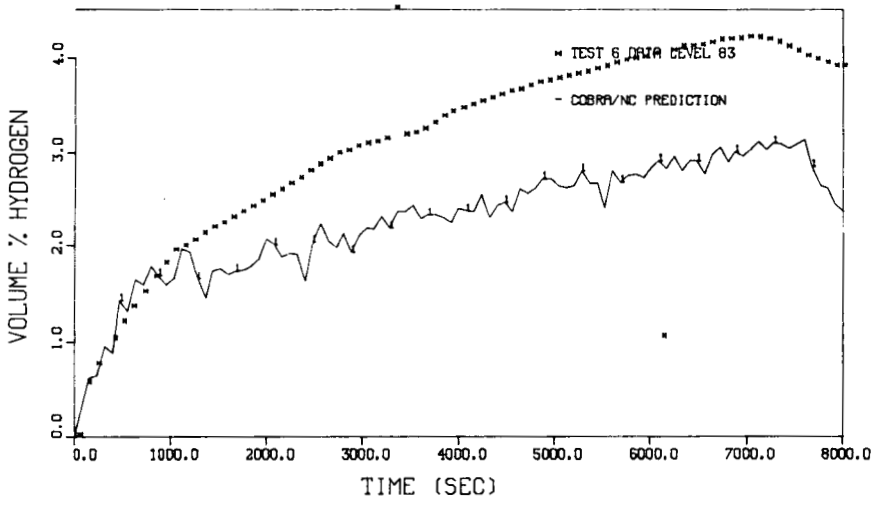


FIGURE 25. Test 6 Hydrogen Concentration in Room 1

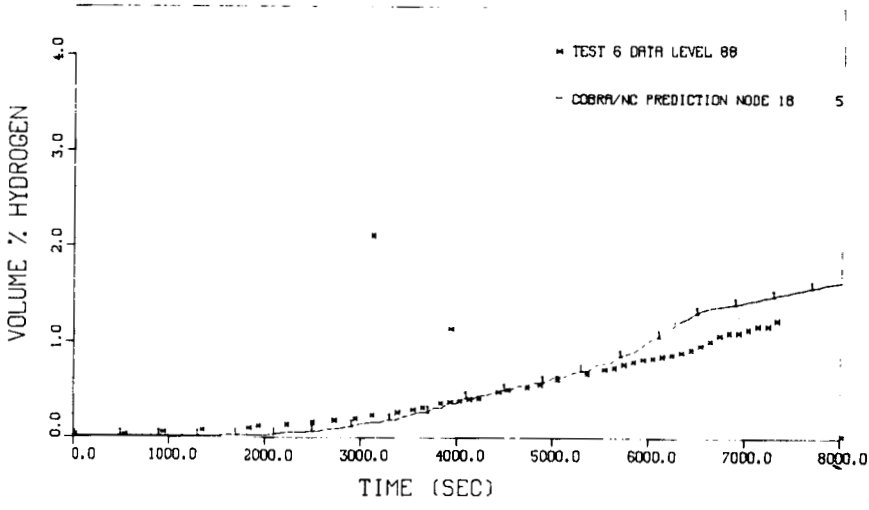


FIGURE 26. Test 6 Hydrogen Concentration in Room 2

APPLICATION OF THE TEMPEST COMPUTER CODE FOR SIMULATING HYDROGEN DISTRIBUTION IN MODEL CONTAINMENT STRUCTURES*

D. S. Trent
L. L. Eyler
Battelle, Pacific Northwest Laboratory

INTRODUCTION

Predicting time-dependent hydrogen concentrations developing in containment structures during the course of a LOCA requires an analytical tool capable of simulating the principal transport mechanisms including buoyant and forced convection, turbulent mixing, heat transfer, and condensation. Additionally, the simulation tool must be able to deal with these transport mechanisms as the hydrogen traverses through the complex intrastructure of a typical reactor containment system. Containment features such as forced air circulation systems, ice condensers, and sprays further complicate the simulation process.

Computer codes previously developed for containment analysis have not dealt with all mechanisms required to handle rapid evolution of large quantities of hydrogen. Such codes have been developed to handle specific aspects of containment analysis such as initial transient dynamical response following a large-break LOCA, hydrogen distribution resulting from radiolysis, and aerosol behavior. The numerical approach of such codes, with a few exceptions, is based on lumped parameter analysis which eliminates several of the basic mechanisms required for resolving short-term hydrogen distribution in containment. Currently, finite-difference codes that have been used for other purposes are being modified to address the hydrogen distribution issue.

The present work deals with assessing the capability of the TEMPEST computer code for predicting hydrogen distribution in a model containment test facility. The TEMPEST computer code was developed by the Battelle, Pacific Northwest Laboratory, and is designed to address a broad spectrum of multi-dimensional hydrothermal problems. TEMPEST solves the three-dimensional, time-dependent equations of turbulent motion and energy transport using state-of-the-art numerical procedures. The code contains a two-equation model for turbulence which follows the k-ε approach. A reliable turbulence model is an important aspect when modeling systems that are substantially characterized by turbulent mixing, such as in the case of confined buoyant plumes.

TEMPEST has received considerable general use and has been assessed with a considerable amount of single-phase experimental data related to natural and forced convection, buoyant and forced plumes/jets, heat transfer and turbulence. Because of the code's rather complete treatment of low-speed, single-phase flow phenomena, applicability to complex structures, and verification history, it appeared to be a good candidate for application in hydrogen distribution studies. Required modification included the addition of an appropriate number of transport equations to handle the expected chemical species, ancillary relationships for computing state variables and additional logic to accommodate user-specified boundary condition input.

The experiments chosen for the data comparison were conducted by the Battelle Institut e.V. and reported by Langer et al.[1,2,3]. The series of experiments conducted by the Battelle Institut involved a total of 23 tests and investigated various geometric configurations, flow

*Work sponsored by U.S. DOE under Contract DE-AC06-76RLO(1830) and EPRI.

rates, and thermal initial conditions. Experimental measurements included hydrogen concentration and temperature history at a number of positions within the test facility. This series of tests provides a good data base for computer code assessment and verification. The computer code RALOC[5,6] has been used to predict a large number of these tests. Additionally, the codes COBRA-NC,[7] and HMS,[8] have also used selected data from the first test series (experiments 1 through 6) for the purpose of code assessment and testing.

A schematic of the experimental facility used for these tests is shown in Figure 1. The cylindrical compartments R1, R2, and R3 were used for the first series of tests (experiments 1 through 6). Ports that connect the cylindrical compartment with the other compartments were blocked off with plates and sealed to form a gas-tight configuration. A constant head water pool at the base of compartment R1 was used to prevent excess pressure buildup in the compartments.

Gas was released to the compartment through a cylindrical cushion 2.5 m in diameter and 0.1 m thick. The gas cushion was constructed of porous canvas with the bottom surface sealed so the gas could only flow vertically. This cushion provided for a uniform, low-velocity source centrally located near the water surface. The hydrogen gas was fed into the cushion from a battery of bottles with the appropriate controls for fine adjustment (see Figure 2).

Hydrogen detectors and thermocouples were placed at various locations within the test compartment as shown in Figure 2. Measurements were controlled by a computerized acquisition system. Results were digitized and recorded on magnetic tape. Procedures, testing, and calibration of the instrumentation is given in Reference 1.

Although, TEMPEST simulation results have been compared with several of these tests, results are presented here only for tests 2, 3, 4, and 6. These tests were selected because they deal with geometric effects, the complexities of stratification/destratification in turbulent flow, and present an excellent challenge for the TEMPEST turbulence model.

Results of these data comparisons illustrate that the TEMPEST computer code is capable of predicting hydrogen concentration history with reasonable accuracy under complex turbulent flow conditions. In this regard, the code should be a useful tool for resolving hydrogen distribution issues in reactor containment systems.

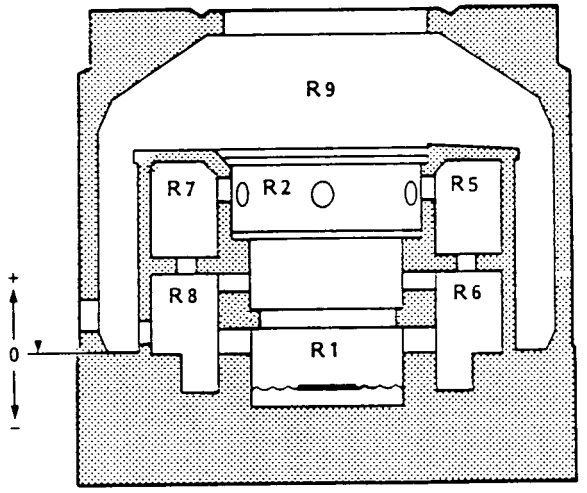


FIGURE 1. Cross Section View of Battelle-Frankfurt Model Containment System

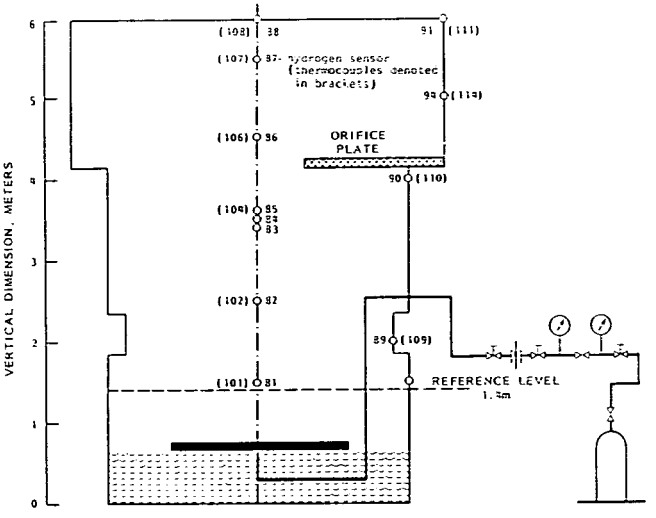


FIGURE 2. Schematic Diagram of Gas Injection System and Location of Pertinent Thermocouples and Hydrogen Sensors

GOVERNING EQUATIONS AND SOLUTION TECHNIQUE

Equations governing momentum, heat, and mass transport solved by TEMPEST are based on the following conservation laws:

1. conservation of mass, including individual species (continuity)
2. conservation of momentum (Newton's Second Law)
3. conservation of energy (First Law of Thermodynamics).

Thermodynamic state relationships of the form

$$\rho = f(P_o, T, \omega_i)$$

are required in addition to other relationships necessary for definition of temperature-dependent materials properties. Empirical relationships are needed to describe drag, film, and mass transfer coefficients for certain simulations.

In the current version of TEMPEST, turbulent flow Reynolds stresses are modeled through an effective viscosity. The Prandtl-Kolmolgorov hypothesis is used to relate the effective viscosity to a velocity and a length scale. In this approach transport equations for the turbulent kinetic energy (k) and the dissipation of turbulent kinetic energy (ξ) are solved to determine the effective turbulent viscosity as

$$\mu_T = C_\mu \rho k^2/\xi$$

PRINCIPAL ASSUMPTIONS

The TEMPEST code simulates flow and thermal fields subject to the following assumptions and/or restrictions:

- fluid is single phase and incompressible (insofar as sonic effects are not considered)
- body forces other than gravity are not considered (forces resulting from an accelerating coordinate system are included)
- fluid is Newtonian (for laminar situations, Navier-Stokes equations apply)
- turbulent flow conservation equations are time averaged and Reynolds stresses are incorporated through appropriate eddy viscosity models
- viscous dissipation is eliminated
- the Boussinesq approximation holds.

Assumptions related to chemical species transport are:

- Mixture conservation equations apply.

- Components of the mixture are in local dynamic and thermodynamic equilibrium.
- Mixture is an ideal gas.
- Concentration difference is the only contribution to chemical potential gradients.
- The mixture eddy diffusivity for mass is related to the mixture eddy diffusivity for momentum by a turbulent Schmidt number, SC_T.

The assumption that concentration differences are the only contribution to chemical potential gradients limits diffusional mass transport to Fick's Law. There are a number of other effects that may contribute to the chemical potential gradient including phenomenological effects described by Onsager's relationships. Such effects are related to the inter-relationships between chemical and thermal gradients, and are usually small but can be important to specific processes. As indicated previously, laminar flow mass transport capability is not fully developed for mixtures and the current version should be applied only to fully turbulent flows or to at most binary mixtures in laminar flow.

CONSERVATION EQUATIONS

Continuity

The equation describing the conservation of mass is

$$\frac{1}{R^{\beta}}\frac{\partial R^{\beta} U}{\partial R} + \frac{1}{R^{\beta}}\frac{\partial W}{\partial X} + \frac{\partial V}{\partial Z} = 0 \qquad (1)$$

where $\beta = 1$ for cylindrical coordinates , $\beta = 0$ for Cartesian coordinates.

Symbols U, W, and V refer to velocity components in the R,X,Z directions, respectively.

Momentum

The equations describing the conservation of momentum in each of the three coordinate directions are:

R- direction component, U:

$$\frac{\partial U}{\partial t} + \frac{1}{R^{\beta}}\frac{\partial}{\partial R}(R^{\beta} UU) + \frac{1}{R^{\beta}}\frac{\partial}{\partial X}(WU) + \frac{\partial}{\partial Z}(VU) - \beta\left(\frac{\rho}{\rho_o}\right)\frac{W^2}{R}$$

$$= \frac{1}{\rho_o}\left[-\frac{\partial P}{\partial R} + \rho g_R + \frac{1}{R^{\beta}}\frac{\partial}{\partial R}\left(R^{\beta}\varepsilon\frac{\partial U}{\partial R}\right) + \frac{1}{R^{2\beta}}\left(\varepsilon\frac{\partial U}{\partial X}\right) + \frac{\partial}{\partial Z}\left(\varepsilon\frac{\partial U}{\partial Z}\right) + S_R\right] \qquad (2)$$

where

$$S_R = -\beta\varepsilon\left(\frac{U}{R^2} + \frac{2}{R^2}\frac{\partial W}{\partial X}\right) + \frac{\partial\varepsilon}{\partial R}\frac{\partial U}{\partial R} + \frac{\partial\varepsilon}{\partial X}\frac{\partial}{\partial R}\left(\frac{W}{R^{\beta}}\right) + \frac{\partial\varepsilon}{\partial Z}\frac{\partial V}{\partial R} - F_R(U)$$

and, $\varepsilon = \mu + \mu_T$, μ = dynamic viscosity , μ_T = turbulent (eddy) viscosity ,

$F_R(U)$ = R-direction flow drag term

X - direction component, W:

$$\frac{\partial W}{\partial t} + \frac{1}{R^\beta}\frac{\partial}{\partial R}(R^\beta UW) + \frac{1}{R^\beta}\frac{\partial}{\partial X}(WW) + \frac{\partial}{\partial Z}(VW) + \beta\left(\frac{\rho}{\rho_o}\right)\frac{UW}{R}$$

$$= \frac{1}{\rho_o}\left[-\frac{1}{R^\beta}\frac{\partial P}{\partial X} + \rho g_X + \frac{1}{R^\beta}\frac{\partial}{\partial R}\left(R^\beta \varepsilon \frac{\partial W}{\partial R}\right) + \frac{1}{R^{2\beta}}\frac{\partial}{\partial X}\left(\varepsilon \frac{\partial W}{\partial X}\right) + \frac{\partial}{\partial Z}\left(\varepsilon \frac{\partial W}{\partial Z}\right) + S_X\right] \quad (3)$$

where

$$S_X = \frac{\beta\varepsilon}{R^2}\left(2\frac{\partial U}{\partial X} - W\right) + \frac{1}{R^\beta}\frac{\partial \varepsilon}{\partial R}\left(\frac{\partial U}{\partial X} - \beta W\right) + \frac{1}{R^{2\beta}}\frac{\partial \varepsilon}{\partial X}\left(\frac{\partial W}{\partial X} + 2\beta U\right) + \frac{1}{R^\beta}\frac{\partial \varepsilon}{\partial Z}\frac{\partial V}{\partial X} - F_X(W)$$

Z - direction component, V:

$$\frac{\partial V}{\partial t} + \frac{1}{R^\beta}\frac{\partial}{\partial R}(R^\beta UV) + \frac{1}{R^\beta}\frac{\partial}{\partial X}(WV) + \frac{\partial}{\partial Z}(VV)$$

$$= \frac{1}{\rho_o}\left[-\frac{\partial P}{\partial Z} + \rho g_Z + \frac{1}{R^\beta}\frac{\partial}{\partial R}\left(R^\beta \varepsilon \frac{\partial V}{\partial R}\right) + \frac{1}{R^{2\beta}}\frac{\partial}{\partial X}\left(\varepsilon \frac{\partial V}{\partial X}\right) + \frac{\partial}{\partial Z}\left(\varepsilon \frac{\partial V}{\partial Z}\right) + S_Z\right] \quad (4)$$

where

$$S_Z = \frac{\partial \varepsilon}{\partial R}\frac{\partial U}{\partial Z} + \frac{1}{R^\beta}\frac{\partial \varepsilon}{\partial X}\frac{\partial W}{\partial Z} + \frac{\partial \varepsilon}{\partial Z}\frac{\partial V}{\partial Z} - F_Z(V)$$

Thermal Energy

The equation describing the conservation of thermal energy is:

$$\rho_o C\left[\frac{\partial T}{\partial t} + \frac{1}{R^\beta}\frac{\partial}{\partial R}(R^\beta UT) + \frac{1}{R^\beta}\frac{\partial}{\partial X}(WT) + \frac{\partial}{\partial Z}(VT)\right]$$

$$= \frac{1}{R^\beta}\frac{\partial}{\partial R}\left(\sigma R^\beta \frac{\partial T}{\partial R}\right) + \frac{1}{R^{2\beta}}\frac{\partial}{\partial X}\left(\sigma \frac{\partial T}{\partial X}\right) + \frac{\partial}{\partial Z}\left(\sigma \frac{\partial T}{\partial Z}\right) + \dot{Q} \quad (5)$$

where

$\sigma = \kappa + \kappa_T$

κ = thermal conductivity

κ_T = turbulent (eddy) thermal conductivity

C = specific heat

$\dot{Q}$ = volumetric heat generation rate

Constituent Transport

The transport equation for the ith component in a mixture of n species (i=1,2,...n) is

$$\frac{\partial \omega_i}{\partial t} + \frac{1}{R^\beta}\frac{\partial}{\partial R}(R^\beta U\omega_i) + \frac{1}{R^\beta}\frac{\partial}{\partial X}(W\omega_i) + \frac{\partial}{\partial Z}(V\omega_i)$$

$$= \frac{1}{R^\beta}\frac{\partial}{\partial R}(D_\omega R^\beta \frac{\partial \omega_i}{\partial R}) + \frac{1}{R^{2\beta}}\frac{\partial}{\partial X}(D_\omega \frac{\partial \omega_i}{\partial X}) + \frac{\partial}{\partial Z}(D_\omega \frac{\partial \omega_i}{\partial Z}) + \dot{\omega}_i \qquad (6)$$

where ω_i is the mass fraction of the ith component defined as

$$\omega_i = \frac{\rho_i}{\rho} \quad \text{and} \quad D_\omega = D_{im} + \frac{\mu_T}{SC_T}, \quad D_{im} = \text{molecular diffusion coefficient of component i,}$$

SC_T = Schmidt number turbulent

It is assumed that the mixture density ρ does not have large spatial variations (i.e., $\nabla\rho$ is small) and thus the component transport Equation (6) is expressed in terms of the mass fraction, ω_i.

TURBULENCE EQUATIONS

Modeled transport equations for turbulent kinetic energy (k) and dissipation of turbulent kinetic energy (ξ) are solved to obtain the turbulent effective viscosity (μ_T). The modeled forms of the equations are:

Turbulent Kinetic Energy

$$\rho_o\left[\frac{\partial k}{\partial t} + \frac{1}{R^\beta}\frac{\partial}{\partial R}(R^\beta Uk) + \frac{1}{R^\beta}\frac{\partial}{\partial X}(Wk) + \frac{\partial}{\partial Z}(Vk)\right]$$

$$= \frac{1}{R^\beta}\frac{\partial}{\partial R}(R^\beta \varepsilon_k \frac{\partial k}{\partial R}) + \frac{1}{R^{2\beta}}\frac{\partial}{\partial X}(\varepsilon_k \frac{\partial k}{\partial X}) + \frac{\partial}{\partial Z}(\varepsilon_k \frac{\partial k}{\partial Z}) - \rho\xi + S_k \qquad (7)$$

where $\varepsilon_k = \mu + \frac{\mu_T}{\sigma_k}$ and $S_k = P_k + G_k$

Shear production:

$$P_k = \mu_T\left\{2\left[\left(\frac{\partial U}{\partial R}\right)^2 + \left(\frac{1}{R^\beta}\frac{\partial W}{\partial X} + \beta\frac{U}{R}\right)^2 + \left(\frac{\partial V}{\partial Z}\right)^2\right]\right.$$

$$\left. + \left(\frac{1}{R^\beta}\frac{\partial U}{\partial X} + \frac{\partial W}{\partial R} - \beta\frac{W}{R}\right)^2 + \left(\frac{\partial U}{\partial Z} + \frac{\partial V}{\partial R}\right)^2 + \left(\frac{\partial W}{\partial Z} + \frac{1}{R^\beta}\frac{\partial V}{\partial X}\right)^2\right\}$$

Buoyant production:

$$G_k = \frac{\mu_T}{\rho\sigma_T}\left(\frac{\partial\rho}{\partial R}g_R + \frac{1}{R^\beta}\frac{\partial\rho}{\partial X}g_X + \frac{\partial\rho}{\partial Z}g_Z\right)$$

Dissipation of Turbulent Kinetic Energy

$$\rho_o\left[\frac{\partial\xi}{\partial t} + \frac{1}{R^\beta}\frac{\partial}{\partial R}(R^\beta U\xi) + \frac{1}{R^\beta}\frac{\partial}{\partial X}(W\xi) + \frac{\partial}{\partial Z}(V\xi)\right]$$

$$= \frac{1}{R^\beta}\frac{\partial}{\partial R}\left(R^\beta \varepsilon_\xi \frac{\partial\xi}{\partial R}\right) + \frac{1}{R^{2\beta}}\frac{\partial}{\partial X}\left(\varepsilon_\xi \frac{\partial\xi}{\partial X}\right) + \frac{\partial}{\partial Z}\left(\varepsilon_\xi \frac{\partial\xi}{\partial Z}\right) + \frac{1}{k}(S_\xi - \rho C_{\xi 2}\xi)\xi \qquad (8)$$

where $\varepsilon_\xi = \mu + \frac{\mu_T}{\sigma_\xi}$ and $S_\xi = C_{\xi 1}P_k + C_{\xi 3}G_k$

The turbulent viscosity, μ_T, is computed using the Prandtl-Kolmolgorov hypothesis:

$$\mu_T = C_\mu \rho k^2/\xi \qquad (9)$$

Recommended turbulent model constants[4] are

$\sigma_T = 0.9$, $\sigma_k = 1.0$, $\sigma_\xi = 1.3$, $C_{\xi 1} = 1.44$, $C_{\xi 2} = 1.92$, $C_{\xi 3} = 1.44$, and $C_\mu = 0.09$

RESULTS

Computed results using TEMPEST have been obtained for the first series of Battelle Institut tests. Data comparisons for tests 2, 3, 4 and 6 are presented here. Test 1 and 5 were base experiments having no interesting features with respect to geometry, source location, or stratification and are not presented. A summary of these tests as given in reference 1 is presented in Table 1 and schematic diagrams of the geometries are illustrated in Figure 3. The strategy of these experiments was to proceed from simplistic conditions (test 1 and 5) to geometric complication (test 2 and 3), the investigation of source location effects and diffusions (test 4), to the most complicated experiment involving both geometric complexity and a thermal inversion layer (test 6). A computer code must model the effects of advection, turbulent and molecular diffusion, and buoyancy with reasonable accuracy to perform well on these four experiments. The hydrogen in both tests 1 and 5 is nearly homogeneously distributed over the long term and therefore does not pose a particular challenge to code performance.

Each of these tests were simulated using the same version of the TEMPEST code. All internal parameters such as the turbulence constants were unchanged and no tuning was conducted to obtain improved results from test to test. Some nodalization studies were performed to investigate this effect on computed results. Generally, it was found, as would be expected, that the noding structure needed to be consistent with the expected phenomena to obtain accurate results.

TABLE 1. Summary of Tests 1 Through 6

Exp. No.	1	2	3	4	5	6
Input time	23' + 3h 07'	3 h 47'	2 h 52'	2 h 10'	8 h 40'	18' + 1 h 48'
Gas mixture N_2/H_2 (vol. %)	68/32	34/66	34/66	34/66	34/66	34/66
Input rate (m^3/hr)	6.0/0.87	1.19	1.22	1.24	0.51	2.35/0.98
Gas volume introduced (m^3)	2.31/2.72	4.51	3.49	2.67	4.44	0.7/1.67
Air volume (m^3)	70.8	71.9	71.4	71.9	71.8	72.0
Compartment temp mean (°C)	18	17	17	22	19	35/19
Gas temp mean (°C)	16/19	19	18.5	25	21	19
Orifice diameter (m)/area (m^2)	-	1.13/1.0	0.62/0.3	-	-	1.13/1.0
Height of source above base (m)	0.6	0.6	0.6	3.4	0.6	0.6
Volume increase due to water removal	1.9	-	-	-	-	-
Experimental goal	Fundamental experiment density convection	Density convection with large opening	Density convection with small opening	Diffusion due to altered input site	Repetition of Exp. 1 with m = const.	Density convection with temperature stratification

Extracted from Reference 1

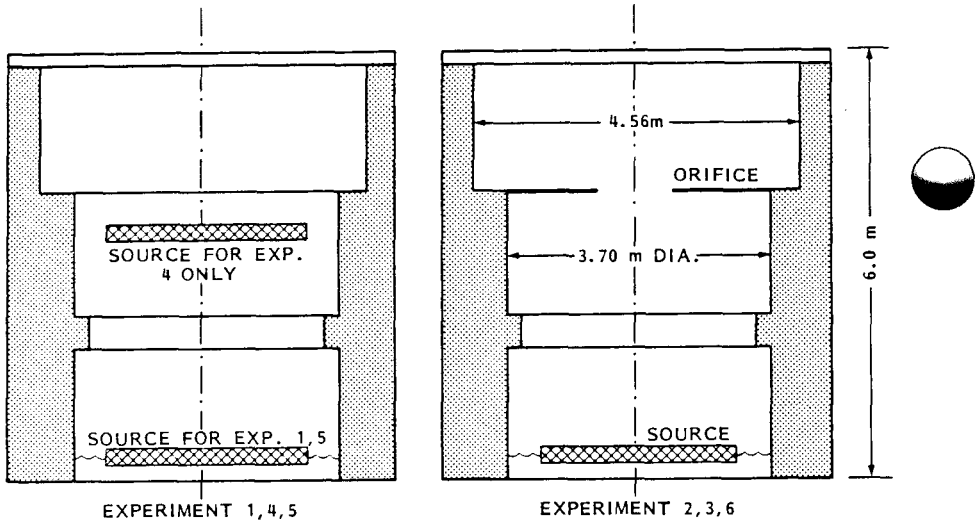


FIGURE 3. Test Configurations for Experiments 1 through 6

Specifically, fairly small finite-difference cells were required in the vicinity of large concentration gradients to obtain good data comparison. Results of the nodalization studies are not presented.

In all cases the simulations were performed using the k-ε turbulence model. Results are also presented using laminar flow assumptions for Tests 2, 3 and 6. Because of the very small mass fraction of hydrogen, molecular transport properties, thermal conductivity, and viscosity of air were used. The molecular diffusion coefficient for the binary system of hydrogen diffusing in to air was obtained from reference (9). This value of 6.11×10^{-5} m^2/sec at 0° centigrade was extrapolated to the test condition using (see reference 10).

$$D_2P_2 = D_1P_1 \left(\frac{T_2}{T_1}\right)^{3/2} \Omega_r$$

where Ω is the ratio of the "collision integrals" for molecular diffusion at temperature T_1, and T_2 but Ω is approximately unity for the temperature extrapolation condition required in this study.

EXPERIMENTS 2 AND 3

Results of experiments 2 and 3 may be compared with each other to illustrate the effect of orifice size on the penetration of hydrogen into the facility upper compartment R2 (see Figure 1). Flow conditions and compartment initial temperature are essentially the same for both cases (Table 1) The hydrogen source causes a buoyant cloud to form that rises under the action

of buoyancy and spreads through turbulent diffusion. As the buoyant plume encounters the partition, a portion will penetrate through the orifice, the remainder spreading laterally along the partition, setting up a recirculation pattern in the lower compartment. Flow that penetrates to the upper compartment will displace the resident mixture, forcing an equal volume downward through the orifice, joining the lateral spread and the recirculation pattern that is set up in the lower compartment. Thus, a countercurrent flow exists in the orifice which is assumed to be symmetric in a two-dimensional computation.

The portion of the plume penetrating the orifice depends on the size of the orifice as well as the plume spread at the orifice elevation. The plume spread depends on the source diameter and elevation above the orifice. Thus, from a computational viewpoint, the plume centerline momentum and concentration must be accurately predicted if penetration and resulting hydrogen concentration in the upper compartment are to be accurately predicted. Since temperature gradients do not exist in these tests, circulation patterns developed in the compartments will keep each compartment at near uniform concentration. A concentration gradient will exist between the compartments in the vicinity of the orifice with the concentration difference depending on the degree of flow penetration. The computation grid system used by TEMPEST for both experiments 2 and 3 is shown in Figure 4.

Figure 5 illustrates the TEMPEST prediction compared to data for the large orifice (test 2). The computer code predicts a concentration difference that is larger than observed in the experiment. Although other factors, such as numerical truncation errors, may be participating in this discrepancy, it is felt that the turbulence model is predicting an effective viscosity that is too large, thus causing a spread rate greater than in the

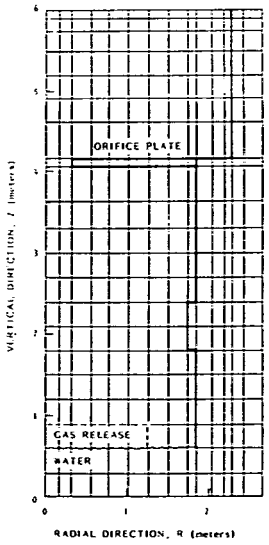


FIGURE 4. Finite-Difference Computational Cell Structure for Battelle-Frankfurt Tests 2 and 3

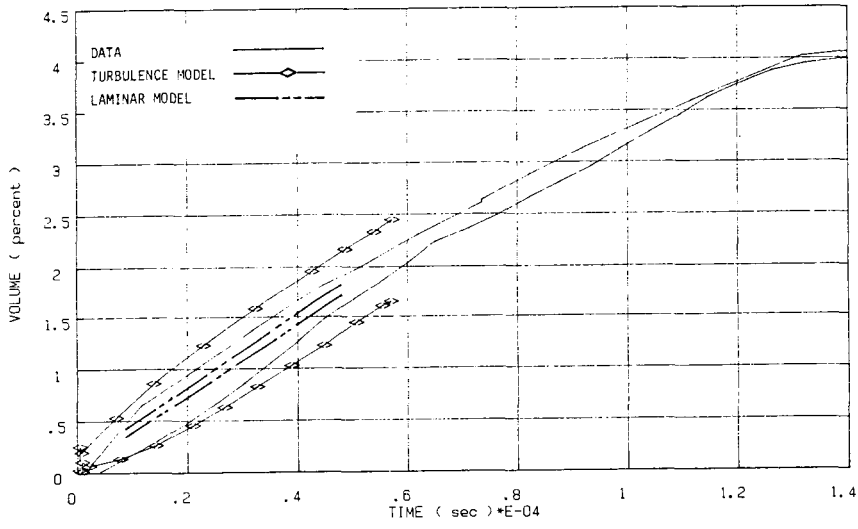


FIGURE 5. Hydrogen Concentration versus Time for Test 2 (Large Orifice)

experiment. Again, the standard set of turbulence constants are used without any adjustment to achieve improved accuracy. By adjusting the constant C_μ the predictions could be improved.

A computation that assumed laminar flow and molecular diffusion is also displayed in Figure 5. This computation shows very little difference in the concentration distribution between the upper and lower compartments. The reason for this outcome is that a laminar plume has very little spread or mixing with the surrounding air and thus penetrates the orifice essentially unimpeded. Laminar assumptions for these tests are, of course, unrealistic, for a system of this size and source strength.

Similar calculations for the small orifice test are illustrated in Figure 6. In this test the orifice dramatically affects penetration of the plume into the upper compartment, causing a substantial difference in concentration between compartments. Again the TEMPEST code overpredicts the orifice effect, although agreement out to 4000 seconds is quite good. It appears that a change in the test flow rate might have occurred between 4000 and 6000 second

A simulation using laminar assumptions is also shown, and, as in test 2, the orifice size has essentially no effect on penetration of the plume to the upper compartment.
Hydrogen concentration contours for tests 2 and 3 at 4000 seconds are shown in Figure 7. Comparison of this information indicates that:

- the concentration in each compartment is fairly uniform (spatial differences are about 0.2 volume percent)
- the concentration gradient is much steeper for the smaller orifice.

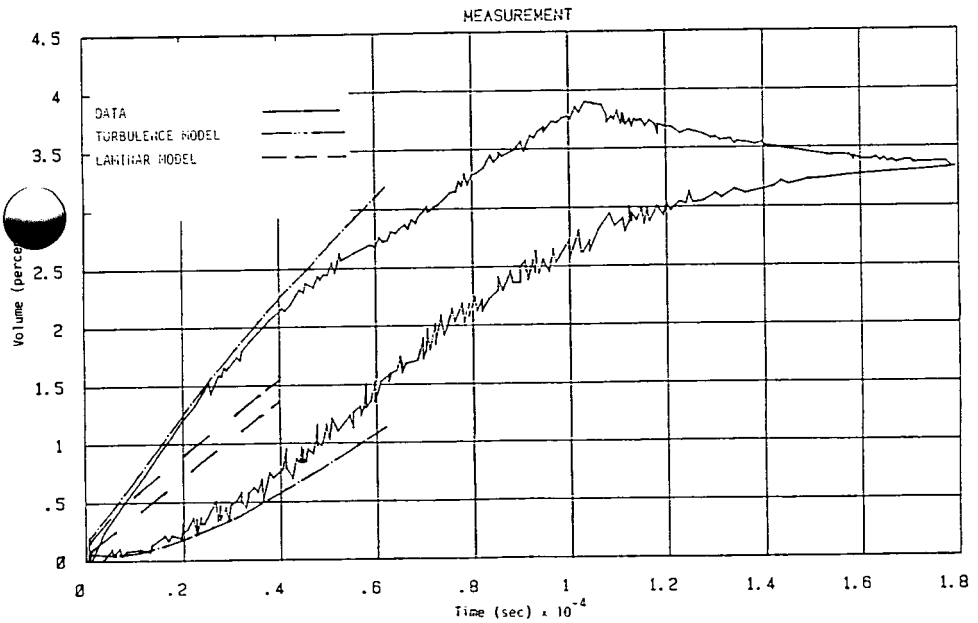


FIGURE 6. Hydrogen Concentration versus Time for Experiment 3 (Small Orifice)

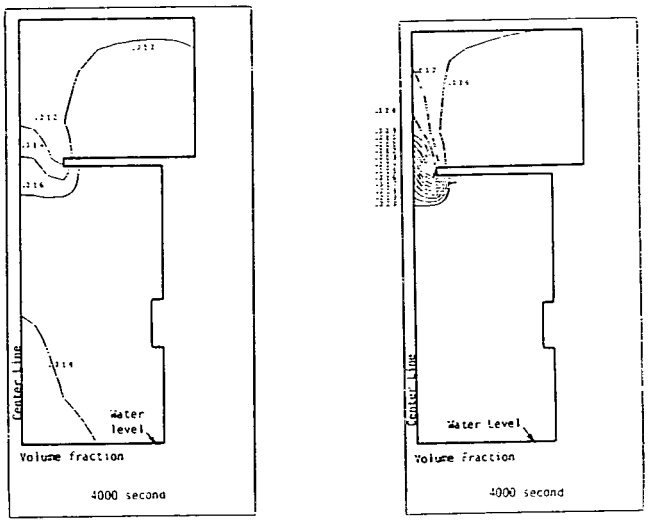


FIGURE 7. Predicted Hydrogen Volume Fraction Contours at 4000 Second for Test 2 and 3

These results indicate that it is necessary to accurately predict turbulent spread of the rising plume. For a buoyant plume, a turbulence model of some form must be employed since the relationship between turbulent diffusivity and elevation above the source are related as $\varepsilon = f(Z)$.

TEST 4

The finite-difference computational cell structure and source location for test 4 is illustrated in Figure 8. In this test the region above the source will set up a strong convection pattern and be fairly well mixed. Hydrogen will penetrate to the lower region by diffusional processes in conjunction with a weak degree of convection through an annular space between the source and wall. The annular width is 0.35 m. Hydrogen penetrating to the lower region will form a stably stratified density structure with weak stratified flow.

Computed results for this case are compared to experimental data as shown in Figure 9 for a transient time out to 12,000 seconds. The computed results for stations 88 and 82 are in good agreement with the data, whereas the results for station 81 predicts a concentration somewhat greater than the data indicate. Again, the turbulence model was employed for this simulation using the standard set of constants. Contours of the predicted turbulent kinetic energy and eddy viscosity are shown in Figure 10 at the time of flow shutoff (7800 seconds). This figure illustrate that there is a high level of turbulent kinetic energy generated in the upper region that is nearly completely suppressed by the density gradient in passing to the lower chamber. Likewise, the predicted eddy viscosity distribution is typical of turbulent cellular convection in the upper region whereas in the lower region the turbulent component of eddy viscosity is suppressed to values comparable to the molecular viscosity. This behavior is an important aspect of the TEMPEST turbulence model and demonstrates the capability of modeling complex turbulent and laminarizing flows in a more realistic fashion than using a constant viscosity. In this particular case, however, using a constant value of molecular diffusivity and laminar flow assumptions, would most likely have produced a reasonably accurate prediction because turbulence plays an insignificant role in development of the lower region density structure.

Hydrogen concentration contours superimposed on velocity vector plots are shown in Figure 11 for various times during the transient. Note that the lower region is stratified whereas the upper region is well mixed. A strong convection pattern exists above the source. Convection in the lower region is typical of a stratified region where the flow follows along equipotential surfaces.

Noding studies were carried out for this case that revealed finer noding in the lower region gave improved results. It is suspected that finer noding between stations 82 and 81 would yield an improved prediction of hydrogen concentration at measuring station 81.

EXPERIMENT 6

The previous experiments investigated the influence of physical features and position of the H_2 source on the resulting H_2 concentration distribution within the test compartments. Test 6 in this series was designed to investigate the effect of thermal stratification on gas flow penetration into an adjacent but warmer compartment. In this case the orifice geometry of experiment 2 was used, but the upper compartment (R2) was heated to create an atmosphere about 16°C warmer (average) than the lower compartment. Thus the rising plume created by hydrogen injection at the bottom of R1 is obstructed by the orifice plate as well as a thermal barrier at the orifice. Had this test been executed with the same flow rate as test 2, results could be directly compared to

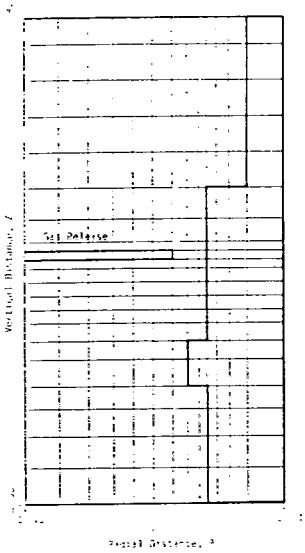


FIGURE 8. Finite-Difference Computational Cell Structure for Experiment 4

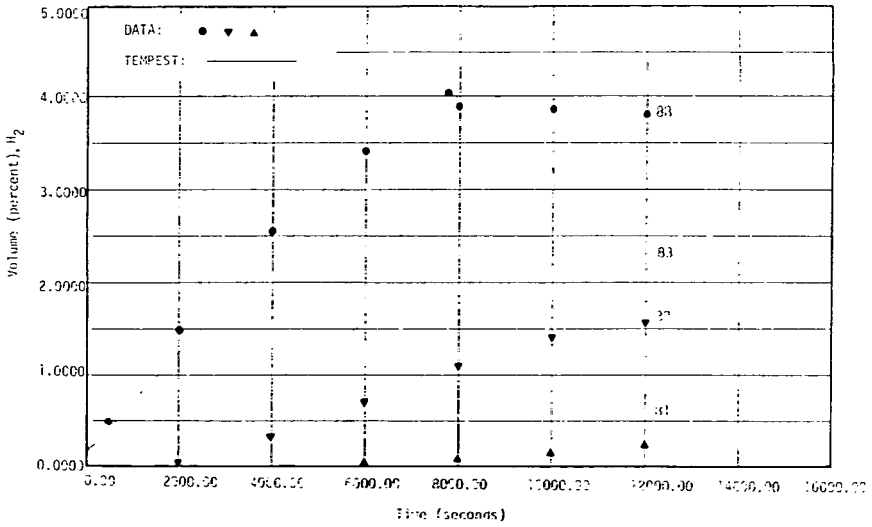


FIGURE 9 Hydrogen Concentration versus Time for Experiment 4

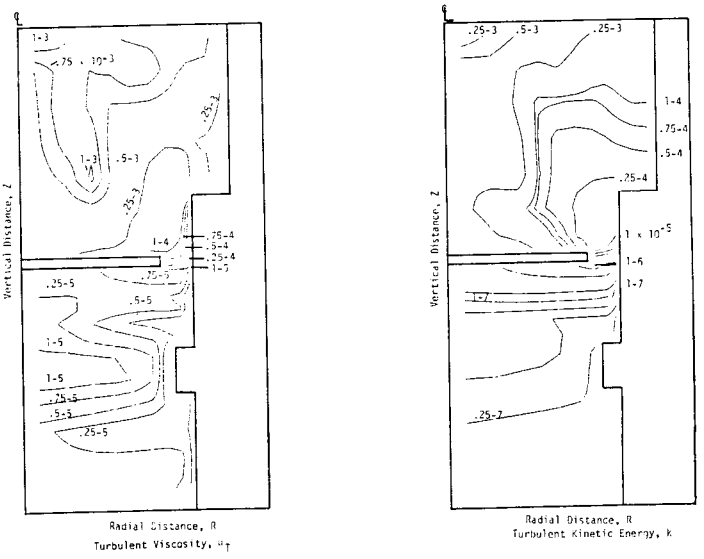


FIGURE 10. Contours of Predicted Turbulent Viscosity and Kinetic Energy for Test 4. 7800 Seconds

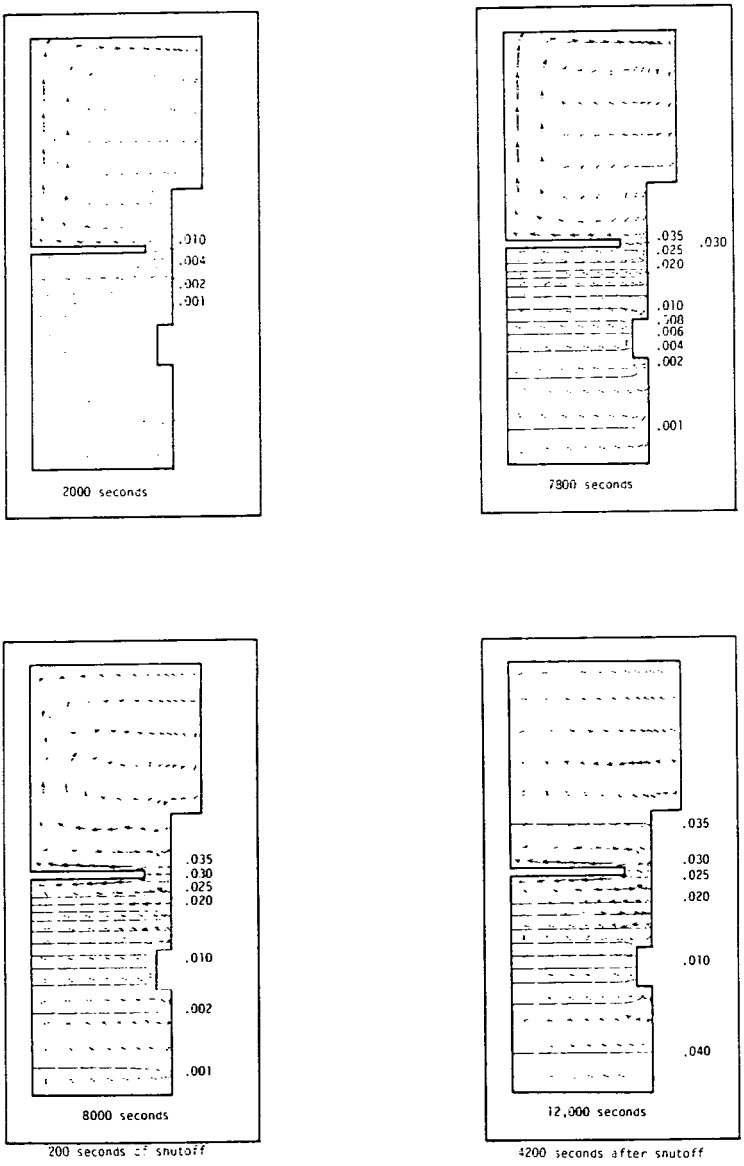


FIGURE 11. Predicted Velocity Vectors and Hydrogen Volume Fraction Contours for Test 4

a thermally homogeneous case with all other conditions being the same (see Table 1). However, a problem developed with the initial H_2 injection,[1] so that the first 1080 seconds of the transient were run at a flow rate about twice that of test 2. Nevertheless, the experiment produced valuable information regarding thermal stratification effects on plume penetration.

The locations of thermocouples and H_2 sensors are shown in Figure 2. A maximum 39°C initial temperature was measured at the top of compartment R2 and approximately 33.5°C was measured just above the orifice. The upper compartment wall temperatures were about 35°C. Initial stratification extended downward through the orifice about to midheight of the lower compartment, where the temperature measured was 19°C. The lower compartment wall temperatures were also about 19°C.

Thermal stratification in the lower compartment that existed initially was destroyed during the first few minutes of injection and temperatures remained fairly steady at about 19°C for the remainder of the test. The difference in temperature from bottom to top of the lower compartment was about 1°C. This was most likely the result of heat transfer from the warmer, lower compartment walls and some interchange with warmer air in the upper compartment. Thermocouple station 110, located near the wall just under the orifice, decreases only slightly in temperature during the course of the experiment. Temperatures in the upper compartment decreased only about 3°C during the test.

Figure 12 illustrates the hydrogen concentration history at the four locations indicated (along with TEMPEST predictions). The data show a rapid buildup of H_2 in the lower compartment, reaching nearly 2% by volume at sensor station 81 after 1080 sec. Concentration at station 90 (near wall) reached about 1.5% at 1080 seconds. Very little H_2 penetrated to the upper compartment during this time. After 1080 sec the injection rate was reduced from 2.35 m^3/sec to 0.98 m^3/sec, which reduced the rate of concentration increase in the lower compartment as shown in Figure 12.

The most important feature revealed in Figure 12 is that the warmer gas in the upper compartment effectively blocks the rising plume from penetrating the orifice. Sensor 86 is just above the orifice in a location having large density stratification caused by both temperature and H_2 concentration gradients. Dynamically, the gas at this location will oscillate because of the competing effects of plume inertia and turbulence, tending to destabilize the flow, and the density gradient, which tends to maintain stability. The larger initial density gradient results in small, high-frequency oscillations. Later, as the density difference is decreased, the oscillations will increase in magnitude and have a lower frequency. Continuous action of the plume's inertia and turbulence will eventually destroy the density gradient and the system will behave as observed in experiment 2.

The finite-difference nodalization structure for experiment 6 is illustrated by Figure 13. As in experiment 4, a fine computational cell structure is used in regions where large gradients are expected. In this case wall heat transfer is considered. Results using the TEMPEST turbulence model are compared with the experimental data, as shown in Figure 12. Although the basic trends of the transient appear to be predicted reasonably well, TEMPEST underpredicts the amount of hydrogen in the lower compartment by approximately 0.5 to 1.0 volume percent. This discrepancy is unresolved but hand-calculated estimates are in better agreement with the computer result than the measured results based on the flow rate indicated in Table 1. Based on these estimates, and that similar problems did not occur in the previous simulations, we believe there may be a discrepancy between the reported flow rate and measurements in this experiment.

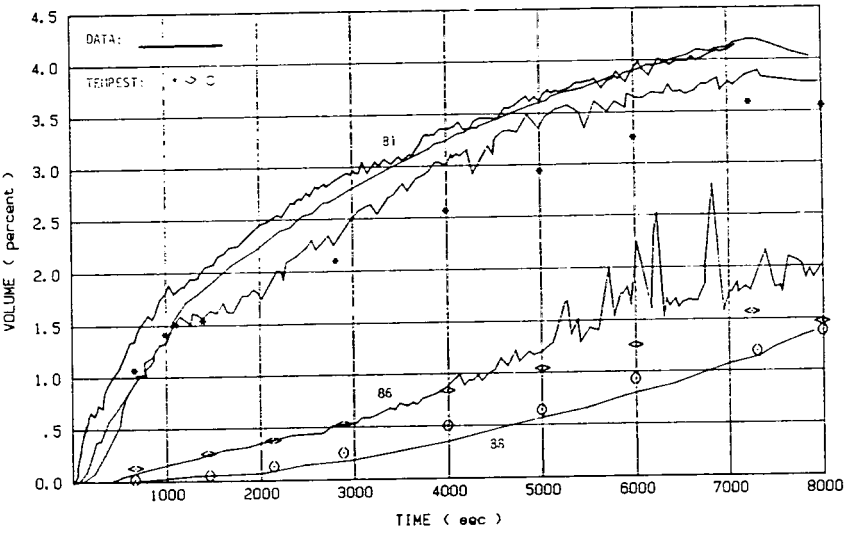


FIGURE 12. Hydrogen Concentration versus Time for Experiment 6

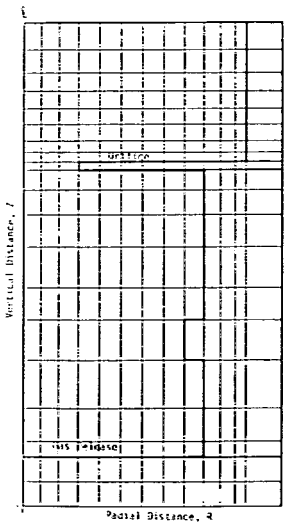


FIGURE 13. Finite-Difference Computational Cell Structure for Experiment 6

Figure 14 shows results for a simulation using laminar flow and molecular diffusion assumptions. This case assumed a discontinuous temperature profile with the upper compartment at 36°C and the lower compartment at 20°C. The results here are quite similar to the turbulent case except for the early penetration of hydrogen through the orifice (station 86). The reason for this is that laminar flow assumptions fail to accurately predict the lower compartment buoyant plume spread. Hence, the high-velocity, small-diameter laminar plume tends to penetrate the stratification layer more effectively than a more diffuse turbulent plume.

Figures 15 illustrates hydrogen concentration and temperature contours superimposed on velocity vectors at 1500 seconds in the turbulent simulation. Note how the upper compartment stratification blocks the plume penetration at the orifice

SUMMARY AND CONCLUSIONS

In this study several aspects of simulating hydrogen distribution in geometric configurations relevant to reactor containment structures were investigated using the TEMPEST computer code. Of particular interest was the performance of the TEMPEST turbulence model in a density-stratified environment. Computed results illustrated that the TEMPEST numerical procedures predicted the measured phenomena with good accuracy under a variety of conditions and that the turbulence model used is a viable approach in complex turbulent flow simulation.

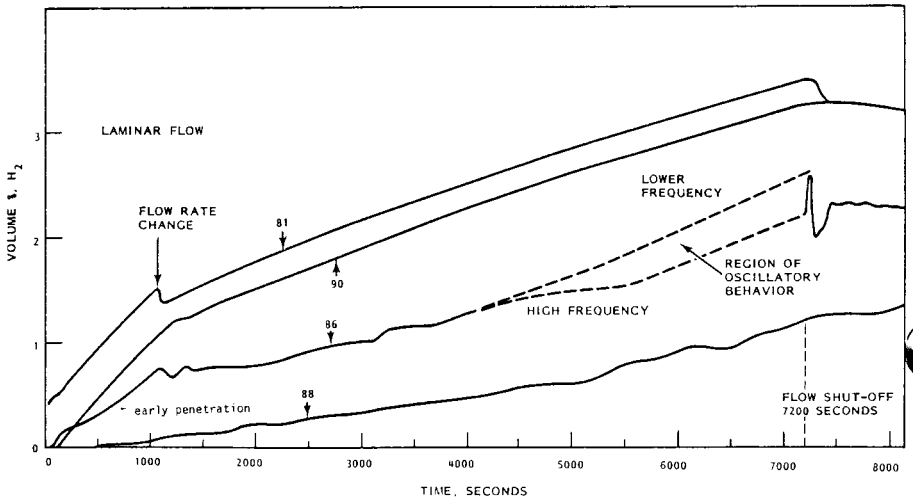
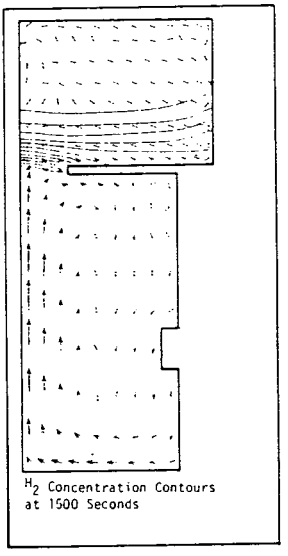


FIGURE 14. Predicted Hydrogen Concentration versus Time for Experiment 6 Using Laminar Flow Modeling



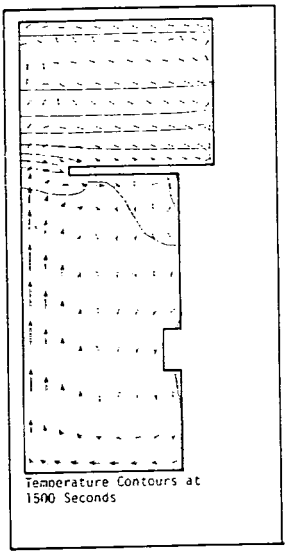


FIGURE 15. Computed Hydrogen Concentration and Temperature Contours at 1500 Seconds. Test 6

REFERENCES

1. G. Langer, R. Jenior, H. G. Wentlandt. "Experimental Investigation of the Hydrogen Distribution in the Containment of a Light Water Reactor Following a Coolant Loss Accident." BF-R-63.363-3. Battelle Institute e.V. Frankfurt, translated October 31, 1980.

2. "Experimental Investigation of the Hydrogen Distribution in a Model Containment (Preliminary Experiments Phase II)." Technical Report BF-R-64.036-1. Federal Ministry for Research and Technology, Bonn, July 1980.

3. "Experimental Investigation of the Hydrogen Distribution in a Model Containment (Preliminary Experiments Phase II)." Technical Report BF-R-64.036-2. Federal Ministry for Research and Technology, Bonn, April 1982.

4. B. E. Launder and D. Spalding. Mathematical Models of Turbulence. Academic Press, London, 1972.

5. Hermann L. Jahn. "RALOC - A New Model for Calculation of Local Hydrogen Concentrations in Subdivided Containments Under LOCA - Aspects." Presented at Thermal Reactor Safety Meeting, Sun Valley, ID, July 1977.

6. Hermann L. Jahn. "Hydrogen Distribution After a Loss-of-Coolant Accident in the Subdivided Containment of Light Water Reactors--Translation." NUREG/CR-1831, SAND80-6031. Sandia National Laboratories, March 1...

7. M. J. Thurgood, K. R. Crowe ... Kelly. "Volume 1: COBRA-TF Equations and Constitutive Models." PNL-4385 (NUREG r ... e assigned). Battelle, Pacific Northwest Laboratory. To be published.

8. J. R. Travis, M. D. Torrey, ... low. "Modeling of H_2 Migration in LWR Containments. LA-UR-81-3171." Los Alamos ... Laboratory, October 1981.

9. R. H. Perry, C. H. Chilton ... Kirkpatrick. 1963. Chemical Engineers' Handbook.

10. J. R. Welty, C. E. Wick, a ... lson. 1969. Fundamentals of Momentum, Heat and Mass Transfer. John Wiley and ...

Development of Mixing Analysis Computer Code on Behavior of Hydrogen in Subcompartmented Containment Vessel after LOCA.

T. Fujimoto*, O. Ukai*, J. Ogata*, M. Kinoshita*, A. Tsuge*
T. Kooriyama**, K. Shimamura**
K. Takahashi***, K. Ōnishi****, S. Inase*****, A. Nakamura******,
T. Morita*******

* Mitsubishi Heavy Industries, L.T.D.
** Mitsubishi Atomic Power Industries, Inc.
*** The Hokkaido Electric Power Co., Inc.
**** The Kansai Electric Power Co., Inc.
***** The Shikoku Electric Power Co., Inc.
****** The Kyushu Electric Power Co., Inc.
******* The Japan Atomic Power Company

Abstract

It is an important problem for safety of light water nuclear reactor plant to evaluate the hydrogen distribution in the containment vessel after loss of coolant accident (LOCA).

A new computer code named MAPHY was developed, which can predict the transient behavior of hydrogen concentration in any subcompartments after LOCA.

MAPHY code shows good agreement with existing data and extensive verification program is undergoing.

Nomenclature

		unit
A	: flow area	(m^2)
C	: concentration of atmosphere component	(-)
C*	: concentration of soluvent component	(-)
Cp	: specific heat	(kcal/kg°C)
D	: diffusion coefficient	(m/h)
d	: equivalent diameter	(m)
f	: friction factor	(-)
f	: vector-valued function	(-)
G	: flow rate	(kg/h)
g	: acceleration of gravity	(m/h^2)
g_c	: conversion factor	($kg*m/kgh^2$)
h	: elevation	(m)
h	: enthalpy	(kcal/kg)
J	: joule constant	(kg·m/kcal)
K	: form loss coefficient	(-)
K	: overall heat transfer coefficient	($kcal/m^2h°C$)
k	: thermal conductivity	(kcal/mh°C)
L	: length between subcompartments	(m)
M	: mass	(kg)
P	: total pressure	(kg/m^2)
p	: partial pressure	(kg/m^2)

Q	: heat input or output	(kcal/h)
R	: gas constant	(kg*·m/kg°C)
T	: temperature	(°C)
t	: time	(h)
Δt	: time step	(h)
U	: total energy in a subcompartment	(kcal)
Vt	: total volume	(m^3)
Va	: free volume	(m^3)
v	: specific volume	(m^3/kg)
$\vec{y}$	: vector of unknown variables	(-)
α	: heat transfer coefficient	(kcal/m^2h°C)
β	: coefficient of thermal expansion	(l/°K)
ρ	: density	(kg/m^3)
μ	: viscosity	(kg/mh)
δ	: width of heat sink	(m)

Subscripts

A	: component of gas	N_2	: nitrogen
dif	: diffusion	n	: node number
eva	: evaporation or condensation	O_2	: oxygen
F,ℓ	: liquid	rec	: recombination
g	: gases and steam	s	: steam
gen	: generation	α	: (α∈T) terminal
H_2	: hydrogen	β	: (β∈I) initial
i	: node number		
j	: node number		
k	: path number		

1. Introduction

Hydrogen generation in light water reactor power plant may endanger integrity of containment vessel under certain circumstances. Especially, the hydrogen distribution after LOCA in a subcompartmented containment vessel is an important problem of reactor safety. Therefore, various studies and developments of evaluation method have been conducted.[1] ~ [2]
Computer code named MAPHY (Mixing Analysis Program of Hydrogen in the Containment Vessel after LOCA) code which can predict the transient behavior of hydrogen concentration in any subcompartments was developed and has been verified.
MAPHY code substitutes node-path in network for subcompartment in the contaiment vessel. Gases in each subcompartment are assumed homogeneously mixed condition and Henry's law was applied when liquid and gas are coexisted.
This paper presents the analytical description of MAPHY code and its verification.

2. Physical model of MAPHY

MAPHY code is applied to long-term hydrogen mixing-10∿100 days-after LOCA.
Therefore, the following assumptions are provided to simplify the problem.

(1) subcompartments in the containment vessel are substituted for node-path in network.



(2) hydrogen, oxygen, nitrogen gases and steam in each subcompartment are homogeneously mixed.

(3) Henry's law can be applied when liquid and gas are coexisted.

(4) steam is always in the saturated condition.

Gases and steam are transfered to others subcompartments by the differences of density, temperature and pressure.
The transfer mechanisms are as follows;

(1) flow caused by pressure difference among subcompartments.

(2) natural convection caused by density difference due to concentration and temperature.

(3) diffusion caused by partial pressure difference.

(4) transportation of resolved gas.

MAPHY can consider the heat sinks and sources that have large influence to the mixing phenomena.
The mechanisms of hydrogen generation are considered following mechanisms;

(1) metal-water reaction
(2) core radiolysis
(3) sump radiolysis
(4) corrosion of Al and Zn

Hydrogen generated by metal-water reaction is given by input data for initial conditions, and hydrogen by others are given by time dependent input data.
In MAPHY code, the effects of safety systems after LOCA (ECCS, containment spray and hydrogen recombiner) can be also considered.



Equations

The basic equations required for calculations are

(1) the momentum equation for the atmosphere flowing through the pathes by the total pressure difference between every two subcompartments.

(2) the diffusion equation for the gas components by the partial pressure difference between every two sub-compartments.

(3) the energy and mass equations for individual components in each subcompartment.
(4) the state equations for the each gas component.

Fig.1 shows the MAPHY's model in a subcompartment.
As the phenomena is assumed to be quasi-stable, the physical properties of atmosphere are dependent on temperature.
All gases are treated as ideal gas.
Only the physical properties of steam are tied to the saturation conditions when the sump or spray exists.
Basic equations of MAPHY code are as follows;

(1) momentum equation

$$\frac{dG_{g.k}}{dt}=\frac{A_k}{L_k}\left\{g_c(p_i-p_j)-\frac{1}{2}\left(K_k+f_k\frac{L_k}{d_k}\right)\frac{|G_{g.k}|G_{g.k}}{\rho_k\cdot A^2_k}+\rho_k\cdot g\cdot(H_i-H_j)\right\}$$

(2) diffusion equation

$$G_{gdif}=\frac{D_k\cdot A_k}{R\cdot L_k}\left(\frac{p_i}{T_i}-\frac{p_j}{T_j}\right)$$

$$\cong\frac{D_k\,A_k}{R\cdot L_k\cdot T}\left(p_i-p_j\right)$$

$$T=\frac{T_i+T_j}{2}$$

in each component

$$G_{H_2dif}=\frac{D_k\cdot A_k}{R_{H_2}\cdot L_k\cdot T}\left(p_{H_2i}-p_{H_2j}\right)$$

$$G_{O_2dif}=\frac{D_k\cdot A_k}{R_{O_2}\cdot L_k\cdot T}\left(p_{O_2i}-p_{O_2j}\right)$$

$$G_{N_2dif}=\frac{D_k\cdot A_k}{R_{N_2}\cdot L_k\cdot T}\left(p_{N_2i}-p_{N_2j}\right)$$

$$G_{sdif}=\frac{D_k\cdot A_k}{R_s\cdot L_k\cdot T}\left(p_{si}-p_{sj}\right)$$

(3) mass conservation equation

$$\frac{dM_f}{dt} = \sum_{\alpha \in T} \{ (1 + C^*_{H_2,\alpha} + C^*_{O_2,\alpha} + C^*_{N_2,\alpha}) \cdot G_{f,\alpha} \} - \sum_{\beta \in I} \{ 1 + C^*_{H_2,\beta} + C^*_{O_2,\beta} + C^*_{N_2,\beta} \} \cdot G_{f,\beta} - G_{eva} + G_{\ell H_2} + G_{\ell O_2} + G_{\ell N_2} + G_{rec}$$

$$\frac{dM_{H_2}}{dt} = \sum_{\alpha \in T} (C_{H_2,\alpha} \cdot G_{g,\alpha} + G_{H_2 dif,\alpha}) - \sum_{\beta \in I} (C_{H_2,\beta} \cdot G_{g,\beta} + G_{H_2 dif,\beta}) + G_{H_2 gen} - G_{H_2 rec} - G_{\ell H_2}$$

$$\frac{dM_{O_2}}{dt} = \sum_{\alpha \in T} (C_{O_2,\alpha} \cdot G_{g,\alpha} + G_{O_2 dif,\alpha}) - \sum_{\beta \in I} (C_{O_2,\beta} \cdot G_{g,\beta} + G_{O_2 dif,\beta}) + G_{O_2 gen} - G_{O_2 rec} - G_{\ell O_2}$$

$$\frac{dM_{N_2}}{dt} = \sum_{\alpha \in T} (C_{N_2,\alpha} \cdot G_{g,\alpha} + G_{N_2 dif,\alpha}) - \sum_{\beta \in I} (C_{N_2,\beta} \cdot G_{g,\beta} + G_{N_2 dif,\beta}) - G_{\ell N_2}$$

$$\frac{dM_s}{dt} = \sum_{\alpha \in T} (C_{s,\alpha} \cdot G_{g,\alpha} + G_{s dif,\alpha}) - \sum_{\beta \in I} (C_{s,\beta} \cdot G_{g,\beta} + G_{s dif,\beta}) + G_{eva}$$

$$G_{eva} = \frac{(G_F + G_{rec}) v_F + G_s \cdot v_s}{v_F - v_s} + \frac{M_F \cdot v'_F + M_s \cdot v'_s}{v_F - v_s} \dot{T}$$

(4) energy conservation equation

In each subcompartment, energy conservation equation is given by

$$\frac{dU}{dt} = \sum_{\alpha \in T} (G_{F,\alpha} \cdot h_{F,\alpha} + G_{g,\alpha} \cdot h_{g,\alpha}) - \sum_{\beta \in I} (G_{F,\beta} h_{F,\beta} + G_{g,\beta} h_{g,\beta}) + Q_n$$

Transforming the equation to the temperature differential equation,

$$\dot{T} = \frac{F_0 - F_1 + F_2 \cdot T}{F_3}$$

$$F_0 = \sum_{\alpha \in T} (G_{F,\alpha} \cdot h_{F,\alpha} + G_{G,\alpha} \cdot h_{g,\alpha}) - \sum_{\beta \in I} (G_{F,\beta} \cdot h_{F,\beta} + G_{G,\beta} \cdot h_{g,\beta}) + Q_n$$

$$F_1 = (G_s + G_0) h_s + (G_F - G_0) \cdot h_F + G_{H_2} \cdot h_{H_2} + G_{O_2} \cdot h_{O_2} + G_{N_2} \cdot h_{N_2}$$

$$F_2 = \frac{V_t}{J} \{ (\dot{M}_{H_2} R_{H_2} + \dot{M}_{O_2} R_{O_2} + \dot{M}_{N_2} R_{N_2}) / V_a + (M_{H_2} R_{H_2} + M_{O_2} R_{O_2} + M_{N_2} R_{N_2}) v_F (G_F - G_0) / V_a^2 \}$$

$$F_3 = C_{pH_2} M_{H_2} + C_{pO_2} M_{O_2} + C_{pN_2} M_{N_2} + (h_s - h_F) \cdot HB + M_s h_s' + M_F h_F'$$
$$- \frac{V_t}{J} \left\{ p_s' + \frac{M_{H_2} R_{H_2} + M_{O_2} R_{O_2} + M_{N_2} R_{N_2}}{V_a} \left(1 + \frac{v_F' \cdot M_F - v_F \cdot G_l}{V_a} T \right) \right\}$$

where
. : time derivative
, : temperature derivative
$G_G = G_g + G_{dif}$

$$G_0 = \frac{(G_F + G_{rec}) v_F + G_s v_s}{v_F - v_s}$$

$$G_1 = \frac{M_F v_F' + M_s v_s'}{v_F - v_s}$$

(5) conditions of gases in a subcompartment

State equations of gases are as follows.

$$p_{H_2} = \frac{M_{H_2} \cdot R_{H_2}}{V_A} T$$

$$p_{O_2} = \frac{M_{O_2} \cdot R_{O_2}}{V_A} T$$

$$p_{N_2} = \frac{M_{N_2} \cdot R_{N_2}}{V_A} T$$

(6) heat sinks and sources

Heat sinks and sources are treated as inside material nodes. The common wall to another subcompartment is divided into two sections at the center of it. The divided sections are regarded as isolated boundary. The wall can be divided into three nodes.
Heat transfer between gas and the wall is

$$Q_1=K_1A_1\cdot(Tg-Tw_1)$$

$$\text{where}\quad \frac{1}{K_1}=\frac{1}{\alpha}+\frac{\delta_1/2}{\lambda_1}$$

In the internal layer of the heat sinks, heat teansfer equation is

$$Qi=Ki\cdot Ai(Tw_{i-1}-Tw_i)$$

$$\text{where}\quad \frac{1}{Ki}=\frac{\delta_{i-1}/2}{\lambda_{i-1}}+\frac{\delta i/2}{\lambda_i}$$

Natural convection and condensation of steam are considered as heat transfer mechanism. In this model, $|Tg-Tw_1|$ is larger than the temperature difference between gas and wall surface, so the heat transfer is promoted and the transition rate of Tg is suppressed.

4. Solution procedure

A governing ordinary differential equation is given by

$$\dot{\mathbf{y}}=\mathbf{f}(t,y)$$

where $\cdot$; derivative with respect to time t
$\mathbf{y}$; vector of unknown variables
$\mathbf{f}$; vector-valued function

Equation of $\dot{\mathbf{y}}$ is approximated with implicit method for time as

$$y_{n+1}-\Delta t\mathbf{f}(t_{n+1},\ \mathbf{y}_{n+1})=\mathbf{y}_n$$

where $t_{n+1}=tn+\Delta t$

If $\mathbf{f}$ is the nonlinear equation about $\mathbf{y}$, fully implicit method which applies Newton-Raphson method is often used. But in this code(MAPHY), second-order process[9] which is suggested by T. Steihaug and A. Wolfbrandt is applied because Newton-Raphson method has no certainty with convergence. And R.E. Scraton's[10] strategy is applied to the control of time step(Δt).

5. Verification

A prelimnary calculation was performed with the experimental configuration of Battelle Frankfurt.[5] This experiment simulated the hydrogen generation of sump radiolysis. The experimental configuration is consist of six sub-compertments which volume are about 30~40 m^3. Three subcompartments have the sump water, and hydrogen and nitrogen mixture, which ratio in volume is 2:1, is injected into one of these subcompartments. The temperature is homogeneously constant at each sub-compartment. This experimental configuration was simulated by nodes and paths shown in Fig.2 in the calculation. Hydrogen mixture was injected from node 10 to node 1 at 0.32 m^3/h. Temperatures of each subcompartment were assumed to be equal, because temperature differences among the subcompartments at the experiment were very small.

Fig.2 shows also the calculation results of hydrogen concentration and gas flow rates. The squared blocks of node ① to node ⑥ represent the subcompartments, and the solid and fat lines 1 to 13 between blocks indicate inter-connections. The directional lines do not show the flow directions, but only initial node to terminal node in the program input.

The flow directions are shown by the sign of the calculational result. Fig.3 shows the comparison of experimental and calculational results. The RALOC's result[5] is also shown in this figure.

The calculational results of MAPHY shows fairly good agreement with the experiment and the analysis by RALOC code, but it is necessary for MAPHY to be verified under other various conditions.

6. Verification program of MAPHY

In order to advance the verification of MAPHY code, a large scale model test program is undergoing at Takasago Technical Institute of Mitsubishi Heavy Industries, Ltd. This program is sponsored by five electric power companies of Japan; The Hokkaido Electric Power Company Inc., The Kansai Electric Power Company Inc., The Shikoku Electric Power Company Inc., The kyushu Electric Power Company Inc., The Japan Atomic Power Company.

6.1. Experimental apparatus

(1) Containment vessel model
A typical Japanese plant had been selected, and the model which simulates its subcompartments and paths was constructed.
The block diagram of these subcompartments and paths are shown in Fig.4. The model containment vessel ø3.5m×14mH) consists of 27 subcompartments. The paths between subcompartments are the same as model plant and the total volume of model containment vessel is about 1/680 as large as the model plant.

(2) Capacity of experimental apparatus
In order to qualitatively simulate the phenomena in a containment vessel after LOCA, the following systems are installed.(see Fig.5)
① containment spray system
② steam and hot water injection system
③ temperature control system of subcompartment's wall.
④ helium (simulated hydrogen gas) injection system

(3) detection and measurement systems
The following physical properties are measured.

①	concentrations of helium (mass spectrography)	: 30 points
②	temperature (Thermo Coupie)	: 400 points
③	velocity	: 10 points
④	pressure	

6.2. Experimets
The experiments are carried out to investigate the effects of the following parameters

① condition of temperature distribution in containment vessel
② condition of helium injection rates and places
③ condition of containment spray
④ condition of steam and water injection
⑤ condition of paths

6.3. Verification plan
Based on the experimental data, MAPHY can be verified about the node classifications, the evaluation method of the pressure loss coefficients and so on.

7. Conclusion

A new computer code named MAPHY was developed, which can predict the transient behavior of hydrogen concentration in any subcompartments of containment vessel after LOCA.

MAPHY code shows good agreement with Battelle's data and extensive verification program, sponsored by five electric power companies of Japan. is undergoing.

References

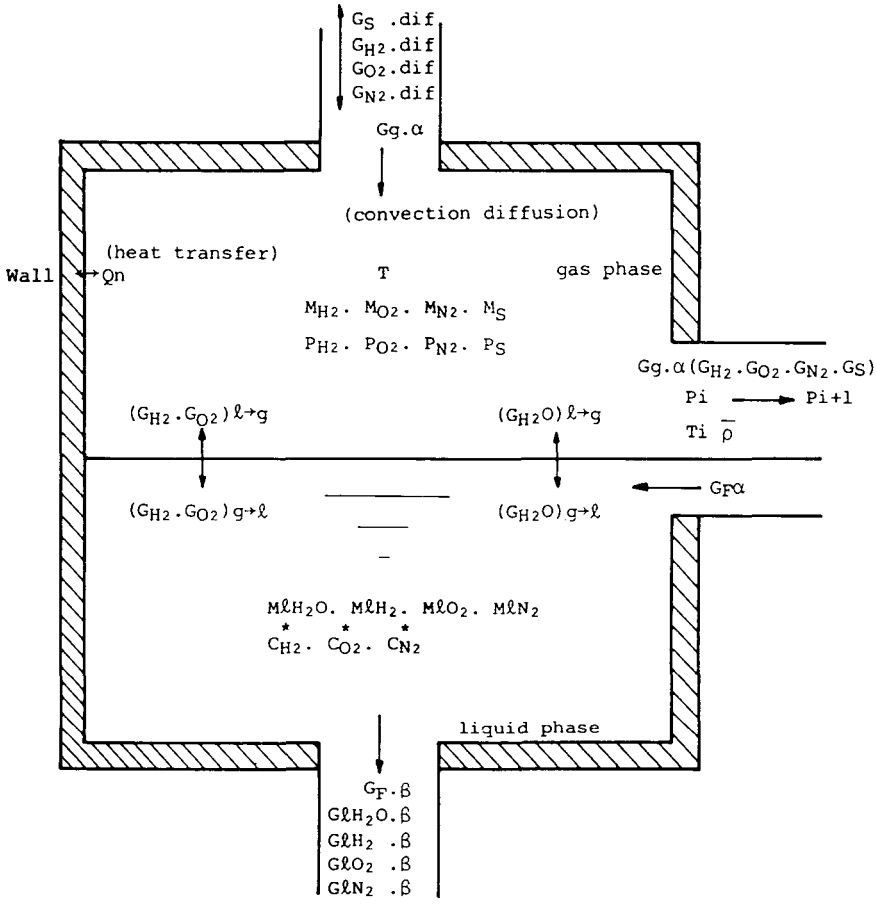
(1) Jahn, H. L., "RALOC-A New Model for Calculation of Local Hydrogen Concentrations in Subdivided Containments under LOCA-Aspects, Thermal Reactor Safety Meeting, Sun Valley July 31-August 5,1977

(2) Jahn, H. L. and G. Langer, "Distribution of Hydrogen Released within Compartmented Containment in Consequence of a LOCA-Analysis and Verification, The 7th WRSR Information Meeting, Gaitherburg(USA), Nov. 5-9,1979

(3) T. Steihaug and A. Wolfbrandt, An attempt to avoid exact Jacobian and Non-linear equations in the numerical solution of stiff differential equations, Mathematics of Computations, Vol 33, No.146(1979), pp521-534

(4) R.E. Scraton, Some L-stable methods for stiff Differential equations, Intern.J. Computer Maths, Vol 9(1981) pp81-87

(5) "Experimental Investigation of the Hydrogen Distribution in a Model Containment (Preliminary Experiments Phase II) Technical Report BF-R-64.036-2, Quick Look Report Test Block 4, Battelle Frankfurt, April, 1981



Gℓ.a	: inlet flow rate of liquid	($H_2O.H_2.O_2.N_2$)
Gℓ.β	: outlet flow rate of liquid	($H_2O.H_2.O_2.N_2$)
G.a	: inlet flow rate of atmosphere	($H_2O.H_2.O_2.N_2$)
G.β	: inlet flow rate of atmosphere	($H_2O.H_2.O_2.N_2$)
Gdif	: diffusion rate	($H_2O.H_2.O_2.N_2$)
(G_{H_2O})ℓ→g	: flow rate by evaporation	
(G_{H_2O})g→ℓ	: flow rate by condensation and recombination	
$(G_{H_2}.G_{O_2})$ℓ→g	: absorption rate	
g→ℓ	: desorption rate	
Mg. M_F	: mass of atmosphere	
C, C*	: concentration	
Pi. Pi+1	: total pressure	
P	: partial pressure	($H_2O.H_2.O_2.N_2$)
ρ	: density	
α	: initial node	
β	: terminal node	

Fig.1 MAPHY's model in a subcompartment

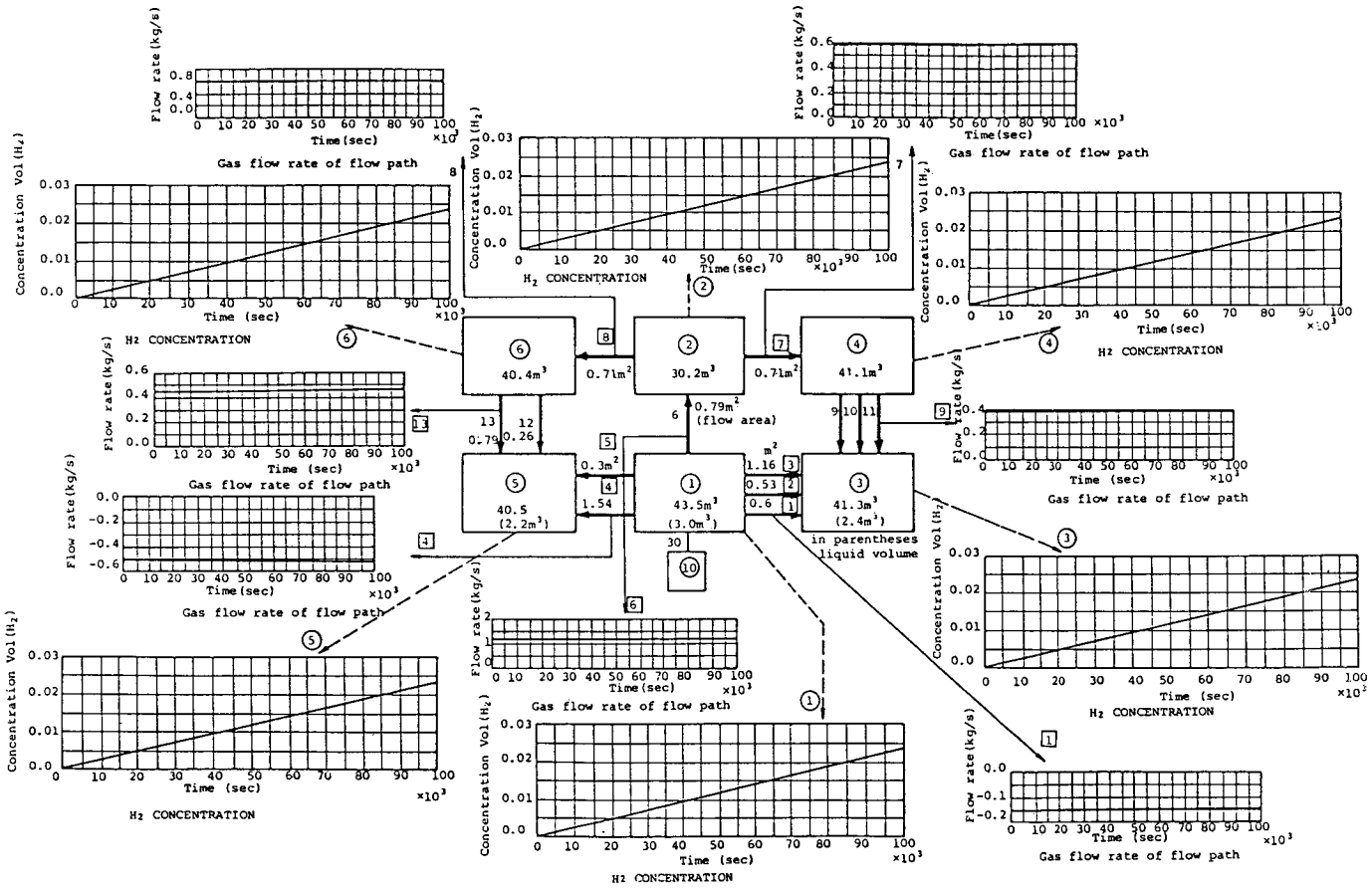


Fig.2 The calculation results(hydrogen concentration in each subcompartment and flow rate of gas)

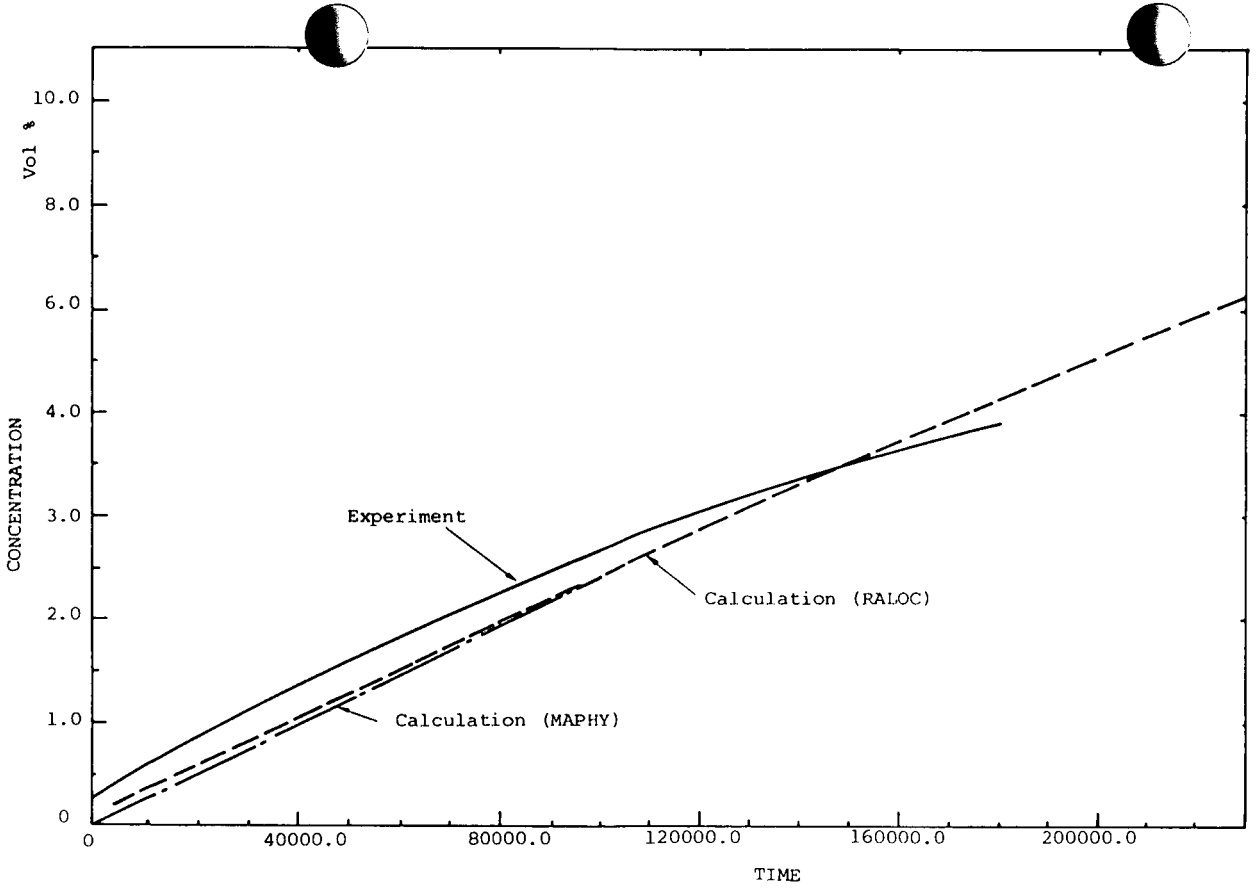


Fig.3 Comparison between Calculation and Experiment (Test No.12 Compartment 1)

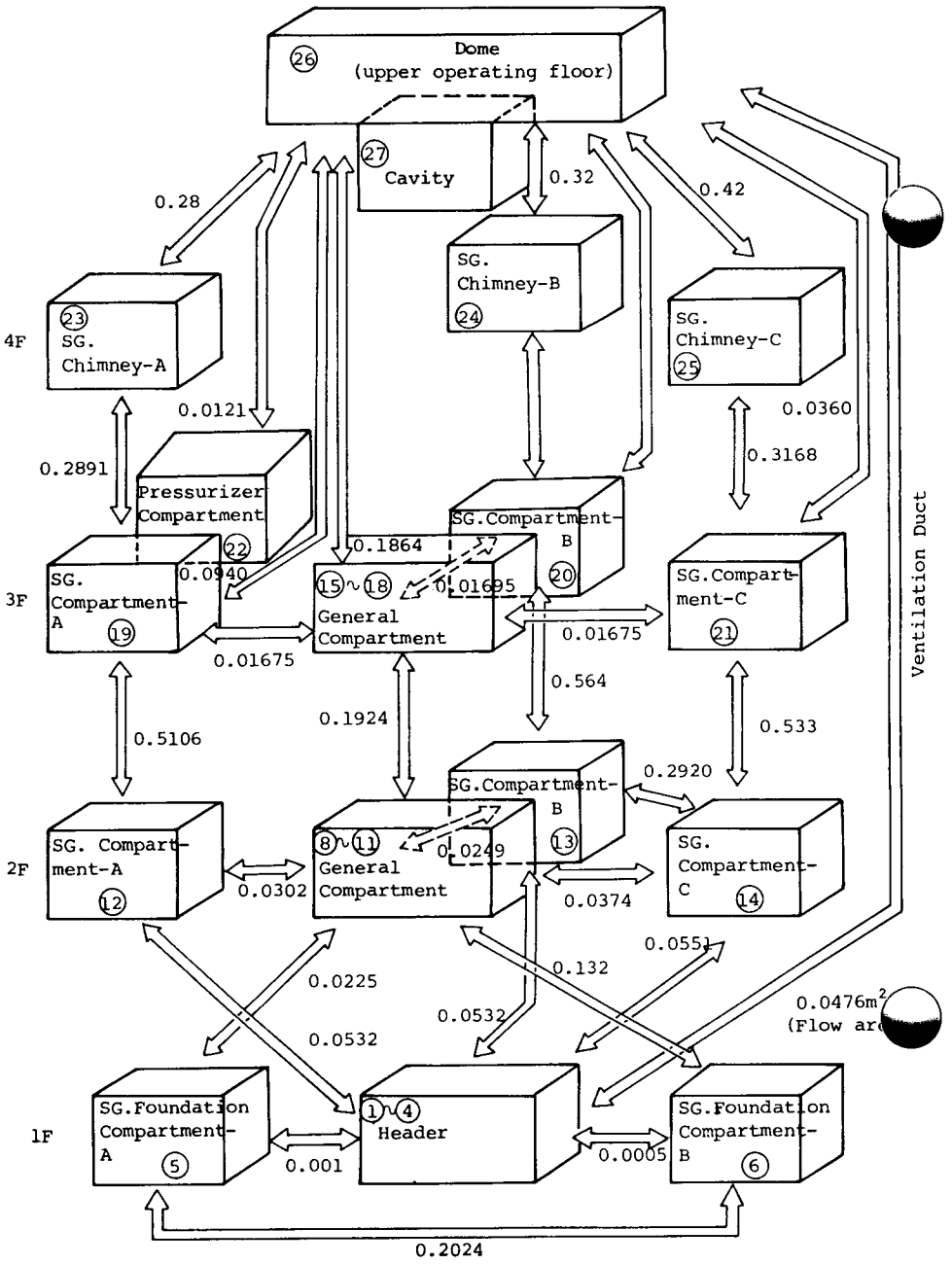


Fig.4 Block Diagram of subcompartments and paths

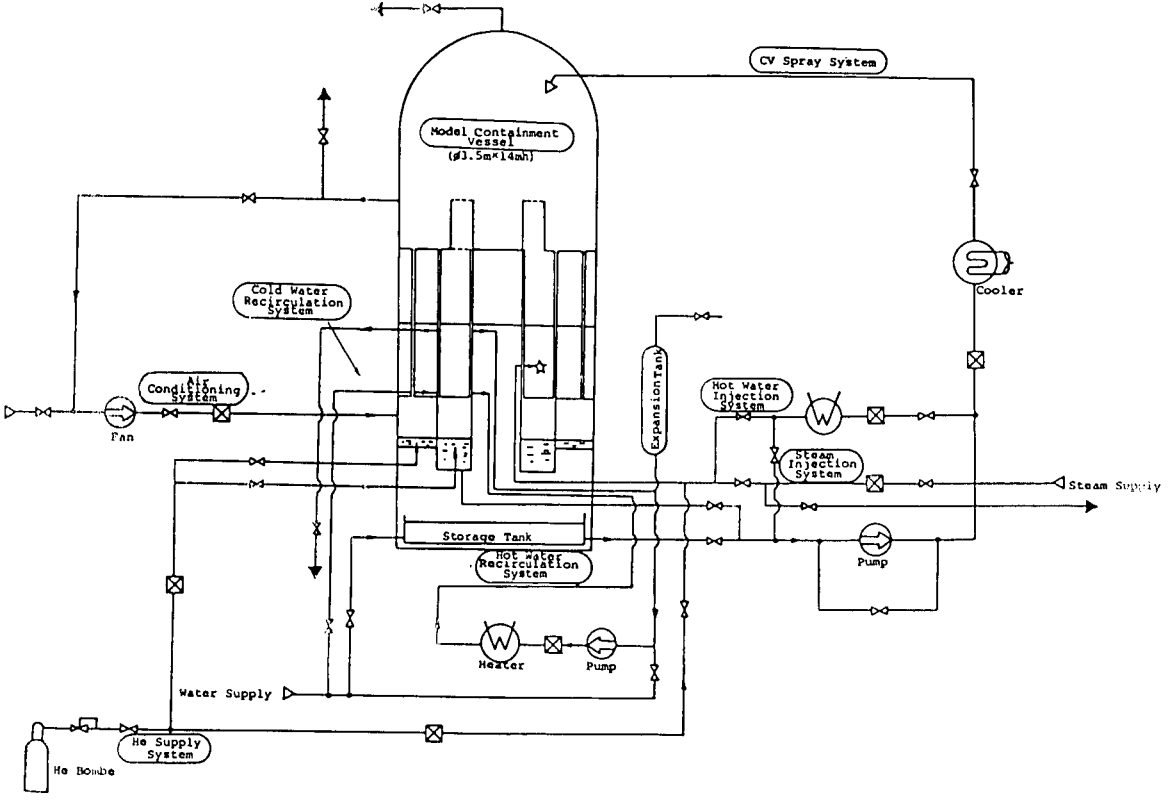


Fig.5 Schematic Diagram of Experimental Apparatus

HYDROGEN MANAGEMENT AND THE METAMORPHOSIS OF NRC POLICY ON SEVERE NUCLEAR ACCIDENT RISK

Harold R. Denton, Director
Office of Nuclear Reactor Regulation
U.S. Nuclear Regulatory Commission
Washington, D.C. 20555

INTRODUCTION

I appreciate the opportunity to address this Second International Workshop on the Impact of Hydrogen on Water Reactor Safety. Many of you may be aware that I am pinchhitting for Commissioner Ahearne, who is pinchhitting for Chairman Palladino. Last June, Commissioner Ahearne presented some cogent remarks to the Workshop on Containment Integrity, which provide an excellent background for my talk on the subject of hydrogen management in the broader perspective of NRC policies being developed to deal with severe nuclear accident risk.[1]

There are now 35 countries throughout the world that have commercial nuclear power plants in operation, under construction, or on order.* This list is almost certain to expand. Yet, whether a healthy political and financial climate can be achieved that would support a vigorous growth in nuclear programs within each of these countries is a challenge of no small dimensions.[2] To an important degree, this outlook will depend on the success of cooperative international efforts such as those reflected in this workshop. The key objectives are to prevent severe nuclear accidents, especially those with serious offsite consequences, and to assure both the public and financial community that the risks of such severe accidents can be controlled.

TOWARD A NEW PERSPECTIVE OF DECISIONMAKING

From the early days of light water reactor developments (at least as early as the Humboldt Bay Nuclear Plant) it was understood that, following a loss-of-coolant accident, hydrogen could accumulate inside the primary reactor containment as a result of: (1) metal-water reaction involving the fuel element cladding; (2) the radiolytic decomposition of the water in the reactor core and the containment sump; (3) the corrosion of certain construction materials by some spray solutions; and (4) possible synergistic effects of chemical, thermal and radiolytic byproducts of accidents on containment protective coatings and electric cable insulation. These areas were debated in licensing reviews and occasionally in licensing hearings for many years. Our design requirements began to stabilize in 1974 with the issuance of 10 CFR 50.46 that set the oxidation of one percent of the core zirconium as a performance objective for emergency core cooling systems.

Controversy flared later on when the Vermont Yankee Appeals Board overturned the staff requirements to inert the containment of that reactor to protect against post-LOCA hydrogen generation. The problem was that the staff used 5 percent metal-water reaction for the containment performance objective,

*Plant capacities of 30 MWe and over, as of June 30, 1982. (Nuclear News, Vol. 25, No. 10, August 1982).

rather than the 1 percent for ECCS. To settle the Vermont Yankee controversy, rules were established to deal with these hydrogen matters in Title 10 of the Code of Federal Regulations (10 CFR) Section 50.44, "Standards for Combustible Gas Control Systems in Light Water Cooled Power Reactors," and General Design Criterion 41, "Containment Atmosphere Cleanup," in Appendix A to 10 CFR Part 50. These rules require that systems be provided to control hydrogen concentrations in the containment atmosphere following a postulated accident to ensure that containment integrity is maintained. The amounts of metal-water reaction treated by this hydrogen rule are trivial by today's standards, being in the range of one to five percent of the core zirconium.

The reason for their triviality is, of course, the small-break, loss-of-coolant accident at Three Mile Island. We threw the design basis of 50.44 out the window on Friday, March 30 when we learned of the hydrogen explosion and the 28 psi pressure spike in the TMI-2 containment some ten hours after the accident began. We then began to learn the hard way that there was much about the phenomenology of hydrogen generation, burning or detonation, as well as the systems interactions affecting accident control measures and containment integrity, that was poorly understood. The Special Inquiry Group established by the NRC to evaluate the TMI-2 accident estimated that the total amount of H_2 generated by the accident was about 990 pounds which is equivalent to 45% of reaction of the fuel cladding with water. However, there was, and still exists, a broad range of uncertainty surrounding this estimate.

In response to the elevated concerns about the adequacy of public protection from accidents such as TMI, and to correct the deficiencies in reactor design, operation and regulation that were revealed by the accident, the NRC established the "TMI-2 Action Plan," NUREG-0660. It was approved by the Commission and published in May 1980. In the Action Plan, Task II.B., "Consideration of Degraded or Melted Cores in Safety Review," identified a number of actions that involve developing and implementing a phased program to include in safety reviews consideration of core degradation and melting beyond the design basis. One of these actions, Task II.B.8, was a "Rulemaking proceeding on degraded core accidents." This was to comprise two separate actions, a long-term rulemaking and an interim rule. The long-term rulemaking was to consider to what extent, if any, nuclear power plants should be designed to deal effectively with degraded core and core-melt accidents and to mitigate the consequences thereof. This rulemaking has evolved into what is now being referred to as the "Severe Accident Rule." A staff proposal for a policy statement on severe accidents and related views on nuclear reactor regulation is currently under review by the Commission.

The other action identified in Task II.B.8 involved an "interim rule" which was to be based on a number of recommendations specifically related to accidents that involve severely damaged or degraded reactor cores. The recommendations were determined by the staff to be of such safety significance that they should be codified by regulation in order to provide assurance that the public health and safety is adequately protected. The staff believed that the changes resulting from these requirements would improve the capability of nuclear power plants to deal with TMI-2 type accidents. The Interim Rule relating to hydrogen control has now been issued in two parts: a final rule (December 2, 1981) and a proposed rule (December 23, 1981). The Final Rule requires principally two

actions: (i) inerting of Mark I and II BWRs, and (ii) installation of H_2 recombiner capability. The owners of the BWR plants with Mark I containments have recently asserted that the requirement for a recombiner capability should not apply to them. Based on a more thorough examination of the radiolysis analysis, they believe that the atmosphere in the Mark I containment can be maintained in the inert condition for an indefinite period.

The Proposed (Part 2) Rule, for which public comment has now been received, involved four proposed measures:

(1) Hydrogen control for BWR Mark III and PWR Ice Condenser Containments.

(2) Survivability and Qualification Standards for Safety Systems and Components that must function during and after a hydrogen burn to establish and maintain safe cold shutdown.

(3) Analyses of LWRs for the consequences of large hydrogen releases corresponding to the metal-water reaction of 75% of the active fuel cladding.

(4) Containment structural integrity requirements.

The Commission approved the hydrogen control measures of the Part-1 Interim Rule on December 2, 1981 and the near term Construction Permit/Manufacturing Rule on January 15, 1982.

Because of the large number of corrective actions already taken that chiefly resulted from the lessons learned through the TMI-2 accident, the urgency for additional actions would appear to be substantially reduced. A new stage of metamorphosis in NRC policy on severe nuclear accident risk is heralded by the Commission's newly established requirements, among other initiatives being taken, that further regulatory actions to reduce risk be evaluated by an analysis of the costs and benefits of risk reduction. As published in January 1982, "US Nuclear Regulatory Commission Policy and Planning Guidance, 1982" (NUREG-0885) specifically states:

> "Requirements imposed on the regulated industry by NRC are to have a positive contribution to safety, not only individually, but also when the requirements are taken as a whole. Requirements proposed to achieve incremental reductions in residual risk should be evaluated on a cost-benefit basis."

A companion administrative initiative was the recent establishment of the Committee to Review Generic Requirements (CRGR). This Committee has the responsbility to review and recommend to the Executive Director for Operations (EDO) approval or disapproval of requirements to be imposed by the NRC staff on one or more classes of power reactors. The CRGR will develop means for controlling the number and nature of the requirements placed by NRC on licensees. The objectives of these controls are to eliminate or remove any unnecessary burdens placed on licensees, reduce the exposure of workers to radiation in implementing some of these requirements, and conserve NRC resources while at

the same time not reducing the levels of protection of public health and safety.

SCIENCE, THE ENDLESS FRONTIER

Implementing the Commission's directive to employ cost-benefit analysis and probabilistic risk assessment (PRA) in justification for further safety modifications poses numerous difficulties. It is important to recognize at the outset that scientific methodology and experimental or frequency data on failure rates for probabilistic assessments of severe accidents and their consequences have important areas of deficiency. Moreover, the estimation of the dollar costs of the safety adders and the various benefits of risk reduction pose additional dimensions of uncertainty for the new basis of decisionmaking. These deficiencies put enormous pressures on the need for expanded research programs by the NRC and industry to improve the quantitative basis for evaluating the risks, costs, and benefits of additional measures to reduce the risks of severe nuclear accidents.

The snowballing requirements for research funding remind me of a book entitled, Science: The Endless Frontier.[3] Written in 1945 by Dr. Vannevar Bush, the book developed the theme that each advance of science that resolved certain mysteries also uncovered new mysteries to be explored. Thus, a moving frontier is created with an endless horizon. It seems to me that Bush's concept of moving frontiers aptly describes the situation with regard to research projects related to an improved information basis for hydrogen management and other aspects of severe accident risk management.

The research projects and experimental findings on hydrogen management issues being reported in this workshop illustrate quite well the diversity of science frontiers and their galloping movement. This is scarcely surprising in view of the many different designs of reactors, containments, and technologies for accident prevention, accident management, and consequence mitigation. Add to this the legion of imaginable scenarios of accident sequences affecting hydrogen generation rates and accident progression phenomenology involving water-metal interactions, steam explosions, fragmented debris and concrete interactions, performance of distributed igniter or recombiner systems, safety equipment survivability, the variety of threats to containment integrity and uncertainties regarding containment performance, and one begins to appreciate the need for considerable research by industry and government in order to execute the Commission-mandated requirement that the risks, costs, and benefi of each proposed safety modification be evaluated as a basis for determining their justification.

Yet, if one can envision an endless progression of research needs, it is also true that funds available to support these needs are not limitless. Accordingly, it is essential that:

(1) Priorities for hydrogen management research be established using cost-benefit analysis in the broader framework of integrated risk assessment of all research candidates affecting the risk mangement of severe nuclear accidents; and,

(2) Effective coordination be established between all such research efforts by industry and government, both within the United States and world-wide, to avoid wasteful duplication of effort and to facilitate the exchange of information useful in setting research priorities.

The NRC has already established a staff function responsible for coordinating the degraded core and severe accident research sponsored by the NRC and the Industry Degraded Core Rulemaking Program (IDCOR).[4,5] Current efforts are under way for an exchange of information with a number of countries regarding their research programs and decisionmaking logic related to the implementation of safety measures affecting accident prevention, accident management, and the assurance of containment integrity.

COMMISSION INITIATIVES IN DEVELOPING SEVERE ACCIDENT POLICIES

Proposed Safety Goals

As I previously noted, the regulatory issues of improved hydrogen management need to be examined in the broader perspective of Commission initiatives in developing severe accident policies. Focusing on one matter of special public concern--namely, nuclear power plant accidents that might release radioactive materials to the environment--the Commission released for public comment on February 1982 a discussion paper on Safety Goals for Nuclear Power Plants.[6] This paper was preceded by several NRC-sponsored workshops involving public input and a number of discussion papers and safety goal proposals.[7,8] The proposed safety goal policy statement was developed in response to the recommendations of the President's Commission on the Accident at Three Mile Island which called for an explicit policy statement on safety philosophy and the role of safety-cost tradeoffs in NRC safety decisions. It was felt that the development of safety goals and a workable implementation plan could lead to more coherent and consistent regulation of nuclear power plants, a more predictable regulatory process, an improved public understanding of the regulatory criteria that the NRC applies, and increased public confidence in the safety of operating plants.

The safety goal discussion paper proposed two qualitative safety goals and four provisional numerical guidelines:

(1) "Individual members of the public should be provided a level of protection from the consequences of nuclear power plant accidents such that no individual bears a significant additional risk to life and health.

(2) Societal risks to life and health from nuclear power plant accidents should be as low as reasonably achievable and should be comparable to or less than the risks of generating electricity by viable competing technologies.

(3) The risk to an individual or to the population in the vicinity of a nuclear power plant site of prompt fatalities that might result from reactor accidents should not exceed one-tenth of one percent (0.1%) of the sum of prompt fatality risks resulting from other accidents to which members of the U.S. population are generally exposed.

(4) The risk to an individual or to the population in the area near a nuclear power plant site of cancer fatalities that might result from reactor accidents should not exceed one-tenth of one percent (0.1%) of the sum of cancer fatality risks resulting from all other causes.

(5) The benefit of an incremental reduction of risk below the numerical guidelines for societal mortality risks should be compared with the associated costs on the basis of $1,000 per man-rem averted.

(6) The likelihood of a nuclear reactor accident that results in a large-scale core melt should normally be less than one in 10,000 per year of reactor operation."

How to bridge between the provisional guideline of a large-scale core melt probability and the numerical guidelines for offsite prompt and latent fatality risks was left open for treatment by the staff within the framework of an implementation plan. There are, of course, numerous uncertainties in building such a bridge. For example:

(1) Should, or how should, the differential risk between these numerical guidelines be allocated between probability of containment failure, probabilities of different scenarios for radiation transport, and exposure probabilities related to different scenarios for emergency evacuation or sheltering?

(2) How should uncertainties regarding source terms be treated--notably iodine removal by sprays or other mechanisms?

(3) How should uncertainties regarding dose-response models be treated?

Regarding the issue of containment failure, there are numerous designs of containment, heat suppression methods and other accident management and consequence mitigation techologies. Obviously, hydrogen management options play an important role in questions of risk allocation and the treatment of uncertainties. The safety goal study by the ACRS suggested a probability goal of 0.01 for a large-scale uncontrolled release, given a large-scale fuel melt, with an upper limit of acceptability of 0.1.[7] Such a zone concept of safety targets, rather than single-point risk allocations between numerical guidelines, provides for some allowance for uncertainties in risk estimation. More importantly, it allows for flexibility in nuclear plant design which permits credits (or risk tradeoffs) to be given for superior safety engineering features in important areas of defense-in-depth design strategies. In fact, a great deal of the controversy over hydrogen control rules surrounds this very question of whether credits should be given for superior accident prevention designs in compensating for weaker or smaller containment designs. These serious questions the Commission will need to consider in finalizing its safety goals and implementation plans as well as other policy developments affecting severe accident risk management including rulemaking for plants of new design as well as backfitting decision criteria for operating reactors or those in the pipeline.

Severe Accident Rules for Reactors of New Design

Another NRC initiative in developing severe accident policy being reviewed by the Commission is the "Proposed Commission Policy Statement on Severe Accidents and Related Views on Nuclear Reactor Regulation." The focal issue is how best to coordinate a final decision on severe accident considerations for existing plants and rulemaking on specific standard designs. The new approach, if approved, would replace the unfocused long-term generic rulemaking envisioned in Task II.B.8 of the TMI Action Plan with severe accident rulemakings on specific standard plant designs and regulatory decisions on classes of existing reactors which may, or may not, include rulemaking.

In the past several years the Commission has required more protection for severe accidents in a number of near-term licensing actions than was envisioned in the TMI Action Plan. Included among these safety measures are a number that deal with hydrogen control for certain classes of reactors such as Mark I and II BWRs and certain plants with ice condenser containments. Moreover, other changes in reactor design and operation are being implemented in accordance with NUREG-0737 ("Clarification of TMI Action Plan Requirements"), thus accomplishing the significant safety improvements mandated by studies of the acident at Three Mile Island.

Considerable momentum has been achieved among a broad scope of regulatory and industry activities that would be supportive of the approach to severe accident decisionmaking embodied in the proposed Commission policy statement on severe accidents. Among these are the following:

(1) The nuclear industry has initiated the Industry Degraded Core Rulemaking (IDCOR) Program that will produce a study of costs and benefits of design features to deal with severe accidents.

(2) NRC's Office of Research has developed a two-phase plan for first producing and later confirming information needed for regulatory decisions on severe accidents.

(3) The safety goal policy statement which I have already discussed has been published for public comment. It would initiate a structured approach for developing more detailed quantitative guidance for systems design affecting severe accident risk based on cost-benefit analyses and demonstration that risk is as low as reasonably achievable (ALARA).

The AIF and several reactor vendors are seeking some statement of Commission policy on referencing of approved standard designs in future CP applications.

The staff considered, but did not include in the proposed Commission policy statement on severe accidents, the question of a numerical guideline on availability of containment function (given a large-scale core melt) by which to judge the adequacy of old and new types of containment. Currently, there is inadequate knowledge to establish numbers appropriate for such guidelines. However, containment failure evaluations have a functional relation to the provisional numerical guidelines for off-site safety consequences in the proposed Commission policy statement on safety goals. Containment failure

evaluations should continue to be performed in the context of probabilistic risk assessments for a representative sample of operating plants and plants under construction and for all future designs. If flexibility in containment design is permitted for new plants, as seems desirable, then integrated risk assessment would indicate a need for tradeoff considerations between accident prevention and consequence mitigation in meeting the numerical guidelines for off-site consequences. For example, if the containment design has a failure probability on the high side, then it should be expected that compensatory features of plant design will excell the core-melt numerical guideline or t other superior consequences mitigation features will have been provided.

PUTTING IT ALL TOGETHER

In conclusion, I would offer the following observations:

(1) In view of the large number of safety actions already implemented, chiefly as a result of lessons learned from the TMI accident, the pendulum is swinging away from urgency for further safety modifications to a regulatory climate of patient and systematic evaluation of need based on an integrated system assessment of severe nuclear accidents and their consequences.

(2) It is essential that decisions on the treatment of hydrogen management and containment integrity issues be examined in the broader perspective of policies under development to deal with severe nuclear accident risks. These include: safety goals and provisional numerical guidelines; policies regarding the use of quantitative probabilistic risk assessment and cost-benefit analysis in safety decisionmaking; the use of rulemaking for the resolution of severe accident issues for new standard plant designs; the development and application of backfitting policy for plants in operation or under construction; and other policy initiatives involving legislative reform and emergency preparedness.

(3) Major uncertainties still exist regarding the quantifications of PRAs and cost-benefit analyses to decide upon safety modifications. Research programs in progress or planned will likely make important contributions to uncertainty reduction. This includes numerous areas of confirmatory research regarding hydrogen generation and accident progression phenomenology as well as predicting the effectiveness of hydrogen management technologies and containment reliability.

(4) Many of us feel that this research effort is more likely to increase th confidence of our decisionmaking rather than lead to major new require ments for severe accident management and consequence mitigation. Howe if the new information indicates otherwise, we shall not hesitate to do what is necessary to protect the health and safety of the public.

(5) Coordination of research between government and industry as well as between countries is essential to eliminating wasteful duplications of research funding. Moreover, the sharing of information regarding severe accident decision criteria would be helpful in establishing research priorities and the desirability of implementing further safety measures or abandoning unnecessary ones.

(6) Despite the large research effort being mounted, it seems rather likely, in keeping with Vannevar Bush's concepts, that numerous residual uncertainties will exist.

Thus, although useful progress will likely be made in bridging the gap between PRA capabilities and the validation of safety goal attainment, I do not foresee this gap being closed in the next five or ten years if rigorous scientific evidence is insisted upon for estimating the probabilities and consequences of severe accident risk. Accordingly, this gap can only be bridged through the exercise of informed judgment with hopefully a narrowing of disagreement among experts as to the ranges of uncertainty through research findings and evaluations of the growing volume of failure data from plant operations.

The quantification of subjective probability judgments concerning certain initiating or promoting events of nuclear accident sequences is not an approach that many scientists or engineers feel comfortable with and remains a problem to be dealt with. In this regard, I would invite your attention to the methods of developing subjective numerical probability estimates in the face of soft information on cause-effect relationships now being used in the Seismic Safety Margins Research Program sponsored by the NRC and conducted by the Lawrence Livermore Laboratory.[9] Regardless of the mixture of hard and soft information, regulatory decisions will continue to be made in the face of residual uncertainties. We in the scientific community must provide the most appropriate objective data and the best informed subjective judgments that we can if the new policy initiatives toward a more quantitative basis for regulatory decision-making regarding severe accident prevention and consequence mitigation are to be successful.

REFERENCES

1. John F. Ahearne, "Remarks before the Workshop on Containment Integrity," Conducted by Sandia Laboratories, Quality Inn, Pentagon City, Virgina, June 8, 1982.

2. Harold R. Denton, "Nuclear Power: Epilogue or Prologue?" The Energy Journal, 4, No. 1, 125-141, January 1983.

3. Vannevar Bush, Science: The Endless Frontier (Washington, D.C.: Government Printing Office, 1945).

4. Nuclear Plant Severe Accident Research Plan, Draft, NUREG-0900, U.S. Nuclear Regulatory Commission (Forthcoming).

5. IDCOR Program Plan, a report prepared by Technology for Energy Corporation (Knoxville, Tenn.) for the Industry Degraded Core Rulemaking Program, sponsored by the nuclear industry (November 1981).

6. Safety Goals for Nuclear Power Plants: A Discussion Paper, NUREG-0880, U.S. Nuclear Regulatory Commission (February 1982).

7. Advisory Committee on Reactor Safeguards, An Approach to Quantitative Safety Goals for Nuclear Power Plants, NUREG-0739, U.S. Nuclear Regulatory Commission (October 1980).

8. Roger Mattson, et al., "Concepts, Problems and Issues in Developing Safety Goals and Objectives for Commercial Nuclear Power," Nuclear Safety, 21, No. 6, 703-716 (November-December 1980).

9. R. W. Mensing, The Use of Subjective Input, Phase I Final Report of the Seismic Safety Margins Research Program (NUREG/CR-2015, Vol. 10), U.S. Nuclear Regulatory Commission, July 1981.

SESSION Va

COMBUSTION MODELLING AND EXPERIMENTS

579/580

Ignition of Hydrogen/Oxygen/Nitrogen Mixtures Exposed To Two Configuration Dependent Ignition Sources

Frank J. Benz
NASA JSC White Sands Test Facility
Las Cruces, NM

ABSTRACT

White Sands Test Facility (WSTF) performed a series of tests to determine the ignition characteristic of hydrogen/oxygen/nitrogen mixtures. The testing was performed to assess the ignition hazard on board the Space Transportation System (STS) from possible leakage of hydrogen, oxygen and nitrogen.

The ignition sources consisted of an exhaust duct that exposed a heated surface through a 1/4 inch crack in the insulation and a heated surface that existed at the bottom of a 0.75-inch diameter, 2-inch long tube. These ignition sources were fabricated to simulate the exhaust duct and the hydrazine injector tube in the Auxiliary Power Unit (APU) on board the STS. The data obtained using these ignition sources were compared with data obtained using common ignition sources such as electrical spark, hot surfaces, etc.

The results indicated that the configuration aspects of the ignition source had significant affects on the ignition characteristics of hydrogen mixtures.

1.0 Introduction

White Sands Test Facility (WSTF) performed a series of tests to determine the ignition characteristic of hydrogen/oxygen/nitrogen mixtures exposed to various ignition sources. The testing was performed to assess the potential ignition hazards on board the Space Transportation System (STS) due to leakage of concentrated hydrogen, oxygen and nitrogen sources.

The program was divided into two parts. The first part was performed in order to evaluate the ignition characteristics of hydrogen using common ignition sources such as spark, hot wire, fused wire, and hot surfaces (ref. 1). These results were reported in January 1981 (ref. 2) at the First workshop on the Impact of Hydrogen on Water Reactor Safety.

The second part of the test program was performed in order to evaluate the ignition characteristics of hydrogen when exposed to two proposed STS potential ignition sources (ref. 3). The data generated from these tests were compared with data generated from the common igniters used in the first part of the test program (spark discharges, hot surface, etc) in an attempt to correlate "standard" type test data with that obtained from simulated "actual situations".

The information presented herein was selected from the tests that was viewed as most applicable to the subject of this workshop; that is, the data that indicated the dependence of hydrogen ignition characteristics upon the configuration of the ignition source.

2.0 Test System Descriptions

One test system was designed to simulate an exhaust duct and the other was designed to simulate a cavity formed around a fuel line. The exhaust duct configuration exposed the hydrogen mixtures to a hot surface through a 1/4 inch gap. The hot cavity configuration exposed hydrogen mixtures to a hot surface through an annular type path.

2.1 Simulated Exhaust Duct

The simulated exhaust duct was constructed as shown in Figure 1. An 8-inch-long, 2-1/2 inch-diameter cylinder fabricated out of Inconel 600 was wrapped with 1-inch-thick Dynaflex insulation which was in turn wrapped with stainless steel foil. The insulation was sectioned such that a 1/4-inch wide gap was left that provided a path to the Inconel cylinder. A copper sleeve containing an electrical cartridge heater was inserted in the cylinder which provided the means for heating the Inconel surface to the test temperature. The duct was attached to a flange assembly and then bolted to a type 304 stainless steel cylindrical chamber with an internal volume of 0.36 ft^3 (see Figure 2). The test chamber was equipped with ports for test fluid ingress and egress, evacuation, pressure and temperature measurements, and a photocell feed-through. The chamber was provided with sources of hydrogen, nitrogen, and oxygen through a facility plumbing system.

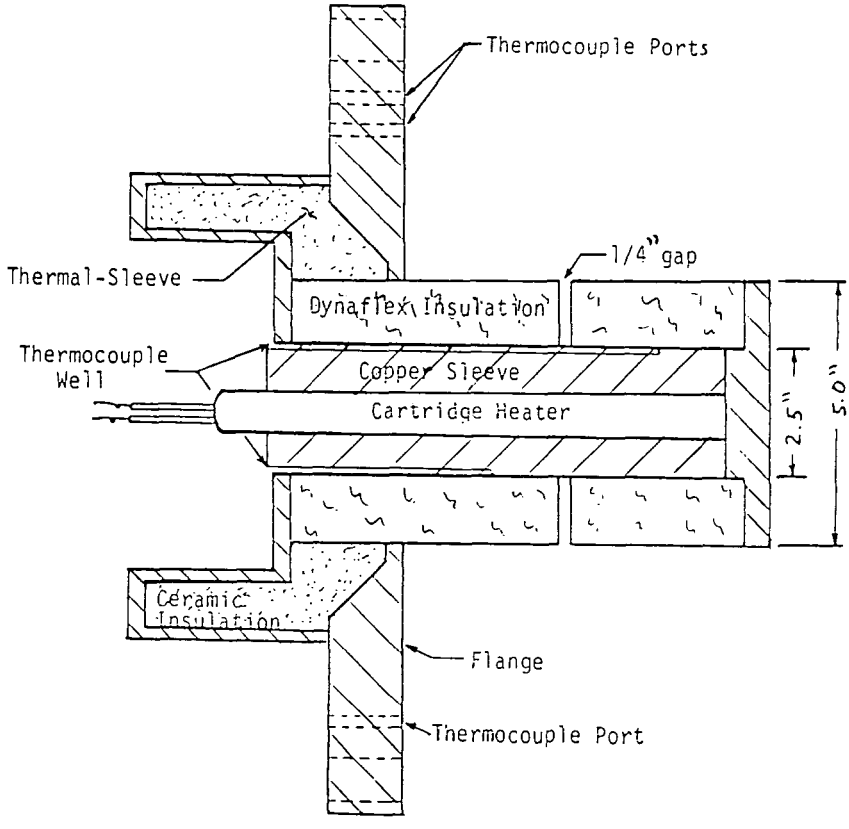


Figure 1
Schematic Depicting Simulated Exhaust Duct Test System

The test system was instrumented to measure pressure, temperature and visible light emission. Pressure was measured with a high resolution 0-200 ± 0.005 psia capacitance manometer and a 0-25 ± 0.25 psia bonded strain gauge pressure transducer. The capacitance manometer was used to establish the test mixtures whereas the bonded strain gauge was used to measure overpressures due to ignitions. Temperatures were measured using stainless steel sheathed, copper constantan thermocouples (refer to Figure 2 for thermocouple placement). Light emission was monitored with a photo conductive photocell through a quartz rod. The photocell had a response from 200 to 2500 manometers in wavelength. Both analog and digital recording devices were utilized to record and display data.

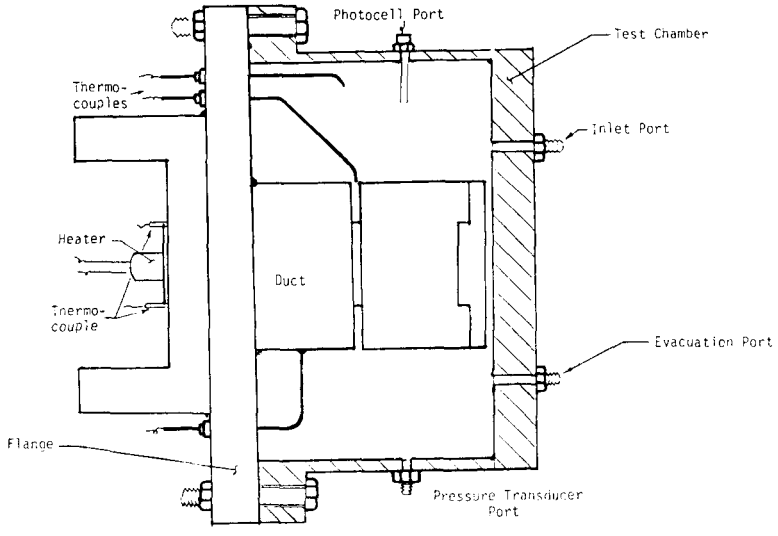


Figure 2
Schematic Depicting Simulated Hot Exhaust
Duct Interface to Test Chamber

2.2 Simulated Hot Cavity

The simulated hot cavity was constructed as shown in Figure 3. A 4.5-inch-diameter, 5-inch-long cylinder fabricated from type 304 stainless steel was closed with a welded baseplate at one end and the other end was fitted with a plate that contained a 0.75-inch diameter tube that extended 2 inches into the cylinder. At the bottom of the tube, a 500-watt cartridge heater was installed that enabled this portion of the tube to be heated. A 0.2-inch-diameter rod was placed in the center of the tube to simulate the feed line and provided an annular path down the tube. The inner cavity of the cylinder was filled with insulation and the entire unit sealed to minimize heat paths other than through the tube. A temperature controller was used in conjunction with the cartridge heater to heat the tube to a maximum temperature of 1350° F. The simulated hot cavity assembly was placed into a cylindrical stainless steel chamber, 22 inches in diameter and 48 inches in length with an internal volume of approximately 10 cubic feet. The cavity assembly was oriented such that the open end was facing vertically

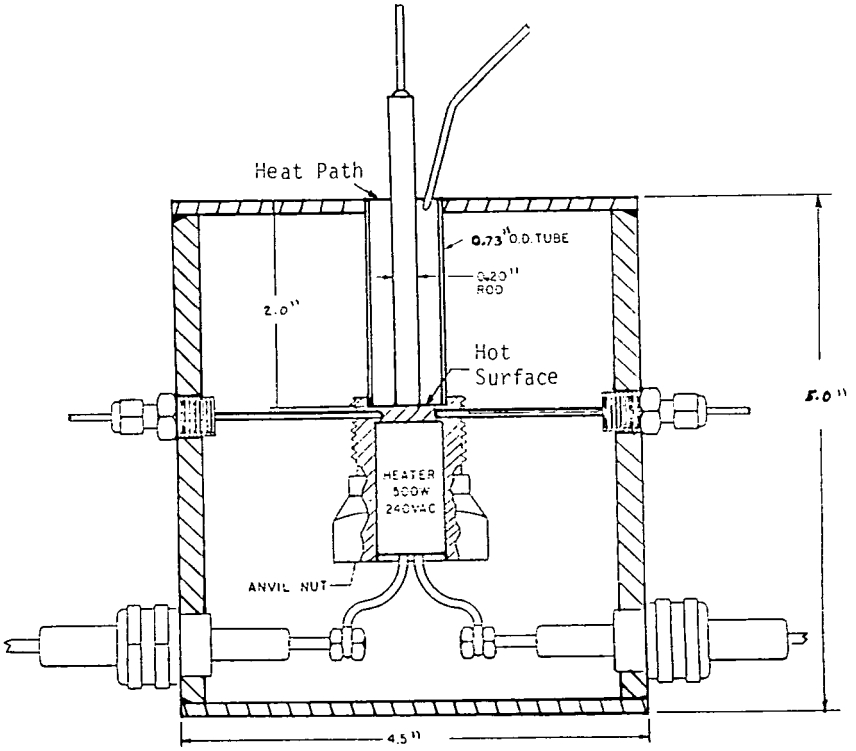


Figure 3
Schematic Depicting Simulated Hot Cavity

upward. The chamber was provided with a port for test fluid ingress and egress, vacuum lines, overpressure relief devices, pressure measurements and electrical feed throughs.

A 0-200 psia capacitance manometer and 0-25 bonded strain gauge were used to measure pressure. Temperatures were measured using type 304 stainless steel iron constantan thermocouples. Thermocouples were placed in the chamber to monitor the gas temperature and in the feedline cavity to measure the hot surface temperature. Light emission from an ignition was monitored with a photoconductive cell that was coupled to the test chamber through a quartz rod. Both analog and digital recording devices were utilized.

3.0 Test Conditions

Testing was performed at ambient laboratory temperature. Each constitutent of the test gas mixture was added such that the mixing temperature was within $\pm$ 1°F of the initial temperature to assure accurate mixture ratios.

A standard excess oxygen/hydrogen/nitrogen mixture was specified for these tests. This mixture consisted of a 1:1.67 hydrogen to oxygen ratio with the balance being nitrogen for mixtures of 10 percent hydrogen and above. Oxygen was maintained at 6 percent when hydrogen mixtures were less than 10 percent.

4.0 Analytical Considerations

Three types of hydrogen ignitions were defined in this test program: ignition, nonpropagating ignition and nonignition.
The following criteria were used to define the three ignitions.

4.1 Ignitions

Ignitions were those events characterized by simultaneous pressure increase, light output, and a temperature increase.

4.2 Nonpropagating Ignitions

A nonpropagating ignition was either observed visually and/or detected by one or more monitoring devices. When observed visually, the ignitions were confined to the area immediately in the vicinity of the igniton source and would extinguish when the ignition source was discontinued. Detection with instruments usually resulted in a high temperature increase near the ignitor, but exhibiting only small photocell response or pressure increase and when power to the igniter was discontinued, response from the instrumentation would discontinue.

4.3 Nonignitions

Nonignition produced no events detectable by either the instrumentation or visual observation.

5.0 Test Procedures

Each of the two test systems was operated using a specific test procedure. Generally, the methods were similar but configuration differences required different procedures. The general test procedures for each system are given below.

5.1 Simulated Hot Cavity

a. Test chamber was evacuated to at least 0.50 psia and then purged by first pressurizing to 25 psia with nitrogen and then evacuating to 1 psia for a total of three times. The chamber was then pressurized

to the designated nitrogen partial pressure.

b. Partial pressures of hydrogen and oxygen were added to the chamber.

c. The mixture was first allowed to temperature stabilize for 5 minutes and the resulting pressure established as the initial test pressure. The cartridge heater was activated and the tube was heated to its maximum temperature.

d. If no ignition was noted during heatup, the maximum temperature was maintained for 10 minutes while continously monitoring for an ignition.

e. If after 10 minutes an ignition did not occur, power to the heater was discontinued. Instrumentation was continued through the first 200 degrees of cool down.

5.2 Simulated Exhaust Duct

a. The exhaust duct test chamber was evacuated to 0.02 psia or less.

b. The partial pressures of hydrogen, oxygen, and nitrogen were added to the test chamber. The mixture was allowed to stabilize for five minutes and the resulting pressure estasblished as the list pressure.

c. The cartridge heater was activated and the duct was heated to its maximum temperature.

d. If no ingition was detected before the exhaust duct reached the test temperature, the duct was maintained at the test temperature for 10 minutes.

e. If ignition of the hydrogen mixture was detected during heating or 10 minute stabilization period, the test was terminated.

6.0 Results and Discussion

6.1 Simulated Exhaust Duct

These tests were performed to identify the temperature at which the exposed heated surface would ignite hydrogen mixtures. The results are presented as a plot of temperature versus percent hydrogen (see Figure 4). Surface temperatures above 1200^{0}F were required to ignite the hydrogen mixtures.

The ignition temperature for the exhaust duct was observed to be independent of the hydrogen concentration over the concentration ranges tested. A comparison of these results with autoignition data taken from the literature (ref. 4) and previously performed tests at WSTF using a hot surface ignitor (ref. 1), is also shown in Figure 4. The ignition

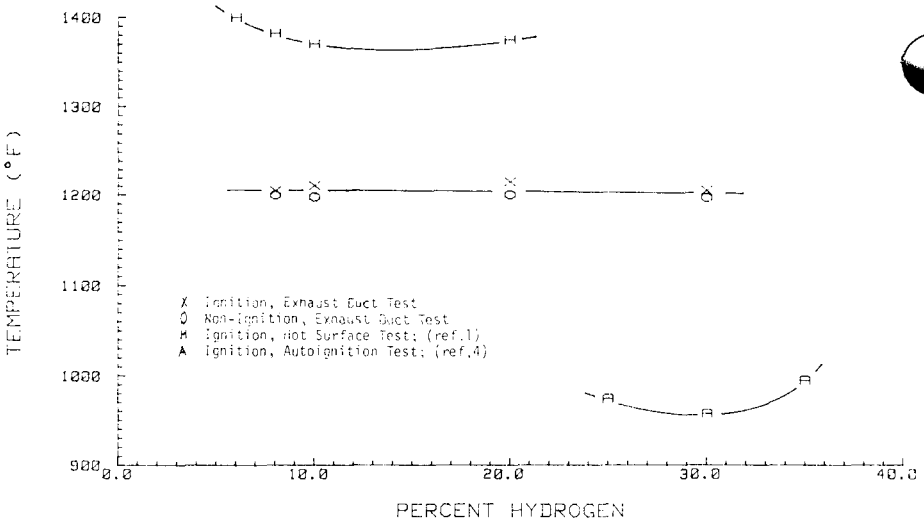


Figure 4
Ignition Results from the Exhaust Duct Test and
Comparison Data from Autoignition and Hot
Surface Igniter Tests

temperatures from both the autoignition tests and the hot surface igniter tests were observed to be much more dependent on the hydrogen concentration than the exhaust duct igniter data. This change in hydrogen ignition characteristic indicates that the configurational nature of the simulated exhaust duct may produce specific ignition limits particular to that configuration. The difference in the magnitude of the ignition temperatures are considered to be due to differences in methodology (autoignition test) and test conditions (hot surface test being performed at 1 psia). This comparison implies that the determination of ignition limits of potentially flammable environments must include the simulated ignition source to attain a true hazard assessment.

6.2 Simulated Hot Cavity

These tests were performed to determine the characteristics of a heated cavity in promoting ignitions in a hydrogen environment. Hydrogen

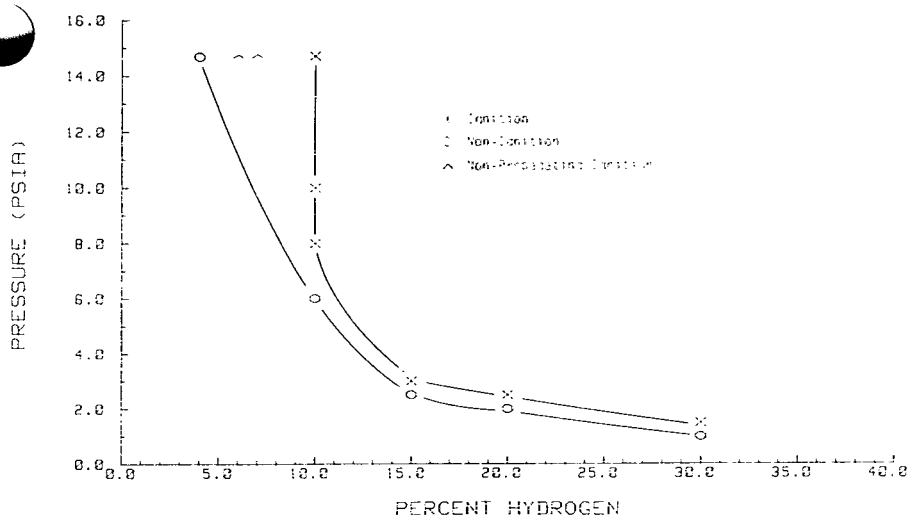


Figure 5
Hot Cavity Test Results

concentration and pressure were varied. The results of this test are given in Figure 5 which is a plot of pressure versus percent hydrogen.

These results represent the minimum parameters (pressure and hydrogen composition) that produced an ignition when the hot surface in the cavity was raised to its maximum temperature (approximately 1360°F). Important to note is the nonpropagating ignitions observed at 14.7 psia. These ignitions were characterized by a large temperature increase (greater than 1000°F) detected by the thermocouple located at the entrance to the cavity. Visual observation of the event was noted as an "oscillating glow" at the cavity entrance. In all cases, instrumentation and visual observation indicated that these ignitions were confined to the cavity and did not propagate to the remaining hydrogen mixture in the chamber. The effect of the nonpropagating ignitions results in a widening of the concentration region between ignitions and nonignitions. This same effect was also observed with other igniters such as electrically heated wires and hot surface (ref. 1, 2). A comparison of the hot cavity igniter data with hot surface and electrical spark igniter data (ref. 1), using similar hydrogen/oxygen/nitrogen mixtures, is given

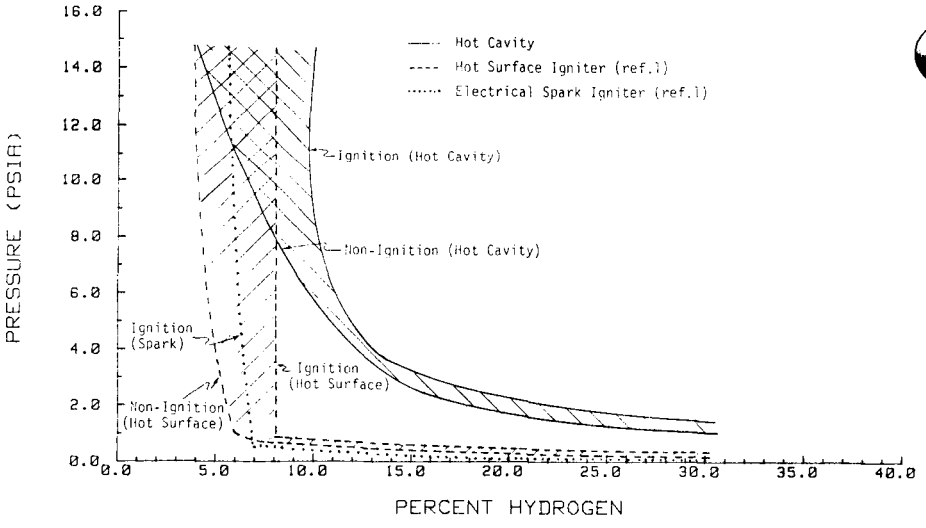


Figure 6
Comparison of Hot Cavity Results with Results from Hot Surface and Electrical Spark Igniter Tests

in Figure 6. Ignition and nonignition data is plotted in the case of the hot cavity and hot surface igniter tests. Only the ignition data for the spark test, is plotted since the difference between ignitions and nonignitions were less than 1 percent hydrogen (ref. 1). Important to the subject of this workshop is the differences observed at the lower concentration limits at 14.7 psia. The ignition data indicates that the spark igniter ignited hydrogen at lower concentrations than the other ignition sources. However, the nonignition concentrations were observed to be lower for the hot cavity and hot surface than the nonigniton concentrations observed for the spark igniter. The occurrance of nonpropagating ignitions is believed to be the cause of the lower nonignition concentrations observed with the hot cavity and the hot surface igniters.

The ignition of hydrogen with the hot cavity igniter was observed to be dependent on the temperature of the hot surface and pressure. Figure 7, which is a plot of pressure versus the surface temperature in the hot cavity that produced ignitions, indicates this dependency for two

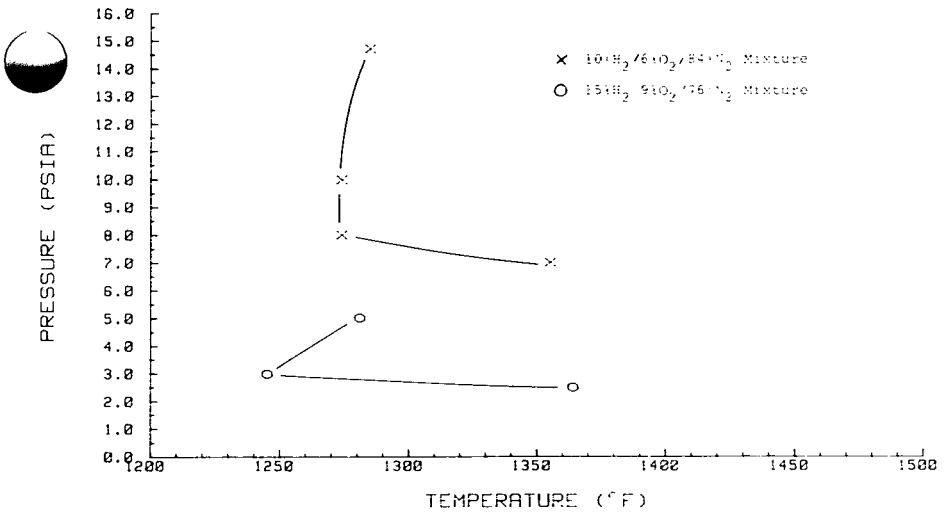


Figure 7
Hot Cavity Surface Ignition Temperature as a Function of Pressure for two Hydrogen Mixtures

hydrogen mixtures. Comparison of these results with the explosion limits reported by Lewis and Von Elbe (ref. 5) show a similarity in trends (see Figure 8). This would suggest that autoignition of hydrogen occurred in the hot cavity. These autoignitions were observed to be dependent on pressure, cavity temperature, and hydrogen composition. Once the hydrogen mixture autoignited, the resulting flame propagated out the hot cavity and provided an ignition source for the remaining hydrogen in the chamber. The flame produced by the autoignition did not always produce ignition of the remaining hydrogen as evidenced by the non-propagating ignitions discussed earlier.

Three test runs using a 10 percent hydrogen mixture produced unexpected results. Ignitions were observed during the cool down phase after the hot cavity surface had been heated to its maximum temperature (approximately 1360^{0}F) and held for 10 minutes. The temperature of the hot surface in the tube during the first cool down ignition was not obtained because recording devices had been turned off. However, after it was noted that an ignition occurred during cool down, the

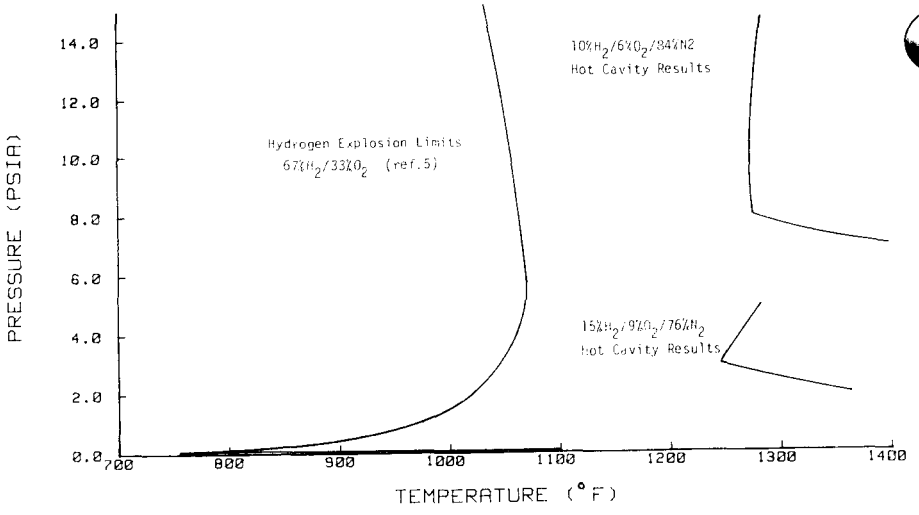


Figure 8
Comparison of Hydrogen Explosion Limits with the Hot Cavity Surface Ignition Temperature Results

recording device was left on for subsequent tests. One "cool down" ignition occurred at 1324°F during a 6 psia test and the other ignition occurred at 1322°F during a 7 psia test.

It is believed that during the cool down phase, the cavity drew in gas from the chamber due to the gas density change in the tube. Hydrogen, having a greater diffusion tendency than oxygen or nitrogen, would be preferentially drawn into the cavity. This would lead to hydrogen enrichment in the cavity and thus increase the ignition potential.

7.0 Conclusion

These tests indicate that use of data obtained from standard igniters such as electrical sparks do not provide all the information necessary to describe the flammable nature of systems. Configuration aspects of the ignition source was shown to significantly affect the ignition process of hydrogen mixtures. The occurance of such an event as non-propagating ignitions, localized autoignitions observed in the hot cavity test, and

ignition observed during cool down in the same test support a philosophy that the configurational nature of the ignition source should be assessed.

Reference

1. Boucher, P.L.; F.J. Benz. Ignitability of Hydrogen/Oxygen/Nitrogen Mixtures at Reduced Pressure. TR-243-001 (Dec. 1980) NASA/White Sands Test Facility, New Mexico

2. Benz, F.J., P.L. Boucher. Flammability Characteristics of Hydrogen/Oxygen/Nitrogen Mixtures at Reduced Pressures. In workshop on the Impact of Hydrogen on Water Reactor Safety, Proc. Vol. III Berman, M. (ed) SAND 81-0661 Sandia Natl. Labs, Albuquerque, New Mexico, Aug. 1981

3. Benz, F.J., P.L. Boucher. Ignition Potential of Hydrogen/Oxygen/Nitrogen Mixtures when Exposed to Simulated Portion of the Auxiliary Power Unit. TR-283-002 (Sept. 82) NASA/White Sands Test Facility, New Mexico

4. Van Dolah, R.W. et al. Review of Fires and Explosion Hazards of Flight Vehicles Combustibles. Bur. Mines Inf. Circ. 8137.1962

5. Lewis, B. G. Von Elbe. Combustion, Flames and Explosions of Gases. 2nd ed. New York. Acedamic Press, 1961

EXTINCTION OF CORRUGATED HYDROGEN/AIR FLAMES

M. Mizomoto, Y. Asaka, S. Ikai
Keio University, Yokohama, Japan

and

C. K. Law
Northwestern University, Evanston, Illinois

ABSTRACT

Recent studies on flammability limits reveal the importance of flow non-uniformity, flame curvature, and molecular and thermal diffusivities in determining the extinguishability and the associated limits of premixed fuel/air flames. In particular, it is found that conditions which favor extinction of a lean flame may cause intensification of a rich flame.

In the present study we have experimentally determined the extinction characteristics and limits of highly curved hydrogen/air flames as represented by the opening of bunsen flame tips. Results show that the tip opens at a constant fuel equivalence ratio of ϕ=1.15, regardless of the velocity and uniformity of the upstream flow. This critical mixture concentration, while being rich, is still on the lean side of that corresponding to the maximum burning velocity (ϕ=1.8), implying that for highly diffusive systems, the relevant reference concentration is that for maximum burning velocity instead of stoichiometry.

I. INTRODUCTION

A major activity in fundamental combustion research over the years has been the attempt to identify the dominant mechanisms responsible for the extinction of laminar premixed flames and the associated extinction/flammability limits. An important extinction mechanism which was recognized quite early (Karlovitz et al. 1953) but has been only recently firmly established is the concept of extinction by stretch. To appreciate its significance let us consider a flame stabilized in the divergent flow field at the stagnation point of a flat surface (Fig. 1). This flow has a constant velocity gradient and therefore well-characterized flow non-uniformity. After ignition, a flat flame can sometimes be established at a finite distance away from the surface where the burning velocity is balanced by the normal velocity of the flow. We are interested to know whether and how this flame can be extinguished by changing the mixture concentration and the flow intensity. We shall assume for simplicity that the fuel-oxidizer mixture can be adequately represented as a one-reactant system controlled by the concentration of the deficient reactant. Thus for this system the relevant binary diffusion coefficient, δ_m, is that for the deficient reactant (say the fuel) and the inert, while the thermal diffusivity, δ_t, is that of the inert.

Let us consider the case of an adiabatic surface so that complications due to downstream heat loss in the presence of an isothermal surface do not exist. If we take a control volume for a section of the flame, as shown in Fig. 1, then since diffusive transport is normal to the flame while convective transport is along the streamlines which are divergent relative to the flame, it is clear that the control volume loses thermal energy to the indicated streamline while gains chemical energy, in the form of the reactant concentration, from it. Thus the flame behavior, in particular its

temperature, depends on the relative rates of heat and mass diffusion, which can be represented by the Lewis number

$$Le = \frac{\delta_t}{\delta_m} = \frac{\lambda}{C_p \rho \delta_m}$$

where λ, C_p, and ρ are respectively the thermal conductivity coefficient, the specific heat at constant pressure, and the density. For Le=1, heat loss and mass gain occur at the same rate such that the flame temperature T_f is the adiabatic flame temperature T_{ad}. However, for $Le \gtrless 1$, we expect $T_f \lessgtr T_{ad}$.

If we attempt to extinguish this flame by increasing the blowing rate, then the flame will be pushed closer to the wall while at the same time suffers stronger diffusional stratification effects. Then for $Le \neq 1$, T_f will further deviate from T_{ad}. Thus it is clear that for Le>1, there exists a critical blowing rate at which T_f has been reduced to such an extent that steady burning ceases to be possible. Extinction in this case occurs when the flame is at a finite distance away from the wall, with the deficient reactant completely depleted in crossing the flame prior to extinction. On the other hand for Le<1, increasing blowing elevates T_f and therefore extinction cannot occur. Eventually the flame will be pushed onto the wall. With the further increase in the blowing rate, reaction cannot be completed because of the reduced residence time. Only then will the flame temperature start to decrease, and will eventually lead to extinction because of incomplete reaction. The above behavior have been recently substantiated through both numerical calculations (Sato and Tsuji, 1978) and experimentation (Ishizuka and Law, 1982). In particular it has been found that extinction of the Le>1 flames seems to occur at a constant stretch rate. Thus positive stretch can extinguish a Le>1 flame but will intensify a Le<1 flame.

In the above example stretch is imposed on a planar flame by a non-uniform flow field. By the same token a curved flame in a uniform flow field

should also suffer stretch; that is an observer stationed at the curved flame will perceive the flow approaching him to be non-uniform. A convenient configuration through which this flame curvature induced stretch can be studied is the tip of the bunsen flame (Fig. 2), which can be easily established in the laboratory. The stretch mechanism which may lead to extinction in the tip region can be explained as follows. For the sake of clarity let us suppress thermal expansion such that the flow lines are not diffracted in crossing the flame-front, as shown schematically in Fig. 2. Thus for a closed tip its concave curvature towards the fresh mixture focuses the heat ahead of the flame. This tends to raise the flame temperature to a value above that corresponding to the adiabatic flame temperature of the mixture. On the other hand, this curvature has a defocusing effect on the reactants approaching the flame. Thus, if the more mobile species is stoichiometrically more abundant in the fresh mixture, then it suffers relatively stronger defocusing and renders the mixture more stoichiometric as it approaches the flame tip. In this case the enhanced preheating coupled with the shift towards stoichiometry will make burning the most intense in the tip region, which has the greatest curvature. Hence tip extinction, or opening, is not possible. However, if the more mobile species is stoichiometrically less abundant, then its concentration is further reduced as the tip is approached. This tends to weaken the burning intensity. In this case tip opening is possible, depending on the relative rates of thermal and mass diffusion for the mixture of interest.

Thus it is clear that the flame tip suffers negative stretch, or compression, in this case. Tip opening is possible for a Le<1 flame and not possible for a Le>1 flame. These behavior have been experimentally verified for hydrocarbon/air flames (Law et al., 1982) in that tip opening occurs for

rich propane/air and butane/air mixtures (Le<1) although for rich methane/air flames the burning is intensified at the tip and therefore opening is not possible. Furthermore, it is shown that opening occurs at a constant fuel equivalence ratio of 1.44 and is independent of the intensity, uniformity, and configuration of the approach flow.

The final form in which stretch can be manifested is for an accelerating flame as in the case of an expanding spherical flame. Here the rate of change of the flame surface area constitutes a stretch rate.

The above discussions amply demonstrate the importance of stretch and preferential diffusion in influencing the temperature, propagation rate, and extinction limits of premixed flames which can be either corrugated, and/or accelerating, and/or situated in a non-uniform flow field. These flame stretch effects, of course, are the strongest when the mixture Lewis number deviates the most from unity as would be the case involving hydrogen combustion. We have therefore extended our study to hydrogen/air mixtures which possess very small Le in the lean case. In the present paper we shall report some preliminary results from hydrogen/air bunsen flame studies. It will be shown that the strong preferential diffusion effect can significantly extend the range of opening of the bunsen flame tips.

II. EXPERIMENTAL SET-UP AND RESULTS

The experiments involve the determination of the laminar flame speed of hydrogen/air mixtures and the concentration limits for the opening of its bunsen flame tips. Two types of bunsen tubes were used. The first (Fig. 3) is a straight tube of 3.99 mm inner diameter situated coaxially within a uniform external shroud flow generated by a contoured nozzle. The flow velocity at the exit of this straight tube is well developed and therefore

parabolic in profile. The second burner (Fig. 4) is a contoured nozzle with the inner diameter at the nozzle exit being 7.08 mm. The velocity profile at the exit is uniform.

The laminar flame velocity was determined by using the nozzle burner to generate a bunsen cone, schlieren photography to define the flame edge, and Laser Doppler Velocimetry (LDV) to determine the flow velocity. The schematic of the optics-burner system is shown in Fig. 5.

Figure 6 summarizes the results on the laminar flame speed of hydrogen/air mixtures as a function of the equivalence ratio ϕ. It is seen that S_u attains its maximum velocity at ϕ=1.8 instead of around the stoichiometric condition of ϕ=1. The shift is well known and has also been recently theoretically confirmed (Sen and Ludford, 1981). The maximum S_u is about 3.1 m/sec. The present results generally agree with the previous ones in the literature except the present measurements are of much greater accuracy.

In determining the concentration limits of tip opening, it is necessary to define the instant at which the flame at the tip is locally extinguished. For hydrocarbon/air flames such a transition is quite sharp and therefore is well defined. However for hydrogen/air flames this transition is not as clear. For example starting with a closed tip configuration at a very rich concentration of, say, ϕ=2.0, the hydrogen concentration is gradually leaned to bring about tip opening. At $\phi \simeq 1.25$ tip opening is observed, although the opening is intermittent. Only until $\phi \simeq 1.10$ does the tip become consistently open. Thus by quantifying the persistence of tip opening as the ratio of the time of tip closing to that of tip opening, we have defined tip opening as the instant at which this time ratio is 0.5.

Figure 7 summarizes results of the concentration limit at tip opening for

both the straight and nozzled tubes with the exit velocities varying from 7 m/sec to 17 m/sec. The velocity range is limited at the lower end by flashback and the upper end by transition to turbulent flow. Also note that the indicated velocity of the straight tube is only an averaged value in that because of its parabolic profile the center velocity which directly influences the tip is higher than the average value.

Figure 7 demonstrates clearly that, similar to the previous hydrocarbon/air flames, the tips of hydrogen/air bunsen flames also open at an almost constant hydrogen concentration, varying from ϕ=1.15 at U_j=7 m/sec to ϕ=1.20 at U_j=17 m/sec. This holds for both the straight and contoured tubes despite the difference in their velocity profiles. Thus the opening is again independent of the flow intensity and distribution.

It is of particular interest to note that while from the simple heat and mass diffusional considerations it is anticipated that hydrogen/air flames should open on the lean side, the present results show that it occurs on the rich side. The apparent contradiction can be reconciled by recognizing that since the maximum flame speed also occurs on the rich side, at ϕ=1.8, therefore the limit of opening, with ϕ=1.15, is still on the lean side of the concentration corresponding to the maximum flame speed. Physically it is reasonable to expect that as the mixture is gradually leaned from ϕ=1.8, the burning intensity continuously decreases until extinction occurs, without regard to the state of stoichiometry. Thus it may be conjectured that the relevant reference state to indicate the tendency for extinction is that of the maximum burning intensity instead of stoichiometry.

Finally, we have also experimentally observed that around the state of tip opening the flame becomes polyhedral (see, e.g., Lewis and von Elbe, 1962) in that ridges start to appear along the bunsen cone. The onset of this mode

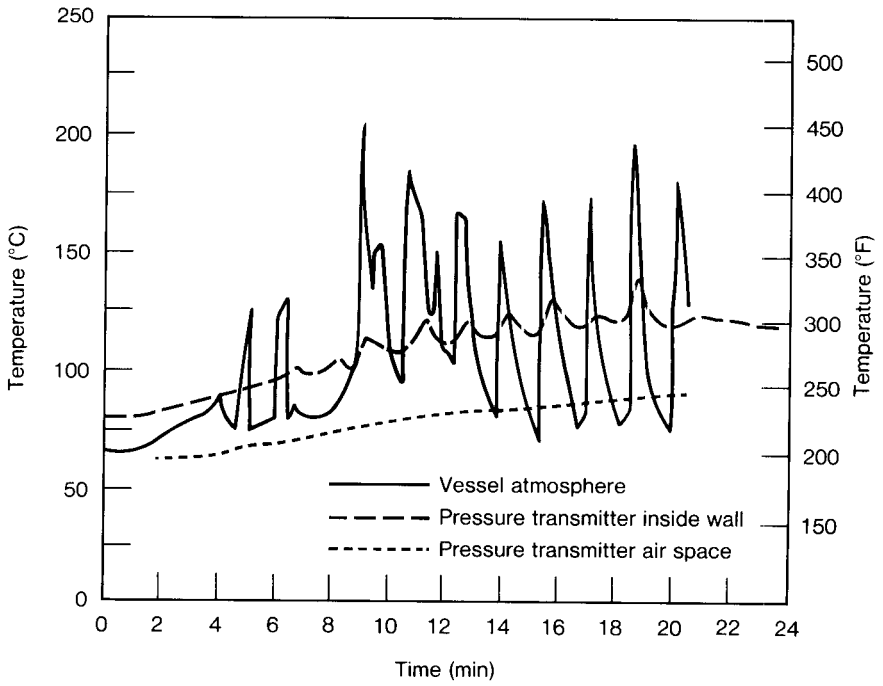


Figure 3. Thermal lag measured on pressure transmitter during dynamic injection test with flowing hydrogen and steam (test 4.4).

of flame instability when extinction is just about to be effected through stretch can also be satisfactorily explained on the basis of preferential diffusion (Sivashinsky, 1976).

III. CONCLUDING REMARKS

In the present investigation we have experimentally demonstrated the importance of flame stretch and preferential diffusion on the extinction of the highly-diffusive hydrogen/air flames. In particular it is shown that there exists a critical concentration, and thereby possibly a critical stretch rate, for the extinction of negatively-stretched hydrogen/air flames which are lean relative to the state of the maximum burning rate. Since an expanding flame suffers positive stretch, we would expect the lean hydrogen/air flames will intensify upon being stretched while the rich flames will extinguish. Further experiments are being conducted to verify the above concepts.

References

Karlovitz, B., Dennisten, D. W., Knapschaefer, D. H., and Wells, F. E. (1953) "Studies on Turbulent Flames," Fourth Symposium on Combustion, Williams and Wilkins, Baltimore, pp. 613-620.

Sato, J. and Tsuji, H. (1978), Proc. of Sixteenth Japanese Symposium on Combustion, pp. 13-15.

Ishizuka, S. and Law, C. K. (1982), "An Experimental Study of Extinction and Stability of Stretched Premixed Flames," to appear in Proc. of Nineteenth Symposium on Combustion.

Law, C. K., Ishizuka, S., and Cho, P. (1982), "On the Opening of Premixed Bunsen Flame Tips," Combust. Sci. Tech. 28, pp. 89-96.

Sen, A. K. and Ludford, G. S. S., "Effects of Mass Diffusion on the Burning Rate of Non-Dilute Mixtures," Eighteenth Symposium on Combustion, The Combustion Institute, pp. 417-424.

Lewis, B. and von Elbe, G. (1961), Combustion, Flames, and Explosion of Gases, Academic Press, N.Y.

Sivashinsky, G. I. (1976), "On a Distorted Flame Front as a Hydrodynamic Discontinuity," Acta Astronautica 3, pp. 889-918.

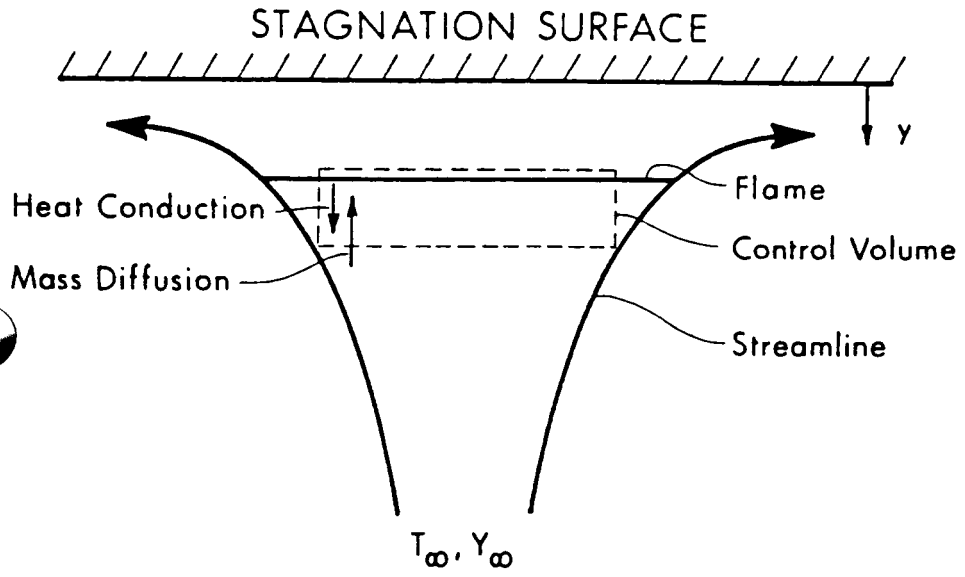


Figure 1. Extinction in Stagnation-Point Flow, Illustrating Stretch Experienced by a Planar Flame in a Non-Uniform Flow.

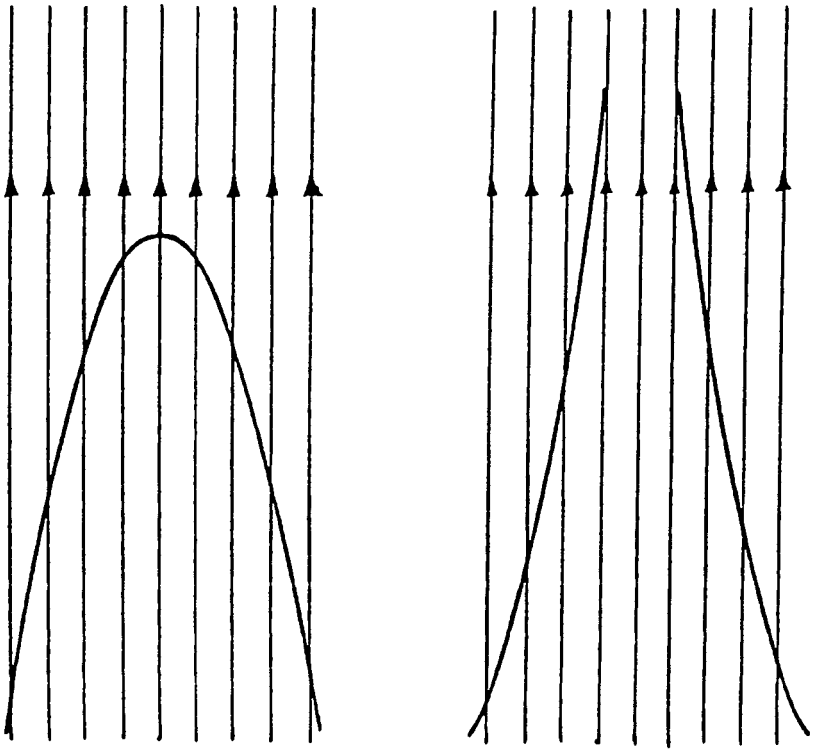


Figure 2. Opening of Bunsen Flame Tip, Illustrating Stretch Experienced by a Curved Flame in a Uniform Flow.

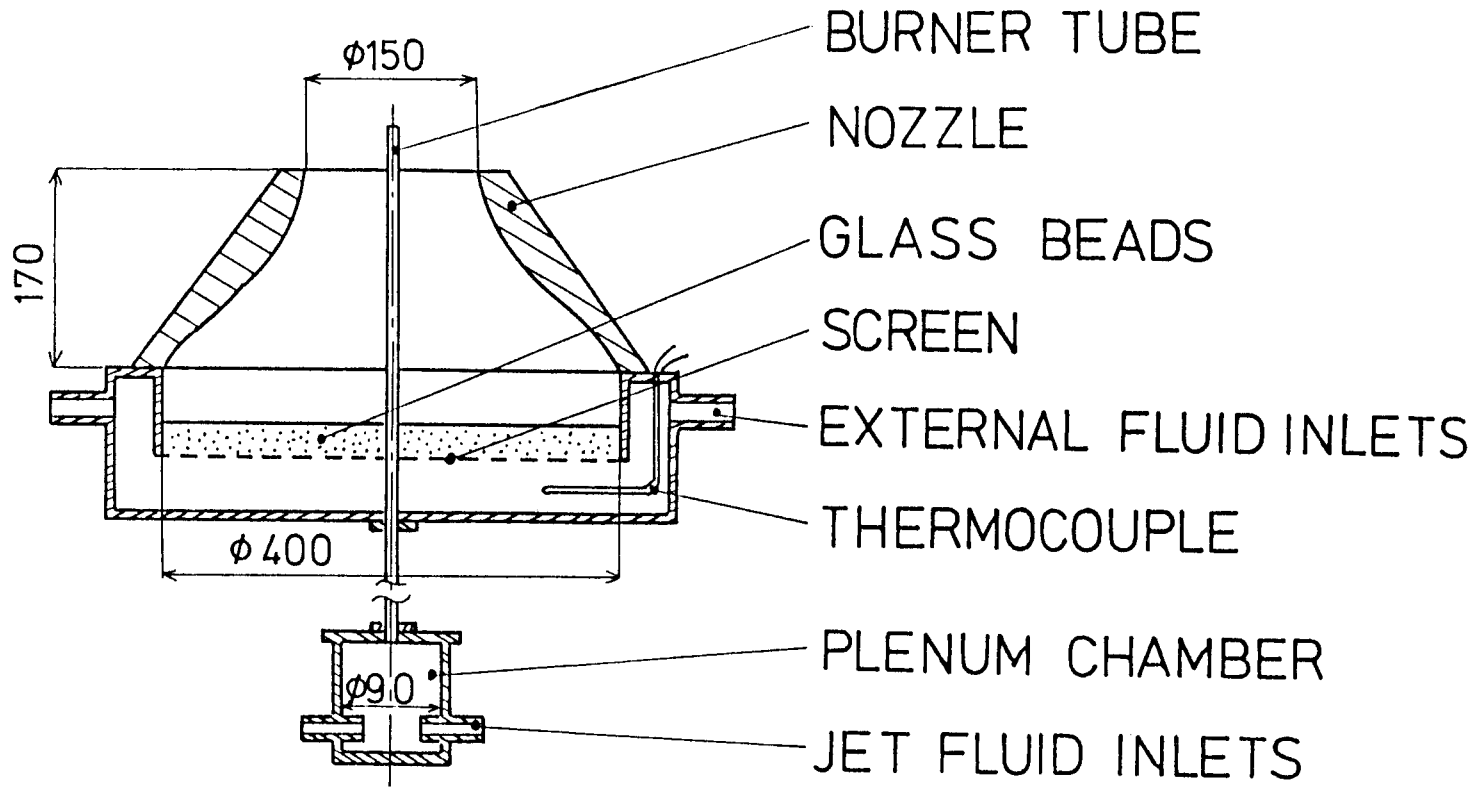


Figure 3. Schematic of the Straight Bunsen Tube

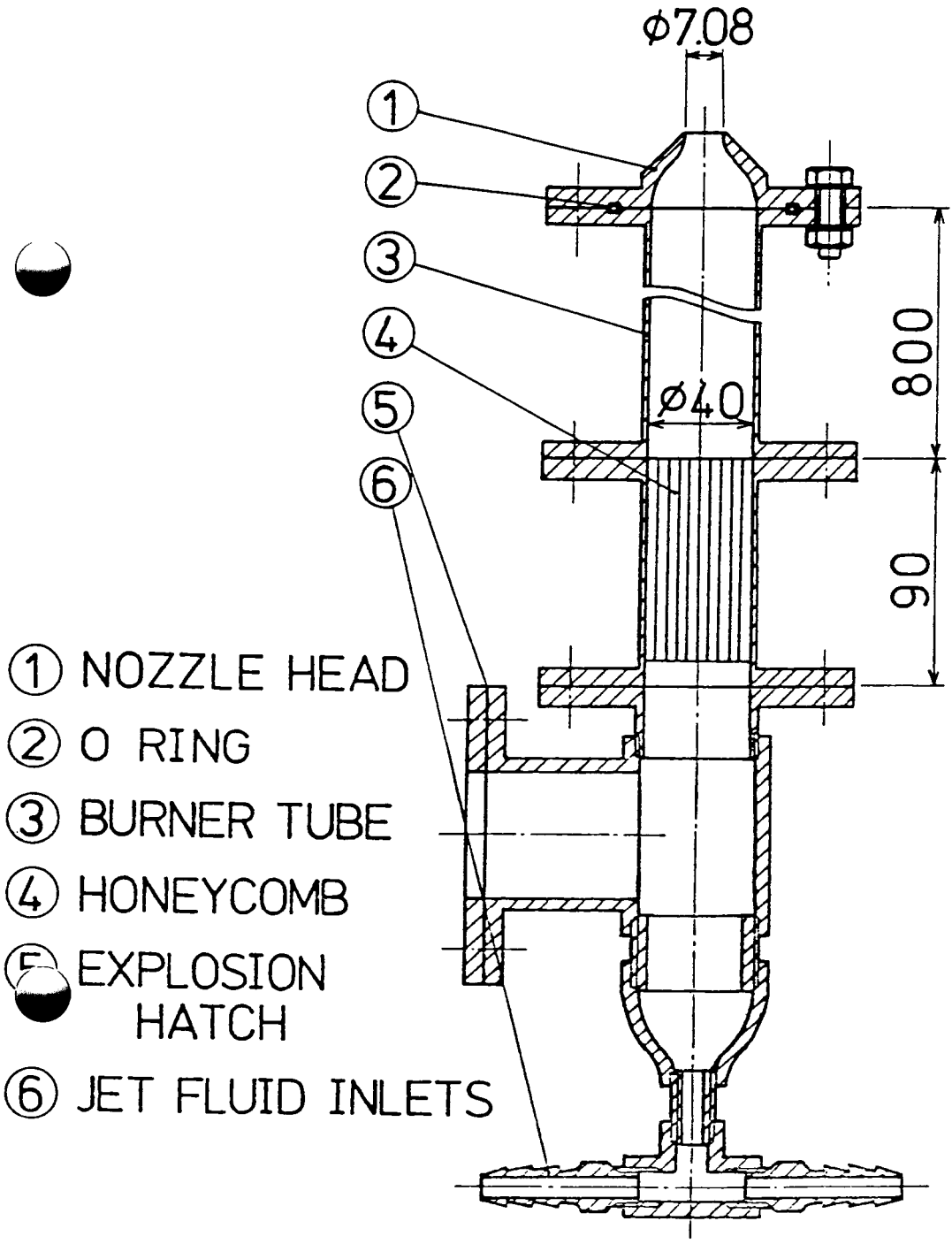


Figure 4. Schematic of the Contoured Bunsen Tube

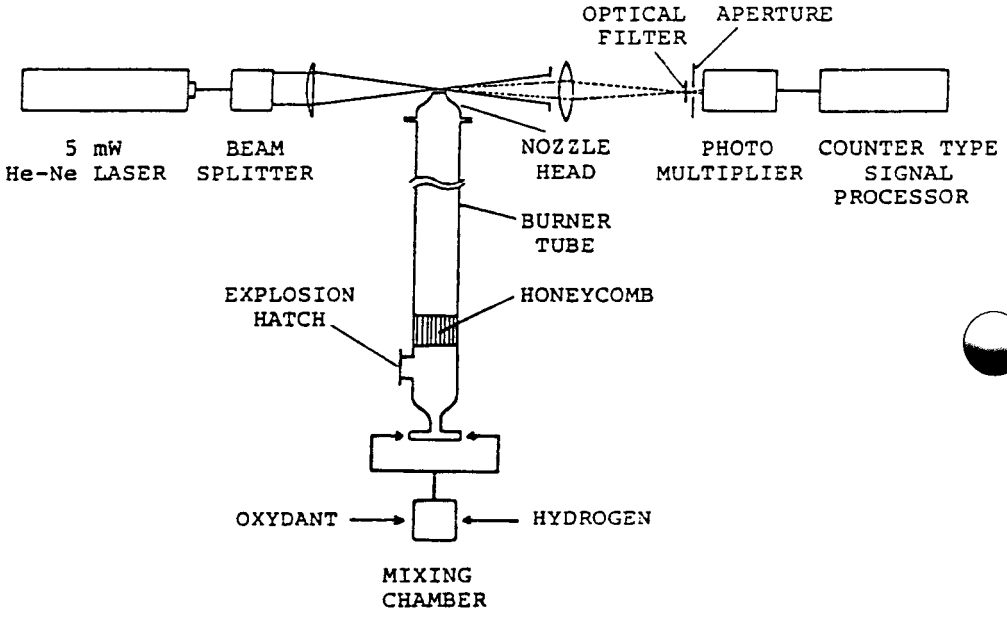


Figure 5. Schematic of the LDV System

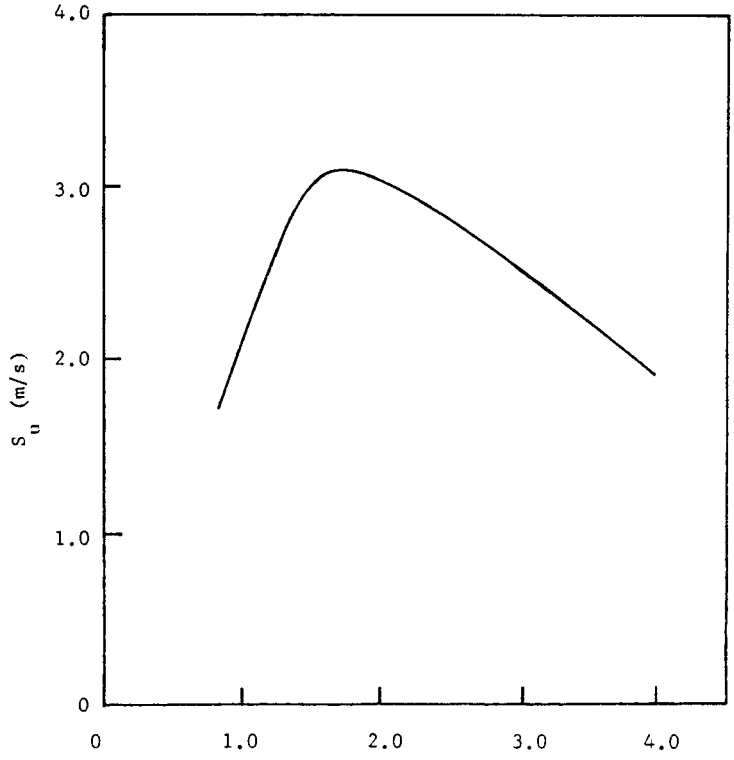


Figure 6. Burning Rate of H_2/Air Flames

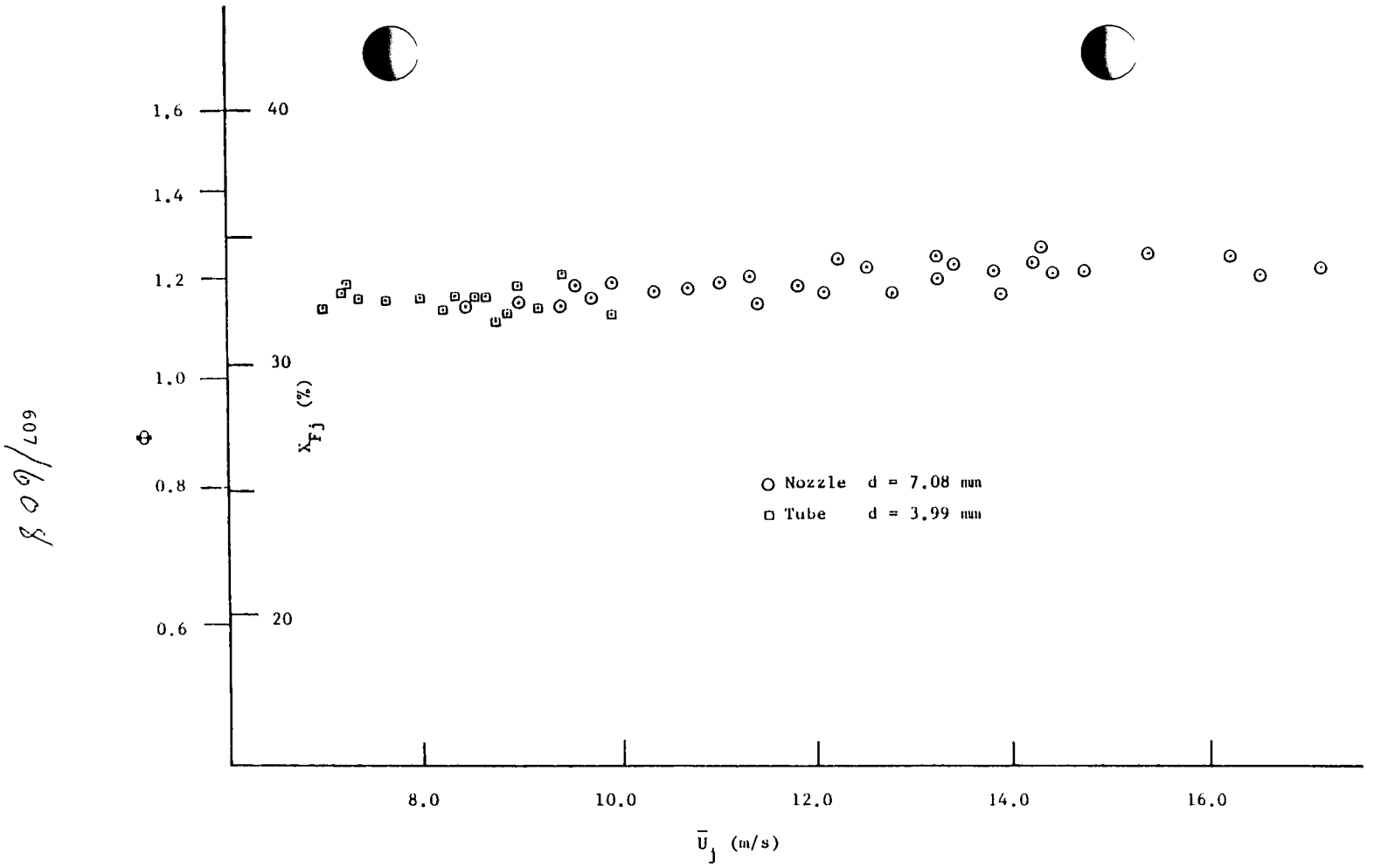


Figure 7. Concentration Limit of the Opening of Hydrogen/Air Bunsen Flame Tips

FLAME TEMPERATURE CRITERIA TESTS

S.S. Tsai, N. J. Liparulo, J. E. Olhoeft,
and D. F. Paddleford
Nuclear Technology Division
Westinghouse Electric Corporation

1.0 INTRODUCTION

Hydrogen combustion in the reactor containment during severe hypothetical accidents has been recognized by the NRC and the nuclear industry as a potential threat to the containment integrity. Data on hydrogen flammability and burning characteristics are important for accurate predictions of the pressure loading on containments due to hydrogen burn.

Hydrogen flammability data on hydrogen-air mixtures at room temperature and atmospheric pressure is abundant[1,2]. The flammability limits for upward, sideward, and downward propagation of flame in quiescent hydrogen-air mixtures are well known. At approximately 8.5 volume percent H_2, ignition via a local spark ignition source will quickly propagate throughout the entire mixture volume. This rapid deflagration within the hydrogen mixture develops a large pressure rise, resulting from nearly complete hydrogen burn. Ignition of hydrogen concentrations below 8.5% in a quiescent air atmosphere generally results in incomplete combustion and low pressure rise. Therefore, 8.5% H_2 is considered as a deflagration limit for hydrogen. A flame temperature of 710°C (1310°F) corresponding to 8.5% H_2, has been proposed by Lewis and Karlovitz as a simple first-order criteria for deflagration (global combustion) under more general conditions.

Westinghouse has used the flame temperature criteria in the COCOCLASS9 code[3] to determine whether a hydrogen-air-steam mixture generated in containment during severe hypothetical accidents could undergo a non-benign combustion. At each time step during accident progression, the flame temperature of the containment atmosphere is calculated in the code and compared with the critical flame temperature of 710°C to determine when the mixture will undergo global combustion. The flame temperature criteria has been used to study the containment response to hydrogen combustion during hypothetical core meltdown accidents for the Zion and Indian Point plants. The criteria is believed to be conservative when applied to hydrogen-air-steam mixtures at elevated temperatures and pressures, as found in post-accident containment atmospheres.

Since the Lewis-Karlovitz "flame temperature criteria" had been based on data obtained from hydrogen flammability tests using hydrogen-air mixtures at room temperature and atmospheric pressure, a test program was conducted at Fenwal Incorporated to evaluate its applicability to a post-accident containment atmosphere at elevated temperature and pressure.

Another objective of this test program was to obtain laminar burning velocities under post-accident containment atmospheric conditions.

These velocities are needed for estimating the hydrogen burn time in containments. This paper presents the results obtained from this test program, which are then used to validate the Lewis-Karlovitz flame temperature criteria.

2.0 FLAME TEMPERATURE CRITERIA TESTS

The tests were planned by Westinghouse, and Combustion and Explosive Research, Inc., and conducted by Fenwal Incorporated, Ashland, Massachusetts from late 1980 through early 1981. This test program consisted of several series of hydrogen burn tests at elevated temperatures and pressures and at various steam concentrations.

2.1 Test Conditions

A matrix of test conditions involving three parameters, namely, initial temperature, initial pressure, and initial steam concentration was selected, which are representative of post-accident containment atmospheric conditions. The following parameter ranges were selected:

initial temperature:	25°C(77°F), 100°C(212°F), 175°C(347°F), 250°C(482°F)
initial pressure:	15, 30, 45, 60 psia
initial steam concentration:	0, 20, 40, 60, 75%*

Each test series represents a combination of the test conditions given above. Each series at the stated conditions was first started at 14% hydrogen, and then decreased to 12%, 10%, 8%, etc., until a threshold was identified. Thirty-two test series were run and provided the data for assessing the deflagration limit.

2.2 Test Facility and Instrumentation

The tests were conducted in a 98 gallon spherical test vessel having a pressure rating of 500 psig with a capability of being heated to 500°F. The vessel was constructed of 316 stainless steel.

The outside surface of the vessel was insulated with 3 inch thick fiberglass insulation. This insulation had an aluminum foil face which was oriented away from the vessel.

Mixing of the various gaseous components was accomplished by means of a five-inch diameter fan which was driven through a magnetic drive by an external air motor.

Steam was supplied to the test vessel from an electrically heated boiler which was self-regulated to maintain a pressure in the range of 15-25 psig. A manually operated control valve was positioned between the boiler and the test vessel.

*Throughout the text, steam concentration is defined as the volume percent of steam in the steam-air mixture (hydrogen not included).

The temperature of the test vessel was controlled by a thermocouple controller which had its sensing element in a well inside the vessel and approximately 6 inches from the vessel wall. The temperature was sensed and recorded from a thermocouple which was in a well inside the vessel and approximately 6 inches from the vessel wall.

Ignition was accomplished by the discharge of two series-wired 525 microfarad capacitors across a pair of electrodes which were located at the center of the test vessel. The capacitors were initially charged to 900 volts.

Transient pressures were monitored by means of two strain-guage pressure transuducers, the output of which were fed to a Consolidated Electrodynamics Corporation recording oscillograph. Timing markers were electronically superimposed on the oscillograph chart, providing a time base to facilitate the determination of the rate of pressure rise. One transducer was calibrated to read relatively low pressures resulting from marginal pressure transients and the other was calibrated to read higher pressures resulting from more complete combustion.

A mercury manometer was used to measure pressures during the loading of gaseous components by the partial pressure method. This apparatus is shown schematically in Figure 1.

2.3 Test Procedure

1. Vessel temperature was stablilized at the specified test temperature.
2. Barometric pressure, relative humidity and ambient temperature were read and recorded.
3. Air, hydrogen and steam were added according to the appropriate partial pressures.
4. The vessel contents were mixed for approximately five minutes.
5. The mixing fan was stopped for approximately two minutes.
6. The ignition source was energized.

2.4 Data Analysis and Evaluation

For each of the 32 test series, the temperature and pressure rises due to hydrogen burn were measured. The laminar burning velocity, S_u, is determined as follows:

$$S_u = \frac{a}{\psi}\left(\frac{1}{r}\cdot\frac{\psi}{\psi-1}\cdot\frac{K}{P_i}\right)^{1/3} \quad \text{(cm/sec)}$$

where a = Radius of test vessel (cm)
r = Ratio of specific heat of unburned gases
ψ = Expansion ratio (P_f/P_i)
K = Constant (psi/sec^3)
P_i = Initial pressure (psia)
P_f = Final pressure (psia)

The constant K is determined as follows:

$$K \approx \frac{\Delta P}{(t-X)^3}$$

where ΔP = Pressure rise (psi) in time t (sec)
X = Correction factor (sec)

and X is determined as follows:

$$X = \frac{(\Delta P_2/\Delta P_1)^{1/3} t_1 - t_2}{(\Delta P_2/\Delta P_1)^{1/3} - 1}$$

where ΔP_1 = Pressure rise (psi) in time t_1 (sec)
ΔP_2 = Pressure rise (psi) in time t_2 (sec)

In the equation given above, ΔP's are chosen such that $\Delta P_2 > \Delta P_1$. The burning velocity thus obtained is a good approximation to the more exact equation given in Reference 7.

In Figure 2 the effect of initial temperature on the maximum pressure rise for 0% H_2O, and 30 psia is shown. The effect of temperature is to lower the deflagration limits because the higher the initial temperature, the lower the energy needed to heat the gas to the critical flame temperature. At low hydrogen concentrations, a higher initial temperature would give rise to a higher flame temperature and hence a higher pressure rise. The effect of initial temperature on chemical kinetics at low hydrogen concentrations is clearly seen in the figure. After the deflagration limit has been reached, the reaction rate no longer controls the maximum pressure rise. Instead, the thermal effect will dominate, i.e., the pressure rises depend on the gas molar number, which is inversely proportional to the initial temperature. Therefore, it is seen from Figure 2 that at high hydrogen concentrations the maximum pressure rise is approximately inversely proportional to the initial temperature (absolute temperature). The approximately constant

slopes at hydrogen concentration higher than 10% indicate that the combustion is nearly complete. In Figure 2, the pressure rise for the 77°F case is consistent with the data obtained by Furno et al.(4).

Figure 3 shows the effect of initial pressure on the maximum pressure rise for 20% H_2O and 347°F. As seen from the figure, the effect of initial pressure on the deflagration limits is insignificant for the pressure range investigated. After the deflagration limit has been reached, the maximum pressure is approximately proportional to the initial pressure or the gas molar number. Again, it is seen that combustion goes to completion at about 10% hydrogen.

Figure 4 shows the effect of steam concentration on the maximum pressure rise for 347°F and 45 psia. Two effects of steam can be identified. The first effect is the thermal effect - steam has about 20-25% higher heat capacity than air. This effect would be accounted for in using a flame temperature approach. The second effect is the chemical kinetic effect - the presence of steam tends to decrease flame temperature and hence retard the reaction rate or extinguish the flame even at high hydrogen concentrations. High radiation heat loss due to high steam content can explain this effect. Consequently, the deflagration limits increase with the increasing steam concentration. At 60% steam concentration, the deflagration limit is about 11% as compared to 8.5% for the dry air cases. For all the 60% H_2O tests, the hydrogen mixtures were successfully ignited.

The laminar burning velocity as a function of hydrogen concentration for the selected ranges of initial temperature, initial pressure, and steam concentration is shown in Figures 5 through 7. In general, the laminar burning velocity increases with increasing hydrogen concentration, increasing initial temperature, decreasing initial pressure, and decreasing steam concentration. Except for 60% steam concentration, the burning velocity increases almost linearly with hydrogen concentration at high hydrogen concentrations. For the ranges of initial conditions investigated, the effect of steam concentration on the burning velocity is much more pronounced than the other effects investigated. It is seen from Figures 5 through 7 that minimum burning velocities exist at low hydrogen concentrations, which are close to the deflagration limits. Because of low burning velocities, reaction rates are low and flames are easily extinguished by disturbances.

3.0 VALIDATION OF FLAME TEMPERATURE CRITERIA

In order to validate the flame temperature criteria, the flame temperature and the theoretical pressure rise for each of the tests were calculated. In the present study, the flame temperature and theoretical pressure rise were calculated by the COBURNA(6) code. In the code, the flame temperature is calculated by equating the heat released by hydrogen combustion with the enthalpy increase of the reaction products. Constant pressure during combustion and complete combustion of hydrogen are assumed (if there is inadequate oxygen supply, then hydrogen is assumed to react until oxygen depletion). The final gas temperature based on the constant volume specific heat is also

calculated in the code. The theoretical pressure rise, in turn, is calculated from the final gas temperature using the ideal gas law for gases and steam tables for H_2O.

For each of the 184 tests conducted to date, the initial test conditions, namely, initial temperature, hydrogen concentration, and steam concentration are input to the COBURNA code to calculate the flame temperature, the theoretical pressure rise, and the ratio of the experimental to the theoretical pressure rise. This ratio is shown in Figures 8 through 16. Complete hydrogen combustion was assumed in the calculations of the theoretical pressure rise. The theoretical pressure rise was chosen to nondimensionalize the experimental pressure rise since the experimental pressure rise will approach the theoretical one at high hydrogen concentrations. The measured pressure rise is lower than the theoretical one, at low hydrogen concentrations, because adiabatic and complete combustion have been assumed for the theoretical calculation.

In Figures 8 through 16, it is seen from the figures that there exist threshold flame temperatures at which the pressure rise ratio increases sharply with the flame temperature. Above these threshold flame temperatures, the pressure ratio approaches one, which corresponds to the complete combustion condition. Below these threshold flame temperatures, the fraction of hydrogen burn is so small that the experimental pressure rise is only a small fraction of the theoretical pressure rise. It is seen from Figures 8 through 16 that these threshold flame temperatures are higher than the 1310°F critical flame temperature chosen by Lewis and Karlovitz. This implies that this flame temperature criteria correctly predicts small pressure rises for mixtures with flame temperatures lower than 1310°F, and hence the criteria is conservative when applied to determine whether a hydrogen mixture will undergo global combustion.

However, the criteria overpredicts the degree of energectics for some mixtures with high steam contents. The 1310°F flame temperature seems to be a good critical flame temperature for the dry air tests. However, as steam concentration increases, the critical flame temperature increases. At the same time, the transition zone widens and the pressure rise ratio decreases with increasing steam concentration. It can be inferred from Figures 8 through 16, at low initial temperatures the critical flame temperature appears to vary linearly with steam concentration. For example, at 212°F the critical flame temperature increases at a rate of about 5°F for each percent increase of steam concentration.

The degree of conservatism of the criteria can be reduced if a critical flame temperature as a function of the steam concentration is specified. A new critical flame temperature as a quadratic function of the steam concentration has been derived by curve fitting the test data. This new criteria corresponds to roughly a 100°F shift upward in the critical flame temperature for each 20% increase in steam concentration.

4.0 SUMMARY AND CONCLUSIONS

The Fenwal flame temperature criteria tests have been conducted and a total of 218 tests have been completed. For the ranges of initial conditions investigated, the maximum pressure rise resulting from combustion of pre-mixed hydrogen-air-steam mixtures strongly depends on the initial conditions. The effects of initial pressure, initial temperature, and steam concentration on both the maximum pressure rise and burning velocity have been identified. The Lewis-Karlovitz flame temperature criteria has been found to be conservative. However, a modified flame temperature criteria has been proposed to reduce the degree of conservatism associated with the 1310°F flame temperature criteria when considerable steam is present. This corresponds to roughly a 100°F shift upward in the critical flame temperature for each 20% steam increase.

The following conclusions may be drawn from the present investigation of the flame temperature criteria:

1. Flame temperatures exhibit a threshold characteristic for the ranges of initial conditions investigated even though the range of the threshold temperatures become wide at high steam concentrations.

2. The threshold flame temperature is a strong function of steam concentration and it increases with increasing steam concentration.

3. The Lewis-Karlovitz flame temperature criteria is valid and found to be conservative.

4. A new flame temperature criteria which is dependent on the steam concentration would be a more accurate representation for the deflagration limit of hydrogen mixtures with high steam content.

ACKNOWLEDGEMENTS

The authors wish to express their sincere gratitude to Messrs. G. Klopp, and Drs. B. Lewis and B. Karlovitz for assistance, suggestions and helpful discussions.

They also would like to thank Commonwealth Edison, and other utilities for providing financial support.

REFERENCES

1. F. C. Howard and G. W. Jones, U.S. Bureau of Mines, Bulletin 503, 1952.

2. Z. M. Shapiro and T. R. Moffette, "Hydrogen Flammability Data and Application to PWR Loss-of-Coolant Accident," WAPD-SC-545, Bettis Plant, September 1957.

3. F. M. Bordelon and E. T. Murphy, "Containment Pressure Analysis Code (COCO)", WCAP-8326, Westinghouse Electric Corporation, July 1974.

4. A. L. Furno, E. B. Cook, J. M. Kuchta, and D. S. Burgess, "Some Observations on Near-Limit Flames," 13th Combustion Symposium (Int.), pp. 593-599, 1970.

5. B. Lewis and B. Karlovitz, "Hydrogen Explosion Hazard of Pressurized Water Nuclear Reactor Containment," report to Westinghouse PWR System Division, January 16, 1980.

6. J. Olhoeft, "COBURNA Program and Comparison to Hydrogen and CO Combustion Experiments," Westinghouse letter MD-MP-808, May 15, 1980.

7. B. Lewis and G. von Elbe, "Combustion, Flames and Explosions of Gases," 2nd ed., Academic Press Inc., 1961.

13.1 CUBIC FOOT SPHERICAL TEST VESSEL FIGURE 1

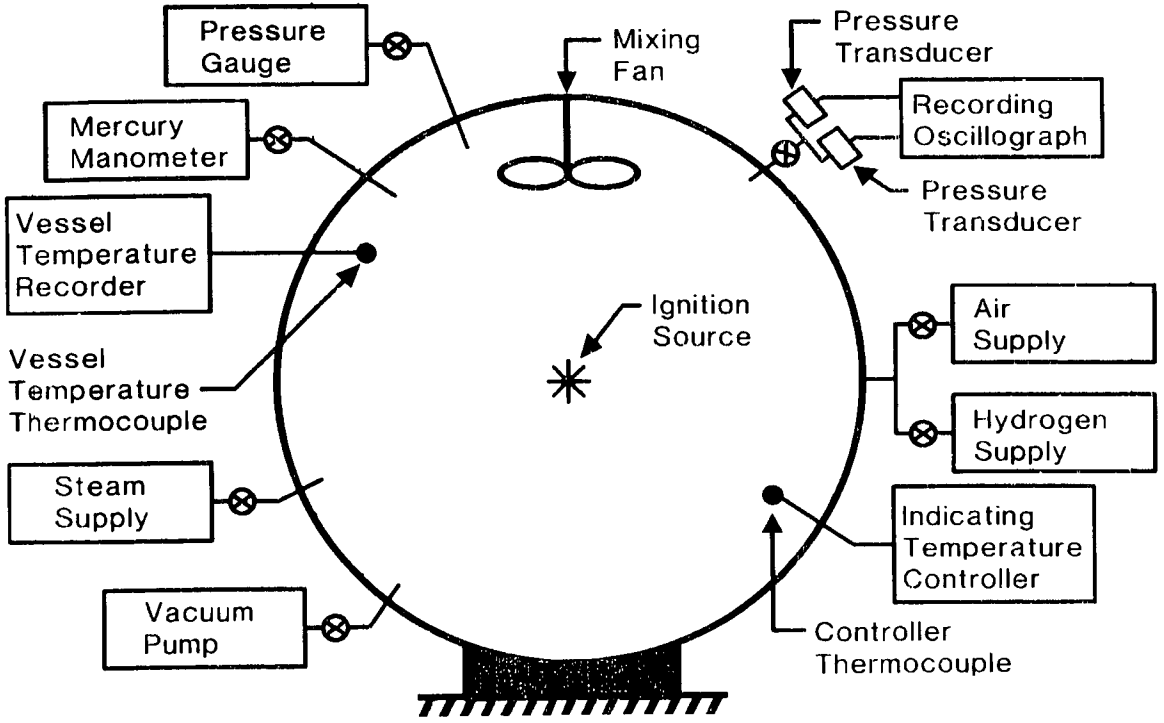
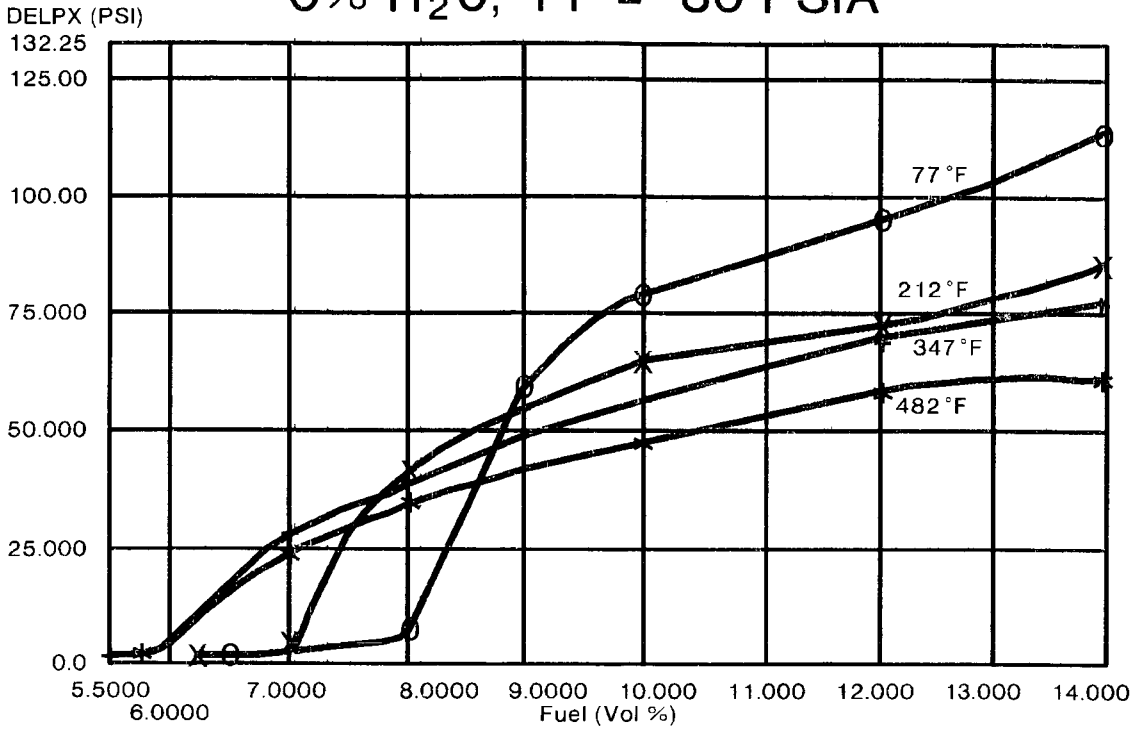


FIGURE 2

EFFECT OF TEMPERATURE FROM 77.0. TO 482.0. °F

0% H_2O, PI = 30 PSIA



403DW02581 15

SEP 82

LN

FIGURE 3

EFFECT OF PRESSURE FROM 15.0 TO 60.0 PSIA

20% H_2O, TI = 347°F

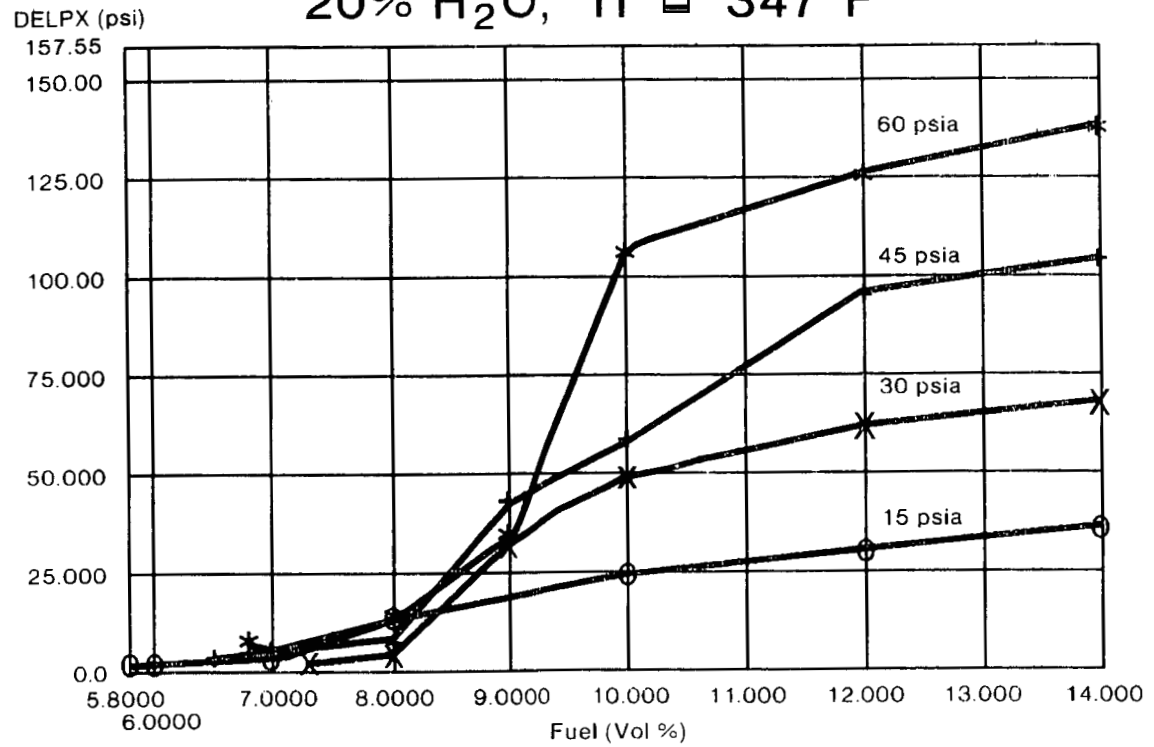
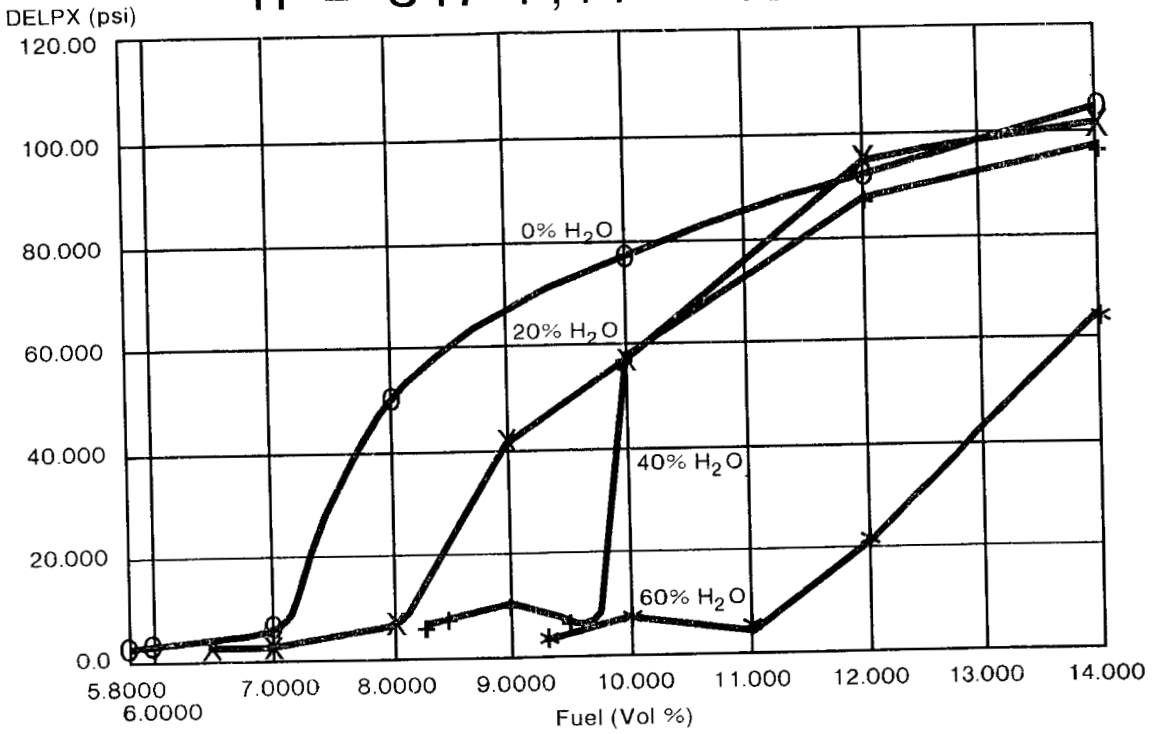


FIGURE 4

EFFECT OF H_2O FROM 0.0 TO 60.0%

TI = 347 °F, PI = 45 PSIA

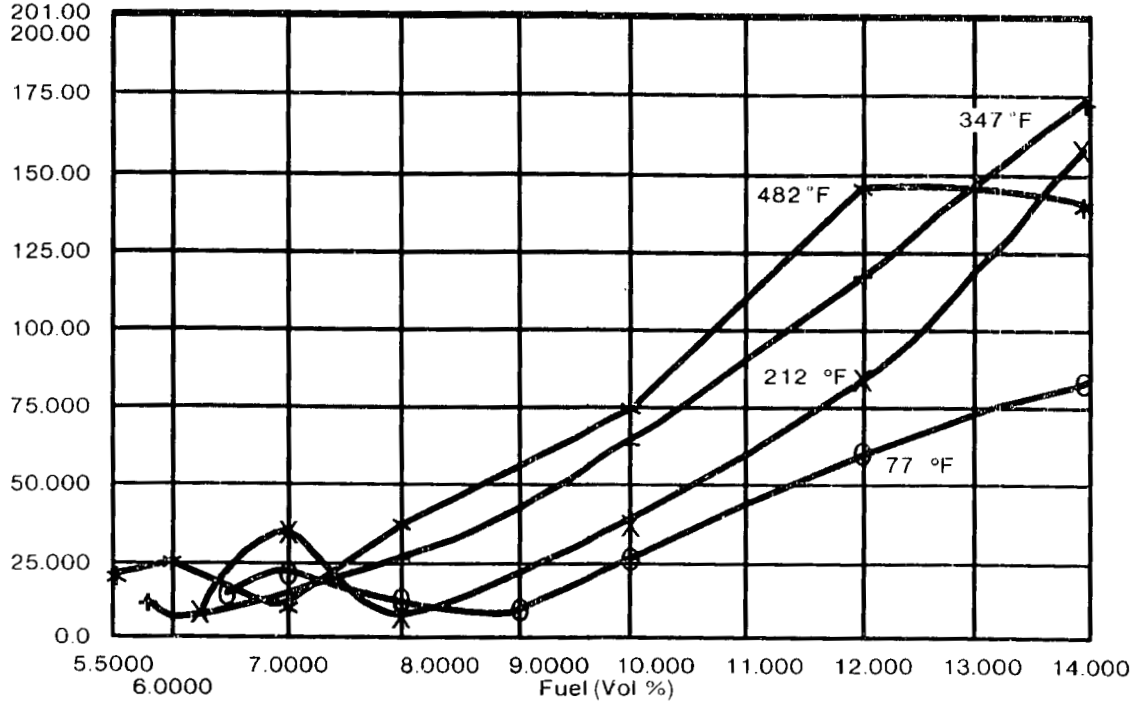


620

FIGURE 5

EFFECT OF TEMPERATURE FROM 77.0. TO 482.0. °F

SU Burning Velocity (CM/Sec) 0% H_2O, PI = 30 PSIA



621

FIGURE 6

EFFECT OF PRESSURE FROM 15.0 TO 60.0 PSIA

20% H_2O, TI = 347°F

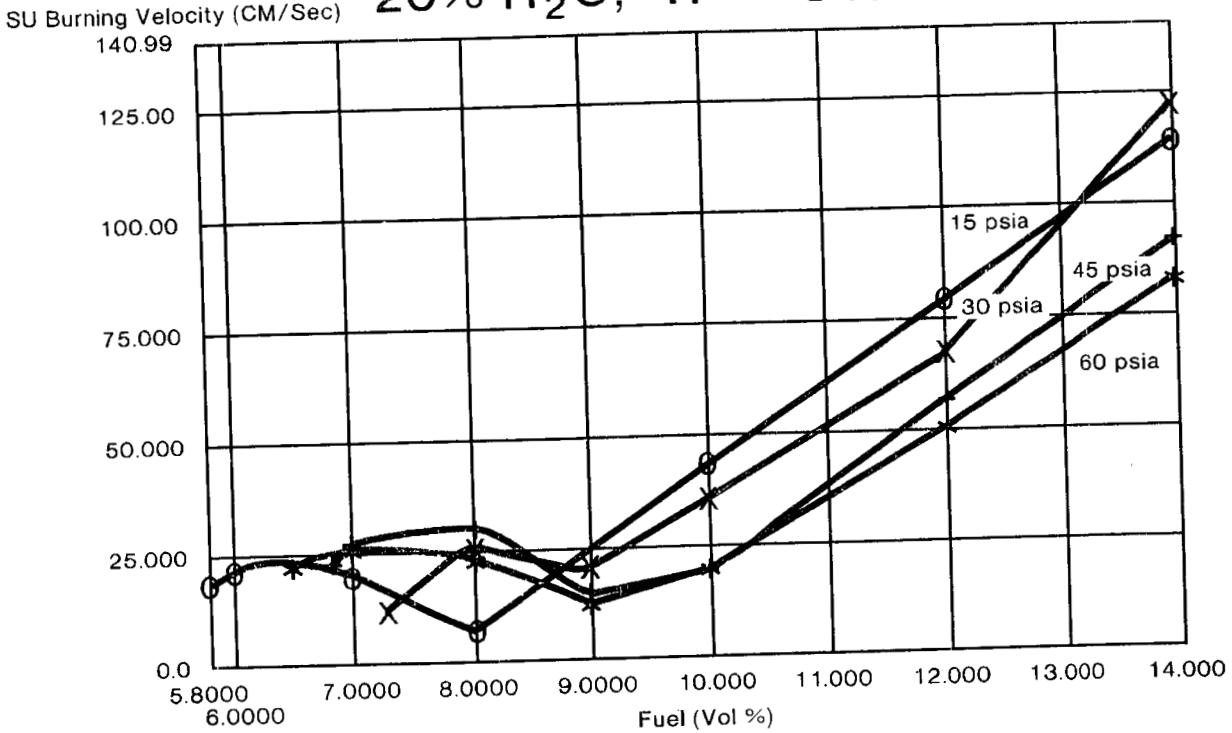


FIGURE 7

EFFECT OF H_2O FROM 0.0 TO 60.0%

TI = 347 °F, PI = 45 PSIA

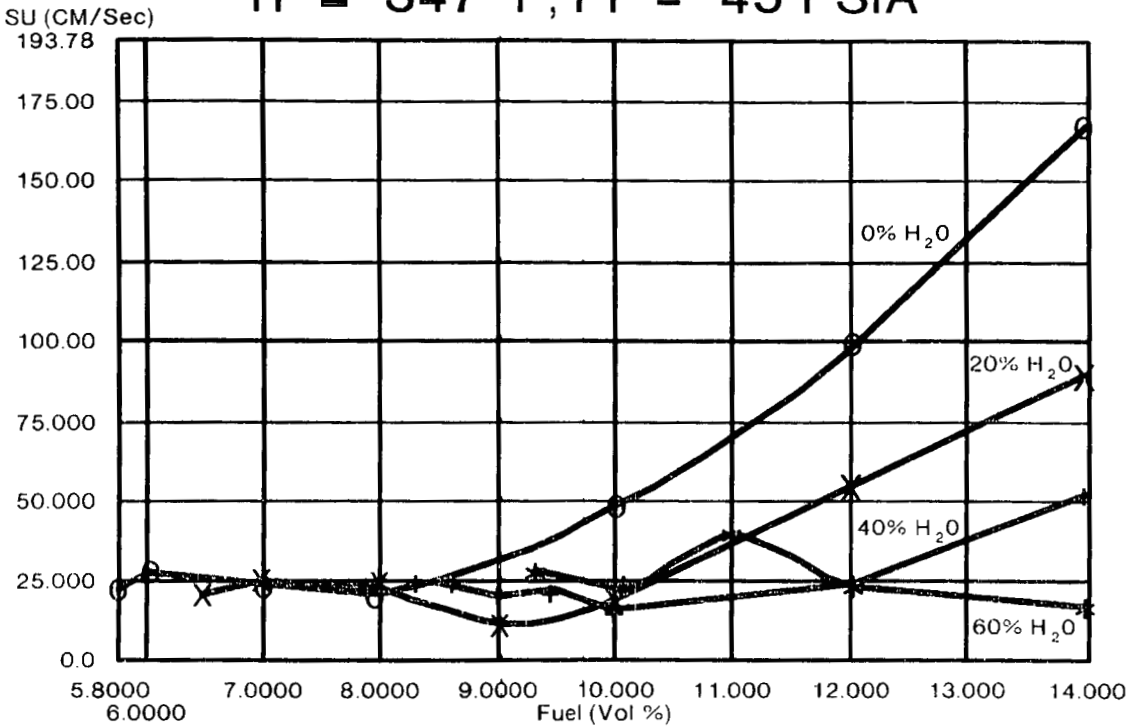
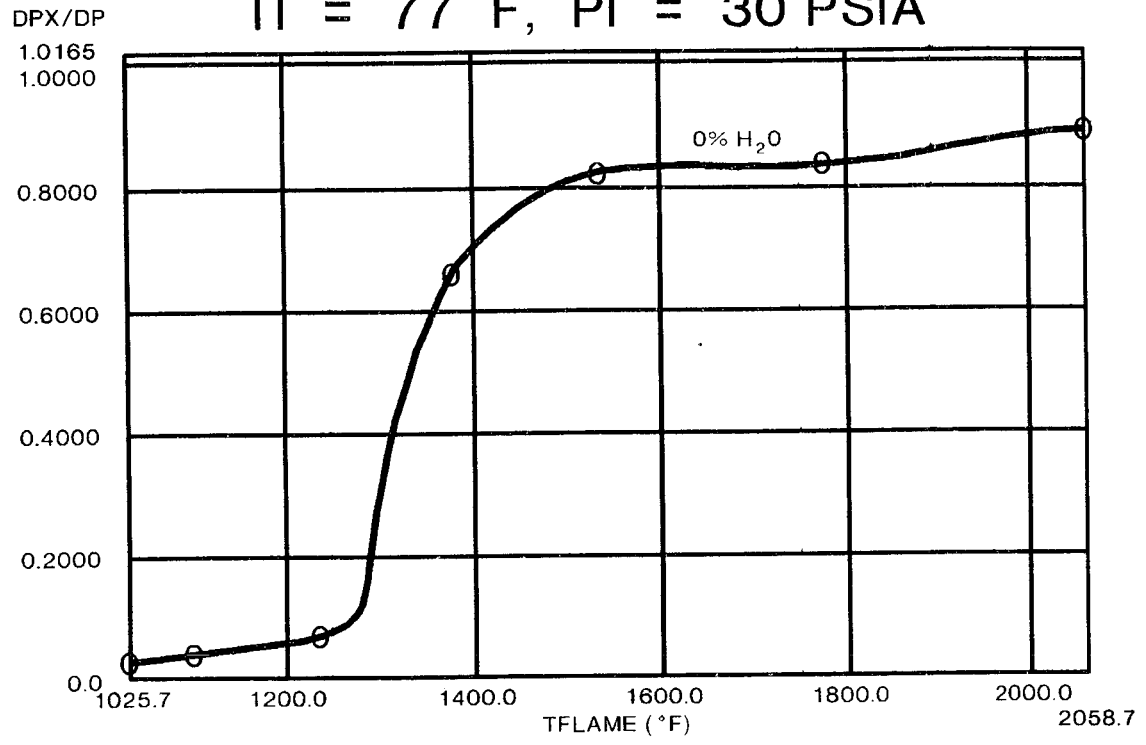


FIGURE 8

EFFECT OF H_2O AT 0%

TI = 77 °F, PI = 30 PSIA



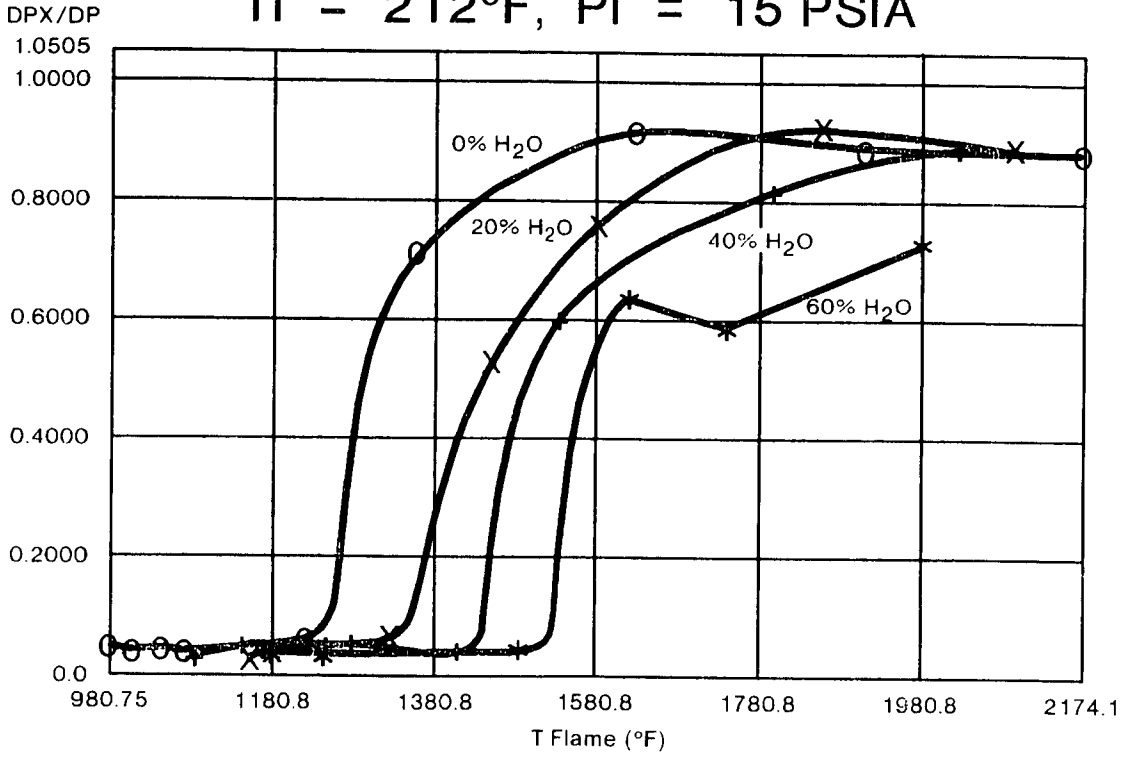
403DW026819

SEP 82

LN

FIGURE 9

EFFECT OF H_2O FROM 0.0 to 60.0%
TI = 212°F, PI = 15 PSIA



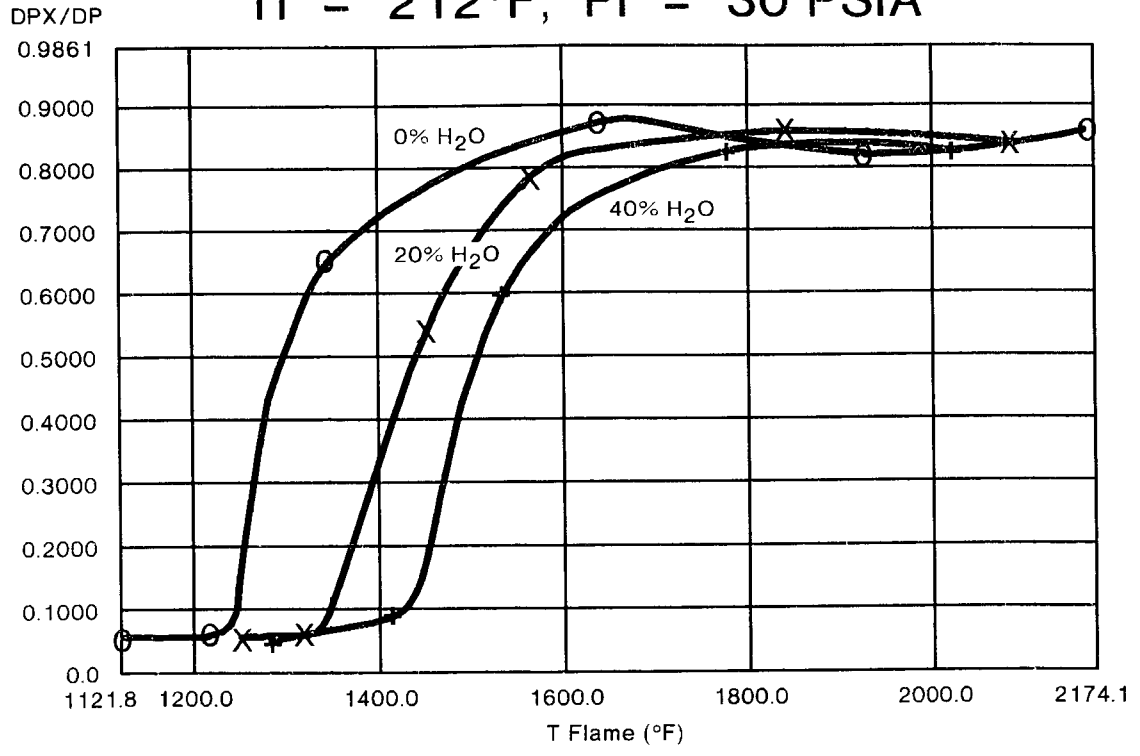
403DW025818

SEP 82

GH

FIGURE 10

EFFECT OF H_2O FROM 0.0 to 60.0%
TI = 212°F, PI = 30 PSIA



403DW025817

SEP 82

GH

FIGURE 11

EFFECT OF H_2O FROM 0.0 to 20.0%
TI = 212°F, PI = 45 PSIA

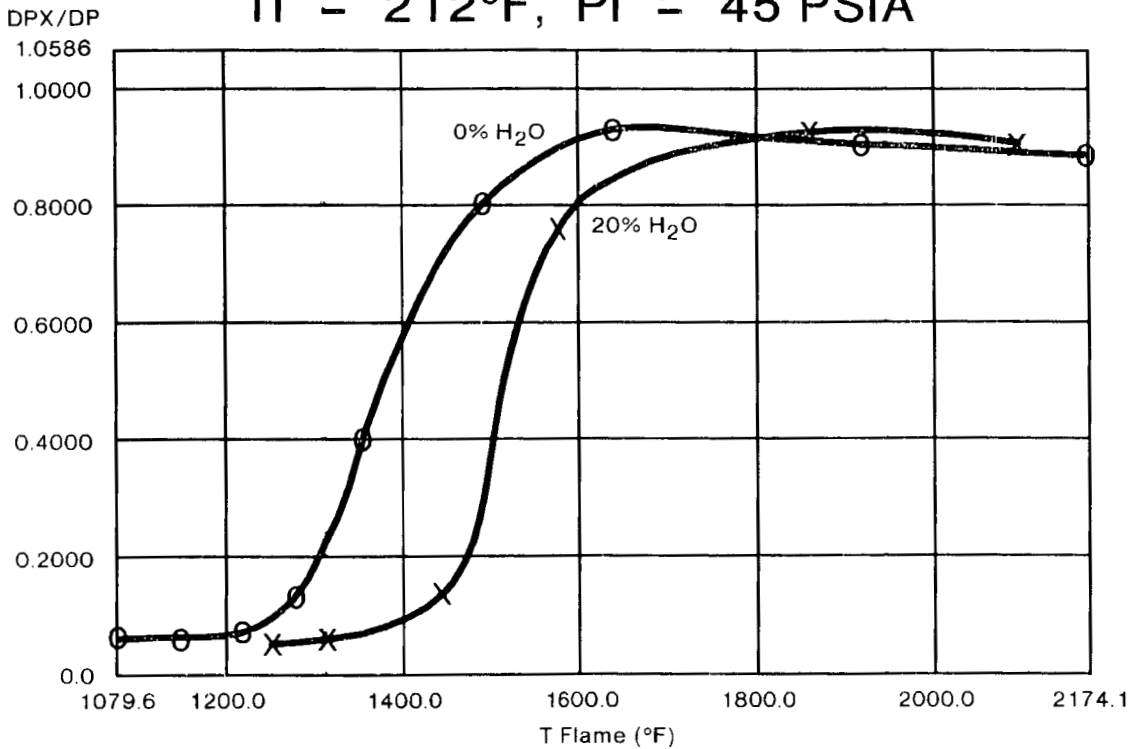


FIGURE 12

EFFECT OF H_2O FROM 0.0 to 60.0%
TI = 347°F, PI = 15 PSIA

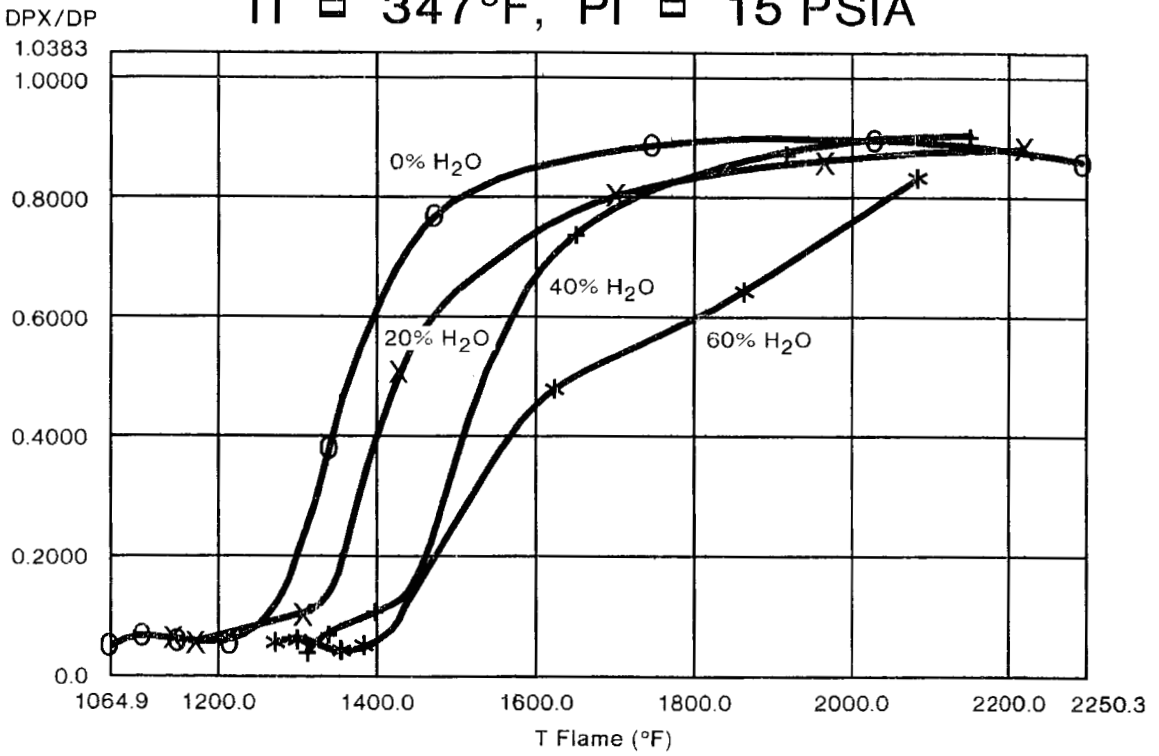


FIGURE 13
EFFECT OF H_2O FROM 0.0 TO 60.0%
TI = 347 °F, PI = 30 PSIA

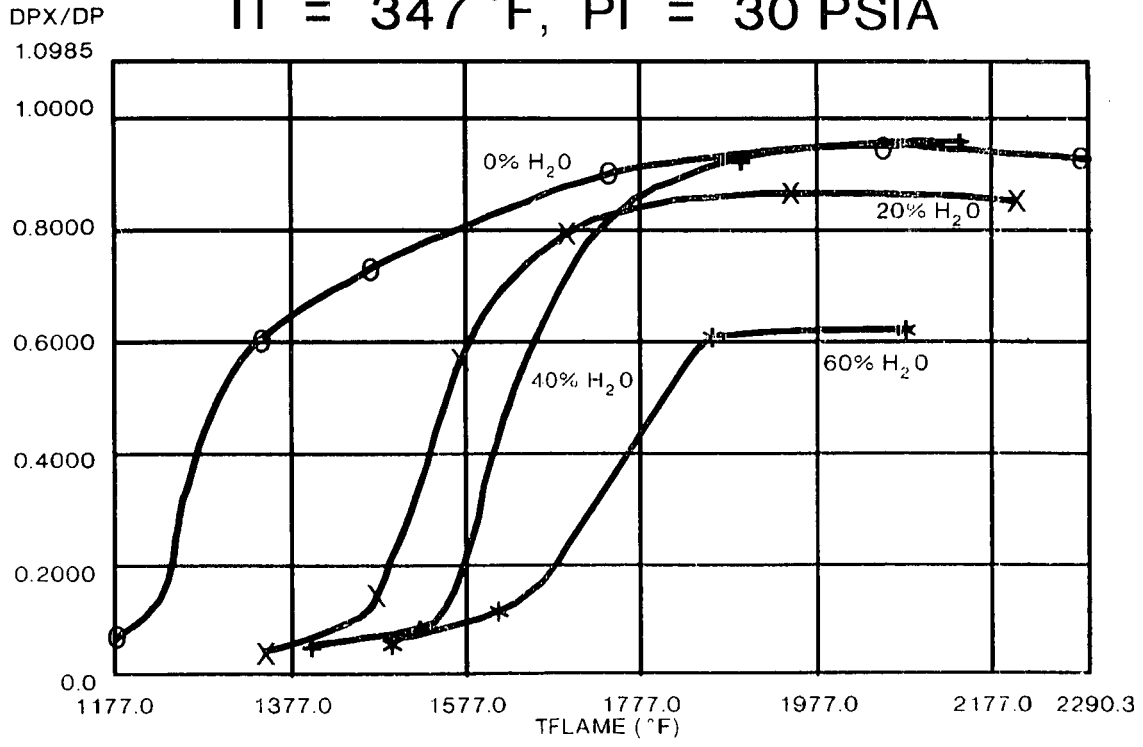


FIGURE 14

EFFECT OF H_2O FROM 0.0 to 60.0%
TI = 347°F, PI = 45 PSIA

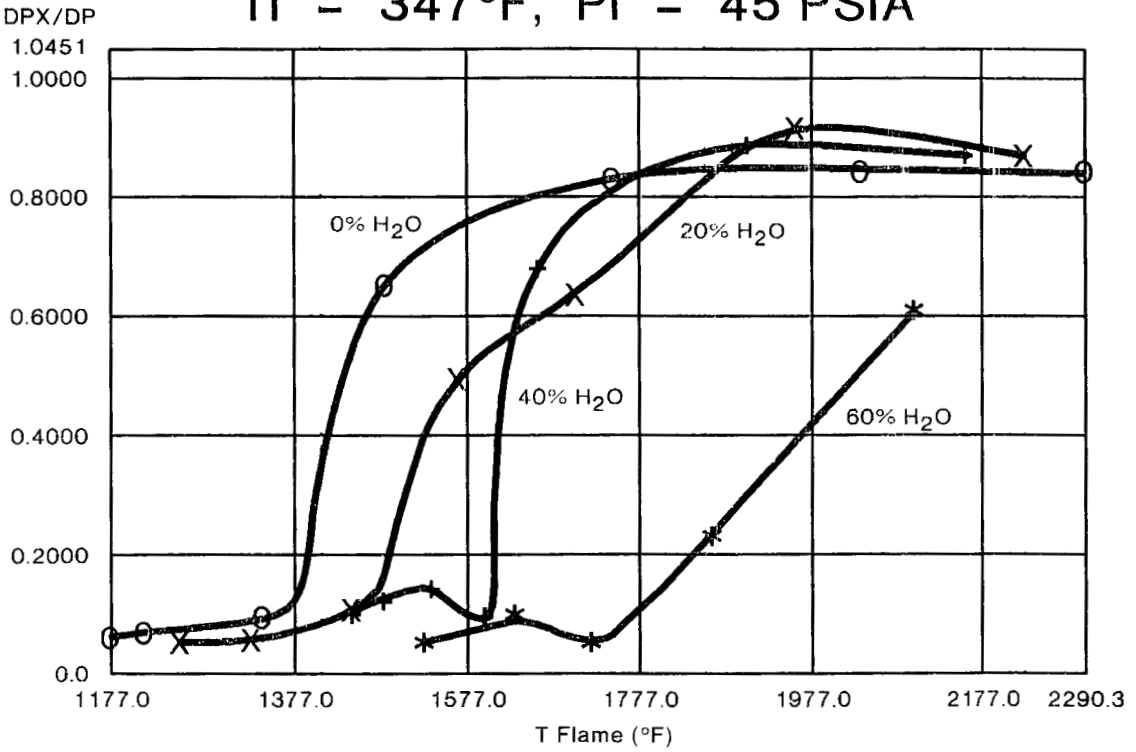
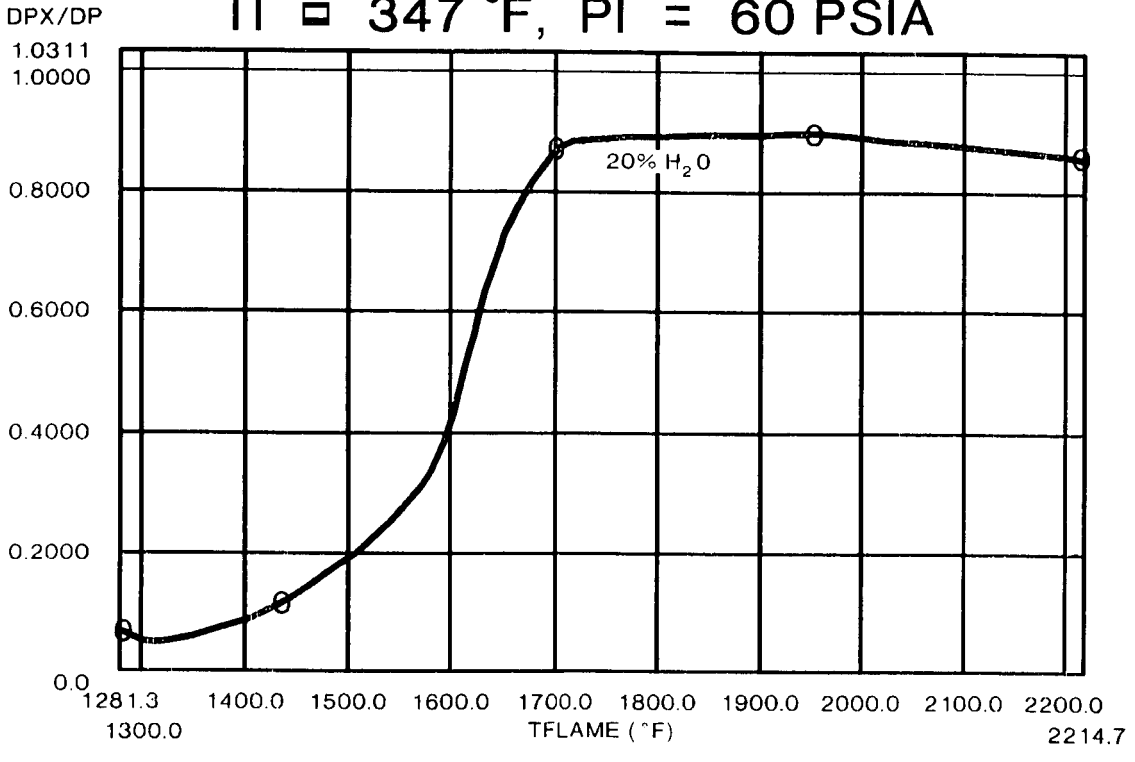


FIGURE 15
EFFECT OF H_2O AT 20.0%
TI = 347 °F, PI = 60 PSIA



403DW02581.2

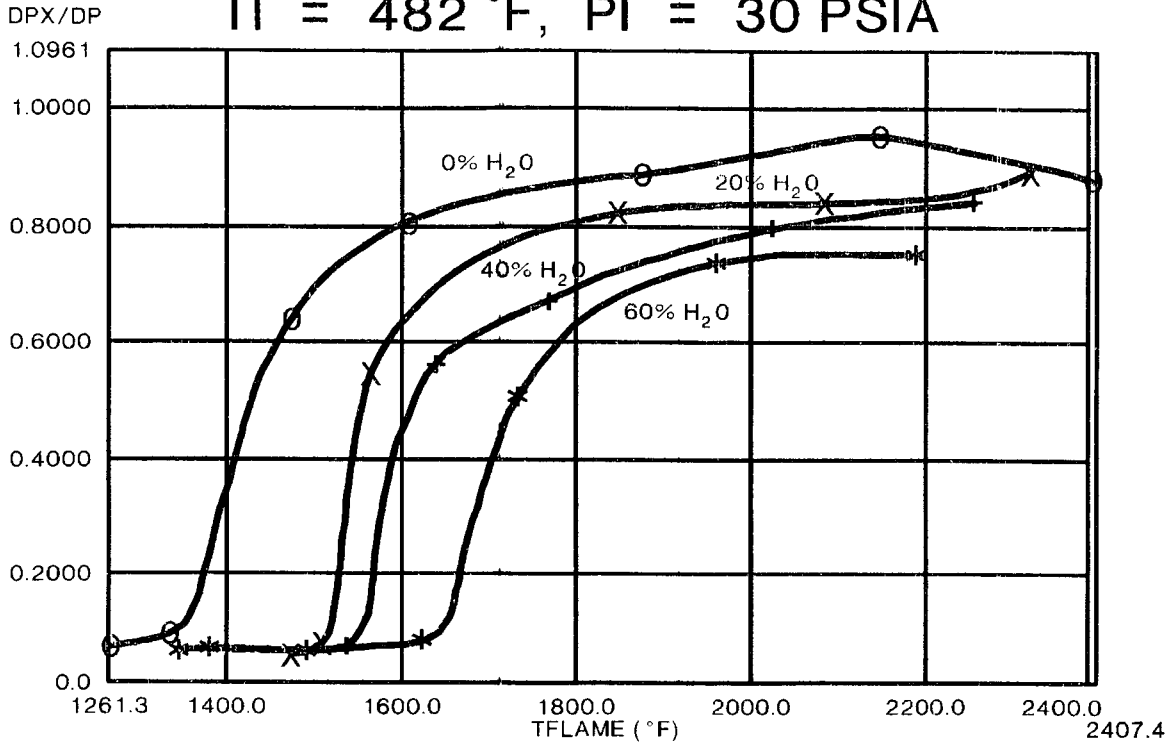
SEP 92

LN

FIGURE 16

EFFECT OF H_2O FROM 0.0 TO 60.0%

TI = 482 °F, PI = 30 PSIA



403DW02681.1

SEP 82

LN

A REVIEW OF RECENT EXPERIMENTS AT WNRE ON HYDROGEN COMBUSTION

by

H. Tamm, R.K. Kumar, W.C. Harrison

Systems Analysis Branch
Whiteshell Nuclear Research Establishment
Atomic Energy of Canada Limited
Pinawa, Manitoba ROE 1LO

1. INTRODUCTION

The Whiteshell Nuclear Research Establishment (WNRE) research program on hydrogen combustion, as related to nuclear safety, was reported at the previous workshop[1,2]. Some utilities have installed deliberate ignition systems to prevent unacceptable pressurization of reactor containments during severe accidents where hydrogen may be produced. Most of the recent experimental work comprises small-scale experiments to determine the range of conditions under which hot-surface ignitors are effective for deliberate ignition, and larger scale experiments to study the nature of combustion following deliberate ignition under various uniform conditions. This work also forms part of the EPRI Hydrogen Control Program, as presented by Thompson[3], and is funded jointly by AECL, EPRI, and Ontario Hydro.

2. SMALL SCALE EXPERIMENTS ON IGNITOR EFFECTIVENESS

Two ignitor types have been studied: the GMAC No.7 glow plug, which is being used in several ice condenser containment systems, and an alternative ignitor manufactured by Tayco. Both ignitors provide a hot surface to ignite mixtures as they become flammable. The glow plug is powered by a 14 volt AC electrical supply, whereas the Tayco ignitor is powered by 120 volts AC.

The experiments were performed with the ignitor at the centre of a 17-L vessel[4], instrumented with pressure transducers and ionization probes to monitor combustion, and thermocouples spot-welded to the ignitor surface to determine the ignition temperature. The experimental procedure consisted of heating the evacuated vessel sufficiently to prevent steam condensation (typically 80-95°C), adding steam, hydrogen, and air to their appropriate partial pressures, and then turning on the power to the ignitor.

Figure 1 shows the concentrations at which the glow plug was tested and also indicates whether ignition was achieved. The criterion for ig-

nition was the detection of a flame by the ionization probe near the top of the vessel. Ignition with a pressure rise of less than 12 kPa was defined as marginal. From these experiments, we can identify ignition-limit curves for both quiescent and (fan-induced) turbulent mixtures to delineate regions of ignitable mixtures. Experiments with the Tayco ignitor, although fewer in number, confirmed that its ignition effectiveness is fully equivalent, within the range considered, to the glow plug.

The surface temperatures at ignition for both the glow plug and the Tayco ignitor are shown as a function of steam concentration in Figure 2. The points above the solid curve are for the glow plug and those below the curve are for the Tayco ignitor. For the range of conditions investigated, ignition temperature was not noticeably affected by hydrogen concentration, turbulence, or the extent of combustion. The increase in ignition temperature with steam concentration is likely due to the higher heat capacity of mixtures containing steam. The ignition temperature for the Tayco ignitor is that of the outer surface of the coil to conform with measurements used to characterize ignitor requirements. Temperatures on the inside surface are likely higher, and this, together with the larger surface area of the Tayco ignitor, is believed to account for its ignition temperatures being lower than those of the glow plug.

3. LARGE-SCALE EXPERIMENTS

Description

The main objectives of the experiments performed in the WNRE Containment Test Facility (CTF) were to: (a) determine the rate and extent of combustion near the lower flammability limits, (b) validate model predictions of large-scale behaviour, (c) determine the effects of turbulence induced by fans or gratings on combustion, and (d) study the effects of confinement geometry and concentration differences on combustion behaviour.

The CTF[1] consists of a 2.3-m diameter sphere, a 6-m long, 0.3-m diameter pipe, and a 5.7-m long, 1.5-m diameter cylinder, all of which can

be interconnected. These vessels can be heated to prevent steam condensation. The sphere only was used for these experiments, with the closed-ended pipe added for experiments involving confinement geometry and concentration differences. Schematics of the experimental arrangement are shown in Figures 3 and 4 for the two cases.

The experiments were performed by evacuating the system, adding the component gases, and, after mixing was achieved, igniting the mixture with one of the spark ignitors located at various points in the system. Four ignitor locations were available, three in the sphere (bottom, centre, top) and one at the closed end of the 6-m pipe. Gas chromatography was used to determine concentrations before and after ignition.

4. RESULTS AND DISCUSSION

(a) Combustion of Mixtures Near the Lower Flammability Limits

The results of these experiments have been presented elsewhere[5] and only a general overview is presented here. Most experiments were performed at 100°C to prevent steam condensation. Small quantities of steam ($\leq$ 15%) were found to have no effect on the nature and extent of combustion with bottom ignition. This is demonstrated in Figure 5 which shows the pressure transients for mixtures containing 8% hydrogen. The results agree with the small scale tests of Liu et al.[2]. Combustion was complete for both dry mixtures and those containing 15% steam, whereas only 38% of the hydrogen was consumed for the mixture containing 30% steam. Steam inhibition is more effective with central ignition, as shown in Figure 6 for 7% hydrogen, where the addition of 15% steam essentially suppressed combustion (less than 0.5% hydrogen consumed). This figure also demonstrates the effectiveness of fan-induced turbulence in increasing the extent and rate of combustion. With fans on, complete combustion was attained with the mixture containing 15% steam. An interesting observation was that faster combustion was achieved with bottom ignition than with central ignition, as demonstrated in Figure 7, contrary to what would be expected in the absence of buoyancy effects (i.e. in mixtures containing more than $\lesssim$ 10% hydrogen).

Figure 8 summarizes the peak overpressures achieved with bottom and top ignition, with and without fan-induced turbulence. Under quiescent conditions, the minimum hydrogen concentration required for top ignition was 8.5%, whereas only 7% hydrogen was required for bottom ignition. The marked effect of turbulence is evident from the peak pressures plotted in this figure. Turbulence provides higher peak pressures because it increases the extent and rate of combustion.

(b) Combustion at Higher Hydrogen Concentrations

Concentrations between 10-42% hydrogen and 0-40% steam were investigated to provide experimental data for validating combustion models based on burning-velocity correlations. More detailed results will be given in Reference (6).

Complete combustion was observed over these concentration ranges in that either all the hydrogen or all the oxygen was consumed. Figure 9 summarizes the experimentally measured peak pressures. As expected, the highest peak pressure for a given steam concentration was observed for stoichiometric ratios of hydrogen and oxygen. The peak pressures decreased with steam concentration, not only because of the increased heat capacity of the mixture but also because of increased radiation heat transfer. Longer combustion times, due to the retarding effect of steam on burning velocity, allow more time for heat losses. Thus, larger deviations in peak pressure from those predicted for adiabatic conditions were observed. For mixtures containing 30% steam, this deviation is significant. For example, the peak pressure obtained for a mixture containing 10% hydrogen and 30% steam was about two-thirds of that calculated for adiabatic conditions.

A surprising result was that the combustion times of dry mixtures containing 29.5% hydrogen and 41.7% hydrogen were almost equal, whereas model predictions would suggest much faster combustion with 41.7% hydrogen due to the higher burning velocity. The reasons for this discrepancy are not clear.

(c) Combustion in the Presence of Gratings

Some experiments were performed to study the effectiveness of gratings in increasing the extent and rate of combustion. Two gratings, perforated metal sheets with 2.5-cm diameter holes occupying 50% of the area, were placed horizontally at the one-third elevations in the sphere. For mixtures containing 6% hydrogen at 100°C, the gratings increased the extent of combustion from 30% to 60% with bottom ignition. As seen in Figure 10, flame acceleration was observed, but the peak pressures were similar, due to the heat absorbed by the gratings. For higher hydrogen concentrations, the peak pressures were actually lower with the gratings present. The limited number of experiments with only one grating configuration precludes any general conclusions.

(d) Combustion with the Pipe-Sphere Configuration

Two ignitor locations, the pipe end and the sphere centre, were used. Some experiments were conducted with a rupture disc separating the pipe and sphere to permit mixtures of different concentrations in the two sections. All experiments were done at room temperature.

With pipe-end ignition and no separation between the pipe and sphere, mixtures at concentrations between the horizontal and downward flammability limits showed very little combustion; Figure 11 shows the case for an 8% hydrogen mixture (chained curve). The flame must have propagated along the top of the pipe, since the thermocouples along the central elevation of the pipe did not detect the flame. When it reached the sphere after ~14 s, a small pressure rise was observed as the flame moved to the top of the sphere and was quenched. This experiment was repeated with one fan in the sphere turned on. Again, no flame detection in the pipe was observed prior to ~13.5 s, but the turbulence now produced complete combustion in the sphere (solid curve of Figure 11), and flashback of the flame into the pipe was detected.

For a given hydrogen concentration, higher flame speeds were observed in the pipe with sphere-centre ignition than with pipe-end ignition.

Figures 12 and 13 show results for a 20% hydrogen mixture ignited at the sphere centre. Comparing the thermocouple outputs of Figure 13 (see Figure 4 for their locations) with the pressure history of Figure 12, one can see the effective flame distortion toward the pipe, since the flame is detected well before combustion in the sphere is complete. (Due to the $\sim$ 10:1 volume ratio between sphere and pipe, the pressure rise is dominated by combustion in the sphere). The pressure transducers in the pipe showed large acoustic pressure oscillations. For a 25% hydrogen mixture, the peak pressure at the pipe end exceeded the predicted adiabatic pressure. However, no detonations were observed.

Some experiments with a rupture disc of $\sim$ 100 kPa (15 psi) rating were performed with pipe-end ignition to investigate the effect of concentration differences between pipe and sphere. Figure 14 shows the result for a 15% hydrogen mixture in the pipe and a 6% hydrogen mixture in the sphere. (Mixtures containing less than 15% hydrogen in the pipe would not rupture the disc). The turbulence produced by the rapid flow into the sphere markedly increased the rate and extent of combustion; thus, combustion in the sphere under quiescent conditions would take 6-8 s, whereas in this case it occurred in about 0.4 s. Nearly 80% of the hydrogen in the sphere was burned.

5. SUMMARY

The WNRE experimental work on hydrogen combustion has been reviewed. It involved both small-scale ignitor effectiveness tests and larger scale combustion behaviour.

The ignition limits for lean hydrogen-air-steam mixtures have been determined with a GMAC glow plug and a Tayco ignitor. Both could ignite mixtures containing up to 50% steam, and, with turbulence, at even higher concentrations. Both ignitors required a higher surface temperature to ignite mixtures as steam concentration was increased.

Larger scale experiments in the Containment Test Facility were done with spark ignition under a variety of configurations and a wide range of hydrogen and steam concentrations. For mixtures near the lower flammability limits, the inhibiting effect of steam for various conditions, and the influence of fan-induced turbulence in increasing the extent and rate of combustion, were discussed. For richer mixtures of hydrogen, higher steam concentrations reduced combustion peak pressures significantly, due largely to heat-transfer effects. The gratings used did not greatly affect combustion, mainly because their effectiveness in absorbing energy counteracted flame-acceleration effects. Experiments with the pipe-sphere combination showed large amplitude acoustic oscillations in the pipe for high (> 20%) hydrogen concentrations.

6. ACKNOWLEDGEMENT

The support of this work by the Electric Power Research Institute and Ontario Hydro through joint funding with AECL-WNRE is gratefully acknowledged. The work of R. MacFarlane, A.G. Skeet, and J.E. Swiddle in performing the experiments is sincerely appreciated.

REFERENCES

1. H. Tamm, D.D.S. Liu and W.C. Harrison, "The WNRE Research Program on Hydrogen Behaviour in Nuclear Reactor Containments", Workshop on the Impact of Hydrogen on Water Reactor Safety, NUREG/CR-2017, SAND81-0661, 1981.

2. D.D.S. Liu, R. MacFarlane and L.J. Clegg, "Some Results of WNRE Experiments on Hydrogen Combustion", ibid.

3. L.B. Thompson, "EPRI Hydrogen Combustion and Control Program", Second International Workshop on the Impact of Hydrogen on Water Reactor Safety, Albuquerque, N.M., October 1982.

4. H. Tamm, R. MacFarlane and D.D.S. Liu, "Ignition Effectiveness of Thermal Heating Devices in Hydrogen-Air-Steam Mixtures", Proceedings of the ANS International Meeting on Thermal Nuclear Reactor Safety, Chicago, Illinois, August 29-September 2, 1982.

5. R.K. Kumar, H. Tamm, W.C. Harrison, J. Swiddle and G. Skeet, "Combustion of Hydrogen-Steam-Air Mixtures Near Lower Flammability Limits", ibid.

6. R.K. Kumar, H. Tamm, W.C. Harrison, G. Skeet and J. Swiddle, "Combustion of Hydrogen at High Concentrations Including the Effect of Obstacles", to be presented at the Second International Topical Meeting on Nuclear Thermal-Hydraulics, Santa Barbara, California, January 1983.

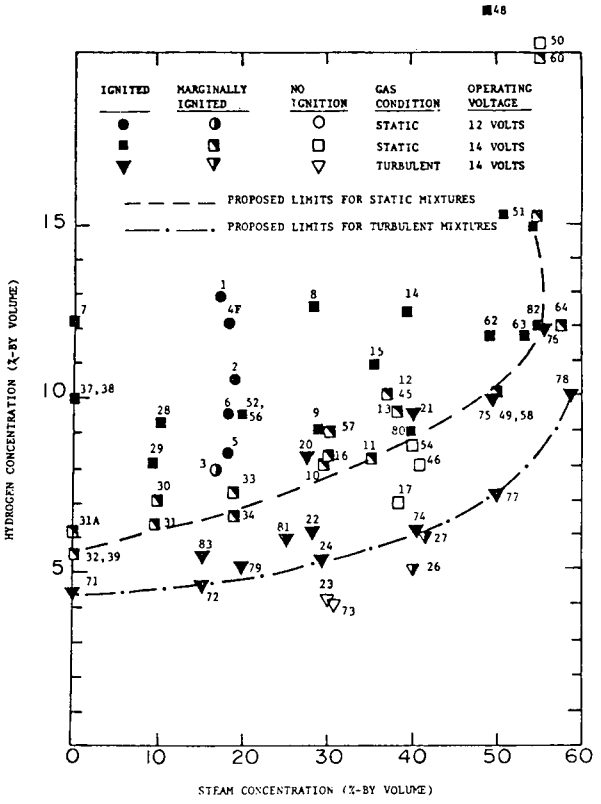


Fig. 1 Ignition Limits of Hydrogen-Air-Steam Mixtures With A Thermal Glow Plug

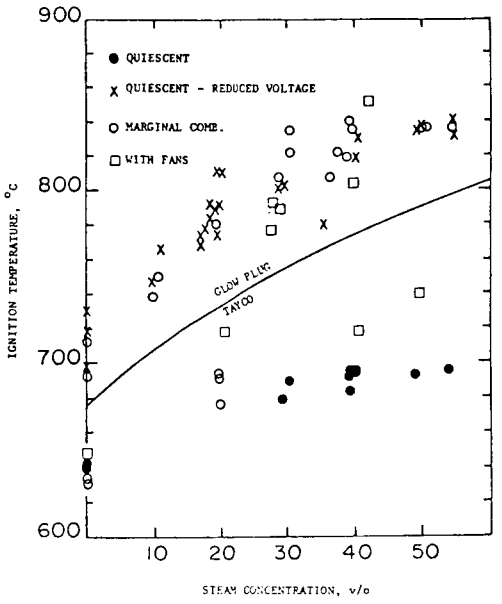


Fig. 2 Surface Temperature at Ignition vs. Steam Concentration

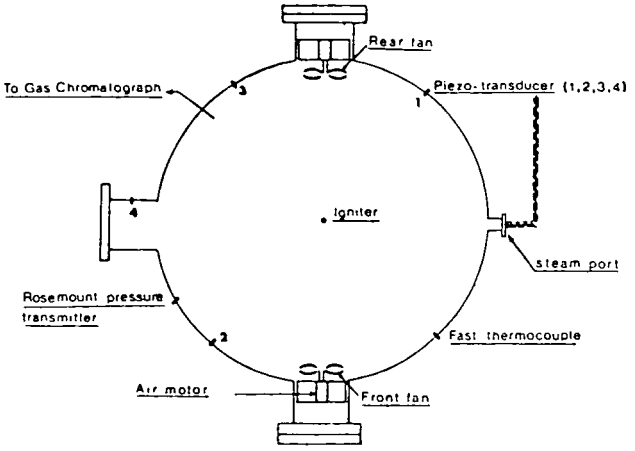


Fig. 3 Arrangement of Fans and Instrumentation in the Sphere (Plan View)

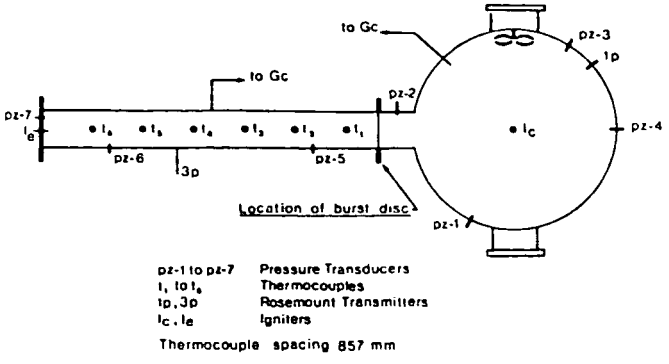


Fig. 4 SCHEMATIC OF THE INSTRUMENTED PIPE & SPHERE

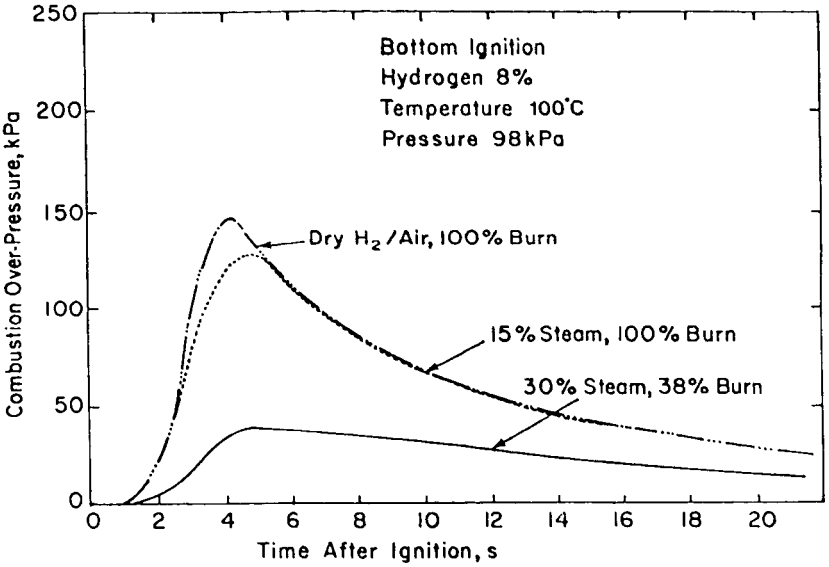


Fig. 5 The Effect of Steam Additions With Bottom Ignition

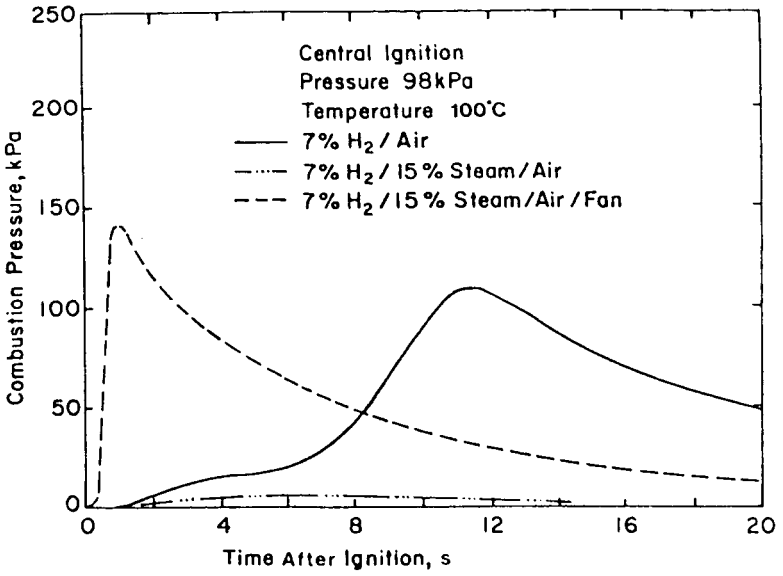


Fig. 6 The Effect of Steam With and Without Turbulence for Central Ignition

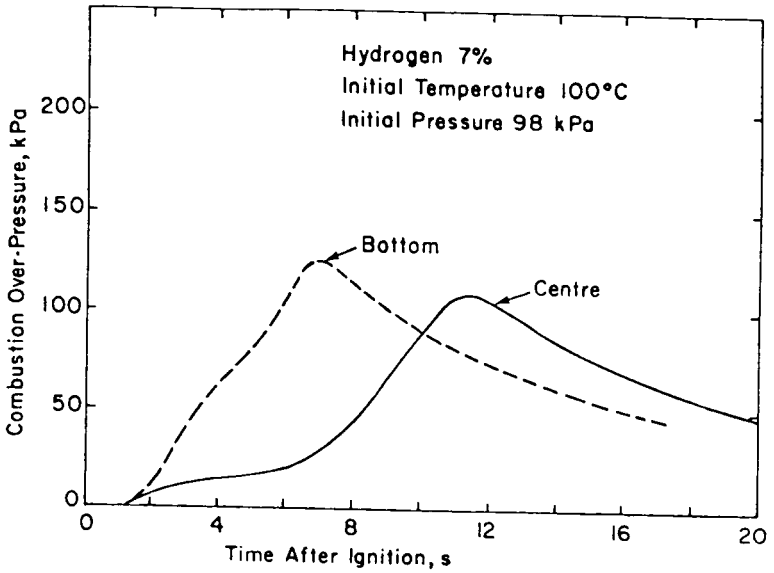


Fig. 7 The Effect of Ignitor Location

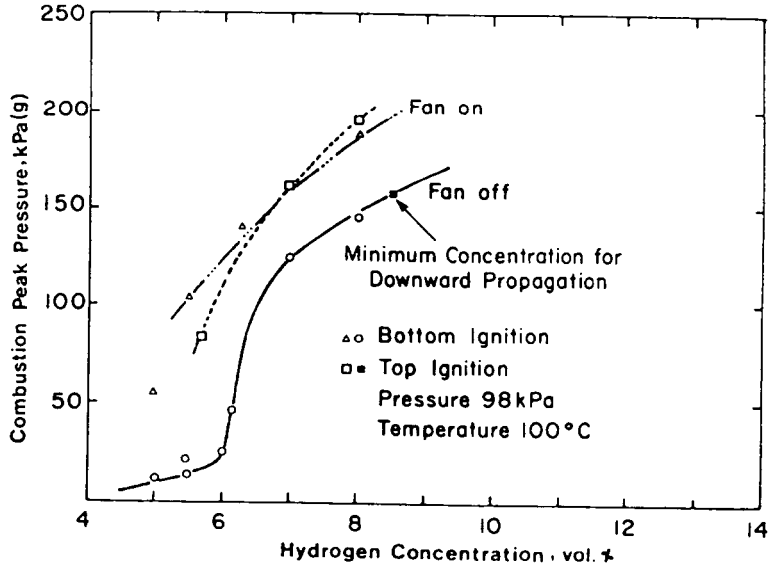


Fig. 8 The Effect of Hydrogen Concentration on Combustion Peak Pressure

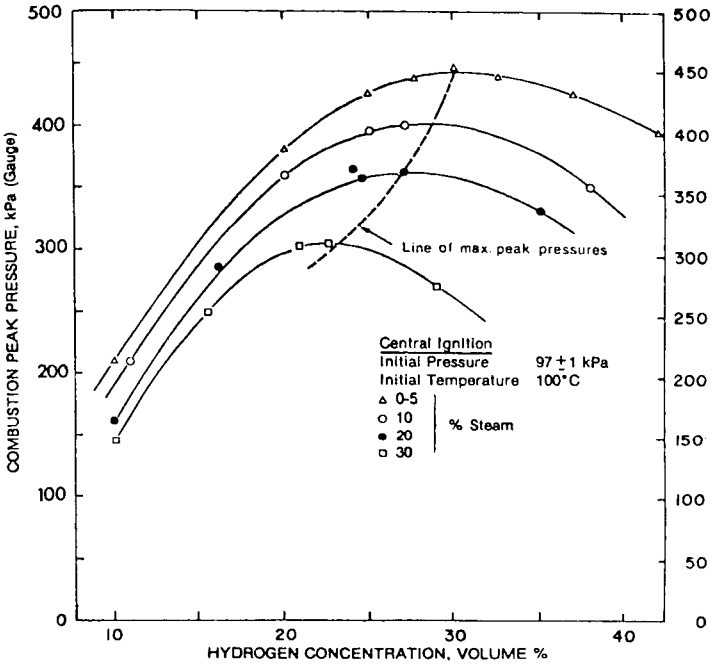


Fig. 9 The Effect of Steam at High Hydrogen Concentrations

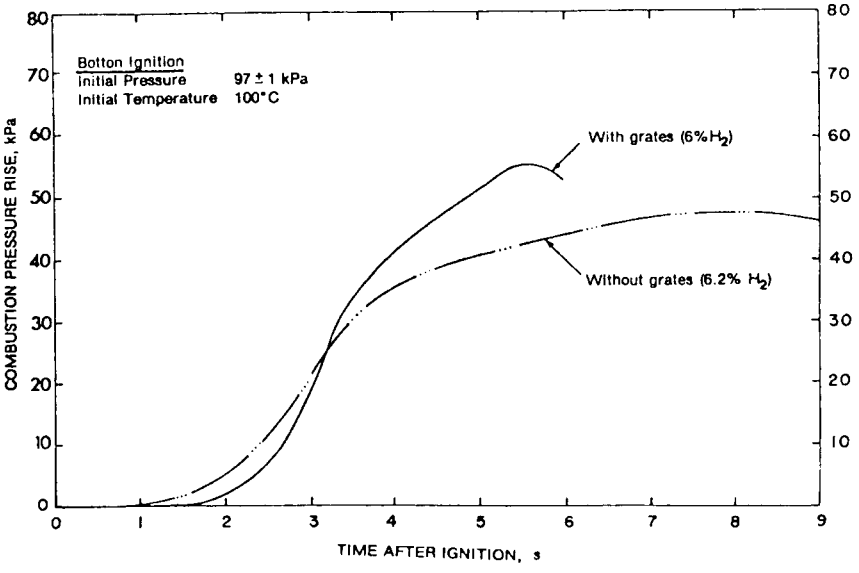


Fig. 10 The effect of Gratings on Combustion at Low Hydrogen Concentrations

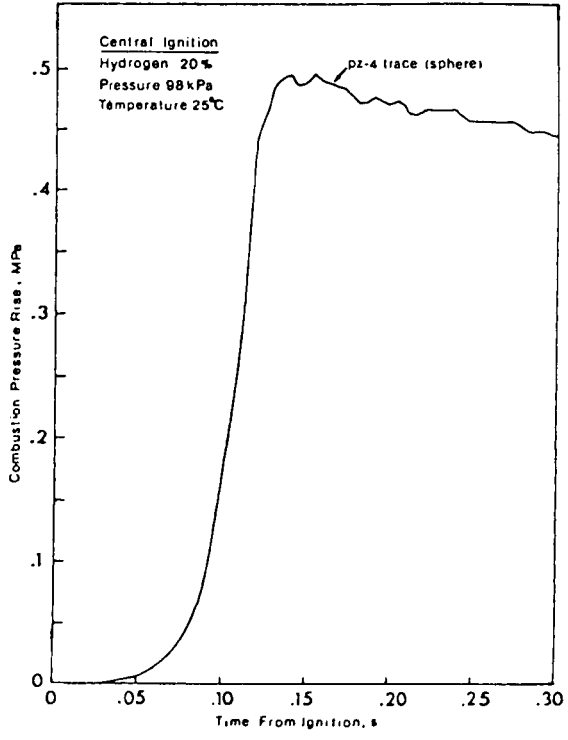


Fig. 12 Pressure Rise in Sphere for Sphere-Central Ignition

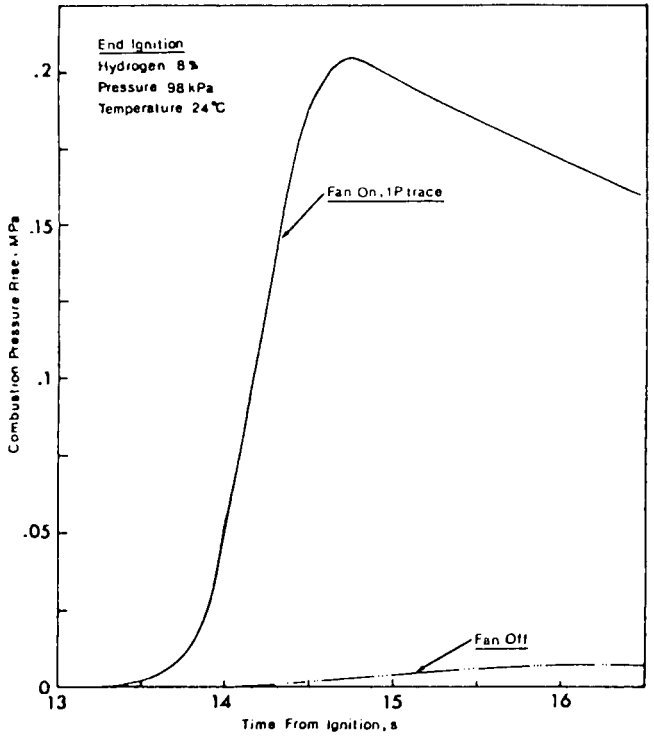


Fig. 11 The Effect of Turbulence for Pipe-End Ignition

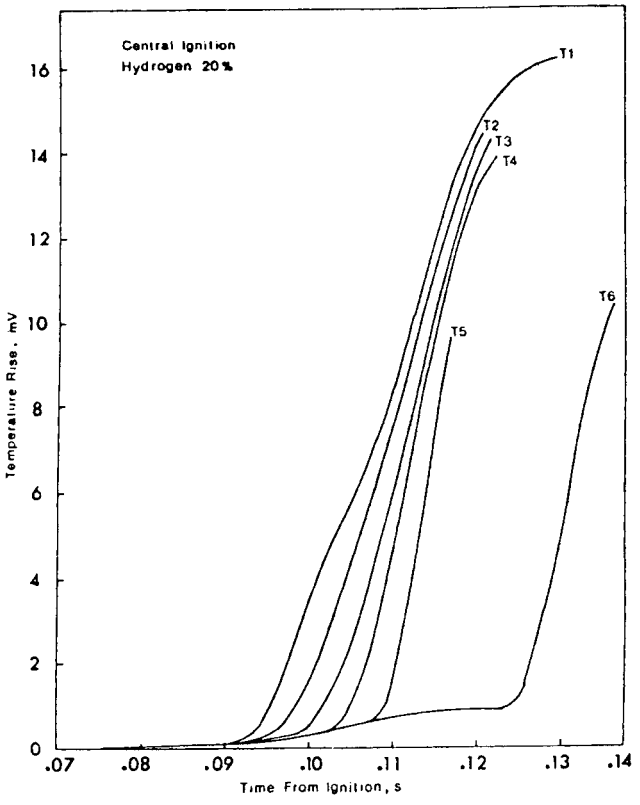


Fig. 13 Flame Detection in Pipe for Sphere-Central Ignition

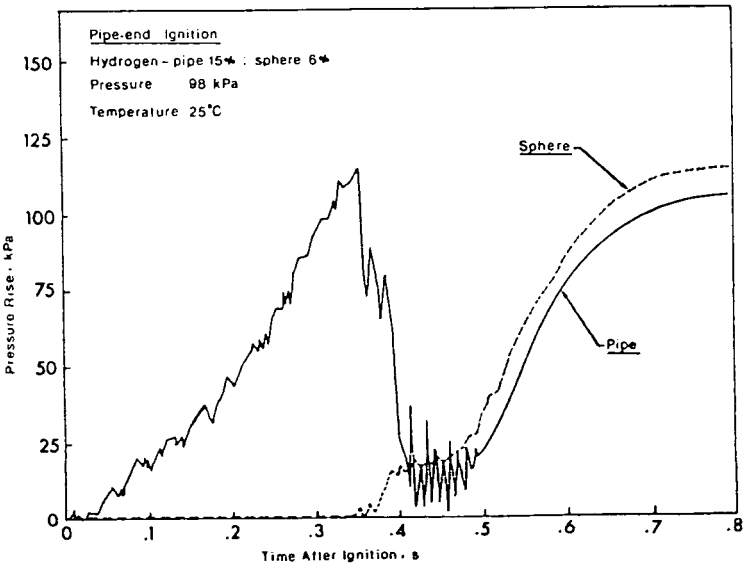


Fig. 14 Pressure Rise in Pipe and Sphere for Combustion With Rupture Disc

HYDROGEN CONTROL TESTS IN INTERMEDIATE SCALE

R.C. Torok and K. Siefert
Acurex Corporation
Mountain View, California 94043

and

L.B. Thompson
EPRI
Palo Alto, California 94304

ABSTRACT

Experiments were conducted to examine the combustion behavior of hydrogen under containment conditions typical of a degraded core accident. Parameters included hydrogen concentration, hydrogen and steam flowrates, water vapor concentration, igniter location, and water spray characteristics. Both premixed combustion and dynamic (continuous injection) tests were conducted in a vessel of 2.1 m (7 ft) internal diameter by 5.2 m (17 ft) high, having a volume of 17.8 m^3 (630 ft^3). Measurements were made of temperature, pressure, flame front propagation, and gas constituent concentration.

The maximum combustion overpressure in the 17 dynamic injection tests was 193 kPa (28 psig) for a case without steam addition to the hydrogen flow and without water sprays or fog. The presence of steam injected with hydrogen substantially lowered the maximum pressure observed. In dynamic tests with water sprays or microfogs, the maximum pressure increase was 34 kPa (5 psi). Microfogs had little effect on overpressures in the premixed combustion tests.

1.0 INTRODUCTION

Deliberate ignition systems have been installed in several PWR ice condenser and BWR Mark III containment buildings for controlling hydrogen following a postulated degraded core accident. Hydrogen would be removed by multiple burns at lean concentrations in order to prevent potentially dangerous hydrogen accumulations and to limit the combustion pressures and temperatures.

The project discussed in this paper was performed principally as an intermediate-scale examination of the deliberate ignition concept to hydrogen control. Hydrogen, steam, and in some cases water fog or spray were continuously injected into a closed vessel which contained a single preactivated ignition source. These experiments were part of EPRI's broader program on hydrogen mixing, combustion, and control, and were co-sponsored by the three owners of PWR ice condenser plants -- American Electric Power, Duke Power, and Tennessee Valley Authority. Other related projects included studies of premixed

combustion at Whiteshell Nuclear Research Laboratories, water fog effects on hydrogen flammability at Factory Mutual Research, and hydrogen mixing and distribution at Westinghouse Hanford Company.*

2.0 TEST FACILITY AND PROCEDURES

The test vessel and mechanical systems are indicated in Figure 1. The cylindrical vessel has a volume of about 18 m^3 (630 ft^3) and dimensions of 2.1 x 5.2 m (7 x 17 ft). The mechanical system provides capabilities for: (1) injection of hydrogen or a hydrogen/steam mixture into the lower portion of the test vessel; (2) supplying water spray or microfog spray through nozzles near the dome; (3) obtaining pre-test and post-test vessel gas samples, and (4) providing means for homogenizing the vessel atmosphere prior to premixed combustion tests.

A propane-fired boiler provided steam for heating the vessel prior to testing, and for concurrent injection of steam with hydrogen. When hydrogen alone was required, the steam line was isolated from the injection line. Steam flowrate was monitored with an annubar flow sensor and a differential pressure gage. Hydrogen flowrate was monitored and controlled with a rotameter and a control valve.

A closed-loop spray system recirculated water from a shallow pool to the spray nozzles by a three horsepower electric motor and a gear pump. A bypass loop was utilized to control the flow rate. A single standard containment Spraco nozzle was used for the spray tests, delivering 57 l/m (15 gpm) with a nozzle pressure difference of 275 kPa (40 psi). Microfog tests were also conducted using 9 Spraco 2163-7604 pinjet nozzles which delivered 4.2 to 5.3 ℓ/min (1.1 to 1.4 gpm) depending on the nozzle pressure used.

An air-operated fan was mounted inside the vessel and was used to help provide a well-mixed atmosphere prior to premixed-combustion tests. Two 10 cm (4 inch) butterfly valves located at the top and near the bottom of the tank and a squirrel-cage blower were used to purge the vessel following a test after post-test gas samples were obtained. Atmosphere samples were passed through a cold trap and silica gel to remove moisture, and then to a glass sample bottle for on-site measurement by gas chromatography.

Three igniter locations were used for placement of glow plug assemblies which were provided by Duke Power Company. The igniters were powered by 110 VAC stepped down to 14 VAC through a transformer located within the igniter box. General Motors Model AC-7G glow plugs were used as the ignition source. Each assembly consists of a galvanized steel enclosure with one hinged side panel. The 5 inch diameter hydrogen injection nozzle was located at half the vessel radius and just below the bottom igniter position.

Test vessl instrumentation was placed as shown in Figure 2. Measurements were made of vessel gas and wall temperatures, pressure, wall strain, and flame front location, in addition to gas concentrations.

*Results of these projects are presented in separate papers at the October 4-7, 1982 Albuquerque Conference and in an overview paper at the opening session.

All temperature measurements within the vessel were made with 76.2 micron (0.003 in.) diameter Type K thermcouples. Four of these thermocouples were located on the centerline of the test vessel and wall thermocouples were welded directly to the vessel inner surface. Pressure measurements were made by both strain gage and piezoelectric transducers.

Instrumentation to detect flame front propagation consisted of 35 thermocouples in a 5 x 7 grid (Figure 2) with a specially designed electronics assembly. The processing circuitry used high input impedance operational amplifier comparators to detect a threshold temperature rise in each thermocouple. Each thermocouple was associated with a distinct output voltage so that the pattern of flame front arrival could be determined.

Two recording systems were used for data acquisition. A twenty-eight channel FM tape recorder was used to record all potentially fast response data. The frequency response was 10 kHz or greater. An Autodata 9 data logger was used to record relatively slow response signals and served as a backup to the FM tape recorder.

3.0 TEST MATRIX, PROCEDURES, AND RESULTS

Both premixed combustion tests and dynamic injection tests were conducted, according to the test matrices give in Tables I and II.* The first three premixed tests were performed for comparison with combustion experiments at other facilities and as reference cases for the later tests with fog spray. The dynamic injection hydrogen control experiments (Table II) were performed to determine the effects of several variables on hydrogen combustion behavior. Igniter location, hydrogen flow rate (with and without steam injection), water spray (on or off) and microfog spray were varied in several combinations.

Three spray rates were utilized. The 57 ℓ/min (15 gpm) rate was achieved with a single Spraco 1713 swirling atomizing nozzle with a nozzle pressure drop of 275 kPa (40 psi). It produces a droplet number-mean diameter of about 200 microns. Secondly a manifold of 9 Spraco 2163-7604 pinjet nozzles were utilized with nozzle pressures of either 140 or 210 kPa (20 or 30 psi). This configuration produced microfog with droplet number-mean diameters of 11 and 8 microns repsectively and total flow rates of 4.2 ℓ/min (1.1 gpm) and 5.3 ℓ/min (1.4 gpm) respectively.

Vessel pre-heating to the target temperature of 70°C (160°F) was accomplished by injecting steam into the vessel. The water spray was utilized to help create a stable and uniform temperature during this preconditioning time period. In premixed combustion tests the fan was then turned on and hydrogen injected to the desired concentration, sprays were turned off and a pre-test gas sample taken. In the dynamic injection tests the glow plug was activated prior to initiation of gas flow.

*Five additional experiments for equipment survivability studies were performed in Test Series 4, reported in Session VIII of this Conference.

3.1 Premixed Combustion Tests

Three premixed combustion tests (Table 1) were conducted as reference cases for later microfog tests. Tests with measured hydrogen concentration of 4.7, 7.8, and 9.7% by volume and initial water vapor of about 26% resulted in peak overpressures of 55, 245, and 330 kPa (8, 36, and 48 psi). Burn completeness was 30, 90, and 99%, respectively. The ignition was at the bottom location in all cases, which should produce the most complete burn in lean-mixture cases.

The tests with microfog resulted in similar overpressures. In tests 3.3 and 3.4 the measured concentrations were 7.2 and 7.6% hydrogen and the overpressures were 275 and 270 kPa in comparison with 245 kPa with no fog. The burns were 99% complete, in contrast to 90% without fog. The results were even more similar in the higher hydrogen concentration cases, overpressures being 325 and 345 kPa in tests 3.1 and 3.2 in contrast to 330 kPa without fog.

Microfog had been expected to lower combustion pressures and temperatures by a heat sink effect. It appears that the density of droplets fine enough to vaporize and absorb energy during the combustion period (about one second) was too low to have an appreciable effect. In the lean mixture test with about 7.5% hydrogen the fog spray may have increased turbulence, enhancing burn completeness. In all cases ignition took place approximately 20 seconds after the igniter was turned on.

3.2 Effects of Igniter Location in Dynamic Tests

The effects of igniter location on hydrogen combustion behavior in tests with continuous injection of dry hydrogen can be seen by comparing Tests 2.3, 2.11, and 2.6 (Table II and Figure 3). When the bottom igniter was activated, hydrogen injected at the half-radius point at about 0.25 m/second bypassed the ignition source, building up throughout the volume until a global burn took place at about 450 seconds. The peak pressure was 193 kPa (28 psi), and other local intermittent combustion took place during this test.

The center igniter position allowed earlier and frequent intermittent local combustion to take place. The highest single overpressure was only 41 kPa (6 psi). The post-test sample contained 0.4% hydrogen, 5.7% oxygen, and 36% water vapor, so the combustion was essentially complete. When the top ignitor was activated, some combustion took place at about 300 seconds as the igniton limit for upward propagation was reached. A volume-average concentration of 4.7% hydrogen had been injected up to that time. As hydrogen was further introduced the limit for downward propagation was apparently reached at about 580 seconds. A global burn took place throughout the vessel, as indicated by the flame front detectors. The peak overpressure was 138 kPa (20 psi).

3.3 Effects of Steam, Water Spray, and Water Fog in Dynamic Tests

The addition of steam or water spray can have a dramatic mitigating effect on combustion in dynamic hydrogen injection tests. Typical effects can be seen in Figure 4 which shows three cases having an activated central igniter. The top curve is for Test 2.11 with dry hydrogen injection (also see Figure 3, center). There are a number of intermittent local burns which consume most of the hydrogen and produce a maximum pressure of 41 kPa (6 psi). In the center

figure, Test 2.10, large quantities of steam have been added to the hydrogen flow, in a mass ratio of 60 to 1. The highest combustion overpressure is reduced slightly to 28 kPa (4 psi), however, the major effect is to make the combustion somewhat more erratic, taking place over a longer time period. In the lower figure, Test 2.9, a water spray is added to the condition of the previous case. Now the multiple combustion events are much more uniform, and peak combustion overpressures are held to less than 20 kPa (3 psi).

Very similar trends are seen with the bottom igniter activated. With injection of dry hydrogen alone the peak combustion pressure is 193 kPa (28 psi) as shown in Figure 3. With the addition of steam injection (Test 2.5) the highest combustion pressure is 31 kPa (4.5 psi). With the addition of both steam and water spray (Test 2.4) the highest pressure is 7 kPa (1 psi).

The effects of water fog are somewhat similar to those of a standard containment spray in dynamic injection tests. Figure 5 shows a case with hydrogen injection and water fog (Test 3.8). The fog spray apparently aided mixing, contributing to local combustion near the igniter and very little overpressure. With the addition of steam injection (Test 3.6, Figure 5) several discrete combustion events are apparent, with maximum overpressures of 34 kPa (5 psi). The events are more spread out and most are stronger than obtained with the much higher water flow rates and larger drops of Test 2.9 (Figure 4).

3.4 Effects of Hydrogen Flowrate in Dynamic Tests

The effect of hydrogen flow rate can be seen in Figure 6 for cases of dry hydrogen injection. The top curve for the low hydrogen flow rate of Test 2.6 shows a global combustion event of 193 kPa (28 psi) at about 450 seconds. The bottom case with triple the flow rate, Test 2.8, resulted in a combustion of 162 kPa (24 psi) at about 130 seconds. Each deflagration occurred at about the same mean-volume percent combustible gas concentration.

With the addition of large quantities of steam the behavior is somewhat more complex as shown in Figure 7. The first major burn in Test 2.7 occurred as expected at one-third the time than for Test 2.5 which had one-third the hydrogen flow rate. The second major combustion occurred at about 830 seconds in both tests, however. Combustion at the intermediate times may have been limited by the high steam injection rates (60 or 20 to 1 in steam to hydrogen mass flow).

4.0 SUMMARY AND CONCLUSIONS

Glow plug igniters were shown to be effective for deliberate ignition of hydrogen in environments of air, steam, water spray and water fog. In premixed combustion experiments the combustion of 7.5% hydrogen by volume was complete with the presence of fog spray and nearly complete without a spray.

Simulation of several degraded core accidents, with continuous injection of hydrogen into a vessel containing an activated igniter, resulted in maximum combustion overpressures of less than 2 atmospheres which is within the apparent capacity of all containment designs. Injection of steam with the hydrogen provides an additional mitigating effect, and water sprays have a dramatic limiting effect on combustion pressures in such experiments. In all cases combustion proceeded until either the hydrogen or oxygen concentrations were reduced to low levels.

Table I

Premixed Combustion Tests[1]

Test No.	H_2 Concentration (v%)	Fog Spray (ℓ/min) 4.2	5.3
1.1	5.0	-	-
1.2	7.5	-	-
4.2	10.7	-	-
3.1	10.7	-	X
3.2	10.7	X	-
3.3	7.5	-	X
3.4	7.5	X	-

(1) Bottom igniter location and initial temperature of 70°C for all tests.

Table II

Dynamic Injection Tests[1]

Test No.	Igniter Location	Gas Injection (kg/min) Hydrogen 0.016	Hydrogen 0.048	Steam 0.96	Water Flow (ℓ/min) Spray 57	Spray 4.2	Fog 5.3
2.2	Top	X	-	X	-	-	-
2.3	Top	X	-	-	-	-	-
2.4	Bottom	X	-	X	X	-	-
2.5	Bottom	X	-	X	-	-	-
2.6	Bottom	X	-	-	-	-	-
2.7	Bottom	-	X	X	-	-	-
2.8	Bottom	-	X	-	-	-	-
2.9	Center	X	-	X	X	-	-
2.10	Center	X	-	X	-	-	-
2.11	Center	X	-	-	-	-	-
3.5	Bottom	X	-	-	-	X	-
3.6	Bottom	X	-	X	-	X	-
3.7	Bottom[2]	X	-	-	-	-	X
3.8	Bottom	-	X	-	-	-	X
3.9	Bottom	X	-	-	-	-	X
3.10	Bottom	X	-	X	-	-	X

(1) All tests began with the glow plug igniter heated to about 930°C with initial vessel atmosphere temperature of 70°C.

(2) Vessel mixing fan on.

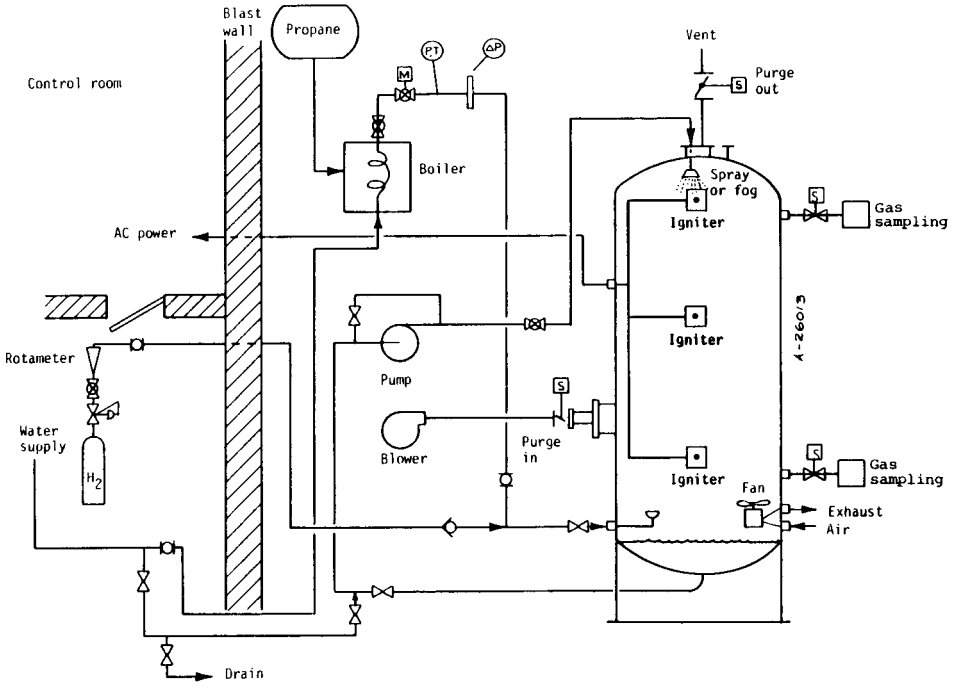


Figure 1--Schematic of hydrogen control test facility.

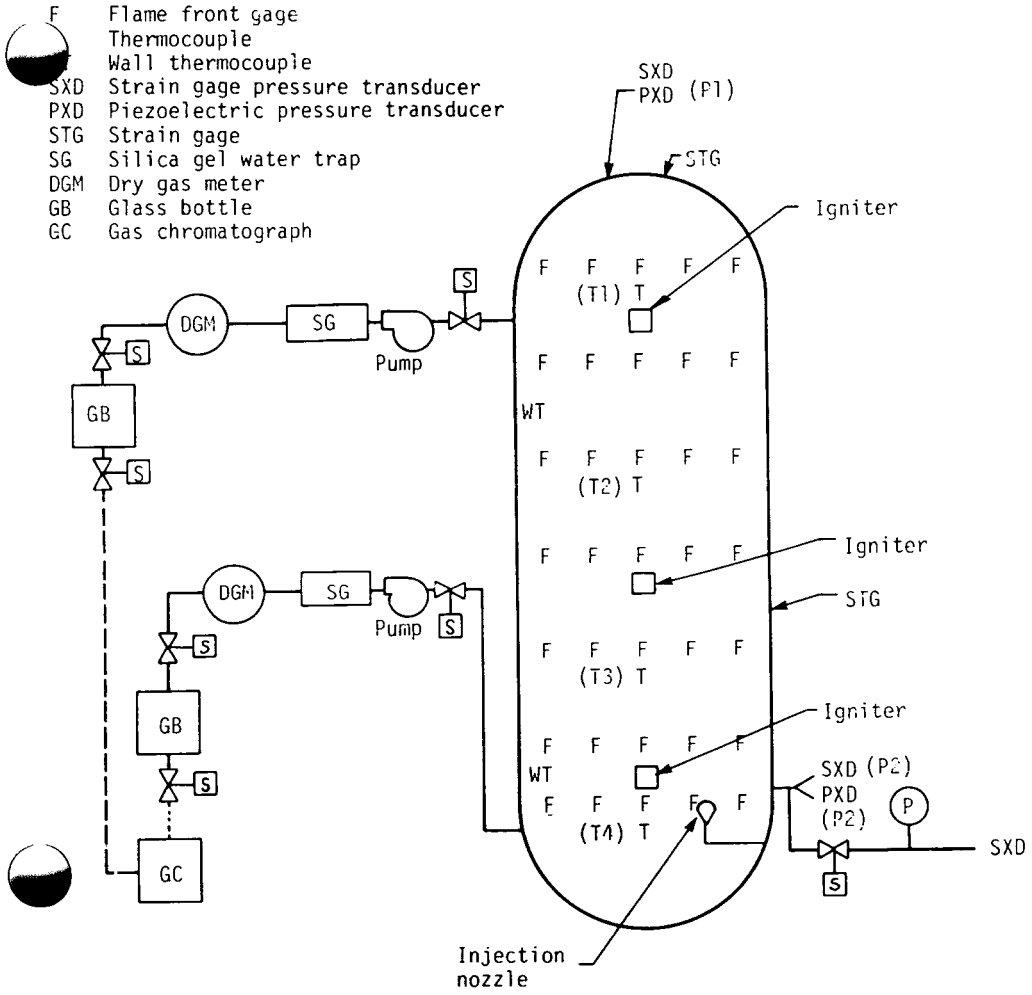


Figure 2--Instrument Locations in 2.1 x 5.2 m tank.

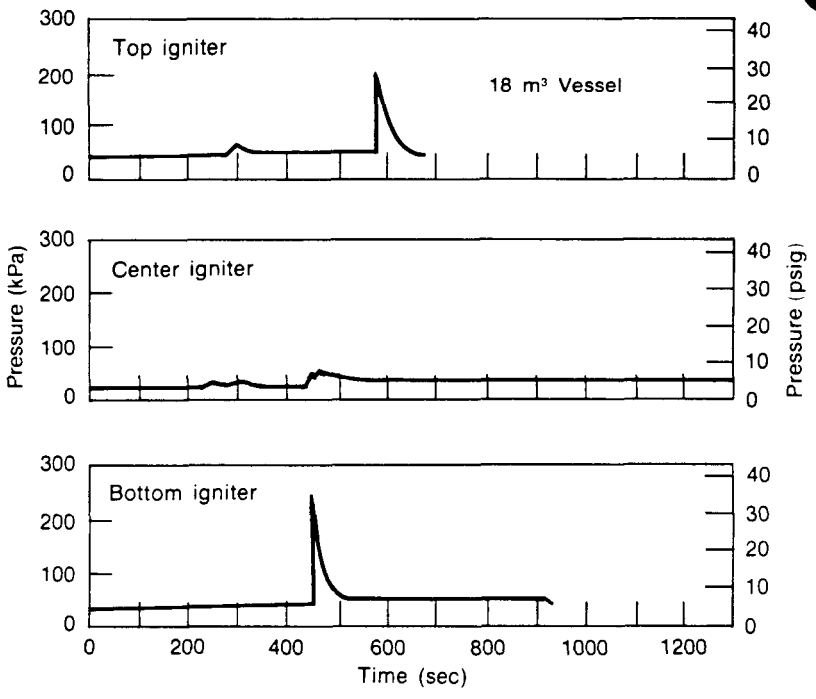


Figure 3--Effect of igniter location in experiments with continuous injection of hydrogen into a 18 m^3 vessel.

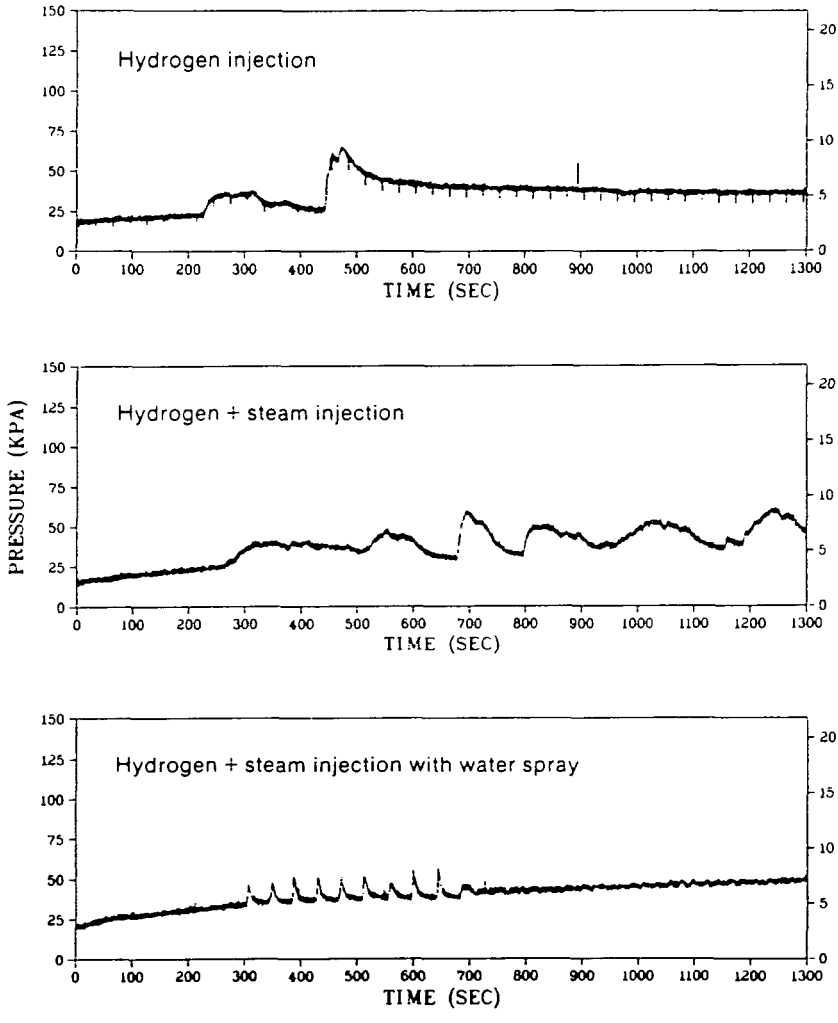


Figure 4--Effects of steam injection and water spray in experiments with a center igniter location and continuous injection of hydrogen into a 18 m^3 vessel.

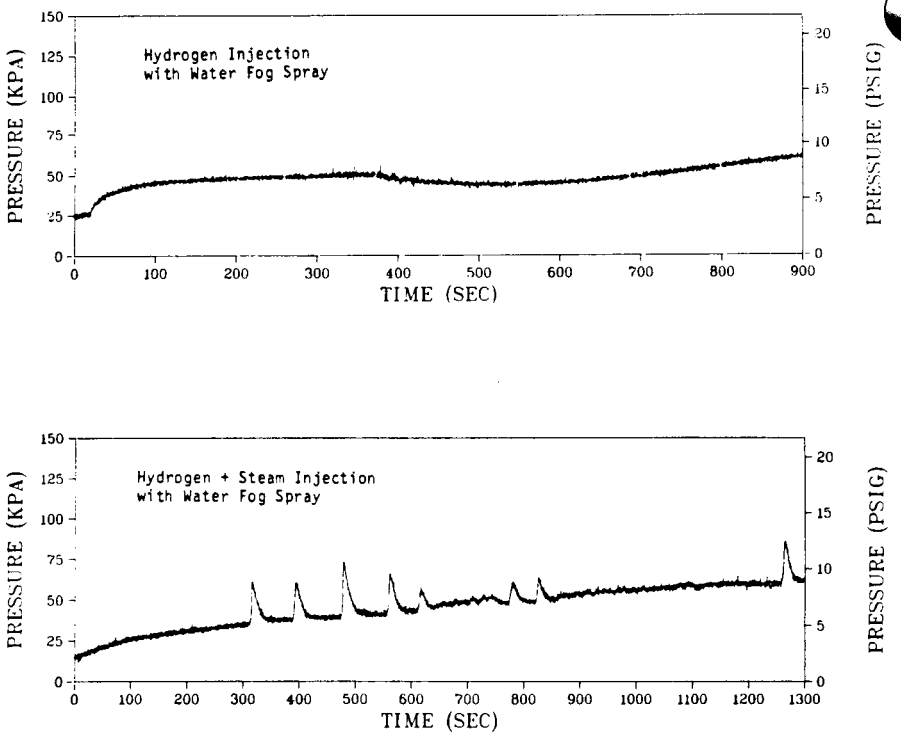
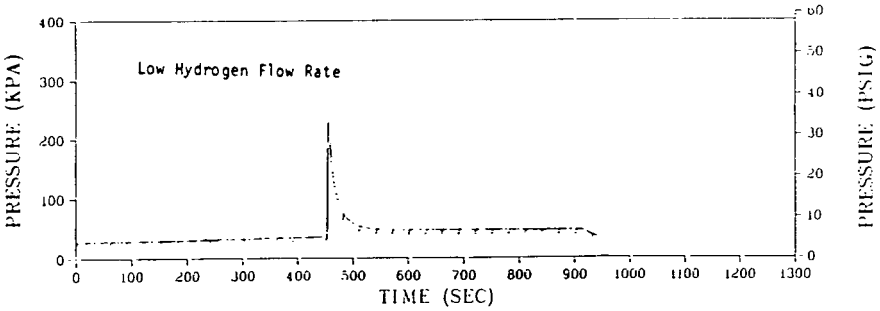


Figure 5--Effects of steam injection and water fog in experiments with a bottom igniter location and continuous injection of hydrogen into a 18 m^3 vessel.



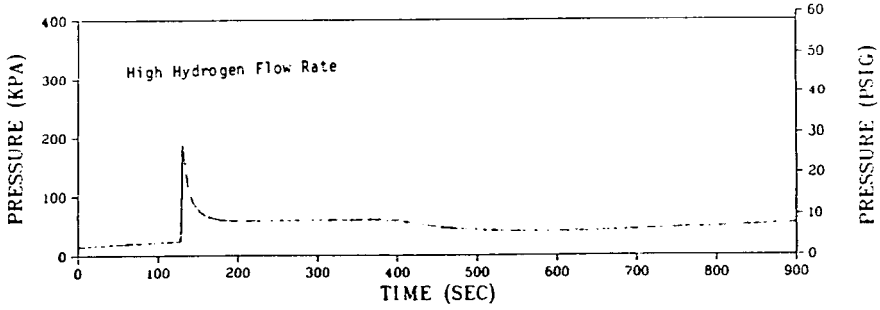


Figure 6--Effects of Hydrogen injection rate into a 18 m^3 vessel. (Tests 2.6 and 2.8)

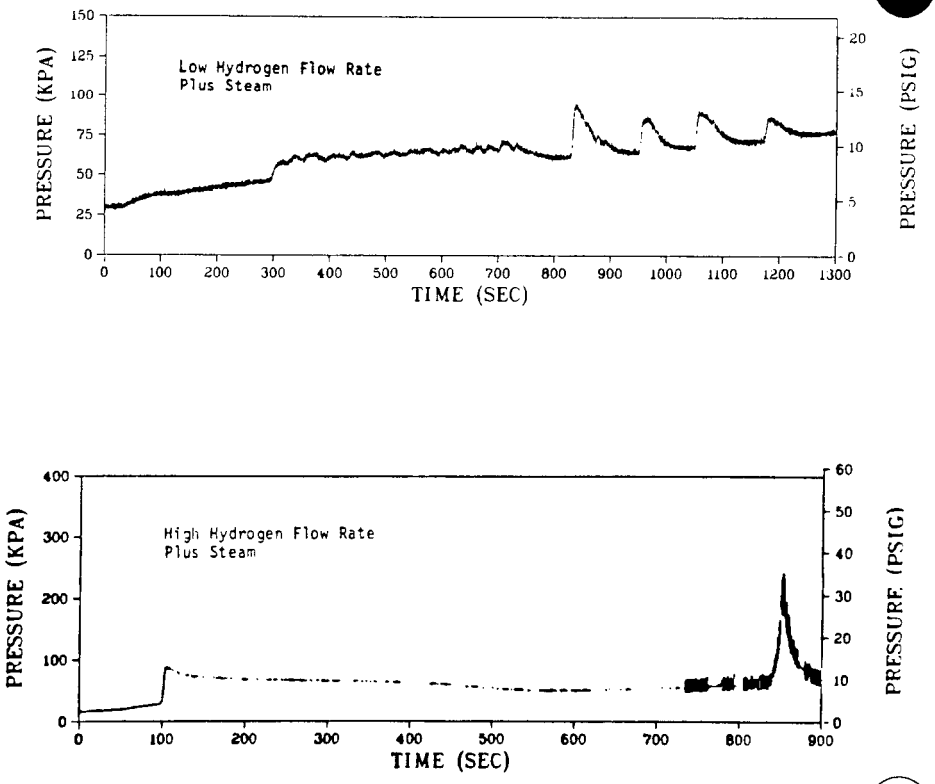


Figure 7--Effects of Steam Injection and Hydrogen Flow Rate into a 18 m^3 vessel.

EXPERIMENTAL RESULTS FROM COMBUSTION OF HYDROGEN:AIR MIXTURES IN AN INTERMEDIATE-SCALE TANK

W. B. Benedick
Shock Wave and Explosive Physics Division

J. C. Cummings
P. G. Prassinos*
Reactor Safety Studies Division
Sandia National Laboratories
Albuquerque, N. M. 87185

Sandia National Laboratories is currently involved in several experimental projects to provide data that will help quantify the threat of hydrogen combustion during LWR accidents. One project which employs several experimental facilities is the Variable Geometry Experimental System (VGES). The purpose of this paper is to present a description of and experimental results from one of these facilities: an intermediate-scale burn tank (~5 m^3). The data provided by this facility can be used in the development of analytical models to predict hydrogen combustion behavior along with providing a means of assessing present and future analytical models.

†This work performed at Sandia National Laboratories supported by the U.S. Nuclear Regulatory Commission.
*Technadyne Engineering Consultants, Albuquerque, New Mexico.

Introduction

To assess the threat from deflagrations, detonations and accelerated flames in hydrogen air mixtures, and to evaluate proposed mitigation schemes in nuclear reactor containment buildings, the intermediate scale experimental apparatus should approximate the length-to-diameter (L/D) ratio of the containment building. Clearly, tubes and pipes are not appropriate, but vertical tanks with a L/D ratio of 2 to 5 would provide a good approximation. Our VGES tank has a L/D ratio of about 4 which is small enough to observe such phenomena a bouyancy effects in the flame kernel, turbulent flow effects on flame propagation, etc. The VGES tank is used to quickly provide scoping data on hydrogen: combustion on an intermediate scale. Our testing format is designed to provide quick answers to NRC questions about effects of igniter type and location, obstacles, water fogs/foams, inert gas dilution, Halons, etc.

The tank and associated instrumentation are shown schematically in Fig. 1. The tank is installed in the ground with only the top end of the cylinder exposed. The tank is 4.3 m long and 1.2 m in diameter with an integral semi-ellipsoidal bottom end and a flanged top. The removable semi-ellopsoidal cover, which adds 0.6 m in length, is secured by 48 large bolts. The tank is made of 1.6-cm-thick alloy steel and is thought to have a yield strength of 4.1 MPa (600 psi) or greater.

The principal instrumentation has been an array of 32 thermocouples (see Fig. 1b) and a dynamic-pressure transducer. The present thermocouples are type K, constructed of 0.03-cm-diameter wire with an exposed 0.08-cm-diameter bead. We have tested several other types and sizes of thermocouples, and we plan to eventually replace the present ones with faster-responding models. A Kulite strain-gauge pressure transducer was used to measure dynamic pressure. The sensitive element of the gage was isolated from the burn by ~2 cm of metal felt and a rubber membrane. The intrinsic frequency response of the gauge is ~150 kHz; however, the mounting technique probably limits the actual response to less than 10 kHz. Both pressure and temperature signals were recorded by a multi-channel, digital data-acquisition system.

In addition to the gas temperature and pressure measurements, gas samples were taken before and after most burns and were analyzed with a GC (gas chromatograph) at Sandia. Comparison of pre-burn GC analyses with expected compositions computed from the partial pressures of air and added hydrogen revealed a systematic difference of 10 to 15% in the total hydrogen content. The uncertainty in the partial pressure method is conservatively estimated to be a factor of 3 less than this. Therefore, we have concluded that a systematic error is present in the GC technique (perhaps due, in part, to the sampling process). Partial-pressure measurements were used to establish the pre-burn hydrogen concentrations.

The tank was equipped with two muffin-type mixing fans (see Fig. 1a), 25 cm in diameter and rated at 0.2 m^3/s (450 cfm). These fans were used to mix the contents of the tank before and after hydrogen addition and also before post-burn gas sampling. Post burn gas sampling was performed both with and without mixing and the large differences in results indicated mixing was essential to obtain representative samples. For some shots, fans were also left running during ignition and combustion to provide a source of turbulence.

Following some experimentation with exposed 300 watt photoflood lamp filaments, the standard 14-volt glowplug (General Motors #7G) used in the Sequoyah IDIS system [1] was selected as an igniter. For most cases, the igniter was located 1.2 m from the tank bottom and on the centerline. To obtain a rapid heat-up, approximately 70 volts was applied for the first 1.5 seconds, then two additional glowplugs (located outside the tank) were switched in series for an additional 3.5 seconds. (Igniter lifetime is greatly reduced when operated in this manner; glowplugs must be replaced every 5-8 shots). Other tests were also conducted with 14 volts applied to the glowplug (~ 20 s required for ignition) and with a high-energy (~ 30 j) spark as an igniter.

Experimental Procedure

Test procedure for each shot was as follows: after the tank was sealed, the fans were turned on for about 600 s to eliminate any thermal stratification of the air. Monitoring the pressure* with a Wallace and Tiernan absolute pressure gage (accurate to about 40 Pa), hydrogen was admitted to the tank until the predetermined final pressure was reached. The fans were left on for another 600 s to insure that the hydrogen and air were completely mixed, then the pre-burn gas sample was taken. For the quiescent burns, the fans were turned off about 600 s prior to ignition. The turbulent, or "fans on", burns were ignited while the fans were still running.

Test Series

We have conducted over 90 tests in the VGES burn tank to date. These experiments were conducted as part of ten tests series (TS) as described below:

- TS #1: Glowplug igniter (located 1.2 m from the tank bottom and on the tank centerline). The glowplug was energized with ~ 70 volts for a few seconds. Sixteen burns with 3.8 - 9.1 percent hydrogen and fans on or off during the burns.

* Note that the ambient air pressure in Albuquerque is roughly 83 kPa (0.83 atm).

- TS #2: Raised glowplug igniter position. Similar to TS #1 except that glowplug was raised to the vertical center of the tank. Eleven burns with 4.8 - 15.3 percent hydrogen and fans on or off during the burns.

- TS #3: Spark igniter. Similar to TS #1 except a spark igniter (~ 30 joules) were used in place of the glowplug. Eight burns with 4.8 - 8.3 percent hydrogen and fans on or off during the burns.

- Test #4: 400-torr air. Similar to TS #3 except the initial pressure of air was reduced to 53 kPa (0.53 atm). Nine burns with 5.6 - 10.7 percent hydrogen and fans on or off during the burns.

- TS #5: 200- and 100-torr air. Similar to TS #3 except the initial pressure of air was reduced to either 26 or 13 kPa (0.26 or 0.13 atm). Six burns with 7.4 - 23.4 percent hydrogen and fans on or off during the burns.

- TS #6: Additional nitrogen (partial pre-inerting). Similar to TS #1 and #3 (either spark or glowplug was used as an igniter) except that the initial pressure of air was reduced to 53 kPa (0.53 atm) and nitrogen was added to bring the total initial pressure to 79 kPa (0.79 atm). Twelve burns with 3.9 - 16.7 percent hydrogen and fans on or off during the burns.

- TS #7: 14-volt glowplug. Similar to TS #1 except that the glowplug was activated with 14 volts for 50 seconds. Six burns with 5.7 - 10.7 percent hydrogen and fans on or off during the burns.

- TS #8: Higher hydrogen concentrations. Similar to TS#1 and #3 (either spark or glowplug was used as an igniter) except that higher hydrogen concentrations were investigated. Nine burns with 9.9 - 18.7 percent hydrogen and fans on or off during the burns.

- TS #9: Additional CO_2 (inerting and steam simulation). Similar to TS #1 except that the initial air pressure was reduced to 53 kPa (0.53 atm), then 20 kPa (0.20 atm) of hydrogen was added (the hydrogen concentration at this point was 27.3 percent), and then CO_2 was added to the mixture. Seven burns with 27 -56 percent CO_2 (27 - 93 kPa) and fans off during the burns.

- TS #10: Equipment survivability (Hydrogen Burn Survivability Program). Similar to TS #1 except that CO_2 (to simulate steam) was added to the mixture for some tests. Equipment in the tank consisted of passive and active calorimeters, conduit (with and without internal wires), and cables. Six burns with 10 or 15 percent hydrogen, 0 or 10 percent CO_2, and fans on or off during the burns.

Results

Initial conditions, principal results, and theoretical peak pressures and temperatures are reported elsewhere[2]. Example raw data from a single thermocouple and pressure gage are shown in Fig. 2. The thermocouple signal exhibits a slow initial rise due to its thermal mass and the finite heat transfer rates from the flame front and combustion products to the wires and bead. The decaying signal at later times reflects the cooling of the combustion products by radiative and convective heat transfer to the tank walls.

The principle use of the thermocouple data was in determining a cross section of the flame-front geometry as a function of time. To do this, the breakaway time t_b, defined in Fig. 2a, was used as the effective time that the flame-front arrived at the thermocouple. Both contour plots (showing iso-arrival-time contours) and space-time (x-t) plots of burn-front trajectories were constructed using these data. Examples of contour plots comparing the "fans on" and "fans off" cases for 7.4 and 10.7% H_2 are shown in Fig. 3. These plots were obtained by fitting a fifth-order polynomial to a fine grid interpolated from the array of t_b values. This procedure was implemented in a computer program specifically written for this purpose. Two space-time plots are shown in Fig. 4 comparing 7.4% hydrogen to 10.7% hydrogen combustion.

It is evident from both the contour and x-t plots that the burns were asymmetric, accelerating as the burn front moved up the tank, and that downward propagation and/or convection of the burned gas occurred in portions of the tank. Effective flame velocities (determined by the transit time from the igniter to the top row of thermocouples) increased rapidly as the initial hydrogen percentage was increased and are factors of 4-10 higher with "fans on" as compared with "fans off". Isolated contours for lean mixes suggest the presence of flame globules which have been observed by other investigators.[3] However, due to the sparseness of the thermocouple grid and the nature of the data reduction procedure, these contour plots yield only a qualitative indication of the flame geometry and should not be given undue emphasis.

The initial rise of the pressure signal (Fig. 2b) is due to the flame propagating outward from the igniter. Since the igniter is left on for ~ 5 seconds, it is possible to have more

than a single flame front or even an extended region of combustion within the tank. This makes the analysis of the pressure signal more difficult than in the case of spark ignition.[3] However, comparing pressure traces and burn contours, it becomes apparent that the time at which the flame-front first arrives at the tank top corresponds closely to the time at which the peak pressure is reached. The subsequent decay of pressure is due to the gas temperature decay caused by heat transfer from the hot combustion products to the cold tank walls.

Both the peak pressure rise, Δp, and the pressure rise time, Δt (defined in Fig. 2b), are useful measures of the burn strength. Two additional "figures of merit" can be defined from these quantities: the mean pressure derivative, $\Delta p/\Delta t$, which can be related to chemical energy release rate; and the ratio of peak pressure rise to initial pressure, $\Delta p/pi$, which can be related to the completeness of combustion.[4] Pressure signals from both "fans on" and "fans off" burns are compared in Fig. 5 for the 5.7 and 7.4% hydrogen cases. The influence of convection and turbulence caused by the fans is clearly shown; Δp is larger, Δt is smaller, and the pressure derivatives have increased by factors of 2-8.

"Effective velocity" data were determined for both upward and downward propagation using thermocouple arrival times from thermocouples located on the tank centerline. Most of the values shown in Fig. 6 were calculated directly from the digitized experimental data using a computer code that we developed.

The normalized peak-pressure data for all of the tests in TS #1-8 are plotted in Fig. 7. We observed no significant differences in peak pressure for a given hydrogen concentration for all of the variables except pre-burn gas motion. Burns with the fans on generally produce a higher peak pressure for hydrogen concentrations below 8 percent. It is important to note that the transducers we are using to record pressure are sensitive to changes in temperature; we believe that, for the burns with $\gtrsim$ 10 percent hydrogen, our values for peak pressure may be low.

Test series #9 was conducted in order to determine: (a) the ability of CO_2 to inert an H_2:air mixture or to mitigate the effects of H_2:air combustion; and (b) the degree to which CO_2 will simulate steam (H_2O) in a "cold" test chamber. Normalized peak-pressure data for the burns in this test series are plotted in Fig. 8.

Conclusion

Much of the data from the first ten test series have been incorporated as technical input to various NRC programs, with some data still being analyzed. In particular, we have used the pressure rise time and flame velocity data to develop a computer code that can predict the temperature and pressure response of a nuclear plant containment building to hydrogen combustion.

An important discovery resulting from these tests was the very significant increase in pressure rise time that occurred for lean hydrogen:air mixtures ignited in a non-quiescent state (fans "on"). Ignition of lean mixtures with the fans "off" also produced a greater pressure increase than that reported in earlier studies.[3] These very significant differences are attributed to geometric effects and igniter location.

Low-pressure test results indicate the feasibility of similar tests proposed for a large sphere (2000m^3) at the Nevada Test Site. The partial pre-inerting, CO_2 inerting, and equipment survivability tests have addressed specific questions posed by the NRC.

References

1. M. Berman, M. P. Sherman, J. C. Cummings, M. R. Baer, and S. K. Griffiths, Analysis of Hydrogen Mitigation for Degraded Core Accidents in the Sequoyah Nuclear Power Plant, NUREG/CR-1762, SAND80-2714 (March 1981).

2. Light Water Reactor Safety Research Program Quarterly Report, January-March 1981, M. Berman, editor, NUREG/CR-2163, SAND81-1216 (July 1981); Light Water Reactor Safety Research Program Semiannual Report, April-September 1981, M. Berman, editor, NUREG/CR-2481, SAND82-0006 (February 1982).

3. A. L. Furno, E. B. Cook, J. M. Kuchta, and D. S. Burgess, 13th Symp. on Comb., Comb. Inst., Pittsburgh (1971).

4. Proceedings of the Workshop on the Impact of Hydrogen on Water Reactor Safety, M. Berman, editor, NUREG/CR-2017, SAND81-0661, Vol. III, 173-212 (September 1981).

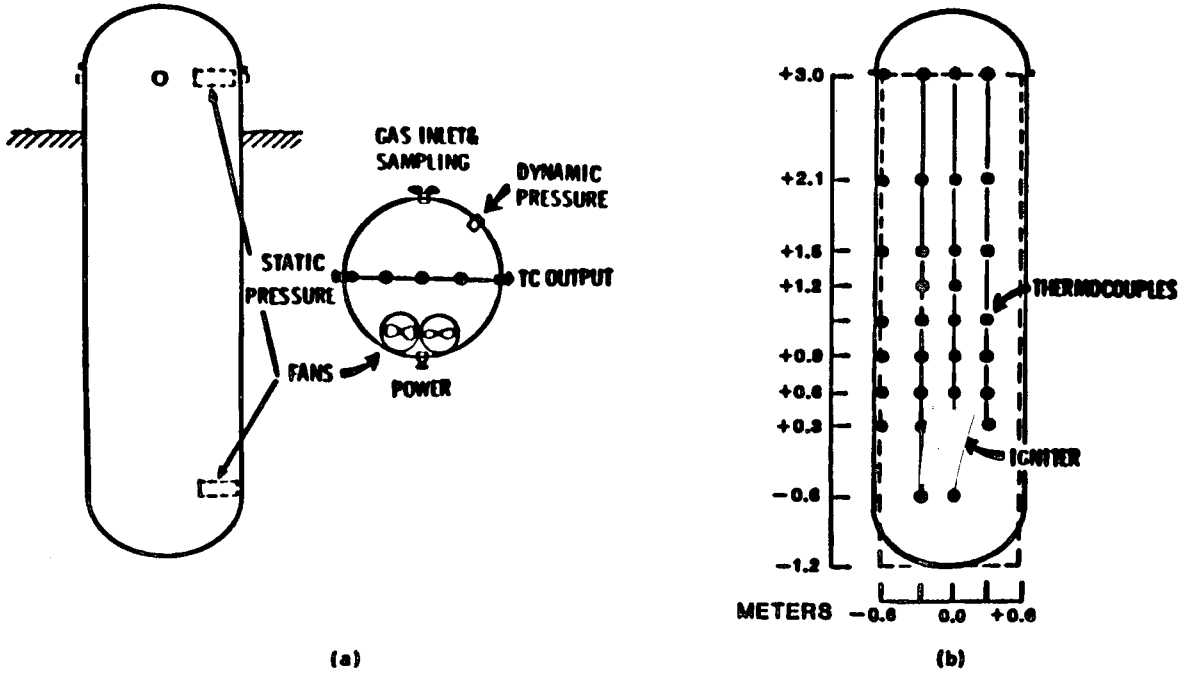
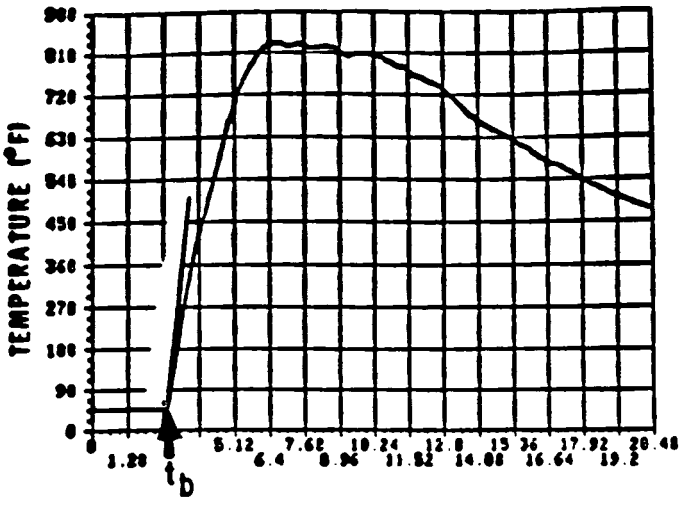
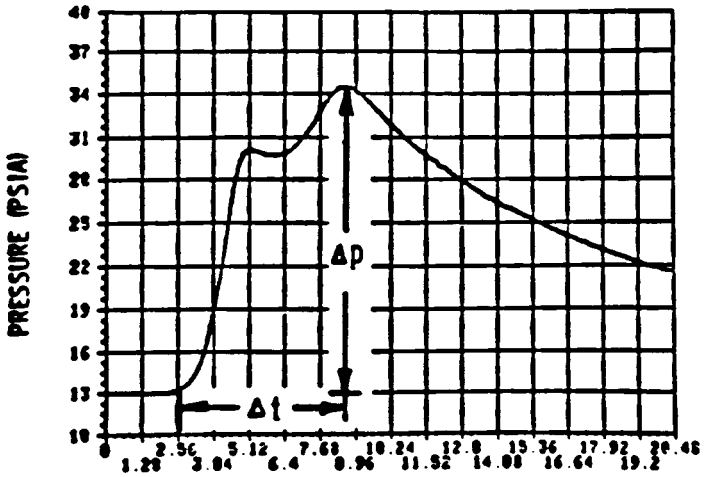


Figure 1. VGES burn tank: (a) setup and (b) thermocouple array.



(a)



(b)

Figure 2. Examples of raw data: (a) thermocouple temperature and (b) tank pressure.

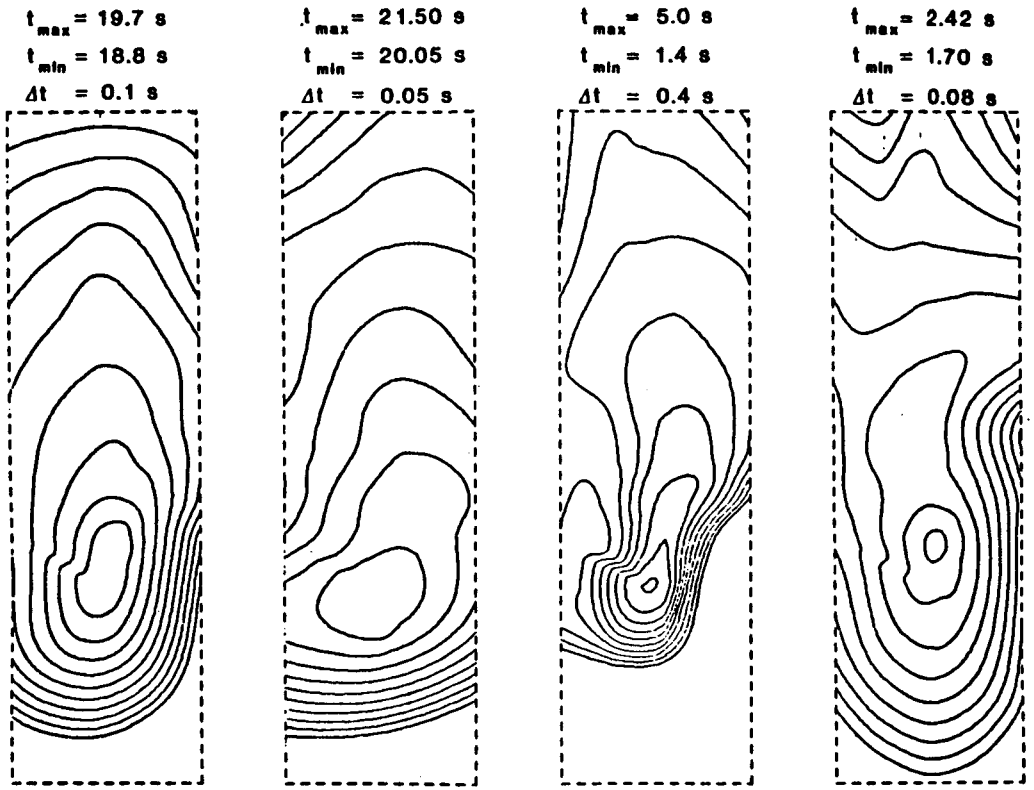


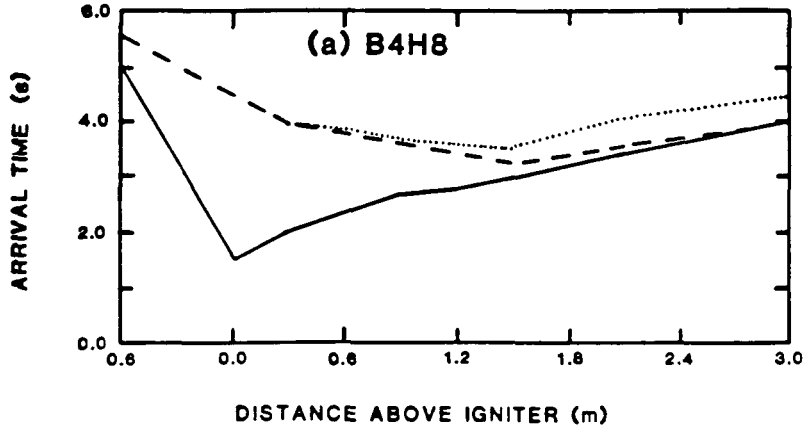
Figure 3. Iso-arrival-time contours for hydrogen:air burns. Dashed lines represent the approximate location of tank walls. The igniter was located at about 0.3 of the tank height from the bottom.

B58H12 - 10.7 % H_2 , fans off.

B59H12 - 10.7 % H_2 , fans on.

B4H8 - 7.4 % H_2 , fans off.

B10H8 - 7.4 % H_2 , fans on.



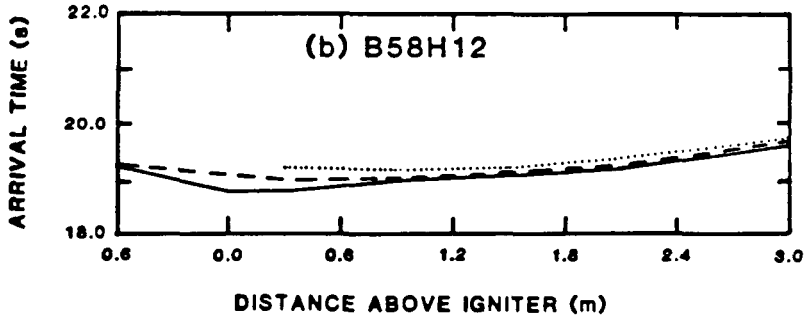
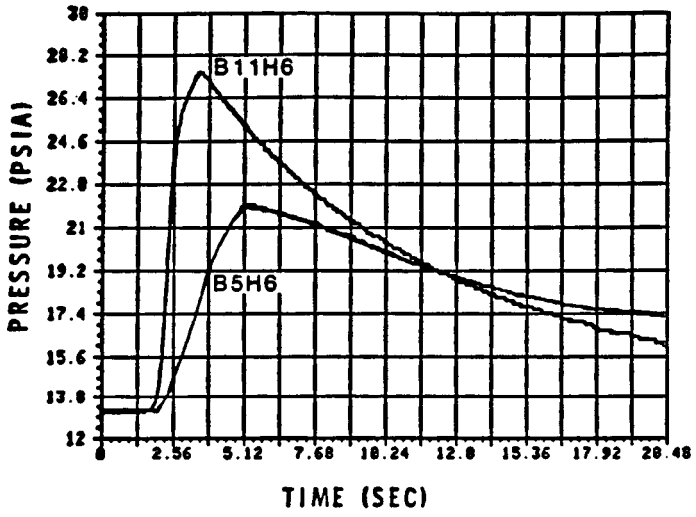


Figure 4. Space-time (x-t) plots for hydrogen:air burns.
(a) B4H8 - 7.4 % H_2 , fans off.
(b) B58H12 - 10.7 % H_2 , fans off.
..... 60 cm from tank centerline,
----- 30 cm from tank centerline,
——— tank centerline.



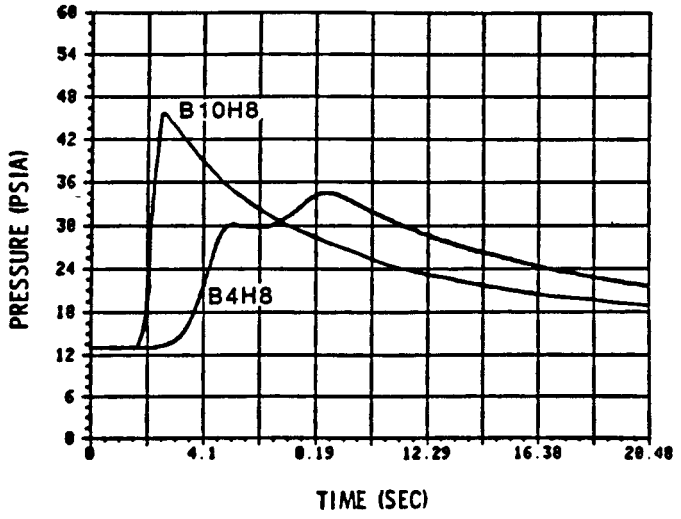


Figure 5. Pressure histories for hydrogen:air burns.

B11H6 - 5.7 % H_2 , fans on.

B5H6 - 5.7 % H_2 , fans off.

B10H8 - 7.4 % H_2 , fans on.

B4H8 - 7.4 % H_2 , fans off.

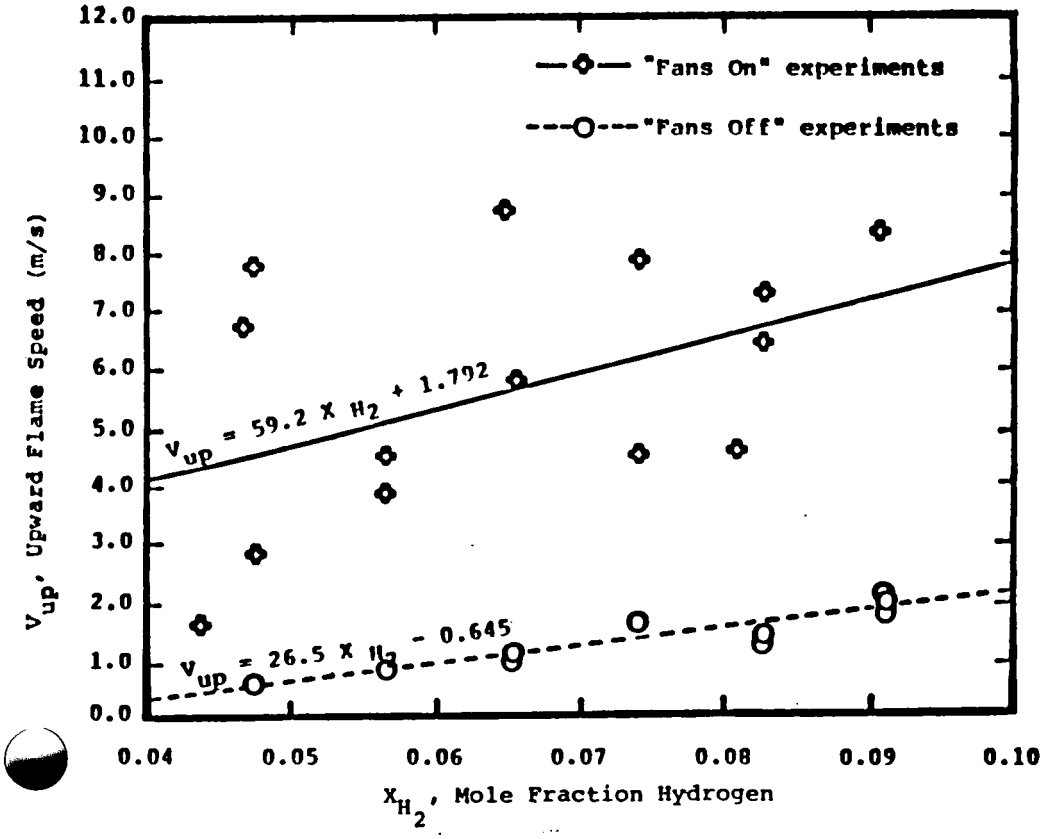


Figure 6. Experimental flame speed for upward propagation.

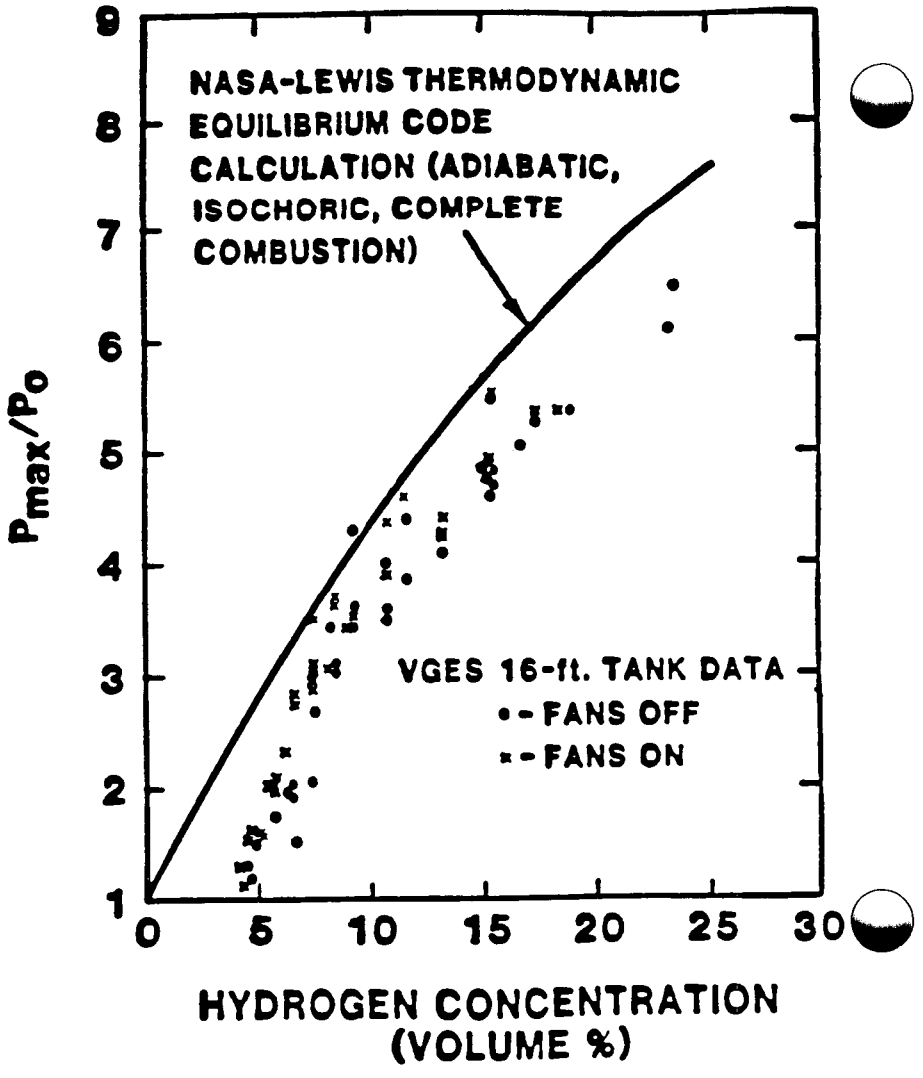


Figure 7. Normalized pressure rise as a function of hydrogen concentration for VGES burn tank tests.

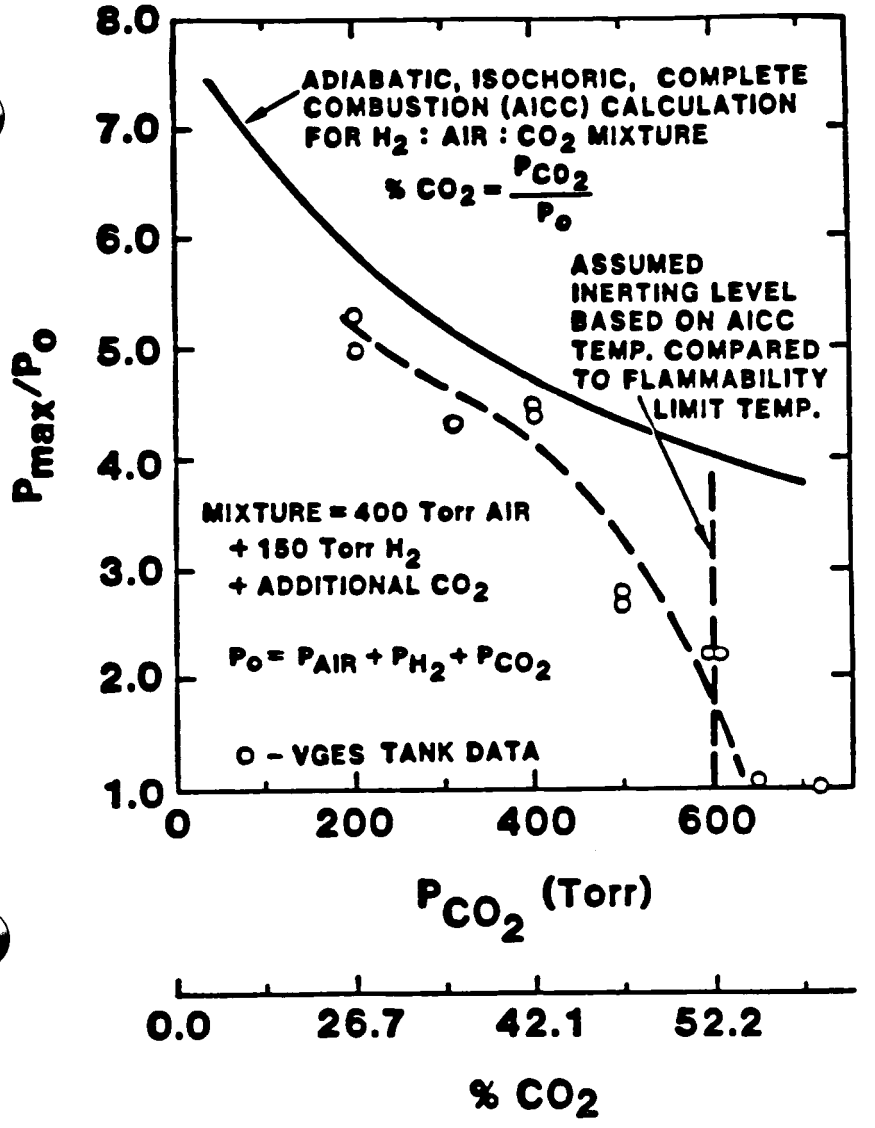


Figure 8. Normalized peak pressure for mixtures of H_2:air:CO_2 .

SESSION Vb

COMBUSTION MODELLING AND EXPERIMENTS

681/6 82

Medium-Scale Combustion Tests of H_2:Air:Steam Systems

S. F. Roller and S. M. Falacy

Sandia National Laboratories

Albuquerque, NM

SAND 82-2390C

ABSTRACT

The first Hydrogen Behavior Program test series, TS #1, is discussed. Combustion of hydrogen and air with and without added steam was done. The ratio of peak to initial pressure is compared to adiabatic, isochoric, complete burn values. The effects of initial temperture and added steam are examined. Future test plans and modifications and additions to instrumentation are discussed.

Sponsored by the
Office of Nuclear Regulatory Research
U. S. Nuclear Regulatory Commission
Washington, D. C. 20555

under FIN No. A-1246 and A-1336

Introduction

The objectives of the Hydrogen Behavior Program are to quantify the threat posed by the hydrogen released during Light Water Reactor (LWR) accidents and to generate information and equipment concepts which will prevent or mitigate that threat. The experimental test plan has been designed to provide verification of and data for analytical models as well as to characterize phenomena that are too complex to be modeled analytically at the present time.

The Fully Instrumented Test Site (FITS) tank is being used to provide data on hydrogen combustion and its mitigation in an intermediate-scale volume in the presence of steam and other diluents. It was originally built for use in the Steam Explosions Program at Sandia under contract with the USNRC.

The tank is a cylinder 3.4 meters high and 1.5 meters in diameter with semi-ellipsoidal heads. It is mounted vertically; the top head is removable and is held in place by 48 1/2" bolts. There are twenty-five access ports of assorted sizes, mostly 6" and 8" diameters. The tank and fittings have been designed to high-pressure boiler standards (1-1/8" thick walls) and have been tested at 300 psi. There is a 250-psi 8"-diameter burst disk in place during all testing.

A number of modifications were done to give the system additional capabilities necessary for hydrogen combustion tests. These include installation of a tank heating system, insulating the tank, providing gas feedthroughs for hydrogen, air, and steam, installing a gas sampling system, and preparing a computer-based data-acquisition system.

The FITS tank was operational for hydrogen combustion experiments in May 1982. The first test series (TS #1) was run for the Hydrogen Burn Survival (HBS) Program. The data were analyzed and reported here by Aragon, McCulloch and Richards[1]. About thirty tests were performed for lean hydrogen (6-15%) and steam (0-40%) burns in air. The initial pressures were greater than ambient and the initial temperatures were about 110°C. Hydrogen Behavior Program instrumentation in these tests was similar to the instrumentation used in the Hydrogen Behavior Program TS #1 discussed below.

In addition to the above instrumentation, special HBS instrumentation included:

* passive calorimeters in several shapes with attached thermocouples,
* 0.5-mil and 5-mil thermocouples to measure gas temperatures,
* thermocouples on the valve and on each mixing fan, and
* Gardon-type heat flux gages.

Hydrogen Behavior Program TS #1 - Description

The first Hydrogen Behavior Program test series was done in July and August 1982. Forty burns were done for the ranges of

* 4-30% hydrogen,
* up to 60% steam,
* initial temperatures of 45°C or 110°C,
* initial pressures greater than ambient, and
* fans off for at least ten minutes before ignition.

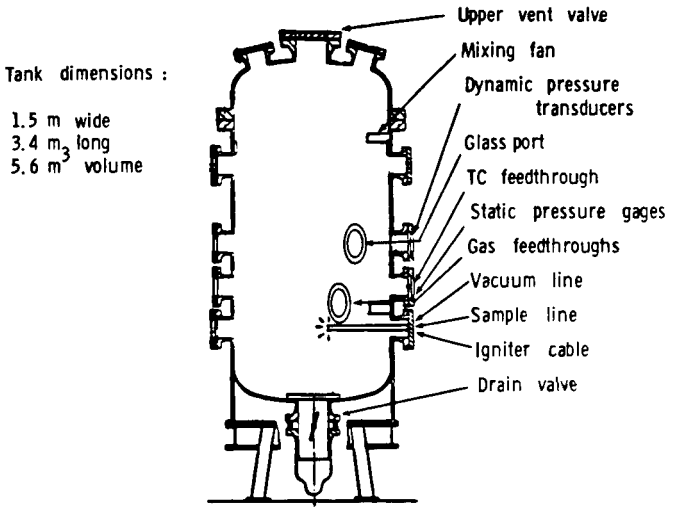


Figure 1. FITS Tank (set up for TS # 1 of the Hydrogen Behavior Program)

Standard instrumentation in the tank included:

* two 0.5-mil thermocouples on a Kapton film,
* thirty-two 12-mil thermocouples,
* four strain-gauge type pressure transducers:
  (a) three air-cooled Precise Sensors with 22–32 kHz resonant frequency
  (b) one Kulite with 80-125 kHz resonant frequency.

The data acquisition system, an LSI 11/23 operating on RT-11 Fortran, used LeCroy analog-to-digital converters. The sampling rates for slow burns were 20 Hz for the 12-mil thermocouples and 500 Hz for the rise and peak of the pressure traces. For fast burns the sampling rates were increased to 200 Hz for the 12-mil thermocouples and 5 kHz for the pressure rise and peak.

The gas composition before the burn was calculated by partial pressure measurements. For "hot" tests with steam added to the pre-burn mixture, the tank was heated to about 110°C before filling to prevent condensation when the steam was added. After the tank was evacuated twice to 1.5 psia with a liquid-ring pump capable of handling the temperatures and condensables, air was allowed into the tank through a vent on the top head. When the pressure stabilized, all valves were closed. Hydrogen was then added to the desired pressure. Before steam was added, the valves in the hydrogen feed line were closed in case ignition occurred accidentally. Steam was added to the desired final pre-burn pressure. During filling the fans were on and were kept on for one minute after the gas feedthrough valve was closed. Condensation was sometimes observed on the glass port used for

monitoring via a video camera, but it usually was gone before the gas was ignited. It was noted that, for higher steam concentrations, it was difficult to reach the desired final pressure. Some of these mixes contained the maximum partial pressure of steam possible at the tank temperature, so it is possible that the steam was condensing in parts of the tank not visible to the video monitor.

Two gas samples were taken before ignition and one was taken after the burn. The sampling bottles and the sampling line were heated. The sample bottle was filled and evacuated to one torr three times before the sample was taken. A sorption pump was used for the evacuation, allowing it to be in the tank room and close to the sample manifold since it contained no spark sources. The sample bottles were taken to Sandia's Analytical Chemistry Division for analysis by gas chromatography. These analyses were done without heating the sample bottles and without measuring the water content. The only measure of the fraction of steam was the partial pressure calculation done for pre-burn compositions.

A comparison of the partial pressure (PP) and gas chromatography (GC) results for hydrogen concentrations is in Table 2. An average of the two GC pre-burn analyses was generally used; however, one of the values was thrown out if it was significantly different from the value that agreed well with the partial pressure calculation. The difference between the partial pressure calculations and the GC analyses, calculated with respect to the PP results as

$$\frac{GC - PP}{PP} \times 100\%,$$

was ± 7% on the average. The trend was for the partial pressure calculation to give the higher hydrogen concentration; only eight of thirty-five GC analyses gave higher values. The high GC results could not be due to leaks in the sampling system. The presence of inhomogeneities in the gas mixture as a function of mixing time will be examined more closely in future work.

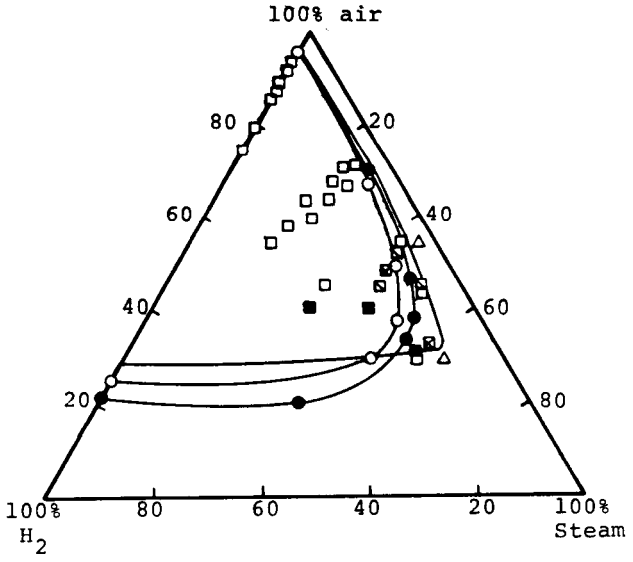
The igniters were located near the bottom of the tank. Ignition was normally by a 32-J spark in this test series. If several discharges did not ignite the mixture, the fans were turned on. If the spark plug still did not ignite the gases, the glow plug was turned on. If, after two minutes, no ignition occurred, the test was recorded as "no burn".

Hydrogen Behavior Program TS #1 - Results

For the test matrix used in this test series (see Figure 2), all but two of the forty tests were ignited. In order to determine the flammability limits for the hydrogen-air-steam system, the matrix needs to be extended to higher steam concentrations for a given hydrogen-air ratio. More accurate gas analysis, as discussed below, will also help in this task.

The pressure transducers used for dynamic pressure measurements were calibrated statically at ambient temperature and at about 100°C before and after the test series. No dynamic calibration was done for this test series; the Sandia Pressure Calibration Laboratory uses Precise Sensor transducers as the standard for their dynamic pressure calibration.

The ratios of maximum pressure to initial (pre-ignition) pressure as measured by the air-cooled Precise Sensors are listed



Flammable Limits (Ref. 2)

——— 75°F - 0 psig

—○—300°F - 0 psig

—●—300°F -100 psig

FITS TS #1

□ burn (1 spark)

▨ burn (more than one spark)

▩ burn (more than one spark and fans on)

■ burn (fans and glow plu

△ no burn

Figure 2 - Hydrogen Behavior Program FITS TS #1
Test Matrix Plotted on the Shapiro-Moffette Diagram

in Table 1 and plotted in Figure 3. The error bars indicate the range of values given by these three transducers. As the plot shows, the pressure ratio decreases as the steam fraction increases for a given percent hydrogen in air. Also, the pressure ratios are higher for the hydrogen-air burns done at initial temperatures of 40-50°C than those for burns at initial temperatures of about 110°C. The magnitude of this effect was about 25%, in agreement with calculations which show that the ratio $\Delta P/P_o$ is inversely proportional to the initial temperature.

A comparison of two pressure traces at about 30% hydrogen is shown in Figure 4. The burn with an initial temperature of 41°C had a higher maximum pressure ratio (9.22) than the burn starting at 111°C (7.09). The same trend for maximum pressure with lower initial temperature was seen at other hydrogen concentrations.

The experimental pressure ratios are compared to theoretical values in Figures 5 to 8. In each of these figures, the abscissa represents the hydrogen content on a dry basis (i.e., without water or steam). The error bars again represent the spread of pressures recorded with the three air-cooled Precise Sensor pressure transducers. One of these (PS 19471) had higher sensitivity and was expected to give the most accurate pressure trace; it tended to give the highest value. It also had an unusual shape at the peak of a few of the traces and usually had a later time for the peak value, as seen

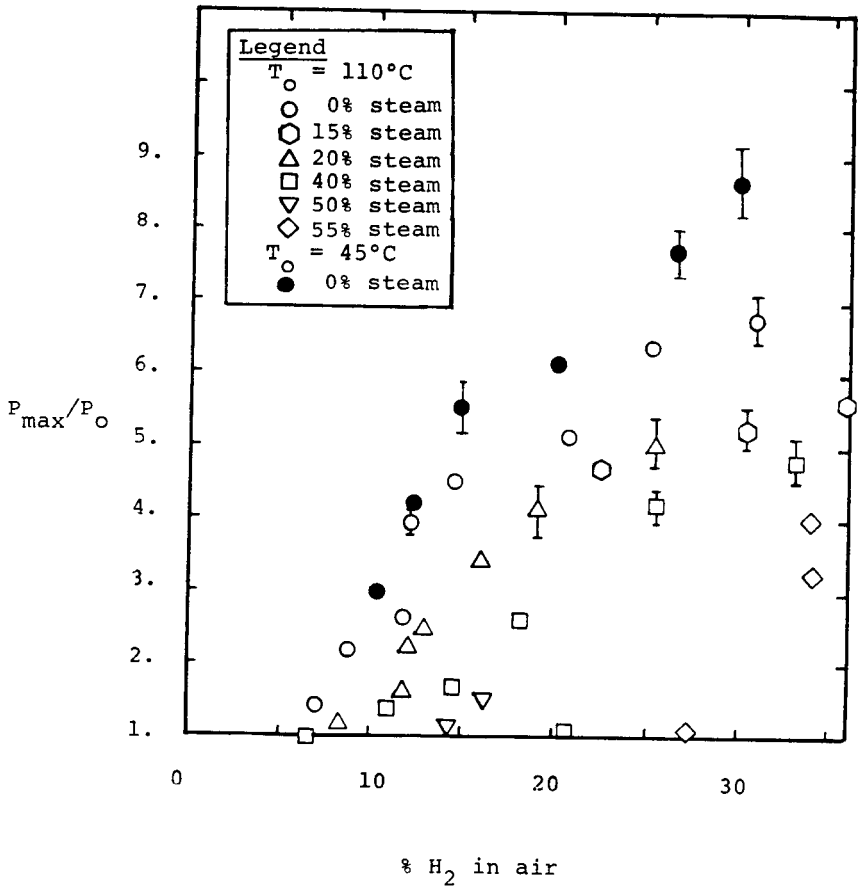


Figure 3. Hydrogen Behavior Program -- FITS TS #1
P_{max}/P_o

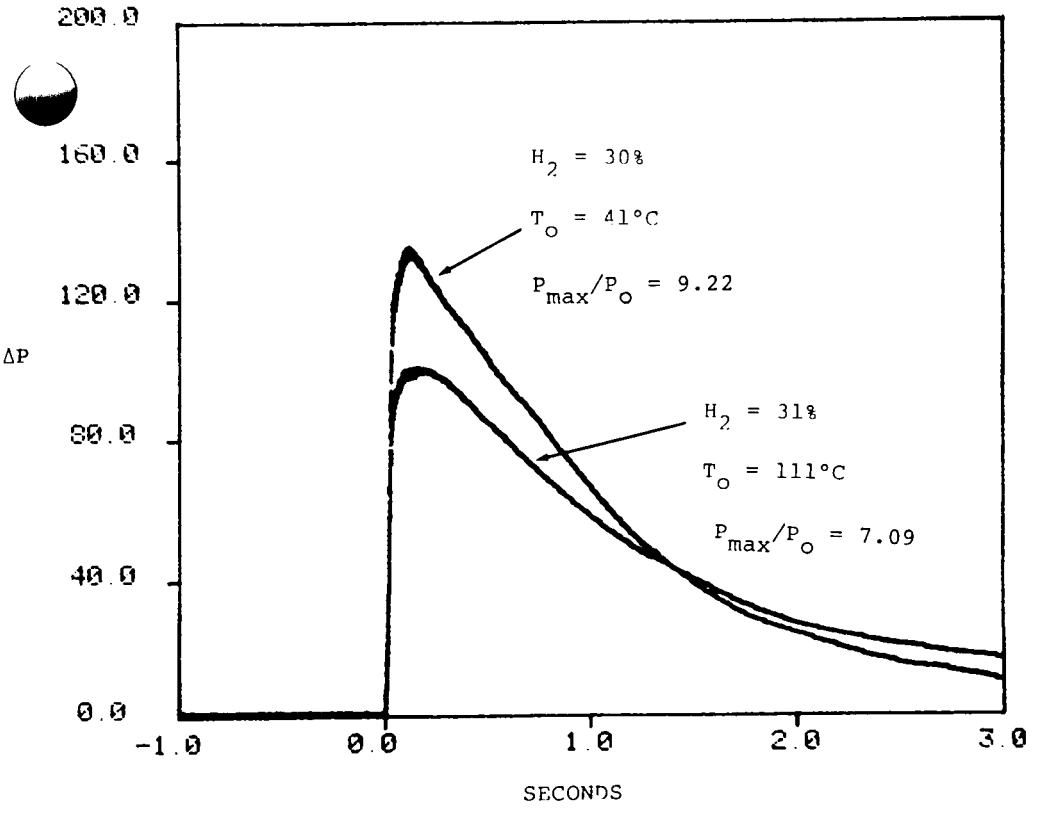


Figure 4. Effect of Temperature on Pressure.

in Table 1, where the time of the peak pressure is listed for PS 16978 and PS 19471. The trend of the values from all three Precise Sensors is similar.

The diaphragm of the Kulite transducer was coated with RTV protect it from the flame, but its response was poor. Peak pressure values from the Kulite were 30% lower than those from the Precise Sensors.

In Figures 5 to 8, the experimental pressure ratios are compared to the theoretical adiabatic, isochoric, complete combustion curves calculated with the NASA complex chemical equilibrium code[3]. The experimental pressure ratios lie below the theoretical curve for hydrogen concentrations in air less than 15%, approaching the theoretical values as the hydrogen percentage increases. For more than 20% hydrogen, the experimental pressure ratios are at or above the theoretical values. This is a result not seen in most previous hydrogen-air combustion tests. Burns done in the Variable Geometry Experimental System (VGES) 16' tank produce experimental data 80 to 100 percent of the theoretical value for hydrogen concentrations greater than ten percent[4] Similar results have been reported for 10 to 45% hydrogen in air at AECL Whiteshell[5] and in the small-scale mini-FITS combustion bomb. One exception is Lowry's test series in a tank at Lawrence Livermore National Laboratories[6]. He measured a pressure ratio greater than the adiabatic value for 12% hydrogen in air. However, his pressure transducers were offset by 6-in. tubes to protect them from thermal transients (see Figure 9).

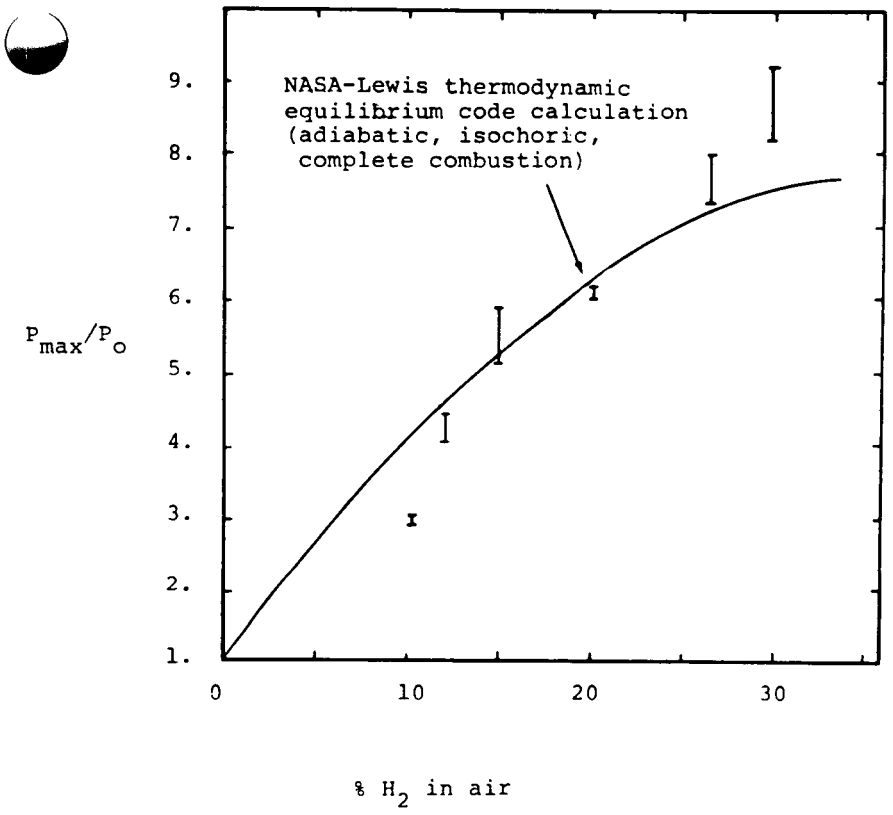


Figure 5. Hydrogen Behavior Program -- FITS TS #1

P_{max}/P_o for 0 - 30% H_2, 0% steam, T_o = 45°C

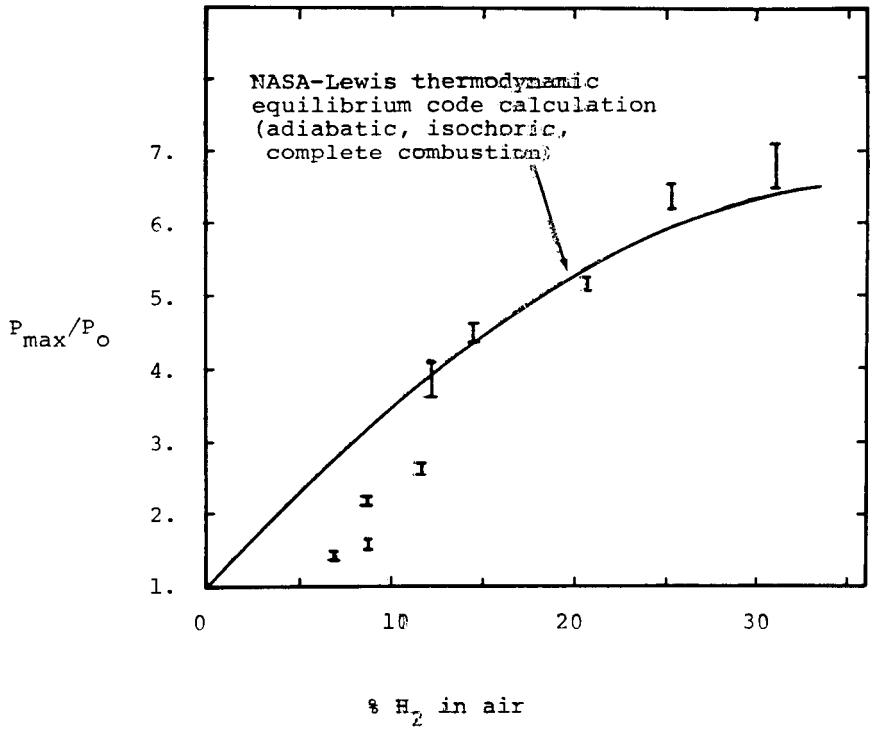


Figure 6. Hydrogen Behavior Program -- FITS TS #1
P_{max}/P_o for 0 - 30% H_2, 0% steam, T_o = 110°C

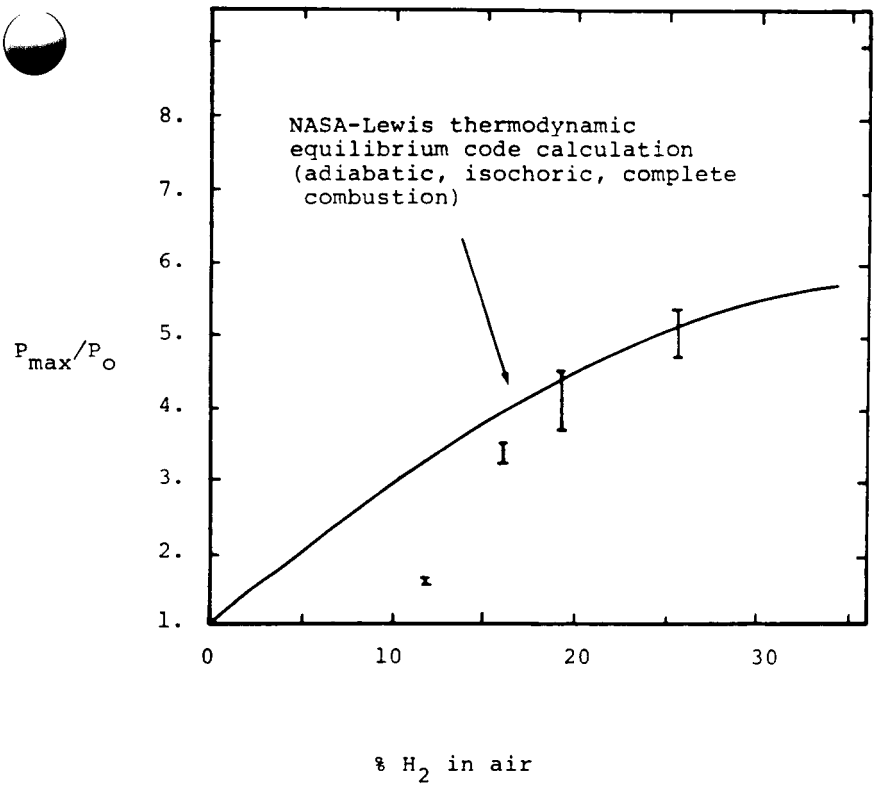


Figure 7. Hydrogen Behavior Program -- FITS TS #1
P_{max}/P_o for 0 - 30% H_2, 20% steam, T_o = 110°C

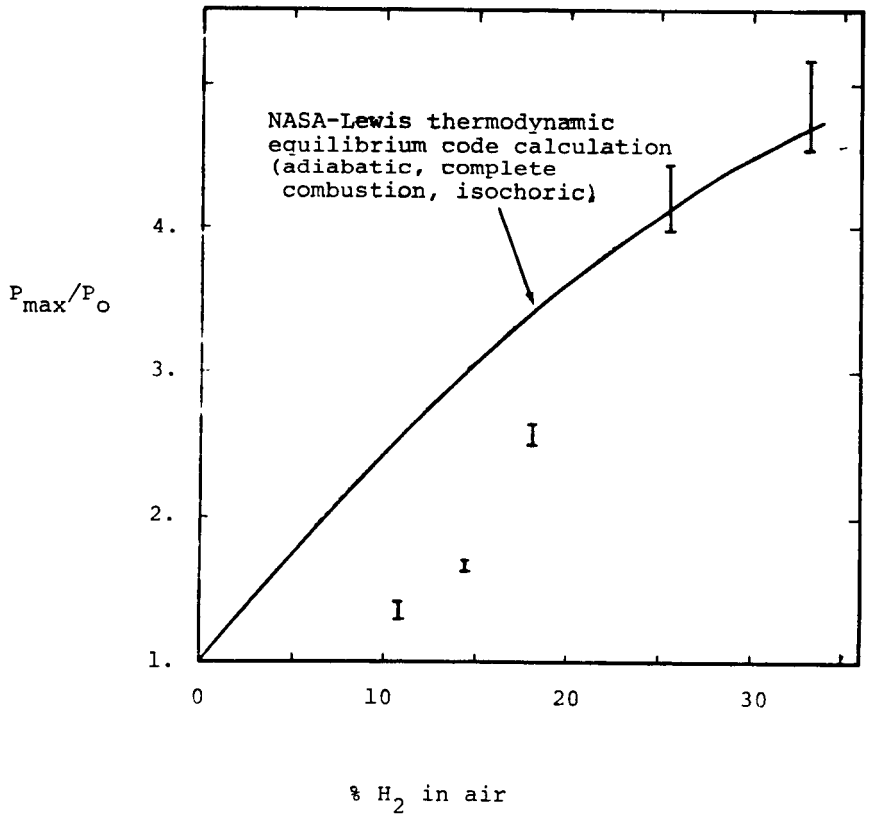


Figure 8. Hydrogen Behavior Program -- FITS TS #1
P_{max}/P_o for 0 - 30% H_2, 40% steam, T_o = 110°C

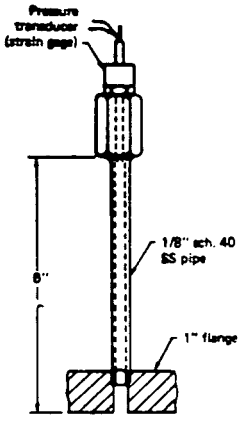


Figure 9a. Pressure transducers were offset by 6-in. tubes to protect them from thermal transients (as shown in Reference 6).

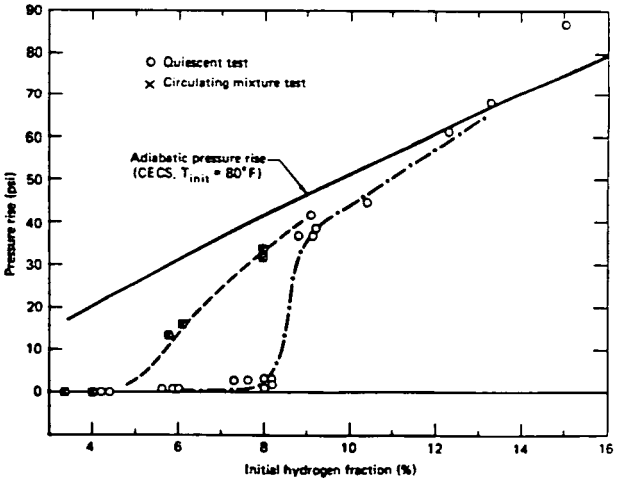


Figure 9b. Pressure rise is shown as a function of hydrogen concentration for dry H_2/air tests (as shown in Reference 6).

FIGURE 9. Lawrence Livermore National Laboratory igniter tests.

One possible explanation of these results is that the air cooling of the diaphragm in the Precise Sensors provides significant protection from the flame effects seen on the Kulite diaphragm, and that the pressures measured in the FITS tank are more correct values, perhaps measuring the effect of dynamic hea on the pressure in fast burns. It has been shown that the effect of heating a strain gage pressure transducer is to lower the gage output[7]. Another possibility is that there is some other error in the Precise Sensor transducer measurements that gives pressures that are too high. This question will be investigated more closely in the next test series, as discussed below.

The finer thermocouples, a 0.5-mil junction on a Kapton film, did not perform as well as expected. They responded more slowly and gave lower peak temperatures than did the 12-mil beaded-type thermocouples. This is probably because the Kapton base and the thermocouple support provided significant thermal inertia. The temperature traces recorded by the 12-mil thermocouples are being used for flame-arrival contour mapping.

Using the GC gas analyses of pre- and post-burn compositions, the extent of the burn was calculated as:

$$\text{fraction burned} = \frac{[H_2]_o - [H_2]_f [N_2]_o / [N_2]_f}{[H_2]_o}$$

where the species in brackets indicate their mole fractions from the GC analyses and the subscripts "o" and "f" mean pre- and post-burn, respectively.

The extent of burn values are tabulated in Table 2 and are plotted in Figure 10. The extent of burn decreases as steam

fraction increases for a given percent hydrogen in air.

Current Improvements

A number of improvements are being implemented for future combustion tests in the FITS tank.

To help resolve the differences in pressure measurements in several facilities as discussed above, some additional transducers and thermal protection of the sensing elements will be used in future test series. Kulite transducers will be used with adapters to hold layers of a felt metal in front of the diaphragm, as has been done in VGES 16' tank burns. Air-cooled Precise Sensors with higher sensitivities will be used. Another type of transducer that will be used is a PCB quartz piezoelectric charge-mode sensor. The model that will be used has a frequency response of 250 kHz. If the correct time constant for the system is used, this transducer can give good resolution of the peak of the pressure trace. If the time constant is too short (less than about 100 times the time to the peak pressure), decay in the circuit will give a low value; if it is too long, the baseline will drift excessively (thermal effects can also cause this).

In future test series in the FITS tank, the pressure transducers will be mounted flush with the tank wall. In past burns, they were mounted at the end of the instrumentation port away from the tank wall. These ports are seven inches deep and seven inches in diameter. Having the transducers mounted flush with the tank wall will eliminate possible interaction of the pressure wave with the instrumentation port.

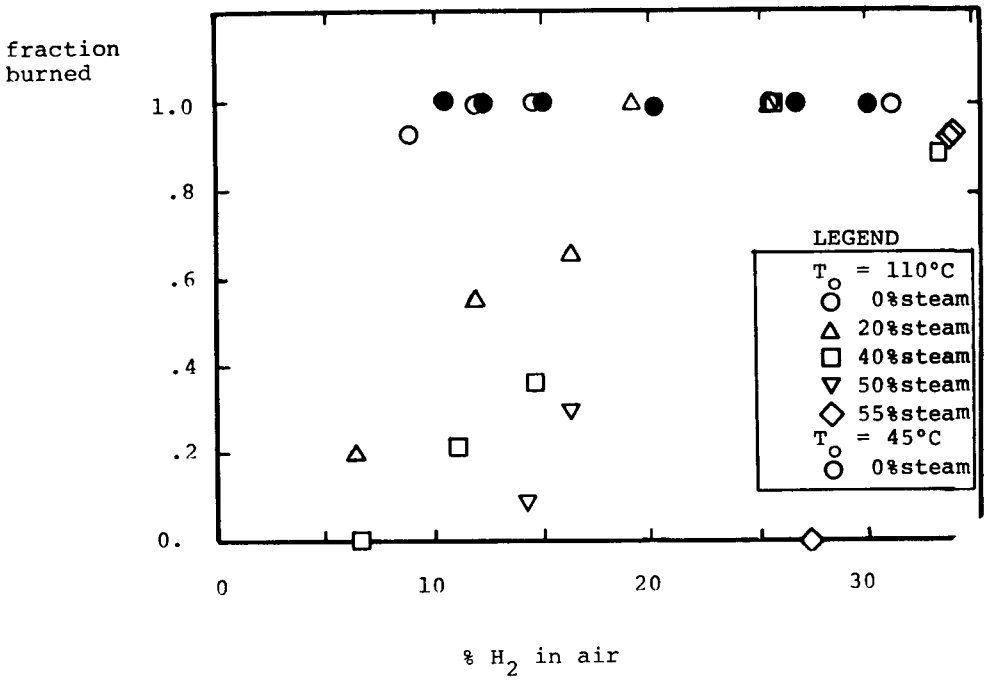


Figure 10. Hydrogen Behavior Program -- FITS TS # 1
ent of Burn

The thermocouples will be mounted on a support designed to give more protection to the wires and less blockage to the gas flow. A range of sizes of beaded-type thermocouples will be used, from two mils to twelve. From the peak temperatures measured by the thermocouples with different response times, a better idea of the peak gas temperatures can be derived.

Thin-film heat flux gages are being designed and built by J. E. Shepherd and O. B. Crump of Sandia. The response time will be about 10 μsec and the heat flux sensitivity will be about 0.1 W/cm^2, appropriate values for the combustion tests to be done in the FITS tank.

Gas sample analysis will be done on-site for future test series. A gas chromatograph has been installed at the test site. It is designed to give good sensitivity for hydrogen as well as the other species present in the system. This system will provide better analyses for several reasons:

* the measurement will be of the amounts of all significant species present, not just a dry analysis excluding the steam fraction,
* the analyses can be done on-site and on-line and can be repeated if necessary, until they converge,
* these samples, analyzed at the time of the test, can be used to determine the mixing needed to achieve a homogeneous composition, and
* the column packings were selected specifically for analysis of the species present in FITS tests.

FY 83 Test Plan

The next Hydrogen Behavior Program test series, due to start in November, will compare hydrogen-air-steam and hydrogen-air-CO_2 burns.

Other test series planned for FY 83 will examine:

* the mitigation effect of water sprays on hydrogen-air combustion over a range of fog densities feasible in the FITS tank, and
* the anomalous thermal igniter experimental results reported by Lowry[6], providing enough spatial and temporal resolution of composition and phase gradients to explain these results (if possible).
* a second test series to be performed for the HBS project.

Summary

Experiments are being done in the FITS tank to provide data on hydrogen combustion and its mitigation. After performing a test series for the Hydrogen Burn Survivability Program, the first Hydrogen Behavior Program test series was done in July and August 1982. Results include:

* pressure ratios were significantly higher for burns started at 45°C than for burns started at 110°C,
* experimental pressure ratios were lower than the theoretical values for hydrogen concentrations below 15% but were on or above the theoretical curve for concentrations in the 15-35% range,
* the Kulite gave peak pressure values 30% below those from the air-cooled Precise Sensor transducers on the average,

- the extent of the burn decreased as the steam fraction increased for a given hydrogen-air ratio.

Improvements are planned in instrumentation and gas sample analysis being done for future test series. The FY 83 test plan was also discussed.

TABLE 1 - Hydrogen Behavior Program - FITS TS #1 - Temperature & Pressur Data

TEST ID 1982	T_{max}, °C (TC17)	Precise Sensor Transducers P_{max}/P_o PS16978	PS19471	PS16979	t_{pmax}, s PS16978	PS19471
7/23 12:30:59	243	1.16	1.18	——	.52	.84
7/23 No Burn	NB[1]	NB	NB	NB	——	——
7/23 16:00:39	325	1.42	1.41	1.40	2.20	2.17
7/23 17:00:59[2]	278	1.31	1.39	1.29	3.42	5.15
7/23 17:44:29	564	2.16	2.18	2.19	3.45	2.14
7/23 18:21:54	736	3.60	3.98	4.07	.83	.83
7/26 15:12:48[3]	187	1.14	1.16	1.13	5.10	2.92
7/27 14:07:42	458	1.65	1.68	1.64	3.69	3.28
7/27 14:53:12[3]	401	1.64	1.68	1.64	——	——
7/27 16:07:03	349	1.51	1.56	1.48	2.85	2.80
7/27 16:45:50	643	2.60	2.70	2.54	2.27	2.61
7/27 18:27:58	627	2.49	2.62	2.71	4.33	4.33
7/28 No Burn	NB	NB	NB	NB	——	——
7/28 14:38:55	675	2.46	2.54	2.46	3.83	3.90
7/28 15:49:56[3,4]	112	1.07	1.08	1.06	1.58	1.76
7/28 17:35:37	741	3.30	3.52	3.54	1.13	1.33
7/28 18:43:41[3,4]	112	1.07	1.12	1.05	1.28	1.71
7/28 20:04:29	773	4.44	4.61	4.39	.47	.43
7/30 15:23:54	885	3.81	4.49	3.73	.76	.78
7/30 17:12:23	1057	5.13	5.22	5.07	.18	.23
7/30 18:01:10[3]	936	4.08	4.42	3.97	.76	.89
7/30 19:06:15	1020	4.74	5.37	——	.24	.40
7/30 20:35:07[3,4,5]	870	——	3.98	——	.71	.84
8/3 15:05:27[3,4,5]	1097	4.55	5.15	4.80	.23	.28
8/3 16:49:51	1170	6.24	6.50	6.34	.13	.19
8/4 09:39:07	1013	4.51	5.37	4.93	.26	.26
8/4 11:34:17	1121	6.46	7.11	6.77	.12	.16
8/4 12:40:52[3,4,5]	961	4.34	4.89	4.52	.17	.26
8/4 13:33:48	868	3.31	3.21	——	2.28	2.37
8/4 14:35:55	1054	5.48	5.73	5.59	.11	.27
8/4 15:26:00	1026	5.18	5.55	5.04	.09	.22
8/4 16:19:32	835	4.70	4.75	——	.31	.31
8/5 11:42:32[6]	1100	8.17	9.20	8.84	.08	.12
8/5 13:28:16[6]	——	7.34	8.02	7.80	.09	.20
8/5 14:41:23[6]	——	6.03	6.20	6.13	.17	.29
8/5 15:31:14[6]	——	5.30	5.89	5.19	.54	.54
8/5 16:23:18[6]	——	4.06	4.37	4.04	.96	1.03
8/5 17:27:01[6]	——	2.98	2.99	——	3.55	3.44

Notes to Tables 1 and 2

1 NB - No burn.
2 Condensation seen on glass port at ignition time.
3 More than one spark needed for ignition.
4 Fans on during burn.
5 Ignition by glow plug.
6 To = 45°C instead of 110°C.
7 Average of two samples unless otherwise noted.
8 Bad value (w/ref. to partial pressure calculations) thrown out.
9 Two post-burn samples were taken on this and previous burns.
10 ND - None detected.

TABLE [redacted] Hydrogen Behavior Program FITS TS #1 - Gas Composition Data

TEST ID 1982		Partial Pressure (PP) Calculations % of Total H_2	Partial Pressure (PP) Calculations % of Total H_2O	Partial Pressure (PP) Calculations % H_2 in Air	Gas Chromatography (GC)[7] Pre-Burn H_2	Pre-Burn O_2+Ar	Pre-Burn N_2	Post-Burn H_2	Post-Burn O_2+Ar	Post-Burn N_2	GC-PP PP	H_2 Fraction Burned
7/23	12:30:59	6.39	22.85	8.28	8.40	12.89	78.71	6.49	18.68	74.84	———	.19
7/23	No Burn	3.75	42.74	6.56	5.62	18.90	75.48	———	———	———	-.14	NB
7/23	16:00:39	6.93	———	6.93	———	———	———	3.75	19.29	76.96	———	———
7/23	17:00:59[2]	6.66	39.12	10.94	10.08	18.74	71.18	8.22	18.21	73.58	-.08	.21
7/23	17:44:29	8.66	———	8.66	6.	19.52	74.76	.52	18.22	81.26	-.22	.93
7/23	18:21:54	12.19	———	12.19	11.48	18.60	70.22	ND[9]	16.83	83.18	-.06	1.00
7/26	15:12:48[3]	7.49	47.31	14.21	12.41	18.28	69.30	11.54[9]	17.75	70.72	-.13	.09
7/27	14:07:42	9.35	20.49	11.76	10.62[8]	19.31	70.07	5.27	17.86	76.87	-.10	.55
7/27	14:53:12[3]	8.77	39.12	14.41	13.23[8]	18.68	68.08	9.09	17.55	73.36	-.08	.36
7/27	16:07:03	8.32	48.62	16.18	16.24	17.64	66.26	12.27	16.12	71.61	.004	.30
7/27	16:45:50	11.76	———	11.76	———	———	———	tr	17.18	82.82	———	1.00
7/27	18:27:58	10.95	39.39	18.06	16.88	17.87	65.25	———	———	———	-.07	———
7/28	No Burn	10.22	59.64	25.33	24.88	15.45	59.68	———	———	———	-.02	NB
7/28	14:38:55	10.21	23.38	13.33	12.58	18.23	69.19	ND	17.36	82.65	-.06	1.00
7/28	15:49:56[3,4]	12.49	39.52	20.65	21.60[8]	6.35	72.05	12.84	17.89	69.27	.05	.38
7/28	17:35:37	12.78	20.17	16.01	15.08	16.29	68.65	5.91	14.54	79.55	-.06	.66
7/28	18:43:41[3,4]	12.27	55.02	27.28	26.72	14.97	58.32	26.38	15.95	57.67	-.02	.002
7/28	20:04:29	14.43	———	14.43	13.64	17.56	68.80	tr	14.54	85.46	-.05	1.00
7/30	15:23:54	15.09	21.17	19.14	20.22[8]	16.58	63.12	tr	11.56	88.44	.06	1.00
7/30	17:12:23	20.64	———	20.64	24.86[8]	15.59	59.55	———	———	———	.20	———
7/30	18:01:10[3]	15.28	40.06	25.49	24.36[8]	15.70	59.94	ND[10]	7.02	92.98	-.04	1.00
7/30	19:06:15	20.27	20.27	25.42	25.80[8]	15.61	58.88	ND	14.16	85.84	.01	1.00
7/30	20:35:07[3,4,5]	15.68	53.82	33.97	31.91	13.96	54.14	4.39	.056	95.05	-.06	.92
8/3	15:05:27[3,4,5]	20.11	39.29	33.13	33.32[8]	14.64	52.04	6.43	1.23	92.34	.01	.89
8/3	16:49:51	25.21	———	25.21	25.15[8]	16.35	58.50	tr	5.26	94.74	-.002	1.00
8/4	09:39:07	25.11	29.76	35.76	35.16[8]	14.00	50.85	8.66	1.99	89.35	-.02	.86
8/4	11:34:17	30.90	———	30.90	29.36[8]	15.66	54.78	tr	1.61	98.39	-.05	1.00
8/4	12:40:52[3,4,5]	30.34	29.94	43.30	43.39	10.38	46.23	24.54	1.08	72.42	.002	.64
8/4	13:33:48	15.42	54.78	34.09	33.51	14.33	52.17	4.38	1.28	94.34	-.02	.93
8/4	14:35:55	30.43	15.24	35.90	———	———	———	6.07	5.93	88.00	———	———
8/4	15:26:00	25.61	15.87	30.43	27.71	15.61	56.60	tr	2.99	97.01	-.09	1.00
8/4	16:19:32	19.24	17.53	23.33	20.65	16.43	62.93	tr	10.32	89.65	-.11	1.00
8/5	11:42:32[6]	29.99	———	29.99	27.17[8]	14.58	58.25	tr	2.35	97.65	-.09	1.00
8/5	13:28:16[6]	26.53	———	26.53	25.00[8]	15.95	59.05	tr	11.87	88.13	-.06	1.00
8/5	14:41:23[6]	20.04	———	20.04	18.53	17.29	63.83	tr	11.80	88.20	-.08	1.00
8/5	15:31:14[6]	14.86	———	14.86	13.23[8]	18.70	68.07	tr	15.06	84.94	-.11	1.00
8/5	16:23:18[6]	12:35	———	12.35	10.97	17.90	71.13	tr	15.74	84.26	-.11	1.00
8/5	17:27:01[6]	10:37	———	10.37	7.66	18.69	73.65	tr	17.66	82.34	-.26	1.00

(Notes are below Table 1.)

References

1. J. Aragon, W. H. McCulloch, B. Richards, "Hydrogen Burn Survival Experiments", presented at the Second International Workshop on Water Reactor Safety, October 3-7, 1982, Albuquerque, NM.

2. Z. M. Shapiro and T. R. Moffette, "Hydrogen Flammability Data and Application to PWR Loss-of-Coolant Accident", WAPD-SC-545, Bettis Plant, September 1957.

3. S. Gordon and B. J. McBride, "Computer Program for Calculation of Complex Chemical Equilibrium Compositions, Rocket Performance, Incident and Reflected Shocks, and Chapman-Jouguet Detonations", NASA SP-273, 1971.

4. W. B. Benedick, J. C. Cummings, and P. G. Prassinos, "Experimental Results from Combustion of Hydrogen: Air Mixtures in an Intermediate Scale Tank", presented at the Second International Workshop on Water Reactor Safety, October 3-7, 1982, Albuquerque, NM.

5. H. Tamm. R. K. Kumar, and W. C. Harrison, "A Review of Recent WNRE Experiments on Hydrogen Combustion", presented at the Second International Workshop on Water Reactor Safety, October 3-7, 1982, Albuquerque, NM.

6. W. E. Lowry, B. R. Bowman, B. W. Davis, "Final Results of the Hydrogen Igniter Experimental Program", NUREG/CR-2486.

7. C. K. Chan and M. E. Simpson, "Thermal-transient Effects on Pressure Measurements", Experimental Mechanics, September 1979, p. 324-330.

WATER FOG INERTING OF HYDROGEN-AIR MIXTURES

Robert G. Zalosh and Satya N. Bajpai*
Factory Mutual Research Corporation
Norwood, Massachusetts 02062

ABSTRACT

Laboratory tests have been conducted to determine the effects of water fog density, droplet diameter and temperature on the lower flammable limit (LFL) of hydrogen-air-steam mixtures. Five different fog nozzles were used to generate dense fogs with volume mean drop diameters ranging from 20 micro-meters to 115 micro-meters. At 20°C, these nozzles marginally raised the hydrogen LFL from 4.0 vol. % hydrogen to typically 4.8%, with one exceptional nozzle producing an LFL of 7.2%. At 50°C, the LFL in the presence of dense fog ranged from 5.0 to 7.9%, while at 70°C, the range was 5.9 to 8.5%. Fog densities required to achieve a given level of partial inerting increased with approximately the second power of average drop diameter, as predicted by a theoretical flame quenching analysis.

INTRODUCTION

One of the hydrogen control methods that has been suggested for reactor buildings is a water fog system, probably in conjunction with a distributed ignition system. The water fog system would fill the containment volume or a critical subcompartment with a high-density fog prior to and during controlled combustion of hydrogen by the distributed ignition system. It has been suggested[1] that heat absorption by the water fog would maintain peak combustion temperatures and pressures at relatively low values as evolved hydrogen is gradually consumed. Adiabatic, isochoric combustion calculations[1] which include fog droplet evaporation effects, indicate that fog concentrations on the order of 10^{-4} g-water/cm^3-gas-mixture can significantly reduce containment pressures compared to dry combustion at the same hydrogen concentration.

The EPRI hydrogen control test program has included intermediate-scale tests to verify the mitigating effects of water fogs and sprays during various

* Presently at Stone & Webster Engineering Corporation, Boston, Massachusetts

combustion scenarios. Prior to conducting these intermediate-scale tests (which are described in the paper by Torok et al[2] at this workshop), Factory Mutual Research (FMRC) was commissioned to determine any inerting effects caused by adding water fogs to normally flammable hydrogen-air mixtures. In particular, laboratory tests were performed to characterize fogs produced by commercial fog nozzles and to ascertain how these fogs influence lower flammable limit (LFL) hydrogen concentrations. The FMRC experimental approach has been similar to that previously used by Sapko et al[3] for methane-air mixtures. Experimental procedures and equipment are described in the following section.

TEST APPARATUS AND EXPERIMENTAL PROCEDURES

Hydrogen-Water Fog Inerting Apparatus

A schematic view of the experimental setup is shown in Figure 1. The inerting tube is a 15-cm i.d., 1 meter long (18-liter) vertical Plexiglas tube. Premixed hydrogen-air mixtures entered the top of the tube in which the fog nozzle was installed. The gas mixture and suspended fog flowed down and out the bottom of the tube through a polypropylene funnel which aided water collection and eliminated air updrafts. Nominal gas mixture flow rates were 10-20 l/min as determined by flow meters in the inerting tube inlet lines.

Five different nozzles were used to obtain a range of fog concentrations and drop sizes. The nozzles were: 1) a SPRACO impingement-type nozzle (#2163-7604), 2) a SPRACO hollow cone nozzle (#2020-1704), 3) a SPRACO hollow cone misting nozzle (#1806-1605), 4) a SPRACO impactor type nozzle (#1405-0604), and 5) a Sonicore (Model 35H) air-driven fog nozzle which used the hydrogen-air mixture as the atomizing medium. Figure 2 is a photograph of these five nozzles. Distilled water for the fog nozzles was supplied from an electrically heated hot water tank pressurized by nitrogen. The fog nozzle is located ~20 cm below the top of the inerting tube.

Ignition electrodes were located at the center of the inerting tube for most tests. The electrodes were machined from a ~6 mm brass rod to produce the needlepoint shape. A spark gap of ~3 mm is allowed between the needle

points. During an ignition attempt, the electrodes were energized by a transformer with secondary coil (i.e., output) voltage of 8,400 V and current of 20 mA. The calculated spark energy is 2.8 Joules/cycle. In a few tests the electrodes were replaced by a glow plug (General Motors Model 7G AC) energized by a 14 Vac transformer. Prior to activating either the ignition electrodes the glow plug, uniform gas and fog concentrations were established in the be by allowing the gas/fog flow to sweep out six tube volume changes.

Flame propagation in the inerting tube was monitored by three chromel-alumel thermocouples with a bead diameter of ~0.3 mm. Two thermocouples were located 5 cm above and 5 cm below the ignition electrodes and the third thermocouple was 15 cm above the electrodes. The beads of all three thermocouples were approximately on the centerline of the inerting tube. Thermocouple response signals were fed to an oscillograph to indicate whether or not the hydrogen-air mixture was ignited. If either of the three thermocouples responded during an ignition attempt, the mixture was considered to be flammable. Actually, only the thermocouples above the igniter indicated the presence of flame; thus, flame propagation was upward only.

Successful ignitions were confirmed by the deployment of three pressure relief vents situated in the closure cap at the top of the flammability tube. The vents which were 4-cm diameter aluminum disks, fluttered as a result of any incipient pressure rise in the tube.

Droplet Size and Concentration Measurement

The droplet size distribution and droplet concentration produced by the fog nozzles were determined by means of a KLD Associates DC-2 Drop Size Measurement Probe. The operation of this KLD Drop Size Measurement Probe is conceptually similar to hot-wire-anemometer operation. Local cooling caused by droplet atachment to a hot wire changes the electrical resistance of the wire. us, the voltage is reduced by an amount proportional to the diameter of the oplet attached to it. With appropriate counting electronics, the droplet size distribution can be obtained. A more complete discussion of the KLD Drop Size measurement technique is provided in a paper by Magnus et al[4].

Drop size measurements using the probe were made in both the inerting tube and in an unconfined fog. In the inerting tube, the probe was located at the ignition location, i.e., about 33 cm below the nozzle. In unconfined fogs, the probe was also located about 33 cm directly below the nozzle centerline.

If droplet velocities are known, fog concentrations can also be obtained from the droplet counts and sample collection time. Thus, the droplet number density may be defined as the number of drops counted divided by the sample volume. The droplet number density, n_i, corresponding to each droplet size interval is calculated by the expression:

$$n_i = \frac{K_i N_i}{v \cdot t \cdot \ell (D_i + d)}, \text{ Drops/cm}^3 \qquad (1)$$

where:

K_i = captive area factor, i.e., small droplet trajectory/velocity deviation caused by wire sensor. The factor is unity for drops >8.7 μm;

N_i = droplets counted in the ith channel;

v = flow velocity (cm/s);

t = counting time interval(s);

ℓ = sensor length (0.1 cm);

D_i = average droplet diameter for the ith channel (varies from 1.3 to 366 μm);

d = sensor wire diameter (5×10^{-4} cm).

Fog mass concentration, $C(g/cm^3)$, is related to the number density distribution by

$$C = \frac{\pi}{6} \rho_w \sum_i n_i D_i^3 \qquad (2)$$

where ρ_w is water density and n_i is given by Eq. (1). Fog volume fraction is calculated similarly, but without the density factor, in Eq. (2).

Fog concentrations computed in this manner are only as accurate as the accuracy of the assumed flow velocity, v, in Eq. (1). Two alternative calculation procedures have been used with two different assumed values for v:

1. The average gas velocity, v_f, flowing through the tube was used. However, this velocity was only 1-2 cm/s, which is less than the terminal velocity, v_t, for the larger drops in the fog.

2. Therefore, a second calculation procedure was also used in which the droplet velocity in Eq. (2) was assumed to be either v_f or v_t, depending on which value was larger for a channel of given size.

In view of the uncertainty involved in using the DC-2 probe data to calculate fog concentration data, another independent method, previously used by Lapko et al[3] was used here also. This consisted of simply collecting water for a known interval in a dish of ~14 cm i.d. inserted into the bottom of the inerting tube such that there was a clearance of ~5 mm between the tube and the collector dish. By knowing the rate of water collection and the volumetric flow of the hydrogen-air mixture, the water/gas flux ratio was calculated. To the extent that the droplet and gas mixture residence times in the tube are comparable, this flux ratio is also a measure of fog concentration.

FOG CONCENTRATION AND DROPLET SIZE DATA

Data from the KLD drop size probe were processed to determine water fog concentration and drop size distributions. Cumulative log-probability plots of the drop size distributions were obtained at various pressures and temperatures. A sample plot is shown here as Fig. 3. The linear relationship shown in these plots implies[5] that the drop diameters satisfied a log-normal distribution. The "average" diameter in these distributions has been represented by number median diameter, number mean diameter, volume mean diameter, and Sauter mean (volume to surface area ratio) diameter. Tabulated values of all these average diameters and the complete set of drop site distribution plots for the various test conditions are provided in the full FMRC report to EPRI[6]. Tables 1 and 2 list values for the number median and volume mean diameters at various nozzle pressures and temperatures.

For a given pressure and temperature, the five nozzles produced average drop sizes that usually increased in the order: Sonicore (air driven) 35 H, Spraco 2163, Spraco 1806, Spraco 2020, and Spraco 1405. For example, at a pressure of 20±5 psig and a temperature of 45±3°C, the volume mean drop diameters for these five nozzles were 22 μm, 35 μm, 43 μm, 50 μm, and 92 μm, respectively.

A comparison (e.g. Fig. (3)) of the drop size measurements made in the tube and on unconfined fogs shows that the drop sizes for all Spraco nozzles

are larger when the measurement is done in the open than when it is done in the tube. For example, under identical operating conditions of 25 psig and water at ~20°C, the number median drop size for Spraco 2020-1704 nozzle was reduced from 8.2 μm measured in open to 4.8 μm measured inside the tube. This shift in distribution can be attributed to droplet breakup in striking and rebounding off the walls of the inerting tube.

For a given nozzle, the average drop size decreased with increasing pressure and with increasing temperature. This effect is illustrated for Spraco nozzles 2163 and 1806 (two comparable nozzles) in Figure (4).

Fog concentrations calculated using the three methods described previously did not always produce the same results. For the Sonicore air-driven nozzle and the Spraco 1405 nozzle, concentrations obtained from the KLD probe data (assuming $v = v_f$) agreed fairly well with concentrations based on the water/air flux ratio. For the other three nozles, the fog concentrations calculated from the probe data with $v = v_f$ were an order of magnitude smaller than those based on flux ratios. This implies that the gas and water drop residence times in the tube are comparable for small-drop fogs (Sonicore nozzle) and large-drop spray (Spraco 1405 nozzle), but the two residence times are quite different for moderate-drop sizes in the range 30-100 μm. Thus, the water collection technique is not a reliable method for determining concentrations of fogs with drops in this size range.

Fog concentration calculations based on probe data with v equal to the larger of either v_f or v_t were often an order of magnitude smaller than concentrations based on the other two techniques. Thus, concentrations based on v_f and v_t ranged from 10^{-5} to 10^{-3} gm water per cm^3 of gas while concentrations based on the other two techniques generally ranged from 10^{-4} to 10^{-2} gm/cm^3.

The discrepancy in fog concentration data is an unfortunate consequence of the inherent inaccuracy in the measurement techniques employed. Other techniques, based on optical attenuation or scattering phenomena are more accurate although more complex, and are recommended if and when more refined mesurements of fog density are warranted. Fog concentration data listed in Tables 1 and 2 were calculated using v_f since v_f is the best estimated droplet velocity in the tube and, therefore, the authors feel this method is the most accurate of the three techniques used. Concentrations based on all three techniques are provided in the full FMRC report.[6]

FOG INERTING DATA

Hydrogen lower flammable limit (LFL) data in the presence of water fog are shown in Tables 1 to 3 for gas/fog temperatures of 20°C, 50°C, and 70°C, respectively. The data represent the results of about 160 tests conducted with the five nozzles operated at pressures of 10-40 psig. The LFL values shown in the last column of Tables 1-3 represent either the midpoint of a pair of "ignition-no ignition" tests or else the concentration for a test with marginal ignition; i.e. thermocouple response but no incipient pressure rise.

For the Spraco hydraulic nozzles at 20°C, the hydrogen LFL was 4.4-5.3 vol % (neglecting any water vapor diluting). These values are only marginally higher than the hydrogen LFL for upward flame propagation in dry air; i.e., 4.0 vol %, which was also verified (a value of 4.08 $\pm$ 0.1% was measured) in the present apparatus using both spark and glow plug igniters. Fog inerting tests with spark and glow plug igniters operated at the same fog and gas concentrations produced equivalent results within the experimental uncertainty ($\pm$ 0.28% H_2) associated with the gap between "ignition - no ignition" concentrations.

The Sonicore air-driven fog nozzle at 20°C caused the hydrogen LFL to increase to 7.2 vol %. This increase is undoubtedly due to the smaller drops produced by the Sonicore nozzle compared to the Spraco hydraulic nozzles.

At 50°C, hydrogen LFL's in the presence of water fog varied from 5.0 to 7.9 vol % depending on nozzle type and pressure. At 70°C, the hydrogen LFL was 5.9-8.5%. The 70°C data were obtained with the glow plug, which was acquired toward the end of the test series.

The observed increase in LFL with increasing temperature is similar to that reported by Sapko et al[3] for water spray inerting/quenching of methane-air mixtures. It can be attributed to the following effects:

1. The hydrogen-air mixture is diluted by additional water vapor, which is presumably present at the saturation values shown in Figure (5).
2. As initial droplet temperatures increase closer to the atmospheric pressure boiling point, i.e., 100°C, the droplets can vaporize more rapidly to quench a growing kernel of flame.
3. The fog characteristic drop size is reduced with increasing temperature. The smaller drops evaporate more rapidly than larger drops to quench an incipient flame.

The water vapor dilution effect can be ascertained by comparing the fog LFL data to Zabetakis' data[7] for hydrogen-water vapor-air mixtures. The comparison is indicated in the following table which shows that water vapor saturated hydrogen LFLs at 20°C and 50°C are lower than the lowest LFLs measured in the presence of dense fogs at these temperatures. Hence, there must have been a significant additional heat sink inerting effect caused by the liquid water content of the fog. At 70°C, on the other hand, the vapor-saturated LFL (7.2%) lies in the middle of the range of the LFLs measured with dense fogs. Thus, water vapor cooling could indeed account for some of the enhanced inerting observed with fogs at 70°C.

Temp	Hydrogen LFL (Dry Vol %)	
	No Fog	
(°C)	Dry-Sat	Dense Fog
20	4.0-4.1	4.6-7.2
50	4.0-4.7	5.0-7.9
70	4.0-7.2	5.9-8.5

For a specific nozzle at a given temperature, the hydrogen LFLs increased with increasing nozzle water pressure as shown in Fig. 6 for the Spraco 2163 and 1405 nozzles. This effect can be attributed both to the smaller drop sizes at higher pressures and to the generally higher fog concentrations at higher pressures.*

* Fog concentrations did not increase monotonically with increasing water pressure because the fog spray angle (as well as flow rate) increases with pressure, so that a larger fraction of the spray strikes the tube wall.

TABLE 1

HYDROGEN-WATER FOG INERTING DATA AT 20°C

Nozzle	Pressure (psig)	Spray Angle (Full)	Drop Size Vol. Mean (Micron)	Drop Size No. Median (Micron)	Conc. $\frac{cm^3 H_2O}{cm^3 Mix}$	Igniter	Hydrogen LFL (vol %)
Spraco	10		111	9.8±	8.1×10^{-4}	Spark	4.42 ± 0.11
2163-7604	20	>60°	54.5	4.7±	3.8×10^{-4}	Spark	4.76 ± 0.31
~60°	25		44.1	3.8±	2.7×10^{-4}	Spark	4.76 ± 0.31
	30	~60°	20.6	1.5±	2.8×10^{-4}	Spark	4.72 ± 0.28
	30	~60°	20.6	1.5±	2.8×10^{-4}	Glow Plug	5.0 ± 0.24
Spraco	10	61°	139	13±	3.6×10^{-3}	Spark	4.64 ± 0.12
2020-1704	20		86.2	6.8±	8.5×10^{-4}	Spark	4.76 ± 0.31
	25		58.4	4.8±	2.9×10^{-4}	Spark	4.76 ± 0.31
	30	80°	35.7	5.6±	1.5×10^{-4}	Spark	5.26 ± 0.19
Spraco	10		136	13±	9.4×10^{-5}	Spark	4.40 ± 0.10
1806-1605	20		59.3	5±	6.0×10^{-5}	Spark	4.76 ± 0.31
	25		66	4±	5.7×10^{-4}	Spark	4.76 ± 0.31
	30	~40°	47.8	6.4±	3.2×10^{-4}	Spark	4.65 ± 0.34
[illegible]eco	10		136	14±	4.5×10^{-3}	Spark	4.64 ± 0.12
1405-0604	20		110	10±	2.2×10^{-2}	Spark	4.76 ± 0.31
(20-30°)	25		114	11±	2.7×10^{-2}	Spark	4.76 ± 0.31
	30	20°	115	14±	3.3×10^{-2}	Spark	5.26 ± 0.19
Sonicore 03514	20		-	5	1.1×10^{-3}	Spark	7.2 ± 0.22

TABLE 2

HYDROGEN-WATER FOG INERTING DATA AT 50°C

Nozzle	Pressure (psi)	Drop Size Vol. Mean (Micron)	Drop Size No. Median (Micron)	Conc. $\frac{cm^3 H_2O}{cm^3 Mix}$	Igniter	Hydrogen (vol %)
Spraco	40	33.1	5.2±	1.4×10^{-4}	Spark	7.19 ± 0.22
2163-7604	30	21.4	4.2±	8.1×10^{-5}	Spark	5.55 ± 0.11
	20	34.5	4.5±	1.9×10^{-4}	Spark	5.55 ± 0.11
Spraco	40	24.5	3.8±	9.3×10^{-5}	Spark	7.19 ± 0.22
2020-1704	30	27.1	4.2±	1.1×10^{-4}	Spark	7.19 ± 0.22
	20	50.3	6.2±	4.0×10^{-4}	Spark	6.32 ± 0.22
Spraco	10	-	-	-	Glow Plug	4.98 ± 0.22
1806-1605	20	43.2	-	9.7×10^{-5}	Glow Plug	5.22 ± 0.42
	30	15.2	-	1.6×10^{-5}	Glow Plug	5.44 ± 0.22
	40	11.2	3±	1.9×10^{-5}	Glow Plug	5.18 ± 0.42
	40	11.2	3±	1.9×10^{-5}	Spark	5.35 ± 0.42
Spraco	40	87.8	9.6±	3.2×10^{-2}	Spark	5.55 ± 0.11
1405-0604	30	91.8	11.5±	2.0×10^{-2}	Spark	5.55 ± 0.11
	25	115	14±	1.7×10^{-2}	Spark	5.55 ± 0
Sonicore	25	24	2.4±	1.1×10^{-3}	Spark	7.93 ± 0.23
035H	20	24.4	2.8±	1.1×10^{-3}	Spark	7.19 ± 0.22

TABLE 3

HYDROGEN-WATER FOG INERTING DATA AT ~70°C

Nozzle	Press. (psi)	Igniter	Hydrogen LFL (vol %)
Spraco	10	Glow Plug	6.76 ± 0.22
2163-7604	20	Glow Plug	7.18 ± 0.22
	30	Glow Plug	7.62 ± 0.22
	40	Glow Plug	8.46 ± 0.22
Spraco	10	Glow Plug	5.88 ± 0.21
1405-0604	20	Glow Plug	6.32 ± 0.21
	30	Glow Plug	7.62 ± 0.21
	40	Glow Plug	7.62 ± 0.21

Water fog densities required to achieve a given level of inerting depend on the fog characteristic drop size. This is shown in Figure 7, which is a plot of fog density (based on probe data with $v = v_f$) versus volume mean diameter for inerting to a hydrogen LFL of 4.76% at 20°C, and 7.2% at 50°C. Although the 50°C data in Figure 7 refer to smaller drops than the 20°C data, best fit lines through both sets of data are approximately colinear on the log-log plot. The data in Figure 7 refer to four nozzles. Data from the fifth nozzle (Spraco 1405) were more scattered than for the other four nozzles, but did indicate that the linear relationship in Figure 7 could possibly be extrapolated to somewhat larger drop diameters and fog densities, as shown in Figure 8. The trend of the data shown in Figures 7 and 8 is analogous to that observed by Sapko, et al with methane (see Figure 3 of Reference 3), except that the fog density in Figures 7 and 8 varies approximately as the second power (instead of linearly) of drop diameter.

ANALYSIS OF INERTING RESULTS

The observed higher LFLs with increasing fog concentrations and with decreasing drop size are qualitatively consistent with the concept of flame

quenching due to the fog heat sink effect. A quantitative analysis is also possible if the following simplifying assumptions are invoked. First, uniform drop size (D) and fog volume fraction (η) distributions are assumed for the fog suspended within a flame kernel. Second, the distinction between inerting and flame quenching is ignored. The latter assumption is not only conservative (for estimating minimum inerting requirements) but it is also probably a reasonable approximation for the laminar flows in the FMRC inerting tube.

With these assumptions, the inerting criterion is tantamount to the transverse heat loss quenching criterion described in the FMRC incomplete combustion model.[8] Hypothesizing that the fog droplets are dominant heat sink, the following equation can be derived [9] from this quenching criterion.

$$\frac{\eta}{D^2} = \frac{1}{6e} \frac{RT_{AD}}{E} \left(\frac{1}{1 - T_O/T_{AD}}\right) \left(\frac{S_u}{a}\right)^2 \frac{1}{Nu} \qquad (3)$$

The notation is: T_{AD} is the adiabatic flame temperature for a particular H_2-air mixture, R is the universal gas constant, E is the combustion reaction activation energy (16 kcal/mole), T_O is the initial gas temperature, S_u is the adiabatic laminar burning velocity of the mixture, a is the mixture thermal diffusivity, and Nu is the Nusselt number for droplet heat transfer. Taking the Reynolds number for the droplet flow field to be based on droplet terminal velocity, the appropriate equation for Nu is [9]:

$$Nu = 2 + 0.818\ (D/D_O)^{0.75} \qquad (4)$$

where D_o is equal to 50 microns, and droplet evaporation has been neglected.

In order to make comparisons with the experimental inerting data, values for S_u, T_{AD}, and a in Eqn (3) were selected for a 7.2 vol % hydrogen-in-air mixture with T_o equal to 50°C. These values are 10.8 cm/sec, 840°K, and 0.10 cm^2/sec, respectively. The resulting equation obtained by inserting Eqn (4) into Eqn (3) is:

$$\eta = \frac{2.3 \times 10^{-7}\ D^2}{2 + 0.818\ (D/50)^{0.75}}\ , \text{ with D in } \mu m \qquad (5)$$

which indicates that η varies as D^2 for small values of D.

Figure 9 shows the comparison between fog volume fractions from Eqn. (9) and those based on the inerting data in Figure 7. The indicated difference between theory and data is certainly within the experimental uncertainty associated with fog concentration measurements.

CONCLUSIONS

1. Dense water fogs applied to hydrogen-air mixtures cause only a marginal increase in the hydrogen lower flammable limit (LFL) concentration at room temperature. Four fog nozzles used in this program caused the hydrogen LFL for upward flame propagation to increase from 4.0 vol % to 4.4-5.3 vol %. Fog generated from an air-driven nozzle (which generated smaller drops than the hydraulic nozzles) resulted in a hydrogen LFL of 7.2% at $20^{\circ}C$.
2. Increasing temperature causes large increases in the hydrogen LFL in the presence of water fog. For a typical hydraulic type fog nozzle used in the project, the hydrogen LFL increased from 4.8 vol % to 7.2 vol % and to 7.6 vol % (based on dry hydrogen-air mixture) as initial temperatures increased from $20^{\circ}C$ to $50^{\circ}C$ and to $70^{\circ}C$. This increased inerting is due in part to water vapor dilution and more importantly to liquid phase water heat sink effects.
3. Fog densities required to achieve a given level of hydrogen inerting are strongly dependent on the characteristic drop size of the fog. For example, required fog densities increased by an order of magnitude (from 10^{-4} gm/cm^3-gas to 10^{-3} gm/cm^3-gas) as volume mean drop diameter increased from about 20 to 100 μm. These results are consistent with a quantitative analysis of flame quenching due to cooling by suspended water droplets.

ACKNOWLEDGEMENT

This effort was funded jointly by EPRI and by TVA, Duke Power, and American Electric Power. The authors are also grateful for the theoretical analysis derived by Dr. Erdem Ural of FMRC.

REFERENCES

1. Berman, M., et al., "Analysis of Hydrogen Mitigation for Degraded Core Accidents in the Sequoyah Nuclear Power Plant," NUREG/CR-17625 and 80-2714, March 1981.
2. Torok, R.C., Siefert, K., and Thomson, L.B., "Hydrogen Control Tests in Intermediate Scale," presented at the Second International Workshop on the Impact of Hydrogen on Water Reactor Safety, October 1982.
3. Sapko, M.J., Furno, A.L. and Kuchta, J.M., "Quenching Methane-Air Ignitions with Water Sprays," Bureau of Mines Report RI8214, 1977.
4. Magnus, D.E., et al., "Sensing of Droplet Size and Concentration in Pollution Control Equipment," Proceedings 4th Joint Conference on Sensing of Environmental Pollutants, American Chemical Society, 1978.
5. Stockham, J.D. and Fochtman, E.G., eds., Particle Size Analysis, Ann Arbor Science, 1977.
6. Zalosh, R.G. and Bajpai, S.N., "The Effect of Water Fogs on the Deliberate Ignition of Hydrogen," EPRI Project 1932-1, NP-2636, November 1982.
7. Zabetakis, M.G. (1956), "Research on the Combustion and Explosion Hazards of Hydrogen-Water Vapor-Air Mixtures," Division of Explosives Technology, Bureau of Mines, Pittsburgh, PA, Report No. 3543 dated September 4, 1956.
8. Zalosh, R.G., Ural, E.A., and Hwa, V.W.S., "Lean Hydrogen-Air-Steam Mixture Combustion Models," presented at Second International Workshop on the Impact of Hydrogen on Water Reactor Safety," October 1982.
9. Ural, E., FMRC Internal Memorandum, September 1982, also presented as "Water Fog Inerting of Flammable Gas-Air Mixtures," Paper #36, 1982 Technical Meeting of the Eastern Section of the Combustion Institut December 1982.

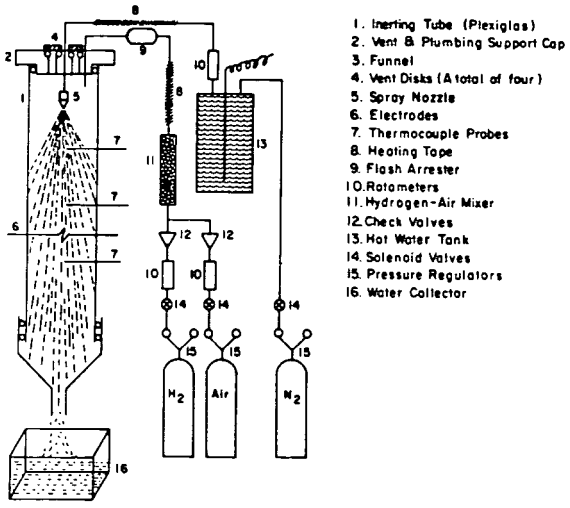


Figure 1 Hydrogen-Water Fog Inerting Experimental Setup

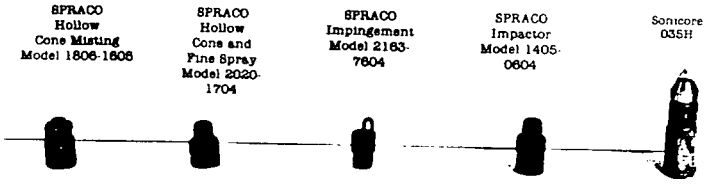


Figure 2 Fog Nozzles Used in Inerting Experiments

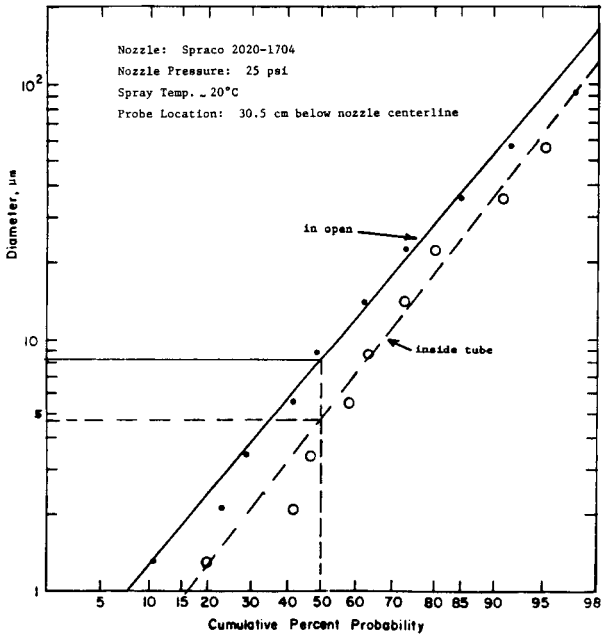


Figure 3 Drop Size Distributions in Tube and in Open

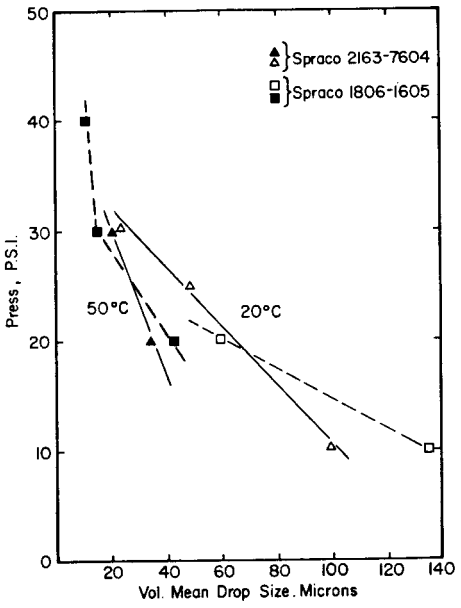


Figure 4 Drop Size Varation with Pressure and Temperature

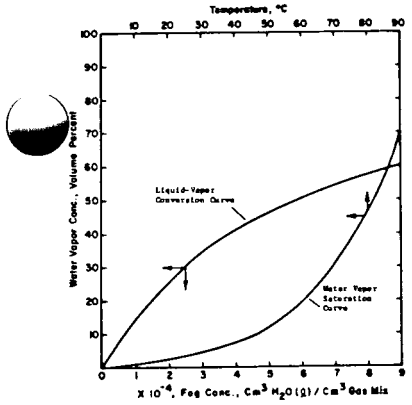


Figure 5 Liquid-Vapor Conversion and Water Vapor Saturation Relationships

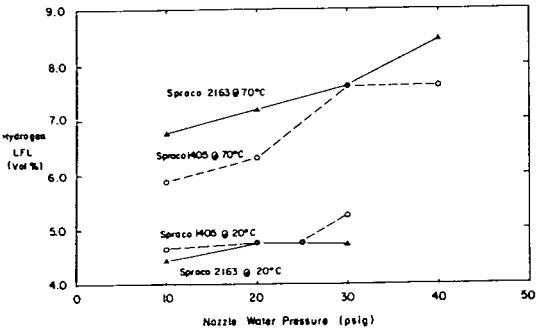


Figure 6 Hydrogen LFL versus Fog Nozzle Water Pressure

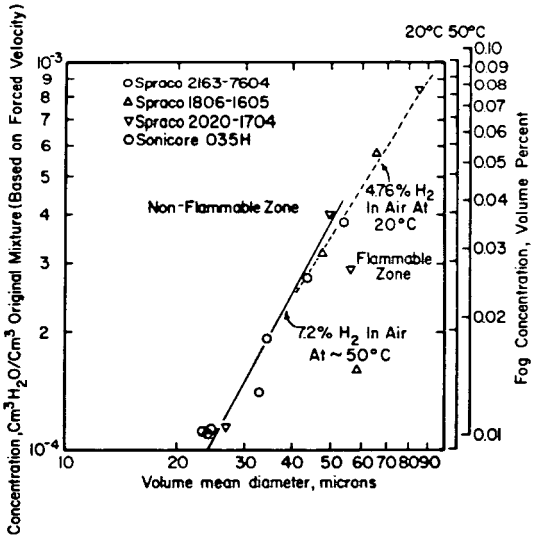


Figure 7 Fog Concentration as a Function of Drop Size to Achieve indicated Inerting Levels

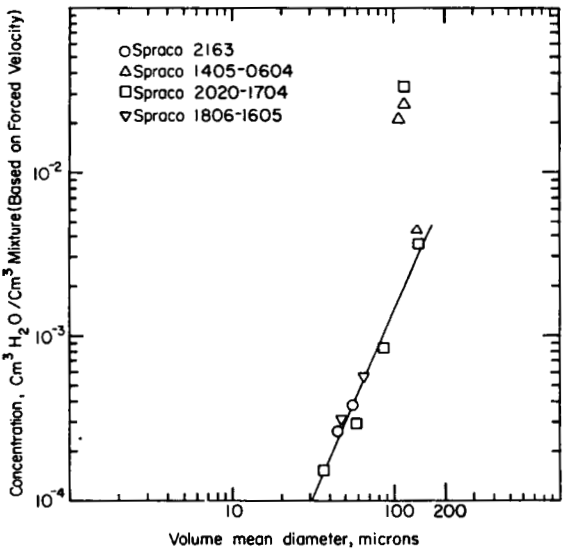


Figure 8 Fog Concentration versus Drop Size Requirements for Inerting to 4.76 Hydrogen at 20°C

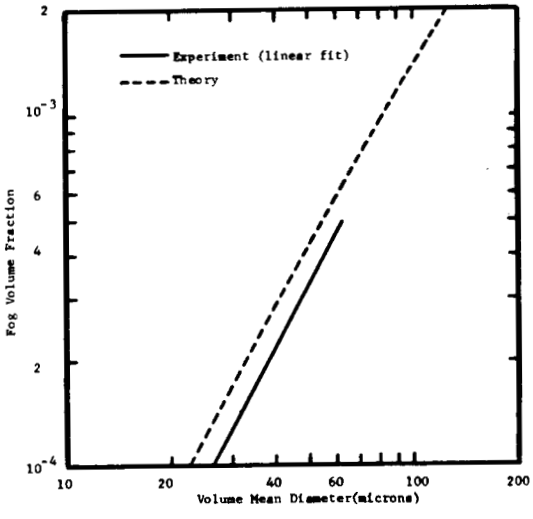


Figure 9 Comparison of Experiment and Theory for 7.2% Hydrogen in Air at 50°C

FOG INERTING CRITERIA FOR HYDROGEN/AIR MIXTURES

S. S. Tsai, and N. J. Liparulo
Risk Assessment Technology
Westinghouse Electric Corporation

ABSTRACT

A distributed ignition system has been proposed to ignite hydrogen at low concentration in the ice condenser containment during severe accidents. The post-accident containment atmosphere could be misty due to fog generation from the break flow and condensation in the ice bed. Thus it is important to establish a fog inerting criterion for effective performance of the ignition system. This paper presents such a criterion that specifies the necessary fogging conditions, i.e., fog concentration and drop size, for inerting a hydrogen/air mixture. The criterion shows that the minimum fog inerting concentration varies with the square of the volume mean fog drop size. The present fog inerting criterion is shown to be in general agreement with the Factory Mutual test data.

1. INTRODUCTION

A distributed ignition system has been proposed to ignite hydrogen at low concentration in the ice condenser containment during severe accidents. The post-accident containment atmosphere may be misty because of fog generation by the break flow and condensation in the ice bed. Thus it is of important to establish a fog inerting criterion for effective performance of the ignition system.

Zalosh and Bajpai[1] have recently conducted hydrogen flammability tests to determine the effect of water fogging on the hydrogen lower flammability limit. In the tests, the minimum fog inerting concentrations for various volume mean drop sizes and hydrogen concentrations were measured. It was found that an 8 vol percent hydrogen mixture could be inerted at high fog concentration. Fog formation may also have been responsible for failure of the two Lawrence Livermore tests[2] at high steam concentrations to ignite hydrogen during the test vessel cool-down period.

The capability of fog droplets in inhibiting combustion or quenching flames is due to their heat absorbing capability - high heat of vaporization and small drop sizes (on the order of 10 μ). Due to the small drop sizes, fog droplets could vaporize rapidly (on the order of miliseconds) within a propagating flame front (~ 1 mm thick). If a substantial amount of these droplets are present, the flame may be quenched.

The critical droplet diameter for quenching a hydrogen flame has been estimated by Sandia National Laboratories[3]. It was assumed that the measured "quenching distance" for a hydrogen flame propagating through a

tube or between plates could be used for fog droplets. This model does not consider heat transfer and combustion occurring between the burned gas and the suspended droplets.

This paper presents a fog inerting criterion that specifies the necessary fogging conditions, i.e., fog concentration and drop size, for inerting a hydrogen/air mixture.

2. FOG INERTING CRITERIA

Recent hydrogen burn experiments[2] conducted at Lawrence Livermore Laboratory indicated that substantial fog formation could occur when saturated steam is discharged into an unheated vessel. It appeared that this fog prevented a glow plug igniter from successfully igniting the hydrogen mixture in the vessel. The ability of fog in inhibiting and quenching a hydrogen combustion can be explained as follows. The fog droplets suspended in the hydrogen-air-steam mixture act as a heat sink that could absorb a large amount of combustion heat by vaporization, greatly reducing the pressure and temperature rises resulting from hydrogen combustion. If droplets are sufficiently small such that they could vaporize inside the thin (1mm) flame front, the flame may be quenched or inhibited. For a flame speed of 2 m/s, the drop residence time is of the order of 0.5×10^{-3} seconds.[3] In such a short period of time, the droplets of initial radius less than about 4 μ will vaporize entirely in the flame front.

The quenching of a propagating flame is also governed by the distance between droplets. As the droplets become closely packed, the total droplet surface area available for energy loss increases. A critical spacing between droplets exists such that a large fraction of the heat released is absorbed, Thus preventing flame propagation. This critical spacing is known as the "quenching distance", which is usually determined by propagating flames in tubes.

2.1 PREVIOUS WORK

The effectiveness of fog droplets in inhibiting or quenching a flame depends on its quenching distance, which was determined by Berman et al.[3] as

$$d_q = [4V/S]_{crit} \qquad (1)$$

where V is the gas volume and S is the heat transfer surface area.

In the suspended fog droplets, this volume-to-surface ratio (i.e., V/S) is equal to $d\,(1-\eta)/6\eta$, where d is the mean droplet diameter and η is the volume fraction of the droplets. When four times this ratio approaches the quenching distance, a critical droplet diameter can be obtained as

$$d_c = \frac{3}{2}\,\frac{\eta d_q}{1-\eta} \qquad (2)$$

Using the quenching distance data for a given volume fraction of water and gas composition, the critical droplet diameter can be determined from Equation (2). The drop sizes less than the critical drop size are capable of quenching a flame.

2.2 PRESENT THEORY

The previous theories do not model the heat transfer and combustion processes occurring between the burned gas and the suspended droplets. A new theory has been developed, which models the heat loss and combustion within a thin flame front.

Consider a hydrogen/air/steam/mist droplets mixture in which a flame is propagating. The flame may be divided into three zones: heating zone, reaction zone, and post-reaction zone as shown in Figure 1. The unburned gas at temperature T_u moves in the reaction zone with the laminar burning velocity S_u. If the unburned gas density is ρ_u, then the constant mass flow rate m is equal to $\rho_u S_u$. The unburned gas is heated to ignition temperature T_i and burned in the reaction zone to reach the flame temperature T_f. The fog droplets will act as a heat sink that reduces the flame temperature. The problem has been formulated and solved by von Karman[4]. In his formulation, three energy equations, which incorporate the heat loss terms, were written for the three zones described above. The solution to these equations yields the following relationship

$$2K\theta_i = \left\{1 - \exp\left(-\frac{1}{2}\mu^2\right)(Y_u - Y_f) \times \left[1 + \sqrt{1 + (4K/\mu)^2}\right]\right\} \times \left\{1 - \frac{1}{\sqrt{1 + K/\mu^2}}\right\} \qquad (3)$$

where $\theta_i = \overline{C}_p (T_i - T_u)/q$

$\mu = \sqrt{\overline{C}_p / \overline{\lambda w}}\ m$

$K\theta_i = (S/\overline{C}_p w)\ \theta_i$

= the ratio of heat loss rate per unit volume to the heat release rate by chemical reaction per unit volume

q = heat of combustion

$\overline{C}_p$ = mean specific heat

$\overline{\lambda}$ = mean heat conductivity

w = reaction rate (mass of fuel consumed per unit time per unit volume)

Y_u = hydrogen mass fraction in the heating zone

Y_f = hydrogen mass fraction in the reaction zone

m = $\rho_u S_u$

A plot of Eq. (3) is shown in Figure 2. It is seen that for a given $K\theta_i$, there is a minimum value of $(Y_u - Y_f)/\theta_i$. Below this minimum value, there is no solution for the $\sqrt{\theta_i}\ \mu$. Therefore, this value is considered as the flammability limit. At the flammability limit, the value of $K\theta_i$ can be determined from Figure 2 or from Eq. 3 as

$$(K)_{crit}\ \theta_i = f\ ((Y_u - Y_f)/\theta_i) \tag{4}$$

A plot of $(K)_{crit}\ \theta_i$ as a function of $(Y_u - Y_f)/\theta_i$ is shown in Figure 3. Equation 4 may be expressed as

$$\frac{n}{d^2} = \frac{q\ \bar{C}_p\ \rho_u^2\ S_u^2\ (Y_u - Y_f)\ f\left(\frac{Y_u - Y_f}{\theta_i}\right)}{12\ \bar{\lambda}^2 (T_i - T_u)} \tag{5}$$

Detailed derivation procedure for Eq. (5) is given in Appendix A. Using the data on S_u from Reference (5) we can calculate the right hand side of Eq. (5) for a given composition and initial gas temperature.

3. VERIFICATION OF THEORIES BY EXPERIMENTS

Experiments have been conducted at Factory Mutual to study the effects of water fog density, droplet diameter, and temperature on the lower flammability limit of hydrogen-air-steam mixtures[2]. The results indicated that most of the fog nozzles tested at 20°C only changed the limit from 4.03 volume percent to 4.76 percent, corresponding to fog concentration in the range of 0.028-0.085 volume percent, and volume mean drop size ranging from 45-90 microns. For the 50°C case, the lower flammability limit increases to 7.2 percent, corresponding to 0.01-0.04 volume percent of fog and 20-50 micron volume mean drop sizes. The results demonstrated that the fog inerting effect is more pronounced at reduced drop sizes and increased temperature.

Figures 4 through 6 show the comparison between the test data and the theoretical predictions. For this comparison, the present theory used the free stream temperature to calculate the thermodynamic properties used in Equation (5). This yielded somewhat higher fog concentrations than those calculated by use of the mean of the flame and free stream temperatures. In Figures 4 and 5, the data suggests a linear relationship between the volume concentration and volume mean drop size on the log-log plot. It also suggests that the minimum fog inerting concentration varies approximately with the square of the volume mean drop size.

The present theory is in good agreement with the Factory Mutual data at 4.76 percent H_2; however, it overpredicts the minimum fog inerting concentration at 7.2 percent H_2. The cause of this discrepancy is still unknown. The discrepancy may be caused by the uncertainty of the data. The following discussion supports this view. The fog droplets are very small and they vaporize very fast in a flame. Therefore, the fog droplets behave as steam except for their larger heat absorption capability. When the fog droplets vaporize, they absorb the heat of vaporization which is much larger than the steam sensible heat. Typically, the heat of vaporization of water is about 1000 Btu/lb and the average specific heat of steam in the temperature range of interest is about 0.48 Btu/lb. It is well known that a hydrogen flame cannot propagate in steam higher than about 64 percent in a steam-air mixture. At 7.9 percent H_2, the adiabatic flame temperature is about 1240°F and therefore the increase of the steam sensible heat is about 540 Btu/lb. Consequently, for the same amount of fog droplets and steam, the fog droplets heat absorption capability is about 1.9 times higher. This means that the fog concentration which is equivalent to 22.1 percent steam in a steam-air mixture is capable of inerting 7.9 percent H_2. This fog inerting volumetric concentration was calculated to be 1.61×10^{-4} ft^3 H_2O/ft^3 mix for 7.9 percent H_2. To inert 7.2 percent H_2, a minimum fog concentration of 1.56×10^{-4} ft^3 H_2O/ft^3 mix equivalent to about 21.3 percent steam in a steam-air mixture is required. These estimates show that the present predictions are reasonable and conservative. The estimates are consistent with Factory Mutual data on 7.9 percent H_2 but not on 7.2 percent H_2.

It should be noted that in the tests three fog concentration measuring techniques were used. These three techniques gave substantially different results. The discrepancy is at least one order of magnitude difference. The fog concentration data presented in Figures 4 through 6 were obtained from one of the techniques. In view of the uncertainty of the data, care must be exercised in using them for fog inerting analysis purposes. They should be used in conjunction with the present fog inerting criterion in the assessment of fog inerting potential in the ice condenser plants. Some uncertainty also exists in the present fog inerting theory. The maximum uncertainty associated with the underprediction of the heat loss and temperature dependence of the thermophysical properties is estimated to be ± 63 percent.

4. SUMMARY AND CONCLUSIONS

A fog inerting criterion has been developed to predict the minimum fog concentration required to inert a given hydrogen concentration and volume mean fog drop size. The present fog inerting criterion has been shown to be in general agreement with the Factory Mutual test data. The criterion shows that the minimum fog inerting concentration varies with the square of the volume mean fog drop size.

ACKNOWLEDGMENTS

The authors wish to express their sincere gratitude to Drs. V. Srinivas, B. Lewis, and B. Karlovitz for assistance, suggestions, and helpful discussions, to Messrs. D. F. Paddleford, R. Bryan, F. G. Hudson, D. Renfro, and K. Shiu for valuable comments.

They also would like to thank TVA, Duke Power, and AEP for providing the financial support.

REFERENCES

1. R. G. Zalosh and S. N. Bajpai, "Water Fog Inerting of Hydrogen - Air Mixtures," EPRI Project Preliminary Rpt. 1932-1, September, 1981.

2. B. Lowry, "Preliminary Results: A Study of Hydrogen Igniters, "ENN80-45, Lawrence Livermore National Laboratory, November 17, 1980.

3. M. Berman, et al., "Analysis of Hydrogen Mitigation for Degraded Core Accidents in the Sequoyah Nuclear Power Plant," Sandia draft report, December 1, 1980.

4. T. von Karman, unpublished notes, 1956.

5. S. S. Tsai, and N. J. Liparulo, "Flame Temperature Criteria Tests," accepted for presentation at the Second Int. Workshop on the Impact of Hydrogen on Water Reactor Safety, Albuquerque, New Mexico, October 3-7, 1982.

APPENDIX A

DERIVATION OF EQUATION (5)

This appendix gives detailed procedures to derive Eq. (5), starting from Eq. (4)

$$(K)_{crit}\,\theta_i = f\,((Y_u - Y_f)/\theta_i) \tag{4}$$

where the ratio of heat loss rate per unit volume to the heat release rate by chemical reaction per unit volume, $(K)_{crit}$, is defined as

$$K_{crit} = S/C_p w \tag{A-1}$$

and the ratio of sensible heat to heat of combustion, θ_i, is defined as

$$\theta_i = C_p\,(T_i - T_u)/q \tag{A-2}$$

To arrive at Eq. (5), it is necessary to assume that all the heat loss is attributed to convection heat transfer to fog droplets of only one drop size. Under this assumption, the rate of heat loss per unit volume per degree, S, may be expressed as

$$S = n\pi d^2 h \tag{A-3}$$

where n = number of drops per unit volume
d = volume mean drop size
h = heat transfer coefficient

It is further assumed that the relative velocity between the droplets and the mixture flow is so small that heat transfer coefficient, h, can be approximated by the conduction limit. In fact, it can be shown that for small drop sizes, convection and radiation are unimportant heat transfer mechanisms at the drop surface. Under this assumption, Eq. (A-3) reduces to

$$S = \frac{12\eta\bar{\lambda}}{d^2} \tag{A-4}$$

where $\bar{\lambda}$ = mean heat conductivity

η = volume fraction of mist droplets $(\frac{n}{6}\,\pi\,d^3)$

The of heat generation per unit volume, w, is related to the laminar buring velocity, S_u, and the thickness of the reaction zone, ℓ, by

$$w = \frac{\rho_u S_u (Y_u - Y_f)}{\ell} \tag{A-5}$$

The thickness of the reaction zone may be approximated by

$$\ell = \frac{\overline{\lambda}}{\rho_u S_u \overline{C}_p} \tag{A-6}$$

Combining Eqs. (A-1), (A-4), (A-5), and (A-6), we have

$$K_{crit} = \frac{12\eta \overline{\lambda}^2}{\rho_u^2 S_u^2 \overline{C}_p^2 (Y_u - Y_f) d^2} \tag{A-7}$$

Substituting Eqs. (A-2) and (A-7) into Eq. (4), we have

$$\frac{\eta}{d^2} = \frac{q \overline{C}_p \rho_u^2 S_u^2}{12 \overline{\lambda}^2 (T_i - T_u)} (Y_u - Y_f) f\left(\frac{Y_u - Y_f}{\theta_i}\right) \tag{5}$$

Q.E.D.

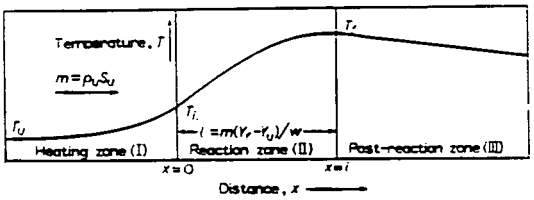


FIGURE 1 SCHEMATIC REPRESENTATION OF TEMPERATURE PROFILE THROUGH THE FLAME FRONT

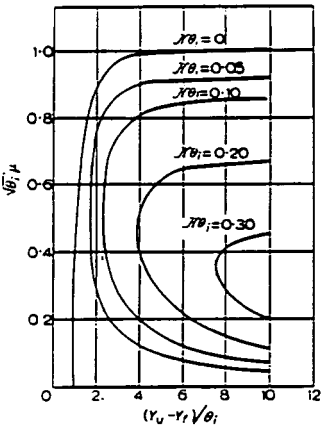


FIGURE 2 THE PARAMETER $\sqrt{\theta_i}\ \mu$ AS A FUNCTION OF $(Y_u - Y_f)/\theta_i$ FOR DIFFERENT VALUES OF $K\theta_i$

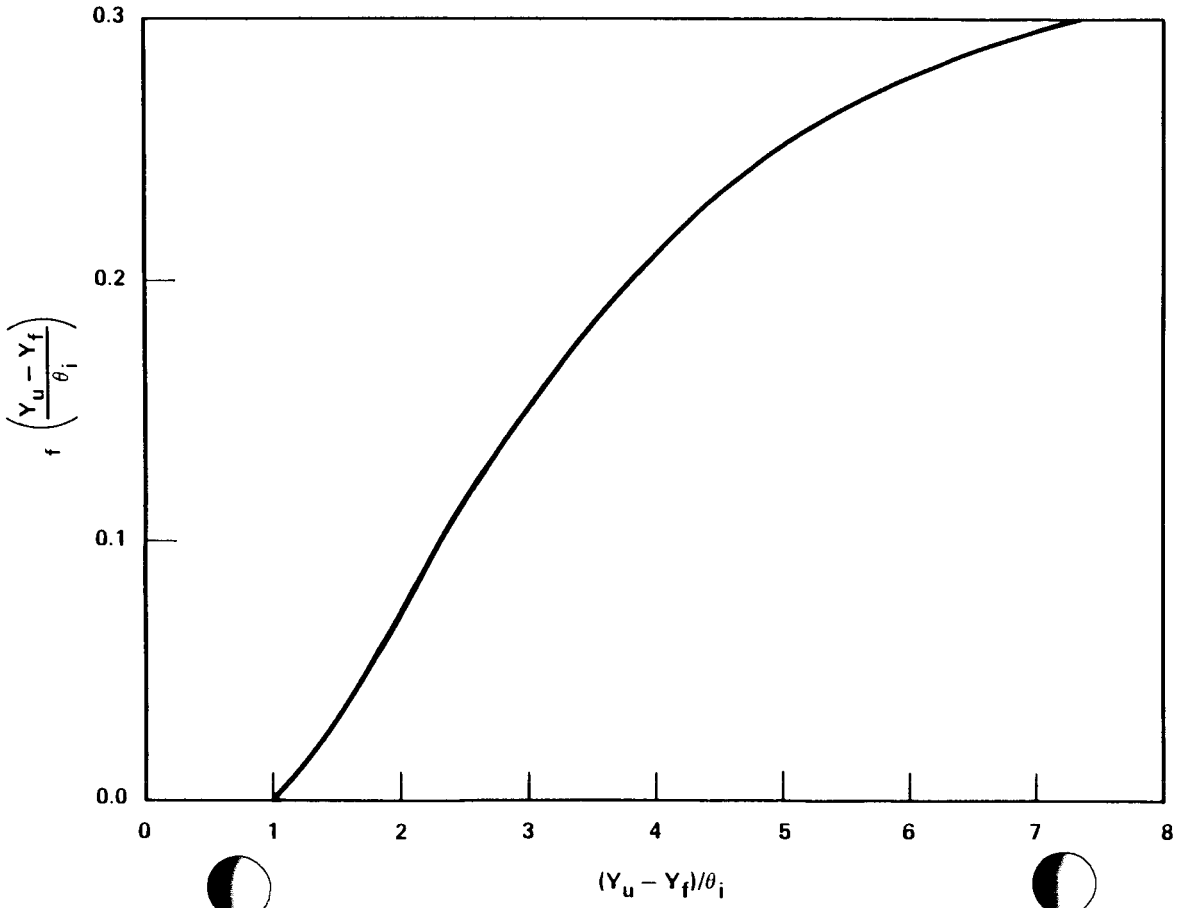


FIGURE 3 (K) θ_i AT THE FLAMMABILITY LIMIT AS A FUNCTION OF $(Y_u - Y_f)/\theta_i$

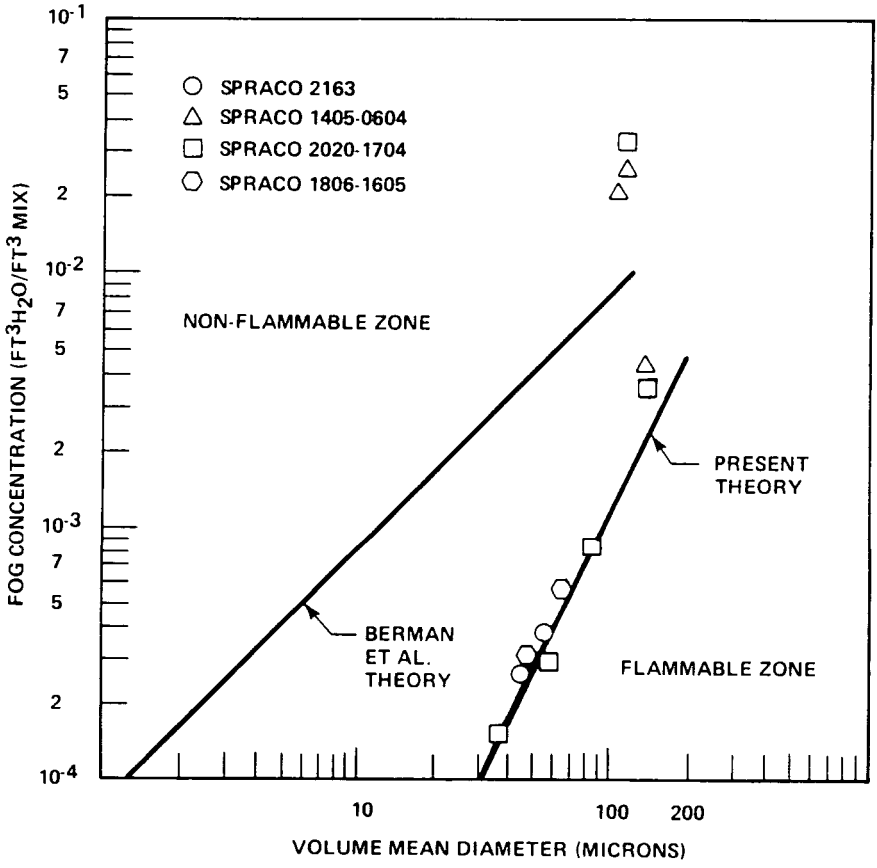


Figure 4. Comparison between Theories and Factory Mutual Fog Inerting Experiments on 4.76 Percent H_2

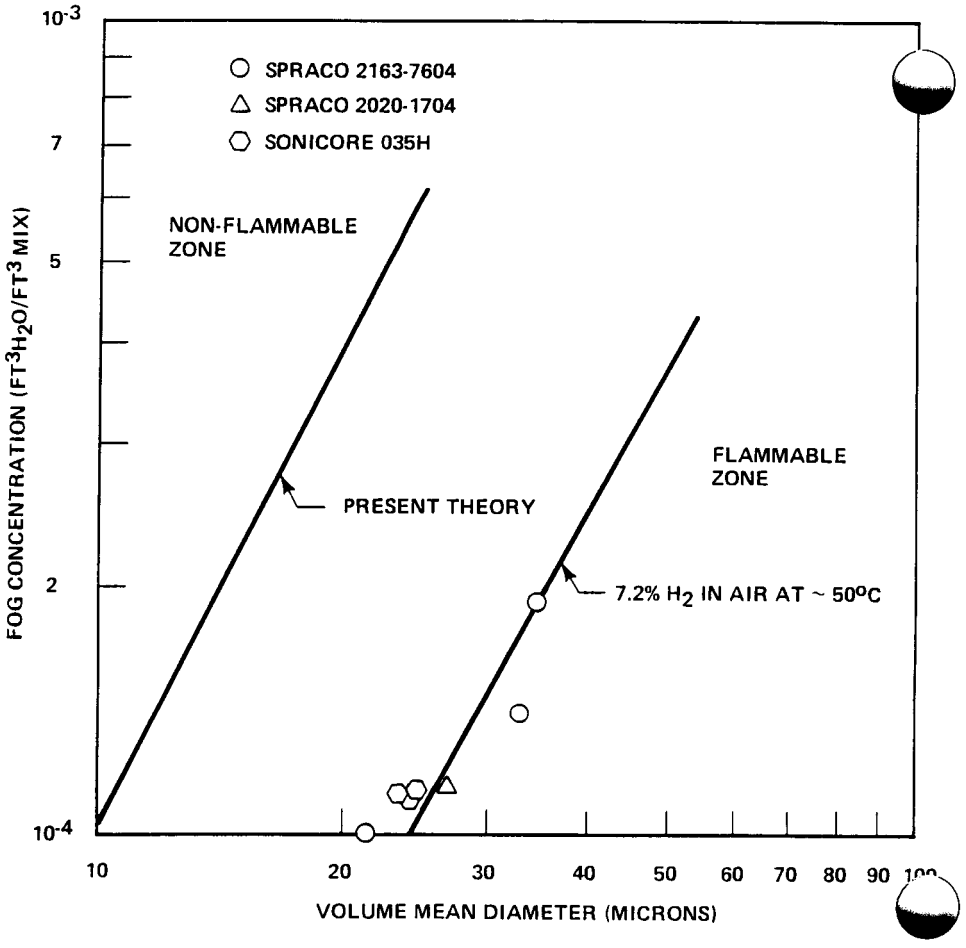


Figure 5. Comparison between the Present Theory and Factory Mutual Fog Inerting Experiments on 7.2 Percent H_2

VAPORIZATION OF SPRAYS IN SUPERHEATED ATMOSPHERES

C. F. Guenther (Bechtel Power Corporation)
R. J. Tosetti (Bechtel National, Inc.)

As a result of the accident that occurred at TMI, concern has been raised as to the potential consequences of hydrogen generation under degraded core conditions. Previous studies (Ref. 1) have addressed the effects that such an event might have on the containment environment of large dry containments. The generation and ignition of hydrogen from such an event could lead to containment atmospheric temperatures on the order of 3000°F for complete combustion of hydrogen resulting from 100% metal-water reaction. At those temperatures, most of the heat is removed by radiation to the containment walls, water sprays, and convection to the walls. The relative effect that each of the heat removal mechanisms has on the containment temperature was addressed in Reference 1. The accurate modeling of each heat transfer mode is necessary to predict the temperature and pressure profiles after the burn. This paper addresses the models used to predict the rate of heat removal by water sprays. The rate at which the sprays remove heat from the containment depends upon a number of interrelated factors: the initial spray temperature, the mass flow rate of the sprays, and the fraction of the spray which vaporizes while falling through the containment atmosphere. In the following discussion, the modeling of spray drop vaporization will be presented.

The rate of drop vaporization is dependent upon the size and temperature of the drop as well as the temperature, pressure, and gaseous composition of the containment atmosphere. The total amount of spray vaporized is also dependent upon the time the drops remain airborne in the containment which is a direct function of the spray fall height. Since the physical parameters such as spray fall height, drop size distribution, and containment atmospheric conditions, needed to accurately predict the behavior of spray drops under post-hydrogen burn conditions can vary from plant to plant, a model, to be useful, must be able to predict the effect of these parameters on the amount vaporized.

A methodology for predicting the behavior of spray drops under various conditions is presented in the following analysis. Such an analysis is necessary in part due to the wide distribution in drop sizes which can originate from a spray nozzle. A typical drop size distribution is given in Table 1 for a Spraco 1713A nozzle. The modeling of spray vaporization is best made by modeling individual drops. A drop is subjected to a rapid temperature increase after it leaves the nozzle and falls through the super-heated atmosphere. As the temperature increases further, it gives up its mass to compensate for the incoming heat flow. The mass loss continues until the drop completely vaporizes or until it reaches the containment sump. The effect that varying fall heights, drop sizes, containment atmospheric moisture content, and containment temperature have on the total fraction of drops vaporized is discussed below. The rate at

which heat is removed from the containment by the sprays can be determined from the following heat balance equation.

$$\frac{dQ}{dt} = F \cdot ((h_{fg} + h_{\ell}) \cdot f + h_{\ell} \cdot (1-f)) \qquad (1)$$

where

Q - quantity of heat (Btu),
F - spray flow rate (lbm/sec),
h_{fg} - heat of vaporization (Btu/lbm),
h_{ℓ} - increased enthalpy due to increase in spray drop temperature prior to vaporization (Btu/lbm),
f - fraction of sprays vaporized.

Once the droplets leave the spray nozzle, they are subjected to gravitational and viscous forces. The viscous forces are a function of the drop velocity (U) and temperature gradients of the containment atmosphere. Due to symmetry, the trajectory of a spherical drop can be modeled in two-dimensional space by Equations 2 and 3. The corresponding geometry upon which Equations 2 and 3 are based is shown in Figure 1.

$$\frac{d^2x}{dt^2} = \frac{-\pi r_o^2 U^2 \rho C_D}{2M} \operatorname{Sin}\theta \qquad (2)$$

$$\frac{d^2z}{dt^2} = \frac{g(\rho_{\ell} - \rho)}{\rho_{\ell}} - \frac{\pi r_o^2 U^2 C_D}{2M} \operatorname{Cos}\theta \qquad (3)$$

where

x - horizontal distance from the nozzle (cm),
z - vertical distance from the nozzle (cm),
r_o - radius of drop (cm),
U - velocity of drop (cm/sec),
ρ - density of containment atmosphere (gm/cm^3),
C_D - drag coefficient for drop of radius r,
M - mass of drop (gm),
ρ_{ℓ} - density of drop (gm/cm^3),
θ - angle between velocity vector and z-axis,
g - gravitational acceleration (980 cm/sec^2).

The first term in Equation 3 describes the gravitational forces while the second term describes the viscous drag forces that act upon the drop. Drop motion in the horizontal direction (X) is subjected to viscous forces only. It should be noted that since vaporization reduces the mass of the drops,

their radii are functions of time.

The rate at which the spray drops vaporize is calculated based upon the conservation of energy. The spray drops were assumed to reach thermal equilibrium at the saturation temperature the instant they left the spray nozzle. The assumption of a rapid equilibrium being attained between the drop and containment atmosphere has been shown to be a good approximation since the time required to reach thermal equilibriam is small compared to the drop residence time (Ref. 2). The equilibrium drop temperature utilized was based upon the steam tables temperature-pressure relationship for saturated steam using the containment pressure determined from the ideal gas law. This methodology for calculating equilibrium drop temperature gives the maximum temperature at which a drop could exist without boiling under the pressure profile of the containment atmosphere.

The rate at which heat enters the drop by convection is given in Equation 4.

$$q'' = h(T_c - T_d) \tag{4}$$

where

q'' - heat flux (cal/sec-cm^2),
h - heat transfer coefficient (cal/cm^2-sec-°C),
T_c - containment temperature (°C),

T_d - equilibrium drop temperature (°C),

Radiant heat transfer to the drop was conservatively neglected to simplify the calculation. The heat transfer coefficient for a sphere was calculated based upon Equation 5 (Ref. 3). Utilizing the heat transfer coefficient of a sphere was a good approximation for the range of drop sizes under consideration since the surface tension of the drops is strong enough to overcome the distorting viscous forces. Results of testing performed by Spraco confirm that in this regime the drops are spherical (Ref. 4).

$$h = \frac{k}{D}\left(2.0 + 0.6\left(\frac{C_p \mu}{k}\right)^{1/3}\left(\frac{DU\rho}{\mu}\right)^{1/2}\right) \tag{5}$$

where

k - thermal conductivity of containment atmosphere (cal/cm-sec-°C),
D - drop diameter (cm),
C_p - heat capacity of containment atmosphere (cal/gm-°C),

μ - viscosity of the containment atmosphere (poise).

The mass-energy balance of the drop is given by Equation 6.

$$dq_i = dm_i \cdot h_{fg} \tag{6}$$

where

dq_i - the amount of energy required to vaporize an amount of water dm of drop i (cal),
dm_i - the incremental loss of mass due to vaporization of drop i (gm),
h_{fg} - heat of vaporization at the temperature of the drop (cal/gm),

The total mass energy balance on the drop can be written by combining Equations 4 and 6.

$$dm_i \cdot h_{fg} = h(T_c - T_d)4\pi r_i^2 dt \tag{7}$$

where

$4\pi r_i^2$ - area of drop i (cm^2)
dt - time increment (sec)

Rearranging Equation 7 we obtain the rate of vaporization.

$$\frac{dm_i}{dt} = \frac{4\pi h(T_c - T_d)r_i^2}{h_{fg}} \tag{8}$$

The rate of change, for the drop radius, can be obtained using the following relation.

$$dm_i = \rho_\ell 4\pi r_i^2 dr_i \tag{9}$$

Substituting Equation 8 into Equation 9, we obtain the following result for the rate at which the spray drop radius changes.

$$\frac{dr_i}{dt} = \frac{h(T_c - T_d)}{\rho_\ell h_{fg}} \tag{10}$$

The coupled differential equations presented thus far, Equations 2, 3, 5,

and 10 cannot be solved analytically. As a result, the above models were solved numerically using the Runge-Kutta method which was utilized because of its accuracy and adaptability to programming techniques. The computer code developed for this analysis is capable of tracking the history of each drop until it either vaporizes or reaches the end of its fall height in the containment. In the following paragraphs, various computational results will be discussed in some detail.

The computer code was utilized to obtain the vaporization fractions for several conditions of airborne water vapor concentrations as a function of the containment temperature. In particular, vaporization fractions were obtained as a function of containment gas temperature, for the initial saturation temperatures of 160, 215, and 285°F. These initial saturation temperatures correspond to vapor concentrations resulting from a small pipe break to a major LOCA. The results of this analysis are presented in Figure 2. The curves presented were found to give an approximate fit, within 10% to the following equation.

$$f = c_1 + c_2 T + c_3 T^2 \qquad (11)$$

where

f - fraction of sprays vaporized,
T - temperature of containment (°F),
c_i - coefficients obtained from fitting (Table 2).

The interesting point to note is the shape of the curves as the water vapor concentration increases. If the concentration of water vapor airborne in the containment is increased, the fraction vaporized will increase as long as the temperature at which the containment atmosphere is saturated is roughly 150°F below the actual containment temperature. The increase in the fraction vaporized is attributed to the drops increased residence time in the containment as a result of the increased density and viscosity of the containment atmosphere. As the containment temperature approaches the saturation temperature, the rate at which the drop is vaporizing decreases and the onset of condensation begins to occur as long as the drop temperature is less than the containment temperature. The previous equation, Equation 11, and its associated coefficients given in Table 2 were derived for a drop fall height of 100 ft and a spray drop size distribution based on a Spraco 1713A nozzle. The use of a fall height of 100 ft, although typical of large dry containments, limits the usefulness of Equation 11. As a result, information was also extracted from the code which gave additional information that will allow the vaporization fraction for various fall heights and drop size distributions to be determined.

The effect of fall height and containment temperature on the vaporization of various spray drops was investigated. A typical spray drop distribution was given in Table 1 for the Spraco 1713A nozzle. Based on any given drop size, Figures 3, 5, and 7 present the fall height required to ensure the complete vaporization of a drop. These curves show the effect that temperature and airborne water levels have on the vaporization of spray drops.

Two interesting observations should be noted at this point. On examining Figure 3, 5, or 7 it can be concluded that increasing the temperature in containment decreases the fall height necessary to achieve complete vaporization. The three figures together indicate the reduction in required fall height achieved by increasing the moisture content of the containment atmosphere for a fixed temperature. The latter observation appears to hold true provided the containment temperature is above the saturation temperature by roughly 150°F. The curves presented in Figures 3, 5, and 7 can be approximated by a power function of the form given by Equation 12.

$$H_f = aD^b \tag{12}$$

where

H_f - fall height required to assure complete vaporization of a spray drop of initial diameter D (ft),
D - initial drop diameter (cm),
a,b - power coefficients (Table 3).

The above formula was found to fit the data to around 10% of its calculated value for fall heights of up to 100 ft. Figures 4, 6, and 8 give the fraction of a spray drop vaporized as a function of drop size. Again the figures indicate that higher containment temperatures and water vapor levels lead to a higher fraction of drops vaporized. The curves presented in Figures 4, 6, and 8 can be approximated by a power function of the form given by Equation 13.

$$F_v = a'D^{b'} \tag{13}$$

where

F_v - fraction of spray drop vaporized,

a',b' - power coefficients (Table 4).

The relation described by Equation 13 gives the fraction of a drop vaporized as a function of its size. The above equation was found to approximate the data to within 10% of the calculated values.

The application of the methodology or data presented in this paper will allow the vaporization fractions to be ascertained for a wide set of conditions. The distribution of spray drop sizes for a particular nozzle can be expressed by a discrete function $n(d_i)$ which gives the number of drops expected for a given drop size diameter d. For any drop fall height in the containment, Equation 12 or Figures 3, 5, and 7 can be used to determine the maximum drop size which can be expected to vaporize completely. All drops smaller than the above specified maximum drop size can be expected to completely vaporize in the containment. Drops greater

in size than the maximum drop size specified previously will only partially vaporize. The amount of partial vaporization for these drops can be obtained with the use of Equation 14, below, or estimated with the aid of Figures 4, 6, and 8 which are based on a 100 ft fall height. The above approximation applies best to the range of drop diameters where the curves in Figures 3, 5, and 7 are somewhat linear or for fall heights greater than 40 ft. The fraction of a drop vaporized for any given fall height can then be specified given the temperature and airborne water vapor concentrations of the containment atmosphere. The equation defining the fraction of a spray drop vaporized is given by Equation 14.

$$F_i = \frac{a'(D_p \cdot d_i)^{b'}}{d_p} \tag{14}$$

where

D_p - drop diameter at which incomplete vaporization just begins to occur in a 100 ft. containment as determined by Equation 12 or Figures 3, 5, or 7 for the specified temperature and water vapor concentration (cm),
d_p - drop diameter at which incomplete vaporization just begins for all height of interest from Equation 12 or Figures 3, 5, or 7 (cm),
d_i - drop diameter of interest for which fraction of vaporization is desired (cm), and
a', b' - the appropriate coefficients corresponding to the specified temperature and water vapor concentration obtained from Table 4.

Once the maximum drop size which will completely vaporize in the containment has been determined, the vaporization fraction for the sprays can be determined by the use of Equation 15.

$$f = \frac{\sum_{i=1}^{m} n_i \cdot d_i^3 + \sum_{j=m+1}^{\ell} n_j \cdot d_j^3 \cdot F_j}{\sum_{i=1}^{\ell} n_i \cdot d_i^3} \tag{15}$$

where

m - number of drops that will completely vaporize, and
ℓ - total number of drop size intervals produced by the nozzle.
All other parameters are as previously defined.

The calculation of the vaporization fraction can be obtained with varying degrees of accuracy using the methods presented. Due to the complexity of the equations, a computer code was designed to calculate the vaporization fraction for a number of different spray parameters. The use of the code to calculate the vaporization fraction in conjunction with a heat transfer code however, would be cumbersome. As a result, the vaporization fraction was calculated for a number of different conditions and the results presented graphically in Figures 3 - 8. The curves indicate the general dependence of the vaporization fraction for a wide variety of conditions. These results will allow a gross determination to be made for the heat removal capability of a given spray system.

References

1 Tosetti, R.J., Guenther, C.F.; Evaluation of H Combustion and Control Under Degraded Core Conditions for Pilgram-2; NUREG/CR-2017, August 1981

Parsly, L.F.; The Heating of Spray Drops in Air-Steam Atmospheres; ORNL-TM-2412; Part VI; January 1970

3 Bennett, C.O., Myers, J.E.; Momentum, Heat, and Mass Transfer; McGraw Hill; 1962

4 Spraco Spec on 1713A Nozzle; Spray Engineering Company; Burlington, Massachusetts

Table 1

Drop Size Distribution for a Spraco 1713A Nozzle
(Based on a Pressure Differential of 40 PSID)

Drop Interval	Diameter (cm)	Number of Drops	Drop Interval	Diameter (cm)	Number of Drops
1	3.75-3	3	41	1.0375-1	4
2	6.25-3	19	42	1.0625-1	4
3	8.75-3	50	43	1.0875-1	3
4	1.125-2	78	44	1.1125-1	3
5	1.375-2	99	45	1.1375-1	4
6	1.625-2	78	46	1.1625-1	3
7	1.875-2	77	47	1.1875-1	3
8	2.125-2	62	48	1.2125-1	4
9	2.375-2	62	49	1.2375-1	3
10	2.625-2	50	50	1.2625-1	0
11	2.875-2	37	51	1.2875-1	0
12	3.125-2	33	52	1.3125-1	2
13	3.375-2	28	53	1.3375-1	2
14	3.625-2	25	54	1.3625-1	0
15	3.875-2	25	55	1.3875-1	0
16	4.125-2	19	56	1.4125-1	1
17	4.375-2	18	57	1.4375-1	1
18	4.625-2	16	58	1.4625-1	0
19	4.875-2	14	59	1.4875-1	0
20	5.125-2	15	60	1.5125-1	0
21	5.375-2	11	61	1.5375-1	0
22	5.625-2	11	62	1.5625-1	0
23	5.875-2	11	63	1.5875-1	0
24	6.125-2	9	64	1.6125-1	1
25	6.375-2	11	65	1.6375-1	0
26	6.625-2	9	66	1.6625-1	0
27	6.875-2	11	67	1.6875-1	0
28	7.125-2	8	68	1.7125-1	0
29	7.375-2	8	69	1.7375-1	2
30	7.625-2	9	(Maximum Drop Interval Analyzed)		
31	7.875-2	7			
32	8.125-2	8			
33	8.375-2	6			
34	8.625-2	6			
35	8.875-2	7			
36	9.125-2	6			
37	9.375-2	6			
38	9.625-2	4			
39	9.875-2	5			
40	1.0125-1	4			

Table 2

Polynomial Coefficients for Defining Vaporization Function for a Spraco 1713A Nozzle

Saturation Temperature	Coefficients		
	c_1	c_2	c_3
160°F	-0.7432	4.381E-3	-2.758E-6
215°F	-1.0000	5.298E-3	-3.455E-6
285°F	-0.9302	5.274E-3	-3.515E-6

$$f = c_1 + c_2T + c_3T^2$$

Table 3

Power Function Coefficients for Determination of Spray Drop Vaporization Fraction as a Function of Fall Height

Saturation Temperature	Containment Temperature							
	300°F		500°F		700°F		900°F	
	a	b	a	b	a	b	a	b
160°F	500770.	2.817	19863.	2.253	9045.	2.177	4895.	2.086
215°F	1010618.	2.934	19575.	2.284	6818.	2.130	3612.	2.038
285°F	(Drop Condense)		16396.	2.300	5792.	2.212	2066.	1.971

$$H_f = aD^b$$

Table 4

Power Function Coefficients for Determination of Spray Drop Fraction Vaporized After Falling 100. ft

Saturation Temperature	Containment Temperature							
	300°F		500°F		700°F		900°F	
	a'	b'	a'	b'	a'	b'	a'	b'
160°F	0.159	-2.148	1.077	-1.910	2.237	-1.828	4.523	-1.632
215°F	0.168	-2.058	1.483	-1.831	3.253	-1.723	10.85	-1.246
285°F	(Drop Condense)		3.400	-1.551	16.09	-1.013	(vaporized)	

$$F_v = a'D^{b'}$$

DIAGRAM INDICATING SPATIAL COORDINATES OF A FALLING DROP USED IN THE TRAJECTORY MODEL

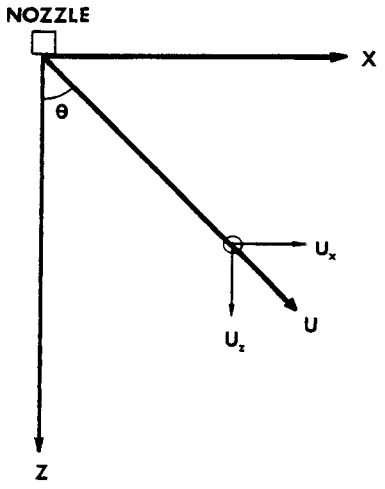


FIGURE 1

FRACTION OF SPRAYS VAPORIZED VS TEMPERATURE FOR A SPRACO 1713A NOZZLE

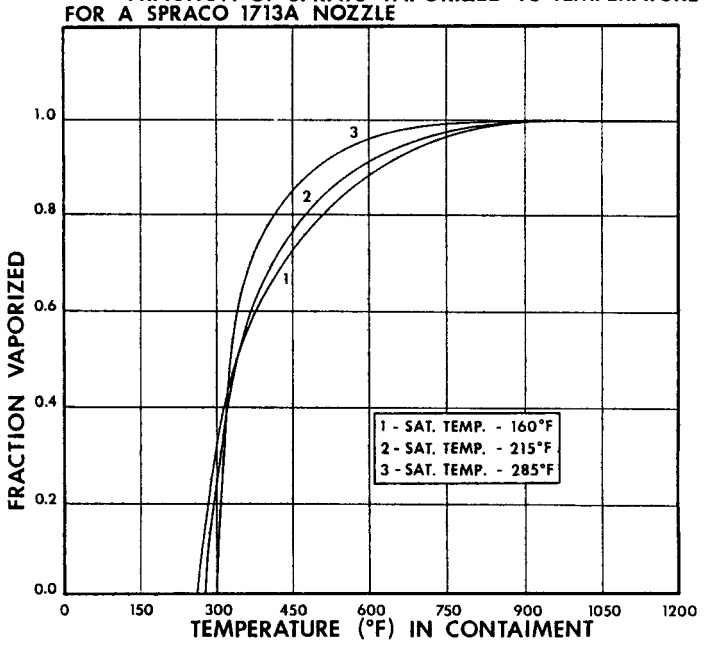


FIGURE 2

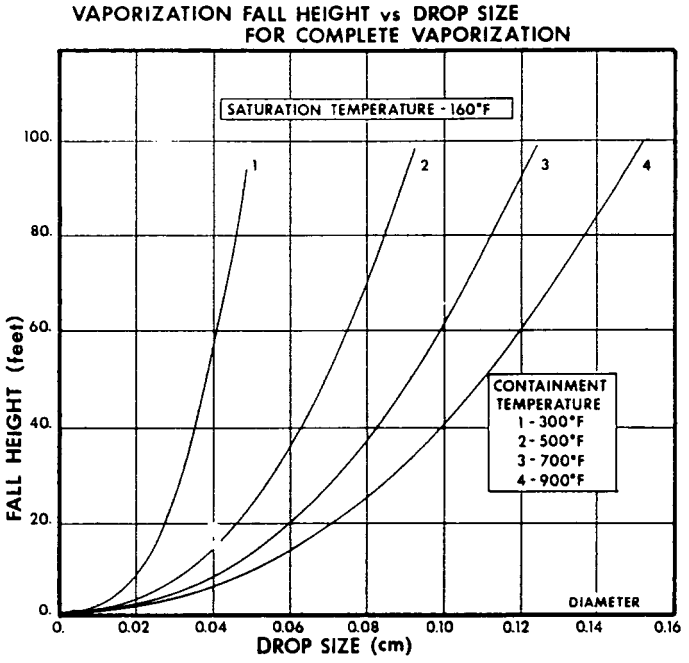


FIGURE 3

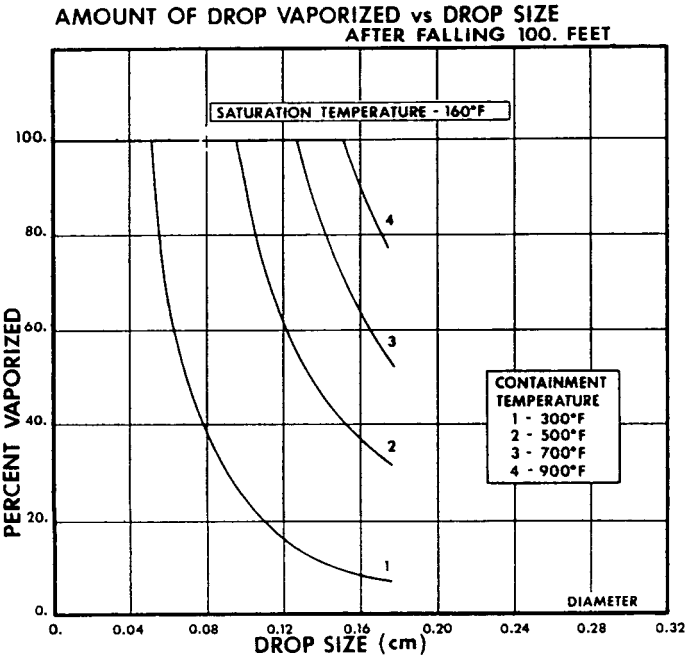


FIGURE 4

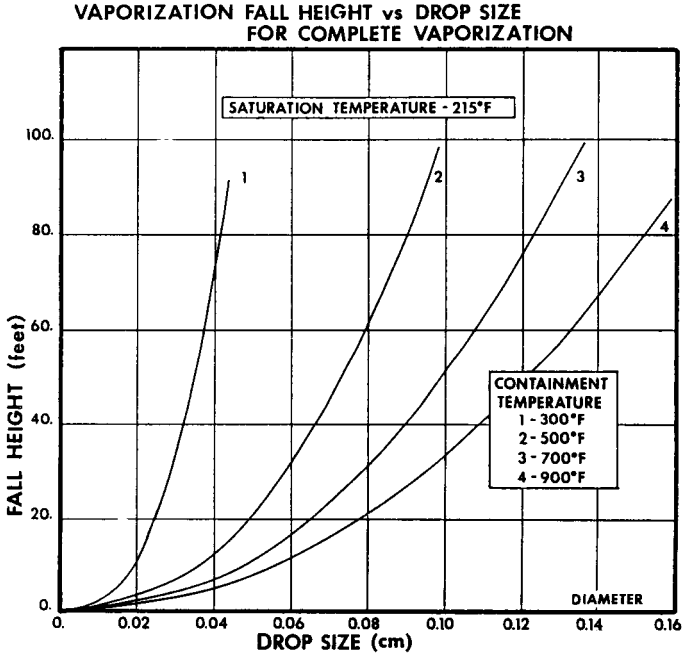


FIGURE 5

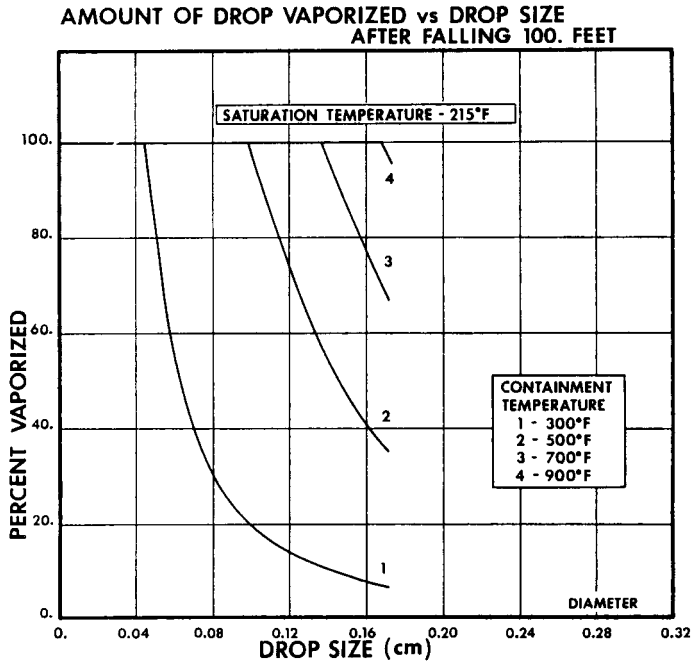


FIGURE 6

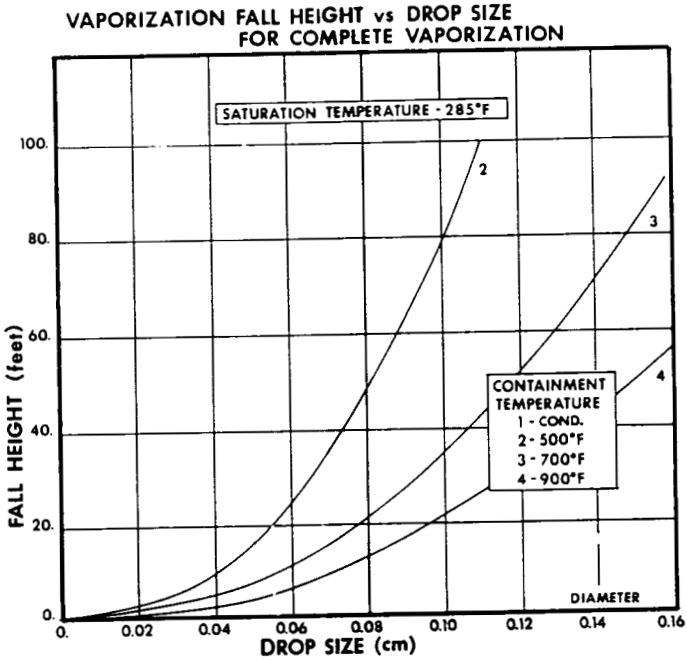


FIGURE 7

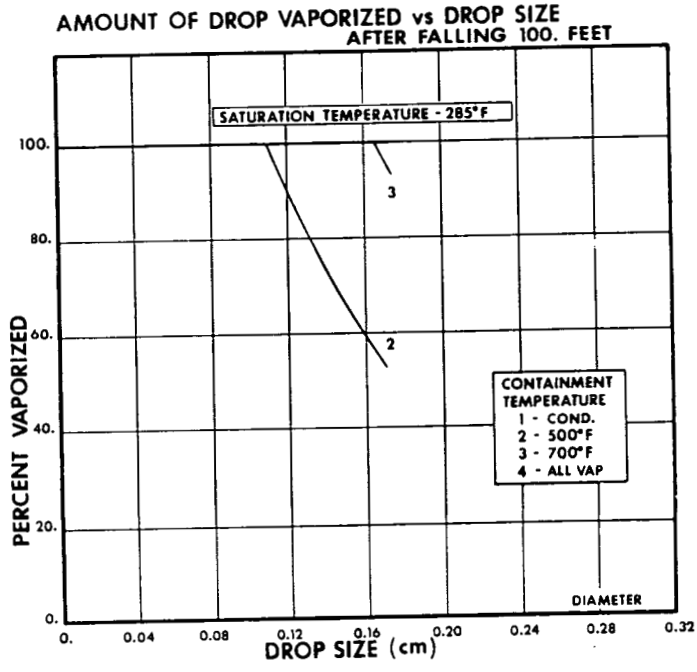


FIGURE 8

755/7 56





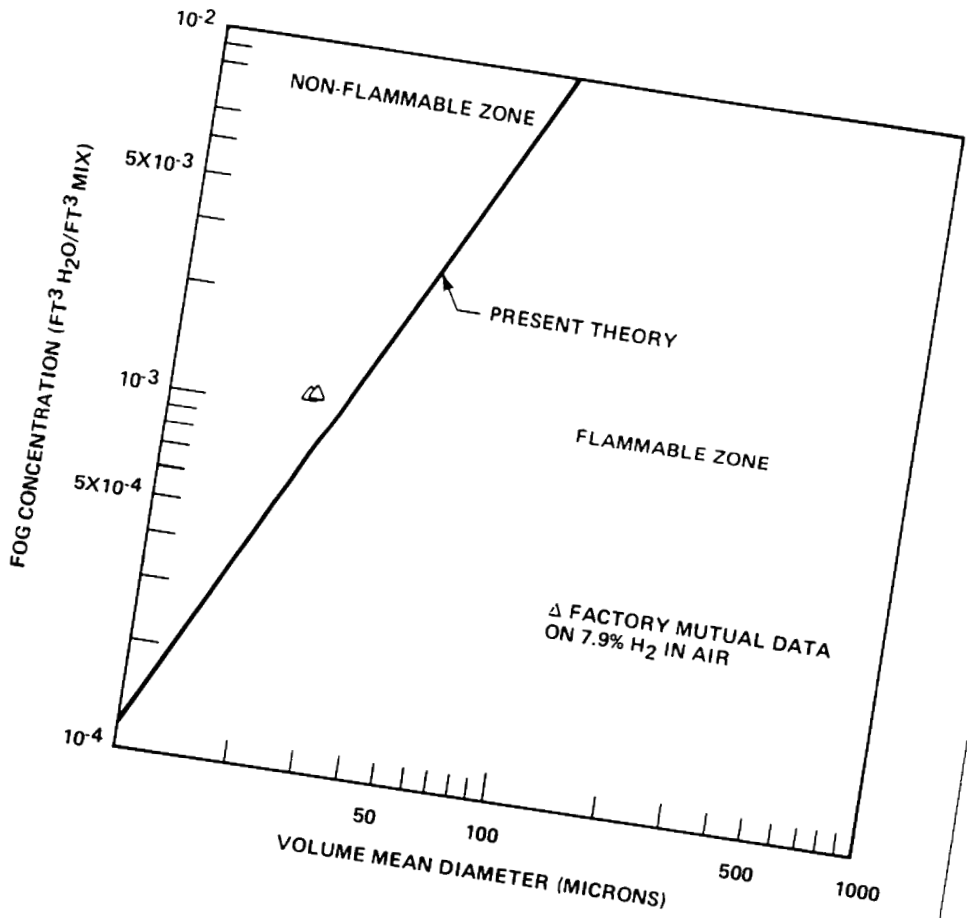


Figure 6. Comparison between the Present Theory and Factory Mutual Fog Inerting Experiments on 7.9 Percent H_2

A HYDRODYNAMIC MODEL OF HYDROGEN FLAME PROPAGATION IN REACTOR VESSELS*

M. R. Baer and A. C. Ratzel
Sandia National Laboratories
Albuquerque, New Mexico 87185

ABSTRACT

A hydrodynamic model for hydrogen flame propagation in reactor geometries is presented. This model is consistent with the theory of slow combustion in which the gasdynamic field equations are treated in the limit of small Mach numbers. To the lowest order, pressure is spatially uniform. The flame is treated as a density and entropy discontinuity which propagates at prescribed burning velocities, corresponding to laminar or turbulent flames. Radiation cooling of the burned combustion gases and possible preheating of the unburned gases during propagation of the flame is included using a molecular gas-band thermal radiation model.

Application of this model has been developed for 1-D variable area flame propagation. Multidimensional effects induced by hydrodynamics and buoyancy are introduced as a correction to the burn velocity (which reflects a modification of planar flame surface to a distorted surface) using experimentally measured pressure-rise time data for hydrogen/air deflagrations in cylindrical vessels. This semi-analytical model of flame propagation reduces to a set of ordinary differential equations which describes the temporal variations of vessel pressure, burned volume and gas entropy. The thermodynamic state of the burned gas immediately following the flame is determined using an isobaric Hugoniot relationship. At other locations the burned gas thermodynamic states are determined using a Lagrangian particle tracking method. Results of a computer code using the method are presented.

*This work performed at Sandia National Laboratories supported by the U. S. Nuclear Regulatory Commission, Office of Nuclear Regulatory Research.

NOMENCLATURE

A	Cross-sectional area
c_v	Specific heat of gas
E	Expansion ratio of unburned gas density to burned gas density
k	Constant in the state-relationship equation; (Equation 9)
L	Length scale of vessel geometry
p	Gas pressure
$\vec{q}_r$	Radiant heat flux vector
Q	Volumetric heat source
R	Gas constant
s	Gas entropy
$\vec{S}$	Surface area vector
t	Time
T	Gas temperature
v	Gas velocity
v_F	Flame speed
V	Volume
x	Length coordinate

Greek

γ	Isentropic index
ψ	Partial volume coordinate
ϕ	Normalized entropy
ρ	Density
μ	Burn velocity

Subscripts

u	Quantity related to unburned volume
b	Quantity related to burned volume
T	Quantity related to total volume
p	Quantity related to a particular parcel of gas
o	Initial gas condition prior to ignition

Superscript

$*$	Quantity related to condition at the flame surface
$\bar{}$	Volume average

INTRODUCTION

To assess the thermal response of reactor components to a deliberate or inadvertent hydrogen burn within a nuclear reactor vessel, the combustion induced thermal environment must be accurately characterized. Estimates of the effects of confined hydrogen/air deflagration are typically based entirely on the thermodynamics of constant volume combustion. Although an adiabatic, isochoric calculation can provide a reasonable estimate of the over-pressure induced by combustion, nonphysical gas temperatures are typically calculated. It is well known that gas

motion occurs during confined combustion and these fluid dynamic effects play a crucial role in establishing the temperature fields [1].

Due to the variety of complex physical and chemical processes which occur during flame propagation, a detailed calculation of transient reactive flow based entirely on first principles is beyond current computational capabilities, even with the best of modern computer hardware [2]. However, certain approximations can be invoked to produce a model which is more amenable to calculation and which retains the strong interaction between chemical release of energy and the dynamics of fluid motion.

The flame propagation model that we use in this study is one which follows the prior work of Sivashinsky [3] and Takeno and Iijima [4]. The fundamental equations of aerothermochemistry are treated in the limit of small Mach number based on the ratio of flame speed to unburned gas sound speed. This approximation greatly simplifies the hydrodynamics associated with deflagration within a confined vessel by ignoring the effect of acoustic/flame interactions. Deflagration of hydrogen and air is typically a low speed phenomena unless disturbed by large scale turbulence effects [5], and thus this limit is easily justified.

The essential combustion physics is modeled by treating the thin flame as a density and entropy discontinuity which propagates at a prescribed rate. Existing data for burn velocity appropriate for laminar [6,7] or turbulent flames [8,9], are used as an input to this formulation and thus resolution of flame structure in the model is unnecessary.

As a flame propagates within an enclosed vessel its surface expands spherically around the ignition location and later is distorted to conform with the confining vessel. If the radius of curvature of the flame is greater than the flame thickness, the hydrodynamics can be treated in a one-dimensional fashion [10]. Multidimensional effects induced by expansion of the combustion products and/or buoyancy effects are added as an empirical correction to the flame shape. This view of flame propagation is formulated to treat variable gas movement of the burned and unburned gas predicted from the equations of motion. The thermodynamic states of the burned and unburned gas are then determined by compression and redistribution by induced gas flows.

Since this model is directed toward determining the thermal fields within the vessel, the model has been expanded to include the effects of thermal radiation energy transfer from the hot burned gas region to the cool unburned gas and to the vessel walls. Typical of large scale fires, the gas is optically thick since the absorption length is much less than the characteristic length of the containment. Consequently, we treat heat loss as a volumetric heat release process in which we utilize an engineering model of thermal radiation. Consistent with the notion

of the Curtis-Godson approximation [11], nonuniform temperature fields are replaced by an equivalent isothermal temperature, and absorption and emission coefficients are determined using molecular exponential wide-band models as detailed by Edwards [12]. A simple energy balance based on enclosure theory is used to determine: 1) the energy lost by the burned gas and 2) the fraction of this energy which is absorbed by the unburned gas (if steam and/or CO_2 is present). A mathematical description of the proposed model follows.

THEORY

Consider an arbitrary enclosed vessel geometry as shown in Figure 1. We shall partition this volume into two regions: the burned and unburned gas regions. Separating these regions is a thin flame which is treated as a density and entropy discontinuity that traverses the vessel. In the derivations to follow we denote conditions in the unburned and burned region, respectively, by the subscripts u and b, and conditions at the flame surface are denoted by the superscript *.

In treating this formulation of slow combustion we use the appropriate gasdynamic equation in which acoustic/flame interactions are ignored. Derivation of these conservation equations can be found in reference 2. The governing equations which apply to both the burned and unburned gas regions are as follows:

Mass: $$\frac{D\rho}{Dt} + \frac{\rho}{A(x)} \frac{\partial}{\partial x}(A(x)v) = 0 \qquad (1)$$

Momentum: $$\frac{\partial p}{\partial x} = 0 \qquad (2)$$

Energy: $$\rho T \frac{Ds}{Dt} = \nabla \cdot \vec{q}_r \qquad (3)$$

State: $$p = R\rho T \qquad (4)$$

where $$\frac{D}{Dt} = \frac{\partial}{\partial t} + v \frac{\partial}{\partial x} \qquad (5)$$

All the variables are defined in the nomenclature. Note that slow combustion limit constrains the pressure within the confined vessel to be only temporally varying. To incorporate the volumetric energy source (or sink) of thermal radiation into the model, the energy equation is integrated over the burned and unburned volumes. Using Green's theorem, the entropy equations are reduced to the following forms:

$$\rho_b T_b \frac{d\bar{s}_b}{dt} = \frac{\oint_b \vec{q}_r \cdot d\vec{S}_b}{V_b} = \frac{Q_b}{V_b} \qquad (6)$$

$$\rho_u T_u \frac{d\bar{s}_u}{dt} = \frac{\oint_u \vec{q}_r \cdot d\vec{s}_u}{V_u} = \frac{Q_u}{V_u} \qquad (7)$$

Consistent with the usual engineering treatment of hot gas thermal radiation, we represent the rate of heat loss from the combustion gases and the absorption of thermal radiation by the [illegible]ned gases using an equivalent isothermal temperature (obtained [illegible] a volumetric weighted average emissive power) and mean beam length for each region. Emission and absorption coefficients are then computed using the appropriate molecular band models for H_2O, CO_2 and CO [12]. The rate of energy loss from the combustion region is then determined by the thermal radiation which is emitted from the burned region through the surface area encompassing the burned volume. In a similar manner the rate of energy transfer to the unburned gas is taken as that fraction of the radiant energy which passes through the flame surface from the burned volume. A determination of the absorption coefficient within the unburned region establishes the energy which can be absorbed by the cool unburned gas. The remaining energy from the combustion region is transmitted to the vessel walls within the burned and unburned gas regions. The enclosure walls are treated as cold blackbody surfaces, and hence the wall radiative transfer to the gas is omitted in this analysis. For further details on the exponential wide-band model formulations utilized in this work, the reader should review the monograph by D. K. Edwards on molecular gas band radiation [12].

For the sake of simplicity, we shall define the normalized entropy variable:

$$\phi = \bar{s}/c_v \qquad (8)$$

and utilize the following thermodynamic state relation for an ideal gas:

$$p = k\rho^{\gamma} e^{\phi} \qquad (9)$$

In contrast to prior work [4], we have found that it is convenient to introduce a partial volume coordinate, which is given as follows:

$$\psi = \frac{\int_0^x A(x)dx}{\int_0^L A(x)dx} \qquad (10)$$

[illegible]otal vessel volume is given by the denominator of Equation (10). By definition, ψ^* represents a particular flame location and denotes the fraction of the vessel volume which has burned. Note that $\psi^* = 0$ conveniently defines the ignition location and $\psi^* = 1$ indicates when complete burning has occurred. The equations of motion are therefore reduced to the following forms:

$$\frac{\partial(Av)}{\partial\psi} = -\frac{V_T}{\gamma_u}\left\{\frac{1}{p}\frac{dp}{dt} - \frac{d\phi_b}{dt}\right\} \qquad (\psi < \psi^*) \qquad (11)$$

$$\frac{\partial(Av)}{\partial\psi} = -\frac{V_T}{\gamma_u}\left\{\frac{1}{p}\frac{dp}{dt} - \frac{d\phi_u}{dt}\right\} \qquad (\psi > \psi^*) \qquad (12)$$

$$\frac{d\phi_b}{dt} = \frac{(\gamma_b - 1)Q_b}{pV_T\psi^*} \qquad (\psi < \psi^*) \qquad (13)$$

$$\frac{d\phi_u}{dt} = \frac{(\gamma_u - 1)Q_u}{pV_T(1-\psi^*)} \qquad (\psi > \psi^*) \qquad (14)$$

The gas velocity fields are obtained by integration of Equations (11) and (12) with the use of appropriate boundary conditions. For the problem of interest we treat an ignition source located near a wall. For enclosed vessels the normal flow at the walls must vanish and thus at $\psi = 0$ and 1, $v = 0$. Therefore,

$$v_b = -\frac{V_T}{A(x)}\frac{\psi}{\gamma_b}\left\{\frac{1}{p}\frac{dp}{dt} - \frac{d\phi_b}{dt}\right\} \qquad (\psi < \psi^*) \qquad (15)$$

and

$$v_u = -\frac{V_T}{A(x)}\frac{(\psi-1)}{\gamma_u}\left\{\frac{1}{p}\frac{dp}{dt} - \frac{d\phi_u}{dt}\right\} \qquad (\psi > \psi^*) \qquad (16)$$

By definition, we introduced the burning velocity, μ, as a given input to the model and thus at the flame surface,

$$v_u^* - v_b^* = \mu(E-1) \qquad (17)$$

where $E = \rho_u^*/\rho_b^*$ is the expansion ratio which is calculated using a Hugoniot relationship at constant pressure. Using Equations (15) and (16), the pressure rise induced by combustion is determined by:

$$\frac{1}{p}\frac{dp}{dt} = \frac{\left\{\frac{\mu(E-1)A^*}{V_T} + \left[\frac{\psi^*}{\gamma_b}\frac{d\phi_b}{dt} + \frac{(1-\psi^*)}{\gamma_u}\frac{d\phi_u}{dt}\right]\right\}}{\left\{\frac{(1-\psi^*)}{\gamma_u} + \frac{\psi^*}{\gamma_b}\right\}} \qquad (18)$$

In addition, the conservation of mass across the flame discontinuity requires that:

$$E(v_u^* - \mathscr{V}_F^*) = (v_b^* - \mathscr{V}_F^*) \qquad (19)$$

where

$$\mathscr{V}_F^* = \frac{V_T}{A^*}\frac{d\psi^*}{dt} \qquad (20)$$

This constraint determines the time rate of change of the burn volume fraction, ψ^*, by combining Equations (15), (16), (19) and (20). The burn volume fraction is thus given as:

$$\frac{d\psi^*}{dt} = \frac{1}{(E-1)} \left\{ \frac{1}{p} \frac{dp}{dt} \left[\frac{\psi^*}{\gamma_b} + \frac{E(1-\psi^*)}{\gamma_u} \right] - \frac{\psi^*}{\gamma_b} \frac{d\phi_b}{dt} - \frac{(1-\psi^*)}{\gamma_u} \frac{d\phi_u}{dt} \right\} \quad (21)$$

To determine the thermodynamic state of the unburned gas as it corresponds to the temporal variation of vessel pressure, we use Equation (9) to define the density and temperature fields:

$$\frac{\rho_u}{\rho_o} = \left\{ \frac{p}{p_o} e^{-(\phi_u - \phi_o)} \right\}^{1/\gamma_u} \quad (22)$$

and

$$\frac{T_u}{T_o} = \left(\frac{p}{p_o} \right)^{(\gamma_u - 1)/\gamma_u} e^{(\phi_u - \phi_o)/\gamma_u} \quad (23)$$

The thermodynamic field within the burned gas region is solved using a Lagrangian particle tracking method. To illustrate this method, consider a particle of gas that burned at a particular time denoted by the subscript p. At this time the gas is located at ϕ_p and its burned gas density is ρ_p. An integration of Equation (15) requires that at later times the gas density must change to conform with the vessel pressure and hot gas entropy. This particle of gas contracts to another location, ϕ_b, such that:

$$\rho_b \phi_b = \rho_p \phi_p \quad (24)$$

Gas density and temperature for this particle of burned gas are then determined using Equation (9):

$$\frac{\rho_b}{\rho_p} = \left(\frac{p}{p_p} e^{-(\phi_b - \phi_p)} \right)^{1/\gamma_b} \quad (25)$$

$$\frac{T_b}{T_p} = \left\{ \frac{p}{p_p} \right\}^{(\gamma_b - 1)/\gamma_b} e^{(\phi_b - \phi_p)/\gamma_b} \quad (26)$$

As an overview of this semi-analytical model, the hydrodynamics of confined vessel flame propagation is simplified to a set of ordinary differential equations which describe the temporal variation of vessel pressure, burned volume, and burned and unburned gas entropy. These equations are solved numerically using a Runge-Kutta integrator. The thermodynamic state of the unignited gas specifies the initial condition for solution to these equations. As the computation is marched forward in time, a Hugoniot calculation is performed to determine flame temperature, burned gas density and burned gas isentropic index. An efficient equilibrium calculational procedure is used and comparison with the Gordon/McBride equilibrium computer code [13] shows agreement well within

1% for all cases studied (from lean to rich mixtures). Also at each time step, absorption and emission coefficients are determined in order to define the temporal variation of the thermal radiative energy transfer.

COMPARISON WITH EXPERIMENTAL DATA

In the context of the model proposed in this study, if we consider flame propagation within a uniform channel, the flame is treated as a planar surface. Three-dimensional gas motions occur during propagation and thus the flame is more realistically represented as a distorted surface. To incorporate multidimensional effects in this model we construct a correction to the flame surface calculation utilizing experimental data.

Two sets of experimental data are available for determining flame surface corrections [14,15]. Of particular interest is the pressure-rise time from ignition to the over-pressure maximum, since this is a measure of the time required for the flame to traverse the enclosed vessel. The data shown in Figure 2 is a plot of pressure-rise time obtained for combustion of various hydrogen/air mixtures within an 11 liter cylindrical vessel (8 cm diameter and 63 cm axial length) [14]. Calculations using the planar surface model are represented by the upper broken curve in Figure 2. The differences between these calculations and the experimental data are used to define a mean correction to the flame surface. Figure 3 presents the ratio of experimental rise time to the planar surface calculated value. This ratio is used as a multiplicative correction to the flame surface area. Calculations using the revised model are represented by the solid line through the data in Figure 2.

To further test this flame surface correction we apply the model, without further manipulation, to a second series of tests within a different geometry which has an effective combustion volume of 4.3 m^3 (enclosed volume of 5.7 m^3) [15]*. Predictions using the flame surface corrections demonstrate reasonable agreement to observed pressure-rise time as seen in Figure 4. Differences seen for the lean mixtures (< 10% H_2 concentrations) correspond to buoyancy effects which cause additional distortion. Flame shape corrections for the lean mixture will be included in the model when additional experimental data become available.

*The vertically aligned cylindrical test vessel was 4.88 m long with a diameter of 1.22 m. The ignition source, either sparkplug or glowplug, was positioned ~1.20 m from the base. Hence, considering only upward propagation of the flame, the physical burn length was 3.68 m and the appropriate burn volume was 4.3 m^3. It should be noted that the concurrent downward flame propagation is assumed to be independent of the upward flame propagation. Future experimental and analytical efforts are planned to evaluate this simplification.

Shown in Figures 5 and 6 are comparisons between model prediction and experimentally measured maximum pressure (normalized by initial pressure) for various H_2/air test burns in the 5.7 m^3 vessel. For the purpose of demonstrating the effect of thermal radiation loss during propagation, the model predictions which include energy loss are compared with isochoric, adiabatic calculations. In Figure 5, the model predictions are bounded by results obtained for the rise times given from the flame surface correlations presented in Figures 3 and 4 (lower curve) and by results obtained from exactly matching the rise times of the experimenal data (upper curve). As seen in this figure, the nonadiabatic calculations reasonably follow the trends of experimental data. Predictions for mixtures less than 8% hydrogen concentration are suspected to be fortuitously coincidental to the data since one expects incomplete combustion to occur for these very lean mixtures. However, for lean hydrogen/air mixtures greater than 8%, the combustion is slow enough to allow an appreciable energy loss during propagation as seen by the reduction in overpressure. As the hydrogen concentrations increase the nonadiabatic calculations approach those without energy loss because the burning becomes progressively more rapid. In Figure 6, the effect of carbon dioxide dilution on the peak pressures is given. In these studies, fixed quantities of hydrogen (150 Torr) and dry air (400 Torr) were mixed with different quantities of carbon dioxide prior to ignition. Lacking flame velocity (pressure-rise time) correlations for combustion in hydrogen-air-carbon dioxide mixtures, we adjusted the burn velocity to match the experimental rise time for each test. The model again overestimates the peak pressure, though the trends are matched for the lower carbon dioxide percentages. Near the assumed inerting level indicated on the figure, the experimental and model predictions deviate, because the model computes pressure rises assuming complete combustion.

SIMULATION RESULTS

To demonstrate model predictions representative of lean hydrogen/air deflagrations, the initial hydrogen concentration is 10% by volume for all the following test cases. (This concentration probably represents an upper bound for deliberate ignition scenarios considered in nuclear reactor containments in the event of hydrogen generation resulting from a loss-of-coolant accident.) Furthermore, only laminar flame propagation is considered in this study, using the experimental burn velocity data of Liu and MacFarlane [6] and the flame correction correlation shown in Figure 2.

A series of typical results for adiabatic combustion in the 5.7 m^3 experimental geometry (described in the previous section) is summarized in Figure 7. Shown in the figure is the spatial variation of gas velocity, density and temperature for different times during the flame propagation. Gas velocity reversal at the flame front location and compressive heating of the combustion gases are clearly seen in this figure.

As discussed previously, the effects of radiation heat transfer from the hot combustion products are important in estimating pressure rise. In addition, the heat loss mechanism may affect the temperature distributions rather dramatically, as shown in Figure 8. For hydrogen-lean deflagrations, the effect of heat loss from the burned gas region overrides gas compressive effects. Hence, the last gas layers consumed by the flame appear to have the highest temperatures following the completion of burning within the vessel. This is completely reversed from the adiabatic calculation, seen in Figure 8, which shows that the gas layers first burned have the highest temperatures. (Boundary layer effects are neglected in this analysis so that the above discussions are not relevant for regions very close to the vessel walls.) Since the combustion time scale determines the extent of radiation cooling during the burn, the effect of this energy loss becomes more significant for large enclosed vessels. In comparing Figures 8b and 8c, for example, the gas temperature at the location where combustion first occurred is reduced by over 200 K when the volume is increased by three orders of magnitude (Figure 8c results were obtained using a cylindrical containment 36.8 m long by 6.1 m radius). Additional scale effects are shown in Figure 9 which gives the temporal variation of burn velocity, pressure, temperature and entropy. In these figures the time variable is normalized by the time required for the flame to completely traverse the vessel volume. The mean temperature in Figure 9c is the temperature based on a weighted emissive power ($\propto T^4$) used for the radiation calculation.

As a final example, we present a model prediction which demonstrates variable flow area effects using an axisymmetric reactor scaled geometry for the Grand Gulf Boiling Water Reactor. (See Figure 10.) Laminar, planar flame propagation is treated using a uniform 10% hydrogen concentration in dry air. Ignition is assumed to occur circumferentially at the base of the containment vessel. The total gas volume and internal surface area of this vessel are 3.79 (10^4) m^3, and 1.12 (10^4) m^2, respectively, representative of the actual Grand Gulf geometry.

Figure 11 summarizes the pressure rise predictions for adiabatic and nonadiabatic combustion analyses in this vessel. As noted previously, the maximum pressure in containment is significantly reduced when the heat losses by radiation are included. Variations due to flow area effects are shown in Figure 12. The large gradients in gas velocity occur due to rapid area changes. These rapid changes in gas velocity represent possible locations of turbulence production, which may potentially cause turbulent flame acceleration.

SUMMARY

A hydrodynamic model for hydrogen flame propagation within enclosed vessels has been developed to investigate the effects of gas motion in establishing the thermal environment induced by hydrogen combustion. Radiation heat transfer has been included

in this work to assess heat loss effects during combustion. Experimental data on pressure-rise time and maximum over-pressure due to combustion have been matched to this theory by introduction of a flame shape correction which empirically adds multi-dimensional effects to the hydrodynamic model. Calculations and experimental data indicate that significant energy loss occurs for confined laminar combustion of hydrogen-lean mixtures burned in large vessels. Furthermore, thermal radiation heat loss during propagation significantly modifies the temperature field induced by gas motion.

Calculations using this simple model are computationally inexpensive and thus a wide variety of parameter studies can be made. Future efforts will address buoyancy effects and turbulent flame propagation when experimental data become available.

ACKNOWLEDGMENT

The authors acknowledge M. P. Sherman and M. J. Wester for their efforts in developing a gas band radiation computer model which was adapted for use in this work.

REFERENCES

1. Garforth, A. M. and Rallis, C. J., "Gas Movement During Flame Propagation in a Constant Volume Bomb", Acta Astronautica, 3, 1976, pp. 879-888.

2. Oran, E. S. and Boris, J. P., "Detailed Modeling of Combustion Systems", Prog. Energy Comb. Sci., 7, 1981, pp. 1-77.

3. Sivashinsky, G. I., "Hydrodynamic Theory of Flame Propagation in an Enclosed Volume", Acta Astronautica, 6, 1969, pp. 631-645.

4. Takeno, T. and Iijima, T., "Theoretical Study of Nonsteady Flame Propagation in Closed Vessels", Progress in Astronautics and Aeronautics, 76, 1979, pp. 578-595.

5. Lee, J. H. S. and Moen, I. O., "The Mechanism of Transition from Deflagration to Detonation in Vapor Cloud Explosions", Prog. Energy Combust. Sci., 6, 1980, pp. 369-389.

6. Liu, D. D. S. and MacFarlane, R., "Laminar Burning Velocity of Hydrogen-Air Flames", to appear in Combustion and Flame.

7. Warnatz, J., "Concentration, Pressure and Temperature Dependence of the Flame Velocity in Hydrogen-Oxygen-Nitrogen Mixtures", Combustion Science and Tech., 26, 1981, pp. 203-213.

8. Kozachenko, L. and Kuznetsov, I., "Burning Velocity in a Turbulent Stream of a Homogeneous Mixture", Combustion, Exp. and Shock Waves, 1, 1965, p. 22.

9. Abdel-Gayed, R. G. and Bradley, D., "Dependence of Turbulent Burning Velocity on Turbulent Reynolds Number and Ratio of Laminar Burning Velocity to R.M.S. Turbulent Velocity", 16th Symposium (International) on Combustion, 1967, pp. 1725-1736.

10. Sivashinsky, G. I., "On a Distorted Flame Front as a Hydrodynamic Discontinuity", Acta Astronautica, 3, 1976, pp. 889-918.

11. Siegel, R. and Howell, J. R., Thermal Radiation Heat Transfer, Second Edition, McGraw Hill Book Co., New York, 1981.

12. Edwards, D. K., "Molecular Gas Band Radiation", Advances in Heat Transfer, 12, T. F. Irvine and J. P. Hartnett, Ed., Academic Press, New York, 1976.

13. Gordon, S. and McBride, B., "Computer Program for Calculation of Complex Chemical Equilibrium Compositions, Rocket Performance, Incident and Reflected Shocks and Chapman-Jouquet Detonations", NASA SP-273, March 1976.

14. Baer, M. R., Griffiths, S. K. and Shepherd, J. E., Hydrogen Combustion in Aqueous Foams, SAND82-0917, to appear in 1982.

15. Berman, M., "Light Water Reactor Safety Research Program Semiannual Report, April-September 1981", SAND82-0006, February 1982.

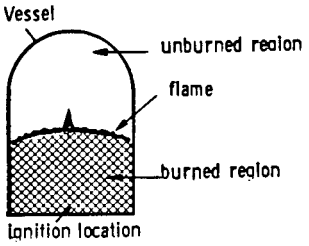


Figure 1. A typical enclosed vessel geometry considered by the model.

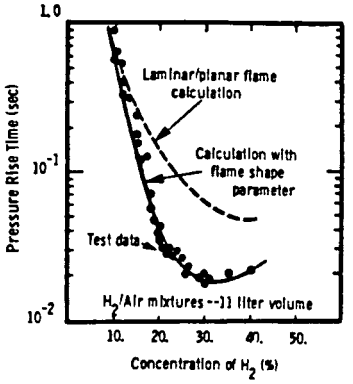


Figure 2. Comparison between theory and experiment with and without flame shape correction in an 11 liter test volume

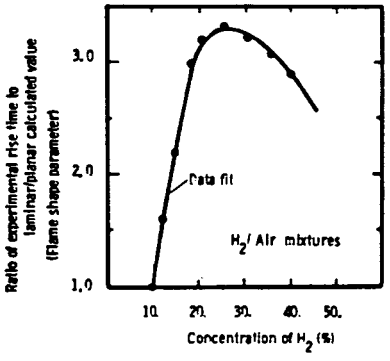


Figure 3. Correction of flame shape as inferred from Figure 2 data in the 11 liter test volume

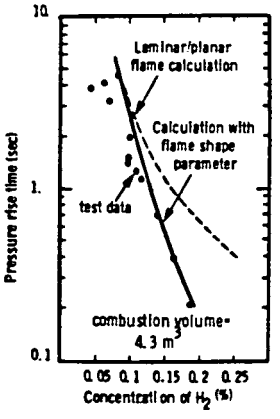


Figure 4. Comparison between theory and experiment for pressure rise time in a combustion volume of 4.3 m^3

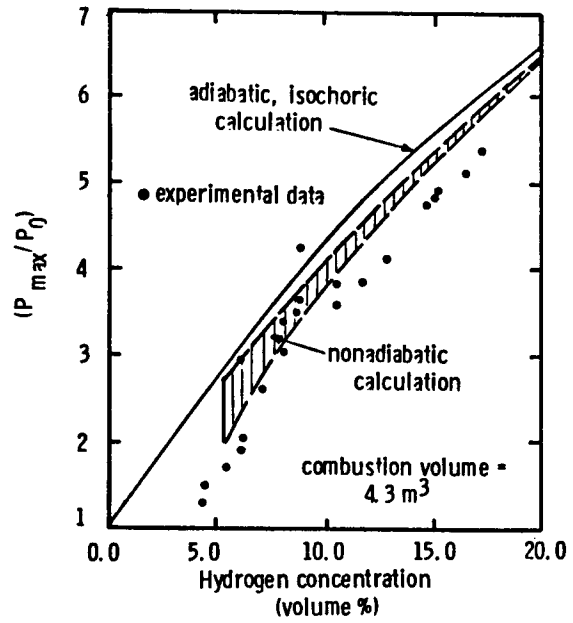


Figure 5. Comparison between theory and experiment for pressure rise resulting from deflagrations of hydrogen-air mixtures in a combustion volume of 4.3 m^3

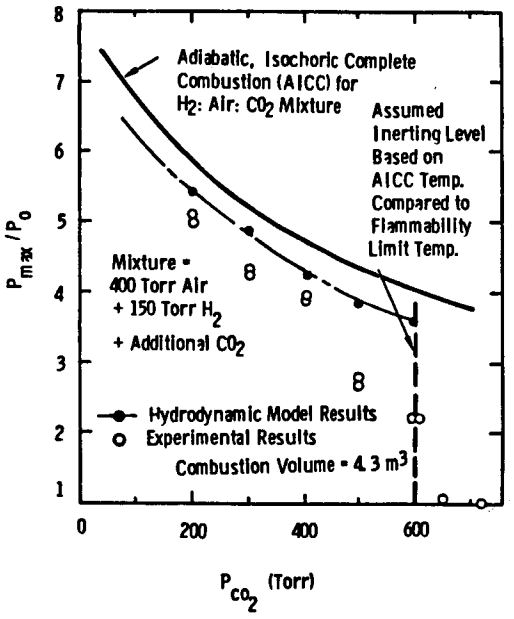


Figure 6. Comparison between theory and experiment for pressure rise resulting from deflagrations of hydrogen-air-carbon dioxide mixtures in a combustion volume of 4.3 m^3

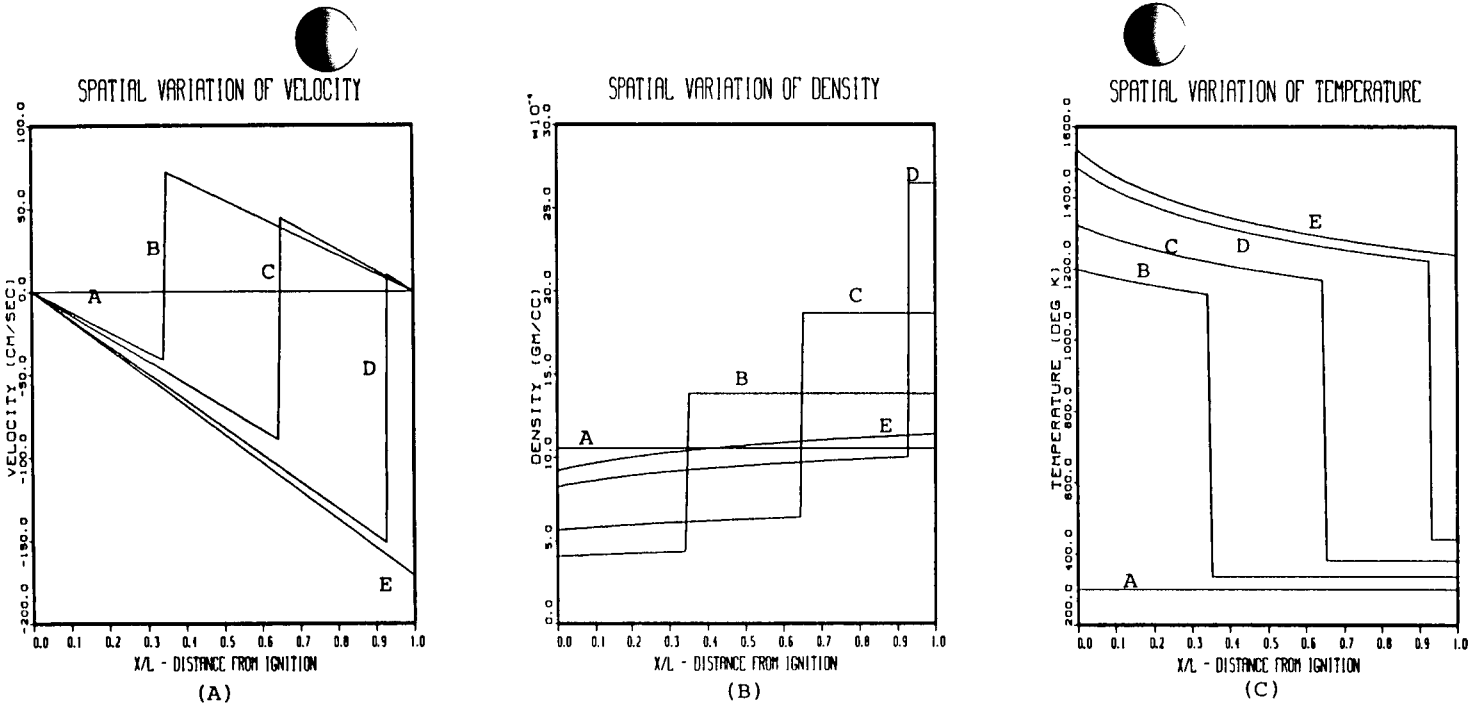
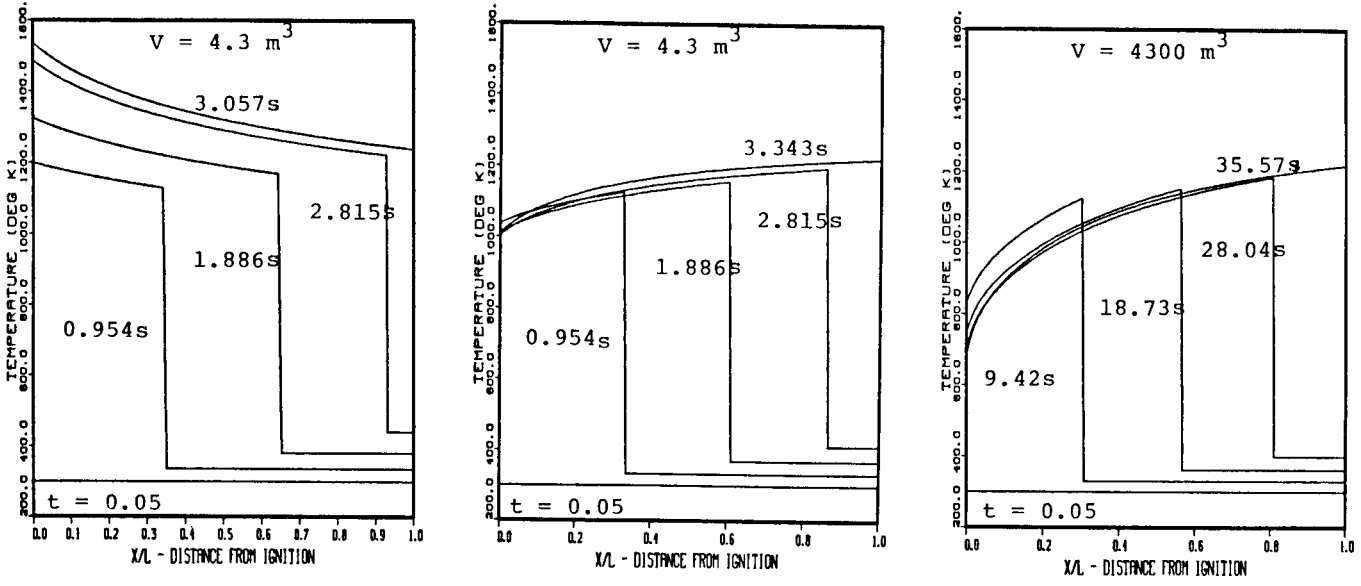


Figure 7: Spatial gas velocity, density and temperature distributions for laminar-adiabatic H_2/air deflagration in a 4.3 m^3 cylindrical vessel: 10% H_2 concentration, humidity ratio = 0.5, and P_o = 1 atm

A: t = 0.0 sec
B: t = 0.954 sec
C: t = 1.886 sec
D: t = 2.815 sec
E: t = 3.057 sec



A: Adiabatic Combustion B: Nonadiabatic Combustion C: Nonadiabatic Combustion

Figure 8. Spatial gas temperature distributions for laminar H_2/air deflagrations: 10% H_2 concentration, humidity ratio of 0.5, P_o = 1 atm.

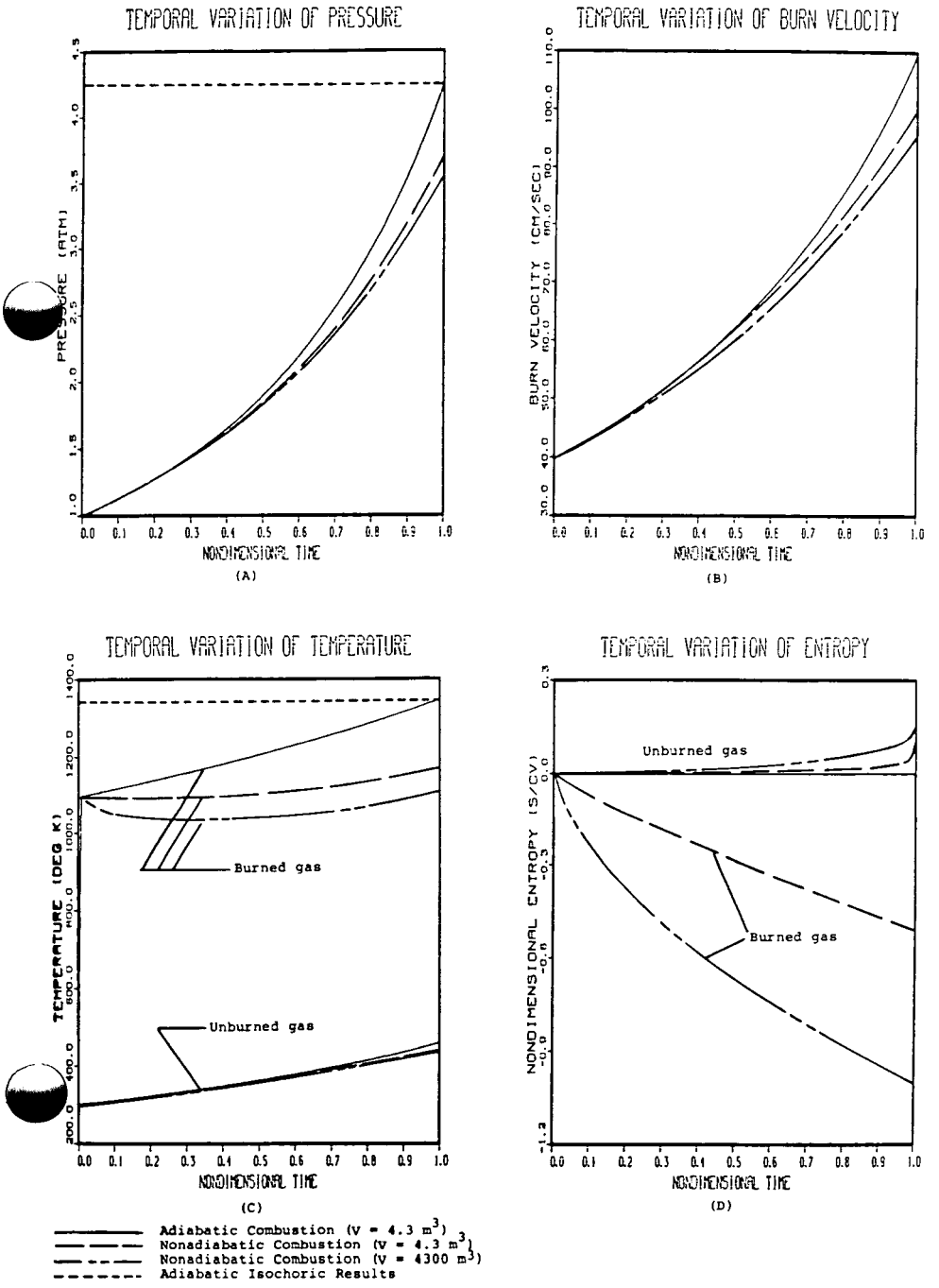


Figure 9. Temporal variation of pressure, burn velocity, mean gas temperature and entropy for laminar H_2/air deflagration: 10% H_2 concentration, humidity ratio of 0.5, P_o = 1.0 atm.

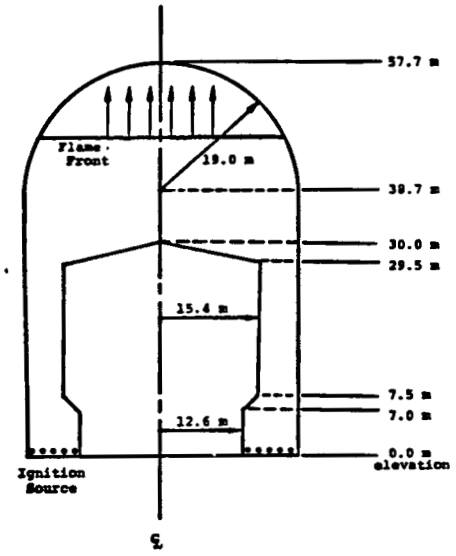


Figure 10. Schematic of the Grand Gulf Boiling Water nuclear reactor containment ($V = 3.79\ (10^4)\ m^3$)

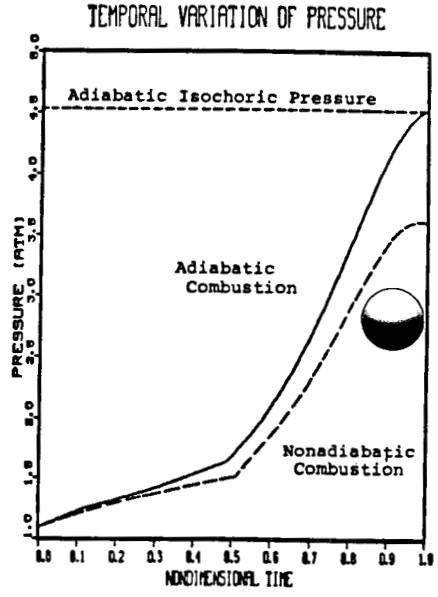
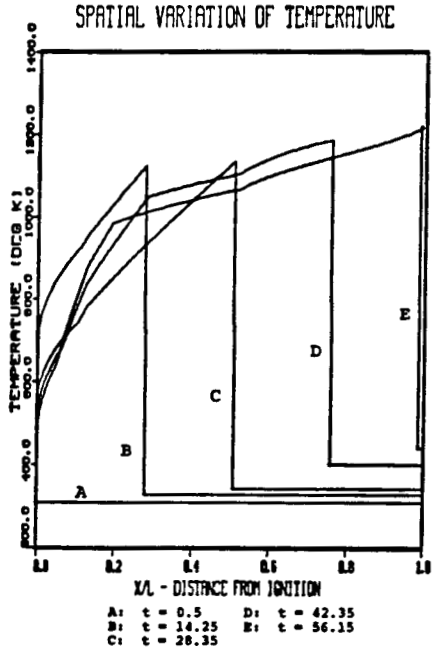


Figure 11. Temporal pressure rise obtained from a 10% H_2/air deflagration in the containment of Figure 10.



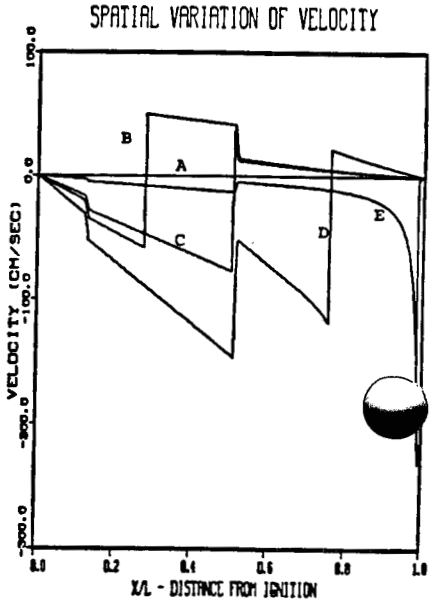


Figure 12. Spatial gas temperature and velocity distributions for 10% H_2/air deflagration in the containment of Figure 10.

TURBULENT CONDENSATION IN THE PRESENCE OF A NONCONDENSIBLE GAS

Michael Corradini
Assistant Professor

Nuclear Engineering Department
University of Wisconsin-Madison

INTRODUCTION

During a postulated loss of coolant accident (LOCA) or a degraded core accident in a light water reactor (LWR) an important concern is to be able to predict the pressure-temperature response in the containment building as steam and possibly gas (e.g. hydrogen) are injected into it. The high energy coolant released from the primary system is a concern because it can significantly contribute to a rise in the containment pressure threatening its structural integrity. During a LOCA the water blowdown flashes to steam as the emergency cooling systems begin to reflood the core. In this case the containment pressure rise due to steam not only affects containment structural integrity, but also impacts the reflood rate in the core; i.e. it establishes the back pressure affecting coolant bypass of the core. In a degraded core accident steam and hydrogen would first be released to the containment. If the concentration of hydrogen increases in the atmosphere to its deflagration limit, it can burn producing superheated steam which can also threaten containment structural integrity.

Current containment designs utilize both active and passive safeguard systems to remove the energy from the atmosphere or to condense the steam. The active systems include containment sprays, fan coolers, ice condensers, low head recirculation pumps and suppression pool cooling. The containment pressure is also reduced by convective heat transfer to the containment walls and internal structural components. If the wall surface temperature is below the dewpoint, the heat transfer can be greatly increased by steam condensation. At a minimum turbulent convective heat transfer will occur due to natural convection currents. Forced convection may be expected due to the flows induced by steam blowdown, containment sprays, fans and possibly by the expansion of combustion gases (e.g. H_2). This latter mode of heat transfer is the general subject of this paper.

Steam condensation in an LWR containment is a complex process dependent on the amount of air locally present, geometry, vapor velocity and the condensation surface [1]. Initially dropwise condensation is expected to occur on the dry cold surface. Because of its unsteady and non-uniform nature dropwise condensation is difficult to model and only experimental trends are measured. It is not expected that it would impact the final containment pressure-temperature response [2]. Dropwise condensation would very quickly change to film condensation. This is the physical situation which will persist throughout the rest of the accident; the steam-condensing as a liquid film on cold surfaces in the presence of air.

A literature review [3,4] indicates that extensive research has been done on film condensation. The original work of Nusselt [5] has been extended to include the effect of interfacial shear, inertia forces, variable properties, energy convective terms and the presence of noncondensible gases. This final effect, the presence of noncondensible gases,

is the most important physical factor affecting condensation heat transfer. The accumulation of noncondensibles at the cold surface near the condensate film inhibits the diffusion of the vapor from the bulk gaseous mixture to the liquid film, thereby reducing the rate of heat transfer. This physical effect requires analysis of the simultaneous heat-mass transfer problem which is distinct from the Nusselt film analysis.

Collier [1] outlines a method to solve the coupled problem based upon kinetic theory diffusion. The final form of this model suggests dimensionless groups to be correlated using experimental data.

Generally solutions to this coupled problem require simplications to be made in the governing heat-mass-momentum equations. One method used the mass diffusion equation; however this technique did not consider the momentum or energy boundary layer.

A common assumption is to consider laminar flow. Sparrow and Eckert [7] solved the mass, momentum and energy equation for a one-dimensional liquid film under the influence of superheated vapor and noncondensible gases. The interfacial shear effect was considered by Koh et al. [8]. The condensation of saturated steam-air mixtures with constant fluid properties was also analyzed [9]. Minkowycz et al. [10] extended this approach to include the effects of interfacial resistance, variable properties, and diffusion for both the liquid film and the steam-air mixture. Sparrow et al. later included the effects of forced convection [11]. Because the LWR containment building is large and the flow probably turbulent, these models are not directly applicable to the current problem.

There has been a number of condensation experiments and correlations with noncondensible gases present. A good review is given by Whitley [4]; in addition he proposes a correlation for forced convection condensation. The most relevant experiments were conducted by Uchida [12] and Tagami [13]. They were conducted in a large vessel at low pressures (0.1 to 0.3 MPa) in which steam was injected into the air atmosphere. The condensing surface was a vertical cylinder (200 mm in diameter with a length of 300 and 900 mm). The condensation heat transfer coefficient was measured as a function of the ratio of the mass of steam to air, the pressure, the condensing length, and noncondensible gas composition (air, nitrogen, argon). The most important effect was the steam to air mass ratio. Based on these tests an empirical correlation was developed which is currently used in LWR licensing calculations. These experimental results were not confirmed at different scales and their theoretical bases are not completely known.

The objective of this paper is twofold. First a condensation model for turbulent flow is derived for both forced and natural convection based upon first principles. Secondly the model developed is compared to the results of Uchida and Tagami tests to gain some insight into the data.

MODEL DEVELOPMENT

Consider the conceptual picture of the condensation process, as shown in Figure 1. The hot gas-vapor mixture transfers energy to the cold wall by two processes. First, the temperature gradient from the bulk to the cold wall provides the driving potential for energy exchange by convective heat transfer (either forced or natural convection) and possibly radiative if the gas temperature is high. Secondly, if the cold wall surface temperature is equal to or below the dewpoint of the gas-vapor mixture (i.e. the vapor saturation temperature at its partial pressure) then the vapor will diffuse through the noncondensible gas component and condense on the cold wall as a liquid transferring energy to the cold wall by latent heat transport.

Once condensation has begun the temperature at the vapor-gas-liquid interface is different from the wall surface temperature; the rate of energy transfer to cold wall is given by the total heat flux

$$q'' = h_{TOT} (T_B - T_w) \tag{1}$$

where h_{TOT} is the overall heat transfer coefficient. This term is in general composed of two heat transfer resistances; the first due to energy transfer through the liquid condensate and the second due to energy transfer in the gas-vapor mixture

$$1/h_{TOT} = 1/h_{film} + 1/h_{gas} \tag{2}$$

One can assume in this analysis that the liquid condensate is in the form of a film flowing down the cold wall. This film condensation concept is valid over most of the course of the heat transfer process, as discussed previously.

The heat transfer coefficient in the gas-vapor mixture is in general made up of three contributions; first, convective heat transfer from the mixture to the film, second, condensation of the steam onto the liquid film, and third, radiation heat transfer from the gas-steam mixture.

$$h_{gas} = h_{conv} + h_{cond} + h_{rad} \tag{3}$$

This final heat transfer coefficient becomes important when the initial gas-vapor mixture is combustible (e.g. hydrogen-steam-air) and after a deflagration the gas-vapor mixture is at high temperatures making radiation an important consideration. In the present model development radiation is neglected. The reader is directed to the current research work of Berman, Sherman, et al. [3] for a discussion of current radiation heat transfer modelling. In this development we concentrate on the development of a turbulent condensation model in forced and natural convection.

The heat transfer coefficient for the flowing film can be modelled a number of ways depending upon whether the film flow is laminar or turbulent [1]. For a laminar condensate film, Nusselt's analysis yields

$$h_{film} = .943 \left[\frac{\rho_l(\rho_l-\rho_g) i_{fg} k_\rho^3}{\mu_\rho L(T_l-T_w)}\right]^{1/4} \quad (4)$$

where L is the vertical length of the cold surface and h_{film} is the average heat transfer coefficient. In practice the film will quickly become turbulent as the wall length increases; therefore, a more complex analysis of a turbulent film is necessary [1]. This will increase the overall heat transfer coefficient. In the present analysis we use the laminar film coefficient to estimate h_{film}. However, as will be demonstrated later in the paper the film coefficient is at least one order of magnitude larger than h_{cond} or h_{conv}, and therefore is a negligible heat transfer resistance. If the more accurate turbulent film coefficient were used this conclusion would be even more apparent.

FORCED CONVECTION

For turbulent forced convection in the gas-vapor mixture the heat transfer coefficient is composed of the condensation, h_{cond}, and convective, h_{conv}, components. To determine the convective heat transfer coefficient, h_{conv}, one can utilize the Reynolds analogy for heat and momentum transfer [14]. The analogy states that the heat transfer coefficient (Stanton number) is proportional to the turbulent wall friction factor, f, and to the ratio of turbulent heat transport to momentum transport,

$$\frac{h_{conv}}{\rho_g c_p v_g} = \frac{f}{2} E_H \quad (5)$$

where E_H is the ratio of the turbulent eddy diffusivity of heat, ε_H, to momentum, ε_M. If one now employs the Coburn analogy between heat transfer and fluid friction, E_H is related to the molecular diffusivity of heat to momentum

$$E_H \cong Pr^{-2/3} \quad (6)$$

The local friction factor for the flat plate is

$$f = 0.0592 \left(\frac{\nu_g}{v_g x}\right)^{1/5} \quad (7)$$

When this is combined with equation 5 and 6 the resultant local heat transfer coefficient is

$$\frac{h_{conv}x}{k_g} = 0.0296\ Re_x^{0.8}\ Pr^{1/3} \tag{8}$$

where $$Re_x = \frac{\rho_g v_g x}{\mu_g} \tag{9}$$

Since $h \sim x^{-0.2}$, the average turbulent convective heat transfer coefficient between x = 0 and x = L is found by integrating equation 8, giving

$$Nu_{FC} \equiv \frac{h_{conv}L}{k_g} = 0.037\ Re_L^{0.8}\ Pr^{1/3} \tag{10}$$

The condensation heat transfer coefficient is defined by the energy transferred to the film condensate by vapor diffusion

$$h_{cond}\ (T_B - T_I) = \dot{m}''_v\ \ (i_B - i_I) \tag{11}$$

where $(i_B - i_I)$ is the change in enthalpy of the vapor flux, $\dot{m}''_v$, which condenses on the cold surface. Now the vapor flux diffusing to the surface can be found in a similar manner as the heat transfer coefficient if one assumes the Reynolds analogy can be applied to mass transfer as well as heat transfer. The analysis would be similar to that for heat transfer as outlined in reference 14. The resultant expression would be

$$\frac{\tau_w}{\rho_g \dot{m}''_v} = \frac{1}{E_D}\ \frac{v_g}{(C_I - C_B)} \tag{12}$$

where E_D is the ratio of turbulent mass transport to momentum transport, τ_w is the wall shear stress, and C is the vapor concentration. If one remembers that

$$C_i = \rho_g X_i \tag{13}$$

$$\tau_w = \frac{f\ \rho_g v_g^2}{2} \tag{14}$$

equ. 12 takes on a form similar to the Stanton number for heat transfer

$$\frac{g}{\rho_g v_g} = \frac{f}{2} E_D \tag{15}$$

where we define g to be the mass transfer coefficient

$$g \equiv \frac{\dot{m}''_v}{(X_B - X_l)} \tag{16}$$

As before one can ssume that E_D is a function of the ratio of molecular diffusivities of mass to momentum

$$E_D = \left(\frac{D\rho_g}{\mu_g}\right)^{2/3} = Sc^{-2/3} \tag{17}$$

Combining equ. 17 with equ. 15 and 7 the average mass transfer coefficient (or Sherwood number) is found to be

$$Sh_{FC} = \frac{g}{\rho_g v_g} = 0.037\ Re_L^{-0.2}\ Sc^{-2/3} \tag{18}$$

where

$$Re_L \equiv \frac{\rho_g v_g L}{\mu_g} \tag{19}$$

The condensation heat transfer coefficient now becomes

$$h_{cond} = \frac{g(x_B - x_l)\ (i_B - i_l)}{(T_B - T_l)} \tag{20}$$

To evaluate these heat and mass transfer coefficients, the transport properties are evaluated at the average film temperature

$$T_f = \frac{T_B + T_l}{2} \tag{21}$$

and average mass fraction

$$X_f = \frac{X_B + X_l}{2} \tag{22}$$

One should note here that the mass transfer coefficient correlation used by Whitley [4] is very similar to this derived model. The only difference being that the mass transfer coefficient is not as dependent on the Schmidt number in Whitley's correlation ($g \sim Sc^{-0.4}$).

NATURAL CONVECTION

The heat and mass transfer coefficient for condensation can also be derived based upon the Reynolds-Colburn analogy. This was done for turbulent convective heat transfer by Eckert et al. [15] for a vertical flat plate. An integral method of solution was applied to a turbulent boundary layer for natural convection assuming the energy and momentum boundary layers are equal. The assumed velocity and temperature profiles were

$$v_x = \Gamma \left(\frac{y}{\delta}\right)^{1/7} \left(1 - \frac{y}{\delta}\right)^4 \tag{24}$$

$$\frac{T - T_B}{T_w - T_B} = 1 - \left(\frac{y}{\delta}\right)^{1/7} \tag{25}$$

where Γ is a characteristic velocity induced by turbulent natural convection. These equations were substituted into the integral momentum and energy balance equations, where the major assumption made was that the local turbulent friction factor for a flat plate for forced convection was similar to that for natural convection. Using this assumption along with the Reynolds-Colburn analogy (equs. 5 and 6)

$$\frac{h_x}{\rho_g \Gamma_x C_{pg}} = \frac{f_x}{2} Pr^{-2/3} \tag{26}$$

an expression was derived for the characteristic velocity for turbulent natural convection. Notice the characteristic velocity replaces the imposed velocity in equ. 26. The resultant local velocity was found to be

$$\Gamma_x = 1.185 \frac{\nu}{x} (Gr_x)^{1/2} \left[1 + 0.494\ Pr^{2/3}\right]^{-1/2} \tag{27}$$

and the boundary layer was found to be equal to

$$\delta_x = 0.565_x (Gr_x)^{-0.1} Pr^{-8/15} \left[1 + 0.494\ Pr^{2/3}\right]^{0.1} \tag{28}$$

where

$$Gr_x \equiv \frac{a\beta\,(T_B - T_w)\,x^3}{\nu^2} \tag{29}$$

When these are substituted into the Reynolds analogy one obtains the average heat transfer coefficient for a plate of length, L,

$$Nu_{NC} = \frac{h_{con}\,L}{k_g} = 0.0246\,Gr_L^{2/5}\,Pr^{7/15}\,[1 + 0.494\,Pr^{2/3}]^{-2/5} \tag{30}$$

The mass transfer coefficient can be derived in a similar manner if one employs the Reynolds analogy

$$\frac{g_x}{\rho_g \Gamma_x} = \frac{f_x}{2}\,Sc^{-2/3} \tag{31}$$

By substituting for the local friction factor

$$f_x = 0.045\,\left(\frac{\nu}{\Gamma_x \delta_x}\right)^{1/4} \tag{32}$$

and utilizing equs. 27 and 28 the local mass transfer coefficient can be found. If one now integrates the equation over the length of the vertical plate, to find the average coefficient, the result is

$$Sh_{NC} = \frac{g}{\rho_g \Gamma_L} = 0.0188\,Re_L^{-1/4}\,Sc^{-2/3} \tag{33}$$

where

$$Re_L \equiv \frac{\rho_g \Gamma_L \delta_L}{\mu_g} \tag{34}$$

$$\Gamma_L = 1.185\,(\nu/L)\,Gr_L^{1/2}\,[1 + 0.494\,Pr^{2/3}]^{-1/2} \tag{35}$$

$$\delta_L = 0.565\,L\,Gr_L^{-0.1}\,Pr^{-8/15}\,[1 + 0.494\,Pr^{2/3}]^{-0.1} \tag{36}$$

Once again the condensation heat transfer coefficient is given by equ. 20.

As before to evaluate these heat and mass transfer coefficients, the transport properties are evaluated at the average film temperature and mass fraction.

One should note that the functional dependence of the heat transfer coefficient and the mass transfer coefficient on the Grashof number are very similar; $h_{conv} \sim Gr^{0.4}$ and $h_{cond} \sim Gr^{0.375}$. This analytical result agrees very well with the empirical data of Akers [16] in which the functional dependence of $h_{cond} + h_{conv}$ on the Grashof number was found to be 0.37.

CORRECTION FOR HIGH MASS TRANSFER RATES

When the mass of vapor becomes a relatively large fraction of the total mass of the gas-vapor mixture, the rate of condensation will increase. As the mass transfer rate increases the momentum, thermal and mass transfer boundary layers will be reduced in size because of the apparent suction effect of the condensation process; this is the exact opposite of the transpiration cooling effect. This reduction in the boundary layer will further increase the temperature and concentration gradients near the wall and increase the heat and mass transfer coefficients. Bird et al. [17] suggest correction factors that could be used to determine the increase in the heat and mass transfer coefficients. The mass transfer coefficient becomes

$$g^* = C_o g \tag{37}$$

where

$$Co \equiv \frac{\ln (R + 1)}{R} \tag{38}$$

and

$$R \equiv \frac{Y_I - Y_B}{1 - Y_I} \tag{39}$$

The convective heat transfer coefficient would become

$$h^*_{conv} = C_o \, h_{conv} \tag{40}$$

where now R is defined to be

$$R \equiv \frac{\dot{m}''_v \, c_{p_v}}{h_{conv}} \tag{41}$$

when this correction factor is applied to the correlations the heat and mass transfer coefficients are increased by 10-50% when the vapor mole

fraction is 20-60% of the mixture. In the following discussion this correction is always included in the calculations.

PARAMETRIC RESULTS

Based on the analysis of the previous section, the heat transfer the cold vertical surface is a function of the steam mass fraction, the characteristic velocity (induced or imposed), the pressure, the length of the surface, and the difference in the bulk and wall temperature. To find the overall heat transfer coefficient one finds the values for h_{film}, h_{conv}, and h_{cond} and combines them as in equ. 3. The film heat transfer coefficient and the condensation heat transfer coefficient is found by iteration on the interface temperature.

The effects of the ratio of gas to vapor mass, velocity, and total pressure are illustrated in Figures 2 and 3 for a steam-air mixture. As the ratio of the air to steam mass increases the heat transfer coefficient decreases; the major reason being that the condensation heat transfer coefficient decreases linearly as the difference in bulk to interface steam mass fractions decreases. Notice that the complete model gives a slightly lower h_{TOT} than the approximate model which assumes that $h_{TOT} \simeq h_{gas}$. This is mainly apparent at high values of h_{TOT} when h_{gas} is of the same order of magnitude as h_{film}. Usually the value of the Nusselt film coefficient ($\sim$ 4000 - 5000 W/m^2k) is more than an order of magnitude larger than h_{gas}. Actually h_{cond} is approximately one to two orders of magnitude larger than h_{conv} (100 to 1). Thus the latent heat term dominates the overall heat transfer process. In the succeeding calculations we use the approximate model because inclusion of the film heat transfer resistance does not significantly affect the numerical results. In fact, if the more applicable turbulent film heat transfer coefficient is used this approximation is even more accurate.

The force convection heat transfer coefficient is directly proportional to the characteristic velocity, $h_{TOT} \sim v_g^{0.8}$. An increase in the total pressure also causes the heat transfer coefficient to increase. The major reason for the increase in h_{TOT} is that the steam-air density increases; Figure 3 illustrates for 0.28 MPa (40 psia) the heat transfer coefficient is 40-50% higher. Finally, one should note that the natural convection coefficient provides the lower bound for the heat transfer coefficient and corresponds to a buoyancy induced velocity of approxi-tely 0.3 to 1 m/s, depending on initial conditions.

An interesting result is illustrated in Figure 4. The effect of surface length is exactly opposite for forced and natural convection. The forced convection coefficient is proportional to $L^{-0.2}$; this indicates that the boundary layer increases as L increases. Conversely the natural convection coefficient is proportional to $L^{0.2}$; this indicates that the buoyancy induced velocity increases as L increases. As the length increases to values appropriate to reactor and containment scale (L > 5 m) the natural convection coefficient becomes equal in magnitude to h_{TOT} for an imposed velocity of 2 m/s. As the figure indicates this is not a strong function of pressure. This suggests that except for a large imposed velocity (e.g. from a LOCA blowdown or hydrogen deflagration) the

the natural convection may be the controlling heat transfer regime to the cold wall.

Figure 5 illustrates the effect of a change in the bulk to wall temperature difference. Assuming that the wall is kept below the dewpoint, as the temperature difference increases h_{TOT} decreases and the heat flux increases. This behavior would persist unless the dewpoint temperature is exceeded; at this point the heat flux would decrease.

These parametric calculations indicate that the primary resistance to energy transfer is primarily in the gas-vapor mixture. This observation should always be checked for the particular system; however, for low pressure steam-air mixtures the present calculations indicate that this approximation is quite valid.

COMPARISON WITH EXPERIMENTAL RESULTS

The best known experimental data which is applied to accident safety analysis of containments is derived from the work of Uchida [12] and Tagami [13]. The experimental program, part of the SAFE project, investigated condensation heat transfer in a steel containment ($\sim$ 45 m^3), at low pressures (0.1 to 0.5 MPa), in the presence of noncondensible gases (varying amount of nitrogen, argon, air). The condensing surface was a vertically positioned cylinder, 0.3 and 0.9 m in length and 0.64 circumference, maintained at a constant temperature (322 K).

In the experimental data reported by Uchida [12] the whole facility was allowed to come to steady state with the heat loss through structures being balanced by steam addition from a boiler, outside containment. The steam entered below a support plate over which the condensing surface was located. The inlet and outlet temperature of the condensing plate cooling water, condensing surface temperature as well as the bulk temperature, were monitored to determine the heat flux and the overall heat transfer coefficient to the condensing surface. Unfortunately no velocity measurements were made to ascertain the imposed circulation rate.

The steady state data of Tagami were also obtained in this manner. In addition, Tagami performed transient condensation experiments in this apparatus with steam and air. The techniques consisted of measuring the heat flux on the vertical surface, the bulk and condensing surface temperatures, the blowdown rate, and the total energy added to the small scale containment. Unfortunately, the imposed velocity and the total containment pressure were not measured; therefore, the data from the experiment not only did not determine the forced convection rate, but also does not allow one to determine the thermodynamic state of the steam-air mixture.

The Uchida steady state data was correlated as a function of only the mass ratio of air to steam

$$h_{TOT_{SS}} = 379 \left({}^{m_g}/_{m_v}\right)^{-0.707} \left({}^{w}/_{m^2 k}\right) \qquad (42)$$

for

$${}^{m_g}/_{m_v} < 20$$

Tagami's steady state data was also correlated as a function of $(^{m_v}/_{m_g})$

$$h_{TOT}^{SS} = 11.4 + 284\ (^{m_v}/_{m_g})\ (^{w}/_{m^2k}) \qquad (43)$$

for $0 < {}^{m_v}/_{m_a} < 1.4$

Tagami's transient maximum heat transfer data was correlated as a function of a dimensional grouping of the energy added, E_A (BTU), divided by the total time for the addition, t_A (sec), and the containment volume, $V_c(ft^3)$,

$$h_{TOT}^{MAX} = 426\ \left[\frac{E_A}{t_A V_c}\right]^{0.6}\ (^{w}/_{m^2k}) \qquad (44)$$

The total heat transfer coefficient is then

$$h_{TOT} = h_{TOT}^{MAX}\ (^{t}/_{t_A})^{1/2} \text{ for } t \leq t_A \qquad (45)$$

and

$$h_{TOT} = h_{TOT}^{SS} + (h_{TOT}^{MAX} - h_{TOT}^{SS})\ \exp\ (-0.5\ (t-t_A)) \qquad (46)$$

for $t \leq t_A$

The condensation model developed in the paper is used to predict the steady state data of Uchida and Tagami (see Figures 6-8). Because no velocities were measured, one must assume various values; in this case an imposed velocity of 2 m/s proved to be adequate giving satisfactory agreement with the published data. The data of Uchida varied two parameters, the total pressure and mass ratio, independently. To match Uchida's data, curves are plotted for the bounding pressures (0.1 & 0.28 MPa) at a velocity of 2-4 m/s. No one curve matches all the data; but the combination of them does bound all the published data. One should note that even though these tests were reported to be for quiescent conditions there probably was an imposed force convection velocity caused by the introduction of steam into the containment vessel. Calculations were done to determine the effect of a change in the noncondensible gas composition; the results indicated relatively little effect on the predicted values (< 5%), and well within the scatter of Uchida's data. One should also note that as the length of the condensing surface was increased (0.3 to 0.9 m) the heat transfer coefficient decreased by about 20% indicating forced convection model functional dependence ($\sim L^{-0.2}$). The natural convection model predicts values for the total heat transfer coefficient lower than observed, as Figure 7 indicates.

CONCLUSION

In this paper a complete condensation model for forced and natural convection is derived by extending the Reynolds-Colburn analogy for heat and mass transfer to mass and momentum transfer. The forced convection model indicates that the total heat transfer coefficient is inversely proportional to the length of the condensing surface ($h_{TOT} \sim L^{-0.2}$), and directly proportional to an increase in the imposed velocity, the total pressure, and the mass ratio of vapor to noncondensible gas. The natural convection coefficient has similar dependencies for the total pressure, mass ratio, and the buoyancy induced velocity; however, it increases as the condensing surface length increases ($h_{TOT} \sim L^{0.2}$). Parametric calculations indicate that at length scales corresponding to the reactor containment environment (> 5 m) the natural convection heat transfer coefficient is larger than forced convection values for moderate imposed velocities ($v_g \sim 2$ m/s and $Re_L \sim 5(10^5)$). This suggests that except for specific events which impose large velocities (LOCA or H_2 deflagration) the natural convection condensation model may better predict the overall heat transfer coefficient.

Finally, the model was compared to the steady state data of Uchida and Tagami [12,13]. The model is in reasonable agreement with data when an imposed velocity of 2 m/s is assumed in the calculations. The data of Tagami indicates a decrease in the heat transfer coefficient by ~20% as the condensing surface length increases; this observation is in agreement with the forced convection model predictions. The natural convection model predicted heat transfer coefficients below the measured values. However, the model does predict the functional dependence on Grashof number ($h_{TOT} \sim Gr^{0.375}$) which is in agreement with the data of Akers [16] ($h_{TOT} \sim Gr^{0.37}$).

REFERENCES

1. J.G. Collier, Convective Boiling and Condensation, McGraw-Hill, London (1981).
2. D.C. Slaughterbeck, Idaho Nuclear Corp. Report IN-1388 (1970).
3. M. Berman, SAND81-1216, No. 1-4, Sandia Laboratories (1981).
4. R.H. Whitley, Masters Thesis, UCLA (1976).
5. W.A. Nusselt, Ziescrhift Ver. Deut. Ing., 60, 541 (1916).
6. A.P. Coburn and T.B. Drew, Trans. Am. Inst. Chem. Engrs., 33, 197 (1937).
7. E.M. Sparrow and E.G. Eckert, AIChE Journal, 7, 473 (1961).
8. J.C. Koh et al., Int. J. Heat Mass Transfer, 2, 69 (1961).
9. E.H. Sparrow, S.H. Lin, J. Heat Transfer, 86, 430 (1964).
10. W.J. Minkowycz and E.M. Sparrow, Int. J. Heat Mass Transfer, 9 (1966).
11. E.M. Sparrow et al., Int. J. of Heat Mass Transfer, 10, 1125 (1967).
12. H. Uchida et al., Proc. Int. Conf. Peaceful Uses of Atomic Energy 13, 93, A/CONF:28/P436 (1965).
13. T. Tagami, Interim Report on Safety Assessments and Facilities Establishment Project for June 1965, No. 1, unpublished work (1965).
14. W.M. Rohsenow, H. Choi, Heat, Mass and Momentum Transfer, Prentice-Hall Publishers, New Jersey (1961).
15. E.G. Eckert, T.W. Jackson, National Advisory Committee Aeronautical Note 2207 (October 1950).
16. W.W. Akers et al., Chem. Eng. Prog., 56, 139 (1960).
17. R.B. Bird et al., Transport Phenomena, Wiley and Sons, Inc., New York (1960).

NOMENCLATURE

a - gravitational acceleration
C - concentration
C_p - specific heat @ const. pressure
D - diffusion coefficient
f - friction factor
g - mass transfer coefficient
Gr - Grasnof No.
i - enthalpy
k - thermal conductivity
L - length of plate
$\dot{m}''$ - mass flux
Nu - Nusselt No.
Pr - Prandtl No.
q'' - heat flux
Re - Reynolds No.
Sc - Schmidt No.
Sh - Sherwood No.
T - temperature
v - velocity
x - distance down the plate
X - mass fraction
y - distance perpendicular to plate
Y - mole fraction
β - temperature coefficient
ζ - characteristic velocity
δ - boundary layer thickness
ε - turbulent diffusivity
μ - dynamic viscosity
ν - kinematic viscosity
ρ - density

Subscripts

B - bulk
conv - convective
cond - condensation
g - gas
I - interface
l - liquid
rad - radiation
tot - total
v - vapor
w - wall

Superscripts

m* or g* indicates correction for high mass transfer rates

Figure 1 Physical picture of condensing surface

Figure 2 Condensation heat transfer coefficient as a function of the mass of air and the gas velocity (P_T = 0.1 MPa)

Figure 3 Condensation heat transfer coefficient as a function of the mass of air and the gas velocity (P_T = 0.28 MPa)

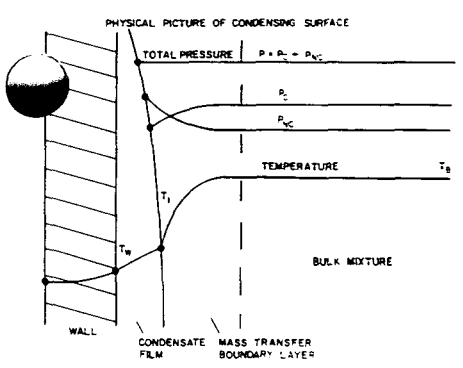
Figure 4 Condensation heat transfer coefficient as a function of condensing surface length

Figure 5 Condensation heat transfer coefficient as a function of the temperature difference

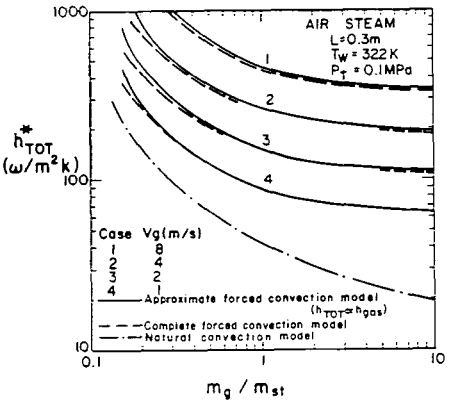
Figure 6 Comparison of the correlation to the data of Uchida

Figure 7 Comparison of the correlation to the data of Tagami (L = 0.3 m)

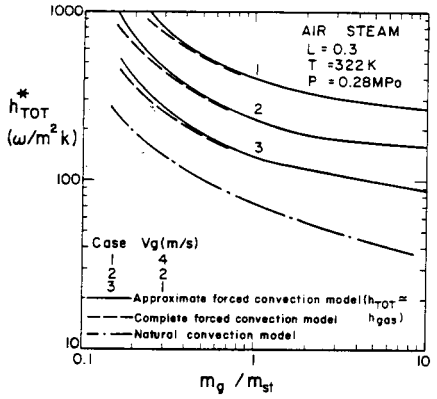
Figure 8 Comparison of the correlation to thedata of Tagami (L = 0.9 m)



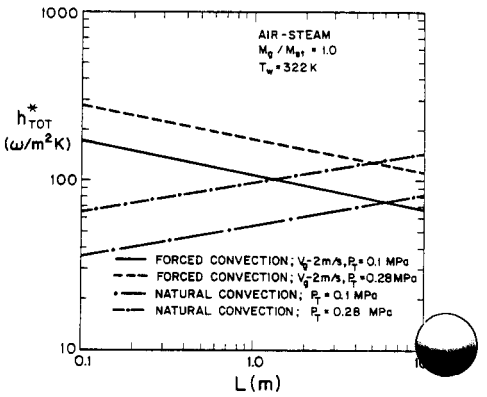
1



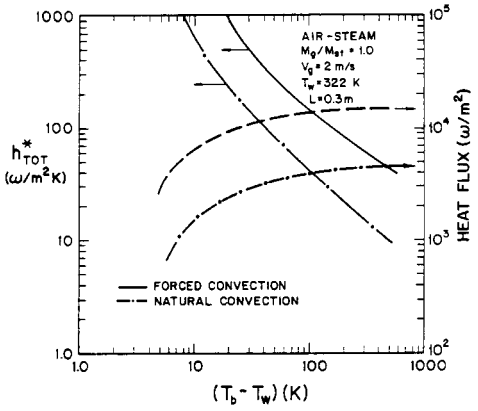
2


AIR STEAM
L = 0.3
T = 322 K
P = 0.28MPa
1
2
3
Case Vg(m/s)
1 4
2 2
3 1
Approximate forced convection model
Complete forced convection model
Natural convection model
h^*_{TOT} $(\omega/m^2 k)$
m_g / m_{st}

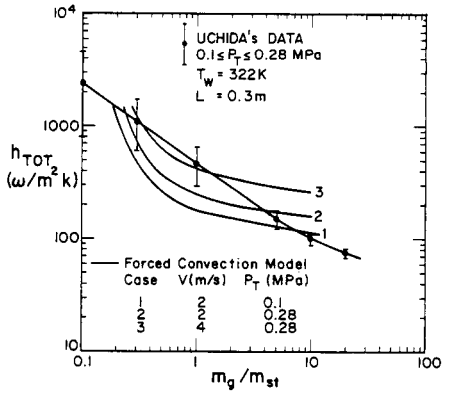
3

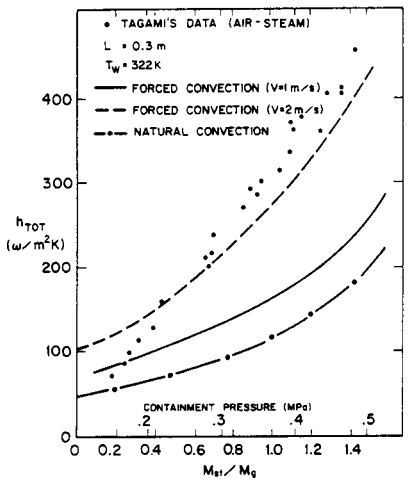

AIR-STEAM
M_g / M_{st} = 1.0
T_w = 322 K
FORCED CONVECTION; V_g=2m/s, P_T= 0.1 MPa
FORCED CONVECTION; V_g=2m/s, P_T=0.28MPa
NATURAL CONVECTION; P_T = 0.1 MPa
NATURAL CONVECTION; P_T = 0.28 MPa
h^*_{TOT} $(\omega/m^2 K)$
L(m)

4

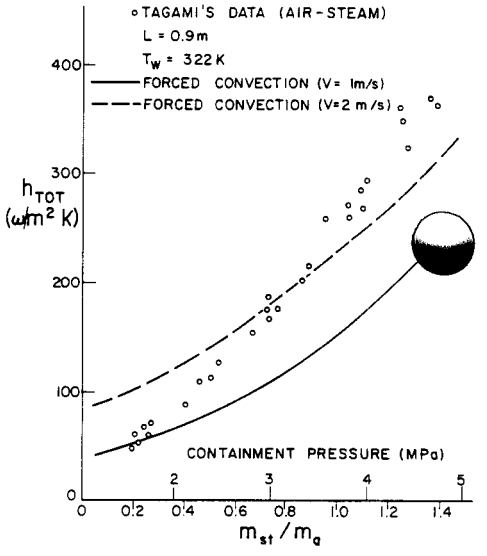

AIR-STEAM
M_g/M_{st} = 1.0
V_g = 2 m/s
T_w = 322 K
L=0.3m
FORCED CONVECTION
NATURAL CONVECTION
h^*_{TOT} $(\omega/m^2 K)$
HEAT FLUX (ω/m^2)
$(T_b - T_w)$ (K)

5


UCHIDA's DATA
$0.1 \le P_T \le 0.28$ MPa
T_w = 322K
L = 0.3m
Forced Convection Model
Case V(m/s) P_T (MPa)
1 2 0.1
2 2 0.28
3 4 0.28
h_{TOT} $(\omega/m^2 k)$
m_g / m_{st}


TAGAMI'S DATA (AIR-STEAM)
L = 0.3 m
T_w = 322K
FORCED CONVECTION (V=1m/s)
FORCED CONVECTION (V=2m/s)
NATURAL CONVECTION
CONTAINMENT PRESSURE (MPa)
h_{TOT} $(\omega/m^2 K)$
M_{st}/M_g

7


TAGAMI'S DATA (AIR-STEAM)
L = 0.9m
T_w = 322 K
FORCED CONVECTION (V= 1m/s)
FORCED CONVECTION (V=2 m/s)
CONTAINMENT PRESSURE (MPa)
h_{TOT} $(\omega/m^2 K)$
m_{st}/m_g

8

SAND82-1285C

Combustion Modeling in MARCH, Developments and Limitations

by
F. E. Haskin
and
W. R. Trebilcock

Sandia National Laboratories
Albuquerque, New Mexico 87185

ABSTRACT

Previous assessments of the MARCH computer code identified various limitations associated with combustion modeling in MARCH. Recent developments have eliminated several of these limitations. The concentrations within a burning compartment can now be sampled every time step to account for changes which occur due to mass transport during a burn. The burn velocity and extent of reaction can be calculated as functions of the hydrogen concentration in the compartment at time of ignition. An "igniter-on" event may now be used to change the ignition threshold at a given point in time. A test for inerting based on high steam and carbon dioxide concentrations has been added. Combustion of carbon monoxide as well as hydrogen may now be treated. Finally, intercompartment flame propagation tests which account for relative compartment location and approximate time delays have been incorporated. Sample calculations, based on the new models, are presented. Remaining limitations and the potential for further improvements in MARCH combustion modeling are discussed.

INTRODUCTION

The MARCH computer code[1] was developed to analyze primary system and containment responses during the course of light-water reactor core-melt accidents from the initiating event through core uncovering, meltdown, vessel breach, and core-concrete interactions. MARCH was designed to be a fast-running code. Its predictions of cause and timing of containment failure were intended to be suitable inputs for use in separate radiological consequence calculations for probabilistic risk assessments.

Because MARCH is a unique, fast-running code capable of treating a variety of reactor and containment types, its usage

has expanded rapidly, and considerable attention has been devoted to identifying its limitations.[2] Efforts have been undertaken at Battelle Columbus Laboratories, Brookhaven National Laboratory, Oak Ridge National Laboratory, Sandia National Laboratories, and the Tennessee Valley Authority to reduce the number and severity of the limitations associated with the most recent public version, MARCH 1.1. Many improvements resulting from these efforts are being incorporated by Battelle Columbus Laboratories into a new version to be called MARCH 2.0.

The purpose of this paper is to describe the combustion models developed at Sandia National Laboratories for inclusion in MARCH 2.0. We also provide some results obtained with these models and discuss the remaining limitations associated with MARCH combustion modeling.

The limitations of MARCH 1.1 which our modifications address are:

1. Poor selection of default ignition criteria
2. No test for inerting due to high steam or carbon dioxide concentrations
3. No accounting for combustible gas transport to and from a burning compartment in estimating the extent of combustion
4. No treatment of carbon monoxide combustion
5. No pre-inerting capability
6. No explicit provision for igniters
7. No intercompartment flame propagation tests
8. No provision for estimating the extent of reaction as a function of hydrogen concentration at ignition
9. No provision for estimating the combustion rate as a function of hydrogen concentration at ignition

DESCRIPTION OF NEW MODELS

LeChatelier's Formula

A simple formula proposed by LeChatelier has been shown to predict the lower limits of flammability (upward flame propagation) for air-hydrogen-carbon monoxide mixtures to within 0.4 percent.[3] Modifying and expanding on an approach proposed in Reference 4, we have used the following form of LeChatelier's formula to characterize thresholds for many important combustion events:

$$x_{H_2} + \frac{L_{H_2}}{L_{CO}} x_{CO} \geq L_{H_2}. \qquad (1)$$

Here, the x's denote the mole fractions of hydrogen and carbon monoxide in the gas mixture. The L's denote the threshold mole fractions for the combustion event being considered, in gas mixtures containing only one (the subscripted) combustible gas. We have applied LeChatelier's formula in tests for ignition, propagation, and completeness. The default limiting mole fractions used for the various events are summarized in Table 1.

Table 1

Default Limiting Mole Fractions for Tests Based on LeChatelier's Formula

Combustion "Event"	L_{H_2}	L_{CO}	L_{H_2}/L_{CO}
Upward Propagation	H2UP = 0.041	CMUP = 0.125	0.328
Horizontal Propagation	H2HZ = 0.06	CMHZ = 0.138	0.435
Ignition with Igniters	H2ON = 0.08	CMON = 0.148	0.541
Complete Combustion	H2XX = 0.08	CMXX = 0.148	0.541
Downward Propagation	H2DN = 0.09	CMDN = 0.150	0.600
Ignition Without Igniters	H2HI = 0.10	CMHI = 0.167	0.600

As discussed later, we make use of the variable y, based on the left hand side of LeChatelier's formula:

$$Y = x_{H_2} + \frac{L^*_{H_2}}{L^*_{CO}} x_{CO} \qquad (2)$$

in our estimate of the extent of reaction and the linear burning rate (flame speed). Here the L*'s denote combustible mole fractions above which burning is likely to be complete in mixtures containing only one (the subscripted) combustible gas ($L^*_{H_2}$ = H2XX and L^*_{CO} = CMXX, see Table 1). In the absence of carbon monoxide, y is equal to the hydrogen mole fraction, x_{H_2}.

Ignition

One test for ignition in our model requires that the mole fractions of hydrogen and carbon monoxide satisfy LeChatelier's formula. The limits, as indicated in Table 1, depend on whether the user wants to approximate ignition with or without igniters. In addition to sufficient combustible gases, ignition requires sufficient oxygen.

$$x_{O_2} \geq \text{HIOXY (0.05 default)} \tag{3}$$

Also, the mole fractions of steam and carbon monoxide must be sufficiently low to preclude inerting:

$$x_{H_2O} + x_{CO_2} \leq \text{HIG (0.55 default)} \tag{4}$$

A specific test for inerting due to the presence of large amounts of nitrogen is not included. However, nitrogen inerting frequently implies insufficient oxygen, and Eq. (3) precludes burning for such cases. The code logic for ignition testing is summarized in Figure 1.

Propagation

The ignition tests are applied to each nonburning compartment at the beginning of each timestep. After ignition in any compartment, burn propagation to a connected compartment is precluded if the atmosphere in that compartment is inerted per Eq. (3) or Eq. (4). The user may specify nonmechanistic burn propagation to all connected compartments which are not inert (by setting input parameter IBURNJ = 2). Alternatively, the user may (by setting IBURNJ = 1) have the code test the combustible mole fractions in noninert, connected compartments using Eq. (1) to determine if burn propagation is possible. The option of precluding the possibility of burn propagation (by setting IBURNJ = 0) is also available to the user.

The code logic for propagation testing is summarized in Figure 2. The user specifies, through an input flow matrix BK(I,J), whether there is a flow path from compartment I to compartment J; whether the flow from compartment I to compartment J is directed upward, horizontally, or downward; and the fraction of a characteristic distance, H2DIST(I), which a burn in compartment I must traverse before propagation into compartment J can occur. The characteristic distance H2DIST(I) is also user-specified and represents the distance traversed by a complete burn in compartment I.

Combustion Rate

In MARCH 1.1 the hydrogen burning subroutine, BURN, surveys all compartment atmospheres until at least one is in the combustible range of hydrogen and oxygen mole fractions. BURN then computes the energy released, DELEN, and the moles consumed, DELOXY and DELHYD, for an instantaneous, adiabatic, constant-volume hydrogen burn. These values are reported back to the containment atmosphere subroutine, MACE. MACE deposits the energy from this exothermic reaction and alters the gas mole fractions at a fixed rate, based on a user-specified time, TBURN. The energy deposition rate is DELEN/TBURN and the rate of hydrogen burning is DELHYD/TBURN. If TBURN is less than the MACE timestep, an adiabatic, constant-volume hydrogen burn is simulated. If TBURN is greater than the MACE timestep, the energy and mole fraction changes are linearly distributed over the time, TBURN. This can lead to errors in predicted pressures, temperatures and mole fractions because gas sources and gas transport between compartments during the burn have no effect on DELEN, DELOXY and DELHYD. Hydrogen flowing into a burning compartment is precluded from participating in the ongoing burn. In fact, cases have been observed in which predicted hydrogen accumulation due to flow from the reactor vessel into a burning compartment has been comparable to the hydrogen consumption over the interval TBURN.

To remove this limitation, our model tests for a change in the rate of combustion at each MACE timestep based on the mole fractions at the beginning of the timestep. The molar combustion rates of hydrogen and carbon monoxide in compartment I are

$$\dot{n}_{H_2} = n_T \dot{y} x_{H_2}/y \tag{5}$$

$$\dot{n}_{CO} = n_T \dot{y} x_{CO}/y \tag{6}$$

where

$$\dot{y} = - y_{max} v/H2DIST(I), \tag{7}$$

n_T = moles of gas in compartment I,

y_{max} = maximum value of y, as defined in Eq. (2), since beginning of the burn,

v = flame speed.

The flame speed has experimentally been observed to be a function of the initial combustible gas concentration. The default function in our model is

$$v = v(y_{max}) = 1.792 + 59.2\ y_{max}\ (m/s). \tag{8}$$

This expression is derived from turbulent hydrogen flame experiments performed at Sandia and is applicable for hydrogen mole fractions below about 10 percent. The application of Eq. (8) to gases containing both hydrogen and carbon monoxide is a modeling hypothesis which has not been tested experimentally.

Extent of Reaction

Once combustion is started in a given compartment, it continues until y, as defined by Eq. (2), decreases to a user-specified or code-computed level, y_{min}. The value of y_{min} depends on the burn limit option specified via the input parameter IBURNL. For IBURNL = 0, continuous burning is approximated and $y_{min} = 0$. For IBURNL = 1, y_{min} = H2LO, a user-specified mole fraction with a default value of zero. For IBURNL = 2, y_{min} is calculated as a function of y_{max} to approximate a linear variation in the extent of reaction from zero percent at $y_{max} = 0$ to 100 percent at $y_{max} = L^*_{H_2}$.

$$y_{min} = \max \left\{ 0, y_{max} \left(1 - y_{max}/L^*_{H_2}\right) \right\} \qquad (9)$$

RESULTS BASED ON NEW MODELS

Large Dry PWR Containment Calculations

The impact of carbon monoxide burning on the containment pressure-temperature response is illustrated below for an S2HF accident sequence in a large dry PWR containment. S2HF denotes a small LOCA (1-1/2" diameter break for the case shown here) involving recirculation failures of both the emergency-core-cooling and containment-spray systems. The accident is discussed in more detail elsewhere.[5] For the results presented here, hydrogen generation before the onset of core-concrete interactions was limited to that from approximately 40 percent Zr oxidation.

Figure 3 compares MARCH-predicted results for two cases: one in which effects of carbon monoxide are ignored (as in the MARCH 1.1 model), and another in which effects of carbon monoxide on ignition, reaction energy, and burn speed are considered in accordance with the models presented above. Complete burning of hydrogen alone is postulated in the first case. Complete burning of both hydrogen and carbon monoxide is postulated in the second case. The ignition threshold is 10 percent hydrogen in the first case and $y \geq 10$ percent in the second case. Accounting for the effects of carbon monoxide yields an earlier burn (~850 versus ~970 minutes) with a higher peak pressure (~7.3 atm versus ~5.8 atm). A second burn with a peak pressure of ~7.8 atm is predicted at ~1130 minutes when CO effects are included.

The results in Figure 3 are based on the INTER core-concrete interactions code which is known[6] to predict high rates of

concrete penetration and carbon monoxide generation relative to the more recently-developed CORDON-MOD1 code. The use of CORCON-MOD1 instead of INTER would have delayed the burns depicted in Figure 3; however, the burns predicted by considering carbon-monoxide effects would still have occurred earlier and resulted in higher pressures than burns predicted without considering carbon-monoxide effects.

BWR Mark III Calculations

Reference 7 includes results from a large number of hydrogen burning calculations for a BWR Mark III containment. Most of the results presented in Reference 7 are based on either the Sandia HECTR code or MARCH 1.1, although some CLASIX results from Reference 8 are also included. Results obtained with our new MARCH combustion models are presented below for two cases: denoted as B-2 and C-3 per Reference 7. The accident considered in both cases involves a transient followed by failure of emergency core cooling and a stuck-open relief valve which discharges steam and hydrogen from the reactor coolant system to the suppression pool. Corresponding results from CLASIX and HECTR are also included below for comparison with our results. The comparisons indicate some points of qualitative agreement; however, they also illustrate some remaining combustion modeling limitations associated with MARCH.

Figure 4 shows the containment pressure responses predicted using our new MARCH models for cases B-2 and C-3. The same hydrogen source term was used for both cases (see Reference 7, Fig. 2.b, source for case B-1). It was developed[8] by extrapolating MARCH results to 75% metal-water reaction. Consistent with the HECTR treatment, we did not model the drywell. (Reference 10 discusses the effects of the drywell based on MARCH 1.1 calculations.) Hydrogen was input directly into a wetwell volume above the suppression pool. The wetwell volume used for case C-3 is more than three times that used for case B-2. The balance of the containment volume in each case was modeled as a single, large upper compartment volume above the wetwell. Table 2 compares the input parameters for the two cases.

Table 2. BWR Mark III Case Descriptions*

	Case B-2	Case C-3
Wetwell Volume m^3	4341	14203
Upper Compartment Volume, m^3	33545	23683
Ignition Limit, % H_2	10	10
Upward Propagation Limit, % H_2	10	4.1
Combustion Completeness, %	100	100
Initial Temperature, K	299.82	299.82
Initial Pressure, atm	1.0	1.0
Flame Speed, m/s	1.8288	7.712
Sprays	On automatically 120 s after first burn	On automatically 120 s after first burn

*For more details, see Reference 7.

Our results for case B-2 predict a series of wetwell burns beginning at approximately 19 minutes and leading to inerting of the wetwell due to oxygen depletion at approximately 52 minutes. In each of the initial wetwell burns, some unreacted hydrogen is forced out of the wetwell into the upper compartment. After wetwell inerting, hydrogen begins to accumulate more rapidly in the upper compartment and an upper-compartment burn is predicted at approximately 67 minutes when the mole fraction of hydrogen reaches 10 percent. The burns which are confined to the wetwell result in lower pressures than the upper compartment burn due to the large volume of the upper compartment relative to the wetwell.

Table 3 compares our results for case B-2 with results predicted by CLASIX and HECTR. All of the codes predict a series of wetwell burns with oxygen being drawn back into the wetwell from the upper compartment after each burn as the wetwell cools down. CLASIX predicts more rapid wetwell cooling and therefore later wetwell inerting and no upper compartment burn. The difference in cooling rates is not clearly understood, but is apparently due to differences in modeling of heat-sinks, radiative and condensing heat transfer, and containment sprays.[7] The hydrogen mole fraction in the upper compartment at the end of the CLASIX run was 8.5 percent.

The MARCH-predicted pressure peaks for case B-2 are lower than the corresponding pressure peaks predicted by HECTR for two reasons. First, MARCH predicts greater reductions in peak pressures due to spray operation. This difference increases with increasing burn time (decreasing flame speed).[7] In our opinion, the HECTR spray model is more realistic. In the absence of sprays, there is generally good agreement between MARCH and HECTR with respect to peak pressure.[7] Second, during the upper compartment burn, HECTR predicts that enough oxygen is forced into the wetwell comparment to overcome oxygen inerting there and permit downward propagation of the burn. Such propagation is not predicted in the MARCH calculations. The MARCH-predicted oxygen mole fraction in the wetwell compartment at the end of the upper compartment burn is ~4.3 percent.

The effects of allocating more of the containment volume to the wetwell and less to the upper compartment are illustrated by the results shown for case C-3 in Figure 4. All of the burns for case C-3 originate in the wetwell. The initial burns are restricted to the wetwell and give rise to moderate peaks (larger than for wetwell burns in case B-2 due to the larger wetwell volume). In each of these initial wetwell burns, some unreacted hydrogen is forced out of the wetwell into the upper compartment. When the hydrogen mole fraction in the upper compartment exceeds 4.1 percent, upward propagation becomes possible resulting in a higher pressure peak for the fourth burn. Table 4 compares our results to HECTR results from Reference 7. CLASIX results were not available for case C-3. HECTR results agree with ours in that HECTR predicts upward propagation during the fourth wetwell burn. As for case B-2, HECTR indicates less suppression of peak pressures due to operation of sprays than does MARCH.

As indicated by the results for cases B-2 and C-3, relatively small differences in compartmentalization or input parameters can produce rather large differences in predicted results. This "ill-conditioning" is not unique to MARCH. The reader interested in such sensitivities should consult Reference 7.

Table 3. Comparison of Results for Case B-2

	CLASIX*	HECTR*	New MARCH Models
Number of Burns			
Wetwell	43	21	14
Upper Compartment	0	1	1
Maximum Temperature, K	1073	1263	1126
Maximum Pressure, atm	1.50	5.40	2.98

*Results taken from Reference 7 for CLASIX Case 2 and HECTR Case B-2'. The HECTR source differs slightly, yielding approximately 8 percent less hydrogen than the source used for CLASIX and MARCH.

Table 4. Comparison of Results for Case C-3

Number of Burns	HECTR*	New MARCH Models
Wetwell	7	8
Upper Compartment	1	1
Maximum Temperature, K	1211	1198
Maximum Pressure, atm	2.86	2.23

*Results taken from Reference 7. The HECTR source differs slightly, yielding approximately 8 percent less hydrogen.

REMAINING LIMITATIONS

Our new MARCH models eliminate the modeling limitations mentioned in the introduction. For problems involving few compartments, our MARCH calculations agree favorably with predictions of the more sophisticated HECTR code. Our capability to treat combustion in atmospheres containing both hydrogen and carbon monoxide is, to knowledge, unique. Nevertheless, a number of combustion modeli limitations remain. Some of these limitations are peculiar to MARCH, whereas, others are more general.

As the comparisons with HECTR indicate, MARCH modeling of compartment sprays can be non-conservative in that unrealistically high pressure suppressions are predicted during burns. In the two-compartment BWR results presented above, MARCH simulated spray cooling in all compartments, but the distribution of sprays between compartments could not be determined. Conversely, for some single-compartment, large-dry-PWR-containment calculations, MARCH does not indicate any pressure reduction due to sprays, apparently because the MARCH logic precludes spray droplet evaporation when the spray droplet fall time exceeds the code's internal time step. Spray modeling is an area in which MARCH improvements appear feasible, and some efforts in this direction are underway at Battelle Columbus Laboratories.

If containment sprays are inactive, radiation heat transfer is the dominant mechanism for energy removal from the gas during a burn. MARCH does not model such radiation heat transfer. This omission is conservative with respect to predicted pressure and temperature peaks. The error introduced is relatively small, especially for large compartments. Modifying MARCH to include such radiation heat transfer seems impractical.

The timing, location, and pressure-temperature peaks of burns depend on the local concentrations of constituent gases which in turn depend on the mixing processes. Mechanisms for mixing include pressure driven mass transfer, convection, and diffusion. MARCH approximates pressure driven mass transfer only, and does so using a fast-running pressure-equilibration model which cannot simulate finite flow resistances between compartments or compartmentalizations having parallel flow paths.[2] These MARCH limitations would be difficult to eliminate. MARCH does not treat mixing due to conv tion or diffusion. Considering the large temperature and assoc density differences which can exist within containments, ignorin convection would tend to underestimate the mixing rates between compartments. Of course, by employing a control-volume approach, MARCH does introduce an artificial mixing in that gas entering a compartment is instantaneously mixed with the contents of the compartment. The more compartments introduced in a problem, the slower the predicted inter-compartment mixing. Convective mixing will be modeled in future versions of HECTR[9]; however, such modeling appears impractical for MARCH.

We have concentrated in this paper on combustion modeling. However, since MARCH is routinely used in a mode which generates hydrogen and carbon monoxide sources, we should point out that there are significant uncertainties and limitations associated with MARCH source terms.(2)

Finally, we wish to emphasize that our models of ignition and propagation thresholds, burning rates, and combustion completeness use very simple relationships which are based on experimentally-observed trends. These relationships are not precise. Furthermore, their use assumes that observed trends can be extrapolated from [illegible]rimental to larger containment geometries or from one gas mixture [illegible]nother. This is particularly true for our models of the effects of carbon monoxide. Such assumptions can only be tested through further research.

REFERENCES

1. R. O. Wooten and H. I. Avci, MARCH (Meltdown Accident Response Characteristics) Code Description and User's Manual, NUREG/CR-1711, BMI-2064, Battelle Columbus Laboratories, October 1980.

2. J. B. Rivard, et al., Interim Technical Assessment of the MARCH Code, NUREG/CR-2285, SAND81-1672, Sandia National Laboratories, November 1981.

3. H. F. Coward, C. W. Carpenter, and W. Payman, Journal of Chemical Society, 115, 27, 1919.

4. R. Joung, R. A. Bari, and W. T. Pratt, "Carbon Monoxide Burning During Core Meltdown Events," Transactions of the American Nuclear Society, 40, p. 606, December 1981.

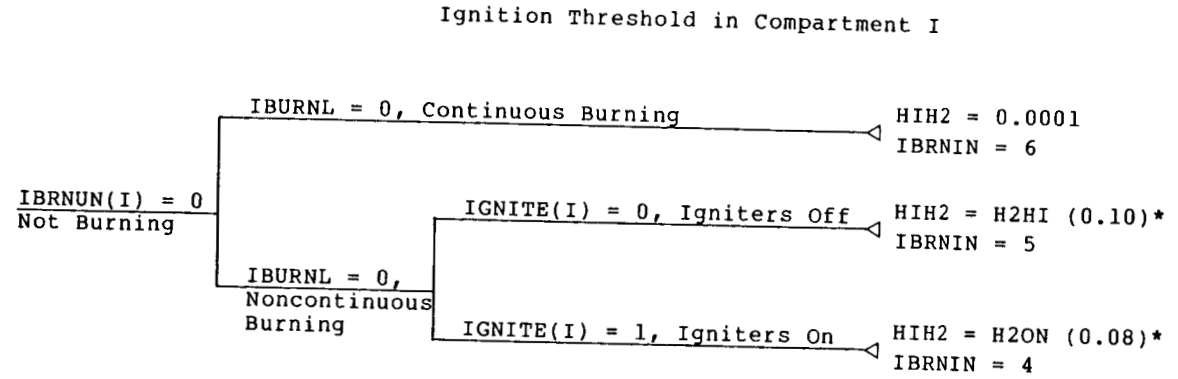
5. F. E. Haskin, J. L. Darby, and W. B. Murfin, Analysis of Hypothetical Severe Core Damage Accidents for the Zion Pressurized Water Reactor, NUREG/CR-1989, SAND81-0504, Sandia National Laboratories, October 1982.

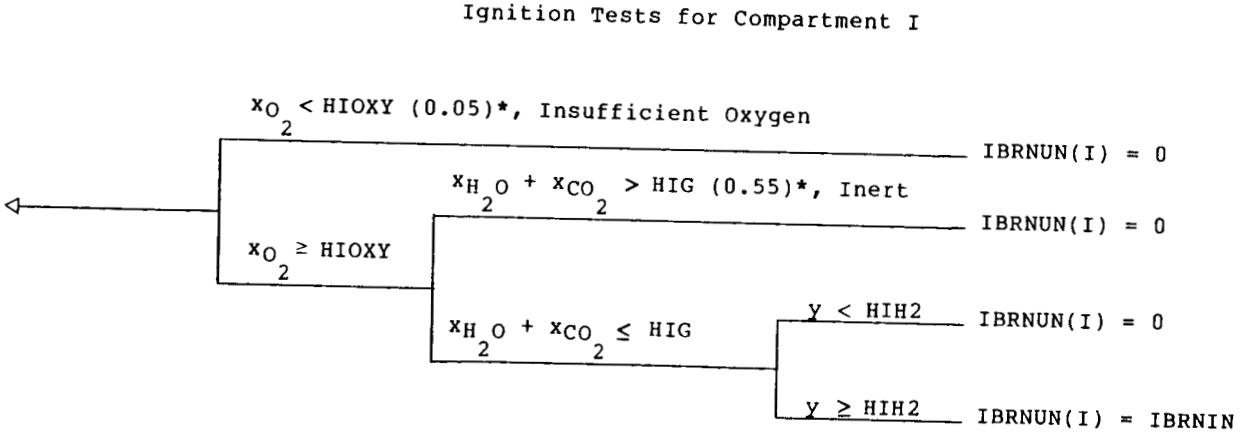
6. F. E. Haskin and C. J. Shaffer, "Impact of Meltdown Modeling Developments on PWR Analyses," SAND-0283C, Proceedings of the International Meeting on Thermal Nuclear Reactor Safety, Chicago, Illinois, August-September 1982.

7. J. C. Cummings, et al., Review of the Grand Gulf Hydrogen Igniter System, NUREG/CR-2530, SAND-0218, Sandia National Laboratories, Draft Report, January 1982.

8. Report on the Grand Gulf Nuclear Station Hydrogen Ignition System, Mississippi Power and Light Company, August 1981.

9. A. L. Camp, M. J. Wester, S. E. Dingman, and M. P. Sherman, "HECTR: A Computer Program for Modelling the Response to Hydrogen Burns in Containments," Proceedings of the Second International Workshop on the Impact of Hydrogen on Water Reactor Safety, Albuquerque, New Mexico, October 1982.





*Default values are indicated in parentheses. Nondefault values should obey the constraints H2HI ≥ H2ON > H2UP > H2LO and H2DN > H2HZ > H2UP.

Figure 1 Ignition Logic for New MARCH Combustion Model

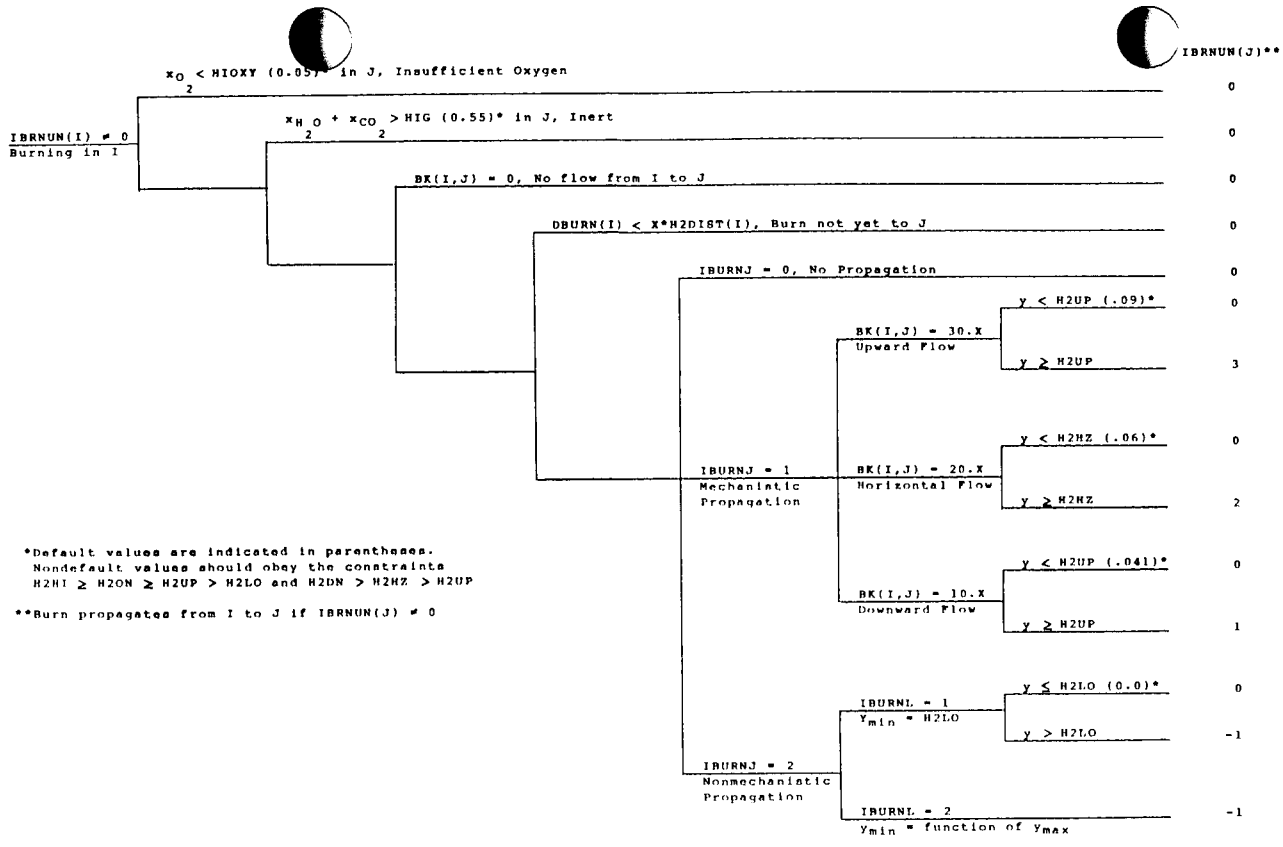


Figure 2 Propagation Logic for New MARCH Combustion Model

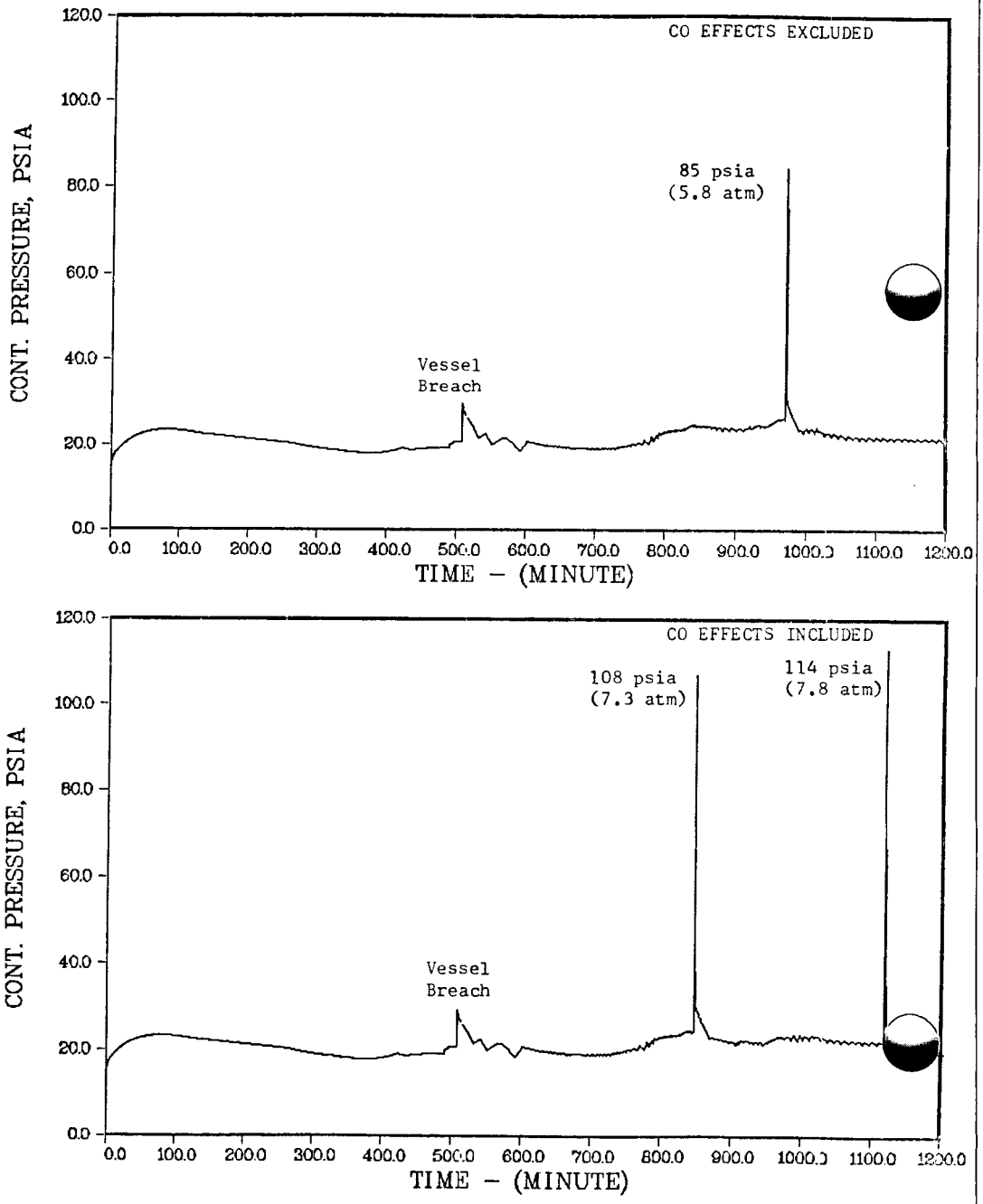


Figure 3 Containment Pressure Response for an S2HF Accident Sequence in a Large, Dry PWR Containment with and without Effects of Carbon Monoxide on Combustion.

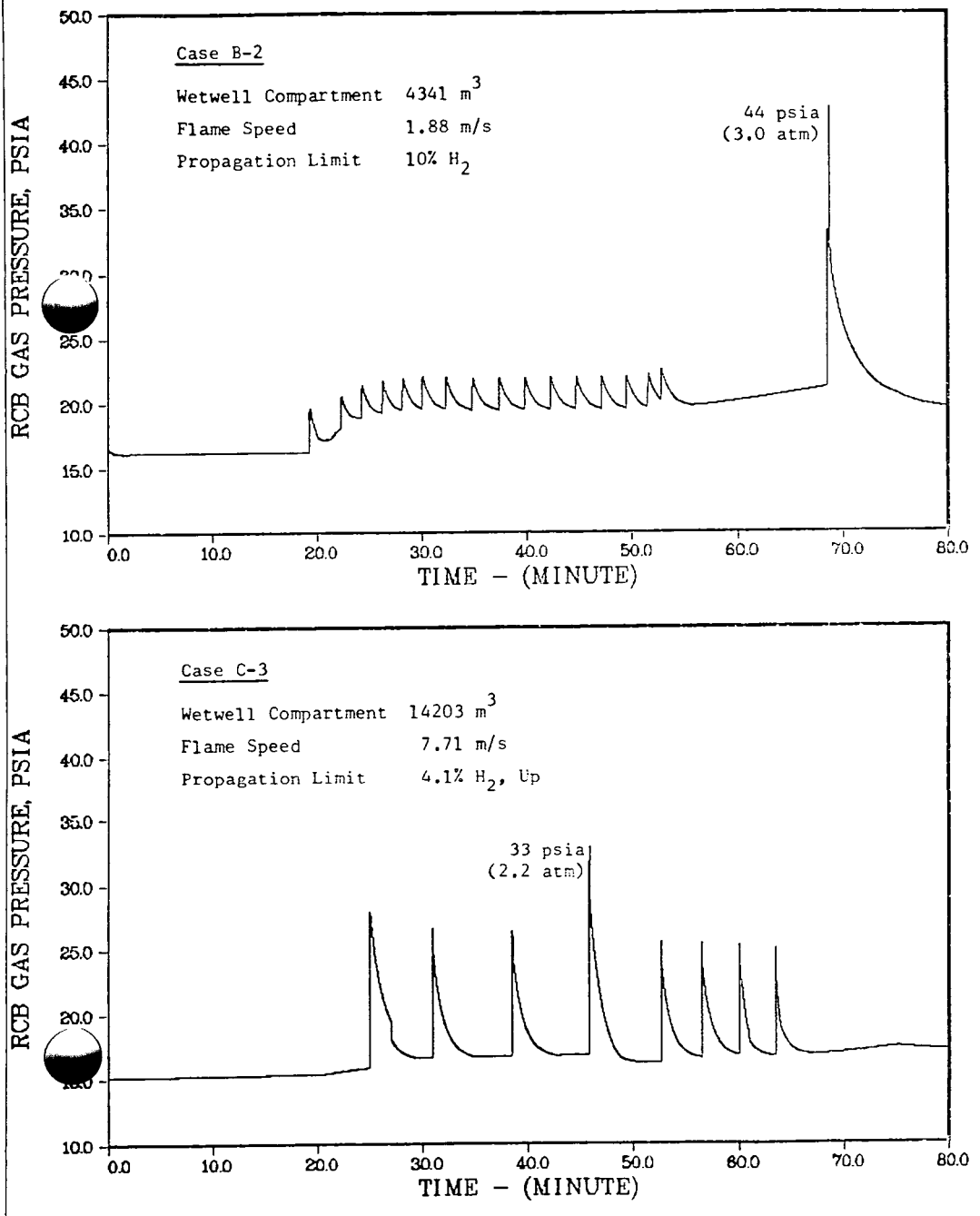


Figure 4 BWR Mark III Containment Pressure for Cases B-2 and C-3





LEAN HYDROGEN-AIR-STEAM MIXTURE COMBUSTION MODELS

Robert G. Zalosh, Erdem A. Ural, and Vicky W.S. Hwa
Factory Mutual Research Corporation
Norwood, Massachusetts 02062

ABSTRACT

Phenomenological flame-propagation models for hydrogen-air-steam mixture deflagrations are described. The models treat the concentration regime in which combustion is complete and the near-lean-limit regime in which buoyant flame propagation and extinction are important. Empirical representations of burning velocities and flame geometries are utilized in both regimes. Transient overpressures calculated with these models are compared to recent data obtained in several test programs. Although reasonable agreement is obtained in many cases, the comparisons suggest that the model could be improved by accounting for self-induced flame turbulence and for radiative heat losses before the flame reaches the vessel wall.

1. INTRODUCTION

Hydrogen combustion computer models are needed to evaluate the consequences of deliberate or accidental ignition of hydrogen-air-steam mixtures within a reactor containment building. Most of the current modeling and experimental efforts, motivated by the Three Mile Island Unit 2 burn on March 28, 1978, have focused on deflagrative combustion of near-uniform, hydrogen-lean mixtures. In order to verify containment integrity, the primary concern has been to determine peak pressures and pressure rise times. However, recently installed deliberate ignition systems have also motivated concern about residual (post-deflagration) hydrogen concentrations and flame heat fluxes on critical equipment.

The simplest approach to hydrogen deflagration modeling is to calculate burned gas temperatures and peak pressures from an adiabatic, isochoric (constant volume) thermochemical energy balance, and to rely upon empirical data for pressure rise times and residual hydrogen concentrations. This is the approach currently employed in the containment response codes such as MARCH[1], HECTR[2], and CLASIX[3]. The major difficulty with this empirical approach is that there does not seem to be any simple data correlation to account for effects of vessel

size and shape, ignition location, and turbulence characteristics. These effects have been observed[4,5] to cause large differences in peak pressure and burn completeness for lean hydrogen concentrations in the range 4-12 vol%. They are also responsible for wide variations in flame speeds and pressure rise times.

As part of the EPRI Hydrogen Combustion and Control Program, Factory Mutual Research Corporation (FMRC) has developed phenomenological flame propagation models for hydrogen-air-steam mixture deflagrations. The FMRC approach has been to make empirical revisions to existing flame propagation models in order to account for the experimentally observed peak pressures, pressure rise times, and hydrogen burn fractions. Hopefully, this approach will result in models that are sufficiently accurate to reproduce and interpret existing data, while also being readily applicable for predictions of future test results and hypothetical containment burn scenarios.

2. FMRC MODEL DESCRIPTIONS

2.1 General Description

The current FMRC models rely upon the following simplifying assumptions:

- A uniform gas mixture exists in the (single) enclosure at the time of ignition.
- There is only one global burn; i.e., no additional hydrogen is released into the containment after ignition.
- Pressure gradients are negligible, i.e., flame speed is small compared to gas mixture sound speed.
- At any instant during the deflagration, a single continuous flame surface separates burned and unburned gases, each at a separate, but uniform, gas temperature.
- Burned and unburned gases satisfy ideal gas relations.
- Unburned gas is compressed isentropically with a constant value of specific heat ratio, γ.

The first three assumptions are consistent with most of the recent test conditions described later in the paper. The last three assumptions are approximations; errors introduced by these approximations are difficult to estimate without resource to more rigorous solutions.

The single burn and single flame front assumptions lead to the following mass conservation equations for burned and unburned gas:

$$\frac{dm_b}{dt} = -\frac{dm_u}{dt} = \rho_u S_u A_f \tag{1}$$

where m_b and m_u are the masses of burned and unburned gas, respectively, at time t; ρ_u is the unburned gas density; S_u is the burning velocity and A_f is the flame surface area. This equation illustrates the importance of an accurate estimate of instantaneous flame surface area as well as burning velocity.

Unburned gas density and temperature, T_u, at any time during the deflagration can be related to the instantaneous pressure, P, via the ideal gas isentropic compression assumption, i.e.,

$$\rho_u = \rho_{uo} \left(\frac{P}{P_o}\right)^{\frac{1}{\gamma}} \tag{2}$$

$$T_u = T_o \left(\frac{P}{P_o}\right)^{\frac{\gamma-1}{\gamma}} \tag{3}$$

where the subscript o denotes preignition values of the thermodynamic variables. From the conservation of volume and ideal gas law:

$$V_o = V_b + \frac{m_u R_u T_u}{P} \tag{4}$$

where V_o = total volume of the vessel;

V_b = volume of burned gas; and

R_u = mass basis gas constant for unburned gas.

Before eqs (1)-(4) can be evaluated, descriptions of flame shape and burned gas thermodynamic properties are required. Separate descriptions are provided in the FMRC models for the complete combustion regime and for the near-lean-limit incomplete combustion regime (corresponding to hydrogen concentrations in the range 4-9 vol% in dry air).

2.2 Complete Combustion Model

In the complete combustion regime, the flame is assumed to propagate as an expanding sphere until it reaches the nearest wall of the vessel. Spherical and spherical cap flame fronts corresponding to this prescription are illustrated in Figure 1 for the cases of central ignition and bottom center ignition in a cylinder with a vertical axis of symmetry.

The adiabatic compression assumption is invoked for burned gas as well as unburned gas in the complete combustion model. This assumption allows the following equation between fractional pressure rise and burned gas fraction to be utilized.

$$\frac{P - P_o}{P_e - P_o} = \frac{m_b}{M_o}$$



where P_e = final pressure when combustion is completed; i.e., adiabatic isochoric thermal equilibrium pressure; and

M_o = initial mass of gas in vessel = $\rho_{uo} V_o$.

Equation (5), which corresponds to the approximate solutions of Bradley and Mitcheson[6] and Lewis and von Elbe[7], is rigorously valid when burned and unburned gases have the same value of γ, and is valid to within (at worst) a few percent when γ_u and γ_b have the usual values of 1.4 and 1.2, respectively. Implementation of eq (5) in the FMRC complete combustion model generally involves a determination of P_e and T_e from an adiabatic thermochemical equilibrium computation accounting for eight chemical species (H_2, O_2, N_2, H_2O, OH, H, O, and N

Calculations of burned gas and pressure rise fractions during the deflagration involve numerical integration of eq (1) with A_f determined from the instantaneous value of m_b and the spherical (or spherical cap) flame surface assumption. In situations involving initially quiescent gas mixtures, the laminar burning velocity correlation of Liu et al[8] has been utilized.

Several simple alternative turbulent burning velocity correlations are available as options in the FMRC model to simulate initially turbulent gas mixtures stirred by a fan. One correlation used for the turbulent/laminar burning velocity ratio is:

$$\frac{S_T}{S_u} = (a + b\, v_F/S_u)^c$$



where v_F is a characteristic fan-induced flow velocity and a, b, c are empirical parameters. When the product b v_F is interpreted as the root-mean-square turbulent velocity fluctuation, eq (6) is a generalization of several of the wrinkled flame (large turbulent macroscale) turbulent burning velocity correlations reviewed by Andrews et al[9]. Typically a and c are both assumed to be unity; however, larger values can be used to also account for flame-induced turbulence. The

value of v_F was initially prescribed to be the fan tip velocity, but now it is taken as the bulk mixing velocity, defined as the nominal fan volumetric flow capacity divided by the enclosure cross-sectional area. Of course, the two different prescriptions require different empirical values for the parameter b.

Another turbulent burning velocity correlation included in the FMRC complete combustion model is:

$$S_T/S_u = \left\{ 1/2 + \sqrt{1/4 + d\ (v_f/S_u)^2} \right\}^{1/2} \qquad (7)$$

where d is another empirical constant of the order 0.10 when v_f is the fan tip speed and about 200 when v_f is the bulk mixing velocity. Equation (7) is consistent with Williams theoretical derivation[10] for the wrinkled-laminar-flame turbulent burning regime. Comparisons of calculated and measured pressure rise times are being conducted for various turbulent hydrogen deflagration experiments in order to determine "best-fit" values of the parameters in eqs (6) and (7).

2.3 Incomplete Combustion Model

Experimental observations (reviewed by Hertzberg[4]) of lean hydrogen-dry air mixture deflagrations in the range 4% to 8% H_2 suggest that there are three complicating factors responsible for less-than-complete combustion of the entire mixture. These factors are: 1) buoyant rise of the propagating fireball; 2) heat losses leading to flame quenching; and 3) noncontiguous flame structures consisting of dispersed flamelets outside of which the combustion reaction itself is incomplete. The first two effects, i.e., buoyancy and flame quenching are included in the FMRC incomplete combustion model. The third effect; i.e., incomplete reaction associated with noncontiguous flamelets, has not been explicitly treated because recent data obtained by Mitani[11], reveal that, although there appear to be large unburned spaces between the flamelets, they consume all but, at most, 6% of the initial hydrogen in the gas mixture reached by the flame prior to extinction.

Buoyant flame propagation effects are incorporated into the FMRC incomplete combustion model via the Crescitelli et al[12] two-phase simulation shown schematically in Figure 2. In the first phase, buoyancy forces cause the expanding flame to propagate upward from the ignition site. This phase terminates when the flame front reaches the top of the vessel. At this time (indicated

as time t_3 in Figure 2) the flame is assumed to suddenly deform into a flat-front downward propagating flame. Cellular flame surfaces are not simulated directly, but there is a provision to "adjust" the nominal smooth flame surface area by an empirical factor to be determined via detailed comparisons of calculated and measured pressure rise times.

Buoyant rise of the flame during the first phase of propagation is determined by the fireball momentum equation:

$$\frac{d}{dt}(M_e v) = (\rho_u - \rho_b)\, g\, V_b - 1/2\, \rho_u\, \pi\, r_b^2\, C_D\, v^2 \qquad (8)$$

where v is the fireball rise velocity, ρ_b is burned gas density, g is gravitational acceleration, r_b is the horizontal fireball radius and C_D is a drag coefficient. The virtual mass, M_e, is included in eq (8) because as the fireball accelerates, some neighboring unburned gas is also accelerated. Thus,

$$M_e = (\rho_b + K\, \rho_u)\, V_b \qquad (9)$$

where K is the added mass coefficient (given by Milne-Thompson[13]) which depends on the shape of the fireball. Originally the flame shape during rise was assumed to be an oblate spheroid, with aspect ratio, ε, given by the following empirical correlation from Crescitelli et al[12] experiments.

$$\varepsilon = \min\left\{1,\ 1.5\text{-}0.5\, \frac{v}{\Gamma S_u}\right\} \qquad (10)$$

where Γ is the unburned/burned gas density ratio. However, eq (10) produced aspect ratios approaching zero when applied to slow-burning hydrogen mixtures in large vessels. Therefore, the following two separate prescriptions were adopted for rising hydrogen flames in large spherical and cylindrical vessels. For spherical vessels, eq (10) was used until the fireball maximum radius of curvature equaled the radius of the sphere. After that time, the fireball maximum radius was held constant as the fireball expanded vertically. For cylindrical vessels, eqs (8)-(10) were used until the fireball reached the sides of the vessel. At this point, eq (8) (which does not account for wall confinement effects) was replaced with the following semi-empirical equation originally proposed by Batchelor[24] for bubbles rising through vertical cylinders:

$$v = 0.48 \sqrt{g R_v (1 - 1/\Gamma)} \tag{11}$$

where R_v is the cylinder radius.

While eq (8) is still applicable (for both spheres and cylinders), the drag coefficient, C_D, is calculated from the correlation:

$$C_D = 2.7 + 12 \nu_u / v r_b \tag{12}$$

(where ν_u is the unburned gas kinematic viscosity) which was originally given for the rise of gas bubbles in liquid fluidized beds[12].

During the first phase, heat losses are assumed to be negligible because burned gas has not yet reached the top of the vessel. Since we also assume ideal gas behavior, constant specific heat ratio, and uniform burned gas temperature, the pressure rise can be determined from eq (5). Thus, the governing equations for the first phase of flame propagation consist of differential eqs (1) and (8), algebraic eqs (2)-(5), (9)-(12) and the associated algebraic equations for flame geometry and mixture burning velocity.

In the second phase, burned gas fills the top portion of the vessel and the flame surface bordering the bottom of the burned gas is assumed to be planar (Figure 2b). Thus, given a vessel geometry and calculated burned gas volume at the end of the first phase, the flame front location, flame surface area, A_f, and the burned gas/vessel wall contact area, A_{bw}, can be determined. Heat loss to the vessel walls, $\dot{Q}_L$, which is assumed to remain at the initial temperature, is currently evaluated using Newton's cooling law,

$$\dot{Q}_L = h A_{bw} (T_b - T_o) \tag{13}$$

where h is an empirical heat transfer coefficient.

Strictly speaking, eq (13) is only applicable for convective and condenson heat transfer. For laboratory-scale vessels, Mitani[11] has shown that convection is the dominant heat transfer mode for near-limit hydrogen-air flames. However, thermal radiation, which is not explicitly described by eq (13), becomes increasingly important as vessel size increases. Approximate calculations performed by the authors indicate that, for a 2-m diameter vessel, heat fluxes due to condensation and radiation are comparable in magnitude (on the order of 8 Watt/cm^2 for 10 vol% hydrogen), and both are somewhat higher

than the heat flux due to natural convection. Unfortunately, calculations based on classical heat transfer correlations do not account for the complicated fluid and thermal effects associated with the fireball reaching the top of the vessel and then propagating downward. For example, interactions between convective motions and the diffusion layer adjacent to the condensed water film on the vessel wall are apparently not accounted for in any published correlations.

In view of the limitations of existing data correlations and theoretical heat transfer analyses, the authors have derived a new correlation based on data from several recent series of hydrogen-air-steam deflagration tests. Heat transfer coefficients were estimated from measured pressure-time curves by calculating the derivative at the inflection point on the decay side of the curves. Data from a total of 15 tests conducted by AECL[14], Fenwal[15] and Sandia[16,17] were included as well as one "full-scale" data point from a report on the TMI incident[18]. The resulting correlation is:

$$Nu = 3.184\times10^{-3}\ \xi_1^{0.90}\ Gr^{0.44}\ Re^{0.24}/\xi_o^{0.075} \qquad (14)$$

where Nu and Gr are the Nusselt and Grashof numbers, respectively, both based on vessel height, H; and Re is $S_u H/\nu_b$. The dimensionless parameters ξ_o and ξ_1 are the flame front position (distance from the top of the vessel) and vessel horizontal dimension, respectively, divided by H.

Using eqs (13) and (14) to evaluate the heat loss term, the burned gas temperature during downward flame propagation is calculated from the energy equation:

$$\frac{d}{dt}\ (m_b\ u_b) = \rho_u\ S_u\ A_f (h_u + \Delta H_c) = \frac{PdV_b}{dt} - \dot{Q}_L \qquad (15)$$

where u_b is burned gas internal energy, h_u is unburned gas enthalpy, and ΔH_c is the heat of combustion. Unburned gas temperatures are evaluated from eq (3), since unburned gas compression is still assumed to be adiabatic.

Due to cooling of the burned gas, the burning velocity is expected to deviate from its adiabatic value, Su_{AD} given by Liu et al[8]. Assuming first order Arrhenius kinetics, the nonadiabatic burning velocity is:

$$\frac{Su}{Su_{AD}} = \exp\left[-\frac{E}{2R}\frac{T_{AD}-T_b}{T_b T_{AD}}\right] \tag{16}$$

where R is the universal gas constant and the value of the overall activation energy, E, for the hydrogen-air burning was taken to be 16 kcal/mole from F[illegible]n and Calcote[19].

The formulation of the problem is not complete unless a flame extinction criterion is defined. Crescitelli et al[12] used the criterion:

$$\left.\frac{Su_{AD}}{Su}\right|_{EX1} = \sqrt{e} \tag{17}$$

which was derived by Frank-Kamenetskii[20] for heat loss within the flame thickness and transverse to the direction of propagation. If the predominant heat loss is taken as a convective loss from burned gas behind the flame front, it can be shown that[21]

$$\left.\frac{Su_{AD}}{Su}\right|_{EX2} = e \tag{18}$$

These two criteria correspond to two simplified cases, and it is not obvious which is more applicable to the present problem. Therefore, in the calculations both are retained and referred to as first and second extinction criteria.

3. COMPARISON OF CALCULATED RESULTS AND EXPERIMENTAL DATA

3.1 Complete Combustion Data

Complete combustion model calculations have been compared to Fenwal[15] and AECL[14] data obtained in spherical vessels and to Sandia[16], Lawrence Livermore[22], and Acurex[23] data in cylindrical vessels. As indicated in Table I, data encompassed hydrogen volumetric concentrations ranging from 7-42% and steam concentrations from 0-40%. Only tests in which there was [illegible]ally complete combustion (as determined by post-test gas samples) were chosen for comparison.

A sample comparison of pressure rise versus time is shown in Figure 3 for conditions with and without the 1500 rpm fan in the AECL 2.3-m diameter sphere. The experimental curves in Figure 3 indicate that turbulence affected not only the time to reach peak pressure but also the peak pressure itself. A higher peak pressure rise within a shorter time was observed with the fan on. In the

theoretical model, turbulence does not influence the maximum pressure; i.e., the adiabatic closed vessel peak pressure rise is 211 kPa (30.6 psig) for an 8% hydrogen mixture, no matter how long it takes to get there. This value is higher than the measured pressure rise with the fan on and 45% higher than the measured rise (26% greater than the peak absolute pressure) without the fan. With the fan on, the pressure rise occurs much faster, both experimentally and theoretically, with empirical turbulent burning velocity coefficients indicated in Figure 3. For other fan-stirred tests, the comparison between calculated and measured pressure rise times showed a root-mean-square deviation of 30-35% depending on the choice of empirical parameters in eqs (6) and (7).

The most obvious explanation for the differences between calculated and measured peak pressures is the effect of heat losses which were neglected in the complete combustion model. Heat losses should be more important for slow burning velocity mixtures since there should be more time available for heat transfer to the vessel walls before combustion is completed. Figure 4 is a plot of percent deviation in peak pressure versus mixture burning velocity. It is evident from Figure 4 that the errors in calculated peak pressures are, indeed, generally larger for slow burning velocities, i.e., for lean mixtures. However, even when the burning velocity approaches 1 m/s (hydrogen concentration about 15 vol%), there are still some deviations of about 16% for cylindrical test vessels. As indicated in Table I, the root-mean-square deviation between calculated and measured peak pressures for all the complete combustion data is about 16%.

Calculated pressure rise times usually exceeded the corresponding measured times for hydrogen concentrations above about 10%, and underestimated measured rise times for hydrogen concentrations less than 10%. The overall root-mean-square (rms) percent difference between calculated and measured rise times is indicated in the last column in Table I for all five intermediate-scale test programs. The Sandia VGES data produced by far the largest rms deviation (109%), possibly because the reported Sandia experimental values do not include the thermocouple delay time to detect glow plug ignition. The rms deviations for the other four test series did not exceed 41%.

TABLE I

COMPARISON OF CALCULATED AND MEASURED PEAK PRESSURES AND

ASURED PEAK PRESSURES AND PRESSURE RISE TIMES FOR COMPLETE COMBUSTION TESTS

Organization	Vessel	D(m)	No. Tests	$\%H_2$ Range	$\%H_2O$ Range	RMS % Deviation P_{max}	RMS % Deviation t_{max}
AECL	Sphere	2.29	21	7-42	0-40	19.9	41.2
Acurex	Cylinder (L/D = 2.42)	2.11	5	7-11	23-33	7.4	-
Fenwal	Sphere	1.93	7	7-13	1-25	9.9	40.5
Livermore	Cylinder (L/D = 2.92)	0.51	5	9-16	0.0	11.4	18.9
Sandia	Cylinder (L/D = 4.0)	1.22	12	9-18	0.0	15.0	108.5
Total			50			15.9%	65.0%
						(38.5% w/o Sandia data)	

3.2 Incomplete Combustion Data

Calculated pressures and burn fractions obtained with the incomplete combustion model have been compared to lean mixture data from the AECL 2.3-m diameter sphere and the Sandia VGES vessel. In Figure 5, the pressure histories calculated with the incomplete combustion model are compared with AECL data for 8% hydrogen with 15 and 30% steam mixtures. The two arrows on each calculated pressure curve ...icate the times for which the first and second flame extinction criteria in ...model are satisfied. The discontinuity in the rate of pressure rise in the calculated curves indicates the end of the first phase where there is a sudden change in the flame surface area. For the 15% steam mixture, the calculated peak pressure and pressure rise time are in approximate agreement with the measured values. For the 30% steam mixture, the calculated maximum overpressure is more than twice the experimental value. This discrepancy may be due to unrealistically high calculated burning velocities when the Liu et al

correlation is applied to mixtures with high steam content*. Even for the 15% steam mixture, the calculated pressure rise is much steeper than the measured rise during the first, i.e., upward phase of flame propagation.

In Figure 6, predicted overpressures with two extinguishment criteria for various H_2-Air mixtures are compared with the AECL data. Both quench criteria produce approximately the same pressures in this case. The calculated rapid increase of peak pressure with increasing hydrogen concentrations in the range 6 to 7 percent is also indicated in the AECL data.

Table II shows the deviations between calculated and measured pressures, rise times and burn fractions for several AECL and Sandia tests. The peak pressures calculated using the first extinction criterion appear to roughly agree with the experimental pressures except for the case of 30% steam as was already mentioned above. The rise times and the burn fractions calculated using the first extinction criterion had root-mean-square deviations with data of 41% and 35%, respectively.

Figure 7 shows the calculated and measured transient overpressure for a 8.4% hydrogen-air mixture ignited in the Sandia VGES vessel. The agreement is surprisingly good particularly in view of the distorted flame front contours measured in the experiments and indicated in the sketch on the left of Figure 7.

In Figure 8, the predicted overpressures using the first quenching criterion are compared with the Sandia data for various mixtures. (Differences between the first and second criteria are not distinguishable in the scale of the figure.) This figure also indicates the sensitivity of the overpressures to the initial hydrogen concentration. Two hydrogen concentration values, based on partial pressures and on gas chromatography were provided by Sandia; the latter gave better agreement with the experiments. Another feature of Figure 8 that is similar to Figure 6, is that the model slightly underpredicts the overpressures for leaner mixtures, (less than 7% H_2) whereas it overpredicts for richer mixtures (above 9% H_2). Possible reasons for these deviations are 1) irregular flame shapes (flamelets) for lean mixtures, and 2) significant first-phase radiation heat losses for richer mixtures.

*Using the Liu et al burning velocity correlation, the complete combustion model also predicted much shorter rise times than the measured values with high steam concentrations.

TABLE II

COMPARISON OF INCOMPLETE COMBUSTION MODEL RESULTS WITH AECL AND SANDIA DATA

Affiliation/ Test No.	$\%X_{H_2}$	$\%X_{H_2O}$	ΔP(atm)	Observed t(s)	Observed % Burn Fraction	% Relative Error (Calc - Obs)/Obs 1st Criterion ΔP	1st Criterion t	1st Criterion Burn Fraction	2nd Criterion ΔP	2nd Criterion t	2nd Criterion Burn Fraction
AECL/113	8	15	1.24	4.9	99	-4.3	-22.7	-20.2	-1.8	-11.4	-3.0
AECL/116	8	30	0.38	5.0	38	112.6	-14.4	39.5	147.1	25.2	108.0
AECL/106	7	0	1.23	7.0	99	-17.0	-43.6	-26.3	-12.6	-31.4	-6.1
AECL/103	6	0	0.267	4.9	30	25.4	-16.7	-16.6	83.0	51.0	53.3
AECL/102	5.5	0	0.237	6.0	26	-49.0	-34.3	-65.4	-33.3	4.0	-42.3
AECL/117	7	0	1.09	11.4	99	-10.4	-61.3	-17.9	-3.3	-52.0	9.5
SNL/B5H6	6.4	0	0.63	4.16	37.6	-42.5	20.2	-43.9	-42.2	34.6	-34.8
SNL/B7H7	7.3	0	0.81	3.20	53.1	-11.1	43.8	-26.9	-10.4	63.1	-13.7
SNL/B4H8	8.4	0	1.46	5.44	-	-8.2	-21.3	-	-7.3	-11.4	-
SNL/B8H9	9.3	0	1.81	5.28	100.	18.8	-29.4	0	18.8	-29.4	0
				Mean Dev. =		1.4	-18.0	-19.7	13.8	4.2	7.9
				RMS Dev. =		45.3	30.3	28.9	57.9	38.1	46.5

CONCLUSIONS

For deflagrations involving the complete combustion of hydrogen, the adiabatic spherical flame propagation model: 1) overpredicts peak pressures with a root-mean-square deviation of about 16%; and 2) predicts pressure rise times with a root-mean-square deviation of 65% (39% excluding the Sandia VGES data) compared to data from 50 tests with initially quiescent hydrogen-air-steam mixtures. The peak pressure deviation is caused by heat loss effects neglected in the adiabatic model, while the rise time deviation is probably due to turbulent flame surface distortion or flame acceleration. In tests with fan-stirred mixtures, the observed peak pressures are closer to the adiabatic equilibrium values, and the measured pressure rise times show similar rms deviations (~35%) compared to calculations with empirical turbulent burning velocity correlations.

For near-lean-limit mixture deflagrations involving flame quenching and residual hydrogen concentrations, peak pressures, rise times and burn fractions calculated with the FMRC incomplete combustion model result in root-mean-square deviations of 18-49% of experimental values. Predictions are better for dry mixtures than for mixtures with high steam content. Differences are probably due to: 1) errors in the empirical burning velocities used for steam-enriched mixtures; 2) neglect of cellular flame surfaces; and 3) omission of flame radiation explicitly in the empirical heat loss correlation derived for this model. All these differences are being addressed in an updated version of the model.

ACKNOWLEDGMENT

This work was sponsored by EPRI under Contract RP-1932-10. Dr. Loren Thompson is the project monitor.

REFERENCES

1. Haskin, F.E. and Trebilcock, W., "Combustion Modelling in MARCH, Developments and Limitations," presented at the Second International Workshop on the Impact of Hydrogen on Water Reactor Safety, October 1982.
2. Camp, A.L. et al, "HECTR: A Computer Program For Modelling the Response to Hydrogen Burns in Containment," presented at the Second International Workshop on the Impact of Hydrogen on Water Reactor Safety, October 1982.
3. Fuls, G.M., "Containment Response to H_2 Combustion," Proceedings of the 1st International Workshop on the Impact of Hydrogen on Water Reactor Safety, January 1981.
4. Hertzberg, M., "Flammability Limits and Pressure Development in H_2-Air Mixtures," Proceedings of the 1st International Workshop on the Impact of Hydrogen on Water Reactor Safety, January 1981, also published as BuMines Pittsburgh Research Center Report 4305, 1981.
5. Bradfute, J.O. and Paulsen, M.P., "Hydrogen Flammability Model Based on Present Data," Proceedings of the Workshop on the Impact of Hydrogen on Water Reactor Safety, Albuquerque, January 1981.
6. Bradley, D. and Mitcheson, A., "Mathematical Solutions for Explosions in Spherical Vessels," Combustion and Flame, Vol. 26, pp. 201-217, 1976.
7. Lewis, B. and von Elbe, G., (1961), Combustion, Flames and Explosions of Gases, Academic Press, 1961.
8. Liu, D., MacFarlane, R. and Clegg, L., "Some Results of WNRE Experiments on Hydrogen Combustion," Systems Analysis Branch of Whiteshall Nuclear Research Establishment, Atomic Energy of Canada Limited, issued as AECL-7046, 1980, also presented at the Workshop on the Impact of Hydrogen on Water Reactor Safety, Albuquerque, January 1981.

Andrews, G.E., Bradley, D., and Levakabamba, S.B., "Turbulence and Turbulent Flame Propagation," Combustion and Flame, Vol. 24, pp. 285-304, 1975.

10. Williams, F.A., "Laminar Flame Instability and Turbulent Flame Propagation," Proceedings of the International Specialists Meeting on Fuel-Air Explosions, U. of Waterloo Press, 1982.
11. Mitani, T., "Studies of Premixed Hydrogen Flames," PhD Thesis, U. of California at San Diego, 1979.

12. Crescitelli, S., Russo, G., Tufano, V., Napolitano, F. and Tranchino, L., "Flame Propagation in Closed Vessels and Flammability Limits," Combustion Science and Technology, 15, 1977.
13. Milne-Thomson, L.M., Theoretical Hydrodynamics, p. 423, 1949.
14. Kumar, R.K., Tamm, H., Harrison, W.C., Swiddle, T., and Skeet, T., "Combustion of Hydrogen-Steam-Air Mixtures Near Lower Flammable Limit," AECL Draft Report, 1982.
15. Dalzell, W.G., "Determination of Ignition Performance of Glow Plug Hydrogen Igniter," Fenwal Inc. Report PSR-914, 1980 (supplemental data provided by J.J. Wilder of TVA).
16. Benedick, W.B., Cummings, J.C., and Prassinos, P.G., "Experimental Results from Combustion of Hydrogen: Air Mixtures in an Intermediate-Scale Tank," Second Intl. Workshop on the Impact of Hydrogen on Water Reactor Safety, 1982.
17. Berman, M., "Light Water Reactor Safety Research Program Semiannual Report," April-September 1981, pp. 318-328, NUREG CR-2481, SAND 82-0006, February 1982.
18. Henrie, J.O. and Postma, A.K., "Analysis of the Three Mile Island (TMI-2) Hydrogen Burn," Rockwell International Draft Report RHO-RE-SA-8P, 1982.
19. Fenn, J.B. and Calcote, H.F., "Activation Energies in High Temperature Combustion," Fourth Symposium (International) on Combustion, p. 231, 1959.
20. Frank-Kamenetskii, D.A., "Diffusion and Heat Transfer in Chemical Kinetics," p. 365, 1969.
21. Sthessel, E.A., Merzhanov, A.G., Maximov, Yu.M, and Maximov, E.I., "Effect of Natural Convection on the Combustion of Volatile Explosives in a Field of Mass Forces," Fizika Goreniya i Vzryva, 9, No. 6, pp. 855-861, 1973.
22. Lowry, W., "Preliminary Results of Thermal Igniter Experiments in H_2-Steam Environments," UCRL-84167, Proceedings,1st International Workshop on Impact of Hydrogen on Water Reactor Safety, January 1981.
23. Torok, R.C., Siefert, K., and Thomson, L.B., "Hydrogen Control Tests in Intermediate Scale," presented at the Second International Workshop on the Impact of Hydrogen on Water Reactor Safety, October 1982.
24. Batchelor, G.K., An Introduction to Fluid Dynamics, p. 978, 1970.

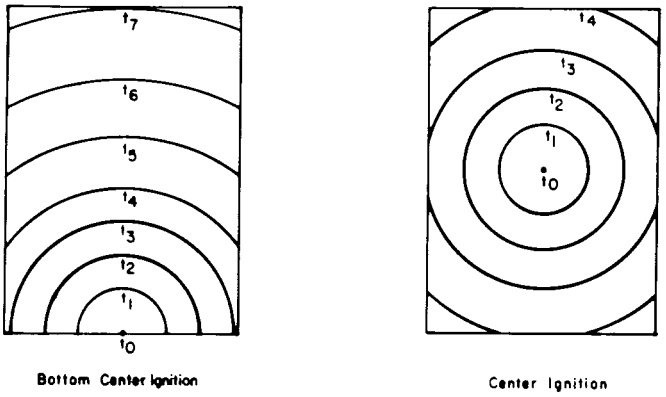


Figure 1 Spherical Flame Progagation in a Cylinder (Complete Combustion Model)

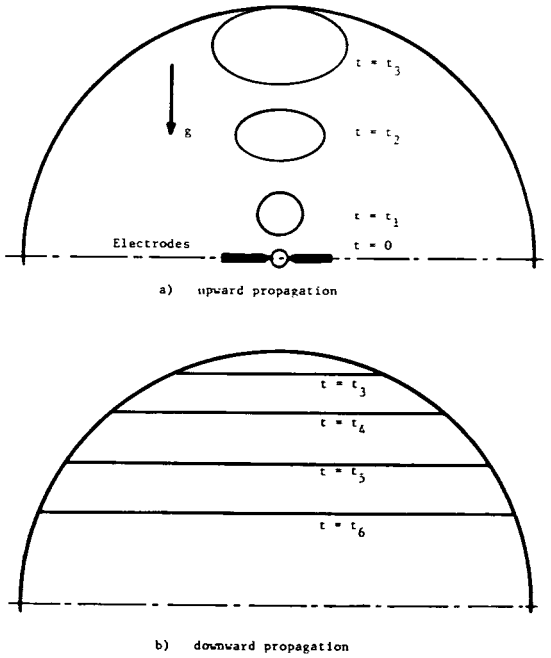


Figure 2 Two Phases of the Flame Propagation ($t_i < t_{i+1}$) in Incomplete Combustion Model

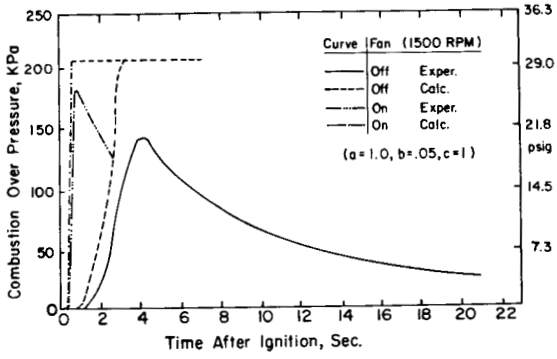


Figure 3 Calculated and measured pressure rise curves, with and without fan-induced turbulence, in the 2.3-m diameter sphere at AECL Whiteshell. Bottom ignition of an 8% hydrogen in air mixture. (Turbulent velocity is based on the fan tip speed.)

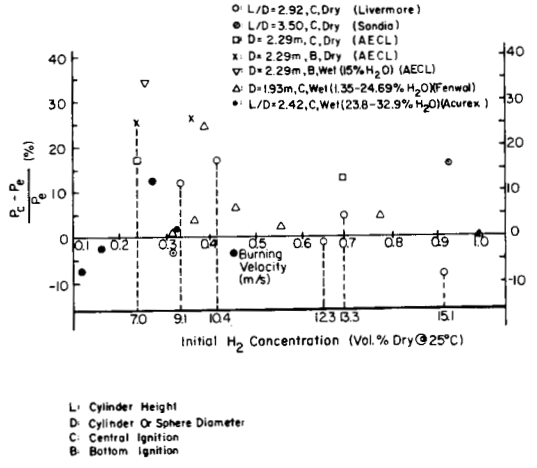


Figure 4 Deviation in Calculated Peak Pressures Versus Mixture Burning Velocity

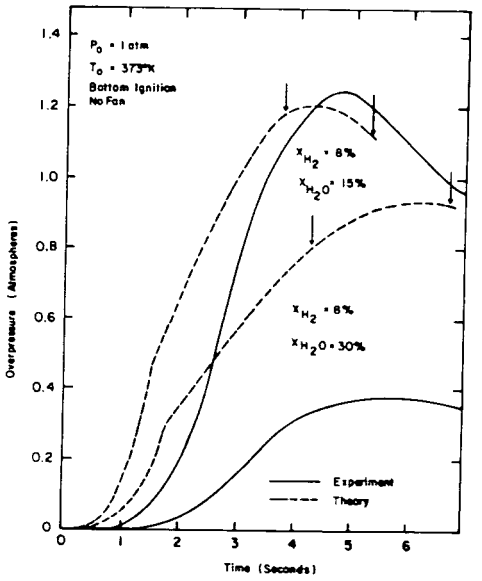


Figure 5 Comparison of the Theory (Broken Lines) with Two AECL Experiments (Solid Lines). Arrows indicate times at which the first and second quenching criteria are satisfied.

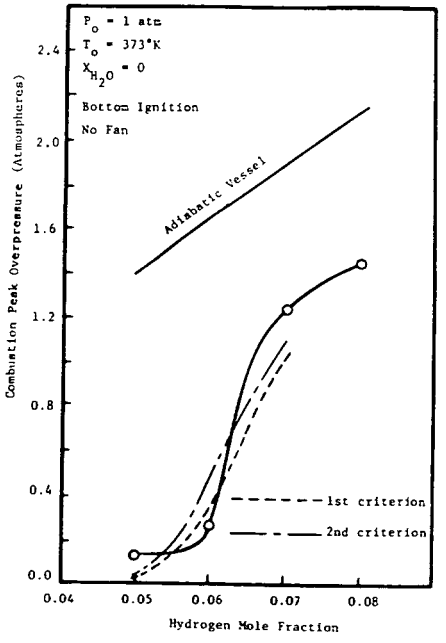


Figure 6 Observed and Predicated Concentration Effect on Hydrogen Burn. (AECL data are indicated with circles. Broken and dashed lines correspond to first and second quenching criteria, respectively.)

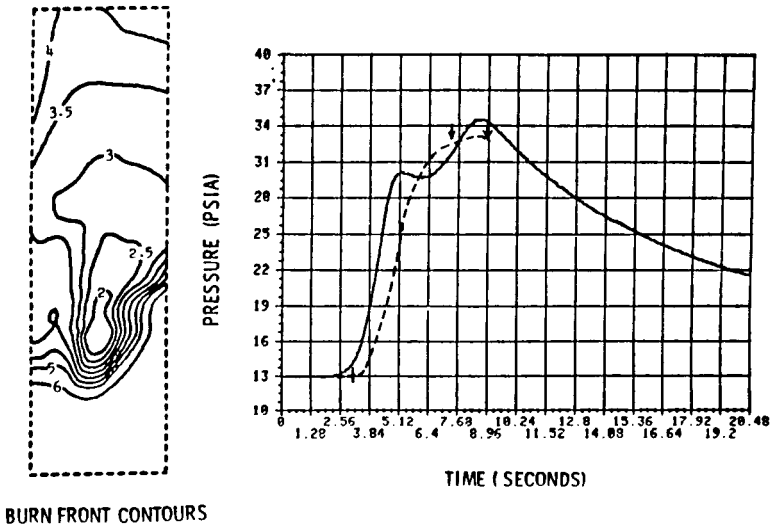


Figure 7 VGES 14 ft Tank-Burn B4H8, X_{HC} = 8.4%

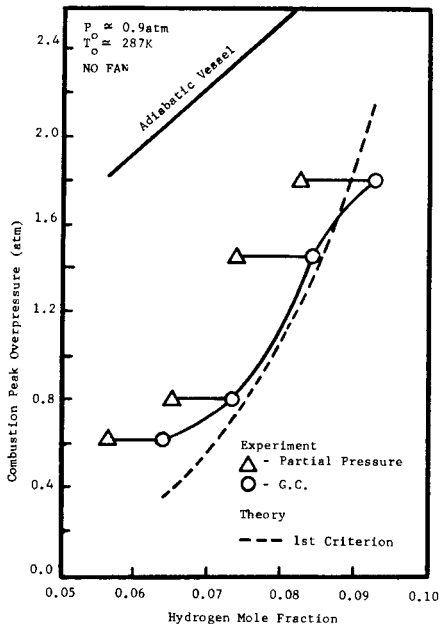


Figure 8 Observed and Predicted Concentration Effect on Hydrogen Burn (Quiescent Sandia Tests)

SAND82-1964C

HECTR: A Computer Program for Modelling the Response to Hydrogen Burns in Containments

Allen L. Camp
Michael J. Wester*
Susan E. Dingman
Martin P. Sherman

Sandia National Laboratories
Albuquerque, NM 87185

*The Dikewood Corporation

ABSTRACT

Sandia National Laboratories is engaged in an NRC-sponsored program to study the problems associated with hydrogen generation in light water reactors. As part of that effort, we have developed a computer program called HECTR (Hydrogen Event: Containment Transient Response), which models hydrogen burns in containments and the associated important heat transfer mechanisms. The purpose of this paper is to summarize the capabilities of HECTR.

Introduction

Sandia National Laboratories is engaged in an NRC-sponsored effort to investigate hydrogen behavior and control in light water reactors. As part of this effort, we are developing analytical models to predict what might happen under certain accident conditions. The purpose of this paper is to describe a computer program called HECTR (Hydrogen Event: Containment Transient Response), which models the response to various accidents involving the release of hydrogen. Some results obtained using HECTR are included in another paper presented at this conference.[1]

HECTR is a fast-running, lumped-volume code, which, in its present form, is most useful for parametric analyses. The code is structured in such a manner that it is extremely flexible, allowing model changes to be implemented with a minimum of difficulty. As data from experimental programs and other code development efforts become available, they will be incorporated in HECTR, allowing HECTR to evolve into a "best-estimate" code.

HECTR currently includes models for hydrogen burns, radiative and convective heat transfer, wall condensation, heat transfer to sprays, wall heat conduction, and ice condensers. Flows between compartments can occur due to pressure gradients or fans. Inertial effects are included. The gases are assumed to be ideal and homogeneous within each compartment. Steam and hydrogen source terms are specified by the user. The structure of the code and each of the various models are discussed in more detail below.

Multicompartment Mass, Energy, and Momentum Equations

The multicompartment model is a system of ordinary differential equations expressing conservation of mass, energy, and momentum. The mass conservation equations are formulated for each of four gas species (water vapor, nitrogen, oxygen, and hydrogen) in each compartment on a molar basis. The conservation of energy equation is written for the total mixture in each compartment. Conservation of momentum is specified at flow junctions, which are the connections between compartments. Gas flow between compartments is caused by pressure differences, gravitational forces, and fans. The gases in each compartment are assumed to be ideal and homogeneous. Compartment interconnections are modelled as orifices with flow resistances.

The independent variable in this model is time, and the governing dependent variables are:

$$N_{ij},\ E_i,\ \text{and}\ F_\ell\ .$$

N_{ij} is the number of moles of the j^{th} species of gas in the i^{th} compartment. E_i is the total internal energy in compartment i and can be expressed by

$$E_i = \sum_{j=1}^{N_{gases}} N_{ij}\, u_{ij} \qquad (N_{gases} = 4) \tag{1}$$

where u_{ij} is the molar internal energy of the j^{th} gas in the i^{th} compartment. F_ℓ is the volumetric flow rate in the ℓ^{th} junction, defined by $F_\ell = A_\ell\, v_\ell$ where A_ℓ is the interconnection area and v_ℓ is the gas velocity at the junction. The conservation equations define the rate of change of each of these three types of variables; therefore, the total number of equations that are solved simultaneously is

$$N_{eqns} = (N_{gases} + 1)\, N_{comps} + N_{juncs} \tag{2}$$

where N_{comps} and N_{juncs} are the number of compartments and the number of flow junctions, respectively.

The conservation equations are given below with the same subscript convention as used above with the sign convention that positive flow in the ℓ^{th} junction is from compartment i to compartment k. Note that the intercompartment fan flows are included separately from the junction flow terms, F_ℓ. A derivation of a momentum equation similar to the one in Equation (4) may be found in Reference 2. Momentum equations similar to the ones presented in Equation (4) and Reference 2 are typical for lumped volume codes.

Conservation of Molar Content:

$$\frac{dN_{ij}}{dt} = -\sum_{\substack{\ell \\ (F_\ell > 0)}} \frac{F_\ell}{V_i} N_{ij} - \sum_{\substack{\ell \\ (F_\ell < 0)}} \frac{F_\ell}{V_k} N_{kj} + \left(\frac{dN_{ij}}{dt}\right)_{\substack{external \\ source}} + \left(\frac{dN_{ij}}{dt}\right)_{chemical} + \left(\frac{dN_{i,H_2O}}{dt}\right)_{\substack{evaporation, \\ condensation}} + \left(\frac{dN_{ij}}{dt}\right)_{fans} \tag{3}$$

Conservation of Momentum:

$$\frac{dF_\ell}{dt} = \frac{1}{\frac{\rho_i L_i}{a_i} + \frac{\rho_k L_k}{a_k}} \left[\left(P_i - P_k\right) + \left(\frac{\rho_i + \rho_k}{2}\right) g(z_i - z_k) - \frac{K_\ell \left(\rho_i + \rho_k\right) F_\ell |F_\ell|}{4A_\ell^2} \right] \tag{4}$$

Conservation of Energy:

$$\frac{dE_i}{dt} = \sum_{j=1}^{N_{gases}} \left[- \sum_{\substack{\ell \\ F_\ell > 0}} \frac{F_\ell}{V_i} N_{ij} h_{ij} - \sum_{\substack{\ell \\ F_\ell < 0}} \frac{F_\ell}{V_k} N_{kj} h_{kj} + \left(\frac{dN_{ij}}{dt}\right)_{\substack{\text{external} \\ \text{source}}} h_{j,\,\text{source}} \right] + \left(\frac{dN_{i,H_2O}}{dt}\right)_{\substack{\text{evaporation,} \\ \text{condensation}}} h_{i,H_2O} - \left(\frac{dQ}{dt}\right)_{\substack{\text{radiation,} \\ \text{convection}}} - \left(\frac{dQ}{dt}\right)_{\text{sprays}} + \left(\frac{dE_i}{dt}\right)_{\text{fans}} \quad (5)$$

Here,

V_i = volume of compartment i (m^3)

$\left(\frac{dN_{ij}}{dt}\right)_{\substack{\text{external} \\ \text{source}}}$ = rate of addition into compartment i from an external source (steam or hydrogen), (moles/s)

$\left(\frac{dN_{ij}}{dt}\right)_{\text{chemical}}$ = chemical molar rate of change due to combustion (moles/s)

$\left(\frac{dN_{i,H_2O}}{dt}\right)_{\substack{\text{evaporation,} \\ \text{condensation}}}$ = rate of change of water vapor due to evaporation from or condensation on the wall surfaces and the spray droplets (moles/s)

$\left(\frac{dN_{ij}}{dt}\right)_{\text{fans}}$ = mass in compartment i due to inter-compartment fans (moles/s) (see Equations 24 and 25)

h_{ij} = enthalpy of the j^{th} gas in compartment i (J/mole)

$h_{j,\,\text{source}}$ = enthalpy of the j^{th} gas evaluated at the source temperature (J/mole)

$\left(\frac{dQ}{dt}\right)_{\text{radiation, convection}}$ = sum of the rates of radiative and convective heat transfer from the gas (J/s)

$\left(\frac{dQ}{dt}\right)_{\text{sprays}}$ = rate of heat transfer from the gas to the spray droplets (J/s)

$\left(\frac{dE_i}{dt}\right)_{\text{fans}}$ = energy addition to compartment i due to intercompartment fans (J/s) (see Equations 26 and 27)

ρ_i = gas density in compartment i (kg/m^3)

L_i = gas path length in compartment i (m)

a_i = effective gas flow area through compartment i (m^2)

P_i = pressure in compartment i (Pascals)

g = acceleration due to gravity (m/s^2)

z_i = elevation of compartment i (m)

K_ℓ = loss coefficient due to flow through the ℓ^{th} junction

A_ℓ = interconnection (flow) area of the ℓ^{th} junction

Method of Solution

The conservation equations are solved using a linearized implicit formulation. This formulation is derived by writing the conservation equations in the general form

$$\frac{d\bar{y}}{dt} = \bar{f}(\bar{y},t) \tag{6}$$

where $\bar{y}$ is a vector of the governing dependent variables (N_i, E_i, and F_ℓ). A Taylor series expansion of $\bar{f}(\bar{y}, t)$ up through first order terms is then performed, producing

$$\frac{d\bar{y}}{dt} \approx \bar{f}(\bar{y}_o,t_o) + \left.\frac{\partial \bar{f}}{\partial \bar{y}}\right|_{\bar{y}_o,t_o} (\bar{y} - \bar{y}_o) \tag{7}$$

where $\bar{y}_o$ is evaluated at t_o and $\partial\bar{f}/\partial\bar{y}$ is the Jacobian of $\bar{f}$. In HECTR, only flow derivatives are included in the Jacobian, while all other terms are set to zero. Finally, applying a finite difference approximation to the left side of Equation (7) yields the linear system of equations

$$\frac{\bar{y} - \bar{y}_o}{\Delta t} = \bar{f}(\bar{y}_o, t_o) + \left.\frac{\partial \bar{f}}{\partial \bar{y}}\right|_{\bar{y}_o, t_o} (y - y_o) \qquad (8)$$

Solving this system determines the updated values for the dependent variables contained in $\bar{y}$ after a time step of length Δt.

The heat transfer is relatively constant over a longer time scale than the time steps, Δt, required to solve the conservation equations. To avoid recalculating the heat transfer rates when they have changed little, the heat transfers due to radiation, convection, sprays, condensation, and wall conduction are held constant over a time step Δt that can be larger than Δt. The small time step, Δt, is controlled such that the maximum pressure change per compartment is 0.01 atm and the sum of the flows leaving a compartment are less than the volume of the compartment. Similarly, the heat transfer time step Δt is controlled such that the maximum compartment temperature change is less than 30 K and the maximum compartment pressure change is less than 0.1 atm. Both time steps are further constrained by user-specified maximums and minimums. Neither time step size is allowed to increase by more than a factor of 1.5 per time step. Problems occurring in this implicit solution technique, involving flow reversals and one-way convections, are successfully dealt with in the program. A simplified flow chart for HECTR is shown in Figure 1.

Hydrogen Burn Model

The hydrogen burn model in HECTR allows combustion to be initiated in a compartment whenever a specified hydrogen concentration is exceeded, provided that the atmosphere in the compartment is not inerted by a shortage of oxygen or an excess steam. Typically, the gas mixture is considered to be inert if the oxygen concentration is less than 5 percent by volume and/or the steam concentration is greater than 55 percent by volume.

The compartment burn time is calculated by dividing a characteristic compartment length by the flame speed. The flame speed, v, is determined from the following experimental correlation

$$v = 59.2\ X + 1.792 \text{ m/s} \qquad (9)$$

where X is the hydrogen mole fraction present in the compartment at the beginning of the burn (v is held constant during the burn). The above correlation was derived from turbulent flame experiments performed in the Sandia VGES 16' ft tank and is valid for hydrogen concentrations below about 10 percent. Other values of the flame speed can be specified, if desired.

The completeness of combustion can either be user specified or determined from the following equation

$$XF = \begin{cases} (1.0 - 12.5\ X)\ X & \text{for } X \leq 0.08 \\ 0.0 & \text{for } X > 0.08 \end{cases} \qquad (10)$$

where XF is the final mole fraction of hydrogen and X is the initial hydrogen mole fraction. The burn is also terminated if all the oxygen in a particular compartment is depleted.

A burn can propagate into adjacent compartments after a specified time delay if the propagation criteria are met in those compartments. These criteria are based upon the hydrogen concentration, and typical values are ≥ 4.1 volume percent hydrogen for upward propagation, ≥ 6 percent for horizontal propagation, and ≥ 9 percent for propagation downward. The oxygen and steam inerting limits hold for propagation as well as ignition.

There are significant uncertainties in the correlations used in the hydrogen burn model. However, HECTR is structured such that the important parameters are easily altered by the user, and it is planned that the correlations will be upgraded as experimental data become available.

Radiative Heat Transfer

The radiative spectrum is broken into seven active wavelength regions, and the emission from steam is considered in each of these regions. Regions in which the gas has no radiative bands, or in which wall emission is negligible are ignored. The bands are determined using an exponential wide-band molecular radiation model.[3] For each band, a gas emissivity is calculated which depends upon temperature, pressure, mole fraction of steam, and mean beam length. For the rest of this discussion, the subscript i will refer to the i^{th} spectral band.

The rate of radiative heat transfer per unit area from the j^{th} surface, q_j, will be the sum of the quantities, q_{ji}, calculated for each spectral band where

$$q_{ji} = \frac{\epsilon_j}{1 - \epsilon_j} (B_{ji} - J_{ji}) \qquad (11)$$

Here, ϵ_j is the emissivity of the j^{th} surface (assumed to be constant; hence, the surfaces are considered to be gray bodies), B_{ji} is the Planck blackbody flux emitted from the j^{th} surface per unit area, and J_{ji} is the radiosity of the j^{th} surface (the rate of radiant heat flux leaving the surface per unit area). The radiosities are determined by solving the following system of N simultaneous equations, where N is the total number of surfaces present

$$\frac{1}{1-\epsilon_j} J_{ji} - \sum_{k=1}^{N} F_{j-k}\, \tau_i(k-j) J_{ki} = \frac{\epsilon_j}{1-\epsilon_j} B_{ji} + \sum_{k=1}^{N} F_{j-k}\, \epsilon_i(k-j) B_{gi}(k-j) \qquad (12)$$

where

F_{j-k} = geometric view factor looking from surface j to surface k

$\epsilon_i(k-j)$ = gas emissivity as a function of the beam length from surface k to surface j

$\tau_i(k-j)$ = gas transmissivity = $1 - \epsilon_i(k-j)$

$B_{gi}(k-j)$ = gas Planck blackbody flux per unit area (W/m^2)

Note that this formulation includes back radiation which can be important if there are large surfaces composed of materials with high reflectivities (e.g., steel).

Convective Heat Transfer

Convective models are included in HECTR for both vertical slab and horizontal pool surfaces. The model for heat transfer on a vertical plane consists of a Nusselt laminar flow solution for wall liquid layers, and either a Couette-type forced turbulent flow model for the air:water-vapor boundary layer or a natural convection turbulent boundary layer correlation. The temperature of the liquid-gas interface, T_{gi}, is varied until the sum of the convective plus radiative heat transfer rates through the gas boundary layer is equal to the heat transfer rate through the liquid. The equilibrium situation is described by

$$\text{maximum } (q_{FC}, q_{NC}) + q_{RAD} = q_F \qquad (13)$$

where q is a heat flux and the subscripts C, NC, RAD, and F refer to forced convection, natural convection, radiation, and the liquid film, respectively. If there is no liquid layer, the interface temperature is set equal to the wall temperature, and terms related to the transport of mass and its associated enthalpy (the first terms on the right-hand side of Equations 15 and 16 below) are dropped in the gas boundary layer correlations.

The correlations used in HECTR are presented below in dimensional form using SI units (q is in W/m^2).[4,5,6]

Nusselt Liquid Layer:

$$q_F = .943\ (T_{gi} - T_w)\ \frac{g_f(\rho_f - \rho_g)h_{fg}K_f^3}{\mu_f L_f(T_{gi} - T_w)}^{1/4} \qquad (14)$$

Forced Convection Gas Boundary Layer:

$$q_{FC} = .037\rho_b U_b Re^{-1/5}\ Sc^{-2/5}\ (MF_{vb}-MF_{vi})[C_{pv}(T_b - T_{gi}) + h_{fg}] \qquad (15)$$

$$\frac{\ln(1+B)}{B} + .037\ K_g\ Re^{4/5}\ Pr^{3/5}\ \frac{T_b - T_{gi}}{L}$$

Natural Convection Gas Boundary Layer:

$$q_{NC} = .0188(\rho_b\Gamma)^{3/4}\left(\frac{\mu_g}{\delta}\right)^{1/4} Sc^{-2/3}(MF_{vb}-MF_{vi})[C_{pv}(T_b-T_{gi}) + h_{fg}]$$

$$\frac{\ln(1+B)}{B} + .0246\ K_g\ Gr^{2/5}\ Pr^{7/15}\ (1+.494\ Pr^{2/3})^{2/5} \qquad (16)$$

$$\frac{T_b - T_{gi}}{L}$$

Here,

T_{gi}, T_w, T_b = liquid-gas interface, wall surface, and bulk gas temperatures (Kelvin)

g = acceleration due to gravity (m/s^2)

ρ_f, ρ_g, ρ_b = liquid, saturated steam, and bulk gas densities (kg/m^3)

h_{fg} = heat of vaporization of the liquid (J/kg)

K_f, K_g = liquid and gas thermal conductivities (W/m-K)

μ_f, μ_g = liquid and gas viscosities (kg/m-s)

L_f = characteristic vertical length of the liquid film (m)

L = characteristic vertical length of the gas boundary layer (m).

U_b = bulk (free-steam) gas velocity (m/s)

Re = Reynolds number based on the length L.
$Re = \rho_b U_b L/\mu_g$

Sc = Schmidt number = $\mu_g/(\rho_b D)$

Pr = Prandtl number = $\mu_g C_p/K_g$

Gr = Grashoff number based on the length L
$Gr = g\beta(T_b - T_{gi})L^3\rho_b^2/\mu_g^2$

D = diffusion coefficient of water vapor through gas (m^2/s)

C_p, C_{pv} = gas and water vapor specific heats (J/kg-K)

β = coefficient of expansion (K^{-1})

MF_{vb}, MF_{vi} = mass fractions of vapor in the bulk gas and at the liquid-gas interface

B = mass transfer driving force = $(MF_{vb} - MF_{vi})/(MF_{vi} - 1)$

Γ = characteristic velocity in the natural convection boundary layer = $1.185\ (\nu_g/L)Gr^{1/2}\ (1 + .5Pr^{2/3})^{-1/2}$, (m/s)

ν_g = gas boundary layer kinematic viscosity (m^2/s)

δ = gas boundary layer thickness = $.565\ L\ Gr^{-1/10}Pr^{-8/15}\ (1 + .5Pr^{2/3})^{1/10}$, (m)

The liquid properties, ρ_f, K_f, and μ_f are computed at a temperature

$$T = T_w + .31(T_{gi} - T_w) \qquad (17)$$

The gas properties ρ_g, K_g, μ_g, D, C_{pv}, and β in Re, Sc, Pr, and Gr are evaluated at a temperature

$$T' = T_{gi} + \frac{1}{3}(T_b - T_{gi}) \tag{18}$$

It has been noted that neglecting the liquid layer and setting $T_{gi} = T_w$ in Equations (15) and (16) generally results in errors of a few percent or less (i.e., the heat transfer resistance in the liquid layer is much less than the resistance in the gas boundary layer). Therefore, some simplification of the current models is planned for the near future.

For liquid pool surfaces, the forced convection correlation of Equation (15) is used with minor modifications to allow for both evaporation from and condensation on the pool surface. A natural convection correlation for pool surfaces will be added in the future.

Wall Conduction

The surfaces in HECTR are treated either as slabs or as lumped masses. In either case, all of the surface properties are assumed to be constant. For those walls considered as slabs, it is assumed that they have insulated rear surfaces. A finite difference formulation is then used to calculate the forward wall surface temperatures given the heat flux to those surfaces. Two different mesh sizes are used inside the slabs. A fine mesh is used near the surface receiving the heat flux to resolve the steep temperature gradients that typically occur there. A coarser mesh is used for the remainder of the wall where the temperature varies more slowly.

The temperature, T, of a surface considered as a lumped mass is given as a function of time by

$$\frac{dT}{dt} = \frac{qA}{mC_p} \tag{19}$$

where

q = incident heat flux (watts/m^2)

m = mass (kg)

C_p = surface material specific heat (J/kg-K)

A = exposed surface area (m^2)

Containment Sprays

The drops from containment sprays are assumed to be isothermal, spherical, and traveling at the terminal velocity corresponding to their instantaneous size and mass. They are tracked through a compartment to the bottom where their final temperature and mass determine the heat and mass transfer rates. A user-specified fraction of the drops that have reached the bottom of a compartment is then allowed to fall into lower compartments. This process is repeated for all drop sizes present in the initial given droplet distribution.

The gas in a compartment is assumed to be homogeneous with none of its properties changing during the fall time of the drops. Therefore, the solutions represent a quasi-steady state model. The differential equations describing drop behavior are valid for both condensation on and evaporation from the drops and are presented below.[7,8]

$$\frac{dm}{dt} = -2\pi \rho_g D(1+.25\ Re^{1/2}\ Sc^{1/3})D_c\ \ln(1+B) \tag{20}$$

$$\frac{dT_d}{dt} = \frac{1}{mC_{PL}}\left[\frac{C_p(T_d - T_b)}{(1+B)^{1/Le}-1} + h_{fg}\right]\frac{dm}{dt} \tag{21}$$

$$\frac{dz}{dt} = \left[\frac{4}{3}\ \frac{(\rho_d - \rho_g)gD}{\rho_g\ C_D}\right]^{1/2} \tag{22}$$

Here,

m = droplet mass (kg)

T_d, T_b = droplet and bulk gas temperatures (K)

z = droplet fall height (m)

t = time (s)

ρ_g, ρ_d = gas and droplet densities (kg/m^3)

D = droplet diameter (m)

Re = Reynolds number

Sc = Schmidt number

Le = Lewis number

D_c = diffusion coefficient (m^2/s)

B = mass transfer driving force
(defined in the Convective Heat Transfer section)

C_{PL}, C_p = droplet and gas specific heats (J/kg-K)

h_{fg} = heat of vaporization of water (J/kg)

g = acceleration due to gravity (m/s^2)

C_d = drag coefficient

The above equations are solved using a standard Runge-Kutta differential equation solver for each drop size. Equations (20) to (22) are valid in all regions of interest.

HECTR also includes a simpler spray model, which is adapted from the more sophisticated model with two additional assumptions. These assumptions are that the drops come instantaneously to the equilibrium temperature and that no droplet properties change during the fall time of the drop. This allows the temperature equation to be discarded and the remaining two equations can be combined as shown in Equation (23)

$$\frac{dm}{dz} = \frac{dm}{dt}\frac{dt}{dz} \tag{23}$$

This simpler model matches the more detailed formulation for small drops, but is less accurate for large drops. This is true because it takes the large drops much longer to reach an equilibrium temperature, and they fall a greater distance during that time. Currently, the choice of spray models is a user input; however, in the future, this choice will come under program control when reasonable criteria are determined for deciding when to use the simpler model in place of the more sophisticated one.

Fan Model

The molar rate of change of the j^{th} gas in the i^{th} compartment due to intercompartment fans is

$$\frac{dN_{ij}}{dt} = \sum_k FN_{kj} \tag{24}$$

where

$$FN_{kj} = \begin{cases} -\frac{FR_{ik}}{V_i} N_{ij} & \text{for } FR_{ik} \geq 0 \\ -\frac{FR_{ik}}{V_k} N_{kj} & \text{for } FR_{ik} < 0 \end{cases} \tag{25}$$

where FR_{ik} is the fan volumetric flow rate from compartment i to compartment k, and the other terms have been defined in a previous section. This flow rate may be either a constant or determined from a pressure head versus flow curve. The energy transfer to compartment i due to the fan is

$$\frac{dE_i}{dt} = \sum_k FE_k \tag{26}$$

where

$$FE = \begin{cases} -\sum_{j=1}^{N_{gases}} \frac{FR_{ik}}{V_i} N_{ij} h_{ij} & \text{for } FR_{ik} \geq 0 \\ -\sum_{j=1}^{N_{gases}} \left(\frac{FR_{ik}}{V_k} N_{kj} h_{ki} \right) + W_{fan} & \text{for } FR_{ik} < 0 \end{cases} \tag{27}$$

where the term W_{fan}, in Equation (27) represents the work performed on the gas by the fan.

Ice Condenser Model

Ice condensers are treated in HECTR as a separate set of volumes. Each ice condenser volume contains an ice surface. The ice is assumed to be at a constant temperature, T_{ice}. The heat transferred to the ice surfaces is determined from the radiative and convective heat transfer models described earlier. The rate of ice melting is then calculated from

$$\frac{dM_{ice}}{dt} = \frac{q}{h_{if}} \tag{28}$$

where q is the sum of the radiative and convective heat transfer rates and h_{if} is the latent heat of fusion of the ice. The heat transfer length, L_{ice}, and area, A_{ice}, are then updated using

$$L_{ice} = L_o \frac{M_{ice}}{M_o} \tag{29}$$

$$A_{ice} = A_o \frac{M_{ice}}{M_o} \tag{30}$$

where L_o, M_o, and A_o are the initial heat transfer length, mass of the ice, and area of the ice, respectively.

The ice condenser model is still under development and will be upgraded to include heatup of the water after the ice is melted. Once all the physical mechanisms are included in the model, it will be assessed against experimental and analytical data that are available to us.

Additional Models and Future Plans

In addition to the models described previously, we will develop detailed models for fan coolers and suppression pools, so that we will be able to model all types of light water reactor containments in detail. Additionally, we will incorporate a one-dimensional flame propagation model to follow a planar flame front moving through a compartment. We plan to add carbon monoxide and carbon dioxide gases to HECTR. Finally, we will continue to upgrade the existing models to incorporate new experimental data and to improve the computational efficiency and flexibility of HECTR.

References

1. S. E. Dingman, M. J. Wester, and A. L. Camp, "Applications of HECTR to Reactor Containments," SAND82-1969C, Sandia National Laboratories, Published in these proceedings.

2. H. L. Jahn, "Hydrogen Distribution After a Loss-of-Coolant Accident in the Subdivided Containment of Light Water Reactors -- Translation," NUREG/CR-1831, SAND80-6031, Sandia National Laboratories (November 1980).

3. D. K. Edwards, "Molecular Gas Band Radiation," Advances in Heat Transfer, Ed. T. F. Irvine, Jr., and J. P. Hartnett, Vol. 12, pp. 115-194, 1976.

4. M. Berman, "Light Water Reactor Safety Research Program Quarterly Report, January-March 1981," Sandia National Laboratories, SAND81-1216, July 1981.

5. R. H. Whitley, "Condensation Heat Transfer in a Pressurized Water Reactor Dry Containment Following a Loss-of-Coolant Accident," University of California at Los Angeles, Master's Thesis (1976).

6. M. L. Corradini, "Turbulent Condensation on a Cold Wall in the Presence of a Noncondensible Gas," Univeristy of Wisconsin-Madison, to be published.

7. Internal Communication from M. R. Baer, April 24, 1980.

8. F. A. Williams, Combustion Theory, Addison-Wesley Publishing Company, Inc., (1965).

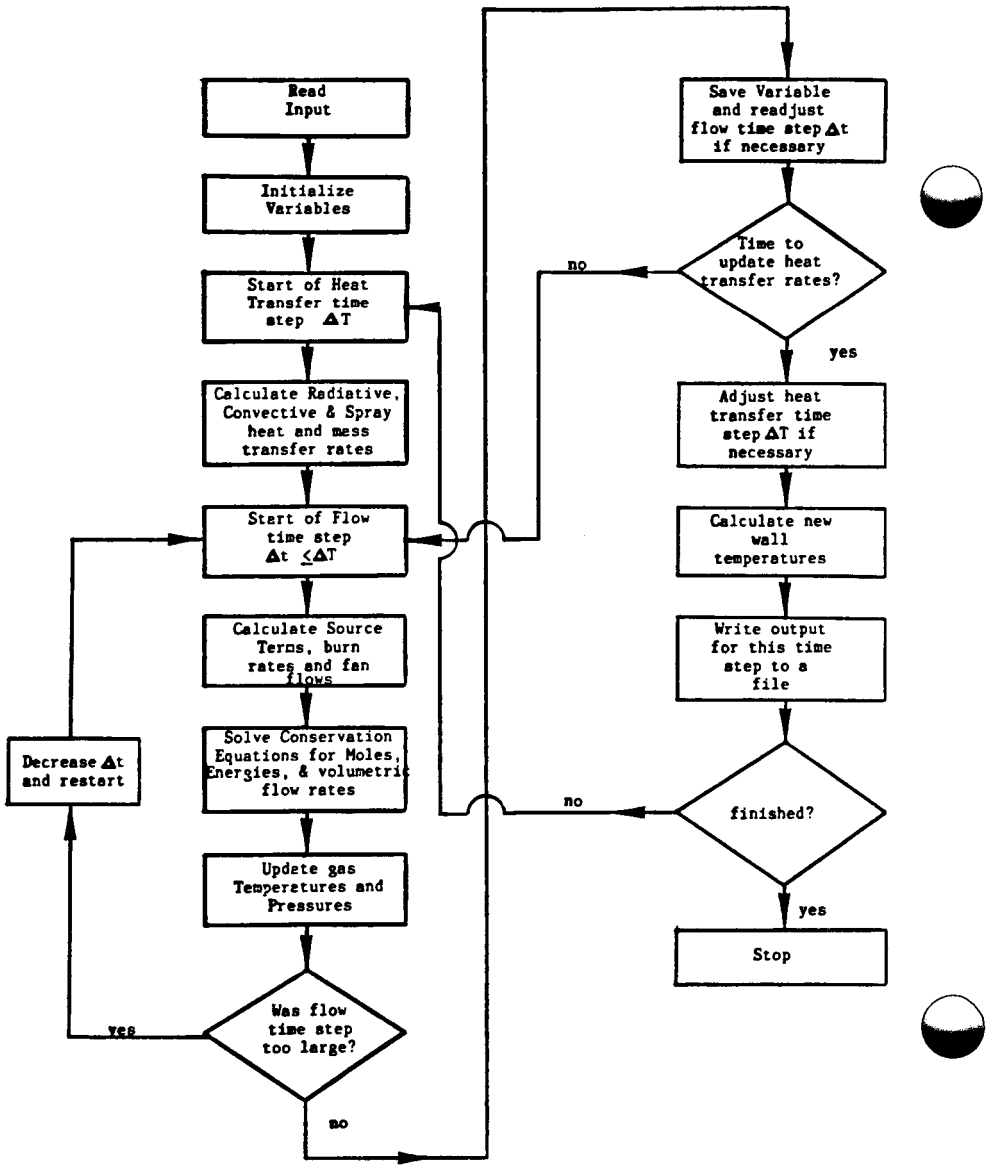


Figure 1, Flow Chart for HECTR

Hydrogen-Steam Flame-Jet Experiments

J. E. Shepherd and O. B. Crump, Jr.

Sandia National Laboratories

Albuquerque, NM

SAND 82-2266C

ABSTRACT

One possible accident scenario involving hydrogen combustion following a LOCA is a turbulent diffusion flame located at the point of release of hydrogen and steam into the containment. A number of unresolved problems associated with such flames are posed and an elementary scaling analysis is presented. A high-temperature, hydrogen-steam jet combustion facility has been constructed at Sandia to investigate these problems; the facility and some preliminary results are described. Finally, a series of calculations of laminar flame speed are presented to show the effect of initial temperature, steam and hydrogen concentration on flame speed.

Sponsored by the
Office of Nuclear Regulatory Research
U. S. Nuclear Regulatory Commission
Washington, D. C. 20555

under FIN No. A-1246 and A-1336

Introduction

A large portion of the recent research on hydrogen combustion in reactor containments has been oriented toward propagating combustion waves, i.e., deflagrations or detonations in a premixed hydrogen-air-steam atmosphere. An alternative combustion problem that may arise is a non-premixed or diffusion flame located at the point-of-release of hydrogen-steam mixtures into the containment (see Figure 1). The jet of steam and hydrogen from the primary system will entrain and mix with the containment atmosphere, and for some range of conditions, burn as a turbulent diffusion flame if ignited. The source of ignition could be accidental (arcing switch contacts) or deliberate (glow plug), and, if the steam-hydrogen mixture is hot enough, spontaneous ignition may occur (autoignition). Such burning hydrogen-steam jets may not only occur in accidental releases, but it has been proposed that deliberate release from a known location (i.e., a high-point vent), combined with deliberate ignition could be used to rid the primary system of accident-produced hydrogen. This has been termed 'deliberate flaring' in analogy to the flaring of unwanted combustible by-products by the chemical processing industry.

Turbulent diffusion flames have been extensively studied in laboratories over the last 30 years, but there are a number of aspects particular to the present problem which have not been investigated. We do not know the concentration limits (steam/hydrogen ratios), jet temperatures and velocities that

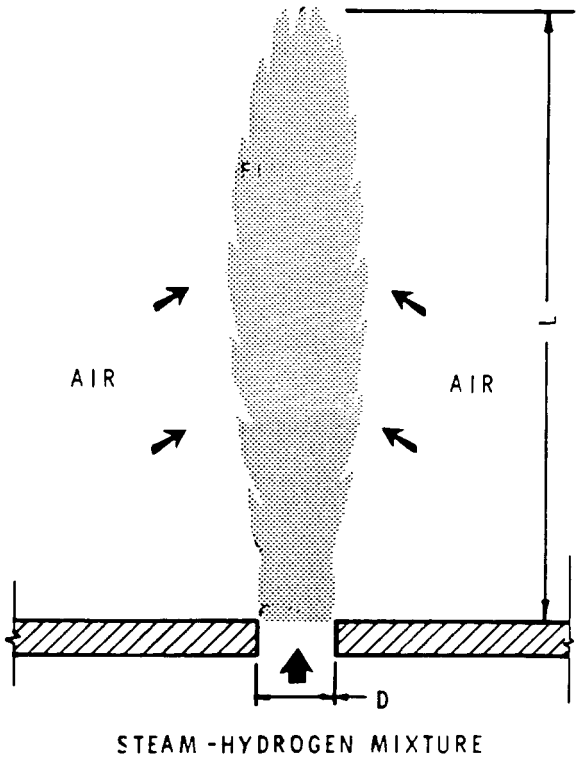


Figure 1 Entrainment into a jet or flame for a simple geometry.

define the region where stable combustion is possible. The temperature, velocity and concentration limits for spontaneous ignition are poorly defined. High-temperature chemical effects of the steam on the combustion kinetics may exist. In addition to these questions of a fundamental nature, very practical engineering problems need to be addressed. What will the convective and radiative heat loads be to components in or near the flame? How will the entrainment of the containment atmosphere and the combustion be affected by the confining and often complex geometry surrounding the flame? As the containment atmosphere is diluted during the burn, how will the flame be affected?

Scaling

To answer some of the basic questions posed above, we have initiated a program at Sandia to experimentally investigate steam-hydrogen diffusion flames at a laboratory scale. Results from these tests will be combined with simple scaling analyses and predicted accident release conditions to scope the problem at reactor scale. Proper scaling from such a small experiment may not be possible when geometric considerations and buoyancy dominate the entrainment into the flame (e.g., burning in the wet well of the Mark III BWR). For that reason, we will primarily consider only those flames where a substantial fraction of the entrainment is due to the forces exerted on the fluid by the jet itself, i.e., momentum-dominated jets. This will be the case when a high-velocity jet is vented through a relatively small opening into a large compartment free of obstructions (e.g., the containment dome).

The principal nondimensional parameter that determines what type of flow is produced by subsonic jets and flames is the ratio of buoyancy forces to inertia forces, the Richardson number or its inverse, the Froude number. If the exit velocity of the jet approaches the local sound speed, then the Mach number will also play an important role; in what follows, we will consider only subsonic flows. Other parameters which may be important are the density ratio (jet fluid/ambient fluid), which determines the effective exit diameter and the Reynolds number, which determines whether the flow is laminar or turbulent.

In the absence of complicating geometric factors and for high enough Reynolds numbers, the Richardson number based on flame length completely determines the character of the flow induced by the flame[1],

$$Ri_L = \frac{g\rho_\infty L^3}{\rho_o U_e^2 D^2} \tag{1}$$

where g is the acceleration due to gravity, ρ_∞ the density of the ambient fluid, U_e the jet exit velocity and D the effective jet diameter. A slightly more convenient parameter to work with is the nondimensional flame length ξ_L

$$\xi_L = Ri^{1/3}. \tag{2}$$

Recent studies[1,2] of turbulent flames conclude that for $\xi_L < 1$, the entrainment into the flame is by forced convection and the jet momentum dominates over buoyancy effects. Forced convection flames are characterized by a length that is independent of the flow

rate and proportional to the diameter of the jet exit (typical hydrogen-air flames are 100-150 diameters long). In contrast, for ξ_L >40 the entrainment into the flame is by natural convection and the buoyancy-induced forces dominate over the initial jet momentum. The flame length is independent of the jet diameter but increases with the flow rate, being proportioned to the total energy output (flow rate times heat of reaction) to the two-fifths power. The thermal radiation output is some fraction of the total energy output[3], typically 0.10 to 0.15 for hydrogen-air flames. Generally, given the jet exit conditions, diameter and flowrate, the flame length and ξ_L can be determined from known empirical correlations (for jets directed vertically upward). An example of such a parametric study for a pure hydrogen jet at 200°C burning in ambient air, is shown in Figure 2. The parameter ranges obtainable in the present facility at SNLA and also that possible in some postulated LOCA's are outlined. Note that both examples involve flow in the transition region $1 < \xi_L < 40$, where neither buoyancy forces nor jet momentum dominates. The jet- momentum-dominated flames have a calculated length of 120 diameters and the buoyancy-dominated flames have a calculated length of

$$L = 23.1 M_o^{2/5} \qquad (3)$$

where M_o is the mass flowrate in kg/s and L is the length in meters.

While there have been a number of experiments on laboratory-scale flames comparable in size to the present facility, there is

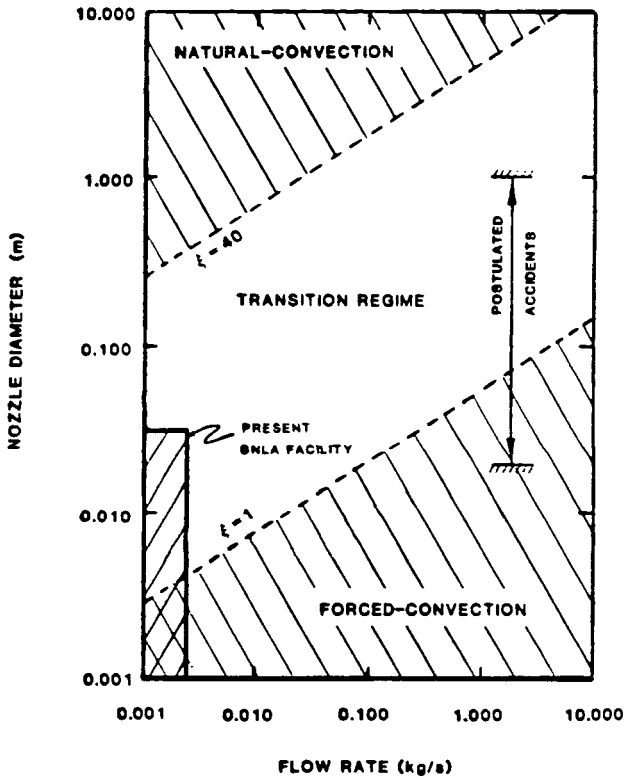


Figure 2 Parameter space for the combustion of a pure hydrogen jet at 200°C in air. The capabilities of the present facility and the relation to postulated accident conditions are shown.

limited data available at the larger scale comparable to the LOCA conditions shown in Figure 2. Most of what is known has been obtained from observations on hydrogen-disposal facilities[4,5] operated in conjunction with rocket motor testing. The ideas and correlations mentioned above appear to have validity at these scales; however, the models have not been extensively tested at these scales and some caution is advised, particularly when dealing with extremely large or small values of ξ_L.

Facility Description

The facility is located at an explosives test site with the jet itself situated within an existing explosives firing chamber (see Figure 3). The chamber is a box 13 ft. long, 11.5 ft. wide, and 7.5 ft. high; constructed of 2" thick steel plate; it is open on one side, which faces a wood and earth barricade. Experimental control and data acquisition equipment are located in an adjoining concrete blockhouse. Data recording and automatic, interactive experiment control is performed by a CAMAC system interfaced to a LSI-11 microprocessor. One important feature of this system is the automatic safety shutdown procedure (in case of an accidental release of hydrogen) programmed into the computer.

Steam is supplied by a small (50 lb/hr maximum flow rate) electrically-fired boiler and hydrogen is supplied by a bottle farm located outside the firing chamber. Both steam and hydrogen pass through separate electrically-powered superheaters capable

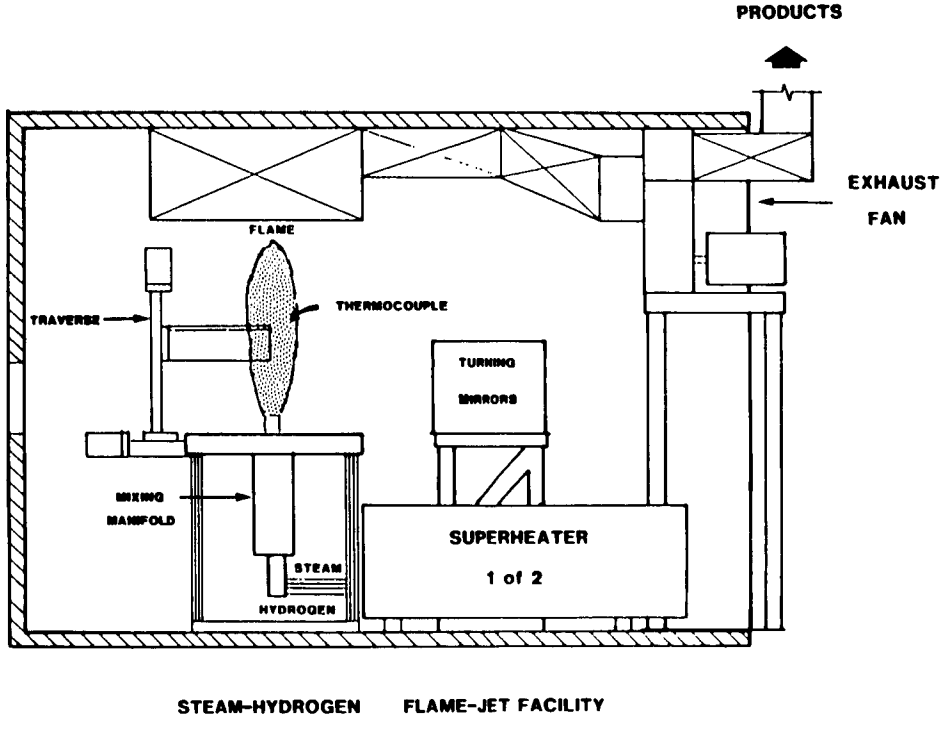


Figure 3 Schematic of flame-jet facility at SNLA.

of raising the gas temperature to 800°C. Steam and hydrogen flow coaxially into the plenum of the flame-jet manifold where the hydrogen is divided into a number of small jets which then mix with the steam. After passing through some flow-management screens and honeycomb, the steam:H_2 mixture exits through a flanged nozzle into the atmosphere. Nozzles are interchangeable so that the contraction shape and ratio can be varied. Initially, very smooth cubic-equation contour nozzles with contraction ratios of 4, 9, and 36 have been used. Later, more abrupt nozzles will be used to simulate actual pipeline breaks and outlets. The jet of hydrogen and steam either spontaneously ignites as it emerges into the atmosphere or, at lower temperatures, an electrical igniter, spark or glow plug is used to initiate combustion. At present, the jet is directed vertically upwards and the hot combustion products are diluted with air, drawn into a duct and exhausted outside of the firing chamber.

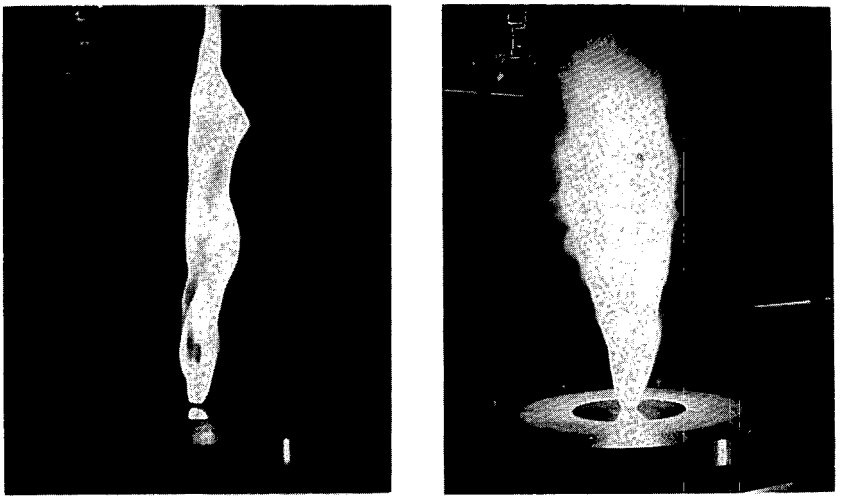
In addition to the standard pressure, temperature, and flowrate instrumentation on the hydrogen and steam supplies, there are specialized diagnostics for the flame-jet itself. Both thermocouple probes and a Pitot-static probe are used to investigate the velocity and temperature profiles. These probes are mounted on a remotely-controlled x-y traversing mechanism and must be water-cooled to withstand the high temperatures of a H_2:air flame (up to 1900°C). Several photographic systems are available to visualize the flame-jet. For Schlieren and shadowgraph photography, both the light source and camera are

located inside the control room and the light is relayed through ports between the blockhouse and firing chamber with turning mirrors. Since these optical systems are stationary, the jet is mounted on a hydraulically-operated lift table in order that the majority of the jet can be visualized. Direct photography of the flame has been accomplished with an ordinary 4" X 5" view camera and high-speed Polaroid film. The flame was made visible by spraying a hydrocarbon aerosol near the base of the flame.

We plan to measure both convective and radiative heat transfer using probes and radiometers. Convective transfer to a cylinder mounted perpendicular to the flow will be measured at different locations within the flow. The total heat transfer will be determined by measuring the temperature increase of water flowing at a known rate through the cylinder. Thermopile-type radiometers will be used to measure the total radiated energy and the radiant energy per unit length of the flame.

Preliminary Results

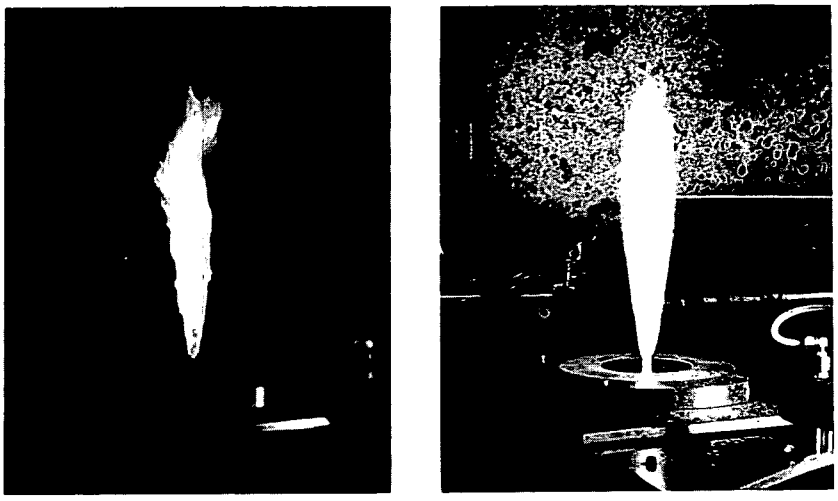
Examples of direct photographs of laminar and turbulent flames are shown in Figures 4 and 5. The exit temperature of the jet was 200°C in both cases and the nozzle diameter was 0.25". In Figure 4, the jet was pure hydrogen flowing at 1.53 SCFM with an exit Reynolds number (based on exit diameter) of 1040 and an exit velocity of 51 m/sec. In Figure 5, the jet was a hydrogen:steam mixture with 2.9 SCFM of H_2 and 3.7 SCFM of steam, an exit Reynolds number of 3020, and an exit velocity of 220 m/sec. Note



a) 1/500 s exposure

b) 1 s exposure

Figure 4 Direct photographs of a laminar flame showing instantaneous and average shape. 1.53 SCFM hydrogen flow at 200°C from a 0.25" diameter nozzle, Reynolds number of 1040 and exit velocity of 51 m/s.



a) 1/250 s exposure

b) 1 s exposure

Figure 5 Direct photographs of a turbulent flame showing instantaneous and average shape. 2.9 SCFM of hydrogen and 3.7 SCFM of steam at 200°C from a 0.25" diameter nozzle, exit Reynolds number of 3070 and exit velocity of 220 m/s.

the dramatic difference in the case of the laminar flame (Figure 4) between the high-speed exposure showing instantaneous flame shape and the long-time exposure showing average flame shape. Obviously, any attempt at theoretical description will have difficulty due to the unsteady fluctuating character of the flow. On the other hand, the fully turbulent flame (Figure 5) is much steadier in an average sense and the smaller-scale turbulent structure appears to dominate the flow.

Temperature measurements have been made using Platinum/Platinum-Rhodium thermocouples. The computer-controlled traversing and recording system was used to sample the temperature at about 200 points on a rectangular grid covering a plane section of flame. This array of measurements was then interpolated to produce a contour plot of the isotherms (Figure 6). The sampled region covers an area 14 inches long by 2 inches wide with the left-hand boundary located at the centerline of the flame-jet and the bottom boundary 1 inch from the jet exit. The outline of a time-exposure photograph taken by the method decribed above is superimposed on the isotherm plot in Figure 6. This particular flame was obtained with a steam flow rate of 1.3 SCFM and a hydrogen flowrate of 2.5 SCFM through a contoured nozzle with a 0.25-inch diameter exit. The gases and piping were at a temperature of 540°C, and the flame was ignited externally by a spark source. At this temperature, the flow was just below the autoignition temperature and would reignite spontaneously if the flow was restarted immediately after being shut off. However, if

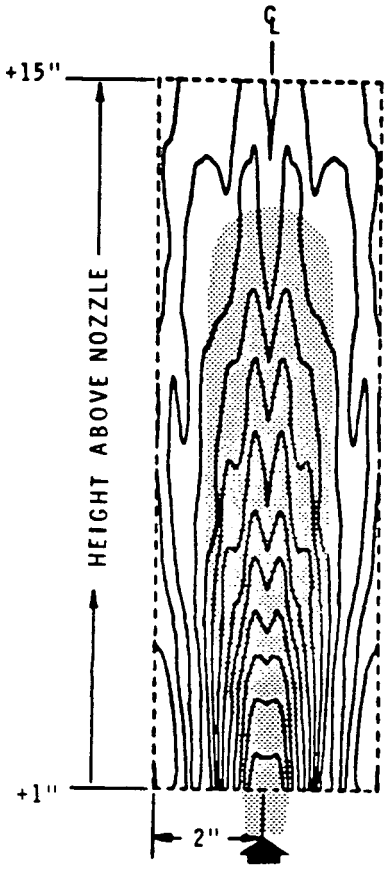


Figure 6 Comparison of instantaneous flame shape to average temperature profile as determined by probe measurements (steam:H_2 jet, exit velocity of 200 m/sec, and exit Reynolds number of 1000). Probe measurements were made from a height of + 1" to + 15" above the nozzle exit and from the centerline (C_L) to + 2" in radius (a mirror image of the temperature profile is shown from the C_L to - 2"). Isotherms are 100°C apart and start at 1400°C closest to the nozzle exit.

the flow was left off for a period of time (greater than one minute), spontaneous re-ignition would not occur.

The effect of increasing the fraction of steam present in the jet flow is to decrease the flame length. Since in the forced-convection regime, the entrainment rate is proportional to the jet exit momentum flux $D^2 {}_o u_e^2$, the amount of air entrained into the jet increases relative to a jet without steam and the same hydrogen flow rate. The greater air entrainment rate results in a stoichiometric fraction of air being mixed in with the jet fluid closer to the nozzle, resulting in a shorter flame.

An example of this effect is shown in Figure 7 for a jet at 200°C from the 0.25" diameter nozzle. The flame lengths were measured photographically and differences in seeding the flame for each picture result in some scatter within the data. However, the trend (indicated by the dashed line) is clear and flames with initial steam fractions as high as 0.9 have been observed. The calculated adiabatic flame temperature at an initial steam fraction of 0.9 and stoichiometric ratio of hydrogen to air is 1050K. This very low flame temperature indicates the marginal nature of these flames. These high-steam-fraction flames are unstable and the maximum fraction of steam which the jet can have and still obtain steady combustion is not known. We have observed steady flames at steam concentrations much higher than simple thermodynamic analyses and laminar flame-speed calculations would indicate possible, suggesting that the high molecular diffusivity of hydrogen plays a substantial role in the mixing processes in these flames.

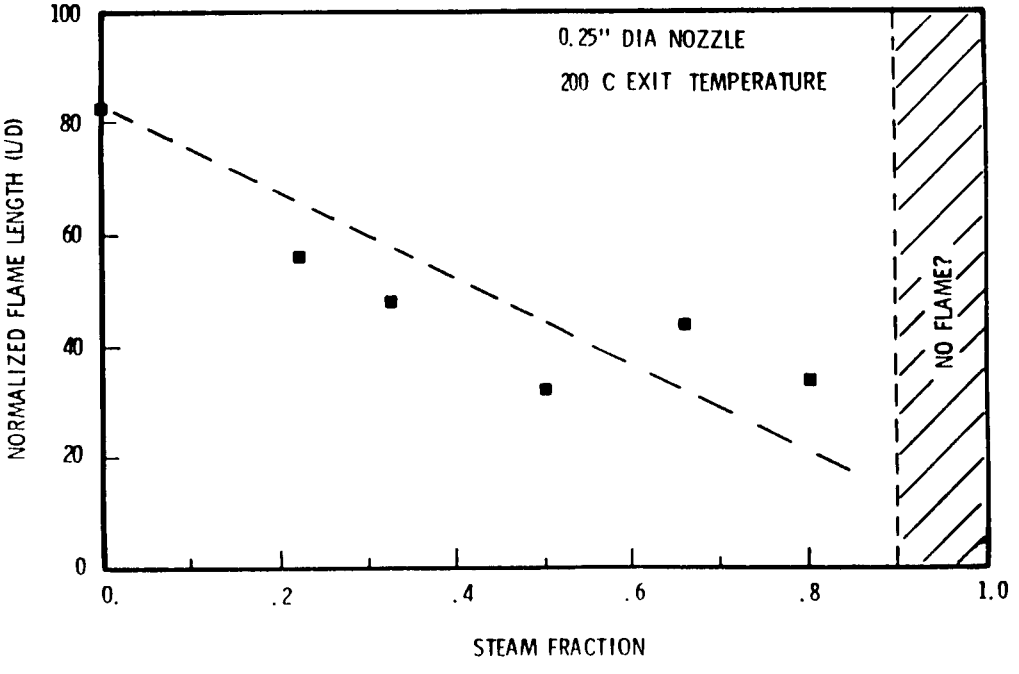


Figure 7 Dependence of visual flame length on steam concentration for 200°C hydrogen-steam jet from 0.25" diameter nozzle.

The converse effect to that discussed above will be observed when burning in diluted or vitiated atmospheres. Generally, the flame length corresponds to that point in the flow where the fuel and oxidizer are in stoichiometric proportions. As a consequence, for the same entrainment rate (jet momentum flux) a jet in a diluted atmosphere will reach a stoichiometric mixture further downstream than in an undiluted atmosphere. For that reason, flames burning in the highly steam-diluted atmospheres expected during a LOCA will be much longer than the flames with the same exit conditions in ambient air.

Flame Stability and Flame Speed Calculations

During experiments with the 0.25-inch diameter nozzle, flame blow out was observed at high flow rates (> 10 SCFM). On the other hand, at higher flow rates with the 0.50-inch diameter nozzle, the flame remained stable. A brief literature search[6,7] has turned up several papers which suggest that absolute stability (the flame will not blow out irrespective of the flow rate) exists for nozzles with exits larger than a critical diameter. Critical diameters have been predicted for hydrogen:air:steam mixtures by Kalghati[6], but this correlation requires knowledge of the laminar burning velocity of hydrogen:air:steam mixtures at elevated initial temperatures. Burning speeds have been measured over a limited range of initial temperatures (20-250^{o}C) and steam concentrations (0-15%) by Liu and McFarlane, but in view of the limited nature of this data base, we feel that it would be desirable to have independent

calculations or measurements for the range of initial temperatures and steam fractions encountered in the present study. Computation of laminar flame speeds is becoming a standard technique and is fairly accurate for hydrogen:air mixtures[9].

The Sandia Livermore laminar flame code developed by Smooke[10] has been used to calculate laminar burning velocities of hydrogen:air:steam mixtures over a wide range of initial compositions and temperatures. These calculations indicate that added steam has primarily a thermodynamic effect (acts as a heat sink) and has a substantial influence on the kinetics only at large steam concentrations. Representative results from our calculations are shown in Figures 8-10. Burning velocity vs. initial hydrogen concentration (for a dry hydrogen:air mixture at an initial temperature of 400 K) is shown in Figure 8; as expected, the maximum burning velocity is at about 42% hydrogen. The effect of initial temperature on the burning velocity of a dry, 30% hydrogen in air mixture is shown in Figure 9. The effect of steam is illustrated in Figure 10 for 30% hydrogen in air mixtures initially at 400 K. On these figures, the extrapolated correlation of Liu and McFarlane is also shown. The extrapolated correlation and our calculations show similar trends except for the dependence on hydrogen concentration (Figure 8). The burning velocities derived from extrapolated correlation are consistently higher than our calculated values. Previous comparisons of calculated and measured burning velocities have also shown this trend and Dixon-Lewis[11] has suggested that there are systematic errors in the measurement technique.

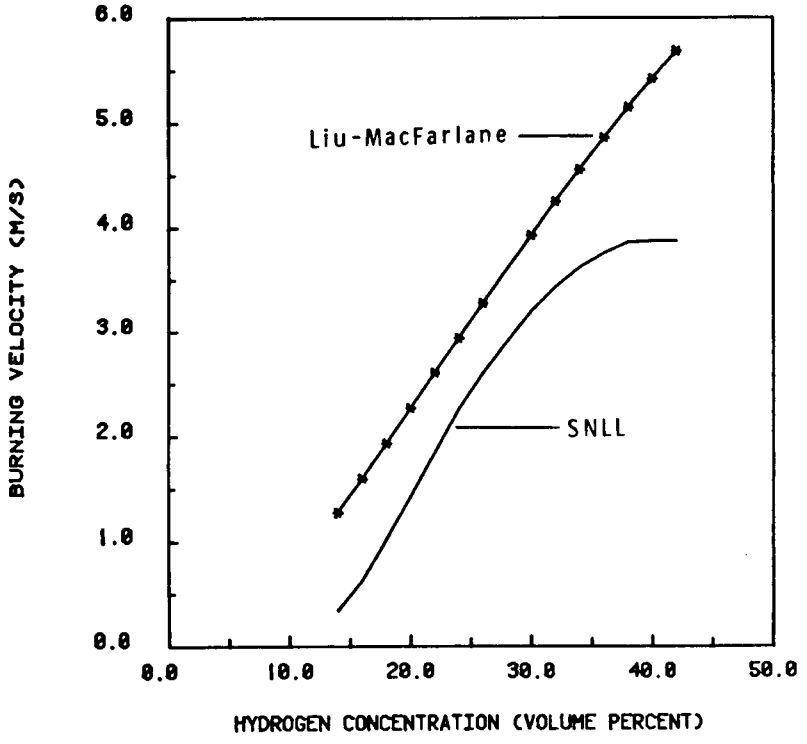


Figure 8 Concentration dependence of laminar burning velocity of hydrogen-air mixtures at 400K. Comparison between calculations by SNLL code and the correlation of experimental results by Liu and McFarlane.

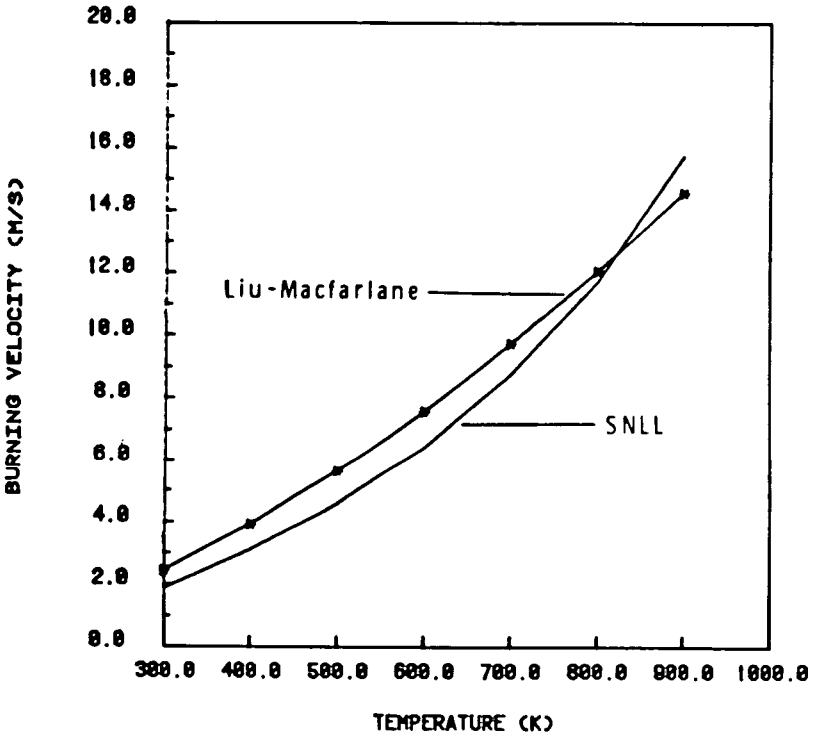


Figure 9 Temperature dependence of the laminar burning velocity of a 30% hydrogen-air mixture. Comparison between calculations by SNLL code and the extrapolated results by Liu and McFarlane.

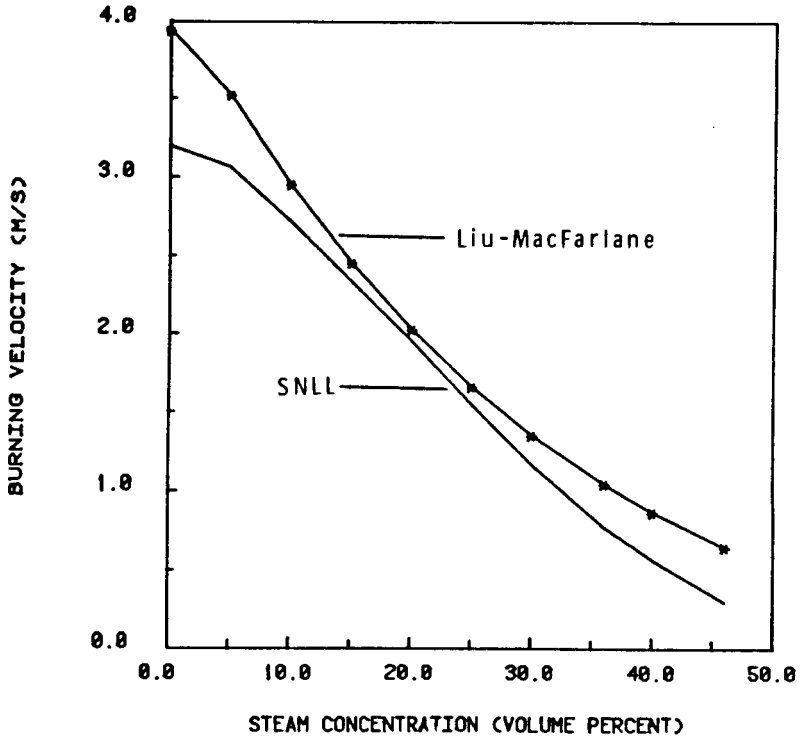


Figure 10 Steam concentration dependence of the laminar burning velocity of a 30% hydrogen-air mixture (constant equivalence ratio). Comparison between calculations by SNLL code and the extrapolated correlation of Liu and McFarlane.

The most comprehensive set of calculations done so far are for 30% (Figure 11) and 42% (Figure 12) hydrogen in air with steam fractions varying from 0-50% and initial temperatures from 400 to 900 K. Calculations were done at 42% hydrogen since that is where the maximum in burning velocity occurs for dry mixtures at room termperature. The hydrogen-air ratio was held fixed as the steam fraction was varied, i.e., the equivalence ratio was held constant (this also applies to Figure 10).

Using the burning velocities shown in Figure 12 as the maximum values in Kalghati's critical blowoff diameter correlation, we have computed critical diameters for pure hydrogen jets as a function of initial temperature. At 300 K, the critical diameter is 0.59 mm and continuously decreases to 0.06 mm at 900 K. Since the flame is absolutely stable for burners with diameters larger than the critical diameter, these very small critical diameters suggest that hydrogen flames are very stable indeed. Of course, as the flame speed decreases with the addition of steam, the critical diameter will increase.

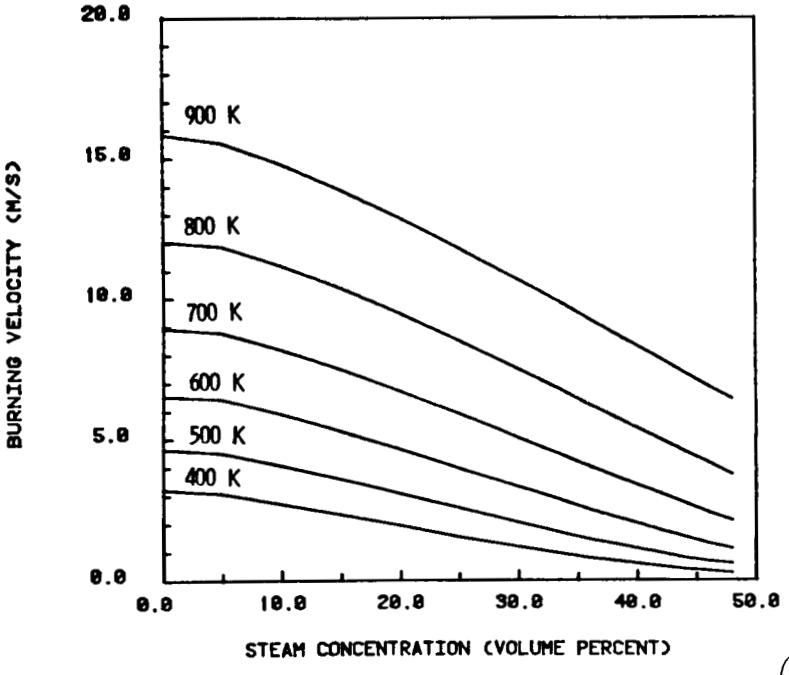


Figure 11 Calculated laminar burning velocities for 30% hydrogen-air mixtures diluted with steam 0-50% (constant hydrogen-air ratio) and at initial temperatures from 400-900 K.

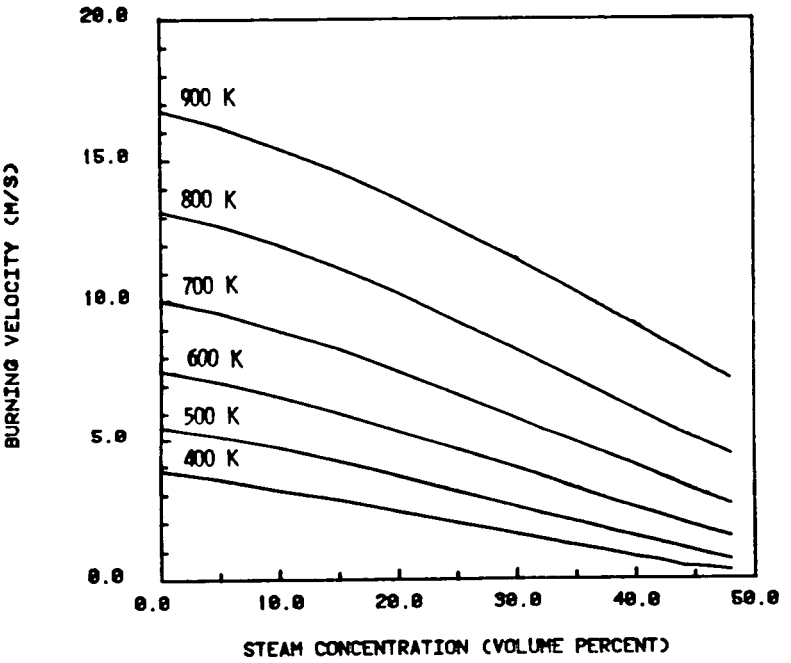


Figure 12 Calculated laminar burning velocities for 42% hydrogen-air mixtures diluted with steam 0-50% (constant hydrogen-air ratio) and at initial temperatures from 400-900 K.

Conclusions

Turbulent diffusion flames may occur inside reactor containments under some hydrogen-producing accident conditions. These flames will originate from steam-hydrogen jets issuing from point-of-release in the primary containment. A scaling analysis of the flames arising from such jets indicates that the flow will be either forced convection, or in the transition regime between forced convection and free convection. To investigate some of the questions about the properties of these flames, a facility has been constructed at Sandia National Laboratories (Albuquerque). In this laboratory-scale facility, flames originated from steam-hydrogen jets at high temperatures and velocities are being investigated. Preliminary results indicate that it is possible to maintain steady flames with initial steam concentrations as high as 90%. Computations of laminar burning velocities for a range of initial temperatures and compositions are reported for steam-hydrogen-air mixtures. Estimates of critical burner diameters indicate that high-temperature hydrogen-steam diffusion flames may be very difficult to blow off.

References

1. Becker, H. A. and Yamazaki, S., "Entrainment, Momentum Flux and Temperature in Vertical Free Turbulent Diffusion Flames", Comb. and Flame 33, 123 (1978).

2. Becker, H. A. and Liang, D., "Visible Length of Vertical Free Turbulent Diffusion Flames", Comb. and Flame 32, 115 (1978).

3. Markstein, G. H. "Scaling of Radiative Characteristics of Turbulent Diffusion Flames", Sixteenth Symposium (International) on Combustion, Combustion Institute, 1407 (1977).

4. Fishburne, E. S. and Pernament, H. S., "The Dynamics and Intensity of Large Hydrogen Fires", Seventeenth Symposium (International) on Combustion, Combustion Institute, 1063 (1979).

5. Thompson, W. R. and Boncore, C. S., "Design and Development of a Test Facility for the Disposal of Hydrogen at High Flow Rates" in Advances in Cryogenic Engineering 12, 207 (1965).

6. Kalghati, G. T., "Blowout Stability of Gaseous Jet Diffusion Flames. Part I: In Still Air", Combustion Science and Technology 26, 233 (1981).

7. Annushkin, Yu. A., and Sverdlov, E. D., "Stability of Submerged Diffusion Flames in Subsonic and Underexpanded Supersonic Gas-Fuel Streams", Combustion, Explosion and Shock Waves 14, 597 (1978).

8. Liu, D.D.S. and McFarlane, R., "Laminar Burning Velocities of Hydrogen-Air Flames. Part II: The Effect of Steam", AECL-7360 (1980).

9. Warnatz, J., "Concentration, Pressure, and Temperature Dependence of the Flame Velocity in Hydrogen-Oxygen-Nitrogen Mixtures", Combustion Science and Technology 26, 203 (1981).

10. Smooke, M. D., "Solution of Burner-Stabilized Pre-Mixed Laminar Flames by Boundary-Value Methods", SAND-8040 (1982).

11. Dixon-Lewis, G., "Kinetic Mechanism, Structure and Properties of Premixed Flames in Hydrogen-Oxygen-Nitrogen Mixtures", Phil. Trans. Roy. Soc. A292, 6 (1979).





SESSSION VI

ACCELERATED FLAMES AND DETONATIONS

871/872







TURBULENT BURNING OF HYDROGEN: UPPER-BOUND CHEMICAL KINETIC MODELS ACCOUNTING FOR THE INFLUENCE OF TEMPERATURE FLUCTUATIONS

by

K. N. Tennankore and H. Tamm

Atomic Energy of Canada Limited
Whiteshell Nuclear Research Establishment
Pinawa, Manitoba ROE 1LO Canada

Issued as AECL-7668

INTRODUCTION AND SCOPE

Simulation of laminar and turbulent combustion is of practical interest in predicting the performance of controlled combustion systems and in estimating the consequences of accidental combustion. Since turbulent combustion is relatively fast, and hence potentially more difficult to control, it is particularly important for safety analysis of systems where potential for burning exists.

Simulation methods for combustion under flowing conditions often use a single reaction model to describe the burning process, which actually comprises many intermediate reactions. Thus, for turbulent combustion, the time-average burning rate, $\dot{r}_b$, is described by a single Arrhenius reaction rate involving the initial reactants,

$$\dot{r}_b = A \exp\left[-E_a/R\bar{T}\right] \; [F] \; [O] \qquad (1)$$

where E_a is an activation energy, $\bar{T}$ is the mean temperature, [F] and [O] are concentrations of the fuel and the oxidizer, R is the universal gas constant, and A is a constant. Since the intermediate reactions are usually described by similar equations, their instantaneous rates have a non-linear dependence on the instantaneous temperature. Also, the mean temperature and the temperature fluctuations vary over a wide range in practical systems, so that Eq. (1) cannot properly describe the overall result of the time-average intermediate reaction rates. Here we present a method to determine upper-bound rates for the overall reaction from the rates for all the intermediate reactions under these conditions. This provides us with an indication of maximum rates of combustion when kinetics control the burning. Further, we illustrate the method by applying it to laminar and turbulent burning of hydrogen in air and in air-water vapour atmospheres.

The upper-bound burning rates can be used directly in prediction procedures based on the conservation equations for mass, momentum, and energy. Mass conservation equations are then solved only for the fuel, oxidizer, and product. The upper-bound rates describe the source or sink terms in these equations. The results based on such a model would enable a conservative analysis of both controlled and accidental combustion.

METHOD FOR DETERMINING UPPER-BOUND RATES

The objective is to determine an upper-bound for the rate of production of a chemical species, say P, from the initial reactants, say A and B, for a specified reaction mechanism described by a number of intermediate series and parallel reactions. The method consists of determining upper-bound rates for the intermediate reactions and then comparing them systematically to obtain an upper-bound rate for the formation of P.

Intermediate Reaction Rates:

The rates of the intermediate reactions are bounded by using maximum values for the concentrations of the reactants. For instance, consider the m^{th} bimolecular reaction in the mechanism given by



$$B + C \rightarrow D$$

rate of formation of D is determined as

$$\dot{r}_D = k_m [B] [C] \qquad (2)$$

where $[B]$ and $[C]$ are the maximum concentrations of B and C, and k_m is the Arrhenius rate constant given by

$$k_m = k_{mo} \exp [- E_m/RT]$$

where k_{mo} is a constant.

Quiescent and Laminar Systems:

The application of Eq. 2 to calculate upper-bounds for the rate of formation of D in quiescent and laminar systems requires specification of the maximum concentrations $[B]$ and $[C]$. Although the correct values of these maximum concentrations can be determined only by solving the set of ordinary differential equations describing the kinetics for a specified pressure and temperature, bounds can be established quite readily as described below.

The maximum values possible for the concentrations of B and C can be determined from the initial composition by directing the reactants to produce the maximum amount possible of B and C in turn. These values upperbound the true maximum concentrations of B and C.

Equilibrium concentrations of B and C can be determined for a specified initial mixture, pressure, and temperature either from kinetic constants or from thermodynamic considerations. These provide lower bounds for the true maximum concentrations of B and C.

Using the maximum values possible for the concentrations of B and C in Eq. 2 will clearly yield the maximum possible rates of formation of D. Such upper-bound rates can be determined for all the intermediate reactions. However, since true maximum concentrations of B and C are not necessarily concurrent, using equilibrium concentrations does not necessarily yield lower bounds for the true maximum rates of formation of D. It merely yields lower bounds for $\dot{r}_D$ as given by Eq. 2.

Turbulent Systems:

In turbulent systems, the variables $[B]$, $[C]$, and T and, therefore, the reaction rate given by Eq. 2 fluctuate. In such cases, every variable is usually decomposed into a mean and a fluctuating component, and the equation is averaged with respect to time to obtain the mean reaction rate.

$$\overline{\dot{r}_D} = \overline{k_m}\overline{[B]}\ \overline{[C]} + \overline{k_m[B]'}\ \overline{[C]} + \overline{k_m[C]'}\overline{[B]} + \overline{k_m[B]'[C]'}$$

where $k_m = k_{mo} \exp\left[-E_m/R(\bar{T} + T')\right]$

and the overbar and prime denote mean and fluctuating components respectively. In this paper we consider the fluctuation intensities of concentration and temperature to be of the same order. The first term on the right side of Eq. 3 is then large compared to the other terms because of the nonlinear dependence of k_m on temperature. Equation 3 can thus be simplified to:

$$\overline{\dot{r}_D} = \overline{k_m}\overline{[B]}\overline{[C]} \qquad (4)$$

The maximum concentrations are estimated in the same way as for quiescent and laminar systems.

Models for $\bar{k}_m$:

For $E_m/R\bar{T} < 1$ and $T'/\bar{T} << 1$, the exponential term in k_m can be rewritten as the product of two terms, and the term containing T' can be expanded as a series, truncated after the second term and averaged with respect to time [1]. This results in:

$$\bar{k}_m = \left[1 + \frac{E_m}{R\bar{T}}\overline{\left(\frac{T'}{\bar{T}}\right)^2}\right] \exp\left[-E/R\bar{T}\right] \qquad (5)$$

For

$$\left(\frac{E_m}{R\bar{T}}\right)\left(\frac{T'}{\bar{T}}\right) \geq 1$$

the higher order terms in the series cannot be neglected. Since higher order correlations cannot be calculated easily, $\bar{k}_m$ is generally considered indeterminate for these cases [1]. However, $\bar{k}_m$ can be upper-bounded for a given distribution of fluctuation intensity by considering the fluctuation to be a generalized Fourier series [2]. For $T'/\bar{T} << 1$,

$$\bar{k}_m < \exp\left[-\frac{E_m}{R\bar{T}}\left(1 + 2\int i_n\, d\omega\right)\right] \qquad (6)$$

where i_n is the spectral intensity, ω is the frequency, and the integration is performed over the frequency range of interest.

For $T'/\bar{T} = 0$ [1], the expression given below can be obtained by following the procedure of reference 2:

$$\bar{k}_m < \exp\left[\frac{-E_m}{R\bar{T}(1+2\int i_n\, d\omega)}\right] \qquad (7)$$

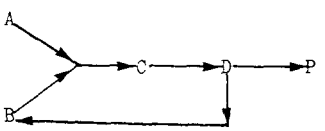
Determination of Overall Rate:

The overall rate of formation of product P is determined by systematically comparing the rates for the formation of various species in the chain leading to P. The procedure involves the following steps:

1) Represent the reaction mechanism as a number of `cycles´ involving intermediate species with the reactions resulting in the product outside the cycle. For instance, consider the reaction set given below:

$$A + B \rightarrow C \quad (a)$$
$$C \rightarrow D \quad (b)$$
$$D \rightarrow P \quad (c)$$
$$D \rightarrow B \quad (d)$$

B produces D through reactions (a) and (b). D produces B through reaction (d). This constitutes a `cycle´ or a closed loop. Product P is produced by reaction (c) which is outside the `cycle´. Thus, BCDB is a `cycle´ in the following figure:

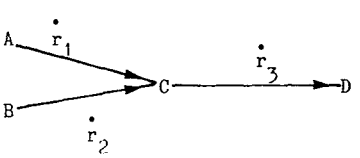


2) Determine the cycle rates by comparing the rates for the intermediate reactions in the cycle. The criteria used in determining the cycle rates are as follows:

a) When two or more reaction paths produce the same species, its rate of formation is the sum of these rates. Consider, for instance, species A and B both producing intermediate species C at rates $\dot{r}_1$ and $\dot{r}_2$. Then:

$$\dot{r}_C = \dot{r}_1 + \dot{r}_2 \qquad (8)$$

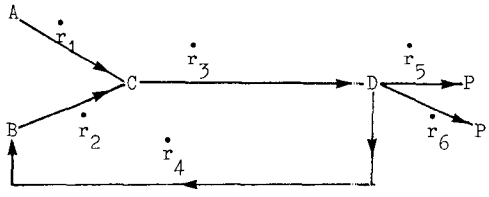
b) When series reactions are involved, the limiting reaction rate determines the rate of formation of the component. Consider species A and B producing species D according to the reaction path shown below:



$$\dot{r}_D = \text{Min}\,[\dot{r}_1 + \dot{r}_2,\ \dot{r}_3] \qquad (9)$$

When intermediate reactions involve more than one intermediate species, the species produced at the fastest rate is considered part of the chain.

3) Include reactions involving initial reactants which form intermediate species but do not form part of the cycle. Determine the overall rate by comparing the cycle rate with the production rate for the species of interest. Consider the reaction scheme shown below:



The rate for the cycle BCDB is

$$\dot{r}_{cy} = \text{Min}\,[\dot{r}_1 + \dot{r}_2, \dot{r}_3, \dot{r}_4] \qquad (10)$$

The overall rate of production of P is

$$\dot{r}_P = \text{Min}\,[\dot{r}_{cy}, \dot{r}_5 + \dot{r}_6] \qquad (11)$$

If there is more than one independent cycle, sum over all cycles.

APPLICATION TO THE BURNING OF HYDROGEN

In this section, we consider the application of the upper-bound method to laminar and turbulent burning of hydrogen in air or air-water vapour atmospheres. The burning of hydrogen according to the overall oxidation reaction,

$$H_2 + 1/2\ O_2 \rightarrow H_2O$$

proceeds via many intermediate reactions. The literature suggests that over 80 such reactions involving intermediate species, namely free radicals, are possible. Since our main interest is in demonstrating the method for determining upper-bound rates, we have chosen the simplified mechanism of 21 reactions suggested by Warnatz [3]. These, together with the reactions that produce the free radicals, H, OH, O, HO_2, and molecular H_2O_2, directly from the initial reactants, are considered in this study to represent the global reaction above. The complete set of reactions is given in Table 1.

The upper-bounds for the rate of formation of H_2O for two different initial mixtures have been obtained based on the reactions in Table 1 and the method outlined in the previous section. One of the mixtures consisted of 20%

H_2 and 80% air by volume. The other was composed of 20% H_2, 60% air, and 20% water vapour by volume. The upper-bound rates for the formation of H_2O were determined for temperatures in the range 500-3000 K, temperature fluctuation intensities of 0 and 30 percent and a pressure of 101 kPa. The reaction cycles determined from the mechanism are shown in Figure 1. The rate constants averaged with respect to time for a fluctuation intensity of 30% were evaluated according to Eq. (7). The calculated overall reaction rates for the formation of H_2O are shown in Figures 2-4.

Figure 2 shows the variation of the upper-bound reaction rates assuming the maximum possible concentrations for the intermediate species and the product, H_2O. The rates decrease with temperature at constant pressure in spite of the exponential increase of most of the intermediate reaction rates. This is due to the decrease in concentration with temperature according to the equation of state. Fluctuations in temperature increase the average reaction rates according to Eq. (7). Consequently, the upper-bound rates increase. A fluctuation intensity of 30% increases the reaction rate up to 70%.

Contrary to expectations, the rates increase when water vapour is present. This is because the maximum concentrations of intermediate species are determined as the maximum possible values based on the initial mixture. The water molecule contains more atoms than H_2, N_2, or O_2, and hence increases the concentrations of H and O radicals.

Figure 3 shows the upper-bound rates determined using equilibrium concentrations for the intermediate species. These concentrations were determined for the two mixtures over the range of temperature at 101 kPa using a NASA code [4].

The reaction rates based on equilibrium concentrations increase rapidly with temperature since equilibrium mole fractions of free radicals increase rapidly with temperature, offsetting the decrease in initial total concentration due to increasing temperature. This, combined with the increase in intermediate reaction rates, increases the upper-bound rates of formation of H_2O.

Temperature fluctuations markedly increase the rates of H_2O formation for hydrogen-air mixtures. The increase is much less for hydrogen-air-steam mixtures. This is due to the following. For hydrogen burning in air-water vapour atmospheres, the limiting reaction is the rate of formation of H_2O (reactions 1, 7, and 10, Table 1). Since these have zero or low activation energies, the influence of temperature fluctuations is small. For hydrogen burning in air, the limiting rate is the cycle rate, which is limited by reactions with large activation energies (reactions 5, 8, 17, and 18). Temperature fluctuations strongly influence these rates and hence the overall rates.

The upper-bound rates for the two different estimates of the concentration of the intermediate species are compared for one set of conditions in Figure 4. The values are widely different at low temperature and converge as temperature increases. The upper-bound rates based on true maximum concentrations should lie between these limits.

Utility of Maximum Burning Rates

In addition to their direct use in prediction procedures for analyzing combustion systems, the maximum burning rates can help assess the relative importance of the various processes that occur during combustion in flow systems. We illustrate this for a stabilized turbulent flame.

Consider the schematic in Figure 5 of a plane, premixed, stabilized, one-dimensional turbulent flame of mean thickness δ. As the combustible mixture flows towards the flame, it is preheated from the initial temperature, T_u, to the ignition temperature, T_i, just before entering the flame zone. The mixture is considered to leave the flame zone completely burnt. The intermediate species and the product diffuse and establish concentration profiles. At steady state, if $\dot{R}$ is the average reaction rate in the flame, mass balance yields [5]

$$\rho_u S_T = \dot{R}\delta \qquad (12)$$

where ρ_u is the unburnt gas density and S_T is the flow velocity of the mixture which is also the turbulent burning velocity.

The unburnt gas temperature increases due to:

1) turbulent diffusive heat transfer from the flame;
2) radiative heat transfer from the flame;
3) heat due to chemical reaction.

Chemical reaction rates in the unburnt gas depend on the concentrations of the various chemical species which in turn depend on turbulent diffusion from the flame zone. Reaction rate R in the flame depends on:

1) the concentrations of the chemical species;
2) the mean temperature;
3) the temperature fluctuation intensity.

It is the balance between these various processes that determines δ for a given density and flow rate of the unburnt gas mixture.

Here we assume the unburnt gas temperature to be primarily increased by turbulent diffusive heat transfer from the flame. Rate of heat transfer from the flame, therefore, can be estimated as:

$$\dot{q} = \rho_f C_{p_f} (\overline{u'T'})_f$$

where u' is the fluctuation in the gas velocity at the flame, and C_p is the heat capacity. Suffix f denotes flame properties. The heat required to raise the unburnt gas temperature from T_u to T_i is given by $\rho_u \bar{C}_p (T_i - T_u)$, where $\bar{C}_p$ is the mean heat capacity in the temperature range T_i to T_u. The turbulent burning velocity can now be expressed as:

$$S_T = \frac{\rho_f C_{p_f} \overline{(u'T')}_f}{\rho_u \bar{C}_p (T_i - T_u)}$$

For example, if we set $(T_i - T_u) = 500$ K, $u' = 10$ m/s, $T' = 200$ K, P = 1 atm., $T_u = 300$ K, and $T_f = 1500$ K, then:

$$S_T \lesssim C_{p_f} / \bar{C}_p \quad \text{m/s}$$

and

$$\rho_u S_T \lesssim 40\ C_{p_f} / \bar{C}_p \quad \text{mol/(m}^2\text{·s)}$$

If $\dot{R}$ is estimated as 10^5 mol/(m^3·s), then from Eq. 12:

$$\delta \lesssim 0.4\ C_{p_f} / \bar{C}_p \quad \text{mm}$$

Experimental values of δ can be used to assess the initial assumption that turbulent diffusive heat transfer is the important mechanism responsible for increasing the temperature of the unburnt gas.

SUMMARY

A method has been presented for estimating overall upper-bound formation rates of a chemical species produced from initial reactants through a number of intermediate reactions. The method determines the overall rates from the rates of intermediate steps. Bounds for the concentrations of intermediate species are used to estimate the rates of the intermediate reactions. The method can be applied to laminar as well as to turbulent systems. Approximation or upperbound models are recommended for estimating the influence of temperature fluctuations on the intermediate reaction rates.

Burning rates of hydrogen for a range of conditions have been estimated using this method. These rates can be directly used in prediction procedures for a conservative analysis of controlled as well as accidental combustion. They can also be used to assess the relative importance of physical processes such as heat transfer and chemical kinetics during combustion in flowing systems.

FUTURE WORK

Realistic estimates for the rates of the various processes described as occurring during turbulent combustion would enable a realistic assessment of their importance. For the purposes of safety analysis, these estimates should be conservative. In this paper we have addressed the problem of estimating chemical reaction rates under turbulent conditions. Future work would consider methods for improving reaction rate estimates and for estimating the rates of remaining processes such as heat transfer and species diffusion.

REFERENCES

1) P.A. Libby and F.A. Williams, "Turbulent Flows Involving Chemical Reactions", Annual Review of Fluid Mechanics, 8, pp. 351-376, 1976.

2) K.N. Tennankore, "Influence of Temperature Fluctuations on the Arrhenius Model for Reactions", Combustion Science and Technology 28, pp. 81-83, 1982.

3) J. Warnatz, "Concentration-, Pressure-, and Temperature-Dependence of the Flame Velocity in Hydrogen-Oxygen-Nitrogen Mixtures", Combustion Science and Technology, 26, pp. 203-210, 1982.

4) "Computer Program for Calculation of Complex Chemical Equilibrium Compositions, Rocket Performance, Incident and Reflected Shock Waves and Chapman-Jouget Detonations", National Aeronautics and Space Administration, Washington, D.C., Report No. N71-37775, 1971.

5) V.S. Arpaci and R.J. Tabaczynski, "Radiation-Affected Laminar Flame Propagation", Combustion and Flame, 46, pp. 315-322, 1982.

6) E. Oran, T. Young, and J. Boris, "Application of Time-Dependent Numerical Methods to the Description of Reactive Shocks", Seventeenth Symposium (International) on Combustion, Combustion Institute, pp. 43-54, 1978.

TABLE 1: Reactions in the H_2-O_2-N_2 System[a]

$k_m = k_{mo} T^B \exp(-E_m/RT)$

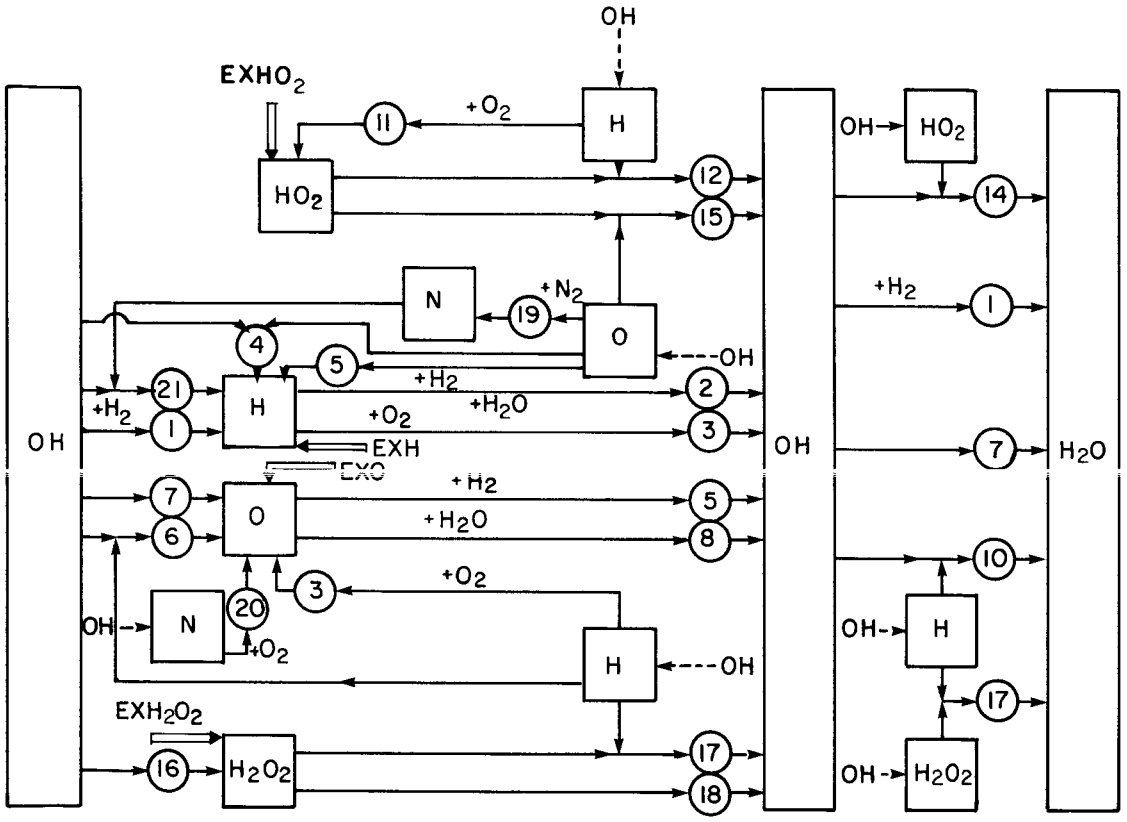
No.	Reaction	k_{mo} (m^3,mol,s)	B	E_m (kJ/mol)
1	$OH+H_2 \rightarrow H_2O+H$	$1.2\ 10^3$	1.3	15.2
2	$H+H_2O \rightarrow OH+H_2$	$4.5\ 10^3$	1.3	78.7
3	$H+O_2 \rightarrow OH+O$	$2.2\ 10^8$	0.0	70.4
4	$OH+O \rightarrow H+O_2$	$1.0\ 10^7$	0.0	0
5	$O+H_2 \rightarrow OH+H$	$1.8\ 10^4$	1.0	37.3
6	$OH+H \rightarrow O+H_2$	$8.3\ 10^3$	1.0	29.1
7	$OH+OH \rightarrow H_2O+O$	$1.5\ 10^3$	1.14	0
8	$H_2O+O \rightarrow OH+OH$	$1.6\ 10^4$	1.14	72.4
9[b]	$H+H+M' \rightarrow H_2+M'$	$9.0\ 10^4$	-0.6	0
10	$H+OH+M' \rightarrow H_2O+M'$	$2.2\ 10^{10}$	-2.0	0
11	$H+O_2+M' \rightarrow HO_2+M'$	$2.3\ 10^6$	0.8	0
12	$H+HO_2 \rightarrow OH+OH$	$1.5\ 10^8$	0.0	4.2
13[b]	$H+HO_2 \rightarrow H_2+O_2$	$2.5\ 10^7$	0.0	2.9
14	$OH+HO_2 \rightarrow H_2O+O_2$	$1.5\ 10^7$	0.0	0
15	$O+HO_2 \rightarrow OH+O_2$	$2.0\ 10^7$	0.0	0
16	$OH+OH+M \rightarrow H_2O_2+M$	$9.1\ 10^2$	0.0	-21.4
17	$H+H_2O_2 \rightarrow H_2O+OH$	$3.2\ 10^8$	0.0	37.5
18	$H_2O_2+M \rightarrow OH+OH+M$	$3.0\ 10^{11}$	0.0	190.0
19	$O+N_2 \rightarrow NO+N$	$1.8\ 10^8$	0.0	319.0
20	$N+O_2 \rightarrow NO+O$	$6.4\ 10^3$	1.0	26.2
21	$N+OH \rightarrow NO+H$	$3.0\ 10^7$	0.0	0
22	$O_2+M \rightarrow O+O+M$	$6.1\ 10^9$	-1.0	248.5
23	$H_2O+M \rightarrow H+OH+M$	$3.5\ 10^9$	0.0	221.3
24	$H_2+M \rightarrow H+H+M$	$2.2\ 10^8$	0.0	202.1
25	$H_2O+O_2 \rightarrow O+H_2O_2$	$3.4\ 10^4$	0.52	187.4
26	$H_2O+O_2 \rightarrow OH+HO_2$	$1.4\ 10^8$	0.17	154.4
27	$H_2+O_2 \rightarrow OH+OH$	$1.7\ 10^7$	0.0	101.3
28	$H_2+O_2 \rightarrow H+HO_2$	$5.5\ 10^7$	0.0	121.8

$[M'] = 6.0\,[H_2O] + [H_2] + 0.4\,[N_2] + 0.4\,[O_2]$

$[M\ ]$ = Total Molar Concentration

a Based on references [3] and [6]

b These reactions form the initial reactants and hence were omitted.



Reaction Number

EXS — Reactions producing species S directly from the initial reactants

OH - - → S — Chain from OH to species S including EXS

Figure 1: Reactions in the H_2-O_2-N_2 System: A Representation as Parallel Cycles.

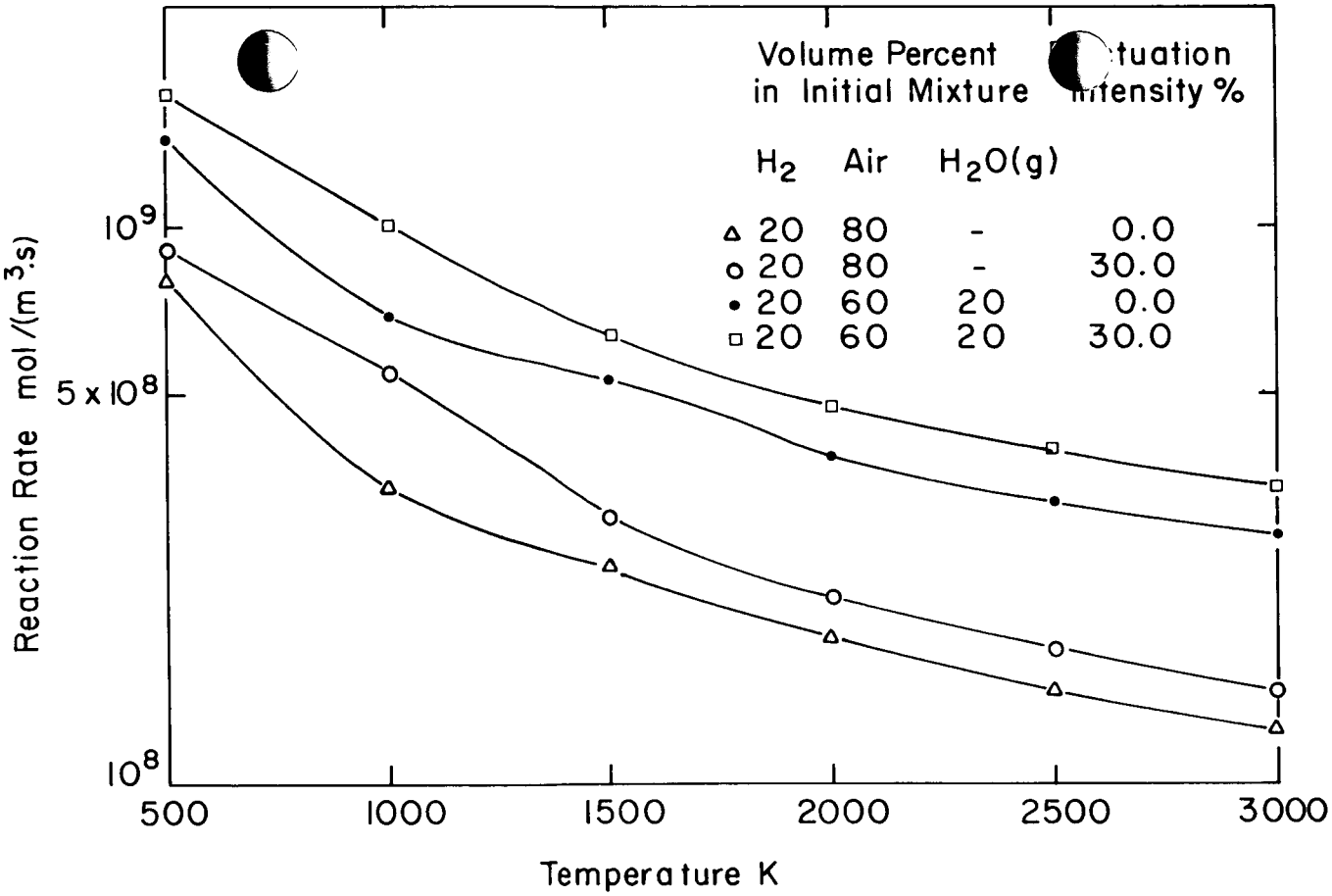


Figure 2: Upper-bound H_2O Formation Rates Based On Absolute Maximum Concentrations For Two Different Initial Mixtures: Variation With Mean Temperature and Temperature Fluctuations.

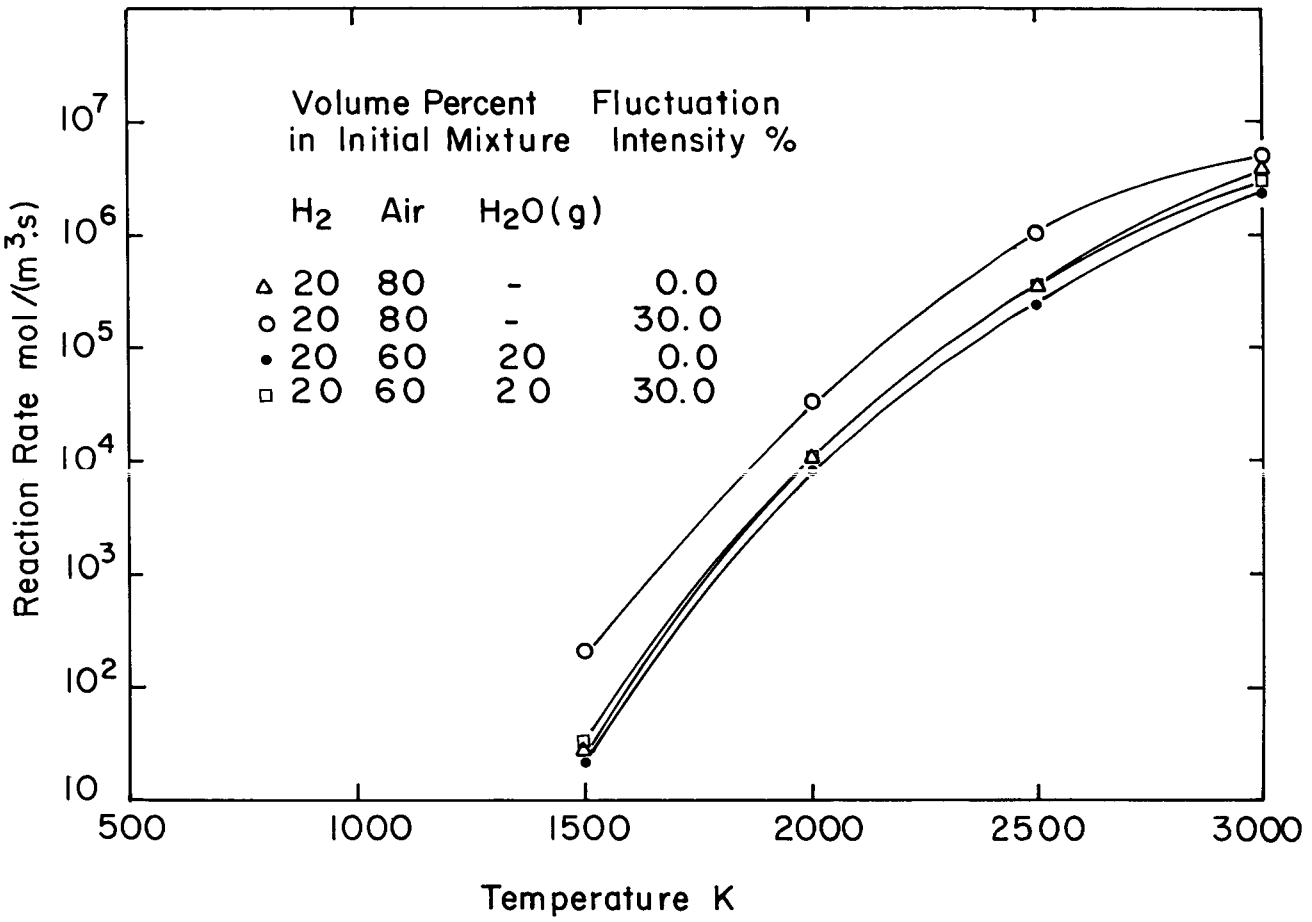


Figure 3: Upper-bound H_2O Formation Rates Based On Equilibrium Concentrations For Two Different Initial Mixtures: Variation with Mean Temp-

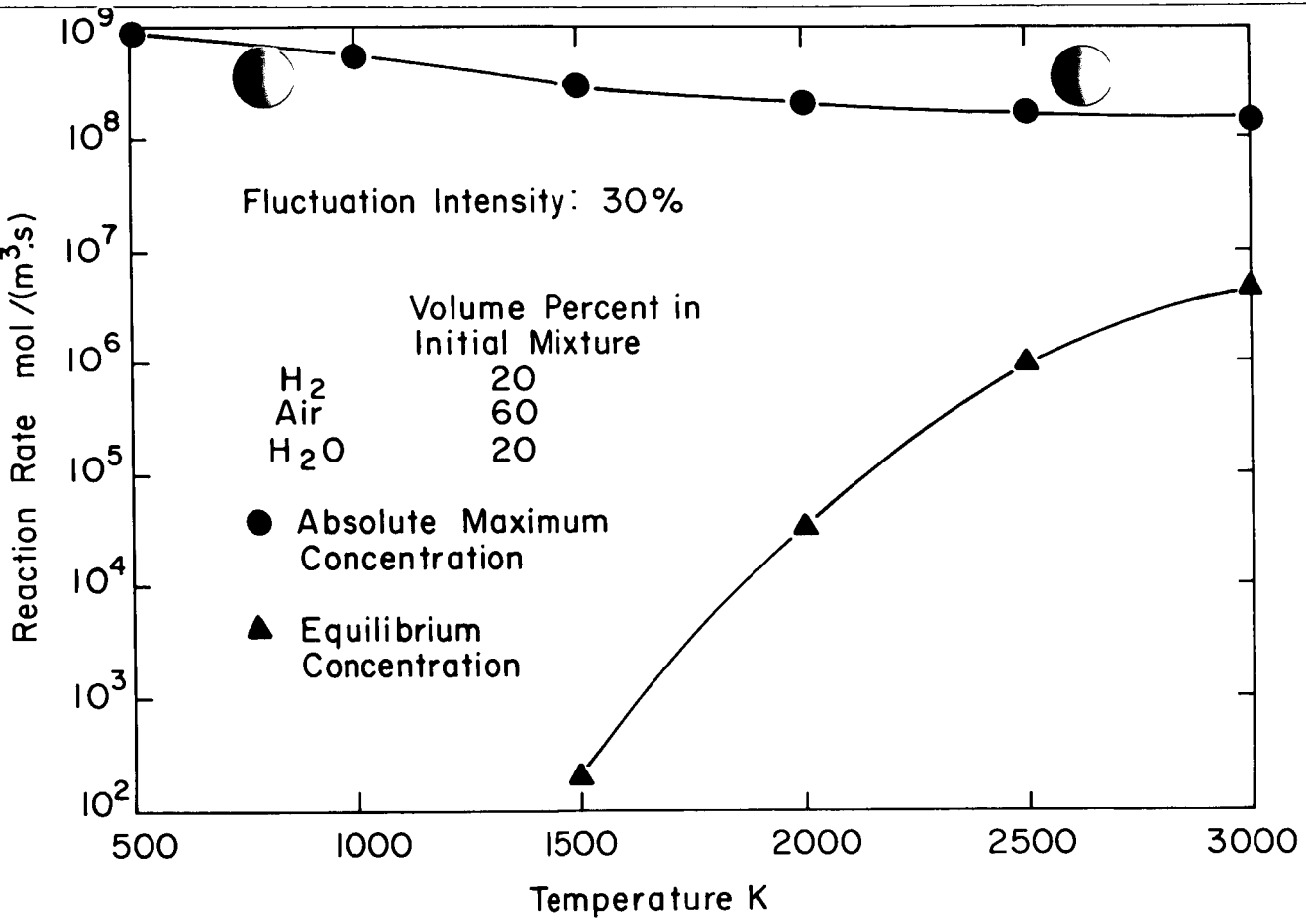


Figure 4: A Comparison of the Upper-Bound Rates Based on Absolute Maximum Concentrations and Equilibrium Concentrations for the Intermediate Species.

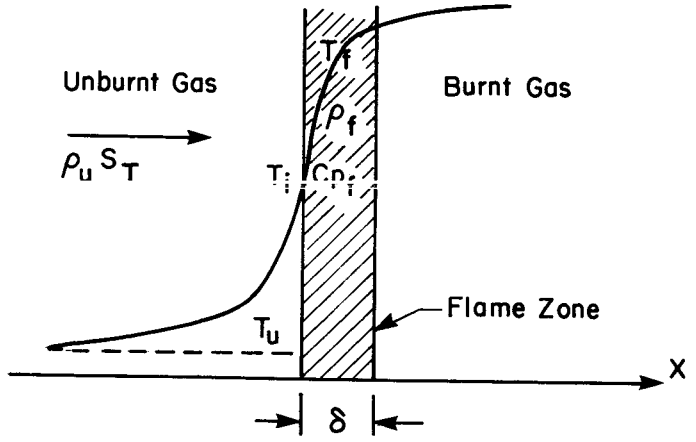


Figure 5: A Schematic Representation of a Plane, Premixed, Stabilized, Turbulent Flame.

Hydrogen-Air Deflagrations: Recent Results

by

John H.S. Lee, Calvin Chan and Romas Knystautas
Shock Wave Physics Research Laboratory
Mechanical Engineering Department
McGill University
Montreal, Canada

Abstract

This paper will summarize the results obtained to date in the joint research program between the Shock Wave Physics Research Laboratory and Sandia National Laboratory (Albuquerque). In the investigation of H_2-air deflagrations, the following problems are being carried out: i) the rate of turbulent flame accelerations by repeated obstacles (orifice plates and wire screens), ii) optimum turbulent flame speeds and transition to detonations, iii) the influence of confinement (or side venting) on the rate of flame acceleration by repeated obstacles, iv) the influence of H_2 concentrations and diluents (CO_2, H_2O) on flame acceleration, v) quenching diameter for the turbulent jet ignition of H_2-air by H_2-air combustion products, vi) influence of strong jet ignition on rate of pressure rise, and vii) the Taylor-Markstein instability mechanism of flame acceleration. Important results and conclusions from each of the above mentioned problems will be described. The experiments are also carried out with other common hydrocarbon fuels (e.g., methane) to provide a basis for comparison to assess the relative hazards of H_2.

1. Introduction

The deflagration mode of combustion is by far more probable than the detonation mode in accidental situations. In any probability risk assessment, it is important to have a realistic estimate of the burning rate. Although a laminar burning velocity can readily be measured or calculated theoretically with a fair degree of accuracy for any given explosive mixture, this parameter does not represent the burning rate under actual conditions. This is due to the fact that the freely propagating flame in an explosion is very sensitive to the gasdynamic flow structure that it generates. Thus, ignition criterion, flammability limits, turbulent burning velocity, etc., are all strongly coupled to the gasdynamic flow parameters (i.e., velocity gradient field, turbulence intensities and scales, etc.) in the unburnt mixture, much more so than the chemical and physical properties. This intercoupling between gasdynamics and combustion for transient deflagrations is far from understood. The objectives of the joint study between the Shock Wave Physics Group at McGill University and Sandia National Laboratories (Albuquerque) are to elucidate these coupling mechanisms and deduce empirical relationships and scaling laws for H_2-air deflagrations. The present paper gives a brief summary of the more important results obtained to date.

2. Flame Accelerations

It is by now well known that obstacles in the path of a propagating flame create turbulence resulting in flame acceleration and high turbulent flame speeds. H_2-air mixtures are particularly sensitive and transition to detonation can easily occur under appropriate confinement and boundary conditions. The objectives of the study are to investigate flame acceleration rates, transition to detonation, maximum turbulent flame speeds and detonation

states under different obstacle environments. The first series of experiments are performed in long circular tubes of various diameters. Spiral coils or repeated circular orifice plates of different blockage ratios $BR = 1 - (d/D)^2$ are inserted into the tube as turbulence generators. The flame speeds (relative to laboratory coordinates) and pressure-time histories are measured for a wide range of H_2 concentrations in air ($10\% \leq H_2 \leq 55\%$).

Typical results for the flame speed versus distance from the ignition source are shown in Fig. 1. A 3 m length of spiral coil (6 mm diameter wire, 5 cm pitch, BR = 0.44) is used for generating turbulence. For all H_2 concentrations, rapid flame acceleration to steady state conditions within the 3 m length of the obstacle region are observed. Depending on the mixture composition, the acceleration to steady state occurs from less than 0.5 m (10 tube diameter) to about 2 m (40 diameters) of flame travel. The final steady turbulent flame speeds range from about a hundred meters per second (10% H_2) to quasi-detonation velocities of the order of 1700 m/sec ($25\% \leq H_2 \leq 45\%$). Upon exiting the obstacle region, the turbulent deflagration either decelerates continuously over the remaining 5 m of the tube for $H_2 \lesssim 17\%$, or after an initial deceleration phase for about a meter of flame travel, the flame re-accelerates back to a normal C-J detonation for $H_2 \gtrsim 17\%$. The critical H_2 concentration where transition to detonation occurs is around 17%, which corresponds closely to the detonability limit for the 5 cm diameter tube used. The detonation cell size for 17% H_2 is 150 mm which agrees very well with the cell size for the single-head spin detonation in a circular tube. As proposed earlier, the criterion for detonability limits in a confined tube is defined by the onset of single-head spinning detonation. Thus, this observation lends further support to the limit criterion proposed for confined detonations in tubes.

For higher H_2 concentrations where quasi-detonations are observed in the obstacle section ($H_2 \gtrsim 30\%$), rapid acceleration to normal C-J conditions occurs immediately upon exiting the obstacle region. This is due to the absence of pressure losses created by the obstacles in the smooth section of the tube. It should be noted that quasi detonations refer to detonation-like phenomenon strongly influenced by boundary conditions. The exact mechanisms of propagation are not known as yet. Turbulence and shock reflections from the obstacles are expected to play important roles.

Pressure-time histories at different locations in the obstacle section show strong pressure spikes manifesting the complex interaction processes between the deflagration and the obstacles. However, a maximum averaged (over the oscillations) value of the pressure can be obtained to represent the state at each location. Figure 2 shows some typical results for the variation of the peak averaged pressure versus distance in the obstacle section. As in the case of the flame speed, the pressure builds up to steady-state values within 0.5 m to 2 m depending on the H_2 concentration. The pressure beyond the 3 m obstacle region either decays slowly or rises rapidly to normal C-J values, depending on whether the deflagration continuously decays ($H_2 \lesssim 17\%$), reaccelerates and undergoes transition to detonation ($H_2 \geq 17\%$) or rapidly transforms from a quasi-detonation to a normal C-J detonation ($H_2 \leq 48\%$).

Figure 3 shows the steady state flame speed in the obstacle section for various H_2 concentrations. Results for three different obstacle configurations are plotted: i) spiral BR = 0.44, ii) orifice plates BR = 0.44, iii) orifice plates with BR = 0.60, and the pitch or plate separation is 5 cm for all three configurations. It is of interest to note that a sharp jump in the steady-state turbulent flame speed occurs around 13% H_2. For $H_2 \lesssim 13\%$, the flame speeds are less than 200 m/sec and not particularly sensitive to

obstacle configuration. For $H_2 \gtrsim 13\%$, the flame speeds jump up sharply to values of the order of the sound speed of the mixture, i.e., ~400 m/sec. For $13\% \lesssim H_2 \lesssim 25\%$, a small dependence on the blockage ratio of the obstacles (i.e., pressure losses) is observed, but the flame speed increases relatively slowly with increasing H_2 concentration. Depending on the blockage ratio of the obstacles, another sharp jump to quasi-detonation velocities (1300 m/sec $\lesssim \dot{R}_f \lesssim$ 1700 m/sec) occurs at H_2 concentrations between 25% and 30%. Turbulent flames and quasi-detonation velocities depend on pressure losses (i.e., blockage ratio). However, it should be pointed out that although the spiral coil and orifice plates may have the same blockage ratio based on the ratio of the open core to the tube area, the spiral in effect causes a smaller pressure loss to the flow. For the case of the high blockage ratio BR = 0.60, the quasi-detonation falls back to the strong turbulent deflagration regime at high H_2 concentrations (i.e., $H_2 \gtrsim 33\%$). For the other two cases shown, it is expected that the quasi-detonation regime should also eventually terminate at the rich end when the mixture becomes less sensitive. For lean mixtures ($H_2 \lesssim 13\%$), the steady state turbulent deflagration velocity appears to be due to the balance between the positive effect of turbulence in augmenting combustion via more rapid mixing and diffusion and the negative effect of quenching. This condition can be characterized by reaction times of the order of the eddy life time. At about 13% H_2, flame temperatures increase to values the order of 1300°K. From kinetic considerations, the competing reaction between the $H + O_2 + M \rightarrow H O_2 + M$ and $H + O_2 \rightarrow OH + O$ appears to change over at around 1300°K in favor of the more rapid OH branching reaction. Thus, a sudden increase in reaction rate at around 13% H_2 may account for the sharp rise in the turbulent deflagration velocity since with the reduction in reaction times quenching now requires a much more rapid mixing rate (i.e., higher turbulence level and a corresponding higher mean flow velocity). In the region where the flame speeds are of the order of the sonic velocity, (i.e.,

13% $\lesssim H_2 \lesssim$ 25% for the particular obstacle configurations investigated), it appears that frictional choking sets the limiting condition. In other words, the pressure losses due to the obstacles impose an upper bound to the maximum unburnt gas flow velocity that is generated by the flame. Hence, different obstacle configurations and blockage ratios that control the pressure loss will give the different results as observed. We may conclude that while the randomization of the mean flow to create turbulence has a positive effect in augmenting the combustion rate, the pressure losses by the very same randominzation process place an upper bound on the mean flow velocity. For sufficiently intense combustion, auto-ignition due to either local shock heating and, or violent turbulent mixing occurs. This gives rise to the second sharp jump in which transition to the quasi-detonation regime occurs. For all the three cases shown, the turbulent flame speed in which transition occurs is around 800 m/sec. For an obstacle configuration where the pressure losses are less severe, this flame speed can be attained at lower H_2 concentrations (e.g., $H_2 \simeq 26\%$ for sprial). For the high pressure loss configurations, transition is delayed since this critical value of the flame speed is not achieved until later ($H_2 \simeq 30\%$ for orifice plates with BR = 0.6). Detonations in the obstacle region are characterized by detonation velocities significantly below that of the normal C-J values in smooth tubes with no pressure losses. For a given obstacle configuration, transition to the quasi-detonation regime occurs in a region around stoichiometric composition extending more to the side since H_2-air mixtures are more sensitive for high H_2 concentrations. The width of this detonation regime depends on pressure losses. It is conceivable that for sufficiently severe pressure losses (very dense obstacle field), transition to detonation may be completely suppressed.

The variation of the maximum averaged pressure with H_2 concentration for the same three obstacle configurations is shown in Fig. 4. Again, little

difference is observed for the different obstacle geometries. A rapid rise in the pressure also occurs at around 13% H_2 corresponding to the flame speed increase discussed previously. However, unlike the flame speed, the averaged pressure does not show a prominent second jump when transition to quasi-detonation occurs at H_2 concentrations between 25% and 30%. Thus, as far as the averaged pressure is concerned, there is little difference between very high speed deflagrations and quasi-detonations. It is reasonable to expect that for supersonic combustion waves, the pressure when averaged out should be about the same for all cases and should correspond to about the constant volume explosion pressure. This is exactly as indicated in Fig. 4 where above 13% H_2, the averaged pressure is slightly above the constant volume explosion value. A small increase to higher values if observed when transition to quasi-detonation occurs in the region $25\% \lesssim H_2 \lesssim 30\%$. In the quasi-detonation regime, the pressure is as expected slightly below the normal C-J detonation pressure due to the pressure losses encountered in propagating through the obstacle array. However, unlike the quasi-detonation velocity, the averaged pressure appears to be quite insensitive to the obstacle configurations. It should be noted that the details in the pressure-time histories that may have represented the transition to the quasi-detonation regime, as well as the influence of obstacle configurations, are lost in the averaging process.

To investigate the effect of scaling, a similar series of experiments are carried out in a 15 cm diameter tube. Results using orifice plates (BR = 0.3875) as obstacles are illustrated in Fig. 5. For comparison, the flame speeds for the 5 cm diameter tube are also shown. The results are almost identical for the two tubes. The two sharp jumps in the flame speed at about 13% H_2 and also at around 25% H_2 where transition to quasi-detonation occurs are found in the 15 cm diameter tube also. Turbulent flame speeds are

almost identical, although for the case of the larger tube, the quasi-detonation velocity is found to be below that of the smaller tube. This suggests that shock reflections and turbulence due to the obstacles are more effective in generating conditions for auto-ignition than the colliding transverse wave mechanism of normal cellular detonation propagation. In the larger tube the core diameter is large as compared to the detonation cell size, thus permitting a sufficiently large number of cells to pass through for a normal detonation. The perturbations by the orifice plates create expansion waves which retard the combustion processes in the core. In the smaller tube, the core (i.e., orifice opening) is of the order of the cell diameter. Thus, the entire combustion is strongly controlled by turbulence and shock reflections which are more effective in rendering ignition. For higher blockage ratios in the larger tube, we may expect the quasi-detonation velocity to increase when the influence of the obstacle in aiding ignition becomes more dominant.

The variation of the averaged overpressure with H_2 concentration for the 15 cm diameter tube is shown in Fig. 6. Again, the result for the 5 cm diameter tube with a similar blockage ratio is shown for comparison. Almost identical results are obtained for the turbulent deflagration regime. However, in contrast to the detonation velocity, the averaged quasi-detonation pressure is higher than the corresponding case for the smaller 5 cm tube. This suggests that for the same blockage ratio, the pressure loss per unit volume is less in the larger tube than in the smaller 5 cm diameter tube.

The acceleration phase in the larger tube is illustrated in Fig. 7, where the flame speed is plotted against distance from the ignition source. Acceleration to steady-state occurs after around 1.5 m of flame travel (10 diameters) and is thus more rapid than the corresponding cases for the smaller tube where steady-state flame velocities occur typically after 40 diameters of propagation. This suggests that increasing the scale of the turbulence

proportionally increases the acceleration rate, but not the final velocity. For $H_2 \gtrsim 25\%$, there appears to be an overshoot in the flame speed to peak values close to those of normal C-J detonations. However, the final quasi-detonation velocities have sub-normal C-J values. The overshoot is typical of all transition processes where the detonation formed is initially highly overdriven. In the larger tube, the core is sufficiently large for a normal transition to occur. However, subsequent propagation is influenced by the losses due to the orifice plate to give sub C-J quasi-detonation velocities. In the smaller tube, the overshoot is also observed, although much less prominently. There the core is small and normal overdriven detonations are probably never formed at the onset of detonation.

The results obtained thus far for the two tubes indicate that larger scales appear to increase the acceleration rate, but the influence on the final steady-state turbulent flame speed is minimal. For $H_2 \gtrsim 13\%$, where the reaction rate is fast, gasdynamics appear to play the dominant role in setting the upper bound for the flame speed. However, for the quenching control regime of $H_2 \leq 13\%$, we should expect scaling to larger dimensions (hence, large eddies and longer lifetimes) to have a more significant influence on the burning rate. Future experiments in the 30 cm diameter tube and in the 4 ft diameter VGES facility at Sandia should be of great value for the lean mixtures.

3. Influence of Confinement on Flame Acceleration

The investigations on flame acceleration described in the previous section were performed in experimental situations where the flame propagation progressed in a fully enclosed environment of a long confining tube. In such a fully confined geometry, the flow of the unburnt gases that develops due to the displacement effect resulting from the increase in the specific volume

across the flame zone, is a maximum. In most practical situations, explosion occurs under partially confined conditions. Confinement here may be defined in terms of the available degree of venting of the gases normal to the direction of flame propagation (e.g., a tube with porous walls). The consequence of side relief by venting is a reduction of the mean flow velocity in the burnt mixture ahead of the flame, thus rendering the turbulent flame acceleration mechanism less effective. One part of the investigation involved some experiments which were carried out in a rectangular channel with one porous wall to determine the effectiveness of side relief on flame acceleration by repeated obstacle arrays. The channel is 12.7 cm x 20.3 cm x 1.22 m long with the top wall of the channel being removable so that it can be replaced by a porous plate of different degree of porosity. Degree of confinement is henceforth defined as the ratio of the closed to the total area of the top plate (i.e., 100% confinement denotes a solid plate, while 0% confinement refers to the complete removal of the top plate itself). Obstacles are in the form of baffle plate (12.7 cm x 5.0 cm) spaced 10 cm apart. Three different obstacle configurations are studied; i) the baffle plates are mounted on the bottom of the channel, ii) the plates are mounted on the centerline and iii) the plates (20.3 cm x 3.1 cm) are staggered alternately along the two side walls of the flame channel. Typical results for the variation of the flame speed with distance are shown in Fig. 8 for the staggered obstacle configuration in 12.7% H_2-air mixtures. With a solid top plate (i.e., 100% confinement), the flame speed increases exponentially; however, steady state is not reached within the 1 meter of available travel. The maximum flame speed obtained is about 200 m/sec. Replacing the solid top plate with a porous one of only 8% porosity (i.e., 92% confinement), a drastic reduction in the flame speed is noted. The flame reaches steady state in about 0.5 m and the maximum steady turbulent flame speed corresponding to 92% confinement is only 14 m/sec. Further increase in porosity of the top plate (e.g., 23% porosity or 77% confinement)

gives only a slight further reduction in the steady state turbulent flame speed (i.e., 8 m/sec). Figure 9 summarizes the results for different obstacle configurations, H_2 concentration and degrees of confinement. The maximum flame speed at 1 m is plotted for the different conditions. For [redacted]% confinement, results for different obstacle configurations indicate that the staggered obstacle arrangement is the most effective giving maximum flame speeds of about 200 m/sec as compared to only 50 m/sec for the configuration when the baffle plates are mounted on the bottom of the channel. A reduction of only 2% H_2 from 12.7% to 10.6% gives a large reduction of the maximum flame speed obtained (e.g., 200 m/sec to 53 m/sec for the same staggered obstacle configuration). The drastic decrease in the turbulent flame speed from about 13% H_2 down towards leaner mixtures can perhaps be attributed to the kinetic mechanisms described previously. Significant decrease in the flame speed for only slight decrease in the degree of confinement is illustrated for the particular case of the staggered obstacle arrangement and for 12.7% H_2. The result from this study clearly indicates the effectiveness of side relief or venting in reducing the flame acceleration. It should also be pointed out that this conclusion is based on very lean mixtures only. For higher H_2 concentrations, the side relief may not be as effective. Once the flame accelerates to sufficiently high speeds so that the pressure build-up can cause choked flow conditions through the porous [redacted]ate openings, venting becomes ineffective. It should also be pointed out that scale will play an important role for lean mixtures. Under large scale conditions, lean mixtures may attain sufficiently high acceleration rates and turbulent flame speeds to cause choking of the vents. When this happens, the side relief provided will become ineffective. Future experiments in the large scale FLAME facility at Sandia will provide more information on the importance of scale.

4. Quenching Diameter for Jet Ignition

A common scenario in an accidental explosion is the transmission of the explosion from one chamber to another. For example, an explosion may start in a closed-in switch box or motor casing and the subsequent venting of the combustion products via small openings can cause ignition of the explosive mixture in the surrounding containment structure or vessel. The problem of the transmission of explosion through a small opening is a complex one consisting of different regimes depending on the initial conditions. For example, if combustion occurs sufficiently slowly in the first chamber so that the pressure difference across the opening is negligible, the transmission is essentially via laminar flame propagation through the opening. The quenching mechanism is based on heat and free radical losses to the wall of the opening and the criterion for the quenching diameter is found to correlate quite well using the Peclet number $Pe = SD/\alpha$ (where S is the laminar burning velocity, D the quenching diameter and α is the thermal diffusivity). For a small pressure build-up across the opening, the transit time for the flame through the opening is reduced. Thus, losses to the wall are reduced and re-ignition past the opening can occur for smaller openings than indicated by the Peclet number. Transmission for this regime is given by the so called MESG values (Maximum experimental safety gap) and a standard apparatus, agreed upon internationally, is used to determine MESG values for different explosion gases. In general, MESG values are slightly smaller than quenching diam from the Peclet regime. However, H_2-air mixtures for example, are sufficiently sensitive that confined explosions even with fairly large vents give rise to large pressure differences across the opening. In fact, except for near limit mixtures, pressures of the order of the constant volume explosion pressure are usually attained. Quenching conditions corresponding to such large pressure differences where the venting is in the form of an under-expanded

supersonic turbulent jet are not well established. In view of its practical significance in accidental H_2-air explosions, a study was carried out to establish the quenching criterion for this supersonic jet ignition regime.

The experiments are carried out in a cylindrical explosion chamber cm diameter and 35 cm long with a smaller ignition chamber (5 cm diameter and 48 cm long) connected to it via a small orifice. Combustion is initiated by a spark in the ignition chamber and the mixture composition is varied for a given orifice diameter until quenching (i.e., no ignition in the main explosion chamber) is obtained. For orifice diameters up to 35 mm, and $13\% \lesssim H_2 \lesssim 60$) the pressure build-up in the ignition chamber is close to the constant volume explosion value to give a strong supersonic jet discharge of hot combustion products for the ignition of the mixture in the main chamber. The results for the variation of the quenching diameter with H_2 concentration are shown in Fig. 10. Also shown is the corresponding overpressure developed across the orifice. In all cases, the overpressure ratio is greater than the critical value of about 0.8 required for a choked discharge. The variation of the quenching diameter with H_2 concentration is in the familiar form of a U-shaped curve. In the range of $25\% \leq H_2 \lesssim 45\%$, the quenching diameter takes on a more or less constant value of 1.2 mm and a sharp increase occurs at about 13% H_2 and 60% H_2 on the lean and rich sides, respectively. The U-shaped behavior bears strong resemblance to the variation of the induction time with H_2 composition. This suggests a direct link between the quenching diameter and the chemical kinetics of the reactions. Following an approach similar to that used in the study of flame stabilization by bluff bodies, a criterion for quenching is proposed based on the characteristic times required for combustion (i.e., t_c) and for turbulent mixing (i.e., t_m). The turbulent mixing time t_m for the present cases can be estimated as being of the order of the transit time of the gas flow through the orifice over a length scale

equal to the orifice diameter. Similarly, the characteristic chemical time scale t_c can be expressed in the form of an Ahrrenius type law. Thus, more precisely the quenching criterion may then be stated as $t_c/t_m \geq \alpha$, where α is some empirical constant whose value depends on the definitions of the reaction time and the mixing time chosen. Such a criterion appears to agree with the experimental observations made.

5. Influence of Strong Jet Ignition on Pressure Development

The pressure development in vessels depends strongly on initial conditions, particularly for sensitive mixtures such as H_2-air. With weak spark or glow plug ignition, the initial flame kernel is laminar and relatively small. High flame speeds may not have developed prior to significant burn out of the available volume of mixture due to the exponential nature of the flame acceleration process. However, with a strong ignition source, the initial flame kernel is large and turbulent. The flame acceleration rate is thus large and rapid acceleration or even transition to detonations may occur even for small volumes. Experiments have been carried out to investigate the influence of strong jet ignition on the maximum rate or pressure rise in closed vessels for H_2-air mixtures. The jet of hot combustion products is from a small ignition chamber in the apparatus arrangement similar to that described in the previous section. Typical experimental results for the maximum rate of pressure rise with H_2 concentrations are shown in Fig. 11 for the case of a 5 mm diameter jet orifice. For comparison purposes, corresponding results using an electric spark for ignition are also shown. It can be observed that a two-fold increase in the rate of pressure rise from about 1000 to 2000 bar/sec at around stoichiometric composition (i.e., $\sim$ 30% H_2) can be obtained with jet ignition. Below around 13% H_2, the effect of jet ignition is minimal and comparable to that from a weak spark. The

sharp increase in the rate of pressure rise occurs at around 13% H_2 indicating the important role played by kinetics even in the ignition process.

6. Conclusions

The present paper gives only a brief summary of the more important results obtained in this program thus far. Details of the individual studies themselves can be found in separate publications. With the interest in lean mixtures from the practical point of view, it is of importance to point out that there appears to be a critical concentration of about 13% H_2 below which the reaction rate decreases sharply rendering flame acceleration mechanisms impotent. However, this is exactly where scaling up to larger dimensions to increase turbulent eddy size and lifetime will produce significant effects in this lean hydrogen region. The demonstration that a small degree of side relief or venting can limit the flame acceleration and impose a bound on the maximum turbulent flame speed that can be attained is also of some significance. However, the experiments thus far are based on lean mixtures (i.e., $H_2 \lesssim 13\%$). For faster burning mixtures, choking occurs and renders the side venting ineffective. Also, the present experiments for lean mixtures are of relatively small scale. Again, in the lean regime of $H_2 \leq 13\%$, scaling up to large dimensions may produce different results. The next phase of the program in extending some of these experiments to larger scale apparatus at Sandia should offer interesting possibilities.

Acknowlegement

Marshall Berman, John Cummings and Bill Benedick have been most helpful in facilitating our carrying out this program. Marshall provided [illegible] moral support whenever needed, John critically

technical advice on experiments and efforts to see that we get the equipment we need, progress would have been painfully slow.

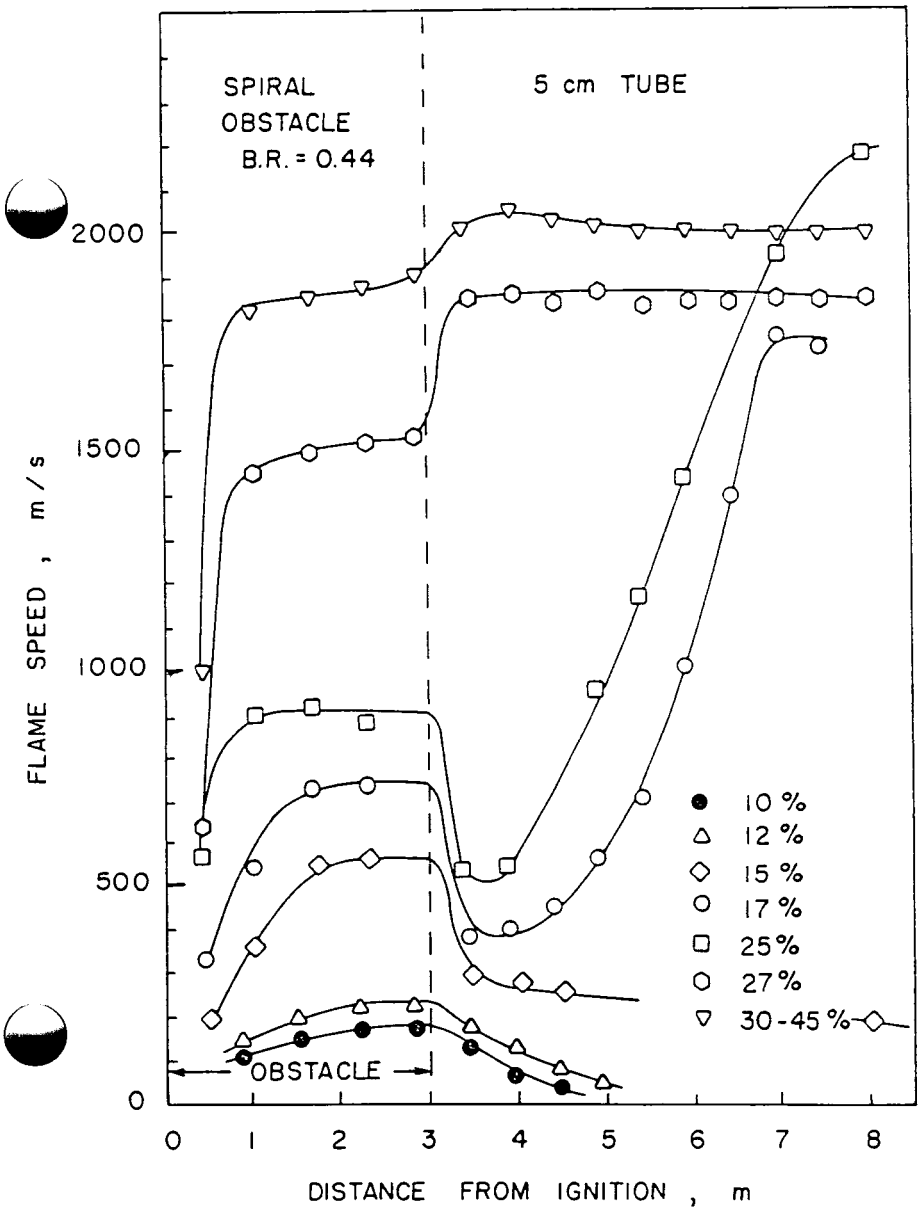


FIG. 1 Flame speed profiles for H_2-air mixtures in a 5 cm diameter tube filled with a spiral obstacle.

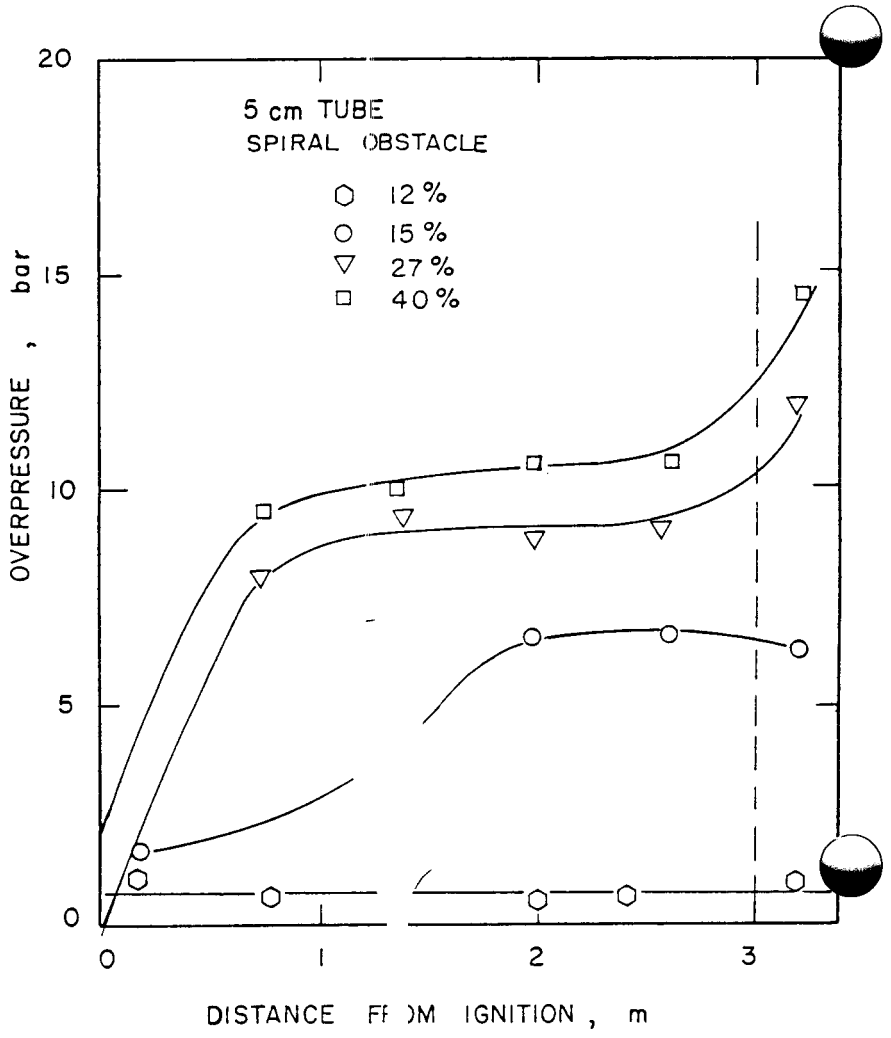


FIG. 2 Overpressures generated by accelerating H_2-air flames.

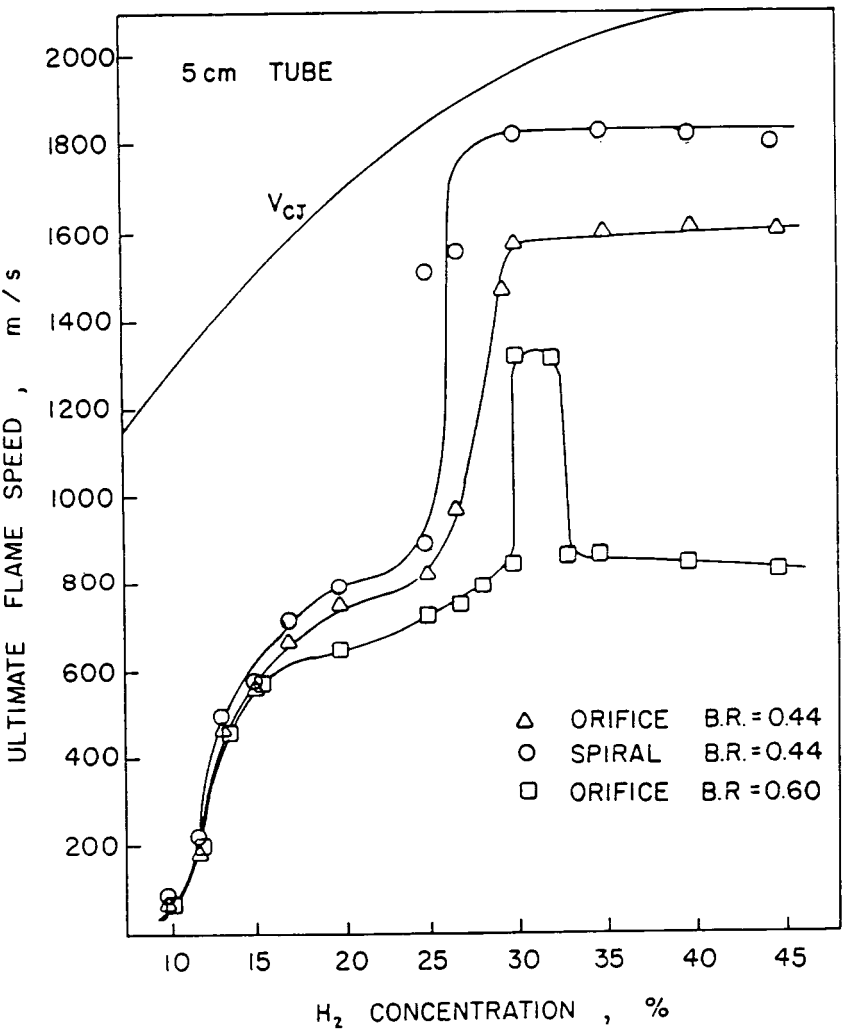


FIG. 3 Ultimate flame speeds for H_2-air mixtures in a 5 cm diameter tube.

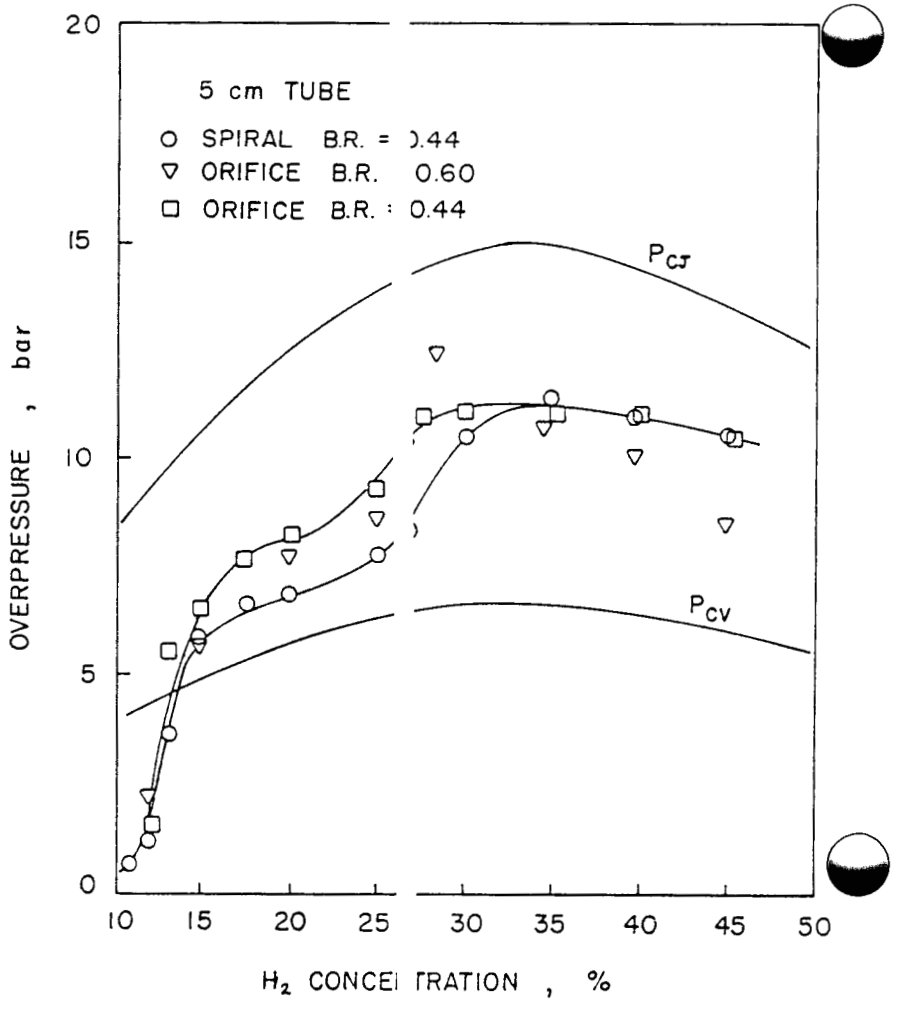


FIG. 4 Ultimate overpr ssure for H_2-air mixtures in a 5 cm diameter t)e.

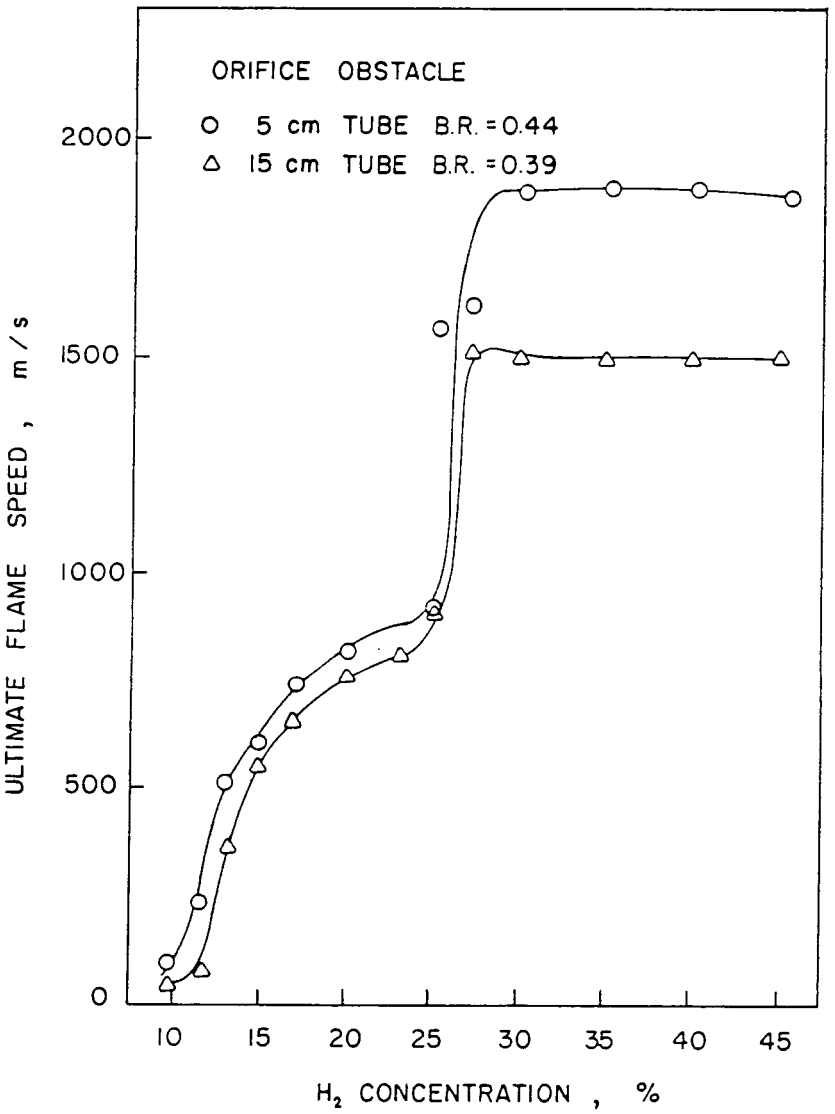


FIG. 5 Ultimate flame speeds for H_2-air mixtures in a 15 cm diameter tube.

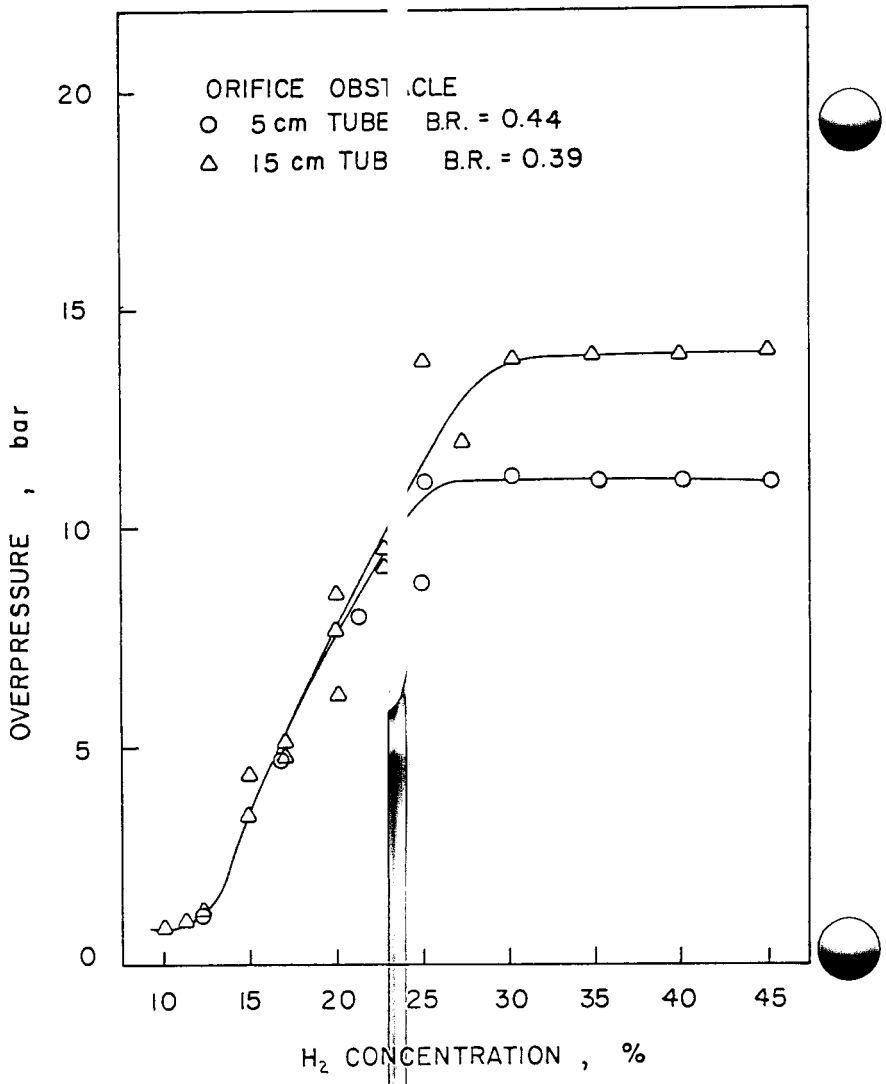


FIG. 6 Ultimate overpressures for H_2-air mixtures in a 15 cm diameter tube.

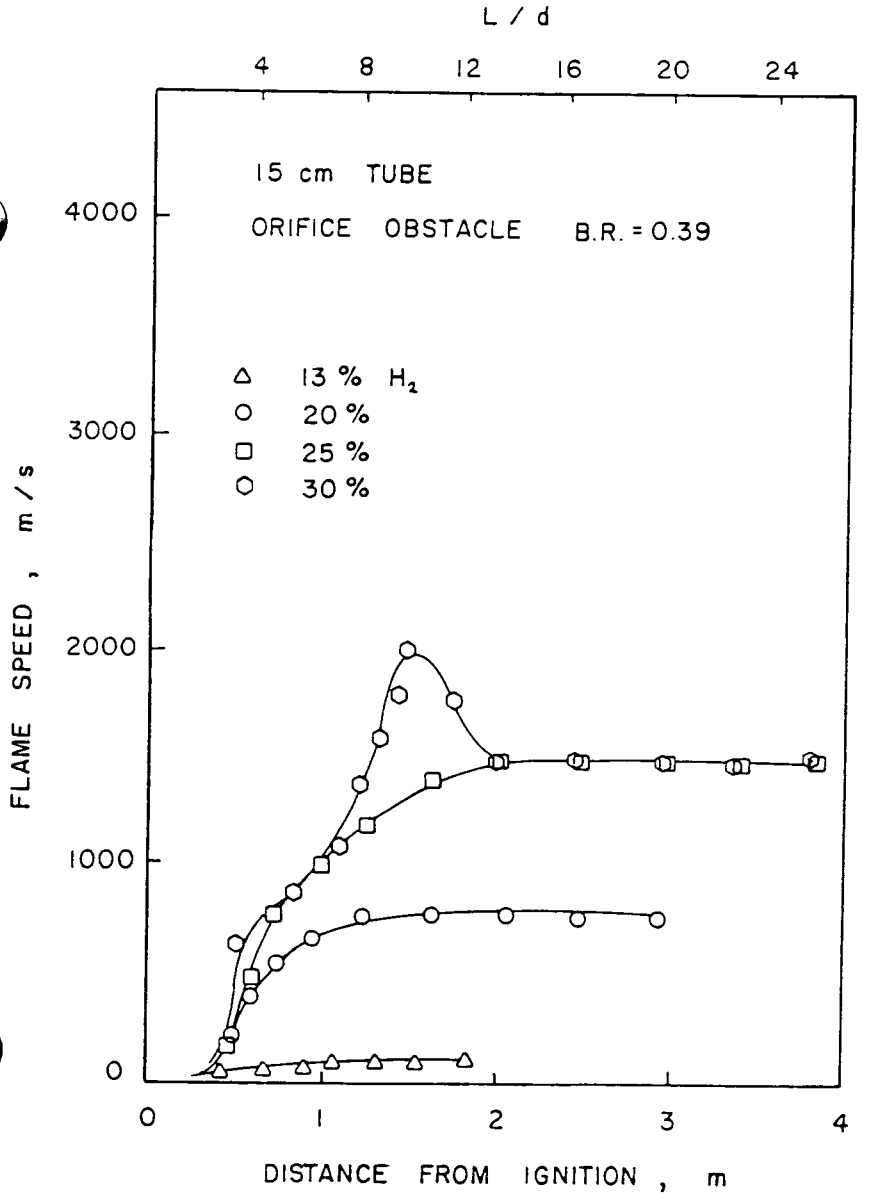


FIG. 7 Flame speed profiles for H_2-air mixtures in a 15 cm diameter tube filled with orifice obstacles.

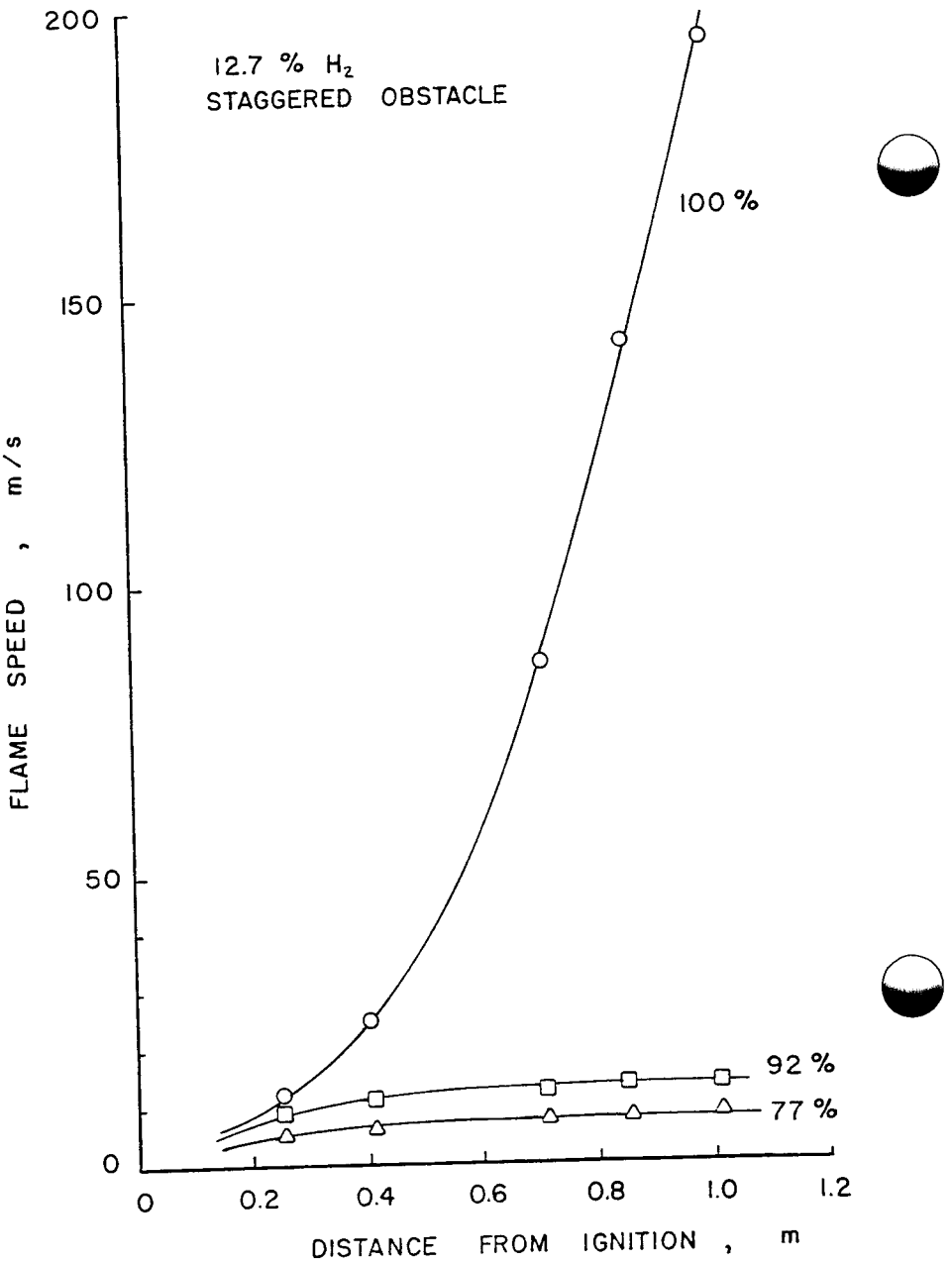


FIG. 8 Flame speed profiles for 12.7% H_2-air mixture under various degrees of confinement.

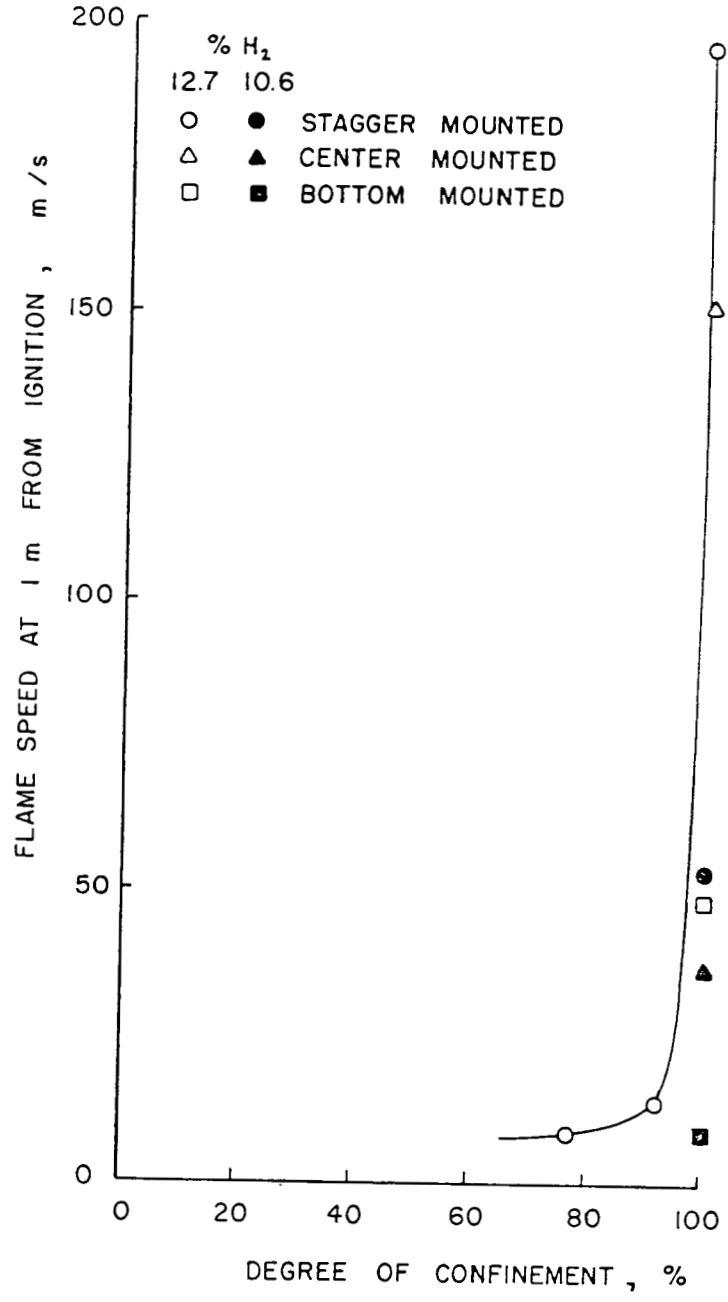


FIG. 9 Influence of confinement on flame acceleration for various obstacle configurations.

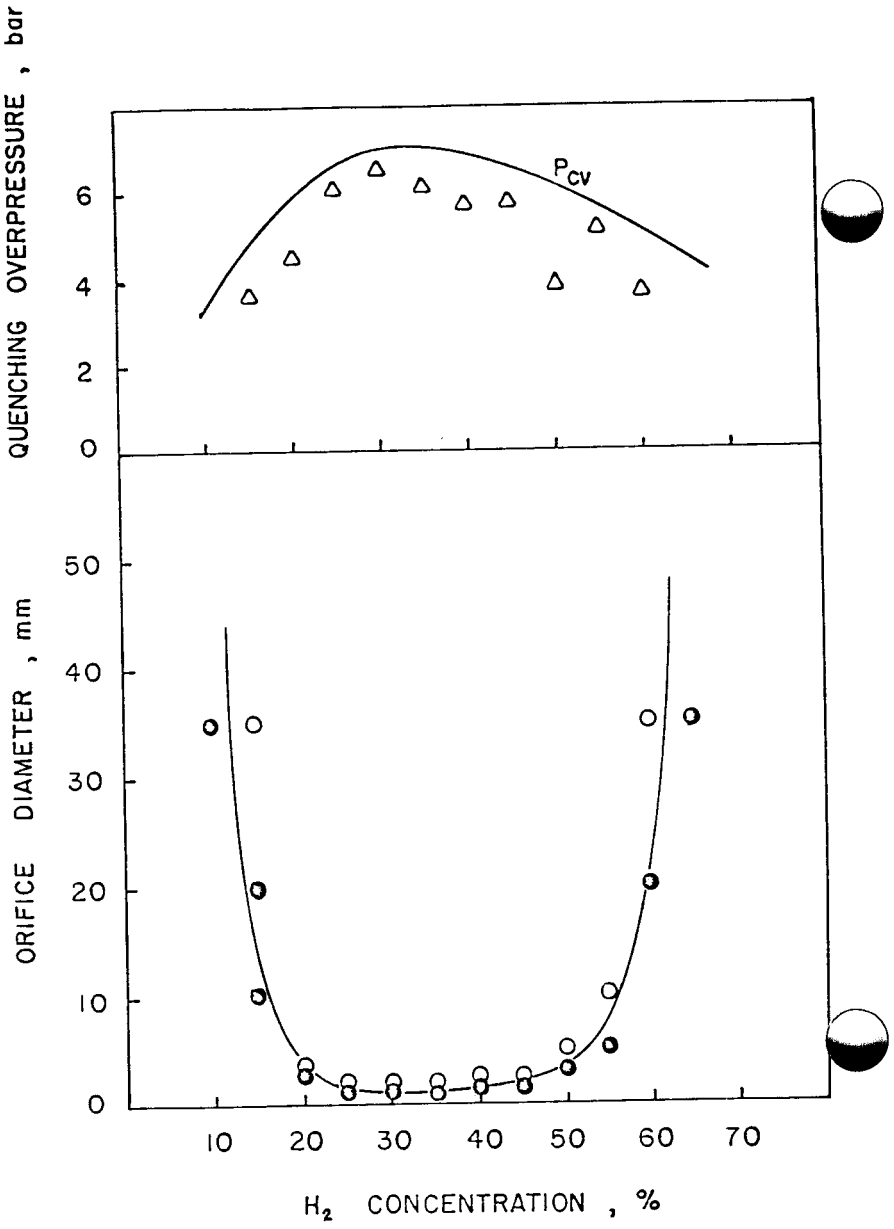


FIG. 10 Quenching diameters for H_2-air mixtures.

Discrete Vortex Simulation of Flame Acceleration Due to Obstacle-Generated Turbulent Flow*

W. T. Ashurst and P. K. Barr
Sandia National Laboratories
Livermore, California

Abstract

This paper describes a numerical simulation of flame acceleration caused by unsteady turbulent flow. A discrete vortex dynamics solution of orifice flow is combined with a simple flame model. We follow the flame motion and couple the chemically-induced volume expansion with the turbulent velocity field in order to obtain the feedback between flow and chemistry. The entrance flow into a chamber is specified for a selected time period at which point the flow is halted and a flame is established. We find that flame speeds are ten to twenty times the laminar value.

Introduction

This paper describes a new modelling effort to explain the phenomenon of flame acceleration due to flow around obstacles that could occur with hydrogen combustion in light water reactor accidents. There is concern that hydrogen produced in a core-melt accident can over-pressurize the containment building if the combustion wave sufficiently increases its velocity during its travels through air ducts and around other equipment in the building. Experiments using combustible gases in channels with internal obstructions have shown flame speeds much larger than the laminar value. Thus, the magnitude and rate of pressure rise could exceed safe values.

The crucial part of the flame acceleration phenomenon is the strength of turbulent flow produced by gas volume expansion due to chemical reaction. Reacting flow in a channel containing obstacles produces large flame acceleration (Moen, et al., 1981). Acceleration occurs because the expanding flow pushes the gas ahead of it around obstacles which creates turbulent flow downstream of the obstacles. Turbulence enhances the mixing of unburnt gas into the flame zone and hence increases the burning rate. This positive feedback accelerates the flow and hence the flame front.

Lee (1982) and his co-workers at McGill University have been conducting flame acceleration tests in various geometries: between two flat plates, in round tubes, and in channels with rectangular cross section. A particular configuration with application to a pressurized water reactor is a 1.2 meter long channel with baffle-type obstacles

*Work supported by U. S. Nuclear Regulatory Commission.

mounted in a staggered fashion on two opposite walls which is a scale model of one section of the annular upper plenum chamber of an ice condenser. They have varied the fuel-air ratio and the degree of confinement of one channel wall (Chan et al., 1982). Experimentally, ionization probes are used to measure flame arrival and from these an apparent flame speed can be calculated. While the laminar burning velocity is 1 to 2 m/s, apparent flame speeds up to 200 m/s have been obtained. However, it is not clear how much of this apparent flame speed is due to convective velocities and how much to turbulence enhancement of flame propagation. Large scale chaotic motion increases the flame surface by folding, and small scale turbulence increases transport within the flame zone. It is possible in our calculations to examine these effects.

Unsteady turbulent flow structure is the key element of our calculation. The distributions of vorticity and volume expansion are defined and the velocity field is obtained from two Poisson equations. The velocity field is restricted to low subsonic values because of the way we solve the momentum equation: constant pressure and infinite sound speed assumed. In this time-dependent flow, we follow the flame front motion and couple the chemically-induced volume expansion into the turbulent flow field. Thus, we have included coupling between the flame and the turbulence. Our flame model is very simple: the flame front moves into the unburnt gas at a constant relative speed. Thus, our results will produce flame acceleration due to increased flame surface but not from changes in flame structure or gas composition. The apparent flame speed and the flow speed along the channel midline are calculated as a function of time in order to compare with arrival time data. In our results we find that the apparent flame speed can be ten or twenty times that of a flat flame in a channel with no baffles. The increased flame surface can easily produce a factor of ten increase while a small exit orifice creates even higher velocities due to the area change.

Method

These calculations use a grid-free numerical method known as "discrete vortex dynamics". This Lagrangian computational technique is currently under development at Sandia National Laboratories for application in turbulent reacting flows. Previous work with the vortex dynamics method has shown its ability to simulate turbulent flow structure in both free and confined geometries. In the free mixing layer the vorticity coalescence and the turbulent shear stress is described without the usual gradient transport assumption of turbulence modelling (Ashurst, 1979). In a channel with a symmetric sudden expansion the vortex method has reproduced the observed steady asymmetric flow (Ashurst, 1981). A new computer program has been written that models the motion of a flame front in a velocity field composed of many vortices (Ashurst, 1982).

Turbulent flow structure can best be characterized by its vorticity. Vorticity has a kinematic definition as the vector curl of velocity: in a boundary layer the velocity gradient normal to the flow is a

measure of the vorticity. Flow downstream of an obstacle is composed of boundary layer vorticity that has escaped from the obstacle (also called vortex shedding). The vorticity equation of motion is derived by taking the vector curl of the Navier-Stokes equation. In two-dimensional flow with no pressure gradients, the equation states that once created the vorticity remains with the fluid mass. In the numerical model, discrete vorticity is created in the obstacle's boundary layer depending on the local freestream velocity. Vortex strength is proportional to the freestream velocity squared times the discrete numerical time step. The velocity field can be calculated from an integration of the vorticity distribution, and thus the vorticity can be advanced in time by calculating the velocity vector at each vortex location. This grid-free feature provides a computational advantage for the discrete vortex method over standard finite-difference techniques, which must resolve the velocity field everywhere and difference the velocity values in order to advance the solution in time.

The flame structure is not calculated, and its motion is assumed to be given by the local gas velocity plus the constant laminar flame speed. Flame quenching is not possible. While the vorticity is calculated in a Lagrangian reference frame, the flame is represented as a discontinuity in an Eulerian mesh. Burn fraction, which ranges from zero to one, is used to construct an appropriate flame surface using a hybrid of the SLIC and VOF algorithms (Barr and Ashurst, 1982). Thus, flame curvature can only be resolved when larger than several mesh cells. The flame geometry gives the distribution of volume expansion due to chemical reaction which is the source term in a Poisson equation for the velocity potential. These model assumptions are similar to those used by Ghoniem et al. (1982). The validity of the interface flame model has been checked against detailed calculations of mass and energy diffusion in a vortex velocity field (Ashurst, 1982). Both methods indicate that at constant turbulence length scale the flame speed increases linearly with turbulence intensity. While the detailed results show increasing flame speed with decreasing length scale (at constant turbulence intensity), the interface model does not. It is reasonable that the interface model can not simulate convective mixing at small length scales since the modeled flame thickness is zero. Ways of improving the interface model are being investigated.

Problem and Results

Recently, Hjertager (1982) calculated the flow in a large scale flame acceleration experiment: a tube 2.5 m in diameter and 10 m long with 5 equally spaced ring baffles (each protruding 0.2 m from the tube wall). Using the classical k-e turbulence model, Hjertager discretized the tube with 15 radial nodes and 30 axial nodes. Thus each baffle was described by 2.5 radial nodes. With this resolution, the details of flame structure shown in Chan et al. (1982) cannot be obtained. Hjertager did obtain qualitative agreement with the pressure and flame speed time history by varying the initial dissipation rate (which is proportional to reaction rate in his

model). Since the vortex dynamics method can describe time-dependent flow structure, we have calculated the turbulence-reaction problem at a more fundamental level with more spatial resolution. But, with more resolution also comes increased computer effort. Therefore, in this study we have focused on just one chamber of a multi-chamber configuration (the volume between two baffles being one chamber). In particular, consider the second chamber: the flow is quiescent until spark ignition which establishes a laminar flame in the first chamber. This produces flow into the second and succeeding chambers. The flame-turbulence interaction commences when the flame reaches the first baffle. As a simple way to investigate flame acceleration, we will concentrate on the second chamber where we can specify the entrance flow and establish a flame in the baffle orifice at a selected time.

Our calculations are focused on one chamber of a multi-chamber experiment. We use planar geometry and consider a channel of height H and a chamber length of 2 H. A 40-by-80 mesh is used for the flame motion. The entrance end has an opening of H/2 symmetrically located which represents one internal baffle and the exit end is unrestricted (an opening of H) or is symmetrically baffled. The combustion that occurs upstream of our chamber is not calculated but its effect is created by prescribing a flow into the chamber at a specified velocity for certain time period. We will call this the injection velocity and the injection time. The injected flow through the entrance baffle hole will create two boundary layers at the hole edges. These boundary layers are modelled by creating discrete vorticity at those locations. The layer's thickness is approximated by randomly varying the nascent vortex location. Each discrete vortex has its vorticity distributed over a non-zero area, which eliminates the infinite velocities that are allowed with a point vortex model. This vorticity area can be related to the viscosity value or Reynolds number of the flow: viscous flow (low Reynolds number) has vorticity distributed over space with small gradients while nearly inviscid flow (high Reynolds number) has vorticity concentrated in small regions and hence has large vorticity gradients. The radius of the vorticity area is randomly selected between zero and 0.01 H. This determines the range of turbulent length scales possible in the vortex motion. The flame's smallest curvature length scale is larger: mesh size of 0.025 H.

At the end of the injection time, the entrance flow is halted and a flame is established in the opening. Initially the chamber is filled with a combustible mixture that produces a density ratio of six across the flame front, and the flame travels at a speed of 0.2 U into the unburnt gas, where U is a characteristic velocity. Without the initial flow, a flat flame would develop and move at a speed of 1.2 U (the density ratio times the burning velocity) and the unburnt gas would be pushed out the chamber exit at speed 1.0 U (the density ratio minus one times burning velocity) if the exit hole is H wide (i.e. no baffle). The velocity U and the channel height H are used to scale all velocities and lengths.

Computer-generated movies showing the vorticity and flame motion provide the best means of understanding the calculational output.

Here selected stills from one such movie will be given. For the short injection times considered the entrance flow vorticity does not occupy a very large fraction of the chamber volume. A smoke-ring like structure is created by the injected flow: two counter-rotating regions of vorticity in planar geometry. Figure 1a shows the velocity vector of each discrete vortex, a total of 600 vortices, as well as the flame surface shortly after ignition. The vorticity appears like two clouds on either side of the orifice, the lower region rotating clockwise and the upper region counter-clockwise. This vorticity [illegible]nfiguration restricts the flame to the midline region until the [illegible]ame gets in front of the vorticity regions (Fig 1d). Then the rotational velocity induced by the vorticity quickly spreads the flame across the entire chamber cross section (Fig 1f). In Figure 1c the vortex regions begin to show deformation due to the volume expansion. The flame moves less rapidly along the midline during its passage between the vorticity regions. This is a result of the selected initial flow condition of a top-hat velocity profile (i. e. all the vorticity is concentrated at the orifice edges). If a jet-type profile had been used instead, then the velocity would have been a maximum along the midline. Because of the vortex random start, the flow does not remain symmetric, and thus the flame leading edge may be on the top or bottom. The flame does not uniformly sweep through the unburnt gas in the chamber, but a portion of the front shoots through the smoke ring and leaves the outer edges unburnt (Fig 1d). Thus, the area of the flame surface becomes many times the cross-sectional area of the channel, which leads to a large burning rate and large velocities associated with the volume expansion.

Figure 2 shows the flame velocity development for the case of an injection velocity of 2 U for a period of 3/4 H/U. During the early flame propagation the front is almost planar, and the flame velocity along the chamber midline is given in Figure 2 for this time period. However, the front soon becomes nonplanar and so the velocity of the leading edge is measured. The volume expansion pushes the unburnt gas out the open chamber end and this velocity is also shown in Figure 2. Without the initial flow, a flat flame front would develop and approach a speed of 1.2 U (density ratio times burning velocity) and would push the unburnt gas out the chamber at speed 1.0 U (density ratio minus one times burning velocity). Because of the initial flow the flame front accelerates to velocities that are fifty times the laminar value and eight times the flat flame value of 1.2 U. The unburnt gas is accelerated to nine times the flat flame value.

[illegible] have varied the injection velocity and time period but have fixed [illegible]e flame speed at 0.2 U. In a series of three calculations the total [illegible]njected mass is constant with value 3/4 (reduced with H and U) while the injected velocity is 2, 1 or 1/2 (all in units of U). A flat flame in the upstream chamber would provide the injection velocity of 2 U since the entrance hole size is H/2. Thus, we have not calculated the initial conditions but prescribe them instead. We also have used a top-hat profile whereas orifice flow does exhibit some streamline curvature (the vena contracta effect). The injected mass is 3/8 of the initial mass in the chamber. Figures 2, 3 and 4 present the apparent flame velocity along the chamber midline and the leading

front value. While all three calculations have the same total injected mass, the largest injection velocity leads to largest flame velocity. Therefore, we fixed the injection velocity at 2 U and varied the injection time in order to determine the maximum flame acceleration. Injection velocity of 2 U for a time period of 3/8 H/U shows the effect of the flame front getting ahead of the turbulent flow region. When this occurs no new flame surface is created and the flame starts to relax back to a flat front and also slows down. This is the cause of the kink in the velocity curves at time 0.7 in Figure 5. Figure 6 presents the velocity development for the case of injection velocity of 2 U for a time of 3/2 H/U. The dashed lines in both Figures 5 and 6 are time-shifted results of Figure 2, the 3/4 H/U injection case. Given a bigger head start with the longer injection time, the vorticity now manages to remain in front of the flame. The fastest apparent flame speed occurs when the flame front can catch the initial vortex region created by the injection (Fig 2). However, for very short injection times the flame can easily catch up with the vorticity but these vortex regions are relativity weak and the flame front passes them and relaxes back to a flat flame geometry with a known speed. On the other hand, when the injection period is long, the flame never catches the most intense part of the turbulent flow (within the chamber) and thus, the flame speed does not become as large (compare Fig 6 with Fig 2). Therefore, there is a particular combination of injection velocity and time period which produces a maximum flame acceleration in a given chamber geometry.

A meaningful way to summarize the calculations is by the flow speed at the chamber exit because this will be the entrance flow for the next chamber in a multi-chamber configuration. The variation of the exit flow velocity with injection velocity for a constant total injected mass can be described by an exponential function with a time constant proportional to the injection velocity. An adequate fit is given by

$$V_{exit} / U = 0.55 \exp(t/\tau)$$

where

$$\tau = 0.185 - 0.057 \ln(U_{injected}).$$

Figure 7 presents this fit (dotted lines) of the exit flow velocities. A note of caution should be expressed in that this fit yields an infinite speed when the injection speed approaches 25 U. However, this unrealistic result is beyond the low subsonic limit of the incompressible flow model that is being used. In fact, for hydrogen-air conditions a Mach number of 0.4 corresponds to a velocity of 12 U. At this Mach number compressibility effects cause an 8% change in density and a 10% change in pressure.

All of the above calculations have no exit baffle, i. e., the opening is H. Calculations have also been done with an exit opening of H/2 located symmetrically like the entrance. Repeating the three injection velocities (Figures 2, 3 and 4) yielded exit flow velocities that scaled inversely with the hole size. This is to be expected in this incompressible flow model if the flame surface is not affected by the exit flow field. Differences in the flame surface did occur as the leading flame edge approached within about H/2 of the exit hole. In

this region the flame velocity was slightly more than twice the previous results.

Conclusions

Numerical simulation of flame acceleration due to large scale turbulent motion has been achieved. The model does not include fine scale turbulence and does not allow the flame structure to change. It was restricted to two-dimensional subsonic flow. We simulated flow in a chamber which is typical of that in the multi-chamber experiments performed by Lee and his co-workers at McGill University. When ignited, the unsteady orifice flow yields a large flame surface and hence velocities many times the laminar burning speed due to the volume expansion. Flame propagation is not one dimensional, thus, amplification over the speed of a flat flame in a duct is not surprising. Large accelerations occur in just one chamber and indicates that compressibility effects will become important.

We have fit the time dependent flow speed as an exponential function of the initial chamber entrance speed. This fit can be used to estimate the flame acceleration. However, the fit does not include the variation of entrance geometry.

There are many possible extensions of the current model. Instead of prescribing the initial entrance flow into a single chamber we could start the calculations with quiescent conditions in a multi-chamber configuration. Also, allowance of side wall venting would be interesting since experiments done at McGill indicate that a small amount of venting behind the flame drastically reduces the flame acceleration. In addition, more chemistry could be included in the flame model: modelling the flame speed as a function of composition and including a provision for flame extinction.

REFERENCES

W. T. Ashurst, 1979, "Numerical Simulation of Turbulent Mixing Layers via Vortex Dynamics," in Turbulent Shear Flows I, edited by F. Durst et al. (Springer-Verlag, Berlin), pp. 402-413.

W. T. Ashurst, 1981, "Vortex Simulation of a Model Turbulent Combustor", in Combustion in Reactive Systems, edited by J. R. Bowen et al., Vol 76 of Progress in Astronautics and Aeronautics, pp. 259-273.

W. T. Ashurst, 1982, "Turbulent Flow Structure Effect on Diffusion and Premixed Flame Propagation", in Proceedings of the Fourth GAMM Conference on Numerical Methods in Fluid Mechanics, edited by H. Vivand, (Friedr. Vieweg & Sohn, Braunschweig/Wiesbaden), also Sandia National Laboratiories Report 81-8785.

P. K. Barr and W. T. Ashurst, 1982, "An Interface Scheme for Turbulent Flame Propagation", Sandia National Laboratories Report 82-8773.

C. Chan, I. O. Moen and J. H. S. Lee, 1982, "Influence of Confinement on Flame Acceleration Due to Repeated Obstacles", accepted for publication in Combustion and Flame.

A. F. Ghoniem, A. J. Chorin and A. K. Oppenheim, 1982, "Numerical Modelling of Turbulent Flow in a Combustion Tunnel", Phil. Trans. R. Soc. London, A 394, 303-325.

B. H. Hjertager, 1982, "Simulation of Transient Compressible Turbulent Reactive Flows", Combustion Science and Technology, vol. 27, pp. 159-170.

J. H. S. Lee, 1982, private communication.

I. O. Moen, M. Donato, R. Knystautas, J. H. Lee and H. Gg. Wagner, 1981, "Turbulent Flame Propagation and Acceleration in the Presence of Obstacles", in Gasdynamics of Detonations and Explosions, edited by J. R. Bowen et al., Vol 75 of Progress in Astronautics and Aeronautics, pp. 33-47.

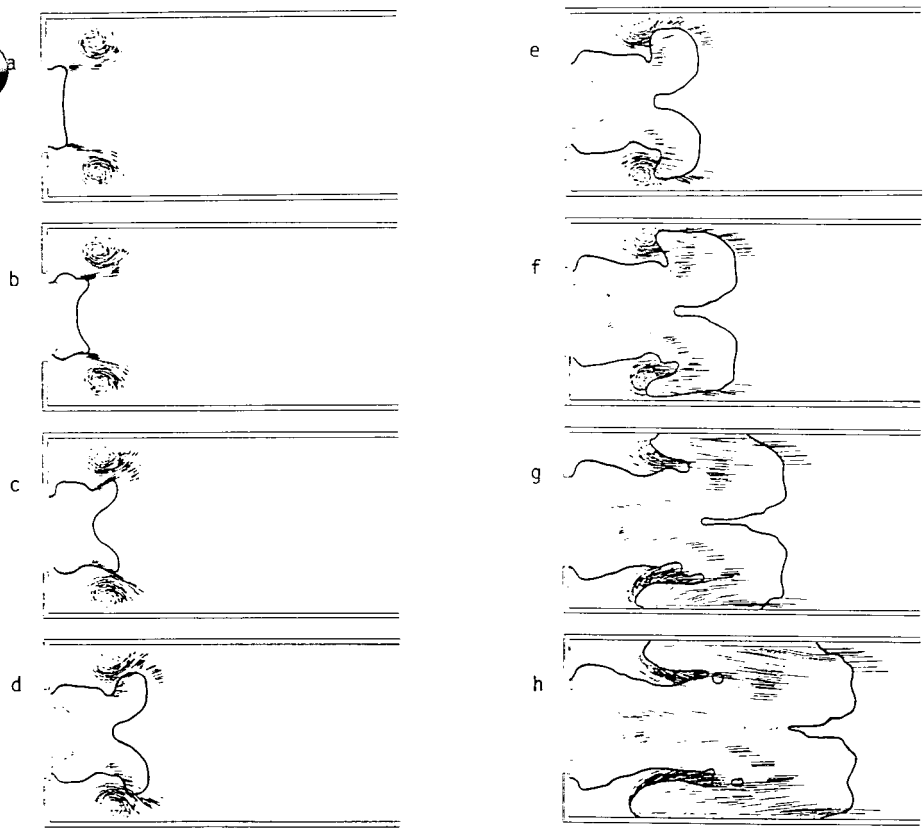


Figure 1. Flame development in a two-dimensional planar channel of height H and length 2 H after ignition across the orifice area (on left). The discrete vorticity which was created by flow injection at speed 2 U through the orifice for a time period of 3/4 H/U is shown by lines scaled to the vorticity velocity. The plot time intervals are 0.05 H/U with the first one at 0.8 H/U (ignition time is 0.75).

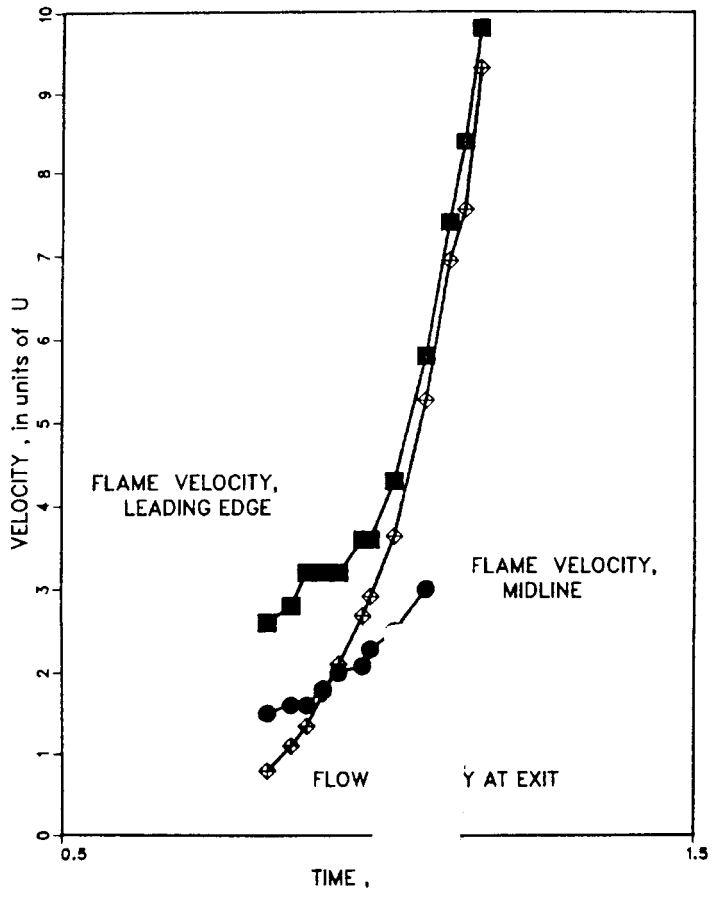


Figure 2. Time development of flam ed in channel; conditions of Figure 1: injec ion velocity of 2 U ction time of 3/4 H/U. While the flame is almost planar the midli elocity is measured, thereafter the leading edge velocity. he exit area is the channel height H.

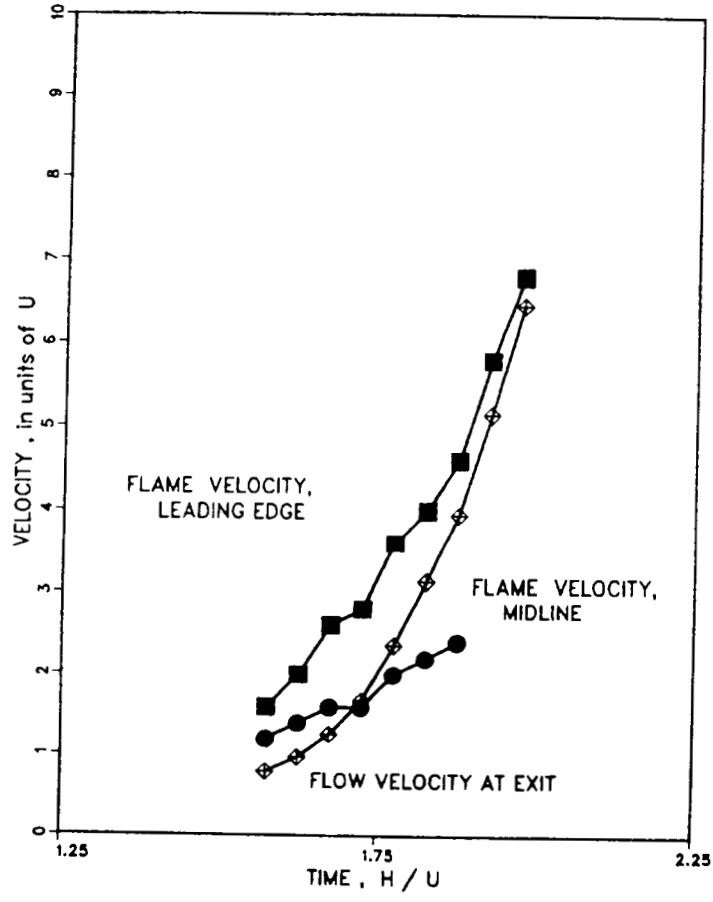


Figure 3. Like Figure 2, but injection speed of U for a period of 3/2 H/U.

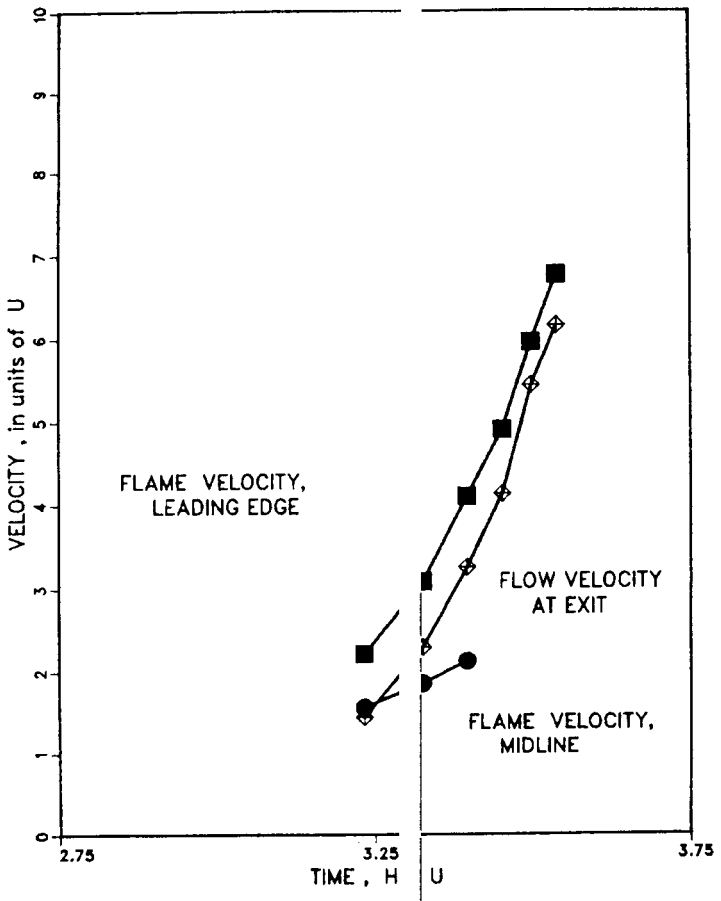


Figure 4. Like Figure 2, but injecti speed of 1/2 U for a period of 3 H/U.

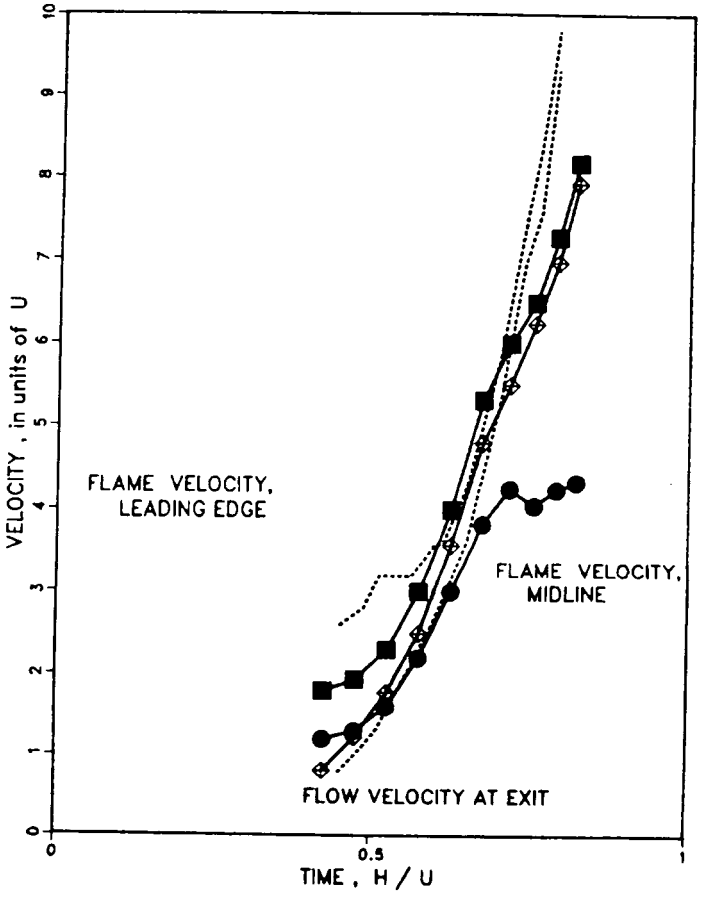


Figure 5. Like Figure 2, but injection time period of 3/8 H/U. The dotted lines are time-shifted results from Figure 2. The decrease in flame acceleration at 0.7 H/U occurs when the flame has engulfed all the injected vorticity and is relaxing back to a flat flame.

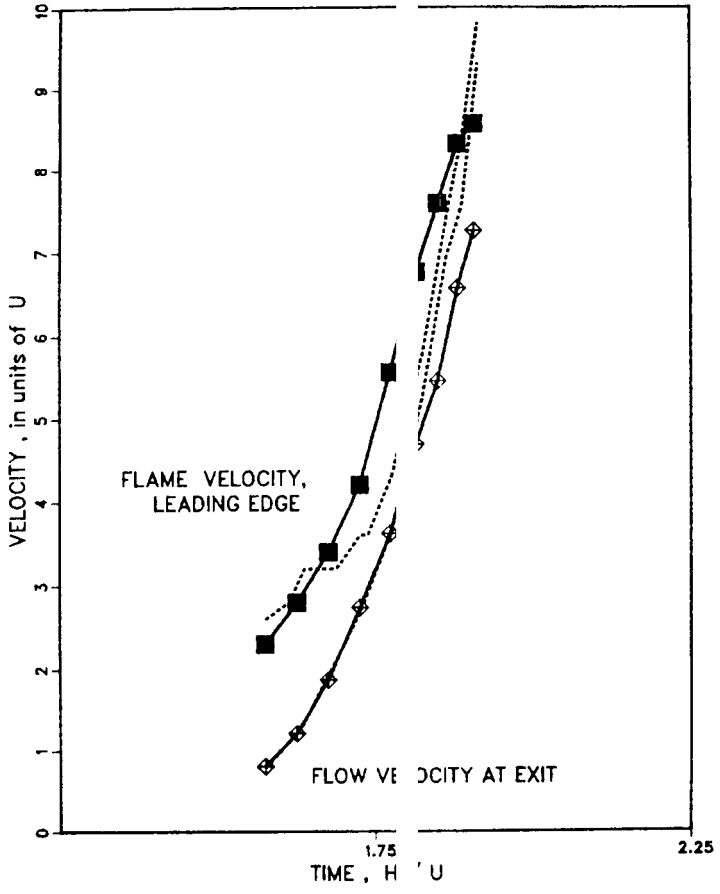


Figure 6. Like Figure 2, but inject n time period of 3/2 H/U. The dotted lines are time-shifted resul from Figure 2. Notice the larger separation between the flow and fla velocity compared to the previous figures. Within the chamb length of 2 H, the flame has not yet caught up with most of the vort ity.

THE RELATION BETWEEN ENERGY AND POWER FOR DIRECT INITIATION OF HYDROGEN-AIR DETONATIONS

by

E. K. Dabora

Department of Mechanical Engineering
University of Connecticut
Storrs, Connecticut 06268

ABSTRACT

A shock tube technique is used to d :ermine the energy and power needed to directly initiate a detonation in a s)ichiometric H_2-air mixture. In this technique the total initiation energy is /aried by varying the driver length whereas the power which is related to th initiating Mach number is varied by changing the pressure ratio between the :iver (He) and the driven gas (H_2-air) which was kept at .5 atmosphere. Three :iver lengths are used, namely 2", 4" and 8". For each driver the pressure ra :o was varied and the location where a CJ velocity is reached is noted. By ext apolation, the conditions necessary for developing a CJ velocity at infinity are then determined. These conditions which can be translated into energy and)wer requirements from each driver are then plotted to determine the relati ıship between these parameters. The resulting relationship is found to be (E :0)(P-27) = 555 J·Kw/cm^4 when the energy, E is expressed in J/cm^2 and the)wer, P in Kw/cm^2. This result indicates also that the minimum initiati ı energy for a planar detonation is 10 J/cm^2. Extension of this result to c :indrical and spherical geometries is made and the results are compared to alues found in the literature.

I. INTRODUCTION

It has been known for some time that the critical energy required the direct initiation of detonations in gaseous systems, is dependent on the method of initiation. Around 1968 Professor John Lee suggested that the critical energy might well depend on the rate of energy input. Indeed in a series of papers Lee and coworkers (1,2,3) have shown this to be the case. More recently Abouseif and Toong (4) were able to show on theoretical grounds that the critical energy does vary with its rate by considering the initiator to be a constant velocity piston. On this basis they were able to reproduce the experimental results of (3) on acetylene - O_2 mixtures at least qualitatively. The experiments of (3) were limited to cylindrical geometry. However, it is conceivable from the work of (4) and the review paper of Lee (5) that the appropriate critical energy for a particular system could be deduced for any geometry: planar, cylindrical or spherical, provided it is known for a particular one. Since in some cases it is easy to conduct experiments in a planar geometry by using the shock tube method of initiation, the results from this technique could well be used at least as a guide in conducting, for example, the more elaborate, therefore more expensive, tests that are usually necessary for the spherical geometry. The purpose of this paper is to describe the experimental technique we used to deduce the relation between initiation energy and power in a planar case, to present the results obtained for the stoichiometric H_2-air mixture and to show how these results could be applied to the spherical geometry.

II. EXPERIMENTA METHOD

1. Experimental Apparatus:

As indicated, the shock tube techni ıe was used to determine the critical energy. In this method a shock wave of .nite strength is induced into t driven section of the shock tube which i prefilled with the desired mixture. The decay or the acceleration of the wav is observed, and if a detonation occurs the location of its initial occurrance i observed.

The shock tube which was used in th study is described in detail in (6). Briefly, the driven section of the ube is 9 ft. long with a 2" x 2" square cross-section. The driver sectio is circular in cross-section providing a driver to driven area ratio, $A_4/A_1 = 1$ 5. Three different length drivers were used namely 2", 4" and 8". The tub operates on the double diaphragm principle to insure diaphragm break up a a desired pressure ratio. In calibrating the tube performance, the sh k strengths obtained corresponded generally to the theoretically calculate shocks for $A_4/A_1 = 1$.

The tube was provided with pressure witches at one foot intervals, starting at .5 ft. from the diaphragm. addition, two piezoelectric pressure transducers are placed at selected locat ns. The wave velocity is measured from time intervals as recorded in a raster d play of the pressure switches as well as from two electronic time interval uni .

2. Theoretical Background: Shock Wave cay:

In the usual use of a shock tube, t driver length is chosen long enough to insure a constant wave velocit throughout the driven section. However, since for our purpose we desire to observe whether a detonation occurs, relatively short drivers were use With a short driver, the rare-

faction wave in the driver, after reflection catches up with the incident shock wave and reduces its velocity if the wave is non-reactive. If the  is reactive as in a detonation, it is expected that the wave will continue to propagate unhampered by the rarefaction wave.

In order to get an approximate value of the decay of the wave, we note that the initiation Mach number of interest is between 3 and 4. For the gases used, helium in the driver and air-H_2 in the driven section, the Mach number obtainable for a given pressure can be determined. Fox (6) has calculated the location at which the rarefaction wave catches up with shock wave as a function of the driver length. The ratio of this critical location over the driver length, X_c/ℓ_4, is found to be 2.8-5.2 for M = 3-4 when the area ratio is 1.65. If after that location the wave is considered as a constant energy blast wave then its decay can be approximated (7) by

$$\frac{dM}{M} = -\frac{\alpha+1}{2}\left(1-\frac{1}{M^2}\right)\frac{dR}{R} \qquad (1)$$

where R is the blast wave distance and α is a geometric factor = 0, 1, 2 for planar, cylindrical or spherical wave. For the shock tube, $\alpha = 0$ and therefore:



$$\frac{dR}{R} = -\frac{M\,dM}{M^2-1} \qquad (2)$$

This equation can be integrated to give:

$$\frac{R}{R_o} = \frac{M_o^2 - 1}{M^2 - 1} \qquad (3)$$

For a 20% decay in M, $R/R_o \cong 1.65$ for M_o 3-5 and for a 50% decay, R/R_o varies from 4.57 to 6.40 when M_o varies om 5 to 3. If R_o is assumed to be the location where the rarefaction vertakes the shock wave, the dr length can then be chosen so that observ le decay could be effected within a reasonable length of the driven sectio For the 6" driver, used for calibration, $M_o = 3.5$, for which X_c/ℓ_4 = $_o/\ell_4 = 4$, 20% decrement is expected at .5 x 4 x 1.65 = 3.3 ft. from the diap agm.

Some tests were conducted to check e predicted velocity decrement and it was found that for $M \cong 3.6$, a decreme of 17% was attained at 6 ft. from the diaphragm. Thus it appears that the xperimental decrement is about half the theoretically predictable decrement.

3. The Relation Between Energy and Pow

In a shock tube, the power is effec vely related to the initiation Mach number and the energy is related to the fective energy stored in the driver. Thus for a given set of driver and drive gases, the power is related to the pressure ratio p_4/p_1 and the energy to t length of the driver.

The rate of energy input to the dri n section must equal the rate of work performed by the driver gas at the terface. Thus the rate per unit area is = $p_2\bar{u}_2$, or the power per unit ar is:

$$P = p_2\bar{u}_2 \qquad (4)$$

$$= p_1(p_2/p_1)(u_1-u_2)$$

$$= (p_2/p_1)(1 - u_2/u_1) u_1$$

$$= (p_2/p_1)(1 - \rho_1/\rho_2) M_1a_1 \qquad (5)$$

Eq. 5 can be written in terms of the shock Mach number after using the shock relations. Thus:

$$P = \left[\frac{2\gamma}{\gamma+1}(M_1^2-1) + 1\right] \left[\frac{2(M_1^2-1)}{(\gamma+1)M_1^2}\right] M_1 p_1 a_1 \qquad (6)$$

The energy involved is equal to this rate multiplied by the time in which this rate is effective. This time is considered to be the time in which the wave propagates until the rarefaction wave reflected from the driver end wall catches-up with the shock front. Thus if X_c is the distance from the diaphragm at which the rarefaction wave reaches the shock front, then the energy per unit area:

$$E = P\, X_c/u_1 \qquad (7)$$

or

$$E = P(X_c/\ell_4)\ell_4/M_1 a_1 \qquad (8)$$

where ℓ_4 is the driver length and X_c/ℓ_4 depends on M_1 for a given combination of gases.

Equations 6 and 7 can also be expressed in a non-dimensional form to obtain

$$\bar{P} = \left[\frac{2\gamma}{\gamma+1}(M_1^2 - 1) + 1\right]\left[\frac{2(M_1^2 - 1)}{(\gamma+1)M_1}\right] \qquad (9)$$

$$\bar{E} = \bar{P}\,\bar{t} \qquad (10)$$

where:

$$\bar{P} = P/p_1 a_1 \qquad (11)$$

and

$$\bar{t} = X_c/u_1 \tau_{CJ} \qquad (12)$$

with τ_{CJ}, the induction time for a Chapman Jouguet detonation taken as the normalizing time, after Ref.(4).

III. EXPERIMENTA RESULTS

The initiation of a stoichiometric xture of H_2-air originally at 0.5 atm. was examined with the three dif rent drivers. Helium was used as the driver gas. The driver pressure is varied to obtain different incident shock strengths and the wave ve city was monitored as the wave proceeded down the tube. The location a which the Chapman-Jouget (CJ) Mach number was reached was noted and th results are shown in Fig. 1. It can be seen that the 8" and 4" result show reasonable variations whereas the 2" results show much scatter. At an rate, the pressure ratio below which detonation is expected to take pla at extremely long distance from the diaphragm can be estimated. The cor sponding initiation Mach number can then be determined and the correspon ng X_c/ℓ_4 is found from (6). Equations 6 and 8 are then used to deter ne the power and energy for initiation. The results are presented i Table I, and plotted in Fig. 2. From this figure the asymptotes of energ and power can be estimated.

Table I

ENERGY AND POWER RELATION F THE INITIATION OF STOICHIOMETRIC H_2-AIR AT p_1 = 0.5 atm.

Driver Length ℓ_4(in)	p_4/p_1	M_1	X_c	ℓ_4	X_c cm	P watts/cm^2	E J/cm^2
2	100	3.90	4.		24.4	10.89×10^4	16.69
4	65	3.55	3.		38.6	8.08×10^4	21.50
8	40	3.2	3.		63	5.78×10^4	27.89

These would correspond to the minimum initiation energy and power. The minimum energy can actually be determined by plotting E vs. X_c, as is done Fig. 3, and finding the intercept. This gives E_{min} = 10 J/cm^2 for a stoichiometric mixture of H_2-air at 0.5 atm. It can also be shown from a plot of P vs. $1/X_c$ that P_{min} = 27 Kw/cm^2 which corresponds to an initiation Mach number of 2.55. The two asymptotic values of E_{min} and P_{min} can be combined to give the following relation between P and E:

$$(E-10)(P-27) = 555 \text{ J}\cdot\text{Kw/cm}^2 \qquad (13)$$

This result shows that the variation of E with P is monotonic, in contrast to the results of (1) and (4) for acetylene-oxygen mixture in cylindrical geometry which exhibit dual values of energy for a given power.

IV. COMPARISON WITH NUMERICAL MODELING

Oran et al (8) used the NRL Reactive Shock Model (9,10) which solves the time-dependent conservation equations coupled to chemical kinetics, to model the experimental phenomenon described above. The model assumes the driver and the driven section to have the same area. The results with respect to the location of the CJ wave are shown in Fig. 4 and compared with the experiment. Both model and experiment are for the 8" driver. One can see that differences in actual values exist but the trend is apparently the same. The differences could be due to the fact that in the experiments, the driver and driven sections have different areas. However, this needs to be ascertained by further experimentation and/or calculations.

The modeling of (8) produces other parameters. Figures 5 and 6 show the wave velocity, the interface velocity and the pressure variation for two driver/driven pressure ratios, namely, 110 and 150. Looking at the pressure variation, it can be seen from Fig. 5 that the wave pressure remains the same for almost one millisec and then decays, whereas in Fig. 6 the pressure, in a short time $\tilde{=}$ 150 μsec, exhibits a variation similar to that of a detonation wave. This then confirms that a pressure ratio of 150 would result in a detonation whereas a pressure ratio of 110 would not, and is indicative of a threshold Mach number or power below which a detonation would not take place.

V. APPLICATION TO OTHER GEOMETRIES

Equations 6 and 7 were derived for a planar wave. If one assumes that the initiation source is a constant velocity piston, the instanteous power for cylindrical and spherical geometries becomes, respectively,

$$P_c = 2\pi\, p_2 \bar{u}_2 (\bar{u}_2 t) \tag{14}$$

and

$$P_s = 4\pi\, p_2 \bar{u}_2 (\bar{u}_2 t)^2 \tag{15}$$

The average power in both cases can then be written as:

$$P_c = \pi\, p_2 \bar{u}_2 (\bar{u}_2 t) \tag{16}$$

$$P_s = \frac{4}{3}\pi\, p_2 \bar{u}_2 (\bar{u}_2 t)^2 \tag{17}$$

Using the same substitutions as was done for Eq. 4, we obtain:

$$P_c = \pi\left[\frac{2\gamma}{\gamma+1}(M_1^2 - 1) + 1\right]\left[\frac{2(M_1^2-1)}{(\gamma+1)M_1^2}\right]^2 M_1^2 a_1^2 p_1 t \qquad (18)$$

$$P_s = \frac{4}{3}\pi\left[\frac{2\gamma}{\gamma+1}(M_1^2 - 1) + 1\right]\left[\frac{2(M_1^2-1)}{(\gamma+1)M_1^2}\right]^3 M_1^3 a_1^3 p_1 t^2 \qquad (19)$$

In nondimensional form these equations and the equation for the planar case can be written in the general form as:

$$\bar{P}_\alpha = \frac{P_\alpha}{(p_1 a_1)(a_1 \tau_{CJ})^\alpha} = k_\alpha\left[\frac{2\gamma}{\gamma+1}(M_1^2 - 1) + 1\right]\left[\frac{2(M_1^2-1)M_1}{(\gamma+1)M_1^2}\right]^{\alpha+1}(\bar{t})^\alpha \qquad (20)$$

Equation 10 for the energy, will continue to be applicable but will have the form:

$$\bar{E}_\alpha = \bar{P}_\alpha \bar{t} \qquad (21)$$

Equation 20 indicates that the average power is independent of time for the planar case but is proportional to the duration and the square of the duration of the initiation source, for the cylindrical and spherical geometry cases respectively. Similar observation can be made regarding the energy, except that the proportionality is to the first, second and third power of the duration for the planar, cylindrical and spherical cases.

In order to check the applicability of our experimental Eq.(13), we note that for a piston that results in an initiation Mach number equal to $M_{CJ} = 4.85$, the Mach of the Chapman-Jouguet detonation of the H_2-air mixture, the power for the planar case is 214 Kw/cm^2 which when used in Eq.13, yields E = 13 J/cm^2. From Eq.7, where X_c/u_1 can be substituted by t, the source duration, t, is found to be 60 usec. This is to be compared with τ_{CJ} for the mixture at .5 atm

which is 1.44 μsec (11). If one assumes that the source duration is to be the same for the other geometrics, it can then be found from Eq.18 and 19 that

$$P_c = 6.41 \quad Mw/cm \tag{22}$$

and

$$P_s = 81 \quad Mw \tag{23}$$

and that the corresponding critical energies

$$E_c = 385 \ J/cm \tag{24}$$

and

$$E_s = 4860 \ J \tag{25}$$

For a mixture at an original pressure equal to 1 atm. the above results must be modified by noting that both energy and power are proportional to the pressure and the source duration raised to an appropriate exponent. If the source duration is assumed to be a constant multiple of the ignition delay then the modification should be related to the ratio of the ignition delays at the two pressures. Again from (11) τ_{CJ} .8 μsec at p = 1 atm. Using the proper proportionality we find that

$$E_c = 238 \ J/cm \tag{26}$$

and

$$E_s = 1670 \ J \tag{27}$$

The critical energy for the direct initiation of H_2-air detonation has been measured by Bull and coworkers (12) and was found to be equivalent to about 1 gm of tetryl or approximately 4700 J. On the other hand Westbrook (13) calculates the critical energy to be ~50 J.

It should be realized however, that in calculating E_s in this paper, we dealt only with piston work. As indicated in (4) the total energy to [illegible]t the piston work is related to the piston work by the factor $\gamma/(\gamma-1)$ which for H_2-air equals to 3.5. Thus the total critical energy predicted in this paper should be 5850 J which compares favorably with Bull's result but is an order of magnitude higher than the prediction of Westbrook.

VI. DISCUSSION

It is well documented now that detonation waves are associated with a cell structure produced by transverse waves which are apparently an intrinsic part of a detonation wave. Recent work to predict the critical energy for initiation is centered around relating this energy to the cell size. However, in many instances, as shown by Bull et al. (14) the problem of determining cell size is a challenging one. Until this is resolved, it appears that the relatively simple method of examining the detonation initiation in a shock tube, as was done here, can offer a relatively simple means of predicting the critical energy for unconfined (spherical) detonations. This statement, however, [illegible] be tempered by the fact that limited data is used here. Certainly, more [illegible] is needed for the refinement of the results.

Another point that must be made, is the fact that our experimental results indicate that the piston work duration is approximately 40 times the induction time. This is in contrast to the numerical results of (4) which shows that a more plausible duration would be equivalent to the induction time. If such a

piston duration were to be assumed here t e predicted critical energy for the spherical case would be orders of mag itude lower than our prediction and would certainly be far off from the e perimental results of Bull (12).

VII. CONCLUS ONS

1. A shock tube method was used to dete nine the relation between critical energy and power necessary for the c rect initiation of a planar detonation in a stoichiometric H_2-ai mixture originally at 1/2 atmosphere.
2. It is shown that the results could b extrapolated to cylindrical and spherical geometries.
3. Based on this extrapolation, the cri ical energy for H_2-air is found to be equal to 5850 J for an unconfi ed detonation, in reasonable agreement with the experimentally f i value of 4700 J.
4. For initiation at a shock Mach num i equal to the CJ Mach number, it is found that the source work should have a duration = 40 times the CJ induction time. This factor needs to be verified for other initiation Mach numbers.

VIII. NOMENCLATURE

a = velocity of sound

E = energy

$\bar{E}$ = non-dimensional energy

k_α = geometric factor ($k_0 = 1$, $k_1 = \pi$, $k_2 = 4\pi/3$

ℓ_4 = driver length

M = Mach number

p = pressure

P = power

$\bar{P}$ = non-dimensional power

R = wave distance from diaphragm

u_1 = wave velocity

u_2 = velocity downstream of wave

$\bar{u}_2$ = convective velocity of gases behind the wave

t = time

$\bar{t}$ = non-dimensional time

X_c = location at which rarefaction wave overtakes shock

α = geometric index = 0 for planar, 1 for cylindrical and 2 for spherical geometry.

γ = ratio of specific heats

ρ = density

τ = induction time

Subscripts

$_4$ = original condition

$_1$ = condition ahead of wave

$_2$ = condition behind wave

$_c$ = cylindrical

$_s$ = spherical

$_{CJ}$ = Chapman-Jouguet

IX. REFERENCES

1. Bach, G., Knystautas, R., and Lee, J. H., Thirteenth Symposium (International) on Combustion, p.1097, The Combustion Institute, Pittsburgh, (1971).

2. Lee, J. H., Knystautas, R., and Guirao, C., Fifteenth Symposium (International) on Combustion, p.53, The Combustion Institute, Pittsburgh, (1975).

3. Knystautas, R., and Lee, J. H., Combust. Flame, v.27: p.221 (1976).

4. Abouseif, G. E. and Toong, T. Y., Combustion and Flame, v.45, p.39 (1982).

5. Lee, J. S. H., Annual Review of Physical Chemistry, v.28, p.75 (1977).

6. Fox, G., "An Experimental Study of the Relaxation Zone Behind Shock Waves in Water-Air Mixtures with Emphasis on Drop Breakup", Ph.D. Dessertation, Department of Mechanical Engineering, University of Connecticut, Storrs, Conn. (1976).

7. Dabora, E. K., "Variable Energy Blast Wave Trajectories - Approximate Solutions", Department of Mechanical Engineering Report, University of Connecticut, Storrs, CT (1973).

8. Oran, E. and Kailasanath, K., private communication.

9. Oran, E. S., Young, T. R., and Boris, J. P., Seventeenth Symposium (International) on Combustion, p.43, The Combustion Institute, 1979.

10. Oran, E. S., and Boris, J. P., Prog. Energy Combust. Sci. 7, 1 (1981).

11. Westbrook, C. K., private communication.

12. Atkinson, R., Bull, D. C. and Shuff, P. J., Combustion and Flame, v.39, p.287 (1980).

13. Westbrook, C. K., "Hydrogen Oxidation Kinetics in Gaseous Detonations", to be published in Combustion Science and Technology.

14. Bull, D. C., Elsworth, J. E. and Shuff, P. J., Combustion and Flame, v.48, p.7 (1982).

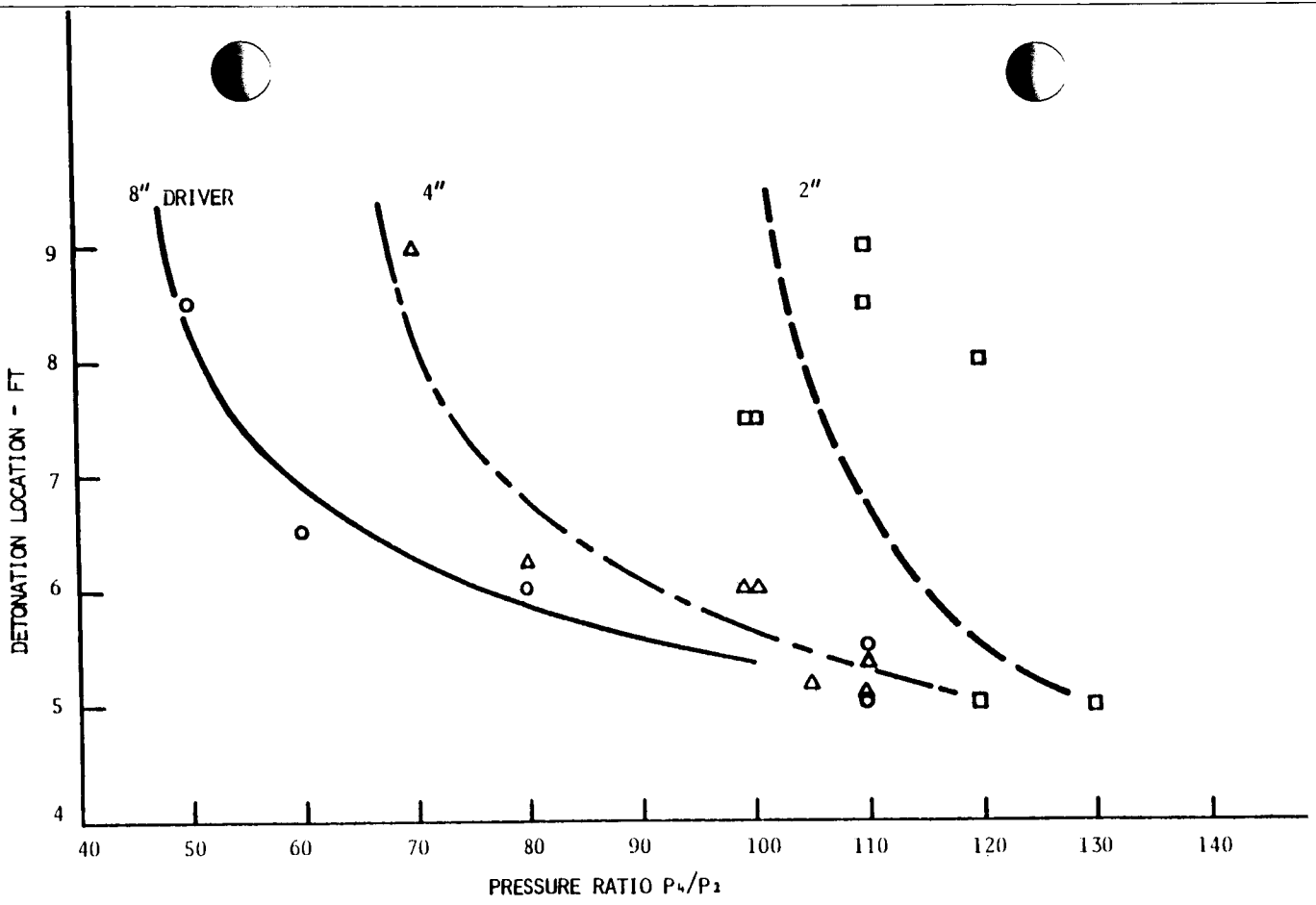
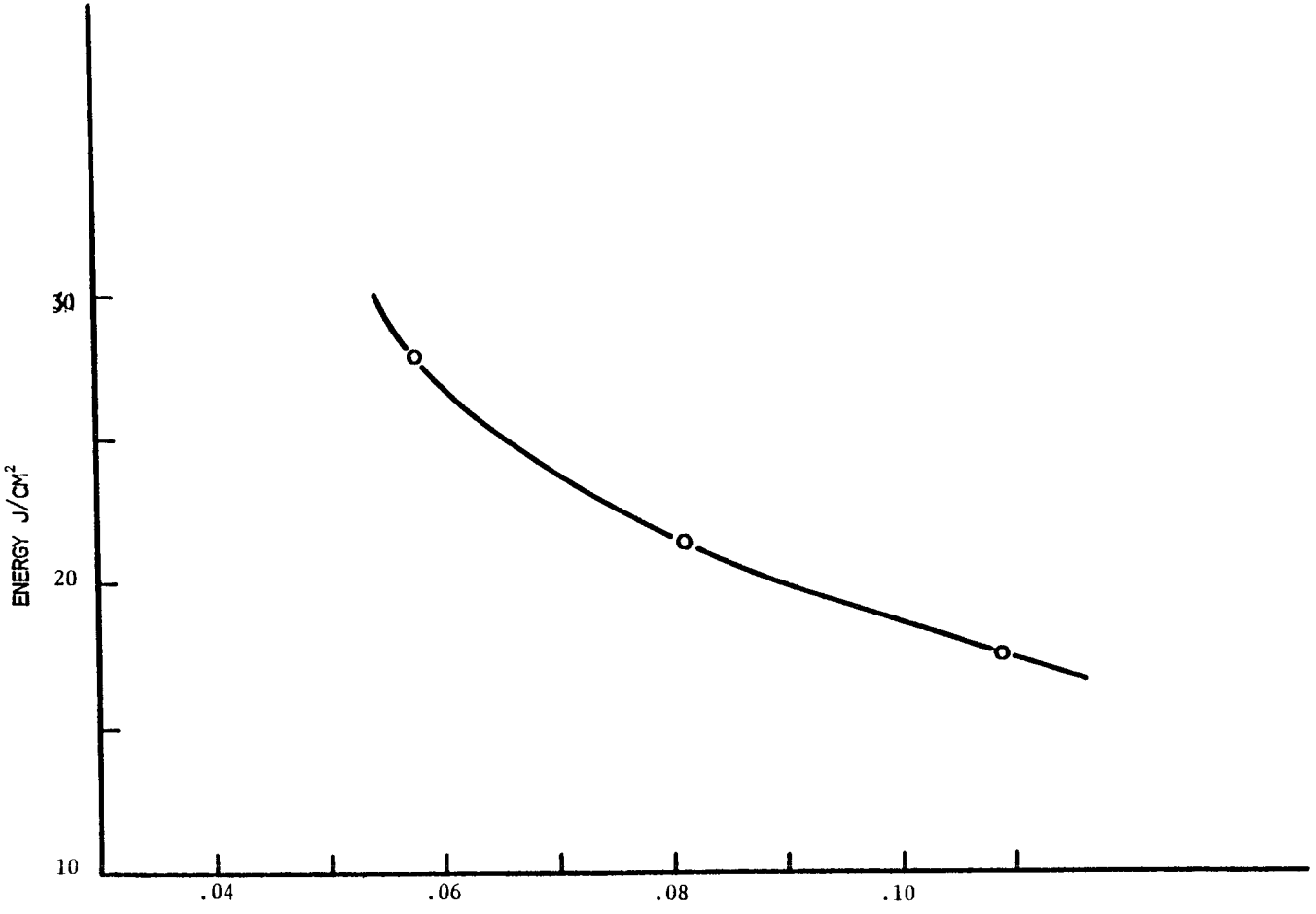


FIG. 1. DETONATION LOCATION VS. DIAPHRAGM PRESSURE RATIO



F[illegible]. ENERGY-POWER RELATION FOR STOICHIOMETRIC H_2-AIR AT P_1 = .5 [illegible]

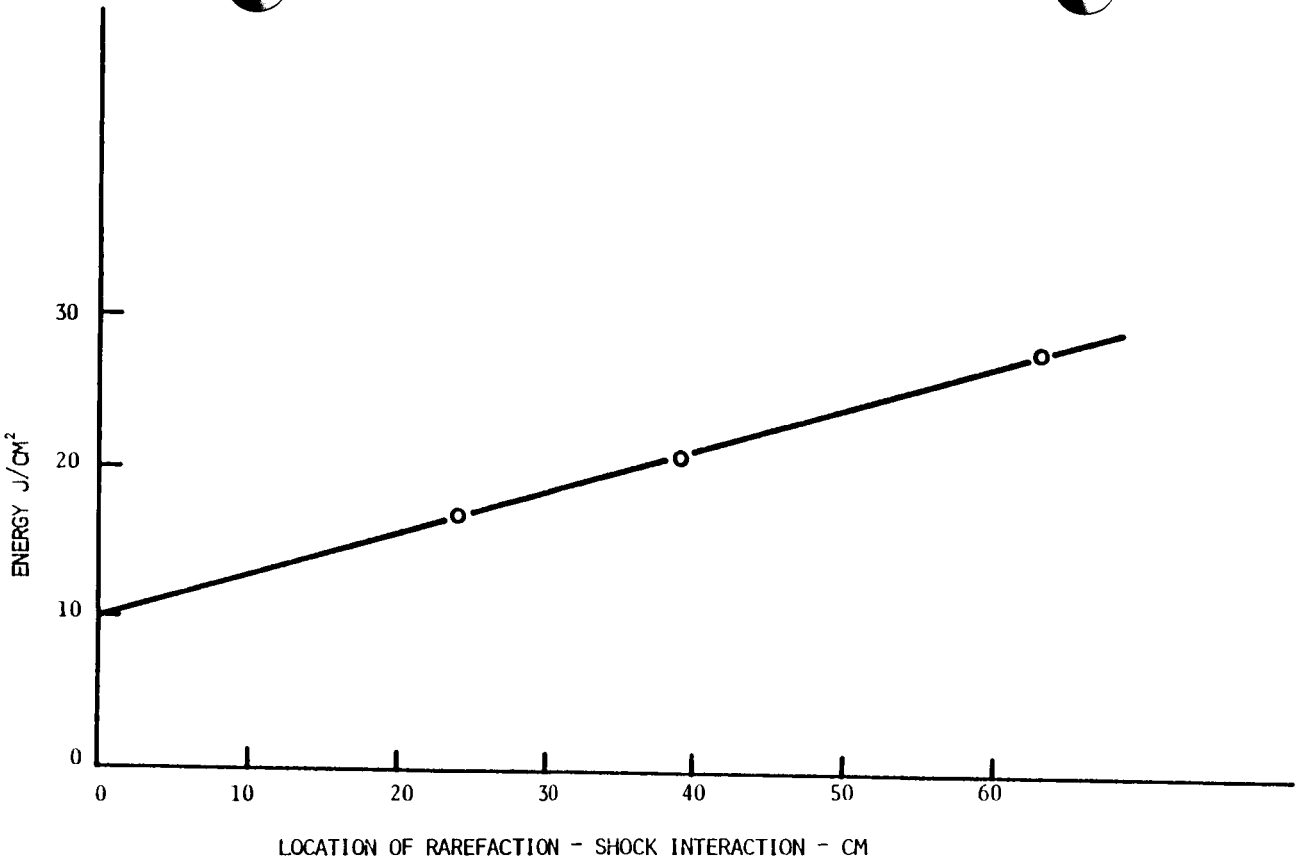


FIG. 3. ENERGY AS RELATED TO RAREFACTION - SHOCK LOCATION

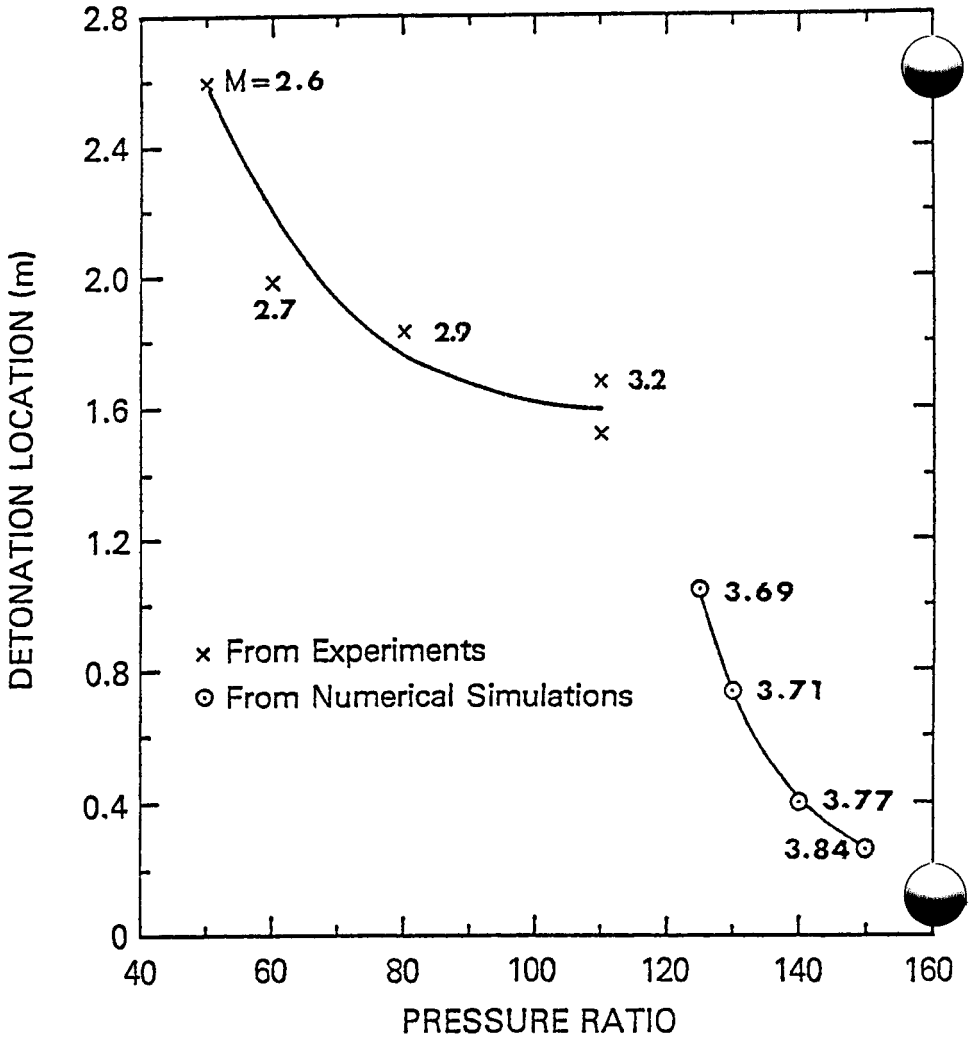


FIG. 4 COMPARISON BETWEEN EXPERIMENTAL RESULTS AND NUMERICAL CALCULATIONS OF REF(8) FOR THE 8'' DRIVER

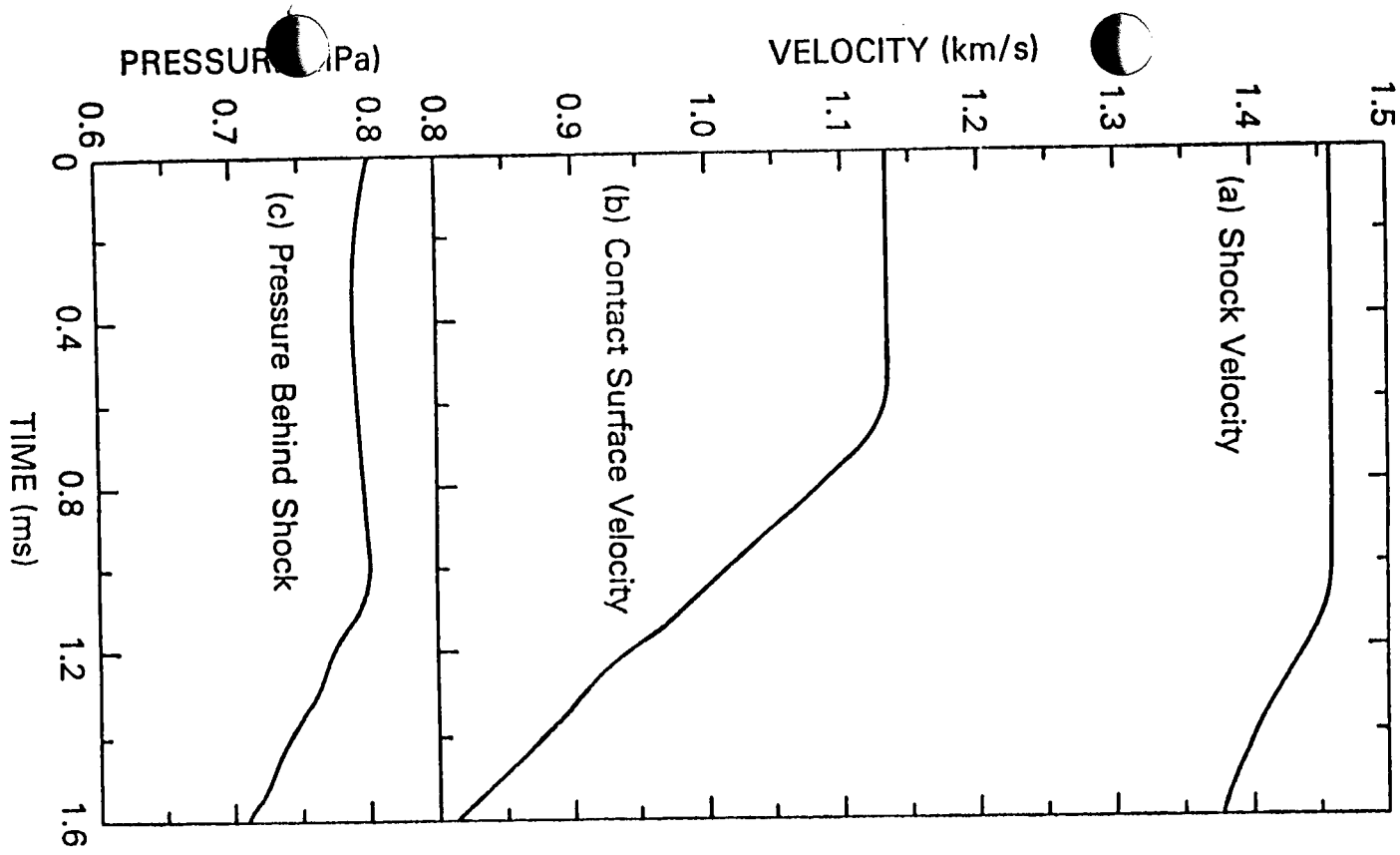


FIG. 5 THE VARIATION OF SHOCK VELOCITY, CONTACT SURFACE VELOCITY AND SHOCK PRESSURE WITH TIME (REF.8). 8" DRIVER, PRESSURE RATIO = 110

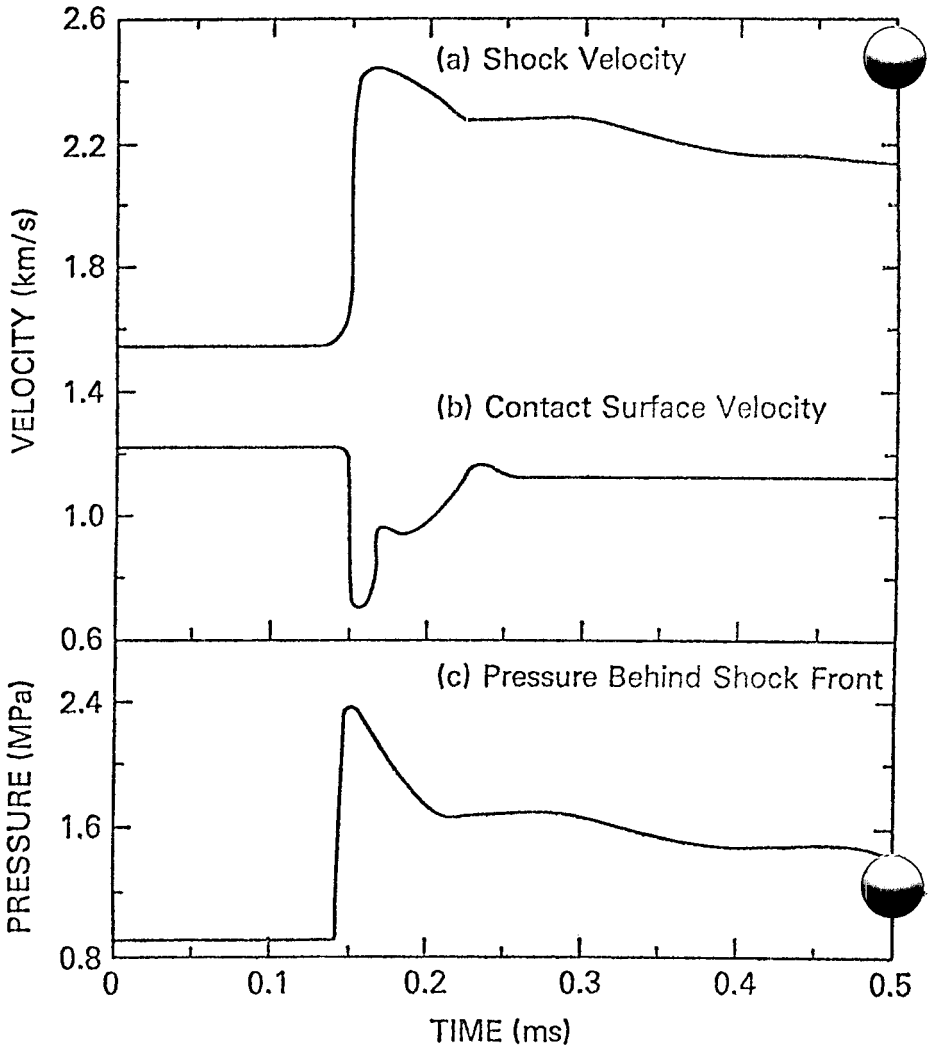


FIG. 6 VARIATION OF SHOCK VELOCITY, CONTACT SURFACE VELOCITY AND SHOCK PRESSURE WITH TIME (REF.8). 8" DRIVER, PRESSURE RATIO = 150

LARGE SCALE HYDROGEN-AIR DETONATIONS†

W. B. Benedick
Sandia National Laboratories
Albuquerque, N. M. 87185

J. H. Lee, R. Knystautas, C. M. Guirao
McGill University
Montreal, P. Q. Canada H3A, 2K6

Abstract

The rich and lean detonation limits of hydrogen-air mixtures are dependent upon critical dimensions of the detonation channel. Extrapolation of laboratory scale hydrogen-air detonations, verified by some large scale detonations, increases confidence for further extrapolation to the very large dimensions associated with reactor containment buildings.

We have complemented the laboratory scale experiments performed at McGill University with large scale experiments. Both rich and lean hydrogen-air mixtures were confined in thin-wall (100μ m) transparent polyethylene envelopes to provide minimum lateral support. The diameter of the envelopes ranged from 0.75 to about 2 m depending upon the mixture under study.

For the critical tube diameter experiments, the polyethylene tube was attached to a steel tube which was generally smaller than the polyethylene tube. High explosive was used to launch a detonation in the steel tube, the emergent detonation wave then propagated into a larger diameter plastic envelope.

We will describe the experimental techniques used to perform these large scale detonation experiments and show some high speed cinematographic records of the experiments. The experimental results will be incorporated into another paper presented by the McGill Univ. experimenters.

†This work performed at Sandia National Laboratories supported by the U. S. Nuclear Regulatory Commission.

The critical tube diameter is the diameter of the smallest tube which will propagate a planar detonation into an unconfined region as an expanding spherical detonation. Experimental evidence[1] indicates that the critical tube diameter is approximately equal to 13 times the detonation cell size, λ. The cell size is a measure of the fundamental signature pattern formed by the transverse shocks which are inherent in a detonation wave, and is a function of the mixture composition. Our work in large-scale detonation tubes is carried out in conjunction with research at McGill University. At McGill, the cell size is measured, as a function of mixture composition, using small-scale detonation tubes. Special emphasis has been placed on lean- and rich near-limit compositions of hydrogen and air. (Direct measurement of the critical tube diameter was made at McGill only for a stoichiometric mixture since 13λ = 20 cm for this mixture, and 20 cm is the diameter of the largest detonation tube at McGill.)

To supplement the McGill detonation cell size measurements, several field-scale experiments were performed using 91-cm and 121-cm diameter steel tubes to launch a planar detonation into a thin-wall (100μm) plastic tube extension attached to one end of the steel tube. The thin-wall polyethylene extension provides minimal support to the propagating detonation wave and may be used to obtain critical-tube-diameter data.

Figure 1 shows the physical layout of the experiment. The 91-cm diameter steel tube was 2.03 m long, and the 121-cm diameter tube was 3.05 m long. DuPont sheet explosive type EL506C1* was used to initiate a hydrogen:air detonation in the steel tube. The total weight of explosive used, including detonator, was 62 g. A plastic hose was used to conduct both air and hydrogen to a point at the rear of the mixing fan.

To the opposite end of the steel tube is attached a long (4.57 m) polyethylene tube. To obtain the desired hydrogen:air mixture, a portion of the polyethylene tube is pulled back over the steel tube and secured to exclude air from this predetermined fraction of the overall length. Air is then introduced to fully inflate this foreshortened tube, whereupon the restraint is released from the polyethylene tube which had been retracted over the steel tube. With the mixing fan running, hydrogen is then introduced to fully inflate the polyethylene tube. The ratio of the retracted length to the overall length represents the hydrogen fraction in the mixture.

Based on the McGill cell-size measurements (see Fig. 2), the critical hydrogen:air mixtures were calculated for the 91- and 121-cm diameter tubes. The tubes were then filled with hydrogen:air mixture which bracketed the critical mixture for each tube diameter. Photometric coverage indicated whether the detonation emerging from the steel tube continued or failed to propagate along the full length of the transparent polyethylene tube extension.

*DuPont EL605C1 sheet explosive is a thin (1 mm), flexible, plastic-bonded explosive containing 63 percent PETN and 8 percent nitrogen cellulose with a detonation velocity of 7 km/sec.

For those tubes of diameters 91 and 121 cm, the (lean) critical fuel concentrations are 19.7 and 18.6 percent H_2, respectively. These large-scale results do fall into the range predicted by cell-size measurements using the $d_c = 13\lambda$ correlation as shown in Fig. 3.

For the rich hydrogen mixtures, our first set of experiments used thin-wall plastic tubes that were the same diameter as the steel tube used to launch the detonation. Detonations were seen to propagate in thin plastic tubes for much richer mixtures than predicted from the McGill cell-size measurements. Because of the high acoustic velocity in the rich mixtures, the propagation distance (~3 m) in the plastic tube may have been insufficient for the detonation to become unstable and fail to propagate. This observation led to a change in experimental technique which employs both larger diameter plastic tubes and longer propagation distances. Larger diameter plastic tube extensions were used in order to minimize the effect of confinement afforded by the tube walls.

The new plastic envelopes (see Fig. 4) were made with a neck the same size as the steel tube, then tapered radially outward over a 60-cm length to a diameter that is 60-cm larger than the steel tube. They were about 6-m long. The neck of the plastic tube was pulled over the steel tube about 70 cm from the throat and attached with tape. The opposite end of the steel tube was closed with a thin polyethylene cover. A vacuum line was attached to the inlet hose in the cover and a vacuum pump was used to pull the plastic tube into the steel tube and to remove all air from the enclosed volume.

Rich hydrogen:air mixtures were then blended in the VGES burn tank. Mixture control was attained by measuring partial pressures of air and hydrogen. The gases were fan mixed in the tank and conducted by hose to the steel/plastic-tube experimental apparatus. Sheet high explosive (100 to 250g) was taped to the polyethylene cover on the steel tube to launch the detonation. When fully inflated with the premixed hydrogen:air, the high explosive was detonated. The hydrogen:air detonation then proceeded down the steel tube and upon emerging, was free to expand into the larger-diameter plastic tube.

With this experimental technique, good agreement with the McGill data was obtained. Allowing for our low ambient pressure (830 kPa, .83 atm), the data points are within 1% of the mixtures predicted by the McGill cell-size measurements, as shown in Fig. 3. For tube diameters of 76, 91, and 121 cm, the (rich) critical fuel concentrations are 52, 53, and 55.5 percent H_2, respectively.

Using the same construction techniques employed for the rich mixtures, lean mixture experiments were also performed with the 76 cm diameter tube. The lean critical fuel concentration was 20% for the 76 cm tube diameter.

References

1. D. H. Edwards, G. O. Thomas, and M. A. Nettleton, J. Fluid Mech. 95, 79 (1979).

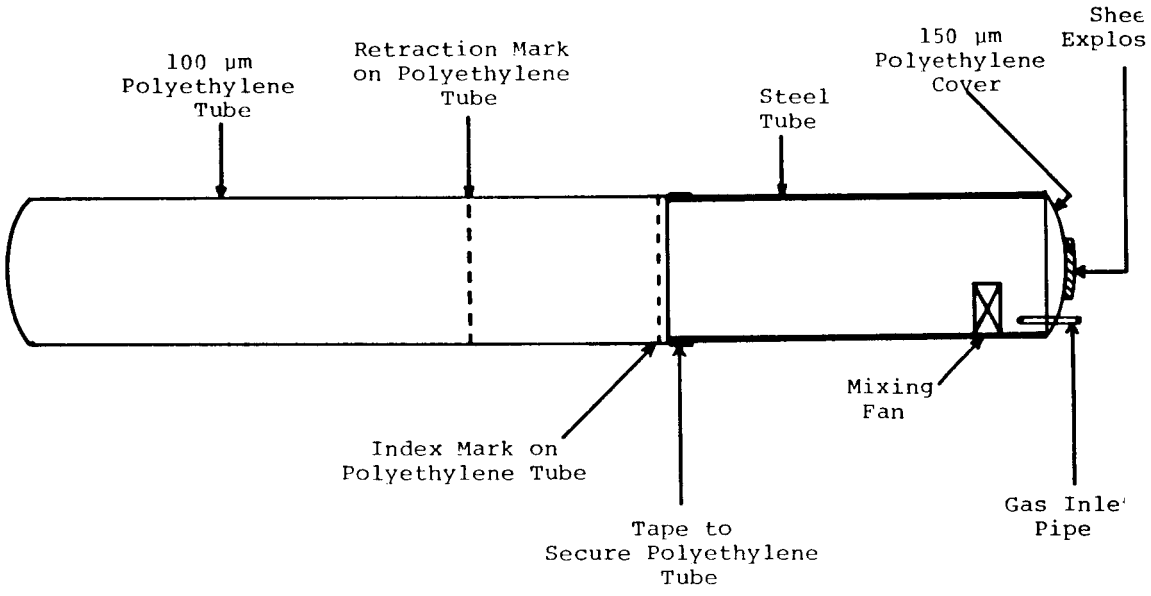


Figure 1, Critical-tube-diameter test facility; first version, polyethylene tube diameter = steel tube diameter.

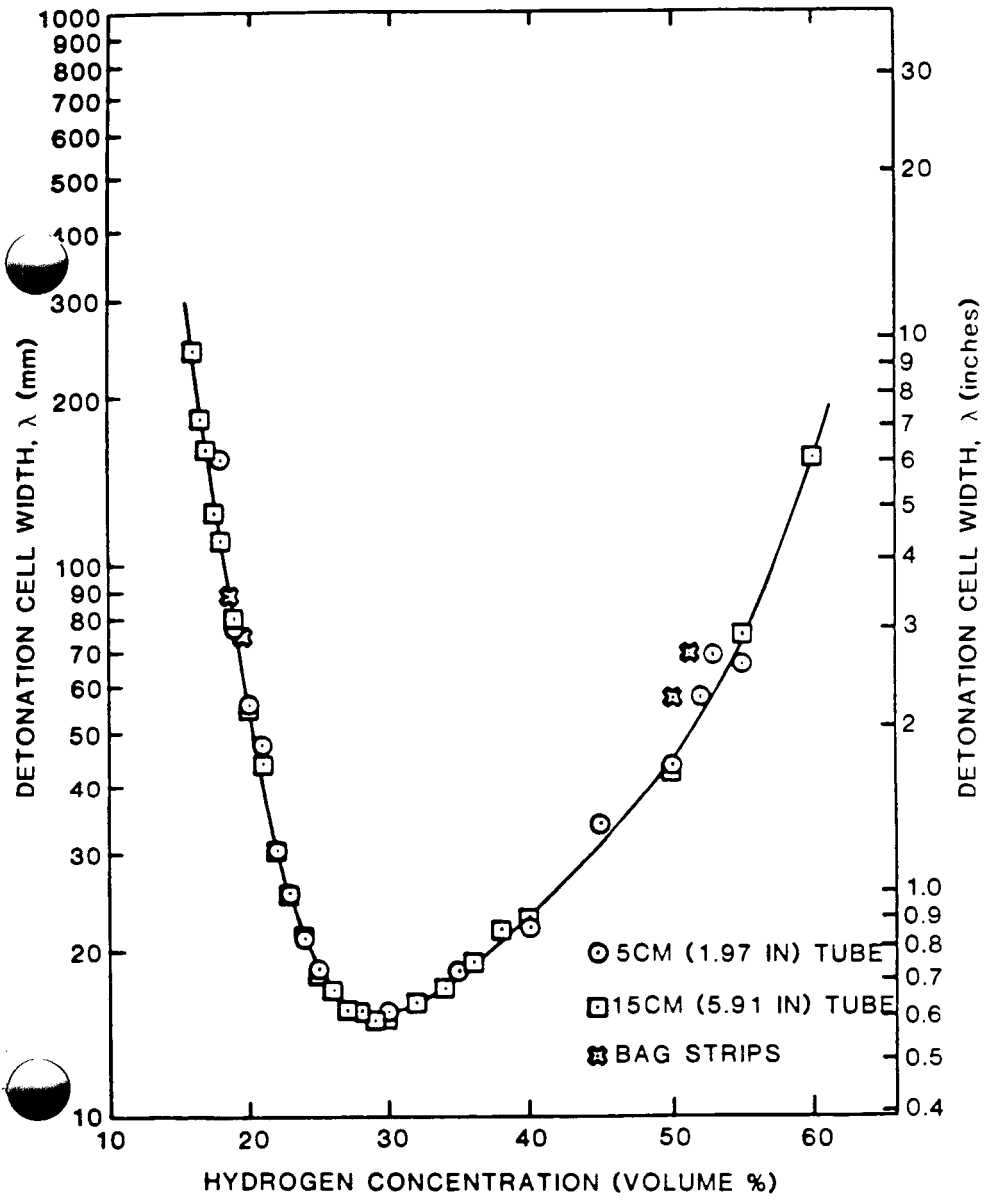


Figure 2, Detonation cell width measurements taken at McGill University (also shown are measurements inferred from polyethylene bag fragments in the Sandia Experiments).

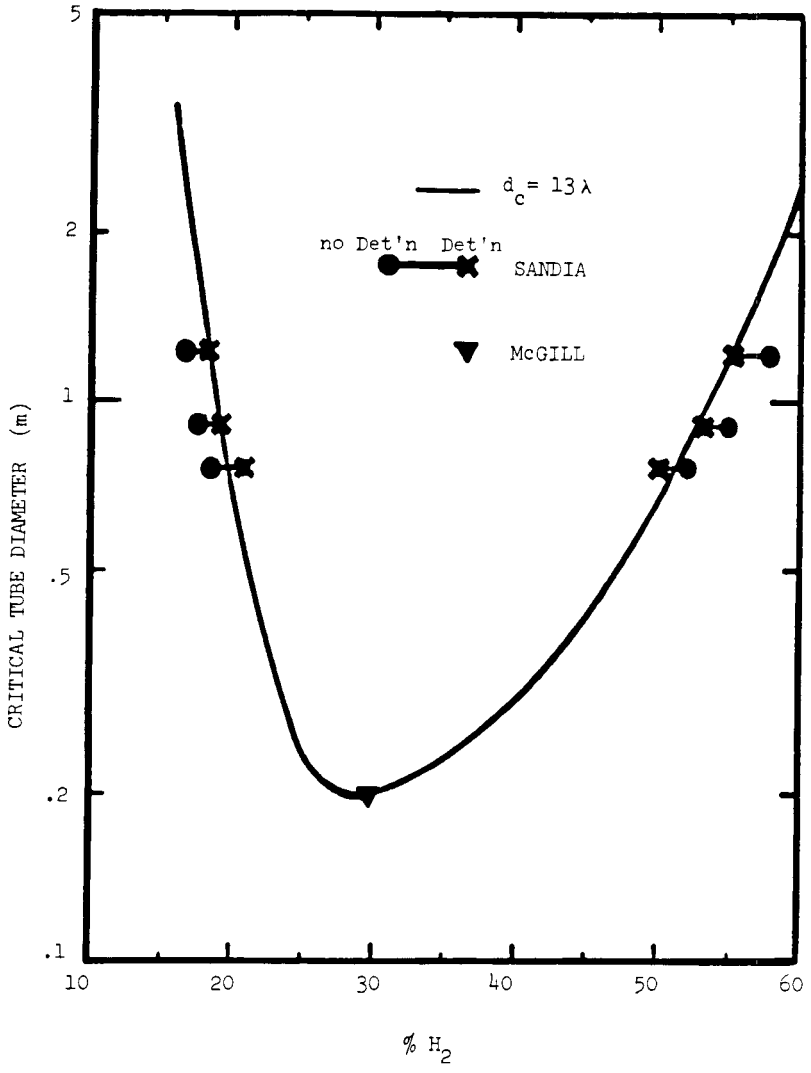


Figure 3, Critical-tube-diameter measurements at Sandia and McGill compared to $d_c = 13\lambda$ correlation.

959/960

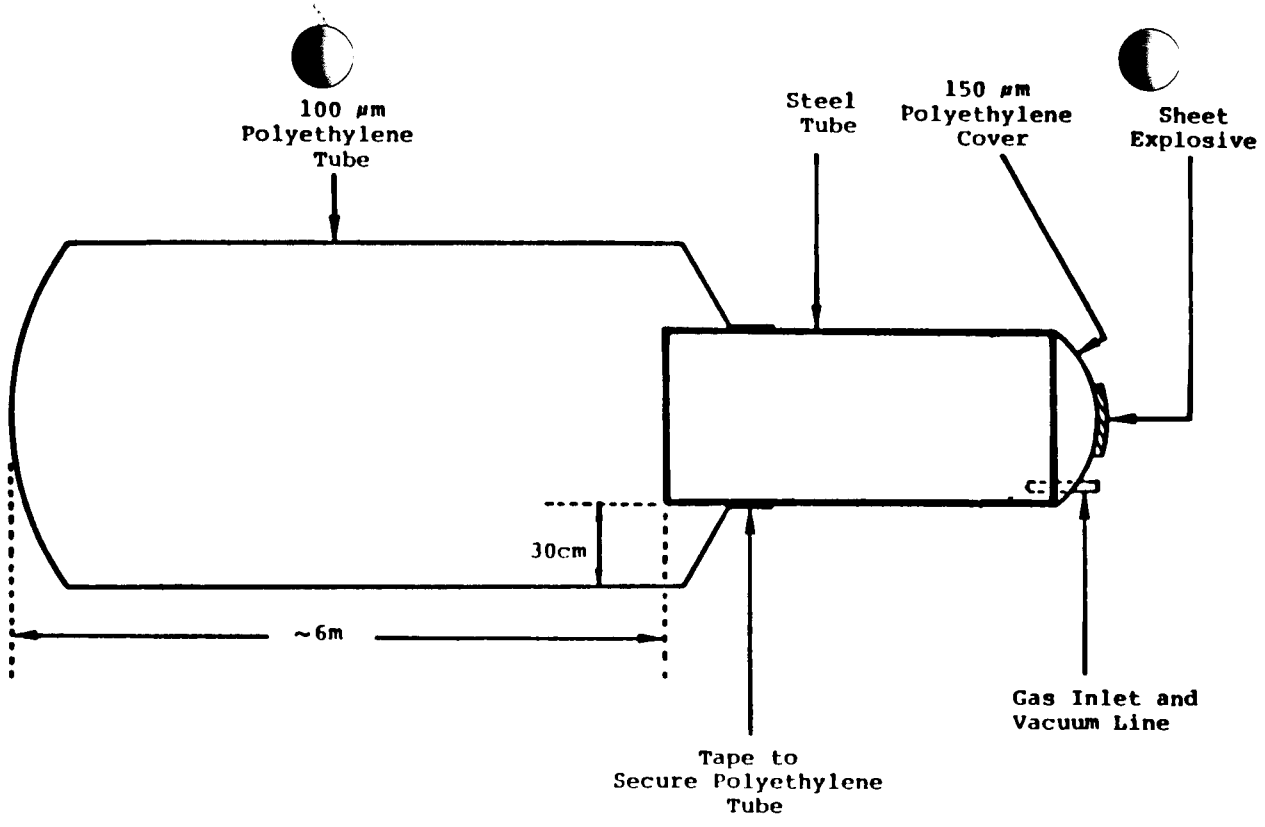


Figure 4, Critical-tube-diameter test facility; second version, polyethylene tube diameter > steel tube diameter.

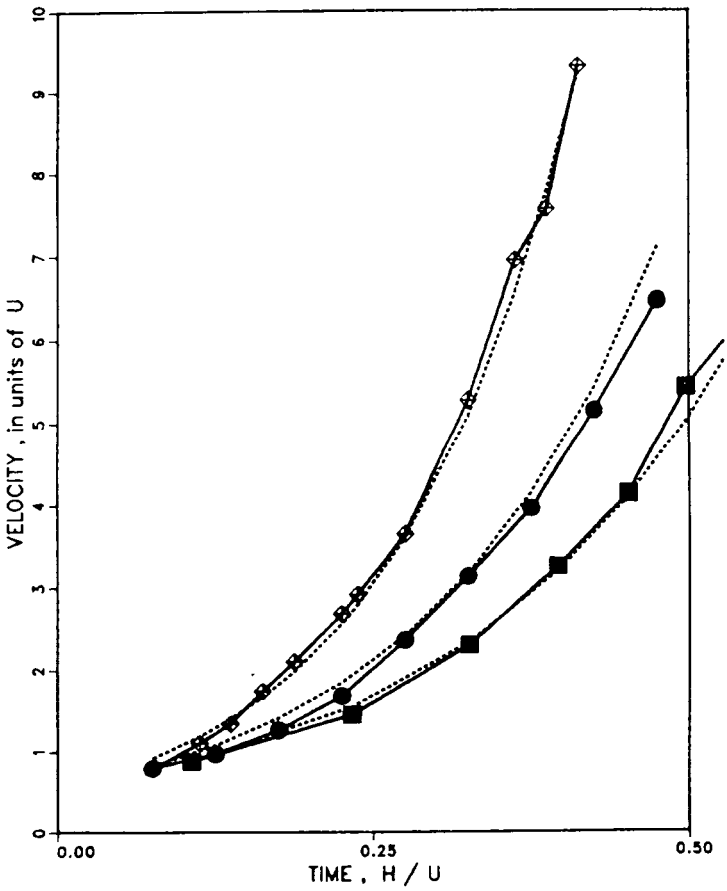


Figure 7. Variation of exit flow velocity with injection velocity with the constraint of constant injected mass. The exit velocities are from Figures 2, 3 and 4 and the dotted lines represent an exponential fit. Chamber configuration is that of Figure 1.




HYDROGEN-AIR DETONATIONS

J. H. S. Lee, R. Knystautas and C. Guirao
Shock Wave Physics Research Laboratory
Mechanical Engineering Deparment
McGill University
Montreal, Canada

and

W. B. Benedick and J. E. Shepherd
Sandia National Laboratories
Albuquerque, New Mexico 87185
SAND82-1864C

ABSTRACT

General gaseous detonation propagation phenomena are briefly discussed. The importance of cellular structure and cell size to detonation initiation, transmission and failure is emphasized. Experimental measurements of cell size λ for hydrogen-air-carbon dioxide mixtures are presented; the hydrogen/air volume ratios range between 0.16 and 1.5 and the carbon dioxide mole fractions are 0, 0.05, 0.10 and 0.15. Cell sizes are a minimum for both diluted and undiluted hydrogen-air mixtures near stoichiometric (i.e., hydrogen/air = 0.4). Minimum cell sizes for carbon dioxide mole fractions of 0, 0.05, 0.10 and 0.15 are 1.51, 2.05, 4.2 and 15.0 cm, respectively. Results of large- and small-scale critical tube diameter (d_c) measurements are presented and show good agreement with the empirical scaling law, $d_c = 13\lambda$. Mean detonation velocities and pressures have been measured and compared to the theoretical Chapman-Jouguet values. Critical energies for direct initiation by high explosives have been calculated from the detonation kernel theory and the measured cell sizes. These energies are in good agreement with previous critical charge mass experiments of Elsworth for hydrogen-air mixtures and demonstrate the remarkable desensitizing action of small amounts of an inert diluent. Addition of 15% carbon dioxide to a stoichiometric hydrogen-air mixture is predicted to raise the critical initiation energy from 5 kJ (1 g tetryl) to 4.1 x 10^3 kJ (820 g tetryl). A comprehensive kinetic scheme for hydrogen oxidation has been used in a one-dimensional reacting flow computation to predict idealized, steady-state reaction zone structures of the ZND detonation model. The calculated reaction zone thickness Δ, determined by the distance behind the shock wave at which the Mach number is 0.95, is found to be approximately proportional to the measured cell size, $\lambda = A\Delta$, where $A \cong 24.2$. Using a slightly more elaborate scaling, this simple model can accurately predict the effect of carbon dioxide dilution on the cell size. No evidence is found in the calculations of a limiting hydrogen concentration below which detonations cannot exist; however, a strong dependence on reaction mechanism and the thermodynamic path is observed for very lean (<15% hydrogen) mixtures.

1. Introduction

Due to the sensitivity of H_2-air mixtures, local detonations cannot be ruled highly improbable. Realistic probability risk assessment requires an accurate knowledge of the dynamic detonation properties of H_2-air mixtures (e.g., detonability limits). Existing data on H_2-air detonations are very limited and are of questionable accuracy since in most cases they were derived from experiments performed in detonation tubes of small dimensions. In an effort to produce reliable information on H_2-air detonations, a joint study between McGill University and Sandia National Laboratories, Albuquerque (SNLA) was initiated. The main objective of the program is to determine the dynamic properties of H_2-air detonations and the effect of inert additives (e.g., CO_2, steam) and inhibitors (halogenated compounds) on these dynamic detonation properties. Dynamic detonation properties refer to those parameters that depend on the sensitivity of the mixture (i.e., detonability limits, initiation energy, critical tube diameter). The equilibrium Chapman-Jouguet (C-J) detonation properties (i.e., detonation velocity, pressure, etc.) based on energetics do not reflect the sensitivity of the explosive mixture. The present paper is a progress report of the current status of the program.

2. Detonation Cell Size

The basic approach used in this program is to determine the characteristic detonation cell size λ. From the cell size, detonation limits and critical tube diameter d_c are deduced. The critical energy for direct initiation E_c is also determined indirectly from the cell size data via the critical tube diameter.

The link between the detonation cell size "λ" and all the dynamic detonation properties has been established only in the past few years. Thus, it would be worthwhile to review briefly these fundamental correlations for the benefit of those not intimately familiar with the recent developments in the field.

Although the mean detonation characteristics (i.e., velocity, pressure) are usually quite close to the values predicted from the equilibrium Chapman-Jouguet theory, the observed structure of the detonation front is far from that given by the one-dimensional Zeldovich-Von Neumann-Döring (ZND) model of a smooth shock front followed by a planar reaction zone. Instead, the detonation front possesses a three-dimensional cellular structure formed by the multiple interactions of transverse shock waves with the main shock front. Figure 1 shows an instantaneous head-on view snapshot obtained when a detonation collides with a glass plate coated with soot. Figure 2 shows the characteristic "fish scale" pattern left on a smoked foil as a cellular detonation sweeps by. The patterns in both of these figures are produced by the motion of the triple-points or shock intersections between the main shock and the transverse waves. The detailed transient structure of the cellular detonation front is described in the papers of Strehlow and co-workers[1-3] among others.[4,5] What concerns us here is that the characteristic cell size of the detonation (which can readily be determined from the "fish scale" pattern left on the smoked foil) gives a direct measure of the overall reaction zone length of the cellular detonation front. The overall chemical reaction zone length corresponds to the length of a detonation cell which is

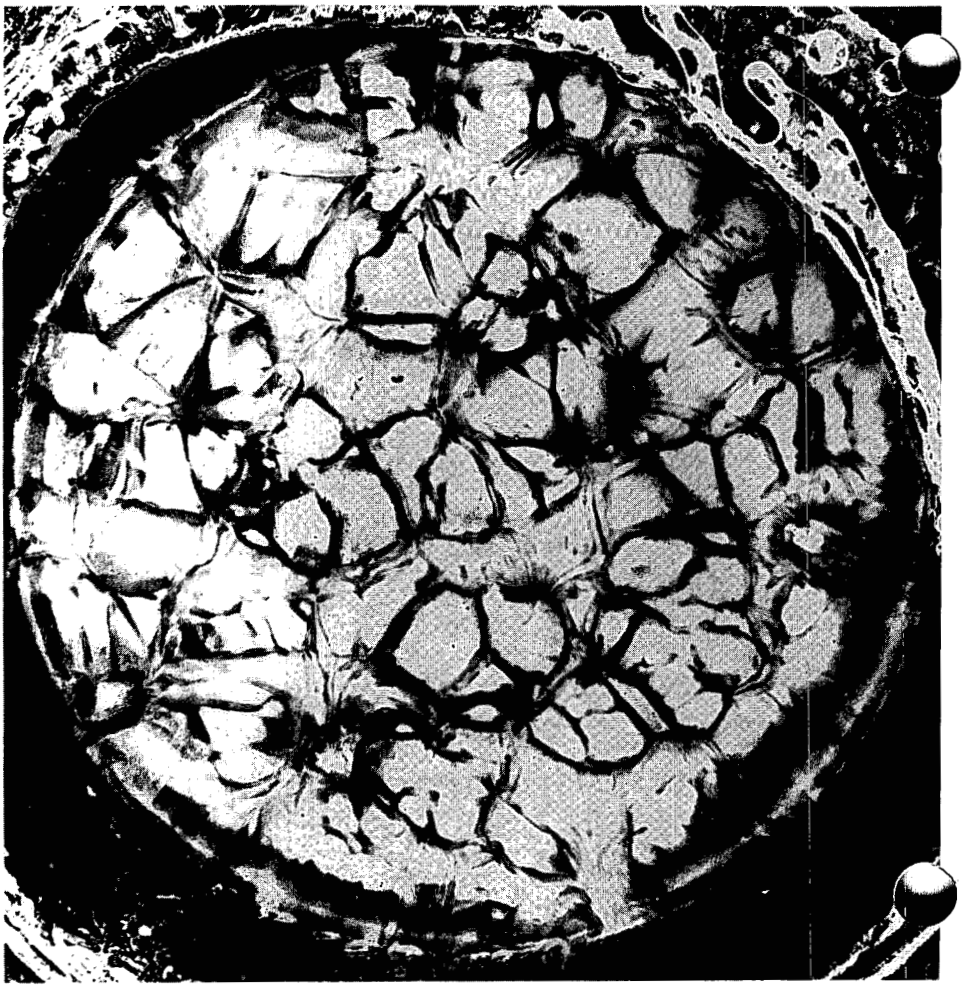


Figure 1. Cellular structure of a detonation front recorded by a head-on impact with a soot-coated glass plate.

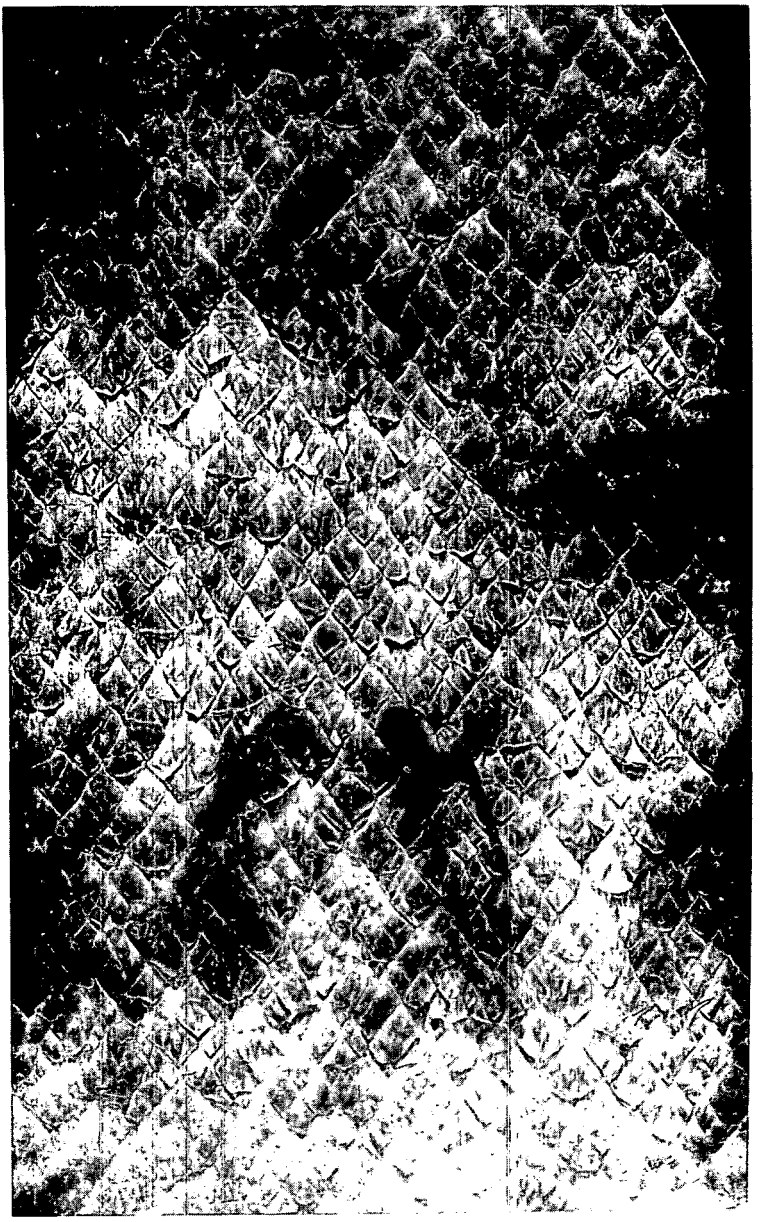


Figure 2. Typical smoked-foil record of detonation cell structure.

approximately 1.6 times the transverse dimension, which we refer to as the cell diameter λ.[6] Note that when the characteristic dimension of the cellular structure is being described, the terms cell size, width and diameter are used interchangeably. However, in all quantitative discussions of cell sizes and in reporting experimental measurements, it is specifically the cell diameter that is being referred to. Since all the important dynamic detonation parameters are functions of the characteristic reaction zone length (or time) of the detonation, the cell size obtained from smoked foil measurements permits a direct estimate of these dynamic parameters.

3. Critical Tube Diameter

The first important dynamic detonation parameter to be correlated to the detonation cell size λ is the critical tube diameter d_c. The critical tube diameter refers to the minimum diameter of a detonation tube from which a planar detonation can emerge into an unconfined volume containing the same mixture, and transform to a spherical detonation without failure and continue to propagate as a detonation. This critical tube diameter is a unique function of the properties of the explosive mixture (i.e., fuel composition, initial thermodynamic states). The correlation between the critical tube diameter and the cell size was first pointed out by Mitrofanov and Soloukhin[7] who, on the basis of their experiments on the diffraction of detonations in low pressure C_2H_2-O_2 mixtures ($p_o \simeq 70$ torr), reported that $d_c \simeq 13\lambda$ for circular tubes and $W_c \simeq 10\lambda$ for a rectangular channel of width W and height approximately W/2.

Edwards et al[8] later repeated experiments in the same mixture and confirmed Mitrofanov's earlier observations. An extensive experimental program in which cell sizes as well as critical tube diameters were measured simultaneously by Knystautas et al.[9] for all the common gaseous fuels (i.e., CH_4, C_2H_2, C_2H_4, C_2H_6, C_2H_6, C_3H_8, [illegible], C_4H_{10}, MAPP and H_2), has firmly established the general validity of the $d_c = 13\lambda$ correlation for these detonable mixtures. The universality of this simple correlation also indicates that a single parameter, λ, can be used to characterize the sensitivity of a given explosive mixture to detonation. In other words, mixtures with the same λ have the same sensitivity. With the simple $d_c = 13\lambda$ correlation, critical tube diameters can be determined via measuring the cell size in an apparatus which is an order of magnitude smaller than that required for the direct measurement of d_c itself.

4. Initiation Energy

In addition to the recent studies on cell size and critical tube diameter, direct measurement of the critical energy E_c required for initiation has been more commonly used to assess the sensitivity of fuel-air mixtures to detonation. The critical initiation energy or equivalently the critical mass of a high explosive charge is usually obtained experimentally in large-scale (5-10 m^3), unconfined geometries (plastic bags) and the results appear as a U-shaped curve when the minimum initiation energy or charge mass is plotted (ordinate) against the fuel composition (abcissa). The minimum energy usually corresponds to the stoichiometric composition. The sharp increase of the critical initiation energy as the fuel composition

deviates from stoichiometry is often used to arbitrarily set the lean and rich limits of detonability. Since the critical charge mass is proportional to the cube of the reaction zone length, the rapid increase in the reaction length as the mixture composition approaches the limits results in extremely large increases in initiation energy. When large quantities of high explosives are used as an initiator, the detonation will initially be strongly overdriven and observations must be made at very large distances to determine if the detonation is truly self-sustaining. Thus, very large-scale experiments are required for the measurements of E_c in insensitive, near-limit mixtures. On the other hand, if E_c is linked to λ, then relatively small-diameter detonation tubes can be used to determine E_c via λ.

Such correlation between E_c and λ has been proposed by Lee et al.[10] The first step is to link E_c with the critical tube diameter d_c. Although a model for this based on the work done by the detonation on the surrounding gas has been proposed earlier by Lee and Matsui,[11] recent developments are based on the idea that a minimum surface energy is required before a planar detonation wave can evolve into a self-sustaining spherical detonation wave without being quenched by expansion waves generated during the diffraction process. This minimum surface energy is equal to product of the energy per unit surface area and the cross-sectional area of the critical tube, $\pi d_c^2/4$. In order to relate this to direct initiation by a high explosive charge, we introduce the concept of a critical detonation kernel.[12] A critical detonation kernel is that volume of reacting gas whose chemical energy release

rate is just sufficient to overcome energy losses and initiate a self-sustaining detonation. For direct initiation by blast waves, the critical detonation kernel is the sphere enclosed by the blast wave when it has decayed to the Chapman-Jouguet velocity. Equating the surface energy of a detonation propagating in a tube of critical size to that of a critical detonation kernel and assuming that the energy per unit surface area is the same, we find that the surface area of the critical detonation kernel must be equal to the cross-sectional area of the critical tube. This implies that the radius R^* of the critical detonation kernel is given by $R^* = d_c/4$. From strong blast wave theory, the blast energy can readily be related to the blast radius and shock strength. Thus, the critical initiation energy can be obtained as

$$E_c = 4\pi\rho_o V_{CJ}^2 I \left(\frac{d_c}{4}\right)^3$$

and with $d_c = 13\lambda$, we write

$$E_c = \frac{2197}{16}\ \pi\rho_o V_{CJ}{}^2 I \lambda^3 \qquad (1)$$

where ρ_o is the initial density of the mixture, V_{CJ} the C-J detonation velocity, λ the cell size and I is a numerical constant (for $\gamma = 1.4$, $I = 0.423$). Expression (1) is the desired correlation between initiation energy E_c and cell size λ mentioned above.

5. Detonation Limits

Detonability limits are usually determined experimentally in tubes. For a given tube diameter, it is found that two limiting fuel concentrations exist (a lean and rich fuel concentration)

beyond which a stable detonation cannot be obtained. Near the limits, detonations are very hard to initiate and strong initiators (i.e. large quantities of high explosives) are required. For this reason, very long tubes must be used to ensure that the influence of the ignitor is negligible; presently, there exists no reliable criterion for determining the minimum tube length for a given ignition source strength. It is also clear that the limits must depend on the tube diameter since losses to the wall cannot be ignored near the limits when the reaction zone length is of the order of the tube diameter. Therefore, limits are only meaningful if the tube diameter is specified and if the tube is long enough for the influence of the igniter to be negligible. Previously reported data that do not specify the tube length, igniter strength and the tube diameter are of limited validity. Moreover, limits for tubes of a certain size are certainly not the same as the limits for unconfined or very large-scale confined detonations. On the basis of recent experiments, Lee et al.[10] have proposed a criterion for detonation limits based on cell size.

Experiments within rigid tubes[13] have confirmed that the limiting condition for the propagation of a stable detonation occurs when the transverse wave structure consists of a single cell, commonly referred to as "single-head spin." In other words, when the mixture composition is varied beyond that corresponding to the onset of single-head spin for the given tube, the detonation is unstable and any finite perturbation will cause the detonation to degenerate into a deflagration. In this case, once the detonation has degenerated, transition back to detonation is no longer possible.

Thus, for a given tube diameter, the detonation limit corresponds to the composition for the onset of spinning detonation. Since spinning detonation in a round tube corresponds to $d = \lambda/\pi$ (where d is the tube diameter), knowledge of the variation of cell size with fuel type and concentration determines the detonability limits for confined detonation in tubes.

For different geometries or degrees of confinement, the composition limits differ. For example, in the case of a detonable mixture of finite thickness W bounded by one solid boundary, the composition limit can be deduced from the critical width of the two-dimensional channel for the successful transformation of a planar detonation into a cylindrical one upon emerging into unconfined space. As mentioned earlier, it is found that the critical width of a channel is approximately 10λ. Thus, based on symmetry considerations, the critical detonable thickness of a gas cloud bounded by one solid surface will correspond to 5λ. Recent experiments at McGill in very large aspect ratio channels indicate that W_c may be substantially less than 10λ instead of nearly equal to it as reported by Mitrofanov and Soloukhin[7] and Edwards et al.[8] who both used channels with aspect ratios near one. Large scale experiments at Sandia are currently being performed to better establish the relationship for this important two-dimensional geometry. In the meantime, the results of Mitrofanov and Edwards can be used to estimate the detonability limits for a large cloud bounded by a solid surface on one side.

For a completely unconfined geometry, the minimum cloud diameter required for spherical detonation must exceed the critical

detonation kernel diameter. Since we have shown above that the detonation kernel diameter D* is related to the critical tube diameter by $D^* = d_c/2$ then the minimum detonable cloud diameter is $D^* = 6.5\ \lambda$. Conversely, for a given size cloud the composition limits of detonability can be estimated from measurements the cell size.

6. Experimental Details

From the remarks above, it is clear that we consider the detonation cell size to be the single most important parameter in determining the dynamic behavior of detonations. For this reason, our experimental and theoretical program has very strongly emphasized the measurement and prediction of cell size in hydrogen-air mixtures over a wide range of concentrations. As a direct check on cell size measurements and the $d_c = 13\ \lambda$ relation, critical tube diameters were also measured. Since critical initiation energies for H_2-air mixtures have already been determined by Atkinson et al.[14] and Elsworth,[15] it will be sufficient to repeat their measurements for near-limit mixtures only in a larger scale apparatus to ensure that stable detonations are indeed achieved. Such experiments will be carried out in the near future at SNLA. Results from these three types of initiation and propagation experiments together with theoretically-based extrapolations will give us a broad data b with which hydrogen detonation hazards can be evaluated.

Cell size measurements were performed at the Shock Wave Physics Laboratory at McGill in three steel tubes (5 cm in diameter x 4 m long, 15 cm in diameter x 6.15 m long and 30 cm in diameter x 17.25 m long). In the two smaller tubes, the explosive mixtures were

prepared in a continuous flow system. The concentrations of the components were controlled by the relative flow rate monitored by flow meters. In the larger tube, the mixture composition was determined by partial pressures and a recirculating pump was used to mix the mixture components. The estimated accuracy of the mixture composition was better than ± 1%.

Direct initiation of detonation was achieved using a solid explosive charge. In the two smaller tubes, a short piece (<50 cm) of tightly coiled primacord (PETN, 22 g/m) detonated by a #8 blasting cap was used. In the larger tube, initiation was with a 20 g charge of solid explosive detonated by a #8 blasting cap.

The diagnostics provided i) average wave velocity measurements via four (five) ionization gauges located along the walls of the 15 cm (30 cm) diameter detonation tube, ii) detonation pressure measurements using piezoelectric pressure transducers[1] located approximately 5.25 m (14 m) from the ignition end of the 15 cm (30 cm) diameter tube, and iii) detonation cell diameter measurements from aluminum foil strips using the smoked foil technique. The lengths of the strips were 30 cm for the 5 cm detonation tube, 35 cm to 75 cm for the 15 cm detonation tube and 2 m for the 30 cm detonation tube. The smallest detonation tube (5 cm in diameter) was not equipped with ionization gauges or pressure transducers.

7. Results

The experimental detonation cell diameter data for H_2-air mixtures measured in the 5 cm, 15 cm and 30 cm diameter tubes are

[1]Model PCB 113A24, sensitivity 5.45 mV/psi, manufactured by PCB Piezotronics, Inc., Buffalo, NY.

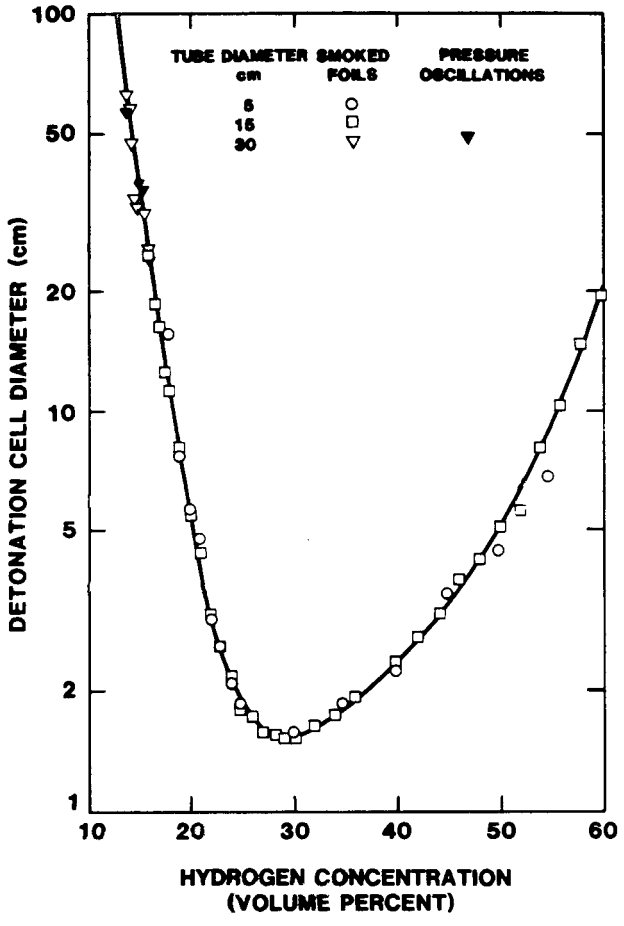


Figure 3. Measured detonation cell diameters (present work) of hydrogen-air mixtures initially at room temperature and atmospheric pressure. Symbols are actual data, the line shown is only an approximate fit.

plotted in Fig. 3 with respect to the hydrogen concentration. The cell diameter data exhibit a characteristic U shape with a minimum cell diameter of 1.5 cm at the stoichiometric composition 29.6% H_2. The maximum cell size that can be observed in a circular tube of diameter D corresponds to the onset of single-head spin detonation, namely when $D \simeq \lambda/\pi$. This means that in the smallest tube used in the present experiment (D = 5 cm), the maximum observable cell size should be approximately 15 cm and indeed the largest cell size measured in the 5 cm tube was 15.5 cm in an 18% H_2-air mixture. Repeating the cell size measurements in the 15 cm tube yields values for λ in very good agreement with the data from the 5 cm tube around the stoichiometric composition. For cells larger than about 5 cm, the results from the 15 cm tube differ slightly from those obtained in the 5 cm tube. As the cell diameters approach the single-head spin size in the small tube, cell sizes obtained from the 15-cm tube are more reliable. Similarly, when $\lambda > 15$ cm, the largest tube (D = 30 cm) gives more reliable results.

Using the 30 cm diameter tube, cell sizes for hydrogen concentrations as low as 13.8% H_2 have been obtained. The value of λ at 13.8% H_2 is about 60 cm as compared to 1.5 cm at stoichiometric composition. Since the present interest in H_2-air detonations centers around the lean limit, no attempt was made to determine the cell size in the 30 cm tube for H_2-rich mixtures. For the richest mixture studies in the 15 cm tube, namely 60% H_2, a cell diameter of 18.9 cm has been measured.

An alternative to determining cell size from the smoked foil records is to use the oscillations in the pressure signals from the PCB transducer mounted flush with the tube wall. Since the cell are centimeters in length and the diameter of the pressure transducer is only a few millimeters, the variations of pressur due to the transverse wave system are clearly evident in the pressure records. The pressure oscillations are observed to last several cycles prior to significant attenuation, so that the period can be determined. The cell length L_c can then be estimated by multiplying the period of the pressure oscillations by the mean detonation velocity, which is the average velocity of the wave system over a cell. From the cell length L_c, the cell diameter is obtained from the empirically determined relationship:[6] $\lambda \approx 0.62\ L_c$. As shown in Fig. 3, cell sizes estimated from pressure oscillations agree very well with those from smoked foil records. We conclude that this is a reliable independent method for measuring λ when it is large compared to the size of the pressure transducer and the transducer and recording system have sufficient time resolution.

One of the most important results of the present investigation is the observation of a stable detonation in the 30-cm tube at a hydrogen concentration of 13.8%. Considering the dramatic increase of cell size as the concentration is decreased, this value is m smaller than the previously reported limits of 18.2% by Breton[1] and 15.3% by Powell, et al.[17] The values of λ obtained in the present investigation for 18.2% and 15.3% hydrogen are 11.1 cm and 30 cm; corresponding minimum tube diameters for stable detonation propagation are 3.53 cm and 9.55 cm. The tube used by Breton

was 2 cm in diameter and that used by Powell et al, 3.7 cm in diameter. Given our present knowledge, it is somewhat surprising that they were able to observe detonations at as low concentrations as they did! The implication is that these detonations were overdriven by strong initiators and were not truly self-sustaining.

Recent experiments[13,18] have shown that even with tube diameters significantly smaller than the single-head spin limit, a single-head spin wave can still be initiated provided a sufficiently strong ignition source is used. Once initiated, the wave decays very slowly while propagating at about the C-J velocity, giving the false impression that a stable detonation is obtained. However, if a finite perturbation (such as an obstruction in the form of an orifice plate or a short length of spiral coil) is placed on the path of the wave, the wave fails immediately downstream of the obstruction and never again transits to a detonation. However, if the tube diameter is larger than that for a stable single-head spin wave (i.e., $D > \lambda/\pi$) the detonation will form again some distance downstream of the obstruction. In the only other study we are aware of that used a tube of large diameter, Zeldovich and Kogarko[21] found a limiting concentration of 15% in a 30 cm diameter tube. The present results in the same size tube are in direct contradiction to this, suggesting either errors in concentration measurement or insufficient initiator energy at concentrations below 15% in their experiments.

Measurements of detonation velocities and pressures were generally found to correspond quite well to the respective theoretical C-J values, particularly near the stoichiometric composition.

Table I

Measured and Calculated Detonation Properties for lean Hydrogen-Air Mixtures.

H_2 (%)	V^* (km/s)	$V_{CJ}^\dagger$ (km/s)	Δp^* (atm)	$\Delta p_{CJ}^\dagger$ (atm)
13.9	1.42	1.45	-	9.1
14	1.51	1.46	-	9.15
14.2	1.59	1.47	-	9.25
14.5	-	1.48	10.92	9.37
15	-	1.51	11.07	9.69
15.5	1.57	1.53	10.61	9.85
16	1.54	1.54	11.7	10.1

* Measured (present work).
† Theoretical (Chapman-Jouguet) calculations.

The experimental results for the average detonation velocity V and pressure Δp measured in the 30 cm tube for the range 14% - 16% H_2 are compared with the theoretical C-J values in Table 1. Both detonation velocity and pressure data agree to within the limits of experimental error with the theoretical values and demonstrate, contrary to earlier results,[19] that detonation velocities do not fall sharply below the C-J values in H_2-lean mixtures (<20% H_2). The earlier results were apparently obtained in short tubes of diameters smaller than λ/π and the detonations observed in these experiments must not have been stable.

From the detonation cell size data obtained in the present investigation, the critical tube diameters were estimated by using the $d_c = 13\lambda$ correlation. Figure 4 shows the variations of the critical tube diameter with H_2 concentration and the U-shaped curve is in essence a 13 times scaled-up version of the cell size curve given in Fig. 3. At the stoichiometric concentration, a critical tube diameter of the order of 20 cm was directly measured in the 0.192 m^3 combustion bomb at McGill.[10] According to the $d_c = 13\lambda$ correlation, this gives a value for λ of 1.54 cm, in excellent agreement with the value of 1.51 cm from the smoked foil records. For off-stoichiometric mixtures, direct measurements of d_c in large-scale tests have been carried out at SNLA and details of the experimental work are reported in an accompanying paper by Benedick.[20] The results for the 76 cm, 91 cm, and 121 cm diameter tubes are shown in Fig. 4. Good agreement is obtained with the prediction $d_c = 13\lambda$ using the cell size data shown in Fig. 3. For example, for the largest diameter tube (D = 121 cm), the critical concentrations

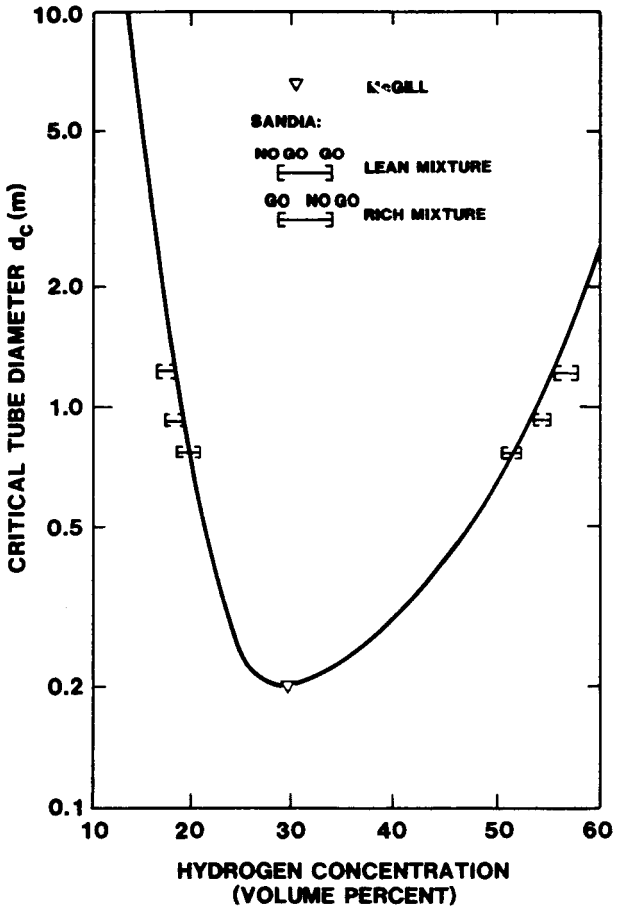


Figure 4. Measured critical tube diameter (present work) for hydrogen-air mixtures initially at room temperature and atmospheric pressure. The line shown is $d_c = 13\lambda$, computed from the approximate fit to λ shown in Fig. 3.

are 18.1% H_2 and 55.5% H_2. The cell sizes corresponding to these H_2 concentrations are 10.5 cm and 9.8 cm respectively and agree well with the value of 9.3 cm obtained by dividing the tube diameter of 121 cm by 13. Thus, the validity of the cell size-critical tube diameter correlation has been established over a wide range of concentrations and length scales for hydrogen-air detonations.

Using the data from the cell size measurements, or equivalently the critical tube diameter measurements, the critical energy for direct initiation of detonation can be estimated from Eq. 1 given in Section 4. The results are compared in Fig. 5 with the experimental data reported by Elsworth.[15] For the stoichiometric composition, the estimated value for the critical charge mass using Eq. 1 is 1.15 g of tetryl (1 g tetryl ≈ 5 kJ), whereas the value reported by Elsworth is 1.1 g. The agreement is excellent for near-stoichiometric compositions. However, the experimental values are consistently lower for less sensitive mixtures for which the critical charge mass becomes large. A possible explanation for this discrepancy is the uncertainty in Elsworth's experiments when the initiation charge is large. In the 1.28 m^3 cylindrical vessel used by Elsworth the wave travel is only of the order of [illegible]m and it would be difficult to assess if the wave was truly self-sustained or still supported by the initiation charge. Larger scale initiation experiments will be carried out in the near future at SNLA for near-limit mixtures.

Using the simple theory of detonability limits outlined in section 5 above, the minimum characteristic dimension (see Fig. 6)

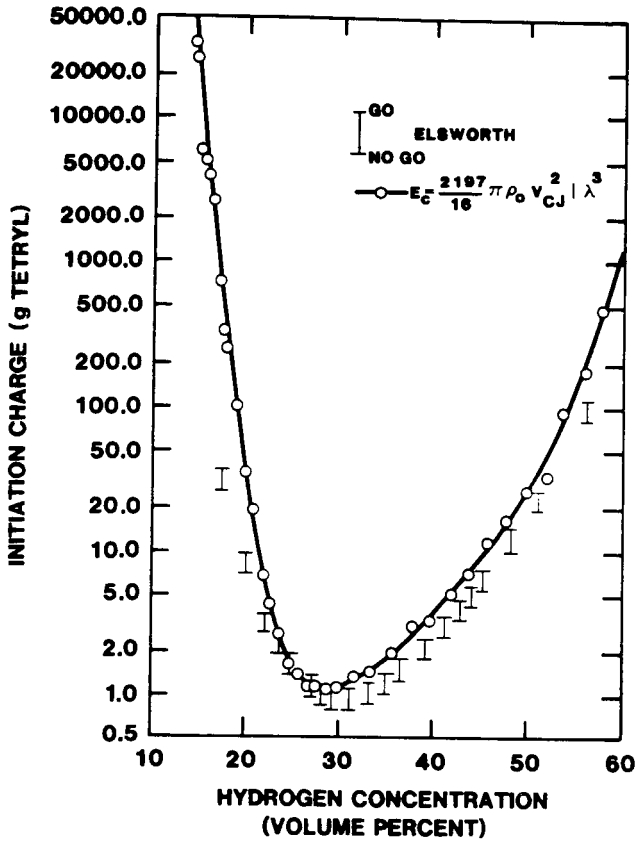


Figure 5. Comparison of critical initiation charge mass for hydrogen-air mixtures initially at room temperature and atmospheric pressure. Experimentally determined explosive charge mass limits by Elsworth[15] are compared to charge masses calculated from cell diameters measured in the present work.

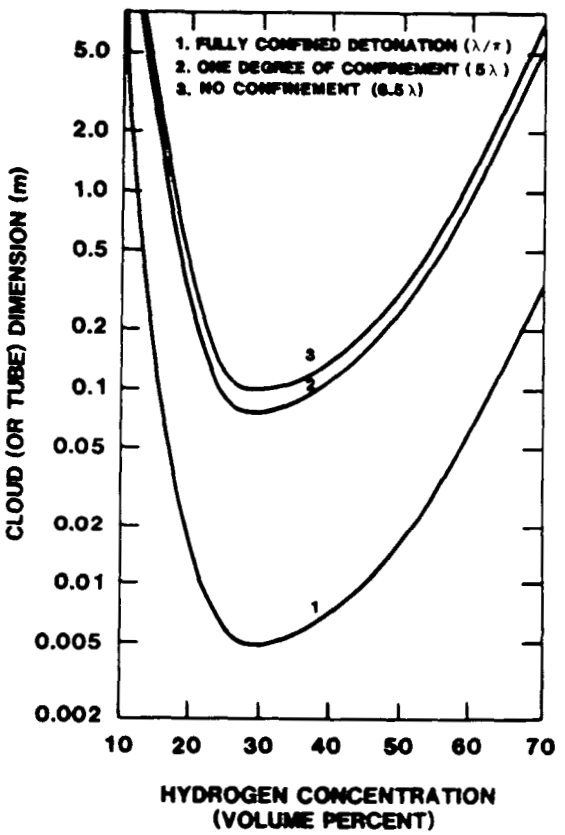


Figure 6. Minimum characteristic dimensions required for detonation initiation with various degrees of confinement as computed from the ad hoc model discussed in the text and the measured cell diameters.

has been calculated as function of hydrogen concentration and degree of confinement from the cell size data presented above. Gas volumes which have concentrations and dimensions above the relevant curve shown in Fig. 6 are able to support steady detonations, while those below are not. Since these curves are simply scaled versions of the cell size data shown in Fig. 3, the characteristic U shape is preserved. The smallest dimensions which can support a detonation occur at the stoichiometric composition where the cell size is a minimum; these dimensions are 0.5, 7.8 and 9.8 cm for fully confined (tubes), confined only in one dimension and completely unconfined, respectively. The smallest dimension which can support steady detonations for very rich or very lean mixtures becomes quite large as the hydrogen concentration approaches the extreme limits. The important question of whether there exists absolute limiting concentrations beyond which steady detonations are not possible has not been addressed in the present work. Very large scale experiments and/or extrapolation of existing data through chemical kineticgasdynamic modelling will be required to establish the exact shape of the cell-size and critical energy curves near the lean (or rich) "limit". Arguments have been presented over the last 25 years for the existence of limiting concentrations but as discussed in the next section, our present kinetic model does not support that conclusion.

The effectiveness of CO_2 as an inert additive for desensitizing H_2-air has been investigated by carrying out detailed measurements of cell sizes in H_2-air mixtures diluted with CO_2. Both 15 cm and 30 cm diameter tubes were used in these experiments. The

composition of the diluted mixture is defined by the hydrogen mole fraction y in the undiluted hydrogen-air mixture and the CO_2 mole fraction x in the diluted mixture. The dilution range extends from x = 0.0 to x = 0.15 in increments of 0.05.

Diluted and undiluted mixture cell size data have been plotted in Fig. 7 with respect to a concentration parameter α defined as the ratio of the hydrogen concentration to the air concentration, i.e. $\alpha = y/(1 - y)$; values of α as a function of y are given in Table 2. Constant values of this parameter are equivalent to constant equivalence ratios (i.e., hydrogen/air ratios) and are independent of dilution whereas the fuel concentration of the mixture decreases with increasing dilution. Since the effect of CO_2 is mainly thermodynamic, the cell size is expected to be primarily a function of equivalence ratio, a conjecture that is supported by the kinetic modelling described below. The cell data plots are similar U-shaped curves which narrow and shift upwards with increasing concentration of CO_2. The cell data exhibit a minimum for $\alpha \approx 0.4$ for undiluted and diluted mixtures (i.e., y = 29.6%, the stoichiometric composition of the undiluted mixture). These minima range from λ = 1.51 cm for 0% CO_2 dilution to λ = 12.1 cm for 15% CO_2 dilution (almost an order of magnitude increase cell size) with λ = 2.05 cm and 4.2 cm for the 5% and 10% CO_2 dilution cases, respectively.

It appears that CO_2 is quite effective in desensitizing H_2-air detonations in lean mixtures. For example, for α = 0.22 (i.e., y = 18% H_2), the cell size of the undiluted mixture is about 11 cm whereas addition of 5% CO_2 increases λ to about 50 cm.

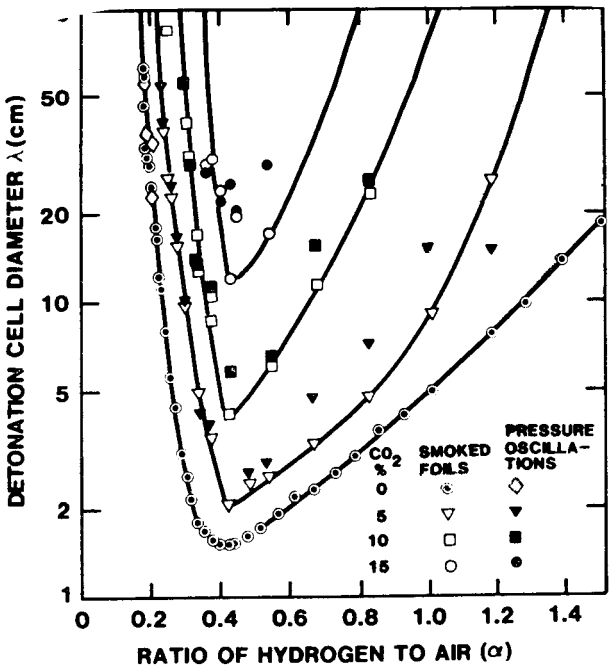


Figure 7. Measured detonation cell diameters (present work) for hydrogen-air-carbon dioxide mixtures initially at room temperature and atmospheric pressure. Symbols are actual data, lines shown are only approximate fits. Results shown are for 0, 5, 10 and 15% CO_2 dilution.

Table II

Concentration Parameters α of H_2-Air-CO_2 Mixtures

$y = H_2$(%)	$\alpha = H_2$/Air	$y = H_2$(%)	$\alpha = H_2$/Air
10	0.111	29	0.408
11	0.0124	29.6	0.420
12	0.136	30	0.429
13	0.149	32	0.471
14	0.163	34	0.515
15	0.176	36	0.563
16	0.191	38	0.613
17	0.205	40	0.667
18	0.220	42	0.724
19	0.235	44	0.786
20	0.250	46	0.852
21	0.266	48	0.923
22	0.282	50	1.0
23	0.299	52	1.083
24	0.316	54	1.174
25	0.333	56	1.273
26	0.351	58	1.381
27	0.370	60	1.50
28	0.389		

This implies that whereas a tube approximately 3.5 cm in diameter can accommodate a stable detonation in an undiluted mixture with 18% H_2, a tube diameter of almost 16 cm is required when 5% CO_2 is added to the undiluted mixture. Since the initiation energy of detonation is proportional to λ^3, the desensitizing effect of CO_2 on initiation is even more dramatic. It can cause an increase in initiation energy by several orders of magnitude.

The effects of CO_2 dilution on the equilibrium detonation properties are much less dramatic as shown in Figs. 8 and 9. The variations of the detonation velocity and pressure have been plotted as a function of the concentration parameter α (defined above) for different amounts of CO_2 dilution (i.e., 5%, 10% and 15% CO_2). There is good agreement between the experimental results and the theoretical C-J values. For $\alpha \approx 0.4$ (i.e., $y \approx 29.5\%$ H_2) a 15% CO_2 dilution reduces detonation velocity and pressure by only about 15% from their values for the undiluted mixture.

Kinetic Modelling

One of the outstanding problems in gaseous detonation theory is the prediction of cell size from the thermodynamic and kinetic properties of the fuel-oxidizer mixture. Ab initio calculations demonstrating the development of cellular structure have recently been performed, but no general conclusions can be drawn from these material-specific results. Past efforts have concentrated on using simplified kinetic models and reaction-zone instability analyses to relate a chemical "induction time" to the cell size. Although detailed quantitative comparisons have generally been unsuccessful, the overall trend is promising and almost all theories point to a

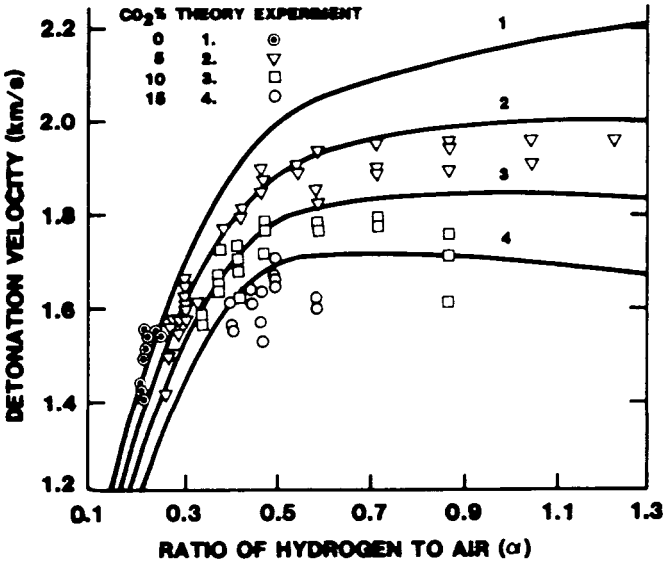


Figure 8. Measured mean detonation velocities (present work) of hydrogen-air-carbon dioxide mixtures compared to Chapman-Jouguet theoretical values (lines). Results shown are for 0, 5, 10 and 15% CO_2 dilution.

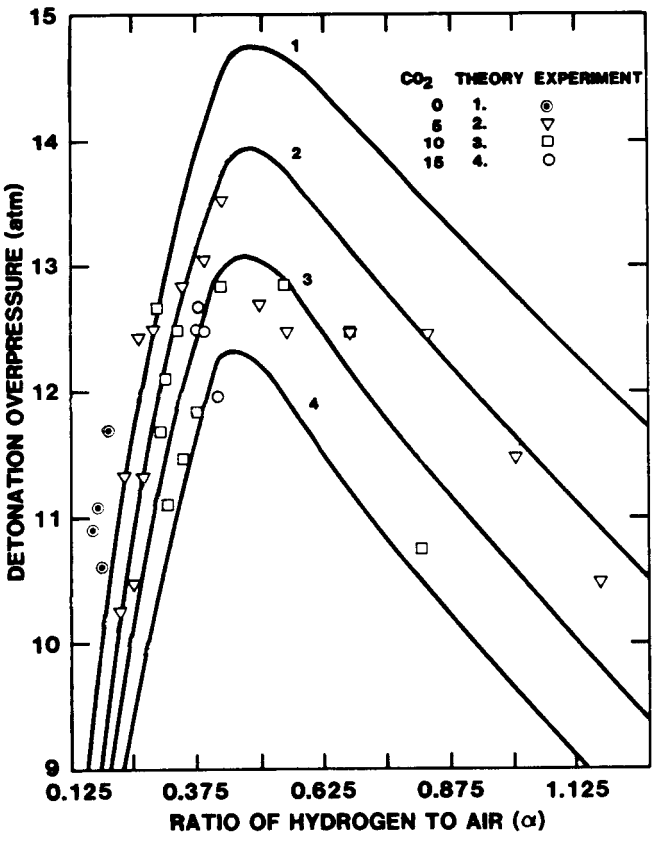


Figure 9. Measured mean detonation overpressures (present work) of hydrogen-air-carbon dioxide mixtures compared to Chapman-Jouguet theoretical values (lines). Results shown are for 0, 5, 10 and 15% CO_2 dilution.

direct correspondence between cell size and reaction zone length. If a reliable method of calculating cell sizes where available, then existing experimental results could be extrapolated to estimate detonability limits and detonation inhibition by additives (i.e.,  ns) and inert diluents (i.e., CO_2, H_2O) could be studied parametrically by relatively inexpensive computer calculations.

We have calculated characteristic reaction zone thicknesses for hydrogen-air-CO_2 detonations using the classical ZND detonation structure model with a comprehensive hydrogen oxidation mechanism using 19 reversible reactions (see Table 3). Details of the calculational method can be found in the accompanying paper by Roller and Shepherd[22]. The ZND model assumes that the detonation structure begins with a reactionless shock wave moving at the C-J velocity followed by a steady, one-dimensional reaction zone terminating in the C-J equilibrium state. Reaction zone temperature profiles are shown in Fig. 10 for 30% hydrogen in air diluted with 0, 5 and 10% CO_2. The shock wave increases the temperature sufficiently to initiate branching chain reactions producing the intermediate species (H, O, OH, HO_2 and H_2O_2). During this induction period, very little energy is released until the temperature rises abruptly as the recombination reactions become important. Almost all of  energy is then deposited in the flow in the relatively short recombination zone; this corresponds to the sharp rise in temperature shown in Fig. 10.

We have examined several different means of defining a characteristic reaction length and have concluded that for the purposes of the present investigation, the distance behind the

Table 3. Hydrogen Oxidation Mechanism

	Reactions	Reaction Rate Constants[a] A	β	E_o
1.	H2+O2=2OH	.170E+14	0.	47780.
2.	OH+H2=H2O+H	.117E+10	1.3000	3626.0
3.	H+O2=OH+O	.513E+17	-.81600	16507.
4.	O+H2=OH+H	.180E+11	1.0000	8826.0
5.	H+O2+M=HO2+M[b]	.210E+19	-1.0000	0.
6.	H+O2+O2=HO2+O2	.670E+20	-1.4200	0.
7.	H+O2+N2=HO2+N2	.670E+20	-1.4200	0.
8.	OH+HO2=H2O+O2	.500E+14	0.	1000.0
9.	H+HO2=2OH	.250E+15	0.	1900.0
10.	O+HO2=O2+OH	.480E+14	0.	1000.0
11.	2OH=O+H2O	.600E+09	1.3000	0.
12.	H2+M=H+H+M[c]	.223E+13	.50000	92600.
13.	O2+M=O+O+M	.185E+12	.50000	95560.
14.	H+OH+M=H2O+M[d]	.750E+24	-2.6000	0.
15.	H+HO2=H2+O2	.250E+14	0.	700.00
16.	HO2+HO2=H2O2+O2	.200E+13	0.	0.
17.	H2O2+M=OH+OH+M	.130E+18	0.	45500.
18.	H2O2+H=HO2+H2	.160E+13	0.	3800.0
19.	H2O2+OH=H2O+HO2	.100E+14	0.	1800.0

a. Reaction rates have the form of $AT^{\beta}e^{-E_o/RT}$. The units are moles, cm, sec, calories and Kelvin. Taken from Miller, et al[26].

b. Efficiencies: H_2O, 21.; H_2, 3.3; O_2, 0.; N_2, 0.

c. Efficiencies: H_2O, 6.; H, 2.; H_2, 3.

d. Efficiencies: H_2O, 20.

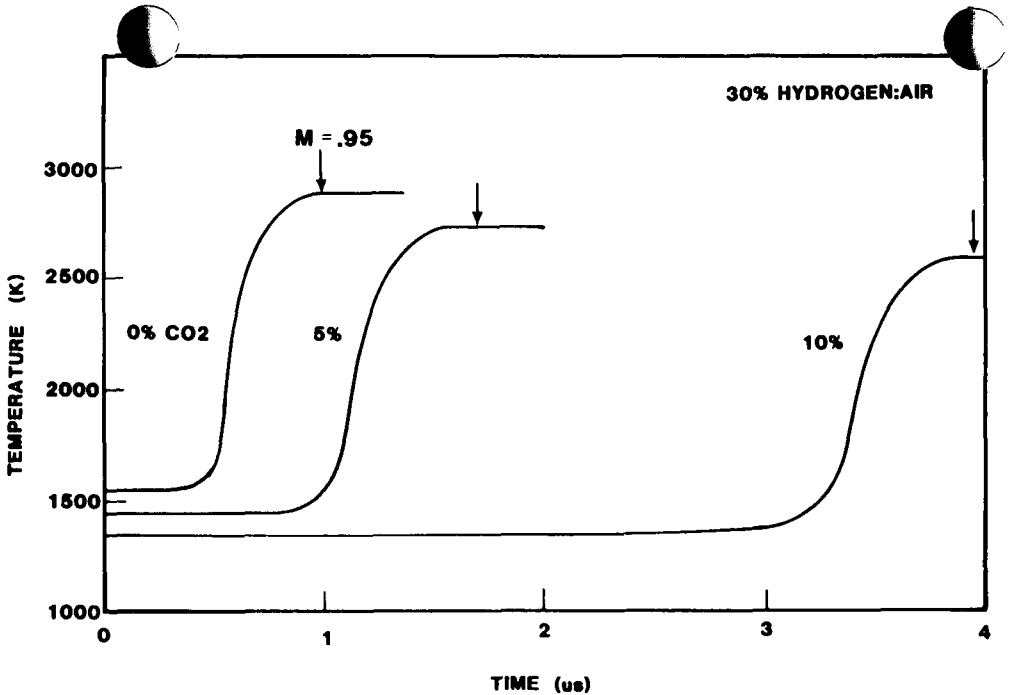


Figure 10. Calculated ZND detonation reaction zone temperature profile for hydrogen-air-carbon dioxide mixtures initially at 300K and 1 atm. Results shown are for 0, 5, and 10% CO_2 dilution. The point where the Mach number, M, reaches 0.95 is shown and indicates the characteristic reaction time (length).

shock at which the Mach number reaches 0.95 is appropriate. This distance is shown in Fig. 10 and corresponds to a distance slightly beyond the point of maximum rate of temperature rise. For concentrations off stoichiometric, the induction zone is so long compared to the recombination zone that the temperature profile practically a square wave. In those cases, our characteristic distance is identical to the distance to the temperature "jump" occurring at the recombination zone. The present choice of reaction zone length yields much better agreement with the cell size data (when appropriately scaled) than more conventional "induction lengths" which correspond to a given concentration of some radical species such as OH.

The reaction lengths Δ have been scaled and compared to cell diameters λ in Fig. 11. All reaction lengths were simply multiplied by a constant chosen so that the scaled length was equal to measured cell diameter at the stoichiometric point, 29.6% H_2. The reaction length at this point is 0.062 cm and the scaling constant is 24.2. These results are in good agreement on the lean side but the scaled lengths are consistently 20-50% smaller than the data on the rich side. Westbrook's recent calculations[23] using a constant volume state and a somewhat different set of reactions are consistent with the present results. His length scale was defined as the distance to the maximum rate of temperature rise.

If the same simple scaling is applied to the H_2-air-CO_2 reaction lengths, similar agreement with the data is achieved with the same discrepancy on the rich side. As mentioned above, we expect

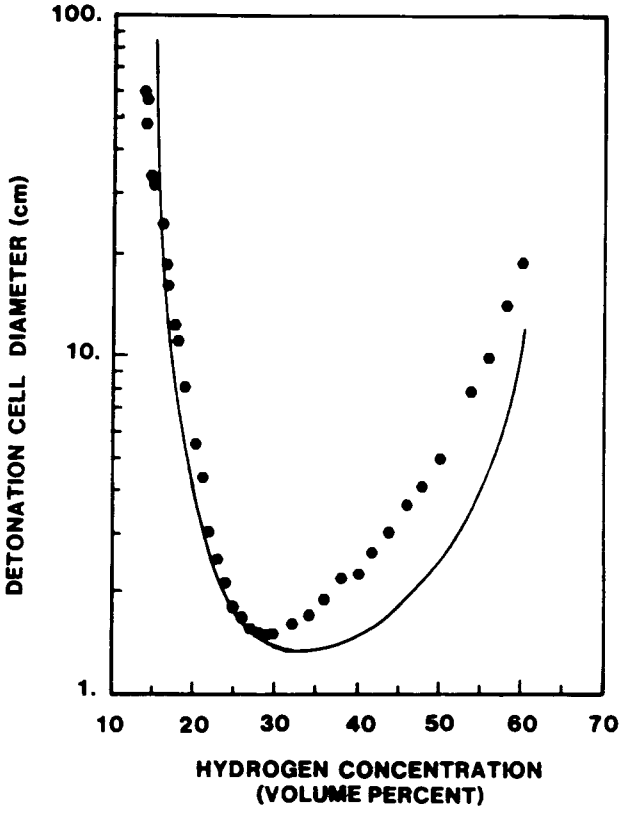


Figure 11. Comparison of experimentally measured cell diameters of the present work (symbols) to the scaled calculated reaction zone lengths (lines) for hydrogen-air mixtures initially at 300K and 1 atm.

that for inert diluents the detonation properties will primarily depend only on the H_2-air ratio. With this in mind, we have attempted to improve the reaction length-cell diameter predictions for CO_2 dilution by using the observed cell diameter-reaction length ratio for H_2-air mixtures at the same equivalence ratio (H_2-air ratio). The results are shown in Fig. 12. The close agreement with the data is encouraging and suggests that this may be a viable technique for predicting the effects of inert diluents.

The effect of the chemical activity of CO_2 has been investigated by carrying out calculations both with and without the dissociation of CO_2 to CO and the interaction with the other species through the reactions

$$CO + O + M = CO_2 + M$$

$$CO + OH = CO_2 + H$$

$$CO + HO_2 = CO_2 + OH$$

$$CO + O_2 = CO_2 + O$$

No dramatic effects were evident and the reaction zone lengths were found to differ by only about 5% from those calculated without these reactions.

The other problem that we have investigated with this model is the question of the existence of an absolute lower concentration limit for detonability. Starting with Belles[24] in 1958, various hypotheses have been suggested for an intrinsic limit derived from the competition between the basic branching chain reaction

$$H + O_2 \rightarrow OH + O$$

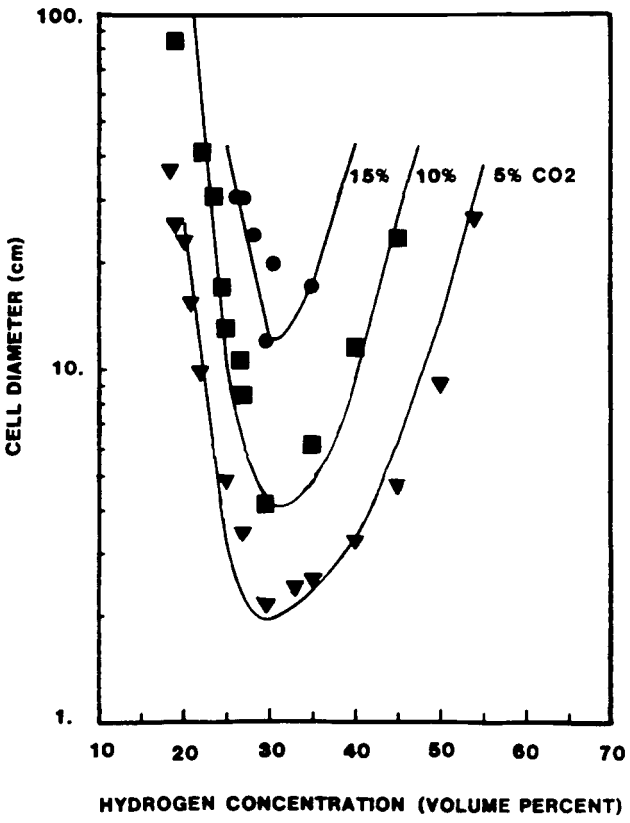


Figure 12. Comparison of experimental cell diameter data for 5, 10 and 15% CO_2 dilution with calculated reaction lengths scaled by the hydrogen-air cell diameter-reaction length ratio at the same equivalence ratio.

and the three-body reaction

$$H + O_2 + M \rightarrow HO_2 + M \ .$$

This, in fact, is the basis for the classical second-explosion limit observed in vessels[25] at much lower temperatures. More recently, Atkinson et al[14] have proposed a limiting value of 13. based on drastic changes in the radical concentration below that concentration. Despite the use of a much more sophisticated kinetic scheme than previous investigators, they apparently chose to carry out the calculation at constant pressure, rather than in a true detonation-structure or constant-volume calculation.

We have performed both types of calculations using the reaction scheme and rates of Atkinson et al, and find that their conclusions would have been drastically altered if a detonation structure calculation had been used. However, if we use the reaction scheme of Table 3 we find similar results for both types of calculations as the hydrogen concentration is varied from 15 to 11%. Reaction zone temperature profiles are shown in Fig. 13 for the ZND structure calculations. A well-defined reaction zone is still obtained at 11% and there is no indication of an intrinsic limit at 13.5%. Besides a lengthening of the reaction zone as the hydrogen concentration is decreased, the radical population shifts so that the species HO_2 and H_2O_2 and surprisingly, H_2O dominate in the induction period. This is an alternate reaction path to the standard branching chain involving OH and these radicals are ultimately consumed in the recombination zone, releasing a substantial fraction of the heat of reaction. Apparently, differences in rate constants and the irreversibility of several reactions involving

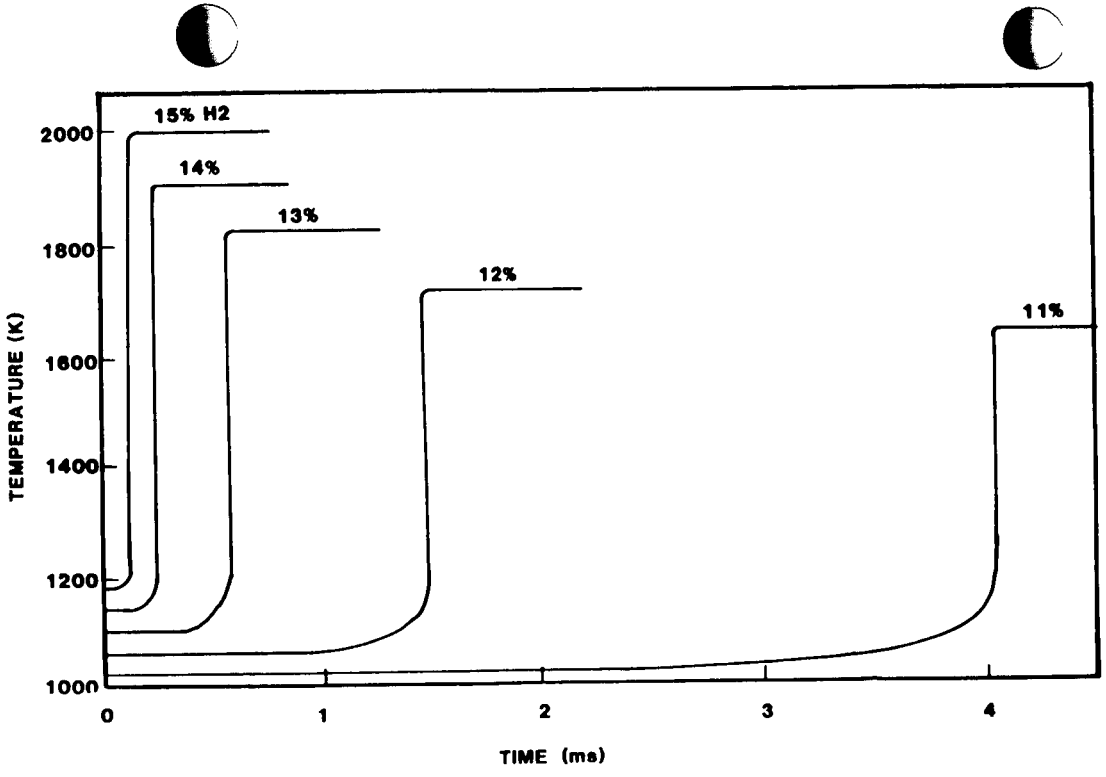


Figure 13. Calculated ZND reaction zone temperature profiles for lean hydrogen-air mixtures initially at 300K and 1 atm.

HO_2 and H_2O_2 in the Atkinson et al scheme are responsible for the dramatically different conclusions.

These results, and in particular, the sensitivity to the thermodynamic path during the reaction (i.e., constant pressure vs. one-dimensional, steady flow) suggest that the ignition behavior of very lean mixtures may depend crucially on the type of initiation. For example, direct initiation may be much easier to achieve than transition to detonation by an accelerating flame, since more pressure relief is available in the latter case.

8. Conclusions

The sensitivity to detonation of atmospheric H_2-air mixtures has been assessed by measuring the fundamental parameter which characterizes the substructure of a detonation, namely, the detonation cell diameter λ. Cell diameters range from 1.51 cm for the stoichiometric mixture (29.6% H_2) to 62 cm for the leanest mixture studied (13.8% H_2) and to 18.9 cm for the richest mixture studied (60% H_2). From cell diameter data, meaningful estimates of the dynamic detonation parameters such as critical tube diameter, critical initiation energy and composition limits have been obtained in small-scale and large-scale experiments as well as through simple analytical models.

Critical tube diameters d_c measured in such experiments demonstrate the validity of the empirical law of Mitrofanov and Soloukhin that the critical tube diameter is of the order of 13 detonation cell diameters, i.e., $d_c \simeq 13\lambda$ for H_2-air mixtures. The smallest critical tube diameter (d_c = 20 cm) corresponds to the stoichiometric composition. The slower increase of critical tube diameter in

hydrogen-rich mixtures considerably increases the detonation hazards of hydrogen-rich mixtures over that of hydrogen-lean systems.

A simple relationship for the initiation energy based on detonation cell diameter predicts reasonably well the critical initiation energies measured in small-scale experiments by Elsworth. For the stoichiometric composition, the model predicts a critical charge mass of 1.15 g of tetryl which is in excellent agreement with the value of 1.1 g reported by Elsworth. For off-stoichiometric mixtures, the model predicts larger initiation charges than the experimental ones. These discrepancies may indicate that the detonations observed in off-stoichiometric mixtures by Elsworth were overdriven and artificially supported during their travel in the limited scale apparatus used by Elsworth. More accurate estimates of the critical charge weight for direct initiation will be provided by future large-scale field tests to be conducted at SNLA, particularly for the less sensitive mixtures.

Criteria for detonability limits based on the detonation cell diameter have been formulated for volumes of mixtures under varying degrees of confinement. For totally confined detonations in tubes, the detonability limits correspond to the onset of single-head spin which determines the minimum tube diameter for the propagation of stable detonation. For circular tubes, the onset of spinning detonation occurs when the tube diameter is approximately equal to the cell diameter divided by π ($D = \lambda/\pi$). For tube diameters less than λ/π, stable detonation can not be maintained. For the detonation limits of 13% H_2 and 70% H_2 predicted by the kinetic model of Atkinson et al., the minimum tube diameters are 0.4 m and

0.3 m, respectively. For totally unconfined detonations, the minimum diameter of the explosive cloud is of the order of 6.5 cell diameters. This criterion follows from i) the empirical observation that the critical tube diameter for continued propagation of a planar detonation into unconfined space and its transformation into a spherical wave without failure is about 13 cell diameters and ii) the minimum detonation kernel surface area must be of the order of the area of the critical tube. For the leanest mixture of 13.8% H_2 used in the present study, the minimum diameter of the explosive cloud is estimated at about 4 m. Therefore, no stable detonation is expected to propagate in a 4 m diameter cloud if the fuel concentration is less than 13.8%. Concentration limits for a cloud resting on a horizontal surface (i.e., one degree of confinement) are determined by a minimum cloud thickness of the order of 5 λ. This is based on the empirical observations of Mitrofanov et al. and Edwards et al. that the successful transmission of a planar detonation and its transformation into a stable cylindrical wave requires a channel width W of about 10 cell diameters. Recent experiments at McGill seem to indicate that $W < 10\lambda$ rather than $\simeq 10\lambda$. In view of the practical importance of this particular geometry, further experiments must be performed to verify the critical conditions under one degree of confinement.

The present study demonstrates the efficiency of CO_2 dilution in drastically reducing the detonation sensitivity of hydrogen-air mixtures. For the largest dilution used in the present experiments, 15% CO_2, the detonation sensitivity (characterized by the detonation cell diameter) of hydrogen-air mixtures ranging from 17% to 35% H_2

(i.e., y = 0.17 - 0.35 where y denotes the hydrogen mole fraction in the undiluted hydrogen-air mixture) is reduced by an order of magnitude.



A smaller dilution (10% CO_2) also increases the cell size in the leanest (y=0.25) and richest (y=0.45) mixtures used in the present experiments by almost an order of magnitude, thus decreasing considerably the detonation potential of these fuel-lean and fuel-rich hydrogen-air mixtures.

Kinetic modelling using the ZND detonation wave structure and a comprehensive hydrogen oxidation scheme has been used to predict cell sizes from calculated reaction zone lengths. Cell sizes in CO_2 diluted mixtures can be accurately predicted if the observed cell diameter reaction length ratio for hydrogen-air mixtures at the same equivalence ratio is used in the comparison. The best agreement is found for a reaction zone length based on the point in the flow where Mach number reaches 0.95. In contrast to previous investigations, no dramatic change in the reaction mechanism is observed near 13.5% hydrogen. However, strong sensitivity to the reaction mechanism details and thermodynamic constraints is noted for very lean mixtures.



Acknowledgement

We wish to acknowledge that this work was sponsored by the Office of Nuclear Regulatory Research, U. S. Nuclear Regulatory Commission, Washington, D. C. 20555, under FIN No. A-1246 and A-1336.

References

1. Strehlow, R. A. Mauer, R. E. and Rajan, S., AIAA J., Vol. 7, No. 2 (1969).

2. Strehlow, R. A. and Engel, C. D., AIAA J., Vol. 7, No. 3 (1969).

3. Strehlow, R. A., Astronautica Acta, Vol. 15 (1970).

4. Voitsekhovskii, B. V., Mitrofanov, V. V. and Topchian, M. E., "The Structure of the Front of Detonations in Gases," Izdvosibirskii Otdelenie Akademiya Nauk SSR, Nov. 1963; transl. in Rept. FTD-MT-64-527 (AD 633-821), Feb. 1966, Wright Patterson Air Force Base, Ohio.

5. Fickett, W. and Davis, W. C., "Detonation," Los Alamos Series in Basic and Applied Sciences, University of Calif. Press (1979).

6. Strehlow, R. A., Comb. Flame; Vol. 12, No. 2 (1968).

7. Mitrofanov, V. V. and Soloukhin, R. I., Soviet Physics-Doklady 9, 12 (1965).

8. Edwards, D. H., Thomas, G. O. and Nettleton, A. A., J. Fluid Mech. 95, part 1 (1979).

9. Knystautas, R. A., Lee, J. H. and Guirao, C. M., "The Critical Tube Diameter for Detonation Failure in Hydrocarbon-Air Mixtures," Comb. Flame (in press).

10. Lee, J. H., Knystautas, R. and Guirao, C. M., "The Link Between Cell Size, Critical Tube Diameter, Initiation Energy and Detonability Limits," Proceedings of the International Specialist Meeting on Fuel-Air Explosion, Montreal, Canada, Nov. 4-6, 1981, Editors: J. H. S. Lee and C. M. Guirao, SM Study No. 16, University of Waterloo, Waterloo, Canada.

11. Lee, J. H. and Matsui, H., Comb. Flame, Vol. 28 (1977).

12. Lee, J. H. S. and Ramamurthi, K., Comb. Flame, Vol. 27 (1976).

13. Moen, I. O., Donato, M., Knystautas, R. and Lee, J. H. S., 18th (International) Symposium on Combustion, The Combustion Institute, p. 1615 (1980).

14. Atkinson, R., Bull, D. C. and Shuff, P. J., Comb. Flame, Vol. 39 (1980).

15. Elsworth, J.: Thornton Research Centre, Private Communication (1981).

16. Breton, J., "Recherches sur la Détonation des Mélanges Gazaus," These, Faculté des Sciences de l'Université de Nancy (1936).

Predictions of Detonability of Hydrogen-Air-Steam Mixtures

S. F. Roller and J. E. Shepherd

Sandia National Laboratories

Albuquerque, NM

SAND 82-2267C

ABSTRACT

In order to realistically assess the detonation hazard of hydrogen-air-steam mixtures, the detonation cell size must be known. Lacking measurements of the cell size, we have developed an estimation technique based on the empirical relationship between calculated reaction zone lengths and measured cell diameters for hydrogen-air mixtures. Reaction zone lengths are calculated from the classical ZND model of one-dimensional detonation using a comprehensive hydrogen oxidation scheme. Both estimated cell diameters and critical initiation energies increase rapidly with either steam or carbon dioxide dilution.

Sponsored by the
Office of Nuclear Regulatory Research
U. S. Nuclear Regulatory Commission
Washington, D. C. 20555

under FIN No. A-1246 and A-1336

INTRODUCTION

Recent studies[1] on gaseous detonation have emphasized the importance of cell size to initiation and propagation phenomena. Simultaneously, detailed kinetic modeling[2] with modern reaction schemes and rates has been used to correlate cell size to a characteristic reaction zone thickness. The predictive capability which emerges from the combination of these efforts is explored in the present study with an emphasis on the hydrogen-air system diluted with water vapor. Characteristic reaction zone lengths are calculated for hydrogen-air mixtures and the relation to cell size determined by comparison to the measurements of Lee et al[3]. Predictions of cell size, critical tube diameter and critical initiation energy for hydrogen-air-water systems are made using this cell size-reaction zone length correlation. These results can be used to realistically evaluate detonation hazards in the steam-filled reactor containments following hydrogen-producing LOCAs.

Reaction-Zone Model

A characteristic reaction-zone thickness was calculated using the classical one-dimensional ZND (Zeldovich-von Neumann-Doering) model of steady-state detonation[4]. In brief, this model postulates an idealized detonation consisting of an unreacted ("frozen") shock propagating at the Chapman-Jouguet (C-J) velocity and followed by a reaction zone governed by the steady, one-dimensional equations of gas dynamics and the appropriate chemical reaction kinetics. Temperatures

and pressures immediately behind the frozen shock are sufficient to initiate reaction through the dissociation of the molecular species. Typically, the reaction zone can be divided into two sections (see Figure 1); the first section is a thermally neutral "timer" or induction zone associated with the production of the radical species (i.e., OH, HO_2 and H_2O_2); and the second section is primarily exothermic and associated with the recombination reactions. At high initial pressures (>0.5 atm), the recombination zone is quite short compared with the induction zone (for off-stoichiometric mixtures) and the reaction zone appears to have a "square-wave" structure. The method used to calculate the reaction zone profiles is outlined below. First, the C-J detonation parameters were calculated using the NASA-Lewis equilibrium chemistry computer code[5]. Second, the conditions behind a frozen shock traveling at the C-J velocity were calculated using this same code. Third, a separate computer code, written specifically for this project, was used to calculate the reaction zone profile behind the frozen shock wave. Fourth and finally, a characteristic reaction zone thickness was determined from the computed profiles. The theoretical basis for computing steady, reactive, one-dimensional flows is comprehensively discussed by Fickett and Davis[4]. Our computer code was based on a variation of one technique they describe. Pressure (p), density (ρ), particle velocity (u) and species mass fractions (y_i), were computed as a function of time by integrating the following set of equations:

1010

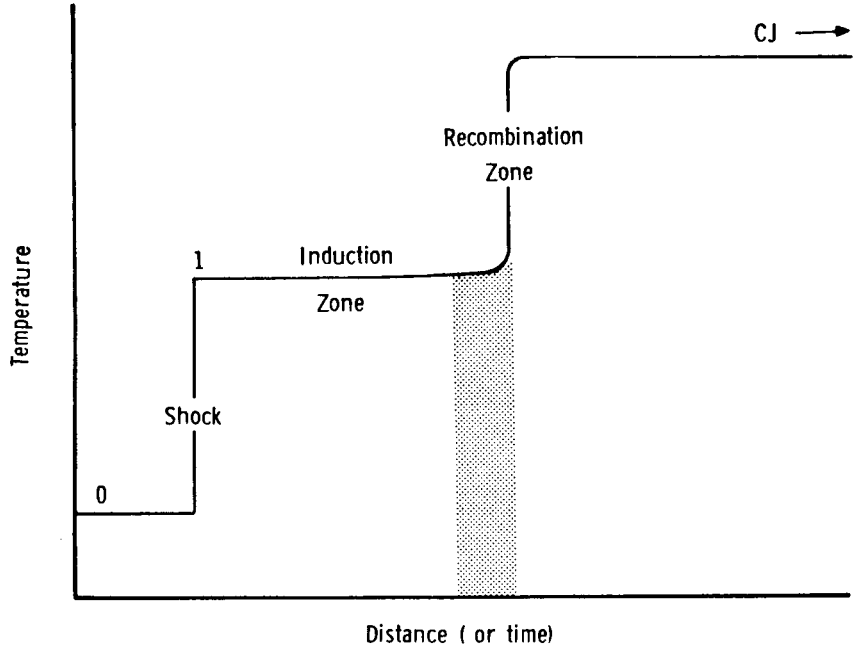


Figure 1. Schematic of the temperature profile in the ZND model of detonation structure.

$$\frac{dp}{dt} = -\frac{u^2\sigma}{\eta}, \tag{1}$$

$$\frac{d\rho}{dt} = -\frac{\sigma}{\eta}, \tag{2}$$

$$\frac{dy_i}{dt} = \frac{W_i\,\omega_i}{\rho}, \tag{3}$$

where σ is the volume rate of change per unit mass due to chemical reaction

$$\sigma = \sum_i \left(\frac{\partial\rho}{\partial y_i} - \frac{\rho}{C_p T}\,h_i\right)\frac{dy_i}{dt} \tag{4}$$

and η is the gasdynamic parameter

$$\eta = 1-M^2 \tag{5}$$

r symbols are W_i, the molecular weight of species i; ω_i, the chemical reaction rate of species i; h_i, the specific enthalpy of species i; C_p, the mixture specific heat at constant pressure, and M, the Mach number u/c.

The particle velocity is computed from the integrated momentum equation at each instant of time

$$u = \sqrt{\frac{\rho_1}{\rho}\left(\frac{p - p_1}{\rho - \rho_1}\right)} \qquad (6)$$

where p_1 and ρ_1 are the preshock pressure and density and the distance from the shock wave is determined by integrating the particle velocity

$$\frac{dx}{dt} = u \qquad (7)$$

Thermodynamic variables were computed using the perfect gas equation of state and internal energies computed from the temperature dependent specific heats given by the JANNAF tables. Calculation of thermodynamic variables and reaction rates was greatly facilitated by using the CHEMKIN subroutine library and symbolic reaction interpreter developed by Kee, et al[6]. This enabled us to rapidly and simply change the reaction mechanism, add or subtract species or alter individual reaction rate coefficients.

The reaction scheme we used is shown in Table 1 and consists of 17 individual reactions with both forward and backward progress considered for each reaction shown. The rates shown were taken from a critical survey of acetylene oxidation by Miller, et al[7], and have been tested individually and as a group in such diverse applications

Table 1. Hydrogen Oxidation Mechanism

	Reactions	Reaction Rate Constants[a] A	β	E_o
1.	H2+O2=2OH	.170E+14	0.	47780.
2.	OH+H2=H2O+H	.117E+10	1.3000	3626.0
3.	H+O2=OH+O	.513E+17	-.81600	16507.
4.	O+H2=OH+H	.180E+11	1.0000	8826.0
5.	H+O2+M=HO2+M[b]	.210E+19	-1.0000	0.
6.	H+O2+O2=HO2+O2	.670E+20	-1.4200	0.
7.	H+O2+N2=HO2+N2	.670E+20	-1.4200	0.
8.	OH+HO2=H2O+O2	.500E+14	0.	1000.0
9.	H+HO2=2OH	.250E+15	0.	1900.0
10.	O+HO2=O2+OH	.480E+14	0.	1000.0
11.	2OH=O+H2O	.600E+09	1.3000	0.
12.	H2+M=H+H+M[c]	.223E+13	.50000	92600.
13.	O2+M=O+O+M	.185E+12	.50000	95560.
14.	H+OH+M=H2O+M[d]	.750E+24	-2.6000	0.
15.	H+HO2=H2+O2	.250E+14	0.	700.00
16.	HO2+HO2=H2O2+O2	.200E+13	0.	0.
17.	H2O2+M=OH+OH+M	.130E+18	0.	45500.
18.	H2O2+H=HO2+H2	.160E+13	0.	3800.0
19.	H2O2+OH=H2O+HO2	.100E+14	0.	1800.0

a. Reaction rates have the form of $AT^{\beta}e^{-E_o/RT}$. The units are moles, cm, sec, calories and Kelvin. Taken from Miller, et al[7].

b. Efficiencies: H_2O, 21.; H_2, 3.3; O_2, 0.; N_2, 0.

c. Efficiencies: H_2O, 6.; H, 2.; H_2, 3.

d. Efficiencies: H_2O, 20.

as low-pressure flames and shock tube studies. In several three-body reactions, increased efficiencies (rate multipliers) are used for certain diluents, particularly H_2O. The mechanism is comprehensive that it allows for production and destruction of the three major intermediate (radical) species OH, HO_2 and H_2O_2; the dissociation and recombination of the reactants H_2 and O_2 and the formation of water products through all of the intermediate channels.

Results

Reaction zone structures have been computed for hydrogen concentrations in air from 10 to 70 percent and steam dilutions up to 30 percent. The results of the equilibrium calculations for C-J properties (detonation velocity, C-J temperature and pressure) together with the temperature and pressure behind the frozen shock are given in Table 2 for steam-diluted mixtures only. The initial conditions were chosen to match those that will be used in future experiments at SNLA; that is, the hydrogen and steam were added to air at initially one Albuquerque atmosphere (nominally 12.8 psia) to obtain the desired mixture mole fractions by partial pressure measurement. The initial temperature was 110°C in all cases.

The post-shock temperatures and pressures were used as initial conditions for the detonation structure calculations. Reaction-zone temperature profiles are shown in Figure 2 for several of the cases listed in Table 2. We have examined several criteria for determining a characteristic reaction zone thickness. Possible methods include the distance (or time) at which some radical concentration (i.e., OH)

Table 2

C-J and Frozen Shock Parameters for H_2-Air-H_2O Detonations

Case No.	%H_2 in Air	%H_2O	P_o (Atm)	V_{CJ} (m/s)	T_{CJ} (K)	P_{CJ} (Atm)	T_s (K)	P_s (Atm)
1	30.0	0	1.186	1972	2980	14.49	1596	25.45
2	22.3	10	1.186	1720	2408	11.73	1364	20.93
3	30.0	10	1.318	1919	2779	15.04	1494	26.51
4	33.4	10	1.384	1961	2789	15.79	1503	27.97
5	44.5	10	1.660	2034	2556	17.30	1434	31.10
6	55.7	10	2.075	2081	2229	18.94	1321	34.15
7	25.1	20	1.384	1739	2349	13.36	1320	23.83
8	30.0	20	1.482	1859	2566	15.64	1394	27.70
9	37.6	20	1.660	1906	2467	16.71	1369	30.01
10	30.1	20	2.075	1935	2150	18.30	1263	32.94
11	30.0	30	1.694	1788	2332	16.26	1292	28.95

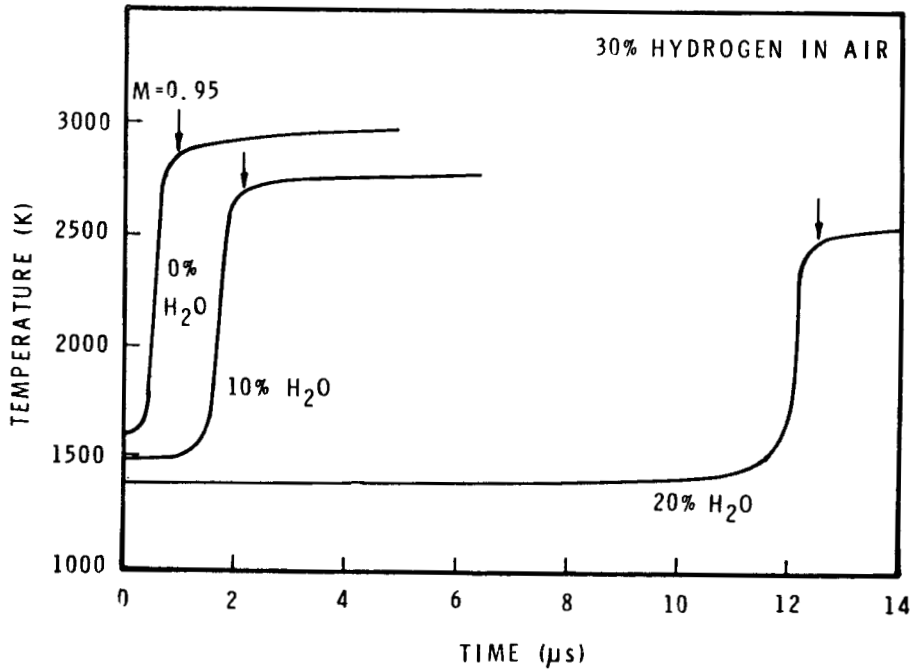


Figure 2. Reaction zone temperature profiles for several hydrogen-air-steam detonations corresponding to the cases listed in Table 1.

reaches a particular value; the first appearance of exothermicity, i.e., when the temperature rises a particular amount or the temperature rate of increase is equal to a particular value; or some measure of the completeness of reaction, i.e., when the Mach number approaches one. All of these methods yield different levels of agreement when the scaled reaction lengths are compared to the measured cell sizes for hydrogen-air mixtures. We have used comparison with the extensive data on cell diameter[3] available for the H_2-air-CO_2 mixtures at room temperature and 1 atm to select among these different criteria. The results of calculations[3] for that system indicate that some measure of the end of the reaction zone is appropriate. In that study, the reaction zone length was defined as the point behind the shock at which the Mach number reaches 0.95. We adopt the same criterion in the present work. The point in the flow at which M = 0.95 is reached is indicated on the temperature profiles in Figure 2.

For hydrogen-air mixtures at 300 K and 1 atm initially, detonation cell diameters from Lee, et al[3] and scaled reaction zone lengths are compared in Figure 3. The reaction lengths were scaled by simply multiplying by a constant chosen so that the scaled values and the data matched at the stoichiometric point. The cell size at this point is 1.51 cm and the reaction zone length is 0.062 cm, yielding a scaling factor of 24.2. Agreement with the data is good on the lean side but the scaled lengths are consistently 20-50% lower than the data on the rich side. These results are consistent with other recent calculations by Westbrook[2], who used a constant density state throughout the reaction zone and a slightly different reaction mechanism. He based his reaction lengths on the points at which the maxi-

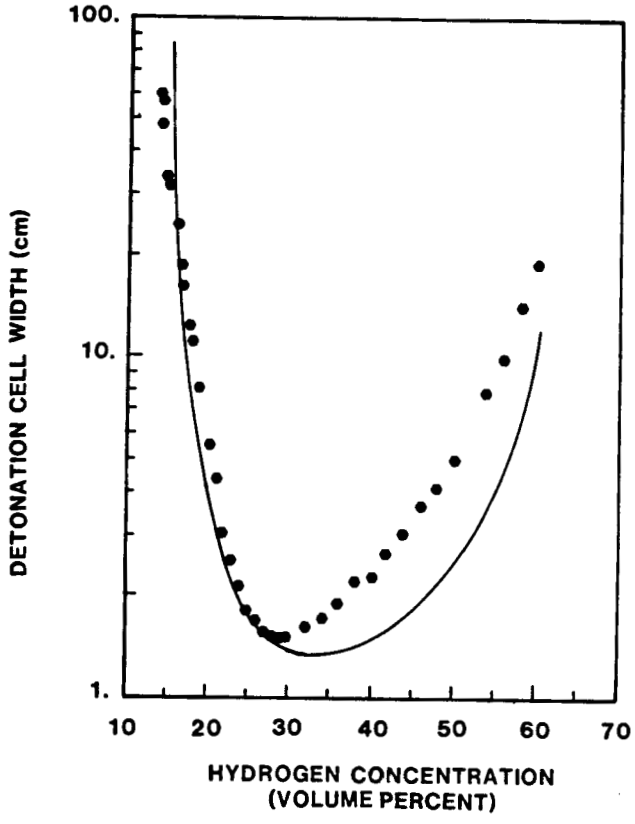


Figure 3. Comparison betwen the measured cell diameters of Lee, et al, and the scaled reaction zone lengths calculated in the present work. Hydrogen-air mixtures only at 300 K and 1 atm initially.

mum rate of temperature rise occurs.

Calculated reaction zone lengths are shown in Figure 4 as a function of the hydrogen percentage in air for 10, 20, and 30 percent steam dilution of the total mixture. For comparison, results[3] for 10, 20 and 30 percent CO_2 dilution of stoichiometric hydrogen-air mixtures are also shown. The minimum reaction zone length occurs near stoichiometric conditions; for 0, 10, 20 and 30 percent steam dilution, the lengths are 0.060, 0.097, 0.47, and 1.97 cm, respectively. Note that for 20 and 30 percent dilution, CO_2 is more effective (greater reaction length) than H_2O as a diluent, while for 10 percent, CO_2 is less effective (shorter reaction length). This can be attributed to the competing effects of the lower post-shock temperatures of CO_2-diluted mixtures and the greater efficiency of H_2O in three-body reactions.

Cell diameters have been computed from the reaction zone lengths by scaling with the observed cell diameter-reaction length ratios in hydrogen-air mixtures at the same equivalence ratio (i.e., the same hydrogen-in-air concentration). The cell diameter-reaction length ratios computed from the data of Lee et al[3] and the present calculations are shown in Figure 5. The dashed line in Figure 5 is the approximate correlation used to compute the cell diameters shown in Figure 5. Computed cell diameters for 30 percent hydrogen-air mixtures diluted with 0, 10, 20 and 30 percent H_2O are 1.44, 2.35, 11.47 and 47.7 cm, respectively. The present scaling method was used with the hydrogen-air-CO_2 system discussed above and produced good agreement with the observed cell diameters for CO_2 concentrations from

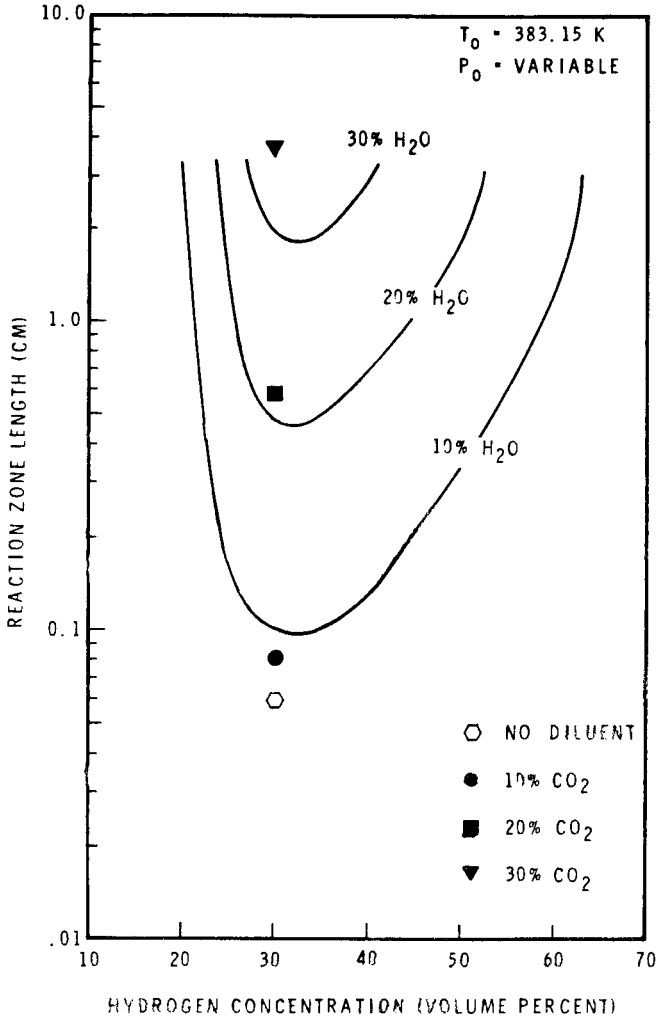


Figure 4. Calculated reaction zone lengths for hydrogen-air-steam mixtures. Hydrogen concentration shown is the percentage of hydrogen in the hydrogen-air component only.

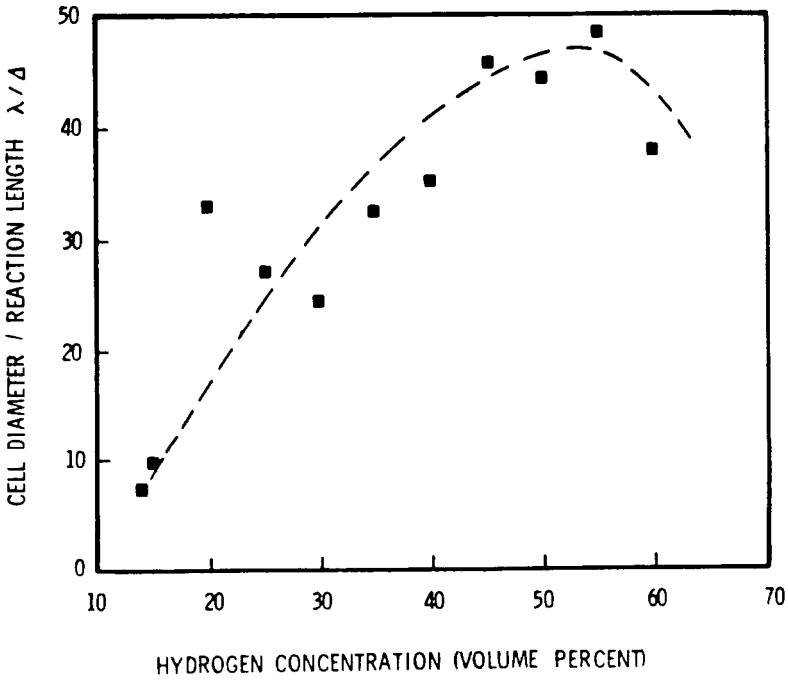


Figure 5. Ratio of observed cell diameters (from Lee, et al) to calculated reaction lengths (present work) for hydrogen-air mixtures initially at 300 K and 1 atm. The dashed line is the approximate ratio used to calculate the cell diameter for hydrogen-air-steam mixtures.

5-15 percent. For chemically inert diluents such as H_2O and CO_2, we expect that most of the variability in the cell size-reaction length ratio will be determined by the equivalence ratio. In fact, H_2O h[illegible] some chemical activity in that it is much more effective than oth[illegible] species as a third body in some recombination reactions (see Table 1). However, calculations deleting this efficiency suggest that this is a negligible effect except for very lean mixtures with high steam fractions.

The critical energy E_c required for direct initiation has been computed from the predicted cell diameters using the detonation kernel model and strong blastwave theory as outlined by Guirao, et al[8]. They find that the critical energy is related to the cube of the cell diameter by

$$E_c = 431\ \rho_o V_{CJ}^2 I \lambda^3 \tag{8}$$

where ρ_o is the gas density ahead of the detonation, V_{CJ} is the C-J detonation velocity, I is the blast integral ($0.6 < I < 1.0$ for hydrogen-air detonations) and λ is the cell diameter.

Critical energies and equivalent tetryl charge mass for direct initiation in stoichiometric hydrogen-air mixtures with 0, 10, 20 and 30 percent steam dilution are show in Table 3. The dramatic incr[illegible] in E_c from 0.78 g of tetryl at 0 percent dilution to 31.8 kg at 30 perc[illegible] dilution illustrates the effectiveness of steam dilution in desensitizing hydrogen-air mixtures. Since the lowest minimum initiation energy occurs near stoichiometric, all other mixtures with the same percentage dilution will require larger initiation energies.

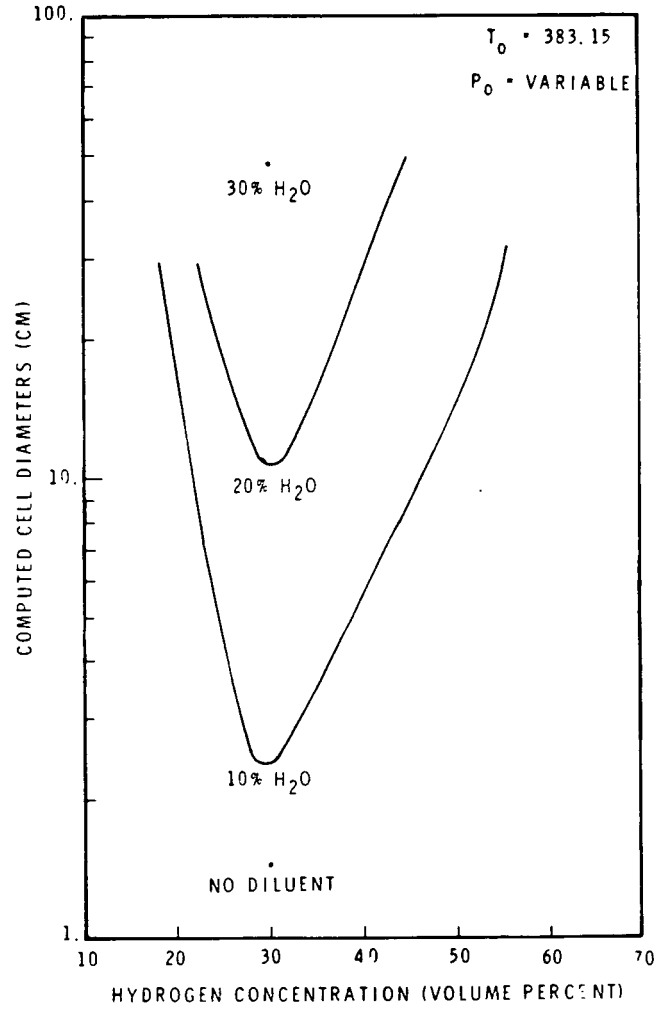


Figure 6. Predicted cell diameters for hydrogen-air-steam mixtures. The hydrogen concentration shown is the percentage of hydrogen in the hydrogen-air component only.

Table 3

Minimum Energy Acquired for Direct Initiation of Detonation in Stoichiometric Hydrogen-Air-Steam Mixtures

% Steam	E_c (kJ)	E_c (g Tetryl)
0	3.92	0.78
10	17.5	3.5
20	2.1×10^3	424
30	1.6×10^5	31.8×10^3

Conclusions

The effect of steam dilution on reaction zone lengths has been computed for hydrogen-air detonations using the classical ZND model of reaction zone struction. Cell diameters have been computed from calculated reaction lengths using an empirical correlation derived from experimental measurements of cell diameter by Lee et al[3] and tested for CO_2-diluted hydrogen-air detonations. Cell diameters for 10, 20 and 30 percent steam dilution of stoichiometric hydrogen-air mixtures initially at 110°C are predicted to be 2.35, 11.47 and 47.7 cm, respectively. Minimum energies and equivalent tetryl charge masses for direct initiation of detonation are calculated using the predicted cell diameters, strong blastwave theory and the detonation kernel model. Critical charge masses for 10, 20 and 30 percent steam dilution of stoichiometric hydrogen-air mixtures initially at 110°C are 3.5 g, 424 g, and 31.8 kg of tetryl, respectively. The present calculations indicate that at high diluent concentrations, CO_2 is slightly more effective than H_2O as a detonation inhibitor. Both CO_2 H_2O (steam) are very effective at increasing the cell diameter and critical initiation energy, resulting in a dramatic inhibition of detonability for diluent concentrations above 20 percent.

References

1. Edwards, D. H., Thomas, G. O. and Nettleton, M. A., "The Diffraction of a Planar Detonation Wave at an Abrupt Area Change", J. Fluid Mech. 95, 1979.

2. Westbrook, C. K., "Hydrogen Oxidation Kinetics in Gaseous Detonations", UCRL-86774, 1981.

3. Lee, J. H. Knystautus, R., Guirao, C., Benedick, W. B. and Shepherd, J. E., "Hydrogen-Air Detonations", Second International Workshop on the Impact of Hydrogen on Water Reactor Safety, Albuquerque, NM, October 3-7, 1981.

4. Fickett, W. and Davis, W. C., Detonation, University of California Press, 1979.

5. Gordon, S. and McBride, B. J., "Computer Program for Calculation of Complex Chemical Equilibrium Compositions, Rocket Performance, Incident and Reflected Shocks and Chapman-Jouguet Detonations", NASA SP-273, 1971.

6. Kee, R. J., Miller, J. A. and Jefferson, T. H., "CHEMKIN: A General-Purpose, Problem-Independent, Transportable Fortran Chemical Kinetics Code Package", SAND80-8003, 1980.

7. Miller, J. A., Mitchell, R. E., Smooke, M. D., and Kee, R. J., "Toward a Comprehensive Chemical Kinetic Mechanism for the Oxidation of Acetylene: Comparison of Model Predictions with Results from Flame and Shock Tube Experiments", presented at the 1982 Spring Meeting of the Western States Section of the Combustion Institute, Paper WSS/CI82-31.

8. Guirao, C. M., Knystautas, R., Lee, J. H., Benedick, W. B. and Berman, M., "Hydrogen-Air Detonations", presented at the Nineteenth Symposium (International) on Combustion, 1982.

SESSION VII

COMBUSTION MITIGATION AND CONTROL

17. Powell, D., Vasatko, H. and Wagner, H. Gg.: AFOSR 69-1095 TR and AD-692900 (1967).

18. Donato, M., "The Influence of Confinement on the Propagation of Near-Limit Detonation Waves," McGill University Ph.D. Thesis, 1982.

19. Schüller, Dissertation, Darmstadt, 1954; also in "Fundamental Data obtained from Shock-Tube Experiments," AGARDograph No. 41, p. 331, Pergamon Press (1961).

20. Benedick, W. B., Lee, J. H., Knystautas, R. and Guirao, C. M., "Large-Scale Hydrogen-Air Detonations," Second International Workshop on the Impact of Hydrogen on Water Reactor Safety, Albuquerque, New Mexico, October 3-7, 1982.

21. Kogarko, S. M. and Zeldovich, Y. B., Dokl. Akad. Nauk SSSR 63 (1948).

22. Roller, S. F. and Shepherd, J. E. "Prediction of Hydrogen-Air-Steam Detonability Limits" Second Intl. Workshop on the Impact of Hydrogen on Water Reactor Safety, Albuquerque, New Mexico, October 3-7, 1982.

23. Westbrook, C. K. "Hydrogen Oxidation Kinetics in Gaseous Detonations" UCRL-86774, 1981.

24. Belles, F. E. "Detonability and Chemical Kinetics: Prediction of Limits of Detonability of Hydrogen," Seventh Symposium (Intl.) on Combustion, 1958.

25. Lewis, B. and von Elbe, G., Combustion, Flames, and Explosions of Gases, Academic Press, New York, 1951.

26. Miller, J. A., Mitchell, R. E., Smooke, M. D., and Kee, R. J., "Toward a Comprehensive Kinetic Mechanism for the Oxidation of Acetylene: Comparison of Model Predictions With Results from Flame and Shock Tube Experiments" presented at the 1982 Spring Meeting of the Western States Section of the Combustion Institute, paper WSS/C1 82-31.

DEVELOPMENT AND TESTING

OF

HYDROGEN IGNITION DEVICES

D. Renfro, TVA
L. Smith, TVA
L. Thompson, EPRI
R. Clever, TRW

This is a Government publication and not subject to copyright.

I. Introduction

Controlled ignition systems for the mitigation of hydrogen produced during degraded core accidents have been installed recently in several light water reactor (LWR) containments. This paper relates the background of the thermal igniter approach and its application to LWR controlled ignition systems. The process used by the Tennessee Valley Authority (TVA) to select a hydrogen mitigation system in general and an igniter type in particular is described. Descriptions of both the Interim Distributed Ignition System (IDIS) and the Permanent Hydrogen Mitigation System (PHMS) installed by TVA are included as examples. Testing of igniter durability at TVA's Singleton Materials Engineering Laboratory and of igniter performance at Atomic Energy of Canada's Whiteshell Nuclear Research Establishment is presented.

In early 1980, the TVA Board of Directors requested the TVA staff to perform an expedited study to identify and evaluate potential degraded core mitigation concepts for the Sequoyah Nuclear Plant which had not yet been licensed for operation. The study was completed within three months and involved identifying mitigation concepts, defining design criteria, producing conceptual designs, performing accident analyses, and evaluating the effectiveness and cost of the concepts. Concepts studied in detail included filtered vented containment, additional containment volume, coupled containment, augmented containment cooling, preinerting with nitrogen, postinerting with Halon, and controlled ignition. The study concluded that controlled ignition was the most viable alternative should a commitment to a mitigation system become necessary. In June 1980, during a visit to the Sequoyah Nuclear Plant by NRC Commissioner Gilinsky, TVA volunteered to install a controlled ignition system. Because of its expedited design and installation schedule and its preliminary justification, it was referred to as the Interim Distributed Ignition System.

II. Controlled Ignition Background

The controlled ignition approach to hydrogen mitigation during degraded core accidents is intended to reliably ignite lean hydrogen-air mixtures throughout the containment to achieve periodic or continuous lean burning. This moderated energy addition rate would allow the active and passive containment heat sinks to absorb the heat of combustion more effectively and reduce the overall containment pressurization. Igniters are distributed throughout the containment in each region at sufficiently close intervals to accomplish this purpose. The devices are to be energized only during potential hydrogen-producing incidents or during testing.

Both spark and thermal (hot surface) devices were initially considered. While either is adequate to initiate combustion, an early decision was made to concentrate on simple thermal igniters. This was to avoid any potential electromagnetic interference from sparks, although subsequent research indicated such effects could probably be overcome.

A flammable mixture can be ignited by a small amount of energy transferred to the mixture locally. The energy must be enough to raise the local gas temperature to an ignition temperture sufficient to cause a self-sustaining reaction, as well as to supply enough additional heat to make up for loss to the surroundings. The tendency of a flame to propagate away from the igniter region is affected primarily by hydrogen concentration, steam and other diluent concentration, and turbulence. Flame propagation and subsequent ignition throughout a surrounding mixture may require slightly higher hydrogen concentrations than needed to achieve local flammability. Areas of investigation have involved the measurement of igniter surface temperature required for hydrogen ignition as a function of various hydrogen-air-steam mixtures.

The thermal igniter must be made of materials which can withstand high temperatures for prolonged periods without oxidizing or otherwise degrading. Thermal igniters normally consist of high-resistance wire surrounded by an insulator and a metallic sheath. The surface temperature potential is determined by the voltage, resistance, insulator properties, sheath geometry, and the temperature of the surroundings. Power requirements may also be a design parameter.

III. Igniter Selection and Development

In June 1980, TVA began looking for a readily available, commercial heater to serve as a thermal igniter in the IDIS. The initial candidate was a 120V ac ceramic core heater theaded for a light bulb socket. Since an existing plant emergency lighting system was utilized as the electric power supply to the IDIS, its application would have been ideal. However, its surface temperature was inadequate, at least as determined by the method of measurement employed at that time - pressure contact of a thermocouple to the heater surface. The next two heaters examined at Singleton were off-the-shelf commercial models in a cylindrical coil configuration. The 120V ac model had an unacceptably short operating life and the 220V ac model failed to reach an adequate surface temperature.

TVA then began examining diesel engine glow plugs from various manufacturers because of their likely reliability and endurance due to extensive development. One of the first diesel glow plugs examined was the General Motors (12V ac) automotive diesel plug available at that time, the AC model 7G plug. Other diesel glow plugs examined included a 12V ac Bosch model, a 12V ac Isuzu model, and a 24V ac General Electric/Caterpillar model. After an initial screening which revealed the need for a gradual break-in or conditioning period, the GM plug was selected as the primary choice for use in the IDIS with the Bosch plug as a backup. Most of the testing subsequently performed on the glow plugs was done on the GM plugs. No modification or further development was necessary since the off-the-shelf plugs demonstrated adequate performance (surface temperature) and durability (cycling,

overvoltage, lifetime, and combustion). The GM AC 7G glow plugs were installed in the IDIS in unit 1 of Sequoyah in August 1980. They also have since been installed in Sequoyah unit 2, Duke Power's McGuire Plant, American Electric Power's D. C. Cook Plant, and in Mississippi Power and Light's Grand Gulf Plant.

In September 1980, TVA received an operating license for Sequoyah unit 1. One of several conditions placed on the license was that by January 31, 1981, "TVA shall by testing and analysis show . . . that an interim hydrogen control system will provide with reasonable assurance protection against breach of containment in the event that a substantial quantity of hydrogen is generated." A further condition required that "for operation of the facility beyond January 31, 1982 (later extended to the first refueling outage), . . . an adequate hydrogen control system for the plant is installed and will perform its intended function in a manner that provides adequate safety margins." Throughout the remainder of 1980 and early 1981, TVA continued to provide justification supporting the capability of the IDIS in compliance with the first condition. At the same time, TVA began a fresh study of alternative candidates for a PHMS in response to the second condition. Concepts evaluated included controlled combustion using thermal igniters, controlled combustion using thermal igniters enhanced by spray fogging, postaccident inerting using Halon, controlled combustion using catalytic combustors, oxygen removal using a gas turbine, and postaccident inerting using carbon dioxide. In May 1981, TVA completed the study and concluded, for a number of reasons, that the best alternative for the PHMS at Sequoyah was controlled combustion with thermal igniters.

With assistance from TVA, the Electric Power Research Institute (EPRI) began exploring the potential for obtaining a suitable 120V ac thermal igniter for use in the PHMS. It should be emphasized that no problems have been encountered with the GM plug by TVA or any of the other utilities that would render it unsuitable for the controlled ignition application. The 120V ac specification was desirable just to simplify the electric power supply to a more standard plant voltage than the low voltage required by the GM glow plug. One of the first candidates was a cylindrical rod heater about 3" long. Preliminary tests revealed that the rod surface temperature decreased with the operating life. Another model examined at about the same time was manufactured at EPRI's request by Tayco Engineering of Long Beach, California. It was configured as a 2" long cylindrical coil heating element. The prototype drew on experience gained by Tayco during the development of heaters for long-life applications in space. Its design was based on criteria supplied to EPRI by TVA that specified a minimum surface temperature of 1500°F within 90 seconds at 120V ac under the extreme postaccident environmental conditions that might be expected in containment. The prototype was delivered to TVA and tested at Singleton. Since it showed promise, a second model was built by Tayco with a pair of support rods inside the coil to maintain its configuration and spacing.

After testing this improved model at Singleton, further modifications were recommended. A third model was built with reduced internal resistance and reduced coil spacing in order to elevate the surface operating temperature. After testing at Singleton, this model was accepted as the one to be produced in quantity for use in the PHMS.

Igniter Physical Descriptions

The igniter used in TVA's IDIS was a standard, off-the-shelf, General Motors AC Model 7G diesel glow plug (see Figure 1). It is approximately 3" in overall length with an Inconel 601-sheathed tip that is about 1" long and 0.2" in diameter. The electrical connector is a spade lug. The automotive design operating voltage is 11V dc, while the IDIS design operating voltage is 12V ac. At 12V ac, the power required is about 95 watts.

The igniter used in TVA's PHMS is a Tayco Engineering heater designed and developed as described previously in section III (see Figure 2). It is approximately 6" in overall length with a cylindrical coil heating element that is about 2.25" long and 0.75" in diameter. The heating element itself is a nichrome wire enclosed in an Inconel 600 sheath that is about 0.125" in diameter. A pair of 0.125" diameter support rods are located within the coil and are welded at each turn. The support rods and igniter housing are all composed of 304 stainless steel. The electrical connector is a two-pin plug. The igniter requires about 525 watts at the design operating voltage of 120V ac.

V. Igniter System Descriptions

The descriptions of TVA's IDIS and PHMS provided here are intended only as two examples of controlled ignition systems. Details of igniter type, installation, or operation may vary between the systems of different plants. TVA's IDIS consisted of GM glow plug assemblies distributed throughout the Sequoyah containment. Each glow plug was mounted so that the tip protruded through a custom metal enclosure (see Figure 3). The enclosure was 8" by 8" by 6" and housed a 120/12-14V ac transformer and all the necessary electrical connections. A sheet metal shield was provided above the igniter tip to prevent direct impingement of containment spray droplets. A copper plate to serve as a heat sink was attached on the face of the enclosure through which the igniter protruded.

The IDIS utilized the existing plant emergency lighting system because of its potential for multiple igniter locations throughout the containment and because it was backed by emergency diesel electric power. Several circuits were used with the number of igniters per circuit ranging from one to eight. The total number of igniters used in the IDIS for Sequoyah unit 1 was 32 and for unit 2 was 45.

The IDIS was designed to be energized immediately following the start of an accident without waiting for a potential hydrogen buildup and to remain energized until the unit reached cold shutdown. The system would have been energized shortly after entry into the procedures of the "Immediate Actions and Diagnostics" Emergency Operating Instruction. All igniters were to be manually activated by breakers at a lighting control panel in the auxiliary building.

The PHMS consists of Tayco igniter assemblies distributed throughout the Sequoyah containment. Each igniter is mounted so that the coil protrudes from a commercially available, NEMA type 4 enclosure (see Figure 4). The enclosure is 10" by 10" by 6" and houses the necessary electrical connections. A spray shield is provided over the igniter coil. However, no copper heat sink was judged to be necessary. No transformer is required in each igniter assembly since each circuit has the proper line voltage of 120V ac.

The PHMS is being installed as a new system because of a desire to customize the igniter coverage by location and to have two redundantly powered igniters at each location. The PHMS power supply is capable of being switched to the emergency diesel generators. There are 32 circuits with two igniters per circuit for a total of 64 igniters in one containment.

The PHMS would be energized immediately following the start of an accident upon the occurrence of any condition which causes the operator to use the "Immediate Actions and Diagnostics" Emergency Operating Instruction. Each of the two trains of igniters would be manually activated by a separate switch in the main control room.

VI. Igniter Durability Tests at Singleton

Three basic types of durability tests were performed on both the GM and Tayco igniters at TVA's Singleton Laboratory: cycling, endurance, and combustion. Although the test sequences were not identical for both types, there was enough overlap for a good comparison of their capabilities.

The cycling tests began with activation in air at a constant voltage until a steady-state igniter surface temperature was reached. Both the GM and Tayco igniters took between 1-2 minutes to reach peak temperature. Then the igniters were deenergized and allowed to cool for 15-20 minutes until close to the ambient temperature. The igniters were reactivated and the cycle repeated. A GM igniter was activated at 10, 12, and 14V ac and the transient surface temperature was recorded (see Figure 5). A GM igniter withstood 10 cycles at 14V ac. The above-design voltage of 14V ac was used for conservatism. The Tayco igniter was activated at 120, 125, 130, and 135V ac for a total of 20 cycles at each voltage and continued to function. For recorded transient surface temperatures at both the design and the highest tested voltage, see Figure 5.

The endurance tests consisted of igniter activation for extended periods. A GM igniter was operated at 14V ac for six consecutive days, and one was operated at 14V ac for two days. The Tayco igniter was activated at 120V ac for one day and later for seven consecutive days. Then it was activated at 135V ac for seven more days. Both the GM and Tayco igniters maintained satisfactory surface temperatures throughout the tests.

The combustion tests consisted of two types-igniter activation in premixed hydrogen-air atmospheres in closed vessels and in flowing mixtures in open combustion tubes. Two cylinders, one with 11 ft^3 and the other with 0.04 ft^3 internal volume, were used for the closed vessel tests. The larger vessel was of carbon steel with an epoxy-coated interior surface while the smaller vessel was of type 316 stainless steel. An igniter was mounted in each vessel through the center of an endplate. Hydrogen concentration in the vessels before and after ignition, the initial temperature, and the transient pressure rise were measured. Two GM igniters were activated in a total of about 50 closed vessel tests with initial hydrogen concentrations ranging from 0-16 volume percent. The igniters survived with no apparent damage and continued to operate.

Two horizontal combustion tubes, one 4' long and 4" in diameter of carbon steel and the other 5' long and 6" in diameter of pyrex glass, were used in over 100 combustion tests with flowing hydrogen-air mixtures. An igniter was mounted in each tube through an endplate at the centerline. A constant 20-scfh stream of various hydrogen-air mixtures was maintained through the tube by passing the gases through a small mixing chamber, then into the tube above the igniter near the end, and out the opposite end. The hydrogen concentration was established and monitored with a gas chromatograph that sampled the stream at the inlet and outlet of the combustion tube. Then the igniter was energized while its surface temperature, as well as the atmospheric temperature approximately one inch above and below it, were recorded throughout the test. A GM igniter was mounted in a combustion tube and activated for 24 hours in a 4-percent hydrogen-air mixture and for 1-2 hours in both an 8- and a 12-percent mixture. Later, a Tayco igniter was mounted in a combustion tube and activated for 24 hours in a 4-percent hydrogen-air mixture, for one hour in both an 8- and a 12-percent mixture and again for 24 hours in a 4-percent mixture. Both igniter types survived these combustion tests and continued to operate satisfactorily, showing no surface deterioration. The same Tayco igniter was intermittently subjected to all of the previously described cycling, lifetime, and combustion tests and continued to operate satisfactorily. Data from these tests will be presented elsewhere.

VII. Igniter Performance Tests at Whiteshell

Two basic types of performance tests were performed on both the GM and Tayco igniter at the Whiteshell Nuclear Research Establishment to determine lower ignition limits and minimum surface temperatures at ignition with various steam concentrations.[1] These

tests and their results are discussed in detail in the paper, "A Review of Recent WNRE Experiments on Hydrogen Combustion," by H. Tamm, et al., also to be submitted to the Second International Workshop on the Impact of Hydrogen on Water Reactor Safety. For this reason, they will simply be summarized here.

The tests were conducted in a roughly spherical 17-liter vessel. Ionization probes were inserted to detect flame propagation, and thermocouples were attached to the surface of the igniters. Steam concentrations were varied from 0-55 percent. The mixtures were introduced into the vessel before the igniters were energized.

Data were compiled from over 50 tests with the GM igniter at various concentrations of hydrogen and steam and with and without forced turbulence (see Figure 6). Each test was characterized by the ionization probe response to flame propagation as either "ignited," "marginally ignited," or "no ignition." Ignition limits for both static and turbulent mixtures were proposed based on the acquired data. Similar data were compiled from about 25 tests with the Tayco igniter (see Figure 7). The proposed ignition limits for the GM igniter are plotted with the Tayco data for comparison. As shown, the performance of the two types of igniters is very similar, with the Tayco ignition limits perhaps being slightly lower. Either igniter was able to ignite dry mixtures with less than 5-percent hydrogen and 50-percent steam mixtures with about 7-percent hydrogen.

During the same test series, data were also recorded on the surface temperature of the igniters. The igniter surface temperatures at the instant of ignition in each of the tests where ignition occurred were compiled for both the GM and Tayco igniters (see Figure 8). The GM igniter surface temperature required for ignition varied from 1280-1350°F for dry mixtures and ranged up to 1535°F for 50-percent steam mixtures. The variation between ignition temperatures for the same igniter and the same steam concentration is due to the differences in hydrogen concentration and degree of turbulence. The required Tayco igniter surface temperature varied from 1165-1200°F for dry mixtures and varied from 1275-1365°F for 50-percent steam mixtures. The Tayco igniter was capable of igniting mixtures at 125-200°F lower surface temperature depending on steam concentration. Both GM and Tayco igniters possess ample margin between their achieved operating temperatures and the minimum surface temperatures required for ignition even at high steam concentrations.

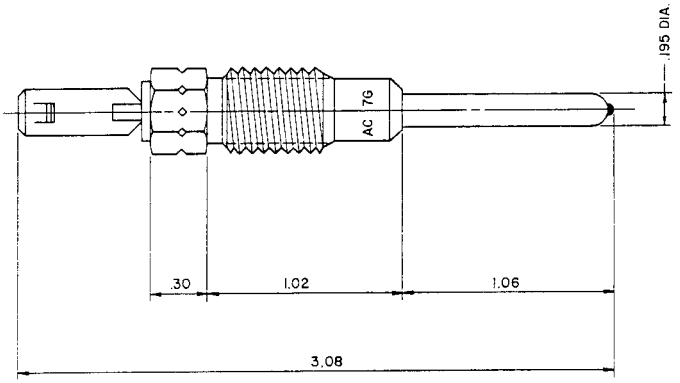
Other combustion performance tests on the GM glow plug were conducted for EPRI by Factory Mutual Research Corporation and Acurex Corporation and are respectively described in the papers "Water Fog Inerting of Hydrogen-Air-Steam Mixtures" by R. Zalosh, et al., and "Hydrogen Control Tests at Intermediate Scale" by R. Torok also to be submitted to the Second International Workshop.[2]

VIII. Summary

Several utilities have recently installed controlled ignition systems in LWR containments for hydrogen mitigation during degraded core accidents. TVA was the first to install such a system. After surveying the off-the-shelf thermal igniter market, the GM AC model 7G diesel glow plug was selected for TVA's IDIS. The GM igniters were installed in custom enclosures with individual transformers and powered by an existing plant lighting system. Later, after evaluating a number of alternative concepts for the PHMS, TVA selected controlled ignition using thermal igniters. A Tayco Engineering igniter was chosen for the PHMS by TVA after several development steps. The Tayco igniters are being installed in standard enclosures without individual transformers since the power supply system provides the 120V ac operating voltage directly. The PHMS has redundant igniters which can be actuated from the main control room. Extensive tests of both durability and performance have been performed on both the GM and Tayco igniters. Both types withstood cycling, endurance, and combustion tests and continued to function satisfactorily. Measurements of lower flammability limits and igniter surface temperatures at ignition showed that the LFL were comparable for the two types and that the Tayco igniter was capable of initiating combustion at lower surface temperatures. In conclusion, the igniter development and testing efforts described here have resulted in two acceptable alternative igniters for use in controlled ignition systems in LWR containments for hydrogen mitigation during degraded core accidents.

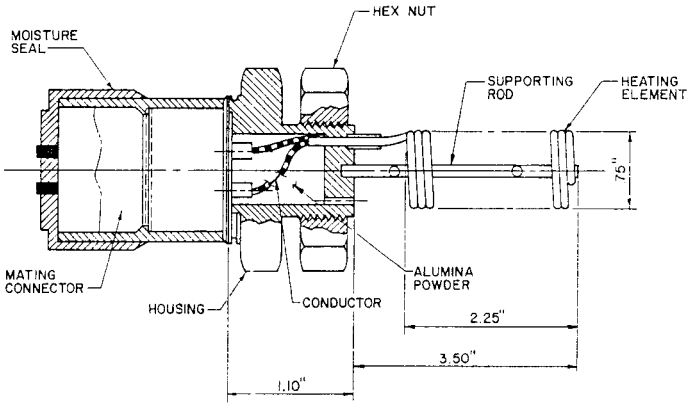
[1]Jointly funded by EPRI, TVA, Duke Power, American Electric Power, Atomic Energy of Canada, Ltd., and Ontario Hydro.

[2]Jointly funded by EPRI, TVA, Duke Power, and American Electric Power.



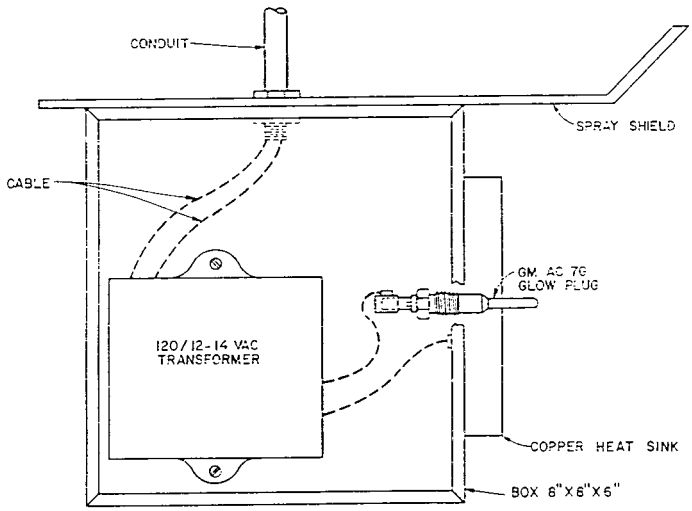
GENERAL MOTORS AC 7G GLOW PLUG

FIGURE 1



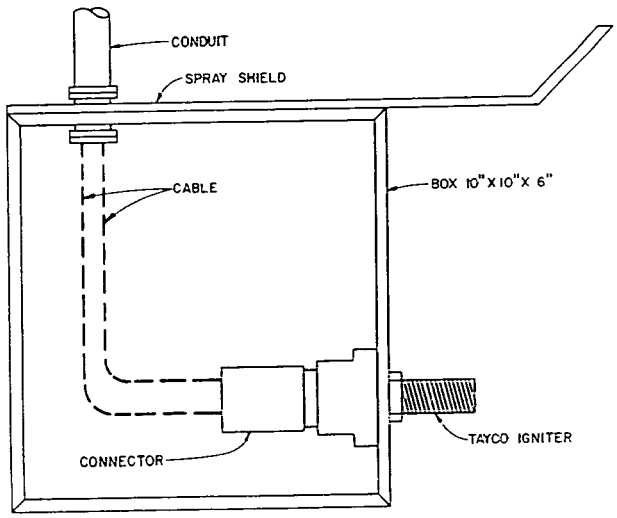
TAYCO THERMAL IGNITER

FIGURE 2



GM IGNITER ASSEMBLY

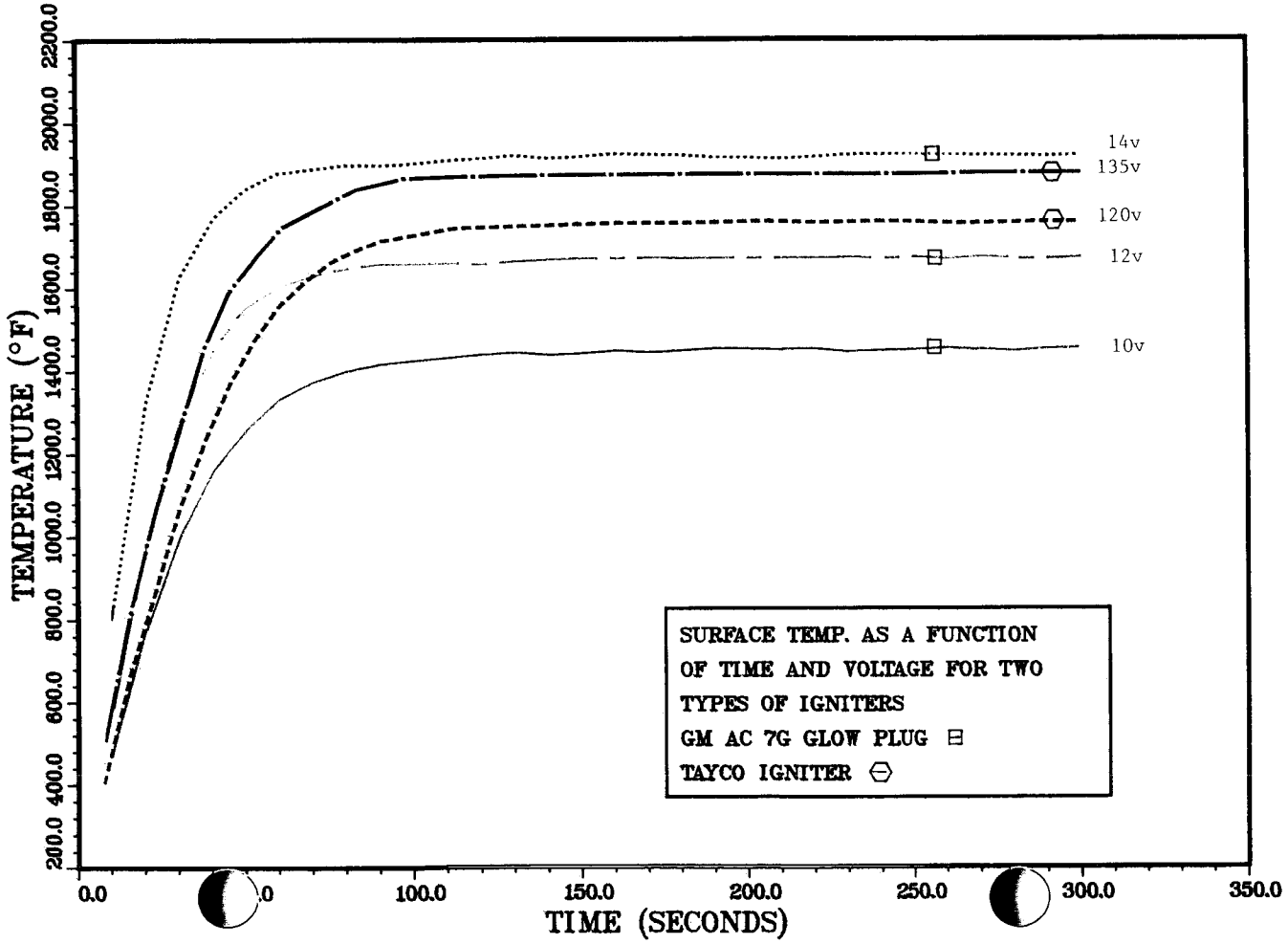
FIGURE 3

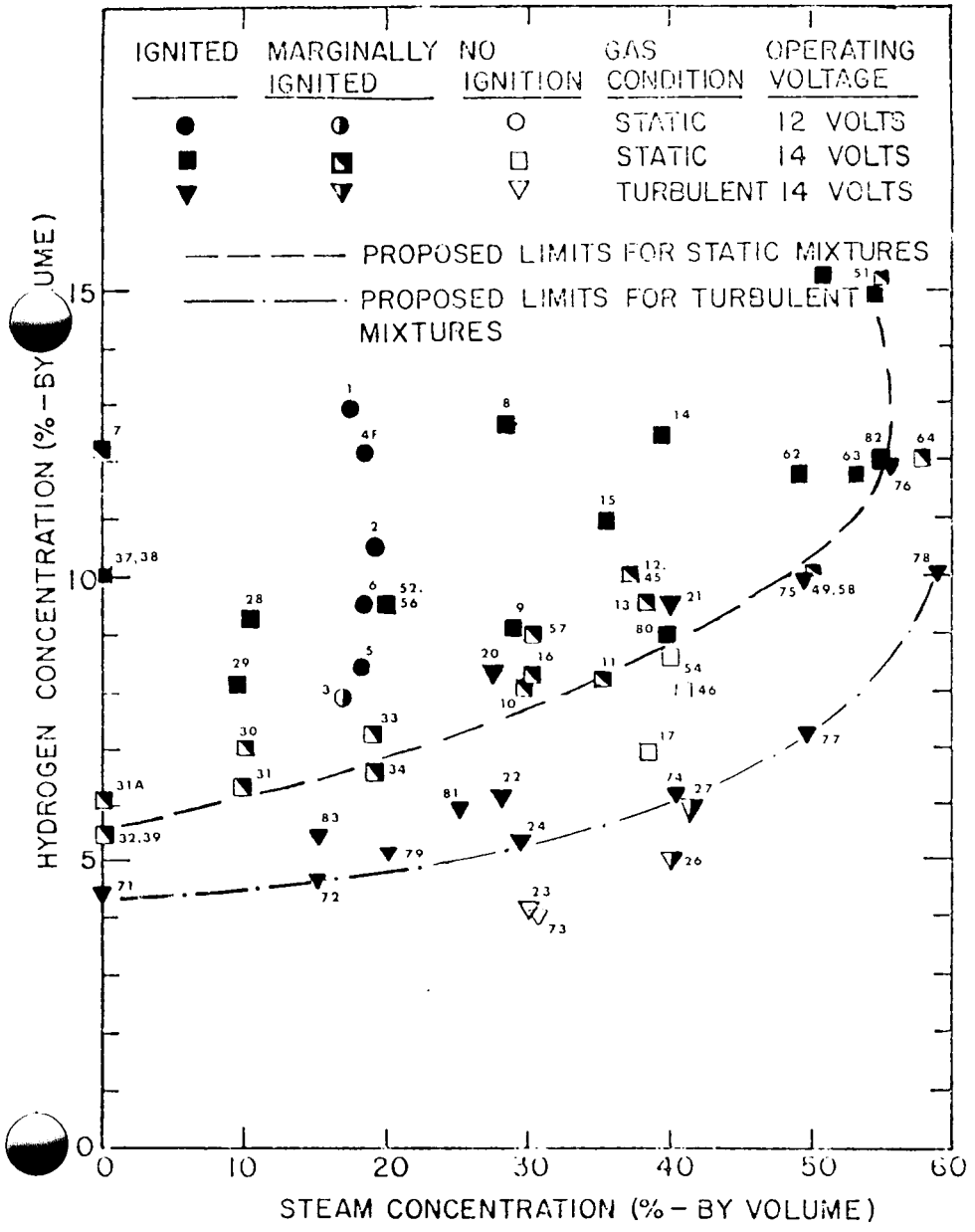


TAYCO IGNITER ASSEMBLY

FIGURE 4

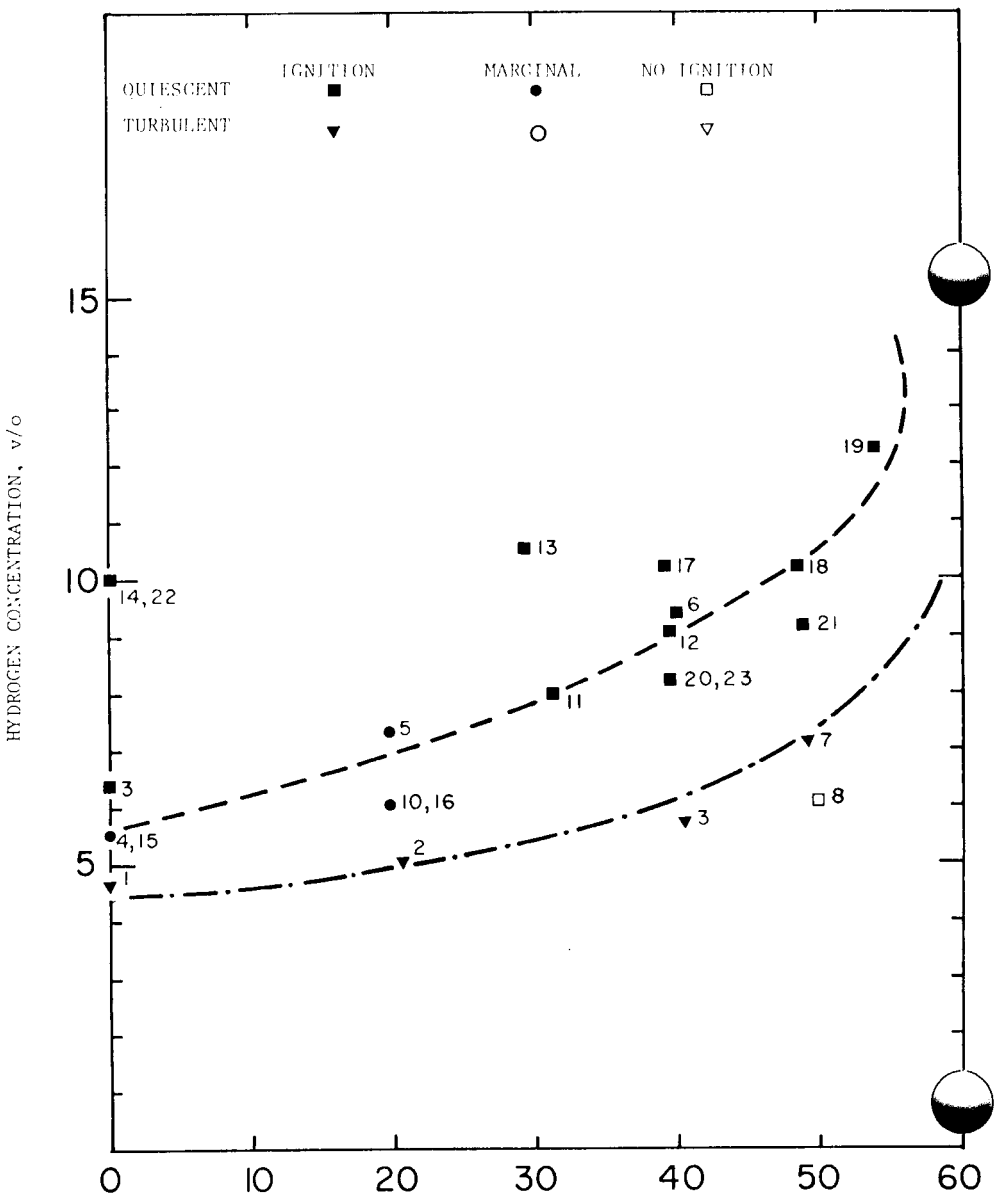
SURFACE TEMPERATURE





THE IGNITION LIMITS OF HYDROGEN/AIR/STEAM MIXTURES USING A GM AC MODEL NO. 7 THERMAL GLOW PLUG LOCATED AT THE CENTRE OF A 17-LITRE QUASI-SPHERICAL VESSEL.

FIGURE 6



The ignition limits of hydrogen/air/steam mixtures using a Tayco igniter located at the center of a 17-liter quasi-spherical vessel. Note that ignition limit lines are for the GM igniter from figure 6.

FIGURE 7

Review of the Grand Gulf Hydrogen Igniter System

John C. Cummings, Allen L. Camp,
Martin P. Sherman, Michael J. Wester,
David Tomasko, Rupert K. Byers, and
Blaine W. Burnham

Sandia National Laboratories
Albuquerque, NM 87185

Introduction

As a result of several investigations of the accident at the Three Mile Island Nuclear Plant (TMI-2) in March of 1979, the U. S. Nuclear Regulatory Commission (NRC) has required that boiling water reactor (BWR) nuclear plants employing the Mark III design be equipped with additional systems to control large quantities of hydrogen. In this regard, the Mississippi Power and Light Company (MP&L) has proposed installation of the Hydrogen Igniter System (HIS) at the Grand Gulf Nuclear Station to burn the hydrogen generated during accidents more severe than the design-basis accidents. The NRC must evaluate the effectiveness and reliability of the proposed HIS as part of the Grand Gulf licensing activities.

In August of 1981, Sandia National Laboratories (SNL) agreed to assist the NRC by making a technical evaluation of the adequacy of the HIS to meet the threat posed by hydrogen combustion at the Grand Gulf Nuclear Station. The technical goals of our evaluation of the design and testing of the HIS were:

1. to assess the adequacy of the location and distribution of igniters;

2. to perform independent calculations of the containment atmosphere pressure and temperature response to hydrogen combustion, and compare these to the calculations performed by the applicant (MP&L has used the CLASIX-3 computer code exclusively);

3. to determine the likelihood (qualitative assessment) and consequences of detonations (in terms of calculating impulsive loads, not in terms of estimating structural failure);

4. to examine and estimate containment (including wetwell) atmosphere mixing;

5. to assess the adequacy of the actuation criteria for the HIS; and

6. to assess the adequacy and completeness of the spectrum of accidents considered in the applicant's evaluation.

As necessary, we were to provide recommendations to the NRC for corrective action or design changes.

Preliminary Report

At the end of August 1981, we submitted a Task 1 Report to the NRC. This report summarized our preliminary evaluation, discussed our technical approach for the Task 2 (draft report) evaluation, and requested additional information in a number of areas. In order to write the preliminary report we had reviewed several MP&L documents (submittals to the NRC regarding the HIS), toured the Grand Gulf Nuclear Station, and performed MARCH computer code calculations for various Grand Gulf accident scenarios.

In our Task 1 Report, we indicated that our evaluation of the adequacy of the HIS would depend heavily on the value of containment failure pressure or "ultimate capacity of the containment." An NRC analysis indicated that 56 psig (71 psia, 4.8 atm) would be an acceptable value. MP&L has reported calculated values from 47 to 67 psig for the ultimate capacity of the containment. Unfortunately, this uncertainty band overlaps with the expected uncertainty in hydrogen-burn pressure associated with the transition from incomplete to complete combustion. For example, the NRC estimate of failure pressure could be exceeded if a *single*, *complete*, *adiabatic*, *isochoric* burn were to take place with eight to nine percent hydrogen distributed homogeneously in the containment air.* Our preliminary conclusion, therefore, was that the uncertainties of the HIS performance overlap with the uncertainties of the calculated failure pressure. Consequently, we stated that more accurate and detailed analyses would be required before an assessment of the HIS adequacy could be made. Our goal was to reduce the uncertainty of the estimates of HIS performance during various scenarios, but we noted that uncertainties would still remain even after we had completed this evaluation.

Draft Report (NUREG/CR-2530) Summary

In January 1982, we submitted a draft report to the NRC for review. Since that time we have made several revisions to the original version and we are currently preparing the final report.

Our technical approach involved the use of several computer codes combined with the engineering judgment of the Sandia staff. The Sandia code HECTR (Hydrogen Event: Containment Transient Response) and the MARCH code (written by Battelle Columbus Laboratory) were used extensively as counterparts to

*The exact hydrogen concentration required to attain 56 psig depends on the preburn pressure (e.g., the addition of the drywell gases to the containment atmosphere increases the initial pressure by 19 percent).

CLASIX-3 in order to calculate the containment atmosphere pressure and temperature response to hydrogen combustion. The German code RALOC was used to investigate mixing effectiveness by calculating the spatial and temporal behavior of the hydrogen concentration (preburn conditions only). The Sandia code CSQ was used to calculate the impulsive loads that would accompany a local detonation.

In summarizing the results of our Task 2 assessment, we must repeat several statements that were made in the preliminary (Task 1) report. First, we used the NRC value of 56 psig for the containment failure pressure. If this value were to increase or decrease by five to ten psi, it could have a significant effect on our evaluation and recommendations. Second, after several months of intensive study and hundreds of computer calculations, we are still left with uncertainties about the adequacy of the HIS. None of the available computer codes (MARCH, CLASIX, and HECTR) is sophisticated enough at present to allow us to predict peak pressures with high precision, and all the codes are very sensitive to certain input parameters and models of phenomena that are simply not known very well.

It is also important to note that we have not analyzed in any significant detail a number of phenomena associated with hydrogen combustion. These include: accelerated flames, missile generation, spatial and temporal nonhomogeneities in gas mixtures, multiple and sequential ignitions, and equipment failures. Theoretical models and computer codes are not presently available as calculational tools to analyze these phenomena. In addition, experimental data are sparse, especially under nuclear plant accident conditions (very large geometrical scales, three-dimensional obstacles and flame paths, concentration gradients in the gas mixture, etc.).

The net result of our evaluation, including uncertainties, can be stated as follows: In our judgment, the currently proposed HIS is "marginally adequate" to meet the threat posed by hydrogen releases within the containment building. By "marginally adequate", we mean the following: In order to calculate the combustion behavior of hydrogen inside the Grand Gulf containment, we must specify a number of parameters for the simple models presently in our computer codes. If each of these parameters is at the optimistic end of its "best-estimate" range, the computer codes predict combustion-generated pressures well below the specified value for failure. If each of these parameters is at the pessimistic end of its "best-estimate" range, the computer codes predict pressures in excess of the assumed failure value. Mid-range values for these parameters will generally result in calculated pressures which are high, but below the specified failure pressure.

Later in this paper, we discuss recommendations for changes to the proposed HIS design which we feel would improve its

ability to meet the hydrogen threat. Several "advanced concepts" that we believe might be desirable alternatives or adjuncts to an igniter system for BWR Mark III plants are discussed in another report.[1]

Several things cause us to judge the HIS to be marginally adequate. There are significant uncertainties in the hydrogen release rate, the degree and rate of mixing within the wetwell/containment (see Fig. 1), and the ignition and propagation behavior of burns. In addition, the availability of the containment spray system is not certain. These items tend to dominate the results of our calculations, and consequently, reliable conclusions are difficult to draw. We do know that if conservative upper bounds or assumptions are made regarding these key items, our calculations indicate the generation of pressure in excess of the assumed failure value.

Hydrogen release rates for accidents in nuclear plants cannot be predicted with confidence at present. Low-pressure (large-break) accidents tend not to produce significant hydrogen prior to total core uncovery due to high steam flow rates which maintain the core temperature below that required for significant metal-water reaction. On the other hand, high-pressure (e.g., small-breaks) accidents tend to have considerably lower steam flow rates which results in higher core temperatures and significant hydrogen generation prior to complete core uncovery. Our present understanding of core behavior during loss-of-coolant accidents is quite limited, primarily due to a lack of knowledge and data concerning core-slump phenomena.

The processes governing production of hydrogen during a degraded-core accident are not well known, and in some respects, are expected to be indeterminate. The hydrogen generation rate will depend on the rate of coolant injection from the Emergency Core Cooling System (ECCS) and the time that the injection begins. The degraded-core models in MARCH can predict very high to very low hydrogen yields, because the predictions are dominated by input assumptions. Until better data and models are produced, we must either accept the (perhaps artificial) conservative upper bound, or select another (equally arbitrary) model.

MP&L used the MARCH code predictions up to the point of core slump (when the rate increases enormously) and then assumed a constant rate equal to the largest previous value.[2] Since the hydrogen release rate is such an important parameter, we recommend further study of the MP&L approach to assess its validity.

The degree and speed of mixing within the wetwell/containment region are very difficult to estimate. Based on engineering judgment, we believe that if containment sprays are operating, the upper dome region will be well mixed. If they are not

operating the mixing is uncertain. Independent of the question of spray operation are the degree and rate of mixing in the annular wetwell region. The computer codes (MARCH, CLASIX, and HECTR) essentially account for only pressure-driven flow between idealized compartments. Unlike RALOC, these codes do not realistically model the post-burn flow and mixing, or natural convective mixing. Consequently, when the codes predict a large number of burns in one region and no burns elsewhere, or oxygen depletion in one region, or a volume filled with hydrogen existing stably below a volume filled with air, the models are demonstrating that they are too crude to provide refined answers.

The ignition and propagation of burns in the containment are obviously phenomena that must be correctly modelled in order to calculate realistic pressure and temperature transients. The computer codes treat these phenomena very simplistically. Consequently, we are forced to specify values for ignition criteria, propagation criteria, combustion completeness, and flame speed. The values we select can have tremendous leverage on the calculations. The combustion processes that would actually occur in containment for our postulated accident scenarios are probably much different than the idealized models. Spatial and temporal gradients in hydrogen, oxygen, and steam concentrations, coupled with discrete igniter locations, would tend to produce a very complex series of local burns which might be less threatening than our calculated "compartment" burns. It is well beyond the current state-of-the-art to model such behavior.

Finally, the issue of whether or not containment sprays operate is very important. It is beyond the scope of this report to determine the quantitative likelihood or probability of spray availability. We can, however, observe the effect of spray availability on our calculations. We conclude that spray operation is very important to plant safety for the accident scenarios (hydrogen release rates in particular) examined in our study. The benefits of containment sprays are threefold: the peak pressure of a single burn will be reduced by spray evaporation if the burn duration is sufficiently long; the baseline pressure for multiple burns will be reduced if the time between burns is sufficiently long; and the thermal environment to which plant equipment will be exposed will be less threatening.

Calculations of the containment atmosphere pressure and temperature response to hydrogen combustion are a very important part of this HIS assessment. But due to the uncertainties discussed above, total reliance on the code calculations is unwarranted. At present, engineering judgment may be as important to the assessment as calculations even though it might appear to be more subjective. A good example of this is the CLASIX-3 sensitivity study[3] of containment sprays. The CLASIX-3 calculations indicate that burns without sprays result in lower peak pressures than with full spray operation. This result is

exactly opposite to our intuition, and in our opinion, is an artifact of the compartment model and input assumptions. Our engineering judgment dictates that, if possible, the sprays should be initiated before significant hydrogen production occurs and remain on until the accident is brought under control.

Comparisons between the various computer codes is difficult because we know little of the calculational models within CLASIX-3 and even MARCH. We have attempted to carry out calculations with MARCH and HECTR that are nearly identical to several CLASIX-3 cases. Unfortunately, we invariably end up comparing "apples to oranges." HECTR has no drywell compartment model; MARCH has a drywell, but only zero-flow-resistance connections to and from it. Since it is not an input for MARCH calculations, the MARCH hydrogen release rate is not the same as that used in HECTR and CLASIX-3. Despite these and other differences, the three codes predict the same general kind of wetwell/containment behavior. (As acknowledged in the CLASIX-3 sensitivity study, the calculational results are sensitive to the user-selected compartment configuration.) Specific differences in calculated pressures and temperatures from the three codes can probably be attributed to differences in modelling and input assumptions for heat and mass transfer. We have some concern regarding the CLASIX-3 calculational models for flow through the drywell vacuum breakers and flow into the drywell through the suppression pool. The CLASIX-3 treatment of heat transfer to and evaporation of the spray droplets is another area of concern.

Regarding detonations inside the Grand Gulf containment building, two conditions must be satisfied simultaneously: a detonable mixture must exist, and an ignition source or mechanism must exist. In our judgment, the likelihood of forming detonable mixtures is small, especially for regions of significant extent. We also currently believe that the likelihood of detonation occurring, either by direct initiation or by transition from deflagration is very small.

Assessment Results and Recommendations

The following sections discuss the results of our evaluation as presented in the draft report. It should be noted that this work did not consider the issue of equipment survivability during and after hydrogen combustion. Since most of the safety/control equipment is located in the wetwell region above the suppression pool, this may be an extremely important issue. Multiple hydrogen burns, continuous burning, and the lack of direct water sprays in the wetwell may lead to significant component temperatures and significant exposure times.

Adequacy of the HIS Design

In our opinion the design of the HIS is basically sound (the deliberate ignition concept, however, is judged to be marginally

adequate to meet the threat posed by hydrogen combustion). We do have a few suggestions that we feel would improve the Grand Gulf system in terms of reliability. The present design[2] calls for a total of about 90 igniters distributed throughout the drywell and wetwell/containment. Redundancy is factored into the design by using two separate power distribution panels (Divisions I and II). Each panel uses two circuit breakers (approximately 23 igniters per breaker) to protect its igniters. The power system is attached to the station diesel generator in case of loss of off-site power.

The igniter distribution and location design is such that: the igniters are no more than ~30' apart if all are operable (except vertically between elevations 209' and 262' in the containment dome, and near the bottom of the drywell); the igniters are no more than ~60' apart if only one Division is operable; all enclosed regions are served by at least one igniter from each Division. The drywell will be served by 18 igniters, 6 each at elevations 146', 161', and 179'. The wetwell distribution of igniters is such that 12 igniters are located near elevation 135', 15 are located near elevation 160', 8 are located near elevation 180', and 19 are located near elevation 204'. In the containment dome there are 8 igniters at elevation 262', 8 at elevation 286', and 2 at elevation 295'.

In our judgment, the HIS design could be improved in two ways: an increased number of circuit breakers (fewer igniters per breaker); and, either a modified igniter support design or an increased number of igniters in the wetwell/containment region. We believe that if a short circuit at one igniter will deactivate 22 other igniters, the circuit breaker design is inadequate. In our opinion, no more than two igniters at any elevation should be protected by the same circuit breaker. This means that a total of six or eight igniters could be protected by one breaker if those igniters are spatially distributed throughout the various regions. We strongly recommend that the drywell igniters be protected by their own circuit breakers, since our preliminary analysis of suppression pool motion during containment burns indicates that significant pool surge may occur inside the drywell.

The present design for igniter housing and support structure such that it tends to limit the effectiveness of combustion nition. In our opinion, the system will reliably ignite hydrogen:air mixtures in the ~ten percent hydrogen* range, but not necessarily in the six to eight percent hydrogen* range. Since it is desirable to burn the hydrogen in containment at the lowest possible mole fraction, the igniters should be positioned so that they can burn out large volumes with upward propagation

*Average concentration in the region served by one igniter (~ 30'x30'x20' = 18,000 ft^3).

of flames. Hydrogen is unique in having a very large difference between the upward and downward flame propagation limits, the upward propagation limit of 4.1 percent being much lower than the downward limit of nine percent.

The design of the igniter housing incorporates a spray shield (horizontal plate with vertical sides) a few inches above the igniter. This shield tends to locally inhibit flame propagation. A much more serious problem for all but those igniters located on the containment dome wall, is that most igniters are located within two feet of ceiling structures. Some of these ceilings are solid concrete, while others are metal gratings. The solid ceilings clearly inhibit the effectiveness of the igniters, and a similar inhibition of igniter effectiveness will occur if the grating area above igniters is covered with equipment. The main point here is not that the igniters won't work as proposed, but that reliable ignition of lean mixtures is questionable for the volume served by a single igniter whenever upward flame propagation is restricted.

We feel that the proper design of a support for an igniter in a specific location should incorporate consideration of the likely flame path. In general, it is desirable to have the igniter away from large solid surfaces, especially those above. If such an approach is not feasible at this time, then we would recommend increasing the number of igniters, especially in the wetwell region (from elevation 135' to 209'). We also recommend that the igniters in the containment dome at elevation 286' be symmetrically staggered in azimuthal position with respect to those at elevation 262', so as to take advantage of the likely flame paths.

Adequacy of the HIS Testing

In our judgment the operational inspection and testing program specified by MP&L for the HIS system[2] is reasonable and adequate (however, the frequency of the periodic testing was never defined). As discussed previously, we feel that the design of the HIS should be changed in several ways. The impact of these design changes to the operational testing program is beneficial. If fewer igniters are powered by one breaker, a change in the current drawn by that breaker is more easily detected and finding the cause of that change is simpler.

Testing of the system design with respect to igniter, transformer, or wiring failure under accident conditions is very important since one failure (short circuit) can shut off a number of igniters. The planned submergence test[2] is a step towards addressing this issue. We feel that it is desirable to test the igniter assembly under accident conditions for extended periods (several hours). These conditions would include hydrogen burn environments, high steam pressures, and water spray impingement.

Hydrogen Combustion Calculations

A wide variety of cases were run using HECTR and MARCH, including cases to examine compartmentalization, flame speed, completeness of combustion, propagation limits, sprays, and the hydrogen source term. Based upon our analysis and a study of the CLASIX analysis presented in Refs. 2 and 3, we have reached the conclusions discussed below.

In most cases the HECTR analysis predicts peak pressures that are much higher than those predicted by the CLASIX analysis.* The CLASIX analysis divided the containment into two compartments: the wetwell region just above the suppression pool and the rest of the containment, including the dome. The CLASIX analysis generally predicts a large number of burns in the wetwell resulting in small pressure rises and no burns in the dome. HECTR generally predicts at least one burn in the dome resulting in high pressures, due to the large volume of the dome relative to the wetwell. The reason that burns are predicted in the dome is that HECTR predicts inerting in the wetwell due to oxygen depletion at an earlier time than CLASIX does. Once the wetwell inerts, hydrogen is transferred from the wetwell to the dome at a higher rate, and burns in the dome occur soon afterward. Both CLASIX and HECTR show that, after a burn in the wetwell, oxygen is drawn back into the wetwell from the dome as the wetwell cools down. HECTR predicts a slightly lower rate of cooling in the wetwell, and thus, inerting occurs a few burns earlier than in the CLASIX analysis. This difference in cooling rate could be due to assumptions regarding passive heat sinks, heat transfer models, or the treatment of containment sprays. Because a small difference in the models or input assumptions can have such a dramatic impact on the results, the problem is "ill-conditioned." Despite the differences in the results, we feel that the behavior of CLASIX and HECTR is similar. Both codes predict eventual wetwell inerting, just at different times (some of the CLASIX cases were close to ignition in the dome at the end of the run). Differences in the heat transfer models appear to be small.

The most significant uncertainty in the analysis involves mixing of hydrogen and oxygen in the containment, and neither HECTR nor CLASIX properly addresses this issue. Both codes include pressure-driven mass transfer, but not convection or diffusion. Therefore, both codes underestimate the rate of mixing. We believe that the actual hydrogen and oxygen concentrations will be more uniform between compartments than predicted.

*A drywell compartment in HECTR might reduce the calculated pressures by 10-15%.

Based upon experimental data, we feel that the flame speed used in the CLASIX analysis is a factor of three or more low. The lower flame speeds result in more time for heat transfer during a burn, particularly if the sprays are on, and correspondingly lower temperatures and pressures. The difference in peak pressure using the CLASIX flame speed as opposed to the HECTR flame speed can be five to fifteen percent depending upon the input assumptions. Flame speeds higher than those used in HECTR, due, for example, to flame acceleration, could result in an additional difference of two to eight percent in peak pressure (not including dynamic loads associated with supersonic flames).

When varying other burn parameters we found that incomplete combustion results in decreased pressure rises; however, the benefit is not always as large as expected due to the fact that burns are more numerous and closer together in time. Additionally, we found that burns propagating from the wetwell into hydrogen concentrations of four to six percent in the dome will probably not produce pressures in excess of the assumed failure pressure. Burns propagating into eight to ten percent hydrogen concentrations in the dome or burns originating in the dome might produce pressures that could threaten containment.

Containment sprays almost always result in a significant reduction in temperature and pressure during a burn. Sprays may have a slight negative effect early in the accident if they enter the containment at a higher temperature than the containment atmosphere and result in an elevation in pressure. However, this effect is small, and we would recommend that the sprays be turned on as early as possible in the accident and remain on until all danger of hydrogen combustion has passed.

The actual number, timing, location, and peak pressures that would be associated with hydrogen burns during a reactor accident depend on the local concentrations of the gases and the mixing processes which produced those concentrations (prior burns, natural and forced convection, H_2 injection rates, etc.). The MARCH, HECTR, and CLASIX computer codes, however, introduce an artificial mixing of the containment atmosphere. The gas entering a compartment is assumed instantly mixed with the contents of the compartment, and hence each compartment atmosphere is homogeneous. Real mixing processes such as natural or forced convection are not considered.* The results of combustion, as predicted by these codes, therefore depend strongly on the compartment model used. The number and arrangement of compartments is somewhat arbitrary. The most "realistic" model will be the one that best approximates the real mixing behavior in containment.

*MP&L does consider a small amount of forced convection in one CLASIX-3 sensitivity case.

For multicompartment models, MARCH predicted a series of burns in the wetwell, the compartment into which hydrogen was introduced from the suppression pool. The inerting of the wetwell by oxygen depletion occurred in all cases and led to the buildup of large hydrogen mole fractions in the wetwell and combustible mole fractions in the upper compartments. In all cases considered but one, burns occurred in the upper containment and led to significant pressure peaks. Most of the cases predicted pressure peaks below the NRC estimate of containment failure pressure, 56 psig (4.8 atm), but some were higher. The results emphasize the importance of those failure-pressure estimates to conclusions drawn from this work.

Detonations at the Grand Gulf Nuclear Station

It appears to us that several conditions could lead to the formation of "detonable" clouds of significant extent. Generally, the igniters would have to be off for some time and other ignition sources (hot surfaces, switching sparks, motor sparks, etc.) would also have to be temporarily off or ineffective. A sudden large increase in the hydrogen release rate or the movement of a large air mass into an oxygen-depleted, hydrogen-rich compartment (e.g., the drywell) might also lead to local regions of detonable proportions. The most likely regions for localized detonations appear to be the drywell and the bottom of the wetwell. Higher wetwell regions could become involved if steam inerting and/or oxygen depletion occurred due to previous combustion events.

Several complicating factors make it difficult to discuss the likelihood of forming a detonable mixture. Hydrogen, oxygen, and steam concentration gradients occur in the vertical (z), radial (r), and azimuthal (θ) directions. This would be true even without combustion. With numerous combustion events occurring throughout the wetwell/containment region at various times, the picture is extremely complex. For each igniter we can envision a sequence of "pulsed" burns in which some hydrogen is locally combusted. A period of mixing follows each burn. In the region between the top of the suppression pool and the first wetwell igniters (z = 135'), the concentration of hydrogen may reach detonable proportions if the hydrogen release rate is high enough. A pulsed burn from z = 135' down to the top of the pool would remove all hydrogen from the region and permit high hydrogen concentrations to form before the new mixture rose to the igniters. The spatial extent of such detonable mixtures would probably be limited.

In our judgment, given current understanding, the likelihood of a detonation occurring, as distinguished from the formation of detonable mixtures, is very small. The probability of a deflagration-to-detonation transition occurring is also probably quite small. However, we feel that some degree of flame acceleration upward through the wetwell obstacles is almost a certainty. The degree of acceleration will depend significantly on

the effectiveness of the igniters in burning very lean mixtures and on the spatial concentration gradients. Measurements in obstacle-filled tubes at McGill[4] indicate that flame acceleration mechanisms function with as little as six percent hydrogen present in air, and that high flame speeds can be achieved (~20 m/s for 8 percent H_2 and ~150 m/s for 10 percent H_2).

The consequences of a detonation occurring in the wetwell the Grand Gulf containment building were calculated using the CSQ computer code. Results, in terms of pressure and impulse histories, are presented in NUREG/CR-2530.

Containment Atmosphere Mixing

Hydrogen transport calculations were made with the computer code RALOC[5]. The objective of these calculations was to provide an estimate of the volumetric hydrogen concentration in the upper compartments of the Grand Gulf containment building when the bottom compartment achieves a reliable combustible hydrogen level at the igniters (assumed to be approximately eight to ten percent). A sensitivity-study approach was used to attain this objective, rather than a best-estimate technique. This was done for two reasons: first, there are large uncertainties associated with the hydrogen release models following a loss-of-coolant accident; second, the RALOC code itself has had only limited assessment to date. It must be noted that all RALOC calculations involve precombustion conditions--no mixing during or after combustion was considered.

Two groups of parameters were varied in this study. The first group contains parameters which test the reliability of the code. These are the maximum time steps allowed during the implicit integration of the differential equations, and the number of zones and connections used to model the Grand Gulf containment (nodalization). The second group consists of physical parameters which are either uncertain in the hydrogen source description, or are known to affect the transport of hydrogen in a containment. They are the amount and rate of hydrogen injection, the hydrogen injection temperature, and the initial temperature distribution present in the containment building.

Although the quantitative results of our RALOC sensitivity studies were somewhat different, the qualitative results were the same. During the injection period, nonhomogeneities existed in the hydrogen volumetric concentrations. Increasing the rate of hydrogen injection, or inverting the temperature distribution (higher temperature at the top of the containment than at the bottom) produced larger asymmetries. (Temperature inversions appear to be possible if containment sprays are inoperable, especially if burns have occurred previously.) When the bottom compartment reached the assumed lower combustion limit of eight

percent, the upper containment levels had hydrogen concentrations between three and six percent, depending on the rate of hydrogen injection and the degree of resolution used in the RALOC nodalization. Once the bottom compartment reached eight percent, an additional five minutes were typically required to bring the upper compartment to the same value. As expected, the hydrogen transport was dominated by convection.

Adequacy of the Actuation Criterion

The stated actuation criterion[2] for the HIS is an indication that the primary vessel water level has fallen to the top of active fuel. Our judgment is that actuation of the HIS at this point in an accident would provide sufficient time for the surface temperature of the igniters to reach an acceptable value for reliable ignition. It should be noted that we have not examined the availability or reliability (under accident conditions) of those systems involved in the primary vessel water level measurement. We are somewhat concerned that the HIS actuation is done manually--apparently without an automatic back up system. Such an automatic activation system might be a desirable addition.

We suggest that MP&L consider incorporating hydrogen detector information into their procedures for containment spray activation and for HIS deactivation. We also recommend that the containment sprays be activated at the same time the HIS is activated or, at the latest, upon indication from the hydrogen detectors of perhaps two percent hydrogen concentration in containment. Our analyses indicate that the sprays are important to the plant safety and should be maintained in operation throughout an accident.

Adequacy of the Spectrum of Accidents

We consider the accident spectrum considered by MP&L in their evaluation to be adequate. Basically, the hydrogen threat to a BWR Mark III plant manifests itself in one of two ways. The release path is either through a break in the drywell and then through the suppression pool, or it is directly into the suppression pool (from the pressure vessel safety relief valves). Due to the uncertainties in hydrogen generation and release rates,* we consider the MP&L approach for this parameter to be reasonable, especially since the effect of increasing the rate was examined in their sensitivity study.[3]

There are several kinds of accidents, not considered by MP&L or Sandia, that present a more severe challenge to the containment integrity. The possibility of significant hydrogen

*As discussed in a number of sections in this paper, the hydrogen generation and release rates are uncertain. The release rate is such a dominant input parameter to our codes that we feel a separate study should address the issue for BWR plants.

releases directly into the wetwell/containment without first traversing the suppression pool is apparently extremely unlikely.[2] Accidents involving loss of all offsite and emergency power are of course much more threatening but less likely. The inclusion of accidents involving the loss of the Residual Heat Removal (RHR) system may not be warranted becau containment failure apparently would occur due to static over-pressurization before core degradation rather than due to hydrogen combustion.[4]

References

1. Light Water Reactor Safety Research Program Semiannual Report, October, 1981-March, 1982, M. Berman, ed., to be published.

2. Letter and attachments from L. F. Dale, MP&L, to H. R. Denton, USNRC (Dec. 21, 1981).

3. CLASIX-3 Containment Response Sensitivity Analysis for the Mississippi Power & Light Grand Gulf Nuclear Station, Offshore Power System Report No. 37A15 (Dec. 1981).

4. Light Water Reactor Safety Research Program Semiannual Report, April-September 1981, M. Berman, ed., NUREG/CR-2481 (Feb. 1982).

5. H. Jahn, "RALOC-MOD1 with 1980 Updates", NRC Translation 654, GRS-A-263 (Jan. 1979).

GRAND GULF NUCLEAR STATION

(BWR MARK III)

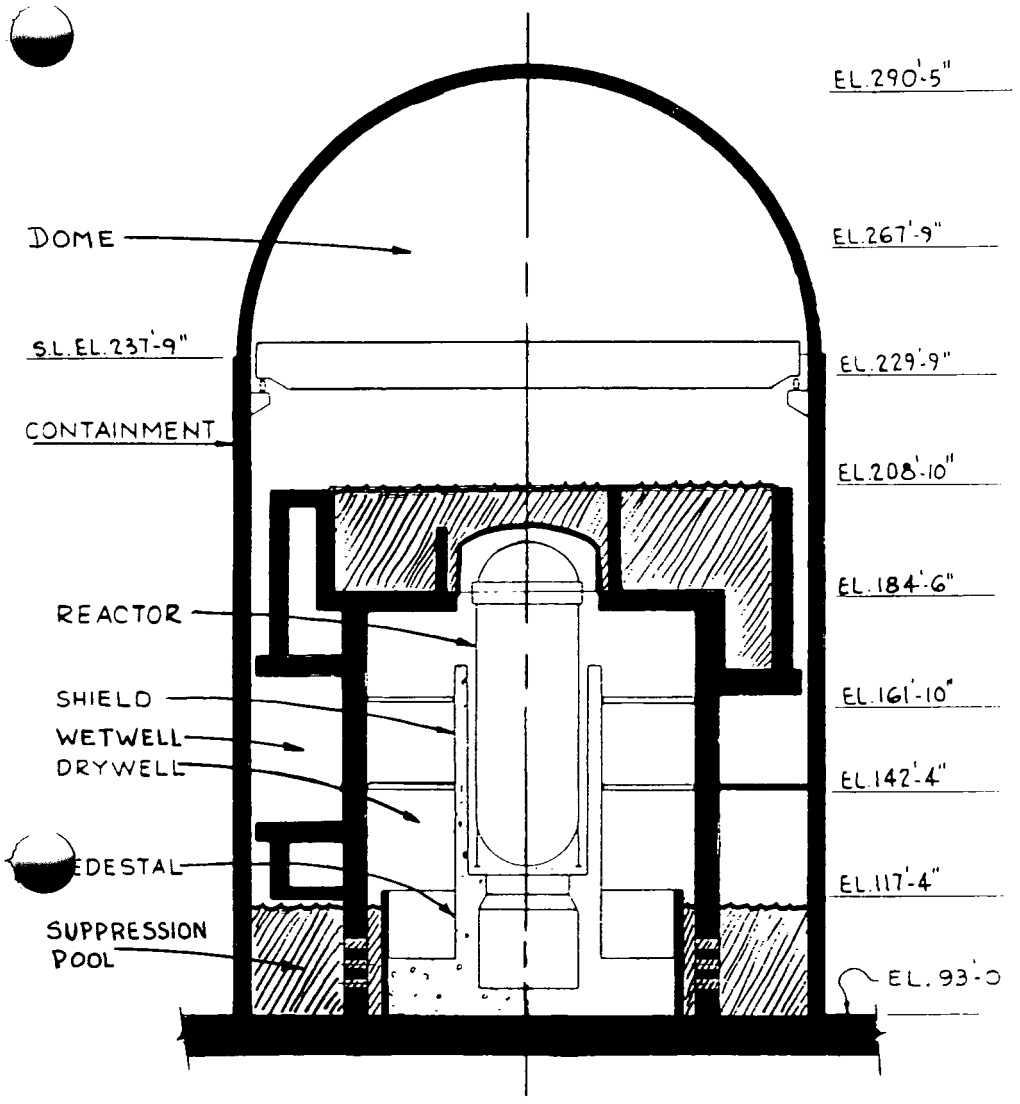


Figure 1. Grand Gulf Nuclear Station (schematic drawing)





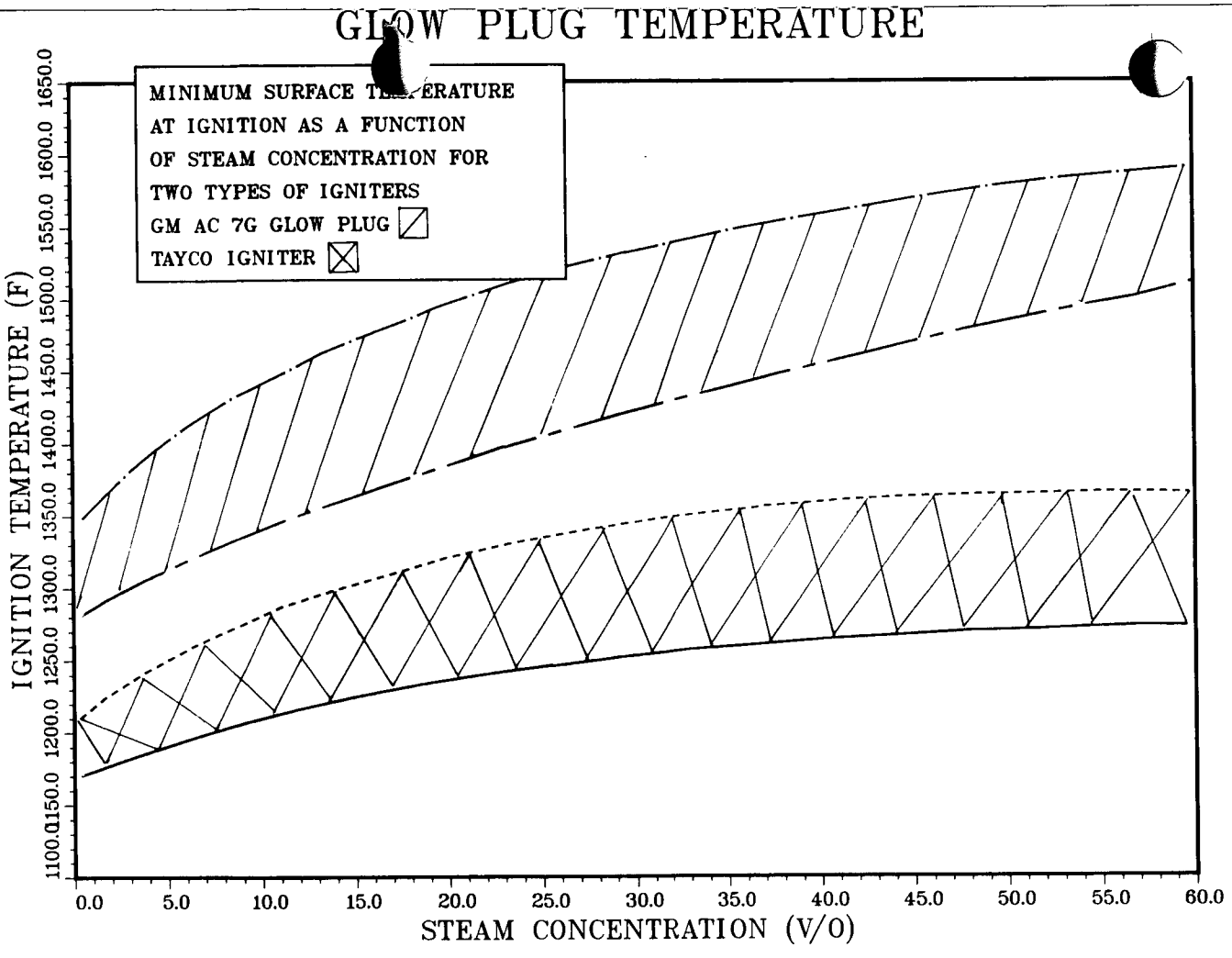

GLOW PLUG TEMPERATURE
MINIMUM SURFACE TEMPERATURE
AT IGNITION AS A FUNCTION
OF STEAM CONCENTRATION FOR
TWO TYPES OF IGNITERS
GM AC 7G GLOW PLUG
TAYCO IGNITER
IGNITION TEMPERATURE (F)
1100.0 1150.0 1200.0 1250.0 1300.0 1350.0 1400.0 1450.0 1500.0 1550.0 1600.0 1650.0
0.0 5.0 10.0 15.0 20.0 25.0 30.0 35.0 40.0 45.0 50.0 55.0 60.0
STEAM CONCENTRATION (V/O)

FIGURE 8





A Technical Evaluation of a Post-Accident CO2 Inerting Hydrogen Control System

M. A. Harris - Bechtel Power Corp.
S. H. Hobbs - Mississippi Power & Light
D. H. Ashton - Bechtel Power Corp.

INTRODUCTION

The accident at TMI-2 pointed out the potential for large quantities of hydrogen gas to be generated, and burned, inside containment following a major accident. Feeling that this represented a significant safety issue, the NRC instructed the owners of nuclear power plants having low design pressure containments, such as the Grand Gulf Nuclear Station (GGNS), to design and install a hydrogen control system. The purpose of the system is to prevent massive hydrogen burns or detonations from rupturing the containment boundary. A number of different control alternatives have been proposed and evaluated. The procedings of the Sandia Hydrogen Workshop (Reference 1) included discussions on water fogging systems, igniter systems, Halon inerting, CO_2 inerting, filtered vented containments, and high expansion foams, among others. In the recently released proposed rule, "Interim Requirements Related to Hydrogen Control" (Reference 2), the NRC stated that for MARK III BWR's now under construction, a post-accident inerting system appeared to be the preferred alternative.

At the time that the design of the GGNS hydrogen control system was begun, only one alternative was found to be technically feasible on the scale required for the Grand Gulf containment — a deliberate hydrogen ignition system (HIS). Other alternatives either lacked the required capabilities and technical development, required lead times longer than acceptable, or would have required extensive back-fit modifications to the nearly completed plant. Similar HIS have also been installed in all ice condenser plants, and laboratory tests have shown this system to be workable and effective (Reference 3).

Nontheless, since the NRC has expressed a preference for a post-accident inerting system, an effort was undertaken to fully document the engineering assessment of the impact of such a system being used at Grand Gulf. This report describes some of the technical problems associated with a carbon dioxide inerting system (CDIS). Some of the issues to be discussed and compared to the HIS are:

- Operational uncertainties, such as:
  - system initiation
  - impact of inadvertent actuation
  - system reliability

- Effect of CO_2 ıg on containment environment, including:
  - containme ısure-temperature analysis
  - discussio ressurization effects
  - discussio mperature effects
  - sensitivi yses

This report will not ı such issues as system cost or constructibility.

II. OPERATIONAL UNCERTAIN

A. System Initiation

Potential problem associated with the actuation of every safety s including the CDIS and HIS, are:

- for which accid ıould the system be activated?
- when should the ı be turned on?
- how should the be activated--manual or automatic?

The decision whether to activate the hydrogen control system for a ccident sequence can be difficult. Some acci ould require relatively prompt action, some may not action for tens of hours, and some might in reality e no action at all. But the requirement is not al vious to the operators. Therefore, it would b rable to have a system which could be turned on fo ccident, without concern over the consequences, the lieving the operators of another crisis decision point preferred system is one which would not adversely i ny accident sequence--turning a benign accident int ere one.

The CDIS is an altern hich may not meet these criteria. Before activating the an operator (or automatic control system) must tain the CDIS will be required since activation may in severe pressure/temperatur transients, as well a quential effects that will be discussed later. Onc DIS is actuated, the decision and consequences will eversible. In comparison, the HIS is a system wl uld be turned on for all accidents, almost imm y, and left on until the operators have time t mine that conditions are safe. The HIS would impact upon the transient, unless it performed it ended function--the burning of hydrogen--which is s desired.

Once a decision is made to activate the hydrogen control system, the question to be answered is: when during the accident must the system be turned on? This is particularly important for the CDIS. If the CDIS is initiated too early, core melt could be induced somewhat earlier, off-site doses might be unnecessarily increased, or recovery efforts oculd be hampered (these issues will be discussed later). On the other hand, the HIS is not as susceptible to this timing decision. If needed, the HIS could be turned on almost immediately.

Finally, the question of how to activate the system--manually or automatically--would probably be the same for both the CDIS and HIS. Presently, it is envisioned that each system would be manually initiated. If sometime in the future a decision were made to require automatic initiation, the HIS could easily accommodate this, while the CDIS may not. As previously discussed, actuation of the CDIS may require decisions or judgements not easily programmed into automatic systems.

B. Impact of Inadvertent Actuation

The impact upon the plant from inadvertent actuation of the hydrogen control system must be determined for each option. The impact of inadvertent actuation of the HIS is simple--there is none. If the HIS actuated accidentally, the effect upon containment environment or other systems would not be noticeable. However, the same cannot be said of the CDIS.

In Section III of this report, a base case CDIS analysis calculating the pressure-temperature effects of the CDIS is presented, with the results shown in Figures 1 and 2. This calculation would also be applicable for an inadvertent actuation analysis. As evident from the figures, the pressure and temperature show wide extremes in just the first 1000 seconds. A discussion of the effects of these pressure/temperature extremes on containment equipment and structures is presented in Section III. Obviously, there would be severe adverse mechanical and economical consequences should the containment be exposed to such a transient.

Of course, the probability that the CO_2 system could accidentally actuate can be made to be rather small with proper design. To further evaluate this problem, an approximation of the probability of inadvertent actuation of a CO_2 inerting system has been made. The basis for this calculation is the CO_2 Inerting System shown in Figure 3. The system works as follows:

1. Upon annunciation c low reactor water level alarm, a key locked switch tuated by the operator to open the discharge valve ne valves on the CO_2 tanks;

2. a timer begins oper also actuating containment evacuation alarms;



3. when the timer reac ro time, an electrical inter- lock is cleared, al the operator to open the contain- ment isolation valv a second set of key locked switches--one switc each isolation valve.

The probability of inac t actuation is estimated to be in the range of 10^{-5} $^{-6}$ per reactor-year. This compares to a probability ut 10^{-3} to 10^{-2} per reactor year for inadvertent ac n of a "normal" safety system (usually caused by oper rror). The reasons for this low probability are:

1. All valves must be via key operated switches; a minimum of three must be opened to allow any CO_2 injection.

2. Should one of the (k discharge valves open, the time delay prevents perator from immediately opening any of the isol valves. A siren also prevents undetected actuatic lone operator.

It should be pointed ou the degree of component independence incorporated into design should preclude significant common mode failures. , no consideration was given to the possibility of o ng some of the interlocks during testing or maintenance ons.

C. System Reliability

The reliability of the en control system is a necessary concern. Three issues primary interest when assessing system reliability:

- the susceptability c system design to mechanical failure;



- the maintainability stability of the system; and,
- how resistant the sy s to human errors.

Both the HIS and the CI ld have a highly reliable system design. The primary fa mechanism for both systems appears to be human error--fail manually initiate or failure to properly realign the m following testing or maintenance. The HIS consi stly of electrical components,

which generally have a high reliability. The CDIS includes a number of valves which could fail, but there can be redundant valves in parallel. One concern with the CDIS is preventing valve or injection line freeze-up, especially after initial injection during the make-up phase when CO_2 may need to be periodically replenished due to leakage and continued hydrogen generation. One advantage of the CDIS is that it would be easier to make it independent of all AC power.

In the area of system maintainability and testability, the HIS has a definite advantage over the CDIS. First of all, since the HIS can be tested from the power source to the system output, most failures can be detected during the routine system maintenance or testing. The HIS can be fully tested quite easily, at virtually anytime. If a failure is detected, repair could be accomplished rather quickly since the system consists primarily of modular electrical components. Should a failure occur locally at an ignitor assembly in the containment, replacement could be made in a relatively short time.

Testing of the CDIS is not as simple as for the HIS. Most of the CDIS will be tested either on a component or subsystem basis. A complete operational test is not advisable. While "puff" testing of the system is possible, this operation would significantly increase the probability of inadvertent actuation. Maintenance of the CDIS will also be more difficult and time consuming. Parts of the system are in contact with low temperature, high pressure CO_2. Should repair of these parts be required, portions of the CDIS may have to be isolated, or depressurized. Cold components would probably have to be warmed before repair could begin. Then this process would have to be reversed after repair is completed.

The reliability of both the CDIS and the HIS could be adversely affected by human errors during maintenance. Any degradation would probably be detected during testing or by inspection. However, both these systems depend upon operator action at a very crucial time--initiation under high stress conditions. System initiation will result after the operators have assessed the situation and determined that events leading to substantial hydrogen generation are unavoidable. Since the CDIS will have such an adverse impact on the containment environment, the operator may delay CO_2 injection as long as possible, hoping some vital system will be recovered (in fact, if a CDIS had been employed at a plant experiencing a TMI type event, it probably would not be actuated). This "waiting-till-the-last-possible-moment" attitude could result in the CDIS not preventing substantial hydrogen burning. On the

other hand, the HIS ca ctuated very early in the accident with no impact upon th equent course of events. An operator should experi ittle anxiety over HIS initiation, and therefore, would r itate to turn it on.

III. EFFECT ON CONTAINMENT NMENT DUE TO CO_2 INERTING

A. Containment Pressu perature Analysis

A detailed analysi performed to determine the containment atmosphere pr -temperature profiles resulting from operation of IS. The basic accident scenario modelled for the C a transient initiated event coupled with a stu safety/relief valve and failure of all emergency c pling. The CO_2 is assumed to be injected direct the containment atmosphere and uniformly dist l. The mass of CO_2 injected was sufficient to in a maximum CO_2 concentration of 60 v/o (a conce on greater than 50 v/o should prohibit hydrogen g). The results of this CDIS base case analysis ncluded in Figures 1 and 2. This accident scen s the same as one of the cases analyzed for the H e results of which are shown in Figures 4 and 5

In addition to the base case analysis, a number of sensitivity run made to assess the effects of changes in analysi lary conditions. This included changes in initial nment temperature, the effect of containment spr e time over which the CO_2 is injected into the ment, and the mode of CO_2 injection. A discus the base case and sensitivity analyses is presen the following sections.

B. Pressure Effects

The base case cont pressure profile is included in Figure 1. The e at the end of the analysis was 33 psia, and w l rising as the atmosphere continued to heat up. ually, the containment atmosphere will reach equilib th the outside air temperatur resulting in a sus pressure of about 37 psia. This 37 psia is 7 ve the containment design pressure, but well bel estimated 70 psia ultimate capacity. In comp the peak pressure for the similar HIS analys bout 50 psia, but unlike the CDIS, this pre s sustained for only a very short period of ti Figure 4). The pressure in the HIS analysis ly drops to about 23 psia, and will continue t ease as the containment temperature drops.

The pressurization resulting from the CO_2 injection is significant for several reasons. First, the higher the containment pressure, the greater the containment leak rate might be. Correspondingly, as the leak rate increases, so does the release of radioactive gases. The only way of depressurizing the containment after CO_2 injection is to vent. Given the experience at TMI-2, intentional venting may not be allowed for quite some time. At the design containment leak rate, the containment would take over a year to naturally depressurize. For some accident sequences, actuation of the CDIS would result in a totally unnecessary increases in offsite radiation doses. Furthermore, if the system were actuated during the DBA LOCA, the CO_2 would add about 28 psig to the LOCA pressure. This would change the entire basis for the containment design.

Operation of the HIS in degraded core accidents will also result in elevated containment pressures. But the pressurization resulting from hydrogen burning is short-lived, and once the burning is complete, the containment will eventually attain a small negative or atmospheric pressure. If no burning occurred, the incremental increase in pressure due to the hydrogen gas would be small. The HIS would have no effect if actuated during the DBA LOCA.

A second problem with the CDIS involves operation of the containment sprays. The CDIS base case assumes the sprays are inoperable. However, if the containment sprays were available and were in the automatic actuation mode they would significantly affect the transient. As shown in Figure 6, once the sprays come on the containment pressure would increase very rapidly. This is due to the spray water being at the same temperature as the suppression pool. For this accident scenario, and a good many others as well, spray actuation will exacerbate the containment transient conditions. Therefore, the question must be raised--should actuation of the containment sprays be inhibited whenever the CDIS actuates?

The containment sprays are usually needed for pressure reduction, by decreasing the steam pressure and containment temperature. For accidents where the CDIS actuates, there would be very little, if any, steam pressure in the containment at the time the sprays come on. The

high pressure is c
mass, not from ste
inhibiting spray a
rate of pressuriz
action. The dange
reverse of present
the containment sp
cisely the reason
tainment pressures
no change from cur

increased non-condensible
s/energy addition. Therefore,
on would actually reduce the
and thus would be the correc
is that this logic is the
safety logic. With the HIS,
ould be initiated for pre-
re there--to reduce high con-
emperatures. This represents
afety practices.

C. Temperature Effects

The base case containm
from actuation of the
minimum temperature ex
-80°F. This is a sign
ture of 80°F. Normall
in a containment are v
will act to mitigate t
is notable in that the
the reverse of other t
system designs (the CD
while safety systems a
temperature increases),
lived. The equipment will have sufficient time to "feel"
the temperature drop.

nperature profile resulting
s shown in Figure 2. The
ed in the containment was
drop from the initial tempera-
eme temperature transients
ort-lived, since safety systems
sient. However, the CDIS
ature transient is not only
ts anticipated by safety
lts in a temperature drop,
rally designed to handle
he CDIS profile is not short-

The rapid cooling of the containment atmosphere has the potential for serious effects on various materials and process fluids inside the containment which will be in locations where the metal and process fluid temperatures follow the atmospheric temperature profile. The following are some of the specific concerns:

- Metals - Rapid cooling may lead to excessive metal contraction resulting in high tensile stresses being generated. Cooling of many carbon steels will lead to transformation from ambient, ductile conditions to notch sensitive, brittle conditions. The combination of these two problems would give rise to a serious potential for brittle fracture. This would be particularly serious with structural steels, pipe and equipment supports, and other items which do not have backup heat sources.

  There would be less concern with piping systems which are full of warm or hot process fluids. The potential brittle fracture problem does not exist with stainless

steels, but small stainless steel process and instrumentation lines could be a problem as described below.

- Coatings - Rapid cooling of surfaces which have been coated could result in cracking and spalling, particularly on surfaces top coated with epoxy over inorganic zinc. Little quantitative data is available on the properties of coatings at temperatures below about -40°F.
- Process Fluids, etc. - None of the process or instrumentation systems are desinged for conditions where the process fluid freezes. This would almost certainly be the situation, however, in small lines which follow the atmospheric temperature profile. However, it was not possible to analyze the effect that the freezing may have on the systems. The freezing would almost certainly give rise to bursts in the piping and tubing which would be very self-evident on subsequent thawing.
- Other Materials - There are probably many other materials inside the containment which; could suffer drastic changes in properties caused by even short low temperature excursions, and which could lead to various failures. Some examples might be--electrical wiring insulation, gasket and sealing materials, intricately machined parts in instruments and gauges.

Burning of hydrogen with the HIS results in a series of extreme temperature spikes (on the order of 1300°F), but these transients are very short-lived (<3 minutes). The equipment does not have time to respond to these spikes, and there is a cooldown period between each burn. While the overall containment temperature steadily increases during the period of hydrogen burning, it has been shown that the critical components will survive the accident (Reference 7).

On the other hand, an additional problem with the CDIS, which is related to the possibility of damaging equipment due to freezing, is that premature actuation may force the plant into a degraded core accident that might otherwise have been avoided. As noted earlier, operators cannot wait too long to initiate the CDIS. In addition, they should not initiate the system too early. Therefore, the operators may have a relatively small "window" during which the CDIS can be confidently actuated. This puts a significant burden upon the operators. The HIS, however, may be actuated anytime before significant amounts of hydrogen have accumulated.

D. Sensitivity Analyses

The basic CDIS transient analysis described in Section III.A could be influenced by many factors. The effect of containment sprays has already been discussed. Other factors considered to have a significant impact on the transient are: 1) the rate of CO_2 injection; 2) the initial containment temperature; and 3) the mode of CO_2 injection into the containment. Additional analyses were made where these parameters were varied. A discussion of each follows.

1. Effect of CO_2 Injection Rate

The CDIS base case analysis assumed that the CO_2 was injected over a 30-minute time period. Two sensitivity analyses were made, varying the time of injection from 15 minutes to 45 minutes. The results of these analyses are included with the base case results in Figures 1 and 2.

Obviously, the longer the CO_2 injection time, the less severe the temperature drop would be. However, even with the 45 minute injection time, the temperature still drops below -50°F. A problem with assuming a longer injection time is that the 30 minute base case time may represent the optimum injection rate. Presently, the hydrogen control system would be activated when the vessel water level drops to the top of the active fuel region (TAF). Analyses in the GE Hydrogen Control Report (Reference 6), for the SORV with no ECCS scenario, show that clad reaction (hydrogen generation) will begin about 16 minutes after the TAF level is reached. Assuming no CO injection, the hydrogen concentration in the wetwell would reach 9 v/o about 30 minutes after the TAF level. With the 30 minute injection time, it takes 12 minutes to reach 50 w/o CO_2 in the containment. Therefore, the containment will be sufficiently inerted before any hydrogen begins accumulating. Assuming a longer injection time might result in significant hydrogen accumulation before the containment is sufficiently inerted.

2. Effect of Initial Containment Temperature

The base case analysis assumed an initial containment temperature of 80°F. Two additional cases were run, one using a 65°F initial temperature, the other using 120°F. The results of the analysis are shown in Figure 7. The temperature profiles for each sensitivity run exhibit the same profile as the base case, except their respective magnitudes differ by the difference in initial temperature. This behavior is attributable

to the containment structures and walls which act as heat sources in the model. The higher the initial containment temperature, the greater the energy stored and ultimately transferred into the containment atmosphere. The pressure profiles also follow the base case profile, with the pressure for the 120°F case usually 1 psi higher than the base case, and the pressure for the 65°F case about .5 psi lower.

3. Mode of CO_2 Injection

The base case assumes that the CO_2 is injected directly into the containment atmosphere, and is uniformly distributed. Of course, there are other possible means of injecting the CO_2 - means such that the severe temperature drop could be reduced or avoided. One is to heat the CO_2 in a preheater. The drawback of this method is that it would probably require some sort of AC-power dependency, for either heating coils or motors. Another possibility is to inject the CO_2 directly into the suppression pool. However, this mode of injection also has several drawbacks. First, it would have to be assured that the injection nozzles would not freeze-up during injection. Second, the containment would still be pressurized to above 37 psia, and would remain so until vented.

IV. SUMMARY

This report has investigated some of the problems associated with a post-accident CO_2 inerting system. Discussions have been presented concerning the operational uncertainties associated with the CDIS, as well as the containment environmental impact resulting from injection of the carbon dioxide. A summary of the issues raised, and the comparison to the hydrogen ignition system, are presented in Table 1. In conclusion, the consequences of employing a CDIS are not considered trivial, and in fact, can be detrimental to plant safety. The deliberate hydrogen ignition system has been proven effective at controlling the accumulation of hydrogen gas, and is clearly preferable to a CDIS.

V. REFERENCES

1. "Proceedings of the Workshop on the Impact of Hydrogen on Water Reactor Safety," held in Albuquerque, New Mexico, January 26-28, 1981, NUREG/CR-2017.
2. "Interim Requirements Related to Hydrogen Control," Federal Register Notice, Volume 46, No. 246, December 23, 1981, pages 62281-85.
3. "Final Results of the Hydrogen Igniter Experimental Program," NUREG/CR-2486, Lawrence Livermore National Laboratory, February 1982.
4. "Report on the Grand Gulf Nuclear Station Hydrogen Ignition System," Mississippi Power and Light Company, August 31, 1981.
5. Allens Creek Nuclear Generating Station PSAR, Amendment No. 59 (June 1981), pages 0-82 through 0-89 and 0-153 through 0-168.
6. "Report on Hydrogen Control Accident Scenarios, Hydrogen Generation Rates, and Equipment Requirements," General Electric Company - Nuclear Engineering Division, presented to the BWR Owner's Group, December 1981.
7. "Report on Equipment Survivability in Support of the Grand Gulf Nuclear Station Hydrogen Igniter System," Mississippi Power and Light Company, January 19, 1982.

Comparison of Carbon Dioxide and Hydrogen Ignition System Characteristics

Item	CDIS	HIS
System Initiation:		
o Accident Scenario	Scenario dependent	Scenario independent
o Time of Initiation	Small "window" during transient	Anytime before H_2 accumulation
o Method of Actuation	Manual--high operator interface	Manual--limited operator interface
Inadvertent Actuation	Severe P/T transient; may damage plant	No impact
System Reliability:		
o Mechanical	High reliability via component redundancy	High reliability via reliable components
o Testing	Partial system or component testing	Full system test capability
o Maintenance	More time-consuming; system may be partially degraded	Quick repair
o Human Error	High--at initiation, operator exposed to high stress decisions, high degree of operator interface required	Low--operator unconcerned about consequences
Pressure Effects:		
o Overpressure	Long-term pressurization above design; significantly higher than HIS	Very short-term pressurization above design; no residual pressurization
o Leak Rate (offsite doses)	Higher than HIS, over much longer period of time	Lower than CDIS, negative pressure soon after burns end
o Spray Actuation	Should be inhibited--reverse of present safety logic	No change in current safety philosophy
o Plant Recovery	Containment must be vented to depressurize	No venting required to depressurize
Temperature Effects	Equipment damaged or failed due to very cold temperature	Equipment would survive short duration temperature spikes

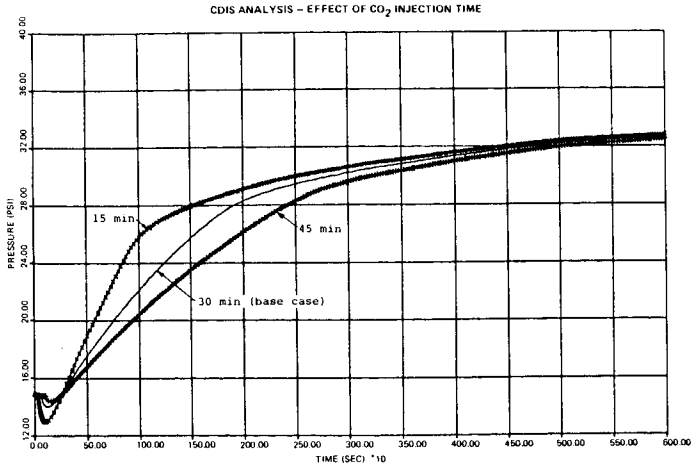


Figure 1

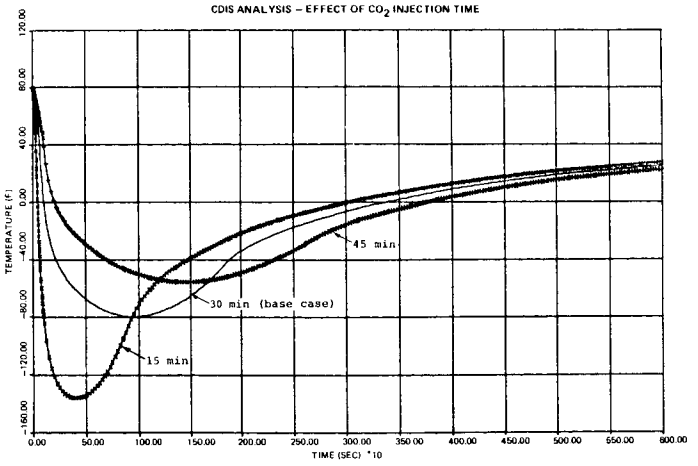


Figure 2

CDIS General Arrangement

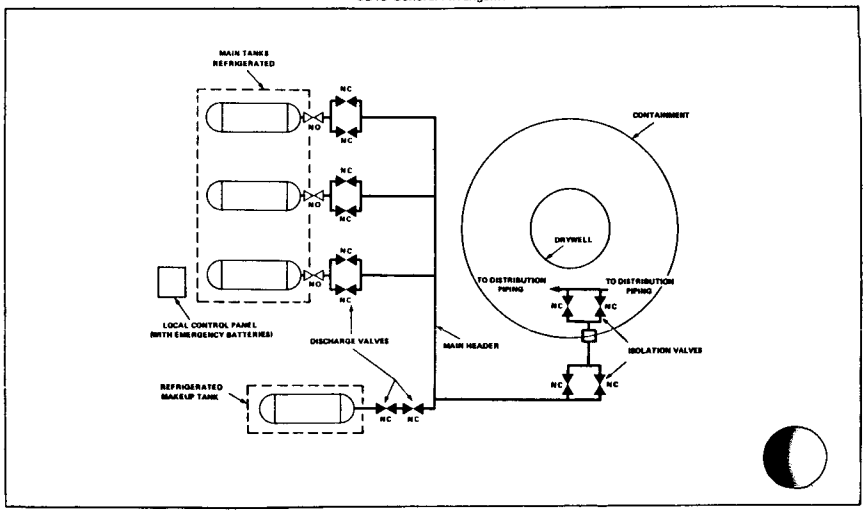


Figure 3

MITIGATION EFFECTS OF CONTINUOUSLY PRESSURIZED, PARTIALLY INERTED CONTAINMENT BUILDING ATMOSPHERES

A. L. Berlad*, R. Jaung and W. T. Pratt
Department of Nuclear Energy
Brookhaven National Laboratory
Upton, New York 11973

ABSTRACT

In this paper we examine the use of a continuously-pressurized, partially inerted containment building atmosphere to mitigate the consequences of potentially severe combustion phenomena. This method differs from (a previously examined scheme of) complete inertion in that it utilizes a continuously-pressurized but only partially inerted containment, thereby providing oxygen partial pressures which are adequate to support respiratory processes, but where inert-to-oxygen ratios are sufficient to provide substantial mitigation of severe combustion events. Human respiratory function in a partially inert atmosphere is determined primarily by the oxygen partial pressure whereas detonability limits (and flammability limits) are determined primarily by the oxygen-inert ratio, for a given stoichiometry. The results of the study show that the method is capable of reliably eliminating hydrogen detonations and all hydrocarbon-based fires. This is prescribed by an atmosphere which will also support normal respiratory functions so that personnel access to the containment building should be unaffected during reactor operation.

I. INTRODUCTION

This paper examines the use of a continuously pressurized, partially inerted containment building atmosphere to mitigate the consequences of potentially destructive combustion phenomena. A previous study [1] considered various schemes to mitigate the consequences of combustion phenomena, which can occur in the containment buildings of Light Water Reactors during postulated degraded core accidents. These schemes are required to mitigate combustion phenomena associated with a wide range of potential accident sequences. The generation rates and relative composition of the combustible gases, non-combustible/non-condensible gases and steam that can be released to the containment vary over a wide range. There is also a potential for local stratification or pocketing of combustible gases. However, if these gases could be ignited and burnt at the lower flammability limits, then the threat to containment integrity is relatively benign. Unfortunately, random ignition sources cannot be relied on to burn the gases at the lower

* Department of Mechanical Engineering, State University of New York at Stony Brook, New York 11794

flammability limits and consequently the potential exists for non-laminar burns or detonations, which can challenge containment integrity.

A number of mitigation schemes have been suggested, which attempt to force combustible gases to ignite at the lower flammability limits (e.g., glow plug igniters). However, there are a number of accident sequences [2] in which combustible gases are released into a steam-inerted containment and glow plugs may not be an appropriate means of control. Other mitigation schemes attempt to suppress combustible gas ignition during the course of the accident (e.g., water mist, Halons). The reliability of these systems under all possible accident conditions has not been demonstrated. A highly reliable scheme [1] which completely eliminates combustion is to continuously inert the containment building atmosphere during reactor operation by introducing an inert gas (e.g., N_2 or CO_2). Complete inertion (at normal atmospheric pressure) to suppress hydrogen combustion implies an atmospheric O_2 concentration which is unable to support normal human respiratory functions. This could increase risk to plant personnel and may reduce the frequency of access to the containment during plant operation. Reduced surveillance can in turn influence the potential for accidents.

In this paper we suggest an alternate scheme which employs a continuously-pressurized but only partially inerted containment where oxygen partial pressures <u>are</u> adequate to support respiratory processes, [3,4] but where inert to oxygen ratios are sufficient to provide substantial mitigation of severe combustion events. For example, continuous inerting (at $p \sim 2$ atm.) with a gas consisting of 1 atm. air plus 1 atm. nitrogen provides a containment atmosphere which supports normal respiratory functions but does not support hydrogen detonations.[5] Also, such an atmosphere will not support electric cable insulation fires [5,6] or other hydrocarbon based fires. Central to the proposed concept is the physiological fact [3,4] that human respiratory function in a partially inert atmosphere is determined primarily by the oxygen partial pressure whereas detonability (and flammability) limits are determined by the oxygen-inert ratio, for a given stoichiometry.

In this paper we examine several cases wherein continuously-pressurized, partially-inerted containment atmospheres are employed to achieve the suppression of selected combustion phenomena <u>as well as</u> maintenance of adequate support for human respiration. In particular, an examination is made of the amount of nitrogen needed to mitigate some of the postulated worst-case scenarios.

It is noted that although 0.21 atm. partial pressure of oxygen is commonly taken as "normal" for respiratory purposes, citizens of Denver and Mexico City function well at an oxygen partial pressure of 0.17 atm. Citizens of Tibet find 0.10 atm. of oxygen to be satisfactory. For accident scenarios where deflagrations as well as detonations are to be avoided, the use of lower-than-"normal" oxygen partial pressures could be employed, in conjunction with the concept of continuously pressurized, partially-inerted atmospheres to help mitigate the problem of containment overpressurization. A specific application to a hypothetical degraded core accident is examined later in this paper.

II. DETONATION AND DEFLAGRATION LIMITS

An extensive body of analysis and experimentation [e.g.7-11] exists which permits identification of the following principal features of detonations and deflagrations, at pressures in the neighborhood of 1 atm. and above:



Composition limits of detonability and flammability are relatively insensitive to moderate variations in total pressure, depending primarily on oxygen-to-inert ratios (as well as fuel concentration).

- Detonability limits for systems involving H_2-CO-CO_2-H_2O-O_2-N_2-hydrocarbons are narrower than flammability limits.

- Addition of an adequate amount of an inert gas (e.g., N_2, He, CO_2, etc.) to a given detonable mixture of the aforementioned kind, may serve to render the modified mixture non-detonable. Additional amounts of inert gas may be added to render the modified mixture non-flammable. For such cases, the original oxygen partial pressure is unmodified, but the combustion behavior (including detonability and flammability) varies with the changes in oxygen-to-inert ratios.

- Despite the absence of universally accepted, comprehensive theories of detonation and of deflagration limits, experimental data and analytic constructs (both) exist which permit identification of whether a given fuel-oxygen-inert mixture is flammable and whether it is detonable (e.g., Appendix A).

The classical features of detonability and flammability for characteristic hydrogen-oxygen-inert and hydrocarbon-oxygen-inert mixtures are summarized in References [8] and [12]. Several observations to be derived from those data are particularly noteworthy for our considerations:

(1) For the case where air, initially at a pressure of one atmosphere, is diluted with about one atmosphere of nitrogen, the resulting mixture, even when a stoichiometric concentration of hydrogen is added, is not able to support the detonation phenomenon.

(2) For the same, partially-inerted oxidizer mixture of (1) above, the approximate "percent additional nitrogen in original atmosphere" is defined to be 50 percent. None of the hydrocarbon species (derived from cable insulation pyrolysis processes) that may occur in containment building atmospheres are flammable at these nitrogen-oxygen ratios (Table I).



(3) When a "vitiated air" of total pressure 1.6 atmospheres and a nitrogen-oxygen ratio of (approximately) 15 is mixed with stoichiometric hydrogen, (at constant volume) the resulting mixture is non-flammable.

It is important to note that all fuel-free oxidizer gas mixtures described in (1)-(3), inclusive, are capable of supporting respiratory processes. Cases (1) and (2) correspond to oxygen partial pressures that are

"normal." Case (3) corresponds to an oxygen partial pressure (0.1 atmosphere) which citizens of Tibet (some 20,000 foot altitude) find adequate. These two oxidizer gas mixtures are illustrative of a class of partially inerted atmospheres that may be employed to eliminate the possibility of unwanted combustion phenomena in containment buildings. The possible burdens that are imposed by this approach derive from the facts that the initial containment operating pressure is above one atmosphere, or the initial oxygen partial pressure is less than 0.21 atmosphere, or both. Whether or not the[redacted] are acceptable trade-offs in a given containment building application depe[redacted] upon the specifics of the particular case. Table II indicates the classic[redacted] range [8] of oxygen and nitrogen partial pressures (and containment total pressures prior to accident onset) where hydrogen detonations or hydrocarbon-based fires are (or are not) possible. Currently proposed detonability limits [10] correspond to somewhat higher inert-to-oxygen ratios. A few particular cases are considered in the following sections.

III. OVERPRESSURE MITIGATION FOR A LARGE DRY CONTAINMENT BUILDING

It is clear that there exists a range of "initial total pressure" and "initial oxygen partial pressure" values which permit both, the adequate support of respiratory processes and the adequate suppression of peak post-accident pressures in containment. Experimental and analytic information, such as that provided in Tables (I), (II), and (A-I), are available to serve in the design and selection of the most advantageous oxygen and nitrogen partial pressures to be employed during normal containment building operation. Thus, if the nitrogen-oxygen ratio is preselected to eliminate burning, the inert-oxygen ratio cannot be degraded by post-accident uncertainties (e.g., nonuniformities, release rates, etc.) in hydrogen evolution. Steam addition can only increase (enhance) the inert-oxygen ratio.

For a majority of accident sequences that lead to core degradation some form of containment cooling is available. Under these circumstances combustible gases can be ignited at the lower flammability limits as they are released to the containment atmosphere. However, we noted in the introduction to this paper that random ignition sources cannot be relied on and consequently the potential exists for non-laminar burns or detonations. It therefore appears desirable to consider the use of a continuously pressurized, partially-inerted containment atmosphere to eliminate the possibility of hydrogen detonations.

However, for those accident sequences initially without containm[redacted] cooling, potentially severe combustion phenomena can occur. Consider a TMLB' (using the nomenclature of WASH-1400) accident sequence. This is a transient initiated accident coupled with a total loss of AC power for an extended period. The reactor core will eventually meltdown unless power is restored and coolant flow returned to the core. It has been shown [2] that as the core degrades and combustible gases are generated they will be released into a steam inerted containment building. Thus H_2 ignition at the lower flammability limits is prevented for these accidents by high steam mole fractions. If power is restored after vessel failure, restoration of containment

cooling can result in detonable mixtures. It is important to prevent detonations under these circumstances. However, the elimination of detonations does not in itself eliminate the possible hazard of overpressurization during H_2 deflagration. This is simply because very large quantities of combustibles can be accumulated during core/concrete interactions for this accident sequence. In fact, the hazard associated with a deflagration under these circumstances is limited by O_2 availability in containment. Therefore, selective reduction of the initial O_2 content serves not only to eliminate the possibility of detonations but also to reduce the total combustion heat release, which lowers the threat to containment integrity for this particular accident sequence.

IV. OVERPRESSURE MITIGATION FOR AN ICE-CONDENSER CONTAINMENT BUILDING

The complete mitigation of combustion-induced pressure effects in ice-condenser containments may be achieved by continuous partial inerting with an oxygen-nitrogen mixture having a total pressure of 1.6 atmosphere and an oxygen partial pressure of 0.10 atmosphere. Such an oxygen partial pressure is adequate to support respiration, but does correspond to less-than-normal oxygen conditions (e.g., the oxygen partial pressure of Tibet). Under such conditions, stoichiometric hydrogen is neither flammable nor detonable. However, the elevated total pressure of the containment building (prior to onset of an accident) represents an elevated initial pressure base from which accident-related steam releases may threaten containment integrity. The possible changes to preservation of containment integrity implied by other than "normal" oxygen and nitrogen partial pressures is considered more comprehensively elsewhere.[14] However, it may be noted here that with the predictable elimination of combustion-related events, a full range of structural design and other standard options may be invoked to secure the integrity of ice-condenser (and other) containment buildings.

V. SUMMARY AND CONCLUSIONS

Containment building atmospheres are generally (with the exception of Mark I and II boiling water reactor containments) operated at "normal" conditions, corresponding closely to a total pressure of one atmosphere, an oxygen partial pressure of 0.21 atmosphere and a nitrogen partial pressure of 0.79 atmosphere. These properties are then used in the study of hypothetical degraded core accidents and their related combustion events.

Under some circumstances, pressure mitigation associated with accident scenarios may be achieved by operating containment atmospheres at conditions other than "normal." Many "abnormal" containment atmospheric conditions may serve as adequate to the human respiratory function. This derives from the facts that the human respiratory function is dominated by the atmospheric oxygen partial pressure and that oxygen partial pressures as low as one half "normal" can be adequate.

Combustion characteristics such as flammability limits (e.g., of hydrocarbon-based cable insulators) and detonability limits for hydrogen-oxygen-nitrogen systems are dominated by fuel-to-oxidizer and inert-to-oxidizer ratios. Accordingly, partially-inerted containment atmospheres can be devised which in a specific application:

1) can adequately sustain human respiratory function, prior to accident onset

2) does not sustain hydrogen detonations; and

3) does not sustain hydrocarbon-based cable insulation fires, and

4) need not sustain hydrogen deflagrations, if so required.

Not all combinations of such initial containment partial pressures (of oxygen and of inert gas) are advantageous, however. Substantially increased initial total pressures may prove unwise in a particular case. Nevertheless, specific combinations of initial partial and total pressure containment conditions can be found which successfully mitigate several combustion accident scenarios. The predictability of such mitigation strategies is strengthened by the selection of containment atmosphere inert-to-oxygen ratios which rule out the possibility of detonations.

VI. ACKNOWLEDGEMENT

This work was carried out under the auspices of the U. S. Nuclear Regulatory Commission. The authors are indebted to Dr. R. A. Bari for many helpful discussions.

VII. REFERENCES

1. A. L. Berlad, M. Sibulkin and C. H. Yang, "Containment Building Hydrogen Control Methods Related to Degraded Core Accidents," Brookhaven National Laboratory Report, BNL-NUREG-28976, (November 1980).

2. R. Jaung, R. A. Bari and W. T. Pratt, "Carbon Monoxide Burning During Core Meltdown Events in a PWR," Trans. Am. Nucl. Soc. 39, 606 (1981).

3. D. P. Dressler, et al., "Biological Effect of Fire Suppression by Nitrogen Pressurization in Enclosed Environments," J. Comb. Toxicology, 4, 314, (August 1977).

4. H. W. Carhart and G. H. Fielding, "Applications of Gaseous Fire Extinguishants in Submarines," p. 239 of Proc. Nat. Acad. Sciences Symp.: "An Appraisal of Halogenated Fire Extinguishing Agents," (1972).

5. A. L. Berlad, W. T. Pratt, R. Bari and R. Jaung, "Method and Apparatus for Suppression of Combustion Hazards in Nuclear Containment Buildings," BNL Patent Disclosure (Patent Pending) (1982).

REFERENCES (cont'd)

6. A. L. Berlad, R. Jaung and W. T. Pratt, "Electric Cable Insulation Pyrolysis and Ignition Resulting From Hypothetical Hydrogen Burns in Nuclear Containment Buildings," these proceedings (1982).

7. R. Jaung, A. L. Berlad and W. T. Pratt, "A Review of Combustion Processes Related to Detonations," Draft BNL Report, (January 1982).

8. H. F. Coward and G. W. Jones, "Limits of Flammability of Gases and Vapors," Bulletin 503, U. S. Bureau of Mines (1952).

9. I. B. Zeldovich and A. S. Kompaneets, "Theory of Detonation," Pub.: Academic Press (1960).

10. R. Atkinson, D. C. Bull and P. J. Shuff, "Combustion and Flame 39, 287 (1980).

11. A. L. Berlad, M. Sibulkin and C. H. Yang, "Hydrogen Combustion Characteristics Related to Reactor Accidents," NUREG/CR-2475, BNL-NUREG-51492, (November 1981).

12. H. G. Wagner, "Fundamental Data Obtained from Shock-Tube Experiments," Pergamon Press. (1961).

13. R. Jaung, A. L. Berlad and W. T. Pratt, "Detonability of Containment Building Atmospheres During Core-Meltdown Accidents," Second International Topical Meeting on Nuclear Reactor Thermal Hydraulics, Santa Barbara, California, (January 11-14, 1983).

14. A. L. Berlad, R. Jaung and W. T. Pratt, "Combustion Hazard Mitigation by Partially-Inerted Containment Building Atmospheres," BNL Report (In Preparation) (1982).

Table I

Turning Points on the Flammability Limit Curves

for Various H/C-O_2-N_2 Mixtures*

FUEL	ORIGINAL ATMOSPHERE					Fuel Conc. in Final Mixture (worst case)
	Air (1 atm.)	N_2 Added	Total Pressure	Total O_2	Total N_2	
	Mole %	Mole %	Atm.	Mole %	Mole %	Mole %
Methane	62	38	1.61	13.0	87.0	6.0
Ethane	55	45	1.82	11.4	88.6	3.6
Propane	57	43	1.75	11.8	88.2	3.0
Butane	59	41	1.69	12.4	87.6	2.5
Pentane	57	43	1.75	11.9	88.1	2.2

* Based on data of Coward & Jones for upward flame propagation (Ref. 8).

Table II

Worst Case

Detonability of Hydrogen (Classical Values) with O_2-N_2 Mixtures

and

Flammability of Hydrocarbons with O_2-N_2 Mixtures

for

Various Total Pressure and $[N_2]$:$[O_2]$ Ratios
(Ref.: Coward & Jones)

P_{Total} atm	P_{O_2} atm	P_{N_2} atm	$\left(\frac{P_{N_2}}{P_{O_2}}\right)$	Detonability w/H_2	Flammability with H/C's
1.00	0.21	0.79	3.7619	Detonable	Flammable
1.50	0.21	1.29	6.1429	"	Non-flammable
1.60	0.21	1.39	6.6190	"	"
1.70	0.21	1.49	7.0952	Non-detonable	"
1.65	0.21	1.4406	6.86	Marginal	Non-flammable
1.50	0.1875	1.3125	7.00	Non-detonable	Non-flammable
1.40	0.1750	1.2250	↓	↓	↓
1.30	0.1625	1.1375			
1.20	0.1500	1.0500			
1.10	0.1375	0.9625			
1.00	0.1250	0.8750	7.00	Non-detonable	Non-flammable

APPENDIX A

DETONABILITY OF H_2-O_2-N_2-CO-H_2O-CO_2 MIXTURES

A range of experimentally determined detonability conditions for mixtures of two or three gaseous species are summarized in References [8] and [12]. More general criteria of detonability are required in order to account for variations in initial temperature and pressure, as well as greater numbers of chemical species as constituents of the gas of interest. Experimentally, it has been found that short post-shock induction times (<10 μsec) always result in a quasi-steady detonation. Very long induction times (>250 μsec) correspond to post-shock chemical kinetic rates which are too small [7] to sustain the large upstream (flame-to-shock) energy fluxes required to maintain a quasi-steady shock wave (of a stable detonation). Addition of nitrogen to an otherwise detonable H_2-O_2 mixture will lengthen the post-shock induction time and will also reduce the flame temperature. The induction time can be determined by a computer program which employs some 23 chemical kinetic equations for the H_2-O_2-N_2-CO-H_2O-CO_2 system.[13] Induction times short enough to sustain a quasi-steady Chapman-Jouguet (C-J) detonation wave also fall within the detonability limits provided by experimentally based correlations.[8]

Table A-1 gives the calculated results for the effect on "induction time" of nitrogen addition to "normal" nitrogen-to-oxygen ratios for several stoichiometric (wet) H_2-O_2-N_2 mixtures. Based on the classical observations, N_2-to-O_2 ratios of 7 are adequate to prevent detonations. Here the relation between induction time and detonability is related further to nitrogen-to-oxygen ratios. The conditions selected correspond to an S_2D accident scenario for an ice-condenser plant (small break loss-of-coolant accident coupled with failure of the active Emergency Core Cooling System in the injection phase).

Table A-1

(P) (atm)	(T) (°K)	(P_{N_2}/P_{O_2}) -	$\left(\text{Induction Time}\right)$ (μsec)	[OH] (ppm)
2.00	330.50	3.770	12.20	210
2.10	328.79	4.147	15.04	168
2.201	327.25	4.524	18.58	133
2.301	325.85	4.901	23.02	105
2.402	324.58	5.278	28.69	82
2.502	323.42	5.655	35.98	64
2.603	322.36	6.032	45.46	50
2.703	321.39	6.409	57.24	38
2.803	320.49	6.786	72.46	30
2.904	319.65	7.163	92.62	23
3.004	318.88	7.540	119.1	17
3.105	318.16	7.917	151.9	13
3.205	317.49	8.294	198.6	10
3.306	316.86	8.671	180.0	8
3.406	316.26	9.048	246.2	7
3.506	315.71	9.425	344.5	6
3.607	315.19	9.802	548.4	4
3.707	314.69	10.179	1145	2

Pressure-Temperature Conditions and Calculated Induction Times for Stoichiometric H_2-O_2-N_2 Mixtures and a Range of N_2-O_2 Ratios for a Postulated S_2D Accident in an Ice Condenser Containment Building

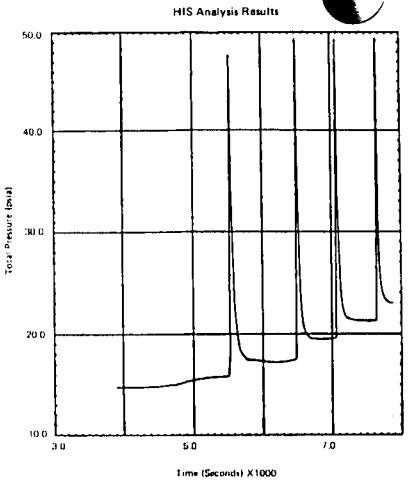


Figure 4
(Reference 4)

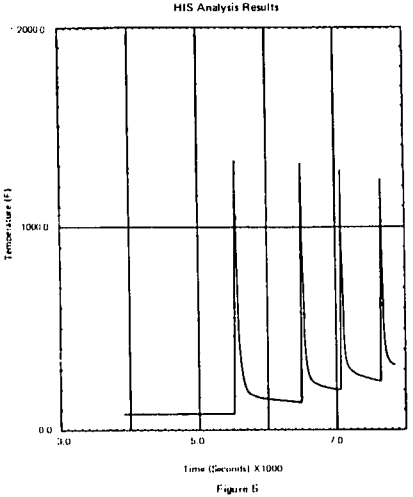


Figure 5
(Reference 4)

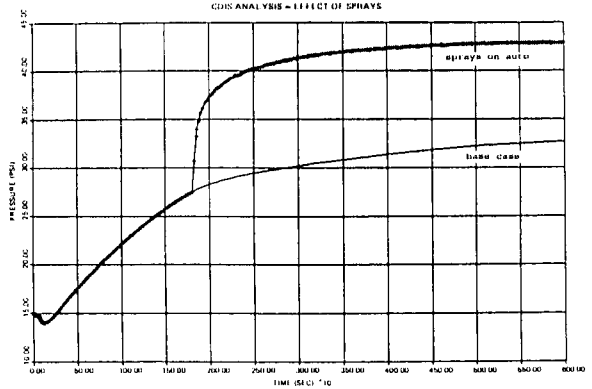


Figure 6

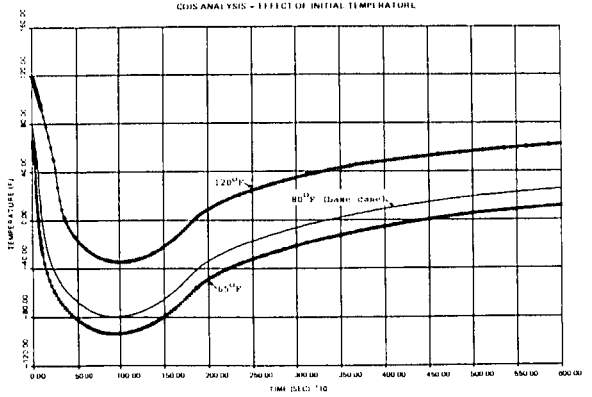


Figure 7

HYDROGEN COMBUSTION IN AQUEOUS FOAMS*

M. R. Baer, S. K. Griffiths and J. E. Shepherd
Sandia National Laboratories
Albuquerque, New Mexico 87185

ABSTRACT

Water fogs are recognized as an effective means to mitigate the effects of large-scale hydrogen combustion that might accompany some loss-of-coolant nuclear reactor accidents. Fogs of sufficiently high density to produce large beneficial effects may, however, be difficult to generate and maintain. An alternate method of suspending the desired mass of water is via high expansion-ratio aqueous foams. Because, in practice, the foam would be generated using the combustible gaseous contents of the containment vessel, combustion occurs inside the foam cells. Although foams generated with inert gas have been well studied for use in fire fighting, little is known about combustion in foams generated with flammable mixtures. To help assess the usefulness of aqueous foams in a mitigation plan, we have conducted several open tube tests and over one hundred closed vessel tests of hydrogen/air combustion with and without foam.

At low and intermediate hydrogen concentrations, the foam has little effect on the ultimate isochoric pressure rise. Above 15% hydrogen concentration, the foam causes a significant reduction in the pressure rise. The maximum effect occurs at about 28% hydrogen (the stoichiometric limit is 29.6% hydrogen) where the peak overpressure is reduced by two and one-half. Despite this overall pressure reduction, the flame speed is increased by up to an order of magnitude for combustion in the foam and strong pressure fluctuations are observed near a hydrogen concentration of 23%.

*This work performed at Sandia National Laboratories supported by the U.S. Department of Energy under contract number DE-AC04-76DP00789 for the U.S. Nuclear Regulatory Commission.

INTRODUCTION

In August 1980, the U.S. Nuclear Regulatory Commission requested a short term study to determine possible schemes to mitigate the effects of deliberate or inadvertent hydrogen combustion in nuclear reactor containment vessels. The objective of this study was to determine various means to reduce pressure and temperature inside a vessel, following combustion of evolved hydrogen gases, to assure no damage to the containment structure and the components within.

Filling the containment volume with a very high-density water fog before ignition of the hydrogen, whether deliberate or inadvertent, appears to provide a variety of benefits during combustion because the vaporization of water is an effective heat sink. Additionally, fogs can scrub undesirable particulate solids from the containment atmosphere.

Experimental work conducted by Carlson, Knight and Henrie [1] demonstrated that a hydrogen/air deflagration can be sustained in a dense fog environment. Enclosed vessel tests using fog volume fractions of 0.05% (volume of water to total volume) clearly indicated that temperature and pressure rise were reduced compared to tests without fog addition.

Isochoric equilibrium calculations confirmed that vaporization of fogs with volume fractions of 0.01 to 0.05% substantially reduces the overpressure during combustion if vaporization occurs during the time in which the flame traverses the vessel. An analytic model of hydrogen/air/steam combustion coupled with water vaporization kinetics was developed [2] to model the dynamics of flame-droplet interactions. Predictions with this model suggested that water droplets less than 200 μm radius can completely vaporize very near the flame front. On the other hand, very small droplets, < 5 μm, could vaporize within the flame reaction zone, influencing flammability and causing thermal quenching of the combustion. Between these two limiting droplet sizes, it appears that water droplets can effectively suppress the adverse effects of combustion if present in a sufficient quantity.

The feasibility of generating and maintaining suitable fogs has been investigated with a numerical model of droplet interactions [2]. Solutions of the governing integro-differential equations show that drop interactions, i.e., collision and coalescence, are critical in determining the behavior of very high-density fogs. For a given injection rate, the settling losses and attainable fog densities differ by several orders of magnitude when drop interactions are and are not considered. Despite constant injection rates, the coalescence of drops also leads to periodic, large-scale rain-out with corresponding oscillations in the quasi-steady fog density. The stability of these fogs is so impaired by drop interactions that fogs of acceptable density may be difficult to maintain with reasonable injection rates. A small scale experimental investigation of fog generation supports this conclusion [3].

In order to circumvent this problem of maintaining high density fogs, we propose the alternate technique of suspending the water with a high expansion-ratio aqueous foam. Adding a small quantity of surfactant to the water results in a relatively stable bubble matrix which can easily suspend a mean water volume fraction of 0.1%. Water drainage from a foam mixture can be substantially lower than the settling loss associated with fogging, a significant advantage in generating and maintaining a foam. Recent work on foam stabilization has demonstrated that drainage can be greatly suppressed by the proper selection of surfactants [4].

Foams generated with entrained air are commonly used for fire fighting and such applications have been extensively studied. There are many commercial foam generators available for such applications and generators have been designed to discharge up to 30 m^3/s [5]. Foam generators are simple devices which are typically composed of an induction fan, spray nozzle and a perforated screen. The water/surfactant solution is sprayed against the screen and air is pushed through the screen by a fan producing a bubble matrix on the downstream side.

Using these generators, fast foam production has been achieved in many large volume applications (i.e., warehouses, aircraft hangers, etc.) and foam depths of 30 m are readily obtained. In one particular application, a warehouse of 42,000 m^3 (1.5×10^6 ft^3) was completely filled with foam in only 7 minutes [6]. Clearly, it has been demonstrated that filling a large containment vessel with a high expansion-ratio foam is a technically feasible alternative to fogging. In addition, foam generation typically requires smaller operating pressures than fogging so that pumping costs can be expected to be significantly lower than those of a fogging system.

In contrast to fire fighting applications in which the water foams contain inert gas, foams generated within the containment vessel will contain combustible gas. Flame spread will occur across a collapsing bubble matrix and the dynamics of the flame/foam interaction will be even more complex and less amenable to analysis than combustion in fogs. A literature survey has suggested that litle is known about combustion of high expansion-ratio aqueous foams generated with a premixed flammable gas. Although the soap bubble technique is a classical means of experimentally determining gaseous burn velocity [7], flame spread across a bubble matrix is an entirely different flame propagation problem. Related studies have been limited to flame propagation using only very few cells [8] or in a foam mixture in which the liquid is combustible [9]. Due to the lack of any fundamental work in this area, we have conducted several open-tube and closed-vessel tests in order to assess the usefulness of aqueous foam in a mitigation scheme.

OPEN TUBE EXPERIMENTS

Experimental Procedure

The open-tube tests were intended primarily as a quick visual examination of foam combustion. Prior to these tests, there was serious doubt as to whether such mixtures would even support combustion. Early tests were conducted using methane so that a visual observation of the flame structure could be made. Tests were also conducted using hydrogen/air filled foams; however, t hydrogen/air flames were virtually nonluminous, so only foam collapse was observed in the tests.

The test burns were performed in a horizontal, 1 m lucite tube, 8 cm in diameter. A small screen-type foam generator was used to fill the tube with a 1000:1 expansion-ratio foam blown with the desired combustion mixture. A detailed description of the foam generator is given in the section on the closed vessel experiments. For safety reasons, only lean hydrogen/air mixtures were burned in the tube. Movies taken with a framing camera at 200 fps were the only diagnostics used on the open tube tests.

Test Results

The most notable observation in these tests was the dramatic difference in character of the flame front with and without foam. Without foams, the visible flame front was laminar, stable and very thin; typically visual thicknesses were on the order of millimeters. Except for the leanest mixtures, the flame was nearly planar and propagated with only minor instabilities and distortion of the front. In contrast to this, when the mixtures were burned in a foam, the flame became extremely unsteady and the visible flame front broadened to ~10 cm. The flame spread in the foam mixtures exhibited marked oscillations and sporadic burning across the diameter of the tube. Close inspection of the movies revealed that the flame moved forward in irregular jumps, developing a pattern of foam cell collapse and rapid consumption of the cell contents followed by a long delay. As the flame moved down the tube, it displayed a very irregular surface with fingers of the flame jetting into individual foam cells. Evidently, the bubble collapse process locally accelerated the flame. Large scale oscillations ahead of the flame were also observed as the flame travelled down the tube. By visually tracking the flame front, a flame velocity was measured and compared with existing data for methane/air. At a concentration of 10% (volume of methane in the total mixture volume), a flame velocity of 56 cm/s was measured experimentally. This represents a factor of two higher than the reported laminar flame velocity [7] and is typical of turbulent flame propagation based on a wrinkled flame theory [10].

Another notable observation in these tests was that very little of the water in the foam appeared to be vaporized. Following a burn, the tube walls were covered with a thick water film and a

large volume of water drained from the tube ends. Several efforts to measure the volume of water vaporized were unsuccessful, and the desire to accurately quantify the amount of water evaporated led to the closed vessel tests described in the next section.

CLOSED VESSEL TESTS

Experimental Procedure

The closed vessel tests were conducted in a small-scale, 11 liter, combustion bomb. The primary purpose was to determine the over-pressures associated with the deflagration of confined hydrogen/air filled aqueous foams. All foam tests used approximately the same foam composition, expansion ratio and uniform bubble size in order to avoid any spurious results introduced by changes in foam characteristics. Baseline tests were also performed using gaseous hydrogen/air mixtures without foam. Various mixtures covering lean to rich concentrations of hydrogen were ignited using both soft (glow plug) and hard (spark and high explosives) ignition sources.

The combustion facility consisted of a combustion bomb, a foam generator and a data acquisition system. See Figure 1. The combustion bomb itself was located inside an explosives testing chamber and operated remotely with air-operated valves. The foam was generated within the combustion vessel. The foam generator section, indicated in Figure 1, served only to premix separate streams of metered dry air with the hydrogen and to disperse a liquid spray of water/surfactant solution. The hydrogen and air were premixed using a porous plug of rigid polymeric foam packed within a 7 x 60 cm plexiglass pipe. The liquid solution of water and surfactant passed through a tube along the center line of this pipe and was dispersed using an adjustable atomizing nozzle set to produce a coarse spray of liquid droplets. The liquid spray passed into the combustion bomb where it impinged on a fixed conical screen located just inside the combustion chamber. The liquid drops wet this perforated surface and foam was produced as the premixed hydrogen/air gas passed through the screen.

The surfactant used in this study was a typical organic fire-fighting agent, MSA type V [11], which was premixed with water to produce a 2% (volume fraction of surfactant) solution. This mixture was held in a storage tank and pumped from the tank using overpressure of air. The flow rate of the solution into the combustion bomb was metered and held constant at 0.5 cm^3/s for all of the foam tests. Dry air and hydrogen were also metered (using rotometers) and these flow rates were adjusted to produce a constant 1000 to 1 expansion-ratio foam.

The first step in each test was to adjust the gas flow rates which purged the combustion vessel and foam generator with the desired gas mixture. After purging, the water/surfactant mixture was added to begin foaming. When the vessel was full, as indicated by the appearance of foam at the drainage valve, the liquid

and gas supplies were simultaneously terminated to avoid producing gaseous pockets within the combustion bomb. The two valves at the inlet and exit of the vessel were closed and the mixture was immediately ignited. In order to minimize the effects of bouyancy during propagation, the combustion vessel was horizontally oriented in all tests. Several preliminary fillings were performed and the system was opened to examine the foam being produced. Visual inspection inside the vessel indicated that a fairly uniform bubble matrix of foam was produced. Bubble cell size was typically 1 cm in diameter.

The ignition source within the vessel was located at the center of the vessel end-plate, opposite the foam generator. Glow plugs and spark ignitors were used in initial tests. Tests conducted with a glow plug showed successful ignition of various foam mixtures; however, the time delay required to heat the glow plug element to the point where ignition occurred was typically 20 s. In order to minimize foam drainage, which would substantially alter the mean foam expansion ratio for these small scale experiments, the glow plug ignition source was abandoned and a spark ignitor was used to produce more prompt initiation. The total energy delivered to the spark gap was approximately 7 J.

Additional tests were conducted using various hard ignition sources. The primary objective here was to observe the effect of the ignition source on flame propagation and to determine if detonation of a foam mixture could be initiated in this small scale combustion bomb. Tests were conducted using an RP2 detonator [12], which is a small detonator containing 40 mg of tetryl and 20 mg of PETN packed around a bridgewire ignitor. A pyrotechnic device which sends out hot particles along with a shock pulse, and an RP2 detonator boosted with 1 g of tetryl were also used. Each test required the installation of a new ignitor and thus fewer tests were conducted with these ignition sources than with the spark source; hard ignition tests were conducted only at a fixed hydrogen concentration of 22%. At this concentration, the spark initiated tests had indicated very rapid deflagration and the potential for detonation.

Transient pressure measurements were made using two Kulite piezo-resistive pressure gages, mounted flush in the vessel end-plate opposite that of the ignitor. These gages could measure overpressures of up to 1 and 3 MPa with a response time of 50 μs. Pressure signatures were recorded on a Nicolet digital oscilloscope and the data were stored on a mini floppy-disk for post-processing on an HP 9825 mini-computer.

Test Results

First, the results of all the tests conducted with the spark ignition source will be described. Results from each test include the maximum overpressure above ambient, rise time and pressure fluctuation amplitude and frequency. Figure 2 displays a typical pressure record, indicating the variables of interest. Several

mixtures were retested and nearly identical pressure records were obtained, assuring repeatability of the tests.

Figure 3 shows the measurements of pressure rise above ambient as a function of hydrogen concentration. Data represented by the solid dots correspond to tests made without foam and the open dots are tests with foam. Vertical bars in the foam data indicate the amplitude of the fluctuating pressure near the pressure maximum. The curve included in Figure 3 is a theoretical calculation of the adiabatic isochoric pressure rise without foam using an ambient pressure of 83 kPa and 300 K initial temperature [13]. Data obtained for hydrogen concentrations exceeding 18% fall reasonably close to the theoretical calculations. At lower mixture concentrations the effects of heat loss during propagation are evident. In all tests, from lean to rich limits, the over-pressure was suppressed to some degree with the addition of foam. In no test was the pressure rise during combustion in foam in excess of that measured in the unfoamed gases of the same hydrogen concentration.

In order to get a better perspective on the effect of foams on pressure rise, the data of Figure 3 were replotted as the ratio of pressure rise with foam to that without foam as a function of hydrogen concentration. Figure 4 displays these results. The curves on this, and the remaining figures, were merely to indicate trends.

At hydrogen concentrations below 10%, the pressure rise was substantially suppressed by the presence of the foam. This reduced overpressure was apparently due to local pockets of unburned combustible foam. No foam mixtures containing less than 7% hydrogen could be ignited; in comparison, the horizontal lean limit flammability limit is 6% for pure gas mixtures [14]. When the vessel was purged following a test burn of very lean foam mixtures, unburned foam was clearly evident.

For hydrogen concentrations between 10% and 12% the combustion in foam appears to be more complete and the overpressure approaches approximately 90% of that measured without foam.

From a 12% to 28% concentration the presence of foam again resulted in a significant reduction of the peak pressure. Several attempts were made to re-initiate a mixture following the first burn and no observable pressure rise was seen, suggesting that the reduction was not due to incomplete combustion, but due to vaporization of the liquid water. In this concentration range it appears that the foam collapse ahead of the propagating flame was vigorous, producing very small water droplets or ligaments which then passed into the flame zone. Vaporization continued in the hot burned region behind the flame which rapidly cooled the combustion gases. Following tests in this intermediate concentration range, the gases purged from the vessel contained a large quantity of condensed steam, indicating that vaporization had indeed occurred. Purging after pure gaseous combustion resulted in a much smaller amount of condensed steam.

Using the overpressure data described above, equilibrium isochoric calculations were made to determine the volume fraction of water as was inferred from the reduction of overpressure observed in the tests. The water volume fraction held in suspension by the foam was 0.1% and this value is thus the maximum fraction which could evaporate. The computed results, shown in Figure 5, reveal that a substantial fraction of the available water was evaporated for mixtures with hydrogen concentration above 15%. Near a concentration of 28%, maximum water evaporation occurred. The peaked functional dependence of vaporization on hydrogen concentration can be readily explained: the temperature of the products in constant volume combustion reaches a maximum near the stoichiometric point and decreases on the lean and rich sides. Since the evaporation rate increases with temperature, the water fraction evaporated must follow a similar trend.

It is noteworthy that these tests were conducted in a small scale vessel in which a relatively short time is available for vaporization. Using the vaporization model described earlier we estimate that a mean droplet size of ~10 μm was necessary to explain the observed rate of vaporization implied by the measured over-pressure reductions. In comparison, a mean droplet size was estimated from a simplified model of foam collapse based on conventional concepts used in foam engineering [15].* This model assumed that the water contained in the foam cell retracts to the junction of the cell walls where a single droplet was formed. For the foam characteristics used in the present experiments, a 600 μm dia droplet would be formed. The corresponding vaporization time of this size droplet was estimated to be ~1 s [2]. Clearly this notion of foam collapse leads to calculated droplet sizes which are much too large to explain the apparent vaporization. A much more disruptive and catastrophic mechanism of foam collapse must take place in order to produce the very fine droplets necessary to explain the apparent vaporization rates. In larger vessels the effects of water vaporization can be expected to be more significant due to longer flame propagation and droplet residence times. Thus, greater reductions of the over-pressure can be expected for larger scale tests.

As suggested by the previous work in an open tube, burning velocity is enhanced by the presence of the foam. To quantify this effect, a characteristic burn velocity can be estimated from the ratio of the vessel length to the pressure rise time from ignition to the pressure extreme. For all tests, the characteristic burning velocity with foam was enhanced over that without foam. Shown in Figure 6 is a plot of the ratio of pressure rise time with foam to that without foam. The inferred burn velocity of foam mixtures is a factor of 3 to 16 greater than the velocity without foam. Near a concentration of 23%, the pressure oscillations reach a maximum and the burn velocities are most enhanced. The significance of this particular concentration is not understood at this time.

The characteristics of the turbulence produced by foam collapse ahead of the flame were estimated using a model in which the energy released by bubble collapse induced local gas jets. This energy was calculated as a product of liquid surface tension times the change of surface area as the bubble matrix contracts to liquid droplets [15]. Thus, the local fluctuation of the gas ahead of the flame were calculated using the following equation:

$$u' = (13.2\gamma/c\rho_g)^{1/2}$$

where the liquid surface tension, γ, was estimated to be approximately 20 to 30 dyne/cm; the bubble cell size, c, was 1 cm in the tests; and the gas density within the bubble cell, ρ_g, was typically 10^{-3} g/cc.

Calculation of the induced gas velocity produced u' = 5 m/s which was the same order as the laminar burn velocity. The computed Reynolds number based on u' and integral scale of the turbulence, which was taken to be the bubble cell diameter, was found to be Re ~3000. According to known correlations of turbulent burn velocity [10], these calculations suggested turbulent burn velocity should be enhanced by a factor of 5. In explaining the enhanced burn velocity to a factor of 16, u' must be increased by a factor of 3. Since these enhanced burn velocities occur at concentrations in which strong pressure oscillations were observed, it is possible that mechanical agitation increased the turbulent intensity.

In no test was evidence of flame acceleration to detonation observed. In contrast to large scale turbulence effects that are known to accelerate flames to detonation [16], foam breakup apparently produces turbulence of the scale of foam bubble size which can decay rapidly. It is uncertain at this time if a detonation could be propagated and maintained in a foam mixture [17], under other conditions. Burn velocity enhancement with foam addition may be different for large scale vessel tests and thus acceleration effects due to foam collapse remain to be clarified.

Since the previous results indicated that large pressure reductions and burn velocity enhancements were associated with the presence of violent pressure oscillations, data on fluctuating pressure amplitude and frequency were taken from the pressure records. Note that some minor oscillations (a few kPa in amplitude) of an acoustic nature were observed in pure gas tests; however, very violent pressure fluctuations of 150 to 200 kPa were observed in several foam tests.

To further examine the origin of these strong pressure oscillations, the amplitude of the pressure oscillation, normalized with maximum overpressure, was plotted in Figure 7 versus the rise time normalized by the frequency of the oscillations, which were typically 500 Hz. Although the data show considerable scatter, it appears that when the pressure rise time becomes com-

parable with the period of the fundamental acoustic mode of the vessel, pressure fluctuations become greatly amplified. These self-excited oscillations are of an acoustic nature and the coupling with combustion which produces amplified oscillations is explained by arguments based on the Rayleigh criteria [18].

Tests were also conducted with explosive ignitors. Tests were first conducted using the RP2 detonator. A preliminary test was conducted using only air in the combustion bomb to determine the pressure induced by the detonator. The measured over-pressure induced by the detonator was, at maximum, about 7 kPa and the pressure wave continues to reverberate in the vessel several cycles (~5 cycles) before complete attenuation. The combustion vessel was then filled with a pure gaseous mixture of 22% hydrogen/air and initiated with the RP2 detonator. The resulting pressure rise was very rapid and the over-pressure saturated the pressure transducers, suggesting that a detonation occurred.

A combustible 22% hydrogen/air filled foam was then tested in the vessel. In repeated tests, the detonator failed to ignite the mixture. The pressure signatures were similar to those observed in the air test, except that the pressure fluctuations were greatly attenuated after only one or two cycles, consistent with the known attenuation for shock waves propagating in foam. Based on calculations of the peak pressure induced by the shock [19], we can conclude that all of the foam in the vessel was collapsed by the explosive ignition source. The collapse pressure of many aqueous foams has been estimated to be approximately 7 kPa. The calculations also show that the foam dramatically reduces the peak shock temperature and heated volume. However, the pressures and temperatures are not so low, nor the heated region too small such that the explosive source should not ignite the hydrogen/air mixture. Thus, on the basis of these limited results, we must conclude that the failure of the mixture to burn was not a consequence of an insufficient source. A candidate explanation of the observed behavior is that the intense shock fragments the foam into very small droplets such that vaporization quenches the flame. This conclusion, if correct, reveals an unusual property; a weak source such as a spark may be more effective than a stronger, explosive source in igniting combustible mixtures in aqueous foam.

Discharging the fireset into the spent detonator several seconds following detonator ignition produced an arc across the bridgewire contacts which initiated the remaining mixture in the vessel. Presumably by this time, much of the suspended water had settled onto the vessel walls. The pressure record was similar to the trace observed in earlier spark tests without foam addition. This tends to confirm that the shock pulse entirely collapsed the foam mixture.

A second series of tests were then made using a $TiH/KClO_4$ pyrotechnic ignition source. These devices contain 60 mg of

pyrotechnic and generate both a shock and incendiary fragments. Ignition was successfully attained and, again, burning did not proceed to detonation. The pressure rise time was not as rapid as that observed using a spark ignitor source, however some burn-rate enhancement was observed. Also, the peak over-pressure was intermediate to those observed in tests with and without foam addition initiated by a spark source. Apparently, the shock pulse collapsed the foam far ahead of the flame front, ...lding residual turbulence levels much lower than those cal-...ated for flame-front/foam interactions.

The final tests conducted used an RP2 detonator boosted with 1 g of tetryl; ignition was achieved but no detonation was produced. The pressure trace suggested that a rapid deflagration occured following initiation of the detonator. We suspect that ignition, in this case, resulted from burning fragments of the tetryl booster being thrown into the vessel by the primary detonator. As with other foam tests, the measured peak overpressure was much smaller than in the baseline hydrogen/air case.

CONCLUSIONS

The results of our open tube and closed vessel experiments show that the lean hydrogen/air flammability limits are not strongly influenced by the presence of the foam. The horizontal lean flammability limit with foam is slightly increased over that for mixes without foam, from about 6% to about 7% hydrogen by volume. The velocity of flame propagation in foam increases markedly with increasing hydrogen concentrations.

Our tests in an 11-liter closed vessel indicate that the foam reduces the post-combustion pressure rise, but not uniformly as the hydrogen concentration is varied. At low hydrogen concentrations, below 10%, the reduction in pressure rise is substantial -- a factor of two or more. We feel this is due to incomplete combustion of the vessel contents, rather than vaporization of water in the foam. Between 10% and 15% hydrogen concentrations, the foam has a small effect on the pressure rise; at 12% the over-pressure for a burn with foam is about 90% of that without foam. Above 15% hydrogen concentration, the foam causes a significant reduction in the pressure rise. Its maximum effect occurs near the stoichiometric limit, at about 28% hydrogen. Here, the over-pressure is reduced by two and one-half. Despite this ...erall pressure reduction, the flame speed is accelerated by ...re than an order of magnitude for combustion in the foam. Associated with the accelerated flame, large amplitude pressure waves develop in the vessel. We believe these waves help break up the foam and, therefore, lead to enhanced vaporization of the water. Above the stoichiometric limit, the beneficial effects of the foam again decrease. For vessels larger than that used in our tests, we speculate that pressure and temperature reductions will be larger and more uniform with varying hydrogen concentrations due to the longer total burn times and, accordingly, longer residence times for heat transfer from the heated gases to the water.

Although the foam tends to accelerate the flame dramatically, we found no evidence of a detonation in these small-scale tests. Even when squibs and detonators were used to initiate combustion, detonations were not obtained in the foam. In no case did we find that the use of the foam resulted in pressures larger than without it at the same hydrogen concentration.

ACKNOWLEDGMENTS

We would like to thank O. B. Crump, Jr. and S. M. Falacy for their assistance in setting up the experimental apparatus and helping conduct the tests. This project was sponsored by the Nuclear Regulatory Commission; Project Managers, Dr. P. Worthington and Dr. J. Larkins.

REFERENCES

1. L. W. Carlson, R. M. Knight and J. O. Henrie, "Flame and Detonation Initiation and Propagation in Various Hydrogen-Air Mixtures With and Without Water Spray", Rockwell Interim Report, AI-73-29, 1973.

2. M. Berman, et al., "Analysis of Hydrogen Mitigation for Degraded Core Accidents in the Sequoyah Nuclear Power Plant", SAND80-2714, March 1981.

3. A. Camp, "X-Ray Measurements of Water Fog Density", to appear as SAND82-1992, NUREG/CR-1992.

4. P. Rand, O. Montoya and A. Kraynik of Sandia National Laboratories have examined foam drainage effects for a variety of surfactant-water mixtures. Most of their work is documented as Sandia National Laboratories memos.

5. Personal communication from P. Rand, Sandia National Laboratories.

6. Data Sheet obtained from Kidde Belleville, Division of Walter Kidde Company, 1977.

7. B. Lewis and G. Von Elbe, Combustion Flames and Explosion of Gases, 2nd Ed., Academic Press, New York, 1961.

8. P. Girard, et al., "Flame Propagation Through Unconfined and Confined Hemispherical Statified Gaseous Mixtures", Sixteenth (Int.) Symposium on Combustion, The Combustion Institute, 1978.

9. A. Thomas, "Flame Propagation Through Air-Fuel Foams", Sixth (Int.) Symposium on Combustion, The Combustion Institute, 1956.

10. R. Abdel-Gayed and D. Bradley, "Dependence of Turbulent Burning Velocity on Turbulent Reynolds Number and Ratio of Laminar Burn Velocity to R.M.S. Velocity", The Sixteenth Symposium (Int.) on Combustion, The Combustion Institute, 1977.

11. M.S.A. Type V is the brand name of a fire fighting surfactant manufactured by the Mine Safety Application Co.

12. The RP2 detonator is a explosive device manufactured by the Reynolds Manufacturing Company.

S. Gordon and B. McBride, "Computer Program for Calculation of Complex Chemical Equilibrium Composition, Rocket Performance, Incident and Reflected Shocks and Chapman-Jouget Detonations", NASA SP-273, 1971.

14. H. F. Coward and G. Jones, "Limits of Flammability of Gases and Vapors", Bulletin 503, Bureau of Mines, U.S. Dept. of Interior, 1952.

15. Personal communication by A. Kraynik of Sandia National Laboratories. Additional background material relevant to aqueous foams can be found in the text by J. J. Bikerman, Foams, Springer-Verlag, 1973.

16. J. H. S. Lee and I. Moen, "The Mechanism of Transition From Deflagration to Detonation in Vapor Cloud Explosions", Prog. Energy Combustion Science, Vol. 6, 1980.

17. Unreported tests have been conducted by W. Benedick of Sandia National Laboratories of tests in which a detonation initiated by a sheet explosive is propagated into a bag of MAPP gas-air filled aqueous foams. Observation of high speed movies indicated that the detonation was not sustained and the reaction wave quickly reduced to a deflagration.

18. R. Strehlow, Fundamentals of Combustion, Int. Textbook Co., 1968, see pages 270-282.

19. S. K. Griffiths, "Shock Wave Propagation in Aqueous Foams", to appear as SAND82-1482.

20. A Ranger and J. Nichols, "Aerodynamic Shattering of Liquid Drops", AIAA J. 7, February 1969, pp 285-290.

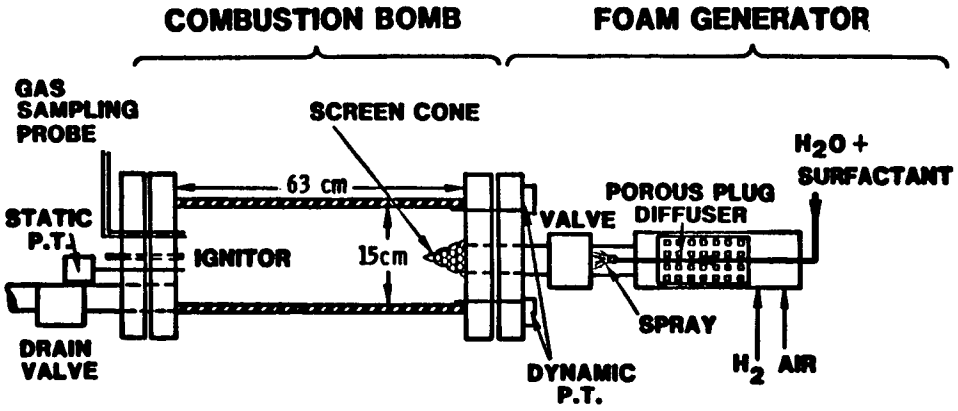


Figure 1. Schematic of the Combustion Bomb Used for Confined Volume Tests

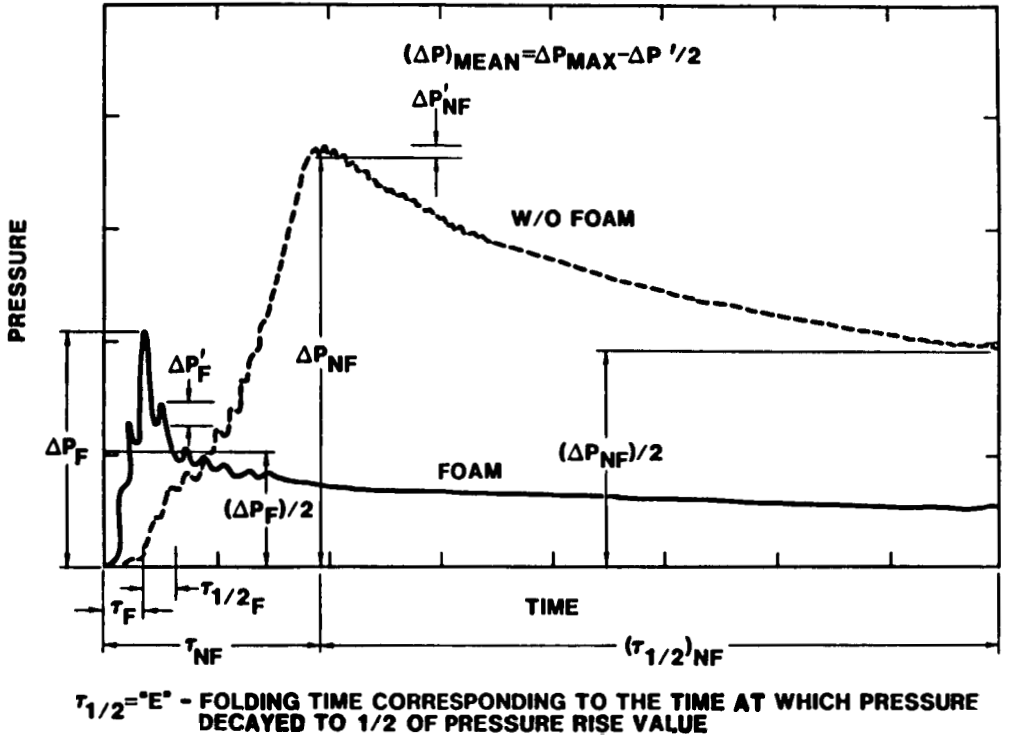


Figure 2. Typical Pressure Records for a Test With and Without Foam Addition Which Shows the Experimental Measurements of Interest

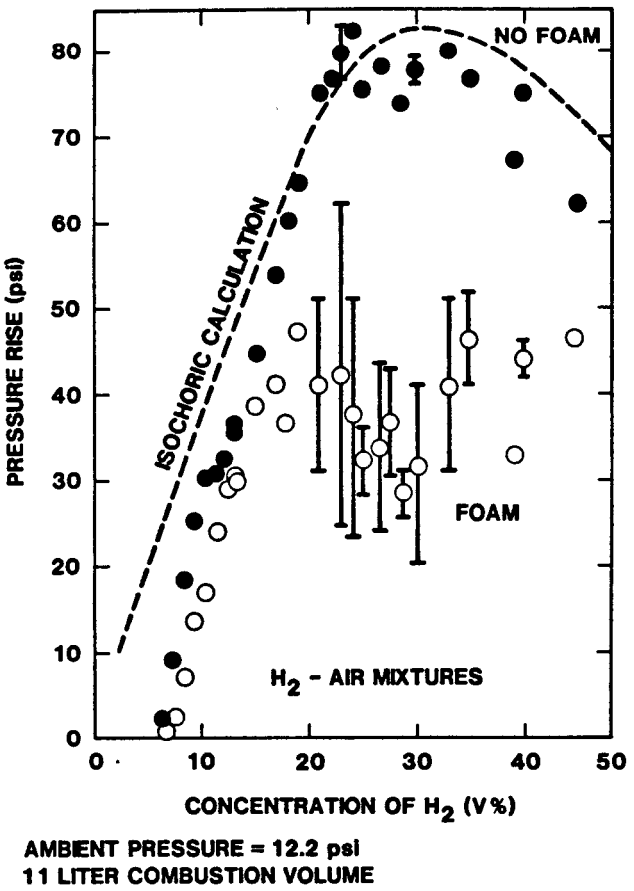


Figure 3. Pressure Rise Above Ambient For Various Concentrations of H_2 With and Without Foam Addition

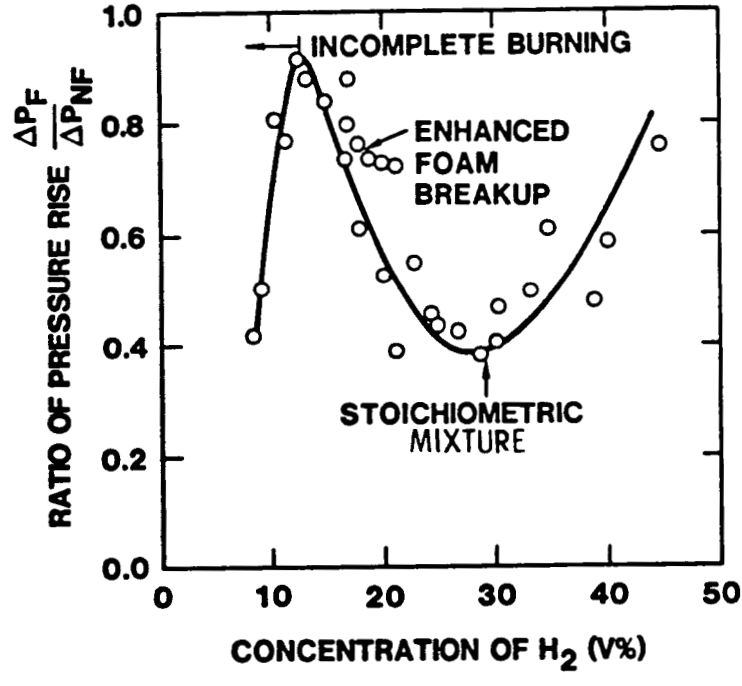


Figure 4. Ratio of Pressure Rise Above Ambient With Foam Addition to That Without Foam Addition vs. Concentration of H_2

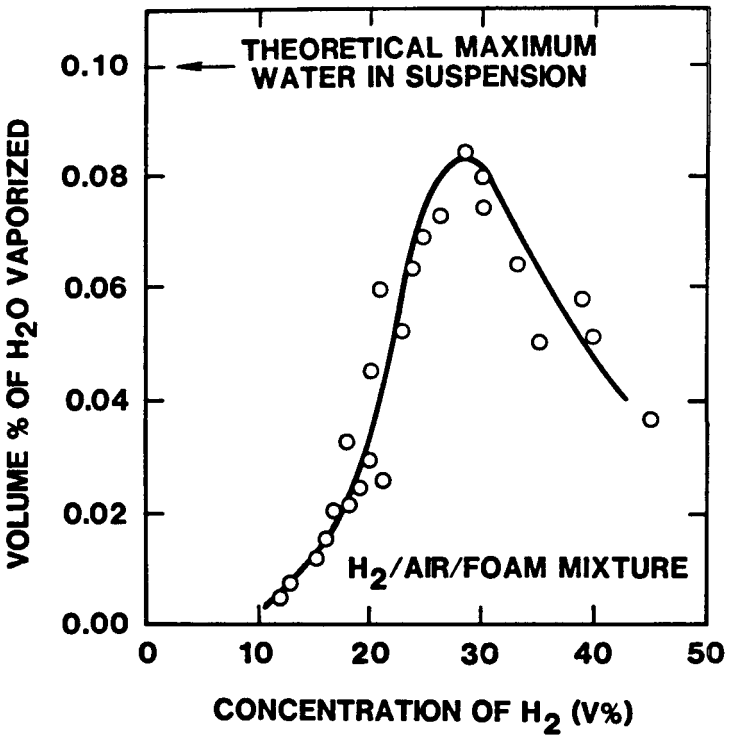


Figure 5. Calculated Water Fraction Vaporized Using the Pressure Data Shown in Figure 3

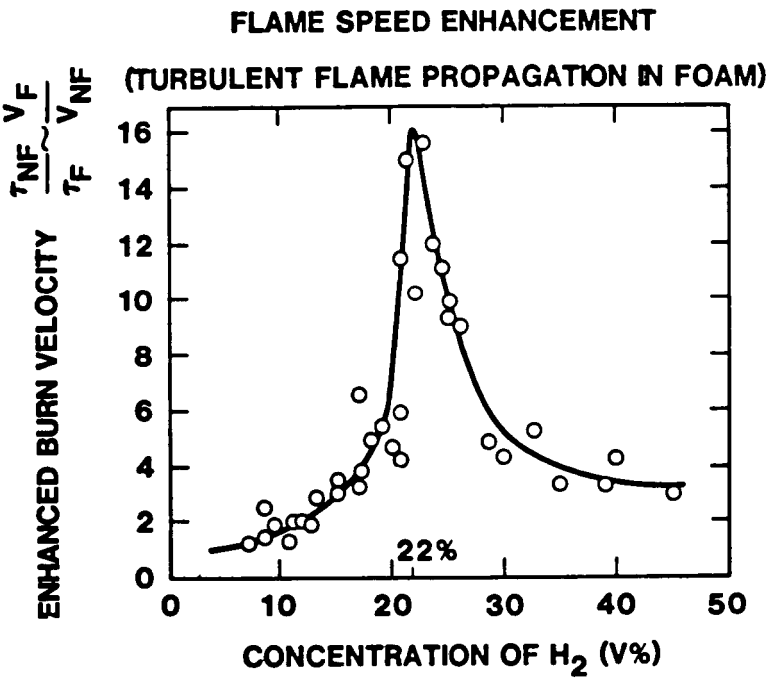


Figure 6. Ratio of Burn Velocity With Foam Addition to That Without for Various Concentrations of H_2

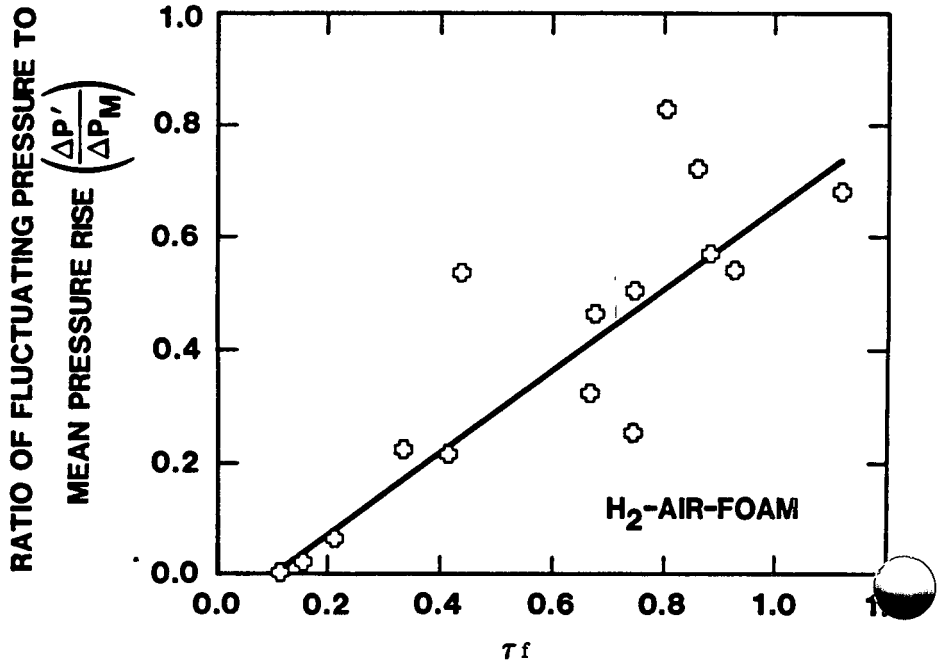


Figure 7. Ratio of Fluctuating Pressure Normalized by Mean Pressure Rise vs. Pressure Rise Time Multiplied by the Frequency, f, of the Pressure Oscillations

STUDY OF HYDROGEN REMOVAL SYSTEMS

W. Baukal, A. Koehling, G. Langer, E. Poeschel

Battelle-Institut e.V., Postfach 90 01 60, 6000 Frankfurt Main 90, Federal Republic of Germany

In 1979, the German Federal Ministry of the Interior initiated a series of studies into the mitigation of consequences of severe (hypothetical) reactor accidents. One of these consequences is the release of hydrogen into the containment atmosphere.

This paper describes the first phase of a hydrogen mitigation study. The first phase was completed in June 1981, a second phase is now under way.

The objective of the first phase was to determine which methods for removing hydrogen and disposing of it in a gradual and controlled manner are available and technically feasible. The safety goal within the first phase of the study was chosen such that the concentration of H_2 in the containment atmosphere should not exceed 4 v/o. The reference basis was a German 1300-MW PWR characterized by a large (approx. 70,000 m^3), dry, multi-compartment containment. Design-basis accidents and hypothetical accidents have been considered.

Hydrogen can be removed or separated from gaseous mixtures by a number of chemical and physical processes (Table 1). The methods and corresponding technical systems have been evaluated with respect to their feasibility for reactor accidents. Combustion as well as catalytic and thermal recombination are the best methods available at present. Chemical absorption in liquid or solid non-metallic or metallic absorbents, adsorption, electro-

chemical methods and separation by non-metallic or metallic membranes were evaluated and found to be less promising.

In the nuclear industry, catalytic recombiners are being used successfully as off-gas purification systems. Catalytic and thermal recombiners are commercially available as hydrogen removal systems for application during and after design-basis accidents (Table 2). In addition, two systems from the non-nuclear industry have been selected for closer consideration: (i) special types of burners developed for removing combustible pollutants from air or off-gas, (ii) completely passive catalytic recombiners used for maintenance-free batteries.

As a limiting case, the rate of hydrogen removal from an accident atmosphere may be set equal to the hydrogen release rate. If the removal system is loaded with the containment atmosphere before the hydrogen concentration has attained a concentration of 4 v/o, the safety goal is reached in any case. Under these premises, the size of the technical system, its throughput and the latest possible loading time after the onset of hydrogen release are governed by the hydrogen relase rate (Fig. 1).

Three fields of application of hydrogen removal systems can be distinguished.

Low release rates: At low release rates, the well-known post-LOCA recombiners with hydrogen removal rates designed up to 4 m^3/h can be used. In this application range, there is no need to transmit and adapt systems from the non-nuclear industry. There are certain system differences among the available recombiners (inside/outside, fixed/portable). These differences, however, are of minor importance for meeting the requirements of a LOCA, compared with the requirements of severe accidents.

Medium release rates: During hypothetical accidents, hydrogen release rates exceeding 4 m^3/h may occur. In a medium range of

release rates, systems selected from the nuclear and non-nuclear industry are in principle suitable. They would have to be scaled up, technically modified and adapted to the particular requirements. There are, however, engineering limits which originate from application and from safety considerations.

We have defined the following limits for the applicability of recombiners and other removal systems: a system intended to be used in hypothetical accidents should (i) be portable or suitable for transportation and (ii) not be operated in continuous standby.

On this basis, the maximum size of a system and the earliest possible time of loading the system with accident atmosphere were estimated. From these engineering limits, the upper limit of hydrogen release which can be controlled by removal methods was deduced. It ranges between 40 and 80 m^3/h H_2, corresponding to a throughput of 1000 to 2000 m^3/h gas mixture.

High release rates: Some scenarios of hypothetical accidents imply a release of hydrogen at rates higher than the above-defined rate of 40 to 80 m^3/h. This may occur, for instance, during degraded core accidents and core meltdown accidents. In these cases, controlled removal of hydrogen by recombiners does not appear feasible.

For this application range, some countermeasures other than controlled removal are under discussion. These methods take into account an accumulation of hydrogen to concentrations higher than 4 v/o, but they avoid ignition of the hydrogen or mitigate the consequences of a hydrogen fire to a tolerable extent. The systems comprise, among others, pre-inerting, post-inerting (by CO_2, N_2 or Halons), removal of oxygen by chemicals or by burning it with an auxiliary fuel, fogging and deliberate ignition.

Before any recommendation can be made, these mitigation methods have to be carefully evaluated with the main view to safety. Introduction of one of the systems must reduce the total risk. This applies also to normal reactor operation. If a mitigation system is operating, it must not cause new safety concerns und reasonably conceivable accident scenarios. The method has to take into account the requirements of the large, dry, multi-compartmented containment. This is at present being investigated in a second stage of the hydrogen mitigation study.

Table 1: Hydrogen Removal and Separation Methods

Combustion

Recombination: thermal
catalytic

Diffusion: polymer membranes, metal membranes

Absorption in non-metals: Ag salts, Pd sols, $NaClO_3$, CuO, resorcinol, quinones, ...

Absorption in metals: metal hydrides

Adsorption

Electrochemical methods: fuel cells

Table 2: Post-LOCA Recombiners

Method	Design features Place[+)]	Installation	Supplier
Catalytic	external	fixed	KWU/Doduco
Catalytic	external	portable	Leybold-Heraeus
Catalytic	external	portable	Air Products and Chemical, Inc.
Thermal	external	portable	Rockwell Internat.
Thermal	internal	fixed	Westinghouse

+) with respect to containment

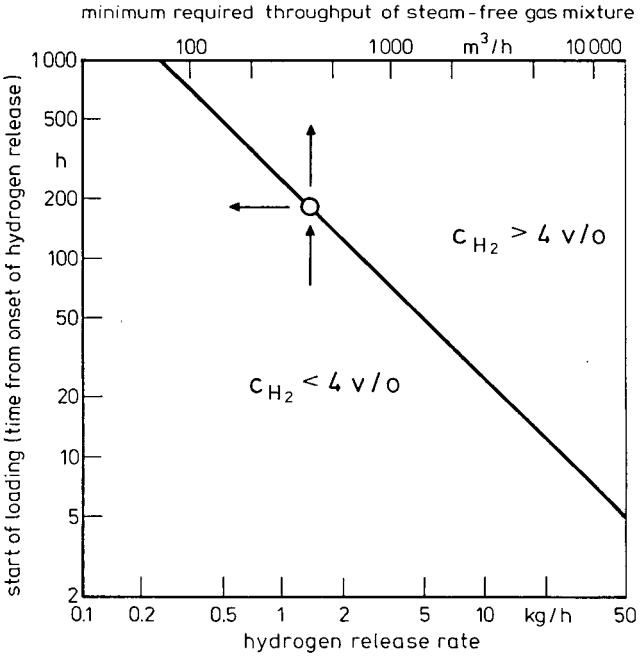


Fig.1: Hydrogen concentration in the containment atmosphere (calculated as free of steam) dependent on hydrogen release and loading of a recombiner

EPRI RESEARCH ON EQUIPMENT SURVIVABILITY UNDER HYDROGEN BURN

G. E. Sliter
Nuclear Power Division
Electric Power Research Institute
P. O. Box 10412
Palo Alto, CA 94303

ABSTRACT

This paper describes two test series sponsored by EPRI to study the effects of hydrogen burn on typical safety-related equipment in nuclear plants. The objective of the tests is to determine whether equipment designed to operate under design basis accident conditions can survive a hydrogen burn environment (i.e., be able to function during and after one or several hydrogen burns). The severity of the environment and the thermal response and operation of the equipment during the tests is monitored. The first series of tests is completed. Seven types of typical Class 1E electrical equipment were subjected to burns of both quiescent and flowing hydrogen, with and without steam, in an intermediate-volume cylindrical vessel. The equipment operated satisfactorily before, during, and after each of six sequential experiments. Measured temperatures at key locations on the equipment did not exceed temperatures specified by the manufacturers as important to operability. The second series of tests is being planned. A wider range of equipment types, both electrical and mechanical, will be subjected to hydrogen burns similar to those in the first series, but in a large-volume spherical vessel. Results of the first test series and plans for the second series are presented.

INTRODUCTION

Safety-related equipment in nuclear plants is designed and qualified to function under the severe environmental conditions produced by design basis accidents such as large- and small-break LOCAs and high-energy-line breaks (HELB). The accident environment at TMI-2, although in almost all respects less severe than the environment for which equipment is normally qualified, included a high-temperature spike from hydrogen burn not addressed by current qualification requirements. The objective of the EPRI research described in this paper is to determine whether equipment conservatively qualified to LOCA and HELB conditions can survive, in addition, the short-term environmental effects produced by the combustion of hydrogen in its vicinity. That is, the equipment must be able to perform its safety-related function during and after one or several hydrogen burns in postulated degraded core accidents.[1]

The research on equipment survivability is being carried out in conjunction with the EPRI Hydrogen Combustion and Control Program described in another paper at this workshop. Equipment experiments are piggy-backed on the main two test series designed to study hydrogen burn phenomena. The first, which is completed[2], was performed in a vessel of relatively small volume with seven types of new electrical equipment. The second, which is being planned, will be performed in a vessel of relatively large volume with a greater variety of both electrical and mechanical equipment, some of it artificially aged to simulate years of prior operation. The first section of this paper describes and summarizes the results of the equipment survivability experiments in the smaller volume. The last section discusses the approach and scope of the experiments in the larger volume. The tests in the large volume are being supported as part of EPRI participation in joint industry research which is using information and data from the TMI-2 accident to improve nuclear plant design, performance, and safety.

INTERMEDIATE-VOLUME EXPERIMENTS

The vessel in the first series of hydrogen burn equipment survivability tests had a cylindrical section 2.1 m (7 feet) in diameter and 5.2 m (17 feet) long. The 17.8 m^3 (630 ft^3) volume called "intermediate" is representative of a compartment in a reactor building, but is small relative to the main open volume in typical containments.

Equipment Specimens. Equipment for the experiments was selected on the basis of its common use as Class 1E safety-related equipment. The specimens contributed by or purchased from manufacturers were of nuclear grade quality; i.e., they were off-the-shelf items that could have been sold for qualification testing or service in a nuclear plant. The following types were selected for the experiments:

---

1. Nuclear Regulatory Commision, Interim Requirements Related to Hydrogen Control, Proposed Rule 10 CFR Part 50, December 1981.

2. R. Torok, W. Wachtler, and K. Seifert, Hydrogen Control Studies, EPRI Final Report, Project RP1939, Acurex Corporation, in preparation.

- o Valve operator (Limitorque, SMB-000-2)
- o Pressure transmitter (Foxboro, NE13DM)
- o Solenoid valve (Asco, NP83 1654E)
- o Limit switch (Namco Controls, EA180-11302)
- o Thermocouple (Conax, Dual Type E)
- o RTD (Weed Instruments, 1B5D/611)
- o Cable (6 samples of Rockbestos and Samuel Moore Dekoran)

The same equipment types had been included in earlier hydrogen burn tests at Fenwal[3] (sponsored by the Tennessee Valley Authority, Duke Power, and American Electric Power). In these tests operability was verified before and after the burns. In the EPRI tests, operability was also monitored remotely during the burns as described below.

The valve operator, designed to control and limit the opening and closing of various types of valves in a nuclear plant, consists of a motor, torque switches, and rotary drum geared limit switches. Operation during the tests was monitored by measuring both the motor current draw for a 25-ft-lb torque and the voltage drop across the limit switch in the open and closed position.

The differential pressure transmitter is used to measure flow, liquid level, or gas pressures up to 51 kPa (7.4 psi). It consists of a stable force-balance system which converts a difference in pressure between the high and low side of the transmitter body to a proportional dc output signal. Operability was monitored by measuring the differential pressure (with a gauge) and the transmitter output voltage.

The solenoid valve is a three-way normally closed valve with 1 cm (3/8 in.) lines used primarily as an isolation valve in the air supply lines of large control valves. When energized by applying 120 VAC to its solenoid coil, it directs air flow from the air supply system to the air operator of the main valve. When de-energized, the air operator pressure is exhausted through a port and the main valve closes. Operability was monitored by measuring the solenoid current draw and the pressure on the outlet and inlet sides.

The limit switch, used extensively in containment areas to determine the position of the moving parts of equipment, consists of a single-pole double-throw switch rated for 2.0 amperes continuous current at 125 VAC. Operation of the switch by a lever opens one circuit and closes another. In the hydrogen burn tests the lever was actuated by the Limitorque valve operator. Operability was monitored by measuring the voltages across the two normally open terminals and two normally closed terminals.

---

3. W. G. Dalzell, "Determination of Ignition Performance Characteristics of Glow Plug Hydrogen Ignitor," Fenwal Inc. Report No. PSR-914 for Westinghouse Electric Corp., November 10, 1980.

The large electrical output of the resistance temperature detector (RTD) allows application in tanks and fluid lines for which a high level of accuracy, sensitivity, and stability is required. The RTD is a transducer that operates on the principle of change in electrical resistance of a platinum wire as a function of temperature change in the wire. The test model was an assembly consisting of a stainless steel closed-end sensor probe, a thermowell for indirect immersion applications, and a cast iron head enclosing a terminal connection block. Operability was checked by conversion of voltage output to temperature and comparison with other vessel air temperature measurements.

The thermocouple is used in applications where accuracy requirements are not as stringent as those provided by RTDs. The assembly is similar to that of the RTD except that the connector enclosure is stainless steel and the probe contains two thermocouple wires for redundancy. Operability was checked in the same manner as for the RTD.

The steel or cast iron enclosures on the active equipment described above ranged in thickness from about 3 mm (1/8 in.) to about 5 mm (3/16 in.).

The electric cables included six lengths of 16-, 18-, and 22-gauge control, instrument, and power cable insulated with polyethylene and jacketed with a neoprene sheath. These cables were passive during the tests, with waterproof seals applied to the cable ends to prevent moisture intrusion. After the tests, standard continuity, insulation resistance, and dielectric strength measurements were made.

Experiment Description. Six sequential survivability experiments were conducted on the equipment specimens described above. The equipment was mounted in a manner recommended by manufacturers onto structural members welded to the test vessel in a central region (Figure 1). Cabling for the active equipment was protected by flexible metal conduit. The passive cable specimens were completely exposed to the burn environments.

The nominal initial condition for each experiment, produced by steam injection, was a saturated atmosphere at 70°C (160°F) representing containment condition at the time of a potential hydrogen burn. In the first two tests, 7.5 percent (Test 4.1) and 10.7 percent (Test 4.2) hydrogen by volume was premixed with vessel air and ignited by a glow plug located near the bottom of the vessel about 2 m (6 feet) below the equipment. These are called premixed combustion tests. In another three tests, hydrogen flowed continuously into the vessel at a measured rate, with the glow plug energized igniting the mixture at intervals between hydrogen buildup. These are called dynamic injection tests. Test 4.3 had a hydrogen flow rate of 0.6 N/min. (0.035 lb/min.); Test 4.4 had the same hydrogen flow along with 9.3 N/min. (2.1 lb/min.) of steam. Test 4.5 had the same steam flow and a higher flow rate, 0.47 N/min. (0.105 lb/min.). The equipment was subjected to hydrogen burn in a sixth test (same as Test 4.4 with water spray superposed) but the equipment was not operated during this test.

Measurements in five tests were made of both vessel environments (hydrogen/steam concentrations and air temperature/pressure) and equipment response (operability measurements described above and equipment temperatures). Twelve

thermocouples monitored temperature histories of equipment enclosure air spaces and of external and internal walls of the enclosures. Temperature and pressure histories were recorded on FM tape, oscillograph, or both. In addition, more than thirty heat-resistive elements (Temp-Plates) indicated whether the peak temperatures on internal component surfaces exceeded selected limits (300, 400, or 450°F) at locations identified by the manufacturers to be important for operability.

Results. All the equipment functioned properly during and after each of five hydrogen burn experiments (by comparison of signals with those in baseline functional tests performed prior to each experiment).

None of the Temp-Plates changed color, indicating that no surface exceeded the selected temperature limits. Also, there was no visible damage or degradation of the equipment surfaces after all six experiments.

In each of the two premixed combustion tests, one global hydrogen burn was recorded, with the vessel temperature rising in about 2 sec. to a peak and then decaying exponentially. In the test with 10.7 percent hydrogen, the maximum air temperature was 900°C (1650°F) and decayed by half the amount it rose in about 7 sec. (see Figure 2). The maximum recorded overpressure in the premixed tests was 331 kPa (48 psi).

In the low-hydrogen-flow dynamic injection test with no steam flow, a single temperature excursion was recorded as in the premixed tests (peak temperature 477°C [890°F] and decay time about 20 sec.). But in the two dynamic injection tests with steam flow, multiple temperature excursions occurred intermittently due to multiple hydrogen built-ups and burns. Figure 3 shows the vessel air temperature history in the test with low hydrogen flow and steam flow. The maximum recorded overpressure in the injection tests was 166 kPa (24 psi) (Test 4.5).

As expected, thermal inertia caused temperatures recorded on equipment surfaces and enclosed air spaces to be substantially lower than vessel air temperature. Typical equipment temperature histories are shown in Figures 2 and 3. None of the recorded surface temperatures on any of the equipment exceeded 241°C (465°F).

The maximum enclosed air space temperature in the premixed combustion tests was 226°C (439°F) within the Conax thermocouple connector enclosure from a burn of 10.7 percent hydrogen. From a burn of 7.5 percent hydrogen, this temperature was only 185°C (365°F). But an interesting anomaly was observed in the measurements of air temperature within the switch enclosure of the valve operator. In the premixed test with 10.7 percent hydrogen, this temperature peaked at 87°C (188°F), whereas in the test with 7.5 percent hydrogen this temperature reached 310°C (590°F). A possible cause of this anomaly is a burn of hydrogen within the enclosure during the test with the lower concentration of hydrogen in the vessel.

Other anomalies were electrical arcing of the valve operator motor observed upon opening the vessel hatch after one of the tests and substantial water penetration into some of the equipment observed when enclosures were opened subsequent to the last test. However, none of the anomalies observed had any apparent effect on the performance of the equipment.

All but one of the six cable samples passed insulation resistance and dielectric strength tests performed upon completion of the six experiments. For the 18-gage Dekoran cable arcing was observed at about 1 kV and the insulation resistance readings were low and unstable, apparently due to moisture penetration through its sealed ends and not from any effects of the hydrogen burns.

Conclusion. The typical Class 1E electrical equipment and cable examined in these experiments survived the cumulative effects of hydrogen burns in six sequential tests in the intermediate-volume vessel with no visible or functional degradation. In addition to the Class 1E equipment, other items of commercial off-the-shelf quality such as the igniters, thermocouples, electrical seal assemblies, copper pressure tubing, and mixing fans survived and remained operational after repeated exposure to the hygrogen environment in 28 experiments.

LARGE-VOLUME EXPERIMENTS

The next series of EPRI hydrogen burn equipment survivability tests will be conducted in a 15.9-m (52-foot) diameter spherical dewar at a DOE facility in Nevada. Its 2100-m^3 (75,000-ft^3) volume is about one-thirtieth the volume of the largest existing reactor containments and is about the same as the volume of the smallest. The dewar is insulated to allow heating to temperatures typical of postulated accident conditions at the time of hydrogen burns. As in the intermediate-volume series, both premixed and dynamic injection experiments are planned. As part of its current effort to prepare a test plan for the equipment survivability tests, Westinghouse Corporation under contract to EPRI will identify prototypical accident scenarios likely to pose the greatest threats to equipment and will select a matrix of experimental conditions that envelope actual conditions.

Equipment Selection. A wider range of equipment types than included in the first series will be selected for the large-volume tests. Among the selection criteria are:

- Common use in nuclear plants, especially TMI-2 (large, dry PWR), Sequoyah Unit 1 (PWR ice condenser), and Grand Gulf Unit 1 (BWR, Mark III).
- Importance to safety of equipment function, especially in terms of need to remain operational following degraded core accidents.
- Suspected vulnerability to hydrogen burn effects.
- Inclusion in previous tests.
- Size and cost.

For items too large to fit through the 61-cm (2-foot) diameter dewar opening or too costly to acquire, analysis will be performed to determine those subcomponents most susceptible to damage from hydrogen burn and these parts will be considered for inclusion in the tests. Although the majority of equipment types selected by the above criteria will be electrical, some mechanical equipment will also be included.

Within the constraints of schedule and cost, some of the equipment will be pre-conditioned to simulate to the extent possible the aging effects of nuclear plant operating environments such as heat, radiation, humidity, and operational cycling.

Experiment Description. In these large-volume experiments, the effects of equipment location and orientation with respect to ignition sites will be investigated by repeating some tests with the equipment repositioned. As in the intermediate-volume experiments, temperatures will be monitored at as many points on the equipment as practical.

Acceptance criteria for equipment survivability and performance will be specified prior to testing. Any differences between these criteria and others more appropriate for equipment qualification will be identified.

A test plan will be generated that will identify the equipment in the tests; its location, orientation, and monitoring; the number of tests; instrumentation and data logging requirements; and the details of each test cycle including vessel temperature profile, chemistry control, hydrogen buildup and ignition time, and sequencing of equipment operation. The test plan is scheduled for completion in early 1983 and the equipment tests in late 1983.

Results. The test results will be combined with those of previous tests and with observations of hydrogen burn damage at TMI-2 to reach general conclusions on survivability. Analytical methods involving heat transfer in the equipment and its environs will be used to interpret and extrapolate the test results to prototypical conditions. An assessment will be made of the overall impact of hydrogen burn test results and data from TMI-2 on current survivability requirements and qualification methods. The key question is whether the conservative methods currently used to qualify equipment in design basis accidents ensure survivability under hydrogen burn in degraded core accidents.

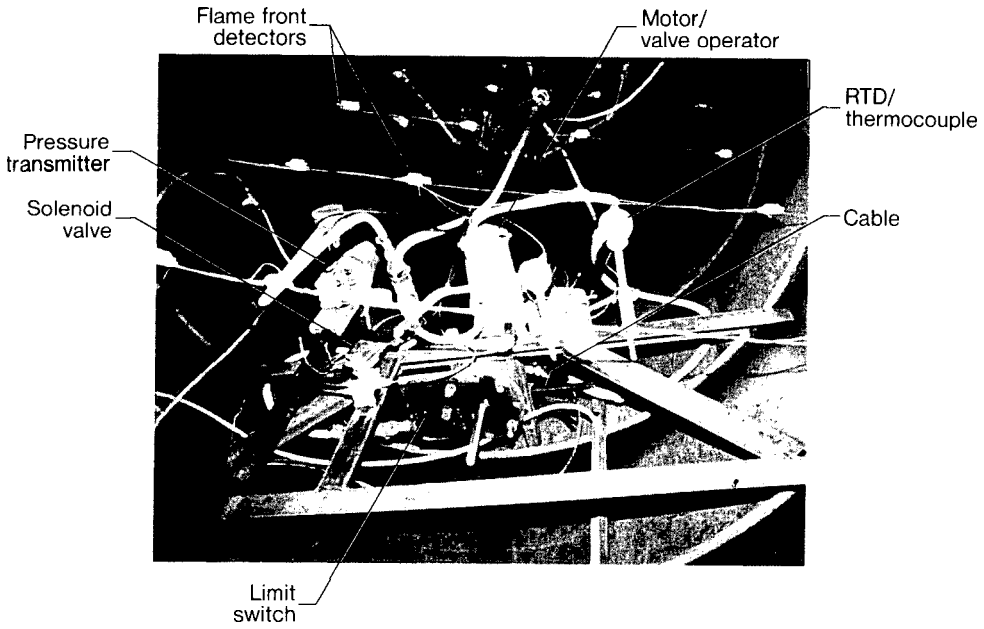


Figure 1 Equipment mounted in intermediate-volume cyclindrical vessel for hydrogen b[illegible] survivability tests.

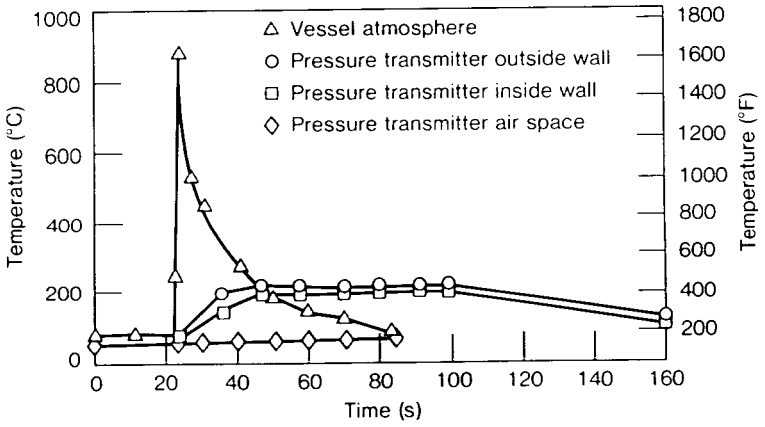


Figure 2. Thermal lag measured on pressure transmitter during premixed test with 10.7 percent hydrogen by volume (test 4.2).

HYDROGEN BURN SURVIVAL

PROGRAM REVIEW

Vincent J. Dandini
William H. McCulloch
David T. Furgal (Editor)
Sandia National Laboratories Division 9445
Albuquerque, NM 87185
operated by
Sandia Corporation
for the
U. S. Department of Energy

Hydrogen Burn Survival Program Review

V. J. Dandini
W. H. McCulloch
D. T. Furgal

ABSTRACT

The hydrogen burn during the Three Mile Island accident[1] has raised a concern that a similar burn resulting from a similar accident in the future could lead to a breach of containment integrity. One method suggested to minimize the possibility of its occurrence is the deliberate ignition of the hydrogen as it is released. In this way, hydrogen concentrations can be kept below levels which would otherwise threaten containment integrity. This mitigation scheme may, however, precipitate a series of hydrogen burns which might have deleterious effects on equipment inside containment. Of particular concern are any components necessary to establish and maintain a safe shutdown condition in the plant.

It is the purpose of the Hydrogen Burn Survival (HBS) program to develop a methodology by which the survivability of safety-related equipment can be evaluated. To this end, experimental and analytical investigations are underway which:

1. Identify the thermal characteristics of the burn environment having an impact on the function of safety-related equipment.

2. Study the responses of safety-related equipment to the hydrogen burn environment.

Experimentation has been carried out in vessels considerably smaller than containment buildings. An important part of the analytical effort has been the development of representative computer models based on observations from these tests and previous work by other investigators. These models will be used eventually to calculate the expected response of safety-related equipment in full-scale reactor containment volumes. Specific goals of the analytical effort are to:

1. Develop models of the heat transfer from the hot cloud of combustion products to the safety equipment and

2. Determine the temperature response of the equipment.

Experimental results were compared with and supplemented by analytical calculations. Both form the basis of a procedure for evaluating equipment survivability and, where possible, recommending possible equipment improvement.

Initial efforts of the HBS program have been directed toward the consideration of equipment in ice condenser PWRs. Specific equipment selected for initial detailed consideration are cables, hydrogen igniters, pressure transmitters, and solenoid valves.

ACKNOWLEDGMENTS

The efforts of several individuals have gone into the Hydrogen Burn Survival program. The authors wish to acknowledge their contributions to this report. They are Lou Cropp, Beth Richard and John Aragon of Sandia Division 9445, Susan Dingman, Division 9441, and Steve Kempka and Art Ratzel of Division 1513.

1.0 INTRODUCTION

The hydrogen burn during the Three Mile Island accident[1] has raised a concern that a similar burn resulting from a similar accident in the future could lead to a breach of containment integrity. One method suggested to minimize the possibility of occurrence is the deliberate ignition of the hydrogen as it is released. In this way, hydrogen concentrations can be kept below levels which would otherwise threaten containment integrity. This mitigation scheme may, however, precipitate a series of hydrogen burns which might have deleterious effects on equipment inside containment. Of particular concern are any components necessary to establish and maintain a safe shutdown condition in the plant.

The purpose of the Hydrogen Burn Survival (HBS) program at Sandia National Laboratories (SNL) is twofold. First, the characteristics of the hydrogen burn environment will be determined. Second, an algorithm will be formulated which can be used to assess the survivability of safety-related equipment exposed to that environment.

2.0 PROGRAM METHODOLOGY

The HBS program at SNL involves parallel experimental and analytical efforts to characterize the hydrogen burn environment in containment. One series of hydrogen burn tests has been conducted in each of two Sandia combustion facilities, the Variable Geometry Experimental System (VGES) and the Fully Instrumented Test System (FITS). These tests, along with a second series planned for the FITS facility, will be used to establish test specifications for small-scale simulations and to help verify the analytical combustion models. These models will then be used to calculate heat flux profiles for full-scale containments. The heat flux profiles will serve as specifications for simulations of the containment environment. Simulations of both the test facilities' exposures and full-scale containment exposures will be conducted at Sandia's Radiant Heat Facility (RHF) and/or the Central Receiver Test Facility (CRTF), a solar test apparatus. All testing will include the exposure of instrumented calorimeters and actual reactor safety equipment. These tests and the verified computer models will yield full-scale component temperature responses. After exposure, component performance will also be verified to determine the degradation, if any, caused by exposure to the environment.

3.0 EXPERIMENTS TO DATE

The first set of experiments was conducted in the VGES facility. The vessel is shown schematically in Figure 3-1. This test series consisted of six burns at 10 and 15% (by volume) hydrogen. Further test descriptions are contained in Table 3-1.

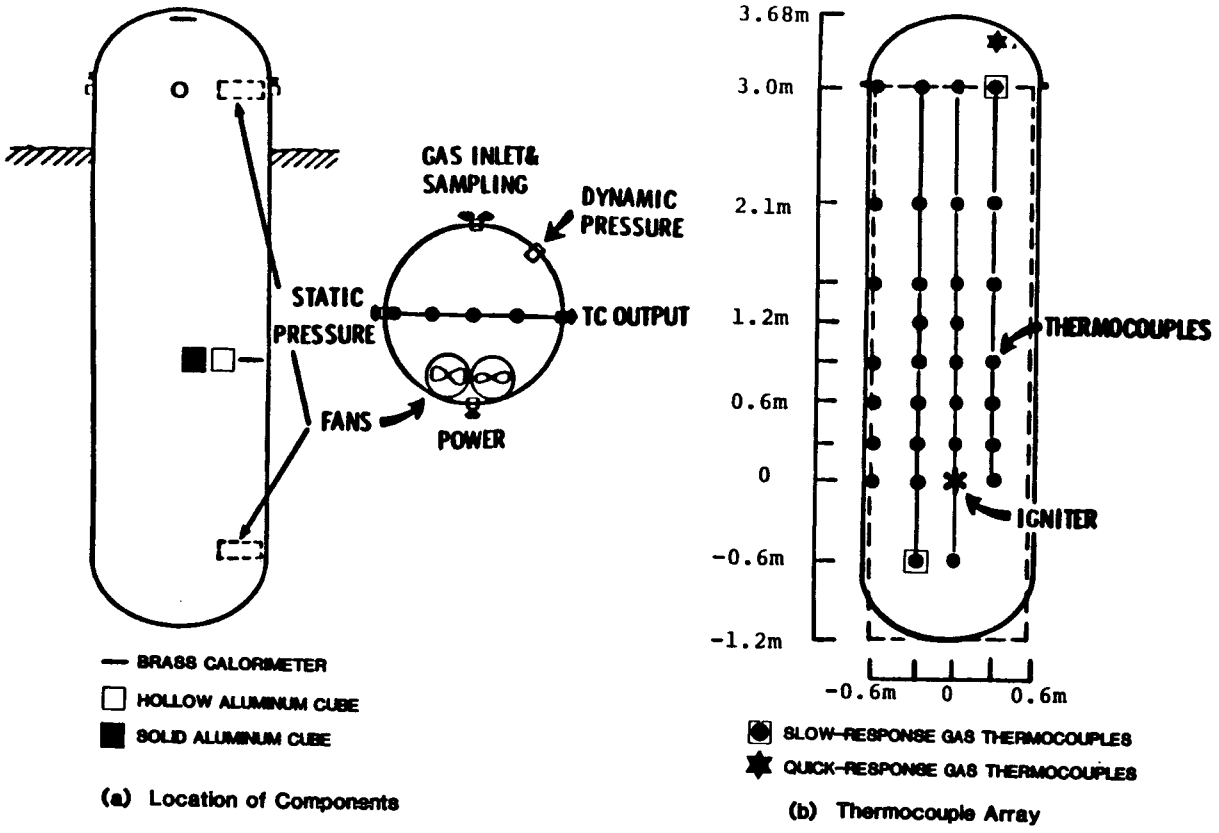


Figure 3-1 Variable Geometry Experimental System (VGES) [2]

Two of the burns also included a 10% (by volume) CO_2 content. The VGES facility cannot accommodate steam injection, therefore, CO_2 was used as a steam substitute. The tests were conducted using either spark or glow plug ignition and with mixing fans on or off.

The VGES tests were designed primarily as scoping experiments and included several calorimeters as surrogates for actual reactor components. A hollow aluminum cube represented equipment having low heat capacities. A solid aluminum cube represented components with larger heat capacities. Several thin plate brass calorimeters were also installed as very responsive, one-dimensional thermal absorbers. The aluminum cubes were black anodized and the brass plate calorimeters were spray coated with a high temperature black paint to maximize heat absorption. Results of the six VGES burns are included in Table 3-1. As might be expected, the presence of the CO_2 substantially lowers the gas temperature. Also, as the hydrogen concentration is increased, the gas temperature rises significantly. The effects of fan air circulation and ignition source were not discernable.

TABLE 3-1

TEST DESCRIPTIONS AND MAXIMUM CALORIMETER TEMPERATURES[2]

Test No.	B88	B89	B90	B91	B92	B93
% H_2	10	10	10	10	15	15
%CO_2	0	0	10	10	0	0
Mixing Fans	OFF	ON	OFF	ON	OFF	ON
Igniter	Spark	Spark	Glow Plug	Glow Plug	Glow Plug	Spark
MAXIMUM TEMPERATURES, ^oF						
Gas	1703.9	1704.6	1447.3	1474.7	2249.7	2198.6
Thin Plate	299.4	293.4	309.5	255.6	365.2	357.2
Hollow Cube	126.9	131.3	132.4	143.2	150.8	158.1
Solid Cube	95.9	89.6	87.4	103.4	******	91.4

The VGES test series indicated a need for improved instrumentation. The thermocouples in the vessel were intended for flame propagation studies in which flame speed was more important than the gas temperature. The thermocouples were constructed of heavy gauge material to survive a large number of burns and as such, had poor transient temperature response. The use of smaller, more responsive thermocouples is preferred when transient gas measurements are needed.

As we began to examine the VGES data and to compare it to calculations, we found that the measurement of heat flux would have been very helpful. Therefore, in subsequent tests some heat flux gauges of differing configurations are to be evaluated, including one of a new design specifically made to be responsive to the very rapid transients typical of hydrogen deflagrations. Once some confidence in the measurement techniques is established, the measured heat flux profiles will serve to corroborate calculations and to specify input conditions for radiant heat tests.

The VGES tests provided an understanding of heat transfer phenomena in combustion environments. These tests indicated modifications in procedures and instrumentation to obtain more meaningful data in the next test series conducted in the (FITS) facility.

The FITS facility, shown in Figure 3-2, offers several advantages over VGES. These include steam injection capability, better instrumentation and data acquisition, higher test repetition rate, vessel pre-heat capability, and generally better control over test parameters.

The first series of tests conducted in the FITS facility consisted of 29 burns with concentrations varying from 6 to 15% (by volume) hydrogen and 0 to 40% (by volume) steam, using spark or glow plug ignition and with or without mixing fans. Data from seven of the tests were determined to be invalid for various reasons. Also, one 8% H_2, 40% steam test failed to ignite.

Detailed evaluation of the data from the FITS tests is the subject of another report;[3] however, some general observations are stated here.

1. Operating the fans during 8 percent burns resulted in higher peak gas temperatures and pressures than with fans off. This phenomena was far less pronounced at higher hydrogen concentrations.

2. There is substantial variation in the calorimeter temperature response for burns with nominally the same initial conditions.

3. The temperature traces from burns at lower hydrogen concentrations are jagged or exhibit several peaks. This indicates irregular combustion, a condition which becomes more noticeable with increasing steam concentration.

Four types of cable and a solenoid valve were also included in the FITS tests. One of the cable samples, which was LOCA qualified, emerged from the exposure in very good condition; the other three, which were not qualified, had severely charred

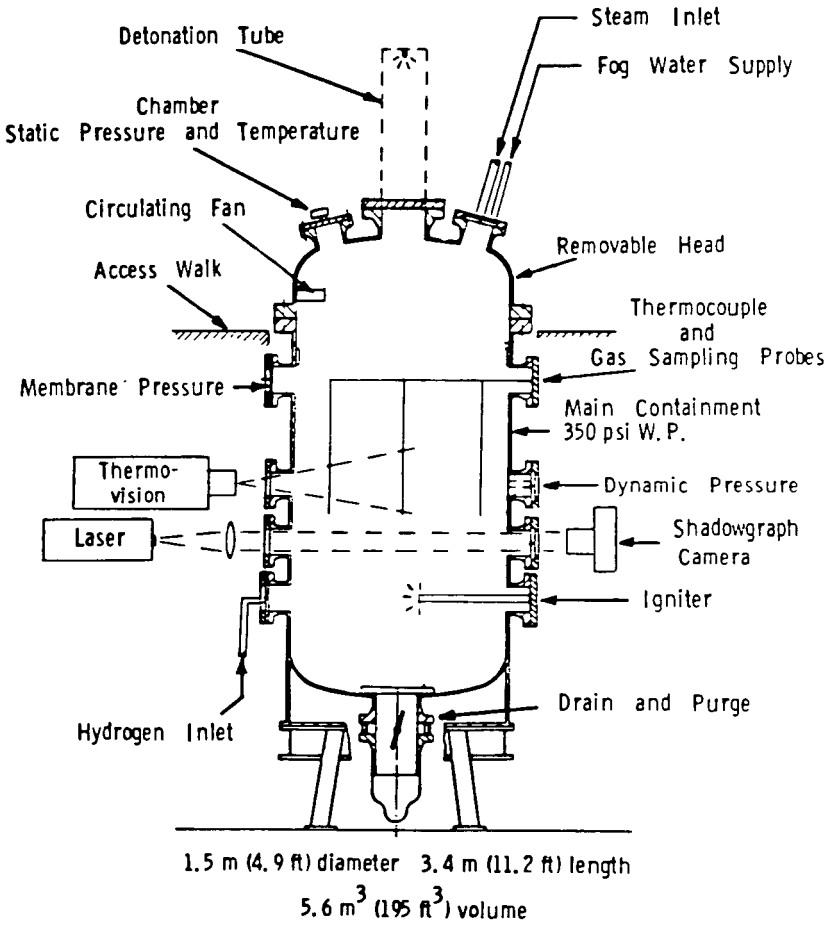


Figure 3-2 Fully Instrumented Test System (FITS) [2]

insulation. The solenoid valve operated well during and after the exposures. The plastic covered conduit used to supply power to the solenoid valve exhibited severe scorching in the area where it attached to the valve housing. However, the portion of conduit which was routed along an aluminum bracket remained unharmed. This, we suspect, was due to the thermal shielding provided by the bracket.

It should be noted that these exposures of actual hardware were not intended to be demonstrations of component responses to expected accident environment. First, the FITS facility is much smaller than containment volumes and presents a substantially milder threat from a contained hydrogen burn.[2] Second, since the test series would have had to be interrupted to remove the components, they were left inside the vessel for all the burns. Third, the sequence of burns separated by gas purging and refilling operations does not represent any identified accident scenario. Actual hardware was included to begin the development of instrumentation techniques and to provide some initial understanding of hardware responses to the environment.

As results from other experiments such as the FLAME facility at Sandia and the Electric Power Research Institute (EPRI) tests at the Nevada Test Site (NTS) become available, they will be included in the HBS effort.

4.0 ANALYTICAL RESULTS

Initial analyses were performed using CORASPN,[4] a code developed at Sandia, which predicts post-deflagration thermal responses in a containment vessel. The code assumes that at any time the temperature is uniform throughout the gas volume. Heat transfer among the walls, components, and gas is by radiation and convection and is taken as uniform over each surface area. CORASPN also accounts for condensation on the vessel walls and components.

As a check on the model, CORASPN results were compared with the outputs of two thermocouples from a 15% hydrogen burn in the VGES test series. Figure 4-1 shows this comparison. The gas temperature profiles calculated by CORASPN show good agreement with the measured data after about ten seconds, but there is s discrepancy earlier. The starting point for the CORASPN calculation was the adiabatic isochoric temperature immediately following the deflagration which is beyond the scale of the figure. The measured temperature profiles indicate a lag associated with thermocouple response.

The CORASPN code was also used to predict the gas temperature profile in the upper compartment of an ice condenser PWR containment without sprays following a postulated 10% hydrogen burn.

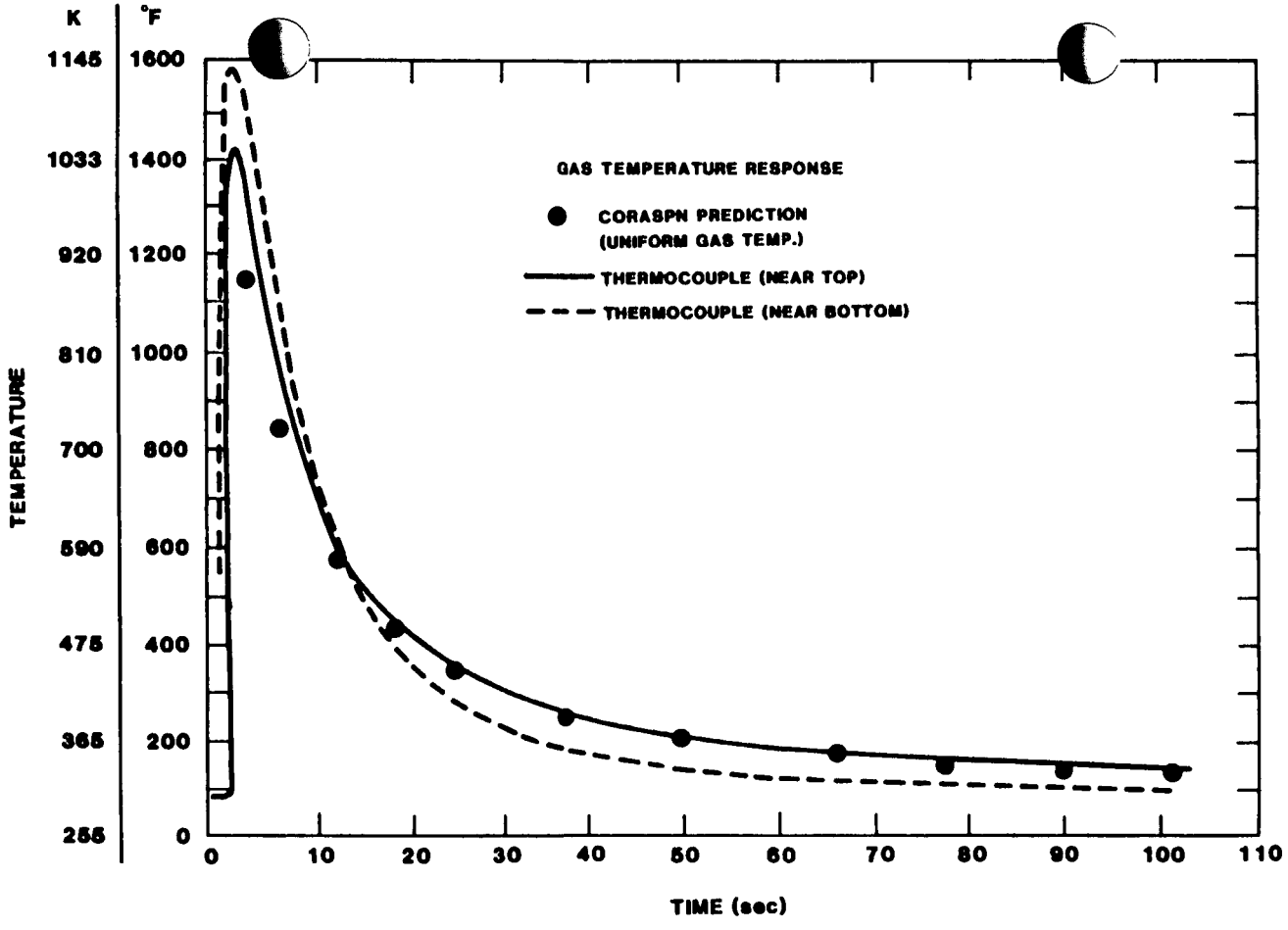


Figure 4-1. Gas Temperature Response Resulting From a 15% Hydrogen Burn in VGES - Predicted vs. Thermocouple Measurements. [2]

Figure 4-2 compares the results of this calculation with the temperature profile from a 15% hydrogen burn in the VGES test series. The cool-down period for the containment volume is larger by orders of magnitude than for the small VGES tank. This indicates that a component in a large containment volume would be exposed to high gas temperatures for a much longer period of time than in a small test volume.

Using heat fluxes calculated by CORASPN, the thermal respo[illegible] of the two cubic aluminum calorimeters used in the VGES tests were calculated for the ice condenser PWR containment using the CINDA-3G[5] code. The environment considered was that of the so-called "S_2D" LOCA with an inoperative spray system. The S_2D accident is a small break LOCA (approximately 2 inches in diameter) with a nonfunctioning emergency core cooling system (ECCS).

Two bounding cases are given here. The lower bound is that of the component with the highest heat capacity in the lowest temperature environment (corresponding to the lower compartment); the upper bound is a low heat capacity component exposed to the more severe thermal environment of an upper compartment burn. The containment spray systems are assumed to be inoperative in both cases. These bounding results are given in Figure 4-3. The solid cube reached a peak temperature of 437 K (211°F) in the lower compartment and the hollow cube in the upper compartment reached 722 K (840°F). This indicates that a component inside such a containment could experience a wide range of temperatures depending on its location and thermal mass. Had an operative spray system been included in the analysis, the upper compartment temperatures would have been significantly lower.

Two new codes with more desirable characteristics are nearing operational status. HECTR[4] and HECTR-ES are second generations of the CORASPN code. The parent code is purely a post combustion code which treats the containment as a single compartment. HECTR models the combustion process and is multi-compartmental. It can also consider multiple burns and the flow dynamics between compartments. HECTR-ES is a parallel improvement on CORASPN. While retaining the single compartment nature of the parent code, it incorporates a multiple burn capability and a one-dimensional flame propagation model which allows a more realistic consideration of heat transfer during the time of the burn. T[illegible] two new codes will eventually be merged into one for use in future HBS analyses. Figure 4-4 gives a HECTR-ES calculation for representative thick and thin wall components exposed to a multiple burn in the upper compartment of an ice condenser containment. The assumptions for the calculation were that the convective velocity was .3 m/sec, there was hydrogen input but no combustion gas removal, and that the containment sprays were inoperative. The combustion region was treated as a single compartment and the rate of hydrogen release into the compartment

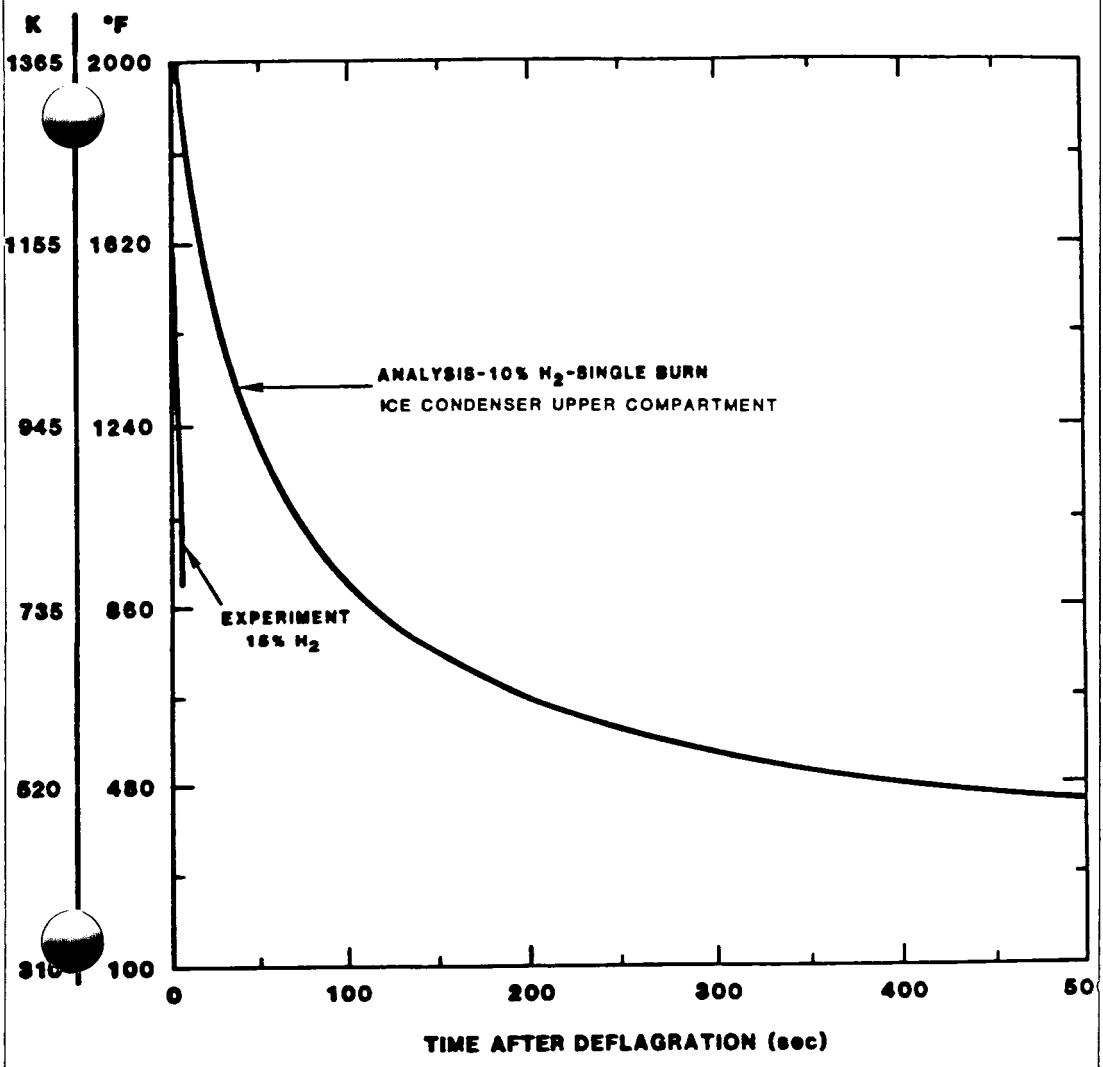


Figure 4-2 Comparison of Temperature Profiles Obtained From VGES Experiments and Ice Condenser Containment Upper Compartment Analysis [2].

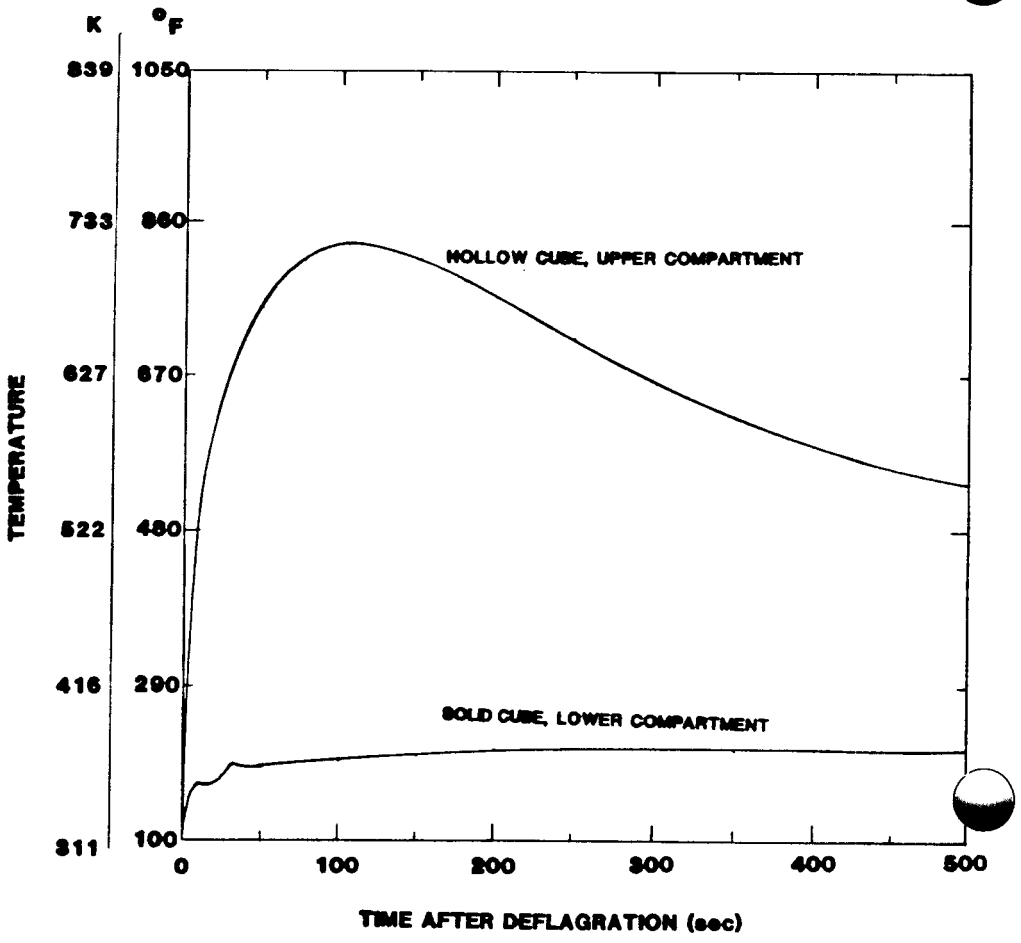


Figure 4-3 Predicted Hypothetical Component Profiles Resulting From a 10% Hydrogen Burn in an Ice Condenser Containment [2]

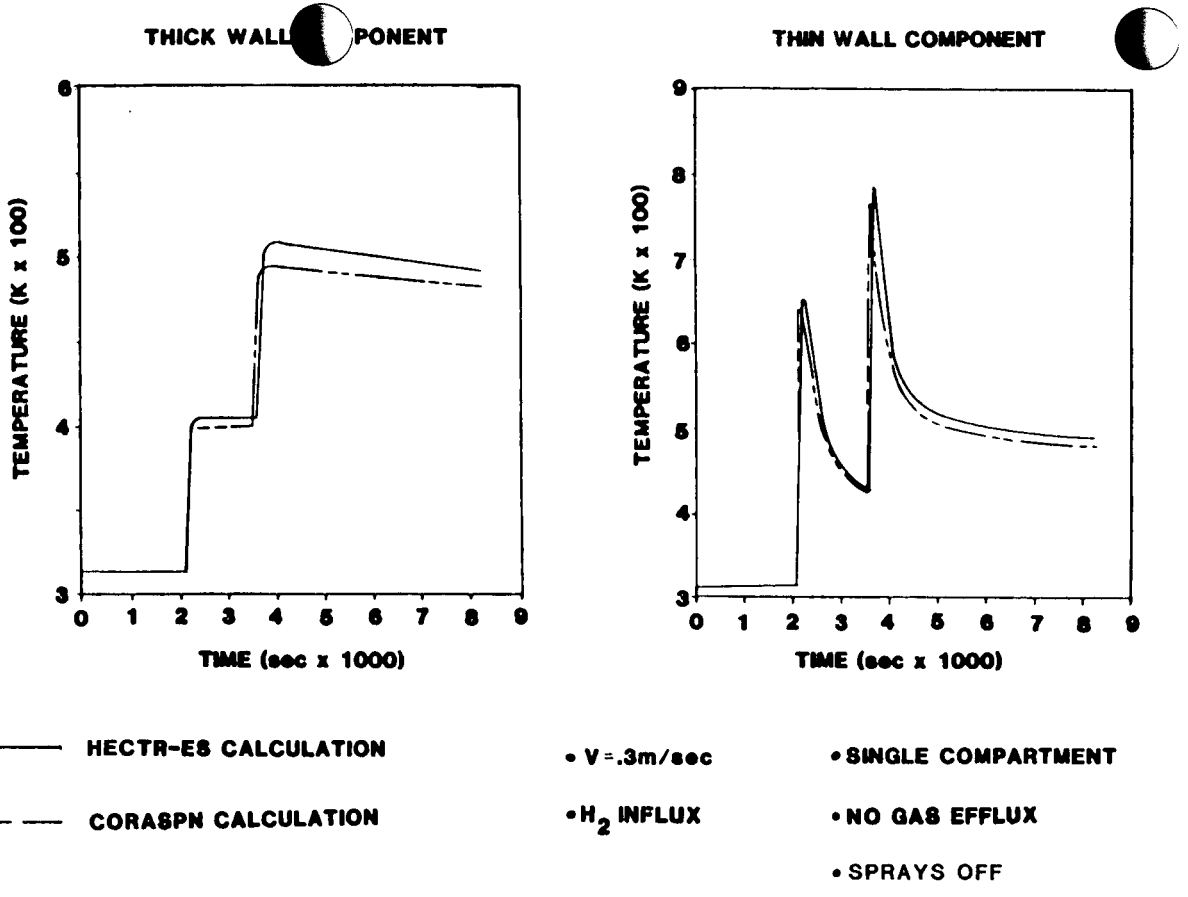


Figure 4-4 Representative Component Responses to Multiple 10% Hydrogen Burns in the Upper Compartment of an Ice Condenser PWR Resulting from an S_2D Accident [6].

was taken from a MARCH[7] calculation. The analysis indicates a higher temperature on the first burn than that predicted by the single burn CORASPN analysis. Even more significant is the elevated temperature produced by the second burn. This effect is due to the short cooling period between burns.

5.0 CONCLUSIONS TO DATE

Although the hydrogen burn environment is not yet completely defined, several conclusions can be drawn from the experiments and analyses conducted to date.

Comparison of the VGES test data and the ice condenser PWR burn given in Figure 4-2 indicates that gas temperatures in full-size containments remain elevated for much longer periods of time than do similar burns in smaller vessels. Differences in component thermal responses to the two environments will, no doubt, be commensurate with differences in the gas temperature profiles.

The CORASPN analysis indicates that, depending on the location in containment, thermal mass, and accident conditions, components may reach temperatures in excess of LOCA qualification guidelines. It must be pointed out that in these analyses the components were taken to be totally exposed to the environment. No consideration was given to the thermal protection provided by structures attached to or near the components. Cable exposed in the FITS tests and equipment removed from the TMI-2 containment have shown that the effects of such protection can be significant.

The use of an improved code, HECTR-ES, indicates that temperature responses are higher than previously predicted by CORASPN and that multiple burns cause a "ratcheting" effect in component temperature due to the small cool-down time between successive burns.

6.0 PLANNED ACTIVITIES

The major component of the hydrogen burn process which poses a threat to equipment survivability is thermal radiation from high temperature water vapor. It is this radiative environment which must be simulated to determine full-scale temperature responses.

Several series of tests are planned at Sandia's Radiant Heat Facility (RHF) and/or the Central Receiver Test Facility (CRTF) to accomplish this objective.

The first test series will duplicate the environment of several of the VGES tests. The heat flux profile corresponding to the temperature profile of one of the VGES flat plate calorimeters will be calculated using the analytical model. The temperature profile will then be duplicated and the heat flux measured. The measured and calculated fluxes will then be compared, verifying the model or suggesting changes.

In the second series of radiant simulation tests, a calorimeter from the FITS tests will be exposed to flux profiles duplicating those measured in FITS. If similar input flux profiles produce similar output temperature profiles, then the solar spectrum, which is employed by the CRTF, will have been confirmed as valid for use in simulating the radiation and convection heat input from the hot gas cloud produced by hydrogen combustion. Since no hydrogen test facilities the size of actual containment buildings exist, full-scale test simulations must be based on analytically determined heat flux inputs.

The final series of tests will expose actual safety-related components to heat flux profiles determined by the combustion models HECTR and HECTR-ES. The profiles will be those for hydrogen combustion in full-scale containments. These tests are expected to confirm component temperature responses predicted by the analytical models.

REFERENCES

1. Alvares, N., Bearson, D., and Eidem, G., Investigation of Hydrogen Burn Damage in the Three Mile Island Unit 2 Reactor Building, GEND-INF-023, Vol. 1, U.S. Department of Energy, June 1982.

2. McCulloch, W. H. et al., Hydrogen Burn Survival: Preliminary Thermal Model and Test Results, NUREG/CR-2730, SAND82-1150, Sandia National Laboratories, July 1982.

3. Richards, E. H., et al., Report on the results of the first test series of FITS tests at Sandia National Laboratories, in preparation.

4. Berman, M., Light Water Safety Research Program Semiannual Report, April-September 1981, NUREG/CR-2481, SNAD82-0006, R3.

5. TN-AP-67-287, Chrysler Improved Numerical Differencing Analyzer (CINDA) for Third Generation Computers, October 1967.

6. Letter: McCulloch (SNLA) to Larkins (NRC/RES) and Parczewski (NRC/NRR), 7-16-82, Subject: Monthly Status Report for June 1982, HBS.

7. Wooten, R. O., Avci, H. J., MARCH (Meltdown Accident Response Characteristics) Code Description and Users Manual, NUREG/CR-1711 (BMI-2064), October 1980.

SESSION VIII

EQUIPMENT SURVIVABILITY

HYDROGEN BURN SURVIVAL EXPERIMENTS:

FITS Series One

Elizabeth H. Richards
William H. McCulloch
John J. Aragon
David T. Furgal (Editor)
Sandia National Laboratories
Albuquerque, NM 87185
operated by
Sandia Corporation
for the
U. S. Department of Energy

Hydrogen Burn Survival Experiments

1.0 INTRODUCTION

A concern evolving from the accident at Three Mile Island is that considerably more hydrogen can be produced in a nuclear reactor accident than had been previously thought. To prevent a severe hydrogen-oxygen reaction from threatening containment integrity, several methods of hydrogen control have been suggested. One such method calls for the intentional ignition of hydrogen before dangerously high concentrations accumulate. The pressures resulting from these low concentration hydrogen burns do not threaten the containment building integrity; however, the survivability of safety-related equipment exposed to the hydrogen burning hydrogen environment is uncertain.

The primary goal of the Hydrogen Burn Survival (HBS) Program at Sandia National Laboratories, Albuquerque, NM, (SNLA) is to develop a method for the NRC to use to analytically evaluate the survivability of safety-related equipment during a hydrogen burn. This method will be developed by establishing calculational models of both the hydrogen burn environment and of component responses to the environment. To demonstrate their credibility, these analytical models must be verified experimentally.

Several series of experiments have been or will be conducted as part of the HBS program. These include medium-scale hydrogen deflagration tests in pressure vessels and hydrogen burn simulation tests at the Sandia Central Receiver Test Facility (CRTF). Program plans also include participation in the larger-scale hydrogen burn experiments conducted by the Electric Power Research Institute (EPRI) at the Nevada Test Site (NTS). Described herein is the first of two series of medium-scale (5.6-m^3) hydrogen burn tests at the SNLA Fully Instrumented Test Site (FITS) facility. This test series is referred to as FITS Series 1.

The purpose of FITS Series 1 is twofold. First, the hydrogen burn environment had to be characterized so that the environment could be simulated in further tests at the CRTF. Second, the tests provide medium-scale verification of the computational models being developed as part of the analytical portion of the HBS program. FITS Series 1 tests treated single burns only; multiple burn phenomenology will be examined in later tests.

This report documents the HBS instrumentation and procedures (test plan) for the FITS Series 1 tests and presents some limited observations. The observations in this report are based on preliminary data. We plan to supplement this information with

additional gas temperature and pressure information from the FITS facility instrumentation. An extensive presentation of FITS Series 1 test results and data analysis will be given in a future report.

2.0 TEST DESCRIPTION

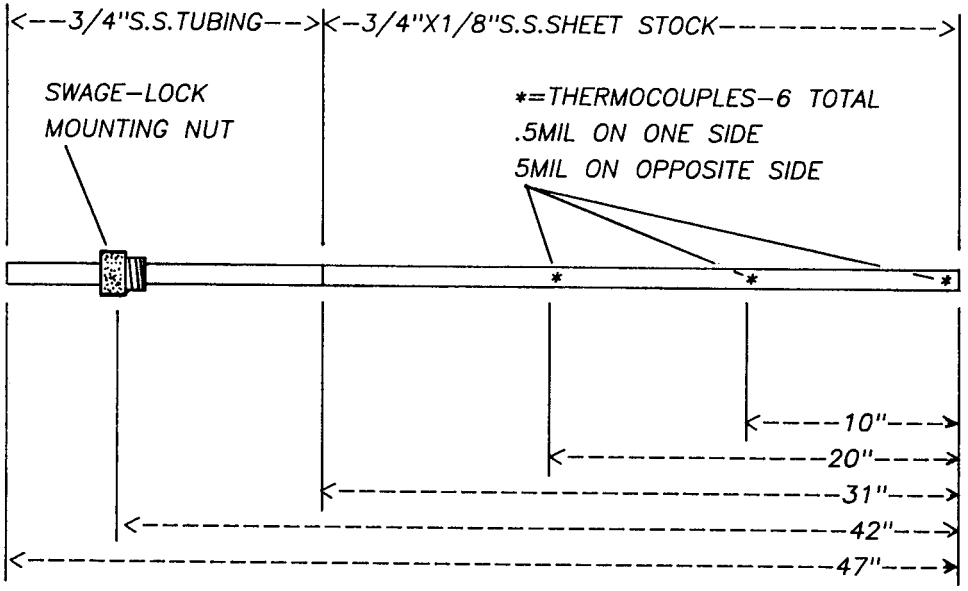
2.1 Facility

Tests were performed at the FITS facility under the direction of Susan Roller and Steve Falacy of SNLA Division 2513 with assistance from Pete Prassinos of SNLA Division 9441. The test vessel is a 5.64-m^3, above ground, steel tank. The exterior of the tank is insulated with two inches of fiberglass insulation. The tank has 25 flanged ports which can be used to accommodate instrumentation or as viewing aperatures. The FITS tank contains an array of 32 12-mil thermocouples to detect flame fronts, two faster response 0.5-mil thermocouples to measure gas temperatures, and 5 pressure transducers. A gas sampling system is set up to determine the gas composition before and after a burn. A closed-circuit television camera provides for visual observation of the burns and for monitoring the occurrence of condensation on the glass port.

2.2 HBS Instrumentation

In addition to the existing FITS facility instrumentation, HBS tests required the addition of 32 data acquisition channels. These provided for two thermocouple probes, each containing 6 spatially arranged thermocouples for gas temperature measurements; 12 calorimeter temperature measurements; and 3 heat flux measurement inputs. The remaining channels were instrumented to measure the temperature responses of a solenoid valve and two mixing fans inside the tank.

Thermocouple Probes - Two thermocouple probes were designed to measure gas temperature at six locations within the FITS tank. Utilizing the flanged ports, one probe was mounted so that it was 1 m (3 ft) from the top of the tank; the second probe was mounted 3 m (10 ft) below the top of the tank. As shown in Figure 1, each probe had three pairs of Type K thermocouples affixed to it. The thermocouples were bent so that the junctions extended into the gas and were not in contact with or shielded by the probe. Each thermocouple pair consisted of a 5-mil beaded thermocouple and a 0.5-mil butt bonded foil thermocouple. This combination was chosen so that we could compare the responses and survivability of the two types. Because of the fast temperature transients which occur, it is desirable to use very small (fast response) thermocouples to measure these gas temperature transients. On the other hand, thermocouples that are too small burn up after just one or two tests. An important feature of the probes is that they are easily replaced through the instrumentation ports without necessitating removal of the tank top.



THERMOCOUPLE PROBE

FIGURE 1

Calorimeters - Two types of calorimeters were used in the tests. Flat plate calorimeters were designed to make their heat transfer characteristics as basic as possible so that post-test analysis could be simplified. Second, three-dimensional calorimeters were constructed to be more representative of real components.

The main component of the flat plate calorimeters is a 0.05-cm (20-mil) thick 15.25-cm (6-in) square brass plate. The front surface is coated with a highly absorptive high temperature flat black paint (Nextel^{TM}: $\alpha = 0.99$). The back surface of the calorimeter was insulated and sealed. Two of these calorimeters were mounted on the inside wall of the tank, one 1.5 m (4 ft) from the top and the other 2.3 m (7.5 ft) from the top, with the back insulated surface facing the wall.

Three intrinsic thermocouples were mounted on the back side of each brass plate, one in the center and the other two 1.9 cm (3/4 in) horizontally off-center. At the outset we had planned to mount a thermocouple on the front side of the flat plate calorimeters, but heat transfer calculations performed by Ben Blackwell of SNLA Division 7537 showed that there would be insignificant temperature differences between the front and back sides. Because of low temperature phase changes inherent in brass, we attempted to use copper plates instead of brass to simplify heat transfer calculations. However, we were unsuccessful at welding thermocouples to the copper plates even when the copper was nickel plated. Therefore, the use of copper plates was abandoned.

Two three dimensional calorimeters were constructed. They were 10.2-cm (4-in) black-anodized aluminum cubes. One of the cubes was hollow, constructed from 0.32-cm (1/8-in) thick aluminum sheet stock. It was used to simulate components that have a low mass and therefore low heat capacity. The other cube was solid, simulating massive components with high heat capacities.

Each cube was instrumented with three thermocouples. Foil thermocouples were bonded to the inside of the hollow cube at two locations and at one location on the outside of the hollow cube. The solid cube was instrumented with beaded thermocouples. They were put into 0.32-cm (1/8-in) holes which were in the same locations as the thermocouples in the hollow cube. The cubes were mounted about 2 m (6.6 ft) from the top of the tank and 0.6 m (2.0 ft) from the wall.

Heat Flux Gages - Previous HBS tests and analyses indicated that the measurement of transient heat fluxes would be valuable for validating analytical models and for specifying input data for the radiant heat simulation tests planned at the CRTF. To begin development of a reliable heat flux measurement technique, some candidate heat flux gages were utilized in FITS Series 1. One of the gages tested was designed to measure only radiative heat flow

(Thermogage Model 8000-12C). To minimize convective and conductive heat transfer from the gas, the gage had an ellipsoidal cavity in front of the sensor and required a continuous air purge to keep the cavity surface clean and dry. The second and third gages were Gardon[1] type circular foil heat flux gages.[2] They had slightly different configurations and calibrations, but both measured net absorbed heat flux.

The first two gages were mounted on a bracket near the tank wall 1 m (3 ft) from the top and were accessible only by removing the top of the tank. The third gage was inserted through an instrumentation port about 2 m (6.6 ft) from the top. The gages all faced across the tank.

Solenoid Valve - To observe the behavior of a "real" component and to gain some experience in instrumenting such components, we mounted a Class 1E qualified solenoid valve about 1 m (3 ft) below the top of the tank. The operation of the valve was checked before and after the test series. The AC current in the coil of the valve was monitored between burns. We mounted a thermocouple inside the valve's electrical enclosure and monitored that temperature during the burns.

Additional Instrumentation - For additional information we bonded two thermocouples to each of the two mixing fans inside the tank to monitor for temperatures during the burns. We also placed several cable specimens, both qualified and unqualified, in the tank along with two types of terminal blocks. The cable samples were included for visual inspection purposes only; mechanical (i.e., tensile) or electrical tests were not performed on the samples.

3.0 TEST PLAN AND PROCEDURES

The documentation describing the operating procedure for the FITS facility is maintained by SNLA Division 2513 and will not be described here. However, the test plan and procedures pertaining to the HBS program tests will be discussed.

3.1 Test Plan

The HBS test plan called for a series of burns to be performed according to the matrix shown in Table 1. This matrix was designed to provide information concerning the effects of varying hydrogen and steam concentrations on the burn environment, the repeatability of the burns, and the effects of turbulence (fans on) during a burn, as well as the component responses to the specific hydrogen burns.

TABLE 1

HBS PROGRAM

FITS SERIES 1

%HYDROGEN	6	7	8	9	10	11	12	15
0% STEAM	YYYX	X	X	YXX	X	X	X	
20% STEAM	X		YXFF		YXF		X	X
40% STEAM	X		XXI		YX		X	

X=VALID TESTS
Y=INVALID TESTS (DUE TO DATA AQUISITION SYSTEM ERRORS)
I=INERTED TESTS
F=TESTS WITH FANS ON

3.2 Procedures

To conserve instrumentation the less severe burns (low hydrogen, high steam concentrations) were executed first followed by the more severe burns (high hydrogen, low steam concentrations). After some of the low concentration burns were completed, we removed the top of the tank and inspected all the test components. The thermocouple probes and cable samples were replaced with new ones. However, due to the inconvenience of removing the tank top we did not do this again for the remainder of the tests. Since the thermocouple probes could be replaced without removing the top, they were replaced at various intervals to assure confidence in the data obtained.

The three flux gages tested presented some problems. The ellipsoidal cavity flux gage was shorted out by water early in the test series. It was replaced by the two circular foil heat flux gages. Readings from these circular foil gages were occasionally interrupted. This, we suspect, was probably the result of electrical shorts caused by condensation. When the circular foil gages once again became operational (presumably after drying out), they appeared to be operating properly.

3.3 Data Acquisition

The data acquisition system at the FITS facility has the capacity for storing about 2000 data points per channel. Sampling 20 times per second, about 90 seconds of data was recorded for each burn. Data sampling was initiated by the increase in pressure associated with a burn. Sufficient time elapsed between tests to output hard copy of some, but often not all, of the data so that it could be scanned for indications of system malfunctions. When malfunctions were found, corrective measures were taken before proceeding with the test sequence.

All of the raw test data from this test series was recorded on floppy discs. To facilitate analysis, the data was transferred to storage files in a SNLA VAX computer system.

4.0 OBSERVATIONS

Although the test information is still in very rough form, several general observations can be made from the analysis of t preliminary data plots:

4.1 Hydrogen Combustion Phenomena

For burns having hydrogen-air mixtures of 8% hydrogen, the tests with turbulence (fans on) produced higher peak gas temperatures and pressures than without. This phenomenon was substantially less pronounced in burns having 10% hydrogen concentration.

There appears to be considerable variation in gas temperatures for burns with nominally the same initial conditions.

The temperature traces for burns with lower hydrogen concentrations (i.e., 6%) are jagged or have several peaks, indicating erratic combustion. This is especially noticeable given higher steam concentrations.

4.2 Gas Temperature Measurements

Time response and survival comparisons were made between the 5-mil and 0.5-mil thermocouples. The data did not clearly indicate that the smaller thermocouples responded more rapidly as had been expected. We believe this is because the 0.5-mil thermocouples were not designed to measure gas temperatures. They were made of foil and were mounted on phenolic. The 5-mil thermocouples were beaded and did not require phenolic. Apparently, the phenolic on the 0.5-mil thermocouples burns off in some cases, but not in others, yielding varying response times. Also, some thermocouples (both 5-mil and 0.5-mil) responded very slowly, indicating that they were too close to the probe (i.e., measuring the probe temperature instead of the gas). Both types of thermocouples survived the test quite well. Only a few 0.5-mil thermocouples failed at the highest H_2 concentration burns.

4.3 Calorimeters

The Nextel™ coating on the flat plate calorimeters did not survive the test series very well. There was some blistering and surface peeling. This, we believe, is as likely to be from the wet environment in the tank as from the high temperatures encountered, and will be addressed in our analyses. No degradation was noted when the calorimeters were checked after the first five burns.

4.4 Flux Gages

Occasionally the circular foil heat flux gages would give no output during a burn. Before performing most of the burns, we verified that the tank walls were heated above 100°C. There appears to be a correlation between the occurrence of this anomaly and the initial wall temperature of the tank. It is possible that water on the gages prevents them from operating properly. Until this anomaly is resolved, the flux measurements from the gages will be viewed with caution.

5.0 FUTURE PLANS

Data from the heat flux gages and thermocouples are stored in the form of input voltages on Sandia's VAX computer system. Once the data is converted to temperatures and heat fluxes, it will be in a form that can be easily manipulated for making comparisons

and trend analysis. We will then look more closely at the effects of hydrogen and steam concentrations on the temperatures and pressures, compare the effects of turbulence during tests, and determine test repeatability. We will study the temperature response of the flat plate calorimeters, calculating the heat fluxes seen by them, and compare those heat fluxes to the heat flux gage measurements and to the calculations based on combustion analyses.

Information from these FITS Series 1 tests will be used to help plan the second series of tests at the FITS facility and the simulation tests at the CRTF. Joe Shepherd of SNLA Division 2513 has developed some new heat flux gages specifically for measuring the transient and peak heat fluxes associated with hydrogen burns; they will provide much needed information concerning convection and radiation during hydrogen burns. Tests using CO_2 instead of steam are also planned. The use of smaller beaded thermocouples (2-mil) is planned for the gas probes to improve gas temperature measurements.

6.0 SUMMARY

The first series of HBS experiments has been completed at the FITS facility. The tests were designed to answer questions about the burn environment and component responses to that environment. Gas temperatures were monitored at various locations within the FITS tank. Once all the data is reduced, heat fluxes will be derived from the flat plate calorimeter responses, and representative component responses from the temperature measurements on the cube calorimeters will be determined. The information gained from FITS Series 1 tests will be used to plan a second series of tests at FITS, to develop a series of hydrogen burn simulation tests at the CRTF, and to provide medium-scale verification of analytical models used for predicting component temperature responses.

SURVIVABILITY OF ESSENTIAL EQUIPMENT AT THE SEQUOYAH NUCLEAR PLANT FOR HYDROGEN BURN TEMPERATURES

Robert H. Bryan, Jr.,
Tennessee Valley Authority

This is a Government publication and not subject to copyright.

Introduction

The ability of equipment to survive hydrogen burns was a principal issue that resulted from TVA's decision to use an igniter system for hydrogen control during degraded core events. To address the issue of equipment survivability at the Sequoyah Nuclear Plant, an evaluation program composed of four main elements was formulated. These elements were:

I. The identification of essential equipment inside the primary containment and its location;

II. The development of anticipated containment environmental profiles;

III. The development and use of analytical models of essential equipment to determine thermal response to the containment profiles; and

IV. The establishment of a test program for proof testing and support of the analyses.

The program was amended during its course to incorporate technical improvements in analytic techniques, test data, and specific NRC concerns. TVA's analysis and testing clearly showed that for lean-limit hydrogen combustion in an ice condenser, plant, survivability of the equipment was assured.

Equipment Selection

A list of equipment essential for safe shutdown of the plant after an accident was developed based on emergency operating instructions and system descriptions. The systems were chosen to assure short and long-term core coolability and the structural and leaktight integrity of the containment (See Table 1).

Establishment of the list preceded a review to determine the location of each component and its physical characteristics. Location was important as the number and magnitude of hydrogen burns varies in different containment compartments. Physical characteristics such as small size, use of heat sensitive components, or low heat capacity were considered in determining components that would be most sensitive to the thermal effects of hydrogen burns. The combination of location and physical characteristics provided a basis to choose a subset of all components from the essential equipment list for detailed analysis and testing. A transmitter, igniter box, exposed (not in conduit) thermocouple and RTD cable, and the igniter system power cable in conduit were the pieces of equipment chosen for the detailed study.

The exposed RTD and thermocouple cable associated with the hot and cold leg temperature monitors and the core exit thermocouples were chosen for detailed evaluation due to their small size and therefore low heat capacity. The igniter power cable in conduit was also chosen due to its small size and location in the upper plenum of the ice condenser where a large number of burns were predicted to occur. The igniter assembly, due to its location in the upper plenum, was also chosen for detailed evaluation. A transmitter was the last item picked for the detailed evaluations. It is relatively small, and heat

sensitive solid-state components were used in its construction. All transmitters located inside containment are in the lower or dead ended compartments.

If this equipment, believed to be the most sensitive to high temperatures, was shown to be able to survive the hydrogen burns associated with a degraded core event, then all the equipment on the essential equipment list would be bounded by these evaluations.

Analysis

Analyses were performed to determine the containment response to hydrogen burns that result from a degraded core event and the thermal response of selected equipment to the containment profile. Hydrogen releases to the containment were assumed to result from a small break LOCA with concurrent failure of the safety injection systems. This event represented the base case for the Sequoyah ignition system.

Analyses were performed using the CLASIX computer code developed by Offshore Power Systems (reference 1) to generate containment atmospheric temperature profiles. Physical features such as the spray system, ice bed, air return fans, and the compartmentalized design of the ice condenser containment were included in the CLASIX model (Figure 1). Burns were allowed to occur in any compartment in which the hydrogen concentration reached a preset value of 8 v/o. Flame speeds of one and six ft/sec were used to evaluate equipment. The results discussed herein were based on the one ft/sec analyses.

Multiple burns were predicted to occur in the ice condenser upper plenum and in the lower compartment with peak atmospheric temperatures of 1114 and 884°F, respectively (Figures 2 and 3). No burns were predicted to occur in other compartments. The temperature peaks in the upper plenum were very brief due to the small quantity of hydrogen consumed in each burn (15-20 pounds), the large vent area available out of the upper plenum, and the relatively cold air (less than 100°F) exiting the ice bed. The equipment analyses were performed using the HEATING5 computer code (reference 2). The CLASIX atmospheric temperature profiles were used as the temperature forcing function input into the HEATING5 models and a separate heat flux was included to model radiation from the flame front at the adiabatic flame temperature for each period of time that a burn was occurring. The transmitter was analyzed using the lower compartment temperature profile. The igniter box was analyzed using the upper plenum temperature profile. The cable in conduit was analyzed using both profiles.

Boundary conditions used in the HEATING5 models were either convection or a combination of radiative and convective heat transfer modes. Radiative heat transfer from the flame to exposed surfaces of the selected equipment was assumed to occur during each burn period. Turbulent free convection heat transfer from the surrounding atmosphere to the equipment's surface was assumed to occur throughout the transient.

The radiative view factor was dependent upon the geometry of the equipment and its location in relation to the propagating flame front. For the purposes of determining the radiative view factor, the

flame front, and the equipment were assumed to be parallel concentric disks of unequal radii. The small disk area was assumed equal to the total exposed surface area of the equipment. The large disc area was determined as a disk whose radius was determined by the flame speed multiplied by the duration of the burn. The flux term was applied to all exposed surfaces.

Two dimensional representations were used to geometrically model the transmitter and igniter box for use in the thermal analyses. The cable in conduit was modeled using a one dimensional representation. Figure 4 shows the igniter assembly and the associated HEATING5 model.

To summarize the results of the HEATING5 analyses, the cable in conduit experienced the highest temperature at 332°F of any of the equipment. This maximum internal temperature calculated for the Barton transmitter was 231°F, and the peak internal temperature for the igniter box was 227°F. Figures 5, 6, 7, and 8 provide the transient results for each piece of equipment. The maximum temperatures predicted to be experienced by the equipment were substantially below manufacturer's maximum operating ranges, confirmatory test data, or NUREG 0588 environmental qualification limits. It was therefore concluded that the equipment would survive repeated hydrogen burns.

Model Verification

Two methods of model verification were used to provide: (1) a comparison of calculated results with the calculated results of other accepted computer programs, and (2) a comparison of calculated results with test-measured results.

The validity of the transmitter model was determined by comparison with the temperature transient analysis performed for the equipment qualification of the transmitter by Westinghouse using the COCO computer program and qualification testing. The Westinghouse results were summarized in topical report WCAP 8936 (reference 3).

The TVA HEATING5 transmitter model was the same one used to predict the transmitter response to the hydrogen burns. The boundary condition used for verification was the instantaneous heat flux from the Westinghouse topical report. Since this heat flux represented the sum of all heat transfer mechanisms at the boundary, no other boundary conditions were assumed.

The graphical comparison of WCAP 8936 and HEATING5 analyses of the initial transient for the internal and external case temperatures are shown in Figures 9 and 10. The curves for both internal and external case temperature show very good agreement. Additionally, both models predict approximately the same long-term maximum temperature. Comparisons of the Westinghouse analysis with the qualification tests were provided in the topical report.

The conservatism of the CLASIX-HEATING5 radiation heat flux modeling technique in predicting thermal responses to hydrogen burns was also verified by modeling a Fenwal test (reference 4). The Fenwal tests showed some teflon insulation surrounding an iron-constantan

thermocouple melted. The verification consisted of modeling the Fenwal thermocouple wire thermal response to a 12-percent volume fraction hydrogen burn. The temperature profiles for the Fenwal test sphere were obtained from CLASIX and were incorporated into the boundary conditions of a one-dimensional HEATING5 model. Radiative, as well as convective, heat transfer was considered in the boundary conditions in exactly the same way as used in the analysis of equipment inside the containment. Computer model results predicted the entire teflon insulation to melt in 1.4 seconds as a result of the single burn in the test.

Confirmatory Equipment Testing

To address concerns raised about the survivability of the exposed incore thermocouple cables and the hot and cold leg RTD cables located in the lower compartment, tests were performed on these cables at TVA's Singleton Laboratory. These tests were designed to confirm that the cables could survive the temperatures to which they would be subjected during a hydrogen burn. Additional testing on the igniter power cables was performed to determine temperature limitations for the Sequoyah Ignition System.

The thermocouple and RTD cables were repeatedly exposed to a high temperature (approximately 1400°F) environment intended to represent the adiabatic flame temperature associated with hydrogen burns in the lower compartment. Constant temperature tests of the igniter power cable were performed for a range of temperatures up to 700°F for 45 minutes which conservatively bounded the integrated heat flux that would result during an actual in plant transient.

Before and after the temperature tests, the cables were each tested to establish the integrity of the cable insulation. These tests consisted of applying 1500V dc for one minute from conductor to conductor and from conductor to shield, and measuring the voltage leakage before and after the cables were subjected to the temperature profile. The value of 1500V dc was chosen as this was the voltage used to test the thermocouple cable before original acceptance from the manufacturer. In addition, each of the test specimens were visually examined for degradation following the temperature tests. Testing details for each cable type are summarized below. No anomalous results were reported.

Thermocouple Cable

The incore thermocouple cables are located in the lower compartment and would be subjected to six burns as shown in Figure 12. To confirm that the thermocouple cable would survive the temperatures produced during the burns, the cable was exposed to the temperature test profile also shown in Figure 12.

The test was conducted in a Lindberg Tube Furnace with a low temperature zone maintained at a constant 300 ± 10°F and a high temperature zone maintained at a constant 1400 ± 25°F. The temperatures of the zones were monitored with 20-gauge chromel-alumel thermocouples. At the beginning of the temperature test, the cables were placed in a 300°F environment for 60 minutes. At the end of this

60-minute period, the cable was transferred to a 1400°F environment for 30 seconds and then back into the 300°F environment for 170 seconds. The 1400°F for 30 seconds followed by the 300°F for 170 seconds cycle was repeated until five cycles were completed. After the fifth cycle, the cable was maintained in a 300°F environment for an additional 60 minutes. The cable was then allowed to cool to ambient temperature.

Prior to the temperature test, a thermocouple junction was formed at one end of the thermocouple cable under test. The frayed edges of the test cable above the thermocouple junction were coated with ceramic paste to seal the end of the cable. Cable temperatures, as measured by the thermocouple itself, increased continuously upon return to the 1400°F region, and decreased continuously upon return to the 300°F zone. The highest temperature recorded from this junction was 1368°F which occurred during the fifth cycle in the 1400°F environment.

In addition, a measurement thermocouple (20-gauge, chromel-alumel) was placed beneath the outer silicone-impregnated fiberglass jacket of the thermocouple cable under test. The temperatures recorded by the measurement thermocouple were, on the average, 242°F below those recorded by the thermocouple junction at the end of the test cable during the time the cable was in the 1400°F environment. The temperatures recorded by the measurement thermocouple were, on the average, 28°F higher than those recorded by the test cable during the time the cable was in the 300°F environment after the first cycle in the 1400°F environment. The difference in these two temperature measurements demonstrated the ability of even the outermost fiberglass jacket to aid in the thermal insulation of the conductors. The cable was designed with three layers of Kapton film, a copper shield with a minimum of 85-percent coverage, and a second silicone impregnated fiberglass braid in addition to the overall fiberglass jacket (see Figure 11). A visual inspection of the cable after the test revealed that the outer jacket had changed color from yellow to gray and the Kapton film had changed from yellow to black. However, the cable successfully passed the 1500V dc test for one minute from conductor to conductor and from conductor to shield described above. Due to the severity of the temperature test and the successful completion of the voltage test, we conclude that the incore thermocouple cables will survive the temperatures produced by hydrogen burns in the lower compartment.

RTD Cable

The hot and cold leg RTD cables are located in the lower compartment and would be subjected to the same environmental conditions as the incore thermocouple cables. The test procedure, temperature profile, and tube furnace used in the thermocouple cable test were utilized in the testing of the RTD cable. The RTD cable is a four-conductor cable designed with two tightly woven stainless steel shields separated by a layer of fiberglass in addition to the insulation on the individual conductors. A measurement thermocouple (20-gauge chromel-alumel) was placed beneath the outer stainless steel shield. The highest temperature recorded by this thermocouple was 1013°F. The lowest temperature recorded by the measurement thermocouple while in the 300°F environment after being exposed to the 1400°F environment for one cycle was 342°F. The measurement thermocouple alternated between

an average temperature of 340 and 933°F as the cable was cycled between the 300 and 1400°F environments. The RTD cable was not energized during the temperature test. A visual inspection of the cable revealed a change in color from yellow to dark gray of the fiberglass braid between the stainless steel shields and a darkening of the insulation on the individual conductors. After the test, the RTD cable successfully passed the 1500V dc voltage test. Due to the severity of the temperature test, we conclude that the hot and cold leg RTD cables will also survive the temperatures produced by hydrogen burns in the lower compartment.

Evaluation of the Test Profile

The test profile for the RTD and thermocouple cables consisted of five burns, whereas CLASIX predicts six lower compartment burns to occur. The tests were performed before mid-year 1981. At that time, five burns were predicted in the lower compartment by CLASIX. Changes to the distributed ignition system and to the containment modeling assumptions resulted in substantial changes to the CLASIX input. These changes resulted in a different number of burns. However, this did not invalidate the test. A comparison of the test profile with the latest CLASIX-predicted profile showed that each burn simulation in the test was substantially longer than was predicted by CLASIX based on a one ft/sec flame speed (Figure 12). In addition, the test temperature before and after the burns was much higher than was expected inside the containment. The test chamber temperature was equal to the adiabatic flame temperature for an 8 v/o hydrogen burn in dry air (1400°F) and was therefore conservative. The radiative heat flux was also much greater in the test than would be seen in a containment. The ceramic tube had an emissivity greater than 0.9, as compared to a steam/gas emissivity of 0.3. This provides a factor of 3 on the test heat flux, as compared to the containment heat flux. The shape factor associated with the test is also greater than would be seen in the containment because the test has a shape factor close to one. The test was therefore conservative in that the temperature used was higher than would be found in containment; the time at high temperature was longer; and the heat transfer was higher than would be present in the containment. Subsequently, the cable passed insulation breakdown tests required of new cable.

Igniter Power Cables

The igniter power cables used for the deliberate ignition system are all enclosed in conduit and were analyzed to show qualification as discussed earlier. The testing performed at Singleton Laboratory on igniter cable was not done to simulate the containment response to hydrogen burns but to determine the ability of the IDIS power cable to withstand high temperatures. The tests showed the power cables could withstand temperatures several hundred degrees higher than the cables would reach as a result of hydrogen burns and still be functional. The tests provided corroborating evidence that the igniter cables, as installed in the plant, would be able to function as intended. Details of the test are provided below.

The test series consisted of placing a section of the igniter cable in a length of conduit and sealing the ends of the conduit. A 20-gauge chromel-alumel thermocouple was also placed in the conduit to monitor

the interior temperature. The conduit was then placed in a Blue M oven, after which the temperature of the oven was raised to a maximum 700 $\pm$ 10°F and maintained at that temperature for 45 minutes. During each test, an iron-constantan thermocouple was used to monitor the temperature of the oven. Approximately 15 minutes after the oven temperature reached the desired test temperature, the thermocouple monitoring the interior temperature of the conduit also reached oven temperature and remained at that temperature for the remainder of the test (approximately 30 minutes). For the 700°F test this interior conduit temperature was 350°F higher than was seen in the containment analysis, showing once again the conservative nature of the test.

After allowing the oven to cool to ambient temperature, the cable was removed and a functional test and a visual inspection of the insulation was performed. The functional test consists of applying 1500V dc between the single conductor and a ground plate to which the cable had been strapped. The cable successfully passed this resistance test. A visual inspection revealed that the PVC jacket which is used for mechanical protection of the insulation had decomposed during the 700°F test. However, the insulation remained fully functional. For tests with maximum temperatures of 600°F or less no visible damage was evidenced and the insulation remained functional.

Conclusions

The analyses and test data supported the conclusion that all essential equipment would survive repeated hydrogen burns. Where equipment had any protection such as the casing of transmitters or conduit for cable, large margins compared to qualification temperatures were present. It was concluded that the survivability of essential equipment had been established for ice condenser containments using deliberate, controlled ignition of hydrogen as the method for hydrogen control during degraded core events.

REFERENCES

1. The CLASIX Computer Program for the Analysis of Reactor Plant Containment Response to Hydrogen Release and Deflagration, OPS Report No. OPS-36A31

2. HEATING5 - An IBM 360 Heat Conduction Program, Oak Ridge National Laboratory, ORNL/CSD/TM-15

3. Westinghouse Topical Report, Environmental Qualification - Instrument Transmitter Temperature Transient Analysis, WCAP-8936 (Proprietary)

4. Sequoyah Nuclear Plant Core Degradation Program, Volume 2, Report on the Safety Evaluation of the Interim Distributed Ignition System, December 15, 1980

E72225.02

TABLE 1
SEQUOYAH ESSENTIAL EQUIPMENT

Equipment	Function
TE-68-18, -41, -60, -83	Cold leg temperature
Hydrogen Igniters	Hydrogen control
[redacted]e exit thermocouples	Information for inadequate core cooling
TE-68, -373 through TE-68-386	For reactor vessel level system
FSV-68-394, -395, -396, -397	Reactor vessel vent valves
Ice condenser seals	Direct steam flow through ice
Penetrations X-003, -111, -113 -112, -054, -079A, -079B	Containment boundary, blind flange with O-ring seal
Electrical penetrations	Containment boundary
Airlock, equipment hatch, and personnel airlock seals	Containment boundary
Containment isolation valves	Containment boundary
LT-3-148, -156, -164, -171, -172, -173, -174, -175	Steam generator level input for control of AFW flow
Air return fans	Containment pressure and hydrogen control
H_2I-43-200, -210	Hydrogen analyzers
FCV-43-201, -202, -207, -208	Allows airflow to hydrogen analyzers
FSV-43-201, -202, -207, -208	Allows associated FCV to open
Ice condenser doors	Allows steam flow through ice bed
[redacted]63-176, -177, -178, -179	Sump level for ECCS switchover
FCV-63-172	Closed position required for proper ECCS flow path
LT-68-320, -355A	Pressurizer level
TE-68-1, -24, -43, -65	Hot leg temperature

E72225.02

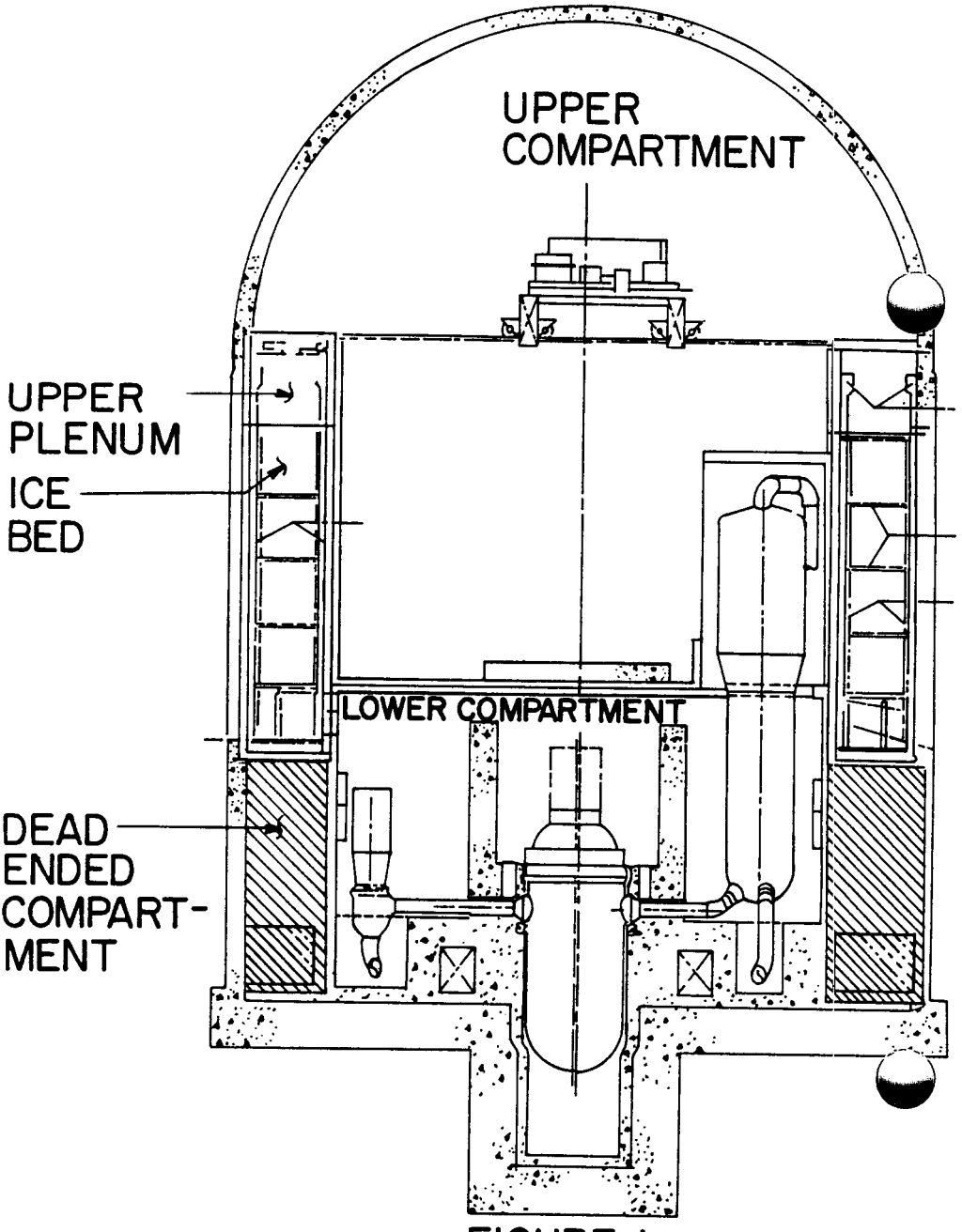


FIGURE 1
CONTAINMENT CROSS
SECTION

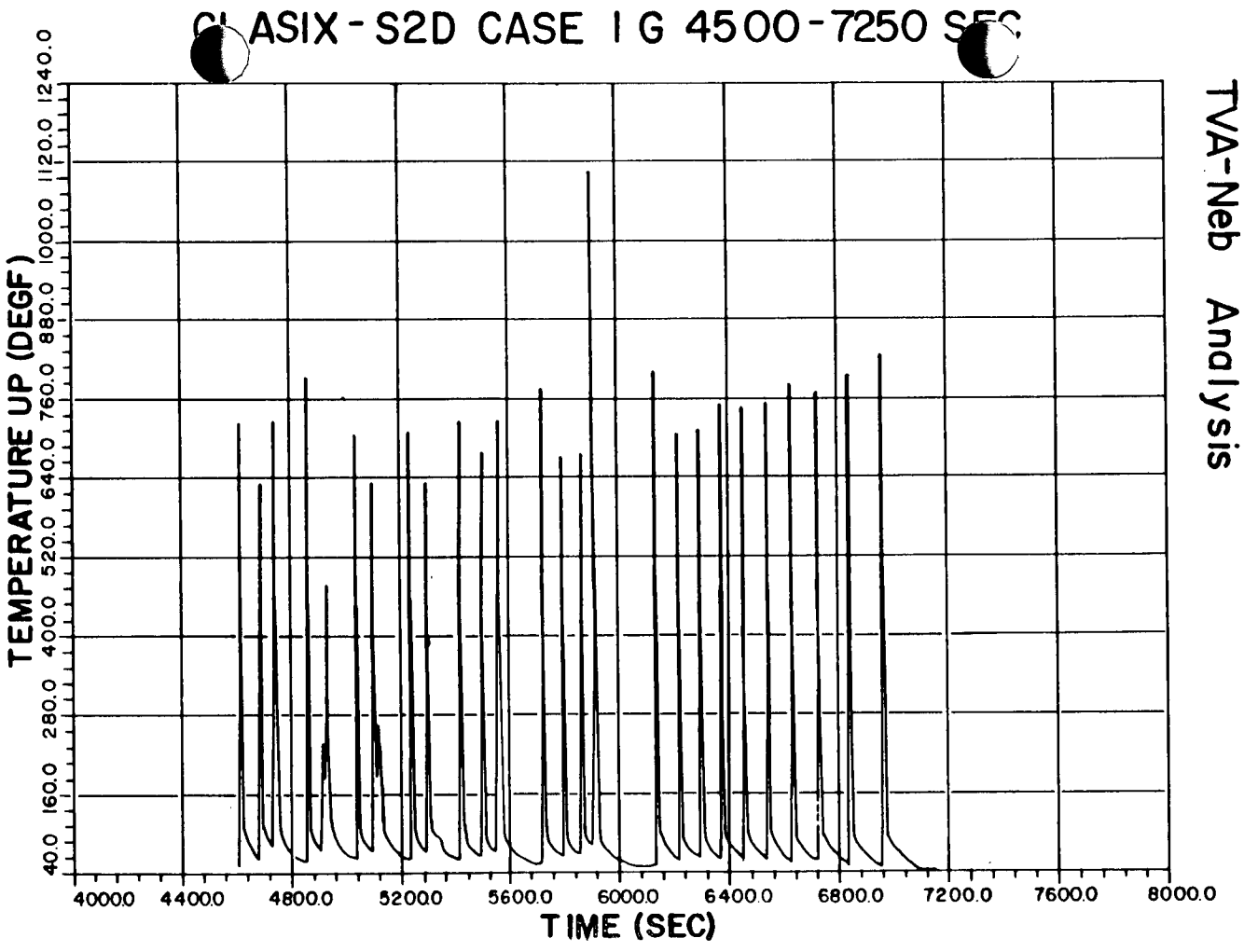

CLASIX-S2D CASE 1G 4500-7250 SEC
TVA-Neb Analysis
TEMPERATURE UP (DEGF)
40.0
160.0
280.0
400.0
520.0
640.0
760.0
880.0
1000.0
1120.0
1240.0
40000.0
44000.0
48000.0
52000.0
56000.0
60000.0
64000.0
68000.0
72000.0
76000.0
80000.0
TIME (SEC)

FIGURE 2

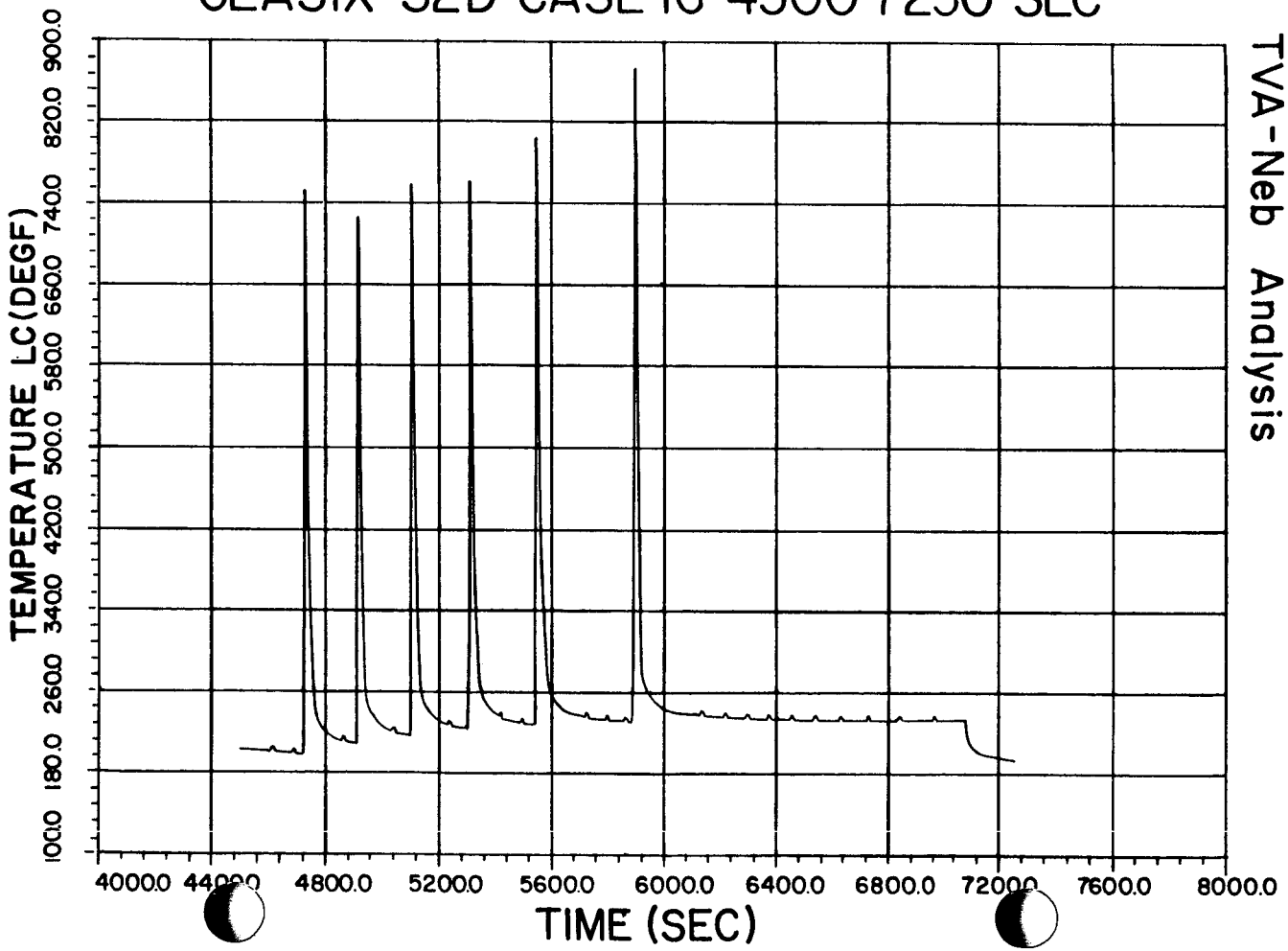

CLASIX S2D CASE IG 4500-7250 SEC
TVA-Neb Analysis
TEMPERATURE LC(DEGF)
100.0 180.0 260.0 340.0 420.0 500.0 580.0 660.0 740.0 820.0 900.0
40000.0 44000.0 4800.0 5200.0 5600.0 6000.0 6400.0 6800.0 7200.0 7600.0 8000.0
TIME (SEC)

FIGURE 3

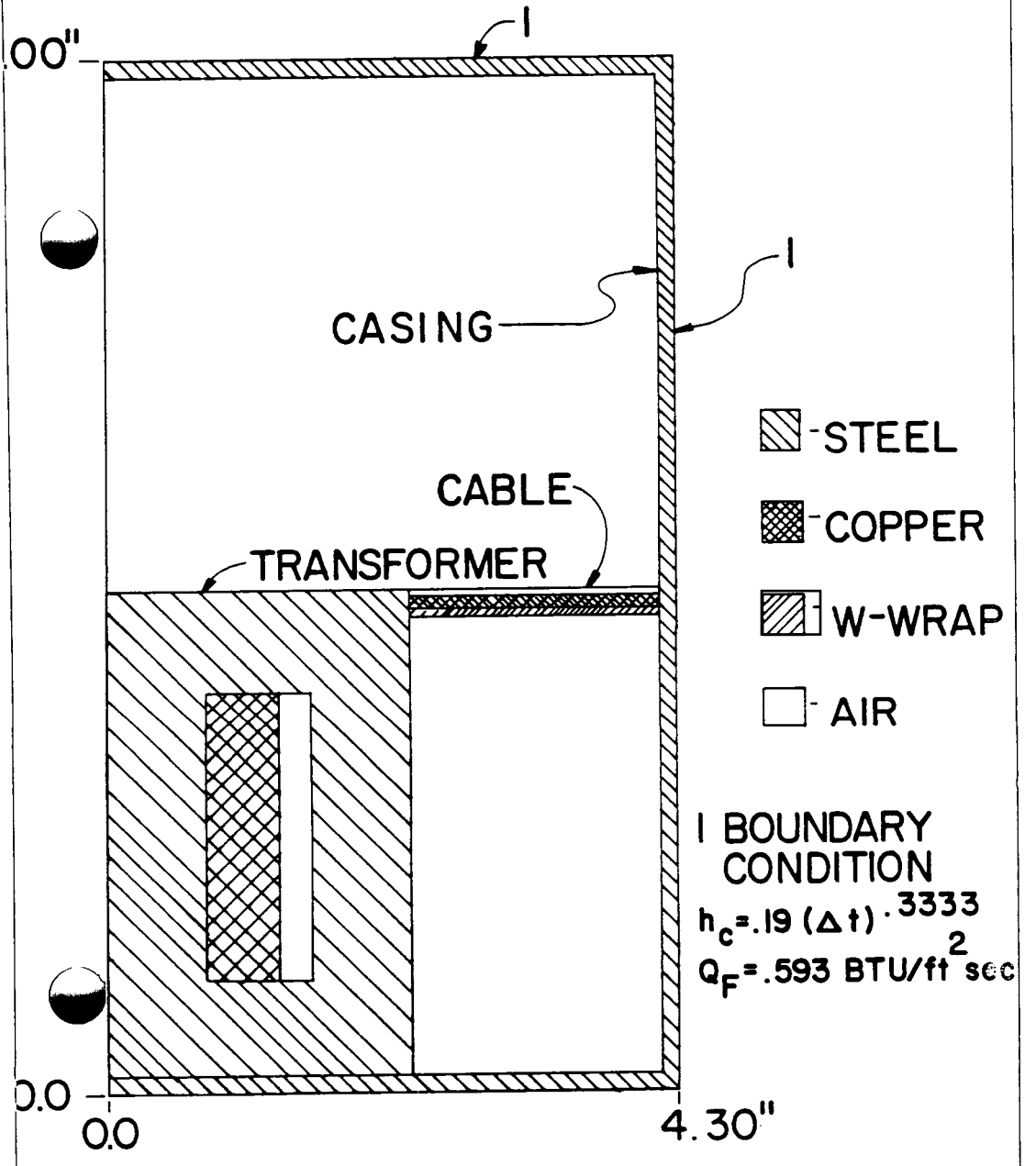

.00"
1
1
CASING
CABLE
TRANSFORMER
STEEL
COPPER
W-WRAP
AIR
I BOUNDARY CONDITION
$h_c = .19 (\Delta t)^{.3333}$
$Q_F = .593$ BTU/ft^2 sec
0.0
0.0
4.30"

FIGURE 4

IGNITER BOX THERMAL RESPONSE (CLASIX 8 VOL %-85 %)

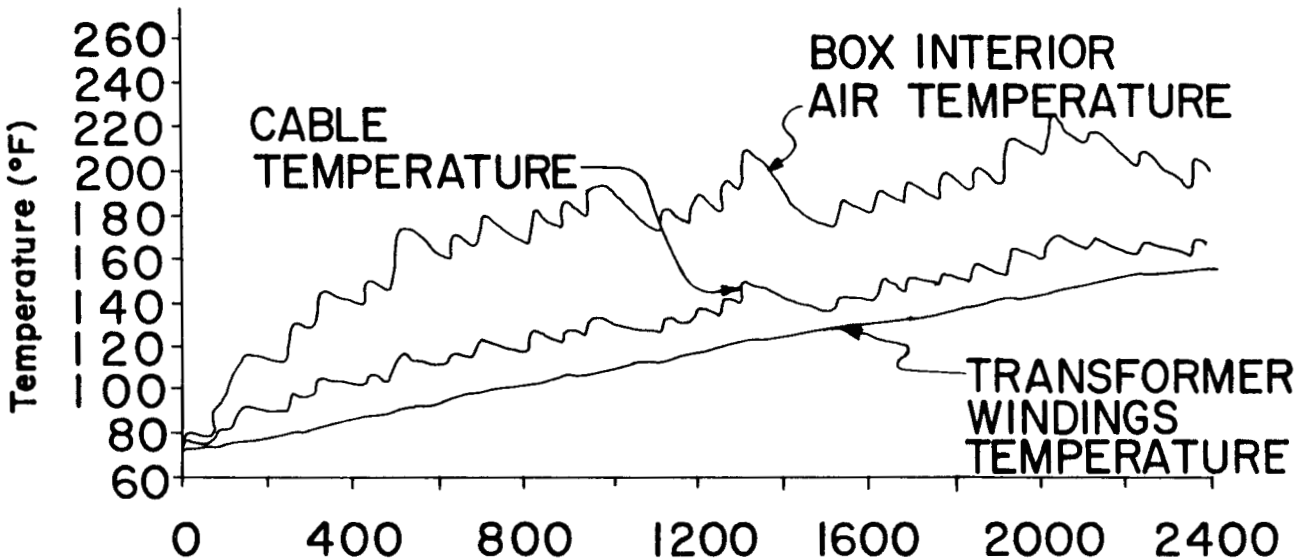
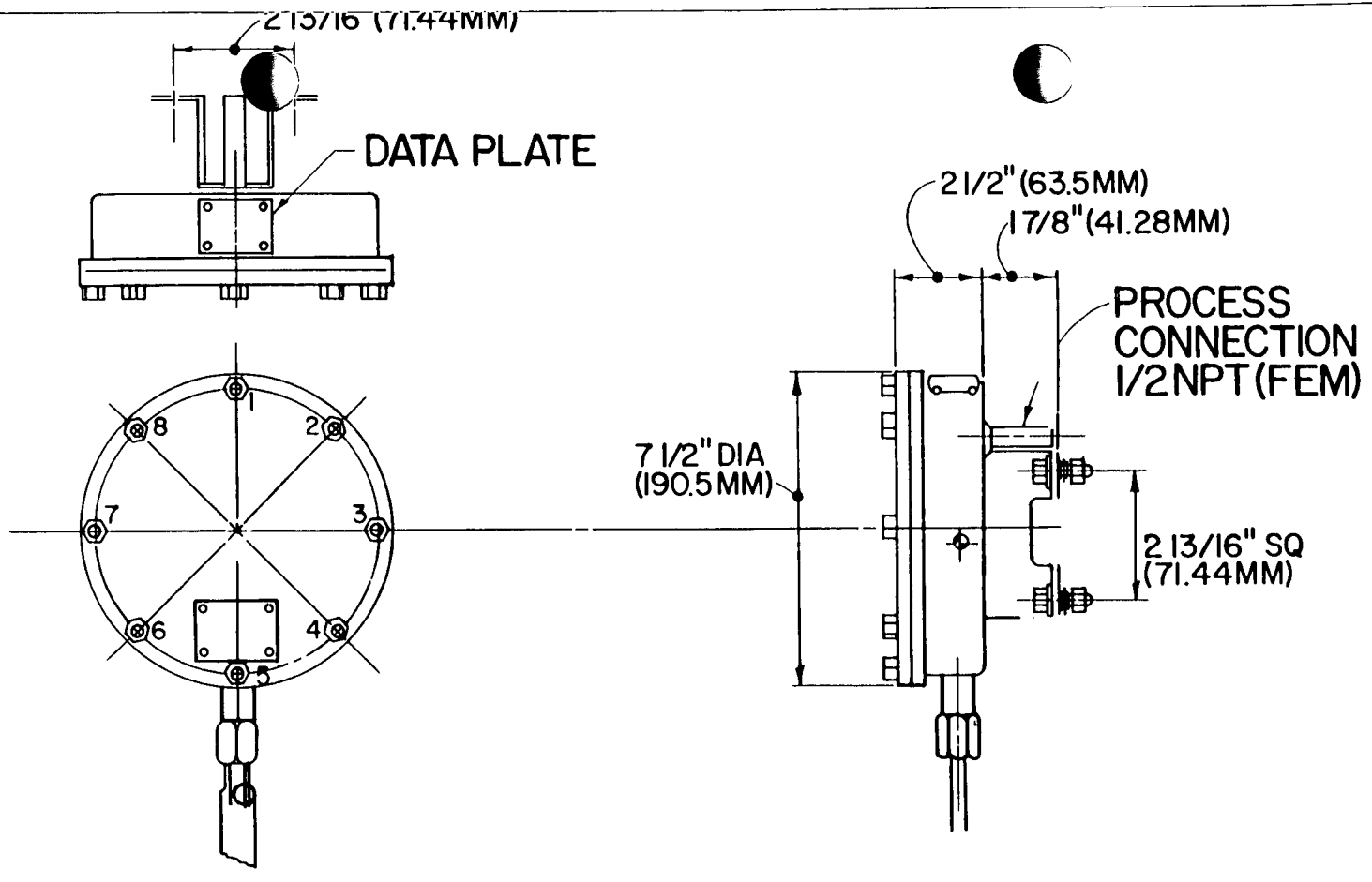


FIGURE 5



FRONT VIEW
WALL MOUNTING

SIDE VIEW
WALL MOUNTING

FIGURE 6

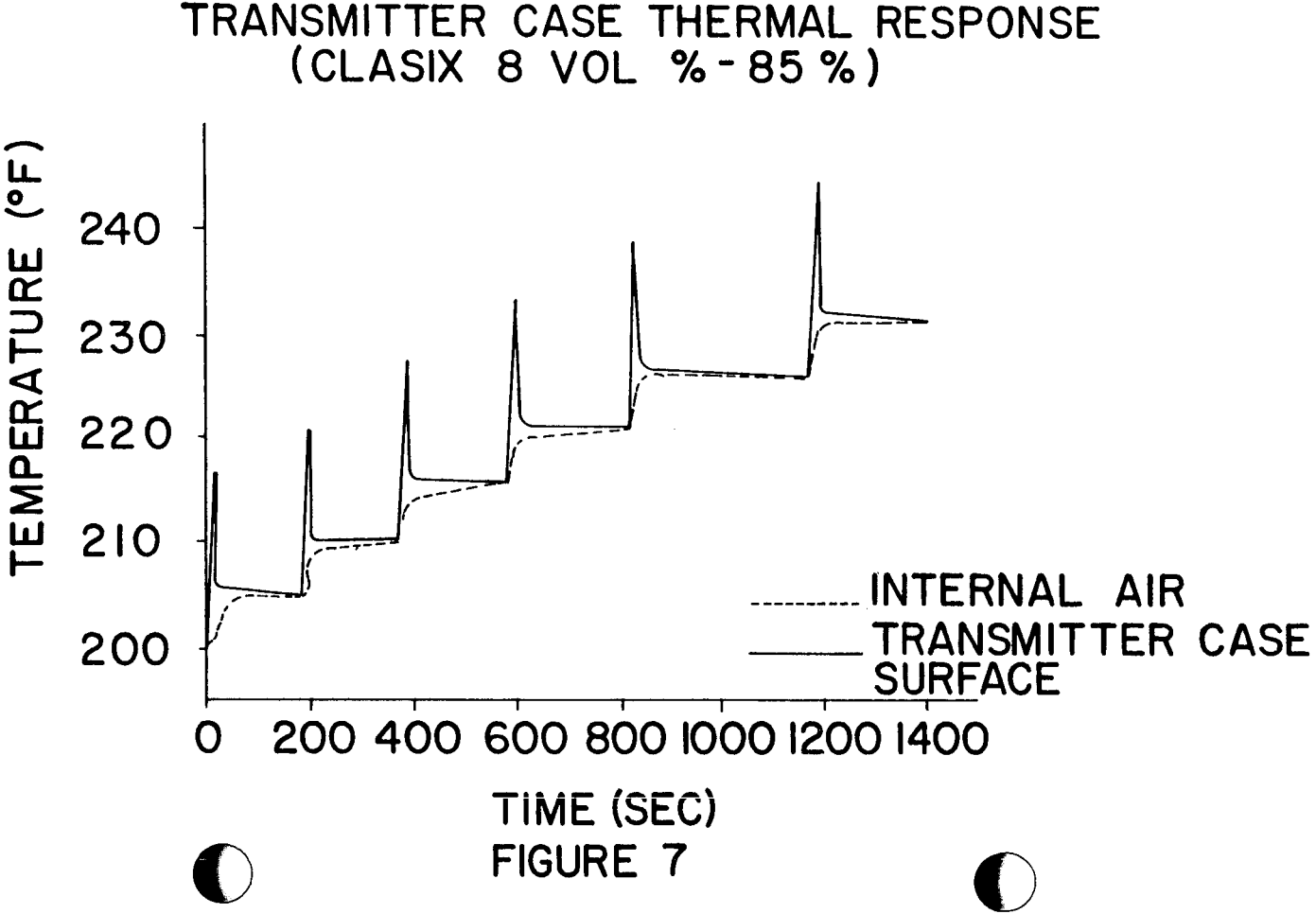
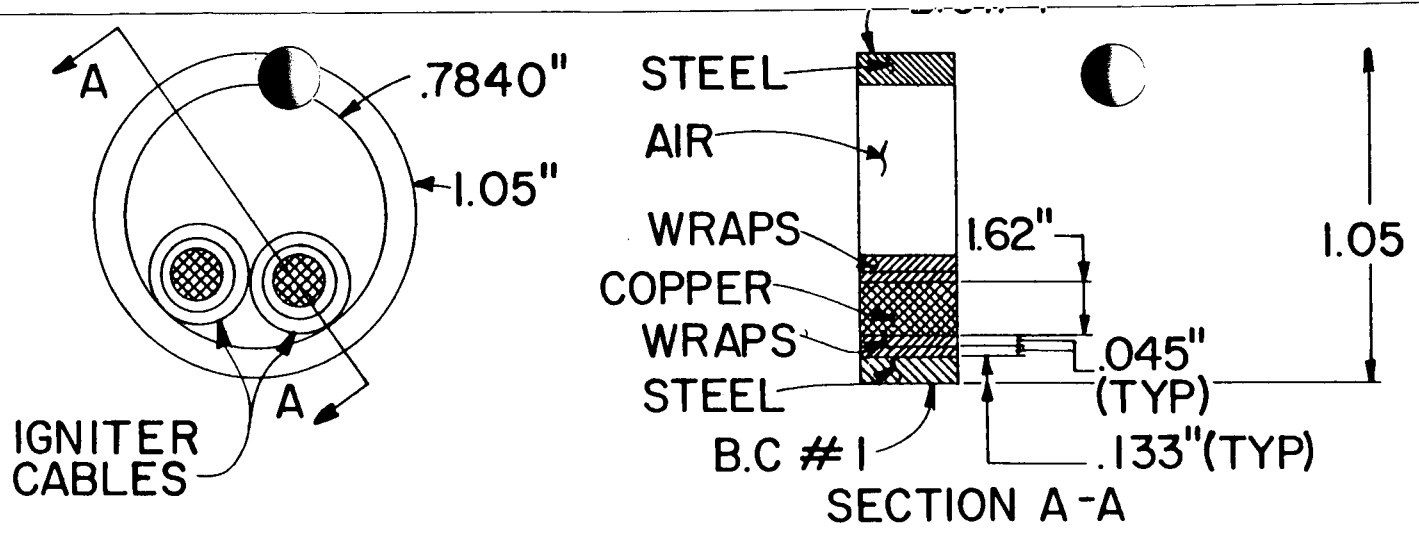

TRANSMITTER CASE THERMAL RESPONSE
(CLASIX 8 VOL %-85 %)
TEMPERATURE (°F)
240
230
220
210
200
0
200
400
600
800
1000
1200
1400
TIME (SEC)
INTERNAL AIR
TRANSMITTER CASE SURFACE

FIGURE 7



CONDUIT AND
IGNITER CABLE

- STEEL
- COPPER
- INSULATING WRAP
- AIR

BC #1-BOUNDARY CONDITION

$h_c = .18\,(\Delta)^{.333}$

$Q_f = .85$ Btu/sec-ft^2

NOTE: SCALE IS DOUBLE

1173

FIGURE 8

CABLE AND CONDUIT THERMAL RESPONSE (CLASIX 8 VOL % - 85 %)

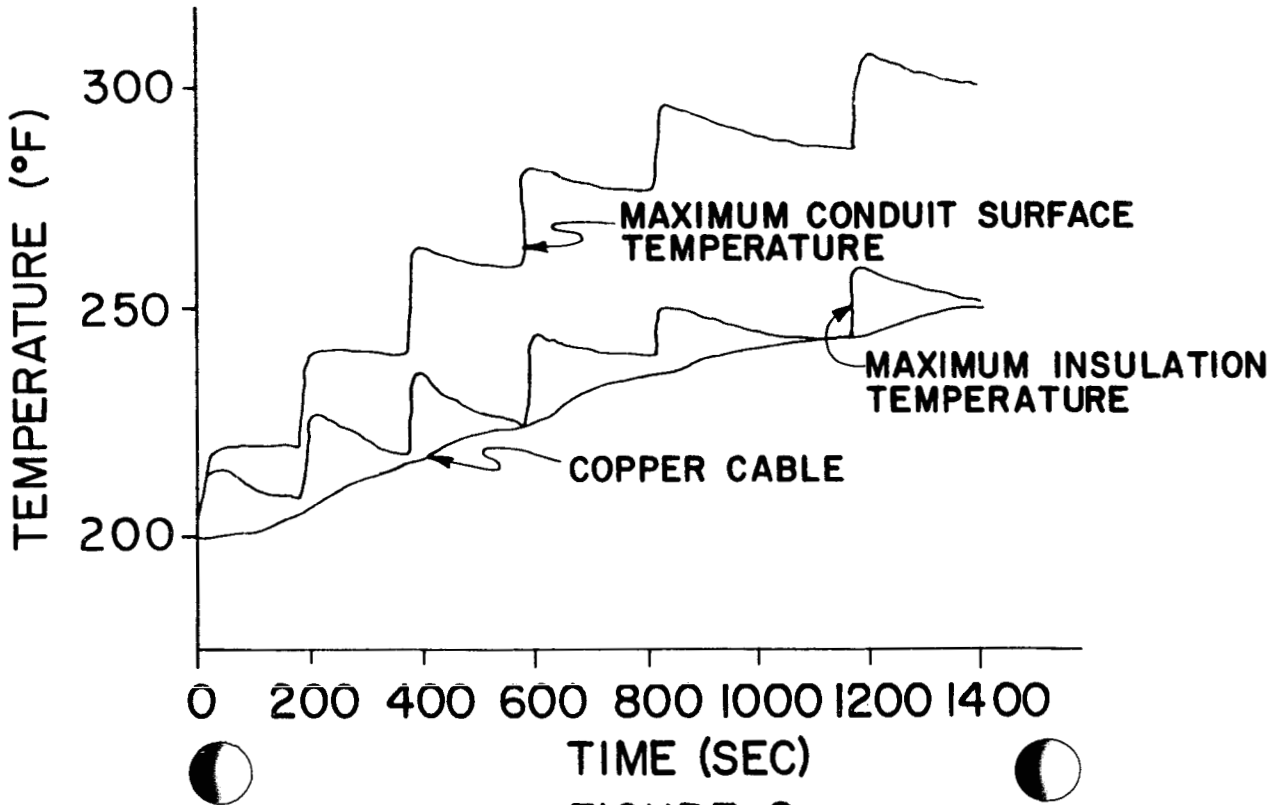


FIGURE 9

CABLE AND CONDUIT THERMAL RESPONSE
(GLASIX 8 VOL % - 85 %)

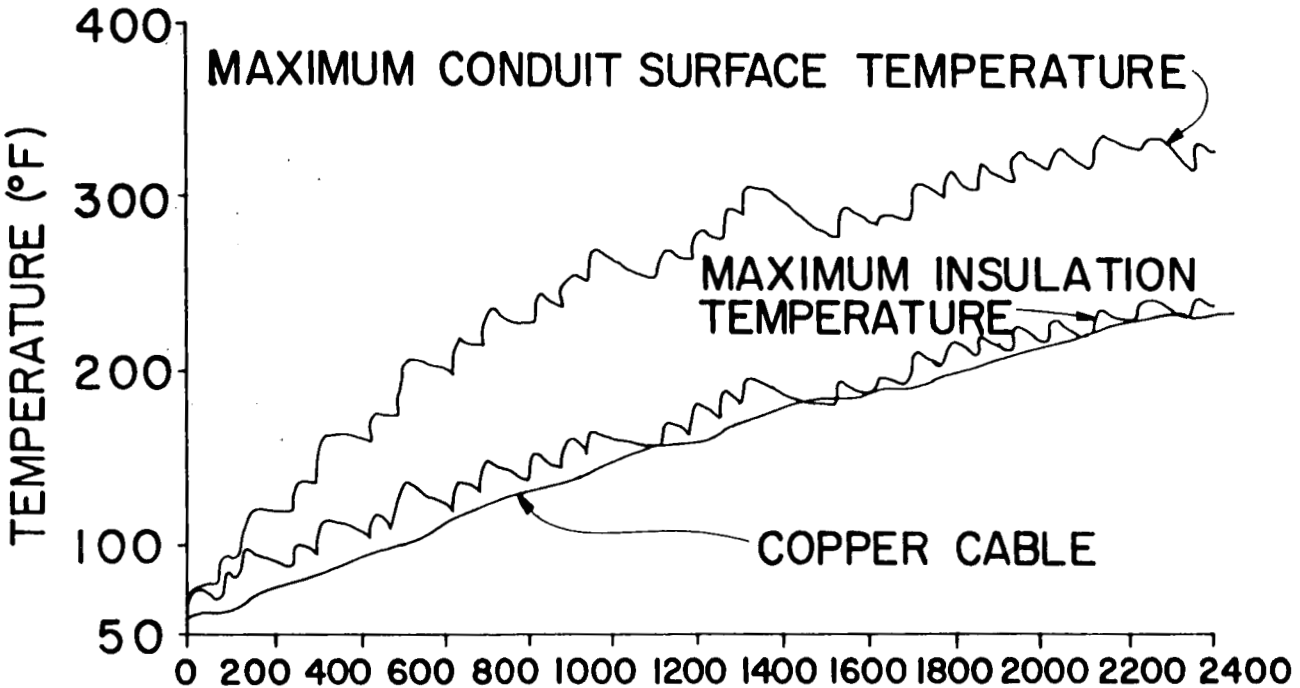


FIGURE 10

TRANSMITTER CASE SURFACE THERMAL RESPONSE

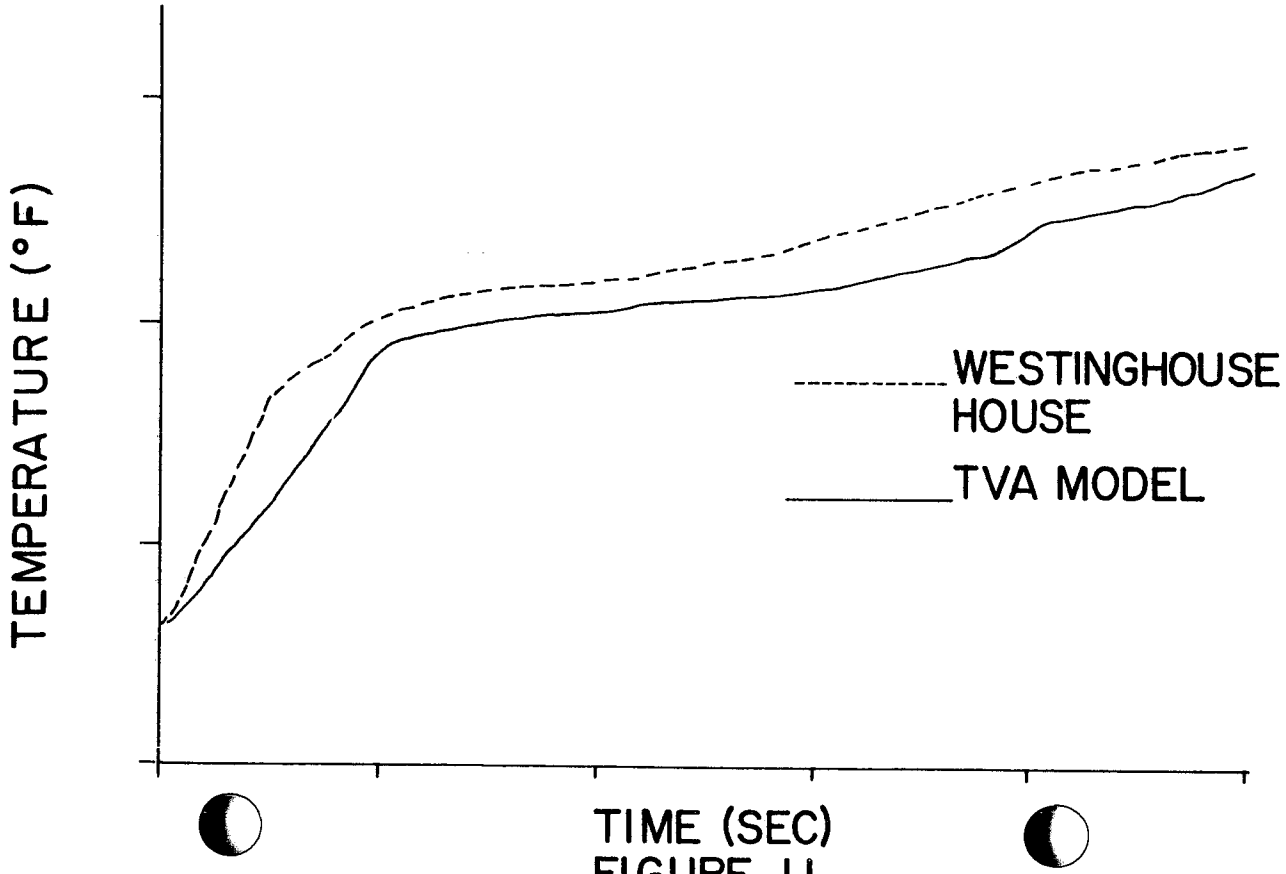


FIGURE 11

TRANSMITTER CASE INTERNAL AIR THERMAL RESPONSE

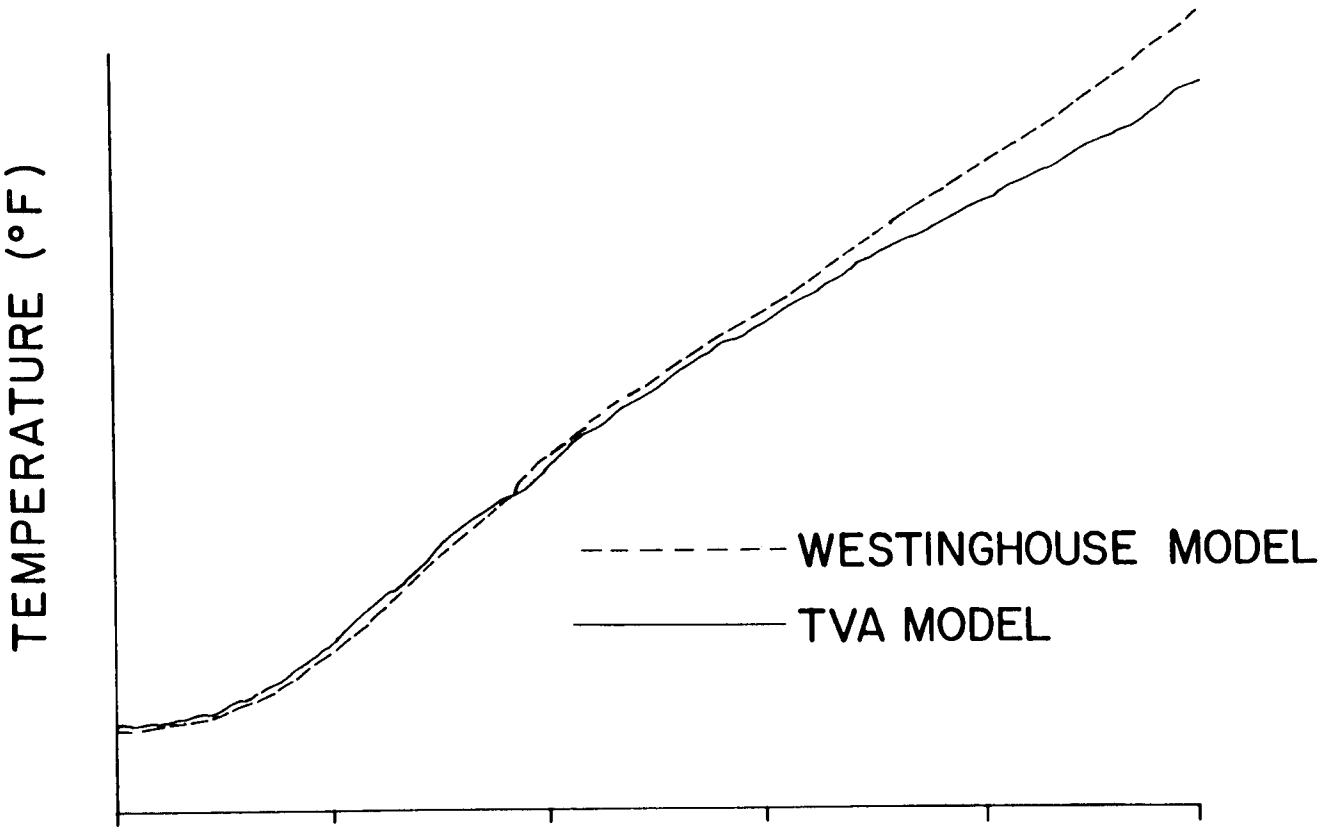


FIGURE 12

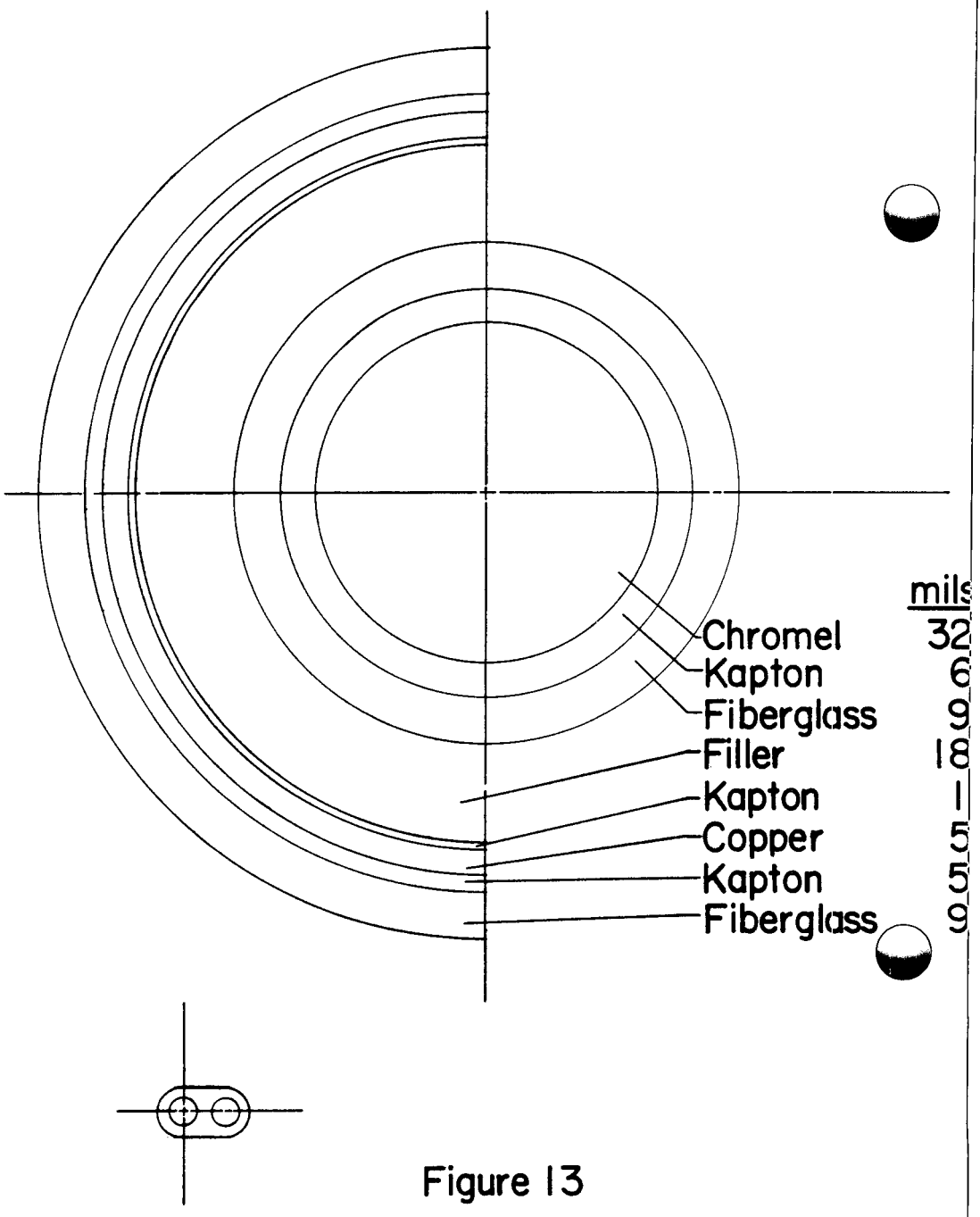

Thermocouple Cable
mils
Chromel 32
Kapton 6
Fiberglass 9
Filler 18
Kapton 1
Copper 5
Kapton 5
Fiberglass 9

Figure 13

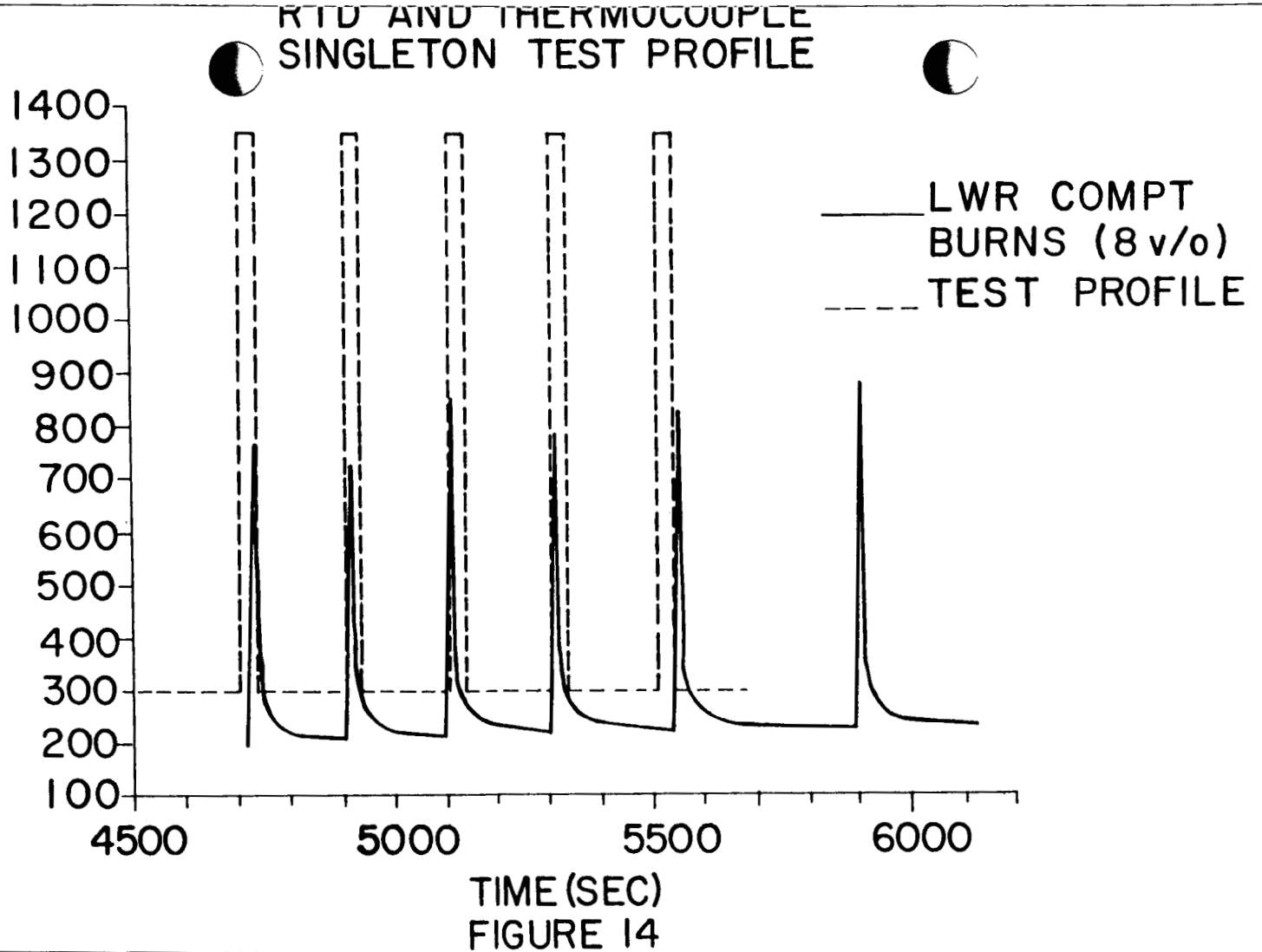


FIGURE 14

08/11/1179

REFERENCES

1. Gardon, Robert, "An Instrument for the Direct Measurement of Intense Thermal Radiation," The Review of Scientific Instruments, Vol. 24, No. 5, May 1953.

2. Brookley, Charles E., "The Circular Foil Heat Flux Gage," Thermogage, Inc., Frostburg, Maryland.

ACKNOWLEDGMENTS

The Hydrogen Burn Survival Program is a team effort, involving several SNLA organizations. In addition to the individuals specifically mentioned in the report, the authors gratefully acknowledge the contributions to this effort by Lou Cropp, Vince Dandini, Steve Kempka and Art Ratzel of Sandia and the staff at the FITS Facility.

AN ANALYSIS OF EQUIPMENT SURVIVABILITY IN HYDROGEN BURN ENVIRONMENTS

P. S. Kepley, Bechtel Power Corporation
S. H. Hobbs, Mississippi Power & Light Company
A. T. Vieira, Bechtel Power Corporation

Introduction

To respond to the NRC rule regarding considerations for degraded core events (Reference 1), a hydrogen control system has been designed and installed at the Grand Gulf Nuclear Station (GGNS). As part of the design program of the hydrogen control system, an equipment survivability study has been conducted. The hydrogen control system at GGNS is a deliberate hydrogen ignition system (HIS). Since the operation of the HIS following a degraded core accident could result in a series of short duration hydrogen burns, the containment environment would experience a corresponding series of temperature spikes (up to 1000 F). The objective of the study was to verify that the equipment that may have an essential role in recovery from a degraded core event would not be rendered inoperable by hydrogen burns resulting from the actuation of the HIS.

To perform this evaluation, a list of required systems has been generated. These systems serve to either ignite the hydrogen and monitor the course of the accident, maintain the containment pressure boundary, or recover the core. A list of these systems is shown in Table 1. Limiting components of these systems have been identified, and they serve as a basis for evaluation of system survivability.

GGNS is a boiling water reactor housed in a Mark III containment. For the purpose of determining the characteristics of a deliberate ignition system, the containment building is divided into three well-defined volumes: the drywell, the wetwell, and the containment (see Figure 1). The drywell contains the reactor vessel and is isolated from the rest of the containment by the suppression pool. The wetwell is the annular region directly above the suppression pool and below the HCU floor. The containment is defined as the remaining free volume.

For this study, two postulated transients have been considered: a LOCA in the drywell or a stuck open relief valve (SORV), along with failure of all decay heat removal systems. In either case, large amounts of hydrogen are released into the wetwell through the suppression pool. With igniters located in the wetwell, a majority of the hydrogen burning will take place in this region, creating a severe local temperature environment.

As the local environment created by the hydrogen burns is well in excess of equipment qualification temperatures, an equipment survivability evaluation is performed. For this evaluation, the thermal response of each limiting component of the required systems is determined based on two burn environments: 1) global burns and 2) the more severe temperature environment of the wetwell. Both cases are considered even if a system or component has been identified as being located well away from the wetwell region. This is done to eliminate questions of which environment should apply to each specific component and to allow single evaluations to be applied to classes of equipment despite locations. Also, in some cases, evaluations are based on comparisons with other similar equipment. The comparisons are made with components that are at least as limiting in regard to thermal characteristics.

Evaluation Method

The thermal response for essential equipment was evaluated using CLASIX-3 (Reference 2) predicted temperature environments. This environment can result from transients involving a stuck open relief valve (SORV): 8 v/o hydrogen, 85 percent hydrogen burn with one train of containment sprays operating and a 6 fps burn speed. The CLASIX-3 analysis predicts that, for the SORV hydrogen release scenario, all hydrogen burning will take place in the wetwell. This results in comparatively mild environments elsewhere in the containment and the drywell. With the exception of the igniters, there is very little essential equipment located in the wetwell. However, the wetwell temperature environment is used to determine the thermal response of the equipment regardless of where it is located. This eliminates any uncertainty about the appropriate temperature environment to be used for any piece of equipment, such as a piece of equipment located just above the wetwell region. To ensure that the thermal response of the equipment is bounding, the equipment is also evaluated using four successive, forced, global, 8 v/o, 85 percent hydrogen burns.

Wetwell Burn Cases

The composite burn transient models 60 successive burns (see Figure 2). Based on the fine detail of these burns, enveloping burn profiles have been developed. The first three burns (which occur at approximately 4850 seconds from the beginning of the transient) are modeled with a 1000 F peak. The temperature exponentially decays back down to 120 F in 13 seconds. There are 130 seconds (peak to peak) between these burns. At 655 seconds after the beginning of the first burn, a set of 12 sequential burns occurs. The peak temperature of this second set of burns is modeled as 800 F with the temperature exponentially decaying to 150 F in 18 seconds. There are 39 seconds (peak to peak) between each of these burns. At 1255 seconds from the beginning of the first burn, the remaining 45 burns are modeled. These burns have a modeled peak temperature of 850 F with 36 seconds between each burn. The 45 burns each exponentially decay down to 180 F in 13 seconds. All 60 burns take 2 seconds to reach their peak temperatures.

Forced Global Burns

The thermal response of essential equipment to postulated multiple global burns has also been evaluated. To provide input for this evaluation, a CLASIX-3 generated temperature profile of a forced containment burn was utilized (see Figure 3). The containment temperature profile which was modeled to envelop this global burn peaks at 800 F in 11 seconds and then exponentially decays back down to 200 F in the subsequent 29 seconds. This burn profile is repeated again at 1000, 1570, and 2170 seconds after the beginning of the first global burn.

Heat transfer to the evaluated components from burn environments was determined based on natural convection and radiation from an absorbing/emitting atmosphere.

Natural convective heat transfer is calculated using the relation:

$$h = hc \ (\Delta T)^{he}$$ (Reference 3)

where,

ΔT is the temperature difference between the surface and the ambient atmosphere

hc and he are, respectively, the coefficient and exponent for the nat convection term

Radiative heat transfer from the burn environment to the equipment is modeled utilizing the methods suggested by Hottel (Reference 4) where,

$$Q = \frac{Es + 1}{2} \sigma\left(E_g \ T_{atmos}^{4} - \alpha_g \ T_{surface}^{4}\right)$$

σ = Stefan-Boltzmann constant

E_s = emissivity of the outside surface

E_g, α_g = are the emissivity and absorptivity of the steam/air environment

T_{atmos} = burn temperatures

$T_{surface}$ = outside surface temperature of the box

The values of emissivity and absorptivity utilized ensure an upper bound of radiative heat transport to the equipment. Sensitivity analyses varying relationships (turbulent, laminar) of natural convection and using forced convection based on the burn velocity of 6 fps are utilized to establish the adequacy of responses obtained.

Modeling of Equipment

The temperature effects on the equipment and its components of repeated hydrogen burns are calculated using a modified version of the HEATING-3 (Reference 5) heat transfer program. The code has been modified to model the thermal response of the equipment to successive hydrogen burns. These modifications allow the code to simulate radiative heat transfer from and to an emitting/absorbing atmosphere. The code has also been modified to use a time-dependent function of atmospheric temperature. This is used to simul the successive hydrogen burns.

For each piece of equipment analyzed, an appropriate HEATING-3 model was constructed. These models, besides considering heat transfer from the burn environment to the exterior of the equipment, also considered conductive, radiative, and convective heat transfer across air spaces to limiting internal components. In these models, best estimate thermal properties were utilized; however, geometric simplifications were chosen to maximize the thermal response of internal limiting components. This was done, for example, by using the minimum thickness of any enclosure and also the minimum distance from the

burn environment to the limiting internal component. The level of detail developed for each model was dependent on the geometry of the component, material makeup, symmetry of the component, and boundary conditions. Sensitivity studies were performed to justify the appropriateness of the modeling assumptions.

The evaluation of the Grand Gulf igniter assembly is presented here as a typical example of the technique used in evaluating equipment. The igniter assembly is an 8- x 8- x 6-inch sealed stainless steel box with a removable access cover. It houses the transformer and terminal strip mounted on a stainless steel plate and also contains the associated wiring. The glow plug extends out through the front and is insulated from the box by the glow plug mount. A spray shield extends over the front of the box to protect the glow plug. The igniter assembly is modeled as being mounted on a 1-inch-thick carbon steel plate. The entire assembly and mounting are assumed to be exposed to the burn environment. The assembly is shown in Figure 4.

A two-dimensional model of the igniter assembly was determined to be the minimum necessary to provide a representative temperature distribution inside the box. The side view of Figure 4 was used for the model. Instead of using a full-scale, two-dimensional model, the box model uses only the lower half of the box. This model, as shown in Figure 5, maximizes the thermal response of the assembly internals. Although the igniter assembly is not symmetrical about the mid-plane, symmetry was assumed using the smaller air gap distance to increase the heat transfer to the transformer. During normal operation, the transformer generates approximately 25 watts of heat. This heat source has been included in the model. The transformer was taken as the limiting component because the igniter assembly materials will not be adversely affected by the burn environment, and all other possible limiting components were analyzed separately.

Figure 6 shows the temperature response of the assembly to the wetwell burn case. The maximum surface temperature for the igniter assembly was 246 F, while the transformer surface reached 210 F. As shown in Figure 7, for the global burn case, the transformer surface reached 183 F and the exterior surface of the assembly reached a maximum temperature of 205 F. All of these temperatures are well below the transformer qualification temperature of 400 F.

Sensitivity Studies

To assure that the reported thermal response of equipment is adequately representative of the actual equipment thermal response, several sensitivity studies have been conducted. These studies involved the following:

a. Calculational time steps and thermal mesh spacings were varied to assure that a convergent solution is obtained.

b. Various modes of convective heat transfer were modeled to determine their impact on the analytical results. Natural convection coefficients that varied as much as 1/3 from the empirical values affected the results by less than 10 F. Forced convection was varied by considering wind speeds from 1 ft/sec to 12 ft/sec (twice the burn

speed). This caused a maximum temperature variation of 10 F. Changing the natural convection coefficient from laminar to turbulent resulted in a negligible change in the maximum temperature of the equipment.

c. Emissivity was varied over its potential range of values (0.7 to 1) causing only a 6 F increase in the maximum temperatures.

d. Various geometrical representations (including a three-dimensional configuration) were modeled, and their effects on the temperature responses were determined.

The results of these studies showed that the analytical response was well represented, as the results did not vary significantly.

Results and Conclusion

The results of the equipment survivability study show that all equipment identified as essential will survive the predicted burn environment. In fact, in all cases, considerable margin exists between the calculated equipment temperatures and the temperatures at which equipment operation has been verified (see Table 2).

In addition to the margin noted between the calculated temperatures and the survival temperatures, a number of other factors and conservatisms are considered in evaluating the conclusions of this report. Among the conservative factors that can be explicitly identified, the following are the most significant:

a. Although the equipment is located throughout the containment, all analyses were performed assuming exposure directly to the most limiting environment (wetwell). This assumption eliminates the need for justifying models of equipment located near or outside the wetwell region.

b. The assumed burn profiles for the wetwell burn are more conservative than the global burn profiles for equipment survivability. The magnitude of the temperature spike is higher, and the total number of spikes is much greater. To verify this conclusion, all analyses were performed assuming exposure to both a wetwell and a global burn environment. In all cases, the wetwell burn profiles resulted equipment surface temperatures that were higher by 20 F to 60

c. The models used in all heat transfer analyses were conservatively constructed. In particular, geometry considerations were often simplified to allow credit for symmetry in the model. For example, in numerous cases, air gaps of varying thicknesses are found inside equipment. To simplify these models, minimum air gaps were used, thus maximizing heat transfer across the gaps to the critical components. In addition, no credit for thermal shielding of equipment was taken, as all exposed surfaces of the equipment were assumed to be completely immersed in the burn environment. The sensitivity studies performed demonstrate that the conclusions reached are not sensitive to the individual parameters defined in the study, varied over their expected range of values.

d. No credit was taken for enhanced cooling that could result from direct impingement of the spray on equipment.

This study justifies the conclusion that the proposed hydrogen control system will not jeopardize the ability of the plant to recover from a degraded core accident. This conclusion is based on analyses using conservative methods and results that have significant margins when compared to maximum allowable temperatures.

References

1. "Advance Notice of Proposed Rulemaking: Domestic Licensing of Production and Utilization Facilities: Consideration of Degraded or Melted Cores in Safety Regulations," Federal Register 45 (193), October 2, 1980.

2. Mississippi Power & Light Company, "Report on the Grand Gulf Nuclear Station Hydrogen Ignition System," August 31, 1981.

3. Chapman, A. J., "Heat Transfer," 2nd Edition, 1967.

4. Hottel, H. C., and Egbert, R. B., "Radiant Heat Transmission from Water Vapor," AIChe Trans., Vol. 38, 1942.

5. Turner, W. D., and Simantov, "HEATING 3 - A UNIVAC 1110 Heat Conduction Program," ORNL-TM-3208, February 1971.

TABLE 1

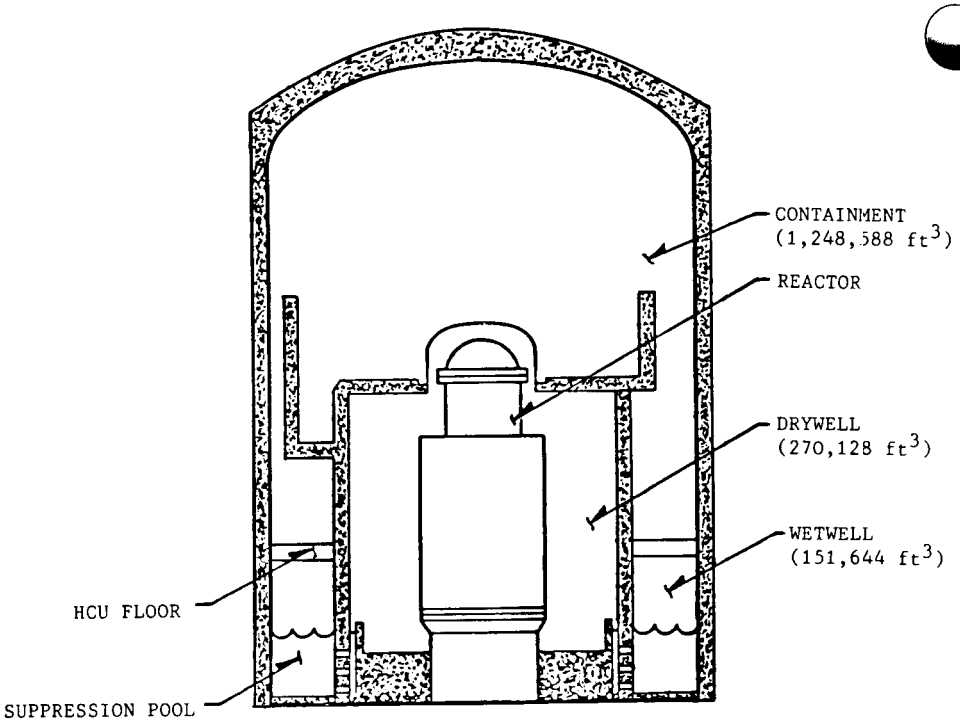
SUMMARY LIST OF REQUIRED SYSTEMS

Containment isolation valves, penetrations, locks, and hatches
Hydrogen igniter system
Hydrogen recombiners, drywell purge compressors, and drywell vacuum breakers
Containment spray (CS) system
Safety relief valves
LPCS, LPCI, and RHR systems
Reactor level and pressure instruments
Hydrogen analyzers
Containment pressure and high-range radiation instruments
Containment and suppression pool temperature instruments
Containment and drywell pressure instruments
Associated instruments and controls
Associated power and control cables
Limit/position indication switches
Main steam inboard isolation valves

TABLE 2

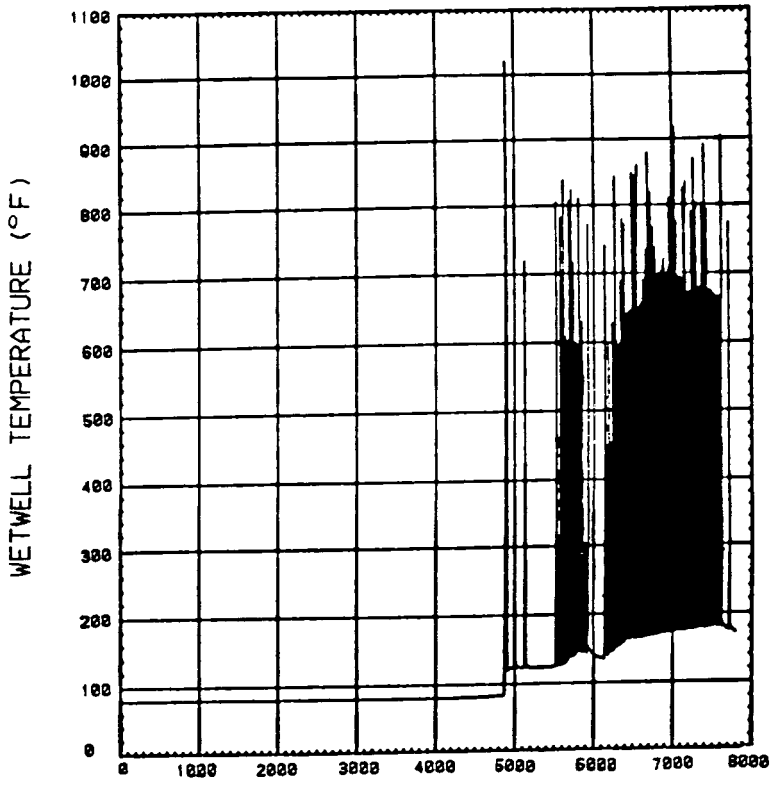
SUMMARY OF RESULTS

Equipment - Limiting Component	Maximum Calculated Surface Temp., F	Maximum Calculated Interior Temp., F	Qualification or Tested Survival Temp., F
Containment Locks and Hatches - seals	216	--	250
Isolation Valve - instrument cables	300	275	320
Electrical Penetrations - cables	300	275	320
Igniter Assembly - transformer	246	210	400
Pressure Transmitter	260	--	303
Pressure Switch	254	--	600
Thermocouple - cables	300	275	320
Radiation Detector - housing	264	--	350
Purge Compressor - motor	184	178	200
Vacuum Breaker - limit switch	212	176	300
Hydrogen Recombiners - cable	300	275	330
Motor Actuators - motor	184	178	200
- switchgear	208	158	200
Air Actuators - solenoid	255	251	330
Limit/Position Switch - gaskets	212	176	300
Cables - w/o conduit	300	275	320
Hydrogen Sampling - fiberglass insulated	--	--	1200
Safety Relief Valves - housing	184	--	340
Containment Sprays - motor actuators	208	158	200



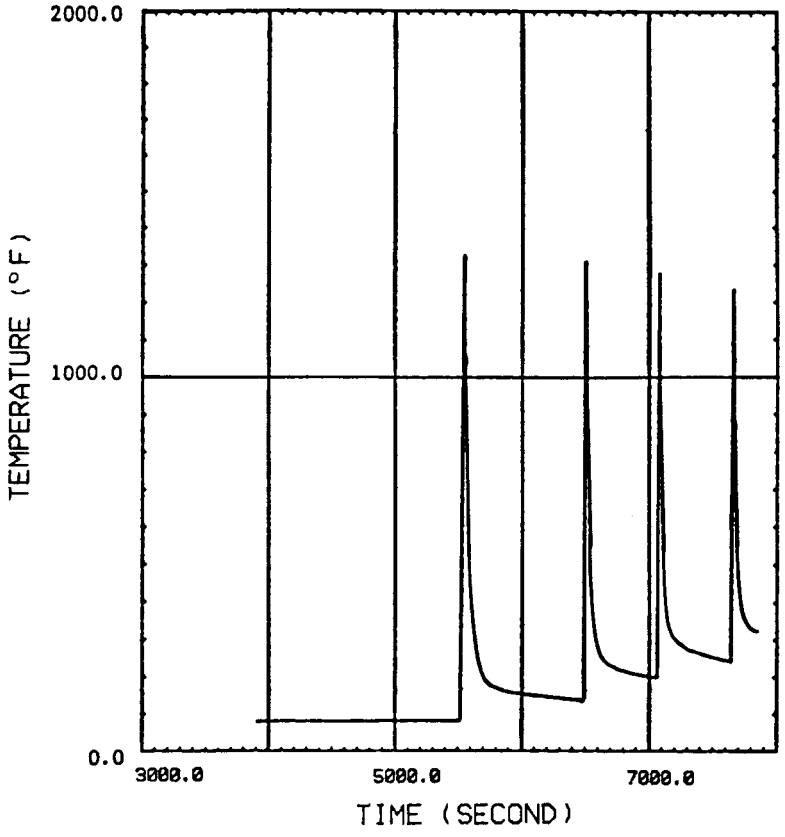
MARK III CONTAINMENT

FIGURE 1



WETWELL TEMPERATURE PROFILE

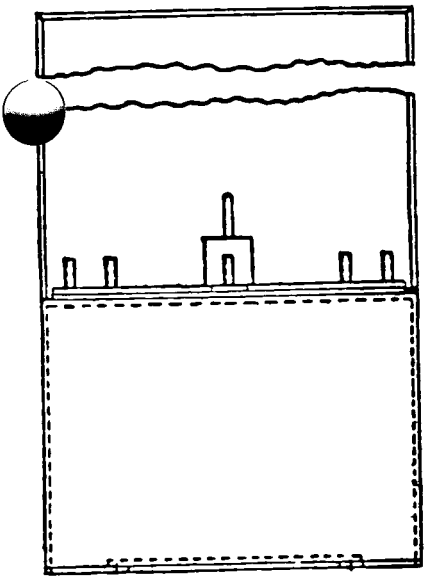
FIGURE 2



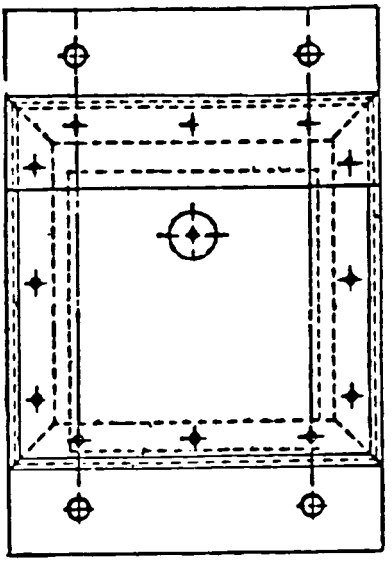
GLOBAL BURN TEMPERATURE PROFILE

FIGURE 3

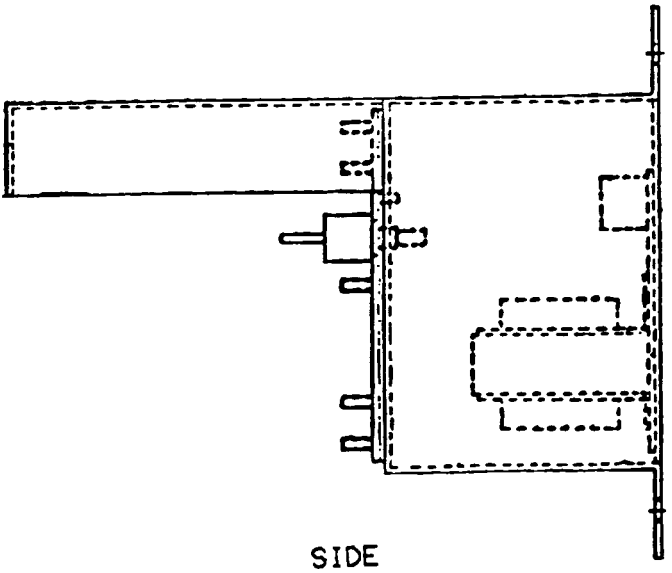
IGNITER BOX



BOTTOM



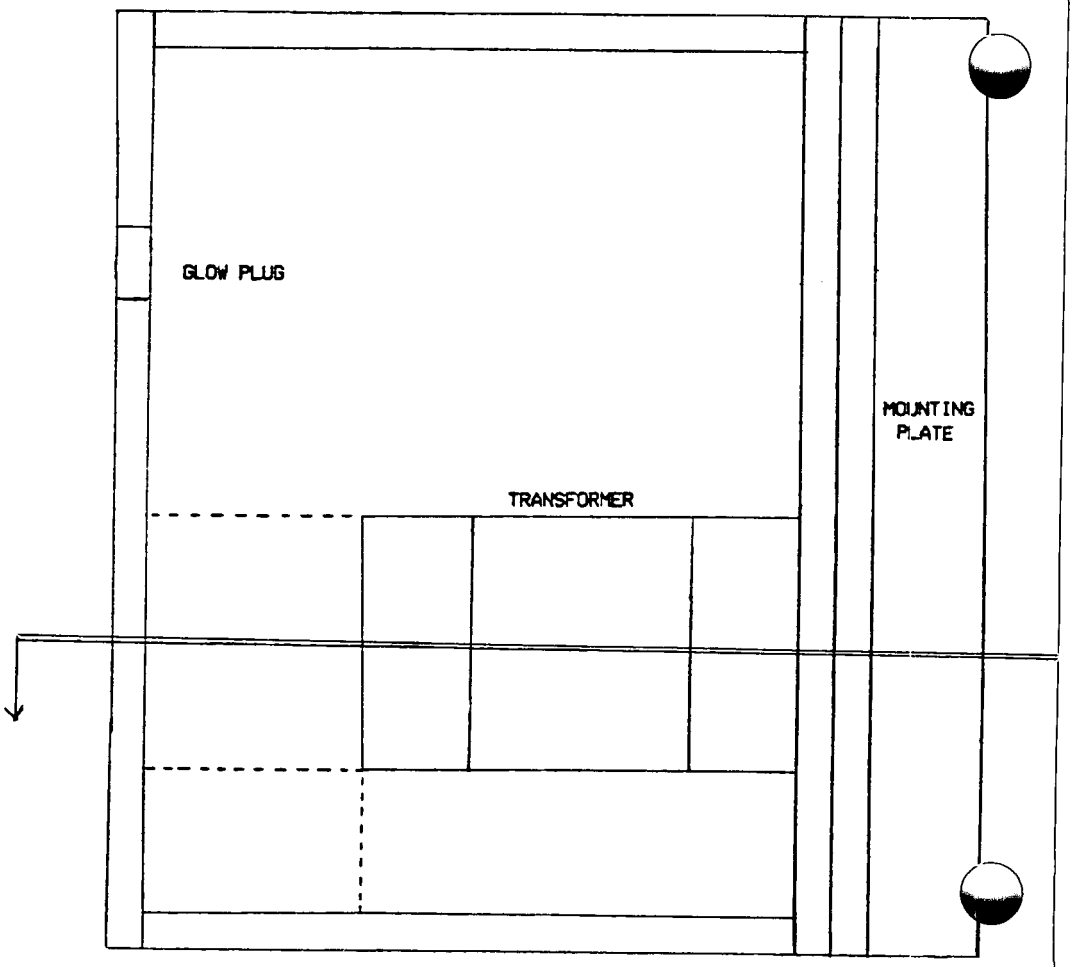
FRONT



SIDE

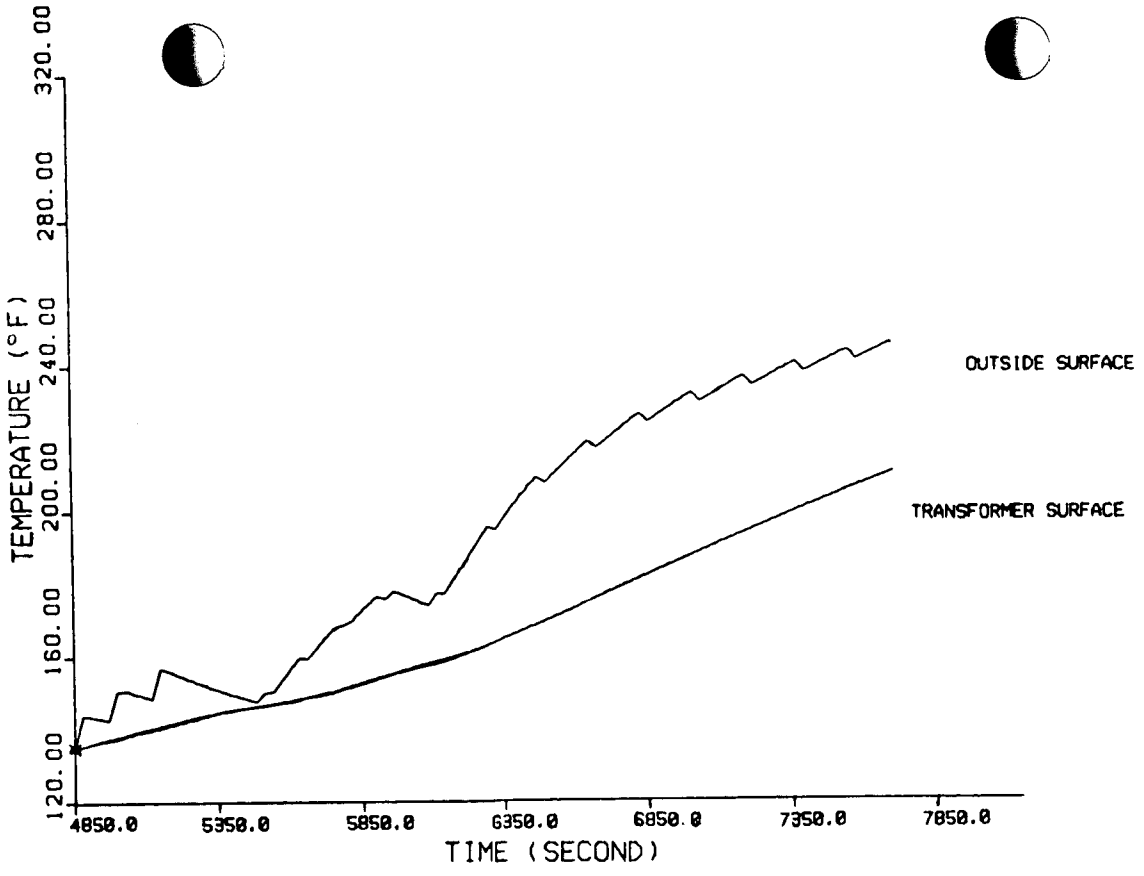
FIGURE 4

TWO DIMENSIONAL IGNITER BOX MODEL



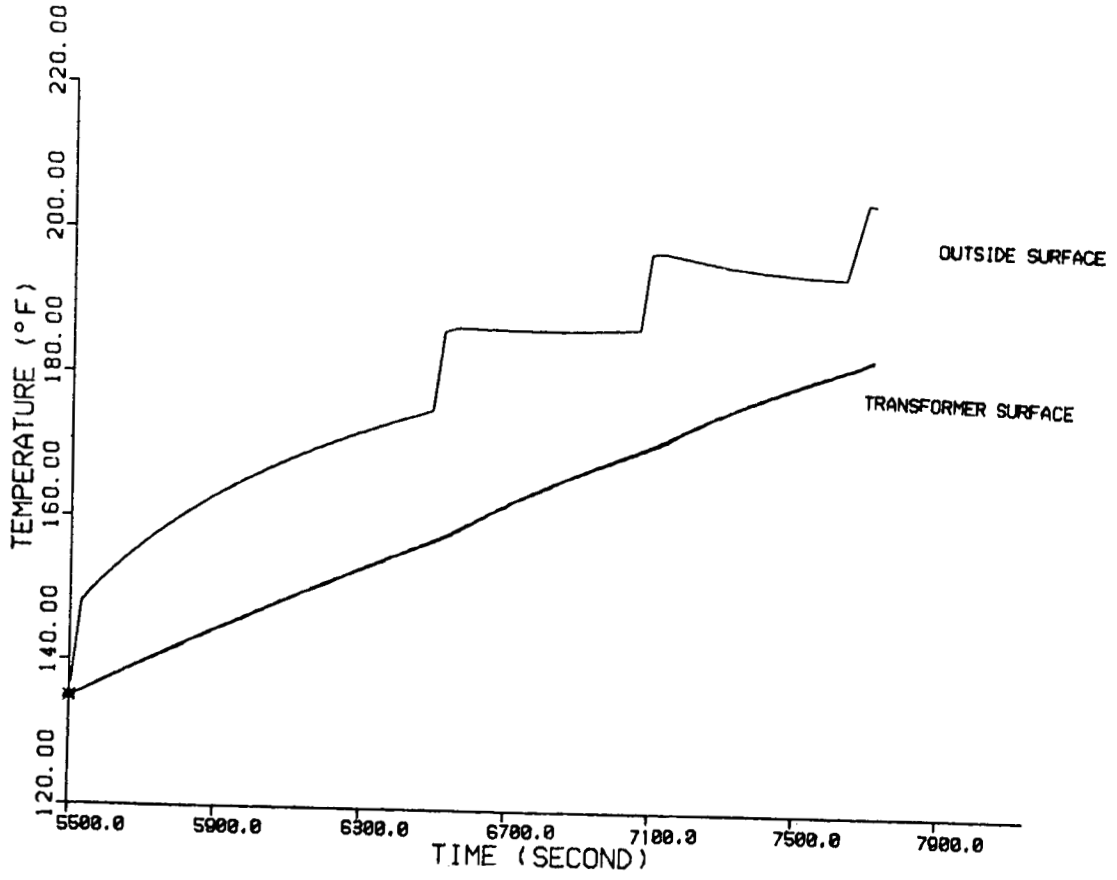
PORTION MODELLED IN THE TWO DIMENSIONAL MODEL

FIGURE 5



IGNITER BOX
WETWELL BURN CASE

FIGURE 6



IGNITER BOX
GLOBAL BURN CASE

FIGURE 7

ELECTRIC CABLE INSULATION PYROLYSIS AND IGNITION RESULTING FROM POTENTIAL HYDROGEN BURN SCENARIOS FOR NUCLEAR CONTAINMENT BUILDINGS

A. L. Berlad*, R. Jaung and W. T. Pratt
Department of Nuclear Energy
Brookhaven National Laboratory
Upton, New York 11973

ABSTRACT

Electric cable insulation in nuclear containment buildings may participate in pyrolysis and combustion processes engendered by hydrogen burn phenomena. This paper examines these pyrolysis/ignition processes of those polymeric materials present in the electric cable insulation and their possible relation to hydrogen burn scenarios.

I. INTRODUCTION AND BACKGROUND

The possibility of synergistic hydrogen burn effects, associated with combustibles other than hydrogen, has been noted earlier.[1,2] Previous investigations at Brookhaven National Laboratory, carried out in connection with the study of "Design Base Fires in Nuclear Power Plants," have provided tabulation of the potential "heat load" (due to complete combustion that may be provided by electric cable insulation materials).[3] For a "typical" nuclear power plant, the containment building is found to contain more than 9,500 Kg (21,000 lbs) of cable insulation.[3] Materials employed as electrical insulators for cables can vary over a wide range.

It has been known for a long time that polymeric materials, such as those encountered in the fabrication of insulation for electrical cables, can undergo a range of processes which lead to combustion. S. L. Madorsky, [4] in an early, comprehensive review of thermal degradation phenomena, summarized the classical experimental characterization of polymeric pyrolysis. Measured rates of molecular degradation and rates of volatilization as functions of temperature, pressure and initial composition are presented for a broad range of organic polymers and their halogenated compounds.[4] In 1971, W. G. Berl and others [5] reviewed the ways in which thermal degradation of polymeric materials may give rise to gaseous species and thereby influence subsequent combustions processes.

Over the last several decades, the combustion of condensed phase, organic materials has been studied extensively. In 1978, Hedges, Baer and Ryan [6] reported on elementary rates of pyrolysis, volatilization, and ignition

* Department of Mechanical Engineering, State University of New York at Stony Brook, New York 11794

of selected polymeric materials. The numerous studies [4-18] concerned with the pyrolysis, ignition and burning of condensed phase organic materials (and their derivates) imply the following features:

(1) In a chemically inert atmosphere, heat transfer to an initially cold organic polymer can lead to degradation of the solid's structure, with one or more of the ensuing processes: depolymerization, melting and gasification, evolution of decomposition product gases, modification of gas phase reactivity.

Temperature-dependent pyrolysis/gasification characteristics for frequently encountered polymeric materials are given in Reference [18]. Results shown are based on Thermogravimetric (TG) methods and/or Differential Thermal Analysis (DTA) methods. As indicated by these and other [5] studies, complex gaseous species are generated by pyrolysis.

(2) In a chemically significant atmosphere (e.g., oxygen-containing) the above noted processes may lead to surface oxidation of the material as well as gas phase oxidation of the products of pyrolysis. Under some circumstances, quasi-steady burning and/or quasi-steady flame spread may be supported by the combustible materials.

(3) The heat transfer processes which support the overall endothermicity of decomposition and volatilization of the original cold polymer may be composed of radiative, convective and conductive fluxes.

(4) In order to characterize the energetics of the ignition of polymeric materials, it has been customary to subject these materials to experimentally measured intense radiative fields. Ignition criteria are then given in terms of (integrated) radiative flux rates [10-13] necessary to achieve "ignition" versus "time to achieve ignition."

(5) Ignition of solids by the complex interaction of a multiplicity of heat transport mechanisms is less well studied than the radiatively induced ignition process. Nevertheless, it is understood that even for the "pure" radiatively induced ignition experiment, conductive-convective cooling by an initially cold atmosphere influences the system's pyrolysis-combustion behavior.

(6) For the case of a hypothetical hydrogen burn in a nuclear containment building, the post-burn convective heat transfer conditions imposed on cable insulators (and other condensed phase combustibles) do not correspond exactly to the experimental conditions previously created in laboratory studies. Laboratory studies of radiatively induced ignition typically employ "normal" room temperature initial conditions. Accordingly, analytic consideration of radiative heat transfer processes only (as in this study) will give rise to calculated ignition times which are longer than those which may actually be encountered in post-hydrogen burn situations.

(7) Radiative ignition of polymeric materials has been found to be influenced by atmospheric composition, pressure, temperature, radiative flux rate, as well as the physical and chemical characteristics of the irradiated material.

Analyses of hypothetical degraded core accidents have been stimulated by the events observed during the recent TMI accident. The work of Reference 2 as well as others [14] consider the consequences of various hypothetical hydrogen release and combustion events. All considered hydrogen burn scenarios imply an elevated temperature and gaseous H_2O in the containment atmosphere. For the nonadiabatic (real) case, peak post-hydrogen burn atmospheric temperatures are transient. Nevertheless, peak temperatures of more than 1700°K can be reached even for hydrogen-air burns containing excess air concentrations.[2,14] Such large containment volumes of hot gases can serve to pyrolyze and gasify (and possibly, burn) part of the more than 9,500 Kg of cable insulation which may reside within the containment building. Quantitative assessment of the interactions between cable insulation pyrolysis/gasification/combustion processes and hypothetical hydrogen burn scenarios is required in order to more adequately identify the temperature and pressure loadings to which containment buildings may be subjected. This paper examines these pyrolysis/ignition processes and their possible relation to hypothetical hydrogen burn scenarios in nuclear containment buildings.

II. THE IGNITION OF COMBUSTIBLE SOLIDS

There are a number of studies concerned with the ignition of large combustible solids. Large fires (in buildings, in forests, etc.) generally involve the ignition of large scale solid materials by energy transport from nearby high temperature gases. The combustible solid's preignition processes are driven by energy transport to the combustible solid and include:

(a) energy deposition "at" the solid's surface by conduction, convection and radiation (for optically opaque solids involving nonabsorbing gaseous pyrolysis products)

(b) volumetric energy deposition (and conversion) in the neighborhood of the solid's surface (where optically active gases and molecular absorbing solids are involved). This is the typical case for polymeric organic materials.

(c) pyrolysis and degradation [4] of the heated solid, giving rise to a high temperature flux of combustible gases entering the gas phase.

As a result of processes (a)-(c) above, frequently encountered ignition (i.e., onset of quasi-steady burning) may occur due to

(a) the combustibility of the high temperature gases generated by the solid, and

(b) the presence of an "ignition source" (flame, or other high temperature neighboring igniter). Where such a small "ignition source" initiates the quasi-steady burning, the ignition process is deemed to be "piloted ignition."

It is also possible that large solid polymeric materials may be ignited by simply being engulfed in a large volume of very hot gases (i.e., combustion products). These serve both to provide the energy flux needed to create a flow of combustible gases from solid's surface and to ignite them.

Pyrolysis-Vaporization Processes

Solid polymeric materials undergo varying kinetic rates of (temperature-dependent) thermal degradation. Studies of the characteristic pyrolysis and vaporization kinetics have been performed by a number of investigations for a broad range of materials.[4,5,7,15] A. D. Baer[15] has suggested that the thermal degradation of a solid (such as a medium density polyethylene of 948 Kg/m^3) can be represented by the global reaction sequence:

(1) $S_1 \xrightarrow{k_{12}} S_2$

(2) $S_2 \xrightarrow{k_{23}} S_3 + G_6$

(3) $S_3 \xrightarrow{k_{34}} S_4 + G_7$

(4) $S_4 \xrightarrow{k_{45}} S_5 + G_8$

(5) $S_1 \xrightarrow{k_{14}} S_4$

Where the schematics (1)-(5) correspond to the rate expression:

$$(6) \qquad \frac{d}{dt}\left[\frac{M_i}{M_{i,o}}\right] = \sum_j A_{ij}\, e^{-E_{ij}/RT} = k_{ij}$$

Here, M_i = mass of the i^{th} species; $M_{i,o}$ = initial mass of the i^{th} species, k_{ij} = rate constant for degradation of i^{th} solid to the j^{th} solid, S_i = molecular solid of the i^{th} species, A_{ij} = Preexponential factor, E_{ij} = activation energy, G_i = molecular gas of i^{th} species.

One may also define (f_{ij}) to be the fraction of the solid S_i which is retained (as a solid) upon degradation to S_j. Thus

$$f_{ij} \equiv \frac{m_{si}-m_{sj}}{m_{si}}$$

Studies by Baer [15] show, for this specific medium density polyethylene, that the following parameters are characteristic:

Reaction Rate	A_{ij}	$E_{ij/R}$	f_{ij}
	sec^{-1}	°K	-
1,2	6.19×10^{4}	8460	1.00
2,3	3.36×10^{5}	8280	0.58
3,4	3.58×10^{9}	16000	0.52
4,5	5.55×10^{6}	12900	0.17
1,4	4.50×10^{12}	25300	1.00

These data may be used, along with independent information regarding local temperature fields, to calculate thermal degradation rates - even for a nonisothermal solid.

Similar sets of kinetic rate expressions may be written for other polymeric materials of interest.[15-17]

Diverse materials may be used in the fabrication of electric cable insulators. Halogenated compounds are frequently employed because of their superior fire resistant characteristics. Uehara and Suzuki [18] studied the gaseous decomposition products given off by heated samples of various chlorinated polyethylene materials. Gaseous species typically found during thermal degradation in the 373°K-773°K range include: Ethylene, Propylene, Ethane, Propane, Butene, Butane, Hydrogen Chloride and Benzene. These are all species which may participate in the dynamics of a hydrogen-air burn. If significant quantities of such species are liberated to a nuclear-containment atmosphere, their effects would extend to influencing containment building peak pressures and temperatures. Table 1 is taken directly from Reference 18 and provides observed activation energies for a spectrum of substituted polyethylenes.

The Ignition Process

Large combustible solids may be ignited in a number of ways. Additionally, successful ignition may lead to several different modes of quasi-steady burning.

The ignition of a large combustible solid by exposure to a localized source of hot gases (e.g., a small flame) is a commonly observed phenomenon. Where successful ignition occurs, there are at least two possible cases of quasi-steady combustion. First, a spatially localized flame may be

established which slowly "burns through" a portion of the large solid - but does not propagate over (and through) the much larger spatial extent of the large combustible mass. For this case of limited, local quasi-steady burning, the scale of the ignition source (and of the portion of the solid eventually consumed by combustion) is small compared to the extent of the entire combustible solid material. Also of substantial significance is the quasi-steady combustion process which spreads, as a wave phenomenon, over the full extent of the large solid. Such a flame spread phenomenon may effectively serve to "ignite" the entirety of the large combustible solid material. Where such a flame spread process is possible, subsequent burning through, in time, of the entirety of the large combustible material is possible.

Other kinds of ignition sources may give rise to quasi-steady combustion phenomena which are generally related to either one, or both, of the two cases cited above.

In order to characterize the flammability of large combustible solids, a number of experimental approaches have been developed. Because of its quantitative nature and ease of utilization radiative ignition of small (several inches on a side) samples of large combustible solids has been a favored experimental method of characterizing the flammability of materials of fundamental and practical interest. In this method (e.g., references 10 and 11) a combustible sample of interest is exposed to a measured, steady-state radiation field (visible-infrared) which provides a known surface energy flux rate (Kw/m^2). Experimental observation is then made of the following parameters:[11]

T_{ig} = ignition delay (sec), q''_o = the imposed steady radative flux rate to the sample surface (Kw/m^2) below which ignition does not occur, q''_e = the effective (imposed) radiative flux rate to the sample surface which leads to ignition of the entire surface (in the presence of a small, pilot flame) at time T_{ig}.

Data so obtained have been correlated[11] by the expression:

$$(\dot{q}''_e = \dot{q}''_o)\ T_{ig} = E_{eff} \tag{7}$$

where

E_{eff} = the effective (integrated) energy required to radiatively ignite the sample of interest.

Although equation (7) must be considered to be an approximation, it has been used to successfully correlate the flammability characteristics of combustible solids - including those of samples of electric cables.[11] For hypothetical post-hydrogen burn conditions, the radiative field is associated with a nonadiabatic containment building and a time-dependent (decaying) temperature field. One may construct a generalization of equation (7) which considers time-dependent radiative fluxes and which reduces (exactly) to the steady state relation for that special case. Equation (8) is such a relationship:

(8) $$\int_0^{T_{ig}} (\dot{q}''_e - \dot{c}''_o)dt = E_{eff}$$

Equation (8) is employed in this study to consider the flammability of previously considered electric cable insulators, when subjected to hypothetical post-hydrogen burn radiative fields in containment building atmospheres.

III. PREVIOUS EXPERIMENTAL RESULTS FOR THE RADIATIVE IGNITION OF CABLE INSULATION

Tewarson, et al. [11] have studied experimentally the radiative ignition of electric cable array samples. Values of their observed and calculated characteristic parameters (from equation (7)) are provided in Table 2. Table 2 shows that the best cable samples require much greater integrated radiative energy inputs in order to achieve ignition. It also shows that all cable samples are flammable - including those which pass IEEE-383 rating tests and including the best sample studied, TEFLON.

Although radiative ignition experiments permit direct characterization of the integrated radiative energy deposition required for ignition, the ignition delay is also prescribed, in part, by other physical processes which are not controlled by the experimenter (unlike the imposed radiative flux rate). An initially cold atmosphere implies "convective cooling" of the heated cable sample during its heat-up period. Additionally, the high intensity radiative source employed in these experiments subtends (at the sample) only a portion of the hemispherical solid angle. Accordingly, in the Tewarson, et al. studies, the heat-up period starts with a cold atmosphere and the cable array sample radiatively and convectively loses heat to the various cold boundaries of the experimental apparatus.

The roles of these convective and (cable surface) radiative loss mechanisms are implicit in the results reported by Tewarson.[11] Tewarson's work [11] also reveals the possible chemical consequences of the radiatively induced ignition and combustion of cable array samples.

The yields observed by Tewarson are associated with massive (realistic) samples of cable arrays under conditions of pyrolysis and subsequent ignition and burning. These results do not (and should not) be the same as those obtained under inert atmospheric conditions (e.g., reference 6).

IV. HYPOTHETICAL POST-HYDROGEN BURN ATMOSPHERIC CONDITIONS FOR A NUCLEAR CONTAINMENT BUILDING

Studies at BNL and elsewhere (e.g., references 2, 14) provide the temperature-pressure-composition conditions of a nuclear containment building atmosphere, subsequent to a hypothetical burn. For a post-deflagration condition associated with a "uniform burn" (hydrogen uniformly distributed in space,

prior to combustion) a high temperature optically active (infrared radiative) atmosphere exists. Where the only fuel involved in the "burn" is hydrogen, the only molecular infrared radiator is the water molecule. For the more complex case where [CO] and other [CO_2] - producing fuels may be present[2,19] partially overlapping infrared (vibration-rotation) bands of [H_2O] and [CO_2] will be active radiators.

Because of the post-burn high temperatures (and large spatial scale of containment building), the radiative flux density impinging upon a cable array sample, located within containment, may be substantial. In order to calculate the radiative flux rates involved, containment atmosphere pressures, temperatures and compositions must be known. Additionally, emissivity data for molecular radiators of significance are also required. In his pioneering contributions, H. Hottel (works summarized in Chapter III of reference 20) provided the appropriate equations of radiative transport. Hottel [20] also provided infrared emissivity data for [CO_2] and [H_2O] which have since been improved upon by Smith and Shen.[21] In a comprehensive study of the infrared emissivities to be employed in gray gas radiative transport models, Smith and Shen provide a compendium of emissivity/absorptivity data for gas temperatures to 3000°K, and for various atmospheric compositions containing [H_2O] and/or [CO_2].

One may combine the experimentally determined cable flammability parameters of Tewarson, et al., the infrared radiative emissivity data of Smith and Shen, a characteristic post-hydrogen burn containment temperature history (e.g., reference 22), and equation (8) - to calculate the expected radiatively-induced ignition times for various cable arrays. Equation (8) has been employed to deduce the delay between the establishment of a hypothetical hydrogen burn's peak temperature and the time at which ignition occurs. Figures (1) and (2) illustrate the ease with which the radiative field (which derives from the post-hydrogen-burn cooling curve given in reference 22) can ignite the very flammable (FMRC-designated) cable array PE/PVC#5. Intersection of the two curves of Figures (2) is not shown and ignition of cable #5 occurs for very early times (less than 3 seconds). The lower curve is based on the FMRC findings for a particularly flammable polyethylene/polyvinylchloride cable (#5) and separates the power-time regime which yields non-ignition (below the curve) from the ignition regime (above the curve). The upper curve gives the infrared radiative power density (based on reference 22 data and Figure 1) imposed on any cable sample, as a function of time. Emissivity data are taken from Smith and Shen's work. Calculations performed consider H_2O to be the only emitting species, neglecting [CO], [CO_2], and other possible infrared sources. As noted earlier, [H_2O], [CO], [CO_2] etc. gases are associated with partially overlapping infrared bands. For these (and other cited reasons) our calculated ignition delays represent upper limit times for the more complex real gas mixtures.

Calculated radiative ignition delays for hypothetical post-hydrogen burn conditions are given in Table (3). All cable array samples for which calculations have been performed are the same as those experimentally studied at FMRC.[11] As noted earlier, ambient atmospheric composition, temperature and pressure can affect the ignition delays observed for polymeric materials. The work of Niioka and Williams [10] and of Ohlemiller and Summerfield [23]

illustrate the effects of oxygen partial pressure and of total pressure on the radiatively induced ignition delay for a selected polymeric material. Similar behavior is to be expected for other polymers. Figures (3) and (4) show how the depleted oxygen concentrations (of a post-hydrogen-burn containment atmosphere) correspond to longer ignition delays. However, the correspondingly higher-than-ambient atmospheric temperatures (of a post-hydrogen-burn containment atmosphere) imply shorter than herein calculated ignition delays. The precise ignition delay effects of the full range of initial atmospheric temperature, pressure and composition variations await further study.

All samples studied (with the possible exception of TEFLON) are readily ignited by the time-dependent radiative fields considered. Thus, ignited samples include several which have successfully satisfied (Pass) the IEEE-383 rating test.

V. PROBLEM CHARACTERIZATION AND MITIGATION

Electric cable insulation in nuclear containment buildings may be pyrolyzed/gasified/burnt as a result of hydrogen burns. The possible effects of such pyrolysis, gasification, and combustion may impact post hydrogen burn environments in containment. These environments can influence the survivability of equipment and the integrity of the containment.

Such consideration should include the cases of "weak" hydrogen burns (less that 10 percent hydrogen) which may/may not lead to cable ignition - but may certainly involve gasification-pyrolysis processes. Even where gasification-pyrolysis of cable insulation does not lead to immediate radiative ignition, the combustible gases liberated (e.g., CH_4 and H_2) may participate in the determination of containment pressure-temperature histories, through hydrogen burns which could occur at subsequent times.

For "strong" hydrogen burns, the energetics of cable pyrolysis/combustion is clearly a determinant of subsequent pressure-temperature histories.

Neither radiatively-induced cable insulation gasification nor radiatively-induced combustion leads to consequences that may be generally ignored. Consider, for example, the pyrolysis and gasification of vinyl chloride. The equilibrum decompositon products are generally specified [5] through the schematics:

(9) $$[2H_2C = CHCl] \rightleftarrows 2HCl + CH_4 + 3C$$

(10) $$CH_4 \rightleftarrows C + 2H_2$$

The equilibrum combustion products are indicated by the irreversible overall process:

(11) $$[H_2C = CHCl] + [2.5O_2] \rightarrow 2CO_2 + HCl + C$$

The mix of cable insulation materials in a given containment building may be a varied one. The mix for a given containment building need not correspond to that for some other containment building. Some cable arrays rest relatively unshielded in cable trays. Other cable arrays may be encased in steel conduit. None of these arrangements is necessarily "safe". Steel conduit is generally a strong absorber of infrared radiation. It displays a very high thermal conductivity and a limited heat capacity. Accordingly, cable samples in steel conduit may be expected to undergo substantial pyrolysis/gasification processes during/after hydrogen burns. Even where "surface burning" of the so encased cable sample is prevented by the steel conduit, escaping pyrolysis products may play a significant role in containment pressure-temperature history (as noted). Non-encased cable samples with an optical view factor of unity correspond to calculations presented above on ignition delays.

There are a number of methods of mitigation or elimination of the possible problems considered. Radiative transfer suppression may be achieved through radiative shielding of cable arrays. Metallic oxides (ceramics) are generally both chemically inert and good radiative reflectors (at moderate temperatures). As such, they may be used to radiatively shield both "naked" and "encased" cable arrays. Also, upgrading of the polymeric quality of a cable insulator is advantageous. Perhaps the most advantageous arrangement is one whereby selected ceramic cable insulation is used instead of the generally encountered hydrocarbon-based polymers. Selected high temperature ceramic insulators combine the highly desirable features of good electrical insulation, chemical inertness over the full temperature range, and substantial infrared reflectivities at moderate temperatures.

VI. ACKNOWLEDGEMENTS

This work was carried out under the auspices of the U. S. Nuclear Regulatory Commission. The authors thank R. A. Bari and J. L. Boccio for helpful discussions and for reviewing and commenting on the manuscript.

VII. REFERENCES

1. A. L. Berlad, M. Sibulkin, and C. H. Yang, "Hydrogen Combustion Characteristics Related to Reactor Accidents," BNL Informal Report, January (1981).

2. W. T. Pratt and R. A. Bari, "Containment Response During Degraded Core Accidents Initiated By Transients and Small Break LOCA in the Zion/Indian Point Reactor Plants," BNL-NUREG-51415, July (1981).

3. I. B. Asp, E. A. MacDougall and R. E. Hall, "Design Base Fires In Nuclear Power Plants," BNL Informal Report: BNL-NUREG-23392, October (1977).

4. S. L. Madorsky, "Thermal Degradation of Organic Polymers," Pub: John Wiley (1964).

REFERENCES (cont'd)

5. D. R. Stull, Fire Research Abstracts and Reviews 13, No. 3, P. 161 (1971).

6. J. E. Hedges, A. D. Baer, and N. W. Ryan, "Pyrolysis and Ignition of Polymers Under Approximated Fire Conditions." XVII Symposium (International) on Combustion p. 1173 (1979) Pub: The Combustion Inititate.

7. S. B. Martin and A. E. Lipska, "A Review of Pyrolysis Techniques for Polymeric Solids". p.207 of Proc. SRI Conf. on Experimental Methods In Fire Research, Pub: S.R.I., May (1974).

8. A. Fernandez-Pello and F. A. Williams, "Experimental Techniques in the Study of Laminar Flame Spread Over Solid Combustibles." Ibid p. 297.

9. A. L. Berlad and C. R. Krishna, "Transport Mechanisms In Fire Spread." Ibid p. 347.

10. T. Niioka and F. A. Williams, "Relationship Between Theory and Experiment for Radiant Ignition of Solids," XVII Symposium (International) on Combustion, p. 1163 (1978).

11. A. Tewarson, J. L. Lee and R. F. Pion, "Categorization of Cable Flammability," Factory Mutual Research Corp., EPRI Report #NP-1200, October (1979).

12. M. Levenson "R & D Status Report on Cable Flammability Research." EPRI Journal, p. 54, May (1980).

13. J. DeRis "Fire Radiation-A Review," XVII Symposium (International) on Combustion p. 1003, Pub: The Combustions Institute, (1979).

14. Anon: "Evaluation of Hydrogen Combustibility and Control Under Degraded Core Conditions," Pilgrim-2 Generating Station, Bechtel Power Corp. Report (San Francisco Power Division), May (1980).

15. A. D. Baer, "Pyrolysis of Polymer Films in Air at High Temperatures and at High Heating Rates," (Private communication). In Press: J. Fire and Flammability (1981).

16. J. F. Rabek, "Comprehensive Chemical Kinetics, (Vol. 14) Degradation of Polymers", edited by C. H. Bamford and C. F. H. Tipper. Pub: Elsevier Scientific Publishing Co., Amsterdam, (1975).

17. Hedges, J. H. "Ignition and Pyrolysis of Polymer Films," PhD. Dissertation, Dept. of Chem. Eng., Univ. of Utah, (1978).

18. Y. Uehara and S. Suzuki, "Effect of Chlorinated-Poylethylene on Thermal Degradation of Polyethylene in an Inert Atmosphere," Proc. C. P. Butler Conference on "Experimental Methods In Fire Research." Stanford Res. Institute, May (1974).

REFERENCES (cont'd)

19. R. Jaung, R. A. Bari and W. T. Pratt, "Carbon Monoxide Burning During Core Meltdown in a PWR," Trans. Am. Nucl. Soc., 39, 606 (1981).

20. W. H. McAdams, "Heat Transmission," Pub: McGraw-Hill, 2nd Ed., (1942).

21. T. F. Smith and Z-F Shen, "Evaluation of Coefficients for the Weighted Sum of Gray Gas Models," Univ. of Iowa, College of Engineering Technical Report E-TFS-80-007, December (1980).

22. Anon. "Evaluation of Hydrogen Combustibility and Control Under Degraded Core Conditions - Pilgrim - 2 Generating Station," Bechtel Power Corp. Report, May (1980).

23. T. J. Ohlemiller and M. Summerfield. AFOSR-TR-69-2147, August (1969).

TABLE (1)*

PYROLYSIS ACTIVATION ENERGIES FOR
PE-C1PE MIXTURES

Material	Activation Energy (K/cal/mol)					
	Melting		Dehydrochlorination		Decomposition	
	TG	DTA	TG	DTA	TG	DTA
PE	-	51.9	-	-	71.7 (59.8)	54.8
20%PC1PE-PE	-	53.8	(32.3)	-	67.5 (64.0)	56.0
50	-		27.8 (32.6)		69.9 (68.0)	
80	-		28.0		65.1	
PC1PE	-		29.4 (32.3)	34.0	59.7 (61.8)	59.6
20%RC1PE-PE	-				68.9	
40	-		28.4		70.6	
60	-		29.0		60.6	
80	-		29.0		64.0	
RC1PE	-		28.4	31.4	61.1	65.9
20%Sb_2O_3-PC1PE			32.0		54.0	
36%			31.7		53.0	
56%			33.3		48.4	

( ) indicate E at $\left(\frac{dT}{dt}\right)$ = 10°C/min.

TG - Thermogravetric

DTA - Differential Thermal Analysis

* Reproduced from Reference 18

TABLE (2)*

IGNITION PARAMETERS FOR CABLE ARRAY SAMPLES

(FMRC DATA)

No.	Cable Sample	E_{eff}[a] (kJ/m^2)	$\dot{q}''_o$[b] (kW/m^2)	IEEE-383 Rating[c]
20	Teflon	8,696	43	Pass
	Polyethylene (granular)[d]	3,744	19	NA
	Polyvinyl chloride (granular)[d]	3,320	21	NA
21	Silicone, glass braid	3,125	29	
	Polyethylene/25%Cℓ (granular)[d]	3,011	26	NA
	Polyethylene/42%Cℓ (granular)[d]	1,969	22	NA
	Polyethylene/36%Cℓ (granular)[d]	1,891	26	NA
13	XPE/FRXPE	1,688	22	Pass
	Polyethylene foam (rigid)[d]	1,641	22	NA
16	XPE/Cℓ·S·PE	1,105	33	
9	PE,PP/FRCℓ·S·PE	890	36	
17	XPE/Neo	826	34	Pass
22	Silicone, glass braid/asbestos	778	14	Pass
	Polyurethane foam (rigid)[d]	772	23	NA
4	PE/PVC	728	36	Fail
5	PE/PVC	347	22	Fail

[a] E_{eff} is defined as the 'effective' energy associated with achieving a flammable cable sample vapor/air mixture near the surface

[b] $\dot{q}''_o$ is defined as the critical heat flux at or below which ignition cannot be achieved

[c] IEEE-383 rating as provided by the suppliers

[d] Research samples

NA - Not applicable

* Reproduced from Reference 11

TABLE (3)

CALCULATED CABLE ARRAY IGNITION TIMES DUE TO POST-HYDROGEN BURN RADIATIVE FIELDS

Cable Designation	Rating (IEEE-383)	E_{eff} KJ/m^2	$\dot{q}''_o$ KW/m^2	T_{ig} (sec)	
				$\%H_2$=19	$\%H_2$=13
TEFLON (#20)	PASS	3696	43	-----	-----
Silicone, Glass Braid (#21)	Research Sample	3125	29	<15	-----
XPE-FRXPE (#13)	PASS	1688	22	≈6	≈26
XPE-NEO (#17)	PASS	826	34	<3	<14
PE-PVC (#5)	FAIL	347	22	<3	≈4
Silicone, Glass Braid, Asbestos (#22)	PASS	778	14	<3	≈9

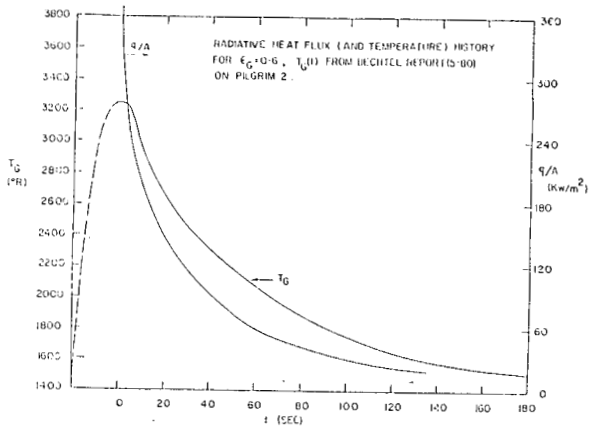


Figure 1 Radiative Heat Flux and Temperature History for a Cable Array in Pilgrim 2 Containment.

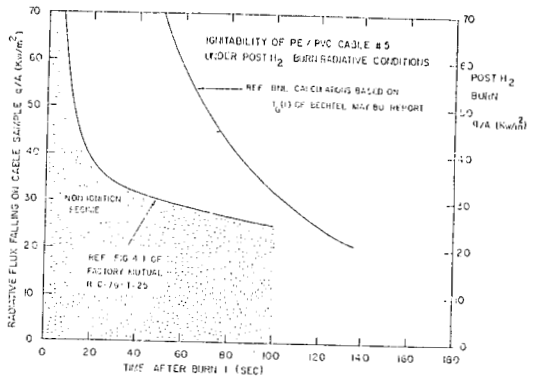


Figure 2 Ignitability of PE/PVC Cable No. 5 Under Post-H_2 Burn Conditions.

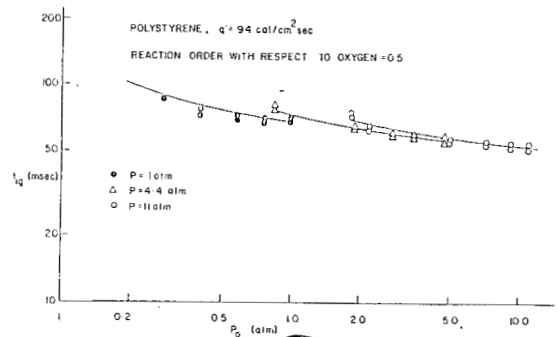


Figure 3 Radiativ[illegible]nduced Ignition Time vs. Oxygen [illegible]artial Pressure for Polystyrene, Over a Range of Total

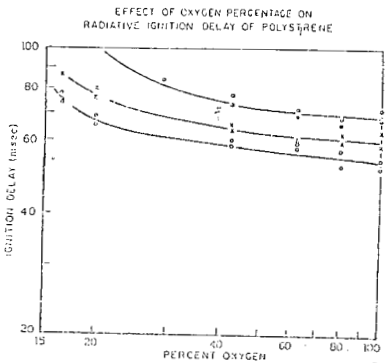


Figure 4 Radiatively Indu[illegible] Ignition Time vs. Percent Oxygen.

REMARKS ON REGULATORY ISSUES OF MAINTAINING CONTAINMENT INTEGRITY

Commissioner John F. Ahearne
U. S. Nuclear Regulatory Commission

Workshop on Containment Integrity

Sandia Laboratories

Quality Inn, Pentagon City, Virginia

June 8, 1982

I would like to speak to you carefully this afternoon about a subject which you know much more about than I do, namely, containment design. Obviously I am not going to provide you with new insights into how best or how better to design containments, nor am I going to offer you solutions to any of the more difficult analysis problems. What I will try to do is provide you the perspective from the Commission, as seen by one Commissioner, on the role of containments and on some of the problems which perhaps you can solve. In order to provide a setting for my remarks, it is necessary for me to review some material. Some of you are very familiar with most of it and most of you are familiar with some of it.

Over the decades in which nuclear power has been under development, there not only has been a change in view as to whether a containment is needed, there also has been a fairly substantial change in the role to be filled by that containment. As you may know, Russia for a long time did not use containments, apparently not believing they were necessary. It is not obvious at the moment whether Russia is shifting to a belief containments are necessary or that containments are necessary to export reactors. Some countries use more elaborate containment systems than we do, for example, Germany. Apparently the British are considering use of a double containment if they go ahead with a PWR.

In the early development of U. S. nuclear power, containments were not seen as absolutely necessary. However, in 1956 Willard Libby, Acting Chairman of the AEC, responding to a question from Senator Hickenlooper on the Joint Committee, stated "it is expected that power reactors such as that now under construction at Shippingport, Pennsylvania will rely more upon the philosophy of containment than isolation as a means of protecting the public against the consequences of an improbable accident. . . . " This was not totally accepted in the industry. In 1958, Atomics International in proposing a small (45 MWth) reactor to be located in Piqua,

Ohio did not propose a containment. The AEC regulatory staff position on that proposal was that experience to date "was inadequate to support this position, even if it might be true. The Regulatory Staff felt that containment was mandatory in a moderately populated region." In this case the site was just outside the city limits and only a few hundred feet from a temporary residential area. In response the company proposed a new type of containment. The ACRS position on this reactor was that "the proposed unconventional type of containment [must be] replaced by a more substantial and dependable system." Subsequently, such a containment was proposed and the ACRS reported favorably.

The current Standard Review Plan for containment functional design describes the containment as "the final barrier against the release of significant amounts of radioactive fission products in the event of an accident." The Standard Review Plan for PWR dry containments states "the primary reactor containment is the final barrier of the defense-in-depth concept to protect against the uncontrolled release of radioactivity. . . ." This description as the final barrier goes back more than twenty years. For example, in 1959 Dr. Beck of the Regulatory Staff wrote "the external containment vessel, as a barrier of last resort against releases of radioactivity to public areas, offers a unique protection, completely independent of all other safety devices and engineering safeguards and its dependability is unaffected by errors in safety analyses and judgement of the reactor assembly. It stands as a visually obvious and intuitively attractive bulwark against the possible consequences of errors in reactor design, malfunction and misoperation which are admittedly present in any human undertaking." Obviously that was before NEPA and the rhetoric of a containment as being attractive has long since been submerged in public opposition against those buildings. Of course, cooling towers have replaced containment buildings as the prime environmental eyesore of a nuclear power plant. Nevertheless, there was a flavor in those comments of Dr. Beck which leads one to believe that perhaps the containment was supposed to operate by itself and perhaps do much more than we currently describe containments as being able to do. And that interpretation would be correct. Containments were thought to be able to do more. The current Standard Review Plan states "[t]he containment design basis includes the effects of stored energy in the reactor coolant system, decay energy, and energy from other sources, such as the secondary system, and metal-water reactions including the

recombination of hydrogen and oxygen. The containment system is not required to be a complete and independent safeguard against a LOCA by itself. . . ." Acceptance criteria for PWR dry containments, include "the containment design pressure should provide at least a 10% margin above the accepted peak calculated containment pressure following a loss of coolant accident. . . ." And "the selection [of the loss of coolant accident for analysis] should result in the highest calculated containment pressure." The highest expected pressure obviously depends upon what type of accident analysis one makes. So, for example, if you assume a 100 percent metal-water reaction of all the zirconium and allow the produced hydrogen to detonate, the pressure can exceed the strengths of current containments.

However, fifteen to twenty years ago it was expected that containments could retain the worst accident. For example, in 1962 a Westinghouse representative gave a paper on facility design in which he described a new concept that had been developed: "the new no leakage Stone and Webster design concept utilizes two layers of steel inside a reinforced concrete vessel. This vessel is designed to withstand the maximum internal pressure generated after rupture of the primary system." He went on to say "the entire structure is designed to withstand the effects of the worst conceivable nuclear incident (generally referred to as the maximum hypothetical accident). . . . Such a hypothetical accident might include core meltdown, sudden release of energy stored in the coolant, or sudden release of energy due to chemical reaction within the reactor." Later, the Consolidated Edison Company in the subsequently withdrawn application for the Ravenswood site described their containment as being able to provide "no leakage of radioactivity even under the worst conceivable accident conditions." These descriptions encompassed core meltdown. The then Director of the AEC Division of Reactor Licensing in 1965 was quoted as indicating to Consolidated Edison "that [the Division of Reactor Licensing and the ACRS] would look at the reactor system itself to see that meltdown is prevented for all including the biggest rupture. Then, the containment is put around it in order that there be protection even if the others fail, and metal-water reactions occur." In this same discussion, the Westinghouse position was given to be "that the containment was satisfactory if the safety injection system does not work at all."

In the mid-1960's this position began to shift, according to Dave Okrent in his fascinating History of the Evolution of Light Water Reactor Safety in the United States (from which most of the historical references in this paper are taken). In approximately 1965 to 1966 discussions began to focus upon containments and core melt. Okrent writes "it seems fair to assume that in the spring of 1965, if there were groups or individuals who made a direct connection between large scale core melting and a loss of containment integrity, it was not a widely held piece of knowledge. . . ." However, by June 1966 the ACRS was unequivocally relating core melt to containment failure. Both Brookhaven and Dr. Beck "had reached the conclusion that for the large water reactors, full scale core melt would be associated with loss of containment integrity. . . " There still was intensive examination by the ACRS, Westinghouse, and General Electric "of the possibility of providing engineered safeguards which would maintain containment integrity in the presence of large scale core melt for the large reactors being considered."

Finally, it is interesting to note that the 1963 AEC Annual Report described the loss of fluid test facility (LOFT) as being designed to prove that the containment would withstand a meltdown. The proposed LOFT test included a meltdown of the nuclear fuel.

After reviewing that history, let me now turn to the Commission's current situation, as we look around for help on ways to analyze and either assess or improve the safety of power plants. A hydrogen explosion at Three Mile Island has caused a major rethinking in the design requirements for containments.

The Commission has come a long way since those days in its understanding of the function of containments. We now are beginning to address standardized plants and future designs. I imagine many designers would much prefer to address what will be the future design. However, I think you should concentrate on better ways to analyze the current designs. It is those which must be reexamined and, if necessary, modified. Over the last two years the Commission has debated containment strengths, with much of the focus being upon ice condenser containments and BWR pressure suppression containments. Both represent containments which are designed to a significantly lower static design pressure than are the large dry containments. These discussions have been driven by the possibility of hydrogen detonation, a

phenomenon which has flared up as a result of the Three Mile Island accident. We really will not know the percentage of hydrogen consumed at Three Mile Island until we get at the core and analyze how much damage actually did occur to the core. Nevertheless, our requirements have a much stronger emphasis on better hydrogen removal and suppression and on better analysis of the effects of hydrogen burn and detonation.

We have debated the strength of containments - not the design pressure, but the actual strength. We have debated regions of plasticity, nonlinear deformation, and the relationship of yield strength to design pressure. We have tried to address failure modes that would occur if there were to be a hydrogen explosion, and the effects of stiffeners, for example, hoops.

The NRC has taken several actions with respect to hydrogen control. We published a two part proposed interim rule on hydrogen control. We have made the first part final: (1) Requiring inerting BWRs with Mark I or II containments; (2) requiring either an internal recombiner or the capability to install an external recombiner for LWRs which rely upon a purge repressurization system as a primary means for controlling combustible gases following a LOCA; and (3) requiring a remotely operable high point vent. The comment period has closed on the second part of the rule. The NRC staff expects to complete the final rule in July and hopes to get it to the Commission in August or September. I do not know what modifications the staff will suggest to the proposed rule. The proposed rule would require that equipment to establish and maintain cold shutdown and containment integrity be able to survive the containment environment after an accident, for example, hydrogen burn. Licensees with ice condenser containments and Mark III BWR's would be required to provide a hydrogen control system capable of handling hydrogen generation assuming 75 percent metal-water reaction. The proposed rule also specified the following acceptance criteria for containments:

(1) Service Level C stress for steel, or Factored Load Category for concrete, for the post accident internal pressurization due either to hydrogen burn or to inerting, assuming CO_2 is used for inerting.

(2) Service Level A stress for steel, or Service Load Category for concrete, for the inadvertent inerting during normal operations.

The other major rulemaking effort affecting containments is the severe accident rulemaking, which at one time was called the degraded core rulemaking. A research plan focusing upon short term goals has been submitted to the Commission. The short term program is to produce an improved methodology for probabilistic risk analysis, to significantly extend the data base so that severe accidents can be assessed, and to develop the data for better estimates of the source term. The Commission would then initiate the severe accident rulemaking based on the information developed under the short term program and the results of the industry IDCOR program.

It is not clear from the Commission perspective whether we are asking containments to go beyond the current design basis or are changing the design basis. It has been suggested that the role of a containment should change, e.g., be built sufficiently strong so that it can withstand whatever might happen inside. The Commission has not reached that position and I do not think it will. If one agrees that the basic containment function has not changed, that is, it is to contain the fission products during an accident but that at some point it might fail, one still has to address whether the design criteria should be changed. In the current design basis accident concept, the containment has been treated differently from other major reactor components, such as the reactor coolant pressure boundary. The accident loads associated with the faulted conditions of the plant are treated as the "normal" conditions for the containment. Since events beyond the current design basis have lower probabilities of occurrence, this "normal" condition for the containment is at the low probability end of operation. Should the same safety margin be required as required for plant systems for the design basis events? If modified, what should it be? If the current approach for design safety margin should be maintained, what is the economical design?

Researchers need to consider alternate containment concepts. The Commission currently has taken the position that either an igniter system or post accident inerting system is required to control the hydrogen generated by the metal-water reaction. This is to take care of a partially degraded core, but it still does not address the full scale core melt event. Is the present containment base mat design adequate or should it be revised to take care of a core melt event? Core catchers at one time were to be included in reactors. The Indian Point design originally had a core

catcher, a refractory lined, water-cooled, stainless steel core catcher device. This was dropped in 1968, with perhaps the AEC Commissioners playing a role in getting it dropped. If neither of the hydrogen control schemes proves adequate, should the containment be designed to accommodate detonations? Could present design concepts result in an economically feasible containment design? Or should some kind of a filtered vent concept be pursued through engineering design? I note that a filtered venting system is being built for the two BWRs at Barseback, Sweden. Other types of containments might be considered. In the very early 1960's, Westinghouse proposed a special containment: "The special features . . . included, in particular, a double containment system with twin liners surrounding an annular space to be held at negative pressure." This was later modified to "a double containment vessel which completely encloses the primary system. Back pumping and monitored leakage of a porous "popcorn" concrete filled space between the containment walls and of all penetrations are provided. The system depends to some extent on keeping the space between the membranes at negative pressure." That is the description of the reactor Westinghouse proposed for the Malibu site, on the coast of Los Angeles. Another construction permit application proposed "double containment for each of the reactor systems and for the spent fuel storage facility. . . These containment structures consist of two steel shells completely surrounded by 5 1/2 feet and 2 1/2 feet of concrete, respectively, with [porous] concrete occupying the annulus between the inner and outer steel membranes." This is the description for the proposed Ravenswood facility, a plant that was proposed to be built in the heart of New York City.

It also is important to study containment failure modes. The risks associated with various failure modes can differ by several orders of magnitude. Realistic failure modes and their associated probabilities are necessary to establish design criteria consistent with the desired margins of safety. Structural engineers and analysts should explore inelastic containment responses to dynamic loadings. The traditional linear elastic, static, or quasi-static analyses are probably no longer adequate to support a PRA for determining the containment failure modes and times to failure. I do not suggest that inelastic behavior should be tolerated in general, but it may be acceptable for some very low probability beyond design basis events, which are the ones to be considered in analyzing the success or failure of a containment. The failure modes and time to failure can significantly affect the source term and emergency planning requirements. TMI analyses have shown that a water-plentiful

environment suppresses release of iodine by several orders of magnitude. Requirements for contingency planning notification systems are driven by the containment failure times. Containment atmospheric temperature and loading calculations should be refined so that structural analysts and designers can use these numbers with confidence to do realistic failure mode studies. There should be more interaction between the people doing thermal hydraulic calculations and those doing containment structural response calculations in order to achieve a safe and economic design.

Finally, members of the containment design community should consider what kind of suggestions they can make regarding safety goals. As you may know, the Commission has published for public comment a proposed policy statement on safety goals for nuclear power plants. It includes qualitative goals and quantitative guidelines. The guidelines address the risk of early and late deaths from nuclear accidents and also provide a plant performance guideline on large scale core melt, namely, "the likelihood of a nuclear reactor accident which results in a large scale core melt should normally be less than one in 10,000 per year of reactor operation." In this safety goal the only mention of containment is following the core melt guideline: "the Commission also recognizes the importance of mitigating the consequences of a core melt accident and continues to emphasize containment, remote siting, and emergency planning as integral parts of the defense-in-depth concept." The Commission effort on safety goals was initiated by a study done by the ACRS, in which the ACRS did suggest goals be placed not only on core damage and fuel failures but also on large scale uncontrolled release from containment. The ACRS study suggested a probability goal of 0.01 for a large scale uncontrolled release, given a large scale fuel melt, with an upper limit of acceptability of 0.1. In asking for public comment on the safety goal the Commission included a series of questions which we requested commenters address. One question is "Should there be added a numerical guideline on availability of containment function, given a large scale core melt?"

Therefore, as you address what better analyses must be done, and do those analyses; as you address what improvements can be made to existing containments, and engineer those improvements; and as you address what safety margins are appropriate for containment analysis and design, perhaps you can also think about what kind of a quantitative goal or guideline ought to be spelled out for containments.

Ahearne, J. F. 1213
Aragon, J. 1145
Asaka, Y. 595
Ashton, D. H. 1061
Ashurst, W. T. 915

Baer, M. R. 191, 77, 1089
Bajpai, S. N. 709
Barr, P. K. 915
Baukal, W. 1109
Benedick, W. B. 665, 953, 961
Benz, F. J. 581
Berlad, A. L. 1077, 1197
Bickel, J. H. 209
Bloom, G. R. 453
Blose, R. 333
Bowers, C. H.
Bryan, R. H. 1157
Butler, W. R. 7
Buxton, L. D. 469

Camp, A. L. 117, 175, 827, 1045
Chan, C. 889
Chung, H. M. 303
Claybrook, S. W. 453
Clever, R. 1029
Cole, R. K. 385
Corradini, M. L. 351, 775
Crump, O. B., Jr., 843
Cummings, J. C. 665, 1045

Dabora, E. K. 931
Dandini, V. J. 1127
Deem, R. E. 145, 161
Denton, H. R. 569
Dickelman, G. J. 131
Dingman, S. E. 175, 827
Dua, S. S. 265

Elliott, J. S. 265
Eyler, L. 531

Falacy, S. M. 683
Fineschi, F. 93
Frid, W. 439
Fuller, E. L. 73
Fuls, G. M. 225
Fujimoto, T. 553
Furgal, D. T. 1127, 1145

Gou, P. F. 265
Griffiths, S. K. 1089
Guenther, C. F. 741
Guirao, C. M. 953, 961
Gunter, A. D. 225

Harris, M. A. 1061
Haskin, F. E. 791
Hankins, D. A. 257, 265
Harrison, W. C. 633
Hassmann, K. 369
Hobbs, S. H. 283, 1061, 1181
Holtzclaw, K. W. 257
Hwa, V. W. S. 807

Ikai, S. 595
Inase, S. 553
Iyer, S. S. 161

Jahn, H. L. 485
Jaung, R. 1077, 1197

Karlberg, G. 439
Kelly, D. P. 385
Kempka, S. N. 191
Kepley, P. S. 1181
Kinoshita, M. 553
Knystautas, R. 889, 953, 961
Koehling, A. 1109
Kooriyama, T. 553
Kumar, R. K. 633
Kupiec, C. F. 117

Langer, G. 1109
Larkins, J. T. 43
Lau, W. 21
Law, C. K. 595
Lee, J. H. S. 889, 953, 961
Liparulo, N. J. 609, 727
Loyola, V. M. 425
Lunt, R. R. 401

Mackenzie, J. S. 401
McCulloch, W. H. 1127, 1145
Mizomoto, M. 595
Morici, A. 93
Morota, T. 553
Muhlestein, L. D. 453

Nakamura, A. 553
Nesbitt, L. B. 265
Niyogi, K. K. 401

Oeata, J. 553
Olhoeft, J. E. 609
Onisi, K. 553

Paddleford, O. F. 609
Papadimitriou, P. 485
Pham, T. V. 485
Poeschel, E. 1109
Postma, A. K. 453
Prassinos, P. G. 665
Pratt, W. T. 317, 1077, 1197

Ratzel, A. C. 191, 757
Reimann, R. 369
Renfro, D. 1029
Richards, B. 1145
Richardson, J. D. 283
Roller, S. F. 683, 1007
Rousseau, K. 145

Schwarzott, W. 369
Shepherd, J. E. 843, 961, 1007, 1089
Sherman, M. P. 827, 1045
Shimamura, K. 553
Siefert, K. 651
Sliter, G. 1117
Smith, L. 1029
Stroupe, E. P. 73
Sundvall, S. B. 439

Takahashi, K 553
Tamm, H. 633, 873
Tarbell, W. W. 333
Taylor, J. J. 1
Tennankore, K. N. 873
Thomas, G. R. 303
Thompson, L. B. 29, 651, 1029
Thurgood, M. J. 509
Tinkler, C. G. 7
Torok, R. C. 651
Tosetti, R. J. 741
Travis, J. R. 489
Trebilcock, W. R. 791
Trent, D. S. 531
Tsai, S. S. 609, 727
Tsuge, A. 553

Ukai, O. 553
Ural, E. 807

Vieira, A. T. 1181

Weber, G. 485
Wester, M. J. 175, 827, 1045
Worthington, P. 43

Yu, W. S. 317

Zalosh, R. G. 709, 807
Zinnari, R. 93